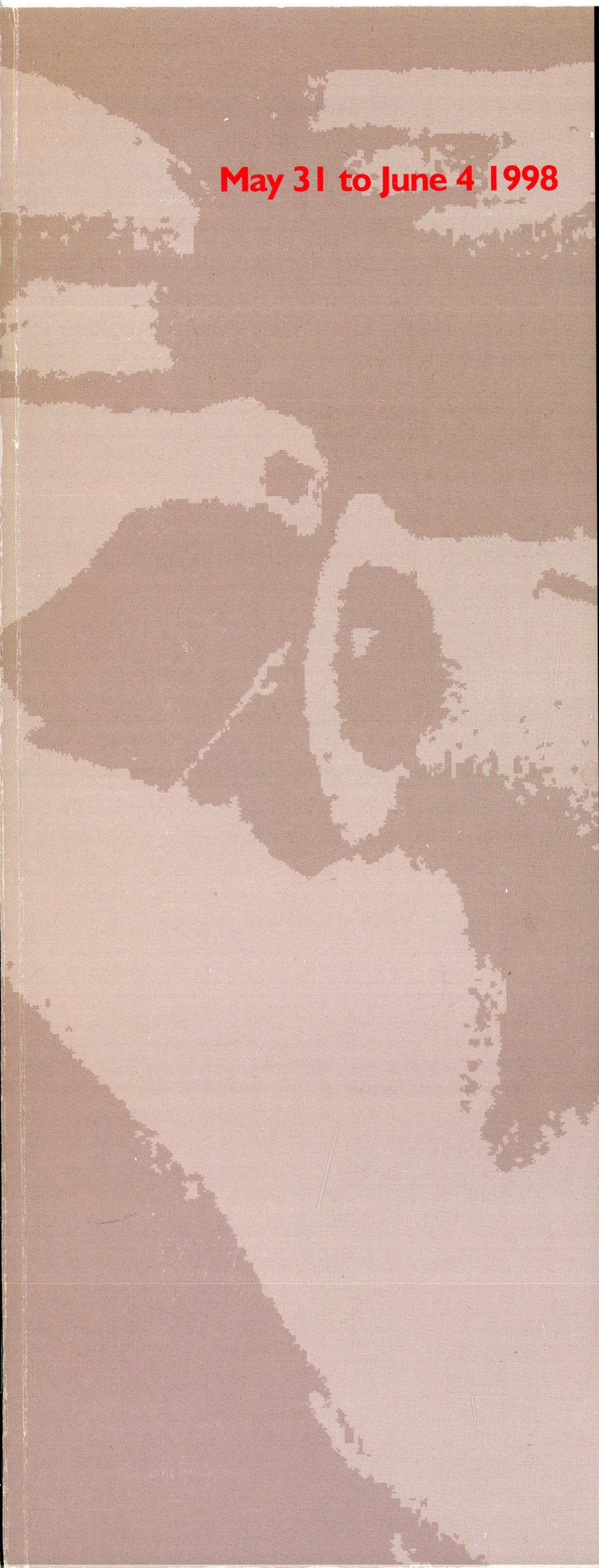

May 31 to June 4 1998

16th International Technical Conference on the Enhanced Safety of Vehicles

Proceedings

Volume 3 of 3

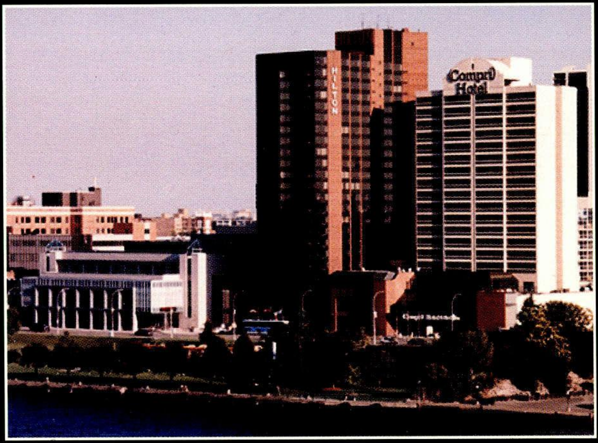

The Cleary
International Centre
Windsor, Ontario
CANADA

ESV
WINDSOR98

16th International Technical Conference on the **Enhanced Safety of Vehicles**

Proceedings Volume 3 of 3

U.S. Department
of Transportation

National Highway
Traffic Safety
Administration

Transport
Canada
Road Safety

Transports
Canada
Sécurité routière

DOT HS 808 759
October 1998

May 31 to June 4 1998

16th International
Technical Conference on the
Enhanced Safety of Vehicles

Proceedings
Volume 3 of 3

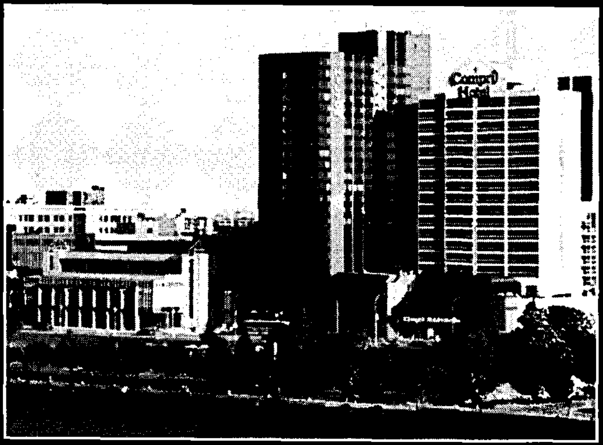

The Cleary
International Centre
Windsor, Ontario
CANADA

ESV
WINDSOR98

How to Use the Conference Proceedings

The first six (6) pages in each of the different sections of the Proceedings are edged in black ink for quick guidance.

Papers in each of the eleven (11) technical sessions have an assigned paper number i.e., 98-S1-O-07, which is representative of the following:

Code **Explanation**
98 = The Year of the Conference
S1 = The Technical Session Number
O = The Type of Paper Presentation (**O**ral, **P**oster, **W**ritten)
07 = The Assigned Paper Number within each Technical Session

When a break in the sequence of an assigned paper number occurs, it is because the paper was (1) withdrawn, (2) rearranged within the session, or (3) transferred to another session.

How to Obtain the Conference Proceedings

The 16th ESV Conference Proceedings are published by the United States Government and distributed globally, currently at no cost. These reports, which detail international harmonization and safety research efforts, have been recognized as the definitive work on motor vehicle safety research. If you are interested in obtaining a copy of the Proceedings, please fill in the form below and mail to:

16th ESV Conference Proceedings
% National Highway Traffic Safety Administration
400 7th Street S.W., Room 6206
Washington, D.C. 20590

Please send a copy of the 16th ESV Conference Proceedings to:

Name: ______________________________

Company Title: ______________________________

Company: ______________________________

Address: ______________________________

City: ______________ State: ______________ Zip Code: ____________

Country: ____________

Telephone: ________________ Telefax: ________________

E-mail: ________________

Introduction

The United States Department of Transportation, National Highway Traffic Safety Administration (NHTSA), Office of Research and Development is the official government agency responsible for the implementation of the International Technical Conferences on the Enhanced Safety of Vehicles (ESV). The Conferences are held approximately every two years and hosted by participating Governments. Delegate and attendee participation includes worldwide governments, automotive industries, motor vehicle research engineers and scientists, medical, insurance, and legal professions, consumers, academia, private corporations, and international media.

The ESV Program originated in 1968 under the North Atlantic Treaty Organization (NATO) Committee on the Challenges of Modern Society, and was implemented through bilateral agreements between the governments of the United States, France, the Federal Republic of Germany, Italy, the United Kingdom, Japan, and Sweden. The participating nations agreed to develop experimental safety vehicles to advance the state-of-the-art technology in automotive engineering and to meet periodically to exchange information on their progress. Since its inception the number of international partners has grown to include the governments of Canada, Australia, the Netherlands, Hungary, Poland, and two international organizations -- the European Enhanced Vehicle-Safety Committee, and the European Commission. A representative from each country and organization serves as a Government Focal Point in support of the Conference.

In 1968 the Conference was known as the International Experimental Safety of Vehicles Conference. Over time, the focus of the Conference shifted from concentration on the development of experimental safety vehicles to broader issues of safety and international cooperation seeking reductions in motor vehicle fatalities and injuries. These issues include program advances such as Pedestrian Safety, Frontal and Side Impact Protection, Biomechanics, Intelligent Transportation Systems, and Vehicle Compatibility. In 1991, the participating governments agreed to change the name of the Conference to "The International Technical Conference on the Enhanced Safety of Vehicles" to reflect the current focus. The 14th ESV Conference, held in Munich, Germany, May, 1994, was the first conference in which the new name was used, and "25 Years of ESV Development" was celebrated.

The 15th ESV Conference, held in Melbourne, Australia, May, 1996, was precedence-setting as well. A new 5-year priority research program known as International Harmonized Research Activities (IHRA) was established under the auspices of the ESV Conference. The program established six international priority research areas; Biomechanics, Advanced Offset Frontal Crash Protection, Vehicle Compatibility, Pedestrian Safety, Intelligent Transportation Systems and recently chosen Side Impact Protection. In May of 1997, NHTSA hosted a Public Workshop to share with its partners the goals and objectives of IHRA. In November of 1997, the ESV Government Focal Points agreed that all participating governments would join in these priority research programs, and that the programs would be governed by an IHRA Steering Committee comprised mainly of the ESV Government Focal Points. Six Working Groups that now exist in each of the priority research areas are led by participating Governments, and are comprised of government and industry experts. The IHRA Steering Committee consisting of Government members meets biannually to review recommendations and research plans being developed by the Working Groups.

This, the 16th ESV Conference hosted by Transport Canada, held in Windsor, Ontario, Canada, May 31-June 4, 1998, was attended by delegates from twenty one (21) different countries. The IHRA Status Reports on the progress of the five priority research areas were presented during this Conference. Well over 300 technical papers were accepted for inclusion in the Conference Proceedings, with international authors representative of sixteen (16) different nations. This Conference also marked the first time scientific poster presentations were given.

The 17th ESV Conference, the first Conference of the 21st Century, will be held in Amsterdam, The Netherlands, in the year 2001. The year was chosen because IHRA will have met the 5-year deadline for reporting their vision, goals, objectives, and achievements under the program.

We thank our international conference participants for their continued interest, dedication and support. It is an outstanding example of the highest regard for automotive safety research we are certain will continue.

International Technical Program Delegates

United States – 16th ESV Conference Sponsor

The Honorable Rodney E. SLATER
Secretary
Department of Transportation

Ricardo MARTINEZ, M.D.
Administrator
National Highway Traffic Safety Administration

Raymond P. OWINGS
Associate Administrator
National Highway Traffic Safety Administration

Donna E. GILMORE
ESV Technical Coordinator
National Highway Traffic Safety Administration

Joseph KANIANTHRA
ESV Historian
Director Office of Vehicle Safety Research
National Highway Traffic Safety Administration

John HINCH
IHRA Secretariat
National Highway Traffic Safety Administration

Rae TYSON
Office of Public & Consumer Affairs
National Highway Traffic Safety Administration

Canada – 16th ESV Conference Host

The Honorable David M. COLLENETTE
Minister
Department of Transport

Nicole PAGEOT
Director General
Road Safety and Motor Vehicle Regulation
Transport Canada

Brian JONAH
Director Motor Vehicle Standards and Research
Transport Canada

Y. Ian NOY
Chief Ergonomics Division
Transport Canada

Vittoria BATTISTA
ESV Program Manager
Transport Canada

Irenka FARMILO
Communications Group
Transport Canada

Laura COOKE
Regional Director, Communications, Ontario Region
Transport Canada

16th ESV Government Focal Points

Peter MAKEHAM
Director
Federal Office of Road Safety
Australia

Y. Ian NOY
Chief Ergonomics Division
Transport Canada
Canada

Viola GROEBNER
Head of Unit - DG III E 5
Automobiles, Other Road Vehicles & Tractors
European Commission

Jean-Pierre MÉDEVIELLE
Deputy General Director
INRETS
France

Bernd FRIEDEL
Chairman, EEVC, Director and Professor
Bundesanstalt für Straßenwesen (BASt)
European Enhanced Vehicle-Safety Committee

K.-H. LENZ
President and Professor
Bundesanstalt für Straßenwesen (BASt)
Germany

International Technical Program Delegates (continued)

Sándor *SZABÓ*
Chief du Bureau ECE
AUTÓKUT
Hungary

Claudio *LOMONACO*
Director General
Ministry of Transport
Italy

Shoji *WATANABE*
Deputy Director, Automobile Division
Ministry of International Trade and Industry
Japan

Gerard J.M. *MEEKEL*
Head of Vehicle Standards Development
Ministry of Transport
The Netherlands

Wojciech *PRZYBYLSKI*
Head of Vehicle Approval and Testing Department
Motor Transport Institute
Poland

Kåre *RUMAR*
Professor
Swedish Road & Transport Research Institute (VTI)
Sweden

Malcolm *FENDICK*
Chief Mechanical Engineer
Department of Transport
United Kingdom

Raymond P. *OWINGS*
Associate Administrator
National Highway Traffic Safety Administration
United States

16th ESV Technical Session Chairpersons

Claudio *LOMONACO*
Director General
Ministry of Transport
Italy

Y. Ian *NOY*
Chief Ergonomics Division
Transport Canada
Canada

Richard *LOWNE*
Research Fellow
Transport Research Laboratory
United Kingdom

Cezary *SZCZEPANIAK*
Professor
Technical University of ŁÓDŻ
Poland

W. Thomas *HOLLOWELL*
Chief Safety Systems Engineering and Analysis
National Highway Traffic Safety Administration
United States

Claes *TINGVALL*
Director of Road Safety
Swedish National Road Adminsitration
Sweden

Rolf *EPPINGER*
Chief National Transportation Biomechanics
Research Center
National Highway Traffic Safety Administration
United States

Dainius J. *DALMOTAS*
Senior Engineer
Road Safety & Motor Vehicle Regulations
Transport Canada
Canada

Keith *SEYER*
Chief Engineer
Vehicle Standards, Research & Development
Federal Office of Road Safety
Australia

Yoshiyuki *MIZUNO*
Director Research Division
Japan Automobile Standards Internationalization
Center
Japan

Bernd *FRIEDEL*
Chairman, EEVC
Director and Professor
Bundesanstalt für Straßenwesen (BASt)
European Enhanced Vehicle-Safety Committee

Table of Contents

Volume 1: Opening Ceremonies Through Technical Session 3

Opening Ceremonies

Welcoming Remarks 1
Nicole Pageot, Director General, Road Safety and Motor Vehicle Regulation, Transport Canada, Canada 1
Raymond P. Owings, Ph.D., Associate Administrator, National Highway Traffic Safety Administration, United States 1

Keynote Addresses 2
Ricardo Martinez, M.D., Administrator, National Highway Traffic Safety Administration, United States 2
The Honorable David M. Collenette, Minister of Transport, Canada 4

U.S. Government Awards Presentations 7
Ricardo Martinez, M.D., Administrator, National Highway Traffic Safety Administration, United States
U.S. Government Awards for Safety Engineering Excellence 7
U.S. Government Special Awards of Appreciation 9
U.S. Government Special Recognition Presentations 10

Government Status Reports 11
Chairperson: Jean-Pierre Médevielle, INRETS, France

Commission of the European Community 11
Herbert Henssler, European Commission

Federal Republic of Germany 15
K.-H.Lenz, Bundesanstalt für Straßenwesen

The European Enhanced Vehicle-Safety Committee (EEVC) 29
Bernd Friedel, Bundesanstalt für Straßenwesen

France 32
Jean-Pierre Médevielle, French National Institute for Research in Transportation and Safety

United Kingdom 35
Keith Rodgers, Department of the Environment Transport and the Regions

Italy 39
Claudio Lomonaco, Ministry of Transport

Japan 42
Shoji Watanabe, Ministry of International Trade and Industry

Australia 44
Peter Makeham, Federal Office of Road Safety

The Netherlands 50
Gerard J.M. Meekel, Ministry of Transport

Sweden 53
Kåre Rumar, Swedish Road and Transport Research Institute (VTI)

Poland 57
Wojciech Przybylski, Instytut Transportu Samochodowego

United States 59
Raymond P. Owings, Ph.D., National Highway Traffic Safety Administration

Canada 79
Nicole Pageot, Transport Canada

International Harmonized Research Activities (IHRA) Status Reports

IHRA Status Reports are located in the Technical Sessions in which they were presented.

Status Report of the Advanced Offset Frontal Crash Protection Working Group . Technical Session 1, p. 146
Claudio Lomonaco, Ministry of Transport, Italy

Status Report of the Intelligent Transportation Systems (ITS) Working Group . . Technical Session 2, p. 360
Y. Ian Noy, Transport Canada, Canada

Status Report of the Vehicle Compatibility Working Group . . . . Technical Session 3, p. 636
Keith Rodgers, Department of the Environment Transport and the Regions, United Kingdom

Status Report of the Biomechanics Working Group . . . . Technical Session 7, p. 1509
Rolf Eppinger, National Highway Traffic Safety Administration, United States

Status Report of the Pedestrian Safety Working Group . . . . Technical Session 10, p. 2120
Yoshiyuki Mizuno, Japan Automobile Standards Internationalization Center, Japan

Invited Speakers Executive Panel

Trends and Priorities in Motor Vehicle Safety for the 21st Century
Moderator: Gerard J.M. Meekel, Head of Vehicle Standards Development, Ministry of Transport, The Netherlands

United States 81
Philip R. Recht, Deputy Administrator, National Highway Traffic Safety Administration

Japan 85
Kazuyoshi Matsumoto, Director, Office of International Affairs, Ministry of Transport

France 88
Christian Steyer, Head of Safety Engineering Department, Renault SA

United States 90
Richard L. Klimisch, Vice President Engineering Affairs, American Automobile Manufacturers Association

Germany 100
Josef Haberl, General Manager Vehicle Safety, BMW AG

The Netherlands 103
Gerard J.M. Meekel, Head of Vehicle Standards Development, Ministry of Transport

Invited Speakers Executive Panel

Human Factors
Moderator: Y. Ian Noy, Chief Ergonomics Division, Transport Canada, Canada

United States 107
R. Wade Allen, Principle Research Engineer, Systems Technology, Inc.

The Netherlands 117
Tom Heijer, Institute for Road Safety Research SWOV

United States 127
Barry H. Kantowitz, Senior Research Scientist, Battelle Human Factors Transportation Center

United States 133
Lidia P. Kostyniuk, Associate Research Scientist, University of Michigan Transportation Research Institute

United Kingdom . . . . (At Time of Printing Paper Not Available)
Andrew Parkes, Principle Research Fellow, Institute for Transport Studies, University of Leeds

Sweden 137
Kåre Rumar, Professor, Swedish Road and Transport Research Institute

Canada 141
Y. Ian Noy, Chief Ergonomics Division, Transport Canada

Technical Session 1

Advanced Frontal and Offset Frontal Protection 145
Chairperson: Claudio Lomonaco, Ministry of Transport, Italy

Oral Presentations

98-S1-O-01
Frontal Offset Crash Test Study Using 50th Percentile Male and 5th Percentile Female Dummies 150
Brian T. Park, Richard M. Morgan, James R. Hackney, John Lee, Sheldon L. Stucki
National Highway Traffic Safety Administration
Johanna C. Lowrie
Conrad Technologies, Inc.
United States

98-S1-O-02
Determination of Frontal Offset Test Conditions Based On Crash Data 164
Sheldon L. Stucki, William T. Hollowell
National Highway Traffic Safety Administration
Osvaldo Fessahaie
Information Systems and Services, Inc.
United States

98-S1-O-03
Offset Test Procedure Development and Comparison 185
Carl L. Ragland
National Highway Traffic Safety Administration
United States

98-S1-O-04
Modeling of an Innovative Frontal Car Structure: Similar Deceleration Curves at Full Overlap, 40 Per Cent Offset and 30 Degrees Collisions 194
W.J. Witteman, R.F.C. Kriens
Eindhoven University of Technology
The Netherlands

98-S1-O-06
Injury Patterns Among Air Bag Equipped Vehicles 213
Jeffrey S. Augenstein, Elana Perdeck, Jami Williamson, James Stratton, Tristam Horton
University of Miami School of Medicine
Kennerly Digges, A. Malliaris
George Washington University
Louis Lombardo
National Highway Traffic Safety Administration
United States

98-S1-O-07
Improving Safety Performance in Frontal Collisions by Changing the Shape of Structural Components . 222
Michael Giess
The Sir Lawrence Wackett Centre for Aerospace Design Technology, RMIT
Josef Tomas
Advea Engineering Pty, Ltd
Australia

98-S1-O-08
The Offset Crash Test - A Comparative Analysis of Test Methods 229
Tomiji Sugimoto, Yoshiji Kadotani, Shigeru Ohmura
Honda R&D Company, Ltd.
Japan

98-S1-O-09
Frontal Impact Protection: Tailoring Safety System Performance by the Prediction of Driver Size and Seated Position 236
Margaret Galer Flyte
Vehicle Safety Research Group Loughborough University
United Kingdom

98-S1-O-10
Simulation of Foot Well Intrusion for Sled Testing 242
Martin Thelen, Ralf Raffauf, Winfried Buss, Willi Roth, Klaus Hillenbrand
PARS, Passive Rückhaltesysteme GmbH
Germany

98-S1-O-11
Predicting Proximity of Driver Head and Thorax to the Steering Wheel 245
Miriam A. Manary, Carol A.C. Flannagan, Matthew P. Reed, Lawrence W. Schneider
University of Michigan Transportation Research Institute
United States

98-S1-O-12
Restraint System Optimisation for Minimum Societal Harm 255
L.J. Sparke
General Motors Holden
Australia

98-S1-O-13
Frontal Impacts with Small Partial Overlap: Real Life Data from Crash Recorders 259
Anders Kullgren, Anders Ydenius
Folksam Research
Claes Tingvall
Swedish National Road Administration
Sweden

98-S1-O-14
Compatibility Study in Frontal Collisions - Mass and Stiffness Ratio 269
Saad A.W. Jawad
ACME Department University of Hertfordshire
United Kingdom

98-S1-O-16
The Effect of Hybrid III Lower Leg Kinematics on Loading Mechanisms and Injury Criteria 275
A.R. Payne
Motor Industry Research Association (MIRA)
J. Green
Rover Group
A.V.Thomas
Jaguar Cars
D. Midoun
Ford Motor Company
United Kingdom

Poster Presentations

98-S1-P-05
Parametric Study on the Effect of the Footwell Geometry, Dynamic Intrusion and Occupant Location on HIII Lower Leg Injury Criteria 283
A.R. Payne, A.R. Lawson, A.R. Hall
Motor Industry Research Association (MIRA)
J. Green
Rover Group
A.V. Thomas
Jaguar Cars
D. Midoun
Ford Motor Company
United Kingdom

98-S1-P-18
An Inflatable Carpet to Reduce the Loading of the Lower Extremities - Evaluation by a New Sled Test Method with Toepan Intrusion 292
Yngve Håland, Erik Hjerpe
Autoliv Research
Per Lövsund
Department of Injury Prevention Chalmers University of Technology
Sweden

Written Papers

98-S1-W-20
Crashworthiness of Aluminum Structured Vehicles 302
Michael J. Wheeler
Alcan International Limited
Canada

98-S1-W-21
Offset Crash Tests - Observations About Vehicle Design and Structural Performance 311
Michael P. Paine
Vehicle Design and Research Pty Limited
Donal McGrane
NSW Roads and Traffic Authority
Jack Haley
NRMA Limited
Australia

98-S1-W-23
Optimized Restraint Systems for Rear Seat Passengers 316
Harald Zellmer, Stefan Lührs, Klaus Brüggemann
Autoliv GmbH Elmshorn
Germany

98-S1-W-26
Patterns of Abdominal Injury in Frontal Automotive Crashes 327
Ali M. Elhagediab
Aerotek Lab Support
Stephen W. Rouhana
General Motors Corporation
United States

98-S1-W-27
The Effect of Airbags on Injuries and Accident Costs 338
Klaus Langwieder, Thomas A. Hummel
GDV Institute for Vehicle Safety
Dieter Anselm
Allianz Center for Technology
Germany

Technical Session 2

Intelligent Transportation Systems (ITS) Collision Avoidance Systems 360
Chairperson: Y. Ian Noy, Transport Canada, Canada

Oral Presentations

98-S2-O-01
Promotion Plan of the Development of Advanced Safety Vehicle (ASV) 367
Shinichi Yahagi, Kanji Nakayama
Ministry of Transport
Japan

98-S2-O-02
Pilot Study of Accident Scenarios on a Driving Simulator 374
Thierry Perron, Christian Thomas, Jean-Yves Le Coz
PSA Peugeot Citroën - RENAULT
Jean Chevennement
RENAULT
Anne Damville, Claire Mautuit
CEESAR
France

98-S2-O-03
Application of Intelligent Transportation Systems to Enhance Vehicle Safety for Elderly and Less Able Travellers 386
S. Ling Suen, C.G.B. Mitchell, Steve Henderson
Transport Canada
Canada

98-S2-O-05
Evaluation of Active Safety Performance of Man-Vehicle System 395
Shun'ichi Doi, Sueharu Nagiri, Yasushi Amano
Toyota Central R&D Laboratories, Inc.
Japan

98-S2-O-06
Relationship Between Driving Behavior and Traffic Accidents - Accident Data Recorder and Driving Monitor Recorder 402
Masaru Ueyama, Sumio Ogawa
National Research Institute of Police Science
Hideo Chikasue, Kizuki Muramatu
Yazaki Meter Company, Limited
Japan

98-S2-O-07
Analysis of the Crash Experience of Vehicles Equipped with Antilock Braking Systems (ABS) - An Update 410
Ellen Hertz, Judith Hilton, Delmas Maxwell Johnson
National Highway Traffic Safety Administration
United States

98-S2-O-08
European Accident Causation Survey (EACS) Methodology 414
Bernard Chenisbest
CEESAR
Norbert Jähn
ACEA
Jean-Yves Le Coz
PSA Peugeot Citroën - Renault
France

98-S2-O-09
A Survey of Canadian Drivers' Knowledge About and Experience with Anti-Lock Brakes 422
Deborah A. Collard, Nigel L. Mortimer
Transport Canada
Canada

98-S2-O-10
Quantifying Head-Up Display (HUD) Pedestrian Detection Benefits for Older Drivers 428
Raymond J. Kiefer
General Motors North American Operations Safety Center
United States

98-S2-O-11
Helping Older Drivers Benefit from In-Vehicle Technologies 438
Michael Perel
National Highway Traffic Safety Administration
United States

98-S2-O-12
Antilock Brake Systems and Risk of Different Types of Crashes in Traffic 445
Leonard Evans
General Motors Global R&D Operations
United States

98-S2-O-34
The Contribution of Onboard Recording Systems to Road Safety and Accident Analysis 462
Gerhard Lehmann
Mannesmann VDO AG
Germany
Alan Cheale
VDO North America LLC
United States

Poster Presentations

98-S2-P-13
Driving Simulator Experiment on Drivers' Behavior and Effectiveness of Danger Warning Against Emergency Braking of Leading Vehicle 467
Hitoshi Soma, Kaneo Hiramatsu
Japan Automobile Research Institute
Japan

98-S2-P-14
Enhancement of Vehicle Stability by Controlling Front Brakes and Engine Torque 476
Yutaka Horiuchi
Honda R&D Company, Ltd.
Japan

98-S2-P-15
Adaptability to Ambient Light Changes for Drowsy Driving Detection Using Image Processing 486
Masayuki Kaneda, Hideo Obara, Tsutomu Nasu
Nissan Motor Company, Ltd.
Japan

98-S2-P-16
Development of Tire Pressure Monitoring System Using Wheel-Speed Sensor Signal 492
Masahiro Yonetani, Kaoru Ohashi
Toyota Motor Corporation
Takaji Umeno
Toyota Central Research & Development Laboratorie, Inc.
Yuichi Inoue
Denso Corporation
Japan

98-S2-P-17
Development of the Brake Assist System 497
Masahiro Hara, Masashi Ohta, Atsushi Yamamoto, Hiroaki Yoshida
Toyota Motor Corporation
Japan

98-S2-P-18
A Test Track Performance Evaluation of Current Production Light Vehicle Antilock Brake Systems . . . 502
Garrick Forkenbrock
Transportation Research Center, Inc.
Mark Flick
Radlinski & Associates Inc.
W. Riley Garrott
National Highway Traffic Safety Administration
United States

98-S2-P-19
Headlamp-Based Vision System and the Vision Task 516
Burkard Wördenweber, Nils Labahn
Hella KG Hueck & Company
Germany

98-S2-P-21
Behavioural Adaptation to Fatigue Warning Systems 521
Alex Vincent, Ian Noy, Andrew Laing
Transport Canada
Canada

98-S2-P-22
Vehicle Design and Injuries Sustained by Female Drivers 537
Michael McFadden
Federal Office of Road Safety
Australia

98-S2-P-23
Visual Performance During Night Driving 541
Alain Priez
Renault
Christophe Brigout, Claire Petit, Lionel Boulommier
AARISTE
France

98-S2-P-24
Driver Behavior in a Throttle Off Situation 546
Alain Priez
Renault
Christophe Brigout, Claire Petit, Lionel Boulommier
AARISTE
France

98-S2-P-27
Design and Construction of a Variable Dynamic Vehicle 552
Lloyd Emery
National Highway Traffic Safety Administration
United States

98-S2-P-30
A Heavy Vehicle Drowsy Driver Detection and Warning System: Scientific Issues and Technical Challenges 562
Paul Stephen Rau
National Highway Traffic Safety Administration
United States

98-S2-P-31
A Collision Warning Algorithm for Rear-End Collisions 566
A.L. Burgett, A. Carter, R.J. Miller, W.G. Najm, D.L. Smith
National Highway Traffic Safety Administration
United States

Written Papers

98-S2-W-29
Application of a Video Analyzer for the Safety Evaluation of an Intelligent Cruise Control System 588
Mark D. Robinson
Scientific Applications International Corporation
Neil Meltzer
Volpe National Transportation Systems Center
United States

98-S2-W-32
Headlamp Performance in Traffic Situation 596
Hans-Joachim Schmidt-Clausen
Darmstadt University of Technology
Thomas Dahlem
Darmstadt University of Technology, Volkswagen AG
Germany

98-S2-W-33
The Requirements for Driver Assistance Systems and their Effects on Real-Life Accidents 602
K. Langwieder
German Insurance Association Institute for Vehicle Safety
U. Frost, Brenner & Münnich Ingenieurgesellschaft, E. Bach
University of Applied Science Dresden
Germany

98-S2-W-35
Analysis of Driver-Vehicle Interactions in an Evasive Manouevre - Results of "Moose Test" Studies . . . 620
Joerg J. Breuer
Daimler-Benz AG
Germany

98-S2-W-36
ABS Performance on Gravel Roads 628
Michael J. Macnabb, Steven Ribarits
University of British Columbia
Nigel Mortimer
Transport Canada
Barry Chafe
Royal Canadian Mounted Police
Canada

Technical Session 3

Vehicle Compatibility 635
Chairperson: Richard Lowne, Transport Research Laboratory, United Kingdom

Oral Presentations

98-S3-O-01
NHTSA's Vehicle Aggressivity and Compatibility Research Program 640
Hampton C. Gabler, William T. Hollowell
National Highway Traffic Safety Administration
United States

98-S3-O-02
Improvement of Crash Compatibility Between Cars 650
Eberhard Faerber
BASt
Germany
Dominique Cesari
INRETS
France
Adrian C. Hobbs, Nial J. Wykes
TRL
United Kingdom
Jos Huibers
TNO
Baudewijn van Kampen
SWOV
The Netherlands
Javier Paez
INSIA
Spain

98-S3-O-03
A Simulation Study on the Major Factors in Compatibility 662
Koji Makino, Takeo Mori, Harutoshi Motojima, Akira Yamamoto
Toyota Motor Corporation
Japan

98-S3-O-04
Compatibility Requirements for Cars in Frontal and Side Impact 667
Nial J. Wykes, Mervyn J. Edwards, C. Adrian Hobbs
Transport Research Laboratory
United Kingdom

98-S3-O-05
Proposal to Improve Compatibility in Head On Collisions 682
Christian Steyer, Marc Delhommeau
Renault SA
Pascal Delannoy
Teuchos
France

98-S3-O-06
Evaluation of Occupant Protection and Compatibility Out of Frontal Crash Tests Against the Deformable Barrier 693
Wilfried Klanner, Bernhard Felsch
ADAC
Germany
Frank van West
AIT/FIA
Belgium

98-S3-O-07
Implementation and Assessment of Measures for Compatible Crash Behavior Using the Aluminum Vehicle as an Example 703
Rodolfo Schoeneburg, Horst Pankalla
AUDI AG
Germany

98-S3-O-08
The Compatibility of Mini Cars in Traffic Accidents 715
Koji Mizuno, Janusz Kajzer
Nagoya University
Japan

98-S3-O-10
Demands for Compatibility of Passenger Vehicles 729
Robert Zobel
Volkswagen AG
Germany

98-S3-O-11
Development of a New Crash-Cushion Concept for Compatibility Purposes of Rigid Obstacles Near the Road 742
Hermann Steffan, Heinz Hoschopf, Bertram C. Geigl, Andreas Moser
Graz University of Technology Institute for Mechanics
Austria

Poster Presentations

98-S3-P-12
Comparison of 10 to 100 km/h Rigid Barrier Impacts 752
Hermann Steffan, Bertram C. Geigl, Andreas Moser, Heinz Hoschopf
Graz University of Technology Institute for Mechanics
Austria

98-S3-P-13
Programmable Deceleration Devices for Automotive Testing 758
Hansjoerg Schinke, Robert Weber, Ulrich Fuehrer
MESSRING
Germany

98-S3-P-14
Calibration of Impact Rigs/Crash-Worthiness Testing of Thin Sheet Metal Boxes 763
Carlo Albertini, George Solomos, Kamel Labibes
European Commission Joint Research Centre
Italy

Table of Contents

Volume 2: Technical Session 4 Through Technical Session 7

Technical Session 4

Truck and Bus Safety, and Fuel System Integrity 769
Chairperson: Cezary Szczepaniak, Vehicle Research Institute, Poland

Oral Presentations

98-S4-O-01
Collision Avoidance Through Improved Communication Between Tractor and Trailor 770
C. James Britell
National Highway Traffic Safety Administration
Alan C. Lesesky
Vehicle Enhancement Systems, Inc.
United States

98-S4-O-02
Safety Measures for the Structure of Trucks and Buses 788
Shinichi Yahagi, Takurou Miyazaki
Ministry of Transport
Japan

98-S4-O-03
Pointers Toward the Improvement of Safety in Buses, Derived from an Analysis of 371 Accidents Involving Buses in Germany and from Crash Test Results 791
F. Alexander Berg, Walter Niewöhner
DEKRA Automobil AG
Germany

98-S4-O-04
Development Possibilities in Relation to ECE Regulation 66 (Bus Rollover Protection) 807
Mátyás Matolcsy
IKARUS Vehicle Manufacturing Company
Hungary

98-S4-O-05
Evaluation of Motor Vehicle Initiation and Propogation, Vehicle Crash and Fire Propogation Test Program 813
Jack L Jensen, Jeffrey Santrock
General Motors Corporation
United States

98-S4-O-06
Stability Augumentation System for the Heavy Duty Commercial Vehicles - Estimation of the Gravity Position with AR Method and Application for Anti-Rollover 828
Hirokazu Okuyama, Fujio Momiyama, Keiichi Kitazawa, Kiyoaki Miyazaki, Ichiro Tsumagari
Hino Motors, Ltd.
Hitoshi Soma
Japan Automobile Research Institute
Toshimichi Takahashi
Toyota Central R&D Labs, Inc.
Japan

98-S4-O-07
Improved Crashworthy Designs for Truck Underride Guards 833
Byron Bloch
Auto Safety Design
United States
Louis Otto Faber Schmutzler
Unicamp State University
Brazil

98-S4-O-08
A Case Study of 214 Fatal Crashes Involving Fire 847
Carl L. Ragland
National Highway Traffic Safety Administration
Hsi-Sheng Hsia
Research and Special Programs Administration
United States

98-S4-O-09
A Look at the NHTSA Minimally Compliant Underride Guard at Impact Speeds Above 30 MPH 856
John E. Tomassoni
JETECH
United States

98-S4-O-10
An Algorithm for Detecting Heavy-Truck Driver Fatigue from Steering Wheel Motion 873
David J. King, David K. Mumford
MacInnis Engineering Associates Ltd.
Gunter P. Siegmund
Canada

98-S4-O-12
Improvement of Car-to-Truck Compatibility in Head-On Collisions 883
Céline Adalian, Jean-Luc Russo, Dominique Césari
INRETS
Hervé Desfontaines
Renault V.I.
France

98-S4-O-13
Heavy Duty Vehicle Crash Test Method in Japan 892
Yoshiriro Sukegawa, Fujio Matsukawa
Japan Automobile Research Institute
Takeshi Kuboike, Motomu Oki
Japan Automobile Manufacturer's Association, Inc.
Japan

98-S4-O-14
Safety of Seats in Minibuses - Proposal for a Dynamic Test 899
Dusan Kecman
Cranfield Impact Centre, Ltd.
James Lenard, Pete Thomas
Vehicle Safety Research Centre
United Kingdom

Poster Presentations

98-S4-P-16
Research Tests to Develop Improved FMVSS 301 Rear Impact Test Procedure 907
Carl L. Ragland
National Highway Traffic Safety Administration
United States

98-S4-P-17
Thermal Properties and Flamability Behavior of Automotive Polymers 911
Ismat A. Abu-Isa, David R. Cummings, Douglas E. LaDue
General Motors Global R&D Operations
A. Tewarson
Factory Mutual Research
United States

98-S4-P-18
European Test Methods for Superstructures of Buses and Coaches Related to ECE R66 (The Applied Hungarian Calculation Method) 920
Sándor Vincze-Pap
AUTÓKUT
Hungary

98-S4-P-19
Simulations of Bus-Seat Impact Tests According to ECE Regulations 927
Sándor Vincze-Pap, Zoltán Tatai
AUTÓKUT
Hungary

98-S4-P-20
Safety Rear Underride Guards with an Optional Reverse Impact Braking System 932
Fred Hope
Hope Technical Developments Ltd.
United Kingdom

98-S4-P-21
Sensitivity of Air-Braked Vehicles to Maintenance Underscores the Need for Reliable Low-Cost Cab-Display Brake Fault Indicator Lamp 940
Daniel D. Filiatrault
Insurance Corporation of British Columbia
Canada

98-S4-P-22
Criteria for the Evaluation of Child Detection Aids at School Bus Stops 958
Michael De Santis
Groupe Cartier
André Chamberland
Les Consultants Génicom
Paul Lemay, Claude Guérette
Transport Canada
Canada

Written Papers

98-S4-W-23
Large Scale Experiment of Contour Marking for Trucks 964
Hans-Joachim Schmidt-Clausen
Darmstadt University of Technology
Germany

Technical Session 5

Advanced Air Bag Technology 971
Chairperson: W. Thomas Hollowell, National Highway Traffic Safety Administration, United States

Oral Presentations

98-S5-O-01
The Influence of European Air Bags on Crash Injury Outcomes 972
James Lenard, Richard Frampton, Pete Thomas
Loughborough University Vehicle Safety Research Centre
United Kingdom

98-S5-O-03
Injuries in Primary and Supplementary Airbag Systems 983
Andrew Morris, Brian Fildes
Monash University Accident Research Centre
Australia
Ken Digges
Kennerly Digges and Associates
United States
Dainius Dalmotas
Transport Canada
Canada
Klaus Langwieder
VDS
Germany

98-S5-O-04
Air Bag Collision Performance in a Restrained Occupant Population 989
Alan German, Dainius J. Dalmotas, Regina M. Hurley
Transport Canada
Canada

98-S5-O-05
Driver Stature Injuries and Airbag Deployment Crashes? -- Analysis of UMTRI Crash Investigations . . 997
Donald F. Huelke
University of Michigan Transportation Research Institute
United States

98-S5-O-06
Assessment of Advanced Air Bag Technology and Less Aggressive Air Bag Designs Through Performance Testing 1003
Glen C. Rains, Aloke Prasad, Lori Summers
National Highway Traffic Safety Administration
United States
Mark Terrell
Federal Office of Road Safety
Australia

98-S5-O-07
Assessments of Air Bag Performance Based on the 5th Percentile Female Hybrid III Crash Test Dummy 1019
Dainius J. Dalmotas
Transport Canada
Canada

98-S5-O-08
Measuring Airbag Injury Risk to Out-of-Position Occupants 1036
Christina R. Morris, David S. Zuby, Adrian K. Lund
Insurance Institute for Highway Safety
United States

98-S5-O-09
Assessment of Forearm Injury Due to a Deploying Driver-Side Air Bag 1044
Christy McKendrew, Margaret H. Hines, Alan Litsky
The Ohio State University
Roger A. Saul
National Highway Traffic Safety Administration
United States

98-S5-O-10
Results of Full-Scale Crash Tests, Stationary Tests and Sled Tests to Analyse the Effects of Air Bags on Passengers With or Without Seat Belts in the Standard Sitting Position and in Out-of-Position Situations 1055
F. Alexander Berg, Bernhard Schmitt, Jörg Epple
DEKRA Automobil AG
Rainer Mattern, Dimitrios Kallieris
University of Heidelberg Institute of Forensic Medicine
Germany

98-S5-O-12
Study of Test Procedure to Evaluate Airbag Deployment Force 1071
Koichi Kamiji, Yoshihiko Morita, Makoto Nagai
Honda R&D Company, Ltd.
Japan

98-S5-O-13
A Smart Airbag System 1080
David S. Breed
Automotive Technologies International, Inc.
United States

98-S5-O-14
The Combination of a New Air Bag Technology with a Belt Load Limiter 1092
Farid Bendjellal, Gilbert Walfisch, Christian Steyer, Jean-Yves Forêt-Bruno, Xavier Trosseille
Renault
France

98-S5-O-15
A Comparison Study of Active Head Restraints for Neck Protection in Rear-End Collisions 1103
Dante Bigi, Alexander Heilig
TRW Occupant Restraint Systems
Germany
Hermann Steffan, Arno Eichberger
University of Technology Graz
Austria

98-S5-O-16
Estimation of OOP from Conditional Probabilities of Airbag Fire-Times and Vehicle Response 1111
Guy S. Nusholtz, Lan Xu, Ronald G. Mosier, Gregory W. Kostyniuk, Pranav D. Patwa
Members of the Advanced Restraint Task Group of the Occupant Safety Research Partnership
United States

Written Papers

98-S5-W-17
Preliminary Experience of Passenger Airbag Deployments in Australia 1122
Andrew Morris, Brian Fildes
Accident Research Centre Monash University
Australia

98-S5-W-19
In-Depth Investigation and Reconstruction of an Air-Bag Induced Child Fatality 1126
Alan German, Dainius Dalmotas, Jean-Louis Comeau, Brian Monk, Pierre Contant
Transport Canada
Michel Gou, Serge Carignan, Louis-Philippe Lussier
École Polytechnique de Montréal
James Newman, Christopher Withnall
Biokinetics & Associates Ltd.
Canada

98-S5-W-20
5th % Female Dummy Upper Extremity Interaction with a Deploying Side Air Bag 1135
Stefan M. Duma, Jeff R. Crandall, Walter D. Pilkey
Automobile Safety Laboratory University of Virginia
United States
Kazuhiro Seki, Takashi Aoki
Honda R&D Company, Ltd.
Japan

98-S5-W-24
Evaluation of Secondary Risk with a New Programed Restraining System (PRS2) 1143
Xavier Trosseille, Farid Bendjellal, Gilbert Walfisch
RENAULT
Jean-Yves Forêt-Bruno, Jean-Yves Le Coz
LAB PSA Peugeot-Citroën Renault
Fabrice Berthevas, Pascal Potier
CEESAR
Jean-Pierre Lassau
Institut d'Anatomie de l'UER Biomédicale des Saints Pères
France

98-S5-W-25
Development of a New Crash Cushion for the Protection of People in Wheelchairs in a Road Accident . 1147
Hartmut Bürger, Jürgen Cordes, Holger Schrimpf
Volkswagen AG
Germany

98-S5-W-29
NHTSA's Advanced Air Bag Technology Research Program 1163
Lori Summers, William T. Hollowell, Glen C. Rains
National Highway Traffic Safety Administration
United States

98-S5-W-30
The Coming Revolution in Air Bag Technology 1175
Byron Bloch
Auto Safety Design
United States

Technical Session 6

Data Collection, Analysis, and Linkage 1191
Chairperson: Claes Tingvall, Swedish National Road Administration, Sweden

Oral Presentations

98-S6-O-02
Air Bag Crash Investigations 1192
Augustus B. Chidester, Kenneth W. Rutland
National Highway Traffic Safety Administration
United States

98-S6-O-04
Pedestrian Injury -- Analysis of the PCDS Field Collision Data 1204
Kristie L. Jarrett
Applied Safety Technologies Corporation (ASTC)
Roger A. Saul
National Highway Traffic Safety Administration
United States

98-S6-O-05
Update on Pedestrian Crash Data Study 1212
Ruth A. Isenberg, Augustus B. Chidester
National Highway Traffic Safety Administration
Steve Mavros
KLD Associates, Inc.
United States

98-S6-O-06
Crash Tests to Reconstruct NASS Cases of Child Fatality/Injury from Air Bags 1226
Sheldon L. Stucki
National Highway Traffic Safety Administration
United States

98-S6-O-07
An Update on the Relationships Between Computed Delta Vs and Impact Speeds for Offset Crash Tests 1234
Joseph M. Nolan, Charles A. Preuss, Sara L. Jones, Brian O'Neill
Insurance Institute for Highway Safety
United States

98-S6-O-08
The Accuracy of CRASH3 for Calculating Collision Severity in Modern European Cars 1242
James Lenard, Barbara Hurley, Pete Thomas
Vehicle Safety Research Centre Loughborough University
United Kingdom

98-S6-O-09
A Review of Crash Severity Assessment Programs Applied to Retrospective Real-World Accident Studies 1250
A.L. Turner
Transport Research Laboratory
United Kingdom

98-S6-O-10
Crash Pulse Recorders in Rear Impacts - Real Life Data 1256
Maria Krafft, Anders Kullgren
Folksam Research and Karolinska Institute
Claes Tingvall
Swedish National Road Administration
Sweden

98-S6-O-12
The Role of Motorsport Safety 1263
Peter G. Wright
Fédération Internationale de l'Automobile
United Kingdom

98-S6-O-13
The Aging of the Australian Car Fleet and Occupant Protection 1269
Lauchlan McIntosh
Australian Automobile Association
Australia

98-S6-O-14
The Risk of Skull/Brain Injuries in Modern Cars 1273
Maria Krafft, Anders Kullgren,
Folksham Insurance Company and Karolinska Institute
Anders Lie, Claes Tingvall
Swedish National Road Administration
Sweden

98-S6-O-50
AIS Unification: The Case for A Unified Injury System for Global Use 1276
Elizabeth Garthe, Nicholas Mango
Garthe Associates
John D. States
United States

Poster Presentations

98-S6-P-15
A Comprehensive Surveillance System to Investigate Targeted Issues in Child Occupant Protection . . . 1291
Flaura K. Winston, Dennis R. Durbin
Children's Hospital of Philadelphia, University of Pennsylvania
Frances D. Bents
Dynamic Science, Inc.
John V. Werner
State Farm Insurance Companies
Esha Bhatia, Rajiv A. Menon, Kristy B. Arbogast
Children's Hospital of Philadelphia
United States

98-S6-P-16
An Approach to the Standardisation of Accident and Injury Registration Systems (STAIRS) in Europe 1298
R. Ross, P. Thomas
Vehicle Safety Research Centre Loughborough University
B. Sexton
Transport Research Laboratory
United Kingdom
D. Otte
Accident Research Unit Medical University of Hannover
I. Koßmann
Bundesanstalt für Strassenwesen
Germany
G. Vallet, J.L. Martin, B. Laumon,
Institut National de Récherche sur les Transports et leur Sécurité
P. Lejeune
CETE, Sud-Oest-Ministere des Transports
France

98-S6-P-18
New "Electronic" Data Collection Methods in the National Automotive Sampling System Crashworthiness Data System 1306
Seymour D. Stern, Marvin M. Stephens, Jr., Kenneth W. Rutland
National Highway Traffic Safety Administration
United States

98-S6-P-20
The Safety Effectiveness of Light-Duty Motor Vehicle Occupant Restraints: Numbers of Occupant Lives Saved and Injuries Prevented by Seat Belts in Road Traffic Collisions in Canada, 1989-1995 . . . 1311
Delbert E. Stewart, Hans R. Arora
Transport Canada
Canada

98-S6-P-21
The CIREN Experience 1325
Jeffrey S. Augenstein
University of Miami School of Medicine, William Lehman Injury Research Center
Kennerly Digges
George Washington University
Gail Cooper
San Diego Department of Health Services
David B. Hoyt
University of California
Brent Eastman
Scripps Memorial Hospital Trauma Services
Andrew Burgess, Pat Dischinger
R. Adams Cowley Shock Trauma Center
Jerry Scally
Volpe National Transportation System Center
Stewart Wang, Lawrence Schnider
University of Michigan
John Siegel, George Loo
UMDNJ, New Jersey Medical School
David Grossman, Fred Rivara
Harborview Injury Prevention and Research Center
Martin Eichelberger, Cathy Gotschall
Children's National Medical Center
Lou Lombardo, Lou Brown, R. Eppinger
National Highway Traffic Safety Administration
United States

Written Papers

98-S6-W-22
Serious Lower Extremity Injuries in Motor Vehicle Crashes, Wisconsin, 1991 - 1994 1328
Trudy A. Karlson, Wayne E. Bigelow, Patricia Beutel
Center for Health Systems Research, UW-Madison
United States

98-S6-W-24
A Half Century of Attempts to Re-Solve Vehicle Occupant Safety: Understanding Seatbelt and Airbag Technology 1337
Wendy Waters, Michael J. Macnabb
New Directions Road Safety Institute
Betty Brown
Insurance Corporation of British Columbia
Canada

98-S6-W-25
Seat-Belt Injuries in Medical and Statistical Perspectives 1347
Richard Bandstra, Uwe Meissner
Volkswagon of America, Inc.
Charles Y. Warner
Collision Safety Engineering, Inc.
Susan Monaghan
Herzfeld and Rubin, P.C.
Robert Mendelsohn
United States
Duncan MacPherson
Canada

98-S6-W-26
A Virtually Exact Calculation of Safety Belt Effectiveness 1360
Carl E. Nash
The George Washington University
United States

98-S6-W-29
Lower Back and Neck Strain Injuries: The Relative Roles of Seat Adjustment and Vehicle/Seat Design 1377
Roy Minton
Transport Research Laboratory
P.A. Murray, M. Pitcher, CSB Galasko
Department of Orthopaedic Surgery University of Manchester
United Kingdom

98-S6-W-30
Review of Vehicle Measures for Reducing Accidents and Injuries 1391
Ian D. Neilson, Ruth Condon
Parliamentary Advisory Council for Transport Safety
United Kingdom

98-S6-W-31
Video Image Processing and Database for Traffic Accident Recording System 1399
Sumio Ogawa, Masaru Ueyama
National Research Institute of Police Science
Japan

98-S6-W-36
Comparison of Young and Adult Driver Crashes in Alaska Using Linked Traffic Crash and Hospital Data 1404
Martha Moore
Alaska Department of Health and Social Services
United States

98-S6-W-37
Pelvic Behavior in Side Collisions: Static and Dynamic Tests on Isolated Pelvic Bones 1412
Hervé Guillemot, Claude Got
CEESAR, European Center of Safety and Risk Analysis
Benoit Besnault, François Lavaste
Laboratory of Biomechanics, ENSAM, Paris
Stéphane Robin, Jean Yves Le Coz
Laboratory of Accidentology and Biomechanics, PSA-Renault
Jean-Pierre Lassau
Laboratory of Anatomy, Faculté des Saint-Pères, Paris
France

98-S6-W-38
Changes in Exposure and Accident Risk for Car Drivers in France 1425
Hélène Fontaine
Institut National de Recherche sur les Transports et leur Sécurité
France

98-S6-W-39
Linking Ontario Collision, Vehicle Registration and Trauma Data 1434
Glenn Robbins
Transport Canada
Canada

98-S6-W-40
Motor Vehicle Data in Canada: Past, Present and Future 1440
Linda Yuen
Transport Canada
Canada

98-S6-W-41
A Statistical Methodological Framework for Estimating, Assessing, Evaluating, Monitoring and Interpreting Road Travel Risk Performance Measure Indicators: A 'Risk Analysis and Evaluation System Model' Combining Traffic Collision and 'Exposure to Risk' Information to Identify 'High Risk' Road Travel Patterns and Characteristics 1445
Delbert E. Stewart
Transport Canada
Canada

98-S6-W-42
Observational Studies of Car Occupants' Positions 1465
M. Mackay, A.M. Hassan, J.R. Hill
Accident Research Centre University of Birmingham
United Kingdom

98-S6-W-43
Logistic Regression Analysis of Lower Limb Injuries in Frontal Crashes 1473
Amin Jibril, Priya Prasad, James Prybylski, Ishwar Parekh, Ernie S. Grush
Ford Motor Company
United States

98-S6-W-45
Field Data Improvements for Fire Safety Research 1486
Joseph P. Lavelle, Douglas W. Kononen, James R. Nelander
General Motors Corporation
United States

98-S6-W-46
A Searchable Transportation Fire Safety Bibliography 1490
Douglas E. LaDue III, Douglas W. Kononen
General Motors Global Research and Development Operations
United States

98-S6-W-48
The Development of the Crash Injury Research and Engineering Network 1493
Jerome T. Scally
Volpe National Transportation Systems Center
Rolf Eppinger, Lou Brown
National Highway Traffic Safety Administration
United States

98-S6-W-49
Epidemiology of the Older Driver -- Some Preliminary Findings from Data Through 1996 1496
Leonard Evans
General Motors Global R&D Operations
Peter H. Gerrish, Bahram Taheri
AV/Nessa LLC
United States

Technical Session 7

Biomechanics - Injury Criteria and Test Procedures 1509
Chairperson: Rolf Eppinger, National Highway Traffic Safety Administration, United States

Oral Presentations

98-S7-O-01
Description and Performance of the Hybrid III Three Year Old, Six-Year-Old and Small Female Crash Test Dummies in Restraint System and Out-of-Position Air Bag Environments 1513
Roger A. Saul, Howard B. Pritz, Joseph McFadden, Stanley H. Backaitis
National Highway Traffic Safety Administration
Heather Hallenbeck, Dan Rhule
Transportation Research Center, Inc.
United States

98-S7-O-02
Performance Evaluation of Impact Responses of the SID-IIs Small Side Impact Dummy 1532
Takeshi Harigae, Masanori Ueno, Masaharu Sasaki, Haruo Ohmae
Japan Automobile Research Institute
Takahiko Uchimura
Japan Automobile Manufacturers Association
Japan

98-S7-O-03
Human Thorax Behaviour for Side Impact. Influence of Impact Masses and Velocities 1542
Youcef Talantikite, Hervé Guillemot
CEESAR
Robert Bouquet, Michelle Ramet
INRETS
Stephane Robin
LAB PSA Peugeot Citröen - Renault
Eric Voiglio
UCBLyon
France

98-S7-O-04
Prediction of Thoracic Injuries in Frontal Collisions 1550
Dimitrios Kallieris, Perla Del Conte-Zerial, Andreas Rizzetti, Rainer Mattern
Institute for Forensic Medicine and Traffic Medicine University of Heidelberg
Germany

98-S7-O-05
Biomechanical Impact Tolerance Characteristics of the Human Neck 1564
Liming M. Voo, Narayan Yoganandan, Frank A. Pintar
Department of Neurosurgery, Medical College of Wisconsin, Department of Veterans Affairs Medical Center
Michael Kleinberger, Rolf H. Eppinger
National Highway Traffic Safety Administration
United States

98-S7-O-06
Seat Designs for Whiplash Injury Lessening 1570
Makoto Sekizuka
Toyota Motor Corporation
Japan

98-S7-O-07
A Sled Test Procedure Proposal to Evaluate the Risk of Neck Injury in Low Speed Rear Impacts Using a New Neck Injury Criterion (NIC) 1579
Ola Boström, Yngve Håland, Rikard Fredriksson
Autoliv Research
Mats Y Svensson, Hugo Mellander
Chalmers University of Technology
Sweden

98-S7-O-08
The Whips Seat - A Car Seat for Improved Protection Against Neck Injuries in Rear End Impacts ... 1586
Björn Lundell, Lotta Jakobsson, Bo Alfredsson
Volvo Car Corporation
Martin Lindström, Lennart Simonsson
Autoliv
Sweden

98-S7-O-09
Lower Leg Injuries Caused by Dynamic Axial Loading and Muscle Testing 1597
Yuichi Kitagawa, Hideaki Ichikawa, Chinmoy Pal
Nissan Motor Company, Ltd.
Japan
Albert I. King, Robert S. Levine
Wayne State University
United States

98-S7-O-10
Axial Impact Characteristics of Dummy and Cadaver Lower Limbs 1608
Shashi M. Kuppa
Conrad Technologies Inc.
Gregg S. Klopp, Jeff R. Crandall, Greg Hall
University of Virginia
N. Yoganandan, F.A. Pintar
Medical College of Wisconsin
Rolf H. Eppinger, Emily Sun, Nopporn Khaewpong, Michael Kleinberger
National Highway Traffic Safety Administration
United States

98-S7-O-11
Improved Measures of Foot and Ankle Injury Risk from the Hybrid III Tibia 1618
Eric R. Welbourne
Transport Canada
Nicholas Shewchenko
Biokinetics and Associates
Canada

98-S7-O-12
The Interaction of Air Bags with Upper Extremity Test Devices 1628
C.R. Bass, S.M. Duma, J.R. Crandall, S. George
University of Virginia
S. Kuppa
Conrad Technologies Inc.
N. Khaewpong, E. Sun, R. Eppinger
National Highway Traffic Safety Administration
United States

98-S7-O-13
Investigation of Inertial Factors Involved in Airbag-Induced Forearm Fractures 1646
Warren N. Hardy, Lawrence W. Schneider
University of Michigan Transportation Research Institute
United States

__Written Papers__

98-S7-W-14
Child Safety in Small and Micro Cars 1660
Reiner Nett, Hermann Appel
Institute of Automotive Engineering Technical University of Berlin
Germany

98-S7-W-16
Pelvis Human Response to Lateral Impact 1665
Robert Bouquet, Michelle Ramet, François Bermond, Yves Caire
INRETS
Youcef Talantikite
CEESAR
Stéphan Robin
LAB
Eric Voiglio
UCBLyon
France

Table of Contents

Volume 3: Technical Session 8 Through Technical Session 11

Technical Session 8

Side Impact Protection and Upper Interior Head Protection 1687
Chairperson: Dainius J. Dalmotas, Transport Canada, Canada

Oral Presentations

98-S8-O-02
Test Methods for Evaluating and Comparing the Performance of Side Impact Barrier Faces 1688
P.J. A. De Coo
TNO
The Netherlands
A.K. Roberts
TRL
United Kingdom
A. Seeck
BASt
Germany
D. Cesari
INRETS
(on behalf of EEVC Working Group 13)
France

98-S8-O-04
Development and Benefits of a Harmonised Dynamic Side Impact Standard 1696
K. Seyer, M. Terrell
Federal Office of Road Safety
B. Fildes, D. Dyte
Monash University Accident Research Centre
Australia
K. Digges
George Washington University
United States

98-S8-O-05
Development of Side Impact Air Bag System for Head and Chest Protection 1708
Takayuki Igarashi, Mitsuo Ehama, Yukisada Sunabashiri
Nissan Motor Company, Ltd.
Japan

98-S8-O-06
Head Impact Protection - New Requirements and Solutions 1713
Michael Menking, F. Porsche
Porsche AG
Germany

98-S8-O-07
Reduction of Head Rotational Motions in Side Impacts Due to the Inflatable Curtain - A Way to Bring Down the Risk of Diffuse Brain Injury 1720
Katarina Bohman, Yngve Håland
Autoliv Research
Bertil Aldman
Chalmers University of Technology
Sweden

98-S8-O-08
Comparative Performance Testing of Passenger Cars Relative to FMVSS 214 and the EU 96/EC/27 Side Impact Regulations: Phase I 1727
Randa Radwan Samaha, Louis N. Molino, Matthew R. Maltese
National Highway Traffic Safety Administration
United States

98-S8-O-14
Benefits of the Inflatable Tubular Structure, An Investigation on the Casualty Abatement Capability of the BMW Head Protection System HPS 1760
Klaus Kompass
Bayerische Motoren Werke AG
Germany
Kennerly Digges
K. Digges and Associates
A. Malliaris
Data Link, Inc.
United States

98-S8-O-33
The Windowbag: An Innovation in Side Impact Protection 1768
Luigi Brambilla, Ingo Kallina, Ulrich Tschäschke
Daimler Benz AG
Germany

Poster Presentations

98-S8-P-11
Upper Interior Head, Face and Neck Injury Experiments 1772
Donald Friedman, Keith Friedman
Friedman Research
United States

98-S8-P-12
Advanced Designs for Side Impact and Rollover Protection 1778
Byron Bloch
Auto Safety Design
United States

Written Papers

98-S8-W-15
An Injury Severity Comparison on Side Impact Crash Tests 1793
Andrea Costanzo
University of Rome "La Sapienza"
Luigi Cicinnati
Fracasso Mechanical Engineering Company
Gennaro Orsi
Biomechanics Engineer Consultant
Italy

98-S8-W-16
Vehicle Design Parameter Study for Side Impacts Using Full Vehicle Simulation 1798
Dong Seok Kim, Chang Hun Lee, Myung Sik Lee
DAEWOO Motor Company, Ltd.
Korea

98-S8-W-17
Design Methods for Adjusting the Side Airbag Sensor and the Car Body 1805
Klaus Friedewald
Volkswagen AG
Germany

98-S8-W-18
Rollover Ejection Mitigation Using an Inflatable Tubular Structure (ITS) 1811
Gershon Yaniv
Simula ASD, Inc.
Stephen Duffy
Transportation Research Corporation
Stephen Summers
National Highway Traffic Safety Administration
United States

98-S8-W-23
Vehicle Far-Side Impact Crashes 1819
Richard Stolinski, Raphael Grzebieta
Departmentof Civil Engineering Monash University
Brian Fildes
Accident Research Centre Monash University
Australia

98-S8-W-25
Development of Moving Deformable Barrier in Japan - Part 2 1827
Masonari Ueno, Takashi Harigae, Haruo Ohmae
Japan Automobile Research Institute
Takahiko Uchimura, Eiji Fujiwara
Japan Automobile Manufacturers Association, Inc.
Japan

98-S8-W-27
The POSIP System - Improving Occupant Protection in Convertibles and Coupes During Side Impacts 1835
Martin Heinz, F. Porsche
Porsche AG
Germany

98-S8-W-29
The Inflatable Curtain (IC) - A New Head Protection System in Side Impacts 1846
Anders Öhlund, Camilla Palmertz, Johnny Korner
Volvo Car Corporation
Magnus Nygren, Katarina Bohman
Autoliv
Sweden

98-S8-W-30
Assessment of Injury Protection Performance of Side Impact Airbags for Out-of-Position and Other than 50th Percentile Adult Male Occupants 1858
Anil V. Khadilkar
Biodynamics Engineering, Inc.
Lonney S. Pauls
Springwater Micro Data Systems
United States

98-S8-W-31
Application of Computer Model as an Engineering Tool for Evaluating Side Impact Design Requirements for Children and Small Adults 1868
Anil V. Khadilkar
Biodynamics Engineering, Inc.
Lonney S. Pauls
Springwater Micro Data Systems
United States

98-S8-W-32
Structure and Padding Optimisation for Side Impact Protection 1889
Marcello Di Leo
Fiat Auto S.p.A.
Italy

98-S8-W-34
Evaluation of Restraints Effectiveness in Simulated Rollover Conditions 1897
Glen Rains
National Highway Traffic Safety Administration
Jeff Elias
Transportation Research Center
Greg Mowry
Simula Automotive Safety Devices Incorporated
United States

Technical Session 9

Biomechanics - Dummy Development and Computer Modeling 1909
Chairperson: Keith Seyer, Federal Office of Road Safety, Australia

Oral Presentations

98-S9-O-01
Design and Development of an Advanced Lower Extremity: ALEX II 1910
Alena V. Hagedorn
Transportation Research Center Inc.
Howard B. Pritz
National Highway Traffic Safety Administration
Michael S. Beebe
Applied Safety Technology Corporation
United States

98-S9-O-03
Optimisation of Vehicle Passive Safety for Occupants with Varying Anthropometry 1919
R. Happee, R. van Haaster
TNO Crash-Safety Research Centre
The Netherlands
L. Michaelsen, R. Hoffmann
EASi Engineering GmbH
Germany

98-S9-O-05
Development and Application of a Side Airbag Computer Model Using the CVS/ATB Multi-Body Dynamics Program 1925
Edwin Sieveka, Jeff Crandall, Stefan Duma, Walter Pilkey
University of Virginia
United States

98-S9-O-07
Development of a Hybrid III Lower Leg Computer Model 1936
Jamie A. Buchanan, Terry McKie, Andrew R. Hall
The Motor Industry Research Association
John Green
Rover Group
Alan Thomas
Jaguar Cars
Djamal Midoun
Ford Motor Company
United Kingdom

98-S9-O-09
Evaluation of THOR Dummy Prototype Performance in HYGE Sled Tests 1945
Masahiro Ito, Koshiro Ono
Japan Automobile Research Institute (JARI)
Yoshihisa Kanno
Japan Automobile Manufacturers Association (JAMA)
Japan
Mark Haffner
National Highway Traffic Safety Administration
Nagarajan Rangarajan, Tariq Shams
GESAC, Inc.
United States

98-S9-O-10
Developing Experimental Cervical Dummy Models for Testing Low-Speed Rear-End Collisions 1954
Noboru Shimamoto, Masatoshi Tanaka
Daihatsu Motor Company, Ltd.
Sadami Tsutsumi, Hiroaki Yoshida, Yoichi Miyajima
Kyoto University
Japan

98-S9-O-11
Dynamic Response and Injury Mechanism in the Human Foot and Ankle and an Analysis of Dummy Biofidelity 1960
Paul Manning, Angus Wallace
The University of Nottingham
Clare Owen, Adrian Roberts, Charles Oakley, Richard Lowne
Transport Research Laboratory
United Kingdom

98-S9-O-12
Design and Performance of the THOR Advanced Frontal Crash Test Dummy Thorax and Abdomen Assemblies 1999
N. Rangarajan, R. White, Jr., T. Shams, D. Beach, J. Fullerton
GESAC, Inc.
M. P. Haffner, R. Eppinger, H. Pritz
National Highway Traffic Safety Administration
D. Rhule
Transportation Research Center, Inc.
United States
D. Dalmotas
Transport Canada
E. Fournier
Biokinetics and Associates, Inc.
Canada

98-S9-O-13
Prospects for Electronic Compliance with Belt Fit Requirements 2011
Y. Ian Noy, Vittoria Battista
Transport Canada
Canada

98-S9-O-15
A High Speed Sensor for Measuring Chest Deflection in Crash Test Dummies 2017
Stephen W. Rouhana
General Motors Global Research and Development Operations
Ali M. Elhagediab, Jeffrey J. Chapp
Aerotek Lab Support
United States

Poster Presentations

98-S9-P-17
Injuries to Pregnant Occupants in Automotive Crashes 2046
Kathleen DeSantis Klinich, Lawrence W. Schneider, Jamie L. Moore
University of Michigan Transportation Research Institute
Mark D. Pearlman
University of Michigan Health Systems
United States

98-S9-P-18
Morphometric Study of the Human Pelvis 2065
Benoît Besnault, François LaVaste
Laboratory of Biomechanics ENSAM
Hervé Guillemot
CEESAR
Stéphane Robin
Jean-Yves Le Coz
Laboratory of Accidentology and Biomechanics, PSA Peugeot-Citroën Renault
France

98-S9-P-19
Geometrical Characterisation of a Seated Occupant 2073
Laurent Chabert
Equipements et Composants pour l'Industrie Automobile
Slah Ghannouchi
Laboratorie d'Anatomie, Faculté de Médecine de Sousse
Claude Cavallero
Laboratorie de Biomécanique Appliqée, Faculté de Médecine Nord, Université de la Méditerranée
France

98-S9-P-26
Finite Element Modelling of Blunt or Non-Contact Head Injuries 2080
A.R. Lawson
MIRA
M.M. Sadeghi
Cranfield Impact Centre
United Kingdom

Written Papers

98-S9-W-20
Fidelity of Anthropometric Test Dummy Necks in Rollover Accidents 2093
Brian Herbst, Stephen Forrest, David Chng
Liability Research Group, SAFE, LLC
Anthony Sances, Jr.
Biomechanics Institute
United States

98-S9-W-24
The Load Path from Upper Legs to Chest in the Hybrid III Dummy; Experiments and Simulations . . . 2098
R. Happee, A.R. Kant
TNO Crash-Safety Research Centre
The Netherlands
E. Abramoski, J. Feustel
Ford Motor Company
United States

98-S9-W-27
A Summary of the Work of the SAE ATD Chest Deflection Task Team 2107
John B. Athey, Joseph S. Balser
General Motors Corporation
United States

Technical Session 10

Pedestrian, Child Restraints, and Motorcycle Safety 2119
Chairperson: Yoshiyuki Mizuno, Japan Automobile Standards Internationalization Center, Japan

Oral Presentations

98-S10-O-02
Injury Pattern of Pedestrians Hit by Cars of Recent Design 2122
Jean-Yves Foret-Bruno, Gerard Raverjon, Jean-Yves Le Coz
Accidentology and Biomechanics Laboratory, PSA-Peugeot-Citroën - Renault
France

98-S10-O-03
Pedestrian Safety Testing Using the EEVC Pedestrian Impactors 2131
Graham J.L. Lawrence, Brian J. Hardy
Transport Research Laboratory
United Kingdom

98-S10-O-04
A Technical Evaluation of the EEVC Proposal on Pedestrian Protection Test Methodology 2145
John Green
Rover Group
(on behalf of ACEA Pedestrian Task Force)
United Kingdom

98-S10-O-05
Validation of Pedestrian Upper Legform Impact Test - Reconstruction of Pedestrian Accidents 2152
Yasuhiro Matsui, Hirotoshi Ishikawa
Japan Automobile Research Institute
Akira Sasaki
Japan Automobile Manufacturers Association, Inc.
Japan

98-S10-O-06
Development of a Non-Frangible Pedestrian Legform Impactor 2168
James R. Marous, David B. Reynolds
Wright State University
Douglas C. Longhitano
The Ohio State University
Roger A. Saul
National Highway Traffic Safety Administration
United States

98-S10-O-07
Use and Misuse of Child Restraint Devices in Michigan 2177
David W. Eby, Lidia P. Kostyniuk
University of Michigan Transportation Research Institute
United States

98-S10-O-09
Development of a Sled Side Impact Test for Child Restraint Systems 2179
I.P. Paton, A.P. Roy
Middlesex University
R. Lowne
Transport Research Laboratory
United Kingdom

98-S10-O-10
Towards Improved Infant Restraint System Requirements 2185
France Legault, Del Stewart
Transport Canada
Canada

98-S10-O-11
Analysis of the Passive Safety of Motorcycles Using Accident Investigations and Crash Tests 2221
F. Alexander Berg, Heiko Bürkle, Frank Schmidts, Jörg Epple
DEKRA Automobil AG
Germany

98-S10-O-12
New Developments in Retrospective Data Bases of Serious Car Crashes and Car Collisions with Pedestrians and Motorcyclists - The Research Activities of the German Insurers (GDV) 2237
Dieter Anselm, Klaus Langwieder, Alexander Sporner
GDV- Institute for Vehicle Safety
Germany

98-S10-O-13
An Overall Evaluation of UKDS Motorcyclist Leg Protectors Based on ISO 13232 2247
Nicholas M. Rogers
International Motorcycle Manufacturers Association
Switzerland
John W. Zellner
Dynamic Research, Inc.
United States

98-S10-O-14
Exploratory Study of an Airbag Concept for a Large Touring Motorcycle 2260
Satoshi Iijima, Soichiro Hosono, Atsuo Ota, Takenori Yamamoto
Honda R&D Company, Ltd.
Japan

98-S10-O-15
Safety Potential of Future Two-Wheel Concepts - A Challenge 2279
Ingo Kalliske, Christoph Albus
Federal Highway Research Institute
Germany

Poster Presentations

98-S10-P-16
The Practicalities of Pedestrian Protection 2293
Keith C. Clemo, Robert G. Davies
Motor Industry Research Association
United Kingdom

98-S10-P-21
Child Restraint Information in the National Automotive Sampling System Crashworthiness Data System 2306
Seymour D. Stern
National Highway Traffic Safety Administration
United States

98-S10-P-29
Motorcycle Helmet Test Headform and Test Apparatus Comparison 2310
David R. Thom, Hugh H. Hurt, Jr., Terry A. Smith
Head Protection Research Laboratory
United States

98-S10-P-30
Testing the Positional Stability of Motorcycle Helmets 2323
Hugh H. Hurt, Jr., David R. Thom, James V. Ouellet
Head Protection Research Laboratory
United States

Written Papers

98-S10-W-17
An Analytical Assessment of Pedestrian Head Impact Protection 2331
Abayomi Otubushin, John Green
Rover Group
United Kingdom

98-S10-W-18
Simulation of Car -Pedestrian Accident for Evaluate Car Structure 2344
Suguru Yoshida, Tetsuo Matsuhashi
Honda R&D Company, Ltd.
Yasuhiro Matsuoka
ESI Japan
Japan

98-S10-W-19
A Study on Pedestrian Impact Test Procedure by Computer Simulation - The Upper Legform to Bonnet Leading Edge Test 2349
Atsuhiro Konosu, Hirotoshi Ishikawa
Japan Automobile Research Institute
Akira Sasaki
Japan Automobile Manufacturers Association, Inc.
Japan

98-S10-W-26
Injury Risk/Benefit Analysis of Motorcyclist Protective Devices Using Computer Simulation and ISO 13232 2357
Scott A. Kebschull, John W. Zellner, Michael Van Auken
Dynamic Research, Inc.
United States
Nicholas M. Rogers
International Motorcycle Manufacturers Association
Switzerland

98-S10-W-27
A New Neck for Motorcycle Crash Testing 2375
Christopher Withnall, Edmund Fournier
Biokinetics and Associates Ltd
Canada

Technical Session 11

New Car Assessment Programs 2385
Chairperson: Bernd Friedel, Bundesanstalt für Straßenwesen (BASt), Germany

Oral Presentations

98-S11-O-01
The Effect of Redesigned Air Bags on Frontal USA NCAP 2386
Brian T. Park, Richard M. Morgan, James R. Hackney
National Highway Traffic Safety Administration
Johanna C. Lowrie
Conrad Technologies, Inc.
United States

98-S11-O-02
Repeatability of Frontal Offset Crash Tests 2400
Susan L. Meyerson, David S. Zuby, Adrian K. Lund
Insurance Institute for Highway Safety
United States

98-S11-O-03
International NCAP Programs in Review 2412
Michael Case
RACV
Michael Griffiths
Road Safety Solutions
Jack Haley
NRMA Ltd
Michael Paine
Vehicle Design and Research
Australia

98-S11-O-04
Evolution of Australian NCAP Results Presentation 2420
Michael Case
RACV
Michael Griffiths
Road Safety Solutions
Jack Haley
NRMA Ltd
Michael Paine
Vehicle Design and Research
Australia

98-S11-O-05
A Scientific Method for Analysing Vehicle Safety 2432
Craig Newland, Günther Scheffel, Mark Armstrong
Autoliv Australia Pty Ltd.
Keith Seyer
Federal Office of Road Safety
Australia

98-S11-O-06
Development of the European New Car Assessment Programme (EURO NCAP) 2439
C. Adrian Hobbs, Paul J. McDonough
Transport Research Laboratory
United Kingdom

98-S11-O-07
Objectives and Experience of Publishing Crash-Tests Results in a European Magazin 2454
Alexander Gulde, Lothar Wech
TÜV Automotive GmbH
Bernd Ostmann
Auto Motor und Sport
Germany

98-S11-O-08
Quality Criteria for Crashworthiness Assessment from Real Accidents 2462
Klaus Langwieder, Hans Bäumler
German Insurance Association Institute for Vehicle Safety
Germany
Brian Fildes
Monash University Accident Research Centre
Australia

98-S11-O-10
Future Directions for Australian NCAP 2479
Christopher G.M. Coxon
Transport South Australia
James W. Hurnall
Queensland Transport
Australia

98-S11-O-11
Improvements in NCAP Results for Australian Vehicles 2484
Christopher G.M. Coxon
Transport South Australia
James W. Hurnall
Queensland Transport
Australia

98-S11-O-12
An Analysis of NCAP Side Impact Crash Data 2490
Hansun Chan, James R. Hackney, Richard M. Morgan
National Highway Traffic Safety Administration
Heather E. Smith
Conrad Technologies, Inc.
United States

98-S11-O-13
Improving US NCAP Consumer Information 2503
Noble N. Bowie, Roger Kurrus, Mary Versailles
National Highway Traffic Safety Administration
United States

98-S11-O-14
Philosophy and Strategy of New Car Assessment Programs To Rate Crashworthiness 2509
Gerhard Lutter, Hermann Appel
ISS Automotive Research
Andre Seeck, Bernd Friedel
Federal Highway Research Institute
Germany

98-S11-O-15
A Simulation Study on Inflation Induced Injury and NCAP with Depowered Air Bag 2518
Toru Kiuchi
Toyota Motor Corporation
Japan

Poster Presentation

98-S11-P-16
Development of a Method of Estimating the Costs of Injuries Predicted by ANCAP Testing in Australia 2526
G. Anthony Ryan, Delia Hendrie, Narelle Mullan
The University of Western Australia Road Accident Prevention Research Unit
Australia

Technical Session 8

Side Impact Protection and Upper Interior Head Protection

Chairperson: Dainius J. Dalmotas, Transport Canada, Canada

TEST METHODS FOR EVALUATING AND COMPARING THE PERFORMANCE OF SIDE IMPACT BARRIER FACES

P.J. A. De Coo
TNO
Netherlands
A.K. Roberts
TRL
United Kingdom
A. Seeck
BASt
Germany
D. Cesari
INRETS
France
on behalf of EEVC Working Group 13
Paper Number 98-S8-O-02

ABSTRACT

Side-impact safety of passenger cars is assessed in Europe in a full-scale test using a moving barrier. The front of this barrier is deformable and represents the stiffness of an 'average' car. The EU Directive 96/27/EC on side impact protection has adopted the EEVC Side Impact Test Procedure, including the original performance specification for the barrier face when impacting a flat dynamometric rigid wall.

The requirements of the deformable barrier face, as laid down in the Directive, are related to geometrical characteristics, deformation characteristics and energy dissipation figures. Due to these limited requirements, many variations are possible in designing a deformable barrier face. As a result, several barrier face designs are in the market. However, research institutes and car manufacturers report significant differences in test results when using these different devices.

It appears that the present approval test is not able to distinguish between the different designs that may perform differently when they impact real vehicles. Therefore, EEVC Working Group 13 has developed a number of tests to evaluate the different designs. In these tests the barrier faces are loaded and deformed in a specific and/or more representative way. Barrier faces of different design have been evaluated. In the paper the set-up and the reasoning behind the tests is presented. Results showing specific differences in performance are demonstrated.

INTRODUCTION

In full-scale side impact testing, a mobile deformable barrier face (MDB) is used to represent the front of the bullet vehicle. Currently[1,2] the EEVC MDB is specified only in terms of general dimensions and dynamic performance, when impacting a flat unyielding load cell wall. As a result of this 'performance only' requirement, several different barrier face designs have been developed. Research institutes and vehicle manufacturers report that different barrier designs, conforming to this specification, can induce different types and amounts of vehicle damage[3], as assessed by the Eurosid-1 dummy.

EEVC Working Group 13 (WG13) have defined a number of alternative test methods for assessing the performance of side impact barrier faces[4]. It also explains the objectives of each test condition and suggest additional desirable features based on current experience. These methods could provide comparative data on various barrier face designs to assist the appropriate authorities to select one or more suitable MDB designs, should a design and performance specification be adopted. The performance of a deformable barrier face can only be fully assessed in a full-scale vehicle impact test. In order to validate fully results of the proposed component based tests it is proposed that full-scale tests are also carried out.

This paper is based on a document prepared by EEVC WG13 and describes tests considered and defined by members of the Working Group and by JASIC. Not all of the tests have been fully evaluated and are subject to possible amendment after preliminary trials.

CURRENT STATUS OF THE MOBILE DEFORMABLE BARRIER FACE

The European Side Impact MDB face is defined by geometrical characteristics, material characteristics and deformation characteristics. A MDB face should meet these requirements by design.

MDB Design

The directive indicates that the barrier should be manufactured from aluminium honeycomb but alternative materials are permitted if equivalence can be demonstrated. In a honeycomb barrier a large volume of air can be trapped during crush, assuming that the ends of the cells are sealed during crush. The performance of the barrier then being crushed will come from a combination of honeycomb crush and the compression/release of entrapped air. In order to reduce test variability it is proposed that the trolley surface, onto which the barrier face is fitted, must be ventilated. [For a barrier design with a continuous solid rear surface it will be redundant feature.]

MDB Manufacturing

Certification, Quality Assurance and Conformity of Production of an MDB are considered to be vitally important areas and suitable procedures should be defined, e.g. barrier manufacturers should be approved to ISO9000 or equivalent. Each barrier should be supplied with traceable certification documentation.

MDB Certification

The certification test for the MDB is a perpendicular full frontal impact into a flat rigid load cell wall at 35kph. There is a large difference between the certification test conditions and the actual side impact test conditions, in that the load cell wall does not simulate the complex deformation characteristics of the structure of the struck vehicle, which can have a large effect on barrier performance. In a vehicle impact, differential crush occurs across the face of the barrier as well as shear and bending forces within it. Thus the current certification test is of very limited use for examining barrier performance under the conditions that it will experience in a vehicle impact. Another limitation of the certification test is that it is carried out at 35kph compared with the vehicle test impact velocity of 50kph, since the deforming element would not be capable of absorbing all of the kinetic energy of the mobile barrier moving at 50kph.

DEVELOPMENT OF ALTERNATIVE TEST METHODS

As a result of the present definition of the certification procedure, many different barrier designs showing identical behaviour in a certification test are possible. In order to study the differences between different barrier designs and construction methods, a number of dynamic tests have been developed. These tests, with other suitable tests, could be used to investigate in a controlled manner the dynamic crush performance of side-impact MDB faces.

Pole Impact Tests

Local intrusion of rigid parts into the barrier was found to be a serious point of concern, especially when this part is located one time in the middle of a barrier block, the next time at an intersection between two blocks. To evaluate this phenomenon, two pole impact tests were originally defined by the working group according to figure 1. The set-up was evaluated by JASIC. For this purpose two fundamentally different barrier designs were tested: a profiled (pyramid-shaped) design and a solid (multi-layered) design. The pyramid design barriers had been manufactured with either a full width or segmented front surface.

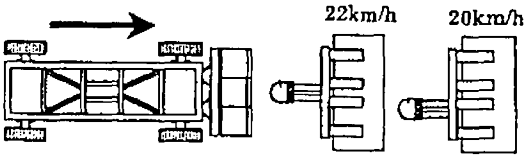

Figure 1: Evaluated test configurations for pole impact

The tests were very severe with very high levels of pole penetration. It was noted that several of the outer blocks became detached from the rear-mounting surface. Total barrier penetration occurred when the pole was offset. In addition, significant differences were observed between barriers manufactured with a continuous front surface and those manufactured with a segmented front.

The evaluation by JASIC showed the need for the pole test but in a slightly different set-up. For that purpose the pole penetration was reduced by adding a rigid wall behind the pole. Additionally, the impact velocity for the centre pole test should be 22kph and 16kph for the offset pole test. The definitive test set-up is shown in the next chapter.

Angled Wall Test

The angled wall test is originally set-up by ACEA/JRC. In this test the wall comprises two symmetrical plates at 30° (left-right symmetrical). This wall profile is not representative of a 'vehicle like' deformed profile (see figure 2). Based on the analysis of twenty side impact tests using fifteen different types/models of vehicles, a new angled rigid wall test was developed by TRL. The analysis examined the post deformation of both vehicles and barrier faces. The aim of the angled walls is to reproduce 'typical' impact deformation on barrier faces, as found in full-scale car tests, so that more realistic performance comparisons can be made between the various barrier designs.

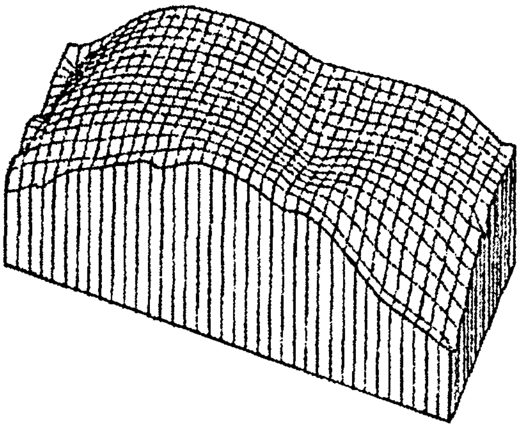

Figure 2: Average profile of 20 crashed barriers.

Seven validation barrier face impact tests, into the new angled wall, have been performed using four designs of aluminium honeycomb barrier face, including both profiled and solid designs. The tests clearly show significant differences in impact performance and barrier failure mechanisms between the different designs of barrier face. Therefore the angled wall test is included in the barrier evaluation programme. The definitive test set-up is shown in the next chapter.

Yielding Wall Test

The interaction between barrier face and car side structure governs the sequence of deformation and deformation pattern. Depending on the stiffness experienced, the barrier or the car will deform. Both structures hit with an originally flat structure. At TNO, a test set-up was developed which also allows the wall to deform. The test produces a convex deformation profile in the barrier.

The impacted wall is replaced by a three-element energy absorbing system. The central element is a rigid plate constrained to move along the longitudinal axis of the mobile barrier with controlled energy absorption. The two outer elements are free-swinging rigid hinged doors whose outer hinges are fixed and whose inner edges bear on the centre plate. The wall at the commencement of the impact is flat. As the barrier loads the wall the centre plate is pushed backwards and the two outer elements swing developing a three surface concave profile.

A series of four tests was carried out to evaluate the discriminating potential of this method. Four different barriers were used, one foam barrier and three profiled barriers. As one of the most important features during side impact is the velocity of the deforming door, the velocity of the central element was monitored.

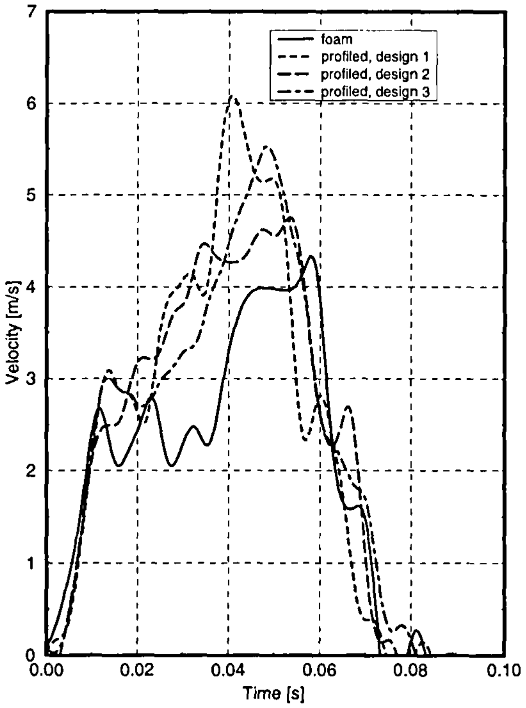

Figure 3: 'Door' velocities with four different barriers.

Figure 3 shows quite different velocities during the time of impact. This justifies the acceptance of this test in the barrier evaluation programme. The definitive test set-up is shown in the next chapter.

BARRIER EVALUATION PROGRAMME

The tests described here should not necessarily be considered to be additional tests or replacements for the certification test in the Directive, but some of them could be used for this purpose if it were considered advisable. It is also acknowledged that the details of the test procedures described below will need to be specified in more detail before they could be used for barrier evaluation.

High Speed Flat Wall Impact Test

This test is a perpendicular impact into a load cell wall. It is fundamentally the same as the current certification procedure, but at the increased velocity of 50kph. To compensate for the increase in energy an additional energy absorption section, covering the full cross sectional area of the barrier, is necessary. The additional element is to be located between the rear face of the test barrier and the impact trolley. The stiffness of the additional section must be uniform across the whole of the rear of the barrier and have a stiffness equivalent to at least twice the stiffest element from which the barrier is constructed. The depth of this additional element must be at least 300mm and should not influence the crush behaviour of the MDB face during the initial impact. It is acknowledged that in this test the barrier face may be totally crushed. The test is used to assess the velocity sensitivity of the barrier's face when compared to the standard 35kph certification test. This test is likely to be able to reproduce better the initial inertial impact stiffness that is experienced in a vehicle test.

Pole Impact Tests

Two pole impact tests are proposed in order to assess the extent to which the barrier face represents that of the front of a real vehicle when impacting a narrow obstacle generating a concentrated force. They are designed to test the ability of the barrier face to transfer impact forces from one part of the barrier to an adjacent part in a similar manner to real vehicles and to test its sensitivity to location of the stiff structure. The pole tests will also be useful for determining the build quality of the barrier, since the outer edges of the barrier will not be directly loaded during the initial phase of the impact.

Central Pole Test - The first of the pole tests is one with a pole located in the centre of the barrier, shown in plan view in figure 4. The test is performed at an impact velocity of 25 kph into a non-deforming pole of 175mm radius, whose apex is 250mm off the surface of the rigid wall. The total barrier mass is 950 kg.

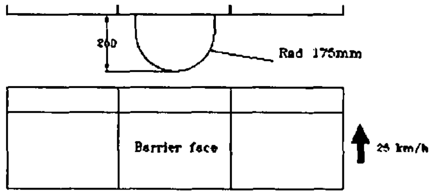

Figure 4. Central pole test.

Offset Pole Test - The second pole test is similar to the central pole test but the pole is offset to one side and is aligned with the division between the centre and edge blocks, figure 5. The offset pole test is performed at the reduced velocity of 20kph. The results of this test will indicate the sensitivity of the MDB face to changes in the location of rigid structures.

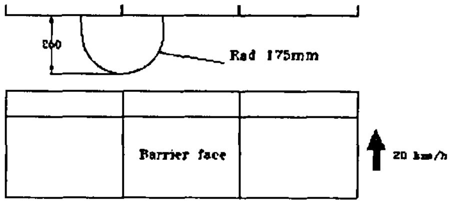

Figure 5. Offset Pole Test.

Rigid Angled Wall Tests

Two test configurations are described at an impact velocity of 35kph. The impact wall is similar to the MDB certification wall, with six load measuring areas but with the addition of rigid elements attached in appropriate places. The purpose of these tests is to examine the dynamic performance of the barrier face with induced shear and bending with longitudinal crush under controlled conditions. The first configuration examines the influence of stiff structures loading the ends of the barrier and the second the influence of a rigid door sill and the override condition. Neither test creates the initial 'vehicle type' loading conditions of full face loading followed by shear and bending, nevertheless the tests will be helpful in studying shear and bending problems, since they would initiate any problems of instability or sensitivity to barrier crush failure. Forces should be measured and can be used for comparative purposes but the prime dynamic evaluation would be from the examination of the dynamic behaviour recorded by high-speed photography. The two tests, the Rigid Edge Loading Test (REL) and Rigid Sill Loading Test (RSL) are specified below.

Rigid Edge Loading Test - The REL test uses the load cell wall with the load cells modified by the addition of rigid wedge shaped blocks, Figure 6. The surface of the wall is wood faced to minimize slip.

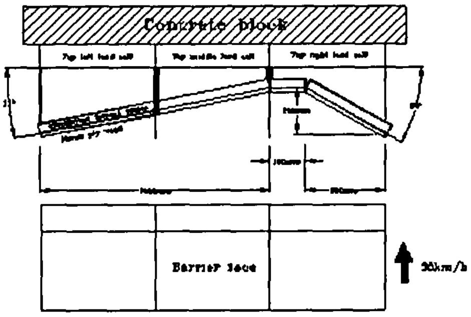

Figure 6. Rigid Edge Loading Test.

The test induces different deformations on each of the outer blocks of the barrier face as will be experienced in vehicle tests. The final deformation profile of the deformable face in plan view is representative of that of the final deformation observed in a typical vehicle impact. However, in a vehicle test the whole face of the barrier is initially loaded at the point of impact, whereas in this test the edges of the barrier are loaded first.

Rigid Sill Loading Test - The RSL test, illustrated in figure 7, simulates an impact into a rigid vehicle sill. It uses the load cell wall with the load cells modified by the addition of rigid wedge shaped blocks mounted on the top three load cells. The surface of the wall is wood faced to minimize slip. The barrier is inverted on the mobile trolley so that the bumper section of the barrier face impacts the simulated sill and is prevented from riding over the sill during the impact. The test induces the type of loading that could be experienced in a vehicle impact, although the loading sequence is not 'car equivalent'.

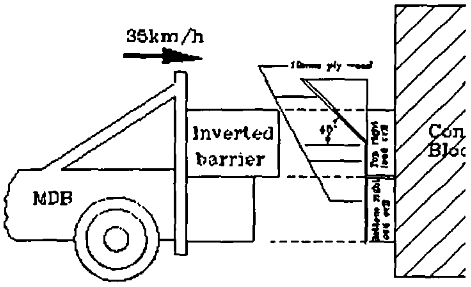

Figure 7. Rigid Sill Loading Test.

Yielding Wall Test

This test configuration will assess the performance of the barrier face in a similar manner to the way a barrier deforms when it impacts a vehicle. In terms of barrier loading sequence, it is considered to be the best of the proposed tests. This test replicates the sequence of initial flat loading followed by differential progressive crush, bending and shear.

In the test, illustrated in Figure 8, the struck vehicle is replaced by a three-element energy absorbing system. The central plate is linearly guided and supported by crumple tubes. The left and right plates are free-swinging rigid hinged doors, at the inner edges supported by the centre plate. The crumple tubes are configured in such a way that barrier loading and deformation in this test simulates that occurring in a vehicle test but produces three flat surfaces compared to the parabolic profile of a vehicle test. The test would be performed at a velocity commensurate with car induced deformation - 50kph. The major assessment of barrier failure would be based on an evaluation of the deformation characteristics obtained by high speed photography, although some comparisons could be made if forces were measured behind the MDB face.

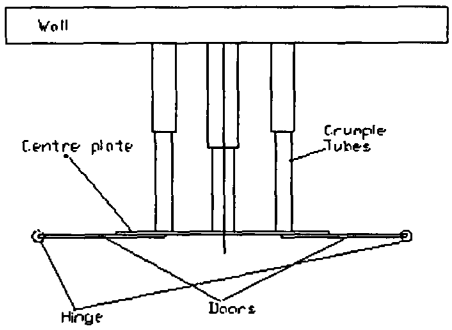

Figure 8. Yielding Wall Test.

Full-scale Vehicle Test

The final MDB evaluation should be based on full-scale vehicle tests where the assessment of barrier performance or variations in performance are based on a) Visual deformation of the barrier. b) Eurosid-1 based parameters at the thorax, abdomen and pelvis levels and c) Vehicle based parameters (acceleration and deformation). The test procedure should be the same as that prescribed in the side impact Directive or Regulation[1,2]. Tests should be performed with the same model of vehicle, using the full range of barrier faces under consideration. In order to eliminate any element of vehicle based bias, the tests should be performed with at least two different types/sizes of vehicle.

ASSESSMENT

Assessment techniques provide a robust methodology to assess the potential performance of any energy absorbing barrier (in particular the European side impact deformable barrier) to deliver a realistic, reliable and repeatable impact to the side of a vehicle, in a legislative test. Some of the tests and evaluation criteria are easy to assess and are thus straightforward to use and to rank the performance of any barrier designs. Other criteria are much more difficult to quantify since they are subjective.

Hereafter criteria related to proper design, dynamic performance and subjective requirements are summarized. In order to evaluate these criteria it is proposed that a group of technical experts on vehicle impact testing could examine the barriers pre and post impact, together with film and transducer data of the tests. The group of experts could then assess the quantifiable and subjective data. They would comment on and rank these aspects of barrier performance and report.

Design Aspects

1. There should be traceable Certification and Conformity of Production data for each individual barrier. The data should preferably be directly associated with the individual barrier rather than by batch or design relationship.
2. The build and manufacturing quality, dimensional control, bonding systems and squareness of construction should be controlled.
3. The front surface of the deformable barrier face should be continuous across the width of the barrier face, thus preventing any object from penetrating the barrier between adjacent blocks or into the blocks without resistance.
4. The barrier material, adhesives and construction should be environmentally stable, covering aspects such as humidity, temperature, UV sensitivity and ageing.
5. The barrier should be sufficiently robust to survive transportation from manufacturer to test facility, to survive pre-impact preparation and the pre-impact acceleration of the trolley.
6. A barrier should deform differentially when subjected to highly localised stresses, at any position. Elements and/or inter layers should not spread the load excessively within the barrier.
7. Post impact barrier disposal should be environmentally satisfactory.

Quantitative Performance Aspects

1. All barrier face designs must fulfil the present requirements as defined in the certification test procedure[1,2].
2. No detachment of component parts or blocks of the barrier shall occur during the crush phase of the impact, although some small opening up of the barrier might be acceptable, after the peak forces have been recorded.
3. The initial stiffness of the barrier face shall be compared with the mean theoretical initial stiffness. The difference should be no greater that 10%. This holds for the certification test. In the high speed flat wall impact test the initial stiffness should be the same as in the 35kph test within a tolerance of [20%]. The variation of absorbed energy distribution for each area, as a

function of the total absorbed barrier energy, from the 35kph test distribution should be less than 10%.

4. The absorbed energy for each block should be determined, if possible. These energies could be used for further evaluation if necessary. If crush forces behind the barrier face on the trolley are measured comparisons can be made.

5. In tests with a symmetrical test configuration the force measurements should be the same for the outer edge blocks. Differences in the instantaneous forces should be no greater than [5%] of the lower measured force.

6. The forces measured at the pole/wall should indicate progressive resistance throughout the period of barrier penetration and not a very rapid rise at the end of the test.

7. In full-scale vehicle tests using different designs of barrier the measured parameters (dummy and vehicle) should not vary by more than 10%. This assessment is made for each make/model of vehicle evaluated.

8. When different designs of barrier are compared the proportion of absorbed energy for each block area and force time history should be similar, if crush forces behind the barrier face on the trolley are measured. This assessment is made for each make/model of vehicle evaluated.

Subjective Requirements

1. The motion and deformations of the barrier face will be examined photographically. A failure would be defined as one 'in which a block or interface moved into an adjacent block or interface inducing a failure in the adjacent member, that could result in a reduction in the for/aft stiffness of that element'.

2. The barrier should fail by crush and not by explosion or other poorly controlled fracture mechanism. Disassembly of the tested barrier may be necessary in order to examine the collapse mechanism(s) of the barrier.

CONCLUSION

The tests and associated assessment techniques should give a clear indication as to the relative merits of the different barrier designs and design concepts. It is possible that the sub system tests will lead to a recommendation for either a single design specification for a MDB face or to a significant tightening up of the existing specifications possibly excluding some generic designs of MDB face. The vehicle tests will indicate whether any unacceptable variability would still exist following such recommendations. It is therefore proposed that if any measured parameter, in the vehicle tests, varies by more than 10% between tests using the 'recommended' barriers, with the same model of vehicle, then a further tightening of the barrier specification should be undertaken, and evaluated as appropriate. If a single design specification were to be recommended then at least two vehicle tests, with each type of vehicle, and barriers from different manufacturing batches, should be undertaken to investigate the reproducibility of the performance of the single barrier design in vehicle tests.

FUTURE WORK

Funding for carrying out the barrier evaluation programme is being sought. It is expected that the programme will start late 1998 and will be completed by the end of 1999.

ACKNOWLEDGEMENTS

EEVC Working Group 13 members are:

- Current members
Mr. Richard Lowne, TRL, chairman
Mr. Adrian Roberts, TRL, secretary
Mr. Andre Seeck, BASt
Mr. Dominique Cesari, INRETS
Mr. Flavio Fossat, FIAT Auto S.p.A.
Mr. Peter de Coo, TNO
Mr. John Oster, Volvo Car Corp.
Mr. William Fan, NHTSA

- Past members
Mr. J. Bloch, Mr. Th. Bourdillon (F)
Mr. A. Benedetto, Mr. S. Canali (I)
Mr. W. Coates, Miss Owen (UK)
Mrs. I. Skogsmo, Mr. J. Sameus (S)

- Observers
Mr. John Green, Rover Group
Mr. Paul Fay, Ford UK
Mr. Francois Guillot, UTAC

The voluntary contribution of JASIC from outside of WG13 to the barrier evaluation programme set-up is greatfully acknowledged.

REFERENCES

1. E.C.E. Regulation No.95. Uniform provisions concerning the approval of vehicles with regard to the protection of occupants in the event of a lateral collision. United Nations Economic and Social Council.

2. Directive 96/27/EC of the European Parliament and of the Council of 20th May 1996 on the protection of occupants of motor vehicles in the event of a side impact and amending Directive 70/156/EEC.

3. Benedetto, A.M.; Experience and Data Analysis on Side Impact testing According to the European Procedure. Proceedings 14th ESV Conference, Munich, 1994, pp 964-985.

4. Owen, C., Roberts, A.K.; Side Impact Barrier Performance Testing, procedures for the assessment of the relative performance of EEVC side impact barrier deformable elements under realistic loading conditions. Version 8. EEVC Working Group 13, April 1998.

DEVELOPMENT AND BENEFITS OF A HARMONISED DYNAMIC SIDE IMPACT STANDARD

K Seyer
M Terrell
Federal Office of Road Safety
Australia
B Fildes
D Dyte
Monash University Accident Research Centre
Australia
K Digges
George Washington University
United States

Paper Number 98-S8-O-04

ABSTRACT

This paper reviews the differences between the US and European regulations and describes the results of the Australian Federal Office of Road Safety's research program to propose a harmonised dynamic side impact standard that combines the better features of the US and European regulations and using the BioSID dummy. The paper also includes a Harm reduction analysis showing the likely benefits of the proposed harmonised standard over the US and European regulations.

INTRODUCTION

After frontal impact crashes, side impacts are the greatest killers of vehicle occupants on Australian roads, accounting for over 25% of fatalities.

Australian Design Rule (ADR) 29/00 - Side Door Strength was introduced in 1977 to provide side impact crash protection. Australia was the only country outside North America to introduce this design requirement.

In 1995, the Federal Office of Road Safety released for comment a draft Australian Design Rule (ADR) for dynamic side impact protection. The draft ADR will be introduced in 1999 and allows compliance to be demonstrated to either the US Federal Motor Vehicle Safety Standard 214 or the Economic Community for Europe Regulation 95.

These two regulations were developed on either side of the Atlantic during the 1980s and early 1990s. Although their intent is the same (to improve side impact protection), their detailed requirements are quite different.

The current situation has forced manufacturers to "fine tune" their designs to ensure compliance with the US or European regulations, depending on the market into which the vehicle is sold. Manufacturers around the world have indicated general support for a single harmonised standard to which the car is designed.

CURRENT OVERSEAS REGULATIONS

The US and European regulations specify two fundamentally different test procedures and test dummies.

Both use a mobile trolley with a deformable face to impact the car being tested. However, the mass of the trolley, specification of the deformable face, test speed, the test dummy and injury criteria are different. While Australian crashed vehicle studies have shown that head and neck injuries are prevalent locally, head injury is only addressed in the European regulation.

US Standard FMVSS 214

The major components of the US dynamic test specified in regulation FMVSS 214 comprise:

- a moving trolley of 3010 lbm (1365 kg),
- a crabbed barrier impact angle of 27 deg,
- a barrier impact speed of 33.5 mph (54 km/h)
- a homogeneous deformable barrier face
- US SID dummies in the front and rear near-side seats.

Trolley Configuration - The trolley mass of 1365 kg was the US average fleet mass when the rule was being developed.

FMVSS 214 calls for the impacting trolley to be "crabbed" at 27 degrees and to strike the test vehicle at an impact speed of 33.5 mph (about 54 km/h). This is illustrated in Figure 1. The velocity component perpendicular to the target vehicle is 30 mph. The crabbed configuration was important to simulate real world intersection crashes where both vehicles are moving. This was subsequently confirmed by Dalmotas (1994) in comparative crash tests undertaken by Transport Canada using North American vehicles.

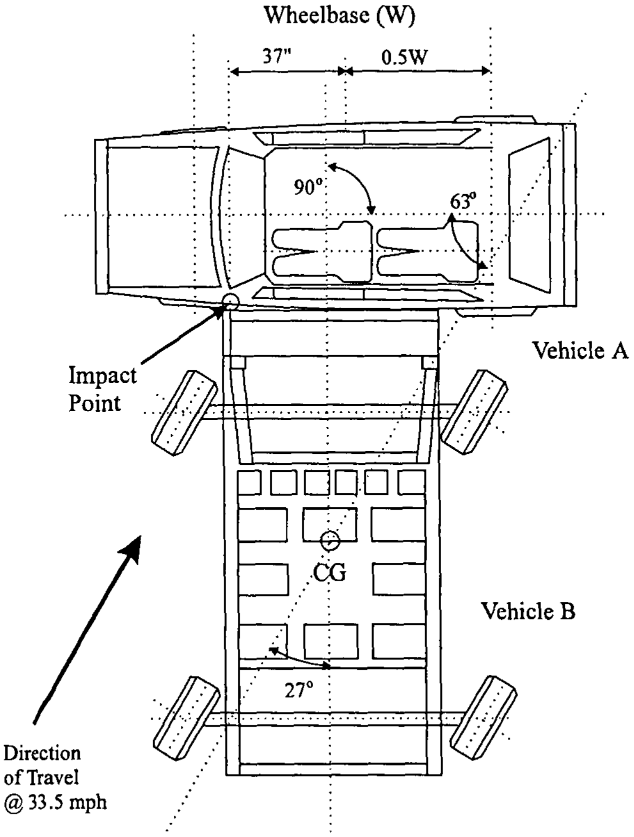
Wheelbase (W)
37"
0.5W
90°
63°
Vehicle A
Impact Point
CG
Vehicle B
27°
Direction of Travel @ 33.5 mph

Figure 1 – US Trolley Configuration

US Deformable Barrier Face - The US barrier construction is essentially homogeneous with a protruding bumper layout as shown in Figure 2. The main section is constructed from 45 psi (±2.5 psi) honeycomb material with the bumper section in 245 psi (±15 psi) aluminium honeycomb material. The US barrier element is considerably stiffer than the European barrier.

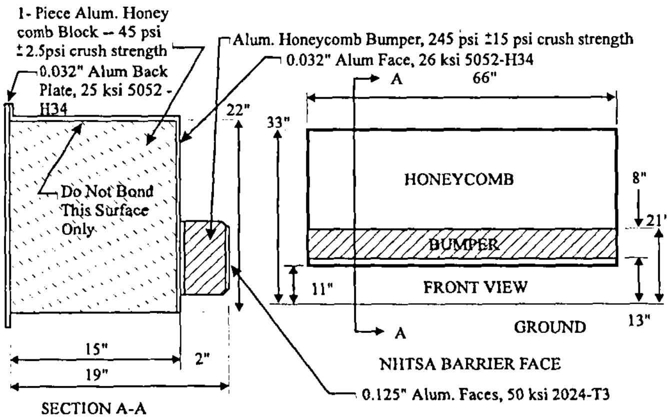
1- Piece Alum. Honey comb Block -- 45 psi ±2.5psi crush strength
0.032" Alum Back Plate, 25 ksi 5052 - H34
Do Not Bond This Surface Only
Alum. Honeycomb Bumper, 245 psi ±15 psi crush strength
0.032" Alum Face, 26 ksi 5052-H34
A
66"
22"
33"
HONEYCOMB
8"
21"
BUMPER
11"
FRONT VIEW
GROUND
13"
A
15"
2"
19"
SECTION A-A
NHTSA BARRIER FACE
0.125" Alum. Faces, 50 ksi 2024-T3

Figure 2 – US Deformable Barrier

The bottom edge of the US barrier is 280 mm from the ground. The bumper element is 330 mm above the ground and the barrier is 1676 mm wide.

The SID Dummy - The US regulation calls for tests involving the Side Impact Dummy (SID) developed by the NHTSA. SID is a modified Hybrid 2 developed specifically for side impact testing after extensive cadaver testing in the US and Germany. Its biofidelity requirements led to unequal masses in the dummy, especially its relatively soft arms which was intended to incorporate rib characteristics.

US Injury Criteria - In developing SID, measurement of deflection forces was difficult because of rotation, therefore acceleration of the thorax and lower spine became the major injury criteria. This has since become a criticism of SID, both outside and inside the US. Delta-V distributions from NASS showed that the 50th percentile was somewhere between 15 and 20 mph which was subsequently adopted as the design speed.

The injury criteria are limited to:

- Peak lateral pelvis acceleration and the
- Thoracic Trauma Index (TTI(d))

where $TTI(d) = {}^1/_2 (G_R + G_{LS})$

G_R = greater of either upper or lower rib accelerations
G_{LS} = lower spine (T12) peak acceleration

The SID dummy criteria was based on hard thorax injuries including liver and kidney injuries but not soft tissue injury in the abdomen. There is no instrumentation available for measuring these injuries other than those covered by rib acceleration.

SID has no provision for specifying any head injury criteria. US accident data shows that the greatest source of severe injury in side impacts is to the head, not the thorax. Therefore, FMVSS 214 does not really address the major source of injury from side impacts. The US have issued a revision to FMVSS 201 which is effectively an upper interior padding standard for side rails and A- and B-pillars aimed at addressing at least part of these head injuries from side impacts.

Impact Point - FMVSS 214 requires the front edge of the impacting barrier to strike the test vehicle at a point dependent on the wheelbase (W) of the vehicle:

- 37 inches (940 mm) forward of the centre of the vehicle's wheelbase, if W ≤ 114 inches (2896 mm),
- 20 inches (508 mm) rearward of the front axle centreline if W > 114 inches.

The majority of cars available in Australia fall into the first category.

ECE Regulation 95

The test procedure was developed by the European Experimental Vehicle Committee (EEVC) and the major components of the dynamic test specified in ECE Regulation 95 comprise:

- a moving trolley of 950 kg (2090 lbm)
- a perpendicular barrier impact
- a barrier impact speed of 50 km/h (30 mph)
- a non-homogeneous deformable barrier face
- EuroSID dummy in the front near side seat only.

Trolley Configuration - The trolley mass is 950 kg which was about the average mass of European vehicles at the time it was developed. There was very little effect observed in testing different masses up to 1100 or 1300 kg because most of the peak loads occur between 35 and 50 msecs and the trolley mass has little influence at that time. The mass of the trolley influences the amount of intrusion but has less effect on dummy performance compared to peak loading.

A perpendicular impact configuration was chosen because some European manufacturers believed this configuration offered best protection to occupants of their vehicles in real world accidents. A perpendicular impact was also the simplest testing option and did not appear to compromise safe vehicle design.

An impact speed of 50 km/h was chosen for the standard based on the distribution of impact speeds observed in real world accidents in Europe.

Canadian tests compared both barriers in crashes to North American vehicles and felt that the US barrier was slightly more representative of US vehicle crashes, particularly those involving MPV's. European tests claim that the European barrier reproduced quite well the worst case outcomes for a European vehicle fleet.

European Deformable Barrier Face - The European barrier design aims to represent the stiffness values of impacting passenger car front structures, ie front longitudinals, engine etc. These values were derived from French testing of representative European passenger car crashes against a rigid barrier wall. Subsequent testing of Japanese cars in Japan showed that these cars also correlated well with these European force characteristics. The barrier face is 1500 mm wide (see Figure 3).

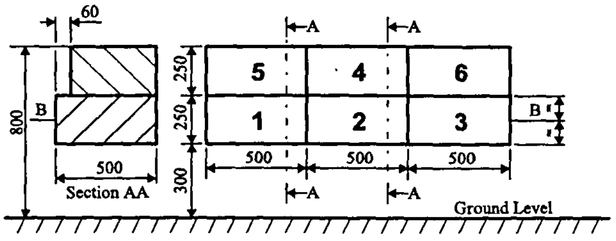

Figure 3 – ECE Deformable Barrier

The height of the barrier was originally set at 300 mm from the ground surface to the lower edge and practically all development work involved in ECE Regulation 95 was based on this barrier height. This was slightly above the bottom edge of the US barrier (280 mm) but below the US barrier's bumper height of 330 mm. Representations by a few European member countries led to the barrier height being lowered to 260 mm when Regulation 95 was first issued. However, the EC Directive for dynamic side impact protection has been finalised with a barrier ground clearance of 300 mm and ECE R95 has reverted to this figure.

EuroSID Dummy - The Europeans felt that there was a need for a more sensitive measuring instrument and injury criteria in side impacts than that offered by SID. As a result, they set about developing EuroSID, a joint exercise involving several European countries. While EuroSID has arms, the specification calls for them to be out-of-the-way during impact to minimise their protective role for the chest.

The EEVC did recommend dummies in both the front and the rear seating positions on the struck side only. However, it seems that most of the development work has been done with only a front seat dummy on-board. The requirement for a rear dummy was subsequently dropped in the ECE regulation.

Dummy Test Criteria - European studies had shown that the most severe injuries in side impacts were to the head, thorax, abdomen and pelvis, so EuroSID was required to detect injuries in these areas.

Head Injury Criteria (HIC) was considered adequate for measuring head injury. For the chest, the Europeans felt that TTI was not appropriate for measuring these injuries and subsequently adopted chest deflection and Viscous Criteria (V*C). Appropriate values of this parameter were determined for EuroSID (European tests showed that a V*C of 1 = 30% to 40% probability of injury for AIS3 or above). Concern has been expressed by some about the repeatability of the Viscous Criteria with the EuroSID dummy so it has been agreed to just record the readings for the first 2 years of the regulation without it being considered as a pass/fail criterion.

Regulation 95 also has abdominal and pelvic injury criteria which limit the peak abdominal and pubic symphysis force as measured by EuroSID.

Impact Point – The impact point of the barrier is centred on the front seat "R-point".

EXAMINING THE FEASIBILITY OF A HARMONISED STANDARD

Australian field data also indicated that side impact crashes caused head, thoracic, abdominal and pelvic injuries. Therefore any harmonised standard from Australia's view needed to address these injuries.

Mobile Deformable Barrier Tests

The first stage of the research program was to conduct crash tests to the following requirements using a vehicle model understood to comply with FMVSS 214 to:

- US FMVSS 214
- ECE Regulation 95
- A harmonised standard described below.

The two tests based on current regulations were conducted in full accordance with test procedures set out for FMVSS 214 and ECE Regulation 95.

Car to Car Tests

A second stage of the program involved two car to car tests with different bullet vehicles for comparison with the mobile barrier tests:

- Ford Falcon as a bullet car.
- Nissan Micra as bullet car.

The Ford Falcon was chosen because it has a stiff front structure and is of the size and mass typical of the vehicles from which the FMVSS 214 barrier was reportedly developed to represent.

The Nissan Micra is of the size and mass typical of the vehicles from which the ECE R95 barrier was reportedly developed to represent.

The impact point for both tests was the front seat R-point (same as R95).

HARMONISED SIDE IMPACT TEST

The harmonised dynamic side impact procedure included the following features:

- BioSID dummies in the front and rear outboard seating positions on the impacted side.
- FMVSS 214 crabbed trolley with ECE R 95 deformable barrier element.
- FMVSS 214 impact geometry.
- ECE Regulation 95 injury criteria to the degree which BioSID is capable of recording.

This test configuration was chosen for the following reasons:

- FMVSS 214 crabbed barrier better reproduces a typical intersection side impact crash.
- FMVSS 214 test configuration requires countermeasures for both front and rear seat occupants.
- BioSID is generally considered to be the more biofidelic dummy.
- ECE R 95 barrier face better represents a vehicle front structure.
- ECE R 95 injury criteria more fully covers the range of injuries seen in side impact crashes.

US experience confirms that the benefits of having a rear dummy are really quite small since occupancy rates, like Australia, are quite low. It would be difficult to justify the need for a rear seat dummy on a cost benefit basis. It should be noted that performance standards will not necessarily guarantee rear seat protection without a rear seat dummy and a separate impact test involving a more rearward impact location.

For this project, a rear BioSID dummy was also used and the benefits determined. Because the US barrier is wider, there are expected to be benefits for smaller cars where the crush profile will encompass the rear seating position.

TEST VEHICLES

Target Vehicle

Ford EF2 Falcon Gli sedans (wheelbase 2791 mm) were used as the target vehicle for all the tests. This vehicle was chosen because it is a high volume Australian produced vehicle claimed to meet the requirements of FMVSS 214.

Seats and trim were removed from the non-impacted side as required to install data acquisition equipment etc. The vehicles were ballasted as necessary to the requirements of the particular test procedure.

Bullet Vehicles

The Ford Falcon was ballasted to the FMVSS 214 test mass and the Nissan Micra was ballasted to the ECE R95 test mass.

TEST RESULTS

The results from the test series were used as part of the input data for MUARC to make Harm benefit calculations.

The injury data is summarised in Table 1. Overlay plots of the following are presented at the end of the paper:

- Vehicle intrusion at H-point
- B-pillar bottom acceleration
- Pelvic acceleration
- Lower spine acceleration
- Upper rib acceleration

The results of the 3 mobile barrier tests and the 2 car to car tests indicated that:

- The onset of vehicle decelerations and dummy readings in the 214 test always led the other tests.
- The onset of vehicle decelerations and dummy readings in the car to car test with the Micra always lagged the other tests.
- The onset of vehicle decelerations and dummy readings in the R95, Hybrid and the car to car test with the Falcon are similar.
- Car/barrier stiffness is more important in determining intrusion and injury severity than whether the impacting car/barrier is crabbed or perpendicular.
- The car/barrier stiffness determines the onset of vehicle decelerations and dummy readings. Higher stiffness means earlier onset.
- Barrier (car) mass does not appear to have an effect on load onset.
- Barrier (car) mass does affect amount of intrusion.
- Spine responses peak between 30-45 msec.
- Rib responses peak between 30-35 msec.

TEST SERIES CONCLUSIONS

The following conclusions have been drawn from the test series:

- Peak dummy responses are reached before 45 msec.
- R95 barrier element's stiffness correlates well with a typical large Australian passenger car.
- Vehicle (barrier) stiffness determines load onset timing.
- Higher stiffness means earlier loading of vehicle structure and dummy.
- Crabbed configuration loads the rear occupant more than a perpendicular impact.

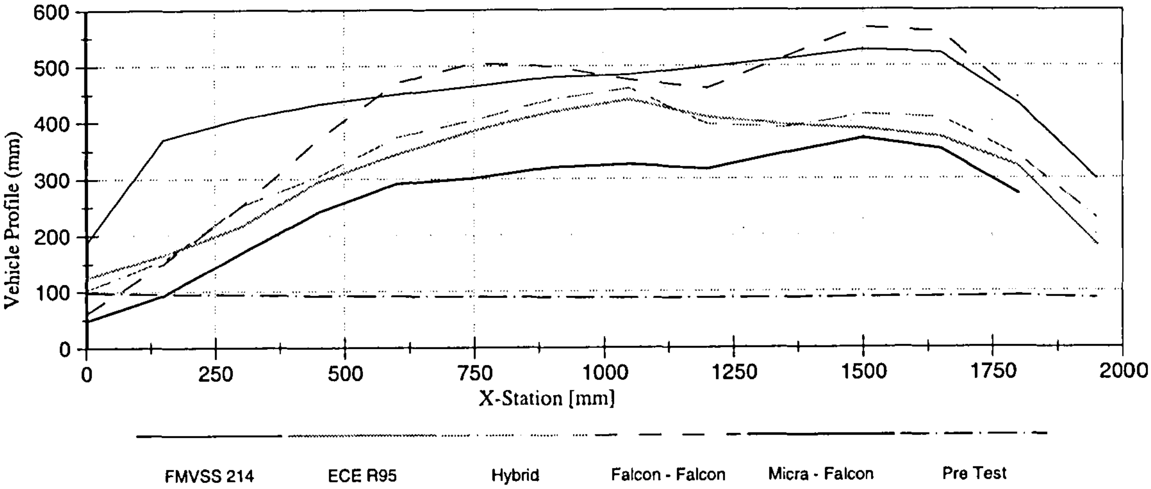

Figure 4 – Vehicle Crush

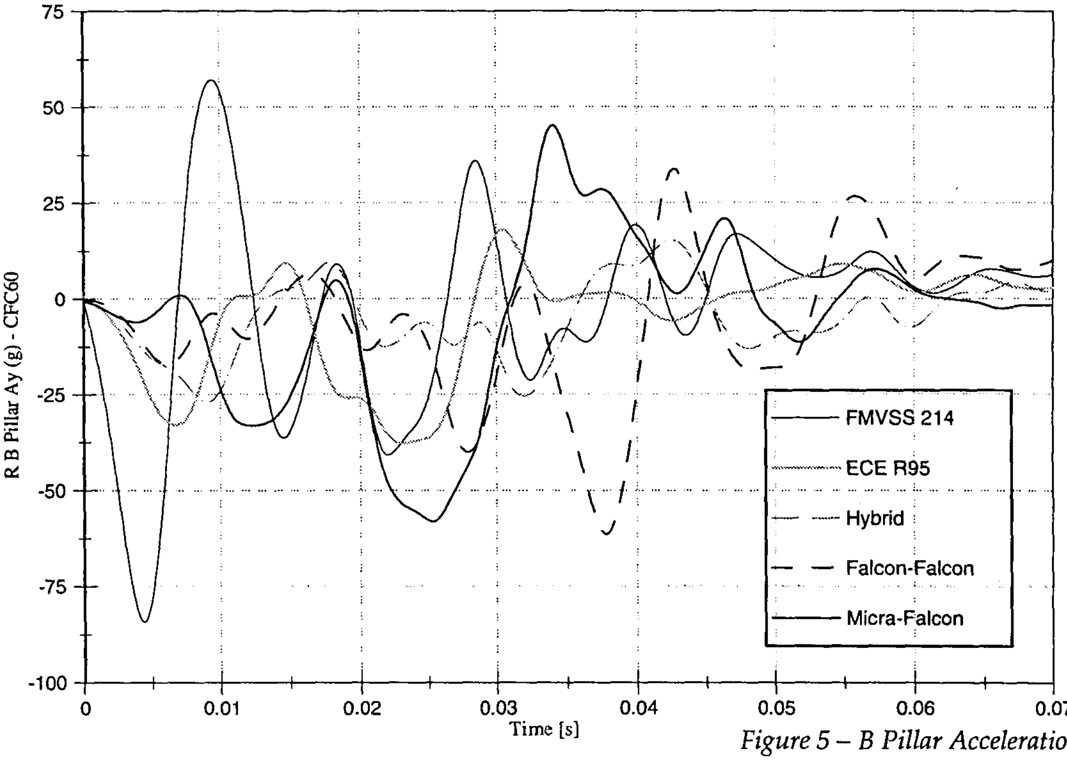

Figure 5 – B Pillar Acceleration

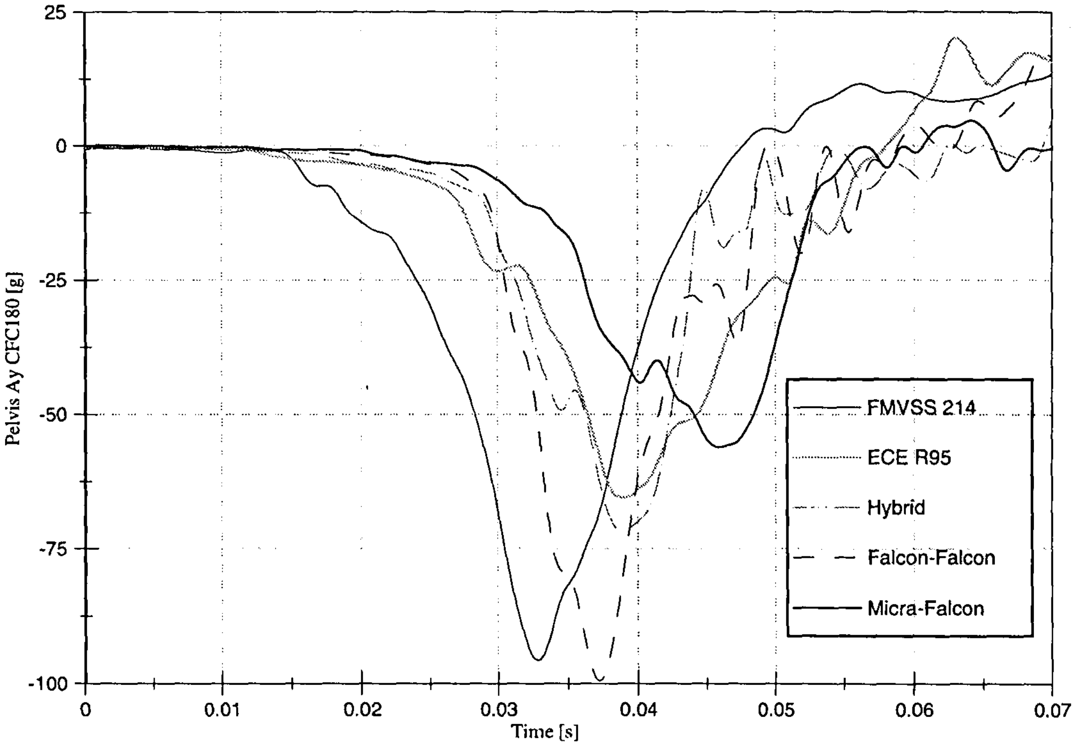

Figure 6 – Pelvis Acceleration

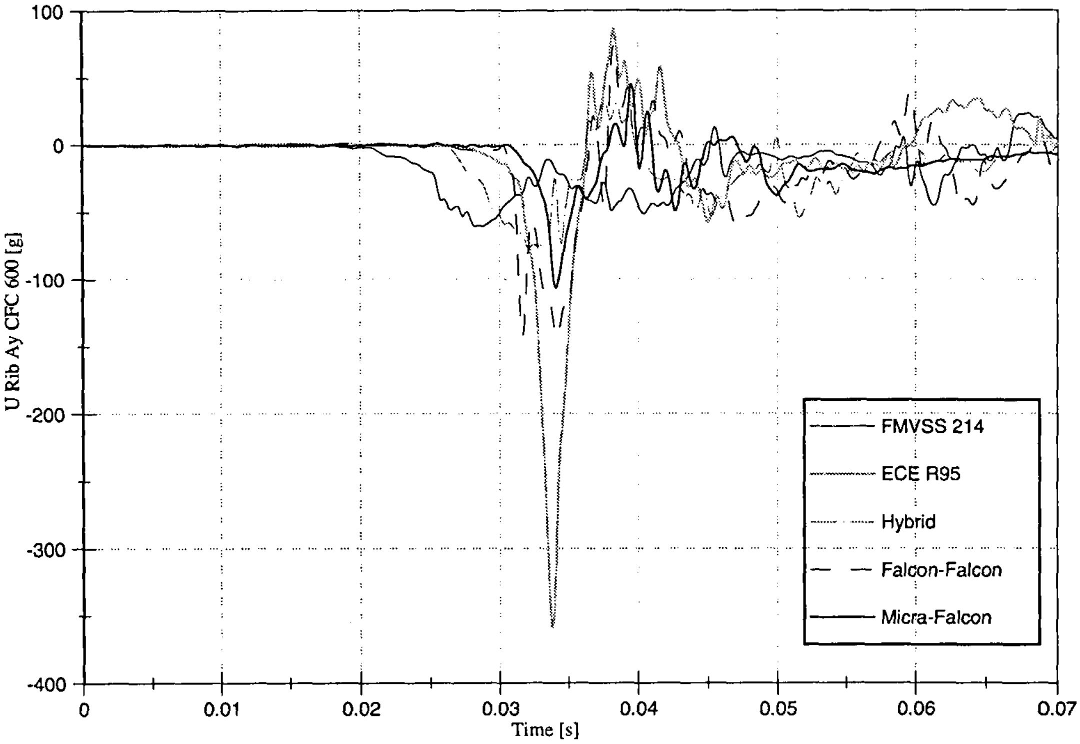

Figure 7 – Upper Rib Acceleration

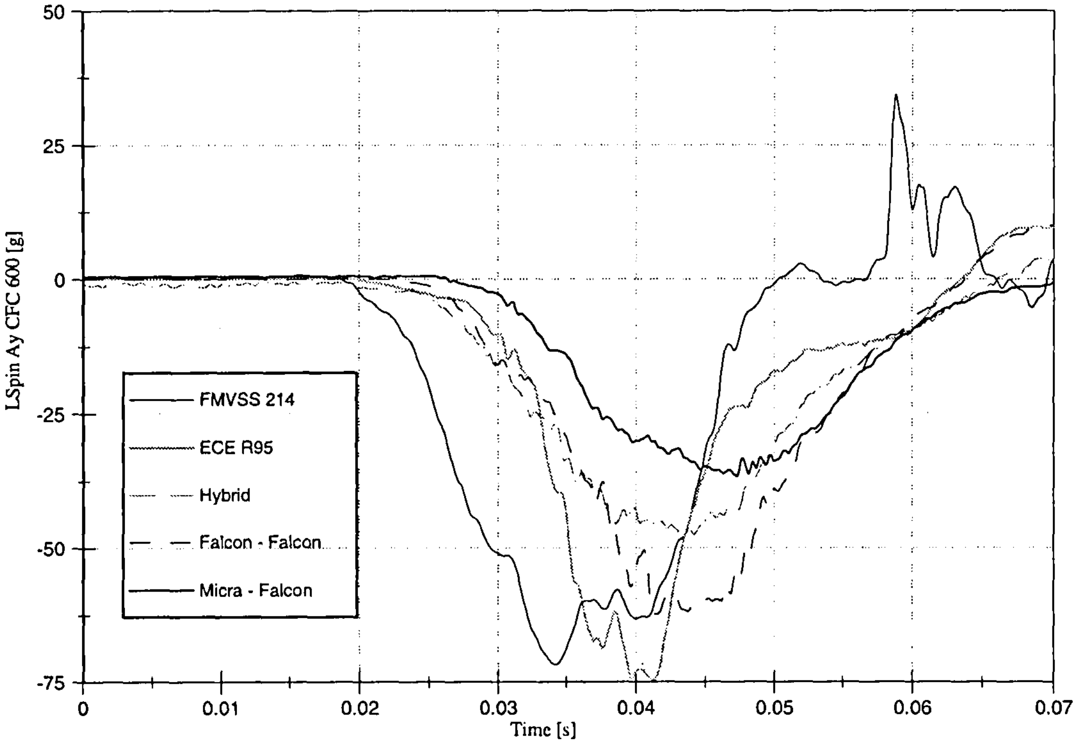

Figure 8 – Lower Spine Acceleration

HARM ANALYSIS

To demonstrate the likely cost effectiveness of the proposed harmonised side impact standard, a Harm benefit analysis was undertaken using the *Harm Reduction* method previously used in other side impact benefit analyses (Fildes et al 1995 and 1996).

The Harm Reduction method has been used previously for estimating the likely benefits of new occupant protection countermeasures (Monash University Accident Research Centre 1992). *Harm* is a road trauma metric which contains both frequency and cost components and is therefore able to express the likely reductions in injuries from the introduction of a new measure into financial benefits.

The systematic building block approach used in this study permitted a body region by contact source analysis of benefits which provided an objective estimate of the consequences of Australia adopting either the existing two candidate regulations or the proposed harmonised side impact standard.

Data Sources Available

An Australia-wide database was necessary to assess the likely injury reductions for both standards. A detailed database was constructed in 1991 of national injury patterns by body regions, restraint conditions and contact sources, along with a series of resultant Harm matrices using BTCE human capital cost estimates (Monash University Accident Research Centre 1992). This comprehensive trauma analysis, based on over 500 real-world crashes examined in the Crash Vehicle File by the Monash University Accident Research Centre, offered a baseline trauma pattern upon which estimates of Harm reductions could be made.

While this database was several years old, it nevertheless was still the most up-to-date source of baseline information available. Moreover, while the numbers of crashes (and hence injuries) have reduced over the last 5 or 6 years, their costs have risen such that the overall cost of trauma is probably still similar to that estimated for 1991. Thus, this database was judged suitable for use in this study, too.

Injury Reductions

As in the previous side impact benefit analysis (Fildes et al, 1996), there was again very little published data available that reported on injury reductions associated with a harmonised standard, apart from the test results reported earlier in this study and some figures published by Dalmotas, Newman and Gibson (1994). Thus, it was deemed necessary again to assemble a panel of international experts to establish the likely injury benefits that would accrue to Australia for the harmonised standard.

A one-day workshop was organised in May 1997 in Washington DC comprising representatives from the car industry, government researchers, representatives of consumer groups and the study team. The workshop provided an up-to-date account of recent side impact regulation developments as well as the likely injury benefits to Australia by adopting the harmonised standard.

It was clear from the discussion at the meeting that many of the assumptions made in the earlier side impact benefit study (Fildes et al 1995) had not been substantiated by more recent published data and experience. Therefore it was decided that part of the task of assessing harmonised benefits should also involve adjusting the earlier figures for FMVSS 214 and ECE 95 in line with more recent expectations.

Relevance Assumptions

Hence, a number of assumptions were agreed to for determining the likely benefits of a hybrid side impact regulation for Australia, as well as more recent expectations for the existing two dynamic side impact standards FMVSS 214 and ECE 95 and these are outlined below.

1. The three standards all requires a test at a crash severity of around 27km/h that will provide benefits at crash speeds up to 64km/h. No benefits are assumed above this speed.

2. The benefits will apply equally to both car-to-car and car-to fixed-objects in side impact collisions.

3. The benefits will apply equally to occupants involved in both non-compartment and compartment struck side impacts.

4. Near-side occupants who sustain AIS 5 or 6 fatal head injuries are excluded from any benefit from the standards. Reductions in chest injuries to occupants who sustain a non-fatal head injury are included.

5. All head injuries (to survivors) in side impacts from contact with the door panel are reduced by 2 AIS and face injuries by 1 AIS over the crash severity range of 0-64km/h. For EuroSID (and BioSID), an additional benefit of 2 AIS applies for head contacts with the side rails.

6. Benefits will apply to the chest, pelvis, femur, shoulder, upper extremity, head and face injuries caused by contact with the door panel, hardware or armrest.

Internal organ benefits will vary depending on the test dummy used.

7. An incremental reduction in TTI or V*C on injuries to the chest from door contacts for near-side occupants can be expressed as a crash severity change.

8. The injury risk curves for TTI and V*C apply to the range of impact speeds for side crashes at severities less than 64km/h for injuries of AIS 3 or greater.

9. Forty-five percent of AIS 3-6 and 90% of AIS 1-2 chest injuries over the crash severity range of 0 to 64km/h are expected to be affected by a side impact standard, based on NHTSA pre-standard crash tests.

10. A reduction of AIS 2 in chest injuries is expected by the use of SID and TTI over the crash severity range and an AIS 3 reduction is expected by the use of EuroSID and V*C measures.

11. It was assumed that there is some heart benefits approximating 25% of that relevant to the hard thorax for SID and EuroSID but 50% for BioSID given its superior injury criteria and test performance.

12. New Australian test data show that V*C is a more critical parameter than TTI and this should lead to additional countermeasures to protect the abdomen. Thus, an overall injury reduction for abdominal injuries of AIS AIS 3 for V*C from EuroSID across the relevant crash severity range is expected (no benefit was claimed for FMVSS214 as SID does not measure abdominal injury).

13. Only upper extremity injuries from contact with the door panel or hardware at or below the crash severity range are relevant. As no test data were available on the likely reductions in contacts, a modest AIS 1 injury reduction is assumed.

14. A dynamic side impact standard will result in the elimination of all injuries with exterior contacts for far-side occupants, ejected through the far-side door over the severity range of 0-40km/h.

15. As the European test procedure does not include a rear seat dummy, no rear seat benefit should be awarded to the ECE Reg 95 standard and similar benefits would apply to front and rear seat occupants in both FMVSS 214 and the proposed Hybrid test.

RESULTS OF THE ANALYSIS

A detailed system of spreadsheets was assembled for calculating the benefits of both the existing and harmonised standards. Relevance figures were assigned by body region and seating position (near- or far-side of the vehicle) and the subsequent Harm units removed were computed. The savings by body region and seating position were then summed to arrive at the total estimate of savings for both standards. Annual Harm saved was converted into Unit Harm benefits using both a 5% and a 7% discount rates with fleet life estimates of 15 and 25 years. The results of the analysis are shown in Table 2 below and discussed below for each of the three regulations.

Revised FMVSS 214 Benefits

The revised benefit estimate for the US standard, FMVSS 214, assuming that all vehicles in the Australian fleet were to comply instantaneously was A$117 million. This is 86% of the original figure previously published (A$136 million) essentially due to reductions in expected savings in abdominal, chest and head injuries because of revised performance criteria. This still a 3.7% reduction in vehicle occupant trauma annually if FMVSS 214 were to apply in Australia. The unit benefit per car would be between $116 and $145.60 per car, depending on the discount rate and fleet life figures used in the calculation. At $100 expected installation cost per vehicle, adopting this standard would still be cost-beneficial.

Revised ECE 95 Benefits

The equivalent revised figure for the European standard is A$122 million each year if all vehicles in the Australia fleet instantly complied. This is also only 83% of the figure originally estimated based on more recent evidence of performance expectations. It should be noted that most of the reduced Harm for the European standard comes from exclusion of any rear seat benefit because of the lack of a rear seat dummy (this was not anticipated at the original workshop held in Munich in 1994). On this basis, the unit Harm benefit would be somewhere between $121.40 and $152.40 per car, would still be cost-beneficial, and would yield a slightly higher reduction in occupant trauma annually of 3.9%.

Harmonised Proposal Benefits

Finally, the harmonised proposal outlined at the start of this paper is expected to save A$142 million annually, based on the assumptions listed by the expert panel. This is 16% greater than ECE 95 and 22% greater than FMVSS

214 because of the expected more stringent test procedure, the inclusion of a rear seat dummy, and the likely improvements from the use of BioSID test dummies. This would amount to an improved 4.5% reduction in vehicle trauma annually and with a unit Harm benefit of between $141.70 and $177.50 per car, would yield a Benefit-Cost-Ratio of 1.5 or greater. The harmonised proposal is clearly superior to either of the two existing standards and would overcome the difficulty of having different side impact standards in different continents.

Benefits for ECE 95 with Rear Dummy

An alternative to the harmonised standard proposal outlined in this paper could be a modified ECE 95 regulation that included a rear seat EuroSID dummy. While this is unlikely to provide all the benefits expected from the harmonised standard, it might nevertheless be a suitable first step to combining the two existing standards that could be acceptable to both regulatory authorities. Naturally, the harmonised standard would still be more desirable in the longer term.

It is difficult to know what additional benefits would accrue to the modified ECE 95 standard because of the lack of test data available on rear seat tests with the European procedure. Results published by Ohmae, Sakurai, Harigae and Watanabe (1989) for one car showed that its performance was well under current requirements for front seat dummies. It might be that with a rear seat dummy installed in a ECE 95 test, some global improvement in rear seat protection would be forthcoming as responsible manufacturers would be expected to respond to this requirement with a range of suitable countermeasures. Assuming a 15% improvement was achieved by this global improvement, the annual benefits in Australia would be A$129 million with a unit Harm saving of between $128.60 and $161.40 per car.

CONCLUSIONS

The harmonised test proposal provides greater benefits than either of the two existing standards and would overcome the difficulty of having different side impact standards in different.

The mass of the impacting trolley does not have an effect on ultimate injury outcome.

For a modified ECE R95 test with a rear seat dummy to realise a benefit for rear seat occupants, it is believed that a crabbed trolley would need to be employed.

There is a strong argument for further research into developing an agreed harmonised regulation on dynamic side impact protection. The two major areas of work would appear to be on:

- An agreed harmonised dummy.
- An agreed harmonised barrier element design (stiffness).

REFERENCES

Australian Design Rules, Third Edition, Australian Department of Transport, Federal Office of Road Safety, Canberra.

Monash University Accident Research Centre (1992). Feasibility of Occupant Protection Measures, Report CR 100, Federal Office of Road Safety, Canberra.

Dalmotas, D (1994). Prospects for the Further Improvement of Side Impact Protection Based on Crash Testing, Proceedings of the 14th International Conference on Enhanced Safety of Vehicles, US Department of Transportation, National Highway Traffic Safety Administration, Washington DC.

Fildes, B.N., Lane, J.C., Lenard J & Vulcan, A.P. (1994). Passenger Cars and Occupant Injury: Side Impact Crashes, Report CR 134, Federal Office of Road Safety, Canberra.

Fildes, B.N & Vulcan, A.P. (1994). Workshop Report on Side Impact Regulations for Australia, Report CR 149, Federal Office of Road Safety, Canberra.

Fildes, B.N., Digges, K., Carr, D., Dyte, D. & Vulcan, A.P. (1995). Side Impact Regulation Benefits, Report CR 154, Federal Office of Road Safety, Canberra.

Fildes B.N., Digges K., Dyte D. & Ganzer S. (1996). Benefits of a frontal offset standard, Report CR 165, Federal Office of Road Safety, Department of Transport, Canberra.

Ohmae H., Sakurai M., Harigae T. & Watanabe K. (1989). Analysis of the influence of various side impact test procedures, Paper 890378, SAE Technical Paper Series, Warrendale, PA.

Seyer K. & Fildes B. (1996). Working towards a harmonised dynamic side impact standard - An Australian perspective, Paper 96-S6-O-05, *The 15th International Technical Conference on Enhanced Safety of Vehicles*, US Department of Transportation, National Highway Traffic Safety Administration, Washington DC.

TABLE 1

Summary of injury data

	FMVSS 214 (US SID)	ECE R95 (EuroSID)	Harmonised (BioSID)	Falcon (BioSID)	Micra (BioSID)	Limit
TTI Driver (g)	64.1	131	75.7	88.2	61.8	85
TTI Passenger (g)	52.3	N/A	57.5	43.4	42.8	85
Pelvic Decel Driver (g)	92.1	64.4	72.3	95.2	56.4	130
Pelvic Decel Passenger (g)	92.0	N/A	44.3	49.1	30.8	130
HPC Driver	N/A	99	147	221	67	1000
HPC Passenger	N/A	N/A	125	289	160	1000
V*C Driver	N/A	1.02	0.80	0.89	0.76	1.0
V*C Passenger	N/A	N/A	0.49	0.22	0.19	1.0
Rib Deflection Driver (mm)	N/A	40.4	42.4	46.8	41.3	42.0
Rib Deflection Passenger (mm)	N/A	N/A	34.0	25.9	22.3	42.0
PSPF Driver (kN)	N/A	1.0	2.59	5.02	2.02	6.0
PSPF Passenger (kN)	N/A	N/A	3.51	0.17	0.23	6.0

LEGEND

Thoracic Trauma Index	*TTI*
Head Performance Criterion	*HPC*
Viscous Criterion	*V*C*
Pubic Symphysis Peak Force	*PSPF*

TABLE 2

Summary Table of Harm Benefits

BODY REGION INJURED		U.S. STANDARD FMVSS 214 $million	EUROPEAN ECE Reg. 95 $million	HARMONISED PROPOSAL $million
HEAD INJURIES	near-side	8.7	9.7	10.8
	far-side	16.1	16.3	18.1
FACIAL INJURIES	near-side	0.6	0.7	0.8
	far-side	0.1	0.1	0.1
HARD THORAX INJURIES	near-side	43.3	43.8	48.8
	far-side	2.9	2.9	3.2
INTERNAL ORGANS	near-side	0.4	3.2	7.2
	far-side	0.3	0.4	0.4
ABDOMINAL INJURIES	near-side	0	5.3	8.4
	far-side	0	0	0
PELVIC INJURIES	near-side	4.4	3.9	4.4
	far-side	0.1	0	0.1
UPPER LIMB INJURIES	near-side	17.0	15.2	17.0
	far-side	3.6	3.2	3.6
LOWER LIMB INJURIES	near-side	17.6	15.8	17.6
	far-side	1.2	1.1	1.2
TOTAL NEAR-SIDE HARM SAVED ($million)		**92.0**	**97.6**	**115.0**
TOTAL FAR-SIDE HARM SAVED ($million)		**24.6**	**24.4**	**27.1**
TOTAL HARM SAVED ANNUALLY ($million)		**116.6**	**122.0**	**142.1**
UNIT HARM - $ per car (7% @ 15yrs)		**$116.00**	**$121.40**	**$141.40**
UNIT HARM - $ per car (5% @ 25yrs)		**$45.60**	**$152.40**	**$177.50**

DEVELOPMENT OF SIDE IMPACT AIR BAG SYSTEM FOR HEAD CHEST PROTECTION

Takayuki Igarashi
Mitsuo Ehama
Yukisada Sunabashiri
Nissan Motor Co.,Ltd
Japan.
Paper Number 98-S8-O-05

ABSTRACT

Most of the Side Impact Air Bag systems in the current market are designed to protect the thorax area only. The new Head and Thorax SRS Side Impact Air Bag system, which Nissan recently introduced into the market, was designed to help provide additional protection for the head in certain side impacts. The system may help protect occupant head contacts when the vehicle collides into a tree, or the high hood of a large striking vehicle. This paper introduces the additional features and function of the new Head and Thorax SRS Side Impact Air Bag system, and some evaluation results in laboratory testing.

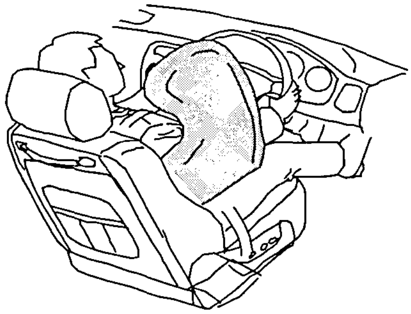

Figure 1. Head & Thorax Side Impact Air Bag

SIDE IMPACT ACCIDENT RESEARCH

Accident statistics in Japan are shown in Figure2. The fatality rate in side impact collisions is rated second (24%) of the total, following frontal impacts, which is 71%.

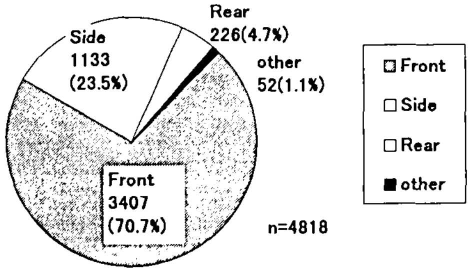

Figure 2. The fatality rate in impact collisions. Accident statistics in Japan(1993).

In side impacts with AIS>3, the occupant in the struck side suffers injury mostly in the head area, second in thorax, third in pelvis, and fourth in the abdomen.

If Head and thorax injuries are combined , they occupy more than 50% of the AIS>3 injuries. (See Figure 3.)

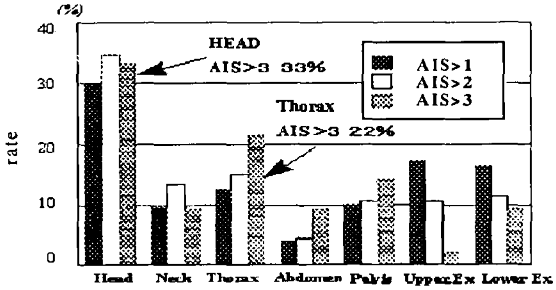

Figure 3. Injury area distribution of the occupant on the struck side in side impacts.

Data source ; National Police Agency, Management and Coordination Agency.

BACKGROUND OF HEAD AND THORAX SRS SIDE IMPAPCT AIR BAG SYSTEM DEVELOPMENT

The result of side impact collision research initiated the development of the Head and Thorax SRS Side Impact Air Bag System to help provide additional protection to the head area in certain side impacts.

CONFIGURATION OF HEAD AND THORAX SRS SIDE IMPACT AIR BAG SYSTEM

The total Hear & Thorax SRS Side Impact Air Bag system diagram is shown in Figure.4

1. A satellite sensor which detects the impact force is located on the bottom of the each center pillar.
2. A control unit, which provides signals for deployment and diagnosis of the whole system is located on the center of the tunnel (control unit is common for frontal impact SRS system).
3. An air bag module which is located in the side of the seat back .
4. A warning light which is installed in the instrument panel to indicate system malfunction.

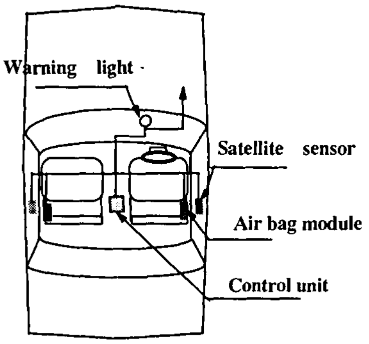
Warning light
Satellite sensor
Air bag module
Control unit

Figure 4. Configuration of Head & Thorax SRS Side Impact Air bag system.

Sequential Event of Air Bag Deployment is described as Follows

1. A satellite sensor in the struck side and a safing sensor in the control unit detect the impact force.
2. If a satellite sensor judges that the impact force is severe enough to deploy the air bag, the control unit provides a signal to the air bag module.
3. The gas produced by the inflator deploys the air bag.

CONFIGURATION OF HEAD AND THORAX SRS SIDE AIR BAG MODULE

Air bag module consists of;

1. Bag to protect Head and Thorax
2. Inflator
3. Housing to secure Bag and Inflator
4. Module tube to protect bag and to control the air bag deployment trajectory.

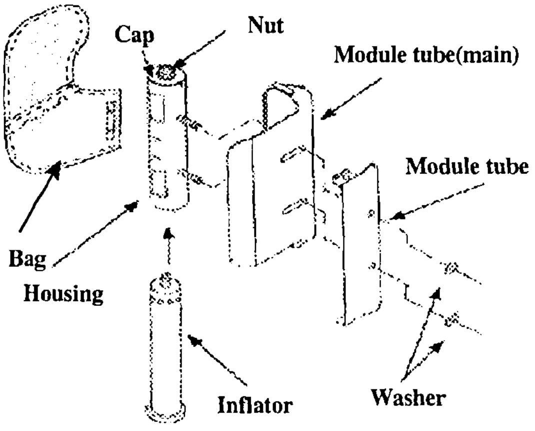
Cap
Nut
Module tube(main)
Module tube
Bag
Housing
Inflator
Washer

Figure 5. Configuration of Air Bag module

The air bag module is attached to the seat back frame and covered by cushion and the trim of the seat back.
When the air bag deploys, air bag deployment force tears the seam and the bag comes out in a forward direction.

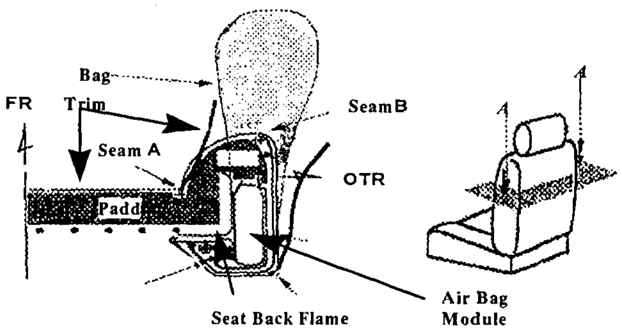
Bag
FR
Trim
Seam A
Padd
SeamB
OTR
Seat Back Flame
Air Bag Module
A
A

Figure 6. Seat back section (A-A)

ADDITIONAL FEATURES OF HEAD AND THORAX SRS SIDE AIR BAG SYSTEM

This newly designed and developed Head and Thorax SRS Side Air Bag has been enlarged to provide additional protection for the head area while still configured for the thorax.
This new Head and thorax SRS Side Impact Air Bag system, is mounted in the seat back to provide consistent performance for the occupant in various fore/aft seat positions which is the same as the current Thorax SRS Side Impact Air Bag system.

BAG DESIGN

Bag shape

Combines thorax protection area and head protection area to make a single air bag shape, providing a larger occupant protection area by using a simple configuration. The deployment shape of a bag was decided from the range of occupant sizes.

Bag folding

The bag folding technique shortened the time for full deployment.
The deployment shape is shown in Figure. 7.

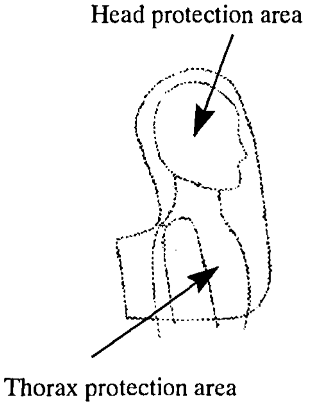
Head protection area
Thorax protection area

Figure 7. Side view of the deployed bag

BAG DEPLOYMENT STEPS

Bag deployment Step.1

Start of the deployment (Signal is sent from control unit to inflator).

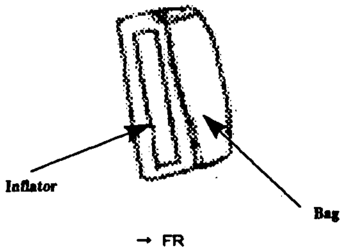

Figure 8.Bag deployment Step.1(time 0msec)

Bag deployment Step.2

Bag deployment pressure tears seat seam and deploys thorax protection area in the forward direction.

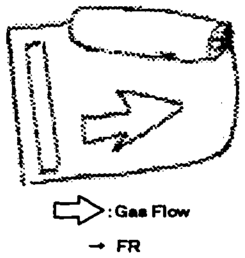

Figure .9 Bag deployment Step.2

Bag deployment Step.3

Gas deploys in the thorax area first, and then partial gas transfers to the head area.

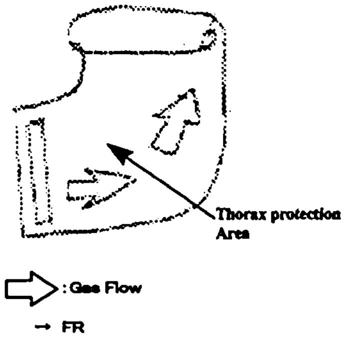

Figure 10. Bag deployment Step.3(after about 8msec)

Bag deployment Step.4

Gas deploys in the head area.(full deployment)

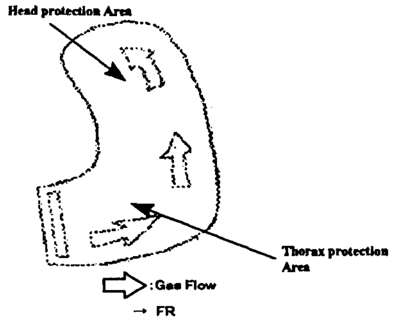

Figure 11.Bag deployment Step.4(after about 20msec)

OCCUPANT PROTECTION PERFORMANCE EVALUATION

Head Protection Performance

There are various kind of head protection performance evaluation tests. We selected a pole impact test as one of the evaluation tests. This test condition simulates that a vehicle crashes into an utility pole or a tree from the side of the vehicle and the occupant head hits into the utility pole or the tree directly. This procedure is under discussion at ISO meetings.

Test results are shown in Figure 12. Deceleration applied for the head was reduced to less than 1/10 of the deceleration applied without Head and Thorax SRS Side Impact Air Bag system.

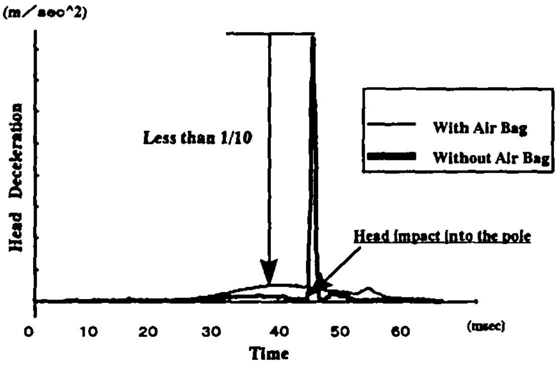

Figure 12. Dummy head deceleration in side pole impact test.

Thorax Protection Performance

The Head and Thorax SRS Side Impact Air Bag System reduces impact force by a maximum of 10~15% in our laboratory testing.

OCCUPANT AIR BAG INTERACTION EVALUATION

Out of Position e Evaluation

To simulate possible O.O.P riding posture, some O.O.P testing was conducted. Among various possible O.O.P postures, three test conditions are evaluated as possible high frequent postures and/or close to the air bag module.

Child Seat Evaluation

In addition to O.O.P test conditions, a child in a child seat was evaluated.

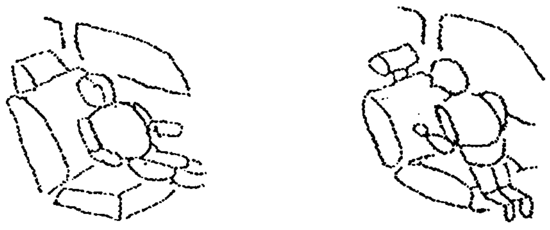

■ Posture.1 (O.O.P) (Close to Door Trim 1)

■ Posture.2 (O.O.P) (Close to Door Trim 2)

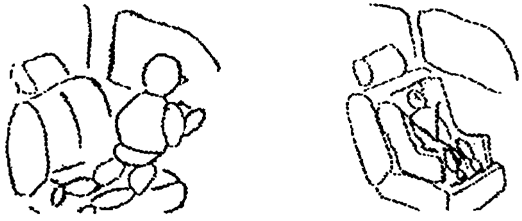

■Posture.3 (O.O.P) (Close to side glass)

■ Posture.4 (Child seat)

Figure.13 O.O.P and child seat test posture(Dummy AC03)

Test Result

O.O.P and child seat test results are shown in Figure.14~17.
As results show, dummy injury numbers are less than IARV(Injury Assessment Reference Values).
The MVSS 208 criteria is used for the IARV.

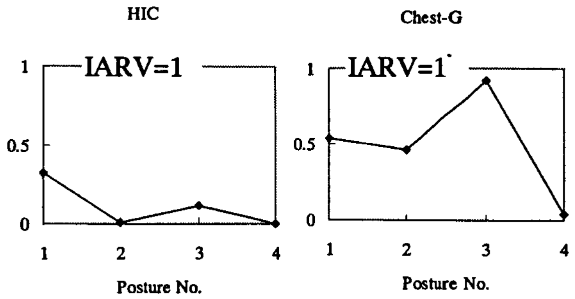

Figure 14. Dummy injury index in o.o.p and child seat test (HIC, Chest G)

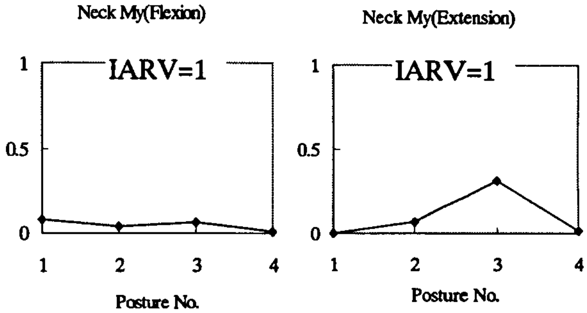

Figure.15 Dummy injury index in o.o.p and child seat test (Neck ;My)

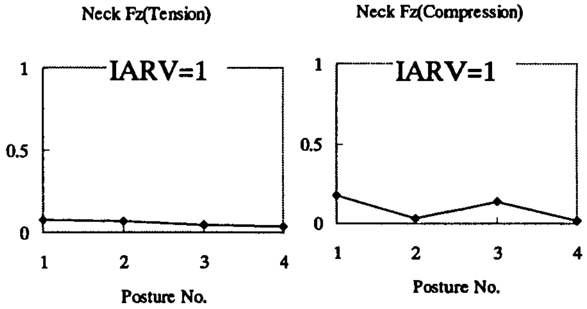

Figure.16 Dummy injury index in o.o.p and child seat test (Neck ;Fz)

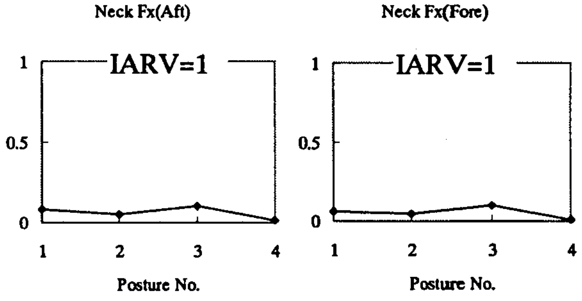

Figure.17 Dummy injury index in o.o.p and child seat test (Neck ;Fx)

ARM/AIR BAG INTERACTION EVALUATION

The test procedure for Arm interaction with side impact airbag is being discussed in the ISO Working Group. For one of the evaluation conditions, there is the elbow on the window sill deployment test condition.

As a part of Airbag interaction evaluation test, the elbow on the window sill condition test was conducted. It was figured that current dummies are not adequate to use for the arm evaluation at the arm and side impact air bag interaction evaluation tests. Since the shoulder joints of existing dummies are not well simulated like the actual human being. This finding was reported to the ISO Working Group meeting. To evaluate the Arm/Airbag interaction, it was agreed to modify the shoulder joint to get better simulation of actual human kinematics.

Human volunteer tests were conducted to evaluate Arm/Airbag Interaction during our development.

Based on the reports from human volunteers, the feeling of impact from Arm/Airbag Interaction is like a slight slap from the side of upper arm and no effect for shoulder and bones. It was concluded that there is a very low risk of arm injuries from Arm/Airbag Interaction.

CONCLUSION

Based on our development and evaluation of the Head and Thorax SRS Side Impact Air Bag System, It was introduced into the Japanese market in September '97, and will be introduced into the US market in Fall of '98.

FUTURE OBJECTIVES

It is very important to evaluate the side effects of the new restraint device before it is introduced into the market, since there are not always adequate evaluation equipment and measuring devices.

In this report the shoulder articulation was discussed, it is desirable to find new necessary improvements and share them among the experts to resolve. The shoulder joint issue is well known among the experts and will be moving towards the favorable solution.

REFERENCE

ISO Technical Report "Road Vehicles-Test Procedures for Evaluating Various Occupant-Interactions with Deploying Side Impact Airbags", ISO TC 22/SC 10/WG3 N130. August 19, 1996.

ISO Technical Report "Road Vehicles - Dynamic Crash Test Procedures for Evaluating Various Occupant - Interactions with Side Impact Airbags when the Impact Object is a Pole, Moving Deformable Barrier, or high - Hooded Vehicle Simulation", ISO TC 22/SC 10/WG3 N131. August 20,1996.

ISO Technical Report "Side Arm/Air Bag Interaction in Static Tests with Combination Autoliv Side Air Bag", ISO TC 22/SC 10/WG3 N166. April 3 1998.

HEAD IMPACT PROTECTION - NEW REQUIREMENTS AND SOLUTIONS

Michael Menking
F. Porsche
Porsche AG
Germany
Paper Number 98-S8-O-06

ABSTRACT

The NHTSA has very substantially extended its existing Part 571 - FMVSS Standard No. 201 "Occupant Protection in Interior Impact" [1]. This extension to the Standard necessitates the development of energy-absorbing trimmings for protection of vehicle occupants in the event of an impact with components in the upper passenger compartment. The publication describes the requirements of the Standard. This paper illustrates development approaches, assisted by numerical simulation, and investigates these experimentally. Dynamic protection systems for reducing the loads on vehicle occupants in the event of an impact are not covered by this publication.

INTRODUCTION

To Porsche, passive safety has always been a very important development aim. The company develops vehicles for a worldwide market which therefore must comply with all worldwide, legally stipulated standards and requirements of the main consumer associations in respect of passive safety in the event of frontal and side impacts, oblique and rear impacts and rollovers.

Protection of the vehicle occupant in the passenger compartment is tested, amongst other things, to Standard FMVSS 201. The amendment to the Standard, which came into force in September 1995 and contains the technical safety requirements in respect of all interior components in the upper passenger compartment, represents an essential extension. The law foresees a step-by-step compliance for manufacturers of vehicles for the American market during the period 1998 through to 2002. Alternatively, the manufacturer may opt for a one-step compliance of the law for all vehicles which then comes into force in September 1999.

NEW REQUIREMENTS OF THE FMVSS 201 - FMH STANDARD

The extension of the Standard is aimed primarily at protecting the unbelted occupant in the event of an impact with components of the vehicle interior. If a vehicle occupant hits an interior component at a speed of up to 24 km/h owing to an accident, the head injury criterion HIC(d) must not exceed a limit value of 1000.

Experimental validation of the requirements is performed with the aid of a modified Hybrid III free-motion headform (FMH). The development and validation tests are conducted in the vehicle on a test stand designed specifically for this test. The following areas of the vehicle interior must be designed in such a manner as to comply with the head injury criterion in the event of an impact of the occupant's head:

- pillar trimmings (A-, B-, C-pillar, rearmost pillar)
- front / rear header
- side rail
- seat belt anchorages, fittings, height-adjuster
- upper roof
- sliding door track
- overhead rollbar
- braces or stiffeners for convertibles

In these areas, different numbers of points are defined which the FMH hits in free motion at a speed of 24 km/h.

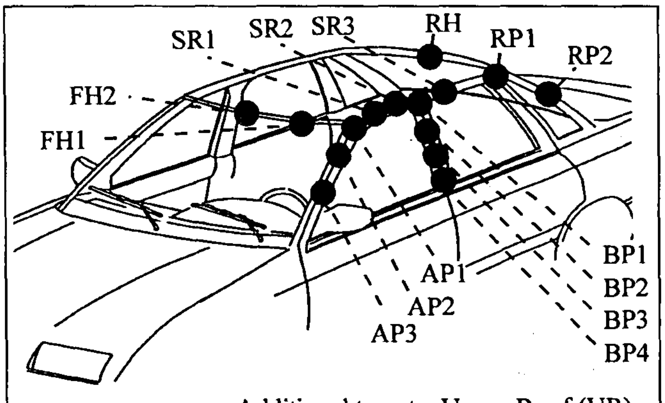

Figure 1. Targets of a conventional vehicle

The test headform must contact the target points with the forehead impact zone within a target radius. The trajectory vector of the FMH is defined by a vertical and horizontal impact angle each. These impact angles are not defined explicitly but as intervals. Consequently, the respective components of the passenger compartment must comply with the requirement criteria of the Standard within a wide variety of test angles. These test angles are determined by the various trajectory vectors of the free-motion headform.

Table 1.
Approach angle limits (only left side)

Target component	Horizontal angle α_H [°]	Vertical angle α_V [°]
Front header	180	0 - 50
Rear header	0 or 360	0 - 50
Side rail	270	0 - 50
Sliding door track	270	0 - 50
A-pillar	195 - 255	-5 - 50
B-pillar	195 - 345	-10 - 50
Other pillar	270	-10 - 50
Rearmost pillar	270 - 345	-10 - 50
Upper roof	any	0 - 50
Rollbar	0 or 180	0 - 50
Brace or stiffener	90 or 270	0 - 50
Seat belt anchorage	any	0 - 50

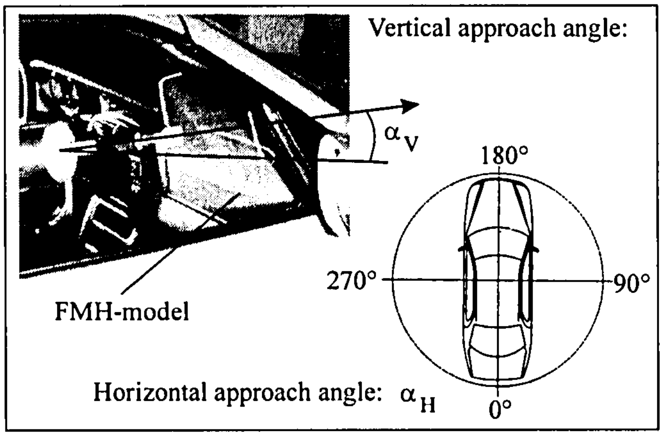

Figure 2. Approach angles of the FMH

DEVELOPMENT CONCEPT FOR COMPLIANCE WITH THE REQUIREMENTS

Developing measures to enhance vehicle safety necessitates the cross-functional cooperation between various technical departments. Styling, Bodyshell Design, Interior Equipment, Numerical Simulation and Safety Testing were included in the development for compliance with Standard FMVSS 201. The measures are aimed at absorbing the kinetic energy of an impacting occupant head by providing for suitable interior trimmings in such a manner that the resulting head accelerations are reduced, thus lowering the head injury criterion to less than 1000.

Basically, various problem-solving approaches are possible and combining them leads to suitable measures:

- The interior must be designed such that "hard areas" are out of reach or are grazed only tangentially.
- In potential impact areas, elements made of energy-absorbing materials must be used .
- Deformation elements optimized in respect of their energy absorption capacity must be used either alternatively or in combination.

Numerical simulation

Numerical simulation is used to reduce the number of possible design variants, optimize the selected variant and, thus shorten the development time.

Impact and crash calculations are conducted at Porsche using the LS-Dyna 3D Finite Element Program. The relevant bodyshell structure, deformation elements and trimmings to be integrated are discretized as finite elements. During simulation, a numerical idealized test headform is launched at a test speed of 24 km/h. Its trajectory vector ends at the target point on the interior structure.

The simulated accelerations at the center of gravity of the test headform and the deformation of the structure are evaluated, analogously to the test. The head injury criterion HIC(d) is determined on the basis of the head accelerations.

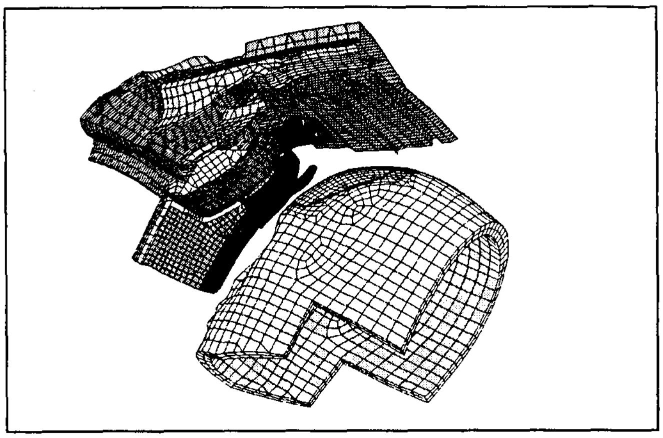

Figure 3. Simulation of a head impact in the area of the B-pillar area

The analysis of the dynamic deformation between the interior trimming and the bodyshell during head contact is of major advantage for design optimization. In the case of complex surfaces with non-constant transitions in particular, the movement of the free-motion headform after initial contact with the target point is influenced by the trajectory vector. This leads to differing head accelerations and, thus, also to differing HIC(d) values.

The concepts for the connection of trimmings, deformation elements and the bodyshell can be varied during the simulation process. Moreover, numerical simulation essential helps to establish the one test combination which - among the wide variety of possible impacts on a target point - leads to a maximum head injury criterion HIC(d).

Numerical simulation offers valuable assistance in impact analysis.

Experimental investigation

Compliance with the legally prescribed requirements in respect of impact protection is tested experimentally. Porsche uses a test bench which was developed specifically for Standard FMVSS 201 - FMH.

The vehicle is prepared for the test and set up on the test bench. With the aid of the test bench equipment, the target points are calibrated and marked in a vehicle-specific coordinate system, either in accordance with the respective CAD data or on the basis of corresponding in-vehicle measurements.

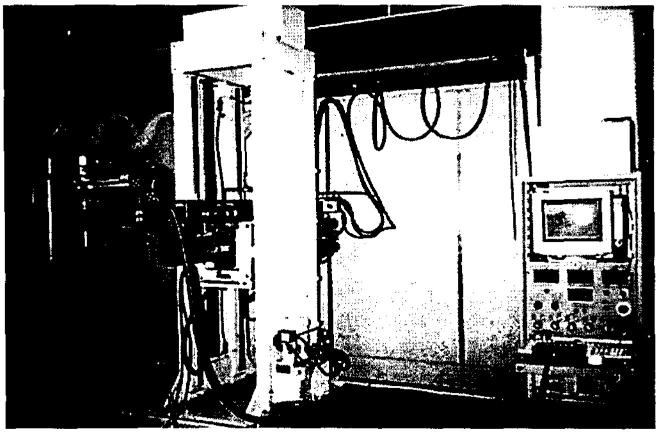

Figure 4. FMH-test facility

Approximately 35 target points must be defined for a conventional vehicle. The target points must be tested within horizontal and vertical impact angles to be determined which define the trajectory vector of the FMH. The Standard generally necessitates testing of a defined target point at differing approach angles (see Figure 2). The number of tests to be performed at a target point can be reduced by analyzing the bodyshell structure, the package conditions between trimming and bodyshell and the trimming contour assuming a "worst-case" situation.

In the vehicle, the test arm is positioned according to the trajectory vector in such a manner that the test headform at the end of the arm moves through an unguided, free-motion trajectory of at least 25 mm before its impact zone contacts the target point. The test headform is accelerated pneumatically. It consists of a modified Hybrid III dummy head with no nose contour. The speed of the test headform on the test bench can be set between 15 km/h and 40 km/h. The legally prescribed speed is 24 km/h.

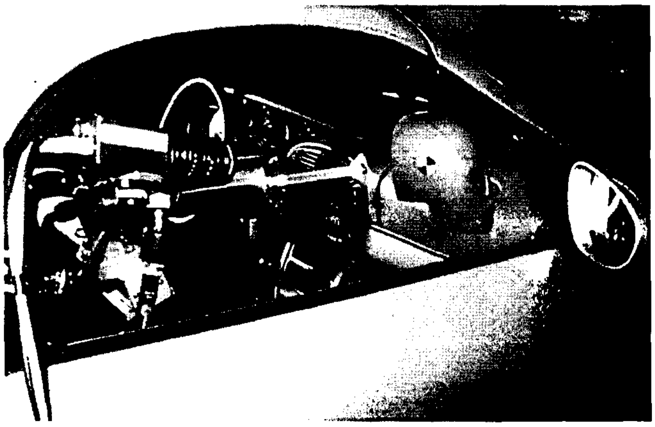

Figure 5. FMH-test

The tests are recorded with a high-speed video camera. The following information is available directly after the impact:

- the position of initial contact point of the test headform and trimming
- the movement of the test head during contact
- the visible deformation of the trimming surface during contact

The evaluation of the measured results covers the impact speed, the head injury criterion HIC(d), the accelerations in the coordinate directions of the trajectory and the resultant acceleration. In addition, the acceleration versus the intrusion depth can be obtained to evaluate the energy absorption quality.

Please refer to [2] for a detailed description of the test procedure.

APPROACHES FOR COMPLIANCE WITH THE REQUIREMENTS

Whilst having the same objectives, the requirements of the extended Standard FMVSS 201 - FMH lead to different measures for different interior components in the upper passenger compartment. Owing to their high stiffnesses and their shape, the pillars of the vehicle necessitate a greater deformation depth than other interior components in the event of a head impact. For reasons of active safety and in order to provide the driver with as unrestricted a field of view as possible, however, it is these components in particular which must retain their optically slim design.

Consequently, the task of Development is to minimize the intrusion depths required for absorbing the kinetic energy, allowing for the biomechanical occupant parameters and their limits. An 'ideal' deformation element consequently features a square-wave characteristic of the stress versus the intrusion depth. This response leads to a constant head acceleration and, thus, to a uniform deceleration of the occupant's head.

Deformation elements deviate from the ideal characteristic of acceleration versus the intrusion depth. The quality of the deformation elements is dependent on the design and the material used. The table below provides an overview.

Table 2.
Deformation elements of different designs

Designation	Parameters
Shell structure	■ material ■ material quality ■ geometry / contour ■ shell thickness ■ joining methods
Rib structure	■ material ■ shape ■ rib thickness ■ distribution
Honeycomb structure	■ material ■ shape ■ cell sizes / radius ■ thickness

Besides the various designs, the material plays a crucial role, too:

Table 3.
Material variants for a deformation element

Material	Parameter
Plastic	■ quality ■ fracture behaviour
Foam	■ quality ■ density
Metal	■ material ■ strength / quality ■ joining behaviour

The selection of a suitable deformation element and material depends on the packaging, the styling of the trimming, the bodyshell structure and the position of the impact area. The properties of certain designs and materials are listed below. The results are based both on quasi-static tests and on head-pendulum and impact tests.

Deformation elements made of foam can be designed and built at low cost. The constancy and amount of stress is dependent on the respective material. 70% max. of the geometrical thickness of the deformation element can made use of. Higher deformation leads to blocking of the foam and, thus, to a progressively increasing stress response. The parameters of foams are largely temperature-dependent. The foam elements are attached to the trimming elements for easy installation.

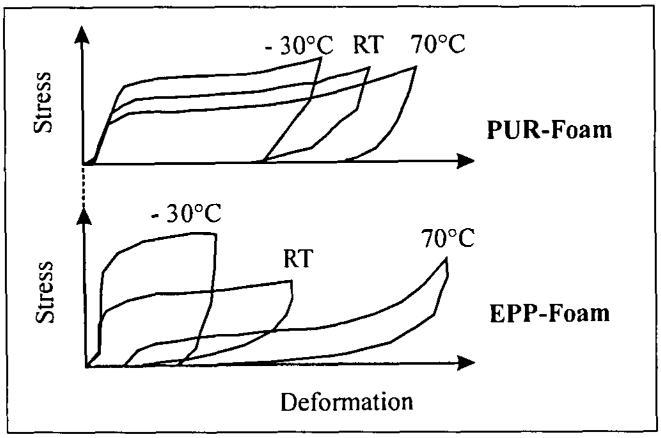

Figure 6. Stress/strain diagram of different foam materials when subject to impact loading [source: Bayer AG]

Metallic deformation elements of shell design absorb energy as a result of local and global deformation. The essential design parameters are the cross-sectional contour and the wall thickness of the shell element. For a given packaging space, these parameters allow high energy absorption with good efficiency at different impact angles. Attachment of the deformation elements is generally complex and performed on the bodyshell. The joining method is dependent on the material and must be adapted to the deformation areas.

When developing a new vehicle, energy-absorbing elements can be integrated in the bodyshell for enhanced stiffness. This helps to further minimize the volume of the energy-absorbing trimmings.

Metallic deformation elements consisting of thin layers are also under investigation. The layers are keyed together. The stress level is homogeneous up to a deformation of 90 % of the element thickness. The stress level can be adjusted as a function of the number of layers. Various concepts are available for attaching the elements. The application of the elements is restricted by packaging considerations and, in particular, by the contour of the bodyshell, trimming and required lead-throughs.

Honeycomb elements are available in various shapes and materials. The honeycombs may consist of aluminum or plastic. The energy absorption results from local collapsing of the honeycomb assembly. The stress/deformation behavior can be adjusted as a function of the diameter resp. the width and the thickness of the honeycombs. The elements respond with a pronounced, virtually constant stress level versus the intrusion depth. The folding zone at this level amounts to approx. 80 % of the honeycomb height. Any stress peaks occurring prior to the initial folding of the honeycombs can be minimized by pre-compression. The application of honeycomb elements is primarily restricted by their shape and, as a result, by producibility considerations. Honeycomb elements with variable honeycomb height can be produced only at very high cost. Honeycomb elements are well-suited for virtually flat areas. For one-dimensionally curved surfaces over-expanding honeycombs, only can be used within certain limits. The diagram below compares some selected designs:

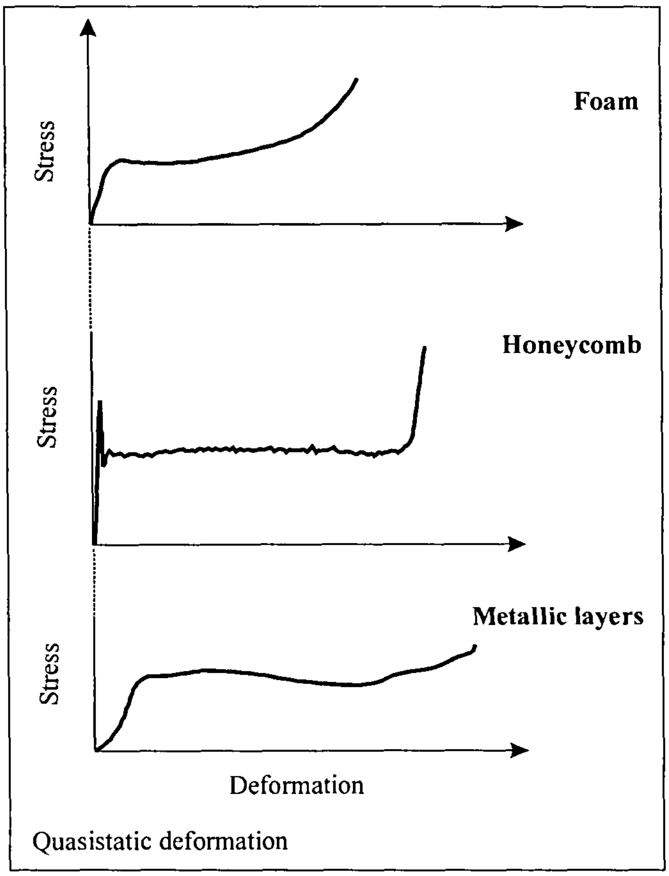

Figure 7. Standardized stress/deformation diagram for various designs

Dynamic investigations of the absorption behavior of the differing designs in an FMH test must always be conducted complete with the trimming elements. Firstly, the trimming element distributes the local loads applied to the target point over the deformation element. Secondly, the shape of the trimming contributes to the overall stiffness of the structure.

One example of an energy-absorption element is the trimming of the rollbar in the Porsche Boxster. Being an open-top vehicle, the Porsche Boxster features an effective roll-over protection system consisting of a high-strength windshield frame and a rollbar. The rigid rollbar made of high-strength, stainless steel is manufactured using an internal high-pressure compression forming process. It's task is to preserve the integrity of the passenger compartment in rollover accidents. In order to further protect the occupant's head in the event of an impact with the rollbar in a rear-end crash, the rollbar has been provided with an energy-absorbing trimming.

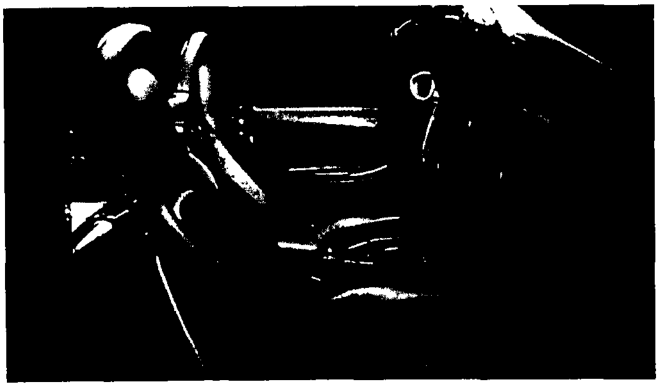

Figure 8. Rollbar of the Porsche Boxsters

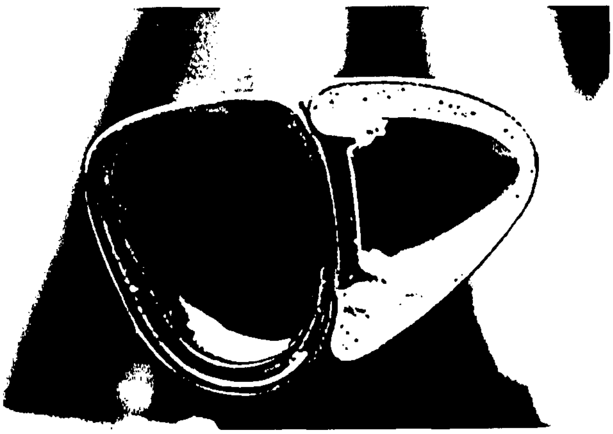

Figure 9: Section through the rollbar and rollbar trimming

The rollbar trimming consists of a metallic deformation element which is provided with a TPO film or leather with expanded plastic on the side facing the occupants. The deformation element is mounted directly on the rollbar structure.

During development, impact tests with the free-motion headform were conducted at an impact speed of 24/h in order to determine the dynamic energy absorption capacity. The results of the FMH test are shown in the following diagrams:

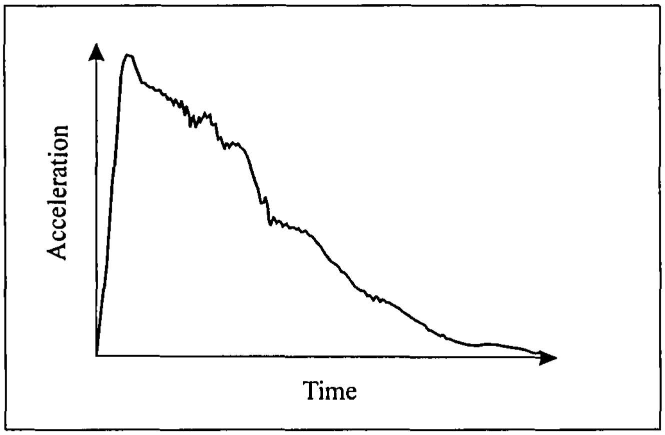

Figure 10: Rollbar: resultant head acceleration versus time

By integrating the characteristic twice, it becomes possible to plot the resultant force versus the intrusion depth on the basis of the head acceleration. The area beneath the curve corresponds to the absorbed kinetic energy of the head.

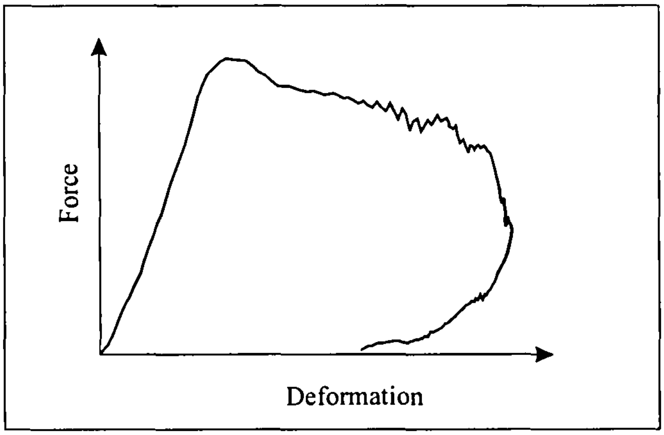

Figure 11. Force/deformation characteristic of the head impact

The complete intrusion depth comprises the plastic deformation of the deformation element, the compression in the connecting area and the elastic deformation of the rollbar.

The diagram also shows a rapid increase in force and a virtually constant force level in the dynamic test. The requirements of the extended Standard FMVSS 201 are met with an adequate safety margin.

CONCLUSION

The extension of Standard FMVSS 201 for protection of the vehicle occupants in the event of an impact with elements in the upper passenger compartment places stringent requirements on interior components in terms of design and energy absorption.

Consequently, the development must be performed in close cooperation between the various technical departments, such as Packaging, Styling, Simulation, Equipment and Safety Testing. The defined development targets are often conflicting ones. For improved energy-absorption and occupant protection, the interior elements must be provided with appropriate intrusion depths, this demand having a considerable influence on styling. At the same time, the occupants' field of view must be as unrestricted as possible and their comfort of movement be preserved.

In the course of preliminary tests, it was possible to acquire know-how as to the particular materials and designs suitable for deformation elements in the interior. To begin with, detailed design investigations and optimizations in the upper passenger compartment are conducted with the aid of numerical simulation. The results of this simulation are then validated and further developed in dynamic vehicle tests on the FMH test bench. These development efforts have led to solutions which allow the additional packaging space required for compliance with the requirements of the extended Standard to be minimized.

In the future, one of the main tasks will be to integrate the required intrusion depths into the packaging of existing subassemblies as far as this is possible, and, at the same time, reduce the number and height of required deformation elements.

REFERENCES

[1] *Code of Federal Regulations - Transportation:* " Standard No. 201: Occupant protection in interior impact", 49 CFR§571.201, 08.04.1997

[2] *U.S Department of Transportation, NHTSA:* "Laboratory Test Procedure for FMVSS 201U", TP201U-01, 1998

[3] *Menking:* "Aufprallschutz für Insassen im Fahrzeuginnenraum", HdT-Tagung "Passive Sicherheit", Essen - Germany, 1997

REDUCTION OF HEAD ROTATIONAL MOTIONS IN SIDE IMPACTS DUE TO THE INFLATABLE CURTAIN - A WAY TO BRING DOWN THE RISK OF DIFFUSE BRAIN INJURY

Katarina Bohman, Yngve Håland
Autoliv Research
Sweden
Bertil Aldman
Chalmers University of Technology
Sweden
Paper number 98-S8-O-07

ABSTRACT

Diffuse brain injuries are very common in side impacts, accounting for more than half of the injuries to the head. These injuries are often sustained in less severe side impacts. An English investigation has shown that diffuse brain injuries often originate from interior contacts, most frequently with the side window. They are believed to be mainly caused by quick head rotational motions.

This paper describes a test method using a Hybrid III dummy head in a wire pendulum. The head impacts a simulated side window or an inflatable device, called the Inflatable Curtain (IC), in front of the window, at different speeds, and at different impact angles. The inflated IC has a thickness of around 70 mm and an internal (over) pressure of 1.5 bar. The head was instrumented with a three axis accelerometer as well as an angular velocity sensor measuring about the vertical (z) axis. The angular acceleration was calculated. The head impact speeds ranged up to 7 m/s, a speed at which the Inflatable Curtain barely bottoms out. The recorded data for linear acceleration, angular acceleration and angular velocity were compared with corresponding threshold values found in the literature.

It was concluded that the Inflatable Curtain has the potential to substantially decrease the risk of sustaining diffuse brain injuries. The IC reduced the maximum linear acceleration and HIC up to 70% and the peak angular acceleration up to 70%, depending on the contact angle between the head and the IC. The peak angular velocity was reduced up to 30%.

INTRODUCTION

Head injuries can be divided into skull fractures, focal brain injuries and diffuse brain injuries. The latter type is the most common. Gennarelli *et al.* (1987) found that over half of the hospitalized patients for head injuries in the United States suffered from diffuse brain injuries. One third of the injuries were fatal. Morris *et al.* (1993) found in another study that 60% of AIS 2+ head injuries in side impacts were of the diffuse brain injury type.

The diffuse brain injuries originate mainly from contact with the interior of the car, especially with the side window (Morris *et al.*, 1993). It was found in the same survey that diffuse brain injuries of AIS2+ level occurred in less severe side collisions with a mean delta-velocity of 32 km/h, than all head injuries of AIS2+ level, with a mean delta-velocity of 43 km/h.

Diffuse brain injuries are believed to be caused by quick rotational motions resulting in critical strains of the axons. These injuries are known as diffuse axonal injuries (DAI). The injuries can be widespread in the brain without any structural disruptions (Gennarelli *et al.*, 1989).

According to a study by DiMasi *et al.*, (1995) a pure translational acceleration of the head will induce very little strain, while a pure rotational acceleration will induce considerably more strain. A combination of translational and rotational accelerations will induce more strain than the rotational acceleration alone. Viano (1997) found similar high strains due to pure rotational acceleration. However, he also found greater strains with pure translational acceleration than DiMasi.

The diffuse brain injuries can cause loss of consciousness during a short or longer period of time. When regaining consciousness there may be irreversible injuries to the axons with loss of physical functions as well as changes of personality (Aldman, 1996).

Injury assessment

The severity and type of diffuse brain damage appears to depend on the magnitude, the duration and the onset rate of the angular acceleration. A short duration of rotational acceleration will require a very high magnitude in order to cause damage to the brain tissue. Conversely, increased acceleration duration can cause brain damage at lower rotational accelerations. When the duration and the amplitude of the acceleration increase, the strain will occur deeper into the brain and cause axonal damage (Gennarelli,1987).

Margulies *et al.* (1992) proposed tolerance levels for diffuse brain injuries in lateral rotational acceleration motions (acceleration about the x-axis). The tolerance is described by the peak angular acceleration (sinewave) and the peak change in angular velocity, which can be reached before a critical level of strain is exceeded. The peak change in angular velocity is the maximum of the integration of the angular acceleration. The strain is linearly increasing with the load and exponentially increasing with the brain size (Margulies *et al.,* 1989). Concussion can be compared with a strain level of 0.05, while tissue disruption occurs at a strain level of 0.2 (Gennarelli *et al.*, 1989).

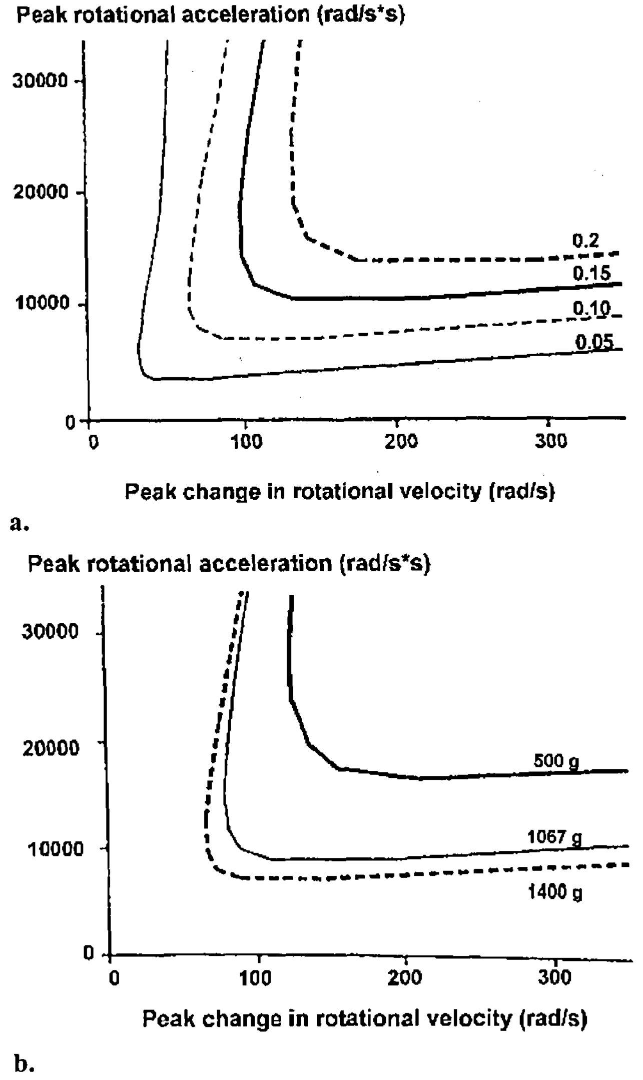

Figure 1. The graphs show the DAI (Diffuse Axonal Injury) thresholds for various strains (Fig. 1a) and for various brain masses (Fig. 1b); peak rotational acceleration as function of peak change in rotational velocity. Redrawn from Margulies *et al.*, 1992.

Gennarelli *et al.* (1987) performed a study concerning the directional dependence of DAI. They concluded that non-centroidal rotation about the longitudinal horizontal x-axis (center of rotation in the lower cervical spine) resulted in the longest traumatic coma. The centroidal rotation about the vertical z-axis was the second worst and non-centroidal rotation about the lateral horizontal y-axis resulted in the shortest traumatic coma (center of rotation in the lower cervical spine).

The Head Injury Criterion (HIC) is based on linear acceleration of the head and can only predict injuries due to forces which are directed through the center of gravity of the head. HIC does not take into account the rotational motion of the head (Gennarelli, 1987).

The aim of this study was to determine the influence the Inflatable Curtain has on the head rotational motion about the vertical z-axis and on the linear acceleration in angled head to side window impacts.

METHODS

Test setup

The test method was based on a Hybrid III dummy head in a wire pendulum. The head was attached above the center of gravity and it was permitted free rotation about the vertical z-axis.

No neck muscle activity was simulated. In these tests, the maximum angular acceleration was reached within 25 ms and the maximum angular velocity within 35 ms. The reaction time of the muscles are normally longer, up to 120 ms (van der Horst *et al.*, 1997). The head was turned up to 30° from its normal forward direction. For a human being, the head is moving freely the first 47°, if the muscles in the neck are not strained (White *et al.*, 1978).

The Inflatable Curtain was mounted on a fixture. A 3 mm thick aluminum plate was attached to the fixture, in order to simulate a side window (Figure 2). The aluminum plate was perpendicular to the ground. A rubber strip was placed between the aluminum plate and the fixture, in order to try to simulate the conditions for a car side window.

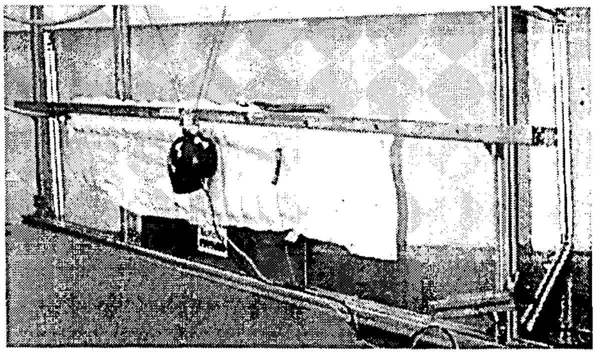

Figure 2. The test rig.

The side window had an angle *a* related to a reference plane (Figure 3). The angle (*a*) was 30° in most tests, but an angle of 45° was also tested. The 30° angle represents the head motion for the driver in a 10 o'clock side impact and the same for the passengers head in a 2 o'clock side impact.

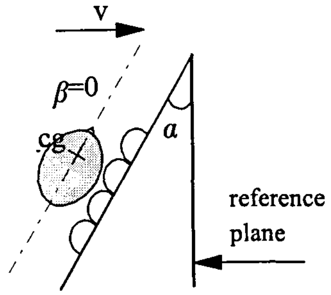

Figure 3 . The test setup from above.

The angle β was defined as the angle between the side window and the center line (x-axis) of the head, through the center of gravity and the nose. The angle β was zero, when the head was parallel with the side window (Figure 3). In this position, it should be noticed that the normal force was not directed through the center of gravity, since this point was located slightly closer to the forehead. The angle β was altered in some of the tests between -30° and +30° (Figure 4).

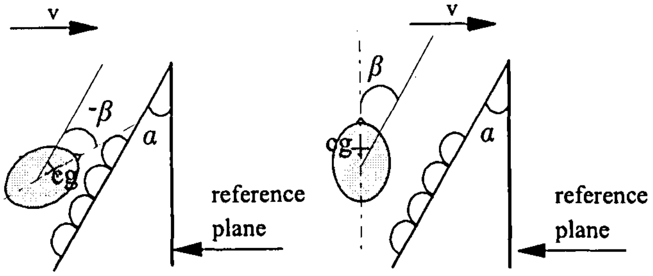

Figure 4. The figure shows how the angle β between the head and the "window" was altered in the tests.

Instrumentation - The head was instrumented with an angular velocity sensor (ARS-01 made by Ata Sensors, USA) and a standard triaxial accelerometer at the center of gravity. The signals were filtered with CFC1000. The angular acceleration was calculated and filtered with CFC180.

A film video camera (KODAK EM, 1000 Hz) was mounted above the head.

The Inflatable Curtain - The IC (Figure 2) had a volume of 12 l and a thickness of 70 mm. It was inflated with compressed air. The internal (over) pressure was 1.5 bar and measured in the front part of the filling duct.

There was no ventilation of the IC except for a small amount of air leaking through the fabric.

The IC had an outer silicon coating. In some tests talc was applied to the surface to study the effect of the friction.

Procedure

The head was dropped from an elevated level, in order to reach a specific velocity (v) at the time of the impact to the "window". The velocity was 3 m/s, 5 m/s or 7 m/s. The velocity of 7 m/s can be equivalent to the impact speed of the head into a fixed object in a 30 km/h car-to-pole/tree collision.

Tests were performed both with and without the IC inside the "window". The influence of the friction of the fabric at various levels of pressure was also tested.

When the head form contacted the IC, there was no simulated lateral bending of the neck. The vertical axis of the head was parallel with simulated window.

RESULTS

Rotational motions

The use of the IC reduced the peak angular acceleration by about 60-70% (Figure 5). The peak angular velocity was reduced less. The reduction being between 2-30% depending on the angle between the head and the IC.

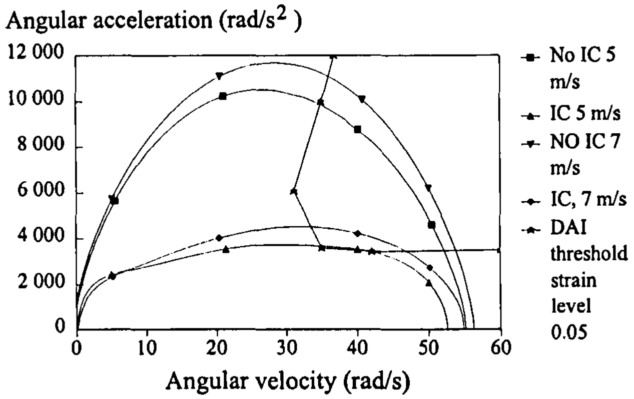

Figure 5. The angular acceleration as function of the angular velocity (simultaneous values) and the peak values. The angle (β) between the head and the IC was 30°. The DAI threshold curve (0.05 strain level) is redrawn from Margulies *et al.* (1992).

Figure 5 shows simultaneous values of the angular acceleration and the angular velocity. The results will be presented as peak angular acceleration and peak angular velocity. It should be noticed that the two peaks do not occur at the same time.

When the impact velocity was increased from 5 m/s to 7 m/s, the peak angular velocity increased 5-10% and the peak angular acceleration 15-25% depending on the angle *β* between the head and the simulated window, with or without the IC (Figure 6).

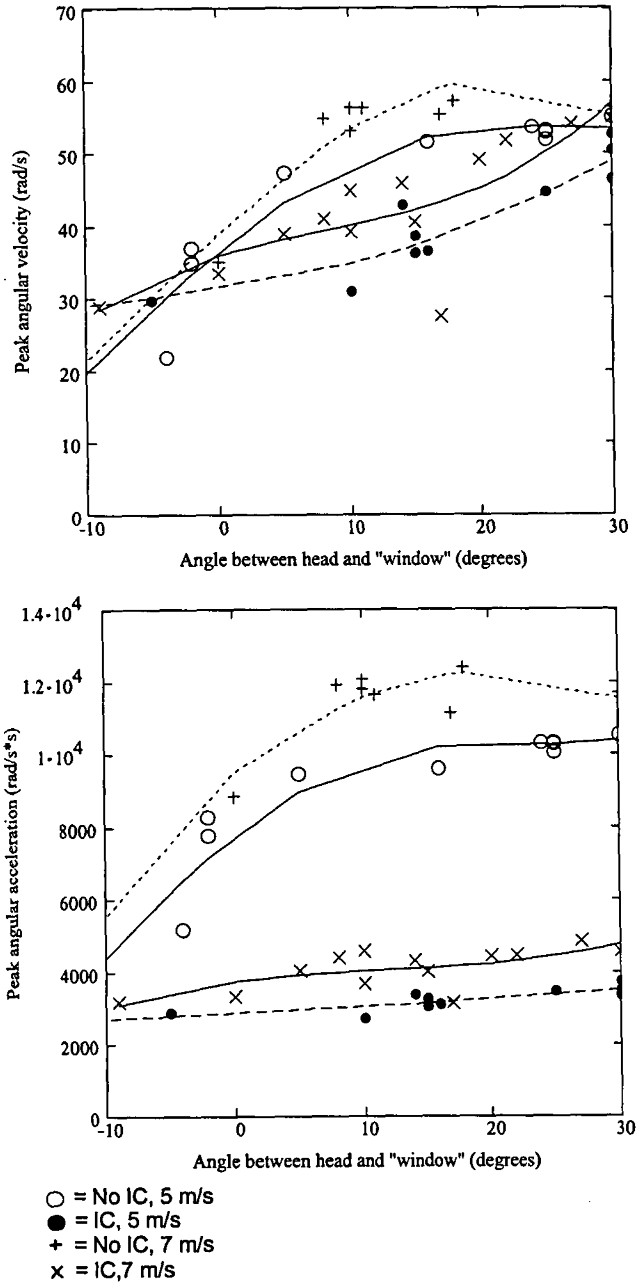

Figure 6. The peak angular velocity and the peak angular acceleration as a function of the angle (*β*) between the head and the "window", with and without IC, at different impact velocities. The angle (*α*) between the IC and the reference plan was 30°.

The angle (*α*) between the reference plane and the simulated side window were tested at 30° and 45°, with the head parallel to the reference plane. Without the IC, the angular acceleration about the z-axis decreased about 35% when the angle increased from 30° to 45° angle, independent of the velocity of the head. With IC, the angular acceleration increased only about 5%.

The angle (*β*) between the head and the "window" was varied between -30° and +30° (see Figure 4). The minimum values were reached at an angle of -20°. That was the angle at which the normal contact force was directed through the center of gravity. The angular acceleration and the velocity both increased with the increase of the angle *β* (Figure 7).

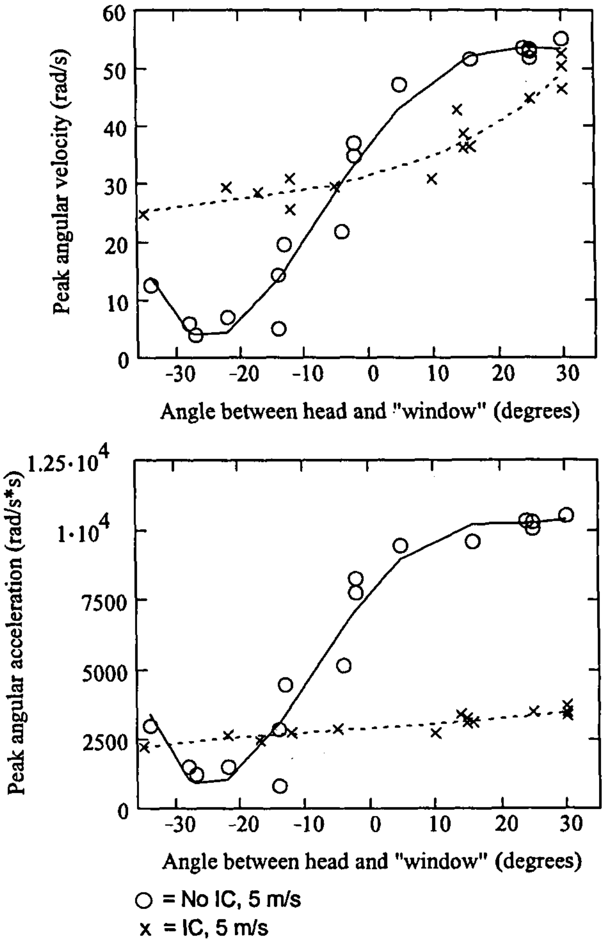

Figure 7. The absolute value of the peak angular velocity and peak angular acceleration as function of the angle (*β*) between the head and the "window", at a contact velocity of 5 m/s.

The angular acceleration, however, did not increase in the same way with the IC as without the IC, when the angle between the head and the "window" was increased

(Figure 7). At -20° the peak angular acceleration and velocity were almost zero, when there was no IC.

Linear motions

The IC reduced the linear acceleration up to 70% (Figure 8).

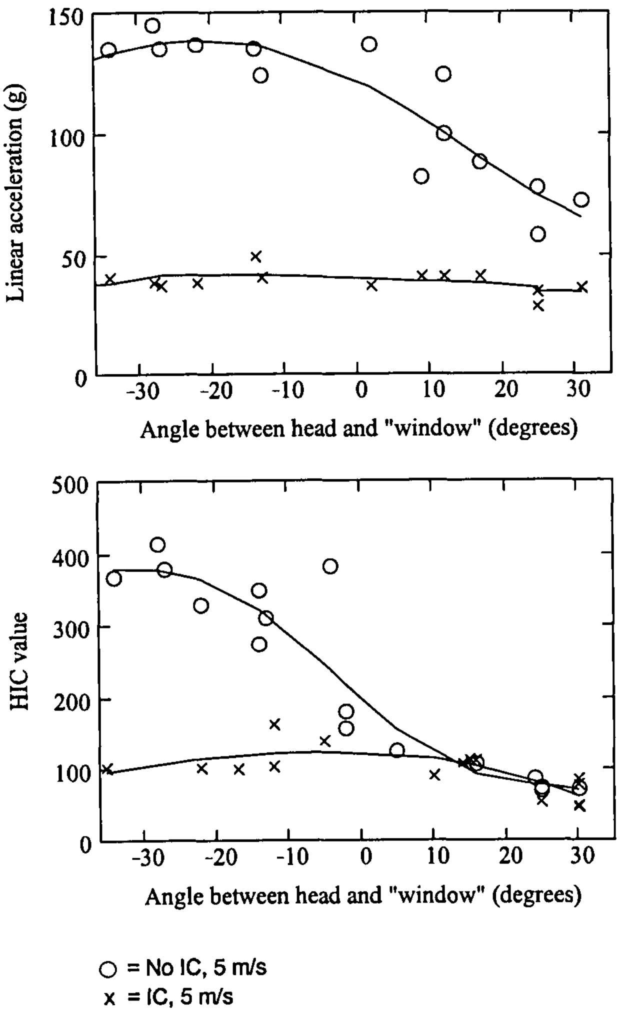

Figure 8. The linear acceleration and the HIC as function of the angle (β) between the head and the "window".

The HIC shows the same characteristic as the linear acceleration, with a reduction up to 70%. The HIC increased as the angle β between the head and the IC decreased (Figure 8). The increase was much smaller with the IC.

DISCUSSION

Rotational motions

Inflatable Curtain - The head angular acceleration was reduced due to the relative "soft" spring characteristics of the IC compared to the "stiff" side window. The angular velocity was mainly influenced by the damping of the IC, which was limited at these impact velocities and impact angles. Moreover, the duration of the rotation was longer with the IC than without, which gave the head more time to reach the angular velocity, despite the lower rotational acceleration.

Figure 5 shows that the risk of diffuse brain injury was mainly reduced by the reduction of the angular acceleration due to the IC.

Angle between the IC and the reference plane - The angular acceleration decreased as the angle (a) increased from 30° to 45°. The angle a had an influence on the head velocity component perpendicular to the IC. The velocity v_y thus decreased as the angle a increased (Figure 9), which explains the reduction of the angular acceleration.

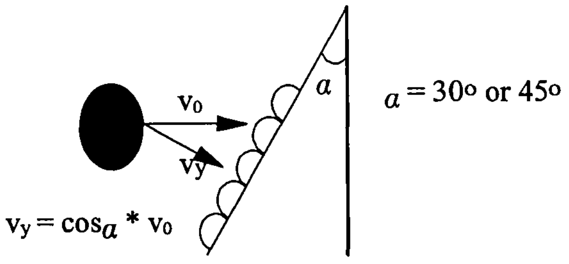

Figure 9. Test conditions.

The peak angular velocity was marginally affected by the change of the angle a from 30° to 45°. The limited energy absorption of the IC in these test conditions means that the kinetic energy of the head form before the impact is transformed to rotational energy after the impact.

Angle between the head and the IC - The torque, the normal contact force times the distance between the contact point and the head center of gravity point, increased with the angle β. This directly increased the angular acceleration. The normal forces were obviously larger than the friction forces.

When the head first came in contact with the IC, it penetrated the IC a couple of millimeters without any large force (15% of the maximum force). The force then increased and the head started to rotate. The distance between the point of contact and the center of gravity, when the head had an angle β of 30° to the side window, was about 7 cm. The effective distance, however, decreased, when the head started to compress the IC. This can explain why the angular acceleration did not vary so much for different β angles with the IC as without the IC.

Pressure of IC - A range of different pressures were tested (between 0.5 bar and 2.0 bar). The angular peak acceleration and velocity decreased both with a reduction in pressure (Figure 10).

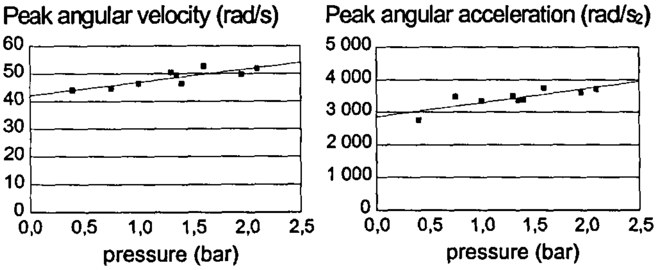

Figure 10. Influence of the pressure of the IC. The angle (β) between head and IC was kept to 30°. The head impact velocity was 5 m/s.

The angular acceleration and angular velocity decreased by about 20%, when the pressure was decreased 75% (from 2.0 bar to 0.5 bar). In order to avoid a bottoming out of the IC at higher impact velocities (7 m/s), the pressure needs to be about 1.5 bar.

Friction - Some additional tests were performed with an IC applied with talc on the surface in order to reduce the friction. The reduction in friction was approximately 80%, from 3.1 to 0.7, when measuring the friction between the fabric and a piece of glass.

The peak angular acceleration increased only between 5% and 10% with the higher friction, independent of the angle between the head and the IC. The angular velocity showed the same small dependency on the friction as the angular acceleration.

Linear motions

The maximum HIC and the maximum linear acceleration were reached, when the angular acceleration and angular velocity had their lowest values. The linear acceleration had its maximum, when the contact force was directed through the center of gravity, which at the same time resulted in the lowest angular acceleration. Vice versa, when the contact point was applied further away from the center of gravity, the linear acceleration decreased and the rotational acceleration increased (Figure 7 and 8).

DiMasi *et al.* (1995) noticed a combined effect between translational and rotational accelerations, when the translational acceleration resulted in a HIC between 800 and 900. In these tests the maximum HIC value was less than 400. This combined effect could not be estimated from these test results. However, it is possible that the strain effects in a human brain at these levels of linear acceleration are small.

CONCLUSIONS

The study has shown that the Inflatable Curtain reduces the angular acceleration as well as the angular velocity of the head in angled head to side window impacts. There was a 2-30% reduction of the peak angular velocity and a 60-70% reduction of the peak angular acceleration in the tests performed. The linear acceleration was reduced up to 70%. It is therefore believed that the IC has the potential to substantially reduce the risk of sustaining diffuse brain injuries in side impacts.

The maximum angular acceleration and angular velocity were both dependent on the perpendicular impact velocity of the head to the side window/IC.

The angle between the head and the IC/window had an influence on both the angular acceleration and angular velocity. However, the influence of the angle was much larger without IC than with.

ACKNOWLEDGMENTS

The authors wish to acknowledge Dr. Ola Boström, Autoliv Research; for his valued contributions.

REFERENCES

Aldman B., " Huvudskador - huvudskydd", Literature in the course in "Teknisk Trafiksäkerhet", Department of Injury Prevention, Chalmers University of Technology, Sweden, 1996, pp. 1-19.

DiMasi F.P., Eppinger R.H., Bandak F.A., "Computational analysis of head impact response under car crash loadings", 39th Stapp Car Crash Conference, USA, 1985, pp. 425-438.

Gennarelli T.A., "Head injury biomechanics: A review", Head injury Mechanisms, Association for the Advancement of Automotive Medicine, 1987, pp. 9-22.

Gennarelli T.A., Thibault L.E., Wiser R., Tomei G., Graham D., Adams J., "Directional dependence of axonal brain injury due to centroidal and non-centroidal acceleration", 31th Stapp Car Crash Conference, USA, 1987, pp. 49-52.

Gennarelli T.A., Thibault, L.E., "Clinical rationale for a head injury angular acceleration criterion", Head injury mechanisms: The need for an angular acceleration criterion, Association for the Advancement of Automotive Medicine, 1989, pp. 5-8.

van der Horst M.J., Thunnissen J.G.M., Happee R., van Haaster R.M.H.P., Wismans J.S.H.M, "The influence of muscle activity on head-neck response during impact", 41th Stapp Car Crash Conference, USA, 1997, pp. 487-508.

Margulies S.S., Thibault L.E., " An analytical model of traumatic diffuse brain injury", Journal of Biomechanical Engineering vol 111, 1989, pp. 241-249.

Margulies S.S., Thibault L.E., "A proposed tolerance criterion for diffuse axonal injury in man", Journal of Biomechanics vol 2. no 8, 1992, pp. 917-923.

Meaney D.F., Thibault L.E., Generalli T.A., "Rotational brain injury tolerance criteria as a function of vehicle crash parameter", Ircobi Conference, France, 1994, pp. 51-62.

Morris A., Hassan A., Mackay M., Hill J., "Head injuries in lateral impact collision", Ircobi Conference, The Netherlands, 1993, pp. 41-56.

Ommaya A.K., Fisch F.J., Mahone R.M., Corrao P., Letcher F., "Comparative tolerances for cerebral concussion by head impact and whiplash injury in primates", International Automobile Safety Conference, SAE, 1970.

Pincemaille Y., Trosseille X., Mack P., Tarrière C., Breton F., Renault B., "Some new data related to human tolerance obtained from volunteer boxers", 33th Stapp Car Crash Conference, USA, 1987, pp. 177-190.

Sparke L.J, "Head and neck injury in side impacts", 15th International Technical Conference on Enhanced Safety of Vehicles (ESV), Australia, 1996, pp. 1252-1256.

Viano D., "Mechanisms of brain injury", Literature in the course in "Teknisk Trafiksäkerhet", Department of Injury Prevention, Chalmers University of Technology, Sweden, 1996.

Viano D., "Brain Injury Biomechanics in Closed-Head Impact", Doctoral thesis, Institute of Clinical Neuroscience, Section on Injury Prevention, Karolinska Institute, Stockholm, Sweden, 1997.

White A.A., Panjabi M., "The basic kinematics of the human spine", Spine 3:12, 1978.

COMPARATIVE PERFORMANCE TESTING OF PASSENGER CARS RELATIVE TO FMVSS 214 AND THE EU 96/EC/27 SIDE IMPACT REGULATIONS: PHASE I

Randa Radwan Samaha
Louis N. Molino
Matthew R. Maltese
National Highway Traffic Safety Administration
Paper Number 98-S8-O-08

ABSTRACT

Based on a long recognized need, the National Highway Traffic Safety Administration (NHTSA) has begun to reexamine the potential for international harmonization of side impact requirements. To this end NHTSA, as directed by the U. S. Congress, has recently submitted a report to the Congress on the agency plans for achieving harmonization of the U. S. and European side impact regulations. The first phase of this plan involves crash testing vehicles compliant to FMVSS 214 to the European Union side impact directive 96/27/EC. This paper presents the results to date of this research. The level of safety performance of the vehicles based on the injury measures of the European and U.S. side impact regulations is assessed.

INTRODUCTION

The National Highway Traffic Safety Administration (NHTSA) has long recognized the need for international harmonization of side impact requirements and the potential of added safety benefits resulting from such harmonization. Although the U.S. and EU side impact regulations ideally address the same safety problem, they differ in test procedures, barriers, dummies, and injury criteria. Recently, the U.S. Congress directed NHTSA to study the differences between the U.S. and proposed European side impact regulations and to develop a plan for achieving harmonization of these regulations. Also, manufacturers believe that these differences lead to different vehicle designs, thus posing undue financial burdens in terms of dual development, testing, manufacturing and distribution of vehicles in various markets.

NHTSA submitted a side impact harmonization plan to the U.S. Congress in April of 1997 [1]. The first phase of the plan is an attempt at assessing whether the safety performance of vehicles is functionally equivalent relative to the European regulation (EU Directive 96/27/EC) and the Federal Motor Vehicle Safety Standard (FMVSS) 214. The Functional Equivalence Assessment Process (Appendix A) was developed by the U. S. and Australia in coordination with foreign governments, industry and consumer groups. NHTSA has recently published a final rule institutionalizing the process [39]. The final rule sets forth the process that the agency will use in comparing U.S. and foreign vehicle safety standards and in determining appropriate rulemaking response, if any. The rule reaffirms NHTSA's policy of actively identifying and adopting those foreign vehicle safety standards that require significantly higher levels of safety performance than the counterpart U. S. standards. The rule also outlines the agency's policy in the case where the comparison indicates that the foreign standard's safety benefits are approximately equal to those of a counterpart U. S. standard.

To begin gathering the data necessary to make the functional equivalence assessment, NHTSA initiated a research program by testing eight U.S. production FMVSS 214 compliant vehicles to the EU Directive 96/27/EC requirement. This paper focuses on the results of the testing in terms of the level of safety performance of the vehicles for both the U.S. and EU regulations.

Current U.S. and European Side Impact Standards

The U.S. regulation on side impact is FMVSS 214; Side Impact Protection [2] addressing thoracic and pelvic fatalities and injuries in vehicle-to-vehicle crashes. The dynamic requirement, or crash test portion of this standard was added in October of 1990. It was phased-in beginning with 1994 model year (MY) cars such that all cars by the 1997 MY had to meet the requirements. Starting with the 1999 MY, trucks, buses, and multipurpose passenger vehicles under 2,721 kg (6000 lbs) must meet the dynamic part of this standard [3].

The European Union (EU) side impact regulation, EU Directive 96/27/EC was approved in October of 1996. It applies to new and redesigned M1 and N1 vehicle types beginning with the 1999 MY. M1 vehicles are those with a capacity of nine or less occupants and would include passenger cars, multipurpose passenger vehicles, and mini buses. N1 vehicles are those with the capacity of carrying up to 3.5 metric tons, e.g. vans and chassis cabs. Vehicles with R-point of lowest seat >700 mm are excluded. All M1 and N1 vehicles starting in the 2004 MY must meet this regulation.

The test procedures of both regulations are similar in that a stationary test vehicle is struck with a moving deformable barrier (MDB). These dynamic test procedures focus on the measurement of anthropomorphic test dummy responses to compute injury criteria. However, the two regulations use different test procedures, barriers, dummies, and injury criteria. Figures 1 and 2 show a schematic of the test setup for the U.S. and EU regulations. Table 1 compares the relevant crash test parameters such as impact direction, impact velocity and barrier face dimensions.

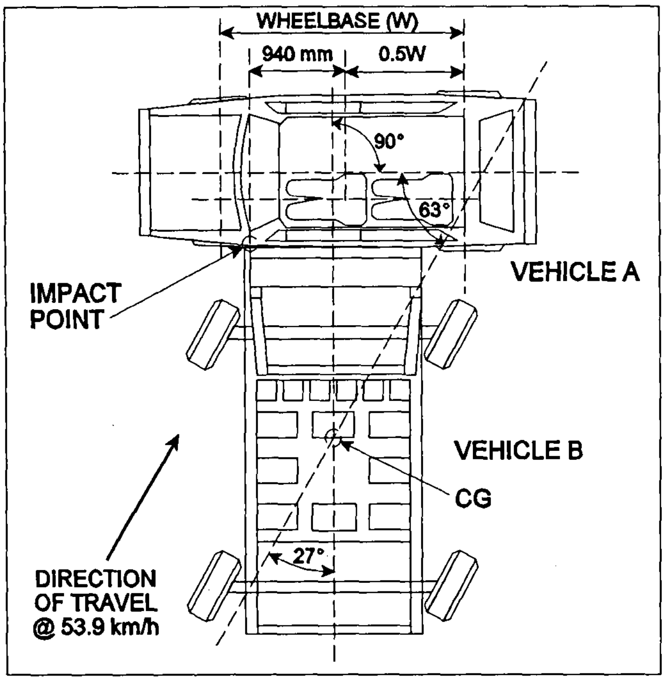

Figure 1. FMVSS 214 Side Impact Test Configuration.

The FMVSS 214 dynamic test simulates the 90 degree impact of a striking vehicle traveling 48.3 km/h into a target vehicle traveling 24.2 km/h. This is achieved by a moving deformable barrier with all wheels rotated 27 degrees (crab angle) from the longitudinal axis, impacting a stationary test vehicle with a 54 km/h closing speed. For a typical passenger car, the left edge of the FMVSS 214 MDB (214MDB) is 940 mm forward of the mid point of the struck vehicle wheel base.

In the EU 96/27/EC dynamic test, the European MDB (EUMDB) impacts the target vehicle at 50 km/h and 90 degrees with no crab angle. This differs from FMVSS 214 in that no attempt is made at simulating the movement of the target vehicle. The lateral striking position is aligned with the occupant seating position rather than the vehicle wheelbase. The EU MDB is centered about the R-point or seating reference point defined as the H-pt for lowest and rearmost driving seat position.

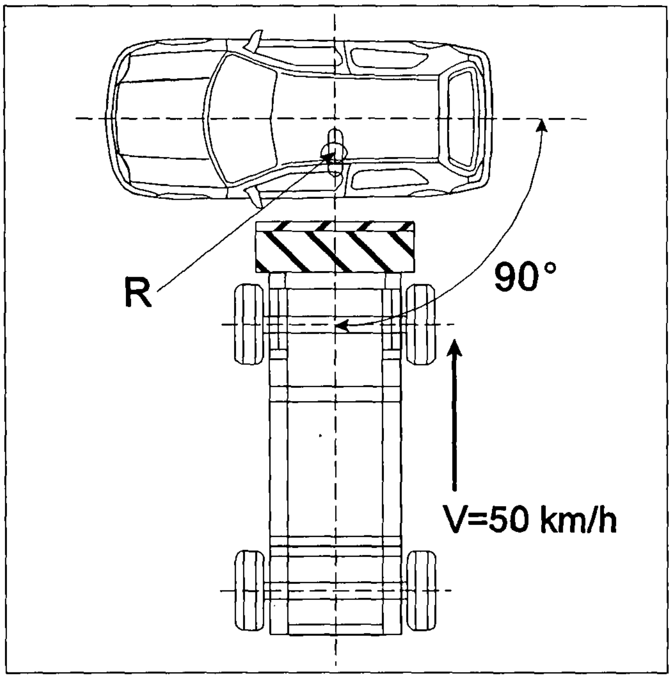

Figure 2. EU 96/27/EC Side Impact Test Configuration.

Table 1.
Crash Test Parameter Comparison

	EU 96/27/EC	FMVSS 214
MDB Mass	950 kg	1367 kg
Velocity Vector	50 kph/90°	54 kph/63°
Impact Point	Centered on R-point*	940 mm from wheelbase center
Barrier Face Ground Height	300 mm	280 mm Bumper 330 mm
Face Width	1500 mm	1676 mm
Barrier Material	Performance Defined	Aluminum Honeycomb

*same as seating reference point

FMVSS 214 and EU 96/27/EC Movable Barriers - The dimensions and material characteristics of the 214MDB face are shown in Figure 3. The aluminum honeycomb of the barrier face is specified by design. The bottom edge of the MDB is 280 mm from the ground. The protruding portion of the barrier simulating a bumper is 330 mm from the ground. The 214MDB has a total mass of 1367 kg initially derived from the weights of passenger cars and lights trucks in the U.S. fleet with a adjustment made assuming a downward trend in vehicle mass due to fuel economy needs [4, pg IIIA-6]. The dimensions of the EUMDB face are given in Figure 4. The European barrier face is segmented into six blocks with force deflection performance characteristics specified in the EU regulation. The lower blocks are stiffer than the top blocks and the center blocks are stiffer than the outboard elements. The EUMDB face is about 20% smaller than the 214MDB in terms of face area. It is also much softer than the 214MDB face on the blocks closest to the sides. The bottom edge is the most forward part of the European MDB and is 300 mm from the ground. The European barrier has a mass of 950 kg , 40% less then the mass for the U.S. barrier.

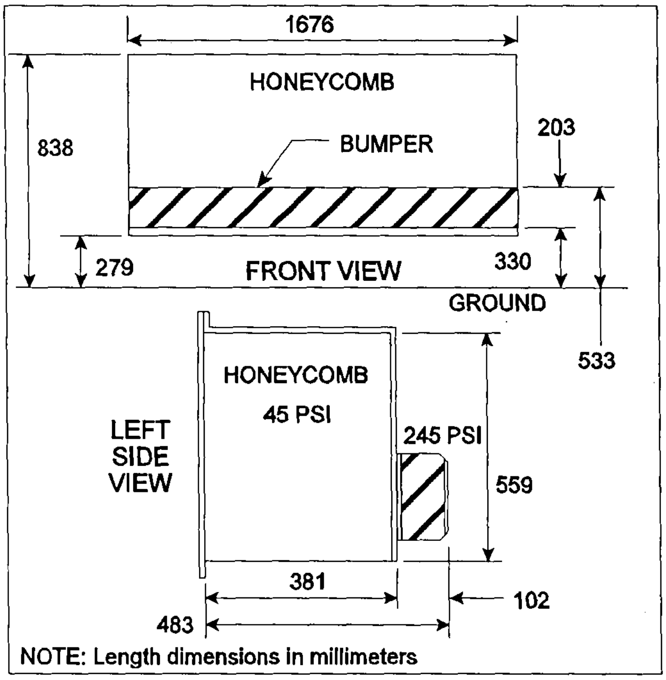

NOTE: Length dimensions in millimeters

Figure 3. FMVSS 214 Side Impact Deformable Barrier Face.

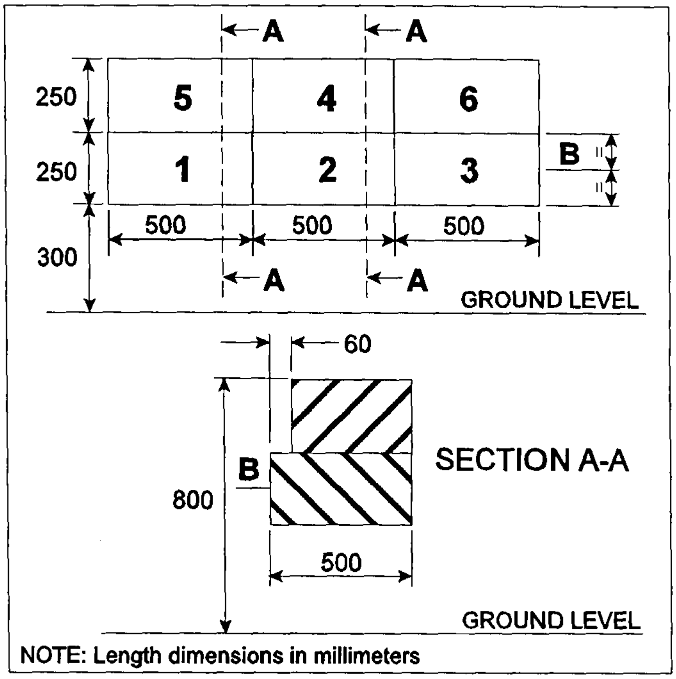

NOTE: Length dimensions in millimeters

Figure 4. EU 96/27/EC Side Impact Deformable Barrier Face.

FMVSS 214 and EU 96/27/EC Dummies and Injury Criteria - In both regulations, successful test performance is determined by dummy injury criteria. However, the regulation differ in both the test dummy and injury criteria. Figure 5 is a schematic of the two side impact dummies, the U.S. side impact dummy (SID) used in FMVSS 214 and the EU dummy EUROSID-1 used in Directive 96/27/EC.

Although both dummies ideally represent a 50th percentile side impact anthropomorphic device, they are based on different designs and have different measurement capabilities. In particular, Eurosid-1 has an articulating half arm, while the response of the arm is folded into the design of the thorax in SID. FMVSS 214 requires that a SID be placed in both the front and rear seats of the test vehicle. The EU Directive requires that only one EUROSID-1 be placed in the front seat. The injury criteria for each regulation, given in Table 2, relate to the measurement capabilities of the dummy used.

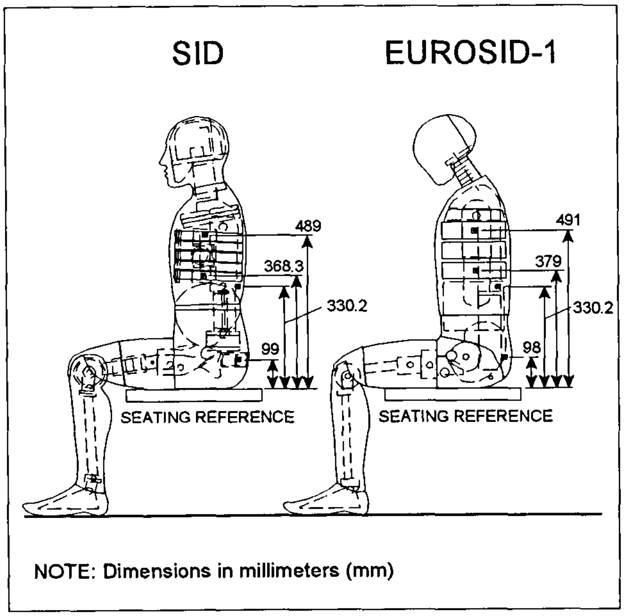

Figure 5 Schematic of Side Impact Dummies of FMVSS 214 and EU 96/27/EC

Table 2.
Test Dummy Injury Criteria

EUROSID-1	U.S. SID
HIC - 1000	
Rib Deflection ≤ 42 mm	TTI ≤ 85 or 90 G
V*C ≤ 1 m/s	
Abdominal Force ≤ 2.5 KN	
Pubic Symphysis Force ≤ 6 KN	Pelvic Accel. ≤ 130 G

SID was designed to measure only the acceleration of the ribs, spine and pelvis to compute thoracic and pelvic injury criteria [20]. The rib and spine accelerations are combined into a single metric called the Thoracic Trauma Index (TTI(d)) which has an 85g limit for 4-door vehicles and a 90g limit for 2-door vehicles. The pelvic acceleration has a 130g limit.

EUROSID-1 has additional measurement capabilities than SID, including force and displacement as well as acceleration based readings [5]. The EU regulation places limits on five dummy criteria to determine vehicle performance. The head protection criteria (HPC) is derived from head acceleration over a head contact time duration and must remain below 1000. A rib deflection criterion (RDC) allows a maximum of 42 mm of deflection in the thorax. A soft tissue viscous criterion (V*C), computed from combined rib deflection and velocity, is to be reported with a proposed limit of 1 m/s. It is worth noting that for the first two years in which EU 96/27/EC becomes effective, V*C values are to reported but not used as a pass/fail criterion . A review of the EU directive is planned in the year 2000 during which the status of V*C as a required injury criteria will be decided. The abdominal peak force (APF) is limited to 2.5 KN. Finally, the pubic symphysis peak force (PSPF), which is in the pelvic region, must be less than 6 kN.

VEHICLE MATRIX

Table 3 lists the U.S. production vehicles that were tested to the EU 96/27/EC requirements. The vehicles were identical in design to vehicles tested to FMVSS 214 in the NHTSA compliance test program. The matrix included four 4-door and four 2-door passenger cars.

Table 3.
FMVSS 214/ EU 96/27/EC Test Matrix

Vehicle		FMVSS 214 test	Side NCAP	Production
1996 Ford Taurus*	4-Dr	1996	Yes	539K
1995 Volvo 850	SW	1995	No	63K
1997 Nissan Sentra	4-Dr	1996	Yes	72K
1997 Hyundai Sonata	4-Dr	1996	Yes	15K
1997 Ford Mustang	2-Dr	1996	No	170K
1997 Lexus SC300	2-Dr	1995	No	13K
1995 Geo Metro	2-Dr	1996	No	58K
1997 Mitsubishi Eclipse	2-Dr	1996	No	111K

*The EU test for the 1996 Taurus was performed by Ford Motor Company.

The selection criteria for the vehicles in order of importance were the following:

1. FMVSS 214 test results were used to provide a range of performance from marginal to good performers within the set of 4-Dr vehicles and correspondingly within the set of 2-Dr vehicles.
2. Vehicles to be tested in the side impact New Car Assessment Program (NCAP) were included as much as possible in order to provide an additional comparative data set at a higher performance level for the current test program and for possible future ECE 95 testing at a higher performance level.
3. Vehicles built or sold by all U. S. manufacturers or their subsidiaries would be represented, and similarly, to the extent possible, for those built or sold by foreign manufacturers.
4. The highest production vehicles would be represented.

EU 96/27/EC TESTS SETUP

With the exception of placing a Eurosid-1 dummy in the rear outboard position, the procedures of the EU 96/27/EC Directive were followed in performing the European side impact tests of the U.S. production vehicles. In addition, experts from TNO, Netherlands, provided training on the latest dummy seating practices. They also provided guidance on common EU 96/2/7EC test set up practices, especially in areas where the EU directive is not specific. Although the seat track position for the front dummy is not specified in the EU Directive, the Eurosid-1 in the driver position was seated in the mid-track position to provide the best comparison with FMVSS 214. In addition, comparison checks of the test vehicle options, test weight and attitude, and dummy H-points and lateral clearances between the FMVSS 214 and EU test setups were performed. This was done to ensure minimum differences in the vehicles, dummy positioning, and test setups for the comparison testing.

The Plascore layered honeycomb construction barrier face, was used for the EU Movable Deformable Barrier (EUMDB) elements. The choice of barrier face was based on a recent evaluation of barrier faces performed through the International Standards Organizations (ISO) working group on Car Collision Test Procedures [6]. The evaluation compared the characteristics of the Cellbond/TRL, Plascore, and AFL/UTAC EUMBD faces and indicated that the Plascore face best fits the force performance corridors specified by EU 96/27/EC. It has been established by various researchers that different EUMDB face designs lead to significantly different vehicle performance results, for both the occupant responses and vehicle intrusion profiles [7,8]. As such, the recently developed honeycomb face from Plascore was chosen to ensure the best currently available fit to EUMDB performance requirements.

In both the 2-Dr Mustang and Eclispe, there was no room to fit a rear Eurosid-1 dummy in the EU tests. In the FMVSS 214 compliance tests, there was no room to fit a rear SID only in the Eclipse. It is worth noting that the Eurosid-1 dummy has a slightly higher seated height specified at 904 ± 7 mm versus 899 ±10 mm for the SID. On the other hand the SID has a wider hip width specified at 373 ±18 mm versus 355 ±5 mm for the Eurosid-1.

Eurosid-1 Calibration Issues - Problems in certification of Eurosid-1 lumbar spine parts were encountered in the set up for the EU vehicle testing. As such, a round robin calibration of three new lumbar spines was performed at three U.S. sites. The results are listed in Appendix A. The base angle output requirements were only met about 50% of the time for two of the parts although the lumbar pendulum pulse requirements were typically met. The differences in base angle outputs were small and consistent suggesting that the new parts were similar in construction but the calibration corridors may be too narrow. The results were presented to TNO and ISO/TC22/SC12/WG5 working group, Anthropomorphic Test Devices, in June of 1997. TNO has initiated a round robin research activity to address this lumbar spine calibration issue.

COMPARISON OF OCCUPANT RESPONSES

The first level of comparison of results was based on the normalized injury criteria of each regulation. Tables 4. and 5. list the computed injury criteria for the FMVSS 214 and EU 96/27/EC tests of the eight vehicles for both the driver and rear dummies. In general, the basis of the comparisons made below was to normalize the computed injury values by the limit of the criteria specified by each regulation. For example, the TTI(d) was normalized by 85 for the 4-Dr vehicles and by 90 for the 2-Dr vehicles, and RDC was normalized by 42 mm. Overall, the results indicate a higher severity for the driver dummy in the EU tests for the RDC thoracic criterion when compared to the TTI(d) in the FMVSS 214 tests. No trend is seen for V*C versus TTI(d). The results also indicate possibly a higher severity for the driver dummy in the 4-Dr vehicles for PelvicG in the FMVSS 214 tests when compared to the PSPF pelvic criterion in the EU tests. This apparent trend is reversed for the driver dummy in the 2-Dr vehicles where a lower severity is indicated for PelvicG when compared to PSPF.

Table 4.
FMVSS 214 and EU 96/27/EC Results (Driver)

	TTI(d)	Pelvic (g)	RDC	Flat Tops	V*C	PSPF (kN)	APF (kN)	HPC	Tstart	Tend	HIC36
	85/90	130	42 mm		1.00	6.0	2.5	1000	(ms)	(ms)	
1997 Ford Mustang 2-Dr	56	65	39.8	yes	0.69	4.827	2.295	33.4	58.9	62.1	85.3
1997 Lexus SC300 2-Dr	63	78	28.1	nd	0.26	2.437	1.409	24.9	63.5	118.3	44.1
1995 Geo Metro 2-DR	80	84	**43.9**	yes	0.65	4.158	1.518	nc			97.1
1997 Mitsubishi Eclipse 2-Dr	82	86	**48.6**	yes	**1.04**	4.097	1.429	nc			94.9
1995 Volvo 850 SW	49	58	29.9	yes	0.38	1.686	0.719	nc			23.5
1996 Ford Taurus 4-Dr	50	61	40.0	yes	0.94	2.196	1.131	67	116.1	145.65	90.8
1997 Nissan Sentra 4-Dr	67	94	**49.0**	yes	**1.32**	4.531	1.029	231.9	42.2	48	389
1997 Hyundai Sonata 4-Dr	70	102	29.7	yes	0.60	3.490	1.369	nc			177.6

* Numbers in bold are in excess of the criterion.
nc= no contact
nd= not determined

Table 5.
FMVSS 214 and EU 96/27/EC Test Results (Rear Passenger)

	TTI(d)	Pelvic (g)	RDC	V*C	PSPF (kN)	APF (kN)	HPC	Tstart	Tend	HIC36
	85/90	130	42 mm	1.00	6.0	2.5	1000	(ms)	(ms)	
1997 Lexus SC300 2-Dr	39	50	10.4	0.04	2.419	0.207	nc			308.6
1995 Geo Metro 2-Dr	69	100	33.5	0.23	3.725	0.110	365.4	38.2	96.7	365.4
1997 Nissan Sentra 4-Dr	51	74	11.4	0.04	5.036	0.576	234.9	61.6	141.6	252
1995 Volvo 850 SW	51	49	6.7	0.01	3.098	0.742	234	58.3	195.4	234
1996 Ford Taurus 4-Dr	57	65	23.6	0.14	1.171	0.594	nc			160.1
1997 Hyundai Sonata 4-Dr	60	102	17.5	0.09	0.673	0.317	nd			188.6

The results also indicate a much lower severity in the EU tests for the rear passenger dummy when both EU thoracic criteria are compared to TTI(d) in the FMVSS 214 tests. No trend is apparent when PSPF was compared against PelvicG for the rear passenger dummy.

Thoracic Injury Criteria

With the caveat that the Eurosid-1 rib deflections which form the basis for computing RDC and V*C are questionable (Refer to section **"Flat-Top"Anomalies in Eurosid-1 Rib Deflection Responses** below), the following observations are made. For the 4-Dr vehicles, the Nissan Sentra driver dummy, exceeded the RDC and V*C criteria (See Figure 6). For the 2-Dr vehicles driver dummy, the Geo Metro exceeded RDC and the Mitsubishi Eclipse exceeded both RDC and V*C.

With the exception of the Sonata and the Lexus SC300, the normalized TTI(d) was on the average 26.8% lower than RDC for the driver dummy. For the Sonata and the Lexus, TTI(d) was 12% and 3% higher than RDC. As to V*C, the results were more of a mismatch, with normalized TTI(d) on the average 27.1% lower than V*C for the driver dummy for four of the vehicles and higher by 27.5% for the remaining four vehicles. There were no apparent trends in these differences for either the 2-Dr or 4-Dr sets of vehicles.

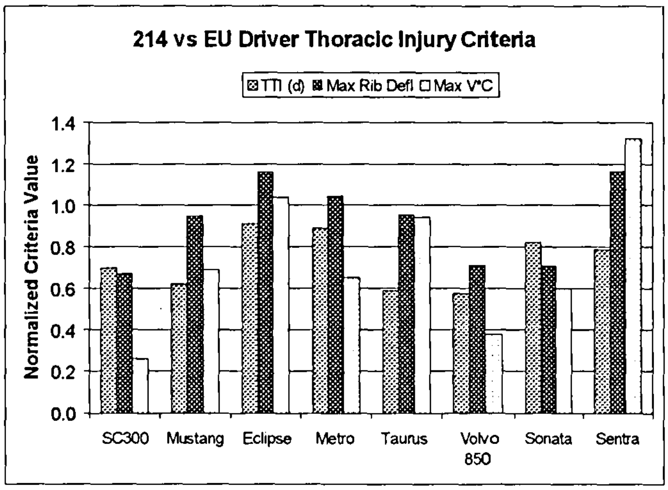

Figure 6.

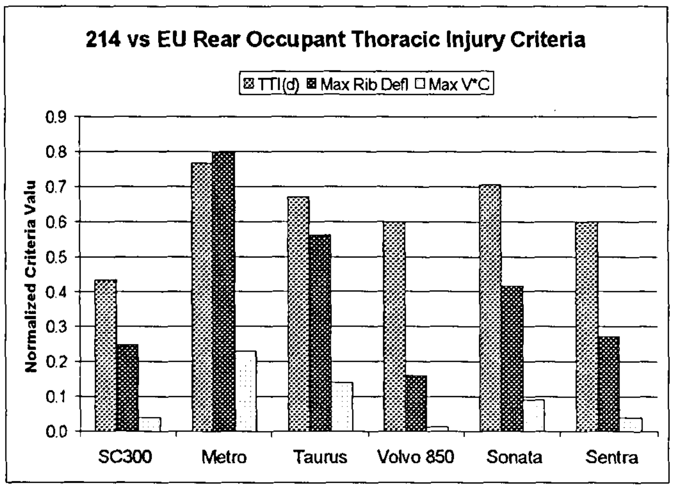

Figure 7.

The average normalized thoracic criteria for the 4-Dr vehicles and the 2-Dr vehicles are listed in Table 6. For the driver dummy, the average normalized TTI(d) and RDC are higher for the 2-Dr vehicles. In contrast the average normalized V*C is lower for the 2-Dr vehicles.

Table 6.
Average Normalized Thoracic Criteria

	4-Dr Vehicle Set		2-Dr Vehicle Set	
	driver dummy	rear dummy	driver dummy	rear dummy*
TTI(d)	69%	64%	78%	60%
RDC	88%	35%	96%	52%
V*C	81%	7%	66%	14%

*average results from only 2 vehicle tests

Pelvic Injury Criteria

For all the vehicles tested and for both front and rear dummy, none of vehicles exceeded the criteria for either regulation (See Figures 8. and 9.). For the driver dummy, the results were more of a mismatch when comparing the results for the two regulations. The normalized PelvicG in the FMVSS 214 tests was on the average 8% higher than PSPF in the EU tests for four of the vehicles and lower by 10% for the other four. When looking at the 4-Dr vehicles separately, PelvicG was on the average greater than PSPF by 16% for three of the four vehicles. The exception was the Sentra, in which PelvicG was less than PSPF by 3%. In contrast, for the 2-Dr vehicles, PelvicG was on the average 12% lower than PSPF for three of the four vehicles for the driver dummy. The exception was the SC300, in which PelvicG was larger than PSPF by 19%.

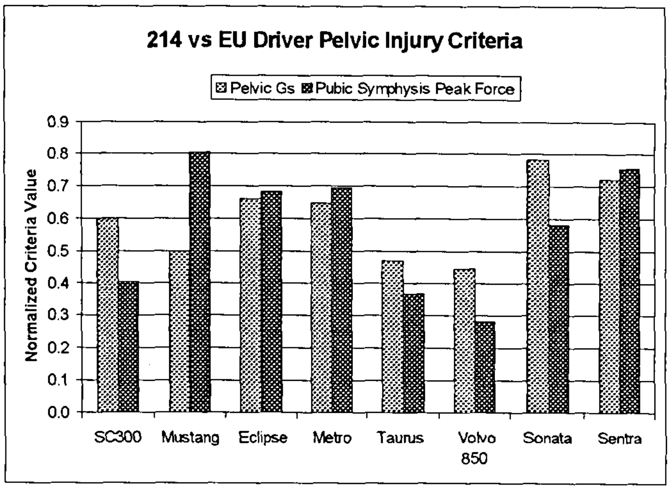

Figure 8.

For the rear passenger dummy, the normalized PelvicG was on the average 38% higher than PSPF for three of the vehicles and lower by 14% for the remaining three. There was no apparent trend in these differences for either the 2-Dr or 4-Dr sets of vehicles.

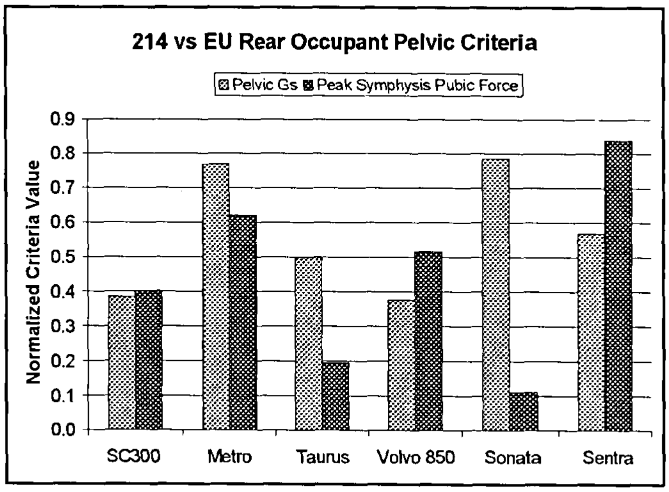

Figure 9.

Abdominal Injury Criterion

For the driver dummy in the EU tests, the Mustang normalized APF was 92% of the limit specified in the regulation and the Volvo APF was 29%. The normalized APF for the remaining six vehicles was clustered closer with an average of 53% of the limit.

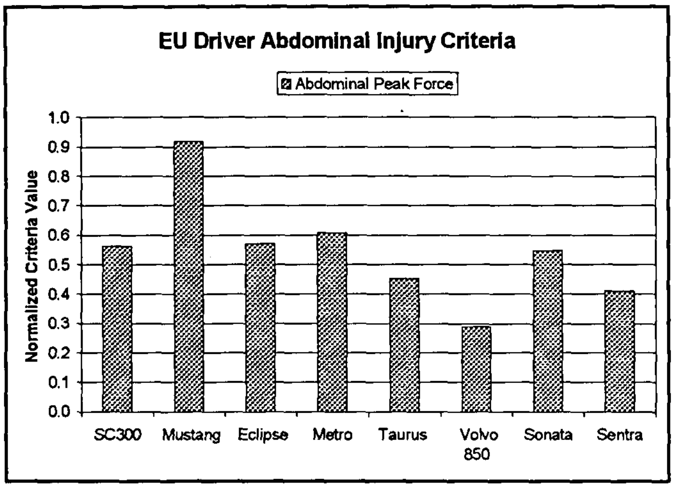

Figure 10.

Overall, the average APF for the driver dummy in 2-Dr vehicles was 67% of the limit. The average APF for the driver dummy for the 4-Dr vehicles was lower at 42 %. In contrast, for the rear dummy, the average APF was only 6.3% of the limit for the 2-Dr vehicles and 22.3% for the 4-Dr vehicles with no value exceeding 30% of the limit. The APF results are presented in Figures 10. and 11.

Head Injury Criterion

For the driver dummy in the EU tests, head contact occurred for four of the eights vehicles, with an average normalized HPC of only 8.9% of the limit specified in the regulation. For the rear dummy, contact occurred for three of the six vehicles with an average HPC of 27.8% of the limit. The normalized HPC and HIC36 values from the EU tests are presented in Figures 12. and 13. HPC is plotted only if head contact occurred.

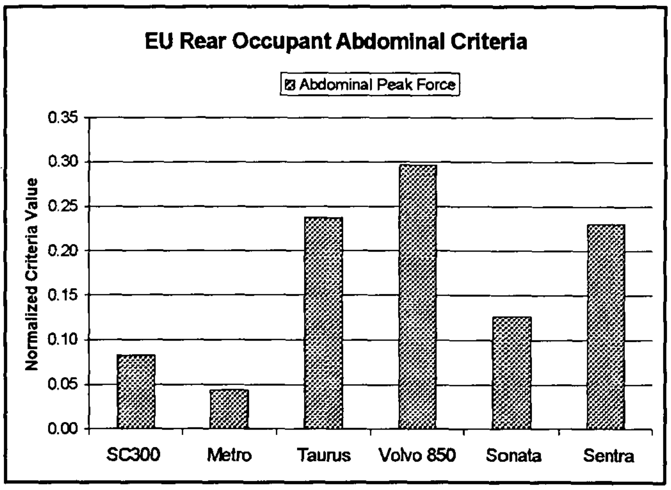

Figure 11.

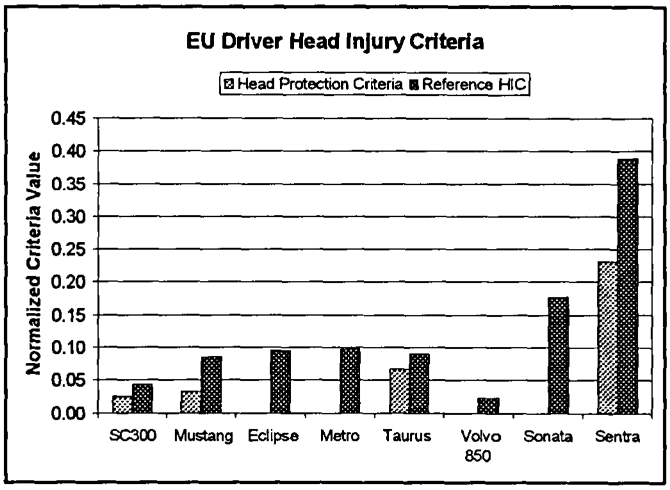

Figure 12.

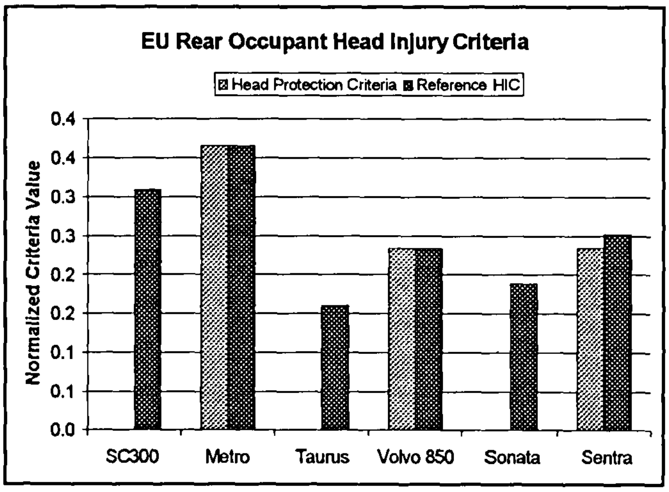

Figure 13.

"Flat-Top"Anomalies in Eurosid-1 Rib Deflection Responses

Figures 15. through 28. present an overlay of the raw (Class 1650) rib displacements for both the front and rear dummy for the vehicles tested. As shown in the figures, sustained peaks (plateaus of flat-tops) as long as 15 ms in at least one of the rib displacement curves are present for the driver Eurosid-1 for all the vehicles tested. These flat-tops are present for the rear dummy in three of the six vehicles. The displacement levels of these plateaus range anywhere from 15 to 50 mm and are below the full range of the rib potentiometers of the dummy.

Lau reported on this phenomenon in a series of Ford LTD crash tests [11]. Using a pneumatic impactor to impact the Eurosid-1, the sustained peaks in the rib displacement were produced but they could not be created with pendulum impact. (Integration of the rib and spine accelerations in the impactor impacts indicated that they were moving away from the impactor at similar speeds.) Henson et al. reported a similar rib deflection problem when testing Pontiac 6000's using the FMVSS 214 procedure with the Eurosid-1 [12]. This was believed to occur when impacts were more rearward than the lateral center of the ribs. The American Automobile Manufacturers Association (AAMA) has highlighted this anomalous rib behavior in their list of mechanical concerns relative to the Eurosid-1 dummy [13]. The AAMA has attributed this behavior to binding in the rib damping modules due to off-axis loading. Transport Canada has recently reproduced this flat-top behavior with the Eurosid-1 ribs with pendulum impacts at -15 degrees from the coronal plane, i.e. posterior or rearward of the center of the ribs [14]. In those tests, the pendulum face contacted the projecting back plate causing an alternative load path through the spine box, however the rib deflections were near their maximum.

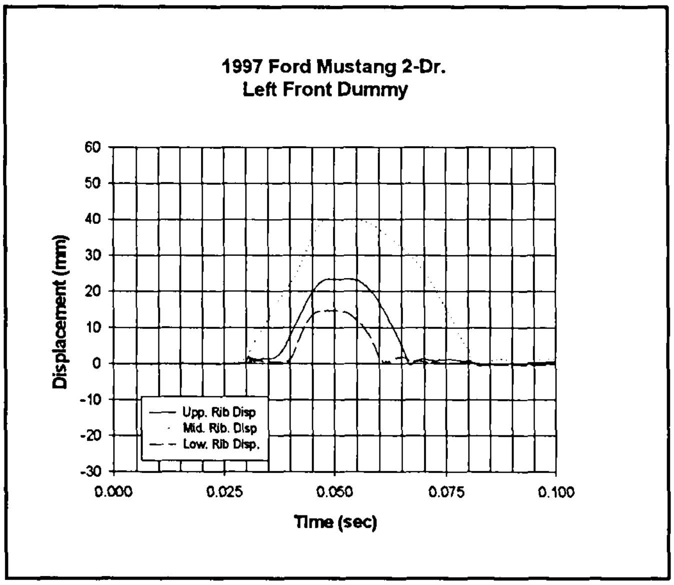

Figure 15.

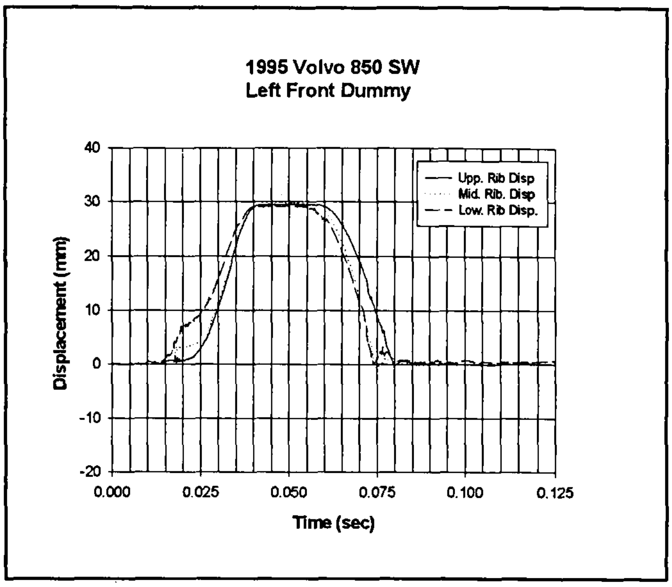

Figure 16.

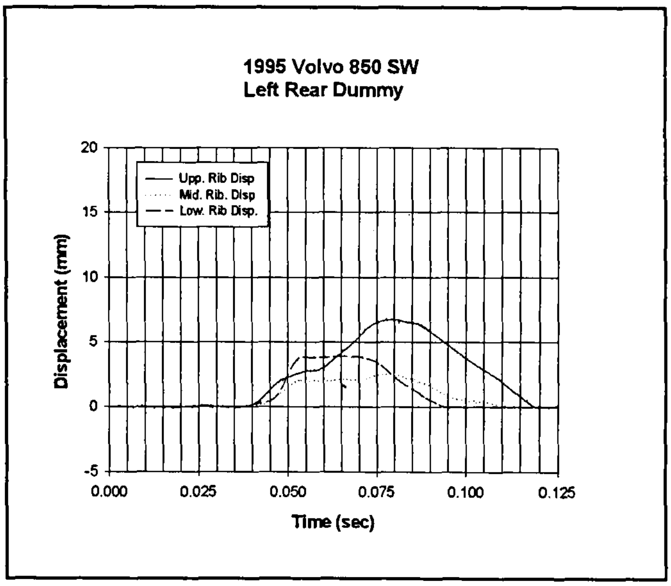

Figure 17.

Review of the high speed film from the series of eight test presented in this paper indicated that dummy rotation was visible in most of the tests. Contact with the intruding door was made more rearward than the lateral center of the ribs on some of the tests, while contact was forward of the center of the ribs in some of the tests suggesting off-axis loading conditions. This flat-top rib behavior of the Eurosid-1 was reproduced and further investigated with bumper pendulum impact tests outside the full vehicle test environment as outlined below.

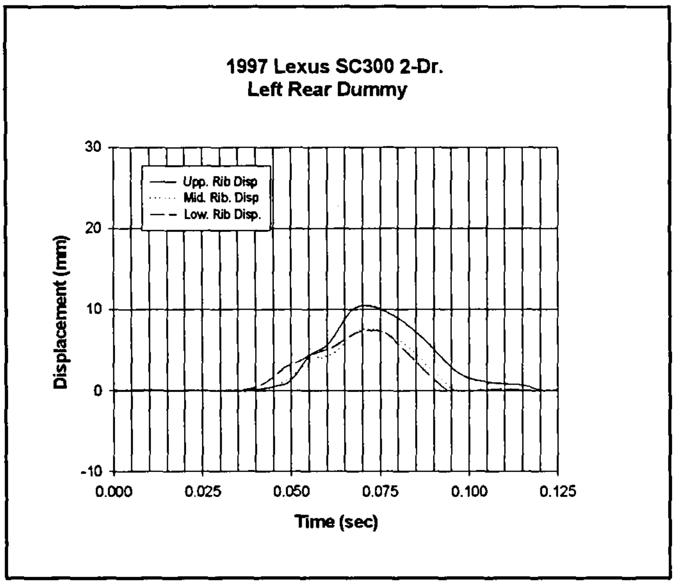

Figure 18.

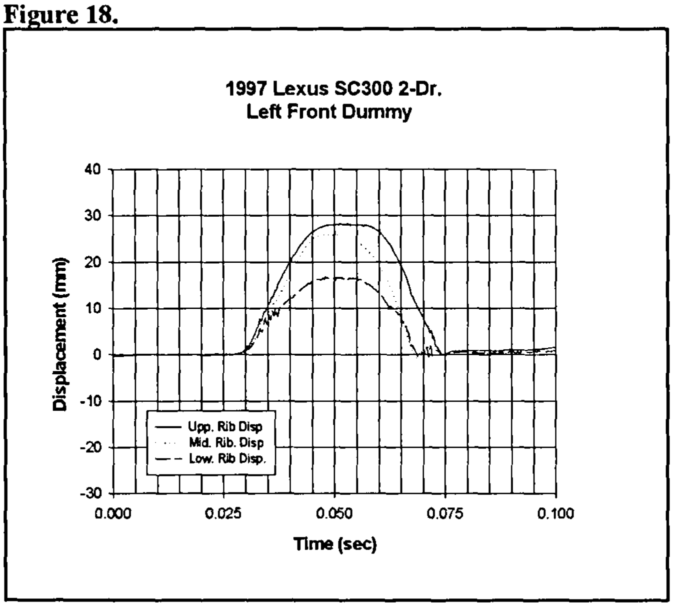

Figure 19.

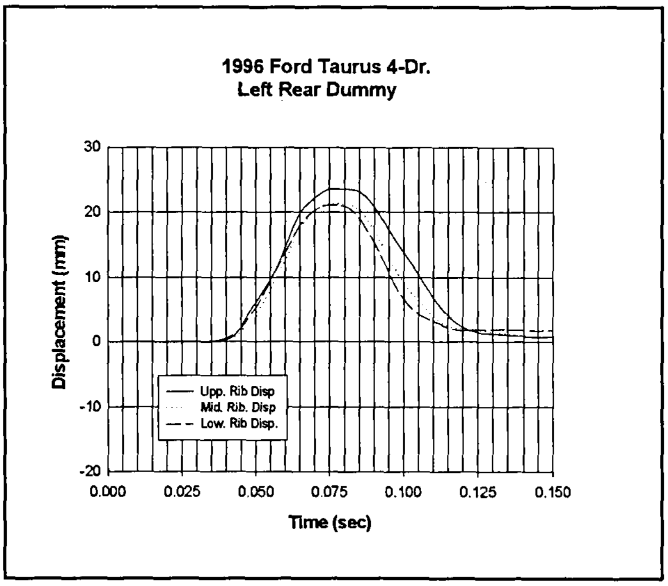

Figure 20.

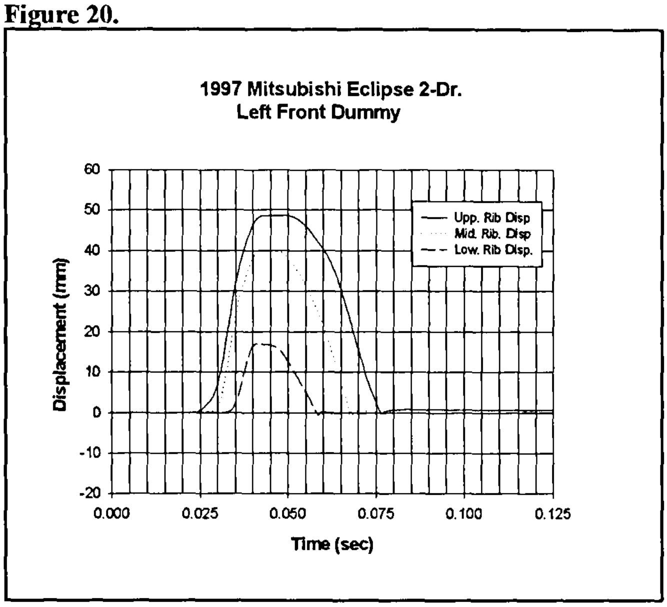

Figure 21.

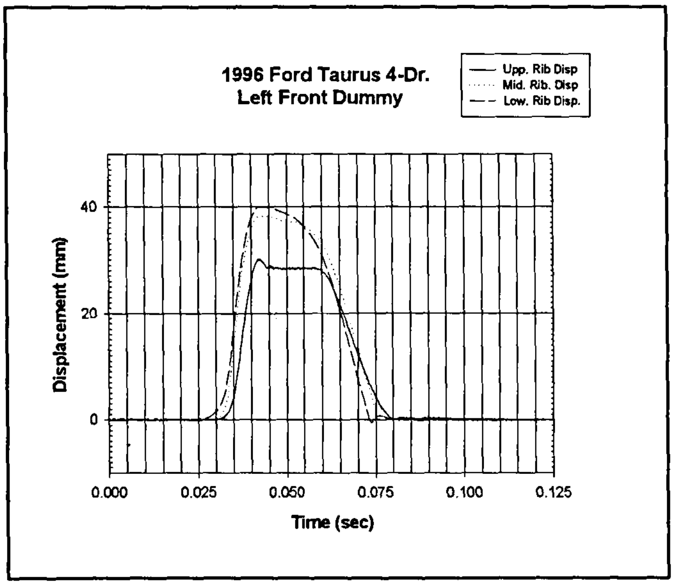

Figure 22.

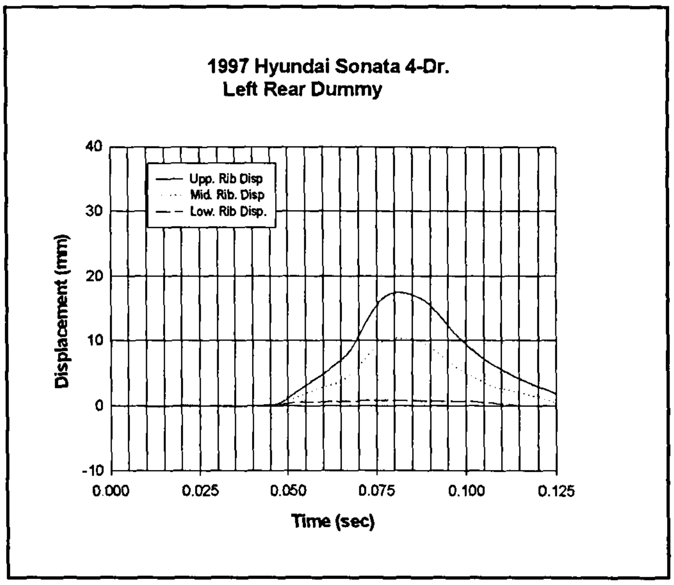

Figure 24.

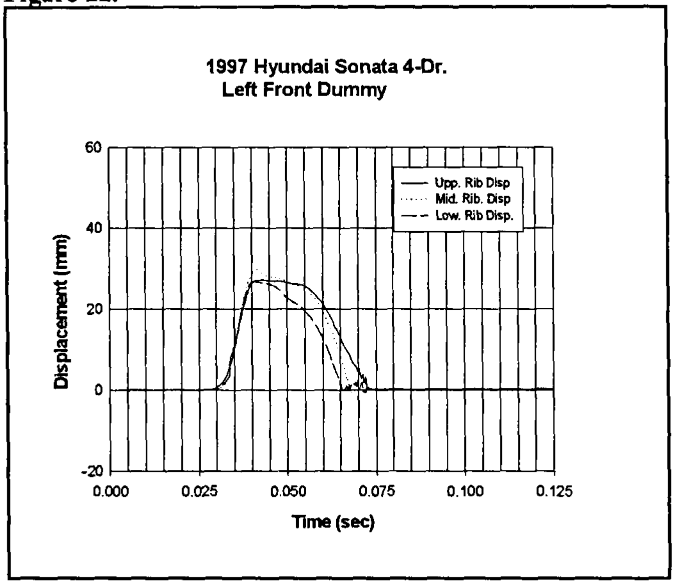

Figure 23.

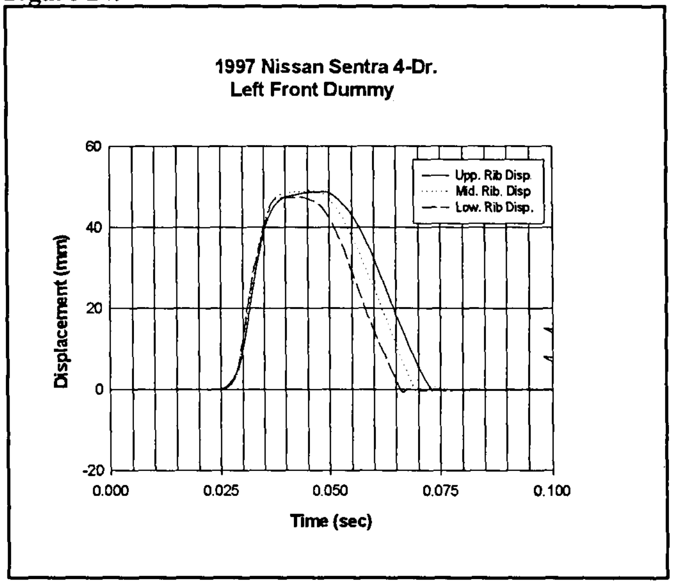

Figure 25.

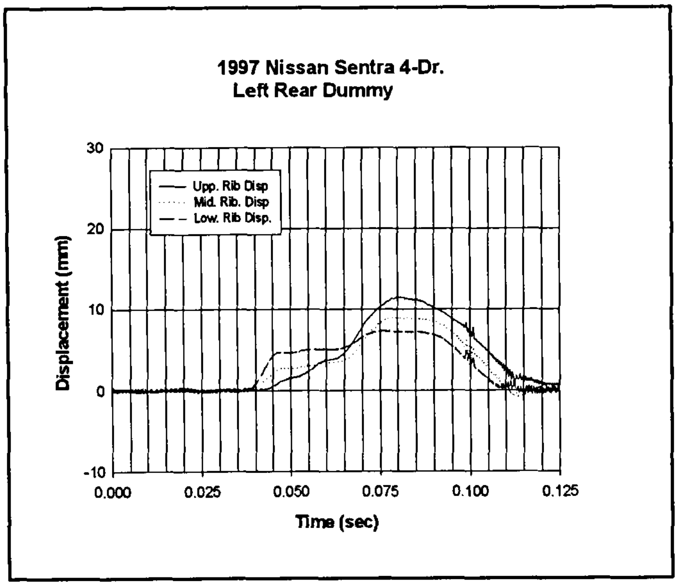

Figure 26.

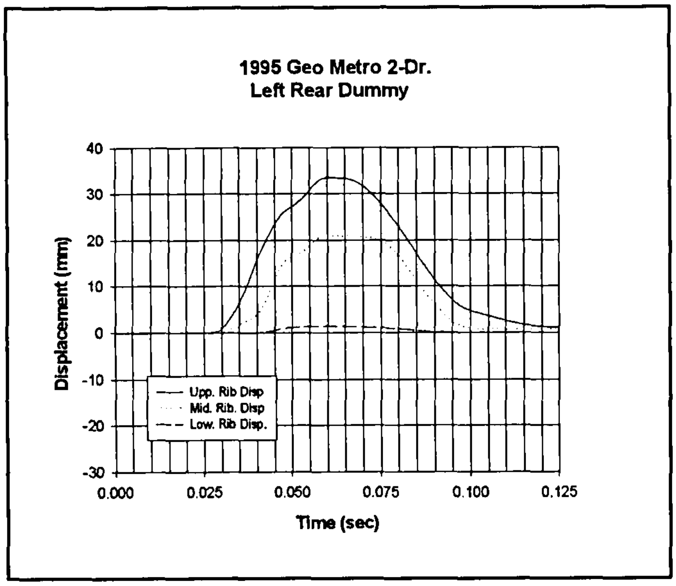

Figure 27.

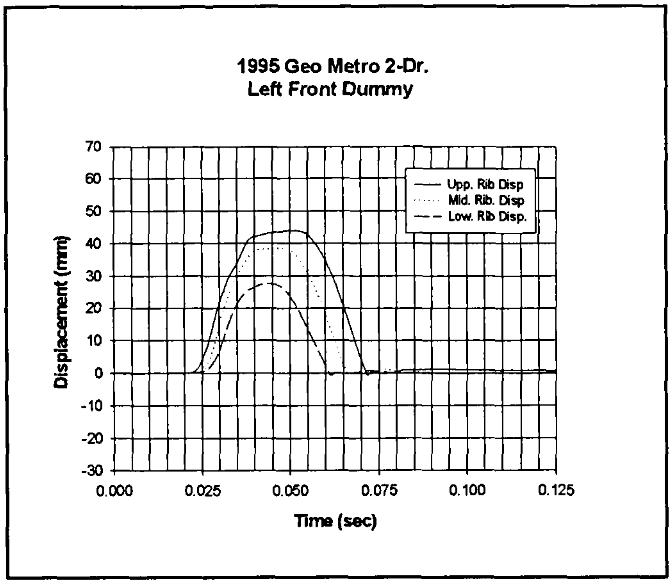

Figure 28.

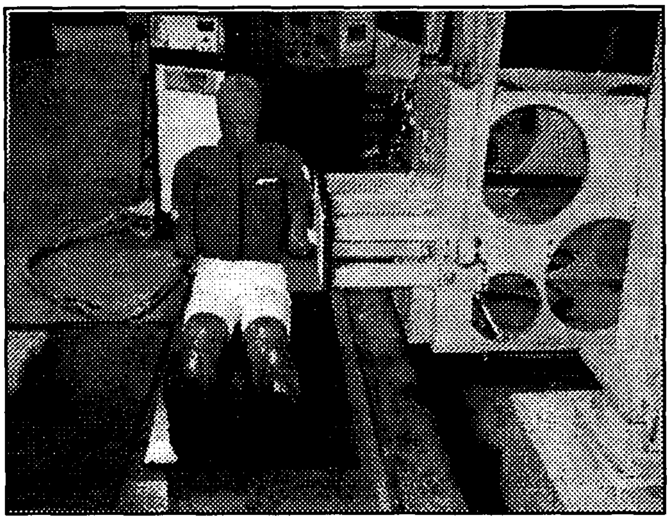

Figure 29. Eurosid-1 Bumper Pendulum Tests Setup.

Eurosid-1 Bumper Pendulum Tests - To further investigate the flat-top behavior in the rib displacement responses, a series of bumper pendulum impact tests with the Eurosid-1 were performed. The general test setup is shown in Figure 29. The part 581 bumper pendulum which has a mass around 907.4 kg was used in all the tests. The bumper pendulum was rotated to a sufficient height and also given an initial velocity via springs to get a closing speed similar to the door contact speeds encountered in the series of EU full scale side impact tests. The test conditions are described in the following:

1. The impact speeds were around 18.2 km/hr.
2. The pendulum impact face was a steel plate with a 3/4" plywood cover, 610 mm wide measured from the seating surface at a height of 239 mm corresponding to the top of the molded pelvis of the Eurosid-1.
3. Based on the review of the full scale crash test films, two impact face heights were used: 239-503 mm (Low Face) & 239-558 mm (High Face) with the seating surface at z = 0. The low face extended from the pelvic/abdomen junction to approximately 1/3 down the arm (arm at 40 degrees) from the shoulder pivot bolt. The high face extended from the pelvic abdomen junction to the center of the shoulder attachment bolt.
4. The dummy was placed on the horizontal flat steel seating surface with legs extended.

5. Tests included +/-15 degrees, and 0 degrees left dummy side impacts (e.g. + 15 degrees is an anterior oblique impact and requires rotating the dummy by +15 degrees about the z-axis using a right-hand coordinate system with x positive in the posterior-anterior direction, and y positive lateral to the left.)

The 18.2 km/hr impact was on the low end of the range of 25-40 km/hr door contact speeds encountered in the EU full scale tests but, as can seen from the following figures, reasonable rib displacements ranges of 10 to 40 mm were achieved as compared to the values obtained in the full scale tests.

As shown in Figures 30. through 34., for both impactor face heights significant flat-top rib deflections responses were present in the +15 degree impact condition, while 0 degree impacts produced a lesser flat-top. The flat-top behavior did not occur for the tests at -15 degrees, neither with the Low Face nor with the High Face.

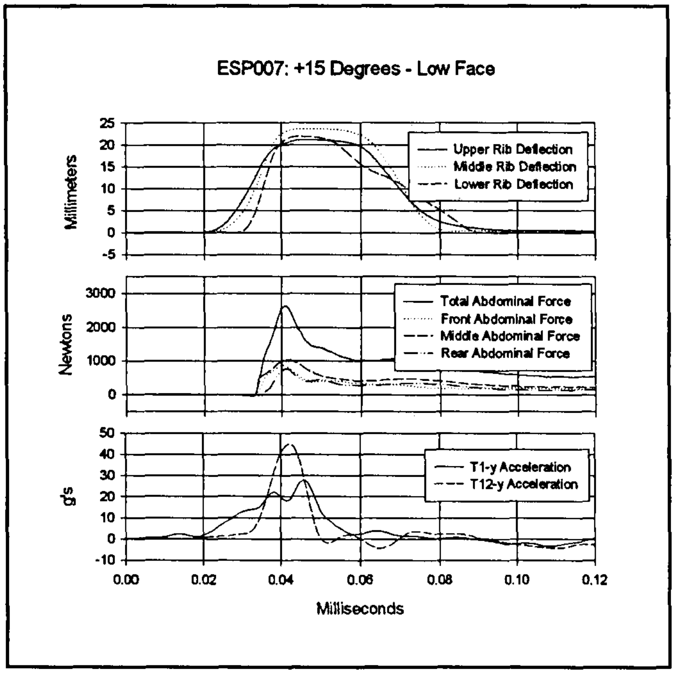

Figure 30.

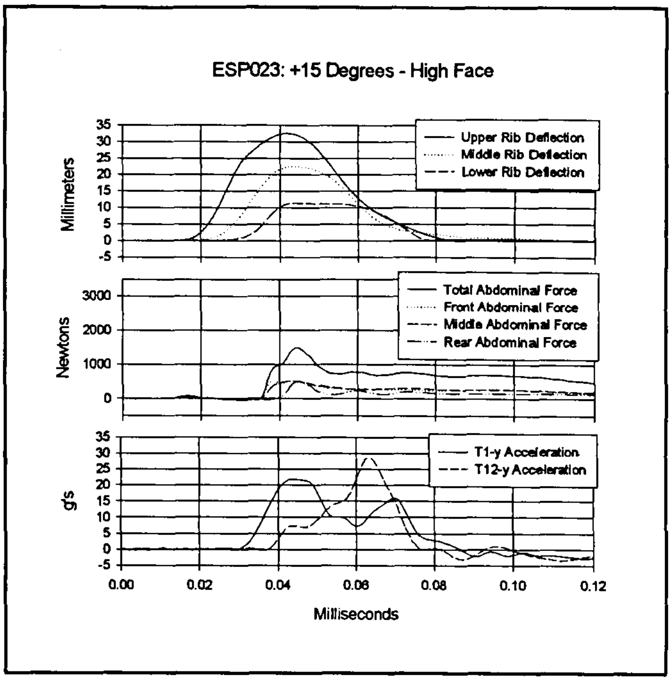

Figure 31.

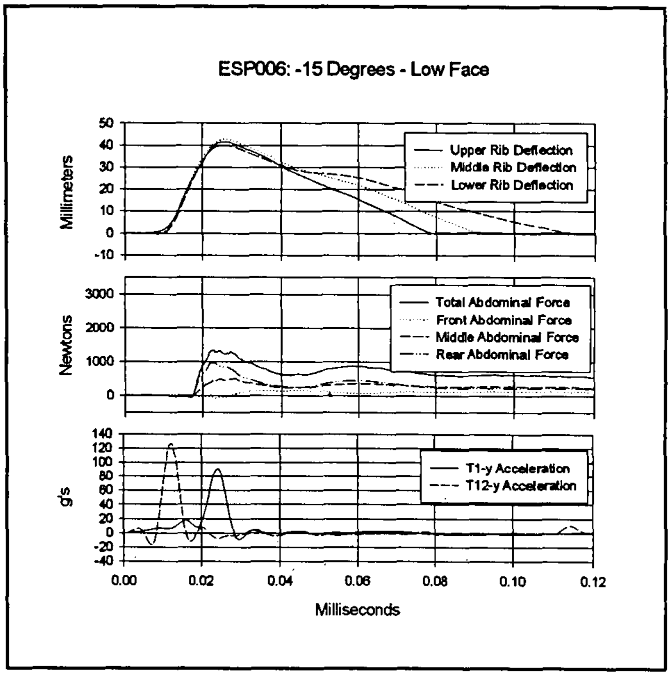

Figure 32.

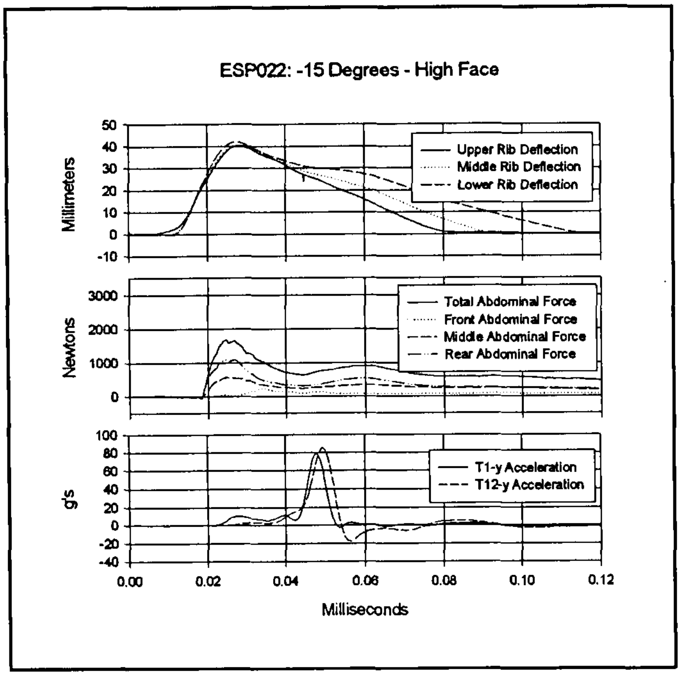

Figure 33.

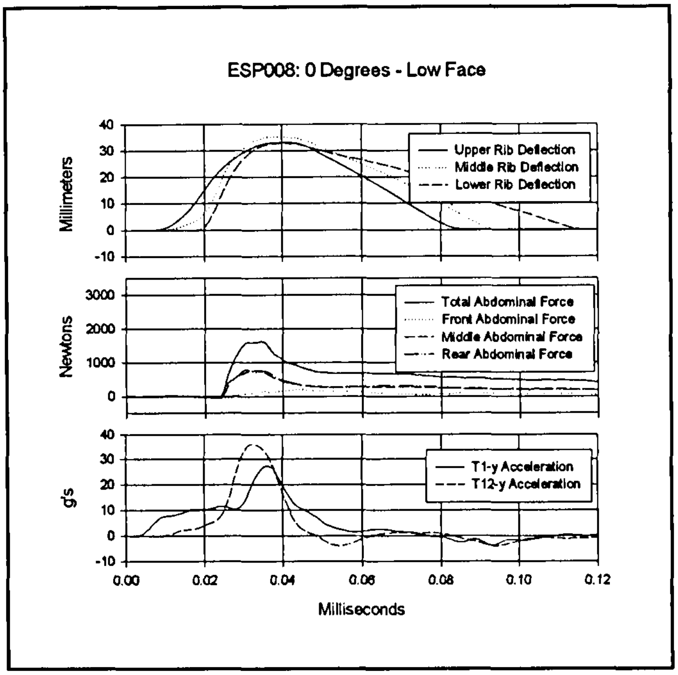

Figure 34.

Based upon this work and that of other researchers, the authors have developed the following hypotheses for the cause of rib flat-tops in the Eurosid-1:

1) Binding of the rib damper module: Henson et al. suggested that moment is transferred across the rib damper in the Eurosid-1 thorax during oblique impact [12]. Such a moment could cause excessive friction between the piston and cylinder wall of the damper, and cause it to bind.

2) Load Bridging: In this test condition, each of the elements of the torso (the shoulder complex, each of the thoracic ribs, abdomen, and possibly the back plate) share the total force transferred to the spine box to accelerate Eurosid-1 through the change of speed of the test. Load bridging can occur when an element's adjacent neighbors experience an increase in stiffness (due to a constitutive relationship in a material or structure, and/or a mechanical binding) and thus the element's deflection is governed by its neighbors. For example, should the upper and lower rib of the Eurosid-1 thorax bind due to some mechanical defect and thus increase their stiffness, the deflection of the middle rib should not exceed that of the upper and lower ribs. Load bridging may be present between a binding shoulder and the abdomen, or the shoulder and pelvis, or direct contact with the back plate, thereby limiting the deflection of the rib modules.

A series of tests was conducted at +15 and 0 degrees to determine the load sharing between the thorax and the abdomen. In these tests the load wall contacted the abdomen and thorax only, while the arm was rotated 180 degrees to point straight up, such that it was not contacted by the impactor. Figures 35. and 36. show the results from these tests, and flat-tops are observed in these conditions. These results show that after the flat-top rib responses, abdominal loads drop off significantly, and then rise again as the thorax begins its expansion. Newton's first law applied to deformable bodies loaded in parallel requires that a) the total load applied equal the sum of the loads carried by each of the bodies, and b) the load one body carries is directly proportional to its stiffness and mass (stress follows elastic modulus and density). Based on this law, we can then conclude from the data that the drop in force on the abdomen indicates an increase in force on the thorax. Thus we would conclude from this test that the flat-top is a result of binding within rib modules or quite possibly of the damper modules themselves. However, this may not be the only mechanism of rib binding in other test environments.

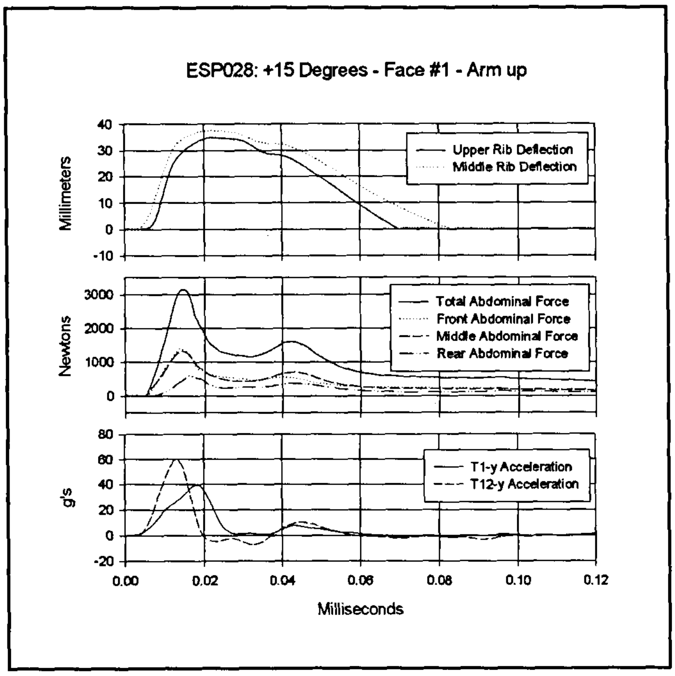

Figure 35.

Another series of tests with the Eurosid-1 was performed with the Eurosid-1 jacket removed at + 15 degrees, the results of which are shown in Figure 37. While these tests were originally designed to permit viewing of the thorax and shoulder during impact, the results indicate that there is a significant change in the dummy behavior between the jacket on and jacket off tests. In Figure 37., the results from three repeat tests at + 15 degrees, with the Eurosid-1 jacket removed in two of the tests, are presented . The results show that the flat-top behavior occurred in all of the three tests. These results indicate that the flat-top behavior is not only reproducible but is also repeatable under the given test conditions.

Other researchers have suggested that the impactor/door surface may come in contact with the back plate of the dummy, thereby off-loading the rib structure and causing a flat-top. Inspection of films from these series of bumper pendulum tests indicate that no impactor-to-back plate contact occurred. Moreover, contact with the back plate is only likely with a combination of oblique posterior loading and excessive rib deflection.

Eurosid-1 Bumper Pendulum Tests with Upgrade Kit -
TNO has recently developed a research kit tool upgrade to address some of the widely accepted mechanical dummy issues with the Eurosid-1 (Refer to section **Eurosid-1 Mechanical Deficiencies**) . The research upgrade kit for the Eurosid-1 addresses a number of minor issues. These include smoothing sharp edges on the projecting torso backplate, use of bumper washers to minimize impacts between the femur shaft and pubic load cell mounting hardware, beveling sharp edges on the clavicle link to prevent binding with the aluminum guide plates of the shoulder assembly, and use of plastic spacers in the lumbar spine and neck similar to those used in the SID. The modifications in this upgrade kit are minor in nature and would not seem tot address the major issues such as alleged binding of the damper in the rib cage, the influence of the kinematics of the shoulder structure on the rib cage deflection, and the deformability of the pelvis bone.

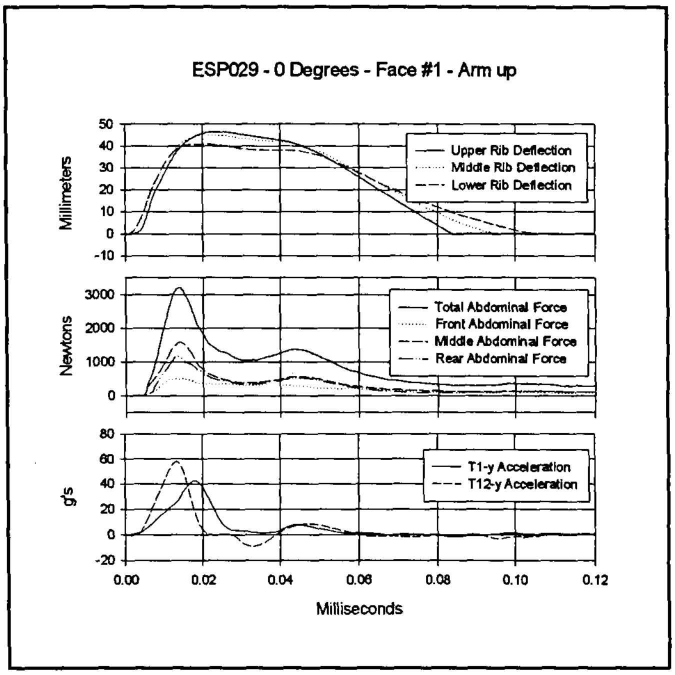

Figure 36.

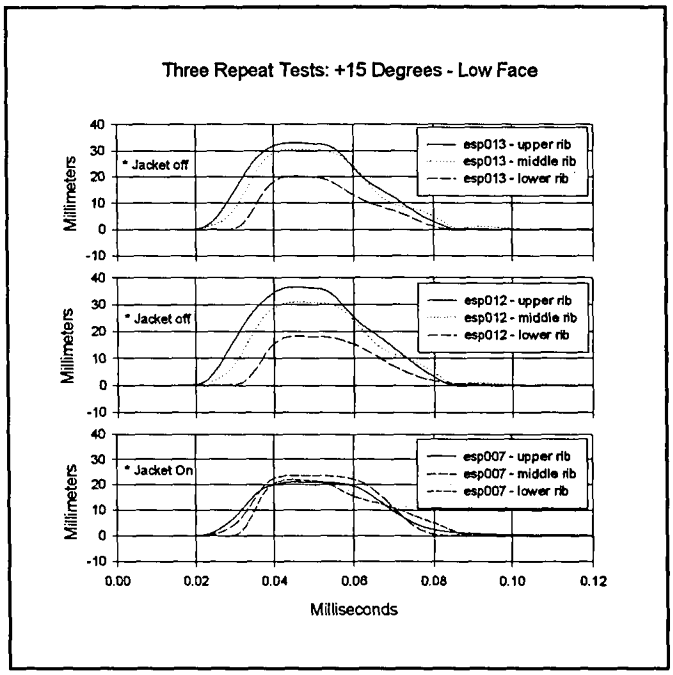

Figure 37.

In April 1998, the Eurosid-1 research upgrade kit was made available to NHTSA for evaluation. To date, a preliminary evaluation was performed through a series of bumper pendulum tests under test conditions similar to those described in the previous section. Tests were performed with the Low Face and were run at + 15 and 0 degrees. The purpose of performing repeat tests with the upgrade kit installed in the Eurosid-1 was to investigate if modifications in the kit address the flat-top anomalies in the rib potentiometer responses.

Figures 38. through 40. show the results from two repeat tests at + 15 degrees and one test at 0 degrees. As can be seen from the figures, the flat-tops are still observed in these conditions.

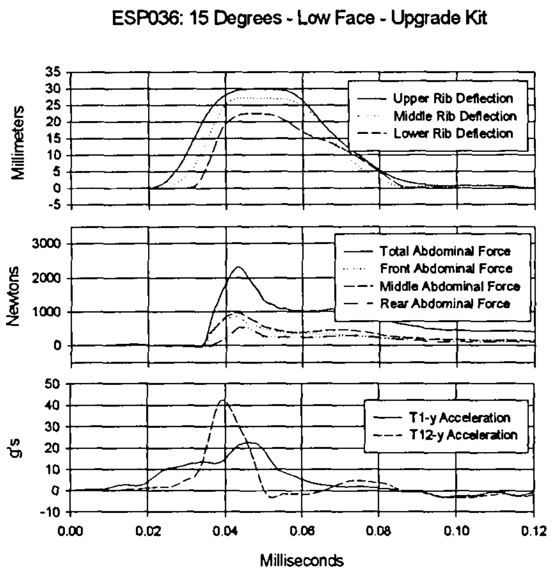

Figure 38.

Conclusions Regarding Eurosid-1 Rib Responses "Flat-Top" Anomalies -

Irrespective of the mechanism causing the anomalous behavior, the flat-top behavior in the rib potentiometer responses indicate that what should be the true peak rib deflections may not be occurring and thus the resulting rib deflections are in doubt. The V*C computation which is based on the rib deflection would also be suspect. In light of this, the RDC and V*C values for the EU 96/27/EC vehicle tests presented in this paper are questionable.

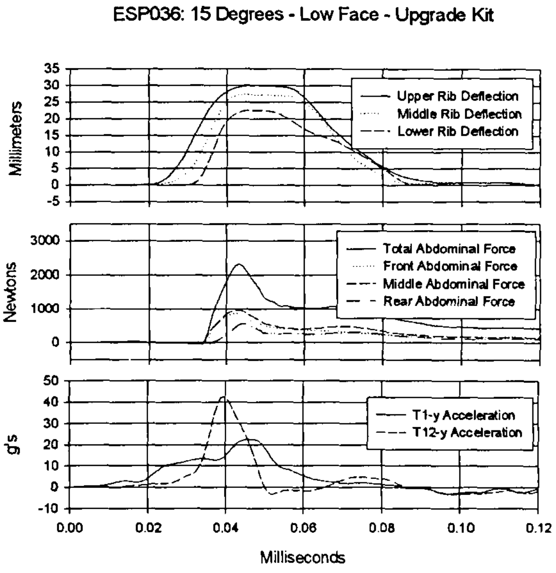

Figure 4.

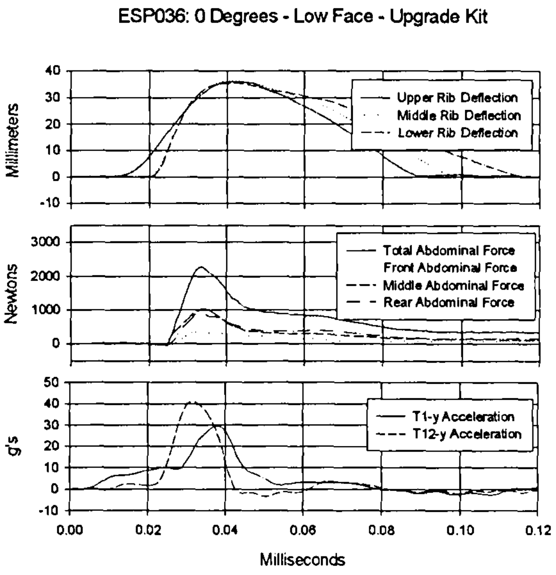

Figure 5.

COMPARISON OF VEHICLE RESPONSES

MDB Engagement - The EUMDB is 176 mm or 10.5 % narrower than the 214MDB and in the EU procedure it is centered on the driver seating reference point while the 214MDB is positioned more forward and is positioned relative to the center of the wheelbase. This resulted in no MDB to A-pillar engagement in the EU tests while the A-pillar was engaged in all of the FMVSS 214 tests. Also, the EUMDB right edge engaged the vehicle rearward of the 214MDB right edge for all of the vehicles tested. (See Table 7.). The vehicle contact areas for the EUMDB and 214MDB, drawn to scale, are shown for the Lexus SC300 and Volvo 850 in Figures 41. and Figures 42. as examples.

Table 7.
FMVSS 214 vs EU 96/27/EC MDB's to Vehicle Contact

Vehicle	Left edge difference* (mm)	Right edge difference* (mm)
Ford Taurus	N/A	N/A
Volvo 850 SW	253	77
Nissan Sentra	274	98
Hyundai Sonata	236	60
Ford Mustang	311	135
Lexus SC300	433	257
Geo Metro	337	161
Mitsubishi Eclipse	358	182

* 214MDB-EUMDB; positive is forward

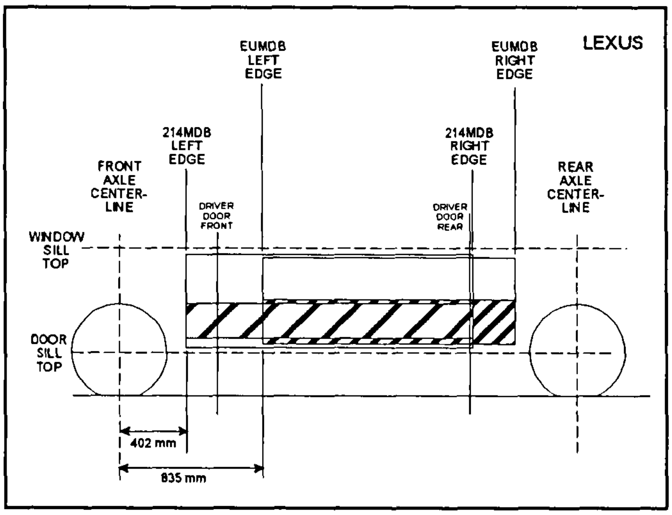
EUMDB LEFT EDGE
EUMDB RIGHT EDGE
LEXUS
214MDB LEFT EDGE
214MDB RIGHT EDGE
FRONT AXLE CENTER-LINE
REAR AXLE CENTER-LINE
DRIVER DOOR FRONT
DRIVER DOOR REAR
WINDOW SILL TOP
DOOR SILL TOP
402 mm
835 mm

Figure 41. Lexus SC300: EUMDB and 214MDB Contact Areas.

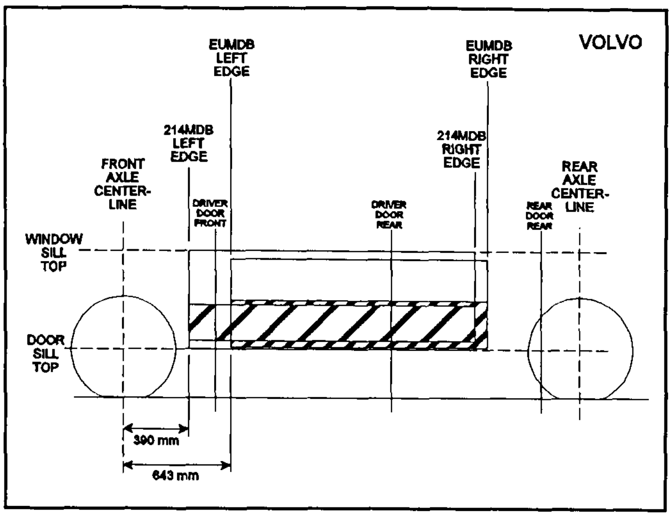
EUMDB LEFT EDGE
EUMDB RIGHT EDGE
VOLVO
214MDB LEFT EDGE
214MDB RIGHT EDGE
FRONT AXLE CENTER-LINE
REAR AXLE CENTER-LINE
DRIVER DOOR FRONT
DRIVER DOOR REAR
REAR DOOR REAR
WINDOW SILL TOP
DOOR SILL TOP
390 mm
643 mm

Figure 42. Volvo 850: EUMDB and 214MDB Contact Area.

Table 8.
Side Intrusion at Door Sill, Driver H-pt, & Mid Door

Vehicle	Door Sill Level max and average crush (mm)		Driver H-pt level max and average crush (mm)		Mid Door level max and average crush (mm)	
	FMVSS 214	EU 96/27/EC	FMVSS 214	EU 96/27/EC	FMVSS 214	EU 96/27/EC
Ford Taurus*	N/A	N/A	N/A	N/A	N/A	N/A
Volvo 850 SW	110 **70**	**150** 69	**284** **220**	264 178	**280** **227**	270 189
Nissan Sentra	166 **125**	**217** 120	310 270	**372** **287**	280 172	**377** **217**
Hyundai Sonata	147 91	**281** **164**	388 **326**	**443** 291	394 **332**	**435** 305
Ford Mustang	132 99	**266** **153**	254 **220**	**333** 211	234 171	**335** **197**
Lexus SC300	**157** **109**	130 100	320 **272**	**330** 216	**351** **239**	304 193
Geo Metro	**160** **112**	112 70	239 **227**	**249** 179	226 **161**	**262** 141
Mitsubishi Eclipse	178 **157**	**196** 107	304 **287**	**333** 265	296 **258**	**333** 248

* Crush profile data was not available for the Taurus EU test

Side Crush Profile Comparison - In order to facilitate comparison with the intrusion profile in the FMVSS 214 tests, pre and post test side crush measurements were collected for the EU tests as specified in the FMVSS 214 test procedure [15]. The maximum side crush at the door sill and mid door levels for the EU and FMVSS 214 tests are presented in Table 8. It is worth noting that relative magnitude for the maximum intrusion at these levels did not correlate with the thoracic and pelvic criteria values for the different vehicles neither for the FMVSS 214 nor for the EU tests. With the exception of the Volvo 850, the maximum static intrusion at the driver H-pt level for the EU tests was on the average 41 mm larger than for the FMVSS 214 tests. At the mid door level, with the exception of the Volvo 850 and Lexus SC300, the maximum static intrusion at the driver H-pt level for the EU tests was on the average 62 mm larger than for the FMVSS 214 tests.

The static crush profiles at the door sill and mid door levels are presented in Figures 43. through 56. In general, in the EU tests, the crush profile is more rounded with larger intrusion around the B-pillar and the rear section of the front door. In the FMVSS 214 tests, the crush profile is more rectangular in shape with the intrusion more evenly distributed along the area of MDB-to-vehicle engagement. This is attributed to the characteristics of the EUMDB and 214MDB and their positioning as described earlier.

At the sill level, with exception of the area around the B-pillar, intrusion was larger for the FMVSS 214 tests of the Metro, SC300, Sentra, and Eclispe. In contrast, the intrusion was significantly larger at the sill level for the EU tests of the Sonata and Mustang.

At the mid door level, also with the exception of the area around the B-pillar, intrusion was larger for the FMVSS 214 tests of the Metro, Sonata, and Eclispe. In contrast, the intrusion was significantly larger at the mid door level for the EU tests of the Sentra and Mustang, specifically around the B-pillar and rear section of front door areas. In fact, the B-pillar was split in half in the EU test of the Mustang.

The Lexus SC300 was the only vehicle which had more intrusion at both the sill and mid door levels for the FMVSS 214 test. For the Volvo 850, which is designed to meet both regulations, intrusion at both levels was comparable for the two regulations. It is worth noting that both the 850 and the SC300 were the best performers in the 4-Dr and 2-Dr vehicles sets relative to the requirements of both regulations.

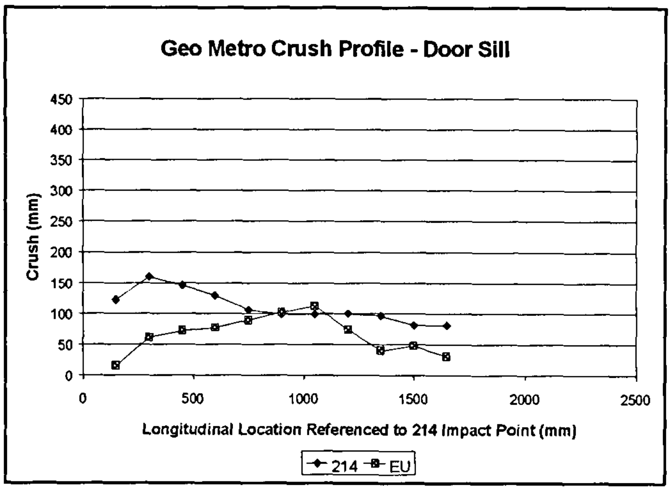

Figure 43.

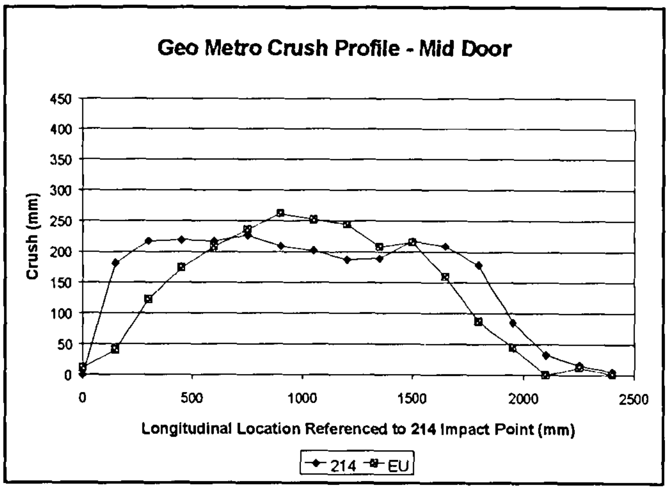

Figure 44.

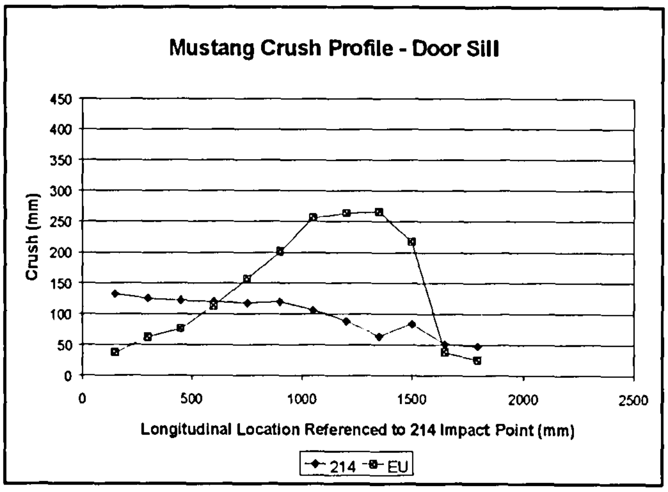

Figure 45.

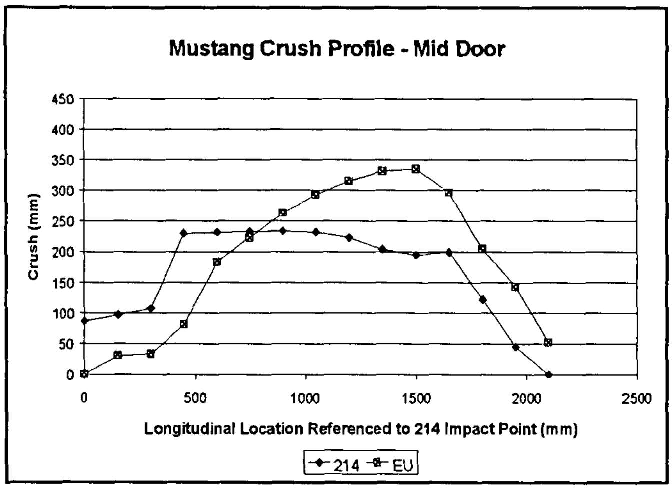

Figure 46.

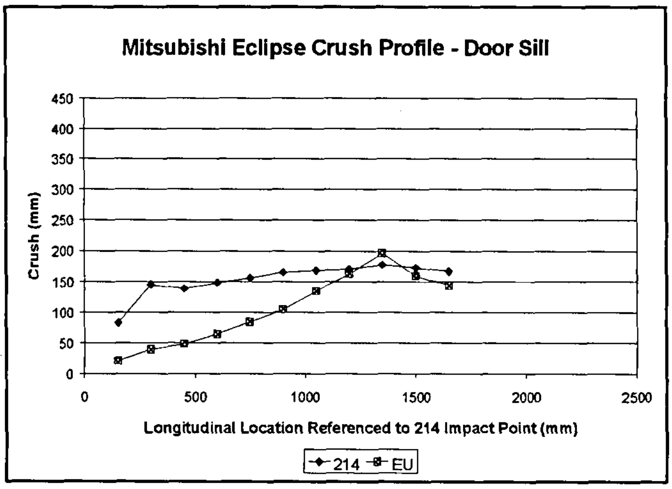

Figure 47.

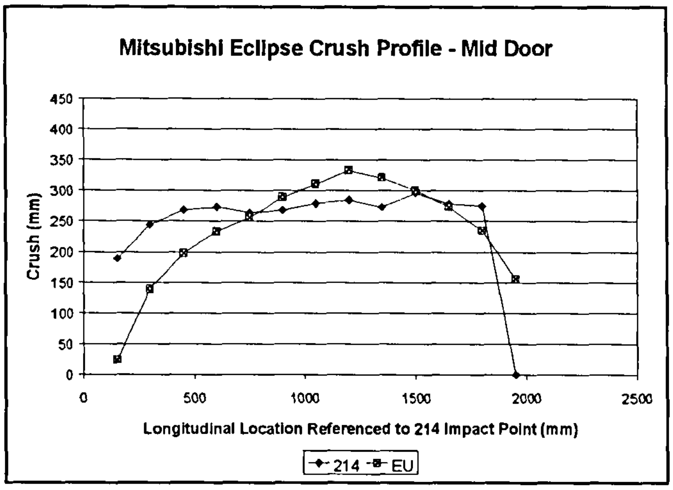

Figure 48.

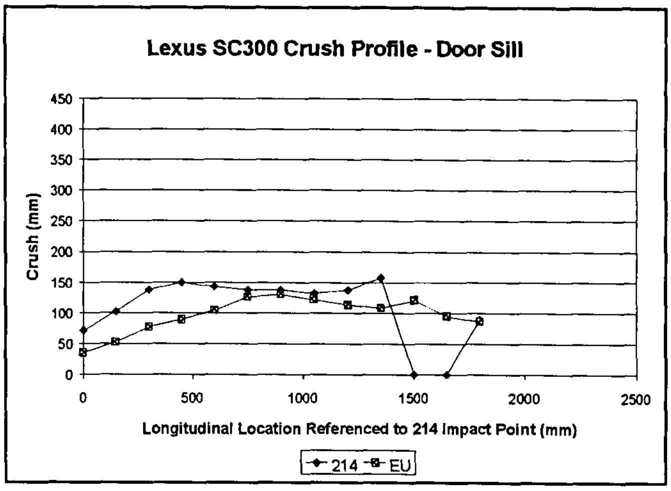

Figure 49.

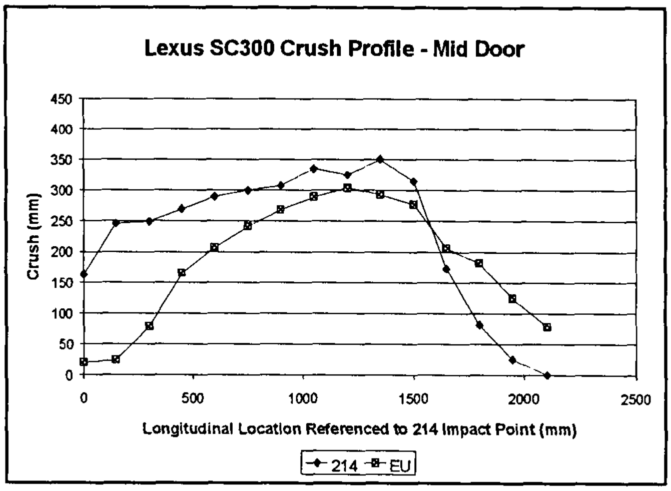

Figure 50.

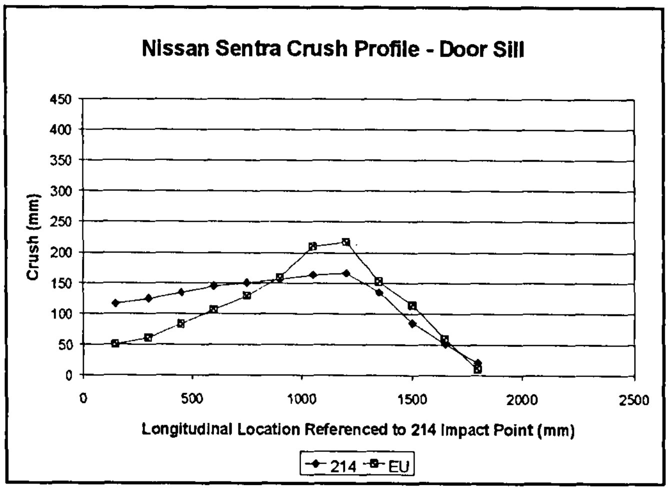

Figure 51.

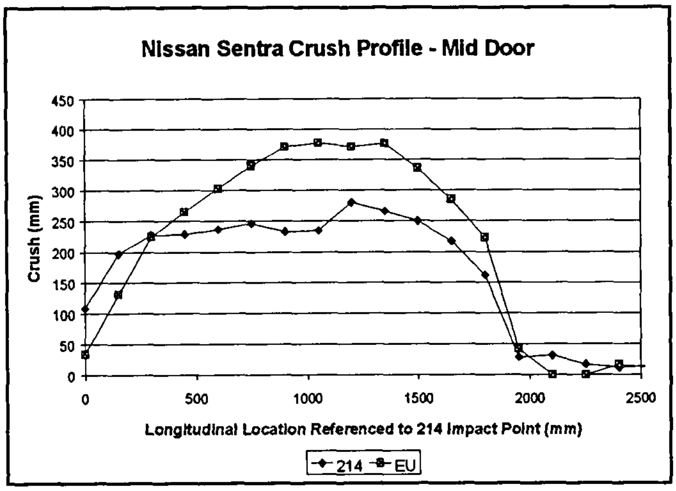

Figure 52.

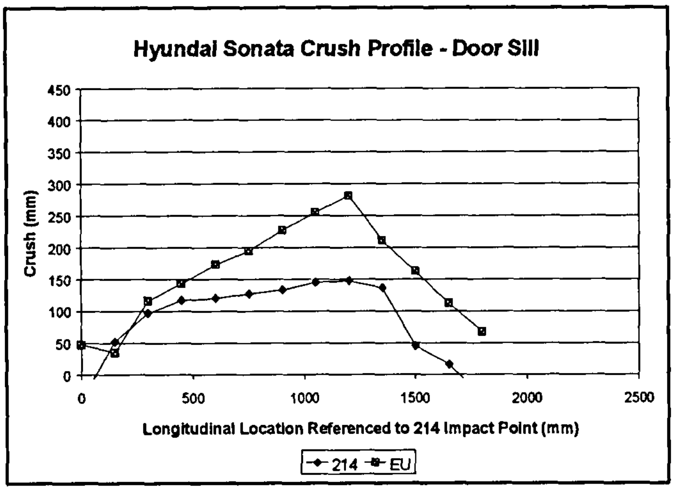

Figure 53.

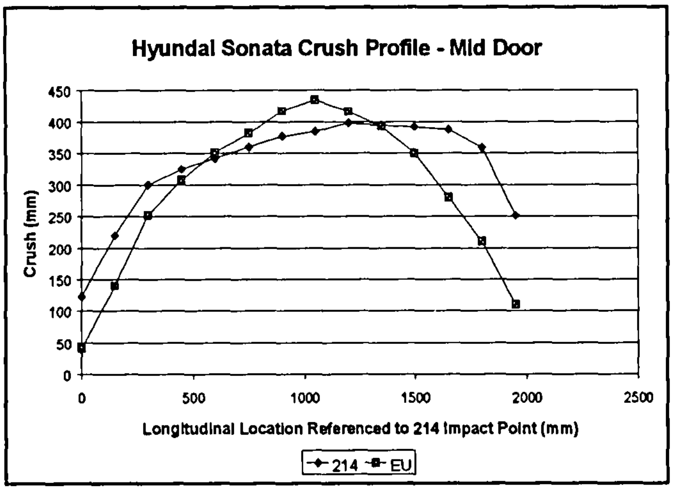

Figure 54.

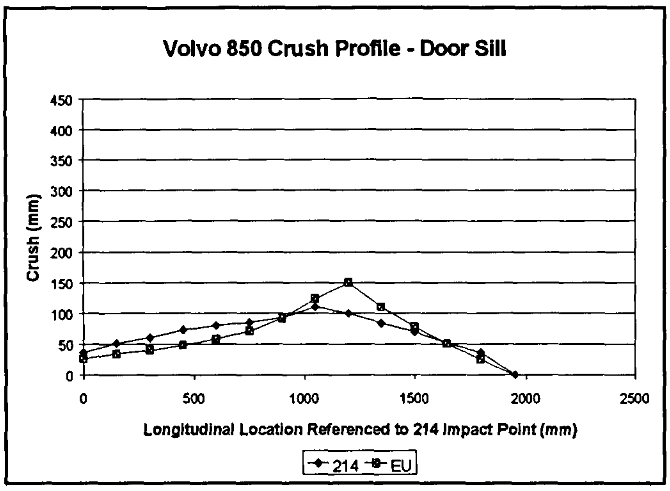

Figure 55.

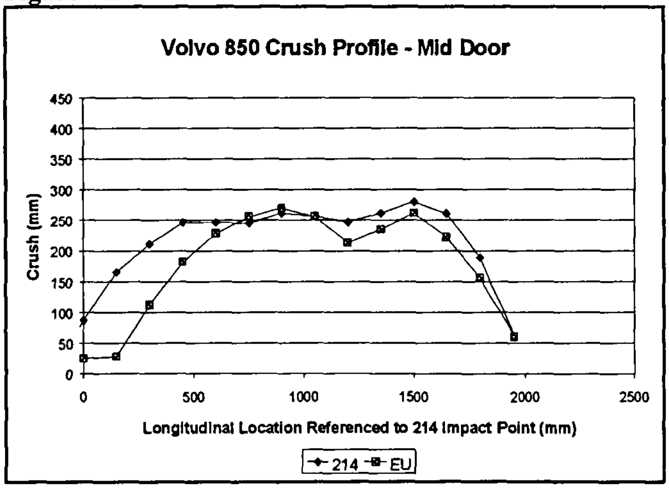

Figure 56.

COMPARISON WITH RELEVANT PREVIOUS RESEARCH

Because of the fluid nature of the European test procedure, the database of full scale vehicle crash tests which can be directly compared to testing performed with the current procedure is limited. The data are further limited if comparisons are required between the same vehicles tested to both the U.S. and EU regulations. Satake et al. reported on 24 full vehicle tests on five Japanese vehicles using the U.S. and (ECE/R.95) procedures [9]. The ECE/R.95 procedure matches that of the EU Directive, however the barrier height was 260 mm rather then 300 mm. Some tests were run at 300 mm for comparison. The barrier face used was made by UTAC of aluminum with a triangular pyramid-shaped design.

In the baseline test, both 4-Dr vehicles exceeded the rib deflection criteria when tested to the ECE. Both 4-Dr vehicles were below the TTI limit in the U.S. test although one was close to it. Comparing the 2-Dr vehicles to the 4-Dr, in the 2-Dr vehicle, the abdominal and pelvic loads increased for the

ECE test, and the rib deflection was lower. For one of these vehicles, the abdominal force exceeded the limit in the ECE test, but for the same vehicle tested to the U.S. procedure, all injury criteria were below their limits. For the other 2-Dr vehicle, the U.S. procedure was more severe, with a very high TTI and pelvic acceleration. The ECE procedure resulted in rib deflection, abdominal loads and pelvic loads at or slightly above the limits. These results were obtained with the barrier height at 260 mm. A 4-Dr vehicle and 2-Dr vehicles were tested with both a 260 and a 300 mm barrier height. All injury criteria were greater for the 300 mm barrier except abdominal force which had about the same result.

The above results may indicate that, for 4-Dr vehicles, the current EU Directive is more difficult to pass than FMVSS 214.

Bergmann et al. also performed tests using the ECE/R.95 procedure [27]. Testing was done at barrier heights of 260 and 300 mm with barrier faces of Kenmont, Fritzmeier, Hexcel and AFL elements. Average results across all tests were determined. Both V*C and RDC for the 4-Dr vehicles were much higher than for the 2-Dr vehicles. V*C was in the vicinity of the criterion limit. However, for APF and PSPF the 2-Dr vehicles had higher values than the 4-Dr.

Beusenberg et al. found a similar dependence on the number of doors a vehicle has when tested to the (EEVC) procedure [10]. Seventeen 4-Dr tests and five two-door tests were analyzed. It is not clear what barrier face construction was used for these tests nor what barrier height was employed. The average and maximum V*C and rib deflection, in general, were below the injury criteria for 2-Dr vehicles. For 4-Dr vehicles the average V*C was above the criteria and the average rib displacement was equal to the criteria. For 2-Dr vehicles the abdominal force was above the criteria. For 4-Dr vehicles the abdominal forces were below the criteria. Pubic loads were higher for 2-Dr vehicles than 4-Dr, but both were well below the criteria.

In the current set of test, it is not clear if the relative severity of each regulation is influenced by the number of vehicle doors. Table 9. gives the vehicle type (2-Dr or 4-Dr) which has the larger normalized injury criteria and the percentage by which it is greater. Also given, is the result of a student's t-test to determine if the difference in the injury criteria is statistically significant. Significance will be determined at $p \leq 0.10$. However, the determination of significance is certainly influenced by the small sample size of 4 vehicles in each category.

The following discussion is limited to the front seat dummy. Some results seem consistent with previous work whereas others do not. This is mainly attributed to barrier height differences and the lack of consistent performance amongst the various European barrier faces. For the EU procedure, the average normalized V*C was 23% greater for 4-Dr vehicles than for 2-Dr vehicles. This is consistent with the results reported in [10] and [27]. However, using a students t-test it is shown that this difference is not significant (p=0.59). The averaged normalized RDC was 7.9% greater for 2-Dr vehicles. This is in contrast to [10] and [27]. This difference is also not significant (p=0.66). For the U.S. procedure, the average normalized TTI was 12% greater for 2-Dr vehicles. This was consistent with results report in [9]. However the difference is not significant (p=0.40). So for the chest injury criteria no consistent or significant difference is evident for either regulation relative to the number of vehicle doors.

For the EU procedure the normalized PSPF was greater for the 2-Dr vehicles by 31% (p=0.31) which is consistent with [9], [10] and [27]. While for the U.S. procedure the normalized PelvicG is nearly the same for both 2-Dr and 4-Dr vehicles, which is not consistent with [9]. Finally, the normalized average APF is 57% greater for 2-Dr vehicles than for 4-Dr vehicles. This difference is considered significant at p=0.053. An increase in APF for 2-Dr vehicles was also reported in [9], [10] and [27].

Table 9.
Vehicle Type With Greater Average Normalized Injury Criteria

	V*C	RDC	TTI	PelvicG	PSPF	APF
No. Doors	4	2	2	4	2	2
% greater	23	7.9	12	0.64	31	57
p	**0.59**	**0.66**	**0.40**	**0.97**	**0.31**	**0.053**

INITIAL ASSESSMENT OF FUNCTIONAL EQUIVALENCE

From NHTSA's perspective, in basic terms, a foreign vehicle safety standard is considered functionally equivalent to a counterpart U.S. standard when the two standards address the same safety need and provide similar safety benefit in the U.S. crash environment. Relative to the European and U.S. side impact regulations, FMVSS 214 has only recently been in full effect for passenger cars and will apply to LTV's by the end of this year, and EU 97/26/EC is not yet in effect. As such, there is currently insufficient real world safety data to assess the effectiveness of either regulations whether in the U.S. or European real world environments.

Data from compliance testing, such as the series presented in this paper, can be used as a surrogate. Injury risk curves would be used to assess occupant risk in the real world from the computed injury criteria obtained via crash testing. Currently, injury risk curves are not available for the abdominal, pelvic, and head EU injury criteria. In addition, due to the volume and quality of the earlier injury and impact data, the EU injury risk functions originally developed for the thoracic region need to be improved [16]. Moreover, those thoracic injury risk functions were based on the responses of the Production Prototype versions of the Eurosid dummy and would need to be updated for the production Eurosid-1.

In addition, the aspect of how well the test conditions and movable deformable barrier of the EU regulation represent the real world U.S. crash environment cannot be overlooked when assessing the relative safety benefit of the two standards. A dynamic crash test requirement in a safety regulation should simulate the crash environment to the extent possible. More importantly, the dynamic requirement should provide for realistic injury causing mechanisms. The representativeness of the EUMDB as the striking vehicle must be considered because a large portion of the U.S. side impact casualties are the result of impacts with light trucks, vans and sports utility vehicles.

Issues in several areas that need to be addressed before any conclusive determination of the functional equivalence of the two side impact regulations are outlined below.

Table 10.
FMVSS 214 vs EU 96/27/EC Criteria: Pass/Fail (P/F)

Vehicle	Dr	214 P/F	214 80%*	EU P/F	EU 80%*
Volvo 850 SW	4	P	P	P	P
Ford Taurus	4	P	P	P	**F**
Nissan Sentra	4	P	P	**F**	**F**
Hyundai Sonata	4	P	**F**	P	P
Ford Mustang	2	P	P	P	**F**
Lexus SC300	2	P	P	P	P
Geo Metro	2	P	**F**	**F**	**F**
Mitsubishi Eclipse	2	P	**F**	**F**	**F**

* 80 % = Exceed 80% of Criteria

Vehicle Issues

In terms of the overall vehicle performance, similar comparative testing of vehicles designed to European requirements would be needed to assess if such vehicles perform well relative to FMVSS 214. The testing presented in this paper is only one part of a general matrix to assess the respective comparative performance. Testing of vehicles designed to both standards and testing of additional vehicles equipped with side air bag systems, which are becoming prevalent in the U.S. fleet, would be a part of this general matrix. The repeatability and reproducibility of testing to both regulations would also need to be addressed.

Vehicle Compliance and Rankings - Based on this series of comparative testing, FMVSS 214 and EU 96/27/EC did not provide similar vehicle performance rankings nor pass/fail results based on the respective thoracic and pelvic criteria (see Tables 10., 11.,and 12.). Overall, the vehicles tested had been chosen based on compliance to FMVSS 214. However, three out of these eight vehicles failed one or two of the EU criteria for the driver.

For statistical confidence to be achieved, certain manufactures require that, as a vehicle design basis, regulation requirements must be met by a margin considerably below the actual limits specified. As such, pass/fail results based on 80% of the criteria were also investigated for this series of comparative testing. Three of the eight vehicles exceeded 80 % of at least one of the FMVSS 214 requirements while five of the vehicles exceeded 80 % of at least one of the EU requirements. The Metro and Eclipse exceeded 80% of one or more of the requirements for both regulations. The Taurus, Sentra, and Mustang exceeded 80% of the requirements of the EU regulation only while the Sonata exceeded 80% the requirements of FMVSS 214 only.

Considering the vehicle rankings for the 4-Dr vehicles based on the driver dummy criteria, FMVSS 214 TTI(d) rated the Hyundai Sonata as fourth, while the EU RDC rated the Sonata as first and the V*C rated it as second. Rankings based on the pelvic criteria for the 4-Dr vehicles were a much better match with only the third and fourth position switched.

Table 11.
FMVSS 214 vs EU 96/27/EC 4-Dr Vehicle Rankings: Driver

Vehicle	TTI rank	RDC rank	V*C rank	PelvG rank	PSPF rank
Volvo 850	1	2	1	1	1
Ford Taurus	2	3	3	2	2
Nissan Sentra	3	4	4	3	4
Hyundai Sonata	4	1	2	4	3

Table 12.
FMVSS 214 vs EU 96/27/EC 2-Dr Vehicle Rankings: Driver

Vehicle	TTI rank	RDC rank	V*C rank	PelvG rank	PSPF rank
Ford Mustang	1	2	3	1	4
Lexus SC300	2	1	1	2	1
Geo Metro	3	3	2	3	3
Mitsubishi Eclipse	4	4	4	4	2

As to vehicle rankings for the 2-Dr vehicles based on the driver dummy criteria, there was a good match for the thoracic criteria with only the first and second position switched. Rankings based on the pelvic criteria were a poor match. PelvicG rated the Ford Mustang as first while PSPF rated the Mustang as fourth. PelvicG rated the Mitsubishi Eclipse as fourth, while PSPF rated the Eclipse as second.

It is worth noting that the Volvo 850 which ranked first amongst the 4-Dr vehicles for the all the injury criteria of both regulations, with the exception of ranking a close second for RDC, was the only vehicle in the matrix tested which was designed to meet both regulation. In addition, it has a side mounted air bag system. As to the Lexus SC300, which ranked first or second amongst the 2-Dr vehicles for both regulations, it was actually designed to meet FMVSS 214. Its good performance relative to the EU requirements may be attributed to its inherent design, with a sporty wider track and considerable crush space between the occupant and inner door, and between the inner and outer door.

Since the relative rankings of the vehicles tested did not look promising, linear regression analysis was applied to evaluate the degree of correlation between the thoracic and pelvic criteria of the two regulations. ρ^2, the regression output that indicates how well one variable can be predicted through a linear transformation of another variable, is presented in Table 13 .

Table 13.
Regression Analysis (ρ^2) of FMVSS 214/EU 92/27/EC Criteria for the 4-Dr/2-Dr Vehicles

	Driver Criteria		Rear Occupant Criteria*	
	TTI(d)	PelvG	TTI(d)	PelvG
RDC	.04/.46	-	.61	-
V*C	.13/.3	-	.61	-
PSPF	-	.77/.11	-	0.17

* Regression was not performed for 2-Dr rear occupant since there was only two data points

Overall, the results indicate mediocre or no correlation between the thoracic and pelvic criteria of the two regulations for the eight vehicles tested. In particular, the correlation for the driver dummy thoracic criteria for both the 4-Dr and 2-Dr vehicles is poor. The correlation for the rear occupant thoracic criteria for the 4-Dr vehicle is mediocre. Finally, the correlation for the driver dummy pelvic criteria is relatively good, $\rho^2=0.77$, for the 4-Dr vehicles but very poor for the 2-Dr vehicles.

Real World Vehicle Issues - In Figure 6., the FMVSS 214 and EU 96/27/EC thoracic injury criteria values are sorted by vehicle weight from left to right for the 2-Dr and 4-Dr vehicles. The vehicle weights are presented in Table 14. below. In the FMVSS 214 tests, TTI(d) exhibited a trend of better performance, i.e. lower values for the heavier vehicles, for both the 2-Dr and 4-Dr vehicles. This is consistent with the real world performance in the U.S. crash environment as indicated by a recent study by Farmer et al. of vehicle-to-vehicle side impact crash study based on 1988-1992 National Accident Sampling System Crashworthiness Data System (NASS/CDS) [17]. The study, which excluded crashes involving rollovers or ejections, indicated that occupants of heavier vehicles were less likely to be seriously injured (AIS $\geq$ 3) in a side impact than occupants of lightweight vehicles. For every extra 45.4 kg in the weight of the subject vehicle, there was a corresponding 7-13% decrease in the odds of serious injury. In contrast, in the EU 96/27/RC tests, the lighter 4-Dr Sonata performed better than the heavier Taurus, while the heavier 2-Dr vehicles performed better overall for the EU thoracic criteria.

Also, in earlier comparative full scale testing by Dalmotas et al., using 1988 U. S. production vehicles, the small Chevrolet Sprint performed much better than the large Chevrolet Caprice and Pontiac Bonville when tested to the European procedure [18]. The matrix of seven vehicles used in the comparative testing by Dalmotas et al. exhibited better performance for the larger vehicles when tested to the FMVSS 214 procedure. This trend was relative to TTI(d), computed from the SID and a production prototype Eurosid which was used as the basis of comparative performance for these tests at Transport Canada. Additional full vehicle testing would be needed to further investigate this possible anomaly in the performance of large vehicles relative to the EU requirements.

Table 14.
Weights of 4-Dr Test Vehicles

Vehicle	Mass (kg)	Wheel Base (mm)
Ford Taurus	1738	2760
Volvo 850	1666	2670
Hyundai Sonata	1540	2700
Nissan Sentra	1307	2535
Lexus SC300	1819	2685
Ford Mustang	1617	2574
Mitsubishi Eclipse	1459	2515
Geo Metro	1039	2365

Application of the Standards - FMVSS 214 becomes 100 percent effective for light trucks, vans, and multiple purpose vehicles (LTV's), a growing proportion of the U.S. fleet, in the 1999 MY. In the EU regulation, vehicles with R-point of lowest seat >700 mm are excluded. The H-points of large pickups, sports utility vehicles, large vans, some of the compact pickups, and the majority of minivans are typically larger than 700 mm. As such, the EU regulation does not apply to the majority of LTV's. The current U.S. crash environment (1988-1996 NASS/CDS and Fatality Automotive Reporting System, (FARS)), when viewed as a yearly average, indicates that LTV occupants, are relatively safe when involved in side crashes, accounting for 14 % of involvement and resulting in 10 % of the severe injuries and the 11 % of the fatalities. Never the less, LTV's are currently 34% of vehicle registrations[1], and their proportion of the U.S. fleet is growing as seen by the trend in market share, with LTV's making up 43% of vehicle sales in 1996. As such, there is a need for the EU regulation to address the LTV vehicle class if it were to become applicable in the U.S. Full vehicle testing of LTV's would then also be needed to assess the relative benefits of the U.S. and EU regulations as applied to LTV'S and in particular assess the adequacy of the EUMDB in such tests.

Movable Deformable Barrier and Test Conditions Issues

MDB Issues - As indicated previously, a dynamic crash test requirement in a safety regulation should simulate the crash environment to the extent possible and should also provide for realistic injury causing mechanisms. As shown in Figure 57., over 43% of the fatalities and 37% of the serious injuries (MAIS ≥ 3) in U.S. light vehicle side impact crashes are in side impacts where an LTV is the striking or bullet vehicle. This is based on a yearly average from the current U.S. crash environment (1988-1996 NASS/CDS and FARS). As shown in Figure 58., when the trend of fatalities in struck vehicles is reviewed from 1980 through 1996 FARS, fatalities in car to car side crashes are decreasing while fatalities in LTV to car side crashes have more than doubled. In fact, a recent study by Gabler and Hollowell indicated that based on 1996 FARS, side impacts in which an LTV was the bullet vehicle resulted in 56.9% of the all the fatalities in side struck light vehicles [25]. This initial assessment, combined with the fact that the LTV population is growing in the U.S. fleet, suggests the following: The MDB in the dynamic test procedure for a side impact regulation in the U.S. should provide for injury causing mechanisms similar to those caused by the LTV vehicle class in order to provide a good representation of the current and future U.S. side crash environment. The MDB weight, stiffness, and geometry characteristics would need to be evaluated on this basis.

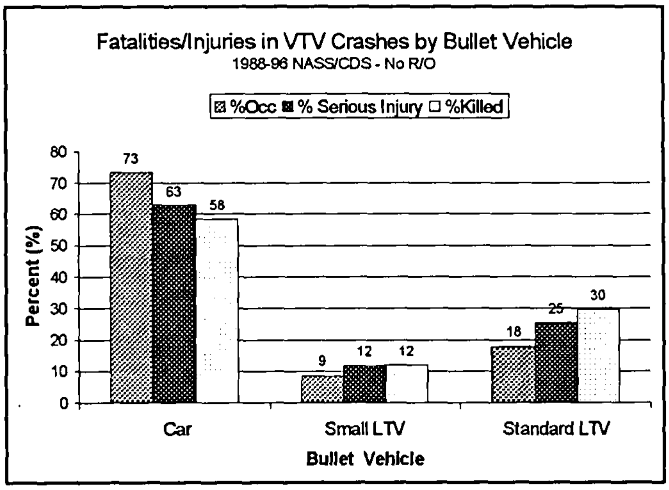

Figure 57.

---

[1] Source R. L. Polk Co, 1996

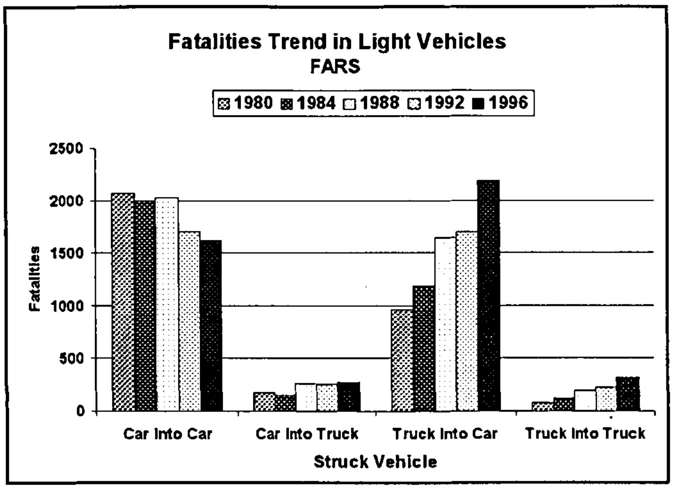

Figure 58.

As a vehicle class, LTVs are heavier on the average as a vehicle class. A study by Kahane of 1985-1993 passenger cars and light trucks indicated that LTVs were on the average heavier by 358 kg than cars with a slowly growing weight mismatch between the two classes [26]. In 1993, the sales averaged mass of LTV at 1770 kg was 422 kg heavier than that of passenger cars at 1348 kg. Figure 59. presents the test weight of the EUMDB and 214MDB along with the average test mass of cars, multipurpose vehicles (MPV) or sport utility vehicles, pickups, and vans in NCAP frontal tests conducted by NHTSA.

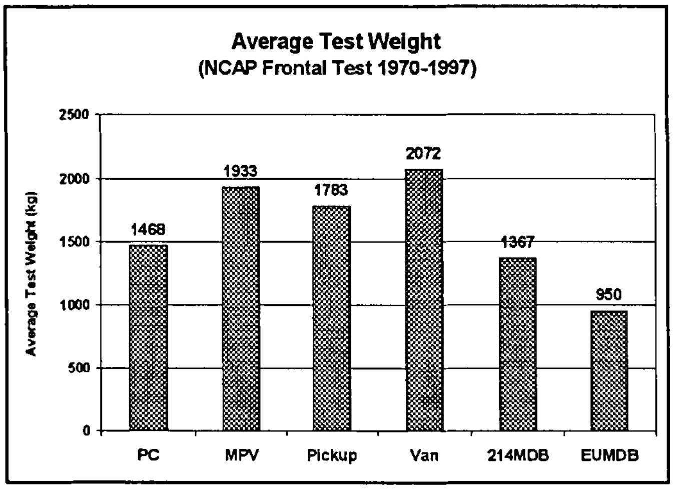

Figure 59.

LTVs also typically have a stiff frame-rail design versus the softer car unibody designs. Figure 60. presents the average stiffness of the Plascore EUMDB calculated from the force deflection performance corridors, and the average stiffness of the 214MDB derived from the force deflection response in a 40 km/h rigid barrier impact. The figure also presents averages of the linear stiffness for cars and LTV vehicle categories based on results from the New Car Assessment Program (NCAP) frontal tests. The quotient of the total barrier force and the corresponding displacement of the occupant compartment was used as a cursory measure of vehicle "linear" stiffness from the NCAP frontal test results. This cursory study indicates that overall, LTVs have about twice the frontal linear stiffness of cars. It is worth noting that the standard deviations in the average linear stiffness for passenger cars and each of the LTV vehicle categories is large. This indicates that there is a wide range of linear stiffness values within each of the vehicle categories. These initial results indicate that the Plascore EUMDB has a frontal stiffness representative of a passenger car and is less stiff than the 214 MDB. Strength comparisons and force versus deflection comparisons of the EUMDB and 214MDB are also presented in Figure 61. and 62.

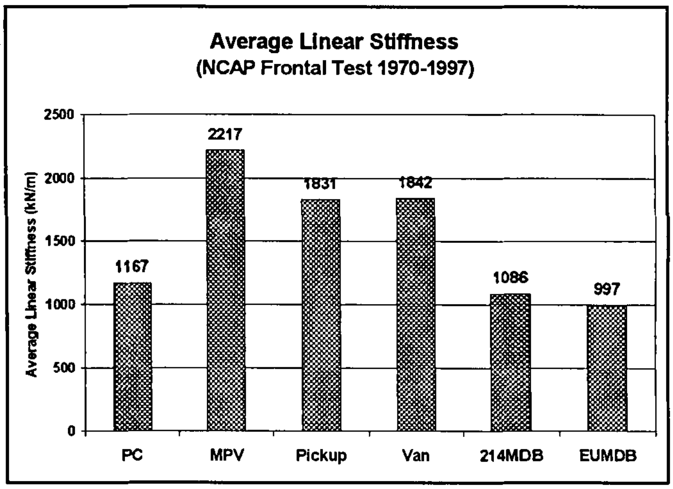

Figure 60.

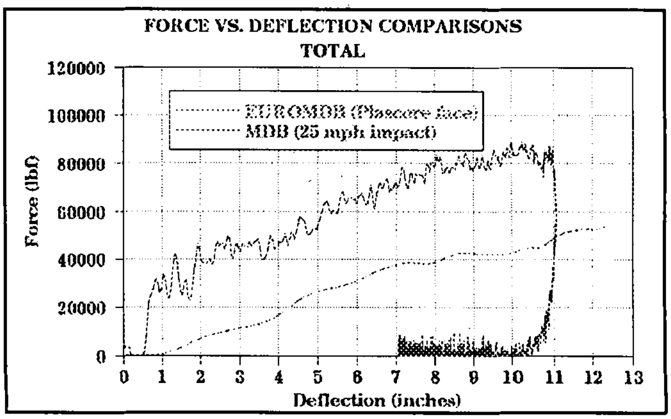

Figure 61. EUMDB and 214MDB Force Deflection Response Comparisons.

As a final note, the geometry of the striking bullet and, as such, a representative side impact MDB should also be addressed. LTV pickup and sports utility vehicles have higher hood height than passenger cars. Also, LTVs typically ride higher than cars. As indicated by the study by Gabler and

Hollowell, the sport utility vehicle category of the LTV class has the highest ride height with an average rocker panel height of 390 mm.

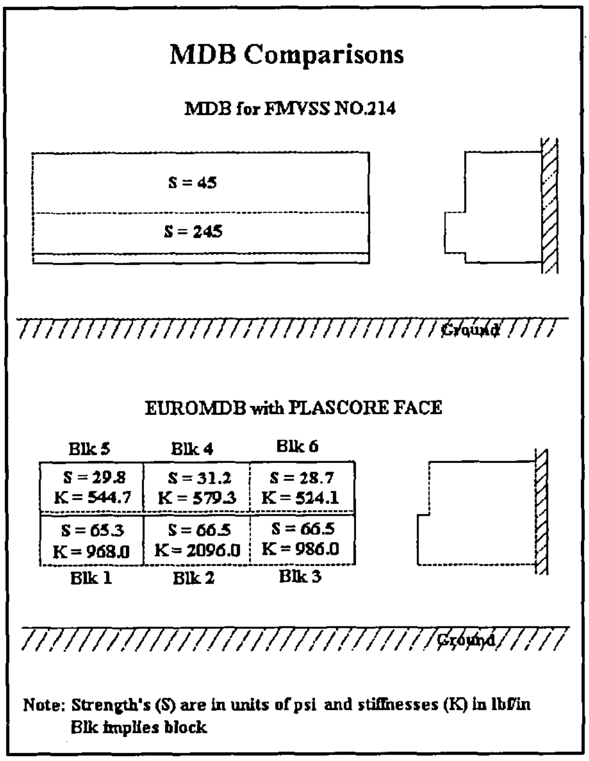

Figure 62. EUMDB and 214MDB Strength Comparisons.

In summary, a quick look at the striking vehicle in the current U.S. crash environment indicates that the EUMDB is inferior to the 214MDB in representing the striking bullet in the current and projected U.S. side crash environment.

Test Conditions Issues - As seen in Figure 63., analysis of the current U.S. side crash environment indicates that the struck vehicle does have a longitudinal component of the change of velocity. This supports the crabbed configuration of the U.S. test procedure. Campbell et al., Satake et al., and Bloch et al. have reported that when the side impact barrier was not crabbed, the injury measures for the front dummy were higher and that the crab angle is a very significant if not the most pervasive factor in the severity of the front dummy loading [28, 9, 29]. As such, the higher thoracic injury measures for front dummy and the high intrusion levels in the area of the rear front door seen in the EU tests, presented in this paper, are not necessarily representative of real vehicle to vehicle side crashes.

In 1991, Dalmotas et al. reported that in a series of vehicle tests performed by Transport Canada, the vehicle deformation patterns or side crush profile produced by the 214MDB in the immediate proximity of the driver's seat, showed closer agreement with vehicle to vehicle damage patterns than those produced by the EUMDB [18].

In 1996, Bergmann et al. reported that in a series of vehicle tests performed by Volkswagen AG, the deformation patterns in the vehicle to vehicle impacts can be compared neither with those in the ECE/R.95 tests nor with those in the FMVSS 214 tests [27]. Nevertheless, the data presented by Bergmann et al. did indicate that the deformation patterns in the FMVSS 214 tests were a closer match than those of the ECE R.95 tests. Bergman et al. also reported that their vehicle to vehicle tests showed severe loading of the struck vehicles in the lower side region, and that the penetration resistance must be increased (safety catch, increased sill overlap area, etc.) for real accidents. They stated that such vehicle design, however, leads to increased thoracic loading in the ECE/R.95 test. They also stated that in the development phase of new vehicles, a vehicle can be well above the injury limits in FMVSS 214 but exhibit very low occupant loadings in ECE/R.95. As mentioned previously, the ECE/R.95 procedure matches that of the current EU Directive, except the barrier height was 260 mm rather then 300 mm.

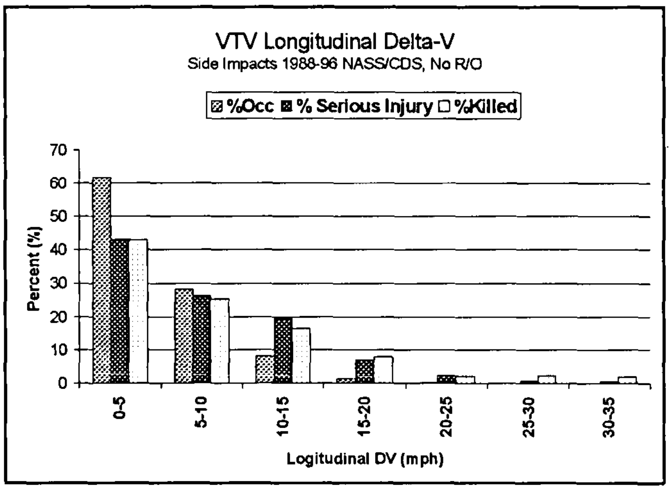

Figure 63.

Injury Criteria Functional Equivalence Issues

Head Protection Criterion Issues - The EU regulation has a head protection criteria while FMVSS 214 does not. The database of FMVSS 214 tests, to date, indicates that for the driver dummy, head contact with the vehicle interior or the MDB does not occur frequently. In the series of tests presented in this paper, HPC averaged less than 10% of the limit for the driver dummy, and less than 30% for the rear dummy with head contact occurring in half the tests. The results imply that, in the context of the current side impact standards, the HPC is not a meaningful or critical criterion. This suggests that neither FMVSS 214 nor EU 96/27/EC provides the correct test conditions to evaluate head injuries in the side impact crash environment.

Abdominal Criterion Issues - The EU regulation has an abdominal criterion while FMVSS 214 does not, and the SID dummy of FMVSS 214 lacks the measurement capabilities even to determine such a criterion. Previous research in this area by Dalmotas et al. [18, 19] indicated that the SID is not sensitive to localized door intrusion, specifically due to the arm rest, which has the potential of causing severe abdominal injuries. The TTI(d) of the SID dummy addresses the hard thorax which includes the liver and spleen. As such, there may be some potential for abdominal protection with vehicle designed to FMVSS 214. However, the cadaveric test conditions, in which TTI was developed, did not include localized loading of the abdominal region [20]. This factor would need to be addressed in assessing functional equivalence.

Thoracic Criteria Issues - Regarding the thoracic criteria, the EU regulation has deflection, or chest compression based criteria while FMVSS 214 has an acceleration based criterion. There has been an ongoing historical debate on which criteria better represent the correct injury mechanism and as such would best predict human occupant injuries.

In earlier research at Wayne Sate University, Cavanaugh et al. argued that C and $V*C_{max}$ are superior to TTI in predicting thoracic injury [21]. In that research, the compression and V*C were calculated for both the arm and the chest and not just the chest as should be done. The results were also based on a small number of cadavers. In recent research at the University of Heidelberg, Kallieris et al. reported that they found the TTI to be the best predictor for the thoracic injury severity [22]. Compression and V*C were also found to be good predictors. Also, in recent research at the Forschungsvereinigung Automobiltechnik FAT, Zobel et al. stated that the overall severity, as reflected by the injury cost scale ICS, is best predicted by TTI, and the European plans to use compression and later V*C are not worth the additional money which they cost the consumer [23].

In more recent research at the Medical College of Wisconsin and the Vehicle Research and Test Center, Pintar et al. concluded that the TTI criterion demonstrated superior injury prediction capability over V*C and C [24]. The data was based on an additional 26 cadaver side impact tests using advanced instrumentation to measure the kinematic variables necessary to generate all current injury criteria measures, including compression, spinal acceleration, V*C and TTI. Additional analyses of the growing database of cadaver tests would be needed to bring closure regarding the merit of the current thoracic injury criteria, and in assessing functional equivalence of the two regulations.

Pelvic Criteria Issue - The EU pelvic criterion is force based while the FMVSS 214 criterion is acceleration based. Further research would be needed to determine which pelvic criterion best addresses real world pelvic injuries.

Side Impact Dummy Issues

Dummy Biofidelity - There is a general consensus in the scientific community that improvements to both biofidelity and instrumentation capabilities of the U.S. SID and the European Eurosid-1 regulation dummies are needed. In 1990, the International Standards Organization (ISO) Working Group on Anthropomorphic Test Devices, ISO/TC22/SC12/WG5, gave the SID an overall rating of 2.34 and the Eurosid an overall rating of 3.22 out of a scale of 10 [30]. The biofidelity rating for the Eurosid-1 has not been fully developed although an estimate of 4.2 has been provided [32]. The ISO ratings for the overall dummy and per body region are listed in Table 15. These ratings correspond to an ISO classification of UNACCEPTABLE for the SID and MARGINAL for both the Eurosid and Eurosid-1 as overall side impact dummies [30]. The 1990 ISO ratings were based on a set of biofidelity requirements that did not account for muscle tone effects which are currently more widely accepted. When the muscle tone effects are taken into account, the overall ratings for SID and Eurosid change to 2.78 and 3.47 respectively. The updated ratings correspond to an ISO classification of MARGINAL for both the SID and Eurosid as overall side impact dummies. Although the other body regions cannot be discounted, it is worth noting that for each of the individual thorax, pelvis and abdomen body regions, the ISO biofidelity ratings of the SID are higher than the Eurosid.

It might be of interest to note, that the most recent addition to the SID of the Hybrid III head and neck for the test purposes of FMVSS 201, Upper Interior Protection, raises the SID ISO biofidelity rating to 3.91 without taking muscle tone into account [38]. If muscle tone were to be added, the SID biofidelity rating would be as high as 4.3.

Table 15.
ISO Biofidelity Ratings of SID and Eurosid [30]

Body Region	SID Ratings Oct 90	SID Ratings Mar 98*	Eurosid Ratings Oct 90	Eurosid Ratings Mar 98*
Head	0.00	0.00	3.33	3.33
Neck	2.31	2.55	3.04	3.70
Thorax	3.19	5.02	4.02	4.78
Shoulder	0.00	0.00	3.42	3.90
Abdomen	4.37	4.38	3.28	3.23
Pelvis	2.76	2.76	2.08	1.76
Overall Dummy	**2.34**	**2.78**	**3.22**	**3.47**

* uses corrected biofidelity equation [31] but is not yet formally accepted by ISO/TC22/SC12/WG5

Eurosid-1 Mechanical Deficiencies - Notwithstanding the biofidelity issues, the Eurosid-1 as referenced by the EU directive has certain mechanical deficiencies as demonstrated by the rib "flat tops" anomalies in the series of tests presented and as indicated by a list of concerns that has been compiled by the American Automobile Manufacturers Association (AAMA) [13]. The AAMA list includes binding in the rib modules as a number one concern. It also includes issues with the Eurosid-1 projecting back plate, bending of the plastic ilium of the pelvis, upper femur contact with the pubic load cell hardware, and clavicle binding in the shoulder assembly. These concerns are widely accepted and TNO has developed a research kit tool upgrade to address some of the outlined Eurosid-1 mechanical dummy issues. As mentioned earlier, the upgrade kit was recently made available to NHTSA for evaluation.

To date, initial evaluation by NHTSA through bumper pendulum testing has demonstrated that the upgrade kit does not address the flat-top anomalies in the rib potentiometer responses. As discussed earlier, those are believed to be partly caused by mechanical binding in the dummy rib cage.

Although minor in nature, it is important to establish how the upgrade kit modifications influence the Eurosid-1 biofidelity and its performance in full scale vehicle testing. To date, TNO has performed only components level testing with the upgrade kit.

Dummy Performance in Higher Severity Testing - The NCAP has been carried out in the United States for almost 20 years. Around the world, other countries have begun their own NCAP programs. Side impact tests were added to the U.S. NCAP starting in 1997. The side impact tests for U.S. NCAP are conducted using the same dynamic specifications as in the FMVSS 214 test procedure but at a higher testing speed. There is an increase of 32% in kinetic energy for the current side impact NCAP test as compared to the FMVSS 214 test. The U.S. SID was evaluated and found to perform in a repeatable and consistent manner in these higher severity crashes before the initiation of the side impact NCAP. It is highly probable that any side impact dummy will be used in higher severity testing. When considering the issues and deficiencies of the Eurosid-1 (or its upgrade or any new side impact dummy), one must consider its performance and durability at the regulation test speed and also at higher test speeds which will be used for umer programs or advanced side impact protection assessments.

Advanced Side Impact Dummy Developments Efforts - The European community is aware of the need to upgrade the Eurosid-1 and has initiated an upgrade project for the dummy, the SID-2000, sponsored by a European Commission consortium [34]. The SID-2000 project was started in March of 1998 with TNO as the project co-coordinator. An upgraded Eurosid-1 prototype is currently the end product in the year 2000. The SID-2000 program will reassess the European crash environment including distribution of injuries by body region, injury criteria, and the need for different size dummies.

In June of 1997, based on a recognized need to harmonize side impact dummies, the ISO Working Group on Anthropomorphic Test Devices, ISO/TC22/SC12/WG5, initiated a work item to develop and standardize a unique technologically advanced mid-sized side impact dummy. A WG5 Task Group, the WorldSID, with a joint three-way chairmanship consisting of the Americas, Europe, and Asia/Pacific, is currently actively performing this work item. The WorldSID Task Group has a target date of a prototype advanced side impact dummy in January 2000. The thrust of the ISO initiative is to develop a common dummy to be produced worldwide. Given the short development time frame, the upgraded dummy is expected to take the best features of existing dummies, one of the main candidates being the 5th percentile SID-IIs dummy that was recently developed by First Technology Safety Systems and the Occupant Safety Research Partnership of the United States Council for Automotive Research [35, 36].

Recently, the European Commission has approved the integration of the SID-2000 project into the ISO WorldSID work item [37]. The SID-2000 consortium is currently considering modifying the project objectives to ensure its compatibility with the WorldSID work item. In the interest of harmonization, it is hoped that the efforts to merge these two dummy development projects succeed such that the end product is one harmonized advanced side impact dummy to be commonly produced and used world wide.

Other Functional Equivalence Issues

The series of tests presented in this paper has shown that a Eurosid-1 dummy placed in the rear seat in the EU procedure undergoes a relatively less severe impact than that seen by the rear SID in FMVSS 214 procedure based on the injury criteria in each regulation. The reason for this is mainly the combination of the EUMDB barrier design (softer on the sides) and uncrabbed 90° impact of the EU test conditions. Lower loadings on a rear outboard seated dummy due to the uncrabbed 90° has been also demonstrated by Satake [9], albeit in that case an uncrabbed FMVSS 214 test condition with SID dummies was investigated. The current U.S. crash environment (based on a 1988-1996 NASS/CDS and FARS study) indicates that rear occupant severe injuries (MAIS ≥ 3) account for only 7.3% of the total severe injuries and 5.1% of the overall fatalities. These low injury rates are at least partially due to the low rear seat occupancy rates. Never the less, it is desirable to require a certain level of protection for the rear occupant by the placement of a rear dummy in a dynamic side impact safety standards. This is mainly due to the premise that, increasingly, the occupants of the rear seat are children whose safety should not be compromised.

Finally, FMVSS 214 has a static crush strength requirement which NHTSA believes provides a certain level of protection against pole or tree impact [26]. This requirement is not currently addressed by the EU directive.

SUMMARY AND CONCLUSIONS

The series of comparative testing, presented in this paper, with current U.S. production vehicles has provided important insights into the performance of vehicles when tested to the requirements of the FMVSS 214 and EU 96/27/EC regulations. However, it can only be viewed as a partial step in determining the overall safety performance of vehicles relative to the two regulations.

The following are concluded from this series of tests:

- Results indicate that vehicles designed to meet FMVSS 214 may not meet EU 96/27/EC.
- Results also indicate that vehicles can be designed to meet both standards.
- Conclusions based on this testing may not be valid due to the measurement anomalies in the Eurosid-1 and the small number of vehicles tested.

Also, the following are highlights of the results from this series of tests:

- Eurosid-1 rib displacements displayed "flat-top" behavior which imply questionable EU 96/27/EC rib deflection (RDC) and soft tissue (V*C) criteria values.
- FMVSS 214 and EU 96/27/EC did not provide similar vehicle performance rankings or pass/fail based on their respective criteria.
- With the caveat of questionable EU thoracic criteria, results indicate a higher severity for the driver dummy in the EU tests for the rib deflection criterion when compared to TTI(d) in the FMVSS 214 tests. No trend is indicated for V*C or the pelvic criterion.
- Results also indicate a much lower severity for rear dummy in the EU tests than in the FMVSS 214 tests for both thoracic criteria. No trend is apparent for the pelvic criterion.
- With the exception of Abdominal Peak Force (ABD) for the Mustang driver dummy, only the V*C and RDC values were relatively high for the EU tests.
- The EU tests crush profile was more rounded, with larger intrusion around the B-pillar and rear front door section, than the FMVSS 214 tests crush profile.

It is important to note that this series of tests is only one part of a general matrix needed to assess the comparative performance of vehicles relative to the two regulations. The general matrix includes testing of European production vehicle to determine how well such vehicles perform relative to FMVSS 214. The matrix also includes testing of vehicles designed for both U.S. and European markets to the requirements of both regulations. Vehicles equipped with side air bag systems would also be part of this matrix as they are becoming prevalent in both the U.S. and European fleet. In addition, since manufacturers seem to design their vehicles for optimum performance in the U.S. NCAP, testing of vehicles to similar higher severity test conditions for both regulations would also be needed. Moreover, a small number of vehicles were tested in this series. A larger number of U.S. production vehicles that more broadly represent the U.S. fleet may need to be tested.

Other issues have also arisen in this research which may in the end confound a definitive functional equivalence determination of the two regulations:

- Light trucks, vans and sports utility vehicles (LTV's) have become a significant and a growing segment of the U.S. fleet. A large portion of the U.S. side impact casualties results from impacts with the LTV class of vehicles. The adequacy of both the FMVSS 214 and the EU movable deformable barrier in representing the striking vehicle in the current and future U.S. crash environment is in question. In particular, the lighter and less stiff EU barrier is less representative of the current and future mix of U.S. vehicles.
- The issue of providing a meaningful test to assess the safety of rear occupants in side impacts is a sensitive one since increasingly the occupants of the rear seat are children whose safety should not be compromised. In this regard, there may be an opportunity for improvements in both regulations, albeit the FMVSS 214 test condition does provide a better loading environment.
- Initial evaluations of the Eurosid-1 research tool kit upgrade, recently developed by TNO, has demonstrated that the upgrade does not address the flat-top anomalies in the rib potentiometer responses. Although minor in nature, it is important to establish how the upgrade kit modifications influence the Eurosid-1 biofidelity and its performance in full scale vehicle testing. One question would be if full scale tests, such as the series presented in this paper, need to be repeated with the upgraded Eurosid-1 to truly assess the comparative performance of vehicles relative to the two side impact regulations.

In terms of struck vehicle deformation patterns, the crush profile in the EU tests was more rounded with larger intrusion around the B-pillar and the rear section of the front door. In the FMVSS 214 tests the crush profile is more rectangular in shape with the intrusion more evenly distributed along the area of barrier-to-vehicle engagement. Earlier research indicates that FMVSS 214 test provides more realistic crush profile when compared to vehicle to vehicle crashes. Notwithstanding the dummy issues, performance in real world crashes for the eight vehicles tested in this series can be assessed by studying real world NASS side impact cases for the same vehicles. Occupant injuries and intrusion profiles would give an indication of which regulation provides a more realistic assessment of this set of vehicles for the U.S. crash environment.

Also, the results from this series of testing were not totally consistent with the relevant full scale testing by other researchers. This is mainly attributed to the fluid nature of the European test procedure, specifically the barrier height changes and the inconsistent performance of the various European barrier faces. Additional comparative full scale testing based on the current European specifications and latest European barrier designs would provide useful data for further assessment.

With the caveats described above, the comparative testing did not provide similar vehicle performance rankings nor pass/fail results based on the respective injury criteria of the two side impact regulations. In fact, there was no direct correlation between the corresponding injury criteria results for the vehicles tested.

On the other hand, the development of an upgraded side impact dummy is planned within two years, whether through the European Commission Consortium SID2000 project or the ISO WorldSID Task Group. The ongoing dummy development efforts reflect the consensus of the world scientific community that, in the interest of safety, an upgraded regulation side impact dummy is needed. Improvements to both biofidelity and instrumentation capabilities of the U.S. SID and the European Eurosid-1 regulation dummies are needed. The Eurosid-1 also has mechanical deficiencies.

In addition, the changes in the composition of the U.S. fleet, with a significant and growing segment of the larger, stiffer, and heavier LTV vehicle class, underscores the need to update the definition of the side impact safety problem in the U.S. crash environment and determine the opportunities for enhancing occupant side impact protection. The test conditions of the dynamic side impact requirement and the characteristics of the striking bullet, i.e. movable deformable barrier, would need to be reassessed relative to the current and future side crash environment. Fixed objects side crashes also need to be studied to investigate additional opportunities for enhancing occupant side impact protection in the U.S. environment.

In conclusion, given the results of the current testing, in particular the measurement anomalies in the Eurosid-1, insufficient data is available at this time to make a tentative determination of functional equivalence of the two side impact standards. Using the NHTSA side impact harmonization plan as a guide, the agency will establish its current position on side impact harmonization based on all available information. From this baseline, a plan will be developed for advancing side impact safety in the U.S. fleet taking into account the level of available resources. It is hoped that the current efforts to merge the European SID2000 and ISO WorldSID dummy development projects succeed and result in an advanced harmonized side impact dummy which can be commonly produced and used world wide. Harmonization research can then focus on evaluating the advanced world side dummy and its application in the next generation side impact safety standard(s). Harmonization of the dummy and injury criteria is a basic premise in achieving a global harmonized side impact regulation. While differences in the fleet composition and crash involvement may preclude totally harmonized test conditions and movable barriers, the use of a single dummy family would significantly alleviate the current burdens of vehicle design, testing, manufacturing, and distribution currently encountered by automobile manufacturers in the growing global market. It should also lead to improved side crash protection world wide.

ACKNOWLEDGMENTS

The authors would like to acknowledge John Fleck and Gary Strassburg of MGA Research, Peiter Van der Veen and Patrick van der Bijl of TNO, Ron Hess of TRCO, Howard Pritz and Tom Grubbs of NHTSA, Tom Trella of VNTSC/RSPA, and Sakis Malliaris of Dubois Associates for their contributions in conducting the testing and analyses presented in this paper.

REFERENCES

1. National Highway Traffic Safety Administration; NHTSA Plan for Achieving Harmonization of the U.S. and European Side Impact Standards, Report to Congress, April 1997.
2. Federal Register, Vol. 55, October 30, 1990, p. 45722.
3. Federal Register, Vol. 60, July 28, 1995, p. 38751.
4. NHTSA "Preliminary Regulatory Impact Analysis: New Requirements for Passenger Cars to Meet a Dynamic Side Impact Test, FMVSS 214," DOT HS 807 220, January 1988.
5. ISO/TC22/SC12/WG5/N256, "Specification Eurosid-1 (January 1990)," April 1990.
6. Scherer, R., Vecchio, M., ISO/TC22/SC10/WG1/N372, October 1996.
7. Benedetto, A. M., "experience and Data Analysis on Side Impact Testing According to the European Procedure", Paper No. 94-S6-O-07, 1994 ESV.
8. Albers, W., Lehmann, D., "Side Impact Requirements in

Paper No. 94-S6-O-07, 1994 ESV.

8. Albers, W., Lehmann, D., "Side Impact Requirements in the USA and Europe - A Critical Comparison", Paper No. 94-S6-O-02, 1994 ESV
9. Satke, K; Analysis of Test Results of Side Collisions Using Actual Vehicles, 1996 ESV.
10. Beusenberg, E.G. Experience of Using Eurosid-1 in Car Side Impacts, 1991 ESV.
11. Lau, I., "An Analysis of the MVMA Sponsored Full Scale Side Impact Tests", 1989 STAPP
12. Henson, S. et al.; Comparison of BIOSID and Eurosid-1 Dummies in Full-Vehicle Crash Tests, 1994 SAE Congress
13. AAMA Eurosid-1 Concerns, ISO/TC22/SC12/WG5 (N533)
14. Dalmotas, D. J., "Eurosid 1 Pendulum Test", Attachments # 1, #2, #3, and #4, Transport Canada, April 1998.
15. Laboratory Test Procedure for FMVSS No. 214 "Dynamic" Side Impact Protection - Passenger Cars, TP-214D-04, August 1995.
16. Lowne R.W., Janssen, E. G., "Thorax Injury Probability Estimation Using Prototype EUROSID," ISO/TC22/SC12/WG5/N271, 1990.
17. Farmer, C. M., Braver, E. R., Mitter E. L., "Two-Vehicle Side Impact Crashes: The Relationship of Vehicle and Crash Characteristics to Injury Severity", Accident Analysis and Prevention, Vol. 29, No. 3, pp. 399-406, 1997.
18. Dalmotas, D., German, A., Gorski Z., Green, R., Nowak, E., "Prospects for Improving Side Impact Protection Based on Canadian Field Accident Data and Crash Testing", SAE Paper 910321.
19. Dalmotas at al., "Side Impact Protection Opportunities", 15th International Conference on the Experimental Safety Vehicles, Paper 96-S6-O-04
20. Eppinger, R. H. , Marcus, J. H. , and Morgan, R. M., "Development of Dummy and Injury Index for NHTSA's thoracic Side Impact Protection Research Program", SAE Paper 840885.
21. Cavanaugh, J. M., Zhu, Y., Huang, Y., and King A., L., "Injury Response of the Thorax in Side Impact Cadaveric Tests", Proceedings of the 37th Stapp Crash Conference SAE, 1993
22. Kallieris, D., Boggasch, F., Mattern, R., "Protection for the Thorax Injury Severity in the 90-Degree Lateral Collision", 14th International Conference on the Experimental Safety Vehicles, Paper 94-S1-O-02, 1994.
23. Zobel, R., Herrmann, R., Wittmüß, A., Zeidler, F., "Prediction of Thoracic Injuries by Means of Accelerations, Deflections, and the Viscous Criteria Derived From Full-Scale Side-Impacts", 14th International Conference on the Experimental Safety Vehicles, Paper 94-S1-O-01, 1994.
24. Pintar, F., Yoganandan, N., Hines, M., Maltese, M., McFadden, J., Saul, R., Eppinger, R., Khaewpong. N., Kleinberger, M., "Chestband Analysis of Human Tolerance to Side Impact", 41st STAPP Car Crash Conference Proceedings, SAE Paper 973320, 1997.
25. Gabler H. C., Hollowell W. T., "The Aggressivity of Light Trucks and Vans in Traffic Crashes", SAE Paper 980908, February 1998.
26. Kahane, C. J., "Relationships Between Vehicle Size and Fatality Risk in Model Year 1985-93 Passenger Cars and Light Trucks", DOT HS 808 570, January 1997.
27. Bergmann R., Bremer C., Wang X., Enßlen A., "Requirements of Comprehensive Side Protection and Their Effects on Car Development", Paper 96-S6-W-16, 1996 ESV
28. Cambell, K. L., Smith E. J. Wasko R., Hensen S. E., "Analysis of the Jama Side Impact Test Data", SAE Paper 892430.
29. Bloch, J. A., Cesari, D., Zac, R., "Influence of Test Procedure Characteristics on the Severity during Side Impacts", Paper 91-S5-O-17, 1991 ESV
30. Mertz H., Irwin, A., "Biofidelity Ratings of SID, EUROSID, and BIOSID", ISO/TC22/SC12/WG5, N288, October 1990.
31. Kirkish, S., ISO/TC22/SC12/WG5 North, Central, and Central American Dummy Advisory Group Meeting, April 17, 1998.
32. Minutes, ISO/TC22/SC12/WG5 (N299), ISO/TC22/SC12/WG5 November 1990.
33. "SID-2000", RTD Basic Research Project, Industrial and Materials Technologies, European Commission Framework Programme IV, ISO/TC22/SC12/WG5 N539, ISO/TC22/SC12/WG5 Meeting, November 1997.
34. Resolution 5, ISO/TC22/SC12/WG5 (N524), ISO/TC22/SC12/WG5 Meeting, June 1997.
35. Daniel, R.P., Irwin, A., Athey, J. Balser, J., Eichbrecht, P.,Hultman, R.W., Kirkish, S., Kneisly, A., Mertz, H., Nusholtz, G., Rouhana, S., Scherer, R., Salloum, M., and Smecka, J., "Technical Specifications of the SID-IIs Dummy," Proceedings of the 39th Stapp Car Crash Conference, SAE Paper 952735, 1995.
36. Kirkish, S., Hultman, R.W., Scherer, R., Daniel, R.P., Rouhana, S., Nusholtz, G., Athey, J., Balser, J., Irwin, A, Mertz, H., Kneisly, A., Eichbrecht, P., "Status of Prove-out Testing of the SID-IIs Alpha-Prototype", 15th International Conference on the Experimental Safety of Vehicles, Paper 96-S10-O-15, 1996.
37. WorldSID Task Group Report to ISO/TC22/SC12/WG5, ISO/TC22/SC12/WG5 Meeting, March 1998.
38. AAMA document, S98-1 NHTSA docket , Comment of January 22, 1998.
39. Federal Register, Vol. 63, 26,508 -1998 (to be codified at Part 553, app. B).

EUROSID LUMBAR CERTIFICATION TESTS

APPENDIX A

Original Lumbar #191

Date	Pulse	Flexion (45-55)	Time (39-53)	Theta A (31-35)	Time (45-55)	Theta B (27-31)	Time (45-55)	Lab	Pass/Fail
05/02/97	ok	49.5	46.4	33.6	49.1	29.4	49.8	FTSS	Pass
05/12/97	99%	52.6	49.5	35.6*	49.5	31.2*	48.3	FTSS	fail
04/09/97	ok	53.3	51.0	37.1*	51.0	32.7*	52.0	MGA	Fail
05/27/97	ok	48.8	50.0	33.2	50.0	29.3	46.0	MGA	Pass
05/29/97	ok	50.9	48.3	35.0	48.6	30.7	47.6	MGA	Pass
05/29/97	ok	50.5	49.3	34.4	49.3	31.3*	45.6	MGA	Fail
02/03/97	ok	49.9	50.1	33.5	49.7	30.5	49.5	TNO**	pass
02/04/97	ok	49.1	47.9	32.9	47.3	30.6	48.3	TNO**	pass
04/11/97	Bit out high	54.1	45.6	37.0*	45.4	32.4*	49.4	TRC	fail
05/13/97	ok	51.4	47.5	35.5*	47.5	31.0	47.5	TRC	fail

*** Does not meet specifications**
**** Original certification**

NOTE 1 : MGA ran with a lighter pendulum base after 4/14 (809 gr vs 1261).
NOTE 2 : MGA ran with a thinner base plate after 5/26 (total pendulum length 72.41 inches)
NOTE 3 : MGA lab temperature prior to 5/30 is 70° F and 68° on 5/30

Lumbar for Eurosid-1 # E1-213

Date	Pulse	Flexion (45-55)	Time (39-53)	Theta A (31-35)	Time (45-55)	Theta B (27-31)	Time (45-55)	Lab	Pass/Fail
05/12/97	ok	48.1	48.5	30.7*	48.1	27.8	47.5	FTSS	Fail
04/04/97	ok	49.5	47.0	32.2	47.0	30.3	45.0	MGA	Pass
05/27/97	ok	46.9	47.0	32.6	49.0	29.2	48.0	MGA	Pass
05/29/97	ok	47.3	47.8	32.6	47.6	29.1	48.1	MGA	Pass
05/30/97	ok	45.7	44.9	31.0	45.6	28.8	46.0	MGA	Pass
05/13/97	ok	47.0	47.0	32.0	47.1	28.3	46.6	TRC	Pass

EUROSID LUMBAR CERTIFICATION TESTS

Replacement Lumbar #183									
Date	Pulse	Flexion (45-55)	Time (39-53)	Theta A (31-35)	Time (45-55)	Theta B (27-31)	Time (45-55)	Lab	Pass/Fail
04/23/97	good	49.0	46.7	32.37	46.6	29.35	47.8	FTSS	Pass
05/12/97	good	49.5	48.0	33.3	47.9	29.5	49.0	FTSS	Pass
04/11/97	good	48.3	42.7	33.1	42.43*	30.10	46.05	MGA	Fail
04/15/97	bad high	50.52	45	35.41*	46.18	31.33*	45.68	MGA	Fail
04/16/97	95% high	52.0	50.4	36.6*	50.4	31.8*	50.7	MGA	Fail
04/29/97 (11:00)	good	47.82	49.0	33.01	49.0	30.86	45.0	MGA	Pass
04/29/97 (20:02)	good	50.47	50.0	34.91	51.0	32.23*	49.0	MGA	Fail
04/30/97	good	50.4	49.0	34.5	49.0	31.9*	48.0	MGA	Fail
04/30/97	good	49.44	49.0	34.03	49.0	31.32*	50.0	MGA	Fail
05/27/97	good	48.8	46.0	33.5	46.0	28.4	46.0	MGA	Pass
05/29/97	good	49.7	48.1	33.6	48.0	30.4	48.6	MGA	Pass
05/29/97 (17:01)	good	49.9	47.4	34.35	47.5	31.46*	45.6	MGA	Fail
05/30/97	good	48.2	46.1	33.0	46.6	30.46	45.9	MGA	Pass
04/18/97	95% high	52.5	44.0	35.2*	43.8*	31.4*	43.5*	TRC	Fail
05/13/97	good	51.6	46.6	34.0	46.8	30.7	46.9	TRC	Pass

BENEFITS OF THE INFLATABLE TUBULAR STRUCTURE
AN INVESTIGATION ON THE CASUALTY ABATEMENT CAPABILITY OF THE BMW HEAD PROTECTION SYSTEM HPS

Klaus Kompass
Bayerische Motoren Werke AG
Germany
Kennerly Digges,
K. Digges and Associates
A. Malliaris
Data Link, Inc.
United States of America
Paper N° 98-S8-O-14

ABSTRACT

Beginning in model year 1997, BMW introduced an innovative head protection system HPS called the Inflatable Tubular Structure (HPS). Tests indicate that the system dramatically reduces the severity of head impacts in side crashes.

This investigation is an evaluation of casualty abatement benefits that are derived from applying injury measures based on the HPS test results to the population in US National Accident Sampling System (NASS/CDS). The results of component and vehicle crash tests are summarized. The procedures for estimating benefits are described along with the benefits in terms of injuries mitigated, maximum injuries to occupants mitigated, and fatalities prevented.

The calculated benefits of the *HPS* in reducing fatalities and the most serious injuries to front seat occupants of passenger cars are:

Casualty Reduction for HPS

Casualty Class	Reductions
Fatalities	*1,344*
AIS 2-5 Injured	*2,598*

The impact mitigation benefits were derived from reducing injuries from head impacts to the following components: A & B pillars, side rails, window frames & glass, and window-pillar interfaces. Approximately 51% of the reductions in fatalities were attributable to the mitigation of head impacts with these components. The remaining 49% of the fatality reductions were associated with mitigation of exterior contacts and prevention of ejection through side windows.

According to the US National Accident Sampling System, the population injured in tow-away motor vehicle crashes suffers an average of about 3 injuries per person. The accounting system used in the tables above does not give credit for injury reduction when the injury is not the most severe of all injuries suffered by an injured person. If the less severe injuries are considered, there is a much larger opportunity for injury reduction. When considering all injuries, the injury reductions for the HPS system are:

HPS Injury Reductions for Front Seat Occupants, All Injuries Considered

Casualty Class	Reductions
AIS 3-6 Injuries	*3,902*
AIS 2-6 Injuries	*8,501*

The benefits cited are over and above the benefits offered by other safety systems. These systems include: frontal air bags, side air bags, FMVSS 214 side impact protection, and FMVSS 201 head protection for the vehicle roof and headers.

THE BMW HEAD PROTECTION SYSTEM HPS

In the opinion of accident researchers, in side-impact collisions top priority should be given to protecting the occupants head. Yet there was no sufficient protection device available so far.

In 1997 BMW started to equip their cars with the so called Head Protection System HPS, also known as ITS, Inflatable Tubular Structure. This device offers the opportunity of deploying a gas filled tubular cushion of about 130 mm in diameter to increase the protection of the head and face. It is offered as standard equipment for the 5 and 7 series and will also be standard fit for the new 3 series car when it is launched in a couple of weeks from now.

The HPS is a unique technology and BMW is the only company to offer an additional protection device for the occupants head and neck. The first ideas were presented at the 14th International Technical Conference on the Enhanced Safety of vehicles ESV in Munich, Germany in 1994. Its function and test results were shown in a presentation at the 15th ESV Conference two years later in Melbourne, Australia.

Since then a lot of improvement has been done and a lot of positive experience has been gained, either from tests but also from statistical analysis and accident researchers are even aware of some real life accidents in which the HPS has performed perfectly in reducing injuries.

The HPS consists of the following components:

- **Inflator** - For the production of the filling medium a pyrotechnical gas generator is installed underneath the instrument panel
- **Flexhose** - a flexible hose leads the gas flow from the inflator to the restraining cushion
- **Bladder** - a gas sealed bladder is filled with the medium and expands its diameter
- **Braid** - surrounding the bladder a braiding texture ensures the tension to contract the system

The undeployed HPS is packaged behind the interior trim parts of the A-pillar and the roof liner of each side of the vehicle. On both ends the system is fixed to the body in white. In case of a side collision with sufficient severity the inflator is activated and the system is filled with gas. During this increase of the tubular structure element, a remarkable tensioning force is created which contracts the tube.

Since the length of the stored system is longer than the shortest distance between the two anchorage points, while contacting the tubular structure is pulled out of the trim and placed in position right beneath the occupants head.

The remarkable tension provided through the effect of a change in the orientation of the fibres in the braiding material restraints the occupant's head without significant neck bending moments.

TESTING FOR EFFECTIVENESS ESTIMATES

BMW conducted a variety of tests to assess the reduction in HIC offered by the HPS. These tests included sled tests with dummies, tests with the Free Motion Headform (FMH) specified in FMVSS 201, and vehicle side impacts with moving barriers and poles. A list of test result samples is shown in Table 1.

Table 1
Test Results Tests With and Without HPS

Test Type	Configuration	Delta-V kph	HIC w HPS	HIC w/o HPS
Vehicle	ECE R 95 Side	20	90	97
Vehicle	FMVSS 214	17.5	212	193
Vehicle	Rigid Pole	30	277	2495
Vehicle	Rigid Pole	32	620	4720
Vehicle	Moving Pole	40	475	1867

The test data shows large reductions in the head injury criteria (HIC) for tests conducted in accordance with US and European side impact procedures. In addition, tests into rigid and moving poles show dramatic HIC reductions - much larger than could be expected with a practical thickness of conventional padding.

Severe crash tests into a rigid pole at 20 mph have been conducted independently by the Insurance Institute for Highway Safety. Results are included in Table 1 (Rigid Pole 32 kph).

Rollover tests conducted by NHTSA have demonstrated the ejection prevention capability of the HPS.

In static deployment tests the HPS was deployed against a dummies head to evaluate potential risks in Out Of Position situations. A 5th percentile female dummy was leant against the side glazing such that the HPS contacted the top of the head when the deployment speed was on its maximum. In this test the maximum axial neck force was .7 kN. This is well below any dangerous values.

APPROACH TO THE BENEFITS ANALYSIS

When deployed, the HPS provides primarily protection of a front seat occupant's head and face against impacts with a car's: A-Pillar, B-Pillar, Side Rail, Window Frame & Glass, Window Pillar Interfaces, and other upper side interior car components.

In addition to casualty abatement as cited above, the HPS, when deployed, is capable of reducing occupant ejections through front side windows. Consequently, the HPS reduces injuries and casualties associated with all external injuring sources, for the ejected occupants at issue.

The first objective of this investigation is to identify all head and face injuries, and injury outcomes in tow-away car crashes, associated with an occupant's crash contacts for which the HPS has the ability to influence.

The second and most important objective of the investigation is the evaluation of casualty abatement benefits that derive from the HPS. More detailed data on the non-applicable contacts may be found in the final report of the study (Digges, 1997).

DATA SOURCES

Due to the demand for high resolution of car, occupant, and injury attributes in this investigation, the NASS/CDS file is the main source of data. The available nationally representative samples in this file, for 1988-1995, include about: 44,000 towaway cars, 91,000 crash involved occupants, and 188,000 injuries, before projection to national estimates.

The sample volumes cited above are generally adequate for addressing the issues of this investigation with sufficient resolution concerning: crash modes, injury attributes including severity and injuring contact, and occupant outcomes.

CATEGORIZATION OF CAR OCCUPANT INJURIES

The annual incidence of car occupant injuries is classified in this investigation on the basis of several injury and occupant attributes, crash configurations, and HPS applicability domains. Specifically the following classes and subclasses are distinguished and applied in the estimation procedure of injury reduction and outcome abatement.

The injuries at issue are head and face injuries, AIS=1-6, due to contacts with upper interior parts and surfaces of cars, specifically: A Pillars, B Pillars, Other Pillars, Window Frames & Glass, Window-Pillar Interfaces, Side Rail, Front Headers, Rear Headers, and injuries to any body region due to exterior contacts of car occupants ejected or partially ejected through the front windows.

The annual US incidence of the cited injuries is: 182,855. This is about 4.6% of the total 4,040,000 injuries sustained each year by car occupants in the US. The balance of injuries (4,040,000 - 182,855) are not at issue here, since these injuries may not be influenced by HPS application.

The universe of injuries at issue here, about 182,855 per year, is partitioned and analyzed in all possible combinations of relevant crash configurations, injuring contacts, and injury severities. A total of 186 combinations of AIS, Injuring Contacts, and Crash Configurations results.

CRASH CONFIGURATIONS

For accounting convenience, eight crash/occupant configurations were defined. Five were configurations in which the HPS can influence the outcome. These are defined as applicable configurations. The crash configurations applicable to ITS mitigation are: (1) No Rollover, No Ejection; (2) Rollover, No Ejection; (3) No Rollover, Ejection; (4) Rollover, Ejection; and (5) Too Severe (Catastrophic Vehicle Damage). The configurations not applicable to HPS protection ar: Front or Rear Header Contacts and Rear Seat Occupants. HPS effectiveness is based on all injuries in the crash configurations listed above which are applicable to HPS deployment.

EXCLUSION OF BENEFITS

Catastrophic crashes are excluded from HPS benefits. These are defined as crashes with either (1) total delta V over 60 mph; or (2) lateral delta V over 40 mph; or (3) extent of damage 4 or higher in CDC scale, when the specific side impact location includes the passenger compartment.

Injuries of rear seat occupants are excluded from HPS benefits, and so are all occupant injuries due to front and rear headers. Such injuries are abated by countermeasures other than the HPS, that may act concurrently. All exterior contact injuries of ejected car occupants benefit from HPS deployment, only if the occupants are ejected via front windows; benefits of qualified ejectees are discounted by 20% in reflection of side effect injuries incurred as a result of retention within the passenger compartment by HPS action.

CONSEQUENCE OF OTHER COUNTERMEASURES

The 1988-1995 NASS data does not adequately reflect the benefits of recently introduced safety improvements. Two of these improvements are: (1) frontal air bags and (2) upper interior head protection. The frontal air bags have been phased in during the past four years, and the upper interior head protection will be phased in during the following four years. Each of these safety systems will reduce the NASS reported level injuries for head and face impacts. Some of the protection provided by these systems supplements the protection provided by the HPS. The presence of the frontal air bag will provide a high level of protection against head and face impact with the A-pillar. The upper interior head protection will reduce the severity head and face impacts with the pillars, side rails and headers. In cases in which it deploys, the

HPS is expected to provide much greater head protection for relevant impacts than that offered by other countermeasures.

A supplemental benefit is applicable in case of no HPS deployment for head and face injuries from contact with the A Pillars. The benefit is achievable by virtue of the main air bag and is applicable for cases of total delta V over 15 mph, i.e. main air bag deployment, irrespective of HPS deployment. The specific benefit is that all head and face injuries due to contact with the A Pillars are reduced to an AIS=1 severity.

Another supplemental benefit is applicable to contacts with A-pillars, B-pillars and side rails in cases of no HPS deployment. Head protective padding on these interior surfaces will limit the HIC to 1000 when tested with the Free Motion Headform (FMH) specified in FMVSS 201, at an impact speeds of 20 km/hr (12 mph).

Adjustments were made to the NASS 1988-95 data to reflect the injury reductions from the two supplemental benefits listed above, under crash conditions in which the HPS does not deploy. The adjustments were made only to contacts which are relevant to HPS protection.

Other safety improvements are likely to enhance the protection offered by HPS. These include improved side impact protection and side air bags for the chest and pelvis. These improvements mitigate the most serious injuries body regions other than the head. The combination of features will further reduce the overall severity of injuries and impairment to the occupant. These improvements do not address head/face injuries and no adjustment for these additional safety features is considered in this analysis.

The increasing use of safety belts in the United States may also reduce injuries in side impacts, irrespective of the HPS. Some of the increases in safety is being offset by the increasing number of light trucks, sport utility vehicles and large cars in US highways. These vehicles increase the severity of side crashes. No adjustment was made for these offsetting factors.

HPS DEPLOYMENT CRITERION

The primary HPS deployment criterion is a lateral delta V of approximately 24 km/hr (15 mph) or higher in planar crashes, irrespective of subsequent rollover. A 30% deployment is applicable for rollovers, based in an analysis of accident data.

HPS Abatement Schedule

Except for the supplemental benefit cited above, the basic mechanism for reduction of head and face injury severities is the large reduction of HIC offered by the HPS when deployed. The HIC associated with a deployed HPS, as a function of lateral delta V, has been determined by test data as shown in the points of Figure 1. The line in this figure represents a best fit to the points, i.e. $HIC=18.8*latdv$, where latdv is in mph.

Figure 1:
Vehicle Crash Severity Vs. HIC for HPS

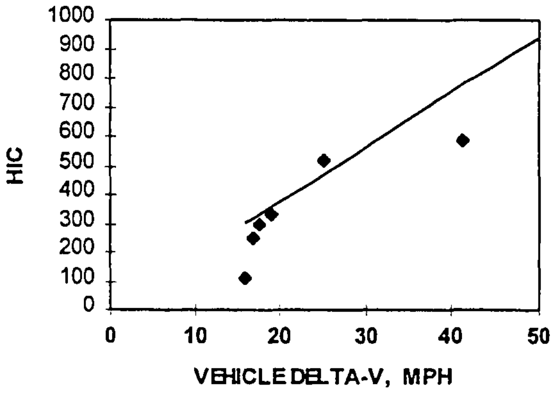

Figure 1 provides the basis for translating the crash severity values for each crash in NASS/CDS to values of HIC experienced by occupants when the HPS is deployed. In turn, the experienced HIC values are translated into sustained head or face injury severities (AIS), as per NHTSA's preferred ways [NHTSA, 1995]. The relationships are:

$$\%AIS1 = 100/[(1+\exp(1.54+(200/hic)-.00650*hic))-(1+\exp(2.49+(200/hic)-.00483*hic))];$$
$$\%AIS2 = 100/[(1+\exp(2.49+(200/hic)-.00483*hic))-(1+\exp(3.39+(200/hic)-.00372*hic))];$$
$$\%AIS3 = 100/[(1+\exp(3.39+(200/hic)-.00372*hic))-(1+\exp(4.90+(200/hic)-.00351*hic))];$$
$$\%AIS4 = 100/[(1+\exp(4.90+(200/hic)-.00351*hic))-(1+\exp(7.82+(200/hic)-.00429*hic))];$$
$$\%AIS5 = 100/[(1+\exp(7.82+(200/hic)-.00429*hic))-(1+\exp(12.24+(200/hic)-.00565*hic))];$$
$$\%AIS6 = 100/[(1+\exp(12.24+(200/hic)-.00565*hic))];$$
$$\%AIS0 = [100-(\%AIS1+\%AIS2+\%AIS3+\%AIS4+\%AIS5+\%AIS6)]$$

where %AIS1, 2, 3, etc. are the projected probabilities, in percent, of head or face injury occurrence at shown AIS severities. The graphical representation of these relationships is shown in Figure 2.

Figure 2:
Relationship Between HIC and Injury Risk

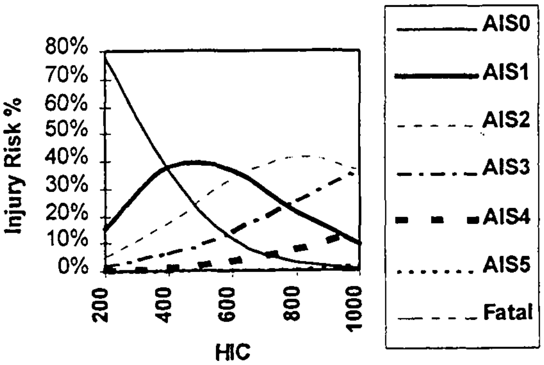

In addition to the reduction of head and face injuries originating from interior contacts, injuries to any body region due to exterior contacts are all but eliminated. Earlier studies indicated an 80% reduction in injuries was attributed to occupant containment within the vehicle (Malliaris, 1985). The mechanism in effect in this case is the HPS prevention of ejection for qualified occupants. BMW studies of accident data indicate that 30% of rollovers have a lateral acceleration of sufficient magnitude to deploy the HPS.

INJURY OUTCOME

The principal benefit of the HPS is to mitigate head and facial injuries. In instances where ejection is not involved, the HPS is assumed to have no influence on mitigating injuries to other body regions. However, for occupants with multiple injuries, the reduction of any of the most severe injuries reduces the risk of death and impairment.

The benefits analysis to follow addresses injury outcomes at three categories - Category 1, *Individual Injuries*; Category 2, *Most Severe Injuries*; and Category 3, *Fatalities.*

Most injured occupants suffer multiple injuries. On average, injured occupants in NASS have 3.4 injuries. It should be noted that NHTSA's benefit analysis for FMVSS 201, considers only those injured occupants whose most severe injury is a head or face injury. No benefits are assigned to reducing head and face injuries present. Consequently, many of the head and face injuries reduced by the countermeasure are not considered. The Category 1, *individual injury*, benefits considers all relative injuries, without regard to the outcome of the injured occupant. This approach may over count the benefits, since a sall number of the injured occupants may die from injuries to body regions which are not influenced by the HPS.

For Category 1, *individual injury*, benefits the appropriate NASS records of crash exposed car occupants are addressed for each injury as implied by configuration, injuring contact, and injury severity. A computer algorithm is applied which incorporates the abatement schedule containing categorical information about: (a) the HPS effectiveness in reducing injury severity based on HIC reduction; (b) applicability limits; and (c) side effects. The first pass is made assuming no HPS action. Subsequently, a second pass is made assuming full HPS action under the conditions and exceptions discussed earlier. Thus are obtained the projected injury reduction benefits offered by an HPS application, and the percent effectiveness of this application, defined as: (before-after)/before.

The Category 2, *most severe injury*, benefits examines the outcomes of injured survivors, by the AIS level of their most severe injury (MAIS). Injury reduction is applied only if the mitigated injury is the most severe injury. This approach under counts the benefits, because reductions in impairment from head injury may not be counted when the head injury is not the most severe injury.

The relatively simple procedure described for evaluating the reduction of individual injuries is not applicable in the evaluation of outcomes, as an occupant's outcome is not the result of a single injury. Rather, it is the collective effect of all injuries incurred by this occupant.

For each injured survivor, the entire set of an occupant's up to 45 injuries is addressed. Each occupant's maximum injury severity and the corresponding classification attributes (injuring contact, injured body region etc.) are determined before, as well as after an abatement schedule has been applied.

An occupant's classification by most severe injury is subject to a further control, namely: no abatement of an applicable injury, e.g. head or face injury by upper interior car component, is registered when there is one or more non-applicable injuries of equal severity for the same occupant.

Thus, counts of occupants by most severe injury, (both before and after abatement application) in conjunction with other injury attributes become the basis for the most straightforward evaluation of outcomes for injured survivors.

The Category 3, *fatality*, benefits are based on fatality risk reductions associated with reducing individual head and face injuries. The procedure followed in the estimation of fatalities, either before or after the application of an abatement schedule, is based on the assignment of a fatality probability for each occupant in the crash records, based on the severities of the three most severe injuries of this occupant, and the occupant's age, irrespective of any other injury attributes.

The fatality probability in question is obtained from and calibrated by all available crash involved car occupant records. For this purpose a logistic regression is applied that models successfully the probability of fatality as a function of the injury severities of an occupant's three most severe injuries, and the occupant's age. With the help of this information a fatality probability is assigned to each and every occupant in the pertinent crash records. The fatality risk is assessed first before and then after application of the instructions provided by the abatement schedule under consideration.

Occupants that have none of their three most severe injuries eliminated or abated, show up with the same fatality probability both before and after application of the abatement schedule. Occupants with injuries that qualify for abatement, show up in the after abatement records with a fatality probability that is reduced with respect to that before abatement.

The sum of all occupants on record, either before or after abatement, with each occupant weighted by the corresponding probability of fatality, is the number of projected fatalities, either before or after abatement. Note that the fatality probability as a weighing factor is applied over and above the familiar inflationary weight, used to derive national estimates from the NASS samples.

This accounting method offers, among other advantages, estimation of fatality reduction, and automated accounting of injuries and injured occupants. At the same time the applied approach prevents double counting of potential benefits, irrespective of abatement schedule complexity.

SUMMARY OF RESULTS

The results of the Category 1, *individual injury* benefits analysis are summarized in Table 2. The annual reduction of AIS 2+ head and face injuries is 6502, with an effectiveness of relevant contacts equal to 34%. The annual reduction of AIS 3+ injuries is 3015, with an effectiveness of relevant contacts equal to 49%.

Table 2
Annual Incidence of Head and Facial Injuries Before and After HPS - Occupants not Ejected

AIS	Before HPS	After HPS	HPS Benefit	% Reduction
6	70	30	40	57%
5	1148	567	581	51%
4	1597	886	711	45%
3	3381	1698	1683	50%
2	12941	9454	3487	27%
2+	19137	12635	6502	34%
3+	6196	3181	3015	49%

In addition, to the head injury reduction, there are injury reductions to all body regions for occupants who are prevented from ejection through side windows by the deployed HPS. The results are summarized in Table 3. The AIS 2+ injury reduction is 1999, with an effectiveness of 32%. For AIS 3+ injuries, the reduction is 887 for an effectiveness of 35%.

Table 3
Annual Incidence of Ejection Injuries With and Without HPS

AIS	Before HPS	After HPS	HPS Benefit	% Reduction
6	129	90	39	30%
5	272	121	151	56%
4	469	302	167	36%
3	1630	1100	530	33%
2	3754	2642	1112	30%
2+	6254	4255	1999	32%
3+	2500	1613	887	35%

The results of the Category 2, *most severe injury*, benefits analysis for non-ejected occupants is summarized in Table 4. This analysis applies the Category 1 injury reductions to each injured survivor in the NASS file, and reduces the maximum AIS (MAIS) for the survivor only when the mitigated injury is their most severe injury.

Table 4
Annual Incidence of Injured Survivors by Max. Injury Severity (MAIS) With and Without HPS for Target Population -Occupants not Ejected

MAIS	Before HPS	After HPS	HPS Benefit	% Reduction
5	432	251	181	42%
4	151	95	56	37%
3	1295	1054	241	19%
2	9812	7855	1957	20%
2+	11690	9255	2435	21%
3+	1878	1400	478	25%

The reductions Category 2, *most severe injury*, by HPS ejection prevention are shown in Table 5.

Table 5
Annual Incidence of Injured Survivors by Max. Injury Severity (MAIS) With and Without HPS for Ejected Population

MAIS	Before HPS	After HPS	HPS Benefit	% Reduction
5	51	12	39	76%
4	56	46	10	18%
3	271	238	33	12%
2	990	909	81	8%
2+	1368	1205	163	12%
3+	378	296	82	22%

The results of the Category 3 (fatality) benefits analysis is summarized in Table 6. This analysis applies the Category 1 injury reductions to each fatally injured occupant in the NASS file, and reduces the fatality risk for those injuries mitigated by the HPS.

Table 6
Annual Incidence of Fatalities With and Without HPS by Shown Target Population

Fatalities	Before HPS	After HPS	HPS Benefit	% Reduction
Non Ejection	1858	1166	692	37%
Ejection	1695	1043	652	38%
Total	3553	2209	1344	38%

A summary table of the total benefits of HPS is shown in Table 7.

Table 7
Summary of Injury and Fatality Reductions by HPS

Totals	Before HPS	After HPS	HPS Benefit	% Reduction
AIS 3+ Injuries	8696	4794	3902	45%
AIS 2+ Injuries	25391	16890	8501	33%
MAIS 3+ Injuries	2256	1696	560	25%
MAIS 2+ Injuries	13058	10460	2598	33%
Fatalities	3553	2209	1344	38%

When examined by crash mode, 23% of the fatality reductions were in crashes which included rollovers. The resulting casualty reductions in rollover crashes are shown in Table 8.

Table 8
Casualty Reduction for HPS in Rollover Crashes

Casualty Class	Reductions
Fatalities	306
AIS 2-5 Injured	382

CONCLUSIONS

The test results of the HPS show dramatic reductions of head injury criteria in very severe crashes. Independent vehicle testing by IIHS demonstrated that injury measures could be drastically reduced in a pole crash which was previously considered unsurvivable. In addition, ejection prevention of the HPS in rollovers has been demonstrated by NHTSA.

Based on the available test data, and the exposure to injuries predicted by NASS/CDS 1988-96, the HPS is estimated to prevent 1,344 fatalities annually if applied to the entire passenger car fleet. In addition, 8,500 AIS 2+ injuries would be mitigated, and 2,500 AIS 2+ injured survivors would have reduced head and face injuries.

The effectiveness of the HPS is estimated at 33% in fatality reduction, 45% for AIS 3+ injuries, and 33% for AIS 2+ injuries.

The estimated HPS casualty reduction is as large as that of the recent US standards in side impact protection and upper interior head protection.

REFERENCES

Digges, K., and Malliaris, A., “Benefits Analysis of the Inflatable Tubular Structure (HPS), Report to BMW, August, 1997.

Malliaris, A., and Digges, K., "Crash Protection Offered by Safety Belts", Proceedings of the Eleventh International Conference on Experimental Safety Vehicles, p.242-252, May 1987.

Kompass K., Haberl J. and Messner G., „Field study on the potential benefit of different side airbag systems“, The 15th International Technical Conference on the Enhanced safety of vehicles, Melbourne, Australia, 1996

NHTSA, 1995, “Final Economic Assessment; FMVSS No. 201, Upper Interior Head Protection”, NHTSA Plans and Policy, June 1995

THE WINDOWBAG: AN INNOVATION IN SIDE IMPACT PROTECTION

Luigi Brambilla
Ingo Kallina
Ulrich Tschäschke
Daimler Benz AG
Sindelfingen
Germany
Paper Number 98-98-0-33

Abstract

A new additional airbag system will provide enhanced protection in side impact collisions. The so - called Window Bag will be installed in some Mercedes cars beginning with the E-Class Sedan for the MY99 and in the new S - Class.

Introduction

First of all, let us consider the global need to further improve side impact protection.

The incidence of side collisions in relationship to the total number of injuries and deaths in car crashes has clearly increased in the last years.

Looking at a summary of the type of collisions involving Mercedes -Benz vehicles with injured occupants over the last 18 years (Figure 1), the average percentage of side impacts is 21% showing an increasing tendency.

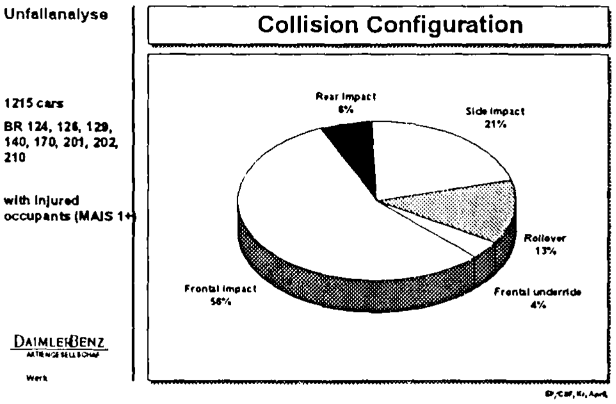

Figure 1: Types of M-B collisions

Much more dramatic is the relevance of side impacts by considering only fatal crashes for the same time period.

In this case, the percentage increase is up to 44% (Figure 2).

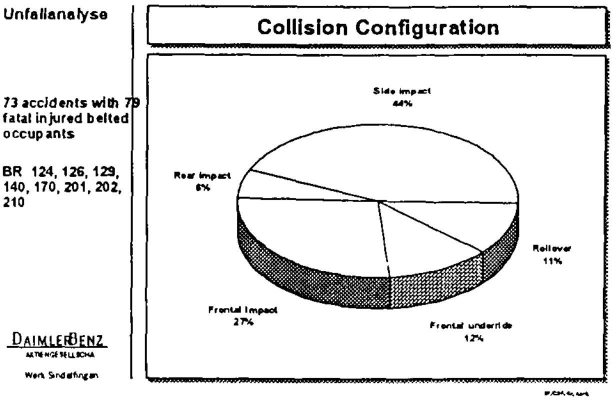

Figure 2: Collision Analysis

This development is mainly related to the improvements made for occupant protection in frontal impacts. Better car structures, restraint systems, and test methods in the last 20 years have continuously reduced the risk to be injured in head - on collisions. As a consequence the relative incidence of side crashes in terms of injuries and deaths has increased. According to this considerations, it is not surprising that car manufacturers have been working for several years on improving side impact safety.

Side impact protection systems

The Daimler-Benz Accident Research Department has shown that the most frequently occurring severe side impact injuries are to the thorax. (Figure 3).

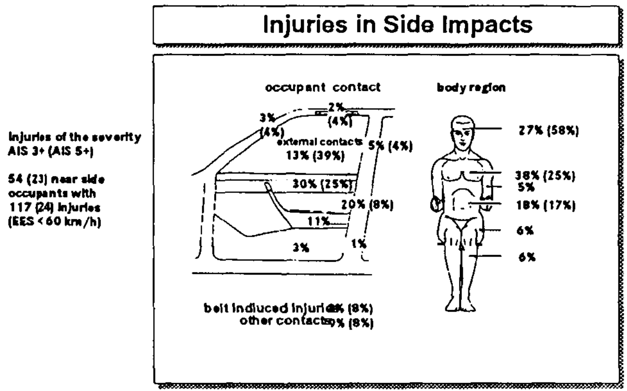

Figure 3: Frequency of side impact injuries

For this reason, Mercedes cars have been equipped beginning with the E - Class in 1995 (or MY96) with side air bags in the front doors.

Side air bags offer an additional protection to the occupant on the struck side.The structural behavior of the car, the interior door, and side wall trim all play a major role to enhance occupant safety in the variety of side impact collisions on the road.

For individuals fatally injured in side impact collisions, the head region shows the largest percentage of injury- 58%, because of the large movement of the head resulting in massive contacts with vehicle or intruding parts.

Furthermore, 48 % of side impacts involving fatalities were single vehicle collisions into a pole or tree.

To reduce the likelihood of severe or fatal injuries in these types of crashes, Daimler-Benz has developed with Autoliv Corporation a unique head protection system which we call the Window Bag.

System Description and Evaluation

The inflated Window Bag consists of a nearly two meter long, thirty-five centimeter wide and six centimeter thick cushion which is intended to protect front and rear occupants on the struck side (Figure 4).

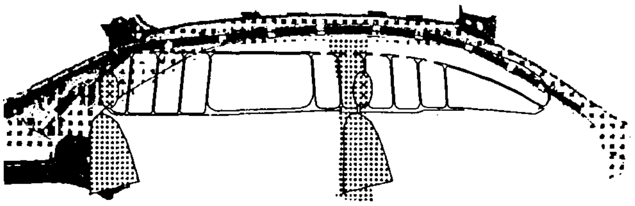

Figure 4: Windowbag

The Window Bag consists of a gas generator, a bag , a thin cover and the mounting hardware. The gas generator is a hybrid type device with 3 grams of composite generant and pressurized argon gas at 300 bar. The air bag is woven as one piece and is made of polyamide fabric with a silicon coating.

The Window Bag is fixed to the A - pillar, the side roof frame, and the C - pillar and is hidden under the corresponding interior trim.

The gas generator is mounted to the C - pillar and is directly connected to the air bag.

Furthermore, the air bag is divided into 9 vertical chambers and when fully deployed covers an occupant's potential contact area with the side of the vehicle. The total overall volume of the Window Bag is twelve liters.

The folded bag is like a flexible tube inside of a thin polyamide cover which includes the gas generator and mounting hardware, and is delivered ready to mount. Plastic mounting clips and brackets allow the air bag unit to be fixed to the car roof and pillars, and also insures a controlled and quick positioning of the Window Bag.

The complete module weighs 1.3 kilograms.

Function and performance

In the case of a side collision where the sensing threshold is reached, the window and side air bags are activated at the same time by an electronic control unit. The control unit measures lateral as well as longitudinal car decelerations and is the same device that activates the driver and passenger air bags in a frontal impact. To quickly sense a side collision, the central unit is assisted by additional deceleration sensing devices on both sides of the car.

After activation the Window Bag inflates along the side wall coming out of the roof trim and expands like a curtain in front of the side windows. The unique design of the gas flow optimally positions and tightens the Window Bag between the A- and the C-pillars in an inflation time of approximately 25 ms at ambient temperature.

The Window Bag's internal pressure has a mean pressure of 1.5 bar.

Out - of - position tests show no additional risk of injury due to the inflating Window Bag's deployment velocity of 50 km/h.

To validate the system efficiency and to optimize the performance, computer programs were run in collaboration with the system supplier. The results, as expected from the collision analysis, clearly showed the most critical case is a side impact of the car into a pole (Figure 5).

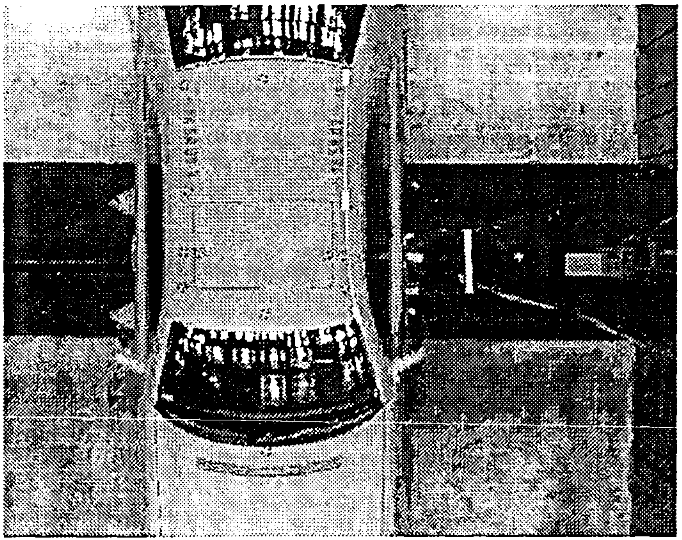

Figure 5, Car to pole crash

Therefore, hardware validation for a car - to - pole crash was conducted first with body in white, and finally with complete cars at an impact speed of about thirty kilometers per hour. The contact area of the pole was aimed at an occupant's head for tests in both the front and in the rear. The pole diameter measured 254 millimeters.

Without the Window Bag, there was massive contact between the head and the intruding pole for the driver, and between the rear passenger's head and the intruding rear car structure. The HIC exceeds 4000 in the front (Figure 6).

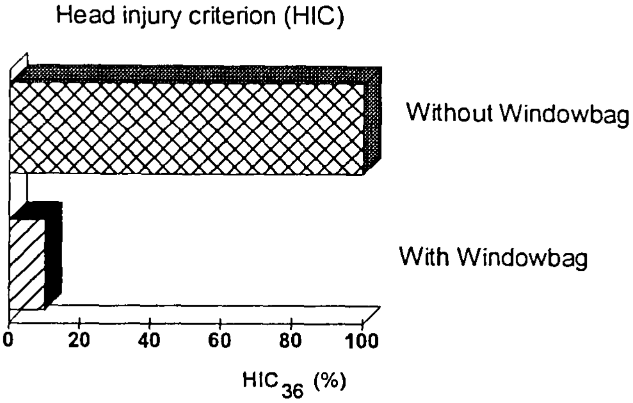

Figure 6: Head Injury Criterion

The Window Bag is able to help avoid severe direct contacts and reduces the HIC values well below the limit of one thousand.

Additionally according to recent studies conducted by Bohmen et al, a device like the Window Bag can also reduce peak angular velocity and acceleration of the head which may contribute to a reduction in brain injuries.

Conclusion

The goal to offer additional protection for the head in side collisions for a front and rear car occupant is fully reached with the introduction of the Window Bag.

This efficiency in reducing injury potential is especially demonstrated in car - to - pole or tree collisions, which according to the Daimler Benz crash statistic causes nearly 50% of the fatalities in side impact collisions.

Due to the large Window Bags's surface, we also expect better protection against contact within the car's interior, the windows, as well as against intruding objects and broken glass independing of occupant size and seating position.

Out - of - position tests did not indicate risk from the inflating Window Bag.

The Window Bag is already recognized as a complement to the additional padding which is necessary to fullfill the FMVSS 201 head impact requirement. For the contact area covered by the Window Bag, a reduced impact speed of 12mph is allowed instead of 19mph.

However, additional protection is also expected in oblique collisions or in rollovers which could occur after a side impact, thereby reducing the risk of head ejection.

Considering that the Window Bag has a great potential to also improve the occupant protection in rollovers, this device is a promising additional inflatable system for overall increased protection in car crashes.

References

Bohman Katarina, Haland Yngve
Autoliv Research
Sweden

Aldman Bertil
Chalmers University of Technology
Sweden

REDUCTION OF HEAD ROTATIONAL MOTIONS IN SIDE IMPACTS DUE TO THE INFLATABLE CURTAIN - A WAY TO BRING DOWN THE RISK OF DIFFUSE BRAIN INJURY

Paper Number 98-S8-O-07

UPPER INTERIOR HEAD, FACE AND NECK INJURY EXPERIMENTS

Donald Friedman
Keith Friedman
Friedman Research
United States
Paper Number 98-S8-P-11

ABSTRACT

Head, face and neck (HFN) injuries associated with upper interior contacts account for a large percentage of all serious to fatal injuries annually. In the past, many of these injuries were the result of unrestrained occupants in rollovers and side impacts. Mandatory belt use laws have helped keep the head and torso inside the vehicle, but HFN injuries in side and rollover accidents persist. Regulatory actions for side and rollover protection deal with torso injuries but head injuries have been addressed only by upper interior padding.

Rollovers have been characterized as violent events and roof crush as the natural consequence of such violence. The original claims were based in part on the "Malibu" experiments, which suggested that head and neck injuries for occupants are unavoidable even with improved roof strength and the use of production restraints.

An analytical effort to understand rollover injuries, using the field accident data of the NASS files and residual headroom as an indicator, was reported by the authors at the 1996 ESV conference in Melbourne, Australia. This work led to a revised theory of rollover head, face and neck (HFN) injury mechanisms and their relationship to, for example, roof crush, headroom, restraint excursion, padding, glazing and vehicle geometry. In an effort to investigate both the original claims and the revised theory, some additional analyses were conducted and a series of experiments were devised.

This paper briefly summarizes the previous work, describes further analyses and experimentally identifies the low crash severity, roof crush, padding and restraint relationship to HFN injury, through physical, computer, and volunteer occupant tests.

The conclusion is that a causal relationship exists between HFN injury and occupant protection system design and performance (including, for example, roof intrusion, vehicle geometry, headroom, restraint excursion, glazing, upper interior padding in combination).

INTRODUCTION

During the sixties and early seventies, the Government and most manufacturers assumed that there was a causal relationship between roof crush, accident and HFN injury severity. [1 2 3]

From the early seventies (when less than 15% of the occupants were using belts), rollover accident investigation researchers confirmed a relationship between roof crush, accident impact severity and occupant HFN injury severity; however, the researchers were inconclusive about whether the injury was a result of the impact severity or the associated roof crush.

Mackay (1970): - [The increased injury associated with increased roof crush] "does not necessarily mean that the roof collapse was the immediate cause of the increased injury; it may be that large amounts of roof collapse are an indication of large collision forces which would have led to serious injury anyway." [4]

The studies of Huelke (1973) showed that, "although roof crush is not necessarily the injury-producing mechanism in rollover accidents, there is a correlation between the amount of roof crush and the severity of injury. This seemingly contradictory finding is explained by the fact that the amount of roof crush is indicative of the impact severity, but the two are not causally related." [5]

Moffatt, (1975) wrote, "If the occupant in these illustrations had suffered neck or head injury, one might be tempted to conclude that the damage caused the injury, and overlook the true mechanics which show that the impact caused the injury and the impact caused the damage, but it was not the damage which caused the injury." [6]

Melvin (1982) wrote "Thus a severe rollover event may produce a severe roof/ground contact, and a severe occupant/roof contact, with the result that both roof intrusion and occupant injuries have occurred but are not directly related." [7]

Strother and Warner then in 1984 carried the point one step further. They pointed out that in side and rollover accidents, it was the occupant's contact velocity with the intrusion that produced the injury, not the change in velocity as in restrained frontal impacts. [8]

In 1985 a summary of 8 unrestrained rollover tests with neck instrumented Hybrid III dummies were interpreted to show "... that roof strength is not an important factor in the mechanics of head/neck injuries in rollovers for unrestrained occupants." In 1990 a similar summary of restrained occupant rollovers and drop tests were published with similar conclusions. These studies are used to demonstrate the apparent violence of rollovers and describe the frequency and mechanism of catastrophic injury to the Hybrid III dummy neck and head in production and rollcaged 1983 Malibu cars. They suggest that such injuries are inevitable and that neither stronger roofs nor restraints will do any good. In 1995 police accident data (which mis-characterizes serious injury) was analyzed in an attempt to validate the experiments and suggest that the conclusions apply to human victims of rollover accidents.[9,10,11]

By reviewing the data on which the interpretation of results was based, the current authors published a series of papers from 1990 to 1995 refuting and casting doubt on the validity of those conclusions. In the process the authors studied the relationship between roof strength and accident severity, and the relationship between roof crush and uninjured, moderate and serious to fatal HFN injury accidents for restrained and unrestrained occupants.[12,13,14,15,16]

The Malibu experiments were also defended and challenged by cadaveric experiments with regard to the biofidelity of the Hybrid III neck for spinal trauma assessment.[17,18,19,20,21,22] Volunteer experiments indicate that the way the human head and neck is held and oriented during impact is quite different than the neck alignment provided by the Hybrid III dummy neck.

In 1995 NHTSA identified negative residual headroom with the use of production restraints as a significant indicator and cause of serious injury.[23]

In 1996 the authors, based on current NASS field accident data, demonstrated a causal relationship between roof crush and serious to fatal HFN injury for restrained occupants.[24] At the same time, Australian accident investigators at Monash University concluded that there is a causal relationship between roof crush and HFN injury, and NHTSA discussed their current research leading to petitioned revision in rollover testing.[25,26]

The authors and associates have recently completed and reported on a number of additional studies characterizing and quantifying the occupant protection factors leading to catastrophic injury in rollovers, including on-going volunteer drop testing.[27,28,29,30] Three additional volunteer drop test series are briefly described here, but separate papers are in preparation.

The objective of this paper is to integrate these latest human injury accident analyses, studies and experiments and supplement our previously published research into this causal relationship issue.

REVIEW OF RECENTLY PUBLISHED DATA

Malibu / Dummy Injury Causation

GM has recently released the Malibu[9,10] instrumentation traces and photographic analysis data. Using the data, the authors assert that rollover tests using the Hybrid III dummy are grossly flawed because injury measurements made on the dummy neck do not correlate with the forces that would be experienced by a human in the same circumstances. Perhaps more interesting, the dummy head would not have been near the roof, if the dummy had been positioned in accordance with the 208 positioning procedure. The Hybrid II and III dummies lack biofidelity for measuring HFN injury in rollovers where the acceleration loads are much lower than in frontal crashes. The measurements of neck compression injury taken from the dummy in those tests indicate neck injury at a rate more than two orders of magnitude greater than occurs in actual crashes. This alone calls into serious question the validity of injury measurement in these experiments.

Nonetheless, there are some useful comparisons between production and rollcaged vehicle driver data that can be made, circumventing the invalid neck data. For instance,if consistent with the field accident data, we assume that a human spine could easily absorb the 2000 newton PII's, but not the 4000 newton PII's, then there were nearly twice as many high energy contacts to unrestrained driver dummies in production vehicles than in rollcaged vehicles.

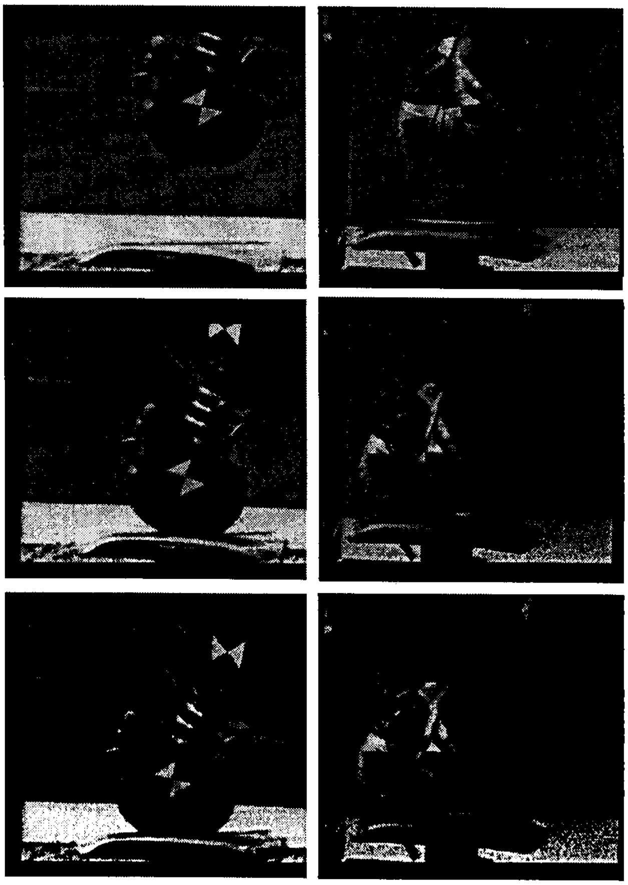

Furthermore, under a similar assumption there were one fifth as many high energy as low energy contacts to the restrained driver dummy overall, and five times as many in production vehicles than in rollcaged vehicles.

There were only two interior head injuries in 16 tests each involving three rolls and two dummies. That is about two in 96 opportunities, both of which occurred to unrestrained dummies.

There was only one flexion injury and that was to a restrained driver in a production car with the most roof crush at a low equivalent velocity.

Assuming a serious lateral neck flexion injury measure is similar to an extension injury measure, there were 10 such injuries to the driver dummy of production vehicle and none to rollcaged vehicle dummies.

For all 10 driver neck loads that were photographically analyzed, the A-pillar/roof rail touch down occurs typically 20 to 50 milliseconds after the neck compression loading peak, as recorded by the technician.

Rollover Injury Data

National Accident Sampling System (NASS) field accident data provides the best source of statistical injury data about real world accidents. A review of that published data shows the estimated number of rollover occupants (1,900,000) and those known to have had head or neck injuries (680,000) based on NASS data for the five year period from 1988 through 1992.[26] Each year about 140,000 (36%) of all occupants are known to have received head, face or neck injuries. Of all occupants in rollovers, more than 96+ percent (96+ %) were not coded as having a serious to fatal HFN injury. Two percent (2%) were coded as having received serious to fatal head or face injuries and one percent (1%) were coded as having received serious to fatal neck injuries. The distribution by restrained or unrestrained occupants is also described.[31] Our studies recognize that the NASS coding protocol requires that a broken neck be coded as an AIS 2 if it is not further specified. Hence those AIS 2 neck injuries in which there is cord damage, neck fracture or dislocation are included in the serious to fatal grouping.

Rollover Residual Headroom Data

NHTSA researchers concluded that there was a causal relationship between restrained HFN injury and "residual headroom," which is the difference between headroom before and after the rollover. The authors' study of "residual headroom" indicates that for unrestrained occupants with upper interior contact, there seems to be little difference (-3.3 to -5.3 cm) in negative residual headroom between minor (AIS 1-2) and severe (AIS 3-6) HFN injury.

For restrained occupants, however, the difference is dramatic. For head, face and neck injuries of AIS 2 or less, the average residual headroom is around plus 3cm (+1 in). For more serious injuries, the average residual headroom is minus 13 cm. (-5 in).

Physically Validated Computer Simulations of Vehicle Rollovers, Rollover Accident Reconstruction and Drop Tests

Using this methodology we consider the relationship between accident impact severity and roof crush and identify the impact velocities which produce the intrusion.[32] The study indicates that 3 to 7 kph (2 to 4mph) is a reasonable estimate of the impact velocities to produce about 150mm (6 in) of roof crush for many on-the-road cars and light trucks from 1988 to 1992. It is also clear that most production vehicle roofs will collapse to the window sill at 10.8 kph (6.7 mph).

Volunteer Neck Injury Testing

Five series of volunteer tests have been conducted.

(1) The first series was in a roll fixture with a pre-depressed (no headroom) roof in which the restrained subject/author with 75 mm of restraint excursion was repeatedly inverted at 2 radians per second without discomfort.[32]

(2) The second series had the subject inverted and suspended by a lap belt in a drop fixture, with the head and neck in a pre-flexed (aligned) orientation touching the roof.

The fixture was then pivoted upward and repeatedly dropped from 50 to 150 mm to a concrete floor without discomfort.

(3) The third series had the authors inverted and suspended by the production door mounted restraint (and a safety lap belt) with their heads near or just touching the non-intruding roof of a 1993 Sunbird compartment, which was then dropped to hardpacked earth from about 225 mm, 500 mm and 925 mm, without discomfort.

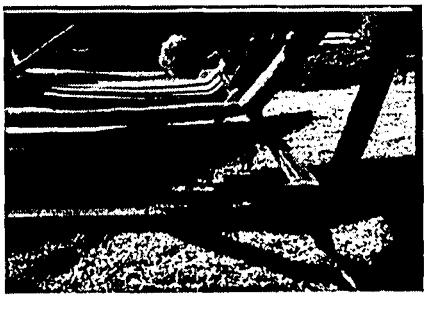

(4) The fourth series with high speed cameras, was conducted by dropping a fully instrumented Hybrid III dummy on its head to an instrumented plate, while restrained by a safety belt on an inverted controlled excursion seat in a drop fixture from 50 mm and 175 mm. The dummy neck compression loads exceeded the Malibu potentially injurious impact criteria. The tests were then repeated with an instrumented author/subject who was uninjured. The results were then compared.

(5) The fifth series also with high speed cameras, was conducted by simultaneously dropping from 300 mm to hardpacked earth, a fully instrumented Hybrid III dummy and a similarly sized author/subject, while they were restrained only by the production belts with their heads just touching the rigidized roof of a 1981 Malibu compartment. The dummy instrumentation recorded catastrophic neck injury while the 71 year old author/subject was uninjured.

HUMAN ROLLOVER INJURY CAUSATION

One aspect and perhaps the crux of the causal issue is whether such low severity rollover impacts generally cause severe HFN injuries as claimed by some researchers? [9,10] A second is, given such low severity impacts, can the occupant protection system do something about it?

The answer to the former question from the frequency and distribution of rollover head, face and neck injuries is NO! The answer to the latter question is yes. In investigated rollovers, 96% of the occupants are not coded as HFN seriously injured. Rollover occupant protection systems in which the elements are compatibly designed to prevent injurious contact are clearly available.

The answer to the former question from the residual headroom analysis is NO! The answer to the latter question is yes. The residual headroom analysis clearly shows that the injury probability for restrained occupants increases with reduction in residual headroom. The implication is that the elements of the rollover occupant protection system must be compatible in order to protect restrained occupants. Unrestrained occupant's injuries are preventable through the use of improved occupant protection system design.

On the basis of the five series of volunteer drop tests from as high as 925 mm (but without significant roof crush), the answer to the former question is NO and the latter is yes!

A fourth No answer to the former question and a yes to the latter question, resulted from analysis of the NASS files for restrained occupants and average roof crush. The table below confirms that the average roof crush for serious to fatal restrained head, face and neck injuries is greater than for those with lesser HFN injury.

Restrained Occupant Injuries	Average Roof Crush		Average Impact Velocity	
	cm	in	kph	mph
None	4.67	1.84	3.0	1.9
No Head, Face, or Neck	6.12	2.41	3.5	2.2
Head, Face and Neck @ AIS 1-2	9.80	3.86	4.5	2.8
Neck @ AIS 2-6	18.38	7.24	6.5	4.0
Head and Face @ AIS 3-6	26.69	10.51	8.5	5.3

HUMAN VOLUNTEER INJURY MECHANISM DEMONSTRATIONS

While those analyses establish that rollover roof impacts are not violent or severe events and that the impact velocities are low, we have developed a basis for explaining why, and demonstrating that the risk of neck injury is reduced with limited roof crush and or reduced belt excursion.

The first series of human volunteer [32] experiments were conducted to illustrate alternative rollover roof crush HFN injury mechanisms in a spit test device. The volunteer is restrained in a spit test machine which is pitched and can be rotated. The machine has a complex pivoted roof structure which can intrude while displacing laterally, intrude while displacing forward and backward, and intrude along a longitudinal crease over the occupant's head from a single sided lateral displacement.

The machine has been used to demonstrate the static energy absorbing, flexing capabilities of the spine with 10 cm (4 in) of roof intrusion without volunteer HFN injury. Those results have recently been extended to demonstrate 14cm (5.5 inches) of intrusion without injury. At the same time it becomes obvious that production restraints are effective in compensating for roof crush. Serious head or face injury is

demonstrated as unlikely as is neck injury, unless the roof and/or the restraint prevents the head, neck and spine from flexing.

A second demonstration mode is the mostly lateral dynamic impact and roof rail displacement with roof panel buckling. Here the roof rail scrubs the ground stopping momentarily from the traveling velocity and a roof buckle is formed and intrudes at twice the speed or more. Serious head and/or face injury is likely unless the roof rail and roof are padded. Similarly, neck or thoracic injury is likely depending on the depth of the buckling roof panel and particularly if the roof keeps the head, neck and spine from flexing.

A third demonstration mode is an impact which results in some roof crush and a rapid change in the rotational velocity. Serious head and/or face injury is likely unless the roof rail and roof are padded; however, neck injury is unlikely.

A fourth demonstration mode is the restrained volunteer dynamic drop tests in a non crushing roof compartment, with and without the head in contact with the roof. These tests correspond to the dummy drop tests conducted in conjunction with the 1985 Malibu paper but not published until 1990. They also correspond to a number of biomechanical drop test studies of unconstrained cadavers and documented studies of head/spinal impacts in sporting events with injurious and non injurious results.

HFN INJURY ROLLOVERS

The following observations provide a foundation for understanding HFN injuries in rollovers:

Most rollovers involve a number of short, low velocity impacts which incrementally scrub off the initial horizontal trip speed and support the rolling vehicle vertically. Occupant contact with the interior of a vehicle as it rolls are also typically benign. As a consequence, the vast majority of occupants in rollovers are HFN uninjured or receive only minor to moderate HFN injury.

The human skull can withstand most such impacts that occur in rollovers without major HFN injury. The remainder of the body—particularly the neck and torso—are highly flexible and resilient. Thus, they can accommodate most of the contact forces and even some intrusion in a rollover.

Rollover tests using Hybrid II and III dummies produce misleading results due to the lack of biofidelity in the flexibility of the dummies' neck and torso.

There are two primary mechanisms of HFN injury to restrained occupants from rollover, and they occur relatively independently of each other.

- Severe head injuries typically occur in rollovers where the head strikes either a rigid part of the interior (such as an unpadded roof rail) or a rigid surface outside the vehicle (such as the road) where the relative speed between the head and the roof or the road is relatively high (6 to 12 ms). This occurs in the interior as a result of roof contact causing lateral intrusion and an abrupt change in roll rate.

- Severe neck compression-flexion injuries typically occur in rollovers in which there is a substantial and rapid reduction in headroom. However, the head, neck and torso, considered as a unit, can flex and foreshorten while absorbing energy. Exceeding the spine's tolerance for such energy absorption may result in injury to the neck—the most vulnerable component of this unit—as it is bent beyond its limits. The bone and ligament structure of the neck is mechanically damaged and consequently can damage the spinal cord.

Rollovers are not inherently violent crashes: that is, the forces generated by most rollovers are within human tolerance limits. Relatively minor modifications to vehicles could substantially reduce the probability of these types of injuries to restrained occupants in rollovers.

THE EFFECT OF THESE STUDIES

Roof to ground contacts in rollovers are foreseeable but not violent events, to a restrained occupant as measured by roof strength, intrusion and/or deformation. Restrained occupant interior contacts in rollovers are in general so low in speed, and so low in force on the head, neck or torso, that the natural compliance of the body resists injury. Catastrophic injury only occurs when the occupant protection system design and/or one of its elements allow excessive interaction between vulnerable body parts and the interior.

Based on these experiments and analyses the claim that catastrophic injury for restrained occupants is the result of diving or torso augmentation and that roof strength or restraint excursion doesn't matter appears to be invalid.

CONCLUSIONS

There is a clear causal relationship between HFN injury and the design and performance of the rollover occupant protection system (including roof crush, vehicle geometry, headroom, restraint excursion, retained side glazing and padding functioning in combination).

REFERENCES

---

[1] *GM's Comments in Response to NPRM Roof Intrusion Standards (FMVSS 216), 1971.*

[2] *Ford Experimental Safety Vehicle, Final Report 1972, Contract No. DOT-OS-20005.*

[3] *GM Experimental Safety Vehicle, Final Report - 1972, Contract No. DOT-OS-00095.*

[4] *Mackay G.M. and Tampen, I.D., Field Studies of Rollover Performance, 1970.*

[5] *Huelke D.F., Injury Causation in Rollover Accidents, 1973.*

[6] *Moffatt E.A., "Occupant Motion in Rollover Collisions," 1975.*

[7] *Melvin, J.W., Discussion of SAE 820244, Crash Protection, SAE SP-513, 1982.*

[8] *Strother and Warner, "Injury and Intrusion in Side Impacts and Rollovers," SAE 840403, 1984.*

[9] *Orlowski K.F., Bundorf R.T., Moffatt T., and Edward A., "Rollover Crash Tests - The Influence of Roof Strength on Injury Mechanics," SAE 851734, 1985.*

[10] *Bahling G.S., Bundorf R.T., Kaspzyk G.S., Moffatt E.A., Orlowski K.F., and Stocke J.E., "Rollover and Drop Tests -- The Influence of Roof Strength on Injury Mechanics Using Belted Dummies," SAE 902314, 1990.*

[11] *Moffatt E.A. and Padmanaban J., "The Relationship Between Vehicle Roof Strength and Occupant Injury in Rollover Crash Data," October 18, 1995.*

[12] *Friedman D. and Friedman K., "Roof Collapse and the Risk of Severe Head and Neck Injury," 13th Experimental Safety Vehicle Conference, 1991.*

[13] *Friedman D., "Mitigation of Head and Neck Trauma," ASME Biomechanics of Trauma Conference, 1993.*

[14] *Friedman D, et al., "Enhanced Safety for Light Trucks and Vans," 14th Enhanced Safety Vehicle Conference, 94-S10-W-24, May 1994.*

[15] *Friedman D. and Friedman K., "The Causal Relationship in Rollover Accidents Between Vehicle Geometry, Intrusion, Padding, Restraints and Head and Neck Injury," Submitted in support of Comments to NHTSA Rollover Prevention Docket No. 91-63; Notice 03, August 16, 1994.*

[16] *Friedman D, Light Truck and Van (LTV) Rollover Safety, Appendix C attached to comments to Docket No. 91-68; Notice 03, re Rollover Prevention, August 16, 1994.*

[17] *Yoganandan N., Sances A., Maiman D., "Spinal Injuries with Vertical Impact, Mechanisms of Head and Spine Trauma," Aloray Publisher, Goshen, New York, 1986.*

[18] *Pintar, Yoganandan, Sances, Reinartz, Harris and Larson, "Kinematic and Anatomical Analysis of the Human Cervical Spinal Column Under Axial Loading," SAE 892436, 1989.*

[19] *Yoganandan N., Maiman D., Pintar FA, Sances A., "Cervical Spine Injuries from Motor Vehicle Accidents", J. Clin Eng 1990*

[20] *Nightingale R, McElhaney J, et al. The Dynamic Response of the Cervical Spine: Buckling, End Conditions and Tolerance in Compressive Impacts, SAE 973344..*

[21] *Sances A Jr., Voo LM: Biofidelity of the Hybrid III Neck for Spinal Trauma Assessment, ASME Adv. Bioeng, 1997.*

[22] *Syson S.R., "Occupant to Roof Contact: Rollovers and Drop Tests," SAE 950654, 1995.*

[23] *Glen C. Rains and Joseph N. Kanianthra, "Determination of the Significance of Roof Crush on Head and Neck Injury to Passenger Vehicle Occupants in Rollover Crashes," SAE 950655, Detroit, Michigan, February 27-March 2, 1995.*

[24] *Friedman K., et al., "Improved Vehicle Design for the Prevention of Severe Head and Neck Injuries to Restrained Occupants in Rollover Accidents," Paper Number 96-S5-O-14, ESV Conference, Melbourne, Australia, 1996.*

[25] *Rechnitzer G. and Lane J., "Rollover Crash Study — Vehicle Design and Occupant Injuries," published as a Monash Univ. report 1994, and at the 15th Technical Conference on Enhanced Safety of Vehicles, May 17, 1996.*

[26] *Summers S., Rains G.C., Wilke D.T., "Current Research in Rollover and Occupant Retention," 15th Technical Conference on Enhanced Safety of Vehicles, May 17, 1996.*

[27] *Meyer, Steven E., "The Effects of Pretensioning of 3-point Safety Belts on Occupants in Rollover Crashes," National Association of Forensic Engineers, 1997.*

[28] *Herbst, et al., "Strength Improvements to Automotive Roof Components," SAE 980209..*

[29] *Friedman, K., "Vehicle Structural Design Utilizing Optimized Finite Element Modeling," SAE 981013.*

[30] *Friedman, D., "Human Subject Experiments in Occupant Response to Rollover with Reduced Headroom," SAE 980212.*

[31] *Friedman, D., "Roof Crush Versus Occupant Injury from 1988 to 1992 NASS," SAE 980210.*

[32] *Friedman, D., "The Relationship Between Vertical Velocity and Roof Crush in Rollover Crashes," SAE 980211.*

ADVANCED DESIGNS FOR SIDE IMPACT AND ROLLOVER PROTECTION

Byron Bloch
Auto Safety Design
United States
Paper Number 98-S8-P-12

ABSTRACT

Every year in the U.S., about 8,000 fatalities occur in side impacts, and about 9,500 fatalities occur in vehicle rollovers. Severe head trauma and spinal cord injuries are the prevalent traumatic injuries that are directly related to the extent of inward crushing or intrusion into the occupant's *"survival space"* and to the rigidity and shape of interior edges and surfaces.

Based on accident evaluations and assessment of available technologies, there are feasible and practical advanced design features for vehicle bodies and interiors that can concurrently enhance both **side-impact protection and rollover roof-integrity protection:**

Strengthened vehicle body by the use of rigid-foam-filled tubular members that strengthen and stiffen the vehicle body, by tripling resistance to bending and compression. Strengthened doors with full-perimeter overlap and multiple latches. Multi-layer laminated floorpans, cross-panels, and roofs of composite materials. Roof tubular members in an interconnected design, with full-length internal stiffeners and/or rigid-foam-filled. Wrap-around stronger seats with taller headrests, and integral seatbelts and belt pre-tensioners that activate in side impacts and when rollovers are initiated. Energy-absorbent closed-cell padding of interior surfaces, some with a metal-air-gap underlayer. Side airbags for torso and head protection. Side window glass-plastic glazing and perimeter bonding, to cushion head impacts and prevent occupant ejection from the vehicle.

The main objects of these safety upgrades are to (A) encourage deflection of the striking vehicle and struck vehicle away from each other, **(B) minimize intrusion** into the occupant's "survival space", **(C) reduce the velocity differential** between the struck vehicle and the occupant kinematic movements, **(D) restrain and cushion the occupant's head and torso,** or allow contact with energy-absorbing materials to maximize distribution of contact forces.

SECTION 1:

SIDE IMPACT PROTECTION

The emphasis on upgraded side impact crashworthiness has been prompted by the 1991 amendment of the United States Federal Motor Vehicle Safety Standard 214 (FMVSS 214). Beginning in the middle to late 1990's, all new cars and vans sold in the U.S. began to phase-in various side-impact features and technology in order to meet a 33.5 MPH dynamic crash test by a deformable moving barrier (DMB), with specific injury-related thresholds applicable to front-seat and rear-seat near-side Side Impact Dummies (SID).

This paper explores the novel integration of various features and technologies that will likely be the leading candidates to upgrade side-impact crashworthiness. Rather than selecting only the *minimal* features to comply with the *minimal* requirements of FMVSS 214 and its limited crash test protocol, there should preferably be an optimal application of features to maximize or optimize side-impact crashworthiness.

These side-impact crashworthiness features include:

- ***The use of internal baffles and rigid-foam-filled tubular members to strengthen and stiffen the vehicle body.***
- ***Strengthened doors with full-perimeter overlap.***
- ***Wrap-around seats with integral seatbelt restraints.***
- ***Foam-cushion energy-absorbent padding of interior surfaces.***
- ***Side airbags for torso and head protection.***
- ***Side-window glass-plastic glazing.***

Since FMVSS 214 is a performance standard, manufacturers have opportunities to be innovative in the designs they adopt in order to comply. The creative use of new vehicle designs, new features, new technologies, new materials, and new manufacturing techniques should be encouraged. From a potential product liability viewpoint, it would be prudent to design for performance levels well above the minimums cited in FMVSS 214, and to include protection for all vehicle occupants, and for a variety of side-impact collision modes.

HISTORICAL BACKGROUND

In the modern era beginning around 1960, various features and technologies have been applied in efforts to make vehicles more crashworthy, to better protect the occupants from traumatic injury in collision accidents.

In the early 1960's, General Motors adopted the full-length *"perimeter frame"* for most of its full-size and mid-size American automobiles, noting that one main function was to protect passengers in side-impact collisions:

> *"Box-section steel members form the frame sides and extend their protective strength from end to end. These husky rails act as steel barriers at the sides of the seats to give you maximum protection all around. You ride cradled within the frame!*

The concept of safely maintaining the occupants' ***"survival space"***, and the use of restraints such as seatbelts and airbags, have been major themes adopted by virtually all automakers (usually with a prod from mandatory regulations, or in response to litigation losses). When a feasible safety technology becomes available, it often takes about twenty years or so before the majority of automakers implement that technology into their mass-produced vehicles. Airbags are such an example, since they were first implemented by GM and Ford in low-volume production (in approximately 12,000 automobiles in the 1973-76 era), then abandoned by GM and Ford.

In the early 1970's, various automakers tried to comply with the initial Experimental Safety Vehicle (ESV) requirements for all prescribed crash modes, including side impacts. Extensive use of structural side-members and cross-members were typically used in a total "cage" design to stiffen and strengthen the vehicle sides and thus help reduce penetration or intrusion into the passengers' ***"survival space".***

In 1984, a U.S. Department of Transportation edict was issued to try to induce a large percentage of states to adopt their own mandatory buckle-up laws, or else passive restraints (airbags or automatic seatbelts) would be federally mandated. Another catalyst was the U.S. government decision to purchase a few thousand cars equipped with driver-side airbags, to which Ford responded with their 1985 Tempo models becoming available with a driver's airbag option. Mercedes also began in 1985 to equip their various models with airbags as standard equipment. Thus stimulated, airbags finally came into mass-production implementation by most auto manufacturers in the early-1990's.

Presently for their 1996 models, virtually all vehicle manufacturers equip all or most of their production cars, pickups, vans, and multi-purpose vehicles with airbags, for the driver and often for the right-front pasenger.

SIDE IMPACT MEASURES STIMULATED BY FMVSS 214, LITIGATION, AND THE ESV PROGRAM

Side impact crashworthiness upgrades are now being implemented in response to the recent amendment of U.S. Federal Motor Vehicle Safety Standard 214 (FMVSS 214). Finally, FMVSS 214 requires dynamic crash testing and measured test dummy loads. A Thoracic Trauma Index (TTI) in the 85-90 g's range for rib, lower spine, and pelvis accelerations, is measured on the Side Impact Dummy (SID). This dynamic test supercedes the "slow push" minimal test which most vehicles met by installing an inner-door beam or tubular member.

Side impact fatalities account for about 32 percent of all vehicle occupant fatalities per year. NHTSA examined accident data from the 1978-1990 era, and concluded that side impacts caused an average of 7,730 fatalities per year, plus an average of 68,600 AIS 3-to-5 level injuries (serious to critical injuries) per year.

Stimulation for auto manufacturers to improve side impact measures has come from a combination of:

- The upgraded FMVSS 214, with its 33.5 MPH side-impact crash test, etc.
- Incentives from product liability cases, which prompt manufacturers to try to design out potential design defects.
- Feasible improvements that have been demonstrated in the Experimental Safety Vehicle (ESV) Program, from 1971 through the present. (The ESV Program has recently been renamed as the *Enhanced* Safety Vehicle Program.)

PERIMETER AND LATERAL STRUCTURAL DESIGN TO MINIMIZE INTRUSION AND ENCOURAGE DEFLECTION

It is important to interconnect virtually all vehicle body structural members so as to efficiently distribute collision loads throughout multiple members and avoid the overload on any one or a few. Structural discontinuities such as hole cutouts, notches, dimpling, overlaps, and spotweld spacing patterns should be minimized to avoid weak zones that would tend to buckle when collision stresses are directly or indirectly applied.

The structural members must take into account the need to **encourage deflection** of the subject vehicle away from other vehicles or stationary objects, as well as to **minimize intrusion** into the subject vehicle's *"survival space"*.

The structural members must take into account the need to **encourage deflection** of the subject vehicle away from other vehicles or stationary objects, as well as to **minimize intrusion** into the subject vehicle's *"survival space"*.

One of the earlier articles about the merits of perimeter strengthening was in *"Side Impact Structures"*, part of the proceedings of the 1968 General Motors Automotive Safety Seminar. The article included the GM illustration that appears below, illustrating the desired principle of delecting one vehicle away from the other. GM's design was essentially a low-weight, high-strength steel corrugated beam that was placed horizontally about mid-way up within the door, along with reinforced structures for further support. GM introduced their inner door beam design into production cars beginning with some 1968 models.

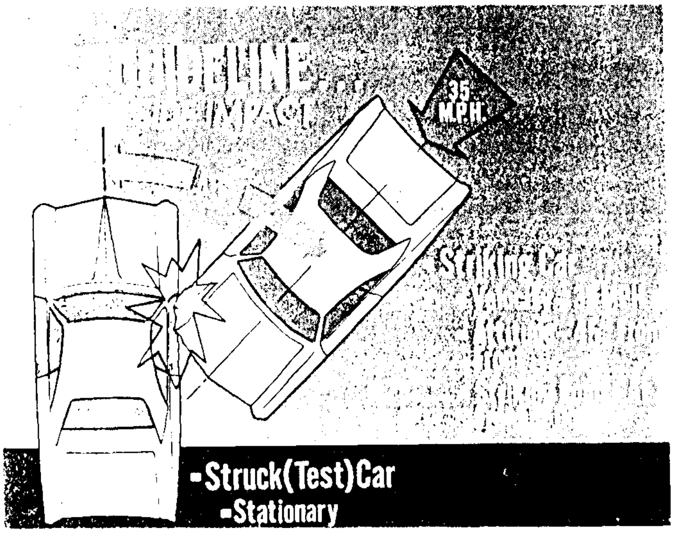

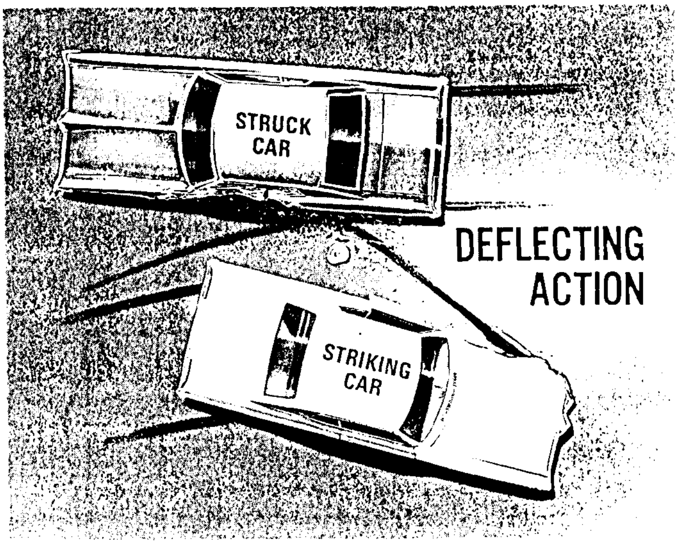

SAFETY DEFECT: A Structural "Gap" or Weak Zone

Too many passenger cars have inadequate versions of "unitized bodies", especially in their failure to include side impact protection. Many vehicles have a structural "gap" between the front and rear subframe members, causing a weakened body in the mid-region of the vehicle where the passengers are located. Thus, another striking vehicle or a tree or pole can excessively intrude directly into the passengers' *"survival space"*, rather than being deflected safely away with minimal intrusion.

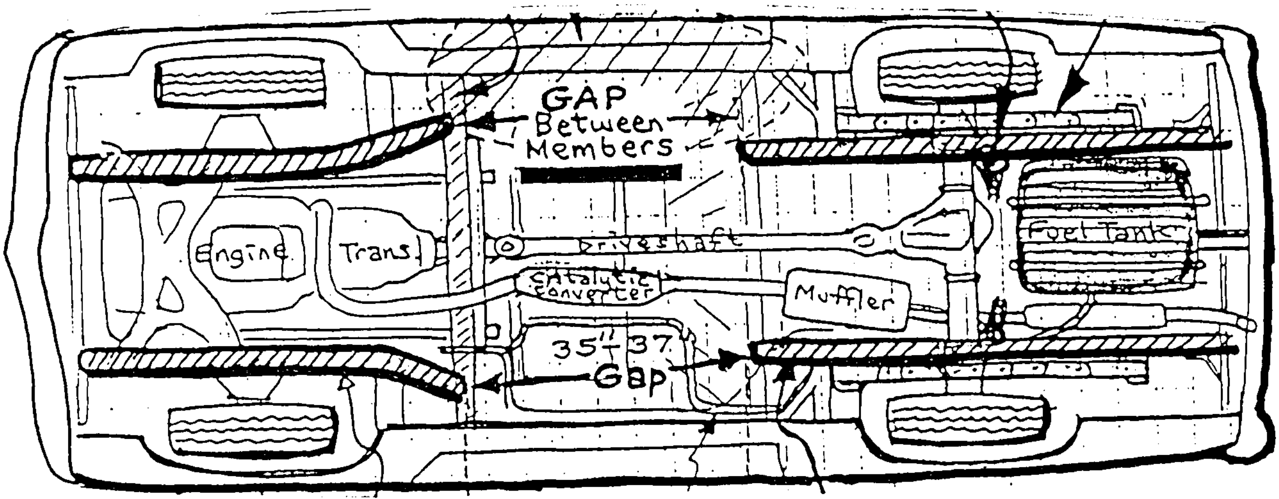
GAP
Between
Members
Engine
Trans.
Driveshaft
Catalytic Converter
Muffler
Fuel Tank
35"-37"
Gap

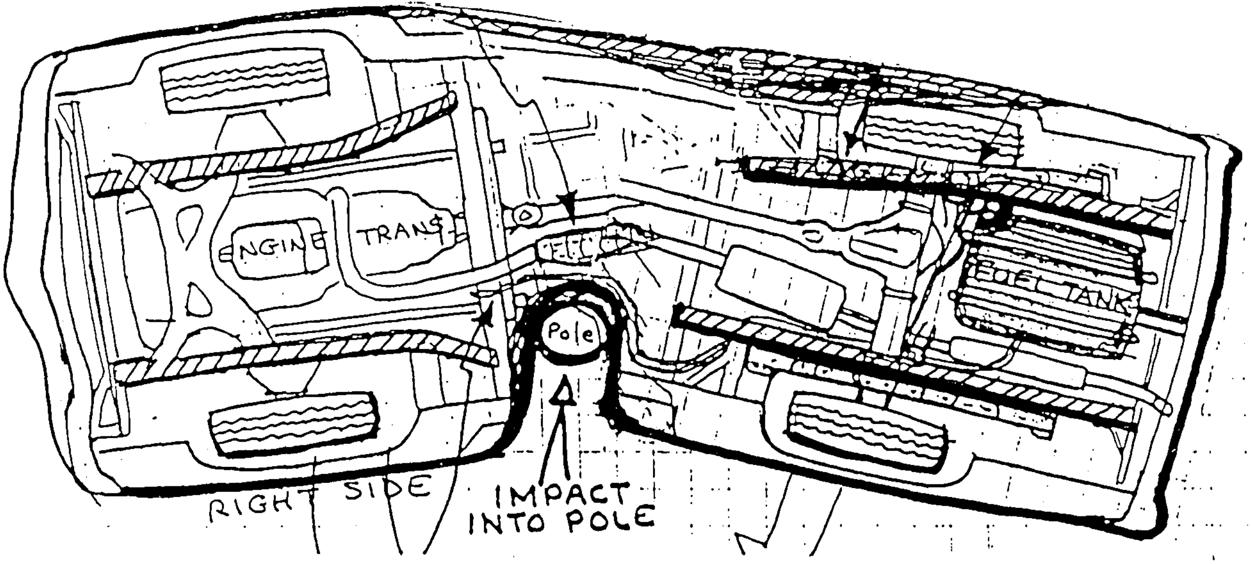
ENGINE
TRANS.
FUEL TANK
Pole
RIGHT SIDE
IMPACT
INTO POLE

Lack of side impact structure to prevent intrusion into survival space

DOORS WITH FULL-PERIMETER OVERLAP

FMVSS 214 first became effective in January 1973 as a requirement for "Side Door Strength - Passenger Cars". It required a "slow push" into the side of the vehicle door so that an inward deformation of no more than 5 inches occurred when the slowly-applied load reached one-and-a-half times the weight of the car, or 5,000 pounds, whichever was less. There was no crash test, no use of instrumented test dummies, nor any specified measure of intrusion into the passenger ***"survival space"***. Most manufacturers met this minimal requirement by adding an inner door beam, typically by a sandwich of corrugated sheetmetal panels, or a steel tube. Too often, such inner door beams were inadequately connected or "floated" within the door.

Improved door structures have typically increased the strength of the door hinges, added stronger door latches (and sometimes a second interlock pin), and strengthened the mid-body B-pillar. Some designs also ***significantly overlap the door*** over the lower rocker section, so that the bottom edge of the door could not be easily pushed inward

The upgraded version of FMVSS 214, retitled as *"Side Impact Protection"*, had a phase-in period from September 1993 (10% of an automaker's production fleet) through September 1996 (100% of the fleet) for compliance. The previous static test ("slow push") has been superceded by more stringent loads applied to the doors, to measure initial, intermediate, and peak crush resistance (not less than three and one half times the vehicle curb weight or 12,000 pounds, whichever is less), required to deform the door inwardly over the initial 6 inches, then 12 inches, then 18 inches of crush.

There is also a new dynamic test in which a deformable moving barrier impacts the side of the target vehicle at 33.5 miles per hour, to measure acceleration loads imparted to seated anthropomorphic test dummies. The basic criterion is the Thorcic Trauma Index (TTI), based on measured acceleration data from the ribs, spine, and pelvis of the test dummy. The calculated TTI shall not exceed 85 g's for 4-door passenger cars, nor 90 g's for 2-door models.

There are no required measurements or criteria in FMVSS 214 for potential head injury, potential neck/spinal injuries. Yet, severe to fatal head and neck/spinal injuries are frequently caused in side-impact collisions, when the occupant's head strikes a tree, pole, or intruding vehicle, or the interior B-pillar or roof-rail or other rigid object. Thus, there is an urgent need to amend and upgrade FMVSS 214 to include such criteria concerning potential injury to the head and neck. Such an upgraded FMVSS 214 should correlate with the new Upper Interior Impact Protection requirements for head injury protection within the recently amended FMVSS 201

INTERNAL BAFFLES AND RIGID-FOAM-FILLED TUBULAR MEMBERS: TRIPLE THE STRENGTH

Most modern-era automobile bodies are of "unitized" design, whereby strategic stampings of sheetmetal are welded into various shapes and interconnections to allow sufficient torsional strength and beam strength. The use of ***internal baffle plates***, to essentially make one larger tube into two smaller tubes by means of a full-length internal partition, adds significantly to the bending resistance and overall strength of that reinforced tubular member.

This strengthening technique can be applied to the roof pillars, roof siderails, windshield header, roof crossmembers, rocker sections, and elsewhere throughout the vehicle body structure, for both side-impact protection as well as for roof strength. These various body elements are, or should be, interconnected to each other, so as to more efficiently distribute any localized forces over a multiplicity of elements, to thereby avoid overloads that would tend to buckle or crush the individual elements. Reinforcing gussets should be used at the junctures where various elements interconnect.

General Motors, Toyota, and Renault tested hollow tubular members that were filled with a rigid polyurethane foam. The technology is basically the insertion of the polyurethane liquid within the thin-sheetmetal tubular structure, then allowing the liquid to expand and fill all voids as it hardens.

Such foam-filled members showed an increase of about three times their original bending strength and compressive strength, at a very negligible weight increase. Various models by Ford (Windstar minivan, Falcon in Australia), Toyota (Lexus LS400), Infiniti, and Nissan (Altima) have utilized such foam-filled members to increase the strength of roof support pillars.

In Australia, the Ford Falcon literature notes:

> *"Strengthened Door Pillars. The A and B pillars are reinforced with a composite material which sets like concrete, and strengthens roof construction."*
> *"Strengthened Roof Construction. Roof crush strength significantly exceeds stringent USA requirements."*

FOAM-CUSHION PADDING OF INTERIOR SURFACES

The data and observations from accident injury evaluations as well as from instrumented anthropomorphic dummies in crash tests, show that expected **traumatic injury levels can be reduced by foam padding, typically supported by yielding sheetmetal beneath the padding**. The basic goals are to distribute loads to the occupant over a broad surface area, and to cushion or lengthen the time of impact deceleration or acceleration experienced by the occupant's head, chest, or entire body. The padded instrument panel upper surfaces, the padded rear-facing backrests of front seats, and the padded knee bolster beneath the instrument panel, are examples of the merits of load-distributing and energy-absorbing padding.

The density of the foam padding, its depth, the area covered, and the underlying denser foam and sheetmetal, are all factors that affect potential injury. Too soft or too shallow a padding, and the protection is progressively reduced and minimal as the crash speeds increase. A novel type of energy-absorbing padding called *"Dynapad"* has been described as closed cells, each with an orifice or other restrictor for the entrapped air to escape as the occupant loads into the padding and compresses the cells and the air within.

Vehicle interior surfaces that need padding include the windshield pillar (A-pillar), the mid-body pillar (B-pillar), the rear window pillar (C-pillar), windshield header, rear window header, and roof siderails. Led by Saab, more vehicles have included complete padded liners for virtually the entire roof.

For enhanced side impact protection, the door itself can utilize semi-rigid foam padding, particularly at the pelvic level and at the shoulder level. Ford used an approximation of such door pads in their 1985 Mondeo-Contour-Mystique vehicles. Many automakers now use foam padding within the doors to enhance side-impact protection, particularly to reduce injuries to the pelvic and torso regions.

STRONGER WRAP-AROUND SEATS WITH INTEGRAL BELT RESTRAINTS

Wrap-around contouring of the front and rear seats can help to restrain the occupant from lateral movement, as well as to offer protection from intrusion or penetrating objects coming from the side. Such wrap-around contouring of the seat backrest would stop at about shoulder height so as not to interfere with the driver's vision to the left and right. Approximations of such contoured seats have occasionally appeared on sportier models by various automakers.

It would be advantageous to integrate the lap and torso seatbelts directly within the seat structure. Thus, the seatbelts would have a better, closer fit to the occupant, without any appreciable gaps as there are with shoulder belts that have their upper mount attached to the mid-body pillar (B-pillar). There are recent or current models from BMW, Mercedes, Chrysler (Sebring convertible, Durango SUV, Ram extended-cab pickup), and some Buick models that have such integrated seatbelts within the strengthened seat.

It is a reflection of the inadequacies of FMVSS 207 on Seating Systems, that too many seats are so weak that they cannot structurally withstand the loads of seatbelts fastened to them. FMVSS 207 requires that a static-load be slowly applied to the seat equal to 20 times the weight of the seat itself, with no dummy on the seat, nor any dynamic test, nor any crash test of the seat mounted in the vehicle. Clearly, it is long overdue the time to significantly upgrade FMVSS 207 to require a dynamic crash test with a seated anthropomorphic test dummy in each seated position of all bucket-style and bench-style seats of the subject vehicle.

The integrated seatbelts should include a **pre-tensioner** that automatically snugs or tightens both the lap and torso belts at the onset of a crash, thereby eliminating dangerous slack or looseness that can allow the occupant's torso to bypass the shoulder belt and impact the steering wheel, the windshield pillars, or other hard edges and surfaces. A belt **force-limiter** should be included to ensure that maximum tolerance belt loads are not exceeded.

The 1997 Cadillac Catera (imported from GM's European Opel operation) featured seatbelt pre-tensioners, as do most of GM's Opel and Vauxhall models in Europe. Yet, the rest of GM's domestic U.S. vehicles lag behind in implementing these more effective seatbelts. The Ford Mondeo cars in Europe have featured seatbelt pre-tensioners since their introduction back in 1994, yet their subsequent U.S. equivalent Ford Contour and Mercury Mystique models do not include seatbelt pre-tensioners.

The delay in adopting seatbelt pre-tensioners in American domestic vehicles is noteworthy and puzzling since GM and Ford had obtained patents for various versions in the 1970's and 1980's, and have been aware of their safety benefits from the ESV program and their own research for about twenty years.

It may have something to do with the tens of millions of GM and Ford cars still on the road with the so-called *"windowshade"* slack-inducing feature that causes the shoulder belts to get dangerously looser as you drive, making such seatbelts less safe and effective in a crash. How do you explain away the alleged merits of those slack-inducing *"windowshade"* seatbelts, while now promoting the safety advantages of *pre-tensioners* that automatically tighten your lap and shoulder belt at the start of a crash?

Clearly, it is important for the lap and shoulder belt to hold the occupant snugly in a side-impact collision situation, to help keep any lateral movements of the torso and head to a minimum. This is necessary for both the collision's near-side occupants as well as for the far-side occupants across the car. This will also help keep the occupants from slamming into each other.

SIDE AIRBAGS FOR TORSO AND HEAD PROTECTION

Automatically inflatable airbags have become widely accepted and utilized for frontal impact protection. Most auto manufacturers refer to airbags as being *"supplemental"* restraints to complement seatbelts, further noting that airbags afford added protection for the head and upper torso in the more severe collisons. These airbags are installed (or stored) within the center of the steering wheel, and in the right-half portion of the instrument panel.

The latest airbag application is for side impact protection. Volvo began utilizing side airbags in 1985, with the airbag installed within the outboard portion of the driver's seat and the right-front passenger's seat. Thus, the Volvo airbag protects the adjacent occupant's torso, and helps keep their head from being impacted by inward intrusion or lateral displacement. The latest Volvo design features a "side curtain" airbag system that inflates downward from the roo-rail, to offer instantaneous protection for the front seat and rear seat occupants.

BMW has recently shown their version of **airbags for side-impact protection**, including the mounting of one airbag within the upper door structure and another tubular-shaped airbag that inflates to offer protection from the windshield pillar to the mid-body pillar. Thus, this second or upper airbag more directly protects the head of the adjacent occupant.

Various side-impact airbags from Volvo, BMW, Mercedes, and Ford show alternatives for mounting the airbag... within the outboard portion of the front seat, or within the door just below the window level, or along the roof siderail (essentailly between the windshield pillar and the mid-body pillar).

The BMW design, first implemented in some of its 1997 models, is especially meritorious in having an upper-level tubular-shaped airbag that protects the head of the driver and right-front passenger. The front anchorage is at the windshield pillar, and the rear anchorage is at the top of the B-pillar. Once inflated, this head-protecting side airbag commendably stays inflated for a prolonged interval to help continue its effectiveness throughout what could be a more complex accident scenario.

It is apparent from crash testing demonstrations and from actual accidents involving Volvo's equipped with side airbags, that reasonable levels of injury reduction can be attained with side impact airbags. The technology is now available to have side impact airbags inflate within 20-to-30 milliseconds of the onset of a side impact to the subject vehicle. There are various storage cavities for the airbags that can be available by feasible redesign of the the seat, the door, or the roofrail. The crash sensors and gas generators have response and actuation times to ensure airbag inflation in sufficient time (e.g., within about 10-to-20 milliseconds).

Side impact airbags for front seat (and also rear seat) occupants are feasible in various designs.... as inflatable protective cushions for the pelvic, torso and/or head regions, as supplemental to lap and torso seatbelts, which may have to be integrated within the front seat (rather than attached to the mid-body pillar) so as to not interfere with the inflating aide-impact airbags.

SIDE-WINDOW GLASS-PLASTIC GLAZING

In a side-impact collision, the tempered side window glass typically shatters or disintegrates into hundreds or thousands of small pebbles. The side window tempered glass is a single sheet, rather than a three-layer sandwich of glass/plastic/glass like the front windshield. Thus, the side window glass does not have any plastic interlayer such as high-penetration-resistant (HPR) butyl plastic to absorb the impact forces of the occupant's head striking it.

In the course of a side-impact collision accident, the easily-shattered side window tempered glass also thereby exposes the occupant's head into being directly impacted by the intruding or striking vehicle.

Among the pioneering advocates for side window glass-plastic glazing was Carl Clarke, who helped demonstrate its merits in a series of comparative crash tests (for both side window and rear window applications). Head injury levels were reduced, as was occupant ejection.

SIDE IMPACT - CONCLUSION

In their efforts to comply with the newly upgraded FMVSS 214 and its dynamic crash test, some automakers will likely utilize stronger side impact structures (door beams, lateral stiffeners in the cowl and floorpan, etc.), semi-rigid or rigid foam blocks strategically located within the doors and pillars, plus a mix of interior energy-absorbing foam padding.

Some manufacturers are obviously going beyond the minimal requirements, such as those that are including side airbags, at the torso level. The latest systems also include a separate side airbag that is critically located at the head level for the driver and passenger.

Rather than settle for compliance with the *minimal* requirements of FMVSS 214, the automakers' efforts should focus on a more comprehensive goal... to ***maximize*** side impact protection for all vehicle occupants, in a ***variety*** of side impact collision modes, and at speeds higher than the prescribed 33.5 MPH.

As demonstrated since the early-1970's in the *Experimental Safety Vehicle (ESV) Program*... now the *Enhanced Safety Vehicle Program*... many automakers have demonstrated feasible means to achieve excellent crashworthiness and occupant protection in 50 mph side impacts. That level of performance, or even higher, should be implemented as each new vehicle is designed and mass produced.

SECTION 2:

ROOF CRUSH IN ROLLOVERS

Every year in the U.S., about 9,500 fatalities occur in vehicle rollovers. Severe head trauma and spinal cord injuries are the prevalent AIS-4/5/6 injuries, and are directly related to the extent of inward and downward crushing or intrusion into the occupant's *"survival space"* and to the rigidity and shape of interior edges and surfaces.

Based on accident evaluations and assessment of available technologies, there are many needless defects and deficiencies in the roof structures of many vehicles. I have personally inspected and evaluated a variety of cars, pickups, and vans that had been involved in rollover accidents. Despite whatever vehicle miscontrol or collision had initiated the rollover, there was extensive buckling and crushing down of the roof. The occupants had often incurred severe to fatal injuries, including severe brain trauma, quadriplegia, and paraplegia.

ROOF STRUCTURE DESIGN DEFECTS

When I personally inspected the accident vehicle's roof structure, I often noted the extensive intrusion into the occupants' "survival space", with the roof having buckled and crushed downward and laterally. The vehicle's upper body and roof strength is essentially a function of the strength and rigidity of the roof pillars and crossmembers and how they all interconnect. Yet, I observed that too many of these vehicles had needless compromises that weakened the integrity of the roof structure.

The windshield pillar (A-pillar) was a thin sheetmetal tube, with either an abbreviated too-short internal reinforcement baffle, or none at all. The mid-body pillar (B-pillar) and rear window pillar (C-pillar) were only moderately reinforced with partial internal baffles, if at all.

In contemporary vehicle design, the windshield pillars are swept back rearward and also angled laterally inward. Such a severe leaning angle reduces the ability of the windshield pillar to support the roof, and thus requires a stronger, stiffer, reinforced pillar with even more reliance on its interconnection to other roof members to better distribute the loads encountered in a rollover accident.

The windshield header (across the top of the windshield), the rear window header, and roof sidemember (along the outboard sides of the roof) were often an "open C" in cross-section, rather than a "closed O" in cross-section. Structurally, a closed tubular section is much stiffer and stronger than an open semi-tubular section.

Further aggravating the roof integrity situation are designs that include too many holes, cutouts, notches, dimples, creases, and other discontinuities... plus a minimal number of widely spaced spotwelds, often poorly located along minimal flanges. Because of these needless design defects, the roof is structurally pre-disposed to buckle and collapse.

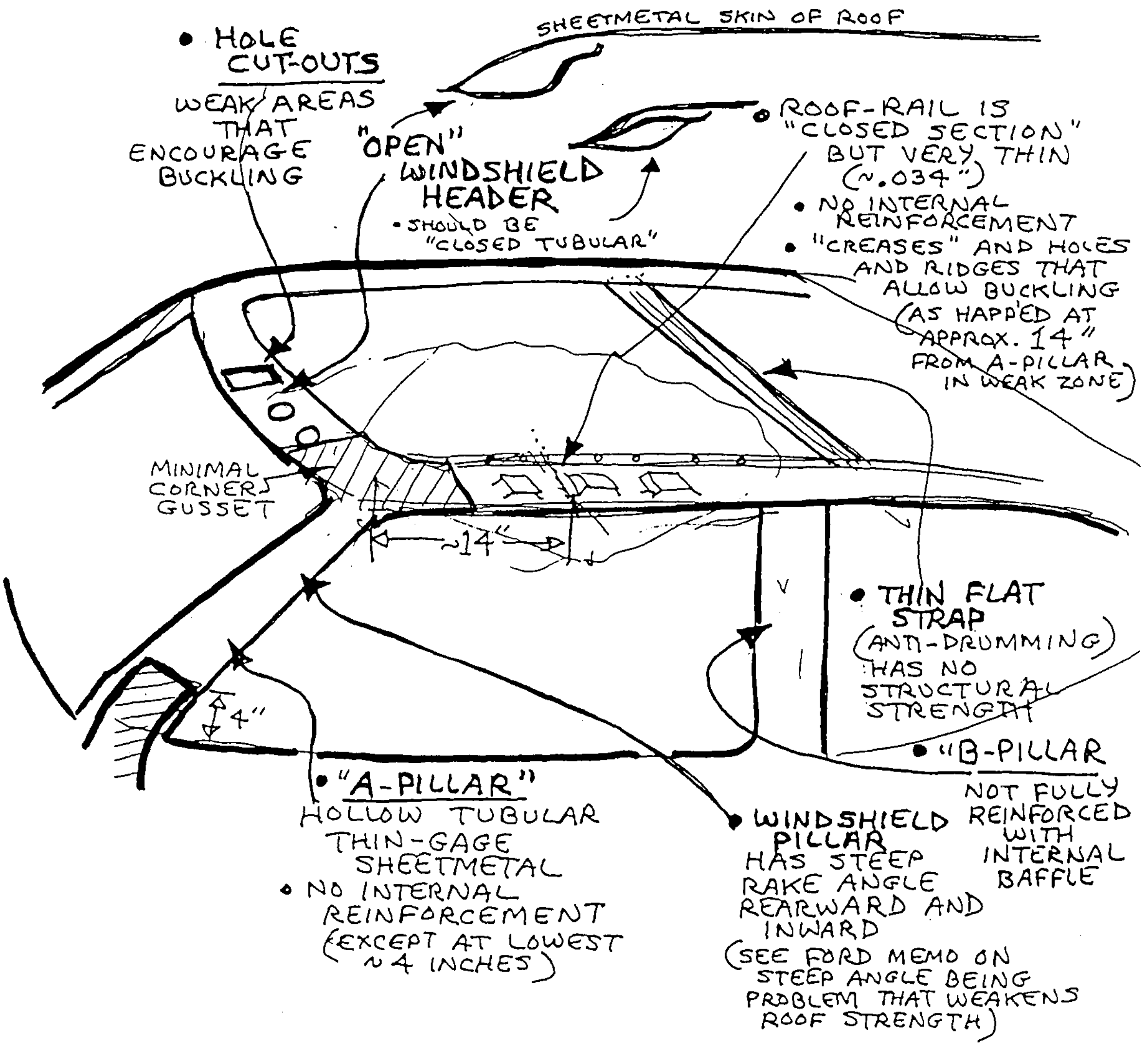
SHEETMETAL SKIN OF ROOF
• HOLE CUT-OUTS
WEAK AREAS THAT ENCOURAGE BUCKLING
"OPEN" WINDSHIELD HEADER
• SHOULD BE "CLOSED TUBULAR"
• ROOF-RAIL IS "CLOSED SECTION" BUT VERY THIN (~.034")
• NO INTERNAL REINFORCEMENT
• "CREASES" AND HOLES AND RIDGES THAT ALLOW BUCKLING (AS HAPP'ED AT APPROX. 14" FROM A-PILLAR IN WEAK ZONE)
MINIMAL CORNERS GUSSET
~14"
4"
• THIN FLAT STRAP (ANTI-DRUMMING) HAS NO STRUCTURAL STRENGTH
• "B-PILLAR NOT FULLY REINFORCED WITH INTERNAL BAFFLE
• "A-PILLAR" HOLLOW TUBULAR THIN-GAGE SHEETMETAL
• NO INTERNAL REINFORCEMENT (EXCEPT AT LOWEST ~4 INCHES)
• WINDSHIELD PILLAR HAS STEEP RAKE ANGLE REARWARD AND INWARD (SEE FORD MEMO ON STEEP ANGLE BEING PROBLEM THAT WEAKENS ROOF STRENGTH)

There is often also minimal interconnection and reinforcement of the roof structure elements. Too many vehicles have only a thin sheetmetal flat strap from B-pillar to B-pillar, serving only as a minimal pseudo stiffener to keep the broad sheetmetal from undulating as the wind rushes across it at highway speeds. Preferably, there should instead be a closed-section rectangular tube structure laterally across the roof from the top of one B-pillar to the other B-pillar. Where the various pillars interconnect with the windshield header and roof siderails, there should also be reinforcing gussets.

FMVSS 216 - ROOF CRUSH RESISTANCE

The U.S. Federal Motor Vehicle Safety Standard (FMVSS) No. 216 is entitled "Roof Crush Resistance - Passenger Cars", and went into effect in August 1973. The purpose of FMVSS 216 is "to reduce the liklihood of roof collapse in a rollover accident" and futher notes that "available data have shown that for non-ejected front seat occupants in rollover accidents, serious injuries are more frequent when the roof collapses."

FMVSS 216 prescribes only a minimal compliance test, which requires a slowly applied load be applied on a slight angle to the front upper corner of the car's roof... and that the test device shall not move more than 5 inches (downward) with an applied force of one and one-half times the vehicle weight, or 5,000 pounds, whichever is less. There is no dynamic vehicle rollover crash test, nor any use of an instrumented anthropomorphic test dummy.

FMVSS 216 was supposed to be initially just a temporary alternative until August 1977, when it would be supeceded by the dynamic rollover crash test required as part of FMVSS 208, entitled "Occupant Crash Protection". The dynamic rollover crash test required the complete vehicle (tilted at 23 degrees), on a moving dolly or sled, to be propelled laterally along a track at 30 miles per hour. The test vehicle would then be released or catapulted off the sled, and it would then laterally roll multiple times on the pavement. With a front seat anthropomorphic test dummy, this dynamic rollover test more closely simulated real-world rollover accidents than does that FMVSS 216 "slow push" to a portion of the roof.

Of interest, virtually all European automakers, including GM-Europe and Ford-Europe, have long conducted and continuously still conduct such dynamic rollover tests per FMVSS 208, as well as the static test of FMVSS 216. U.S. automakers and most Japanese automakers have instead designed their roof structures in accordance with the FMVSS 216 requirements only.

Data from the U.S. Fatal Accident Reporting System (FARS) and elsewhere affirmed there was a strong relationship between injury severeity in rollover accidents and the extent of roof crush. A 1982 SAE Report entitled "Light Vehicle Occupant Protection - Top and Rear Structures and Interiors" by Fan and Jettner, both of NHTSA, urged that further efforts be undertaken and that "it is projected that a high safety benefit could be expected when both the roof crush resistance and the roof interior padding are upgraded simultaneously."

Since then, NHTSA established Docket No. 91-68 in 1991, for rulemaking, and has established new requirements for Upper Interior Head Protection within FMVSS 201. The 5-year phase-in begins September 1998. There is currently proposed rulemaking to expand requirements for Dynamic Head Protection Systems such as airbags.

VEHICLE ROLLOVER TESTING

Commencing in 1983, through 1990, NHTSA conducted some 24 full-scale rollover crash tests to investigate vehicle dynamics and and occupant kinematics. Various recent-vintage cars, pickups, and vans were tested, mostly in sled-propelled lateral rollovers at 30 miles per hour, with a fully-instrumented test dummy seated in the front seat. Some were restrained by the existing seatbelt, while others were unrestrained.

In their late-1991/1992 report entitled "Vehicle and Occupant Response in Rollover Crash Tests", by Obergefell, Kaleps, and Johnson, the authors note among their conclusions:

"Most of the tests resulted in significant roof crush. Often the body was trapped by the roof crush. In these cases the head/neck system was vulnerable to large loads from the roof. These loads did not always result in high head accelerations; therefore, it is important that neck loads be measured in rollover testing."

"These tests provide greatly needed data on vehicle and occupant dynamics during automobile from three different testing procedures. They demonstrated the variability of rollover results, the difficulty of controlling the test conditions, the tendency for significant roof crush, and the danger to the head and neck region of the body."

This 1983-1992 project by NHTSA again pointed out what has been clearly and repeatedly demonstrated for at least the past 27 years: that roof crush in rollover accidents can obviously cause severe head and neck injuries. The tested vehicles either had to comply with the FMVSS 216 "slow push" partial-roof test, or in the case of pickups and vans, they were even exempt from that minimal 216 test. Compliance with FMVSS 216 didn't seem to help when those same vehicles were rollover tested. Again, the point must be emphasized that it is imperative to test roof structures in dynamic rollover crash tests, with instrumented test dummies.

Historically, a 1968 Ford Motor Company memo is most revealing on this issue:

"A significant number of accidents result in roof damage."

"People are injured by roof collapse."

"It is obvious that occupants that are restrained in upright positions are more susceptible to injury from a collapsing roof than unrestrained occupants who are free to tumble about the interior of the vehicle. It seems unjust to penalize people wearing effective restraint systems by exposing them to more severe rollover injuries than they might expect with no restraints."

A SAFER ROOF STRUCTURE

The quest for a safer roof structure must include the automaker's commitment to fully demonstrate and validate the planned vehicle's injury-reduction capabilities by dynamic rollover testing with instrumented anthropomorphic test dummies.

The entire roof structure should be designed as an integrated cage structure that will maximally protect the occupants' *"survival space"* within. The appropriate place to begin is with the proverbial *"clean sheet of paper"* when the particular car, sport-utility-vehicle (SUV), van, or pickup truck is initially conceived. The integrity of maintaining the passenger compartment *"survival space"* must be a mandatory design and performance requirement from the inception, rather than by subsequent piecemeal efforts to correct various structural weaknesses.

The various design defects that are discussed earlier should all hopefully be eliminated from the vehicle's very beginnings. Open-section windshield headers and roof siderails should become closed-section designs, with internal baffle reinforcements. Analogously, the A, B, and C pillars should all be closed-section tubular members that are reinforced their full length, with internal baffles and with rigid foam if needed. The roof lateral crossmembers should be closed-section structural members, not just thin flat straps. The interconnections should be reinforced with gussets that strengthen and stiffen all joints.

Various design innovations should be devised and developed to enhance roof strength and eliminate buckling and crushing downward. Many different approaches have been proposed, some have been implemented, and others that are feasible have yet to be fully developed.

One concept uses full structural arches that span laterally across the vehicle. This is similar to the Republic Industries Safety Car of the late-1960's, then revisited and refined by many others... the Honda ESV, the General Motors ESV, the Minicars RSV, and many other variations on the theme of multiple interconnected arches to form a strong roll-cage construction.

In the early-1970's, many General Motors passenger cars utilized a double-layer roof construction. This design was essentially a sandwich type construction that combined an outer roof with a novel inner roof. While GM boasted of its strength abilities, there was undoubtedly a weight consideration that probably helped alter GM roofs back to single-layer designs, particularly as weight reduction and fuel efficiency became major influences in the mid-1970's.

Interestingly, many GM passenger cars of the early-1970's era featured padded windshield pillars, in a proclaimed effort to help reduce head injuries in a crash, and possibly foreshadowing the anticipated requirements of the then-pending FMVSS 208 for Occupant Protection. By the mid-1970's, the padded windshield pillars were abandoned, and were replaced with various renditions of hard-surface windshield pillars without any energy-absorbing foam.

The need for upgraded crashworthiness measures for side impact protection, and roof crush resistance in rollover accidents, is clear. The continuing epidemic of deaths and severe injuries warrants a dedicated commitment by vehicle safety professionals, automakers, and governmnet agencies worldwide.

AN INJURY SEVERITY COMPARISON ON SIDE IMPACT CRASH TESTS

Andrea Costanzo
University of Rome "La Sapienza"
Luigi Cicinnati
Fracasso Mechanical Engineering Company
Gennaro Orsi
Biomechanics Engineer Consultant
Italy
Paper Number 98-S8-W-15

ABSTRACT

The objective of this study is to analyze the type and entity of injuries caused to the occupants of the vehicles involved in accidental impacts against guardrails with the high containment level. At present, the installation of highway guardrails requires the maintaining of some specific control rules imposing some verifications of the characteristics of the chosen vehicle, the dynamic parameters of impacts and the behaviors during the crash.

The results of the crash tests carried out for the different types of guardrails, concerning the trajectory and the acceleration of the vehicle during the impact as well as of the damages suffered by the vehicle itself, do not allow establishing any precise element regarding the possible injuries to the occupants of the vehicle.

The aspect of the relationship between the damages to the vehicle and the injuries which could be caused to the occupants is the main problem to be solved, in order to find out some new solutions for improving road safety. In the field of impacts against the guardrails, this consideration arouses a greater concern, because the components of the speed and the accelerations transversal to the direction of the crash, cause lateral solicitations on the body of the occupant which can have more serious consequences.

Within the framework of studies and research in road traumatology carried out at the University "La Sapienza" in Rome, scientific research has been promoted with the aim of studying the behavior of vehicles and their occupants during accidental impacts against guardrails. Two crash tests on two different types of guardrails were carried out following the European norm EN 1317 parameters. The results were described and discussed.

INTRODUCTION

In order to identify in simple terms the principal aspects to be emphasized in the research as well as the results to be pursued, the following considerations may be made:

- It is necessary to verify the coherence of the standards currently applicable for installation of the barriers at maximum stress values tolerable on the human body in its many parts;
- It is necessary to single out a concept of correlation between the behavior of the vehicle in the impact and the stressful agents transmitted to the occupants in their typology and entity;
- It is hoped that the research may lead to a normalization of the methodolgy to be followed in the use of barriers and in the limits to impose on the various classes of vehicles in order to lower the risks of more serious injuries. For this purpose an exchange organized on the basis of the homogeneity of the data available at all the international organizations in charge of expressway safety should contribute to improve passive safety in a notable manner.

Material and Method

In order to realize a research program that cannot and must not be limited to the mere two tests performed, it has firstly been necessary to set up certain points of reference, both to achieve a coherency with similar activities carried out in other countries and to have a guarantee in the future of the homogeneity of the collected data and their reliability. The first point was to establish which standards were in force concerning the matter and what legislative prospects existed, above all for the international aspects. The reference specifications available today for the purpose of this research and which give to the matter of impacts against barriers an adequate scientific rigour are essentially two:

- the European standard EN 1317
- the United States specification NCHRP Report 350

The requirements provided for in the applicable specifications essentially regard the total mass of the vehicle, its geometric characteristics and, in particular, the height from the ground of the center of gravity, the velocity and the impact angle. The acclereations and the velocities verifiable on the vehicle and those transferred to the occupants represent the parameters to be controlled as well as the trajectories. In the specific case of this research, however having a limited period of time available, it has been decided to effect two tests on two kinds of barriers - two fundamental types currently used and precisely:

- 3n fracasso steel barrier,
- New Jersey barrier in prefabricated concrete.

Both barriers are the traffic divider type and both perform extermely well with respect to their restraining qualities.

The choice of an automobile has been singled out as the Peugeot 205xA in consideration of its wide diffusion and above all because this model complies with the aforementioned specifications taken as reference for this study, both in terms of mass and height of the center of gravity from the ground.

The two tests were performed (one for each barrier) in conditions of perfect homogeneity, with an impact velocity of 100 km/h and an impact angle of 20°.

The two tests were performed by placing an anthropometric dummy (Ibrid II model) mounted and equipped with instruments inside the automobile, once in the passenger's seat for the impact test at the right and once in the driver's seat for the impact test at the left. In fact, the regulation prescribes that the dummy is to be positioned in the automobile on the side of the impact. For the purpose of exploiting the maximum experience acquired in the sector and establishing presuppositions for future programs with possible exchange of information, the collaboration of the French laboratory, L.I.E.R., in Lyon, was requested - a laboratory where the tests were physically performed and the results obtained were discussed.

The parametric characteristics to pursue and evaluate in an impact test against barriers are indeed many and include both the velocity and the accelerations verifiable on the vehicle and on the dummy as well as the indices of deformation of certain significant parts such as the cockpit, the dashboard and the bumpers of the automobile.

With a view to this study, greater importance was given to the aspect of the accelerations verifiable in the various points of the vehicle and the dummy, integrating the results with a quantitative and qualitative examination with respect to the evaluation of the damages suffered by the vehicle and by the barrier in the collision, and by the shifting of the dummy inside the automobile.

This combined theoretical-experimental examination has made it possible to draw certain considerations which allow stabilizing basic concepts regarding the behavior of the occupant of the vehicle in the crash and the injuries to which he is exposed.

In order to proceed by degrees to a research program founded on new bases which also make it possible to include the damages to which the person is exposed in the specifications of evaluation of the impacts on barriers, it was necessary, as a first step, to examine more closely the comparison of the applicable standards.

The aspect of the accelerations suffered by the vehicle in the collision has been taken as a basic parameter to execute the above-mentioned comparison in the sense that the maximum tolerable values for the acceleration along the three reference axes, or their combination, allow us to evaluate the forces which the hypothetical occupant and the inside of the vehicle reciprocally exchange and the degree of safety to be reached in the various cases.

Behavior of the vehicle in the impacts - The tests carried out have revealed that it is possible to study the behavior of the vehicle, both in terms of trajectory as well as accelerations.

The significant data may be summarized and commented as follows:

- the accelerations found along the three axes present sensible differences in the two tests performed, with greater accelerations in the transverse and vertical direction;
- with reference to the periods of time, the acceleration peaks present values that merit closer examination.

In the 3n fracasso steel barrier impact test the damages suffered by the vehicle in the impact on the right side, i.e. with the dummy in the passenger seat, can be ascribable to the range of normal accidents.

The entire right side and, in particular, the right front part were found damaged, from the lights to the bumper, the front wheel, the windshield, and the side window glasses. Other details may be seen in the attached photographs (Fig. 1a,b,c and Fig. 2a,b,c).

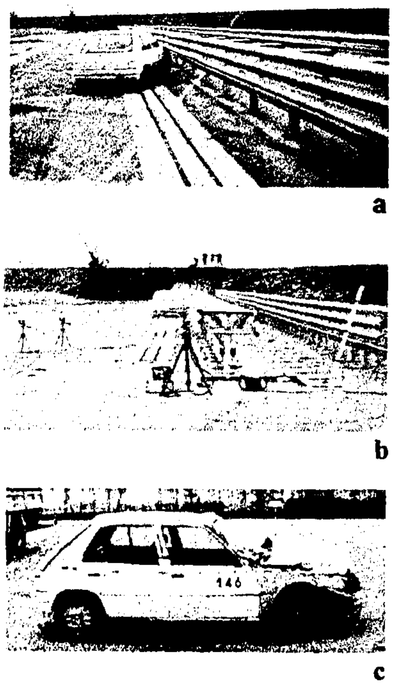

Fig. 1 - Impact on the 3n Fracasso steel barrier

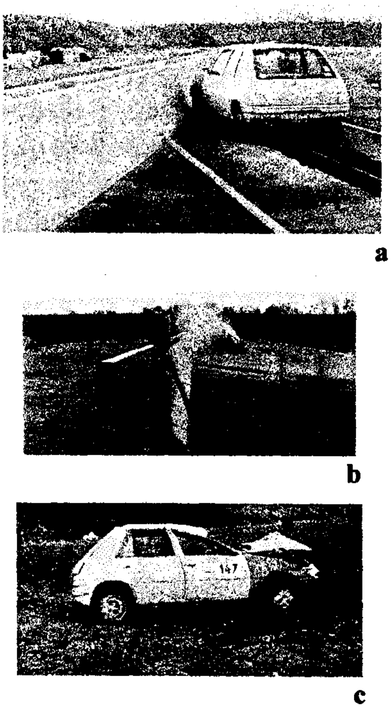

Fig. 2- Impact on the New Jersey concrete barrier.

It was also useful to localize the damages suffered by the barrier itself. The collision had created a recess in the barrier along the steel beam for a stretch of about 7.5 m and with a maximum 0.15 m deflection; the energy dissipators have undergone the programmed breaking of the diaphragms necessary for the absorption of the crash, with this result :

ASI$_t$ (Acceleration Severity Index) = $\sqrt{\left(\frac{\bar{a}_x}{\hat{a}_x}\right)^2+\left(\frac{\bar{a}_y}{\hat{a}_y}\right)^2+\left(\frac{\bar{a}_z}{\hat{a}_z}\right)^2}$ = 0.95 and

$\sqrt{a_x^2+a_y^2+a_z^2}$ = 19.8g as evidenced by the accelerometric traces (Fig. 3a,b,).

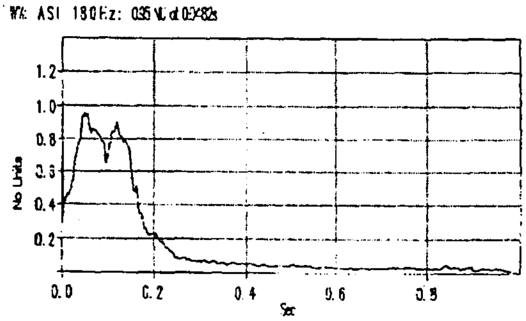

Fig. 3a

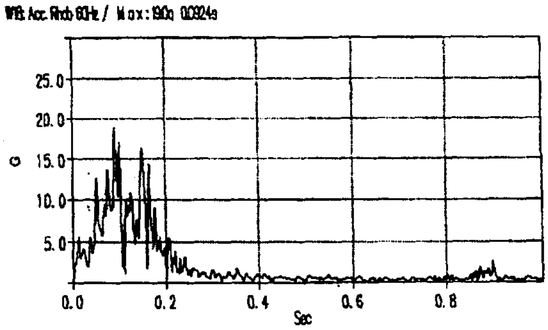

Fig. 3b- Central Reserve 3n Barrier

In the tests performed on a New Jersey concrete barrier with the impact on the left side of the vehicle and the dummy placed in the driver's seat, the damages suffered by the vehicle in the first phase of the impact have not been unlike those seen in the first test.

However, it should be pointed out that in this case a series of rollovers occurred which further damaged both sides of the vehicle.

The damages suffered by the barrier in this case as compared with those relative to the steel barrier may be evidenced by a minor recess (0,025 m compared with the 0,15 m of the other) and a larger area involved in the barriervehicle contact (12.4 m compared with 7.5 m in the preceding test), demonstrating a lesser absorption of energy, with ASI$_t$ = 1.34 and

$\sqrt{a_x^2+a_y^2+a_z^2}$ = 25g as seen by the accelerometric traces (Fig. 4a,b).

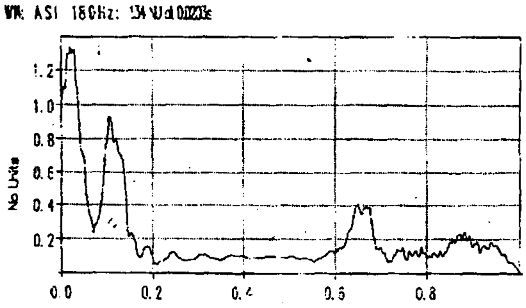

Fig. 4a

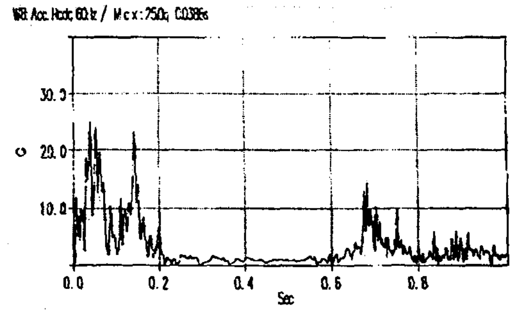

Fig. 4b- Double row prefab-concrete barrier

It is also to be pointed out that the breakage of barrier elements did not occur in either case, nor did either vehicle jump the barrier.

Behavior of the dummy - The purpose of this study in regard to the dummy creates, among other exigencies, the need to identify certain specific anomolies in the movements and rotations it undergoes during the evolutions of the impact. Besides the acceleration values seen in certain significant parts of the body, its behavior was concentrated on movements and, in this respect, the following considerations may be made:

- in the tests performed with the impact on the right side of the vehicle (3n fracasso steel guardrail) the dummy, simulating the passenger, demonstrated a significant lateral inclination of the trunk towards the part opposite the impact and a shifting of the lower limbs towards the car door; the pelvis remained well-positioned as it was protected by the abdominal strip of the safety belt;
- in the impact against the concrete barrier, i.e. with the left side of the vehicle, the dummy, placed in the driver's seat, showed a marked loss of balance of the trunk towards the door and an evident bruise on the head in the left frontoparietal region - which is also a sign of the rolling over of the vehicle consequent on the impact against the barrier.

The two tests, although evidencing the above-mentioned difference, have given a clear indication of the effect of the lateral components of accelerations and this must be taken into consideration in establishing the limits to foresee in impacts, either in terms of velocity or of the lateral mechanisms, which will be specified below.

CONCLUSIONS

The study was seen to be worthwhile and interesting, both concerning the prospects of what must still be done and in the terms of application of the procedures and standards available to date.

The most significant aspects may be summarized as follows:

A) Among the selected parameters in the recording of data characteristic of the impact against barriers, a particularly important role is played by the acceleration severity index (ASI_t) as established by the EN 1317 European specification:

$$ASI_t = \sqrt{\left(\frac{a_x}{12}\right)^2 + \left(\frac{a_y}{9}\right)^2 + \left(\frac{a_z}{10}\right)^2}$$

Where a_x, a_y, and a_z are the components of the accelerations, expressed in g, in the three directions.

This index foresees ≤ 1 values for the best safety conditions with respect to the occupants but which can be accepted up to 1.4 levels only for uses of limited extension, with conditions of lesser security.

The NCHRP-Report 350 United States Standard provides for the occupant velocity measurement O.I.V. (Occupant Impact Velocity) as well as measurement of the acceleration the occupant is exposed to: O.R.A. (Occupant Ridedown Acceleration).

B) The two standards quoted in this study, in addition to the specific one concerning the combined maximum acceleration indicated earlier, do not refer to the acceleration persistence time on the area of the human body under examination.

A more thorough examination could lead to estimating the acceleration-time effect and its consequences on the human organism. In particular, when considering cerebral concussions, the inertia of the mobile mass in the cranium undoubtedly feels the effects of the application times of the forces.

On the other hand, these considerations are well-known in the study of biomechanics; one only needs to widen the range of parameters to be accounted for in the evaluation of impacts on barriers;

C) An analysis of the values of the three acceleration components, together with the evidence concerning the movements and rotations undergone by the dummy in the impact, require a more thorough study of the damages to persons.

In particular, transversal acceleration component is the most culpable, responsible for the injuries that can be caused, both in the impact against the strucutres and in the stress phenomena due to the forces of energy.

The problem of the whiplash in the typology of lateral accelerations requires greater attention, as evidenced on various occasions.

D) The necessity to study in detail the problem of impacts against highway guardrails appears most opportune from several points of view, as already pointed out in this study. If we wish to utilize this matured experience we must see to it that the results gained are homogeneous - and to do this it is necessary to establish a common basis of specifications and applicable standards.

BIBLIOGRAPHY

COSTANZO A.: Rapport d'essai/barriere terreplein central FRA/BSI-04/146, L.I.E.R. - Laboratoire d'essais INRETS Equipements de la route, Lyon, 1997

COSTANZO A.: Rapport d'essai/separateur beton double file prefabrique FRA/SMV/01/147, L.I.E.R.
- Laboratoire d'essais INRETS Equipements de la route, Lyon, 1997

COSTANZO A.: Il colpo di frusta cervicale. Approccio medico-ingegneristico per la valutazione del danno. Convegno Internazionale SARA, Roma, 11-12 aprile 1997.

CICINNATI L.: Full scale testing of an Italian barrier to the new European standards, and a comparison with US specifications. WORLD HIGHWAYS, ROUTES DU MONDE - January/February 1996 - ROUTE ONE, PUBLISHING LTD.

CICINNATI L.: Sicurezza e resistenza delle barriere stradali, Rivista "Dimensione strada", Azienda Nazionale Autonoma delle Strade, ANAS, anno I, n° 1, genn/febb. 1993.

CICINNATI L.: Rapport d'essai/glissière de sécurité routière, INRETS-FR/BSI-06/741, Laboratoire d'essai INRETS, Equipements de la route, LYON, 1993

CICINNATI L.: Rapport d'essai/glissière de sécurité routière, INRETS-FRA/BSI-01/006, Laboratoire d'essai INRETS, Equipements de la route, LYON, 1993

CICINNATI L.: Versuchsbericht - Anfahrversuch an Stahlschutzplanken BASt-TÜV, BASt 97 7 D 07/SCHE, 1997, Prufinstitut TÜV BAYERN SACHSEN, München, 1997

LUND A.K.: Impatti contro barriere deformabili: valutazioni della sicurezza dei veicoli, Convegno Internazionale SARA, Roma, 11-12 aprile 1997.

VEHICLE DESIGN PARAMETER STUDY FOR SIDE IMPACTS USING FULL VEHICLE SIMULATION

Dong Seok Kim
Chang Hun Lee
Myung Sik Lee
DAEWOO Motor Company, LTD
Korea
Paper Number 98-S8-W-16

ABSTRACT

This paper describes a study that was conducted to determine sensitivity of several design factors for reducing injury values of occupants upon side impact using Taguchi method. The full mid-sized vehicle finite element model is used for the analysis under two different side impact standards - SINCAP and ECE-R 95. The design factors that may have major effect on side impacts were selected and L_8 orthogonal array was set up for analysis.

Analysis results show that strengthening the passenger compartment improve occupant protection, especially adding a pusher foam is significantly lowering the injury values in SINCAP. No single factor has major effects on rib deflection which is considered as critical occupant injury criterion in ECE-R 95.

Taguchi method was found to be a useful tool, although its usage may be limited in crash analysis, for predicting the effect of various design factors on structure.

INTRODUCTION

Currently, vehicle manufactures are confronted with two different international standards(FMVSS 214 & ECE-R 95) for the dynamic side impact test. In this respect, vehicle manufactures put a lot of efforts to develop their vehicles that meet the requirements of both existing standards. The problem is that these standards differ not only in their test conditions but also in the construction of dummies and its injury criteria. Moreover, those who design cars to meet the European side impact standard have experienced more difficulty than they expected since 'conventional wisdom' which is applied to meet Federal Motor Vehicle Safety Standard(FMVSS) 214 standard and has proven to be worked is ineffective to meet ECE-R 95 standard[1]. Therefore, a study was initiated to gain a better understanding of how design factors on vehicle structure affect on these standards.

To evaluate the effects of all design factors on side impact using 'one-factor-at-a-time' methods would require a large number of case studies. As an alternative, the Taguchi method was considered. The time and costs required for analysis would be substantially reduced by using this method, but its use in crash analysis is very limited. Such a detailed approach of all steps in Taguchi method would not be cost and time-effective for full vehicle finite element model analysis. Therefore, a study was designed with a simplified Taguchi method. In this study, mean analysis approach was used rather than signal-to-noise(S/N) ratio approach. Also, the optimum setting of design factors and confirmation analysis were not performed here.

USE OF TAGUCHI METHOD

In this study, Taguchi method is being utilized to determine sensitivity of several design factors for side structure. The design factors that may have major effects on side impact were selected and L_8 orthogonal array was set up for analysis. The factors selected for the study included door outer pusher foam, rocker reinforcement extension, B-pillar reinforcement, door trim padding, floor cross-member front, floor cross-member rear and B-pillar reinforcement lower. These factors and their chosen number of levels are listed in table1.

Table 1.
Design Factors

Label	Factor	Levels	
A	Existence of pusher foam	1	2
B	Rocker reinforcement extension	1	2
C	Upgrade of B-Pillar reinforcement thickness	1	2
D	Existence of door trim padding	1	2
E	Existence of floor cross-member front	1	2
F	Existence of floor cross-member rear	1	2
G	Existence of B-pillar reinforcement lower	1	2

Table 2 illustrates the L_8 orthogonal array formats that was used in this study[3].

Table 2.
L_8 Orthogonal Array

	A	B	C	D	E	F	G
	1	2	3	4	5	6	7
1	1	1	1	1	1	1	1
2	1	1	1	2	2	2	2
3	1	2	2	1	1	2	2
4	1	2	2	2	2	1	1
5	2	1	2	1	2	1	2
6	2	1	2	2	1	2	1
7	2	2	1	1	2	2	1
8	2	2	1	2	1	1	2

In accordance with L_8 orthogonal array, the full mid-sized vehicle finite element model(Fig. 1) is modified and used for analysis under two different side impact standards - SINCAP and ECE-R 95.

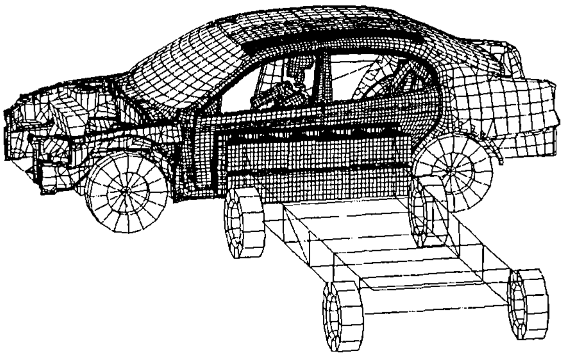

Figure 1. Full Vehicle Finite Element Model

A series of analysis was carried out to investigate the effects of design factors which would be major effect on occupant injury under side impact. Two standards were involved in this study - SINCAP and ECE-R 95.

SIDE IMPACT NEW CAR ASSESSMENT PROGRAM (SINCAP)

In 1997, The National Highway Traffic Safety Administration(NHTSA) releases side impact crash test results. These results brought enough attention to auto makers since their vehicles on the market are selected and being tested under severer condition than FMVSS214 and their results are published to consumers. According to the NHTSA's test results, just 15 percent of 17 tested cars earned four stars - none scored five stars[2]. The agency suspects that such publication will give auto makers a motivation to improve side crash protection in their vehicles just as the frontal crash protection score increases 83 percent high, equivalent to four or five stars, from 28 percent when its test was first started.

The SINCAP crash test simulates a typical intersection collision between two vehicles. Forces are measured on two crash dummies when moving deformable barrier(MDB) is 27 ° angled into the side of car at 38.5mph(Fig. 2). This is 5mph faster than the speed regulated in compliance with FMVSS214.

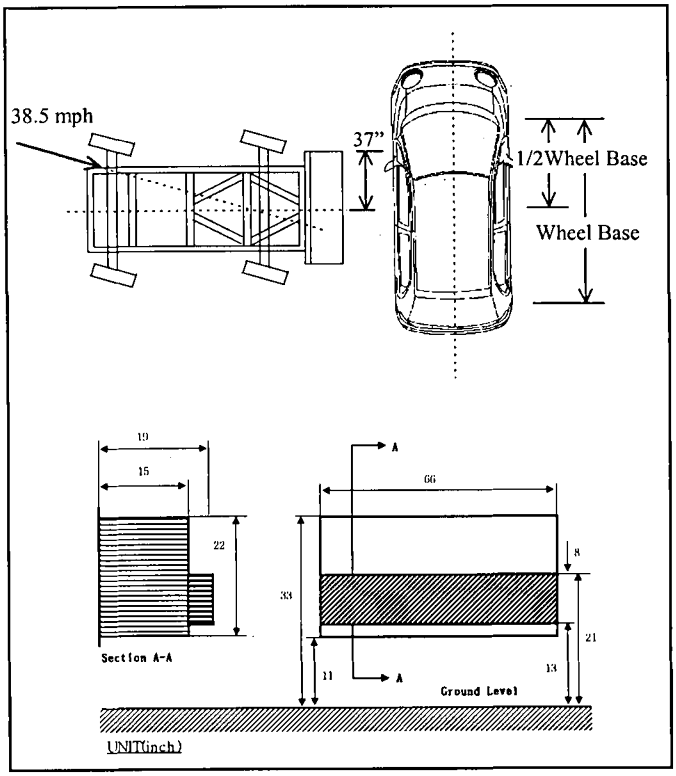

Figure 2. SINCAP Test Condition.

For injury criteria, star ratings are assigned as follows,

★★★★★	TTI ≤ 57
★★★★	57 < TTI ≤ 72
★★★	72 < TTI ≤ 91
★★	91 < TTI ≤ 98
★	98 < TTI

Fill Vehicle Test

In order to see how 5mph difference will affect the crashworthiness of vehicle and injury criteria, tests were performed with different impact speed conditions.

Figure 3 shows the comparison of occupant injuries between FMVSS214 and SINCAP. As it can be clearly seen in this figure, the injury values are dramatically increased, almost twice for rear dummy, for 5mph difference crash speed. Therefore, it would not give satisfactory results in SINCAP test if auto makers only develop their car to meet FMVSS214 requirements.

Also, the conventional wisdom such as strengthening the passenger compartment and restraint system that applied to meet FMVSS214 would work for SINCAP remains in question. This is the one of main reasons for using SINCAP test conditions for the study. The study will give design requirements, in detail, for comprehensive side protection in SINCAP.

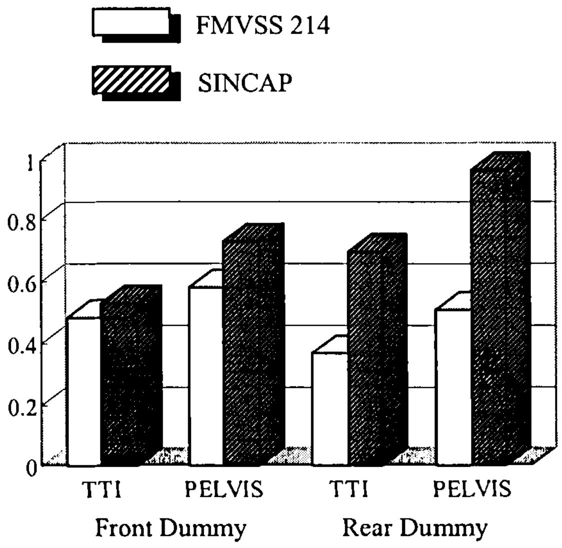

Figure 3. Injury values for FMVSS214 and SINCAP

Full Vehicle Model Structural Computation

Figure 4 shows the deformed vehicle structure from the computational results of base model(case 2) and 7 additional analyses were performed in accordance with orthogonal array.

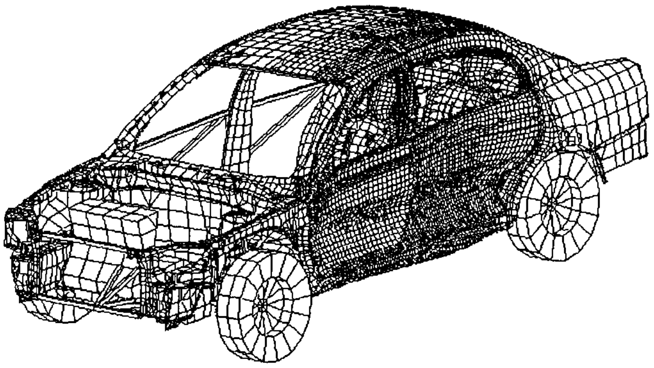

Figure 4. The Deformed Vehicle Structure, SINCAP

The injury values of SINCAP from eight compositions are presented in table 3 and 5, front and rear dummy respectively. Response tables based on mean analysis were calculated to identify the most significant control factors. Table 4 and 6 show the contribution of the control factors in analysis results. The results are classified as "the bigger variation of between two levels, the more effects on side impact."

Analyses Results for Front Dummy

The most significant control parameter influencing TTI is pusher foam in SINCAP, which accounted for 11.7% of the mean variation. The rest factors are accounted for less than 5% of variation. This is probably due to the fact that the most factors involve with strength of structures that below the H-point level. Upgrading of B-pillar reinforcement thickness (factor C) considered to affect on TTI values is less sensitive than expected.

For pelvis acceleration, pusher foam is also the most significant parameter producing 23.1% of the variation, followed by floor cross member rear, and B-pillar reinforcement at 16.5% and 11.2%, respectively. Overall, all factors can be effective for lowering pelvis acceleration, and optimal setting would give more reduction.

Table 3.

Normalized analysis result for front dummy

	Lower Spine	Upper Rib	Lower Rib	TTI	Pelvis
1	**1.10**	**0.98**	**1.05**	**1.07**	**1.34**
2	**1.00**	**1.00**	**1.00**	**1.00**	**1.00**
3	**0.98**	**1.03**	**0.99**	**1.01**	**0.93**
4	**1.01**	**0.99**	**0.92**	**1.00**	**1.05**
5	**0.90**	**0.77**	**0.82**	**0.85**	**0.89**
6	**0.93**	**0.90**	**0.83**	**0.92**	**0.77**
7	**0.96**	**0.84**	**0.86**	**0.91**	**0.83**
8	**0.89**	**0.98**	**0.81**	**0.93**	**0.91**

Note : Case 2 is Base Model

Table 4.

Response Table for Front Dummy

TTI

	A	B	C	D	E	F	G
1	1.020	0.960	0.978	0.960	0.982	0.966	0.974
2	0.903	0.962	0.944	0.963	0.941	0.957	0.936
Delta	0.117	0.002	0.034	0.003	0.041	0.009	0.038

Pelvis

	A	B	C	D	E	F	G
1	1.081	1.000	1.021	0.999	0.989	1.048	0.997
2	0.850	0.931	0.909	0.932	0.942	0.883	0.889
Delta	0.231	0.069	0.112	0.067	0.047	0.165	0.108

Analyses Results for Rear Dummy

Pusher foam does not take into accounts for rear dummy since it was only applied to front door. The control parameter influencing TTI is B-pillar reinforcement, which accounted for 6.2% of the mean variation. Similarly, 5.4% of the variation was due to floor cross member rear and 5.0% was due to floor cross member front.

For pelvis acceleration, door trim padding was the most significant parameter producing 24.8% of the variation, followed by floor cross member front , and floor cross member rear at 9.5% and 8.8%, respectively.

From results above, every factor has some degree of sensitivity to the occupant injury. Specially, adding a pusher foam or door trim padding are substantially effective to lowering both TTI and pelvis acceleration.

Table 5.

Normalized analysis results for rear dummy

	Lower Spine	Upper Rib	Lower Rib	TTI	Pelvis
1	0.97	1.15	0.89	1.00	1.35
2	1.00	1.00	1.00	1.00	1.00
3	1.16	0.90	0.87	1.00	1.39
4	0.87	1.02	0.82	0.89	1.05
5	0.95	0.88	0.80	0.87	1.10
6	0.86	1.19	1.02	0.97	1.13
7	1.09	1.03	0.88	0.99	1.36
8	0.94	1.01	1.02	0.98	1.03

Table 6.

Response table for rear dummy

TTI

	A	B	C	D	E	F	G
1	N/A	0.960	0.993	0.964	0.987	0.935	0.962
2	N/A	0.964	0.931	0.960	0.937	0.989	0.968
Delta	N/A	0.004	0.062	0.004	0.050	0.054	0.006

Pelvis

	A	B	C	D	E	F	G
1	N/A	1.145	1.184	1.300	1.223	1.132	1.222
2	N/A	1.207	1.167	1.052	1.128	1.220	1.168
Delta	N/A	0.062	0.017	0.248	0.095	0.088	0.054

EUROPEAN SIDE IMPACT (ECE-R 95)

ECE-R 95 test involves a side collision with EURO-Moving Deformable Barrier at an angle of 90 ° and a test speed of 50km/h. Its impact position to the target vehicle is relative to the seating position of the driver, R-Point, shown in Figure 5.

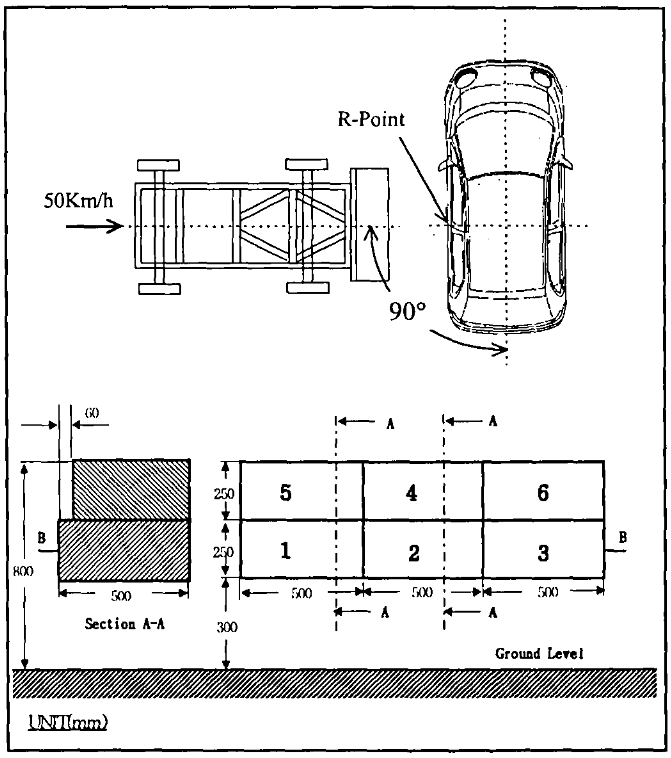

Figure 5. ECE-R 95 test condition.

The dummy used in ECE-R 95 is EUROSID dummy and its injury criteria cover maximum acceleration level to the head, rib deflection limits and peak forces to the abdomen and pelvis as follow,

Criteria for ECE-R 95

Head	HPC	< 1000
Thorax	Deflection	< 42 mm
	VC_{max}	< 1 m/s
Pelvis	PSFP	< 6.0 KN
Abdomen	APF	< 2.5KN

Full Vehicle Model Structural Computation

Figure 6 shows the deformed vehicle structure after impacting with European side impact test condition. It is also computational results of base model(case 2).

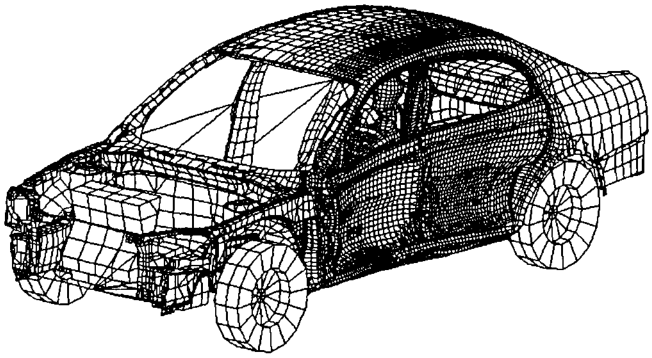

Figure 6. The Deformed Vehicle Structure, ECE-R 95

The injury values of ECE-R 95 from eight compositions are presented in table 7. Response tables were calculated to identify the most significant control factors. Table 8 shows the contribution of the control factors in analysis results.

Analyses Results

It is interesting to note that no single factor has significant effects on rib deflection which is considered as the most critical injury criterion in European side impact. However, strengthening the passenger compartment in lower level (factor E and F) slightly increase the rib deflection which is the conflicting results of federal regulation.

The effective control parameter for Viscous Criterion was a pusher foam which is accounted for 10.4 % of the variation. Even though floor cross member rear and B-pillar reinforcement lead 8.2% and 5.1% of variation respectively, it gives an adverse effects on injury values.

Eliminating factors which weaken the lower level of passenger compartment structure will give lower Viscous Criterion and rib deflection values. This result might be supporting the ideas that increasing the penetration of passenger compartment at the lower level relative to the upper will give significant reduction in thoracic loading[4]. It means that such a design concept should be made at the early stage of vehicle structure development in order to effectively fulfill the European side impact requirements.

Every factor has some degree of sensitivity to the abdomen and pubic forces, so it would not be any problems to control these injury values. Also analysis results show their injury values much lower than its requirements. These would not be considered as critical injury criteria .

Table 7.

Normalized analysis results

	Rib deflection	Rib V.C.	Abdomen Force	Pubic Force
1	0.89	1.02	0.78	0.94
2	1.00	1.00	1.00	1.00
3	0.96	1.08	0.99	1.11
4	0.93	1.04	1.06	1.08
5	0.94	0.86	0.96	0.99
6	0.91	0.96	0.96	1.20
7	0.92	1.05	0.83	1.07
8	0.94	0.85	1.00	1.24

Table 8.

Response table

Rib Deflection

	A	B	C	D	E	F	G
1	0.945	0.934	0.937	0.928	0.925	0.922	0.913
2	0.926	0.938	0.935	0.946	0.946	0.950	0.945
Delta	0.019	0.004	0.002	0.018	0.021	0.028	0.032

Viscous Criterion

	A	B	C	D	E	F	G
1	1.035	0.961	0.981	1.004	0.979	0.942	1.019
2	0.931	1.006	0.985	0.963	0.987	1.024	0.968
Delta	0.104	0.045	0.004	0.041	0.008	0.082	0.051

Abdomen Force

	A	B	C	D	E	F	G
1	0.960	0.927	0.903	0.893	0.933	0.952	0.908
2	0.938	0.972	0.995	1.005	0.965	0.945	0.958
Delta	0.022	0.045	0.092	0.112	0.032	0.007	0.049

Pubic Force

	A	B	C	D	E	F	G
1	1.032	1.031	1.064	1.027	1.122	1.063	1.072
2	1.124	1.126	1.093	1.130	1.035	1.094	1.101
Delta	0.092	0.095	0.029	0.103	0.087	0.031	0.029

CONCLUSION

The study was conducted to determine sensitivity of several design factors for reducing injury values of occupants under two different side impact conditions - SINCAP and ECE-R 95.

From SINCAP analysis results, every factor has some degree of sensitivity to the occupant injury. Specially, adding a pusher foam or door trim padding are substantially reducing both TTI and pelvis acceleration. However, the design principles should mainly focus on reducing TTI values since the injury values in SINCAP are based on TTI.

For ECE-R 95, no single factor can improve rib deflection which is considered as critical injury values. So, the major change of side structure would be required in such a way that increasing the penetration of passenger compartment at the lower level relative to the upper. Therefore, such a design concept should be made at the early stage of vehicle structure development in order to effectively fulfill the European side impact requirements.

As mentioned above, each factor has some degree of sensitivity to the occupant injury upon side impacts. Some factors are more sensitive than others and would give more effects on injury consequently. However, single factor can not solve the various requirements on side impacts. The proper combination of each factor will give more reliable results than single factor alone.

REFERENCES

1. C. Adrian Hobbs, “Dispelling the Misconceptions about Side Impact Protection”, SAE Technical Report, No. 950879, 1995
2. “NHTSA Release First Side-Impact Crash Test Results”, Highway & Vehicle/Safety Report, April 28, 1997
3. G. Taguchi and S. Konishi, “Orthogonal Arrays and Linear Graphs”, The American Supplier Institute
4. Rolf Bergmann, Claudia Bremer, Xuefeng Wang, Arnold Enblen, “Requirements of Comprehensive Side Protection and their Effects on Car”, ESV Technical paper, Volkswagen AG, No. 96-S6-W-16

DESIGN METHODS FOR ADJUSTING THE SIDE AIRBAG SENSOR AND THE CAR BODY

Klaus Friedewald
Volkswagen AG
Germany
Paper Number 98-S8-W-17

ABSTRACT

Now that side airbags are used to protect chest and head of the occupants, reliable detection of side impacts is of great importance. Compared to frontal collisions of the same impact speed, side collisions take only the third of time. Thus detection of a side impact at 50 km/h has to be done in less than 5 ms after the first contact. This challenging task cannot be achieved with a single crash sensor in the middle of the car, as used for the ignition of frontal airbags, but requires specialized sensors for the side impact detection.

At present two different principles of sensors are ready for production: devices that measure deformations and devices that use accelerations. Volkswagen utilizes acceleration-based sensors because they are less sensitive in regard to the impact points. However, placing this type of sensors is an extremely critical task. The pros and cons of some typical mounting locations like doors, sills or cross members are discussed in this paper. Also discussed are methods for optimizing the car in order to shorten the sensing time. They include the analysis of the transmissibility of shocks by experimental methods and the numerical calculation by FEM.

The airbag controlling computer processes the accelerations measured by the sensor and decides whether the airbag should be employed. The evaluation algorithm has to be designed for a specific car body. Not only the behavior of the car body in case of violent side collisions has to be taken into account, but unintended firing in case of light traffic accidents or abnormal driving conditions also has to be prevented.

By employing acceleration based side impact sensors a secure ignition of side airbags is possible. However, an adjustment by modifying merely the software of the controller does not lead to acceptable results. A good performance of the side impact protection system requires an adjustment of all components involved, i.e. the car body, the hardware of the sensor / controller and the software algorithm.

INTRODUCTION

After having greatly improved the safety for passengers in frontal collisions, due in no small part to the wide use of airbags, one of the current major development areas is improving passenger safety in side collisions. Here again airbags look like a very promising means to reduce the risk of injury.

An airbag's effectiveness depends to a great extent upon the timing of its ignition. The earlier the ignition of the airbag after the collision, the greater the advantages of the airbag's restraint. Compared to frontal collisions, side collisions require a much faster airbag reaction time. In a typical frontal collision at 50 km/h against a wall the first contact between the driver and airbag is 50 ms after the start of the crash. The inflation of the airbag requires approximately 25 ms. This means that the gas generator must be ignited approximately 10 ms to 30 ms after the crash has begun.

In the case of a side collision at 50 km/h, as defined in the EEVC statutes, the door typically already reaches the passengers after 20 ms. Due to the smaller volume of the side airbag, in comparison to a front airbag, the inflation time takes 10 ms. In order that the side airbag can still come between the door and the passenger, the gas generator must be ignited after only 5 ms after the crash begins, figure 1.

Despite the very short time allowed for the detection of the impact, unintended firing in the case of light traffic accidents or abnormal driving conditions must be avoided. The use of a common crash sensor placed in the middle of the car, as used for front airbags, is not sufficient. The development of a faster and more reliable side collision sensor is therefore of prime importance.

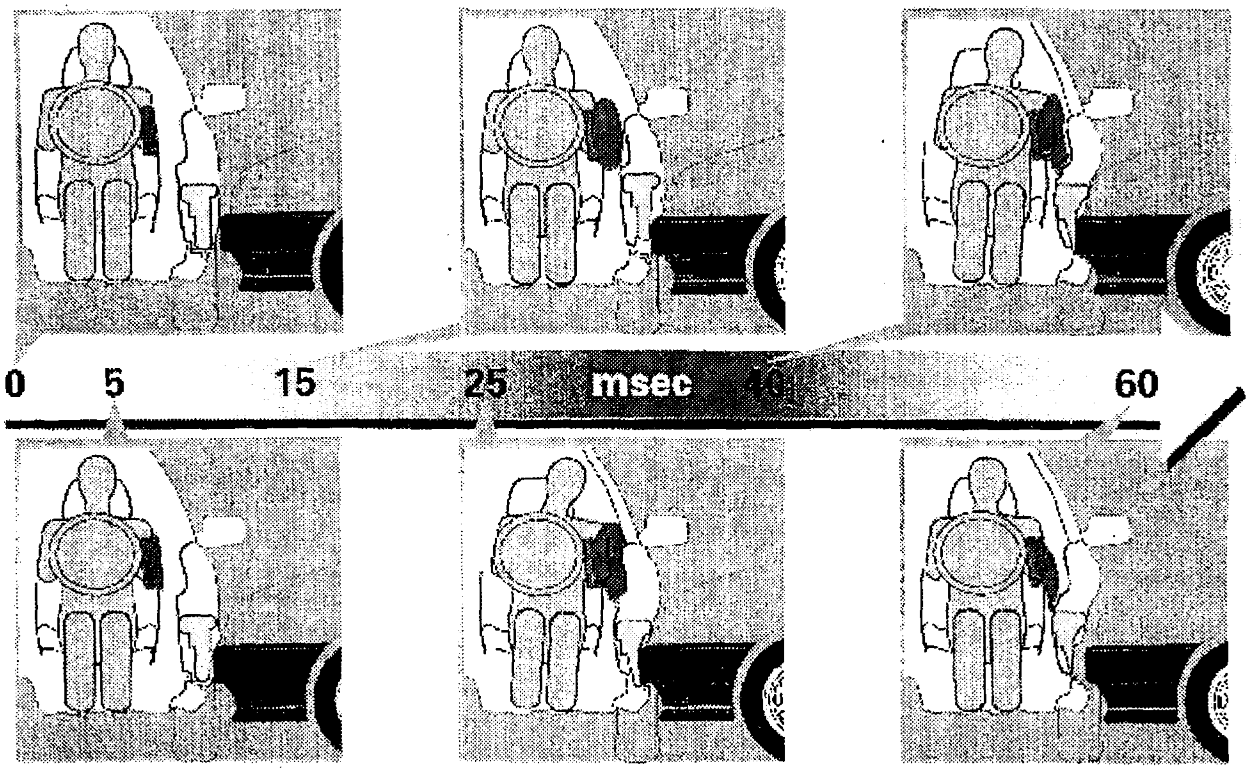

Figure 1. Typical Timing Diagram of a Side Airbag.

PRINCIPLES OF SENSORS

In recognizing a side collision different physical effects can be used. The current side airbag sensors are either deformation or acceleration oriented. Both methods have their advantages and disadvantages. Improvement of the protection offered through airbags is expected in the future through the development of pre-crash sensors, which are to send a crash signal before the actual contact.

Deformation Oriented Systems

A statistical analysis of side collisions has shown those most severe injuries with an injury degree of AIS$\geq$ 3 are chest injuries [1]. This same analysis also categorizes passenger injuries by the type of collision. In the majority of cases the door of the crashed car was hit. A Thorax airbag that is ignited when the door is hugely deformed can in many cases protect the passengers from severe injuries.

The crash is recognized by a simple switch that closes when the car body is deformed beyond a certain degree [2]. This system allows for a very fast recognition of severe accidents. However, due to the crash contacts digital character it is ineffective in the case of moderate accidents, in which a side airbag could already provide protection.

An alternative procedure is based on measuring the difference in volume of the hit door in a side collision [3,4]. In comparison to the switch this system has the advantage that it not only takes into account the absolute degree of the deformation, but also the speed of the deformation in determining the degree of the accident. Due to the analog character of the system moderate accidents can also be recognized.

All of the deformation-based methods have the disadvantage that they heavily depend on the location of the collision. This system can not recognize a severe accident with a collision location in front of or behind the door.

Acceleration Oriented Systems

Just as for frontal crash sensors, these systems are based on measuring the acceleration of the vehicle. The mounting location is of critical importance for a quick employment of the airbag. A mounting location in the middle of the car, as is usually the case for frontal crash recognition, is not sufficient for recognizing a side collision due to the great distance to the collision zone.

This can be improved by using additional acceleration measurement locations near the sill. In comparison to deformation oriented sensors, acceleration oriented sensors can also recognize a collision in the area of the trunk or motor. In addition light traffic accidents and severe deformations, which do not pose a danger to the passengers, can be better recognized.

Pre-Crash Sensors

Pre-crash sensors are still in the development stage [5,6]. Such sensors constantly observe the immediate area surrounding the vehicle and send a signal to the airbag control unit prior to a collision. For this purpose sensors based on infrared, laser or radar are being examined.

The largest problem with all of these methods is guaranteeing a sufficiently high enough reliability for actual accidents. It is not sufficient to simply recognize a possible collision, but also the type of the collision partner has to be detected early enough. For example, the ignition of an airbag when a cat jumps onto the vehicle is unacceptable. In addition such things as fog or radar rays may not influence the crash sensor.

POSITIONING OF ACCELERATION SENSORS

Due to the advantages described above Volkswagen makes use of the acceleration-based system for its side airbags. Various locations can be used for the positioning of the sensors:

On the Tunnel

This location is often used for the detection of frontal collisions. A side collision, however, results in a relatively late signal, and weak amplitude. Therefore, this position is not advisable for the recognition of a side crash. However, the acceleration measured from this position can be used as an additional criterion in judging how severe the collision is (safing function).

In the Door

In this position an early strong signal is sent. However, this area experiences great deformations in a side crash. This can result in the acceleration sensor being turned in the course of the crash, so that a directional placing of the measured accelerations is no longer possible. In addition a sensor placed in the deformation zone has a high risk of being destroyed. Therefore, this position also does not appear to be advantageous.

On a Seat Cross Member

The ideal position for an acceleration sensor is as close as possible to the place of the collision, without being within the deformation zone. In Volkswagen vehicles there is a massive seat cross member underneath the front seats, figure 2. This secures the survival space of the passengers, and at the same time serves as a mounting location for the acceleration sensor.

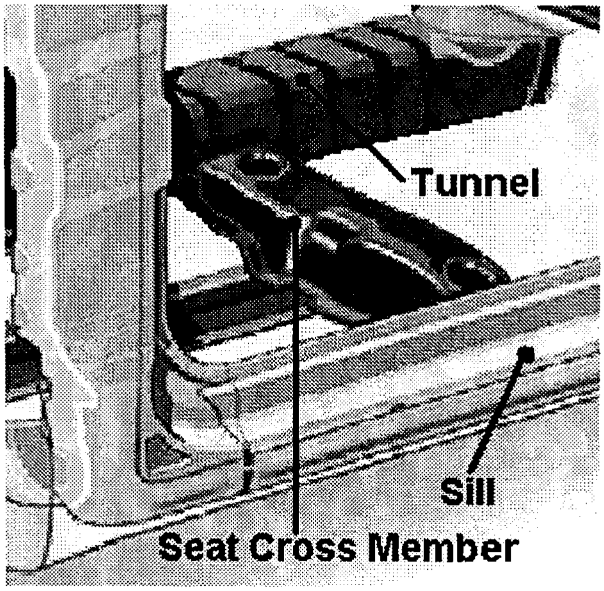

Figure 2. Seat Cross Member.

In the case of a side collision in the area of the trunk or hood the absolute time for the detection of the crash is longer than for a collision with the door. However, the time available for inflating the airbag is also significantly greater due to the lower level of deformation and the slower progress in the front seat area [1]. Therefore, even in these cases the side airbag can reach its full protective effect.

OPTIMIZATION OF THE CAR BODY

For frontal crash controllers, usually the adjustment to the car body is done by modifying the software. The more precise timing requirements of side airbags can only be fulfilled by taking into account the impulse transfer in the construction phase of the car body.

General Construction Principles

A hard and stiff structure is best for the impulse transfer. Therefore, VW has chosen to make the cross section of the seat cross member in the area between the collision zone and the sensor as large as possible, and the connection to the sill inflexible.

Close attention should be paid to the construction of beads in the floor pan. Beads should never cut the direction of the impulse in the impulse transfer area, since otherwise the impulse waves will be weakened or redirected. However, these requirements can contradict the requirements of the frontal crash. In such a case the locating of the sensor and the construction of the beads should be so aligned that longitudinal beads do not cross between the sill and the sensor.

During the critical phase of the crash for the passengers, the crash opponents' acceleration is only reduced minimally. At a collision speed of 50 km/h the crash opponent enters a vehicle hit in a side collision at a rate of 15 mm/ms. An air gap of 15 mm between the body parts carrying the impulse thereby causes a delay of the transfer of the signal by 1 ms! Therefore, a collision should, if possible, not take place on metal membranes such as side parts or outer door metal, but instead on parts supported by members. A car production with small range of tolerance, i.e. with narrow gap measurements between the door and sill, contributes to a fast airbag ignition.

FEM Simulation Calculations

With the help of numerical FEM simulations it is possible to determine how the vehicle will react in a side collision at a very early stage in the vehicle's development, figure 3. Calculating the acceleration impulses at various mounting locations can make a rough positioning of the acceleration sensors. The simulation calculations also supply information on the path of the signal transfer for a particular mounting location.

However, the signal transfer is influenced by many factors that are difficult to simulate numerically, such as the reaction of welding points. Therefore, the FEM calculations can only be used to compare evaluations. Today, an exact calculation of the ignition time isn't possible through computer simulations only.

Experimental Sensitivity Analysis

The sensitivity analysis is a good experimental method for optimization in detail. The body in white is hit with an instrumented hammer, picture 4. The acceleration is measured at the relevant points on the body in white and is compared with the acceleration of the

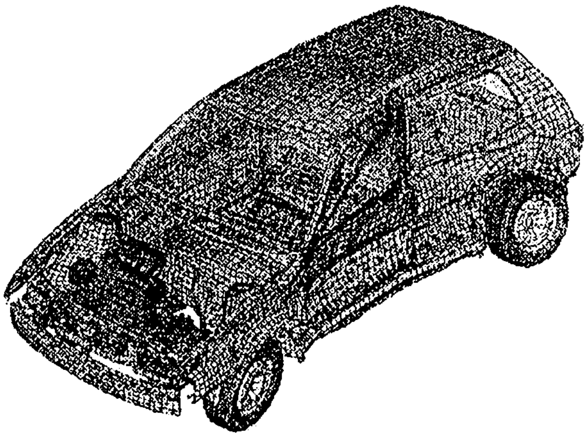

Figure 3. FEM Side Impact Simulation.

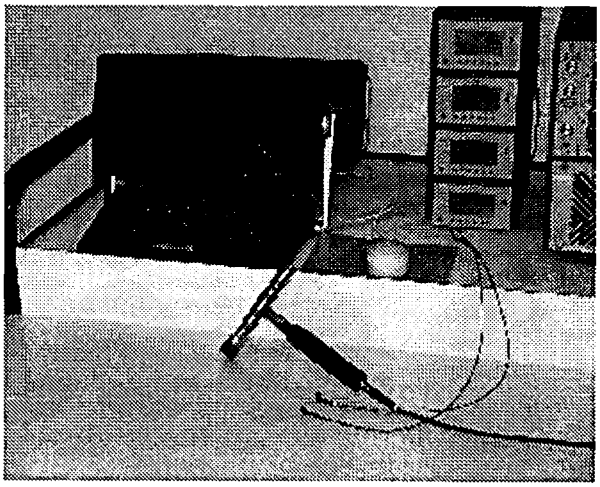

Figure 4. Instrumented Hammer.

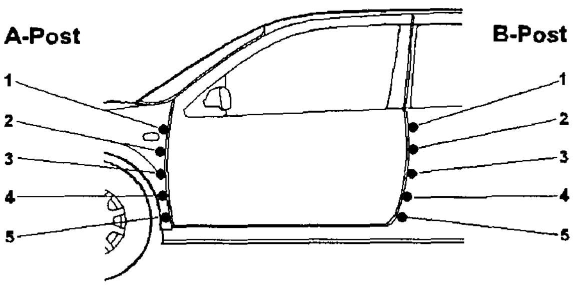

Figure 5. Sensitivity Analysis: Points under Test.

hammer. Through this procedure the most suitable location for mounting the crash sensor can be determined.

The vehicle body itself can also be improved with the help of this method. Transfer functions for various points on the A and B columns are determined, figures 5 and 6. For this particular type of vehicle the height for the best signal transfer is at point 4. In order to transfer the acceleration impulses as quickly as possible from the columns to the sensor the door beam should be at this height.

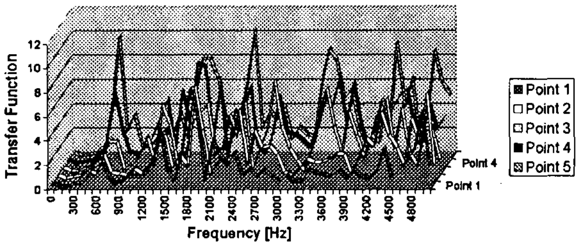

Figure 6. Sensitivity of the A-Post.

INFLUENCE OF THE CONTROLLER

The 5 ms available to ignite the airbag is so minimal that the amount of time needed by the controlling computer to process the measurements can not be ignored. Already the initiator of the processing chain, the A/D-converter, causes a delay lying in the range of a tenth of a ms.

Also the transferal of information between the satellite sensors on the seat cross member and the sensors mounted on the main body require a similar amount of time. A faster communicationsprotocol would result in greater sensitivity to electro-magnetic rays. An increase in speed is difficult to achieve since an unintended firing can in no case be accepted.

A field for optimization is not only offered by the controller's hardware. The evaluation algorithm itself exercises great influence over the speed of the ignition. Problems occur in differentiating between light and violent accidents. A criterion based solely on the level of acceleration that ignites the airbag after a certain value has been exceeded results in a fast ignition, but also ignites in the case of light accidents.

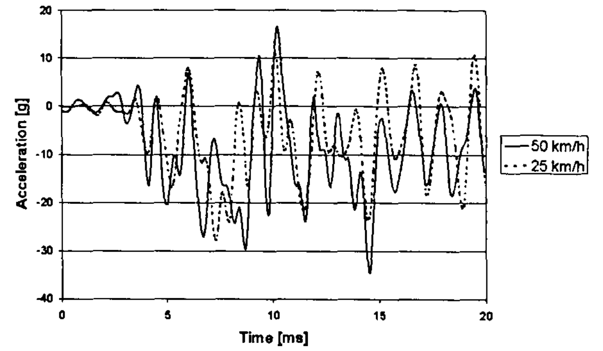

Figure 7. 50 km/h and 25 km/h Crash Tests.

In figure 7 the time history of acceleration of a 50 km/h European side crash is compared with a 25 km/h crash test. It is easy to see that the maximums in acceleration for both tests are at the same level. There is only a minor influence of the crash speed, since the contact force between both parties of the accident during the first phase of the collision is determined primarily by the stiffness of the bodies in white.

As a result the peak value of the vehicle acceleration is also only slightly dependent on the speed of the collision. A greater speed is mostly noticeable in the duration of the deceleration, not in its value. Therefore, a processing of the maximum value is only suitable as a "safing function", i.e. as a secondary criteria to avoid unintended firing.

In order to avoid an unintended ignition with some certainty an evaluation algorithm must use the course of the acceleration over a long time period. This of course negatively influences the ignition time. Therefore, an algorithm that classifies the level of the accident over as short a period of time as possible offers considerable advantages in speed.

CONCLUSION

The prompt ignition of a side airbag poses a challenging task for all involved components. A lot of development time must be placed in making the components for the vehicle body, sensors, controlling hardware and last, but not least the controlling software. By employing a well-tuned acceleration oriented sensor system passengers can also be given the full protection potential of an airbag in a side collision.

REFERENCES

[1] Hassan, A.; Morris, A.; Mackay, M.; Haland, Y.: "Injury Severity in Side Impacts - Implications for Side Impact Airbag". Proc. IRCOBI 1995, Brunnen, Switzerland, pp. 353-364.

[2] Pilhall, S.; Korner, J.; Ouchterlony, B.: "SIPSBAG - A New, Seat-Mounted Side Impact Airbag System". Proc. 14th ESV Conference 1994, Munich, Germany, pp. 1026-1034.

[3] Härtl, A.; Mader, G.; Pfau, L.: "New Sensor Concepts for Reliable Detection of Side-Impact Collisions". Proc. 14th ESV Conference 1994, Munich, Germany, pp. 1035-1038.

[4] Härtl, A.; Mader, G.; Pfau, L.; Wolfram, B.: "Physically Different Sensor Concepts for reliable Detection of Side-Impact Collisions". Proc. SAE-Conf. 1995, Detroit, USA, pp. 107-110.

[5] Swihart, W.; Lawrence, A.: "Investigation of Sensor Requirements and Expected Benefits of Predictive Crash Sensing". Proc. SAE-Conf. 1995, Detroit, USA, pp. 95-106.

[6] Jost, K.: "Sensor Technology Review". Automotive Engineering, Vol. 103, No. 9, p. 39-49.

ROLLOVER EJECTION MITIGATION USING AN INFLATABLE TUBULAR STRUCTURE (ITS’)

Gershon Yaniv
Simula ASD, Incorporated
Stephen Duffy
TRC
Stephen Summers
National Highway Traffic Safety Administration
United States
Paper Number 98-S8-W-18

ABSTRACT

The National Highway Safety Administration (NHTSA) and Simula Automotive Safety Devices (ASD-Simula) are conducting a joint research program to evaluate the effectiveness of the Inflatable Tubular Structure (ITS^{â}) in mitigating ejection during rollover crashes. This research program involves full scale dynamic testing, component testing, simulation, and crash case reviews. All aspects of the program will be analyzed to evaluate the safety potential for ejection mitigation. The preliminary tests show that the ITS can be highly effective in mitigating complete occupant ejection, but cannot prevent arm ejections in rollover crashes.

INTRODUCTION

The ITS is a roof mounted inflatable safety device intended to provide head and neck protection in side impact crashes. When deployed, the ITS covers up a portion of the side window of the vehicle. Unlike conventional air bags, the ITS remains inflated for many seconds, well longer than the typical duration of a rollover crash. Due to its special configuration, the ITS does not require a reaction surface to function and retain the occupant inside the vehicle.

On average, annually 7,741 rollover involved fatalities were reported by the Fatal Analysis Reporting System (FARS) between 1988 and 1996. There were also between 43,000 and 58,000 annual rollover involved incapacitating injuries for the same time period, as reported by NASS GES. Approximately 59 percent of the rollover fatalities came from the 10 percent of the rollover involved occupants who are ejected, or partially ejected from the vehicle. Of these rollover involved ejections, 56 percent of the fatalities, and 49 percent of the seriously injured occupants, are ejected through the side windows. Significant safety improvement can be established by reducing ejection through side windows. Considering all accident types, an average of 7,741 people are killed, and 9,211 people are seriously injured each year in passenger car, light trucks, and vans in crashes involving ejection through side windows (NASS CDS 1988-1996).

The significant potential safety benefit is the impetus for the effort to find a device mitigating side window ejection.

SYSTEM DESCRIPTION

General

The ITS distinguishes itself from conventional air bag restraint systems in several critical areas. Basically, it is a fabric tube rigidly mounted at each end. Upon inflation, the patented design and construction method cause the tube to significantly increase in cross-section or diameter, while at the same time significantly shortening its length. Consequently, the ITS pulls itself from its stored location into the desired occupant restraint position while developing high tensile loads between its mounting locations. Because of the high tensile loads and internal pressure, the ITS provides significant restraint without relying on a bearing surface.

In order to function properly, the ITS must get shorter in length, since the stowed length, in all applications, L_o, is longer than the deployed length, L_1 . The ratio of deployed length L_1 to stowed length L_o is one of the most critical functional parameters of the ITS and is called the slack ratio. This shortening function is accomplished by using a specially woven fabric which significantly contracts in length and increases in diameter as internal pressure is realized (Figure 1). During the pressure build-up, an axial tension force is developed, since the fixed endpoints prevent the ITS from contracting freely.

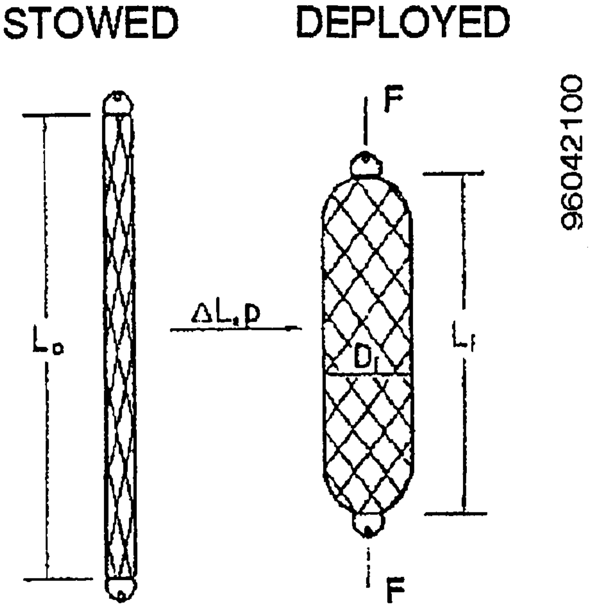

Figure 1 - Inflatable Tubular Structure principle of operation

The development of appropriate pressure and axial tension enable the ITS to perform its two main functions:

> 1) In the absence of a bearing surface, the tension indirectly provides the reaction forces. This way, the ITS can prevent the occupant's head, torso, or legs (depending on the application) from moving into a crash intrusion zone, i.e., reducing the hazard of the occupant's hitting internal and external objects.
>
> 2) The pressurized, inflated ITS provides a cushion to blunt the impact and provide the normal restraint function of controlling occupant deceleration.

Unlike conventional air bags, which deflate in less than 100 ms from the start of deployment, the ITS is not vented. Since the pressure of the ITS is well over 1 bar, the relatively slow reduction in gas volume due to cooling allows the ITS to provide protection for several seconds.

One of the main applications is for side impact crashes. In this application, the Inflatable Tubular Structure (ITS) is intended to provide protection to the head and neck of car occupants in a side impact and in multiple-impact crashes and to reduce the chance of ejection in roll-over crashes.

System Description

The ITS is fixed to the "A" pillar at one end and to the roof rail aft of the "B" pillar at the other end, as shown in figure 2. A gas generator is electrically connected to a side-impact crash sensor which ignites the gas generator if the impact intensity exceeds a predetermined level.

The detailed packaging and the specific location of the gas generator are vehicle-dependent to facilitate optimum integration. The gas generator fills the tubular structure with gas. As the tube inflates, it gets bigger in diameter and shorter in length (Figure 3), and pulls itself out from under the headliner (not shown in Figure 2). The ITS positions itself between the head of the occupant and the side of the vehicle and any intruding objects.

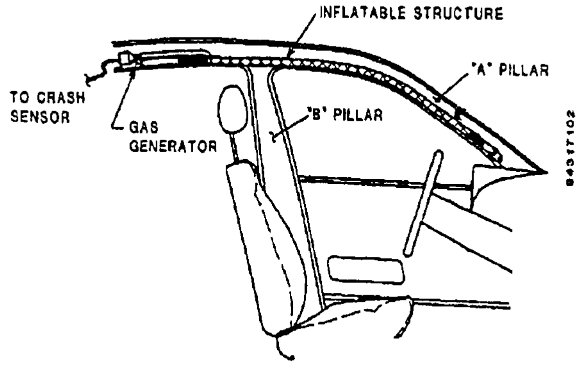

Figure 2 – Inflatable Tubular Structure in a stored position

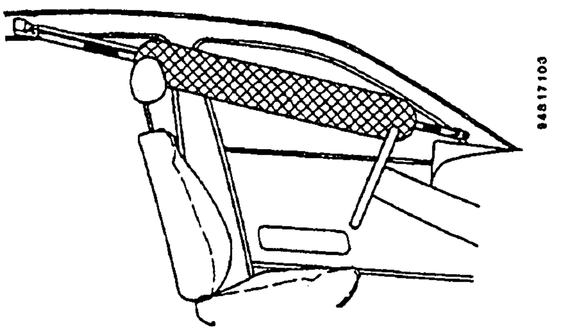

Figure 3 – Inflatable Tubular Structure in a deployed position

The location of the ITS end points at the "A" pillar and the roof rail determine the protection zone of coverage. The position and the orientation of the ITS were selected to protect a wide range of occupant sizes. Figure 4 shows how both 5th-percentile and 95th-percentile occupants would be protected without the need to perform any adjustments to the ITS.

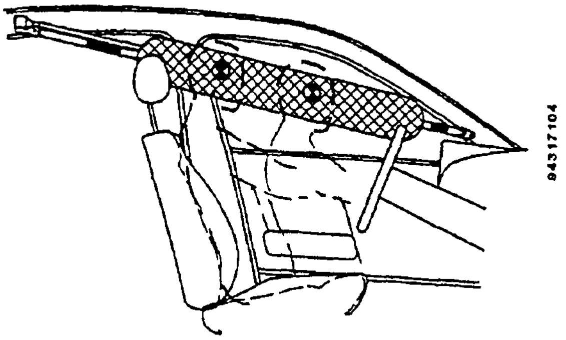

Figure 4 – Inflatable Tubular Structure Protection for 5th through 95th percentile occupants

FMVSS 208 DOLLY ROLLOVER TESTS

Test Methodology

Three dolly rollover tests were conducted per FMVSS 208 criteria using one 1993 and two 1994 Ford Explorers. In this test, the vehicle is held tilted at an angle of 23 degrees and is slid in a transverse direction along the test track. The dolly has an initial velocity of 48 kph (30 mph) and is rapidly decelerated to initiate the vehicle rollover. Each vehicle was launched from the dolly fixture into a lateral roll with the left side (driver) down (see Figure 5). This test method was chosen because it was most likely to produce an occupant ejection.

Each vehicle was equipped with ITS devices adjacent to both front passenger seating positions. The doors were locked and windows rolled down prior to testing. The first two tests utilized two unbelted Hybrid-III dummies in the front seating positions. The passenger side dummy was restrained with a lap/shoulder belt in the third test while the driver side dummy remained unrestrained. The dummies were instrumented with tri-axial accelerometers in the head, chest and pelvis, a chest deflection potentiometer, and a Hybrid III neck transducer which measures axial tension and compression, anterior-posterior shear and bending moment, and lateral shear and bending moment. The movement of the dummies was documented by 5 onboard cameras.

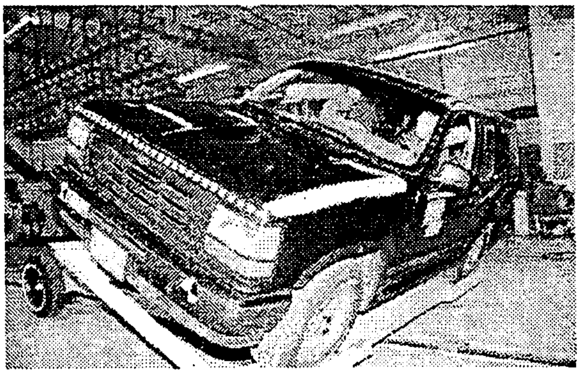

Figure 5 -- FMVSS 208 Rollover Dolly Fixture

The ITS devices were mounted to the dash panel and the rear seat belt mounts on the vehicle side header. Because the inflation time had not been evaluated for the first two tests, the ITS devices were inflated just prior to the start of the test. After analyzing these tests, a rollover sensing device was used in the third test to deploy the ITS systems, via a gas generator, at a predetermined point during the early stages of roll. The ITS devices in the first test measured 6 inches in diameter when fully inflated. The size and location of the ITS for the second rollover test were modified slightly. The front anchor points were moved inboard about 5 inches and the diameter of the ITS on the driver side was increased by 1 inch while the passenger side utilized a slightly more oval shaped device as shown in Figures 6a and 6b. In the third test, the anchor points remained the same while the ITS devices matched those of the first test.

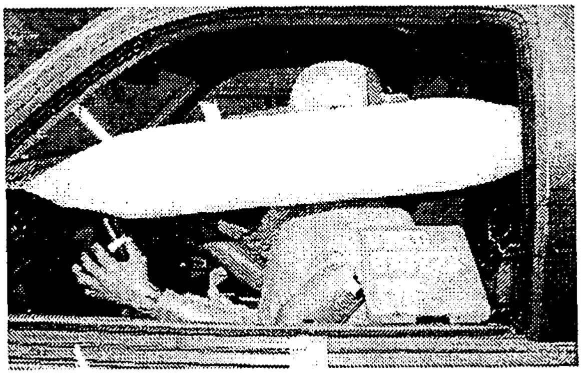

Figure 6a -- Driver Side ITS Used in Second Test

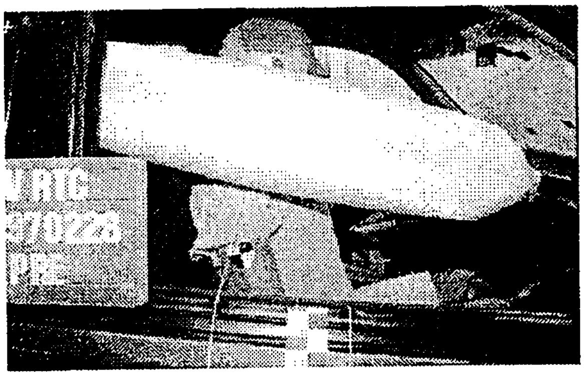

Figure 6b -- Passenger Side ITS Used in Second Test

Results of First Rollover Test

The event trigger signal was lost during the release stages of the cart resulting in lost data in the early stages of the rollover event. This also prevents knowing the event's true time zero. However, reasonable approximations of the entire event can be made by analyzing the data from the second and third tests. The test did provide excellent vehicle and occupant kinematics for evaluating the safety potential of the ITS devices. The vehicle rolled 11 quarter turns and came to rest on the passenger side. The test lasted approximately 4.5 seconds with peak roll velocities reaching 6.34 rad/sec early in the event (approximately 1.4 seconds). The driver side of the roof was exposed to the ground first followed by the passenger side.

The vehicle's rotation kept the dummies high in their seats and against the side interior throughout the entire test. The driver dummy made significant contact with the roof for an extended period of time. As the test, progressed the dummy orientated itself so the buttocks moved out the window opening. The high speed films show that significant excursion out the side window was prevented by the ITS system which reduced the open area (see Figure 7a). The passenger dummy contacted the ITS with its shoulder before impacting its head against the roof side rail. It is evident that the ITS system controlled the dummy's kinematics. Throughout most of the event, the lower arm of the passenger dummy remained out the window, below the ITS device, and made frequent contact with the ground. As seen in Figure 7b, the dummy's head was supported by the ITS, preventing movement outboard through the window.

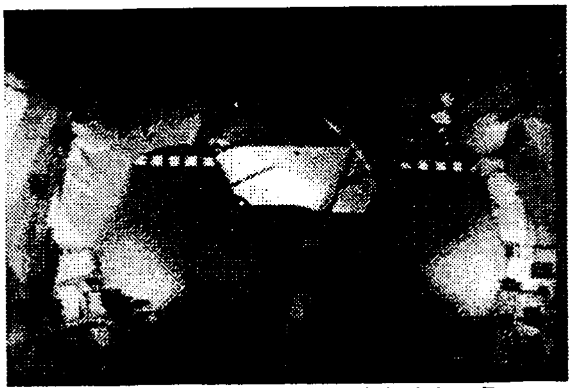

Figure 7a -- Driver Side ITS Minimizing Dummy Excursion Out Window Opening

Although the dummies experienced repeated head impacts with the vehicle's interior compartment, no significant HIC numbers were recorded. This also applies to the chest deflection measurements. However, the high compressive axial loads recorded by the neck transducer indicate that there is a strong probability of neck injury, which is typical to unbelted occupants in such rollover events. The dummies' injury measurements are shown in Table 1 along with injury threshold values. Because of the loss of time zero in the event, it is not possible to determine from film analysis whether these high compressive neck loads occurred as a result of impacts with the ITS or the vehicle interior.

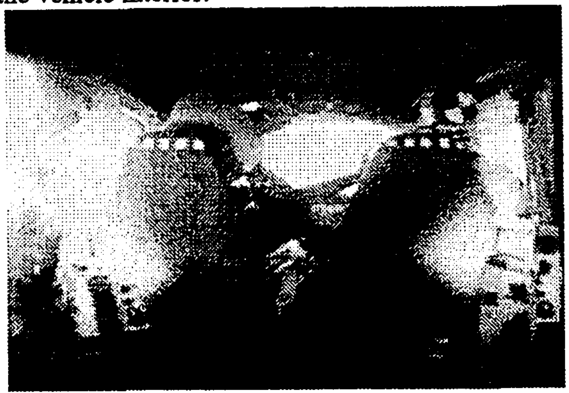

Figure 7b -- Passenger Side ITS Preventing Dummy Head Excursion Through Window

INJURY MEASURE	DRIVER	PASSENGER	INJURY THRESHOLD
HIC	26.2	19.5	1000
3 ms Chest G's	14.3	14.6	60
Chest Deflection, mm	4.6	1.4	50
Maximum Upper Neck Shear Force (fore/aft), N	365 / 561	278 / 413	1100 / 1100
Maximum Upper Neck Shear Force (lateral), N *	564	802	
Maximum Upper Neck			

Tension/Compression, N	417 / 1212	306 / 1838	1100 / 1100
Maximum Upper Neck Bending (flex./ext.), N-M	27 / 56	88 / 15	190 / 57
Maximum Upper Neck Bending (lateral), N-M *	61	44	

*No injury Criteria Exists

Table 1 -- Injury Measurements for First Rollover Test

The driver side dummy made two significant contacts with the driver side ITS. The tension was measured in the ITS webbing and is shown if Figure 8a. During the first roll, the driver's lower shoulder impacted the ITS and on the second roll, the dummy's pelvis contacted the ITS device.

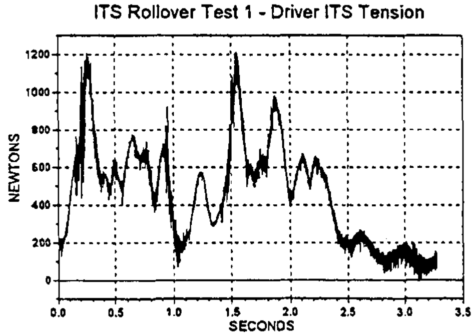

Figure 8a -- Driver Side ITS Webbing Tension

The passenger dummy's neck/shoulder region engaged the ITS throughout most of the test. The tension measurement in the passenger side ITS device is shown in Figure 8b. The tension values in both driver and passenger ITS units indicate significant loading by the dummies. This may suggest that in absence of the ITS, the dummy segments would have been moving outboard through the window opening.

From the occupant kinematics, it appeared that the desired location of the ITS was to position itself between the head and shoulder, thus limiting dummy movement towards the vehicle roof. The high speed films showed that the ITS did not remain over the middle part of the window opening but was instead positioned over the top of the opening. This allowed the dummy more vertical movement with a greater potential for high compressive neck loads. This could be attributed to loss in web tension due to roof deformation. These observations were addressed in the second rollover test.

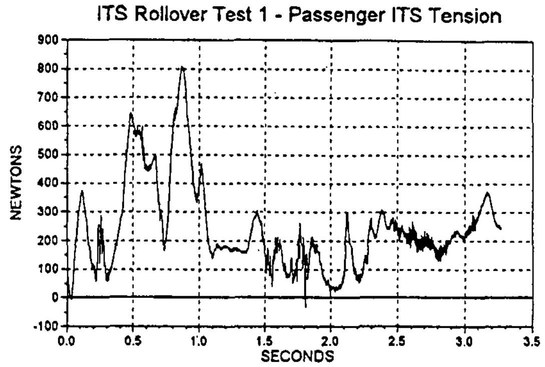

Figure 8b -- Passenger Side ITS Webbing Tension

Results of Second Rollover Test

Prior to running the second rollover test, the ITS system's front anchor points were moved inboard 5 inches to position the ITS closer to the head. This positioning is actually more in line with passenger vehicles. However, because the sides of the SUV are usually more vertical and not bent inboard as much as a passenger car, the ITS system's positioning with respect to the head was two far outboard in the first test. In addition, the system's rear anchor point was positioned 6 inches down from the roof to minimize the effect of roof deformation on the ITS tension.

The second rollover test also provided excellent vehicle and occupant kinematics for evaluating the safety potential of the ITS system. The vehicle rolled 10 quarter turns and came to rest on the roof. The test lasted approximately 6 seconds with peak roll velocities reaching 7.34 rad/sec 1.675 seconds after the roll was initiated.

As the rotational velocity developed, the unrestrained dummies left their seated position and moved towards the upper door and roof areas. Both dummies engaged the ITS system with their neck/shoulder regions. It appears as though the combination of improved inboard positioning and a larger ITS system improved the ejection mitigation capabilities and reduced the vertical movement of both dummies. However, this positioning did not prevent total vertical movement as the force of the dummies were able to move the ITS systems from the desired location over the middle of the window opening to near the top. Both dummies recorded high axial compressive neck loads at several points throughout the test. Table 2 lists the dummies' injury measurements and injury threshold values.

INJURY MEASURE	DRIVER	PASSENGER	INJURY THRESHOLD
HIC	89	43.8	1000
3 ms Chest G's	32.5	18.8	60
Chest Deflection, mm	3.7	4.5	50
Maximum Upper Neck Shear Force (fore/aft), N	245 / 168	530 / 645	1100 / 1100
Maximum Upper Neck Shear Force (lateral), N *	525	1276	
Maximum Upper Neck Tension/Compression, N	768 / 1199	522 / 5114	1100 / 1100
Maximum Upper Neck Bending (flex./ext.), N-M	12 /17	60 / 31	190 / 57
Maximum Upper Neck Bending (lateral), N-M *	80	89	

* No injury Criteria Exists

Table 2 -- Injury Measurements for Second ITS Rollover Test

The measurements indicate that there was a low likelihood of serious head of chest injury but a strong probability of neck injury. Film analysis showed that the injurious neck loads were caused by dummy contact with the vehicle roof. Figure 9 shows the vehicle's orientation along with the passenger dummy's position during which high neck loads were recorded. The vehicle's orientation is typical for many of the high neck load recordings. Film analysis shows that in the majority of ground impacts where the dummy recorded high axial neck loads, the dummy essentially remained in contact with the same part of the vehicle perimeter and simply pressed harder against it as the roof struck the ground.

High compressive neck loads also occurred where the unrestrained dummy moved laterally inboard, towards the impacted side of the vehicle, and did not gain from the restricting action of the ITS in the vertical direction. Figure 10 shows the vehicle and dummy positions for this scenario.

Throughout the test, the outboard arm of both dummies remained outside the vehicle and experienced contact with the ground on several occasions

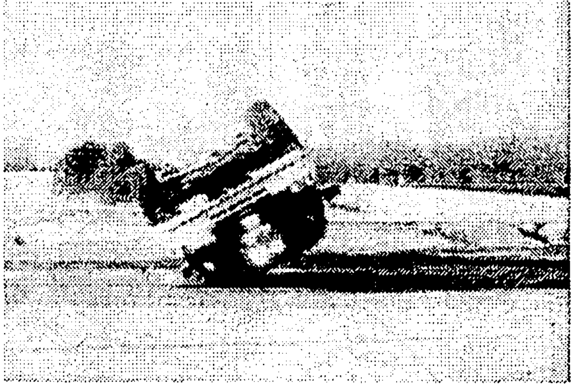

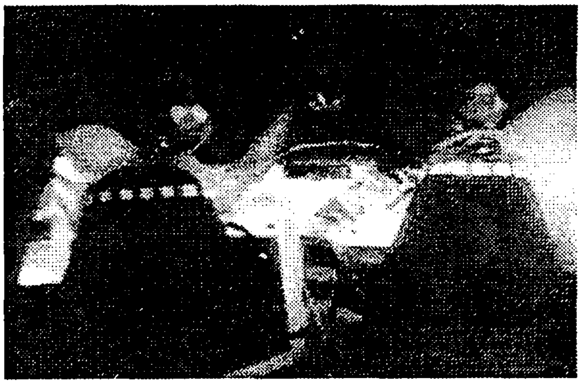

Figure 9 -- Vehicle Orientation and Corresponding Driver Side Dummy Position in Which High Compressive Neck Loads Typically Occurred

Figures 11a and 11b show the tension loads on the ITS webbing as the driver and passenger dummy interacts with the ITS. The high peak loads correspond with the dummy loading it sideways. The significant tension values on both the driver and passenger ITS units indicate a significant loading of the ITS by the dummies. This may suggest that in the absence of the ITS, the dummy segments would have been moving the window opening.

It is reasoned that if the occupant were to be held by seat belt during the rollover event, the efficiency of the ITS would be increased - allowing the ITS to support the occupant at all times, thereby mitigating not only ejection, but also further reducing injury do to contact with the interior of the car.

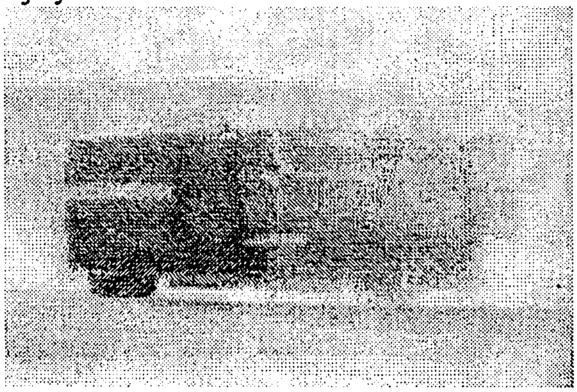

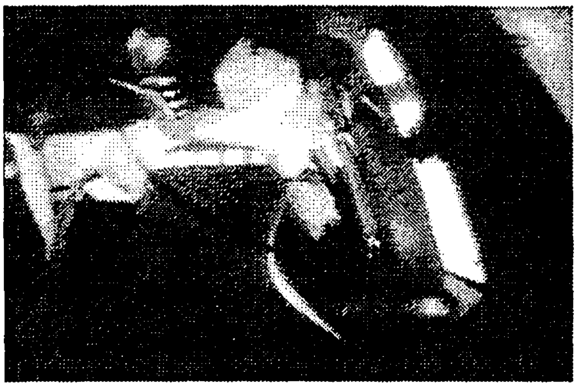

Figure 10 -- Vehicle Orientation and Corresponding Passenger Side Dummy Position in Which High Compressive Neck Loads Occurred

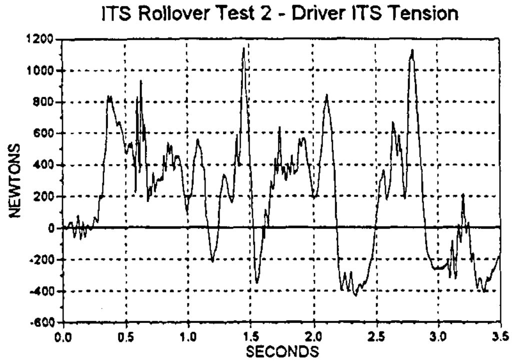

Figure 11a -- Driver Side ITS Webbing Tension

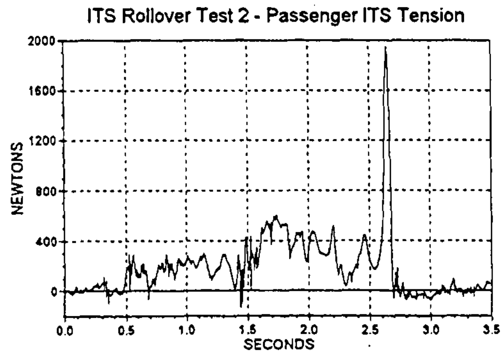

Figure 11b -- Passenger Side ITS Webbing Tension

Results of Third Rollover Test

The primary purpose of the third rollover test was to investigate the characteristics of the occupant/ITS interaction using a fully functional ITS system. A roll sensor was incorporated that initiated deployment of the ITS by means of a gas generator. The system was designed to inflate when the sensor (and therefore vehicle) rotated 35 degrees with respect to horizontal. This number was arbitrarily chosen after analyzing the films from the previous tests. At this point in the test, the dummies have not yet left their seats, nor have any body segments begun to move outboard toward the vehicle perimeter. The inflator received an external signal at 250 milliseconds as a backup precaution. Although the anchor positions were identical to the previous test, the smaller diameter ITS system was chosen for both driver and passenger. The passenger dummy was also restrained by a lab/shoulder belt.

As in the previous tests, this test provided excellent vehicle and occupant kinematics for evaluating the ITS system's safety potential. The vehicle rolled 12 quarter turns and came to rest on its wheels. Unfortunately, the angular rate gyroscope, used to measure roll velocity, failed in the early stages of the test. Analysis of the film and sensor data indicated that airbag deployment was the result of the sensor signal. Both ITS systems deployed and were in position over the window opening prior to any dummy contact.

The driver dummy lifted off the seat and moved toward the perimeter of the vehicle, constrained by the upper door and roof areas. The dummy's neck/shoulder area contacted the ITS throughout most of the test and positioned the bag over the upper area of the window opening. The passenger dummy moved more laterally towards the window opening and made contact with the deployed airbag in the neck/shoulder region and remained there for most of the test. The dummy's vertical movement was significantly reduced by the lap/shoulder belt. Both dummies' outboard arm remained outside the vehicle's perimeter throughout the test with each outboard shoulder appearing to make ground contact at various times.

The dummies' injury measurements are listed in Table 3 along with injury threshold values. As was the case for the previous tests, the rollover caused no significant head or chest injuries.

INJURY MEASURE	DRIVER	PASSENGER	INJURY THRESHOLD
HIC	138	82	1000
3 ms Chest G's	21.8	16.7	60
Chest Deflection, mm	1.8	1.4	50
Maximum Upper Neck Shear Force (fore/aft), N	352 / 762	3843 / 1046	1100 / 1100
Maximum Upper Neck Shear Force (lateral), N *	913	3379	

Maximum Upper Neck Tension/Compression, N	823 / 4703	1093 / 850	1100 / 1100
Maximum Upper Neck Bending (flex./ext.), N-M	27 / 22	33 / 3.4	190 / 57
Maximum Upper Neck Bending (lateral), N-M *	79.4	33	

* No injury Criteria Exists

Table 3 -- injury Measurements for Third Rollover Test

The driver recorded high axial compressive neck loads at several points during the test. Film analysis showed that the majority of these high loads occurred when the dummy head was in contact with the roof rail area and experienced a large force in the neck due to displacement of the vehicle structure. The passenger dummy did not experience any significant axial neck loads. This is attributed to the restraining effect of the lap/shoulder belt. However, high shear forces were recorded which were the result of severe roof crush on the passenger side.

Summary of Test Results

The three full scale rollover tests have demonstrated that the ITS has significant potential for reducing complete ejections during rollover crashes. However, there is a significant potential for arm ejections. From 1988 through 1996, NASS CDS reported an annual average of four occupants with AIS 2 or greater arm injuries due to external contact during rollover. These cases are weighted to an annual estimate of 13 rollover involved occupants with AIS 2 or greater arm injuries due to external contact. These full scale tests also demonstrated a significant potential for neck injury for non ejected occupants.

Simulation Results

MADYMO simulations were conducted for the first two rollover tests. These simulations were validated against the test results and then rerun without the ITS present to evaluate if ejection were indeed prevented.

The baseline simulations were validated to reproduce the occupant kinematics measured in the two tests. When the ITS devices were removed, all four of the unbelted occupants in the first two tests were ejected.

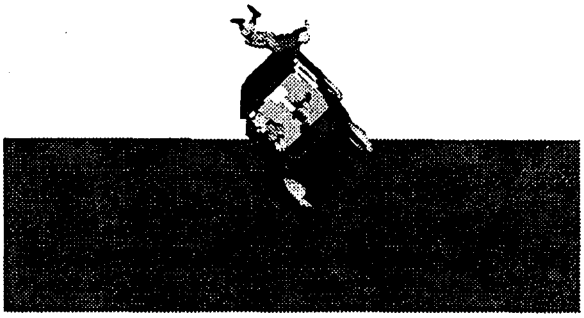

Figure 12 -- Driver Ejection during simulation of the first rollover test without an ITS

Future Research

The baseline testing has establish the potential of ejection mitigation using the ITS. Further work is needed to optimize the ITS location and deployment timing for rollover accidents. Toward this end, the ITS will be tested in a more repeatable rollover test device so that optimizations studies can be conducted.

CONCLUSIONS

The ITS devices have demonstrated a strong potential for reducing side window ejection in rollover crashes. While the kinematics of any single rollover crash are generally not repeatable, the general nature of this mitigation concept should result in significant safety benefits. The potential benefit of the ITS should be further realized in light of the fact that it had been developed for side impact head protection. Therefore, ejection mitigation and head contact with the interior of the car are additional benefits of the same single safety device. Follow on research will focus on optimizing the safety performance of the ITS in rollover environments.

VEHICLE FAR-SIDE IMPACT CRASHES

Richard Stolinski
Raphael Grzebieta
Department of Civil Engineering
Monash University, Clayton
Australia
Brian Fildes
Accident Research Centre
Monash University, Clayton
Australia.

Paper 98-S8-W-23

ABSTRACT

This is a summary of a paper which first appeared in the International Journal of Crashworthiness under the title: "Side Impact Protection - Occupants in the Far-Side Seat", Vol. 3, No. 2, pp 93-122. Readers are directed to the full paper for a more comprehensive discussion of the issues presented here.

Much of the applied vehicle side impact occupant protection research to date has concentrated on occupants seated beside the struck side of vehicles. These occupants are defined as 'near-side' occupants. Real world crash evidence however has shown that occupants seated on the side away from the struck side, defined as 'far-side' occupants, are still subject to a risk of injury. This paper examines side impact epidemiology from an injury causation perspective, and endeavours to explain evidence indicating head injuries and seat belt related injuries constitute a significant proportion of all far-side impact injuries. Injury mechanisms and key dynamic parameters governing injury severity are detailed. Computer models simulating the dynamic motion of vehicle far-side occupants are described. Occupant kinematics and injury parameters from the models are then compared with real world crash case studies. The paper finally suggests vehicle design strategies which may reduce far-side injuries. Some alternative restraint systems are proposed as potential countermeasures to reduce occupant injuries.

INTRODUCTION

Vehicle occupants are particularly vulnerable in side crashes. Australian studies by Fildes et al [1,2] have revealed that side impact crashes accounted for 25 percent of all injury crashes and 40 percent of serious injury crashes where an occupant was either hospitalised or killed. Vehicle side impact occupant protection research has concentrated mostly on the occupants seated beside the struck side of the vehicle. These occupants are defined as near-side occupants. All regulatory side impact test standards focus exclusively on this scenario and rely on an assessment provided by one test intended to represent one point in the spectrum of real world near-side impact crashes.

Real world crash evidence however has shown that far-side occupants as illustrated in Figure 1, are still subject to a risk of injury. The study by Fildes et al noted that around 40 percent of restrained side impact crash casualties were far-side occupants. Relatively little research literature is available that addresses protection of far-side occupants. The scope of this paper thus addresses far-side occupants where there may be opportunities for improved occupant protection.

Before any countermeasures to problems of vehicle far-side impact crashworthiness can be proposed however, it is first necessary to establish clear injury patterns which characterise the problem. It then becomes possible to identify the injury mechanisms and finally propose countermeasure strategies which can address these specific injury processes.

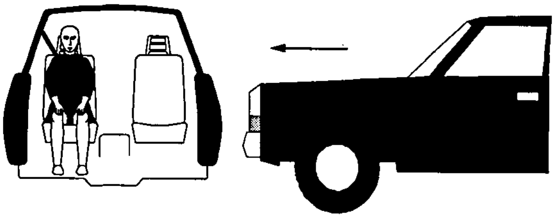

Figure 1. Far-Side Impact Crash Configuration

SIDE IMPACT STATISTICS

Ginpil et al [3], examined data relating to crashes occurring in Australia in 1990 where at least one occupant fatality resulted from an impact to the side of the vehicle. They reported that 79 percent of occupants in the sample were killed in near-side impacts compared to 36 percent of occupants killed in far-side impacts. Further, this study reported that far-side fatalities were more likely to sustain serious head injuries than near-side fatalities. The report detailed 26 percent of far-side fatalities sustained severe injuries only to the head and no other region, compared with only 18 percent for near-side fatalities. Mackay et al [4] using UK field accident data discussed the relative importance of head injuries for restrained far-side occupants. The report highlighted the issue of torso restraint and detailed a frequent mechanism where far-side occupants can slip out of their chest restraint to make head contact with structures on the opposite side of the vehicle cabin. Based on a study sample of 51 head injury cases, 35 percent were judged to have come out of their seat belt. Mackay also reported frequent far-side occupant injuries to chest and abdominal body regions from excessive seat belt loads caused by the upper torso slipping from the shoulder belt. The reported mechanism of the upper torso flailing about in the cabin was considered a key element in the further investigation of far-side impact occupant injury.

Subsequent sections of this paper deal with a closer examination of Australian injured occupant cases. Mathematical computer modelling simulations of these cases have been developed which attempt to reconstruct the essential mechanisms and provide a basis for the selection of potential countermeasure designs.

CRASHED VEHICLE CASE STUDIES

Crashed Vehicle File

Side impact case studies by Fildes et al [1] detailed vehicle crash parameters together with injury distributions for a sample of hospitalised and killed occupants in Australian crashes. These case studies were based on a sample of 198 side impact crashes of passenger vehicles. The study investigated 234 injured or killed occupants and formed part of the Monash University Accident Research Centre's (MUARC) crashed vehicle file collected for the Australian Federal Office of Road Safety (FORS). The whole FORS sample compiled at the time of writing included 134 restrained occupants in near-side impacts and 52 restrained occupants in far-side impacts.

Detailed information about the nature of each crash together with vehicle deformations and likely injury sources were recorded by MUARC researchers. Additionally, estimated vehicle delta-V values were derived using the Crash-3 computer program. Injuries to various body regions were coded according to the Abbreviated Injury Scale (AIS), documented by the American Association for Automotive Medicine, [5]. AIS is a "threat-to-life" scale ranging from AIS1 (minor severity) to AIS6 (non-survivable).

Far-Side Case Study Sample

The sample of occupants killed or injured in far-side cases collected by MUARC was examined to establish parameter patterns relevant to far-side impacts which typically lead to injury. The entry criterion for the far-side sample was based on primary impact damage on the side opposite where the injured or killed occupants were seated. To expedite this review, a subset of the overall MUARC crashed vehicle file published as one page summaries was analysed. As the prime interest of this study is on restrained occupants, cases where seat belts were judged not to have been used, were excluded. A sample of 45 restrained cases classified as far-side impacts by MUARC was thus used. The sample of injured and killed occupants comprised 26 males and 18 females. In the sample, 36 occupants were drivers and 9 were passengers (2 in rear seats). Further, 16 of these far-side occupants were seated beside adjacent (near-side) occupants, whereas 29 far-side occupants were not adjacent to any other occupant. The median occupant age in the far-side sample was around 30 years.

Case Study Vehicle Impact Data

The vehicle impact information from the case study sample was used to specify the significant impact conditions applied in subsequent computer modelling simulations. Figure 2 shows the sample's distribution of objects the car containing the subject far-side occupant impacted with, or was impacted by. Most cases involved impacts with other cars. Impacts with fixed objects such as trees and poles are notable as are impacts with heavier vehicles such as four wheel drives which are included in the light truck category. Most impacts occurred to the mid sections of the subject vehicles.

The sample of vehicles comprised almost equal proportions of vehicle size/weight categories. The numbers of small (under 900 kg), medium (900 to 1200 kg) and large (over 1200 kg) passenger cars in the sample were 14, 15 and 16 cases respectively. Figure 3 shows the distribution of vehicle mass ratios.

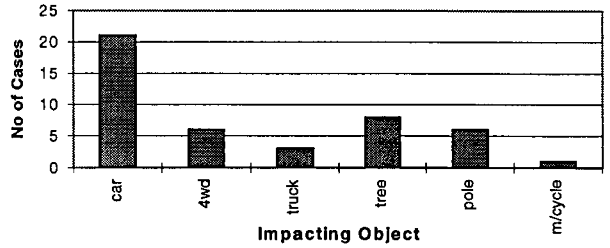

Figure 2. Histogram of Impacted/Impacting Objects, n = 45

The mass ratio in these cases was defined as the mass of the far-side occupant's vehicle divided by the mass of the impacting vehicle. Around half of the cases in the sample have vehicle mass ratios under 0.9.

Figure 5 shows the distribution of the impacting object's directional angle α with the side of the subject occupants' car as defined in Figure 4. Most cases were classified as pure side impacts where the directional impact angle was around 90 degrees. The sample is however skewed towards angles less than 90 degrees where a rearward orientated velocity component relative to the occupant's car was present at the time of impact.

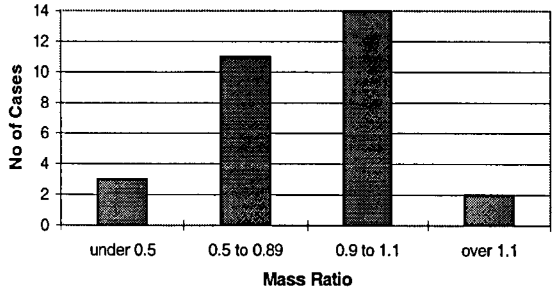

Figure 3. Histogram of Impacting Vehicle Mass Ratios, n = 30 (subject vehicle mass/impacting vehicle mass)

Figure 6 shows the cumulative distribution of the maximum cabin intrusion for all cases in the far-side injury sample. Intrusion exceeded 400 mm in around half of the cases. In around 20 percent of the cases, the maximum intrusion exceeded 625 mm which is equivalent to half of the cabin width of a typical small car. Interestingly, 20 percent of far-side injury cases were recorded where no intrusion was noted

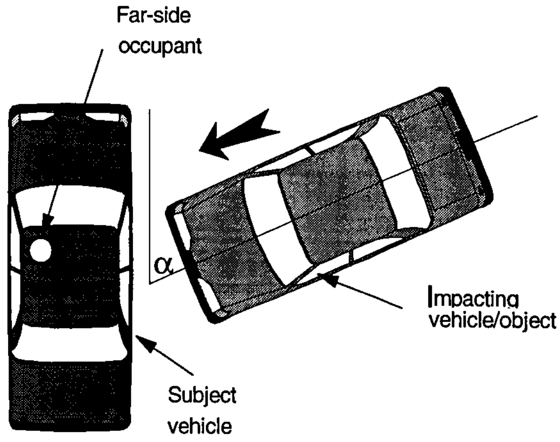

Figure 4. Definition of Impact Geometry

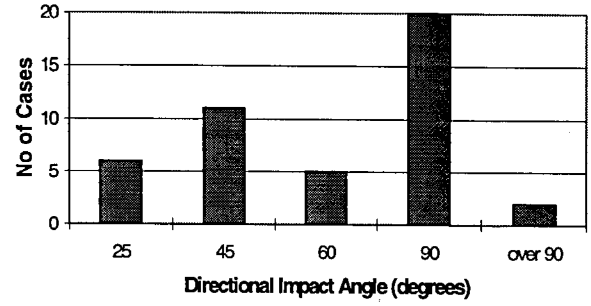

Figure 5. Histogram of Directional Impact Angle α, n = 45

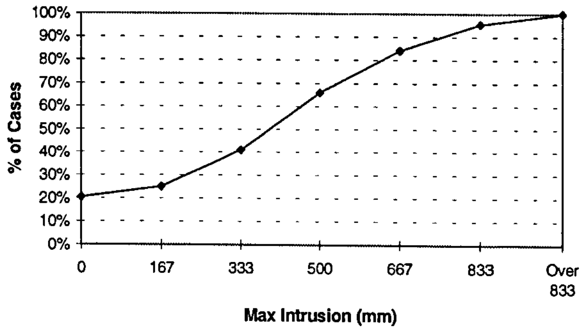

Figure 6. Cumulative Distribution of Max Intrusion for All Cases, n = 45

Figure 7 shows delta-V distributions for light truck or car into car impacts. These vehicle crash delta-V values were calculated by MUARC using the Crash-3 computer program. It was not possible to calculate estimates of delta-V in all cases, thus Figure 7 is based on data from 22 far-side impact cases. In the sample, 80 percent of cases have estimated delta-Vs under 60 km/h, with half of the cases having delta-Vs estimated under 40 km/h.

Based on the case study vehicle impact data, suitable test conditions to conduct subsequent dynamic simulation modelling evaluations of far-side impacts were established. These conditions were considered representative of important segments within the spectrum of real world crashes. Car to car simulation cases were initially investigated with a medium size 1000 kg car. An impacting vehicle mass higher than the far-side occupant's car was chosen, with a vehicle mass ratio of 0.9. Impact into the far-side occupant car's mid section at an angle of 90 degrees was considered representative. Delta-Vs below 60 km/h were also considered relevant for the investigation.

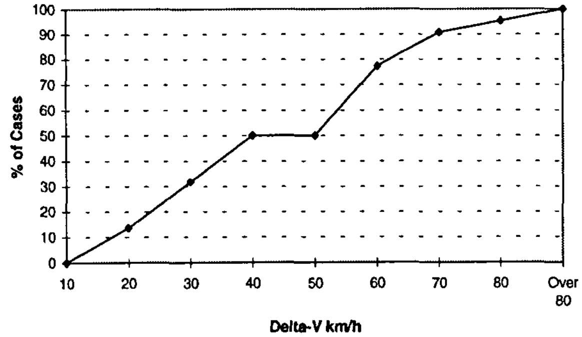

Figure 7. Cumulative Distribution of Delta-V for Light Truck or Car into Car Impact Cases, n = 22

Case Study Occupant Injury Data

Occupant injury data from the far-side study case study sample was used to verify whether simulation load measurements correctly predicted occupant injuries that would be expected in similar real-world situations. Details of injury severity outcomes and observed injury loading mechanisms from the sample of restrained far-side occupants are provided in Stolinski et al [6]. The following is a summary of the findings.

The typical motion of a relatively unrestrained upper torso pre-disposes far-side occupants to a risk of head injuries as the torso rotates across the cabin interior and the head contacts the vehicle's far side or instrument panel. Further, as the shoulder and chest slips out from under the sash part of a three point seat belt, belt loads can be concentrated on the body region impinged by the lap belt. Another mechanism observed in high severity impacts is direct contact with the intruding object. Where intrusion approaches half the width of the car cabin, direct contact with an intruding object may be unavoidable. An additional important mechanism is direct contact with adjacent occupants. It is possible that an adjacent near-side occupant may shield the far-side occupant from intruding objects or the vehicle's far-side, however the impacts between occupants themselves would certainly involve some risk of injury.

FAR-SIDE OCCUPANT/VEHICLE DYNAMICS

Injury Tolerance

Questions arise as to what levels of the key dynamic measures of head velocity and lap seat belt load are critical. Kanianthra et al [7] and NHTSA [8] in the development of the US Upper Interior Head Protection Standard - FMVSS No. 201, selected a free motion headform impact test velocity of 15 mph (6.7 m/s) for the evaluation of interior padding materials. This test speed was established on the basis of US National Accident Sampling System (NASS) data, where it was noted to be the average occupant speed relative to the cabin interior at which the onset of serious injuries (between AIS 2 and AIS 3) are likely to occur. McIntosh et al [9] conducted studies on head impact tolerance in side impacts using cadaver tests and computer simulations. Findings indicated that at impact velocities in excess of *6 m/s*, head injuries of an AIS 3 level were likely. McIntosh et al proposed tolerance levels of maximum head acceleration of 150 g and HIC of 750. The authors suggested that even with padding, the likelihood of brain injury was not reduced at these higher velocities.

Leung et al [10] proposed lap belt injury tolerance loads. Using cadaver tests, injuries were observed for lap-belt tension loads higher than *3 kN*. Although this tolerance load was established with respect to frontal collision kinematics, it is considered that a lateral impact tolerance load may not differ too significantly. It is thought that during impact, the body rotates around its vertical axis so that the belt loads still primarily impinge on the forward portion of the abdomen. Nevertheless some fundamental research to better establish lateral impact tolerance loads still needs to be carried out.

Occupant Dynamics - Sled Test Computer Model

A model of a restrained occupant in a far-side impact sled test situation was developed using the TNO MADYMO occupant/vehicle crash simulation computer program. As previously noted, the mechanism of occupants slipping out of their seat belts is crucial to the realistic modelling of far-side occupant motion. It was therefore necessary to use a finite element seat belt model capable of simulating seat belt slip. The occupant in the sled test was simulated using a multi-body 50th percentile Hybrid III ellipsoid model from the MADYMO dummy database [11]. The finite element seat belt was available as a MADYMO application and is detailed in the MADYMO Applications Manual [12]. The seat structure was simulated using plane elements with dummy-seat and dummy-belt contact interaction characteristics established experimentally by TNO [12].

As a validation exercise, initial modelling was done to replicate a series of sled tests in a General Motors Research Laboratories program by Horsch et al [13]. Sled test response data from both Hybrid II dummies and cadavers was published by Horsch making comparisons possible with the computer model output data. As in the sled test program, *a 100 ms, 10g square acceleration pulse* was applied in the MADYMO model.

Figure 8 shows the computer model simulation kinematics that compared favourably with a sled test run using an unembalmed cadaver [6]. A comparison of responses from the Horsch test series [13] with the computer model simulation responses is summarised in Table 1. Head acceleration levels from the dynamic motion itself are well below published injury tolerance levels. However if the head were to contact an interior cabin structure at a velocity exceeding 6 m/s, as observed in the simulation, injury would be expected. It is noted that measured maximum lap belt loads are above the abdominal injury tolerance levels suggested by Leung.

Occupant Dynamics - Car Test Computer Model

A sled test scenario is somewhat limited as real vehicle lateral impacts also involve varying levels of rotational acceleration. A full car model also provides the opportunity to model more realistic acceleration pulses developed during the interaction of two colliding vehicles. Further, it was considered useful in subsequent studies, to develop the capability to model interactions between the far-side occupant and adjacent near-side occupants in the car. It was therefore decided to assemble a full car and occupant simulation model to further study far-side occupant dynamics in full vehicle side impact situations.

This model was developed [6] by integrating the sled test model, described in the previous section with a car side impact model originally developed to simulate an ECE R95 [14,15] side impact test at 50 km/h. Centre console and floor transmission tunnel surfaces were added to the model for far-side side occupant contact interaction as these structures are present in most cars and are considered important to modelling correct occupant dynamics.

Table 1.
Comparison of Sled Test and Computer Model Peak Responses

Dynamic Parameter	Sled Tests	Computer Simulation
Shoulder Belt Load (kN)	2.6 - 4.1	5.0
Inboard Lap Belt Load (kN)*	1.9 - 4.1	2.8
Outboard Lap Belt Load (kN)**	2.3 - 4.3	4.7
Upper Torso Acceleration (g)	19 - 23	20
Head Acceleration (g)	33 - 42	26
Head Velocity (m/s)	-	9.1

* Inboard Lap Belt Load - (adjacent dummy's right side)

**Outboard Lap Belt Load - (adjacent dummy's left side)

The full car and occupant computer model was run in a number of test cases and the results are detailed in Table 2. The model at this stage has only been run with the far-side occupant in the vehicle. A 1000 kg car with a 1111 kg impacting barrier (mass ratio = 0.9) was used. The subject car containing the far-side occupant was impacted mid section by the mobile barrier at 90 degrees.

It was observed that for far-side occupants where the upper torso is relatively unrestrained, head velocities were closely related to the car delta-Vs. The simulation results show that at an impact speed of 40 km/h, neither the head velocity nor the lap belt load exceeded previously established tolerance values. At 50 km/h, the head velocity exceeded the tolerance value. At 60 km/h, *both* the head velocity and the lap belt loads exceeded the tolerance values. The 60 km/h test speed resulted in only a 31 km/h delta-V of the impacted car. Delta-Vs up to this level in the MUARC far-side injury sample, as detailed in Figure 7, accounted for less than half of the injured occupants. Accordingly, the majority of injured cases occurred beyond this level of delta-V. This is consistent with the simulation findings that injury tolerance levels are certainly exceeded beyond this level of crash severity.

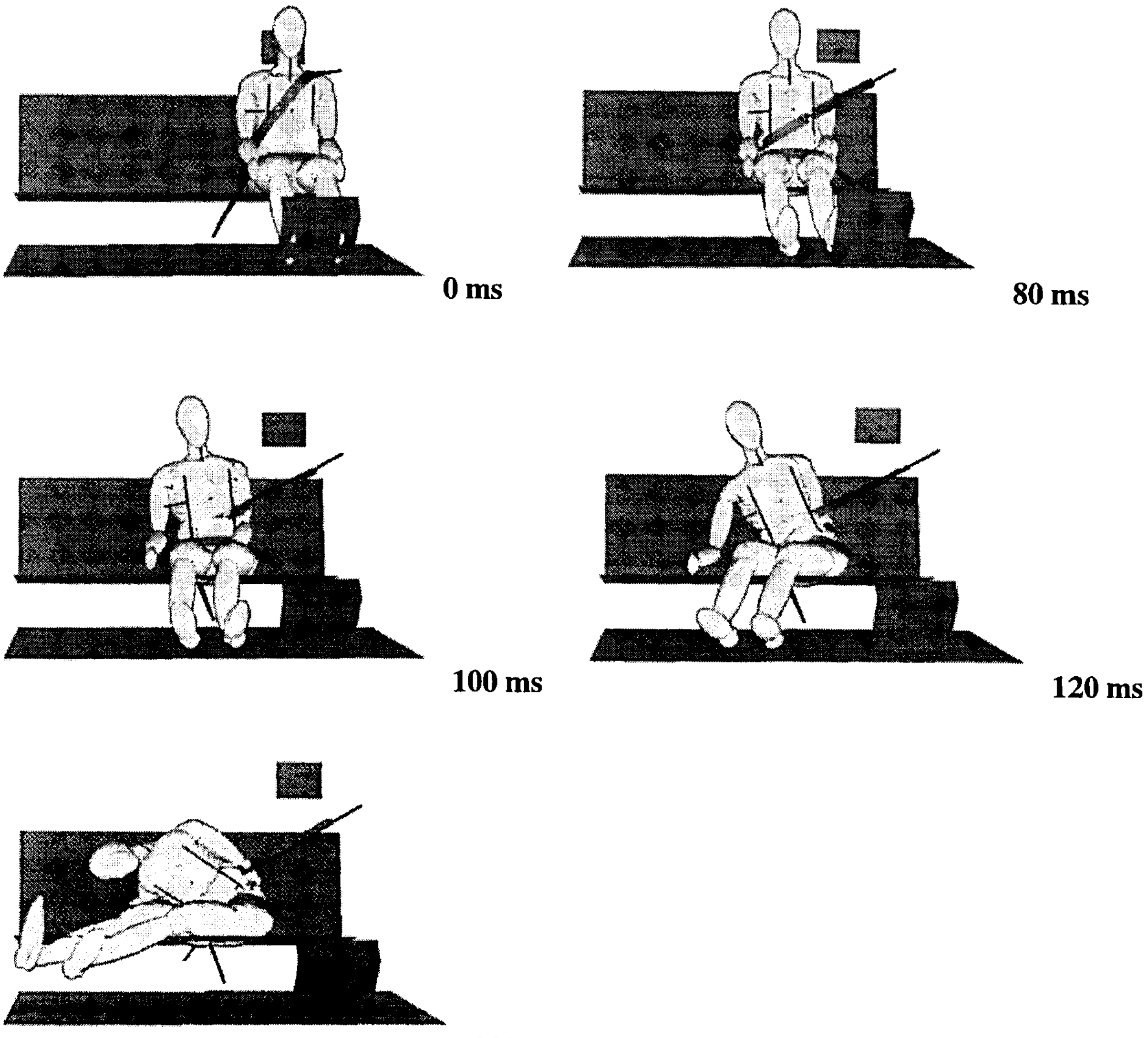

0 ms

80 ms

100 ms

120 ms

200 ms

Figure 8. Dynamic Motion in Far-Sided Impact Sled Test from MADYMO Simulation of Hybrid III Dummy During 10g Side Impact Pulse.

Table 2.
Peak Responses of Far-Side Occupant in the Car Test Computer Model

Impact Speed (km/h	Head Velocity (m/s)*	Lap Belt Load (kN)**	Car Acceleration (g)***	Car Delta-V (km/h, m/s)
40	5.3	1.4	10.5	20.4, 5.7
50	7.3	2.3	12.6	25.9, 7.2
60	9.1	3.5	14.6	31.1, 8.6

* head velocity relative to the car interior, ** outboard lap belt load, *** lateral acceleration measured at the car's centre of gravity

FAR-SIDE INJURY COUNTERMEASURES

Seat Belt Pretensioners

If better upper torso lateral restraint could be provided, the level of torso swing could be reduced, causing either fewer head impacts to occur with the cabin interior or at least at lower impact velocities. Seat belt pretensioning of the sash belt that is activated during lateral impacts may be effective in delaying or reducing the extent of seat belt slip.

Reduction of sash belt slip would also be expected to reduce the concentration of lap belt loading by maintaining more belt loading on the upper torso.

Lateral Wing Seat Bolsters

Another countermeasure could be the provision of highly defined lateral 'wing' torso restraints that are built into seat structures. This design configuration is common in motor sport. Together with a full harness, this design provides a high level of lateral occupant restraint for racing drivers. It appears likely however that comfort issues could lead to serious difficulties in consumer acceptance of this configuration. Careful design of inboard lateral bolsters would be needed to ensure their acceptability in passenger vehicle applications.

As such designs provide more torso restraint, further research is needed to establish whether unacceptable inertial loads are transferred to the unrestrained head/neck of far-side occupants. The human neck model developed by de Jager [16] may be useful in this regard. It will also be important to ensure that thoracic loads on far-side occupants do not exceed tolerance levels.

Reverse Geometry Seat Belts

Another potentially effective countermeasure against far-side head impacts worth considering may be the provision of reverse geometry integrated seat belts. This design configuration has been implemented in the rear seats of some BMW passenger vehicles. Some tests have shown however that belt/neck loads could be excessive with this seat belt configuration. Horsch et al [13], who conducted cadaver sled tests, indicated that serious C5-C6-C7 cervical spine injuries could occur. Conversely, Kallieris et al [17], using cadavers in full vehicle side impact tests, concluded that application of reverse geometry seat belts did not cause neck injuries beyond AIS level 1. It appears therefore that more research is still needed into the biomechanical effects of reverse geometry seat belts and potential benefits for far-side occupants. Reverse geometry integrated seat belts would however incur cost and weight penalties for vehicles because more complex seat and re-inforced floor structures would need to be designed.

Inflatable Restraint Systems

Alternative solutions, involving inflatable airbag restraint systems using existing technology may be possible. This way, existing consumer expectations of comfort and space would not need to be compromised. A basic problem with inflatable systems is the need to provide surfaces or supports for an airbag to react against whilst restraining an occupant. It is possible that an inflatable curtain devices originally intended for protection of near-side occupants could also provide protection for far-side occupants by providing a buffer against head impacts with far-side structures.

CONCLUSIONS

In far-side impact situations, a key mechanism leading to injury is the upper torso slipping out of the shoulder belt. As a result, excessive head velocities can develop in the car together with excessive lap belt loads. This process is considered responsible for many of the head and abdominal injuries observed in far-side impact occupant injury case studies. Head velocities relative to the car interior exceeding 6 m/s and lap belt loads higher than 3 kN have been shown to be critical values, above which, head or abdominal injuries are likely. Other important loading mechanisms include direct contact with intruding objects and contact with adjacent occupants.

The simulation studies described in this paper have shown that with impact velocities at or above 60 km/h (with delta-Vs exceeding 31 km/h), critical values of head velocity relative to the car interior or lap belt load can be exceeded in some crash situations. This is consistent with real world case studies, where most injury cases in the sample were noted to occur above this level of crash severity.

Some alternative restraint systems have been proposed as potential countermeasures to reduce far-side impact injuries. These include seat belt pretensioners which are activated by lateral acceleration, lateral wing seat bolsters, reverse geometry seat belts and inflatable devices. Further research is recommended to investigate the usefulness of these countermeasures, particularly to ensure that neck injury tolerance loads are not exceeded.

Further research work is also recommended to examine:

- larger sample sizes of real world far-side injury cases;
- abdominal injury mechanisms from the lap belt under lateral impact loading;
- injury mechanisms during adjacent occupant interactions and contact with intruding structures;
- issues of eccentric and angled vehicle impact geometry;
- effects of pole and tree impacts.

Consideration should be given to the inclusion of a far-side occupant dummy in future side impact design rule test standards.

Finally, it has been shown that opportunities exist for the development of new and innovative restraint systems.

ACKNOWLEDGMENTS

The authors wish to thank Stefan Nordin and Robert Judd of Autoliv Australia P/L for advice on restraint system technologies that were discussed in this paper and Dr. Clive Chirwa, editor of I.J. Crash for allowing the paper to be published in the ESV proceeding in summary form.

REFERENCES

1. B Fildes, J Lane, J Lenard, P Vulcan, 'Passenger Cars and Occupant Injury: Side Impact Crashes', *Australian Federal Office of Road Safety*, Report No. CR134, 1994.

2. B Fildes, K Digges, D Carr, D Dyte, P Vulcan, 'Side Impact Regulation Benefits', *Australian Federal Office of Road Safety*, Report No. CR154, 1995.

3. S Ginpil, R G Attewell, A Jonas, 'Crashes Resulting in Car Occupant Fatalities: Side Impacts', *Australian Federal Office of Road Safety*, Report No. OR15, 1995.

4. G M Mackay, J Hill, S Parkin, J A R Munns, 'Restrained Occupants on the Non-Struck Side in Lateral Collisions', *Proceedings of 13th ESV Conference*, Paris, France, 1991.

5. American Association for Automotive Medicine, 'The Abbreviated Injury Scale: 1990 Revision' , Illinois.

6. R Stolinski, R Grzebieta, B Fildes, 'Side Impact Protection - Occupants in the Far-Side Seat', *International Journal of Crashworthiness*, Vol.3 No. 2, pp 93-122, 1998.

7. J N Kanianthra, W Fan, G Rains, 'Upper Interior Head Impact Protection of Occupants in Real World Crashes', *Proceedings of 15th ESV Conference*, Melbourne Australia, 1996.

8. NHTSA, 'FMVSS No. 201 - Upper Interior Head Protection - Final Economic Assessment', *NHTSA Office of Regulatory Analysis*, 1995.

9. A S McIntosh, N L Svensson, D Kallieris, R Mattern, G Krabbel, K Ikels, 'Head Impact Tolerance in Side Impacts, *Proceedings of 15th ESV Conference*, Melbourne Australia, 1996.

10. Y C Leung, C Tarriere, D Lestrelin, C Got, F Guillon, A Patel, 'Submarining Injuries of Three Point Belted Occupants in Frontal Collisions - Description, Mechanisms and Protection, SAE Paper No 821158.

11. TNO, 'MADYMO Database Manual - Version 5.2', *TNO Road-Vehicles Research Institute*, 1996.

12. TNO, 'MADYMO Applications Manual - Version 5.2', *TNO Road-Vehicles Research Institute*, 1996.

13. J Horsch, D Schneider, C Kroell, 'Response of Belt Restrained Subjects in Simulated Lateral Impact', SAE Paper No 791005.

14. P J A de Coo, E G Janssen, A P Goudswaard, J Wismans, M Rashidy, 'Simulation Model for Vehicle Performance Improvement in Lateral Collisions', *Proceedings of 13th ESV Conference*, Paris, France, 1991.

15. ECE Regulation No.95, Uniform Provisions concerning the Approval of Vehicles with regard to the Protection of the Occupants in the event of a Lateral Collision, October 1995.

16. M de Jager, 'Mathematical Head-Neck Models for Acceleration Impacts', *Eindhoven University of Technology*, PhD Thesis, 1996.

17. D Kallieris, G Schmidt, 'Neck Response and Injury Assessment Using Cadavers and the US-SID for Far-Side Lateral Impacts of Rear Seat Occupants with Inboard Anchored Shoulder Belts', *Proceedings of 34th Stapp Car Crash Conference*, Paper No 902313.

DEVELOPMENT OF MOVING DEFORMABLE BARRIER IN JAPAN - PART 2 -

Masanori Ueno
Takeshi Harigae
Haruo Ohmae
Japan Automobile Research Institute
Takahiko Uchimura
Eiji Fujiwara
Japan Automobile Manufacturers Association, Inc.
Japan

Paper Number 98-S8-W-25

ABSTRACT

The reduction of occupant injury to side collision is a major subject worldwide.

Extensive research into this subject is now being carried out, mainly in the US, Europe and Japan. As a result, vigorous discussion has come out during various types of international conferences promoting international conformity such as WP29/GRSP, ISO and ESV International Conference.

However, international harmonization of test method has not yet been attained. The US method and European-Japanese methods are different in Moving Deformable Barrier (MDB), the dummy and the injury criteria.

Japanese developed barriers are made mainly of an aluminum honeycomb structure and proved to be of high repeatability in the calibration tests which are the test procedure for Japanese Safety Standard scheduled to be issued on October 1998.

INTRODUCTION

In October 1998 it was decided to be introduced and be put into effect the ECE Reg.95 side impact test procedure in Japan. In this side impact test procedure, the MDB simulating a colliding vehicle strikes the side of a test vehicle. An absorbing material called a deformable barrier is attached to the front of the MDB. The specifications of the deformable barrier, e.g. dimensions, dynamic deflection characteristics, which correspond to those of the typical passenger vehicle, have been set forth. There are, however, no satisfactory dynamic deflection characteristics in the deformable barriers, which have been developed up to the present time, both domestically and outside of the country. If the deformable barrier is left as is, the execution of the testing is likely to be hindered. Therefore, the development of a new deformable barrier is a matter of great urgency.

The deformable barrier used in the past studies for developing side impact test procedure in Japan fails in satisfactorily meeting the performance required for part of the force deflection characteristics. The authors have already reported about this deformable barrier in 15th-ESV International Conference, etc.

Based on the foregoing, a new deformable barrier, which perfectly satisfies the performance required for the calibration test, has been developed. This paper reports on the structure of this recently developed deformable barrier and its calibration test results.

OUTLINE OF THE SIDE IMPACT TEST

Existing methods are the US method (FMVSS 214) and the European method (ECE Reg.95) for the side impact test procedure. Of these methods, Japanese government decided to adopt the ECE Reg.95. The outlines of the test procedure and calibration test for the deformable barrier in ECE Reg.95 are briefly explained here.

Test Configuration

In the ECE Reg.95 test, a MDB, as shown in Figure 1, is applied to collide at an impact velocity of 50 km/h with the side of a standstill test vehicle. The MDB collides laterally at right angles to the test vehicle. The weight of the MDB is designed to be 950 kg including the deformable barrier, measuring instruments, and the like. The collision position is designed so that the centerline of the MDB coincides with the R-point (a hip point when a sheet is set at the rearmost position). The height of the deformable barrier is designed so that the lower end thereof has a ground clearance of 260 mm (300 mm in future). The dummy used for the side impact test is the EUROSID-1, which is mounted on the front seat on the collision side (generally the driver's seat).

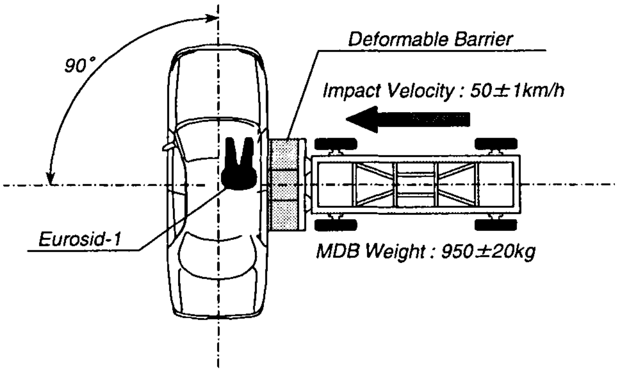

Figure 1. Test configuration of ECE Regulation No.95.

Requirements

Items evaluated for injuries on the dummy, as shown in Table 1, are stipulated by a Head Performance Criterion (HPC, corresponding to a HIC in the frontal impact test), Rib Deflection Criterion (RDC), Abdominal Peak Force (APF), and Pubic Symphysis Peak Force (PSPF). As the criteria for each item, the HPC is 1,000 or less in the same manner as HIC in the frontal impact test, RDC is 42 mm or less, APF is 2.5 kN or less, and PSPF is 6.0 kN or less. In addition to these items, it is expected that in Europe, the Viscous Criterion (V*C) will be adopted in future with the planned criterion being 1.0 m/s or less.

Evaluation items for the body of the vehicle include occurrence of opening of the door during collision, door-opening capability after collision, rescue operability for the dummy, and occurrence of fuel leakage.

Calibration Method for Deformable Barrier

The deformable barrier has a structure of six segments consisting of a matrix of two rows and three columns of blocks. The dimensions of the deformable barrier are width and height 1,500 mm and 500 mm respectively. The depths of the lower blocks and upper blocks are 500 mm and 440 mm respectively. Therefore, a projection corresponding to a bumper is 60

Table 1.
Injury Criteria of ECE Regulation No.95

Body Segment	*Name of Injury Criteria*	*Standard Value*	*Measuring Point*
Head	*HPC* *(Head Performance Criterion)*	*less than 1000*	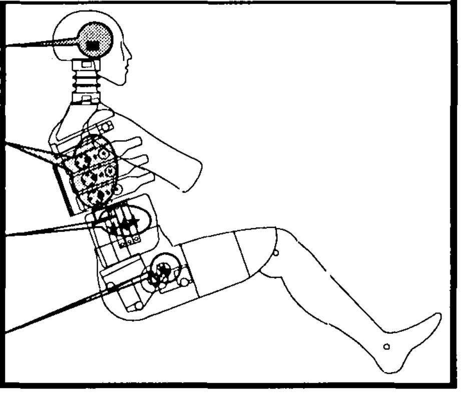
Thorax	*RDC* *(Rib Deflection Criterion)*	*less than 42 mm*	
Abdomen	*APF* *(Abdominal Peak Force)*	*less than 2.5 kN*	
Pelvis	*PSPF* *(Pubic Symphysis Peak Force)*	*less than 6.0 kN*	

mm in length. These dimensions were determined based on investigative results from European vehicles using 1976 models. Based on the investigative results, the dynamic force-deflection characteristics were also determined. In addition, the investigation on Japanese vehicles using 1993 models resulted in the same dimensions and force-deflection characteristics.

In ECE Reg.95, a barrier impact test as shown in Figure 2 is defined as a deformable barrier calibration test. In this calibration method, a MDB weighing 950 ±20 kg is collided at an impact velocity of 35±2 km/h with a rigid barrier equipped in six surface segments with load cells. The calibration results are evaluated by the force- deflection characteristics and dissipated energy of the total barrier and each blocks, and the permanent deflection of the middle intersecting surface of the lower blocks (Level B) as shown in Table 2. In this test procedure, discrepancy of the impact point is required to be within ±10 mm in both vertical and lateral directions to obtain the correct characteristics of the blocks.

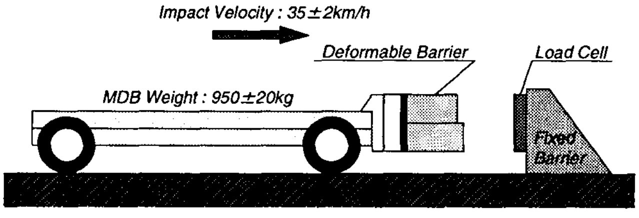

* Impact alignment shall be accurate to within 10 mm.

Figure 2. Calibration test configuration of ECE Regulation No.95.

Table 2.

The Requirement Characteristics of Deformable Barrier for ECE Regulation No.95

Dissipated Energy		Force-Deflection Characteristics
Block 1 (kJ)	10±2	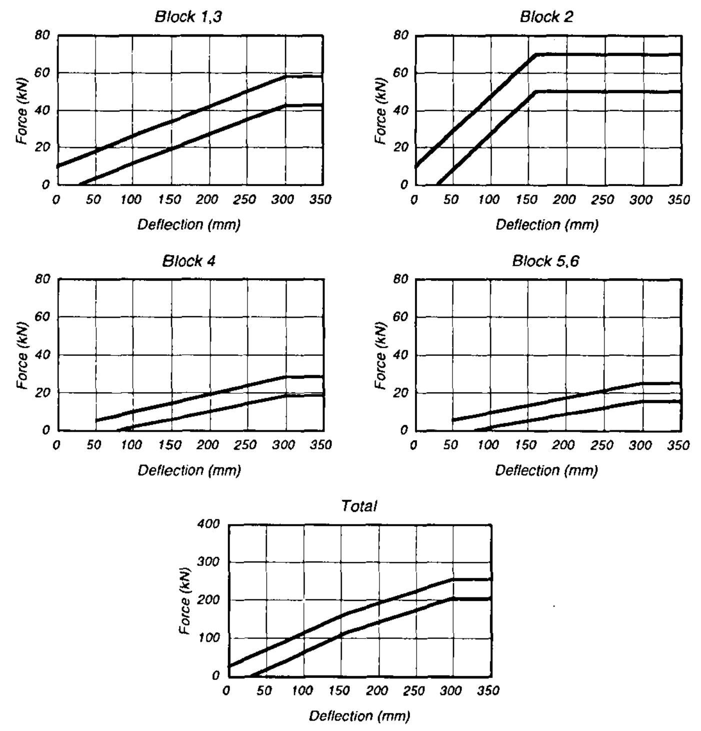
Block 2 (kJ)	14±2	
Block 3 (kJ)	10±2	
Block 4 (kJ)	4±1	
Block 5 (kJ)	3.5±1	
Block 6 (kJ)	3.5±1	
Total (kJ)	45±5	
Deflection of Level B (mm)	330±20	

DEVELOPMENT OF DEFORMABLE BARRIER

The development of the deformable barrier was carried out by JAMA/JARI in collaboration with the Showa Aircraft Industry Co., Ltd. and The Yokohama Rubber Co., Ltd. The deformable barrier with the following characteristics was designed.

- Superior reproducibility.
- Easiness in observation of deflection mode after collision.
- Stable performances against temperature, humidity, etc.
- Light weight, easily handled.

Structure of Deformable Barrier

The deformable barriers, which have been developed both domestically and outside of the country so far are classified into three types, specifically, a hard formed urethane, pyramid shaped aluminum honeycomb, and multi-layered aluminum honeycomb.

As is confirmed from the experience of conducting side impact tests so far, the hard forming urethane deformable barrier breaks into pieces during collision so that the deflection mode cannot be analyzed and the characteristics greatly change with changes in environmental conditions. The pyramid shaped honeycomb deformable barrier produces differences in the results of injuries in the dummy, depending on the position of collision. Based on these results, the aluminum honeycomb was selected as the material and a multi-layered structure was designed to develop a deformable barrier.

Deformable Barrier Developed by Showa Aircraft Industry Co., Ltd. - The structure of a deformable barrier developed by the Showa Aircraft Industry Co., Ltd. is shown in Figure 3. This

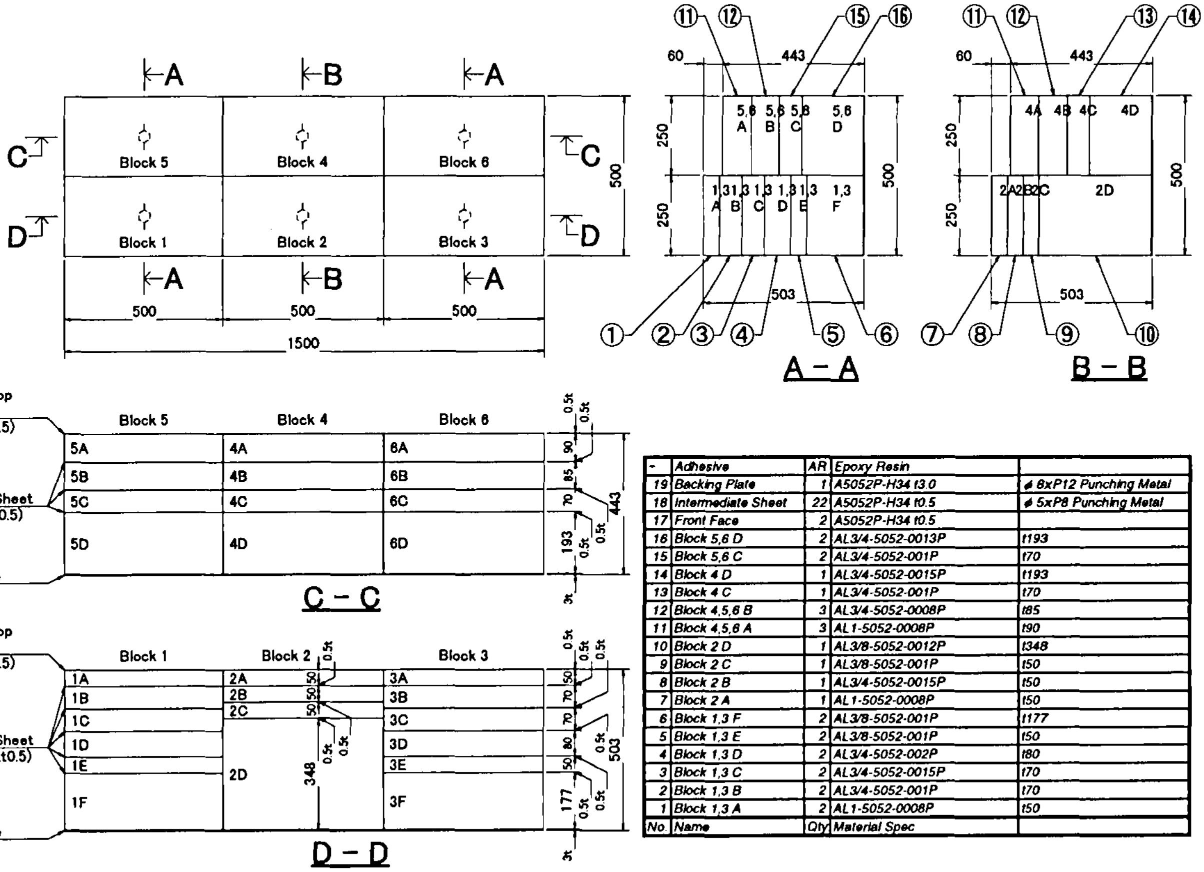
A
B
A
C
D
Block 5
Block 4
Block 6
Block 1
Block 2
Block 3
500
1500
250
443
503
60
A - A
B - B
C - C
D - D
Front Face Top Sheet (250x1500xt0.5)
Intermidiate Sheet 9-(250x500xt0.5)
Intermidiate Sheet 13-(250x500xt0.5)
Backing Plate
5A
5B
5C
5D
4A
4B
4C
4D
6A
6B
6C
6D
1A
1B
1C
1D
1E
1F
2A
2B
2C
2D
3A
3B
3C
3D
3E
3F
①
②
③
④
⑤
⑥
⑦
⑧
⑨
⑩
⑪
⑫
⑬
⑭
⑮
⑯
⑰
⑱
⑲

No.	Name	Qty	Material Spec	
-	Adhesive	AR	Epoxy Resin	
19	Backing Plate	1	A5052P-H34 t3.0	ɸ 8xP12 Punching Metal
18	Intermediate Sheet	22	A5052P-H34 t0.5	ɸ 5xP8 Punching Metal
17	Front Face	2	A5052P-H34 t0.5	
16	Block 5,6 D	2	AL3/4-5052-0013P	t193
15	Block 5,6 C	2	AL3/4-5052-001P	t70
14	Block 4 D	1	AL3/4-5052-0015P	t193
13	Block 4 C	1	AL3/4-5052-001P	t70
12	Block 4,5,6 B	3	AL3/4-5052-0008P	t85
11	Block 4,5,6 A	3	AL1-5052-0008P	t90
10	Block 2 D	1	AL3/8-5052-0012P	t348
9	Block 2 C	1	AL3/8-5052-001P	t50
8	Block 2 B	1	AL3/4-5052-0015P	t50
7	Block 2 A	1	AL1-5052-0008P	t50
6	Block 1,3 F	2	AL3/8-5052-001P	t177
5	Block 1,3 E	2	AL3/8-5052-001P	t50
4	Block 1,3 D	2	AL3/4-5052-002P	t80
3	Block 1,3 C	2	AL3/4-5052-0015P	t70
2	Block 1,3 B	2	AL3/4-5052-001P	t70
1	Block 1,3 A	2	AL1-5052-0008P	t50

Figure 3. The structure and the configuration of the deformable barrier developed by Showa Aircraft Industry Co., Ltd.

deformable barrier is a modification of the deformable barrier which was reported at the 15th-ESV International Conference. As shown in Figure 3, the deformable barrier incorporates 4 to 6 layers of a honeycomb block of different cell size and foil thickness. The aluminum honeycomb is stretched in the lateral direction when the deformable barrier is fabricated. The aluminum honeycomb material is AL5052, which is commonly used in Japan. Each honeycomb block is pre-crashed by 5 mm so that the initial peak of the aluminum honeycomb in a collision is eliminated. The honeycomb blocks are attached to each other using an epoxy resin based adhesive through an aluminum punching sheet with a length of 250 mm, width of 500 mm, and thickness of 0.5 mm with 5mm diameter holes as the intermediate sheet. Also used are an aluminum punching plate with a length of 500 mm, width of 1,500 mm, and thickness of 3 mm with 8 mm diameter holes, as the back plate. And two aluminum plates with a length of 250 mm, with of 1,500 mm, and thickness of 0.5 mm as the front plate. The weight of this deformable barrier is as low as about 17 kg because all materials forming the deformable barrier are aluminum.

Deformable Barrier Developed by The Yokohama Rubber Co., Ltd. - A deformable barrier developed by The Yokohama Rubber Co., Ltd. is shown in Figure 4. The deformable barrier is basically the same as that developed by the Showa Aircraft Industry Co., Ltd. However, each honeycomb, which differs from that manufactured by the Showa Aircraft Industry Co., Ltd., has the same cell size. Changing the foil thickness and aluminum materials controls the characteristics. The aluminum honeycomb is stretched in the vertical direction when the deformable barrier is fabricated. Two types of aluminum materials, specifically, AL5052 and AL3003 are used as the aluminum honeycomb material. Each honeycomb

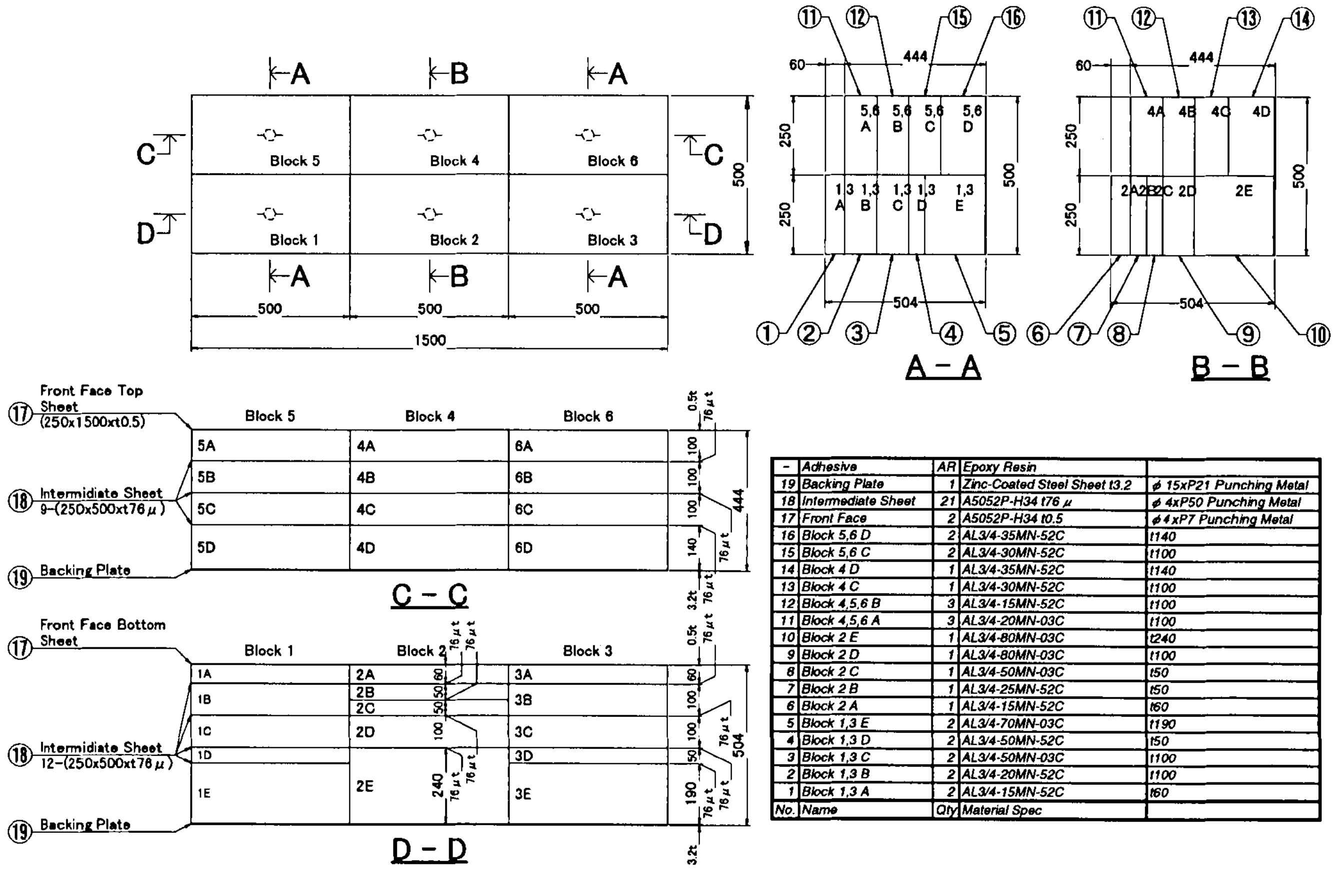

-	Adhesive	AR	Epoxy Resin	
19	Backing Plate	1	Zinc-Coated Steel Sheet t3.2	ϕ 15xP21 Punching Metal
18	Intermediate Sheet	21	A5052P-H34 t76 μ	ϕ 4xP50 Punching Metal
17	Front Face	2	A5052P-H34 t0.5	ϕ 4xP7 Punching Metal
16	Block 5,6 D	2	AL3/4-35MN-52C	t140
15	Block 5,6 C	2	AL3/4-30MN-52C	t100
14	Block 4 D	1	AL3/4-35MN-52C	t140
13	Block 4 C	1	AL3/4-30MN-52C	t100
12	Block 4,5,6 B	3	AL3/4-15MN-52C	t100
11	Block 4,5,6 A	3	AL3/4-20MN-03C	t100
10	Block 2 E	1	AL3/4-80MN-03C	t240
9	Block 2 D	1	AL3/4-80MN-03C	t100
8	Block 2 C	1	AL3/4-50MN-03C	t50
7	Block 2 B	1	AL3/4-25MN-52C	t50
6	Block 2 A	1	AL3/4-15MN-52C	t60
5	Block 1,3 E	2	AL3/4-70MN-03C	t190
4	Block 1,3 D	2	AL3/4-50MN-52C	t50
3	Block 1,3 C	2	AL3/4-50MN-03C	t100
2	Block 1,3 B	2	AL3/4-20MN-52C	t100
1	Block 1,3 A	2	AL3/4-15MN-52C	t60
No.	Name	Qty	Material Spec	

Figure 4. The structure and the configuration of the deformable barrier developed by The Yokohama Rubber Co., Ltd.

block is also pre-crashed. The honeycomb blocks are attached using an epoxy resin based adhesive through an aluminum punching sheet with a length of 250 mm, width of 500 mm, and thickness of 76 μ m and with 4 mm diameter holes as the intermediate sheet. Also used are a steel punching plate which is zinc-plated and has a length of 500 mm, width of 1,500 mm, and thickness of 3.2 mm and with 15 mm diameter holes as the back plate. And two aluminum punching plates with a length of 250 mm, width of 1,500 mm, and thickness of 0.5 mm and with 4 mm diameter holes as the front plate. The weight of this deformable barrier is as low as about 22 kg, although it is heavier than that manufactured by the Showa Aircraft Industry Co., Ltd. because the steel plate is used as the back plate.

Test Results

The calibration tests were carried out twice for every deformable barrier and four times in total to

Table 3.

The Accuracy of the Calibration Test,

the Dissipated Energy and the Deflection at the Level B

		Showa Aircraft Industry Co., Ltd.		The Yokohama Rubber Co., Ltd.		Requirement Value
Test No.		S1	S2	Y1	Y2	
MDB Weight (kg)		949	948	956	956	950±20
Impact Velocity (km/h)		35.1	34.9	35.1	35.0	35±2
Discrepacy of Impact Point (mm) *	Vertical	0	3	7	5	±10
	Lateral	-5	-2	0	3	±10
Disipated Energy (kJ)	Block 1	10.0	9.1	10.8	10.5	10±2
	Block 2	15.5	15.6	15.1	14.8	14±2
	Block 3	9.7	9.6	10.8	10.4	10±2
	Block 4	4.3	4.1	4.1	4.0	4±1
	Block 5	3.4	3.3	4.0	3.9	3.5±1
	Block 6	3.6	3.5	4.0	4.0	3.5±1
	Total	46.5	45.1	48.8	47.6	45±5
Diflection of Level B (mm)		325	320	328	328	330±20

* ; The vertical direction is positive to upper, and the lateral direction is positive to right.

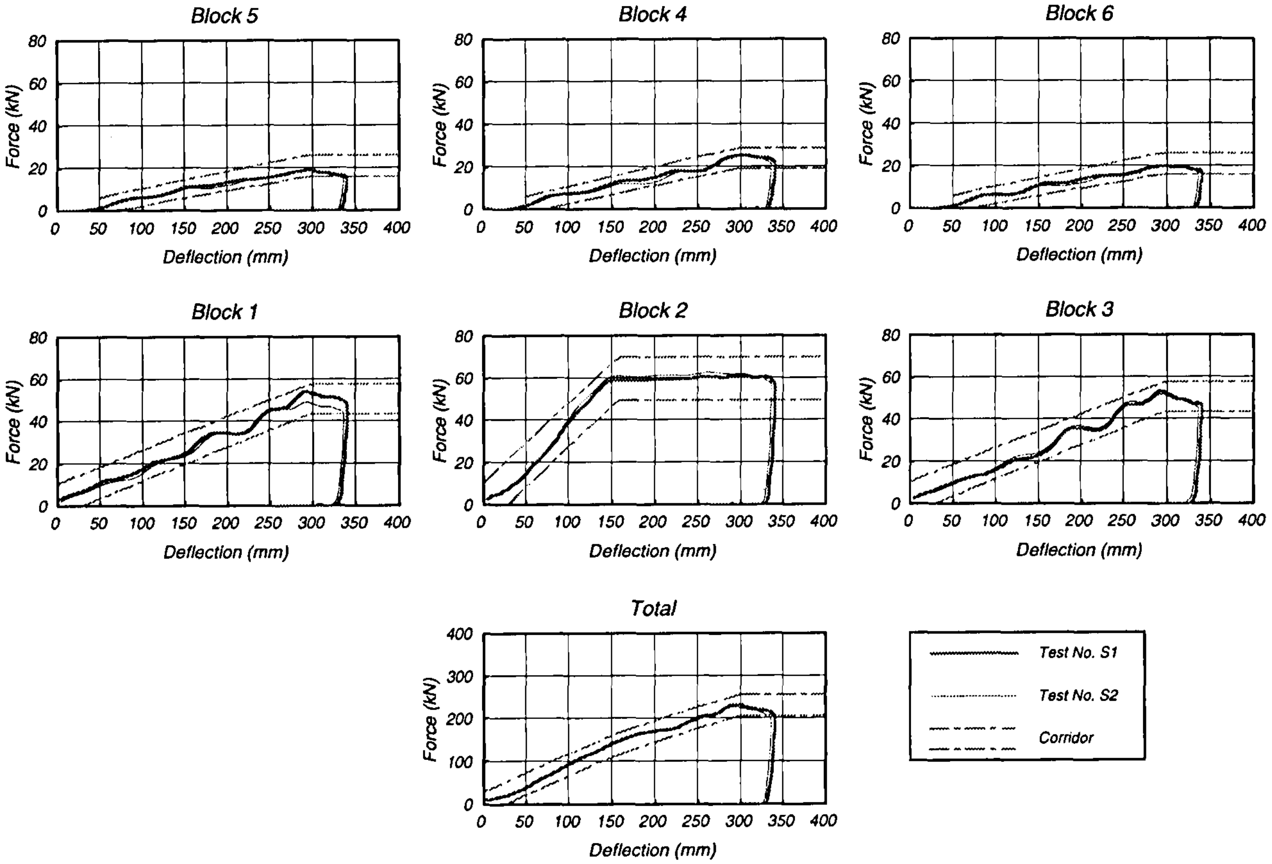

Figure 5. The force-deflection characteristics of the deformable barrier developed by Showa Aircraft Industry Co., Ild.

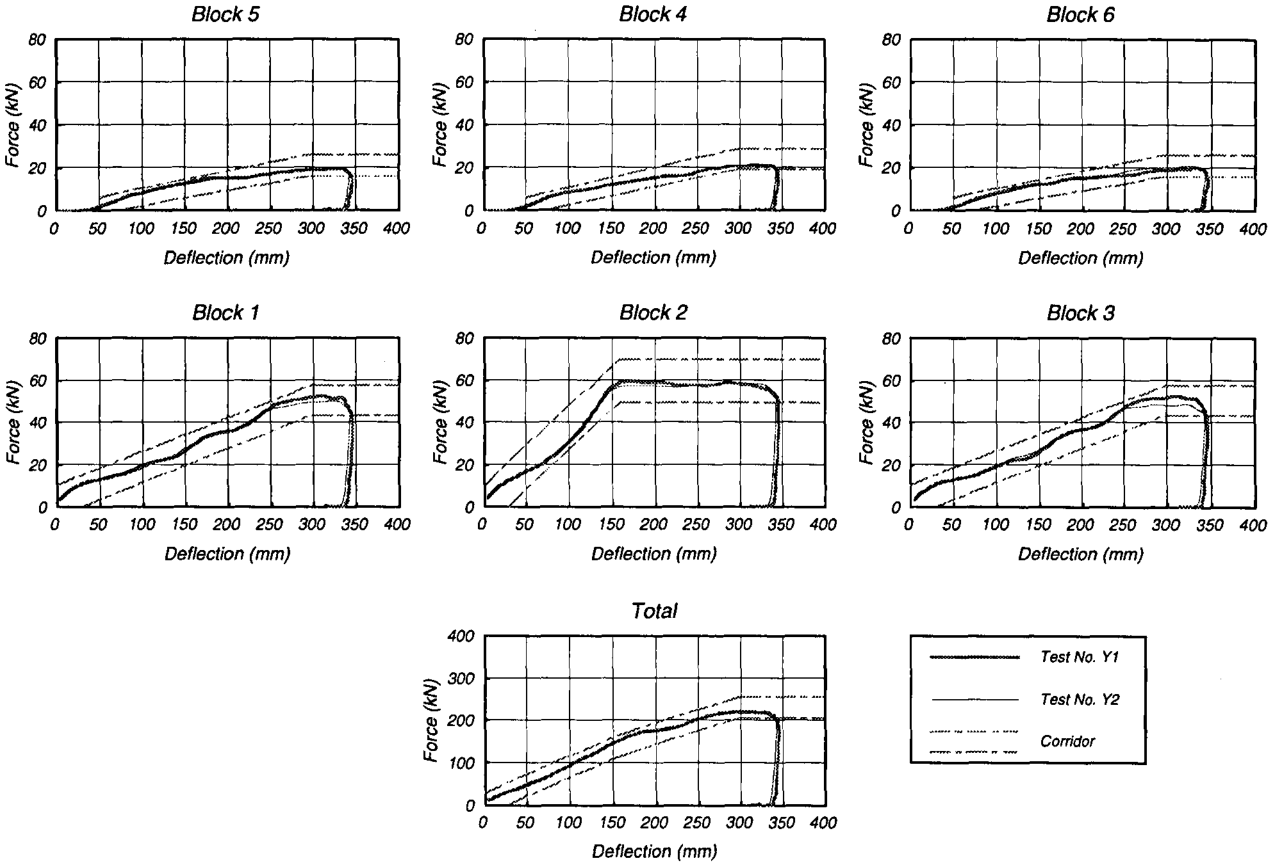

Figure 6. The force-deflection characteristics of the deformable barrier developed by The Yokohama Rubber Co., Ltd.

confirm the reproducibility. The accuracy of the calibration test, the amount of dissipated energy and the deflection at the level B are shown in Table 3. The force-deflection characteristics of the deformable barriers developed by the Showa Aircraft Industry Co., Ltd. and The Yokohama Rubber Co., Ltd. are shown in Figures 5 and 6 respectively.

As shown in Table 3, the results of the amount of dissipated energy and deflection at the level B also sufficiently satisfied the performance requirements. As for the reproducibility, the block 1 of the deformable barrier developed by the Showa Aircraft Industry Co., Ltd. showed some differences in the amount of dissipated energy but this will be no problem on a practical level.

As shown in Figure 5, the force-deflection characteristics of the deformable barrier of the Showa Aircraft Industry Co., Ltd. satisfies the performance requirements in all blocks. There were some differences in reproducibility when the deflection of the block 1 was above 275 mm but this was no problem on a practical level. Other blocks showed excellent results. Some segments of the deformable barrier which was reported at the 15th-ESV International Conference had characteristics which did not fall in the corridor above 320 mm. This improvement ensures that the characteristics of such segments also fall in the corridor.

As shown in Figure 6, the force-deflection characteristics of all blocks of the deformable barrier of The Yokohama Rubber Co., Ltd. satisfied the performance requirements. Although the characteristics of the upper blocks was near the upper limit of the corridor when the deflection was in a range from about 75 mm to 175 mm. Slight differences in reproducibility were observed in the blocks 1 and 2 when the deflection was in the vicinity of 300 mm. Excellent results were obtained as a whole.

SUMMARY

This time we developed a deformable barrier for a side impact test in collaboration with two domestic corporations to obtain the deformable barriers, which satisfied the performance requirements for the test procedure. This deformable barrier can also satisfy the design concept. The developed deformable barrier had sufficient reproducibility and the deflection mode after collision could be analyzed because of the use of aluminum honeycomb. Also, the deformable barrier had stable performance against temperature, humidity, etc., and had a weight as low as around 20 kg.

CONCLUSION

As mentioned at the beginning, a deformable barrier, which satisfies the performance required for the ECE Reg.95 has not yet been developed. Despite continued similar efforts to develop a deformable barrier in many foreign countries including Europe, there has been no report of success in the development of a deformable barrier which meets these requirements. The deformable barrier deficiently meeting the requirements which was developed through these studies in Japan could be applied in the fields of type approval tests or developments tests for new-model cars which will be implemented in the future.

There are signs that EEVC/WG13 in Europe will stipulate the structural requirements of the deformable barrier used in the ECE Reg.95. The ECE Reg.95 is a test procedure with almost the same content as the method which Japanese government will introduce. So Japanese government and JAMA will participate in this project with the consent of the EC commission. It is expected that the studies in Japan could advance after ascertaining the trend in Europe to develop a new deformable barrier as needed.

Finally, special thanks are also due to the Showa Aircraft Industry Co., Ltd. and The Yokohama Rubber Co., Ltd. for their valuable cooperation in the development of the deformable barrier.

REFERENCES

ECE Regulation 95, "Uniform Provisions Concerning the Approval of Vehicles with Regard to the Protection of the Occupants in the Event of a Lateral Collision".

NHTSA, "Final Regulatory Impact Analysis New Requirements for Passenger Cars to Meet a Dynamic Side Impact FMVSS 214".

EEVC Working Group, "Structure Improved Side Impact Protection in Europe", 9th ESV Conference, November 1982.

E.Chapoux, J.C.Jolys, R.Dargaud, "An Approach for the Design of a Deformable Mobile Barrier to Evaluate the Protection Afforded to Occupants of a Passenger Car Involved in a Side Collision", 9th ESV Conference, November 1982.

D.R.Gebbels, "The CCMC Mobile Deformable Barrier for Lateral Collision Testing", 10th ESV Conference, July 1985.

H.Ohmae, M.Sakurai, Y.Nakamura, K.Watanabe, "A Study on Energy-Absorbing Units of MDB for Side Impact Test", 11th ESV Conference, May 1987.

M.Ueno, H.Ohmae, T.Harigae, K.Satake, T.Yamaguchi, E.Fujiwara, "Development of Moving Deformable Barrier in Japan", 15th ESV Conference, No.96-S6-O-06, May 1996.

N.Esumi, K.Satake, H.Ohmae, T.harigae, M.Ueno, "Research Concerning Vehicle Occupant Protection for Lateral Collision - Accident Analysis of Lateral Collision and Vehicle Characteristics in the Japanese Market -", 15th ESV Conference, No.96-S6-O-02, May 1996.

THE POSIP SYSTEM - IMPROVING OCCUPANT PROTECTION IN CONVERTIBLES AND COUPES DURING SIDE IMPACTS

Martin Heinz
F. Porsche
Porsche AG
Germany
Paper Number 98-S8-W-27

Abstract

In recent years, passive safety has been continuously improved. Legal requirements and demands regarding occupant protection in side impacts exist. A lot of reinforcements for the BIW of the cars have been constantly optimized, based on the results of static and dynamic tests.

A new developed part of the occupant protection is a door-based side-airbag system combined with an energy-absorbing door, named POSIP, i.e. POrsche Side Impact Protection system.

The side-airbag module includes a totally new 30 l two-chamber airbag which covers a big part of the upper door area. This side airbag has been designed to reduce both the head and thorax loads also in side pole impacts.

For the first time in automotive history, a standard head protection system is offered which can be installed regardless of the roof design. The POSIP system also protects the occupants of convertibles or of cars with novel roof concepts when involved in side impact pole crashes.

1 Introduction

In many markets today, passive safety is one of the criteria which, along with an appealing styling and sporty performances, make an essential contribution to the success of a car concept. The occupant protection is a primary target in automotive engineering.

Over the last 10 years, occupant protection has been considerably improved, mainly with regard to frontal collisions. Accident research, mathematical analysis and lab tests yielded valuable experiences which have helped to further optimize the cars and their components in terms of passive safety.

In 1986 already, Porsche started setting new standards, being the first European car maker to launch a series car with standard driver and front-passenger airbags on the North American market.

According to the results of pertinent accident research, side collisions are the second most frequent type of accidents after frontal collisions. As accident analyses and injury statistics show, it should be possible to further improve the occupant protection during side impacts.

2 Demands on the side structure

Compliance with the legal requirements regarding occupant protection in side impacts must be demonstrated in static tests and in dynamic side impact tests with moving barriers or moving cars.

2.1 Static side impact test

In the USA, the quality of passenger protection in side collisions is checked by performing a static compression test according to the first part of FMVSS 214 /1/. A test rigid steel cylinder is pressed against the outer door panel in order to demonstrate that the BIW offers a deformation-dependent minimum intrusion resistance. At the same time, this test serves to verify the strength of doors, hinges and locks.

2.2 Dynamic testing using a moving barrier

There are two different side impact tests available, whose rules take into account the vehicle populations and accident conditions existing when the tests were first introduced. This explains the differences between the two tests and the results they are expected to yield.

In the USA, occupant protection in lateral collisions is checked in accordance with part 2 of FMVSS 214 /1/ using a dynamic side impact test. The driver or passenger side of the standing car is impacted by a deformable barrier moving at an angle. The test is performed with one dummy each on the front and rear seats. The barrier hits the side of the car at a speed of about 54 km/h (33.54 mph) and at an angle of 27° (Figure 1). This test configuration simulates a right-angle 50 km/h (30 mph) impact of the barrier with the car moving ahead at half that speed. The characteristic data of the barrier, that is the mass of 1,396 kg, the ground clearance of 0.2794 m, the height of the deformation element of 0.8382 m and the stiffness rather correspond to those of a light-duty truck.

To measure the occupant loads, the US Side Impact Dummy (US-SID) is used. This new dummy has been developed from the Hybrid II frontal impact dummy and provided with a newly designed thorax. For the thorax and lap, corresponding load limits have been stipulated and must be complied with.

The NHTSA (National Highway Traffic Safety Administration) also performs side impact tests at an impact speed of 38.0 mph or 61.2 km/h respectively. These are the so-called NCAP tests.

The countries of the European Union use 96/97/EG /2/ - a method which is comparable to the American FMVSS 214. However, the 950 kg barrier is considerably less heavy, the ground clearance is 0.3 m and the upper edge of the deformation element is 0.760 m above the ground. With this configuration, the barrier corresponds to the average European automobile. The deformable EEVC barrier hits the standing car at a right angle and an impact speed of 50 km/h (Figure 2). ECE-R 95 shows the same configuration with the difference that the ground clearance of the barrier is only 0.260 m /3/.

The test is performed using the EUROSID 1 (European Side Impact Dummy) with no hands and forearms, developed especially for this test and allowing the abdominal loads on the front passenger to be more efficiently measured.

2.3 Dynamic tests with the car moving

The revised version of FMVSS 201 which will be published soon includes a lateral pole impact /4/ under Option 3: the car moving at a 90° angle to its longitudinal axis collides with a rigid 10 inch (254 mm) diameter pole (fig. 3). The collision speed is 18 mph (29 km/h). The car is positioned in such a way that the point of impact is at the center-of-gravity level of the head of the dummy sitting on the front seat.

The dummy to be used for this test is to be a combination of the Hybrid III head/neck structure and the US-SID from FMVSS 214. Besides the dummy, the pole diameter, too, is worth mentioning: contrary to the 305 mm pole diameter prescribed for the static compression test under FMVSS 214, the dynamic test described above uses a pole diameter of 254 mm.

It should be noted that an ISO procedure currently under way, requires the pole diameter to be 350 mm /5/. Which reason exist, that the diameter of the pole have a range between 254 and 350 mm ?

For car-to-car side collisions, no standardized test conditions exist. Therefore, this type of test is carried out to the instructions of each individual automotive manufacturer.

2.4 Safety test results

When comparing the moving-barrier tests after the ECE-R 95 and the FMVSS 214 test conditions, we find that both the resulting deformations to the car and the loads on the dummies are quite different from each other.

The side impact according to FMVSS 214 produces a bellied indentation between the front and rear wheels of the impacted car which evenly increases in longitudinal direction from the A to the B post. The intrusion depth is greatest in the lower portion of the door where the bumper profile of the barrier causes a very clear indentation which is about 50 mm deeper than the damage caused to the vehicle's side structure by the main barrier element.

When tested according to 96/27/EG or ECE-R 95, the impacted car shows a strong deformation of the door ahead of the B-post and between the B-post and the rear wheel. The deepest side structure deformation is found in the center of the door. The bumper profile of the barrier does not leave any particularly pronounced marks.

ECE-R 95 and FMVSS 214 result in different intrusions when used on the same type of car and the dummies respond differently to the loads caused by the intruding side structures.

The US-SID, when tested to FMVSS 214, is particularly sensitive to the intrusion speed at the moment of impact with the side structure. The thorax and pelvis acceleration measurements are quite reliable whereas the rib deformation results are less informative. What is important about this dummy is that the thorax loads are averaged using the Thoracic Trauma Index (TTI) as an evaluation criterion. The US-SID receives particular protection through a resilient, padded inner door lining and a stiff body structure which lowers the intrusion velocity.

The EUROSID 1 dummy used for the european test measures rib deformations, abdominal and pelvic forces as well as head loads. Rib acceleration measurements, however, do not yield any conclusive results. If the side structure of the car is not hit perpendicularly, the EUROSID 1 dummy might yield too low load values. The side structure deformations caused by this test differ from those of the American regulations and place higher loads on the dummy's thorax. The loads depend on the intrusion depth of the side structure and the duration of the contact between the side structure and dummy. It is necessary to minimize the intrusion velocity by providing for a stiff side structure.

3 Possibilities for effective occupant protection in side impacts

In a side collision, the available deformation zone of the impacted car is far smaller than in a frontal collision. Therefore, one of the most vital demands for an efficient occupant protection in side impacts is to provide for a stiff lateral body structure. A stiff body structure lowers the intrusion velocity of the impacted car side and thus can reduce the loads on the vehicle occupants.

Occupant protection is particularly efficient if the body side structure complies with the static and dynamic regulations of both, FMVSS 214 and ECE-R 95. The protective effect can be further improved by using appropriate occupant restraint systems.

3.1 Improvements to the vehicle side structure

Vehicle side structures have to meet very stringent demands. To realize further improvements numerous detail solutions must be found.

The hinges and locks, for example, must be able to transmit the collision forces to the body structure. The minimum breaking force levels stipulated in FMVSS 206 /6/ are sufficient for that purpose.

The reinforcing elements required for compliance with FMVSS 214 have been installed in all Porsche series cars sold worldwide since model year 1985. The upper door area of the Porsche cars is additionally stiffened by a profile fixed to the window channel.

Under normal circumstances and due to its low position, the door sill is not hit by an impacting car or barrier. Nevertheless, the door sill must be designed for high stiffness since it plays an important role in pole collisions.

Another essential safety feature is the transverse reinforcement of the vehicle floor which allows the occupants' survival space to be maintained and the impact energy to be transmitted to the floor structure. This reinforcement is achieved through solidly dimensioned seat cross members at the front and rear which stiffen the area between the door sill and the center tunnel. The lower side of the center tunnel itself is closed by means of add-on members which minimize the tunnel deformations and allow forces to be transferred to the floor structure opposite of the impacted side.

The energy absorbing capacity in a side collision can be enhanced by providing for reinforcements of the doors, seats and body structure which, at the same time, lower the differential speed between the intruding door and the occupant thus reducing the dynamic and static deformations of the body. These measures are particularly beneficial as far as the thorax protection is concerned.

Thanks to these measures the impact forces are transmitted to the body structure via the A and B posts, the door sill and the floor. In that way, the entire side and floor structure is used for energy absorption with the rear seat structure serving as an additional reinforcement.

The seats, too, are vital elements when it comes to preserve the occupants' survival space. The transverse stiffness of the seat back and, above all, of the supporting structure should be high enough to reduce the risk of injuries to the pelvis.

Another essential aspect is the precise positioning of the inner door panel, door reinforcement and door lining elements relative to each other. If a car must also meet the provisions of FMVSS 214, it would make little sense to weaken the body at pelvis level and allow for higher loads on the pelvis and abdomen in order to reduce the thorax loads.

3.2 Restraint systems

In 1990, Porsche started an advanced engineering project to find out whether the protective potential of the existing side structures could be further enhanced through additional occupant protection systems like paddings or side airbags. In doing so, special attention was paid to the performance characteristics of airbag deployment components and mechanisms. The ultimate target was to develop a side airbag which would provide protection not only to the occupant's thorax but also to his head and be operational both in sedans and convertibles /7/.

3.3 New feature for occupant protection in side impacts

For its new car lines (Boxster, 911 Coupé /8,9/, 911 Convertible /10/) Porsche is offering an additional occupant protection device, the so-called 'POSIP' system with POSIP standing for POrsche Side Impact Protection. This novel side airbag system combined with an energy-absorbing door trim is available for the two front occupants.

The unique feature of the side airbag system is the integral protection of the thorax and head during side impacts including collisions with a pole or a tree. The Porsche convertible is the first one of its kind worldwide to also provide a head protection feature. It is complemented by an energy-absorbing door panel laid out to reduce the loads on the pelvis. The first POSIP was installed in a production car in April 1997 (Fig. 4).

4 The components of the side airbag system

The development of the side airbag complete with its cover and the integration of the system into the car required the redesign or modification of numerous parts from such areas as interior equipment, electrics, BIW and safety.

The POSIP side airbag module is fastened to the inner door panel at front-passenger level and covered by the door trim. What is visible to the occupant's eyes is just the cover of the side airbag module with an incorporated black clip carrying the 'AIRBAG' inscription.

The airbag module is screened by a cover harmoniously incorporated into the door trim. It is an apparent safety item which gives the occupants the reassurance they need. The airbag cover is available with a leather-finish only which is friendly to the touch and whose colour is matched with that of the interior trim. The visible tear seam is located in the center of the cover. The POSIP system is available for both the TPO and the leather-lined door trim panel (fig. 5).

The one-piece plastic cover is an injection-moulded element. Porsche's upholstering specialists provide it with a lining of low-shrinkage leather. The making of the tear seam is computer-controlled and documented in all details. Two additional ornamental seams run parallel to the tear seam. After having been sewn together, the leather lining is bonded onto the cover which is then incorporated into the door trim panel in compliance with the customer's order. POSIP is the first side airbag system to use a hinged cover - a solution which allows a precisely defined opening to be created for the unfolding airbag.

POSIP uses a novel hybrid gas generator located inside the airbag. With this particular gas generation technology the pyrotechnical elements account for as little as 4.7 grams of the overall mass. The gas comes from a pressure reservoir filled with argon and helium. This gas generation method which is currently used by few vehicle manufacturers only has been especially chosen for recycling and ecological reasons.

The airbag has a volume of 30 l. The inner face of the polyamide fabric is provided with a thin silicon lining. The airbag includes all the elements needed for a controlled deployment, i.e. the retaining strap, tear seam, darts and interpanels which include the pressure valve and exhaust opening. The airbag is both folded and rolled. It is mounted in a painted steel housing and protected by an additional covering which features all the required warning inscriptions. The housing is provided with one integrated bolting point used to fasten the lower retaining plate of the airbag cover to the door panel. An ejection channel integrated into the steel housing secures the correct positioning of the airbag. Further deployment of the airbag is controlled by the multifunctional retaining strap which has an integrated tear seam. This strap is located at thorax level and serves to limit the expansion of the airbag towards the cockpit center (fig. 6).

Even with the side windows down or shattered, the airbag continues to deploy vertically upwards and rearwards. When hit by the passenger, the upper part of the airbag is supported by the window channel or the intruding object respectively.

The triggering system of the side airbag is composed of the triggering unit on the center tunnel and two outside sensors at the RH and LH sills. In a lateral collision, the sensor on the impacted side activates the central unit which, in turn, triggers the airbag, provided that the signals recorded by the central unit and the safing sensor exceed a given threshold. In general, the airbag on the impacted side only is activated. This configuration allows the side airbag system to be triggered also by an impact outside of the passenger compartment.

To activate the side airbag, an impact higher then a certain threshold is required. Depending on the signals recorded during the collision, the chosen triggering/sensing concept ensures triggering times of about 5 ms and more.

No more than 8 to 9 ms after having been triggered the deploying airbag passes the shoulder point of the occupant whose seat is assumed to be adjusted to center position. Now follows the deployment of the part which protects the occupant's head. About 15 to 18 ms after having been fired the side airbag has reached its fully deployed volume (Fig. 7).

The POSIP airbag forms a flat cushion between the occupant and the inner door panel. The airbag exhaust gas load on the vehicle occupants is very low, since the hybrid gas generator is a low-emission one and the airbag does not have any additional exhaust opening. The airbag has been laid out to provide protection over the entire seat adjustment range and is shaped in a way so as to additionally shield the occupant's head regardless of the roof design.

If a Porsche child seat system is used, the front-passenger side and front airbags are simultaneously deactivated via an additional belt latch.

5 Development strategy

Almost from the beginning, POSIP development had mainly relied on testing. The amount of numerical simulations was gradually reduced as worked progressed.

Therefore, side airbag development was done mainly on the acceleration sled for which two different side impact configurations are available.

Since 1990, a configuration exists which allows the dummy and seat to be mounted freely on the sled whereas the side structure complete with the door, door trim and side airbag module are firmly fixed to the sled (fig. 8). This set-up is used to investigate the deployment conditions of the airbag and its protection potential at various intrusion velocities. The main advantage is that tests can be performed in rapid succession since only the seat, door trim and airbag module must be replaced. One of the drawbacks of this set-up is that the velocity-time response is limited. In the sled test, the occupant is farther away from the door panel than during a real car crash. This configuration is suitable for the simulation of impact speeds up to 7.5 ms and large-surface side-structure intrusions which are typical for FMVSS 214.

The second set-up uses a sled-on-sled structure /11/, which allows side impacts to be simulated even better: The impacting structure is located on a secondary sled which is accelerated by colliding with the primary sled (fig. 9). The intrusion velocity can be more easily adapted to real test conditions. However, with this set-up the representation of the collision process is more expensive. One of its advantages is that it is well suited for tests to ECE-R 95.

The POSIP system was submitted to additional crash tests using various test configurations (Fig. 10).

6 Conclusion

The POSIP system represents an mayor progress in occupant protection during side collisions. It protects the front passenger's thorax and head over the entire seat adjustment range and regardless of the roof design. For the first time in convertible history, an airbag system has been conceived which covers the side window area at occupant level and efficiently protects the occupant's head also in an open car.

7 Acknowledgments

The development of the POSIP system has been a team approach. We owe thanks to our module suppliers Breed Rückhaltesysteme für Fahrzeugsicherheit GmbH, Raunheim, D, Peguform GmbH, Bötzingen, D and Temic Telefunken microelectronic GmbH, Ingolstadt, D as well as the staff from all the departments of Porsche AG involved in the project.

8 References

1 FMVSS Code of Federal Regulations, Part 571.214
2 Richtlinie 96/97/EG Amtsblatt der Europäischen Gemeinschaften Nr. L 169/1-38
3 ECE-R 95 20.07.1995
4 49 CFR 571 and 572 Docket 92-28 Not. 6 FR Vol. 61 Nr. 46 p. 9136-9138.
5 ISO/TC 22/SC 10/WG 3 ISO Technical Report: Road Vehicles - Test Procedures for evaluating various occupant-interactions with deploying side impact air bags.
6 FMVSS Code of Federal Regulations, Part 571.206

7 U. Tautenhahn, M. Heinz, H. Brandsch: Side Protection Systems - State of the Art and Outlook on Future Trends, XXV Fisita Congress, Beijing, Ch, 1994, Paper 945171.

8 H. Petri, T. Posch, H. Eberhardt, H. Klamser: Passive Sicherheit des neuen 911 Carrera, Sonderheft Porsche 911 Carrera der Zeitschriften ATZ 12/97 und MTZ 12/97, S. 44 - 51.

9 L. Hamm: The Body of the New Porsche 911, IBEC International Body Engineering Conference (Section: Advanced body concept and development conference), Stuttgart, D, 1997.

10 H. Rohardt, M. Heinz, K. Pfertner: Die Karosserie des Porsche 911 Carrera Cabriolet - ein weiterer Höhepunkt in der Evolution des Porsche 911, VDI-Tagung 'Entwicklungen im Karosseriebau' (VDI-Bericht 1398), Hamburg, D, 1998.

11 D. Stein, A. Wesolowski, U. Bendig: Sled on a Sled - Die Entwicklung eines Prüfaufbaus zur Simulation des Seitenaufpralls, in: Bedeutung der Rückhaltesysteme in der passiven Fahrzeugsicherheit, Essen, D, 1995.

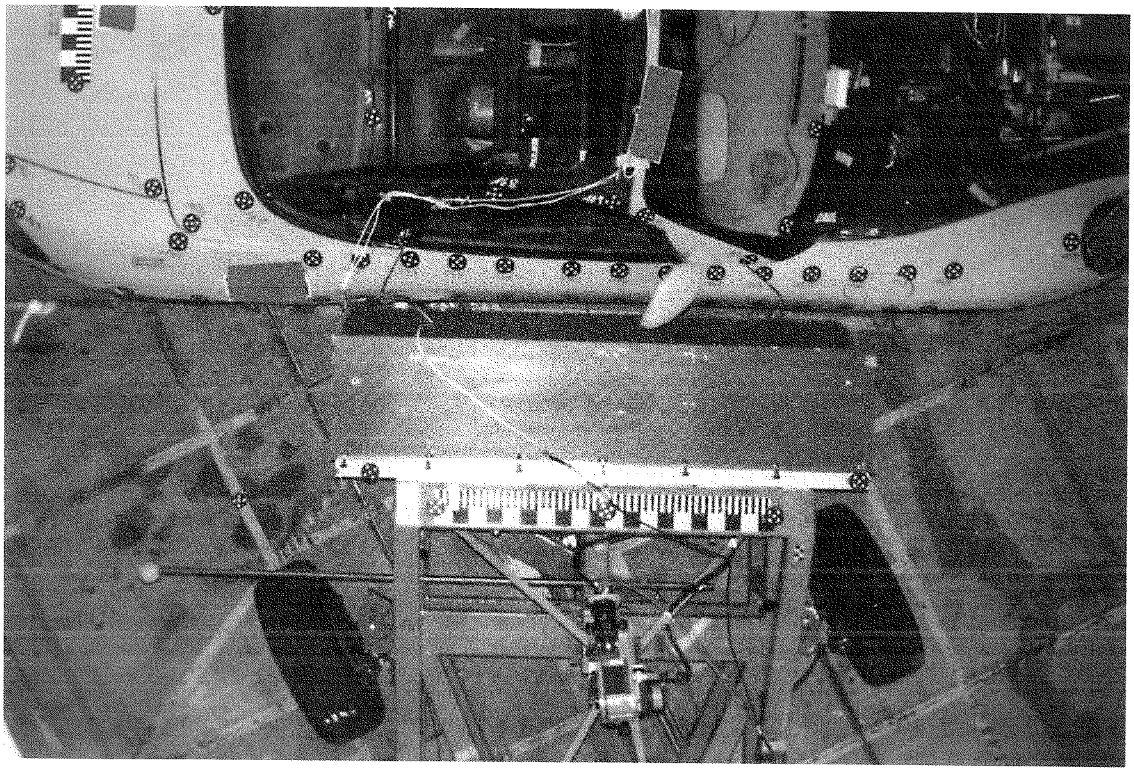

Fig. 1: Test configuration FMVSS 214

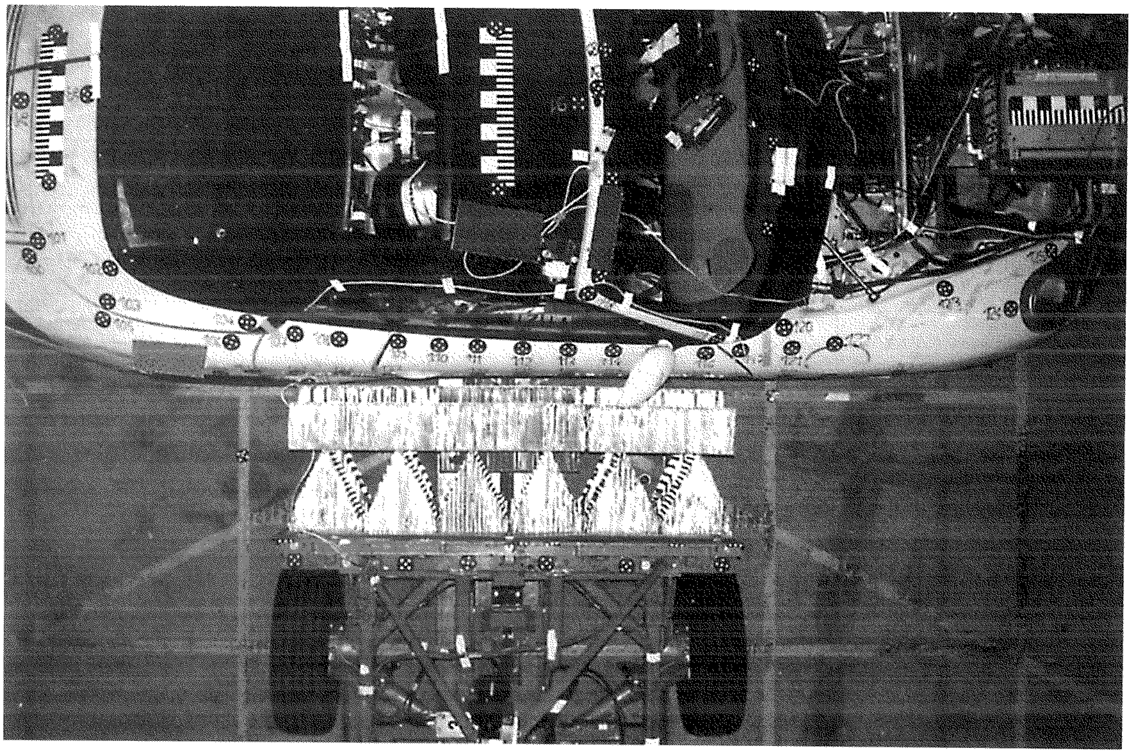

Fig. 2: Test configuration 96/97/EG

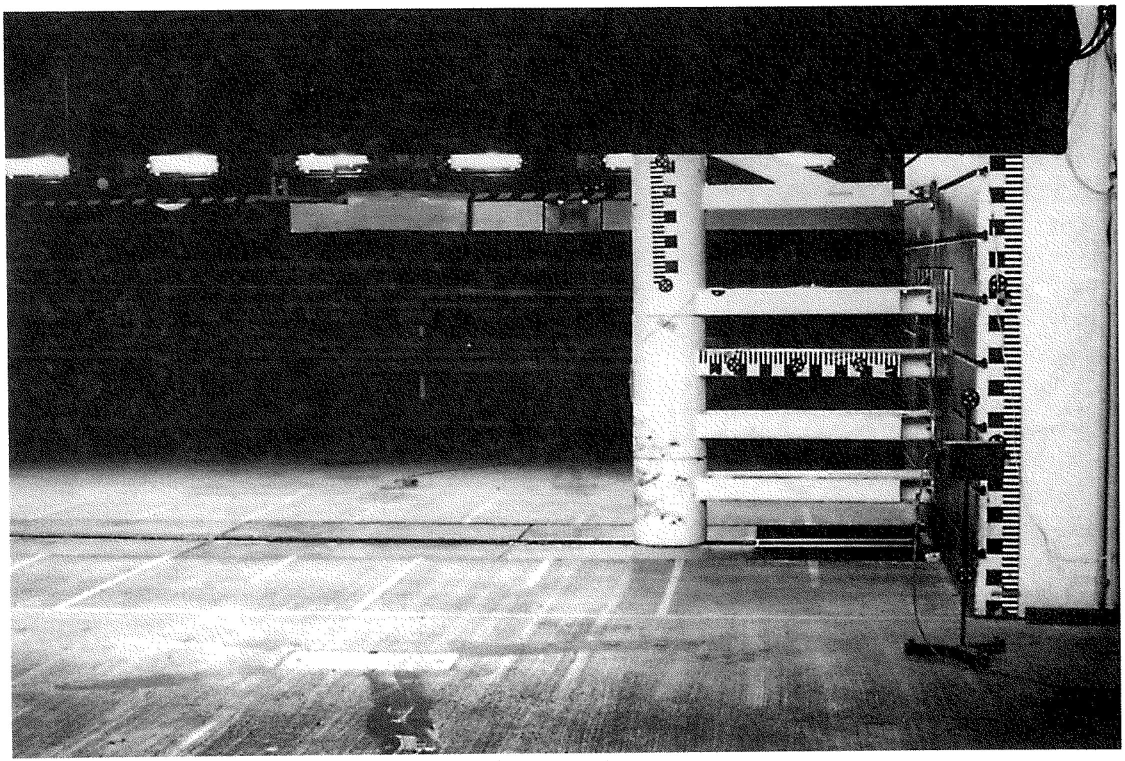

Fig. 3: Test configuration FMVSS 201 (Diameter ∅ 300 mm)

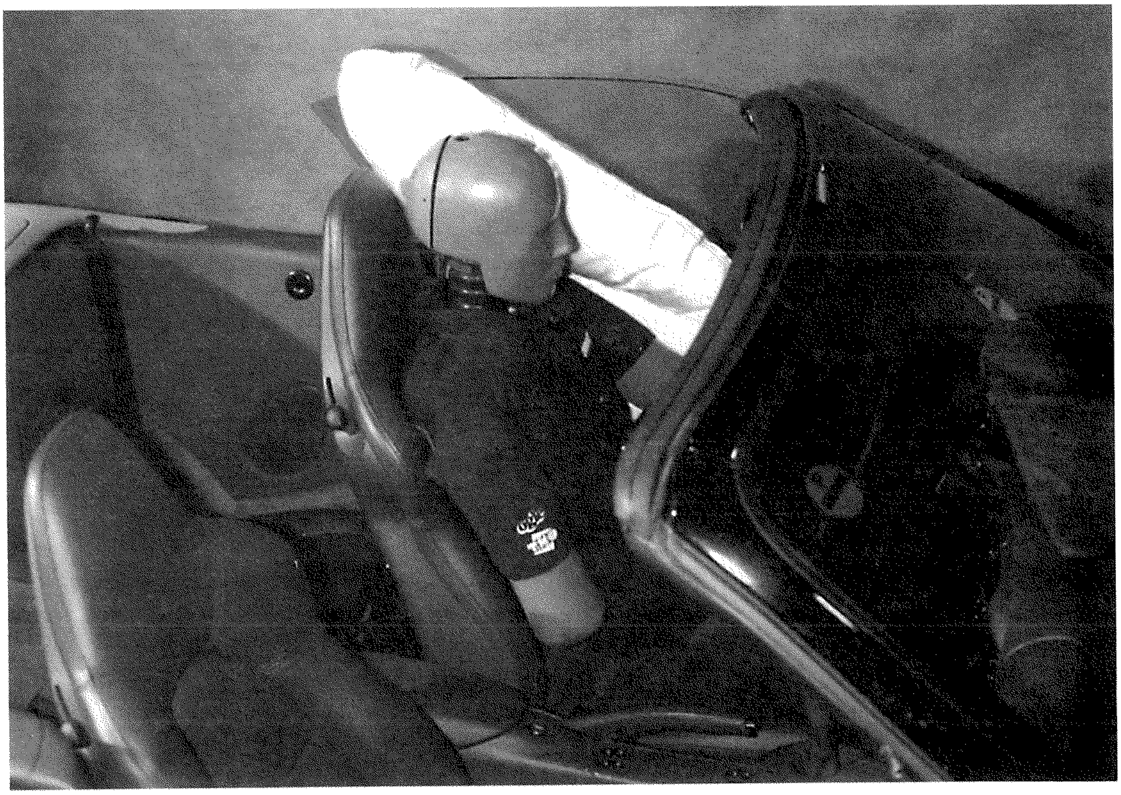

Fig. 4: The inflated cushion of the POSIP airbag in a convertible

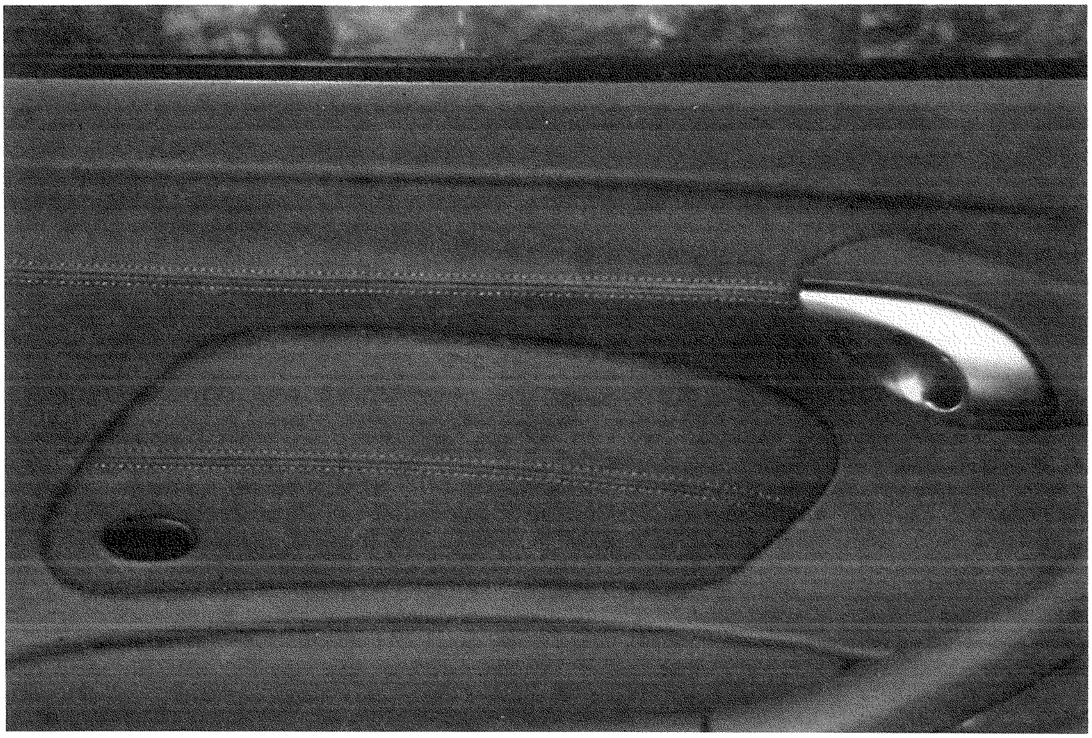

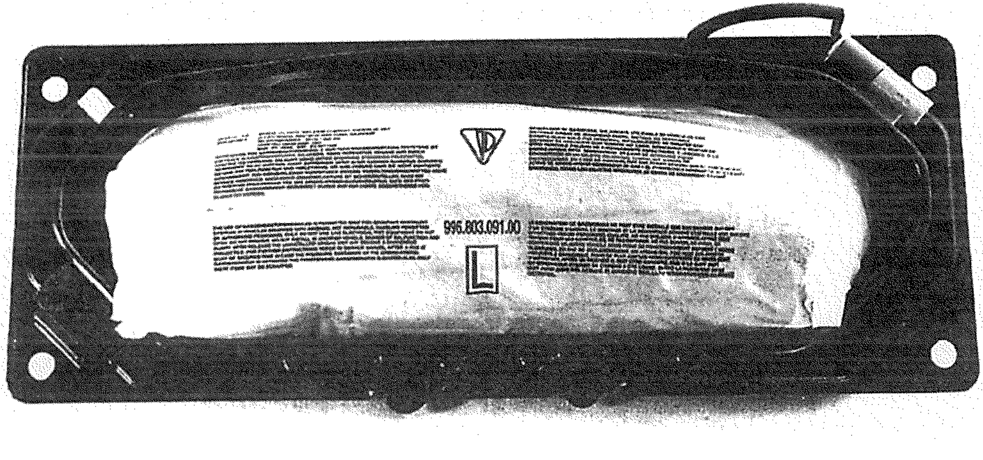
996.803.091.00
L

Fig. 6: The side airbag module

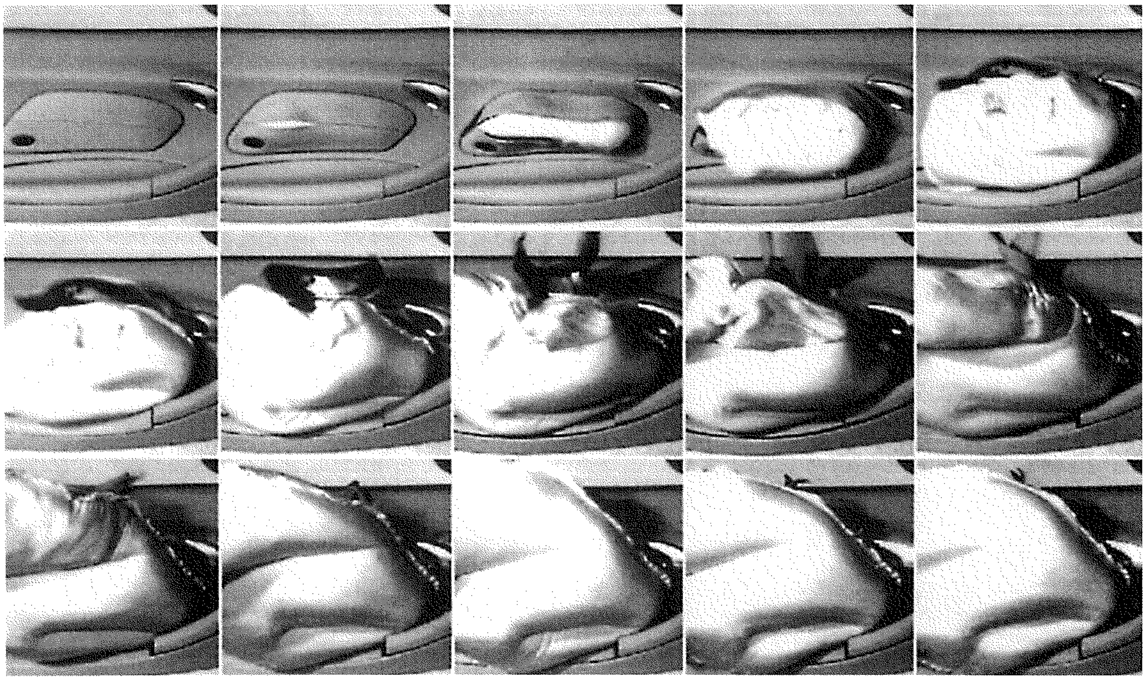

Fig. 7: Airbag deployment with no side windows

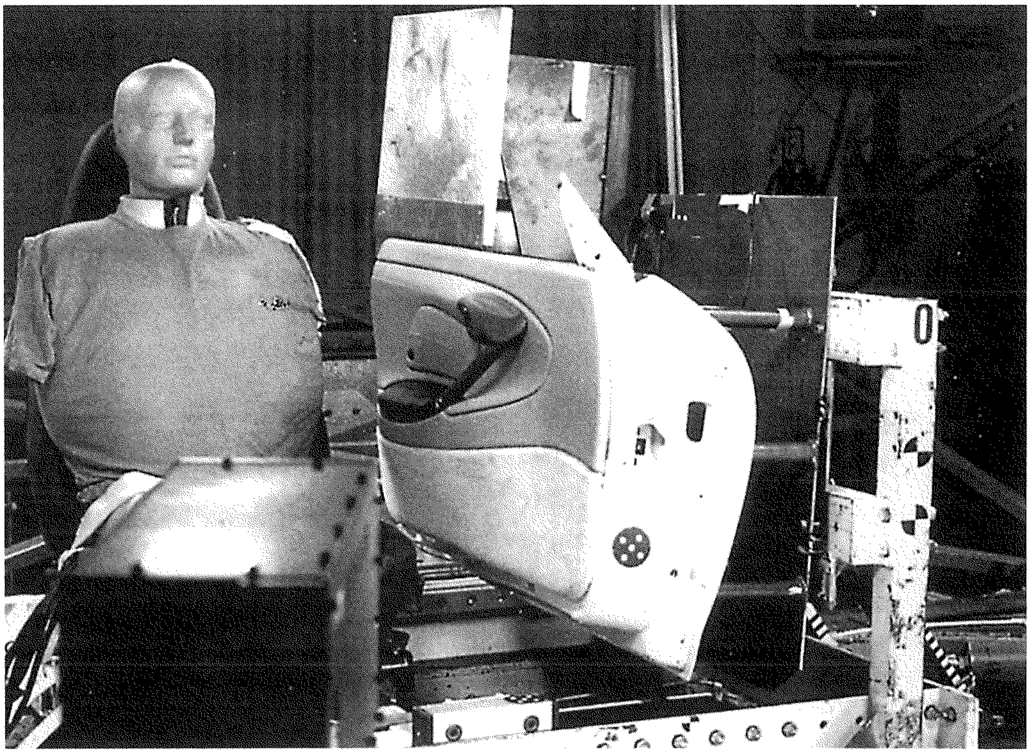

Fig. 8: Sled test configuration 1

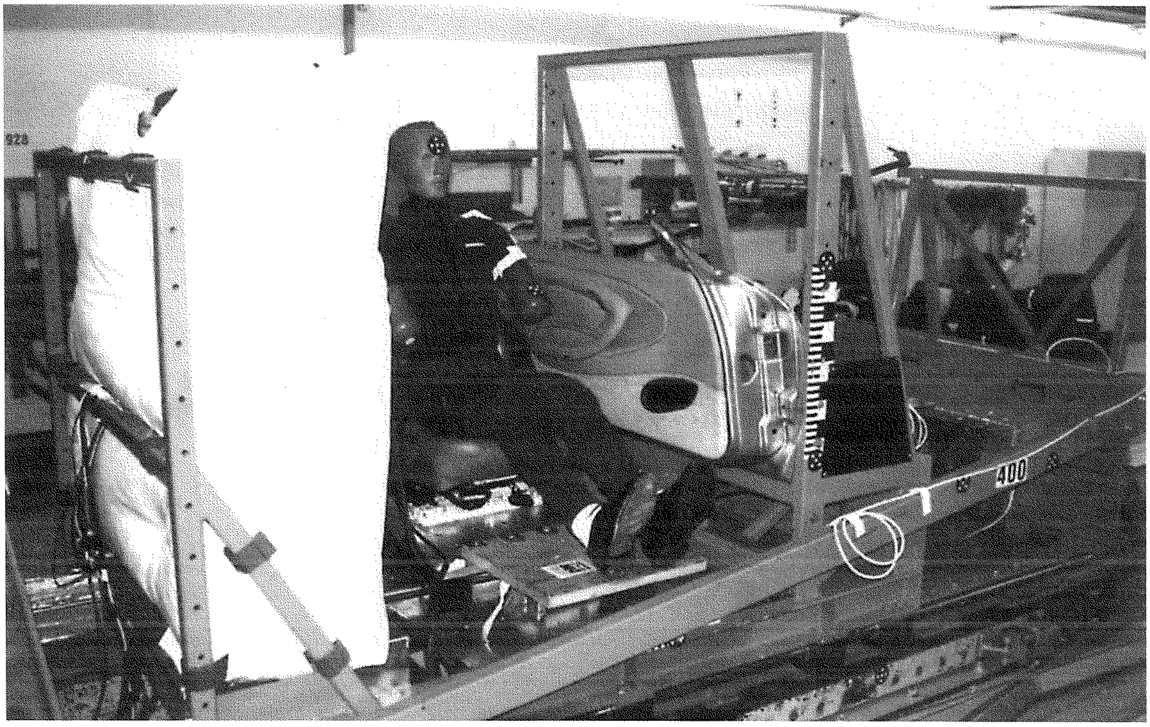

Fig. 9: Sled test configuration 2

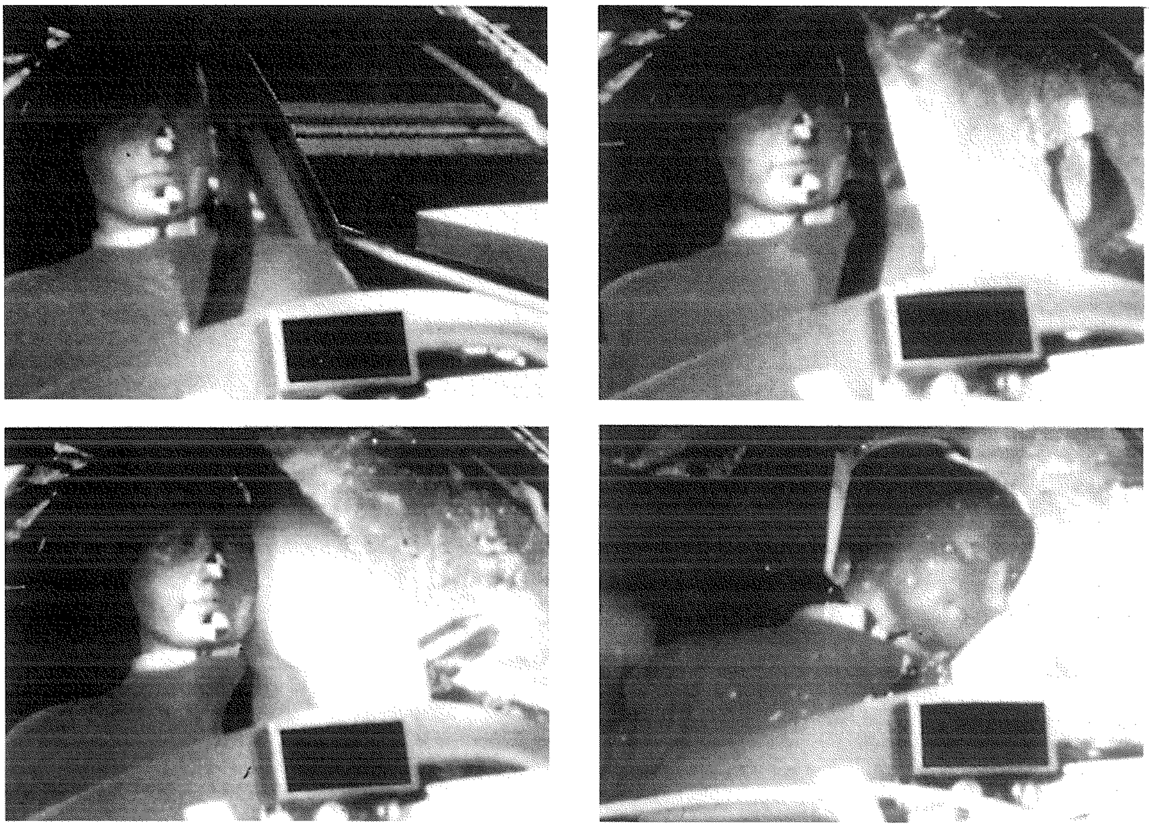

Fig. 10: Example for a airbag deployment in a FMVSS 214 crash test

The Inflatable Curtain (IC) - A New Head Protection System in Side Impacts

Anders Öhlund
Camilla Palmertz
Johnny Korner
Volvo Car Corporation
Magnus Nygren
Katarina Bohman
Autoliv
Sweden

Paper Number 98 S8 W 29

ABSTRACT

Car accident investigations have shown that the head, the chest and the abdomen are the three most vulnerable body regions in side impacts, when serious-to-fatal (MAIS 3-6) injuries are considered. Injuries are much more common to occupants seated on the struck side than to those on the non-struck side. The development of new side impact protection systems has therefore been focused on struck side occupants.

The first airbag system for side impact protection, jointly developed by Volvo and Autoliv, was introduced on the market in 1994. The SIPS bag is seat-mounted and protects mainly the chest and the abdomen, and also to some extent the head, since the head's lateral relative displacement is reduced by the side airbag, thereby keeping the head inside the car's outer profile. However, if an external object is exposed in the head area, for example in a truck-to-car side impact or in a single car collision into a pole or a tree, there is a need for an additional head protection device.

Such a device, called the Inflatable Curtain (IC), jointly developed by Volvo and Autoliv, is described in this paper. The IC is an additional improvement to Volvo's unique SIPS and SIPS bag systems. It consists of two layers of fabric in what is known as one-piece woven technology. The IC is folded into a thin package, and is attached to the roof rail and the upper part of the A-pillar. When inflated, it covers the upper half of the side window, from the A to the C pillars, thereby substantially increasing head protection for both front- and rear-seat occupants. The performance and effects of the IC, in car-to-car and single car side impacts, are presented and discussed in the paper.

INTRODUCTION

Although frontal impacts still account for the largest number of injuries in crash statistics, approximately 25% of all serious-to-fatal injuries are incurred in side impact collisions, Figure 1[1]).

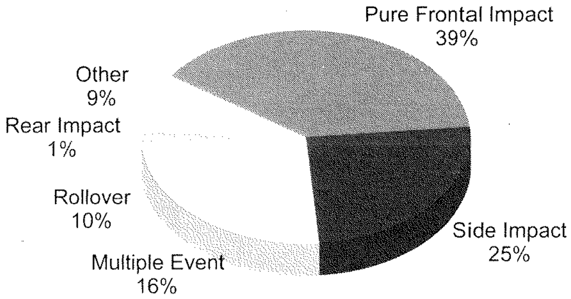

Figure 1. Distribution of serious-to-fatal crashes (MAIS 3+) by impact type. (n=1.997 occupants)

Today, frontal crash safety has been refined to such a degree that the safety benefits of a given design effort aimed at improving side impact protection are probably higher than the benefits of an increased design effort on enhanced frontal crash safety. One reason for this is that severe injuries sustained in side impacts occur over a fairly wide range of crash severities, with a relatively high frequency of injuries occurring even at low severities. Consequently, there is much to gain in terms of injury reduction by improving the side impact protection characteristics, not only at high crash severities but also in the low-medium range of the crash severity distribution.

---

[1] The statistics in Figures 1 - 6 are derived from Volvo's accident data base, containing 27.500 crashes (1976-98) involving Volvo cars (only) in Sweden. The cases are selected according to a repair cost criterion. In case of an injury accident where someone has received medical attention, occupant injury data is acquired from medical case records. Of the 46.800 Volvo occupants involved in the crashes, 61% were uninjured, 34% sustained minor-to-moderate injury (MAIS 1-2), and 4% sustained serious-to-fatal injury (MAIS 3-6).

Structural reinforcements are needed to reduce the velocity of the intruding side structure in car-to-car impacts, and to provide a base on which interior energy absorbents will work satisfactorily. With the SIPS system, Mellander H. et al [1], Volvo took a first step towards increased occupant protection against side impacts by reinforcing many systems of the car, including the doors, the B pillars, the floor, the floor tunnel, the roof, and the seats. Energy-absorbing elements were also added to the car interior inside the door panels.

The SIPS bag, as described by Pilhall S. et al [7], was introduced in 1994 as standard equipment in the front seats of Volvo cars, as the first supplement to the basic Side Impact Protection System (SIPS). The bag was primarily designed to further reduce chest, abdominal and pelvic injuries, with only a moderate potential for reduction of head injuries.

Providing further interior energy absorption elements, in one form or another (foam, bags, etc.), offers a great potential for injury reduction, since this method is effective both in car-to-car impacts and in side collisions with trucks and other undeformable objects (e.g. poles, trees). These collision objects account for a considerable proportion of the severe occupant injuries in side impacts (Figure 2).

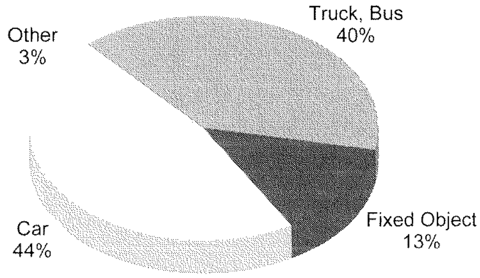

Figure 2. Distribution of serious-to-fatal side impacts (MAIS 3+) by collision object. (n=499 occupants)

In other data bases [2,3,4,5,6], the proportion of fixed objects is often higher, due to variations in road environment between countries, and the proportion of trucks/buses is lower. Together, however these collision objects still account for approximately half of the serious-to-fatal side impacts, though.

In collisions with trucks and fixed objects, body stiffness and strength are of lesser importance, since the collision object is undeformable. Interior energy-absorbing components, however, can considerably improve occupant protection by smoothing out the contact phase between the occupant and the interior side structure of the car.

The risk of sustaining an injury to the head, chest, abdomen, and pelvis is higher in side impacts than in other crash types (Figure 3). Head protection in frontal collisions has been continually improved through such development as the deformable steering wheel, collapsible steering column, increased belt use, and the introduction of frontal airbags. Today therefore, there is a higher risk of head injury in side collisions than in other crash types, especially when colliding with a truck or a fixed object.

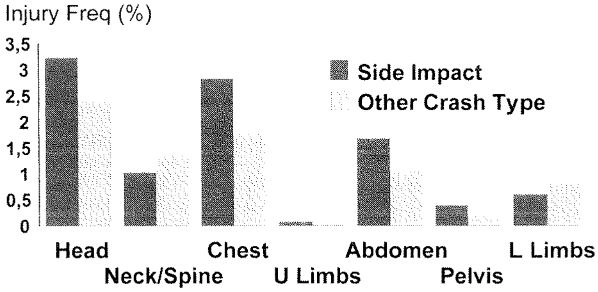

Figure 3. Injury frequency (AIS 3+) by body region (all collision objects). (n=46.856 occupants)

Head injuries are at least as common as chest injuries in side impacts, see Figure 3. This finding is supported by results from a number of sources around the world [5,8,9,10,11]. Consequently, it is highly desirable to examine the possibility of further increasing head protection in side impacts. The need for a head protection device is especially urgent in side impacts against trucks/buses and fixed objects, which together account for almost 60% of the serious-to-fatal head injuries to occupants seated on the impacted side (Figure 4)

Morris et al [12] found that almost half of all head injuries (AIS 2+) in side impacts originated from exterior contacts against other vehicles, poles, trees, etc. Door glass was the most frequent interior contact source. The severe injuries (AIS 4+) were more frequently caused by exterior sources than by interior sources.

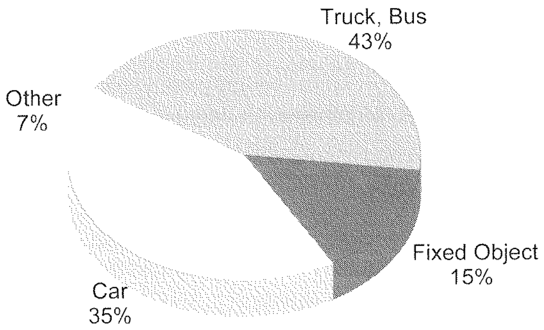

Figure 4. Distribution of collision objects among near-side occupants sustaining (AIS 3+) head injury in side impacts. (n=172 occupants)

An effective head protection device must cover both the front seats and the rear seat, since the risk of head injury is equally high for front or rear seat occupants (Figure 5, Volvo data base).

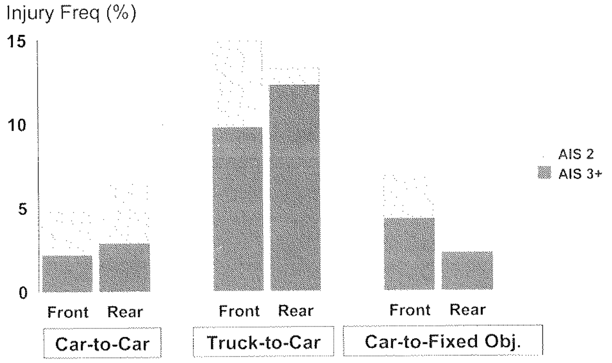

Figure 5. Head injury frequency (%) by seating position and collision object.
(3.414 front seat, 606 rear seat near-side occupants)

The types of head injury (AIS 2+) sustained by near-side occupants are mainly concussions, fractures, brain hemorrhages, brain edemas, and crush injuries (Figure 6); injuries that indicate hard head contact. Similar results were found by Morris et al [12].

In Volvo's data base, the majority (62%) of the concussions are of moderate severity (AIS 2), 35% are serious (AIS 3), and 3% are severe-to-critical (AIS 4-5).

The fractures involve a much higher threat to life: 24% AIS 2, 15% AIS 3, and 61% AIS 4-6. Of the brain hemorrhages, 69% are (AIS 4-6). The crush injuries are exclusively critical-to-fatal (AIS 5-6) as are most of the brain edemas. The ruptures (of the brain stem) are all fatal (AIS 6).

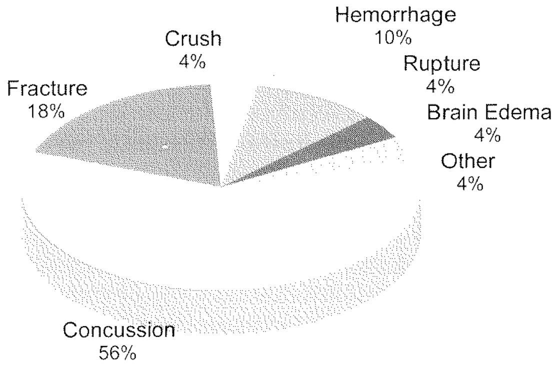

Figure 6. Distribution of AIS 2+ head injuries by injury type.
(n=302 front & rear seat near-side occupants)

Neck injuries in side impacts are mainly of low injury severity in terms of threat to life, AIS 1. These injuries occur at all crash severities. More serious neck injuries (AIS 2+) are very rare (less than 1% injury frequency to near-side occupants). They are more likely to occur at high crash severities, most often in combination with head injury. Most of these (very rare) AIS 2+ neck injuries (73%) consist of fractures AIS 2-5 to the cervical vertebrae (C1-C7), 20% are ruptures AIS 5-6 of vertebrae C1-C4, and 7% are luxations, nerve injuries and pain AIS 2-3.

In view of the accident data presented above, it is obvious that there is an urgent need to further increase head and also neck protection in side impacts. The objective of this paper is to describe the development, design, function, and protective performance of a new dynamic head protection system, the Inflatable Curtain (IC), jointly developed by Volvo and Autoliv. The aim is to considerably reduce the risk of serious-to-fatal head and neck injuries in side impacts – for front seat as well as rear seat occupants, and especially in collisions against fixed objects (poles, trees) and trucks/buses.

DESCRIPTION OF THE INFLATABLE CURTAIN

Main Components

The system consists of two main components, (Figures 7 and 8).

The Bag, manufactured through "One-Piece-Woven" technique. Due to the technique, the bag can be folded in a thin package in the car. The bag is impregnated with a special silicone that makes it possible to maintain an adequate pressure in the bag. Thereby, significant protection is obtained also in multiple accidents. To reduce friction, a thin layer of material (light weight non-woven material) is laminated to the silicone. This makes it easier for the bag to unfold during deployment. The low friction also contributes to avoid adhesive contacts to the occupants.

The Gas Generator is of hybrid type, using a pyrotechnic propellant. When activated by a sensor, gas is generated to open a mechanism that leads into a pressure vessel containing inert gases, 95% argon and 5% helium. The cold gases in the vessel are mixed with the hot gases generated by the propellant. The result is a low temperature of the gas filling the IC, which is important for maintaining a good pressure in the bag. The gas generator is placed in the D-pillar.

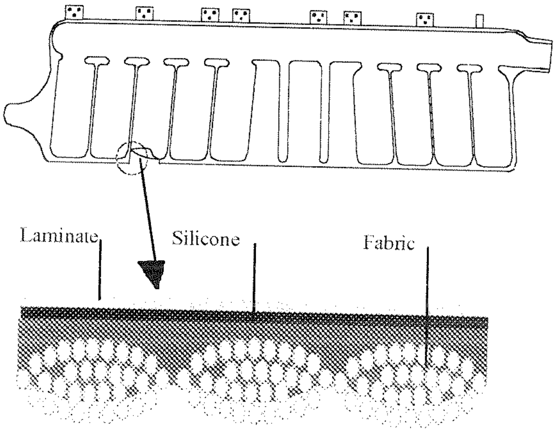

Figure 7. The IC bag.

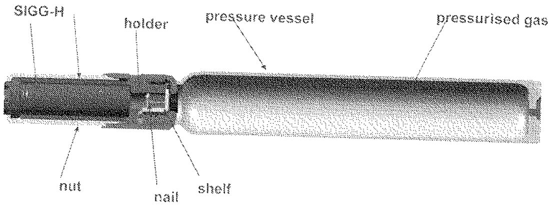

Figure 8. The IC gas generator.

Covering Area

One of the basic principles of the system is to provide an adequate protection area to occupants in both the front and the rear seats. Various occupant sizes and seating positions should also be considered. The protection area can be divided into two different types (Figure 9).

1) The zone where the head is likely to be directly exposed to the pillars, the roof rails, the door glass, and objects outside the car. Impact energy absorbtion is needed in this area.

2) The rest of the area "only" helps protect the occupants by keeping the head inside the compartment, and by preventing glass or similar objects from intruding into the area of the occupants head.

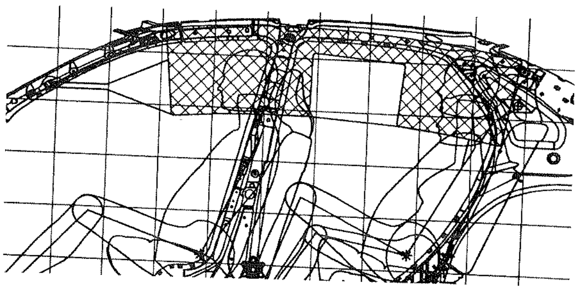

Figure 9. IC covering area.

Timing Performance

An airbag-based side impact protection system has to be very fast in terms of position performance, due to the very limited distances between the occupants and the interior of the car. This is valid for both chest/pelvis protection and head protection. In order to protect the occupants, the IC must be fully deployed after about 30 ms from initial crash contact in high severity side collisions.

The IC is fully deployed at about 25 ms after ignition of the inflator (Figure 10.).

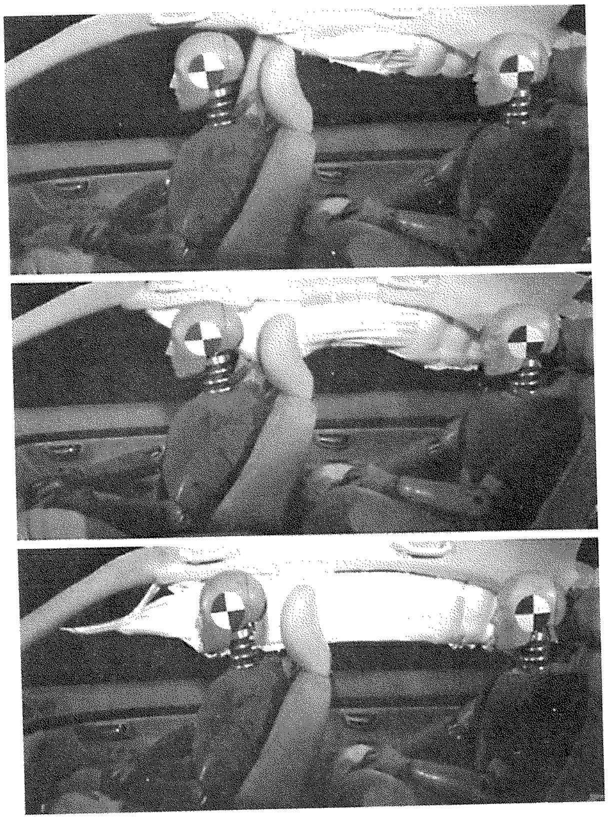

Figure 10. IC deployment at 12, 17 and 24 ms, after ignition of the inflator.

In addition to the time for complete positioning, the bag pressure time history is an important parameter. Both in terms of the time for reaching "working pressure", and for how long the bag remains inflated. (Figure 11).

At about 40 ms, the maximum pressure is reached. The remaining pressure, is adequate in providing protection for at least 3 seconds in crash situations beyond an initial side impact.

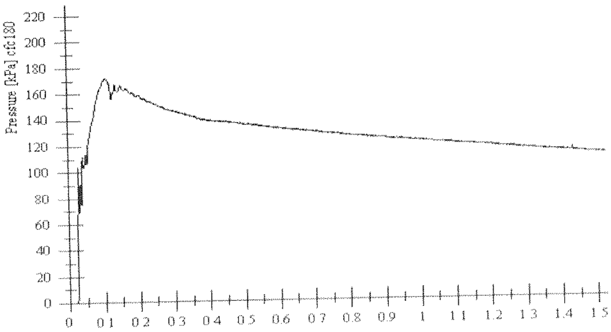

Figure 11. Bag pressure vs. time.

METHODS

Due to the specific area being quite new, and to the relative complex "field accident situation", there are not yet any generally established methods for developing dynamically deployed protection systems for improved head protection in side collisions.

However, there are tools to examine the head protection performance in some relevant situations.

In the preparatory analysis of the IC system's function and energy absorbtion properties, a simple pendulum test set-up was used to take the first development steps. Developments have then continued, mainly with pole impact sled tests and full-scale crash tests. It is thought that the pole impact mainly cover even truck/bus impact.

Pendulum Test

Depending on dummy type, crash mode, and car structure, the head will have an angular direction relative to the torso. The neck loadings will also help the head reduce its velocity. This will result in a number of different possible velocities towards an external object or against a protection device.

The method makes use of a pendulum to which a head form, with a weight of 6,8 kg and diameter of 165 mm, is attached. The head form moves in a pendulum motion and hits the impact object and the IC, in the head form's lowest point where there is a horizontal velocity component only. Behind the IC, a stiff undeformable block is placed which simulates an external contact surfaces.

For the first rough tests, an assumption has been made that the head is angled approximately 30 degrees towards the torso. This gives a horizontal velocity of 7 m/s, corresponding to a pole test at 32 km/h, which has served as an upper limit in the initial tests.

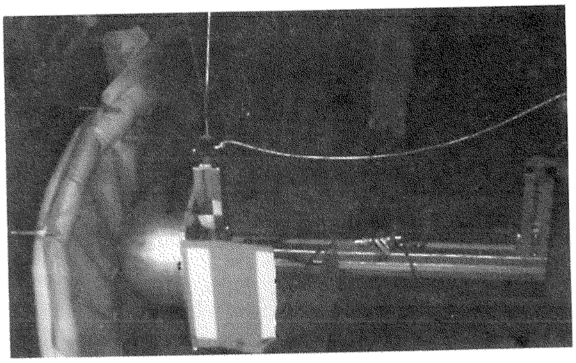

Figure 12. Pendulum test set-up.

It should be noticed, that the head form has a slightly higher weight (6,8 kg) than a real head (about 5 kg), therefore an impact velocity of 7 m/s will correspond to a slightly higher impact velocity for a real head.

Free Motion Headform (FMH) According to FMVSS 201.

The need for improved head protection has led NHTSA to establish new requirements for Upper Interior Impact Protection, in FMVSS 201. These requirements are to be phased in over five years, beginning September 1, 1998. Originally, the requirement defined a number of specific target points (Figure 13) at which a Free Motion Headform's (FMH) HIC(d) criteria must not exceed 1000, when impacting the points at 15 mph (6.7 m/s).

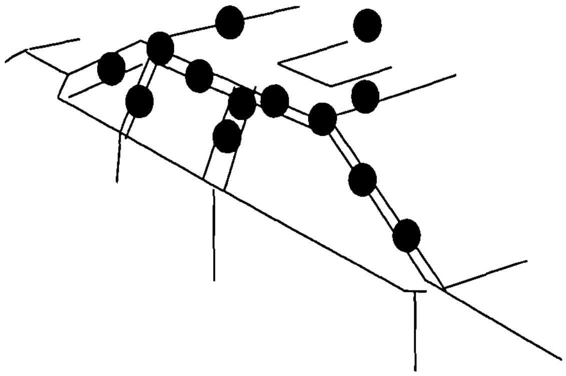

Figure 13. Target points defined in FMVSS 201.

However, since making this rule, NHTSA has subsequently published a Notice of Proposed Rulemaking, in August 26, 1997, that makes possible, but does not mandate, some alternative requirements to use as possible options for "Dynamic Head Protection Systems".

One of these options, a full scale side impact into a fixed pole, also takes into consideration crash situations in which the occupants directly impact an external object.

By using the FMH test set-up, it is possible to evaluate the HIC-reducing effects of the IC, over a wide range of bag pressures and impact velocities, in a way that is both simple and adequate.

In order to isolate the evaluation of the HIC performance vs bag pressure, a fixed block was used, positioned outside the front door window, simulating a rigid external crash object. The FMH head was directed at this fixed block. The FMH head then impacted the IC, which covered the fixed block (Figure 14).

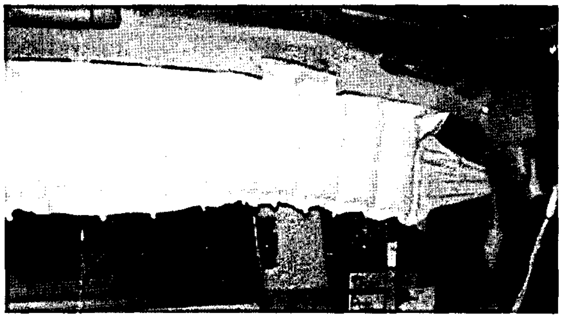

Figure 14. FMH test set-up (head to the right).

Tests have been conducted at two different impact velocities and at bag pressures from 100 to 300 kPa.

Pole Impact Sled Test

The pole impact sled test method (Figure 15),.is based on a full-scale test with a Volvo 850 which is crashed into a pole at 28 km/h. The pole has a diameter of 300 mm. The dummy values measured (Eurosid dummy) have been used as a reference for the development of the pole method.

In the method, the predeformed car body and the pole are placed in a fixed position. The seat including a SIPS bag, and a dummy are placed on a sled and crashed against the pole at chosen velocities. Between each test, door padding is changed to achieve the right torso responses.

Figure 15. Pole impact sled test set-up.

There is a reaction time difference between the pole impact sled method and the full-scale of approximately 8 ms, corresponding to the time for door deformation. This is compensated for by selecting trigger time to reach a good correlation.

In the test series, two different dummies have been used: Eurosid and the US-SID/H3 according to NHTSA's proposal for FMVSS 201, option 3. The primary response measured was head acceleration. In tests with the US-SID/H3 dummy, neck forces were also measured. Head rotation acceleration was measured in test series at 32km/h.

Computer Simulated Pole Impact

In order to predict the relationship between pressure and HIC, and to get a better understanding of this relationship, a mathematical model was developed. The model consists of vehicle structure, intruding pole, dummy, sidebag and IC (Figure 16).

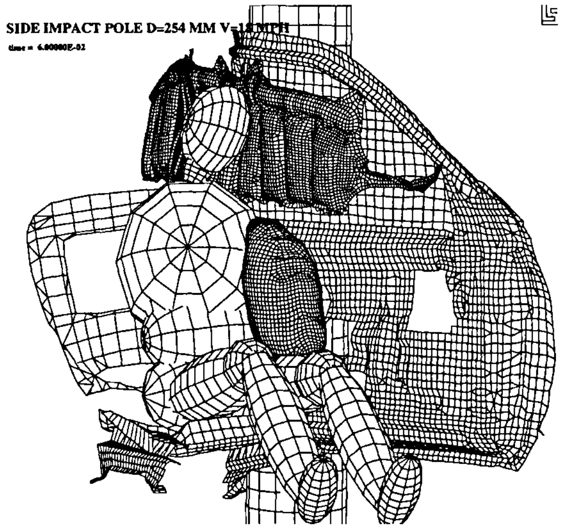

Figure 16. Computer Simulated Pole Impact.

The hybrid approach was chosen for the model development. The vehicle structure was modeled by means of finite elements, while the dummy and pole were modeled by means of rigid bodies. The number of elements and nodes in the model were 64447 and 64778, respectively. The dummy was a model of the US-SID dummy. The pole was a model of a luminary pole, with a diameter of 254 mm. In the simulations, the center of the pole was lined up with the center of gravity of the head and the vehicle traveled sideways towards the pole, with an initial velocity of 18 mph (29 km/h). The initial velocity was not varied in the study. The pressure in the IC, however, was varied from 180 kPa to 240 kPa.

RESULTS

Pendulum Test

HIC vs Cell Thickness - To position the bag quickly and at the same time achieve good injury reduction, the width of the cells is an important parameter in optimization. Performance tests have been conducted in a pendulum rig to produce an indication of the HIC reduction. In the tests, the thickness of the vertical cells and the velocity of the head form have been varied. In all tests the bag pressure was 150 kPa.

The result indicated good injury reduction in all cases (Figure 17).

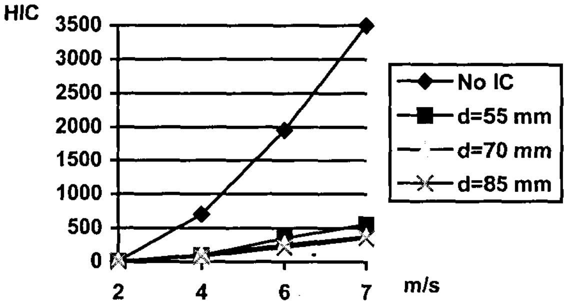

Figure 17. HIC vs velocity, at different cell thicknesses.

A cell with thickness of 85 mm gives a HIC reduction of approximately 90%, at all tested velocities.

A cell with a thickness of 70 mm gives a reduction of 88%, and a cell thickness of 55 mm gives a reduction of approximately 84%.

If the thickness of the cell is increased too much, there will be an unacceptable variations in head loading when comparing an impact to the top of a chamber or between two chambers. Besides, there will be other negative effects, such as increased time to positioning and increased bag volume, which will require an increased gas generator capacity in order to reach an adequate pressure.

A thickness of 70 mm and a pressure higher than 1.5 bar kept the head form from bottoming out the IC at an impacting velocity of 7 m/s.

Absorption of Impact Energy - By throttling the inlet to the vertical cells, the energy absorbtion can be increased. When the head hits the curtain, an amount of work has to be performed to push the air out of the vertical cell to the rest of the curtain. By throttling the inlets, the amount of work is increased (Figure 18).

The absorption in the pendulum tests only takes into account the lateral velocity. When testing with a dummy, in full scale tests, other parameters influence the absorption such as rotation, neck moments, stiffness in the neck etc. However, if the inlets are throttled too much, the time to position and pressurize the curtain will be delayed.

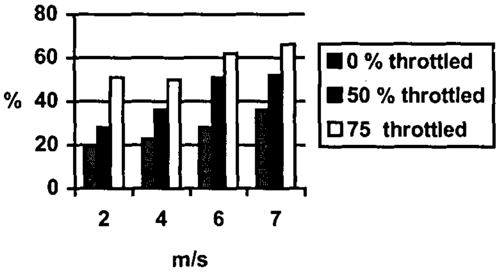

Figure 18. Energy absorption vs impact velocity, at different throttle rates.

Free Motion Headform (FMH), According to FMVSS 201

At "normal working pressure"(140 to 160 kPa), (Figure 12) the HIC(d) value was about 600 at 15,5 mph and around 400 at 12,5 mph (Figure 19). At the lower impact speed, the HIC(d) was about constant in the tested interval.

Two effects were seen at the higher velocity. The performance was quite constant down to about 150 kPa, when the head started to bottom up into the fixed block. On the other hand, the HIC(d) values started to increase when the pressure had exceeded 250 kPa.

The results indicate that the pressure level 160 to 220 kPa is favorable to cover impact velocity up to 15 mph.

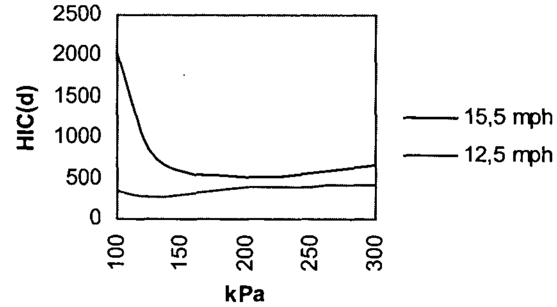

Figure 19. HIC(d) vs bag pressure

Pole Impact Sled Test

There was a major reduction of the HIC value, as well as the head acceleration maximum value, with the IC, at both impact velocities in the simulated pole impact using the Eurosid dummy. The duration of the acceleration were increased (Figure 20). The same tendencies were also found in the simulated pole impact with the US-SID/H3 dummy. The risk of skull fractures were reduced almost 100%, according to risk curves by Mertz H. et al. [17].

The maximum head angular acceleration and the maximum head angular velocity was reduced by the IC, both around the x-axis and the z-axis (Table 1).

In simulated FMVSS 214 sled tests, the neck loading duration decreased with the IC (Figure 21).Computer Simulated Pole Impact

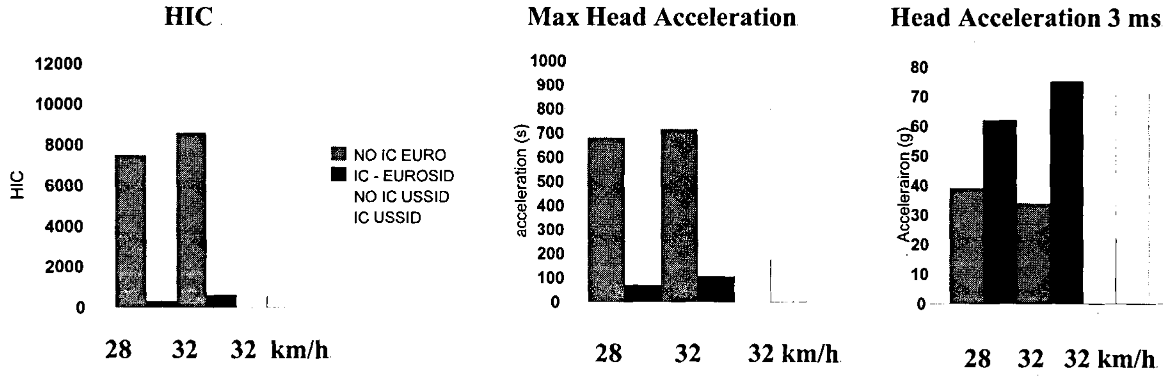

Figure 20. Head acceleration results from pole impact with the Eurosid at two different impact velocities.

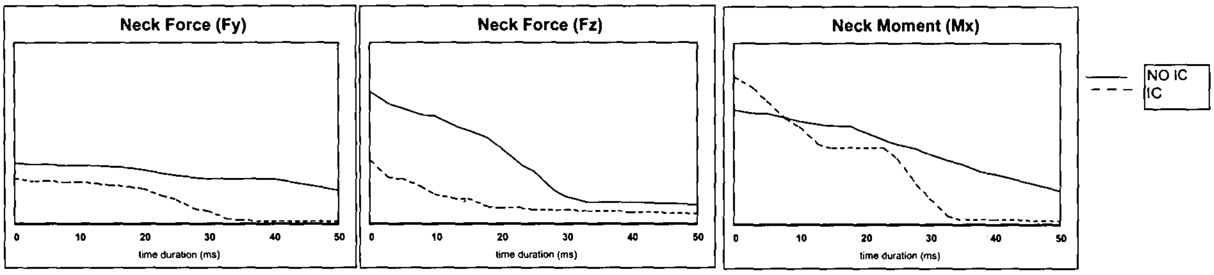

Figure 21. Neck loadings from simulated barrier sled tests with the US-SID/H3 dummy.

Table 1.
Head Angular Acceleration Results from Simulated Pole Impact with the Eurosid dummy at an Impact Velocity of 32 km/h.

	NO IC	IC
Angular acceleration around x-axis (rad/s*s)	42 500	8 200
Angular velocity around x-axis (rad/s)	39	33
Angular acceleration around z-axis (rad/s*s)	3 500	2 100
Angular velocity around z-axis (rad/s)	19	15

Computer Simulated Pole Impact

For all pressures, the HIC was below the injury criterion level of 1000. The HIC value was reduced with reduced pressure. The results indicted that further reductions in HIC could be achieved with a pressure lower than the 180 kPa used in the study (Figure 22).

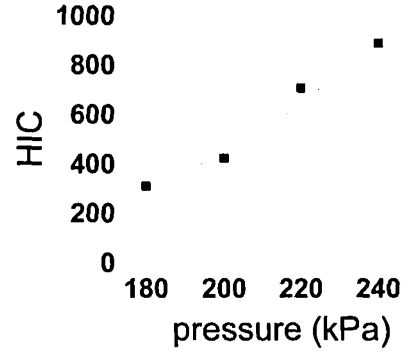

Figure 22. HIC(d) vs bag pressure.

DISCUSSION

Pole Impact Sled Test

Linear acceleration of the head - The maximum head acceleration was reduced with the IC and that was mainly due to the decreased contact force. The IC supported by the pole had much softer force-deflection characteristics than the pole itself, resulting in a much lower contact force. The IC has a thickness of 70 mm resulting in about 10 ms head contact before the head has reached its minimum distance to the pole. The velocity of the head was reduced continuously during the 10 ms penetration into the IC.

In the 28 km/h pole impact, the head velocity started to decrease (around 25 ms after car-to-pole impact) when the thorax came into contact with the side airbag. About 15 ms later, the head came into contact with the IC, and the head velocity was reduced continuously and rather smoothly, falling to zero in approximately 10 ms. Without the IC, the head velocity decreased slowly, due to the torso contact with the side airbag, but when the head came in contact with the pole, the velocity of the head decreased to zero within 1 ms, which explains the high HIC values. With the IC, the head velocity was reduced in 10 ms (Figure 23).

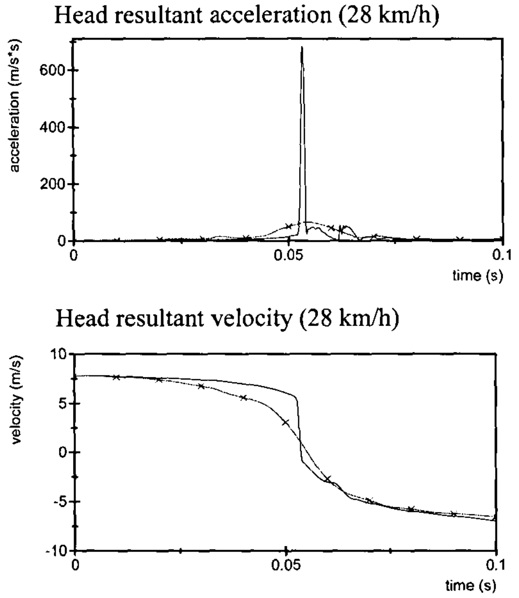
Head resultant acceleration (28 km/h)

Head resultant velocity (28 km/h)

Figure 23. Head acceleration and head velocity change in pole impact sled test at 28 km/h using the EuroSid dummy, with and without the IC.

The same tendencies were shown at both impact velocities, but the dummy values were higher at 32 km/h.

The 3 ms head acceleration value increased with the use of the IC, but it was still below the recommended injury threshold (65-94% of the injury threshold of 80g FMVSS 201). The IC decreased the peak acceleration but increased the duration of the acceleration.

That Dynamic Head Protection Systems, such as the IC, offer a great potential for reduction of head injury risks is supported by NHTSA's findings, which are published in the NPRM (August 26, 1998) for Upper Interior Impact Protection in FMVSS 201.

Angular acceleration of the head - The angular acceleration and velocity around the x-axis were reduced with the IC, both in the impact direction as well as the rebound, in the simulated pole impact with the Eurosid at an impact velocity of 32 km/h (see figure 24).

A considerable reduction (80%) of the angular acceleration was found with the IC, while the angular velocity showed a smaller reduction of about 15%. Margulies et al [13] proposed a criterion tolerance for diffuse brain injury, with an angular acceleration below 4000 rad/s^2 and an angular velocity below 40 rad/s. These injury thresholds indicate a reduced risk for sustaining diffuse brain injuries with the IC.

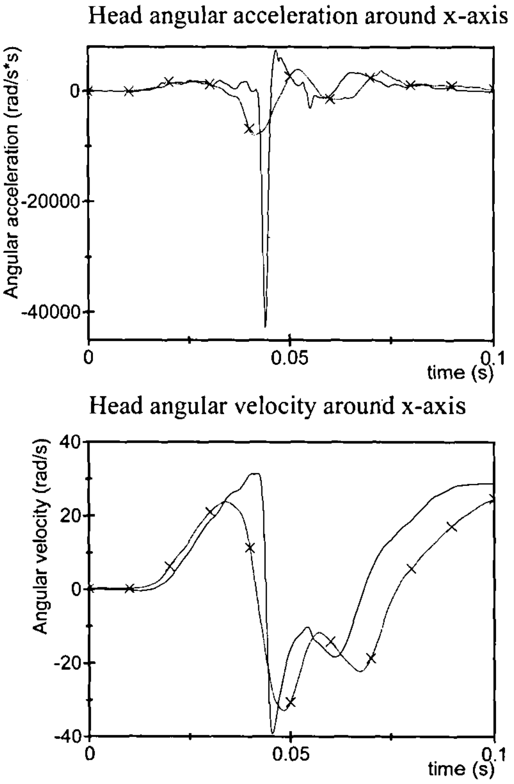
Head angular acceleration around x-axis

Head angular velocity around x-axis

Figure 24. Head rotational motions at a pole impact 32 km/h, with the Eurosid dummy, with and without the IC.

The z-axis angular acceleration was also reduced due to the IC, about 50 %, but the amplitudes were not as high as around the x-axis. These results agree with the findings of Bohman et al. [14], that the angular acceleration around the z-axis showed a significant reduction with the IC.

Neck loading - In simulated barrier (FMVSS 214) sled tests, the neck loading as well as the head acceleration were different compared to the pole impact since there was no head impact, neither with the interior nor the exterior of the car body. Without the IC the head was partly ejected, while the head was kept inside the car with the IC. The tests were run with side thorax airbag.

There was a different pattern in the neck loading with and without the IC. The neck loading without the IC had a slightly higher lateral shear force than with the IC. The neck tension was, however, about twice as high without the IC, mainly due to the inertia loading when the head moved out of the car window. The neck loadings, with or without the IC, were below the Injury Assessment Reference Values (IARV) suggested by Mertz H., [15]. The main difference was found in the increased duration of the load without the IC, especially the lateral shear force (Figure 21).

The neck moment (Mx) was slightly higher with the IC, due to the early contact between the head and the IC, which restricted the head motion out of the window. For duration longer than 8 ms, the moment without the IC was higher than with the IC. The neck moments where compared to average values of the IARV, Mertz H., [15].

In the simulated pole impact tests at 32 km/h, the neck loadings were generally lower than in the barrier tests, except for the compression of the neck without the IC, that exceeded IARV. The neck compression was reduced 73% with the IC.

Evaluation of Possible Airbag-Induced Injuries

The IC has been tested in various ways to eliminate any kind of induced injuries. One of the test methods has focused on the out-of-position situations, (i.e. when the occupant is not properly seated). The occupant can, for instance, be leaning towards the interior side.

To evaluate these situations, tests with different occupant sizes in different occupant positions were conducted. Child dummies were also included.

No harmful values have been measured, that is, they are below the injury criteria, IARV [15].

The IC is designed so that its power decreases the further it unfolds down the side of the car. This means that smaller occupants, often children, who are more sensitive, especially in their necks, see Tarriere C. [16], will receive lighter contact with the deploying curtain.

Future Development

During the past 10 years in car development, crash safety performance has been improved a lot. In spite of this fact, there is a potential to improve the safety standards even further in the future.

For example, new sensor technologies will probably create an extended use of different safety devices. For the IC system, rollover sensors may be used to further utilize the protection potential the system offers.

CONCLUSIONS

The Inflatable Curtain is the first dynamic head protection system developed to offer improved protection for both the front and rear seat outboard positions.

The IC system specifically helps reduce the risk of serious-to-fatal head injuries, especially in side collisions with rigid and/or heavy objects. The results also indicate a reduction of head angular acceleration, thus reducing the risk of diffuse brain injuries. In side impacts, the IC keeps the head inside the car, preventing the head from hitting exterior surfaces, such as the front of an impacting vehicle

The IC also reduces the levels and durations of the various neck loadings.

ACKNOWLEDGMENTS

The authors would like to take this opportunity to pay special tribute to their colleagues at Volvo Car Corporation; Thomas Appelgren, Nils Dahlgren, Lars Bergström and Peter Möller at the Interior Design Department, and Jan Ivarsson and Anders Kling at the Safety Center for their valuable contribution to the development of the IC.

The authors also wish to thank Henrik Bengtsson, Leif Hoverberg, Yngve Håland, Fredrik Kjell, Fredrik Lundgren, Bengt Pipkorn and Anders Åström at Autoliv for their tireless contributions to the development of the IC, from the basic idea to a production ready system.

The authors further wish to thank the colleagues at Collin & Aikman, Becker Group and VOV for contributing to the development of the IC.

CONTACT

For information, contact the main author or any of the Volvo co-authors at:

Volvo Car Corporation
S405 08 Goteborg, Sweden
Phone +46 31 59 00 00

REFERENCES

(1) Mellander H., Ivarsson J., Korner J. and Nilsson S., "Side impact protection system - A description of the technical solutions and the statistical and experimental tools". 12th International Technical Conference on Enhanced Safety of Vehicles, Gothenburg, Sweden, 1989.

(2) Duignan P., Griffith M., Williams S., "Side Impacts in Australia". 15th International Technical Conference on Enhanced Safety of Vehicles, Melbourne, Australia, 1996.

(3) Hassan A., Morris A., Mackay M., Håland, Y., " Injury Severity in Side Impacts – Implications for Side Impact Airbag". IRCOBI Conference, Brunnen, Switzerland, 1995.

(4) Kompaß K., Harberl J., Meßner G., "Field Study on the Potential Benefit of Different Side Airbag Systems". 15th International Technical Conference on Enhanced Safety of Vehicles, Melbourne, Australia, 1996.

(5) Lestina D. & Gloyns P., "Fatally Injured Occupants in Side Impact Crashes". 13th International Technical Conference on Enhanced Safety of Vehicles, Paris, France, 1991.

(6) Rouhana S. & Foster M., "Lateral Impact - An Analysis of the Statistics in the NCSS". Proceedings of the 29th STAPP Car Crash Conference, Paper No 851727, Washington D.C., USA, 1985.

(7) Pilhall S., Korner J. and Ouchterlony B., "SIPSBAG - A new, seat-mounted side impact airbag system". 14th International Technical Conference on Enhanced Safety of Vehicles, Munich, Germany, 1994.

(8) Sparke L.J., "An Australian Perspective on Side Impact Protection". 15th International Technical Conference on Enhanced Safety of Vehicles, Melbourne, Australia, 1996.

(9) Harms P.L., Renouf M., Thomas P.D., et al, "Injuries to Restrained Occupants: What are the Outstanding Problems?" 11th International Technical Conference on Enhanced Safety of Vehicles, Washington D.C., USA, 1987.

(10) Huelke D.F., "Near Side Passenger Car Impacts – CDC, AIS & Body Areas Injured (NASS Data)". SAE International Congress and Exposition, Paper No 900374, Detroit, USA, 1990.

(11) Insurance Institute for Highway Safety, "Side Impact Standard Will Reduce Deaths". IIHS Status Report, Vol. 25, No. 10, Nov. 17, 1990.

(12) Morris A., Hassan A., Mackay M., Hill J., "Head injuries in lateral impact collision", Ircobi Conference, The Netherlands, 1993.

(13) Margulies S.S. and Thibault L.E., "A proposed tolerance criterion for diffuse axonal injury in man", Journal of Biomechanics, Vol. 2, No. 8, 917-923, 1992.

(14) Bohman K., Håland Y., Aldman B., "Reduction of head rotational motions in side impacts due to the inflatable curtain - a way to bring down the risk of diffuse brain injuries". 16th International Technical Conference on Enhanced Safety of Vehicles, Windsor, Canada, 1998.

(15) Mertz H., "Injury Assessment Values Used to Evaluate Hybrid III Response Measurements" 1984, Published in SAE PT-44, 1994

(16) Tarriere C., "Children are Not Miniature Aldults". IRCOBI Conference, Brunnen, Switzerland, 1995.

(17) Mertz H., Prasad P., Irwin A., "Injury Risk Curves for Children and Adults in Frontal and Rear Collisions". 41th Stapp Car Crash Conference, 1997.

ASSESSMENT OF INJURY PROTECTION PERFORMANCE OF SIDE IMPACT AIRBAGS FOR OUT-OF-POSITION AND OTHER THAN 50TH PERCENTILE ADULT MALE OCCUPANTS

Anil V. Khadilkar
Biodynamics Engineering, Inc.
Lonney S. Pauls
Springwater Micro Data Systems
United States
Paper No. 98-S8-W-30

ABSTRACT

The recent real-world experience with the frontal airbags and their sometimes unfortunate interaction with small size adults and children led to the analytical efforts and the results reported in this paper.

The focus of this paper is an analytical study investigating the side impact protection performance of side airbags in interaction with, out-of-position occupants. The study evaluates interaction of the two extreme size occupants including a 3 year old child, and a small 5th percentile adult female. The objective is to identify any potential problems with the side impact airbags in real world scenarios. To date, a considerable amount of research has been invested in developing and evaluating occupant protection systems for both frontal and side impacts. However, the majority of this research has focused on the 50th percentile adult male occupant size, who is properly seated in his seat. The current study validates the computer model using available test data and then assesses the side impact protection performance of the side airbags for the selected conditions.

A computer modeling system, SIFEM, is used to simulate various side impact scenarios of interest and to evaluate several vehicle designs. Candidate designs include currently on the market side airbag systems and those reported in technical literature. System performance is measured in terms of injury criteria (e.g., HIC, TTI, peak chest acceleration, peak pelvic acceleration, occupant kinematics, etc.).

SIFEM computer model is designed to take advantage of finite element and lumped mass modeling techniques. The model simulates interior occupant protection systems including padding, and airbag systems. Airbag system with user-selected bag shape and inflator flow characteristics are modeled. Simplified stretch and deployment algorithms model the bag deployment and its interaction with the occupants. Bagslap, catapult (membrane) and contact pressure phases are also modeled.

INTRODUCTION

A computer modeling system, SIFEM, was used to simulate selected impact event and to evaluate occupant configuration of interest. This paper is a companion paper with another paper in this conference (Reference 1) by the same two authors. The paper in reference 1 describes in greater detail SIFEM model, restraint configuration and the vehicle impact scenario. Only the highlights of those details are presented in this paper. In this study, SIFEM was used as an evaluation tool.

Crash Scenario

The Crash Scenario used for this study consisted of an actual full scale crash test conducted at the Vehicle Research Test Center of East Liberty, Ohio (Reference 2). The test consisted of a 1988 Hyundai Excel 4-door sedan impacted by NHTSA's moving deformable barrier. The intersection collision simulated an impact with striking vehicle traveling at 30 mph, and struck vehicle at 15 mph, colliding at an angle of 90 degrees on the driver side.

Occupant Simulation

The SIFEM data base includes the basic SID (50th percentile adult male dummy) and SIDIIs dummy (5th percentile adult female dummy). Currently, there are no standard side impact dummies available for 3 year old child and 95th percentile adult male. For those two sizes, we created scaled 'theoretical' dummies. The details of the scaling technique are available in reference 1.

A Cautionary Note

The results presented in this study provide great insight into the problems that were studied. Caution and care, however, must be used in interpreting the results presented in this study, because of its limited nature, and the assumptions made during the course of it. The readers are advised to review references 1 and 2 to fully understand the databases used in this study.

Injury Measures

The occupant model calculates the following injury measures:

- Head Injury Criterion, (HIC);
- Peak Chest Acceleration (3 msec clip);
- Peak Femur Load, (PFL);
- Peak Pelvic Load, (PPL);
- Hip Acceleration;
- Viscous Criterion V*C, (each rib and abdomen);
- Thoracic Trauma Index, TTI;
- Hip Joint Load - Displacement, Velocity and Acceleration, (fore and aft and side to side)
- Neck Moment and Head Rotation (fore and aft and side to side)

SIDE IMPACT AIRBAG DESIGNS

Side impact airbags are relatively new. Information on their configuration, design, sensing, and characteristics is still scarce in the published literature. Currently, there are three main configurations of side airbag designs (References 3 and 4). They are:

1. Inflatable airbags similar in principle to the frontal airbags that are deployed from the seat or the door panel;
2. Curtain type thin airbags that deploy from the doorliner downwards in between A- and C- (or B-) Pillar which keeps door glass out and occupant head inside ; and
3. Head Impact Protection (HPS) which is a sausage type inflated device which provides head protection.

This study considers only the first type described above.

Sensing Techniques

Several sensing techniques are identified for the production and planned airbags (References 3 and 4). These include mechanical triggers, pressure inside door cavity, electronic 'g' sensors, etc. NHTSA-conducted side impact tests appear to indicate that on some of the compliance and NCAP tests both left and right side airbags deployed during impact. On the remaining tests, only the impacted side airbags deployed.

Sensing, Trigger and Deployment Times

Side impact configuration is such that for effective protection; sensing, trigger and deployment times have to be shorter than those available for the frontal impact airbags.

All above factors make the issues involved in side impact protection and use of airbags, demanding, technically challenging and complex.

FRONTAL AIRBAG EXPERIENCE

Several articles (References 5,6,7, 8, and 9) have addressed the issues involved in inadvertent airbag related injuries in frontal impacts. After studying the issues involved the following of those issues are applicable to the side impact airbag scenario. They are:

- Inadvertent airbag firing;
- Out-of-position occupant; and
- Unnecessary airbag firing.

Inadvertent Airbag Firings

As seen in NHTSA crash tests, the non-impacted side airbags may deploy during side impact crashes. Similarly, one or both side airbags may deploy during rollovers crashes.

Also of concern is the issue, if the airbags will deploy for relatively minor side impacts. Rather than waiting for the field experience, side impact protection designers must be looking at these issues right now before it becomes a potential safety and societal cost issue.

One more concern is reported frontal air bag deployment in FMVSS 214 type side impact tests (Reference 6). In those tests the impacted vehicle is stationary, but the crabbed Moving Deformable Barrier (MDB) simulates 90 degree intersection collision with both vehicles moving. The calculated delta-V's for the impacted vehicles appeared to be below the threshold for airbag deployment. One wonders if similar occurrence can manifest itself in side impact airbag real-world environment.

Out-of -Position Occupant

Vehicle occupant can very easily be in a position, that is not similar to a crash test Side Impact Dummy, meticulously positioned by a trained test technician. Even properly restrained vehicle occupant can have his upper or lower extremities in harm's way in the path of the deploying airbag.

A person can be dozing off with head and shoulders against the B-Pillar, door, or against the stowed airbag.

Unnecessary Airbag Deployment

This category is different than the inadvertent deployment category. Included in here are low level side interactions that may cause localized moderate damage, some distance forward or rearward and away from the occupant not necessarily requiring side impact airbag deployment and protection.

Authors have been involved in evaluation of several sideswipe kind crashes (Reference 10). The sideswipes can occur at urban city-driving-speeds and also at freeway speeds. There are instances in which the sideswipes have resulted in substantial dollar damage to the vehicle. The extensive dollar damage results from three factors. The first factor is that relatively weak, side structure is involved in the vehicular interaction. The second factor is that the damage can extend over longer length, covering several expensive parts. The third factor is that even though, at times the damage is superficial with limited depth, the repair and/or replacement cost is higher because of the extent of the overall damage.

Biodynamics Engineering, Inc. conducted a sideswipe crash test involving a passenger car and a garbage truck. An instrumented volunteer was the driver of the passenger car. The test data will be presented in reference 10 conference. The results and the data show that the evaluated sideswipe crash was not injury causing event, despite the high dollar repair costs. The deployed side airbag (or airbags) would have further added to the dollar costs without any need for occupant protection, and may have created some harm to the occupant.

The issues identified here are certainly noteworthy, and side airbag designers must have addressed these in their design. The issue this paper focuses on is the issue of what happens to the out-of-position occupants during the unnecessary airbag deployment.

The two cases considered are:

Case No. 1: A case of 3-year old child, not-in a child-safety-seat, but in a booster seat, and leaning to the side against the airbag is considered as a purely theoretical, lower end extreme. The performance comparison is made by simulating side impact airbag, first optimized for the 50th percentile adult male and then for the 3-year old child.

Case No. 2: A case of a 5th percentile adult female is considered. The effect of a deploying airbag is evaluated when she is leaning to the side against the stowed airbag.

The case of 95th percentile adult male was not evaluated in this study. In both considered cases, the occupant is assumed to be restrained. The airbag deployment takes place without any damage to the side structure of the vehicle, to simulate inadvertent airbag deployment. Hence, any trauma imparted to the occupant is solely due to the deployment of the airbag. The side window is assumed to be rolled down and in an open position during the simulation runs.

SIMULATION RESULTS AND DISCUSSION

The kinematics of the selected occupants and the simulation results are presented in Figures 1 to 3 and are summarized in Table 1.

Figure 1 shows kinematics of a 3 year old child, on booster seat, restrained, and leaning against the side when the side airbag is deployed without any side structural damage. The airbag characteristics for this simulation are optimized for the requirements of the of 50th percentile adult male.

Figure 2 shows the kinematics of the same 3-year old, with same seating configuration. In Figure 2, the airbag characteristics are optimized for the requirements of the 3-year old child.

A comparison of the kinematics in Figures 1 and 2, distinctly shows different interaction between the child and the airbag in two cases, and the influence of the higher power airbag in Figure 1. The simulation of 3 year old child is based on SIDIIs family and hence the dummy arm is simulated.

Figure 3 shows the baseline and reference kinematics of a 50th percentile adult male in interaction with the side impact airbag that is optimized for the 50th percentile adult male. A comparison of Figures 1, 2, and 3 gives visual difference and distinct variations between the kinematics of 3 year old and the 50th percentile adult male in interaction with the side airbags with different selected characteristics.

The kinematics of the 5th percentile adult female are not shown here, but, as is to be expected they lie in between the kinematics shown in Figures 1 and 3.

Table 1 has four columns. The first column shows the Injury Measure and the Units. The second column shows the results of the simulation corresponding to the kinematics shown in Figure 1. Hence it is for 3-year old child in interaction with the side airbag that is optimized for the 50th percentile adult male. The column four shows the results corresponding to the kinematics shown in Figure 2. Hence it is for the 3-year old child in interaction with the airbag that is optimized for the 3-year old child.

The third column in Table 1 summarizes the results of the simulation where a 5th percentile female, fully restrained leaning against the side is interacting with side airbag that is optimized for the 50th percentile adult male.

In discussing the results, the known thresholds for the 50th percentile adult male, such as HIC = 1000 are used in the discussion. Most cases the corresponding threshold values for 3-year old child or the 5th percentile adult female are not universally identified and accepted.

3-Year Old Child (Columns 2 and 4, Table 1)

The HIC value is low for both cases. Same is the case with the peak chest 'g' (PCG) value.

The Thoracic Trauma Index (TTI) values are high even for the 50th percentile adult male. TTI values are a little lower in column four, but they are still high, particularly for the 3-year old.

Viscous Criterion (V*C) values are low in column four. A value of 1 Meter/second is considered a threshold. In column two, V*C values are low for the upper and middle rib, but is relatively high for the lower rib.

Hip level forces and accelerations appear to be relatively low and not an area of concern in both columns two and four.

Viscous Criterion values for the abdomen taken in conjunction with the force show high value in column two, and this is an area of concern. This occupant is simulated with the arm. It is seen the arm mass interacts with the ribs and the abdominal area and produces high level interaction. As is seen in column four, the optimization of the airbag for the 3-year old, dramatically reduces the injury measures in the abdominal region.

The rib displacement values are moderately high for the 3 year old. Typically, a value of 1.6 inches is considered as a threshold for the 50th percentile adult male as a design guideline.

The hip joint acceleration, velocity and displacement are relatively low, both in columns two and four.

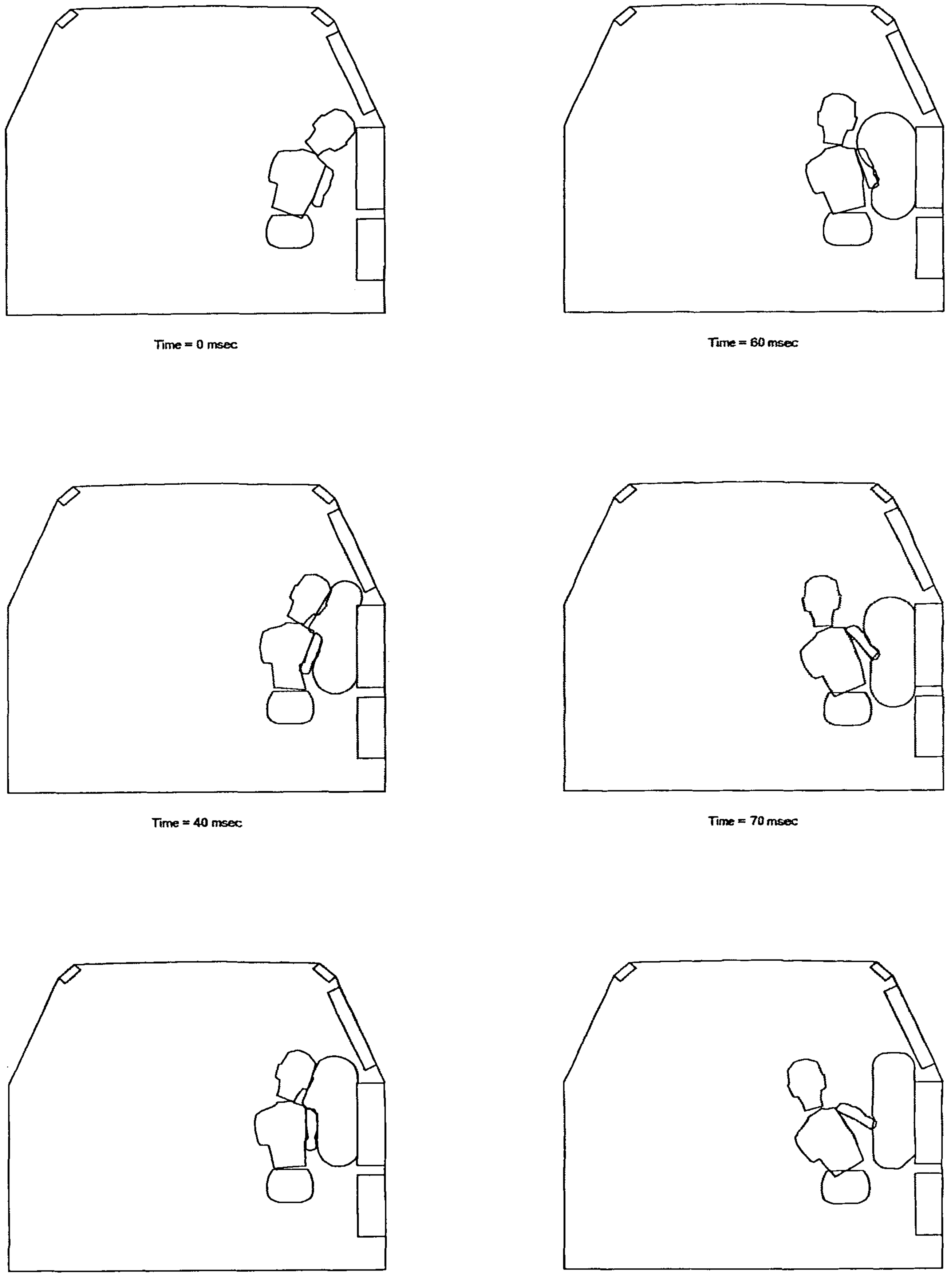

Time = 0 msec

Time = 60 msec

Time = 40 msec

Time = 70 msec

Time = 50 msec

Time = 80 msec

Figure 1. Occupant Trajectory, 3 Year Old Child with Airbag Optimized for 50th Percentile Adult Male

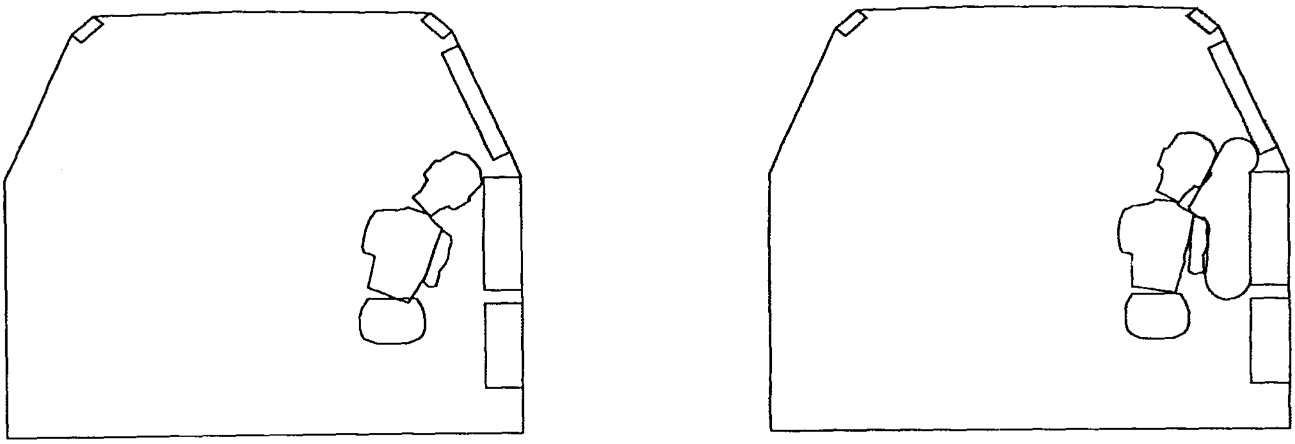

Time = 0 msec

Time = 60 msec

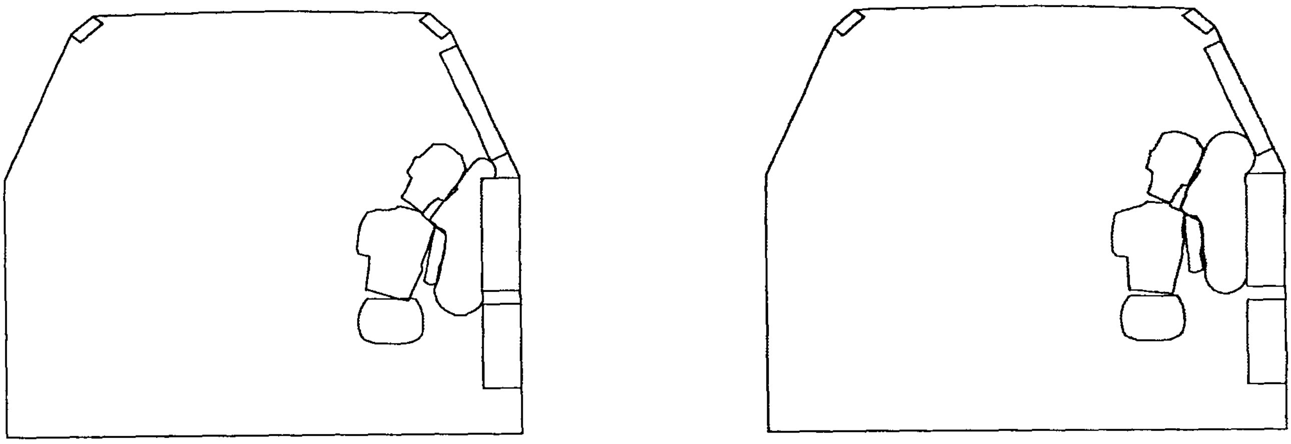

Time = 40 msec

Time = 70 msec

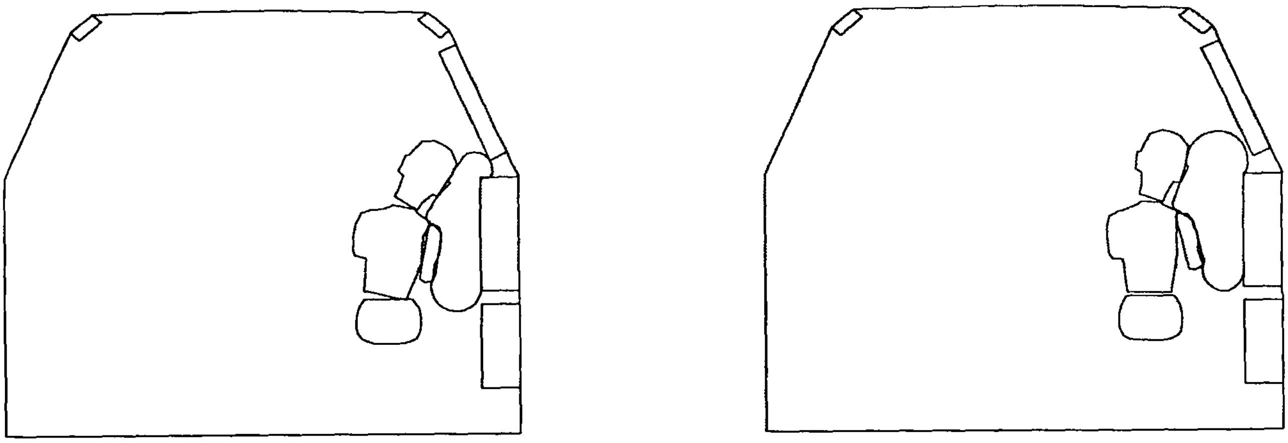

Time = 50 msec

Time = 80 msec

Figure 2. Occupant Trajectory, 3 Year Old Child with Airbag Optimized for 3 Year Old Child

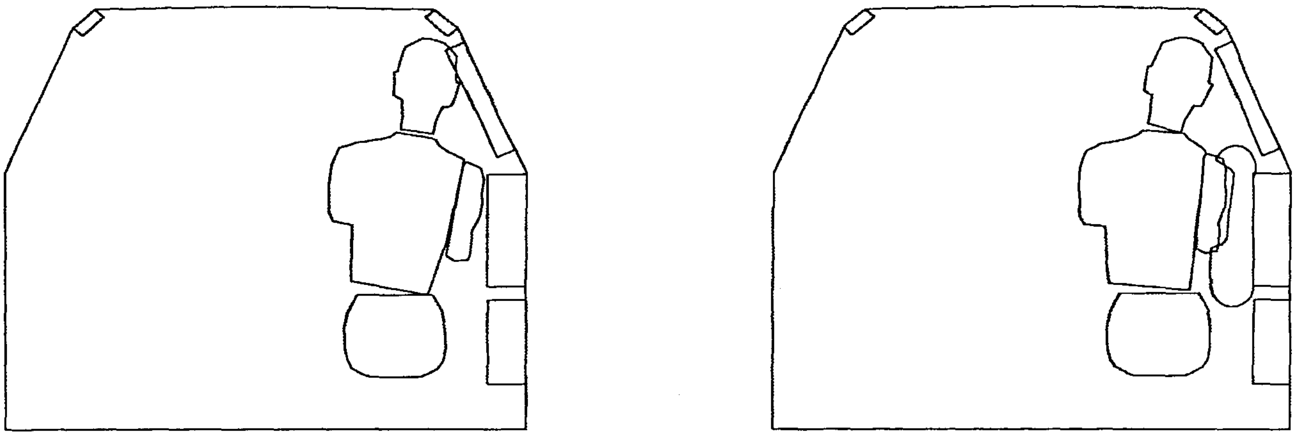

Time = 0 msec

Time = 60 msec

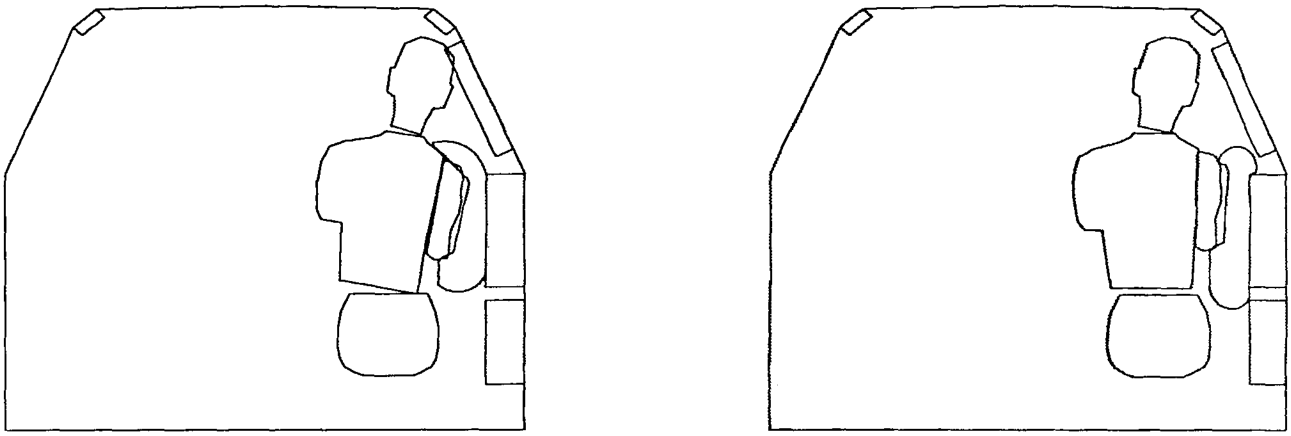

Time = 40 msec

Time = 70 msec

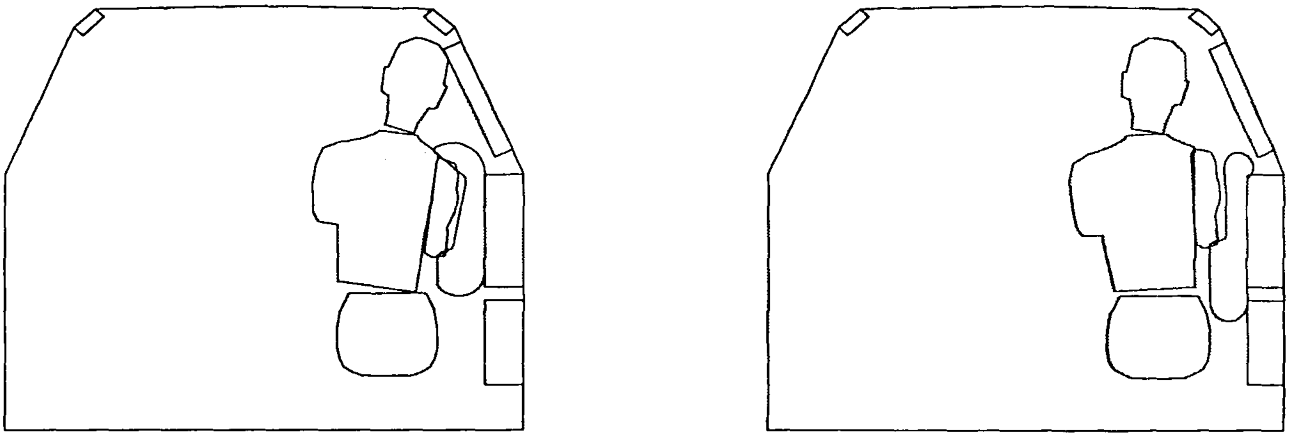

Time = 50 msec

Time = 80 msec

Figure 3. Occupant Trajectory, 5th Percentile Adult Female with Airbag Optimized for 50th Percentile Adult Male

Table 1. Summary of Results

Measure	03 Year Old[1]	05th Percentile[1]	3 Year Old Child[2]
HIC	50.4	37.5	4.9
PCG-3ms (g's)	22.88	19.06	17.34
TTIup (g's)	91.53	64.44	86.54
TTImid (g's)	97.14	65.61	70.26
TTIlow (g's)	105.6	67.61	92.22
V*Cup (M/s)	.1866	.076	.1106
V*Cmid (M/s)	.3902	.115	.1420
V*Clow (M/s)	.7361	.3041	.1633
HipF (lbf)	11.26	0	0
HipA (g's)	+9.5/-9.5	+2.7/-4.0	+3.0/-4.2
AbdF(lbf)	-133.3	-6.5	-3.87
V*Cabd (M/s)	2.481	.5662	.1056
DispRibu (in)	-.4377	-.3434	-.3900
DispRibm (in)	-.7211	-.5155	-.3900
DispRibl (in)	-1.1445	-.8424	-.4186
DispAbd (in)	-1.750	-1.00	-.200
HipJntA (in/s^2)	+22/-16	+2.8/-3.0	+7.5/-10.
HipJntV (in/s)	+10/-12	+5.4/-7.1	+8.9/-9.2
HipJntD (in)	+.05/-.18	-0.2	+.09/-.12
BagP (lb/in^2)	6.5	7.0	2.0
HipRestrY (lbf)	+118/-110	+135/-119	+12/-30
HipRestrZ (lbf)	+180	+210	+39/-7
WSPen (in)	0	0	0

[1] Airbag Optimized for 50th percentile Occupant.

[2] Airbag Optimized for 3 Year Old Child Occupant.

The next line shows the bag pressure, (BagP). This incidentally is not the initial pressure, but is the sustained pressure when the airbag interacts with the occupant.

The next two lines show the hip restraint forces in Y and Z directions. These account for the restraint system and the seat contour and the center console, etc.

The last line shows the side window penetration (WSPen). Obviously, without any side crush the values in all three columns are 0.

5th Percentile Female (Column three in Table 1)

The injury measures for the 5th percentile female are relatively low across all lines and body segments. This statement is true for head, chest 'g', ribs, abdomen, hip joint and hip restraint.

It needs to be reiterated here that these low results are with the airbag left optimized for the 50th percentile adult male.

The presented results show that the SIFEM computer model can be exercised for selected configurations and the results obtained can provide designers meaningful data and information.

The benefits of optimization of the airbag for the 3-year provide only limited benefits when unnecessary or inadvertent airbag deployment takes place.

CONCLUSIONS

1. The 3-year old child, in a booster seat, seat belt restrained, and leaning to the side, does not fair well when a side airbag inadvertently deploys.
2. With a side airbag that is optimized for the 50th percentile adult male, the TTI at all three levels, abdominal interaction and the middle and the lower rib lateral displacement are the areas of concern.
3. The situation is somewhat improved when the side airbag is optimized for the 3-year old. The improvement shows in the abdominal and the rib lateral displacement injury measures. The TTI, however stays relatively high.
4. The 5th percentile female is not that adversely affected, as is the 3 year old, by the inadvertent side airbag deployment.
5. The 3 year old's thoracic interaction with the side airbag needs further evaluation to confirm the results seen in this limited scope study.
6. Versatility and value of the computer model, SIFEM is seen in the types of evaluations undertaken by this study.
7. The analytical effort towards more rigorous validation of the model must be continued.
8. Also to be undertaken will be continued effort in the simulation with more accurate design and performance parameters and the more recent test data. The future efforts will include other scenarios of interest.
9. Once again, it needs to be emphasized, that the results presented here are valid within the constraints of the database used in this model.

REFERENCES

1. Khadilkar A. V. And L. Pauls, "Application of a Model as an Engineering Tool for Evaluating Side Impact Design Requirements for Children and Small Adults". Paper No. 98-S8-W-31, Sixteenth International Technical Conference on Enhanced Safety of Vehicles, June 1998.

2. N. A. El-Habash, Vehicle Research And Test Center, "Evaluation of the BIOSID Dummy, MDB-To-Car Side Impact Test of a 26 degree Crabbed MDB Into a 1988 Hyundai Excel 4-door Sedan at 33.7 mph", Final Report, Contract No. DTNH22-88-C-07292, June 1990.

3. Insurance Institute for Highway Safety, "BMW's New HPS Protects Heads from Serious Injury in SIDE Impact Crashes", Status Report, December 27,1997.

4. NHTSA Internet, "New Occupant Protection Technology in 1998 Vehicles", Undated.

5. Parents for Safer Air Bags, "The Air Bag Crisis Causes and Solutions", October 1997.

6. Hansun Chan, "Frontal Air Bag Deployment in Side Crashes", SAE Paper No. 980910, February 1998.

7. Carley Ward, "Airbag Injuries and Simulation of Occupant Airbag Interaction Using MADYMO Computer Simulation Software", presented to the American Bar Association 7th Annual Meeting, Phoenix, Arizona. March 1997.

8. G. Schroeder, J. Eidam, "Typical Injuries Caused by Air-bag in Out-of-Position Situations - An Experimental Study", 1997 IRCOBI, Hannover (Germany), September 1997.

9. F.A. Berg, B. Schmitt, J., Epple, "Dummy-Loadin Caused by an Airbag in Simulated Out-of-Position Situations", 1997 IRCOBI, Hannover (Germany), September 1997.

10. Khadilkar A. V. et al, "Dynamic Response of Vehicles and Occupants During Full-Scale Sideswipe Tests", To Be Presented at ASME Winter Meeting in Anaheim, California in November 1998.

APPLICATION OF A COMPUTER MODEL AS AN ENGINEERING TOOL FOR EVALUATING SIDE IMPACT DESIGN REQUIREMENTS FOR CHILDREN AND SMALL ADULTS

Anil V. Khadilkar
Biodynamics Engineering Inc.
Lonney S. Pauls
Springwater Micro Data Systems
United States

Paper Number 98-S8-W-31

ABSTRACT

This paper describes a computer modeling system and its application in evaluating several vehicle designs for side impact protection of children and small adults.

INTRODUCTION

An analytical study was undertaken to investigate the problem of protecting small vehicle occupants in side impacts. Because the vast majority of the side impact research to date has focused on the 50th percentile adult male, design insights for small and very large occupant sizes are sorely lacking. The main objective for the current study was to evaluate the side impact design requirements for the smaller occupant sizes. A secondary objective was to evaluate the performance of candidate designs for the very large occupant population, represented by the 95th percentile adult male.

A computer modeling system, SIFEM, was used to simulate the impact event and to evaluate the vehicle design concepts of interest. The design concepts included: interior padding, a hip restraint device and an airbag system. Data from selected side impact tests were first used to validate the model then extrapolations were made to the crash condition, occupant sizes, and vehicle designs of interest.

THE DESIGN PROBLEM

Padding systems play an important role in protecting vehicle occupants during a collision. This is especially true in side impacts where the occupant is very likely to make contact with the interior surfaces of the vehicle. Even when fully restrained by a conventional seat belt, the upper torso of the occupant is free to rotate about the hip joint and make direct contact with the intruding surfaces. Although energy absorbing materials mounted to these surfaces provide a measure of protection for the occupant, they are not a panacea. Padding systems in general do not offer equal protection for all occupant sizes. What is adequate for a large occupant may be inadequate and even harmful to the very small occupant. The converse is also true. In addition, there are areas in the vehicle interior where the use of padding is not even a practical consideration (e.g., the window areas).

Trajectory control is an important factor in the design of occupant restraints for frontal impacts. Out-of-phase loading of body components during impact can introduce secondary effects such as whiplash, excessive body movement and harsh contacts with the vehicle interior. In side impacts, body phasing and trajectory control are also important design considerations, as will be shown later in this paper.

In side impacts, the reactive surfaces generally exclude the side window areas. Current side window glazing materials do not provide a reliable surface since they are often destroyed during impact. Also, the window can be left in the open position by the occupant. Because of this, the area below the window opening usually becomes the primary supporting surface for padding and airbag systems. For large occupants, this forces the reaction loads below the torso c.g., causing the occupant's upper torso and head to rotate into (and sometimes through) the window opening during impact, as illustrated in Figure 1. This allows the occupant's head to make direct contact with the impacting vehicle or with the stiff lower edge of the window. Several new inflatable concepts such as the airbag curtain and the ITS (Inflator Tubular Structure) are currently being considered by several automobile manufacturers as possible solutions to this problem. These concepts are beyond the scope of this study.

For small children, the reaction forces are generally closer to the torso c.g., however, the occupant's head and torso can still rotate onto the lower edge of the window if the torso and hip reactions are not properly phased (see Figure 2).

Airbag systems have become the norm in modern safety systems. For frontal impacts, history has proven that airbag systems are an effective and reliable means for protecting occupants in real life accidents. History has also proven, however, that airbag systems do not automatically provide equal protection for all occupant sizes. Deaths of small children have occurred even in relatively mild impacts. These fatalities have been attributed directly to the performance of the airbag. The lesson here is that an airbag system designed for one occupant size will not automatically work satisfactorily for another. History clearly shows us that what is needed in the design process is a true systems approach. An approach that will optimize the performance of the airbag over a range of occupant sizes, rather than on a specific

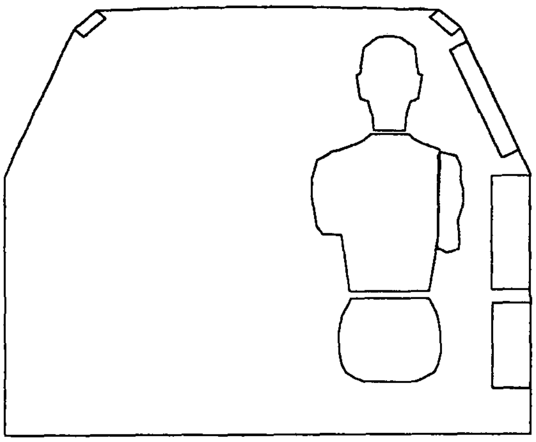

Time = 0 msec

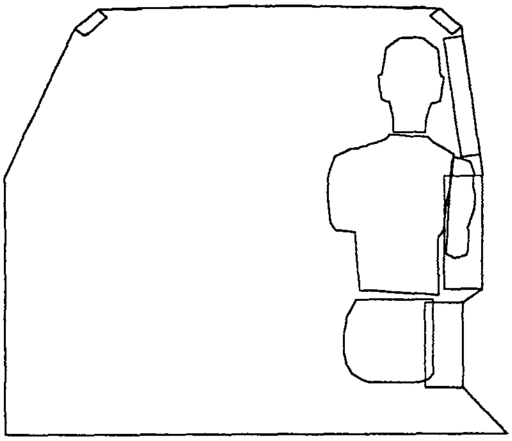

Time = 40 msec

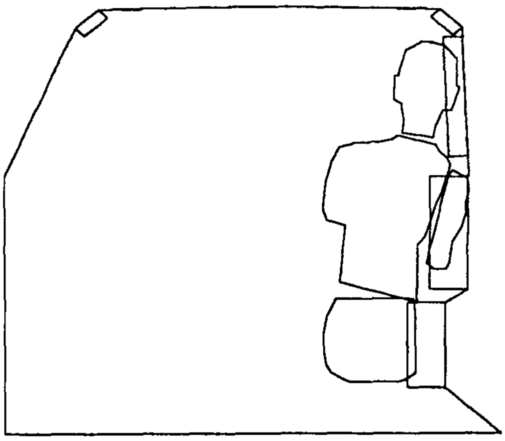

Time = 50 msec

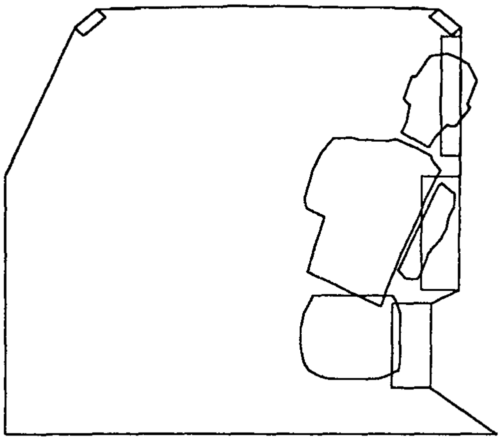

Time = 60 msec

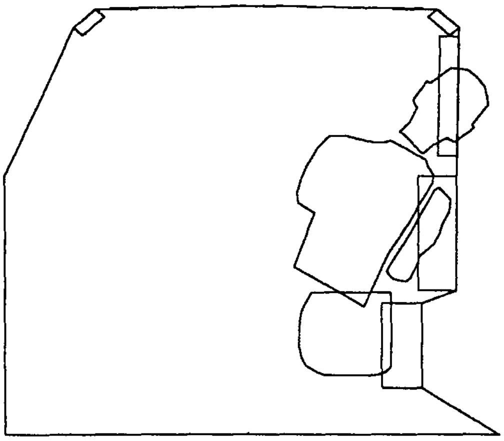

Time = 70 msec

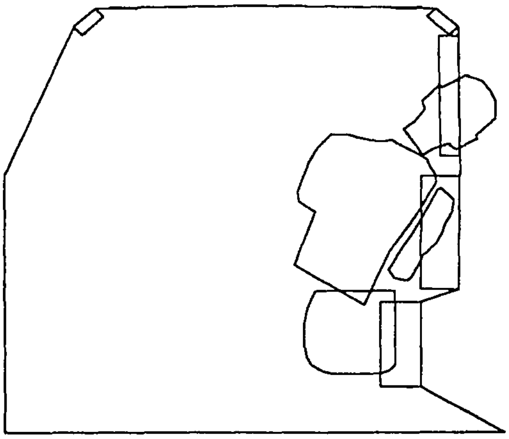

Time = 80 msec

Figure 1. Occupant trajectory, 50th percentile adult male.

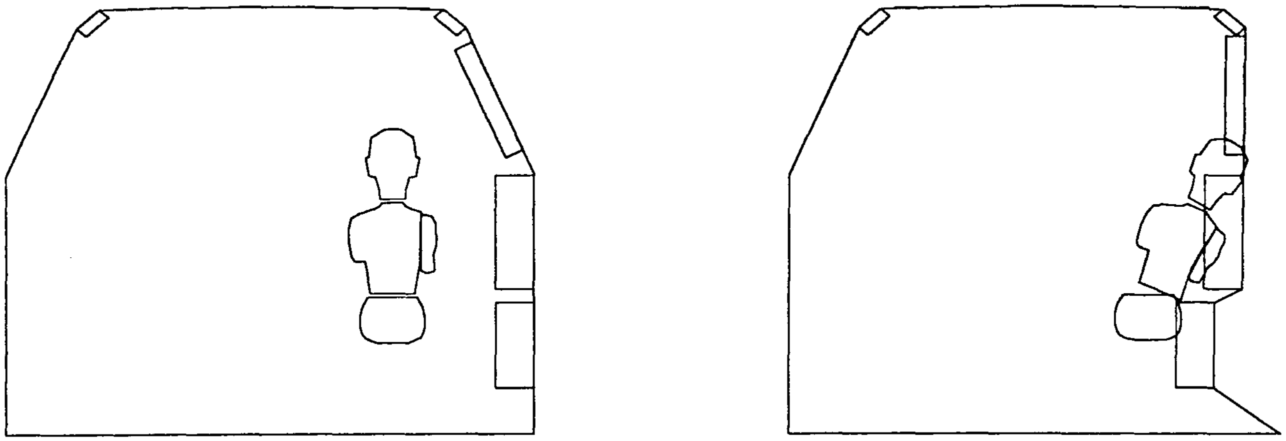

Time = 0 msec

Time = 60 msec

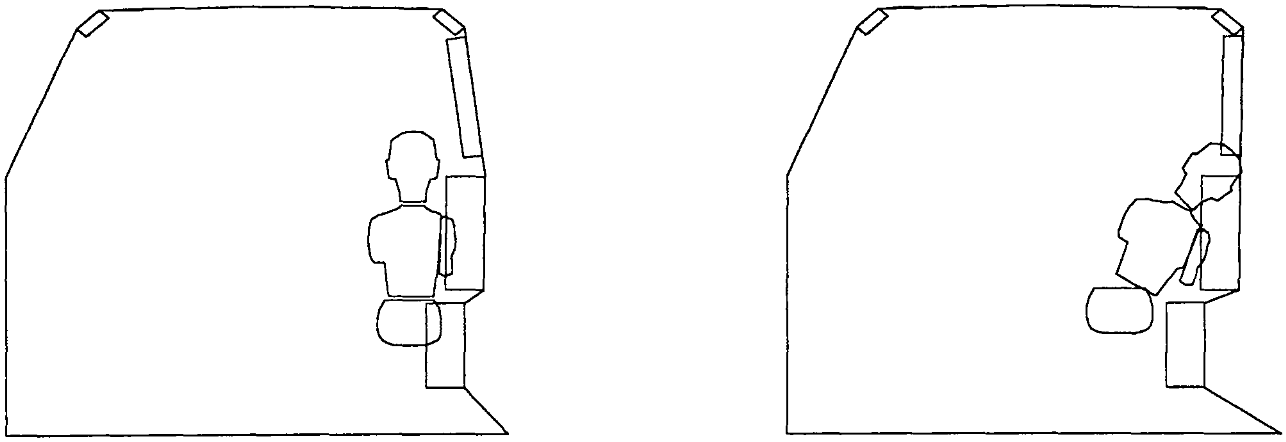

Time = 40 msec

Time = 70 msec

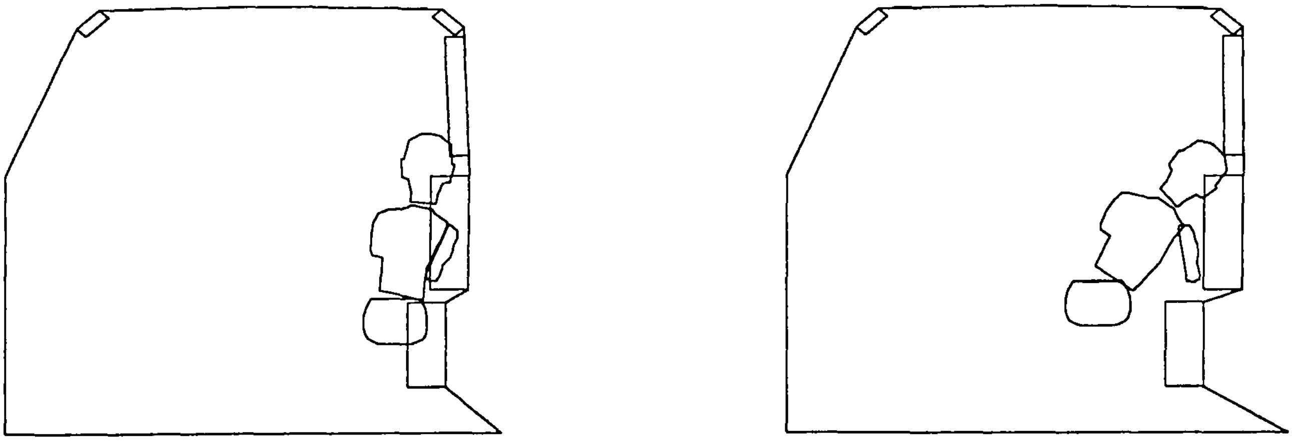

Time = 50 msec

Time = 80 msec

Figure 2. Occupant trajectory, 3 year old child.

size. This observation, no doubt, carries over into the side impact realm as well.

In the current study SIFEM was used as our main systems design tool. SIFEM models real life side impact accidents and simulates the performance of several occupant restraint concepts. These concepts include:

1. Energy Absorbing Padding (upper door, lower door and B-pillar)
2. Window Glazing (as an energy absorbing surface)
3. Hip Restraint Device (horizontal and vertical control)
3. Airbag Systems
4. Pressurized Padding Systems.

ANALYTICAL APPROACH

In this study we limited our scope to one crash condition and three restraint design concepts. The design concepts included door padding, a hip restraint device and a combination head/torso airbag system. This section describes the analytical approach.

Crash Scenario

The side impact event for this study consists of an intersection collision with the striking vehicle traveling at 30 mph and the struck vehicle traveling at 15 mph. The orientation angle of the striking vehicle is 90 degrees with respect to the longitudinal axis of the struck vehicle. This crash scenario was represented by an actual full scale crash test conducted by the Vehicle Research and Test Center of East Liberty Ohio (Reference 1). This test consisted of 1988 Hyundai Excel 4-door sedan impacted on its side by a NHTSA moving deformable barrier.

The referenced test provided the acceleration histories for the passenger compartment and the driver side door. This information was used in SIFEM to represent the baseline vehicle design. Figure 3 shows the acceleration-time history and Figure 4 the velocity-time history for the door assembly. It should be noted that this data represents a production vehicle, not a vehicle that has been structurally optimized for side impact.

Padding System

The padding system consists of energy absorbing materials mounted onto the upper and lower surfaces of the door (below the window opening). The padding material was limited to a single class, one having relatively "flat" pressure-displacement characteristics and little strain-rate effects. Several materials fitting this class are metal and paper honeycombs and some rigid foams. Because of their nearly ideal energy absorbing characteristics, these materials have found wide use in past safety research (e.g., References 2 and 3) . In the current study we assumed two crush strength values for the candidate material, 140 kPa (20 psi) and 280 kPa (40 psi). Reference 3 indicates that paper honeycomb materials having these crush strength levels were used in a sled test evaluation of the SID-IIs dummy, presumably to simulate an actual padded interior of a vehicle. Reference 2 documents the results of dynamic testing with child and adult body forms on paper honeycomb material (KNC1-80(0) EDF, Kraft paper). This material had a static and dynamic crush strength of approximately 30 psi. The test results indicate a relatively flat pressure-displacement curve for approximately 75 percent of the material thickness, when the material begins to "bottom-out". This characteristic was modeled in SIFEM.

Hip Restraint Device

The hip restraint model in SIFEM consists of three non-linear springs acting against the hip mass. Two springs act in the horizontal direction (side-side and fore-aft) and the other in the vertical direction. Each spring can be assigned arbitrary force-displacement characteristics (both tension and compression), with hysteresis effects. With this arrangement, SIFEM can simulate a lap belted occupant and an occupant interacting with various interior surfaces such as the seat-back, seat cushion and a center console made from an energy absorbing material.

Airbag System

The airbag system in this study represents a current state-of-the-art design. The geometry and size of the airbag was based on information from Reference 3. The cited reference indicates that an airbag system "chosen to be representative of an advanced technology" was being used to evaluate the performance of the new SID-IIs, 5th percentile adult female dummy. The airbag is a combination chest-head side impact system having a static volume of approximately 20-30 liters. Photographs indicate that the static depth of the bag is approximately 6 inches. Figure 5 shows the static geometry of this airbag, as modeled in SIFEM. This geometry was selected as the baseline design. Reference 3 does not provide detailed information concerning the performance of the airbag inflator so we made the assumption that the flow rate history of the inflator is trapezoidal (see Figure 6) with the time period, corresponding to the "flat" portion of the curve, a variable to be evaluated. We also assumed that the working pressure for the bag was limited to a value in the neighborhood of 15 psig.

A series of computer runs were conducted to derive the inflator flow and bag venting characteristics for this

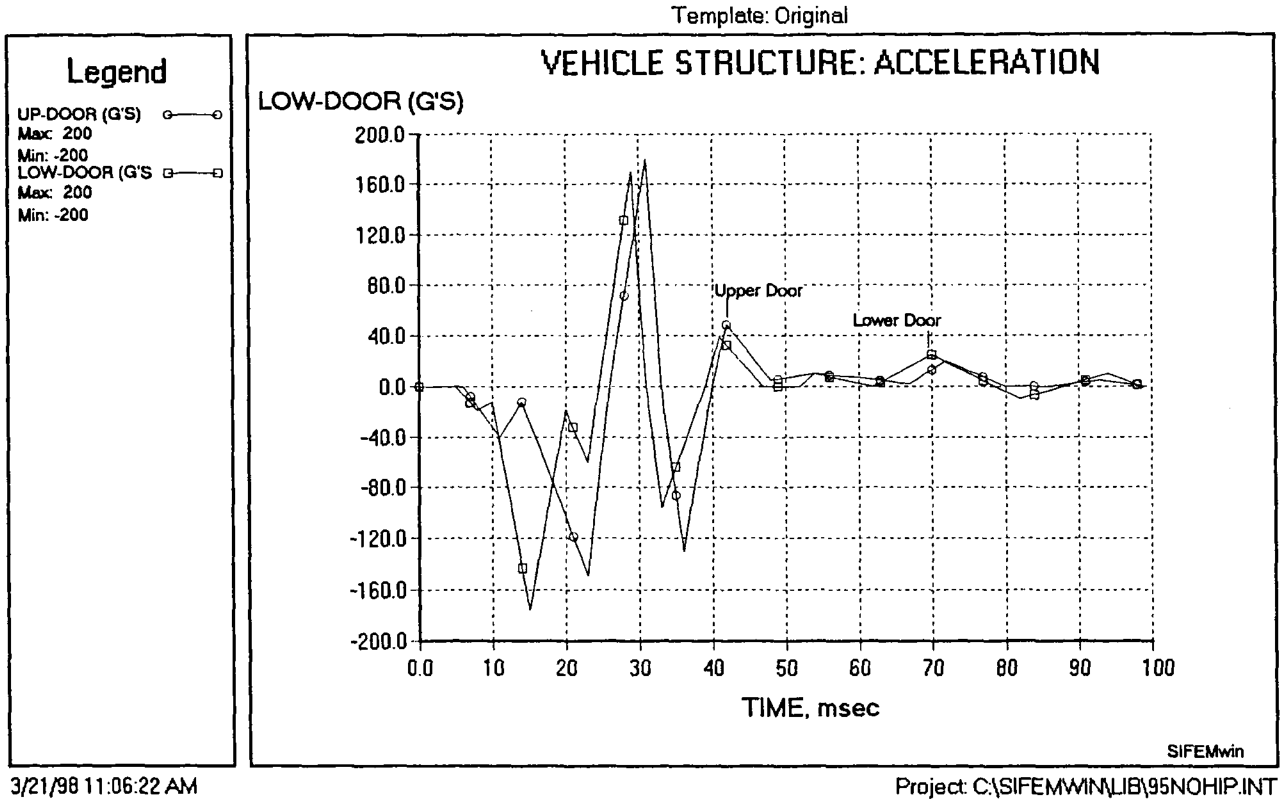

Figure 3. Door acceleration, baseline vehicle.

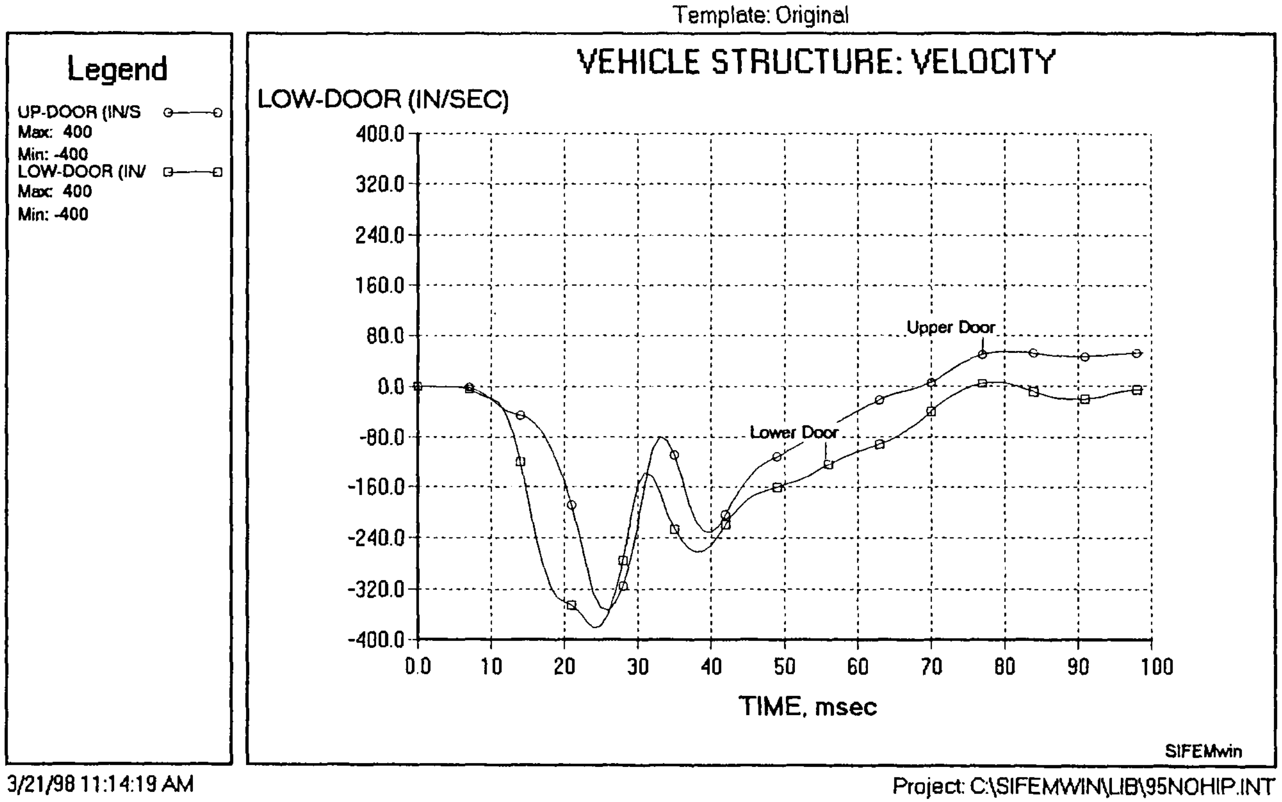

Figure 4. Door velocity, baseline vehicle.

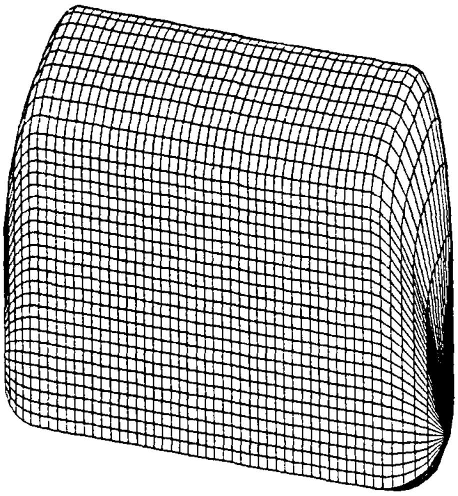

Figure 5. Airbag geometry modeled in SIFEM.

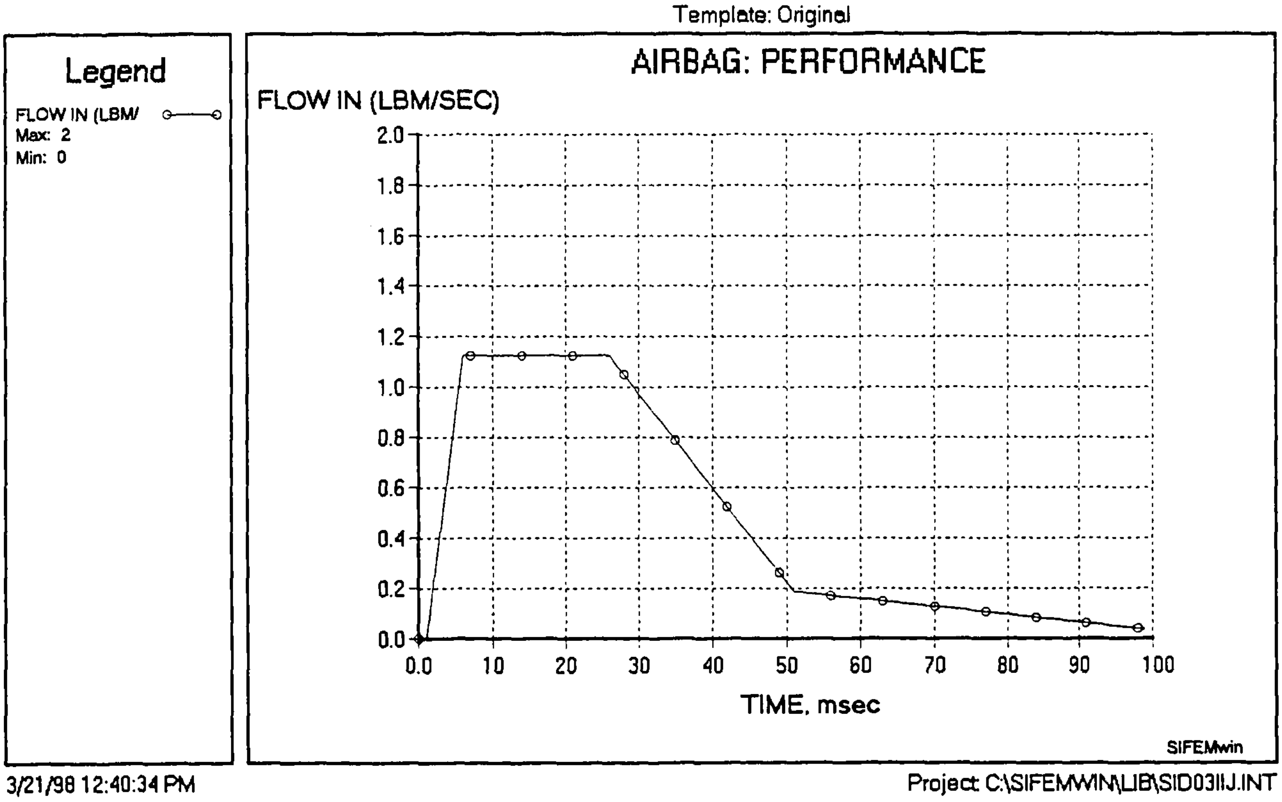

Figure 6. Inflator flow characteristics modeled in SIFEM.

study. Combinations of inflator flow and bag venting were investigated to evaluate the effects of high-flow/high-venting and low-flow/low-venting on system performance. These characteristics were also varied to derive the near optimum combinations for the occupant sizes of interest.

Occupant Simulation

To make this study applicable for the full size range of occupants, it was necessary to make some basic assumptions. Currently there are no standard side impact dummies representing the small 3 year old child and the large 95th percentile adult male. For these occupant sizes we were forced to create our own "theoretical" dummies.

In prior validation work, a SIFEM database was developed for the SID dummy (50th percentile adult male) and the SID-IIs dummy (05th percentile adult female). This database has been checked against available design and test data (References 3-8) and has been found to give good and reasonable simulation results. A simplified scaling rule was used to expand this database to include the 95th percentile and the 3 year old occupant sizes. The scaling rule is based on the assumption that the stiffness and damping characteristics of a given body part are proportional to the component mass. Further, we assumed that the overall geometry and mass distribution for our fictitious dummies are identical to the 95th percentile and 3 year old frontal impact dummy counterpart. The rib mass and the spring and damping characteristics for the various body parts were scaled from the SIFEM database, based upon the assumed mass distribution. The 95th percentile dummy was scaled from the SID data set and the 3 year old child dummy was scaled from the SID-IIs data set. Thus, our 95th percentile adult male dummy is armless and contains hydraulic dampers to represent the force-displacement characteristics of the rib-cage (like the SID). The 3 year old child dummy has a pivoting arm and a spring steel rib cage (no hydraulic dampers) like the SID-IIs.

A Cautionary Note

Because of the assumptions made in this study, caution must be taken when interpreting and using the results. Future side impact dummies may be constructed differently and may not have the same characteristics assumed herein. The main objective for this study was to gain additional insight and knowledge concerning side impacts, not to derive specifications or hard and fast rules for design. This work must be updated as new and improved side impact dummies are made available.

MODEL DESCRIPTION

SIFEM is a Windows$^{(R)}$ based modeling system designed for use on micro computers. SIFEM uses the lumped mass and finite element methods for simulating the occupant and vehicle interactions during a side impact event. The model simulates the performance of padding, airbag and a hip restraint systems. Figure 7 illustrates the side-side portion of the model. A similar model is used to simulate the fore-aft movement of the occupant in oblique and crabbed steering side impacts where a significant longitudinal acceleration component is imposed on the vehicle

Padding materials with arbitrary pressure v.s. displacement and hysteresis characteristics are modeled. by SIFEM. Padded surfaces include the upper and lower areas of the door, the B-pillar and a hip restraining surface (i.e., a center console or a lap belt). The side window is modeled as a nonlinear, energy absorbing surface, having arbitrary force v.s. displacement characteristics. The interactions of the occupant with these surfaces are modeled with sufficient detail to account for: occupant size, sitting location and posture, geometry of the major body parts (head, upper and lower torso, hip and upper arm) and the instantaneous orientation and geometry of each energy absorbing surface within the vehicle interior. The model uses the Adams-Moulton predictor-corrector method to solve the equations of motion.

Figure 8 illustrates the SIFEM airbag model. The airbag cushion is modeled using surface elements. The statically deployed shape of the bag is designed using a built-in CAD routine. The shape of the bag can be arbitrary (along with the inflator flow characteristics). The shape of the bag is defined with over 3500 surface elements. Simplified stretch and deployment algorithms are used to model the interaction of the airbag surface with the occupant and other interior surfaces of the vehicle. Bagslap, catapult (membrane) and pressure contact phases are all modeled in the program.

SIFEM allows the user to model the full size range of occupants. The occupant model simulates the stiffness of the following body parts:

- Cranial (head impacts)
- Neck (side-side and fore-aft directions)
- Shoulder/Arm
- Arm Flesh
- Rib (three rib masses, includes arm interaction)
- Abdomen (includes arm interaction)
- Pelvic Girdle
- Hip Joint (side-side and fore-aft directions)

Modeling options include "no-arm" and "with-arm" configurations. The "no-arm" configuration removes the arm mass from the simulation. This allows the rib masses and the abdominal spring to directly contact the vehicle and airbag surfaces. The "with-arm" option includes the

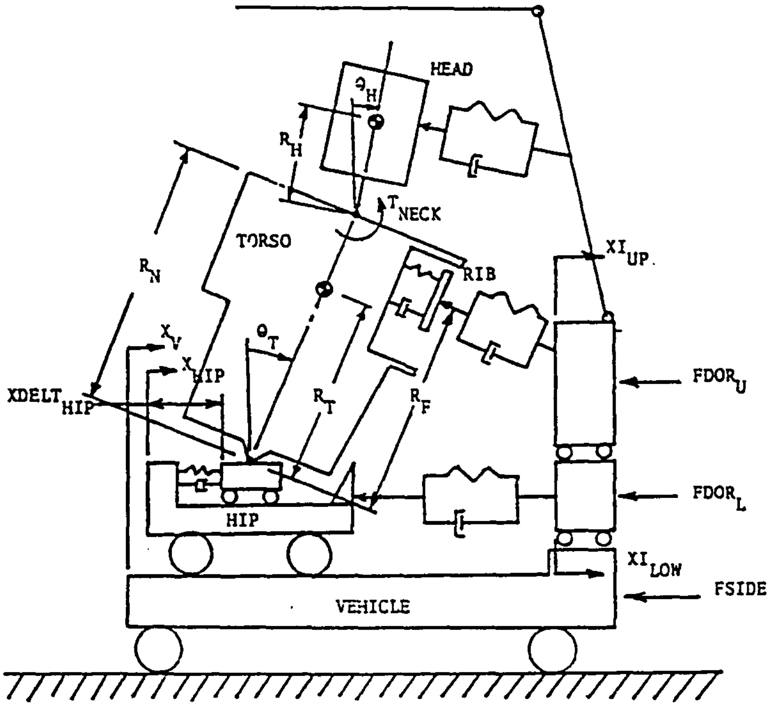
HEAD
Θ_H
R_H
T_{NECK}
TORSO
R_N
RIB
XI_{UP}
X_V
X_{HIP}
Θ_T
$XDELT_{HIP}$
R_T
R_F
$FDOR_U$
$FDOR_L$
HIP
XI_{LOW}
FSIDE
VEHICLE

Figure 7. SIFEM model (side-side portion).

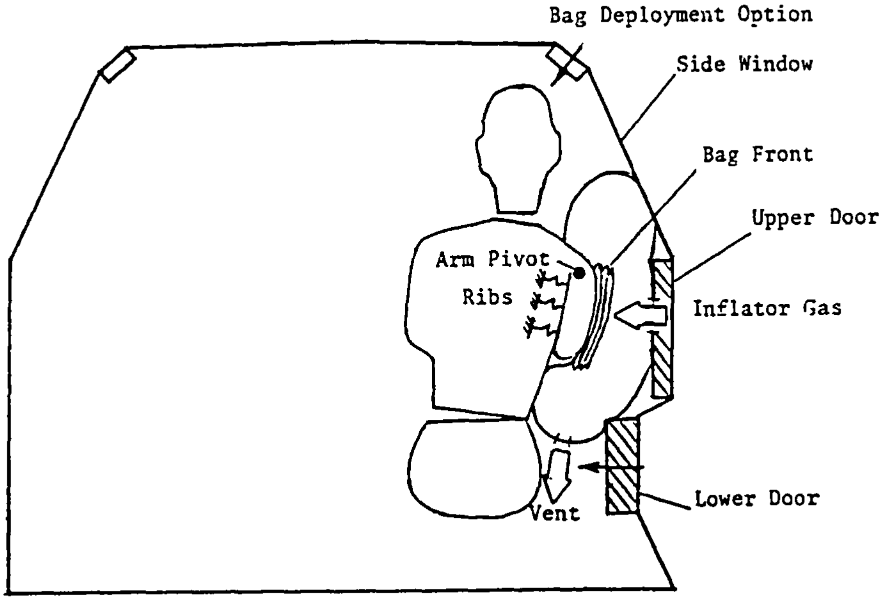
Bag Deployment Option
Side Window
Bag Front
Upper Door
Arm Pivot
Ribs
Inflator Gas
Vent
Lower Door

Figure 8. SIFEM airbag model.

arm mass in the simulation to account for its interactions with the vehicle interior and the upper torso mass. The occupant model calculates the following injury measures:

- Head Injury Criteria HIC
- Peak Chest Acceleration (3 msec clip)
- Peak Femur Load PFL
- Peak Pelvic Load PPL
- Hip Acceleration
- Viscous Criteria V*C (each rib plus abdomen)
- Thoracic Trauma Index TTI (each rib)
- Hip Joint Load, Displacement, Velocity and Acceleration (fore-aft and side-side)
- Neck Moment and Head Rotation (fore-aft and side-side)

MODEL VALIDATION

Prior to this study a validation effort was conducted using SIFEM. Although this effort was not exhaustive, good success was achieved in modeling various full scale crash tests and sled tests involving the SID and SID-IIs dummies. Some of these tests are reported in References 3 through 8. It is premature at this point to claim full model validation for SIFEM, however, the results to date do indicate that SIFEM is capable of providing reasonable simulations for both the SID and SID-IIs dummies. This validation work will continue as new and more detailed test data are made available.

SIFEM SIMULATIONS

Three occupant restraint designs were evaluated in this study. The designs were: 1) door padding, 2) a hip restraint device and 3) an airbag system. For the simulations herein, it was assumed that the occupant is normally seated in the seating position adjacent to the door. It was also assumed that the child occupant was seated on a booster seat in a normal, upright position. The window was assumed to be in the open position for all computer runs.

Door Padding (baseline design)

The baseline design for this study was energy absorbing padding material mounted to the interior surface of the door. Two cases were evaluated. Case #1 consisted of 140 kPa (20 psi) material for the torso padding and 280 kPa (40 psi) material for the hip padding. Case #2 was reversed with 280 kPa (40 psi) material for the torso pad and 140 kPa (20 psi) material for the hip pad.

Case #1 - The simulation results for Case #1 are summarized in Figures 1 and 2 and Table 1. As indicated in Figures 1 and 2, this design allows the occupant to rotate into the door and side window area during impact. Figure 1 shows the trajectory for the 50th percentile occupant and Figure 2 shows the trajectory for the child. For the larger occupant sizes, the head actually rotates through the plane of the window (see Figure 1) and eventually strikes the lower window sill. The maximum window penetration occurs for the 50th percentile occupant size (see Table 1, WSPen=2.8 inches). For the small child occupant, the head rotates directly onto the window sill (see Figure 2).

The trajectories displayed in Figures 1 and 2 are undesirable since they expose the occupant to possible head injuries. The clockwise rotation of the occupant is a result of the reaction loads acting too low on the occupant. This action is further enhanced by the current padding design with its relatively "soft" torso pad and "hard" hip pad.

Additional details of the simulation can be obtained by examining the data in Table 1. To help us in this examination, we will divide the data into the following groups:

1. Head
2. Rib/Spinal-Mass
3. Abdomen
4. Hip/Hip Joint

For the head data group two measures apply, HIC and window penetration WSPen. The data in Table 1 shows that for this data group the trend of lower HIC with increasing occupant size is broken by the 50th percentile occupant. Closer examination shows that this occupant impacts the window sill more solidly than either the 5th percentile or the 95th percentile, causing the increase in HIC. The 50th percentile occupant size also has more window penetration, as indicated by the WSPen measure.

For the Rib/Spinal-Mass group the key measures are: Thoracic Trauma Index TTI, Viscous Criteria V*C, rib displacement DispRib and peak chest acceleration (3msec clip) PCG. The three rib masses in the model are identified in the table as upper, middle and lower. The data in Table 1 shows TTI decreasing with increasing occupant size, except for the 5th percentile female occupant size. This occupant size seems to have unusually low values compared to the two larger occupants. More detailed examination of the data indicates that the larger occupants are "bottoming-out" the torso padding and are "working" the padding material at significantly higher contact stresses.

For the V*C measures, the trend is not clear. The small child appears to respond most favorably for this data group. There are several explanations for this. First, the larger occupants are "bottoming out" the padding and the loading rates for their rib springs are higher due to the increase in the stiffness of the padding. Second, the child occupant may be benefiting from favorable effects

Table 1.
Simulation Results for Baseline Design, Case #1,
Torso Pad = 140 kPa (20 psi), Hip Pad = 280 kPa (40 psi)

Measure	03 Year Old	05th Percentile	50th Percentile	95th percentile
HIC	333.5	182.5	248.3	70.2
PCG-3ms (g's)	66.9	60.44	61.38	63.6
TTIup (g's)	130.0	73.9	90.74	85.7
TTImid (g's)	139.0	67.8	99.3	95.4
TTIlow (g's)	136.0	85.7	111.0	101.9
V*Cup (M/s)	.2537	.5447	.4648	.4019
V*Cmid (M/s)	.5148	1.0662	.8682	.9044
V*Clow (M/s)	.8608	1.4353	1.2731	1.3643
HipF (lbf)	1035	2478	3361	3851
HipA (g's)	-85	-68	-70	-68
AbdF(lbf)	-25.2	-16.7	-119.1	-166.5
V*Cabd (M/s)	1.0254	2.0614	.4518	.3965
DispRibu (in)	-.5330	-1.110	-1.7610	-1.7434
DispRibm (in)	-.8100	-1.5190	-1.9296	-2.0712
DispRibl (in)	-1.105	-1.9580	-2.0849	-2.2867
DispAbd (in)	-1.200	-2.500	-.6600	-.6200
HipJntA (in/s^2)	+56/-64	+24/-28	+33/-36	+24/-34
HipJntV (in/s)	+80/-36	+48/-9	+79/-16	+40/-10
HipJntD (in)	+2.4	+.93	+1.0	+.40
BagP (lb/in^2)	-----	-----	-----	-----
HipRestrY (lbf)	0	0	0	0
HipRestrZ (lbf)	0	0	0	0
WSPen (in)	0	-.376	-1.397	.-6997

resulting from the dynamic response of the arm mass. The larger male occupants (represented by a SID type dummy) do not have articulating arms. For these occupants the mass of the arm is added to the rib mass and the ribs are allowed to make direct contact with the padded surface during impact. Also, the rib springs for these larger occupants are represented by hydraulic dampers and the resulting spring-mass system is highly damped. For the smaller occupants (represented by the SID-IIs dummy type) the arm mass translates and rotates at its connection point with the shoulder spring and interacts with both the padded surface of the vehicle and the rib and abdomen springs comprising the occupant's torso. For these occupants the rib springs represent a steel-spring structure (i.e., the SID-IIs design) and are not as highly damped as the ribs in the SID design. Although both the child and the 05th percentile occupants have similar rib and arm designs, the small child appears to perform better in this category. This may be a result of the child's lighter and more responsive spinal mass, which helps to reduce the rib displacements.

The abdomen data group is represented by the abdomen force AbdF, abdomen viscous criteria V*Cabd and the abdomen displacement DispAbd (see Table 1). The data in Table 1 shows that the smaller occupant sizes are clearly at a disadvantage here. The abdomen V*C and displacement values are significantly higher than those for the larger occupants. This is the result of the arm mass interacting with the abdomen spring. This interaction is modeled In SIFEM by proportioning the area associated with the arm/abdomen contact to the total area of the abdomen spring. This explains the lower abdomen forces and large deformations for these smaller occupants. For the larger occupants (no arm mass) the entire abdomen spring is allowed to make contact with the padding.

The results for this case indicate a potential for serious abdominal injuries from the oscillating arm mass. Relatively large penetrations of the abdomen can be induced due to the small contact areas involved. The high loading rate imposed on the abdominal spring, by the arm mass, drives the V*Cabd parameter to its high value. It is not known how accurately these results reflect real life. Further research and study is needed in this area.

The hip and hip-joint data group is represented by the hip force HipF, hip acceleration HipA and hip joint parameters. The hip-joint parameters are associated with the acceleration HipJntA, velocity HipJntV and displacement HipJntD of the hip joint spring. For the current padding design the small child occupant does not perform as well in this data group as the others.

Simulation Results, Case #2 - For this design the padding materials were reversed so that the 280 kPa (40 psi) material was positioned for the torso and the 140 kPa (20 psi) material positioned for the hip. The results of the simulations are summarized in Table 2.

A general observation for this case is that the trajectories for all occupant sizes were significantly improved. The occupant remains in a more upright posture during impact, compared to Case #1. This improved trajectory is reflected in the lower HIC and window penetration WSPen values (see Table 2). The improved posture helps to reduce the risk of head injuries by reducing the window penetration and the hard contact with the window sill (larger occupants). Note, the HIC value for the child occupant remains relatively high at 325. The reason for this is that the initial height of the child's head is nearly the same height as the window sill (see Figure 2) and solid contact with it is unavoidable.

We can gain more insight to the effects of the design change by comparing the data in Table 2 with the data in Table 1. To help us with this comparison, a three point rating method is introduced in Table 2. The rating values are: B=Better, S=Same or W=Worse. With this method we can quickly evaluate the effects of the design change and identify the effected parameters. For our comparison we will again divide the data into groups.

For the head data group (HIC and WSPen), all occupant sizes appear to benefit from the design change (although the benefit for the child occupant is not that significant).

For the rib/spinal mass data group (TTI, V*C, DispRib and PCG), the TTI values seem to improve across the board while the V*C, DispRib and PCG parameters have mixed results. In general, the larger occupants seem to perform better in this data group.

The abdomen data group (AbdF, V*Cabd and DispAbd), received W ratings for the two small occupants and a mixed rating for the larger occupants. The only gain was the V*Cabd parameter for the two larger occupant sizes. The stiffer torso padding appears to have increased the risk for the abdomen.

The hip and hip-joint data group(HipF, HipA, HipJntA, HipJntV and HipJntD) received a W rating for the child and a mixed rating for the other sizes. All of the occupant sizes (except for the child) received a B rating for the hip joint parameters. The larger occupants (except for the 95th percentile) received B ratings for the HipF and HipA parameters. Note that the 95th percentile occupant size begins to "bottom-out" the hip padding.

An overall view of the data in Table 2 indicates that this design change provides significant benefits for the larger occupants but makes matters worse for the small child (except for some minor improvements in the HIC, TTI, and HipJntD parameters).

Hip Restraint Design

Table 2.
Simulation Results for Baseline Design, Case #2,
Torso Pad = 280 kPa (40 psi), Hip Pad = 140 kPa (20 psi)

Measure	03 Year Old		05th Percentile		50th Percentile		95th percentile	
HIC	325.1	(B)	75.2	(B)	47.5	(B)	55.6	(B)
PCG-3ms (g's)	73.28	(W)	39.89	(B)	45.41	(B)	45.74	(B)
TTIup (g's)	128.3	(B)	66.98	(B)	67.14	(B)	73.16	(B)
TTImid (g's)	127.3	(B)	65.14	(B)	81.22	(B)	75.78	(B)
TTIlow (g's)	146.8	(W)	77.06	(B)	81.69	(B)	75.68	(B)
V*Cup (M/s)	.4961	(W)	.4448	(B)	.5266	(W)	.4678	(W)
V*Cmid (M/s)	1.9042	(W)	1.0191	(B)	.8626	(B)	.7044	(B)
V*Clow (M/s)	3.0772	(W)	2.0465	(W)	.9164	(B)	.7877	(B)
HipF (lbf)	1196	(W)	1878	(B)	1978	(B)	4619	(W)
HipA (g's)	-130	(W)	-60	(B)	-53	(B)	-82	(W)
AbdF(lbf)	-57.7	(W)	-22.4	(W)	-143.6	(W)	-234.4	(W)
V*Cabd (M/s)	5.00	(W)	4.218	(W)	.3548	(B)	.3493	(B)
DispRibu (in)	-.8836	(W)	-1.0530	(B)	-1.8563	(W)	-1.8424	(W)
DispRibm (in)	-1.5970	(W)	-1.9068	(W)	-1.9651	(W)	-1.9779	(B)
DispRibl (in)	-1.9529	(W)	-2.7326	(W)	-1.9784	(B)	-2.1149	(B)
DispAbd (in)	-2.80	(W)	-3.30	(W)	-.730	(W)	-.690	(W)
HipJntA (in/s^2)	+100/-82	(W)	+20/-22	(B)	+8/-14	(B)	+21/-16	(B)
HipJntV (in/s)	+115/-30	(W)	+22/-18	(B)	+9.7/-5.5	(B)	+28/-18	(B)
HipJntD (in)	+1.790	(B)	+.430	(B)	+.200	(B)	+.200/-.200	(B)
BagP (lb/in^2)	-----		-----		-----		-----	
HipRestrY (lbf)	0		0		0		0	
HipRestrZ (lbf)	0		0		0		0	
WSPen (in)	0	(S)	0	(B)	-.4740	(B)	-.060	(B)

NOTE: Scores are for comparison with baseline padding design in Table 1
B=Better
S=Same
W=Worse

For the hip restraint simulations we assumed the padding configuration for Case #2 above (i.e., 280 kPa torso padding and 140 kPa hip padding).

Two hip restraint designs were evaluated. The first design is a linear device where the hip reaction force is proportional to the hip displacement (i.e., an elastic energy absorber). The second design is a nonlinear device where the hip reaction force is relatively constant (independent of hip displacement) and hysteresis effects during rebound are included (i.e., a near perfect energy absorber). Both designs were "tuned" to give a maximum hip displacement of approximately 3.5 inches for the worst case scenario (95th percentile occupant).

Linear Device - The simulation results for the linear hip restraint design are summarized in Table 3. We can compare these results with our baseline padding design in Table 2, to evaluate the design change. Lets make our comparison by data groups.

For the head data group (HIC and WSPEN), a W rating was received for all occupant sizes, except for the child (WSPEN rating of S). Details of the simulations show that the main cause for this poor rating is the multiple loading of the hip mass. The hip mass is first loaded by the door then by the hip restraint. This creates a slight whipping action of the head mass with corresponding increases in the head acceleration and HIC. The slight increase in window penetration also reflects this action.

For the Rib/Spinal Mass group (TTI, V*C, DispRib and PCG), the ratings are mixed. The TTI values improved for the 95th percentile occupant size but received W ratings for the other sizes (except for the child's TTIup value, which received a B rating).

The V*C parameters, in general, improved for all sizes, except for the upper rib which received a W rating (05th percentile female an exception). Apparently the addition of the hip restraint causes the occupant to lean slightly more toward the door during impact (note the slight increase in the WSPEN parameter). This tends to load up the upper rib (occupants without an articulating arm) and the shoulder spring (occupants with an articulating arm). For occupants with an articulating arm, the phasing of the shoulder displacement and the rotation of the arm will determine the rib loading. For the child case, it appears that the maximum displacement of the shoulder spring is more in phase with the maximum rotation of the arm, causing the higher loading of the upper rib spring. The 05th percentile occupant appears to be benefiting from a more "out of phase" response of the arm mass

The PCG parameter received a W rating for all sizes except the small child. The small child appears to be benefiting here from its more responsive torso mass, perhaps receiving a greater benefit from the 3 msec clip.

The abdomen data group (AbdF, V*Cabd and DispAbd) received B ratings for all occupant sizes. The hip restraint appears to provide a real benefit for this data group.

The hip and hip-joint data group (HipF, HipA, HipJntA, HipJntV and HipJntD) received a mixed rating. The hip force HipF parameter received W rating for all occupant sizes while the hip acceleration parameter HipA received a S or B rating across the board. The hip-joint parameters (HipJntA, HipJntV and HipJntD) received a W rating for all occupant sizes except for the child occupant, which received an S or B rating. It is expected that this group would show some performance reduction due to the added energy being transferred to the hip-joint by the hip restraint. The child occupant seems to benefit slightly here.

Nonlinear Device- The simulation results for the nonlinear hip restraint design are summarized in Table 4. Comparing this data with the data for the linear hip restraint design in Table 3, we see that the 95th percentile occupant size appears to have received little benefit from this design change. The other occupant sizes received some benefit, primarily in the reduction of the TTI parameters.

An Overview of the Padding and Hip Restraint Designs - In our evaluation of the padding and hip restraint designs we observed some modest gains for the larger occupant sizes (50th and 95th percentile). Most of the improvement came from switching the padding so that the stiffer (280kPa) padding material is positioned for the torso and the softer (140kPa) padding for the hip. This helped to prevent the large occupants from "bottoming out" the torso padding. It also helped to improve the trajectory for all occupant sizes.

Although we have seen some small areas of improvement for the smaller occupant sizes, these occupants are not adequately protected by any of the designs evaluated so far. The critical areas for the smaller occupants are the TTI and V*C parameters. The high TTI and V*C values appear to be associated with the articulating arm mass.

Airbag System

The airbag system in this study represents a "state of the art" design. Some details of the design are presented above. Two cases were evaluated. For Case #1, the airbag system was optimized for the 50th percentile occupant size. The optimization was carried out by trial and error. The flow characteristics of the inflator and the vent characteristics of the bag were varied until the injury

Table 3.
Simulation Results for Elastic Hip Restraint, Torso Pad = 280 kPa (40 psi), Hip Pad = 140 kPa (20 psi)

Measure	03 Year Old		05th Percentile		50th Percentile		95th percentile	
HIC	479.6	(W)	112.8	(W)	54.5	(W)	62.0	(W)
PCG-3ms (g's)	67.34	(B)	47.56	(W)	46.41	(W)	46.68	(W)
TTIup (g's)	126.67	(B)	81.48	(W)	70.97	(W)	68.01	(B)
TTImid (g's)	143.7	(W)	89.02	(W)	83.6	(W)	69.98	(B)
TTIlow (g's)	189.58	(W)	91.67	(W)	84.21	(W)	70.03	(B)
V*Cup (M/s)	.9979	(W)	.3169	(B)	.6880	(W)	.5696	(W)
V*Cmid (M/s)	1.2849	(B)	.8325	(B)	.7834	(B)	.6434	(B)
V*Clow (M/s)	1.7875	(B)	1.4943	(B)	.8171	(B)	.7028	(B)
HipF (lbf)	1401	(W)	2038.8	(W)	3262	(W)	[1]4583.3+	(W)
HipA (g's)	+90/-100	(B)	+41/-55	(B)	+32/-54	(S)	+31/-46	(B)
AbdF(lbf)	-46.17	(B)	-17.94	(B)	0	(B)	-42.20	(B)
V*Cabd (M/s)	2.7582	(B)	2.5911	(B)	0	(B)	.1201	(B)
DispRibu (in)	-1.0911	(W)	-.9415	(B)	-1.9141	(W)	-1.9255	(W)
DispRibm (in)	-1.3094	(B)	-1.6723	(B)	-1.9438	(B)	-1.9574	(B)
DispRibl (in)	-1.5946	(B)	-2.2476	(B)	-1.9339	(B)	-1.9956	(B)
DispAbd (in)	-2.2	(B)	-2.7	(B)	0	(B)	-.39	(B)
HipJntA (in/s^2)	+85/-100	(S)	+24.5/-12	(W)	+29/-21	(W)	+28/-9	(W)
HipJntV (in/s)	+57/-80	(B)	+36/-55	(W)	+83/-86	(W)	+10/-65	(W)
HipJntD (in)	+1.0	(B)	+.52/-.52	(W)	+.5/-1.65	(W)	+.2/-1.65	(W)
BagP (lb/in^2)	-----		-----		-----		-----	
HipRestrY (lbf)	+350/-1200		+900/-2400		+850/-3250		+950/-3500	
HipRestrZ (lbf)	+290/-20		+190/-10		+180/-10		+36/-8	
WSPen (in)	0	(S)	-.0438	(W)	-1.310	(W)	-.3140	(W)

NOTE: Scores are for comparison with baseline padding design in Table 2
B=Better
S=Same
W=Worse

[1] Data still rising at end of computer run.

Table 4.
Simulation Results for Inelastic Hip Restraint, Torso Pad = 280 kPa (40 psi), Hip Pad = 140 kPa (20 psi)

Measure	03 Year Old		05th Percentile		50th Percentile		95th percentile	
HIC	333.5	(B)	110.7	(B)	55.9	(W)	63.0	(W)
PCG-3ms (g's)	73.10	(W)	39.89	(B)	45.38	(B)	45.70	(B)
TTIup (g's)	128.48	(W)	69.40	(B)	67.10	(B)	73.14	(W)
TTImid (g's)	127.48	(B)	65.14	(B)	81.21	(B)	75.77	(W)
TTIlow (g's)	147.0	(B)	77.05	(B)	81.68	(B)	75.67	(W)
V*Cup (M/s)	.4998	(B)	.4344	(W)	.5232	(B)	.4664	(B)
V*Cmid (M/s)	1.9053	(W)	1.0192	(W)	.8627	(W)	.7044	(W)
V*Clow (M/s)	3.0784	(W)	2.0477	(W)	.9165	(W)	.7877	(W)
HipF (lbf)	1198.2	(B)	1878.2	(B)	3112.2	(B)	4619.8	(W)
HipA (g's)	+110/-140	(W)	+58/-58	(W)	+57/-55	(W)	+42/-82	(W)
AbdF(lbf)	-57.64	(W)	-22.38	(W)	-143.2	(W)	-233.9	(W)
V*Cabd (M/s)	4.9894	(W)	4.2163	(W)	.3540	(W)	.3489	(W)
DispRibu (in)	-.8842	(B)	-1.0521	(W)	-1.8564	(B)	-1.8411	(B)
DispRibm (in)	-1.5964	(W)	-1.9066	(W)	-1.9653	(W)	-1.9780	(W)
DispRibl (in)	-1.9522	(W)	-2.7316	(W)	-1.9785	(W)	-2.1149	(W)
DispAbd (in)	-2.800	(W)	-3.400	(W)	-.7200	(W)	-.700	(W)
HipJntA (in/s^2)	+80/-86	(B)	+38/-30	(W)	+39/-54	(W)	+26/-58	(W)
HipJntV (in/s)	+83/-93	(W)	+23/-63	(W)	+30/-116	(W)	+49/-79	(W)
HipJntD (in)	+1.0	(S)	+.4/-.65	(W)	-1.5	(B)	-1.79	(W)
BagP (lb/in^2)	-----		-----		-----		-----	
HipRestrY (lbf)	-950		-2175.2		-3780		-4068	
HipRestrZ (lbf)	+220/-10		-16		+95/-100		-19	
WSPen (in)	0	(S)	0	(B)	-.8580	(B)	-.0966	(B)

NOTE: Scores are for comparison with the elastic hip restraint design in Table 3
B=Better
S=Same
W=Worse

measures for the occupant were minimized. The airbag configuration was then fixed and the remaining occupant sizes simulated. For Case #2, the process was repeated now optimizing for the 3 year old child.

Case #1, Airbag Optimized for the 50th Percentile Occupant Size - Table 5 summarizes the results for this case. To evaluate this design we will compare the data in Table 5 with the data for the elastic hip restraint design in Table 3. Again we will make our comparison by data groups.

A general overview of the data in Table 5 shows us that all occupant sizes benefit from this airbag design since all sizes receive some reductions in their injury measures. Closer examination, however, shows us that some problem areas have been created as well. We will discuss these problem areas as we make our comparison.

The head data group (HIC and WSPen) shows improved performance across the board. All occupant sizes receive a benefit here. Note that the improvement on HIC is greater for the small occupant sizes. The larger occupants already had relatively low HIC values (Table 3). The larger occupants benefit more from a reduced window penetration (i.e., lower WSPen).

The rib/spinal-mass data group (TTI, V*C, DispRib and PCG) also show improved performance across the board, for all sizes. Note, the only W rating in this group are the V*Clow and DispRibL parameters for the child, 05th percentile and 95th percentile occupant sizes. The 50th percentile occupant size performed the best in this group (this is not surprising since the airbag was optimized for this size). Note also that although the small child and 05th percentile occupants benefit here from the design, the TTI and V*C parameters are still high.

The abdomen data group (AbdF, V*Cabd and DispAbd) received a relatively poor rating for all occupant sizes. Although the child occupant receives a B rating for V*Cabd and DispAbd, the reduction is not very much and their values still remain high (same for the 05th percentile). The larger occupants receive a W rating for all parameters in this data group, indicating that this airbag loads the abdominal spring more than the referenced padding design (Table 3).

The hip/hip-joint data group (HipF, HipA, HipJntA, HipJntV and HipJntD) show a relatively good rating. The two larger occupant sizes received all B ratings. The small child occupant received only one W rating (hip joint velocity). The 05th percentile female size rated the lowest in this data group.

Case #2, Airbag Optimized for 3 Year Old Child The results for this case are summarized in Table 6. Figure 9 shows the response sequence for the small child occupant (only the center slice of the bag is shown in the figure).

The results in Table 6 show that for the first time in this study the child TTI and V*C measures have been reduced to reasonable levels (based on current design standards). One exception is V*Cabd which is still relatively high (.855 m/sec). Note, to achieve this improved performance for the child occupant, the pressure in the airbag had to be reduced to 4.5 psig. Note also that the larger occupants now do not perform very well since the airbag is too "soft". Their responses approach that of the reference design (no airbag), summarized in Table 3.

CONCLUSIONS

In this study we evaluated several occupant restraint concepts for side impact protection. The concepts included interior padding, a hip restraint device and an airbag system. The performance of the candidate designs were evaluated for the full size range of occupants (3 year old child, 5th percentile adult female, 50th percentile adult male and 95th percentile adult male).

The results of this study seem to confirm our initial suspicion that occupant size is an extremely important factor in the design of crashworthy interiors for automobiles A design that works for one occupant size may be counter-productive for another. Extreme caution is needed in the design process and a systems analysis approach is truly warranted.

In this study we evaluated two padding designs. Both designs made use of a class of materials having near perfect energy absorbing characteristics ("flat" force-displacement characteristics, with hysteresis effects). These materials include crushable foams and paper honeycombs. This study indicates that although these near perfect padding materials can provide a good measure of protection for large occupants (see Table 2), they are generally too stiff for the smaller occupants and do not provide adequate protection for the small size group.

This study also evaluated the effects of a hip restraint device. The results show that a hip restraint device improves the posture of the occupant during impact, reducing the penetration of the head into the side window opening. It also prevents serious secondary impacts with other parts of the vehicle interior, following the primary impact. Some of the injury measures also showed some improvement (compare Table 3 with Table 2). Others, however, became worse. In general, the hip restraint designs evaluated herein were not able to significantly improve upon the padding performance summarized in Table 2. The larger occupants continued to perform fairly well while the small occupants did not.

The airbag system evaluated herein represents the size and shape of a current state-of-the-art design. Two design conditions were evaluated: 1) system optimized

Table 5.
Simulation Results for Airbag System Optimized for 50th Percentile Adult Male. Torso Pad = 280 kPa (40 psi), Hip Pad = 140 kPa (20 psi), Elastic Hip Restraint

Measure	03 Year Old		05th Percentile		50th Percentile		95th percentile	
HIC	120.6	(B)	50.7	(B)	37.4	(B)	59.9	(B)
PCG-3ms (g's)	34.59	(B)	32.68	(B)	37.27	(B)	37.17	(B)
TTIup (g's)	118.4	(B)	78.38	(B)	56.88	(B)	50.3	(B)
TTImid (g's)	105.2	(B)	77.39	(B)	48.57	(B)	59.15	(B)
TTIlow (g's)	121.8	(B)	117.8	(W)	48.91	(B)	61.15	(B)
V*Cup (M/s)	.1282	(B)	.2999	(B)	.4775	(B)	.4239	(B)
V*Cmid (M/s)	.6198	(B)	.8417	(W)	.4679	(B)	.6140	(B)
V*Clow (M/s)	1.3691	(B)	1.7826	(W)	.5746	(B)	.8145	(W)
HipF (lbf)	1186.9	(B)	2525	(W)	1678.6	(B)	1948.8	(B)
HipA (g's)	+46/-100	(B)	+36/-72	(W)	+21/-46	(B)	+18/-40	(B)
AbdF(lbf)	-139.9	(W)	-295.7	(W)	-908.2	(W)	-1015.3	(W)
V*Cabd (M/s)	2.344	(B)	2.642	(W)	.5660	(W)	.6400	(W)
DispRibu (in)	-.4858	(B)	-.9388	(B)	-1.8884	(B)	-1.895	(B)
DispRibm (in)	-1.1011	(B)	-1.6304	(B)	-1.9134	(B)	-1.9591	(S)
DispRibl (in)	-1.6829	(W)	-2.1482	(B)	-1.9330	(S)	-2.0276	(W)
DispAbd (in)	-2.00	(B)	-2.9	(W)	-.85	(W)	-.85	(W)
HipJntA (in/s^2)	+32/-46	(B)	+12/-24	(S)	+18.5/-10	(B)	+9.0/-10.0	(B)
HipJntV (in/s)	+85/-72	(W)	+30/-40	(B)	+19/-46	(B)	+12./-29.	(B)
HipJntD (in)	+.9/-.4	(B)	+.65	(W)	-1.00	(B)	-.88	(B)
BagP (lb/in^2)	8.0		11.0		14.0		16.0	
HipRestrY (lbf)	-680		-1700		-1400		-1400	
HipRestrZ (lbf)	-26		-39		+360		+85	
WSPen (in)	0	(S)	0	(B)	0	(B)	0	(B)

NOTE: Scores are for comparison with the elastic hip restraint design in Table 3

B=Better
S=Same
W=Worse

Table 6.
Simulation Results for Airbag System Optimized for 03 year old Child.
Torso Pad = 280 kPa (40 psi), Hip Pad = 140 kPa (20 psi),
Elastic Hip Restraint

Measure	03 Year Old		05th Percentile		50th Percentile		95th percentile	
HIC	52.3	(B)	108.5	(W)	57.3	(W)	67.9	(W)
PCG 3ms (g's)	32.57	(B)	45.2	(W)	45.8	(W)	46.3	(W)
TTIup (g's)	74.07	(B)	71.57	(B)	66.67	(W)	72.48	(W)
TTImid (g's)	50.68	(B)	77.85	(W)	79.8	(W)	72.0	(W)
TTIlow (g's)	55.7	(B)	79.09	(B)	85.04	(W)	71.73	(W)
V*Cup (M/s)	.3229	(W)	.3271	(W)	.67	(W)	.5506	(W)
V*Cmid (M/s)	.3820	(B)	.8681	(W)	.75	(W)	.6248	(W)
V*Clow (M/s)	.4368	(B)	1.7202	(B)	.84	(W)	.7355	(B)
HipF (lbf)	1020.2	(B)	1818.5	(B)	3350.7	(W)	4506.7	(W)
HipA (g's)	+46/-57	(B)	+47/-56	(B)	+36/-55	(W)	+30/-47	(W)
AbdF(lbf)	-60.19	(B)	-107.63	(B)	-223.0	(B)	-345.8	(B)
V*Cabd (M/s)	.8553	(B)	2.5805	(B)	.140	(B)	.1871	(B)
DispRibu (in)	-.7414	(W)	-.9989	(W)	-1.92	(W)	-1.9333	(W)
DispRibm (in)	-.9428	(B)	-1.642	(W)	-1.95	(W)	-1.9834	(W)
DispRibl (in)	-1.1439	(B)	-2.2196	(W)	-1.96	(W)	-2.0219	(B)
DispAbd (in)	-1.25	(B)	-2.8	(B)	-.50	(B)	-.52	(B)
HipJntA (in/s^2)	+32/-24	(B)	+16/-13	(B)	+31/-18	(W)	+25/-9	(W)
HipJntV (in/s)	+30/-57	(B)	+34/-55	(W)	+100/-200	(W)	+5/-64	(W)
HipJntD (in)	+.48/-.55	(B)	+.52/-.4	(B)	+.3/-1.8	(W)	+.1/-1.8	(W)
BagP (lb/in^2)	4.5		4.5		5.8		6.8	
HipRestrY (lbf)	+300/-920	(W)	+900/-2400	(W)	+800/-3300	(W)	+900/-3500	(W)
HipRestrZ (lbf)	+39/-8	(W)	+110/-10	(W)	+180	(B)	+48/-8	(B)
WSPen (in)	0	(S)	0	(S)	-.45	(W)	-.0147	(W)

NOTE: Scores are for comparison with the elastic hip restraint design and airbag optimized for 50th percentile inTable 5

B=Better
S=Same
W=Worse

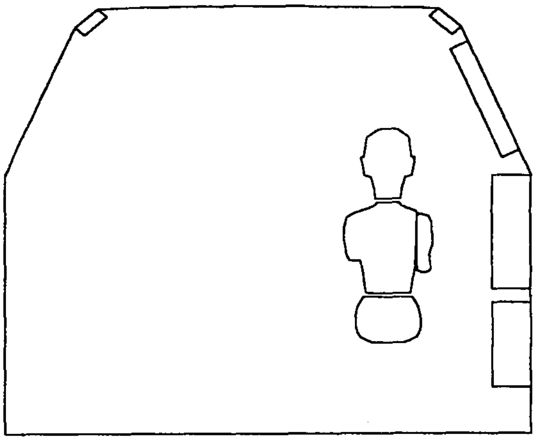

Time = 0 msec

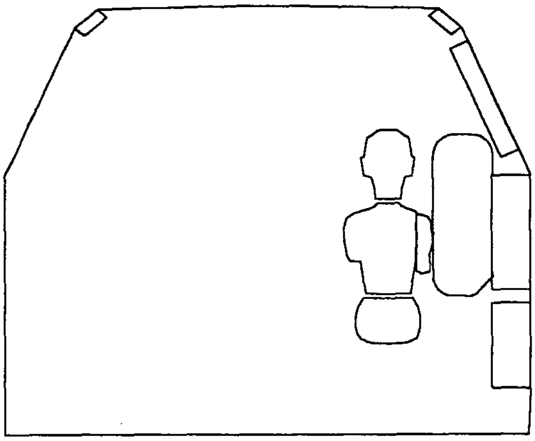

Time = 10 msec

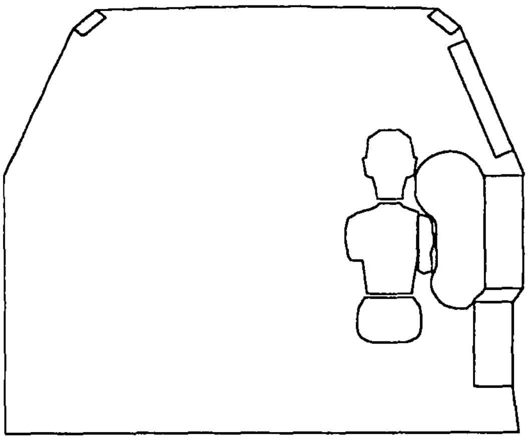

Time = 20 msec

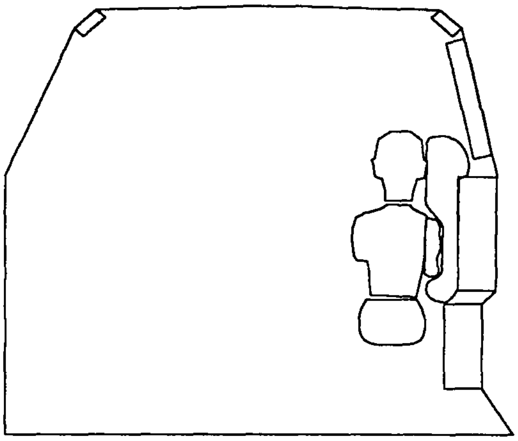

Time = 30 msec

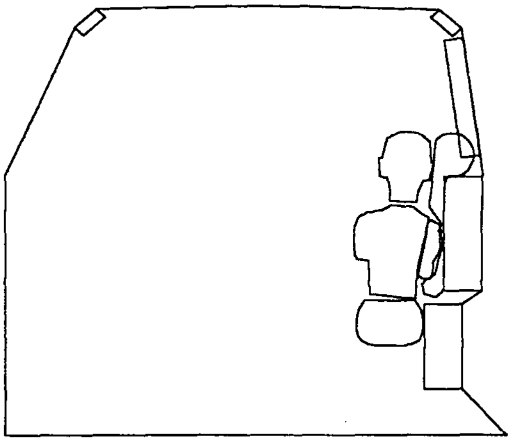

Time = 40 msec

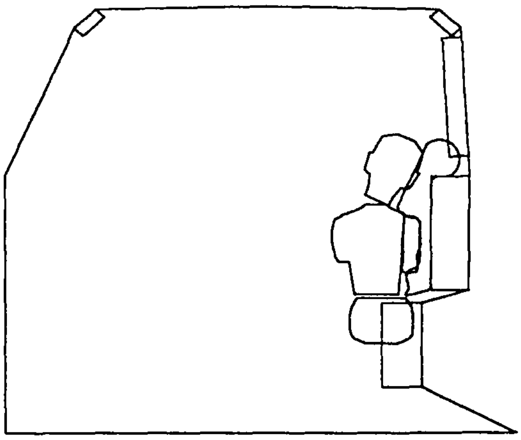

Time = 95 msec

Figure 9. Occupant trajectory with airbag, 3 year old child.

for the 50th percentile adult male occupant and 2) system optimized for the 3 year old child. The results show that each occupant size has its own optimum operating condition. The 50th percentile occupant size requires a bag pressure of approximately 14 psi (see Table 5) while the 3 year old child requires a pressure of only 4.5 psi (see Table 6). Obviously, to protect the full size range of occupants, a "smart" system is needed to adjust to the size of the seated occupant..

Several safety design issues surfaced during the course of this study and are worthy of mention here. First, the study shows that a hip restraint device serves several very positive functions in side impacts. It helps to control the posture of the occupant during impact and thereby reduces the head penetration into the side window area. It also helps to prevent serious secondary impacts with the vehicle interior. However, computer simulations show that a hip restraint adds energy to the hip joint of the occupant during impact. Further research is needed to evaluate the hip joint tolerance of humans in side impacts.

Second, computer simulations in this study show that the pivoting arm mass can be a source of injury to the rib cage and abdomen of the occupant. During impact the arm mass oscillates and transfers energy between the door padding and the rib cage and abdomen areas of the occupant's torso. Large torso penetrations can result because of the relatively small contact areas involved. Further research is needed to determined how important these interactions are in real impacts.

Finally, in our evaluation of the airbag system it has become even more apparent that a "smart" design is needed to protect the full size range of occupants. This will require an inflator that can sense and adjust its flow characteristics to accommodate the size of the seated occupant. The design of such an inflator will require that each stage of the inflator be targeted and optimized for a specific size group. Further research is needed to determine the size groups required to effectively cover the full range of occupants.

REFERENCES

1. N.A. El-Habash, Vehicle Research and Test Center, "Evaluation of the BIOSID Dummy, MDB-To-Car Side Impact Test of a 26 degree Crabbed Moving Deformable Barrier Into a 1988 Hyundai Excel 4-door Sedan at 33.7 Mph", Final Report, Contract Number DTNH22-88-C-07292, June 1990.

2. Lonney S. Pauls, ASL Engineering, "Identification of Superior Energy Absorbing Materials for School Bus Interiors", Final Report, Contract Number DOT-HS-7-01664, July 1979.

3. S. L. Kirkish, et.al., Occupant Safety Research Partnership, and Michael Salloum, First Technology Safety Systems, "Status of Prove-Out Testing of The SID-IIs Alpha-Prototype", Paper No. 96-S10-O-15, Fifteenth International Technical Conference on Enhanced Safety of Vehicles, May 1996.

4. Daniel, R.P., et.al., Occupant Safety Research Partnership and Salloum, M., Smrcka,J., First Technology Safety Systems, "Technical Specifications of the SID-IIs Dummy", SAE Paper No 952735, 39th Stapp Car Crash Conference, Nov. 1995.

5. Midoun, D.E., Abramoski, E., Rao, M.K, and Kalldindi, R., :Development of a Finite Element Based Model of the Side Impact Dummy", SAE Paper 930444.

6. Hasegawa, J., Fukatsu, T., and Katsumata, T., "Side Impact Simulation Analysis Using and Improved Occupant Model", Proceedings of the Twelfth International Conference on Experimental Safety Vehicles, May 1989, Paper No. 89-5A-0-017.

7. Kirkpatrick, S.W., Homes, B.S., Hollowell, W.T., Gabler, H.C., Trella, T.J., "Finite Element Modeling of the Side Impact Dummy (SID)", SAE Paper 930104.

8. Sakurai, M., Harigae, T., Ohmae, H., JARI and Nakamura, Y., Watanabe, K., JAMA, "Study on Side Impact Test Methods", Paper No. 89-5A-0-020, The 12th International Technical Conference on Experimental Safety Vehicles, May 1989.

9. Olsson, J.A., Skotte, L.G, Electrolux Autoliv AB and Svensson, S.E, Volvo Car Corp., "Air Bag System for Side Impact Protection", Paper No. 89-5A-0-029, The Twelfth International Technical Conference on Experimental Safety Vehicles, May 1989.

STRUCTURE AND PADDING OPTIMISATION FOR SIDE IMPACT PROTECTION

Marcello Di Leo
Fiat Auto S.p.A.
Italy
Paper Number 98-S8-W-32

ABSTRACT

This paper aims to show methods to design and optimise vehicle side structure and padding to improve side impact protection.

To limit injuries at thorax level, intrusion profile during impact must perform a negative vertical tilt: a way to obtain this is to avoid B pillar deforming above R point. A static analysis may be useful to determine a proper distribution along B pillar axis of sections' moments of inertia.

A good structural behaviour is necessary but not sufficient to perform good results in side impact. A proper control of padding stiffness is very important especially for abdomen protection.

A method to evaluate the stiffness of padding at thorax level is proposed. A similar method is used to determine failure load of armrest for abdomen protection.

INTRODUCTION

European side-impact test regulation, which is going to be compulsory from 1st October 1998, has become popular due to EURO-NCAP safety rating. This one asks for heavy requirements especially for thorax and abdomen protection. Is it possible to comply with them in standard cars, for the benefit of all customers, and without adopting a side-bag, which has got very high development costs?

Some production vehicles with bio-mechanical values near to Euro-NCAP requirements already exist, but this happens only under very precise conditions and several parameters must be taken into account.

PARAMETERS AFFECTING PERFORMANCE.

It is well known from literature that an intrusion profile which shows a negative vertical tilt is the best one to comply with regulation requirements ([1], [2], [3], [7],[14]) while padding behaviour must be controlled properly ([4], [5], [6], [8], [9], [10], [11], [12], [13]).

The effect of the first one is to reduce side intrusion speed, relative to the thorax, both by limiting the deformation at thorax level and by favouring the intrusion at pelvis level to push the dummy away from the side.

The effect of the second one is to limit acceleration of the ribs and load on abdomen.

Using MADYMO software and DOE technique it is possible to show what are the most important parameters on the performance.

A MADYMO model was generated and correlated to a crash test. Three factors were considered with a variation range as detailed below:

- upper door velocity: between the baseline intruding velocity profile and a profile which includes a reduction of 5 m/s on the first peak (Figure 1);

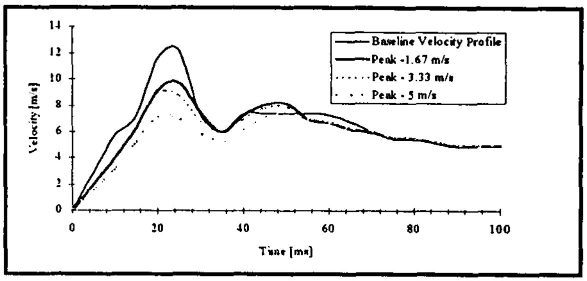

Figure 1. Velocity profiles used in the study.

- upper door stiffness: between 80 kN/m and 40 kN/m (Figure 2);

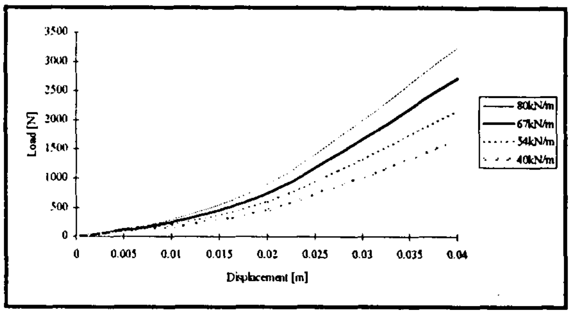

Figure 2. Upper door stiffness characteristics

- Lower distance from the occupant: from the baseline correlated position to 100 mm closer to occupant (Figure 3).

The experimental matrix that was generated is shown in Table 1. Table 1 shows also the results on middle rib (other ribs have similar behaviour). Results on abdomen are meaningless because of correlation problems and a parametric analysis can't be done.

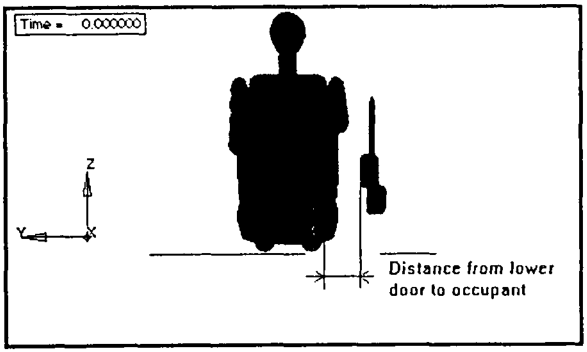

Figure3. Lower door position geometry

Table 1.
Simulation Matrix and results
Note^1 : Value is reduction in the first peak (m/s)
Note^2 : Value is movement closer to the occupant (mm)

Simulation	Upper Door Stiff. (kN/m)	Upper Door Velocity Profile ^{1}	Dist. lower Door to Occupant ^{2}	Mid Rib Def. [mm]	Mid Rib VC [m/s]
Baseline	80	0	0	36	0.47
C1	80	-5	66	5	0.01
C2	54	-5	0	4	0.02
C3	54	0	100	29	0.25
C4	67	-5	100	4	0.01
C5	80	-3.3	100	16	0.17
C6	54	-3.3	66	10	0.06
C7	40	-5	100	5	0.02
C8	67	-3.3	33	14	0.1
C9	80	-1.67	0	26	0.3
C10	80	0	0	36	0.47
C11	40	-3.3	0	20	0.2
C12	40	0	66	14	0.09
C13	80	-5	100	3	0.01
C14	67	0	0	36	0.42
C15	80	0	100	26	0.23
C16	40	0	0	28	0.35
C17	67	-1.67	66	9	0.05
C18	80	0	33	20	0.23
C19	54	-1.67	33	15	0.12
C20	80	-5	0	4	0.01
C21	40	-5	33	5	0.02
C22	40	-5	0	7	0.04
C23	40	-1.67	100	22	0.22
C24	40	0	100	30	0.23
C25	67	0	66	14	0.11

The results show that varying upper door trim stiffness from 80 kN/m to 40 kN/m. VC and rib deflection don't vary so much while upper door velocity profile (i.e. impact speed against thorax) and lower door position level have got main effects. This can be seen in Figures 4 and 5 for middle rib deflection and VC. The lower door position has a non-linear effect on the lower rib deflection, with the minimum injury criteria reached when the position in about 50 mm closer to the occupant.

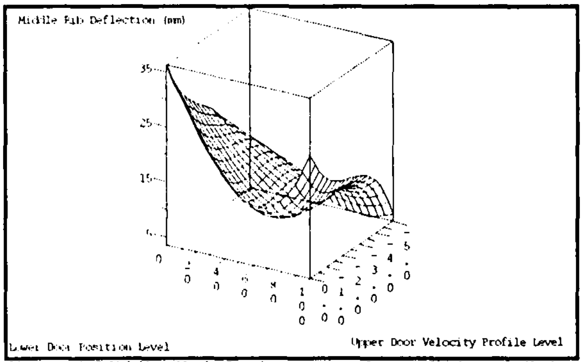

Figure 4. Middle rib deflection: upper door velocity profile level versus lower door position level for middle rib.

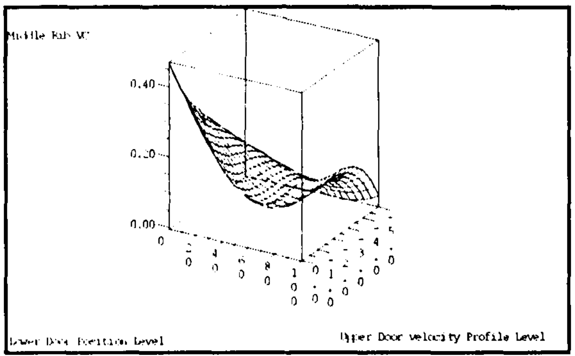

Figure 5. Middle rib VC: upper door velocity profile level versus lower door position level for middle rib.

The upper door velocity profiles should be minimised to further reduce the response results.

Other ribs has got similar behaviour even if the described effect are not the same for all of them because of kinematics effects (for example for a trim with higher stiffness the kinematics show more rotation of the dummies arm across the body and away from the door than a lower stiffness trim).

Let's analyse deeper the effect of lower door distance to occupant. If we consider speed of door relative to ribs' one at the impact time and the difference between contact times against pelvis and thorax it is possible to fill Table 2. It can be seen that the minimum values of rib deflection and VC correspond to a Δv of about 6 m/s and to a Δt of about 10 ms.

Table 2. Relation between contact times, impact speed and bio-mechanical results (MADYMO analysis)

Simu-lation	Contact times [ms]		Speed at t_2 [ms] (^{1} average)		Δt (t_2-t_1)	Δv (v_2-v_1)	Results on ribs (average)	
	Pelv (t_1)	Thor (t_2)	Rib^1 (v_1)	Door (v_2)			Defl [mm]	VC [m/s]
Baseline	24	28	0.1	8.26	4	8.16	38	0.6
33 mm closer	22	28	0.1	8.26	6	8.16	22	0.32
66 mm closer	20	30	1.25	7.5	10	6.25	16	0.16
100 mm closer	14	30	0.98	7.5	16	6.52	28	0.3

This confirms that to obtain good results on thorax pelvis must be hit before than the thorax in order to push away dummy from the intruding side. But if this Δt is higher than 10 ms, kinematics of dummy may worsen results: this will be confirmed on experimental basis and related to the intrusion profile.

As final comment although results on abdomen were meaningless, nevertheless it is evident that armrest must have an influence on abdomen performance: this will be seen on experimental basis.

INTRUSION PROFILE

Several papers deal with the deformation of side structure ([1], [2], [3], [7], [14]) and do confirm the short study described before: it comes out that the most appropriate intrusion profile has a low intrusion at thorax level and a higher intrusion at pelvis level. The relation between biomechanical performance and intrusion profile can be seen comparing two production vehicles in their two doors and four doors versions.

To make such a comparison an *INTRUSION PROFILE INDEX (I.P.I.)* has been defined (see Appendix 1): it says how near real profile is to the theoretical one: theoretical profile is defined as the profile coming from the rigid rotation of side structure around an axis along superior sill for a given intrusion at pelvis level. IPI can be dynamic (measured through accelerometers on the struck side as described in [3]) or static (measured at the end of test). In the following it will be referred to dynamic IPI evaluated ad the time of the first impact, generally against pelvis.

Table 3 shows the relation between IPI and bio-mechanical performance in the said cars.

It is clear that a dynamic IPI of at least 60% on the door must be reached in order to obtain a Δv lower then 10 m/s. With such values good bio-mechanical results look like to be easily achieved. In four doors cars, where B pillar can interfere with dummy, also a dynamic IPI of at least 60% to 80% must be guaranteed and maintained during the whole impact.

Table 3. Relation between contact times, impact speed, intrusion profile and bio-mechanical results (experimental analysis)
Note^1: differences in time and in speed as defined before for table 2.

Vehicle	Rib values (average)		Forces [kN]		Dynamic IPI		Δt^1 [ms]	Δv^1 [m/s]
	Defl. [mm]	VC [mm]	Abd.	PSF	Door	B pillar		
A 4 doors	31	0.8	1.7	3	50%	80%	3	12
A 2 doors	26	0.4	2.1	4	95%	-	10	7.4
B 4 doors	35	0.5	2.2	3	60%	60%	6	10
B 2 doors	19	0.2	1.5	4.3	60%	-	10	5.8

In a two doors car dynamic IPI is mainly related to inertial effects of the door ([1]), while in a four doors car general intrusion profile is related to structural stability of B pillar.

Through FEM analysis ([7]) it can be seen that during crash MDB transfers momentum through the doors to B pillar. In particular rearward door charges it through its hinges: if load through lower hinge favours appropriate intrusion profile, load through upper hinge can make B pillar unstable. These two loads can be considered concentrated in two points (the hinges), and the load through the upper hinge is the worst one.

Loading quasi-statically at upper hinge level B pillars of several production vehicles It could be stated that this very simple loading condition is able to put in evidence structural instabilities that can occur during dynamic impact.

This is a very helpful and easy way of designing B pillar correctly from the very early stages of project, much before FEM analysis of side impact can be performed, as many details of the structure don't need to be known.

In the followings the develeped method to characterise B pillar will be described. Both experimental and mathematical analysis can be performed.

- B pillar can be isolated and constrained and loaded as shown in Figure 7;
- measurements of intrusions at roof level, R point level and 390 mm higher, are taken through potentiometers (Figure 7);
- *I.P.I.* in respect of R point intrusion can be evaluated: just the first 50 mm of intrusion are enough to establish local plastic hinges (Figure 8).

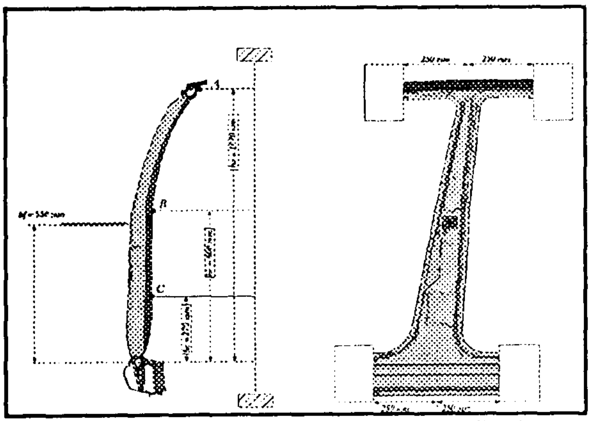

Figure 7. Example of constraining and loading of a B pillar.

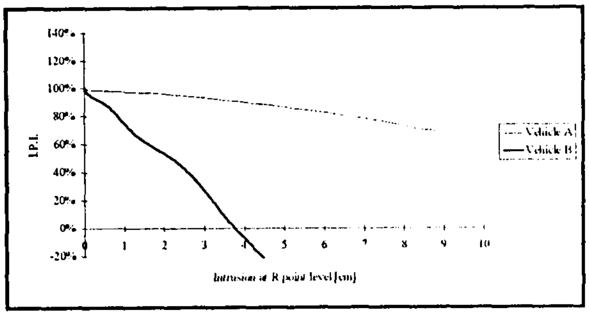

Figure 8. Example of IPI calculated on the basis of a quasi-static loading (FEM analysis).

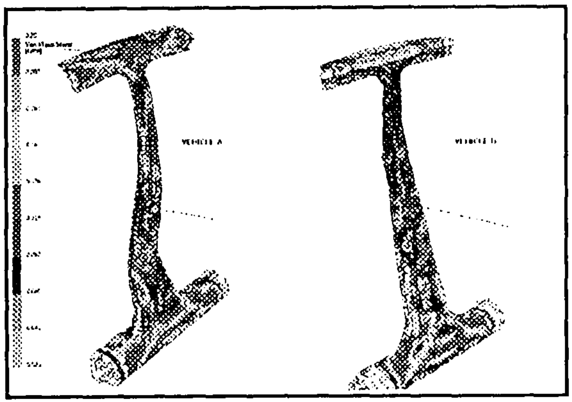

Figure 9. Comparison between the deformations of the B pillars of two vehicle after a quasi-static loading.

Figure 9 shows the comparison of deformations of B pillars of two production vehicles when loaded quasi-statically (FEM analysis). When the deformation is good for side impact protection then the main plastic hinge occurs below R point level (vehicle A). Possible problems may occur when there is a plastic hinge at higher level (vehicle B). IPI detects very well the two situations (Figure 8): in fact IPI for vehicle B decrease quickly, while for vehicle A it is much more stable.

Figure 10 shows the real deformation after a crash test for the vehicle B: plastic hinge is in the place where the quasi-static analysis found it.

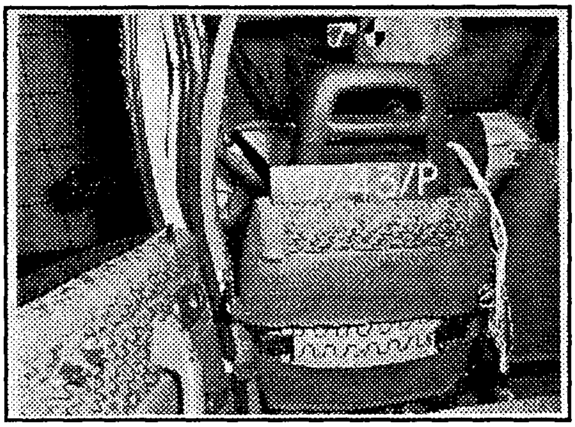

Figure 10. B pillar deformation after a crash test: the upper plastic hinge has been correctly detected through quasi-static analysis

As we are looking for possible instabilities of B pillar when loaded in the described way, a linear analysis can be performed: a simplified method using arch beams theory and few geometrical information has been developed in order to find the most critical sections.

B pillar is considered as a two hinges arch and the problem is considered plane: because of this it is possible to use equations coming from static; even if these are hard hypotheses, if the pillar is designed for this case it will deform in the desired way in the static test. Nevertheless some corrective factors must be introduced to take into account that constraints aren't perfect hinges.

Then bending moments (M) distribution along the pillar can be found and, dividing it by the inertia module (W), the tension distribution can be calculated.

Comparison between tension distribution calculated in such a way and the same calculated via FE models show good agreement (Figures 11 and 12).

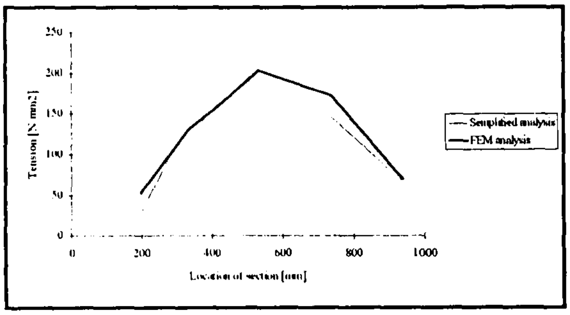

Figure 11. Tension distribution along the beam calculated via simplified analysis and via FEM analysis for B pillar of vehicle A.

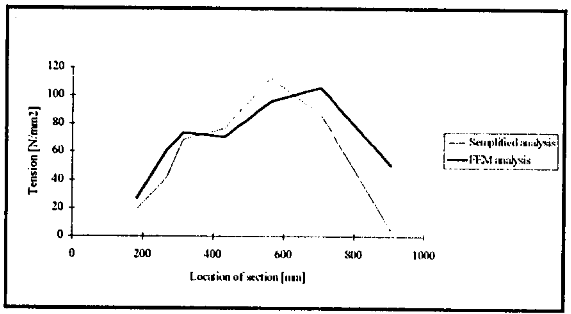

Figure 11. Tension distribution along the beam calculated via simplified analysis and via FEM analysis for B pillar of vehicle B.

Instabilities of B pillar pointed out by simplified analysis are in the sections where M/W is maximum. Then the following design criteria can be expressed:

- critical section where instability occurs must be located under R point level;
- alternatively, stress (M/W) in critical section must be higher then yield stress, while in other sections (i.e. upper then R point level) it must be lower.

This method is useful in the very early stages of design when only the style concept of a new project is available and main dimensions have to be determined.

The same can be applied to a two doors vehicle in order to have a good intrusion profile of bc pillar, being this important mainly for protection of backward occupants: the loading point, anyway, must be considered at 200 mm higher then R point level.

PADDING CHARACTERISTICS

Several papers deal with padding stiffness ([4], [5], [6], [8], [9], [10], [11], [12], [13]) and with methods to evaluate it, but they generally refer it to FMVSS214.

DOE study demonstrated that bio-mechanical parameters at thorax level aren't very much affected by padding stiffness. In [12] and [13] indications of padding stiffness for thorax protection are present and were used to define a specification for side trim panels.

For abdomen protection a correlation between collapse force of armrest and force values measured in side impact tests was found (see table 3).

Table 4. Comparison between failure load of armrest and abdomen force in side impact test.

Vehicle	Failure load at armrest [kN]	Abdomen force in side-impact test [kN]
A	2.5	1.7
B	2.8	2.1
C	3.3	2.3

In this paragraph an experimental method to characterise side trim panels will be described. It will be shown also how a side panel designed to comply with certain specifications will affect bio-mechanical performance.

Let's define *thorax area* the very area hit by the ribs of an Euro-SID, when it is installed in car as defined by regulation and the seat is moved through all its possible positions. In [12] and [13] for a range of 60 to 100 kN/m stiffness was investigated in such an area. To evaluate stiffness of a real panel the following method was developed in FIAT.

A rib-form with the shape of an Euro-SID (i.e. 120 mm × 40 mm) was built and mounted on a trolley suitable to the MTS machine for Body Block test. The mass of the whole trolley and rib-form was 4.3 kg (see Figure 12 and 13).

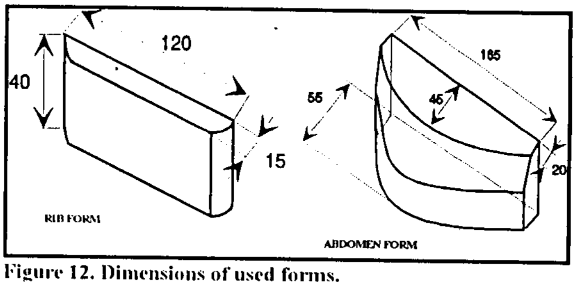

Figure 12. Dimensions of used forms.

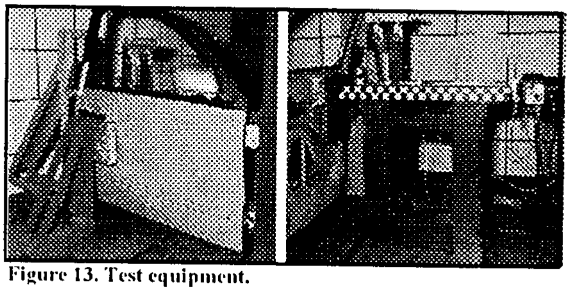

Figure 13. Test equipment.

The form was thrown against the door rigidly mounted through its hinges and latch. Some other constraints are put in order to limit deflection of the door itself. The speed was specified at 24.1 km/h like in the partial test of Regulation, but a range between 20 and 24 km/h was accepted for practical reasons.

The deceleration of the form was measured and used to determine an average stiffness which is related both to door and padding: this was done transforming deceleration results in global parameters like force and energy. By these two quantities it is possible to calculate an average stiffness, sample by sample, using the simple relations of a linear spring, i.e.

$$F = k \times X \quad \text{and} \quad E = \tfrac{1}{2} k \times X^2$$

then

$$k = \tfrac{1}{2} F^2 / E.$$

The maximum value obtained can be considered as the searched value.

Several tests on production panels were performed and values from 60 kN/m to 290 kN/m were found. The highest values were generally found at the fixation points of the panel to the door structure, while the lowest values correspond to the most flexible panels.

Drawing a graph Force vs. Energy, several typical results can be compared (see Figure 14).

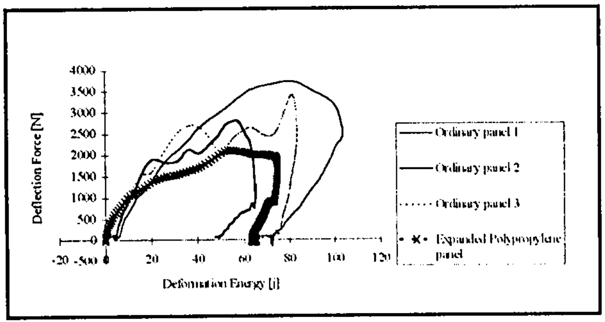

Figure 14. Panel characteristic at thorax level: comparison between current production side panels and Expanded Polypropylene panel.

A similar method was used to determine collapse force of armrest. For this a different form was used, to reproduce abdomen shape (see Figure 12). Measured deceleration is used to calculate a force vs. form's displacement. Several panels were tested and a range from 1.8 kN to 3.7 kN was found (see Table 4 and Figure 15).

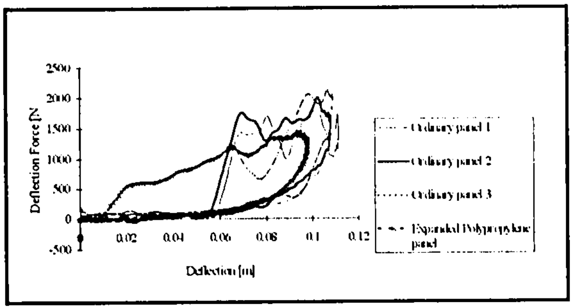

Figure 14. Panel characteristic at abdomen level (armrest): comparison between current production side panels and Expanded Polypropylene panel.

Using the said methods several absorbing materials were tested too. After a proposal from ADLER-PLASTICS® a prototype panel, entirely made with expanded polypropylene, was built. The chosen density was 20 g/l and the thickness at thorax level was 50 mm with internal gaps to reach a global stiffness of 40 kN/m, which is about 25% of the average measured stiffness (see Figure 14).

Finally a maximum force of 1.4 kN was measured at the armrest (see Figure 15).

The same kind of panel was used to perform a full scale side impact test using a production car. The results are summarised in table 5 against standard car.

Table 5. Results of side impact crashes with standard and prototype door panels.

Panel	HPC	Rib deflection [mm]		Rib VC [m/s]		Force [kN]	
		Min.	Max.	Min.	Max.	Abd.	Pelv.
Stand.	300	29	33	0.7	0.9	1.7	3.1
Proto.	340	38	43	1.04	1.16	0.98	3.8

It can be seen a general worsening of thorax performance. This is coherent with the parametric analysis: in fact panel stiffness didn't improve the performance and a slight difference in impact speed worsened it.

Abdomen force was very much reduced by the use of a very soft armrest: a maximum failure load of 1.4 kN must be guaranteed in order to have abdominal force lower than 1 kN in the crash test.

Pelvis and head performance changed within experimental variability.

CONCLUSIONS

An analytical study supported by experimental evidence and by laboratory tests demonstrated that the main parameters which influence bio-mechanical performance in side-impacts are upper door velocity against thorax, lower distance from occupant (pelvis level) and failure load of armrest. Upper door stiffness doesn't appear as an important parameter.

Upper door velocity is influenced by structural behaviour of B pillar (in four door cars): a design specification for B pillar has been developed applying simple static analysis in order to guarantee stability of B pillar during impact.

Lower distance to occupant at pelvis level must be reduced by at least 50 mm, in respect to standard geometry, to achieve good performance at thorax level: this is an important item for design preliminary work. Use of foams and other absorbing materials should be validated.

An experimental methodology for characterisation of trim stiffness has been proposed. At abdomen level failure load of armrest can be measured: it comes out that door armrest must be designed to guarantee a maximum failure load of 1.4 kN to obtain a maximum abdomen load of less than 1 kN in side-impact crash.

At thorax level proposed test is very sensitive to change in stiffness of the panel but it shows poor correlation with side impact test results. This could means that methodology must be improved.

AKNOWLEDGMENTS

Author would like to thank ADLER-PLASTICS® for the help for the support given in defining the proper characteristics of the tested panels.

APPENDIX: INTRUSION PROFILE INDEX

To measure intrusion profile an *INTRUSION PROFILE INDEX (I.P.I.)* has been defined: it says how near is real profile to the theoretical one; theoretical profile is defined as the profile coming from the rigid rotation of B pillar around superior sill for a given intrusion at pelvis level.

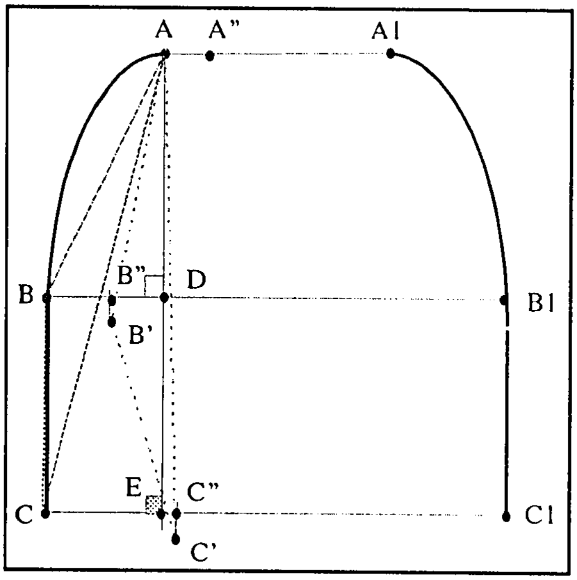

Figure A1. Sketch for definition of IPI.

Refer to Figure A1 where:

AA_1 = roof width before crash;
BB_1 = internal width at thorax level before crash;
CC_1 = internal width at R point level before crash;
$A"A_1$ = roof width after crash;
$B"B_1$ = internal width at thorax level after crash;
$C"C_1$ = internal width at R point level after crash.

Theoretical intrusion profile is obtained through rigid rotation of triangle ABC around A when C moves inward as much as in the crash test. With trigonometry it is possible to calculate how B moves inward in a theoretical profile. Then real B" position relative to B_1 and the theoretical one $B"_t$ can be compared. For mathematical reasons it is better to refer to the areas of polygons $AB"_tC"C_1B_1A_1$ and $A"B"_tC"C_1B_1A_1$. The ratio of these two areas is the desired IPI.

REFERENCES

[1] C.A. Hobbs, "Rationale an Development of EEVC Laterale Impact Test Procedure", IMechE, 1989.

[2] C.A. Hobbs, "The influence of car structures and padding on side impact injuries", 12th ESV (1989) 89-5A-O-026

[3] A.M. Benedetto, "Experience and Data Analysis on Side Impact Testing According to European Procedure", 14th ESV (1994) 94-S6-O-07

[4] H. Matsumoto, H. Tanaka, "The Effect of Door Structure on Occupant Injury in Side Impact", 13th ESV (1991) S5-O-03

[5] A.I. King, Y. Huang, J.M. Cavanaugh, "Protection of Occupants Against Side Impact, 13th ESV (1991) S5-O-04

[6] Y. Håland, B. Pipkorn, "The Protective Effect of Airbags and Padding in Side Impacts - Evaluation by a New Subsystem Test Method", 13th ESV (1991) S5-O-06

[7] A. Inagaki et al., "A Resolution of Side Impact Phenomena by Means of Dynamic Nonlinear FEM Simulation and a Study of Vehicle Body Structure", 13th ESV (1991) S5-O-14

[8] J. Kanaianthra, G.C. Rains, "Innovative Padding Design for Side Impact Protection", 14th ESV (1994) 94-S6-O-11

[9] L. Lorenzo, S. Burr, K. Fennessy-Ketola, "Integrated Inner Door Panel/Energy Absorber Design for Side Impact Occupant Protection", International Congress & Exposition, Detroit, Michigan, February 26-29, 1996, SAE Paper No. 960151

[10] M. Ueno, S. Ugawa, "Study on static/Dynamic Conversion Factor in the Door Inner in the Side-Impact Crash", SAE Paper No. 931978

[11] D.J. Dalmotas, C. Withnall, T. Gibson, "Side Impact Protection Opportunities", 15th ESV (1996), 96-S6-O-04

[12] D.C. Viano, "Evaluation of the Benefit of Energy-

Absorbing Material in Side Impact Protection: Part II", Proceedings of the 31st Stapp Car Conference, SAE Technical Paper 872213 (1987)

[13] Y. Håland, B. Pipkorn, "A Parametric Study of a Side Airbag System to meet Deflection Based Criteria" in "Car-to-Car Side Impacts", thesis for the degree of Doctor of Philosophy, Department of Injury Prevention, Chalmers University of Technology, S-412 96 GÖteborg, Sweden (1994)

[14] R. Bergmann, C. Bremer, X. Wang, A. Enßlen, "Requirements of Comprehensive Side Protection and Their Effects on Car Development", 15th ESV (1996), 96-S6-W-16

EVALUATION OF RESTRAINTS EFFECTIVENESS IN SIMULATED ROLLOVER CONDITIONS

Glen Rains
National Highway Traffic Safety Administration
Jeff Elias
Transportation Research Center
Greg Mowry
Simula Automotive Safety Devices Incorporated
United States
Paper Number 98-S8-W-34

ABSTRACT

A series of tests were conducted to determine the effectiveness of belt restraints in reducing occupant excursion in rollover crashes. A typical 3-point lap and shoulder belt configuration was tested as the baseline restraint. The baseline restraint was compared to an inflatable restraint to determine how well excursion could be reduced over current belt systems in a simulated rollover. A device called the rollover restraints tester (RRT) was used to simulate rollover conditions and to evaluate the effectiveness of restraints to prevent occupant head excursion. Vertical head excursion of a 50th percentile H-III male dummy was reduced by as much as 75 percent with the inflatable restraint.

INTRODUCTION

The lap and shoulder belt is the single most important safety device built for passenger vehicles. It is estimated that safety belts are responsible for saving over 85,000 lives from 1982 to 1996 [1]. Until the last decade, the belt system was largely unchanged. However, seat belt performance has improved recently due to the introduction of electronic and automatic locking retractors. Even greater improvements are being made with the introduction of belt pre-tensioners, load limiters and web grabbers which are improving the energy management capabilities of the restraint system. In general, these enhancements are being developed for frontal impacts and are not optimized for rollover crashes.

Most of the benefits from belt restraints are realized in frontal crashes and ejection mitigation in rollover collisions. However, the performance of restraints in rollovers also prevent impact with the vehicle's interior structure. Previous analysis of rollover crashes in NHTSA's National Automobile Sampling System [2], suggest that occupant impacts within the vehicle interior are a result of intrusion into the survival space and occupant excursion which are caused by the vehicle motion during rollover. Most restraints, by their design, do not securely hold the occupant in the seat. Consequently, we can assume that restraints that provide better coupling of the occupant with the seat, can control relative movement of the occupant with the seat thereby mitigating a large number of injuries from interior impacts.

Recently, several projects have reported investigations into effective restraint in rollovers crashes. Arndt et al [3] conducted vertical drop tests using a H-III 95th male dummy and human volunteers. It was discovered that higher lap-belt angles reduced vertical excursion when subjected to a uni-directional acceleration. Arndt et al.[4] also conducted testing to study seat belt restraint belt slack and its correlation to occupant excursion. As expected, shortening the web length reduced occupant excursion. There were also effects from spool out and seat belt anchorage location that were restraint design dependent. Another analysis was conducted by Cooper et al.[5] using a Head Excursion Test Device. It was found that the lap belt anchorage angle had a significant effect on vertical head excursion when simulating the angular roll rate in a rollover crash. It was also discovered that the anthropomorphic test device (ATD) had less vertical and lateral excursion when compared to cadavers tested in the same configuration. In 1996, NHTSA announced a program to evaluate rollover restraints in a component test fixture [6]. This device, referred to as the rollover restraint tester (RRT), was used in this study to examine seat belt restraints for the possibility of improving restraint effectiveness over current systems. Current technology used to enhance safety in frontal crashes, may be applicable to rollover collisions, since the basic restraint requirements for frontal crashes are the same for rollover crashes. The restraint should effectively couple the occupant to the vehicle/seat to control occupant motion within a vehicle during the rollover event. The objectives of the testing with the RRT were to determine:

1. The relative importance of D-ring adjustment position for improving occupant retention when exposed to rollover forces.
2. The reduction in occupant excursion during rollover with the use of an inflatable tubular torso restraint (ITTR).

TEST METHODOLOGY

Description and Operation of RRT

Real-world crash data indicated that the typical range of roll rate in a vehicle roll-over collision was 180°/sec (0.5 rev/sec) up to about 360°/sec (1.0 rev/sec), but could be as high 540 degrees/sec (1.5 rev/sec).

The rollover restraints tester (RRT) modeled a rollover condition in which the vehicle becomes airbourne at the initiation of the roll, then impacts on the roof structure after rotating approximately 180°. Pre-test photographs of the seated dummy are shown in Figures 1 and 2. Tape markers on the head were used to digitize the dummy's head movement during the simulated rollover. A reference grid behind the dummy's head was used to aid in the digitizing process.

The main features of the RRT (Figure 3) consist of 1) a support framework, 2) a counter-balanced test platform with a pivot axle, 3) a free weight and drop tower assembly, and 4) a shock tower. The support framework was rigidily attached to the floor and braced to minimize any movement of the structure. The platform itself was constructed of 100 mm box beams mounted to a 50 mm axle at the pivot point. Both seat height and lateral positioning from the roll center could be adjusted as required.

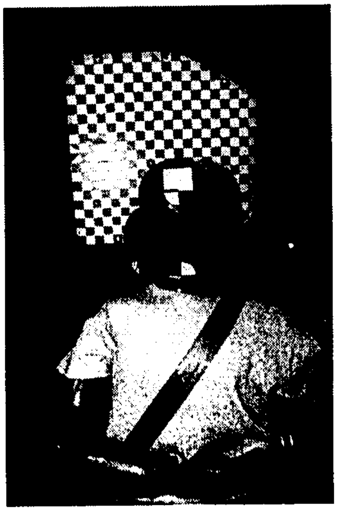
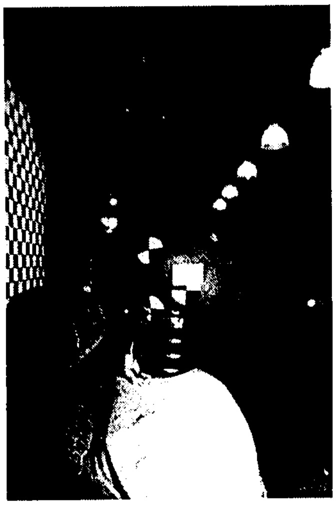
Figure 1. Dummy front view. Figure 2. Dummy side view.

The weight of the dummy and seat fixture was counter-balanced with the use of weights on the opposite wing of the platform. This design allowed the driving force of the free-weight to apply a constant acceleration pulse to the platform as it rotates 180° through the gravity field. Although the location of the center of rotation of the RRT could be somewhat different from that of an actual vehicle during rollover, this was considered a representative set-up which incorporated rollover forces and impact forces expected in a rollover collision.

Due to the relatively large lumped masses of the test components (ie. dummy, test seat, and related counter-balancing mass), the mass moment of inertia of the system was sensitive to the lateral positioning of the seat. Reducing the roll radius enhanced the velocity performance for a given drop weight, while reduction of the moment arm of the counter-balance mass significantly reduced loading stresses on the platform. For the testing reported in this paper, the seats were mounted such that the center of the seat was 610 mm from the pivot axis. This distance represented a fairly short radius of rotation typical of a compact or sub-compact vehicle.

The drop tower and free-weight system provided the motive force for the RRT (Figure 3). A cable attached to the suspended weight was routed through a system of pulleys and spooled around the large circular plate attached to the back of the platform. The radius of this circular plate provided the moment arm for the suspended weight to act upon in order to accelerate the platform. An array of 9 standard automotive piston shocks were used to catch and slow the free-weight at the end of the drop. The angular velocity (impact speed) for the RRT can be modified by varying the mass (force generating the acceleration) and/or the drop height (duration of the acceleration pulse) of the free-weight. In the current configuration, angular velocities of 180°/second up to 290°/second were generated with various combinations of drop height and drop weight.

The shock tower was used to simulate the impact of a vehicle's roof with the ground. The tower consisted of a height adjustable supporting framework housing two hydraulic shock absorbers manufactured by Enertrols Inc. The stiffness of these units were adjusted to simulate a range of roof structure

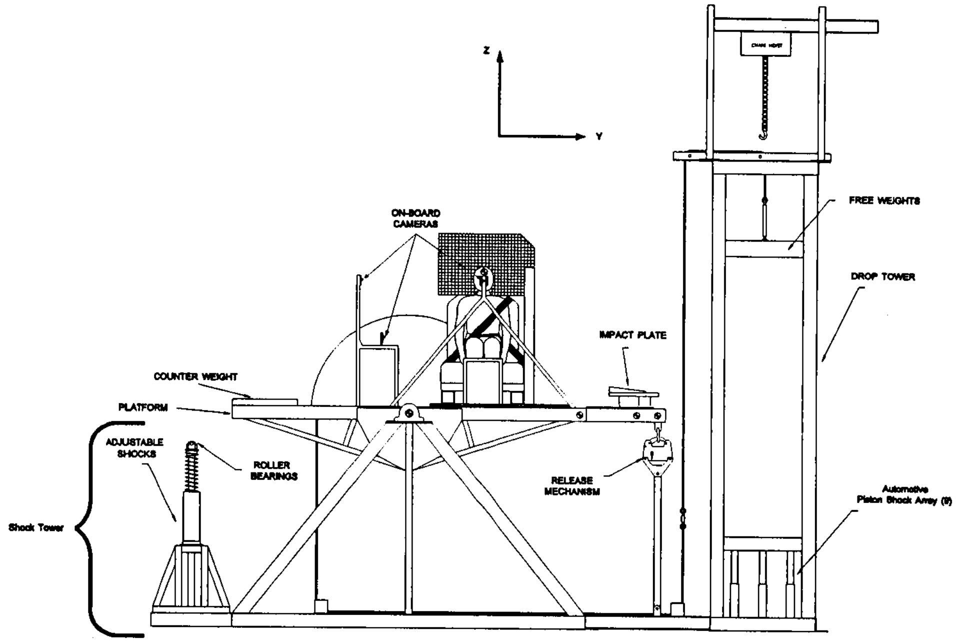
Z
Y
ON-BOARD CAMERAS
FREE WEIGHTS
DROP TOWER
IMPACT PLATE
COUNTER WEIGHT
PLATFORM
ADJUSTABLE SHOCKS
ROLLER BEARINGS
RELEASE MECHANISM
Automotive Piston Shock Array (9)
Shock Tower

Figure 3. Schematic of RRT fixture.

force/deflection (rigidity) characteristics. The unit was capable of a maximum displacement stroke of about 254 mm in its current configuration. The height adjustment of the shock tower allowed adjustment of the angle of impact and the degree of rotation before impact. Increasing the height of the tower decreased the degree of rotation before impact occurred and modified the angle or attitude of the dummy at which that impact occurred.

A checkerboard of 25 mm (1 inch) squares was used as a reference grid behind the dummy's head to help track dummy vertical and lateral excursion with the on-board cameras. There were three on-board cameras tracking the Y-Z plane head movement, X-Z plane head movement, and X-Z plane pelvic movement. The video recording was then used to digitize dummy vertical and lateral excursion. The Y- and Z- axes are shown in Figure 3. The positive X-axis iss normal out of the page. A 50th percentile H-III male dummy was used for all testing.

Restraint Characteristics

Two restraint systems were examined. One off-the-shelf system and one experimental design. An off-the-shelf lap and shoulder belt incorporating inertial reel locks and an adjustable D-ring was used as the baseline system. There were no energy management enhancements. This type of restraint is currently available in most makes and models of cars. The adjustable D-ring is becoming a popular enhancement to obtain a proper fit of the shoulder belt for varying sized occupants.

The experimental restraint was the Inflatable Tubular Torso Restraint (ITTR), developed by Simula Automotive Safety Devices, Inc. This device consisted of the integration of an inflatable section into the shoulder belt portion of a conventional three-point restraint system. The ITTR augmented a standard three-point seat-belt system to allow the shoulder-belt portion to inflate during impact. This increased the diameter and decreased the length, which not only cushions and protects the occupant, but pre-tensions the seat belt. The technology on which the ITTR was based includes a low permeable liner which allowed the unit to remain inflated for at least 7 seconds, and a braided cover which provided the shape change mechanism for the unit.

TEST MATRIX

The matrix of tests conducted with the aforementioned safety belt restraints is shown in Table 1.

Table 1.
Matrix of Tests

Seat Configuration	D-Ring Position	ITTR*	Reps
Lap and Shoulder	Upper		3
Lap and Shoulder	Mid		3
Lap and Shoulder	Lower		3
Lap and Shoulder	Upper	Yes	2
Lap and Shoulder	Lower	Yes	2

*Inflatable Tubular Torso Restraint (ITTR)

TEST INSTRUMENTATION

Systron-Donner roll rate sensors were mounted at the X, Y, and Z roll axis of the RRT platform. High g accelerometers were mounted along the X, Y, and Z coordinate axis using a standard triaxial mounting block. A 24 inch string potentiometer was attached to the pivot axis of the platform. As the platform rotated, the potentiometer string spooled onto a measured radius on the axis. A computer algorithm was then used to convert this measured linear output into an angle of rotation of the platform. An array of three 50,000 pound load cells were mounted to the impact plate. The total force of the impact was determined by the summation of the three individual load cell measurements. A 14 inch linear potentiometer was mounted to the adjustable shocks so that shock compression was measured during impact. Load cells were attached to the lap and shoulder belt to measure belt loads.

Dummy instrumentation included triaxial head, chest, and pelvic accelerometers, upper neck load cell, and triaxial angular roll rate sensors in the spine of the dummy.

Static Test Procedure

Pre-test static measurements of the dummy in the upright and upside down positions were made prior to each individual dynamic rollover test run. These measurements provided information on the belt slack in the restraint. The pre-test procedure for the static upside down measurements consisted of rotating the platform slowly, with the dummy in place on the seat, until the platform impact plate was in contact with the roller bearings atop the adjustable shock absorbers. While the dummy was completely upside down in this position, measurements of the static excursion in the X, Y and Z axis were recorded. Once the pre-test static measurements were made in the upside down condition, the RRT platform was rotated back, to the pre-test upright position of the dummy for the dynamic test.

Dynamic Test Procedure

The sequence of events for a typical dynamic test will now be described. The free-falling mass, which was housed in the drop tower, then began to descend which rotated the platform. The platform accelerated to within 7- 10° of actual impact with the shock tower, then the free-falling mass impacted the shock absorber array at the bottom of the shock tower. The platform coasted at constant angular velocity until impact with the shock tower. At impact, the angular velocity dropped sharply as the platform was decelerated by the impact into the shock tower. The "stiffness" or damping of the adjustable shocks determined force/deflection characteristics of the impact. A high stiffness setting resulted in less overall deflection simulating a more rigid roof while a lower setting simulated a softer or more compliant roof. For the tests conducted in this study a somewhat softer or less rigid roof structure was simulated. Typical displacements for the adjustable shock absorbers ranged from approximately 190 to 230 mm.

The event mark for this test was the initial contact of the impact plate with the roller bearings on the adjustable shocks at 180° of platform rotation. The system was configured to collect approximately two seconds of pre-event data and 0.8 seconds of post-event data to record the entire rollover event. Post-test pictures and static dummy head excursion off the seat were then measured. Video of the rollover event was captured for the head and pelvic area. These videos were digitized to obtain maximum excursion values and traces of the dummy head and pelvis in the X, Y and Z-axis.

RESTRAINT PERFORMANCE TEST RESULTS

Kinematics During Rollover Test

Dummy kinematics are dictated by the actions of gravitational and rotational forces. The dummy was initially sitting upright in a 1 g gravity field. As the platform rotates, the dummy's orientation in this gravity field also rotated with an increasingly larger force vector directed towards the center of rotation. Occupant loading or force due to gravity in the vertical (Z-axis) axis shifted from a positive 1 g to zero g's (at 90° rotation) to -1 g (at 180° rotation). As a result, the dummy moved inward (falls) toward the "interior" of the vehicle.

As angular velocity for the platform increased, the normal and tangential accelerations (rotational forces) created by the rotational motion began to increase adding force vectors to the gravitational force. The tangential acceleration for the dummy was aligned with the Z-axis of the platform and was a function of the dummy's distance from the center of rotation and the angular velocity of the platform. The normal acceleration causes a centripetal force outward from the center of rotation. As a result of this force, the dummy had a steadily increasing tendency (as angular velocity increased) to move outwards towards the "exterior" of the vehicle.

D-ring Adjustment of Baseline Restraint

The baseline lap and shoulder belt system was adjusted to three D-ring adjustment positions. The total span between the upper and lower adjustment was 95 mm. This adjustment was incorporated to determine the effect of D-ring adjustment on excursion. It was not intended as a recommendation on how much adjustment was necessary. Lap belt angle and length were held constant. Shoulder belt angle and length were changed as the D-ring was raised or lowered. Three tests were conducted for each D-ring adjustment position, for a total of nine tests.

The nine tests and their maximum roll rates, impact forces onto the adjustable shocks, and the adjustable shock deflections are shown in Table 2. Roll rate varied 3% for all nine tests. Impact force and shock deflection for the upper (952 mm) and lower (857 mm) D-ring adjustment position were within 2% of one another. Force and deflection were almost 10% different in the mid D-ring adjustment position when compared to the high and low position. As a result, the tests with the D-ring adjustment in the mid-position do not have the same impact conditions as the upper and lower D-ring adjustment position tests that could affect the comparison. Consequently, only the upper and lower D-ring adjustment positions were focused on in the analysis of the results.

X-, Y- and Z-direction head excursions for the baseline restraint is shown for all nine tests in Tables 3, 4, and 5, respectively. Static pre-test head excursion measurements, post-test and maximum dynamic head excursion are shown. Maximum dynamic head excursions were taken from digitized video, and are reported in the last column of each table. Each group of repeat tests were averaged and these averages used to make comparisons.

The post-test X- and Z-direction head excursion measurements were higher than the pre-test static excursion measurements. The dynamic loads stretched the restraints and allowed the dummy to have more post-test excursion. Post-test Y-direction head excursion was significantly less than the pre-test excursion measurement. The dynamic forces moved the dummy inboard more than the static test, but the dummy rebounded to the outboard side and came to rest at a position close to the original upright position.

The dynamic forces during the test caused the X-, Y- and Z-direction maximum head excursions to increase significantly over the static pre-test and post-test measurements. The greatest increase over the static measurement was in the X-direction. In the static rollover, gravitational forces do not act in the X-direction and most head movement was from the torso rotating back into the seat. The dynamic rollover however, caused a much higher rate of rotation of the torso back into the seat which caused the neck to bend

Table 2.
Platform Measurements for Baseline Tests with Adjustable D-ring

Test #	D-ring Position	D-ring Height above Platform (mm)	Roll Rate (deg/s)	Max. Impact Force (N)	Adjustable Shock Deflection (mm)
55	Upper	952	257	58669	238
56	Upper	952	256	58647	233
57	Upper	952	259	59443	267
Average			**257**	**58920**	**246**
48	Middle	914	260	56979	286
49	Middle	914	257	52526	278
50	Midle	914	260	50480	275
Average			**259**	**53329**	**280**
58	Lower	857	254	58358	276
59	Lower	857	258	65670	228
60	Lower	857	255	53109	265
Average			**256**	**59046**	**256**

Table 3.
Baseline Restraint X-axis Head Excursion

Test #	D-ring Position	Static Test (mm)	Dynamic Test (mm)	
			Post-Test	Maximum
55	Upper	64	57	133
56	Upper	67	73	148
57	Upper	60	73	153
Average		**64**	**68**	**145**
48	Mid	57	67	182
49	Mid	57	57	160
50	Mid	60	67	170
Average		**58**	**64**	**171**
58	Lower	57	98	223
59	Lower	64	83	155
60	Lower	60	102	175
Average		**60**	**94**	**184**

Table 4.
Baseline Restraint Y-axis Head Excursion

Test #	D-ring Position	Static Test (mm)	Dynamic Test (mm)	
			Post-Test	Maximum
55	Upper	117	19	182
56	Upper	124	35	187
57	Upper	127	48	203
Average		**123**	**34**	**191**
48	Mid	102	32	188
49	Mid	114	19	190
50	Mid	108	16	181
Average		**108**	**22**	**186**
58	Lower	98	57	203
59	Lower	105	32	236
60	Lower	127	64	226
Average		**110**	**51**	**222**

Table 5.
Baseline Restraint Z-axis Head Excursion

Test #	D-ring Position	Static Test (mm)	Dynamic Test (mm)	
			Post-Test	Maximum
55	Upper	51	143	146
56	Upper	48	133	131
57	Upper	51	98	119
Average		**50**	**125**	**132**
48	Mid	60	130	120
49	Mid	57	127	130
50	Mid	44	130	123
Average		**54**	**129**	**124**
58	Lower	76	140	154
59	Lower	64	127	147
60	Lower	57	114	130
Average		**66**	**127**	**144**

and increase head X-direction movement. Z-direction motion was also much higher in the dynamic test. In this case, dummy loading against the restraints was increased dynamically which allowed the dummy to come off the seat much more than in the static rollover.

D-ring adjustment position had a significant effect on the pre-test occupant excursions. The pre-test Z-direction static excursion increased 24% from the upper to lower D-ring adjustment position.

However, the post-test head excursion was similar for each D-ring adjustment position. Maximum dynamic Z-direction head excursions were within 20 mm for all three D-ring adjustment positions.

The X-, Y- and Z- direction maximum dynamic head excursion increased from the upper to lower D-ring adjustment position (when excluding the mid-position measurements). It appeared there was some adverse consequences to wearing the belt at its lowest position for the 50th percentile male dummy. The lower D-ring adjustment position allowed the shoulder belt to slide off the shoulder more easily during the rollover test. This resulted in the belt going from the top of the shoulder to in front of the shoulder and allowed the upper torso to push down on the shoulder restraint and rotate forward and side-to-side. When the restraint is in the upper position, it fits the 50th percentile shoulder better and stays over the shoulder, improving the restraint during the rollover. This result was counter-intuitive to the expected result. It was expected that the shorter belt length in the lower anchorage position would have less slack and result in less excursion. Additional testing with different sized dummies could verify the correlation between occupant size, D-ring adjustment position, and resulting occupant excursion.

Dynamic Comparison of Restraints Effectiveness

Using the same roll rate and adjustable shock stiffness, a series of tests with the ITTR were conducted at the upper and lower D-ring adjustment positions. Two tests were conducted for each test condition. The results of vertical head excursion from the dynamic tests with the ITTR are shown in Table 6, along with a comparison to the baseline results at the same D-ring adjustment positions. When the ITTR was inflated, the dummy was pushed into the seat 19 mm. Since the excursion measurements were made after the ITTR was inflated, the total excursion measured and recorded in Table 6 is 19mm more than the net vertical excursion from the nominal seating position.

The ITTR substantially reduced vertical excursion when compared to the baseline 3-point restraint. In the upper D-ring adjustment position, the vertical excursion was reduced from 132 mm to 32 mm on average. Similarly, when the D-ring was set to its lowest adjustment position, the vertical excursion was reduced from 144 mm to 53 mm on average. Vertical excursion was higher for both belt systems when the D-ring anchorage was in the lower position, particularly with the ITTR. Although, this was attributed to the belt fitting the shoulder of the 50th percentile male dummy better in the upper D-ring adjustment position, it may not be the reason for the same trend in the ITTR. The design of this experimental unit was such that the tension in the shoulder belt would be higher in the upper D-ring adjustment position. This resulted in a reduction in excursion. Consequently, a better shoulder belt fit was probably a contributing factor to reduced occupant excursion, but it most probably was not the only factor.

The tighter coupling of the occupant to the seat from the ITTR did not result in large increases in neck loads. Neck tension forces went down when comparing the ITTR to the 3-point baseline restraint, and were well below the 3300 N threshold for neck axial tension currently used in FMVSS No. 208. There was an increase in the neck shear load caused by the increased head acceleration when the torso was restricted during impact of the RRT platform. But, the shear loads were very small in comparison to possible injury thresholds.

Traces of X, Y, and Z-direction excursions for baseline and ITTR tests in the upper and lower D-ring adjustment position are shown in Figures 4 through 9. Figures 4 through 6 are traces of the results with the baseline restraint and ITTR in the upper D-ring adjustment position. Figures 7 through 9 are the corresponding plots to the tests with the lower D-ring adjustment position. Each graph shows all the tests conducted at that condition. As indicated by the overlay of the tests on the graphs, the dummy motion was highly repeatable for the conditions tested.

In the upper D-ring adjustment position, head X-direction excursion began about 0.6 seconds before the peak excursion with the baseline restraint (Figure 4). However, the ITTR restricted motion until impact with the shock tower. The ITTR also limited motion in the X-direction to approximately 80 mm, compared to 130 mm for the baseline restraint. Y-direction head motion represented the dummy moving side-to-side. The initial motion in the baseline restraint was negative

Table 6.
Baseline and ITTR Z-axis Head Excursion and Neck Loads

ITTR Results				
Test #	D-ring Position	Maximum Dynamic Vertical Excursion (mm)	Maximum Neck Tension (N)	Maximum Neck Shear [x-force] (N)
51	Upper	37	1810	572
52	Upper	27	1724	534
Average		**32**	**1767**	**553**
53	Lower	42	1888	588
54	Lower	64	1834	536
Average		**53**	**1861**	**562**
Baseline Results (Averages)				
55,56,57	Upper	132	2147	434
58,59,60	Lower	144	2144	407

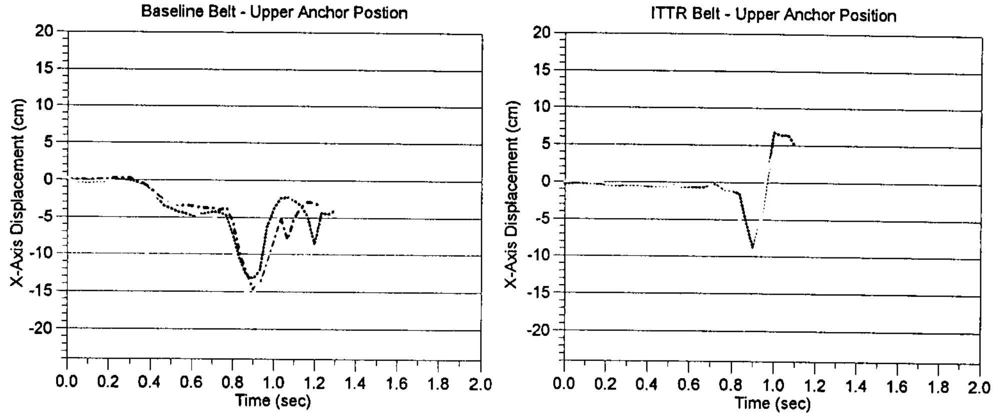

Figure 4. X-axis excursion in upper d-ring adjustment position.

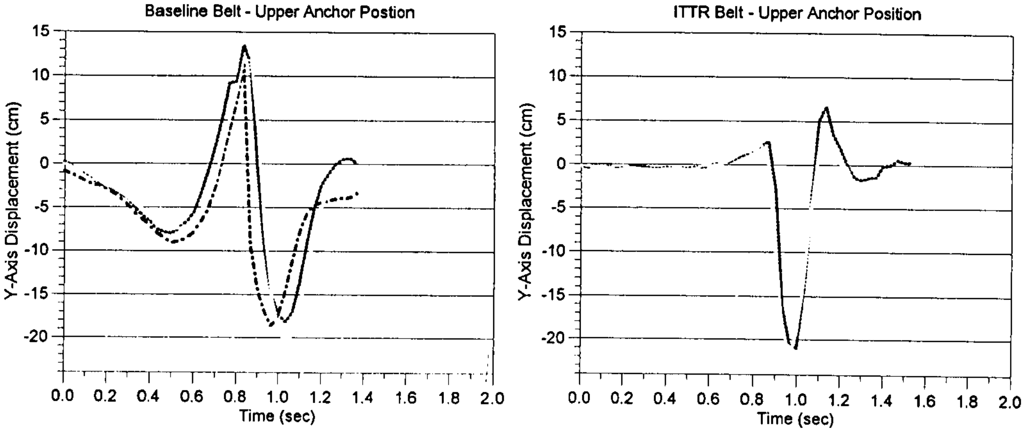

Figure 5. Y-axis excursion in upper d-ring adjustment position.

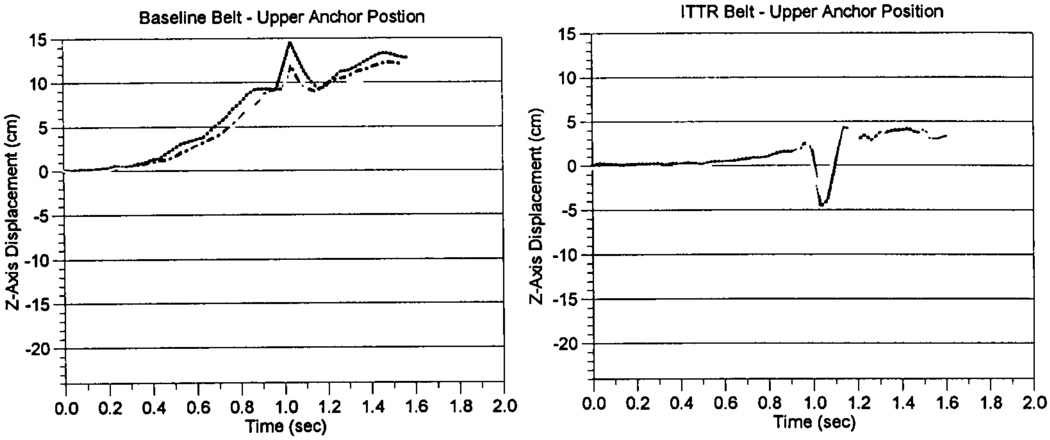

Figure 6. Z-axis excursion in upper d-ring adjustment position.

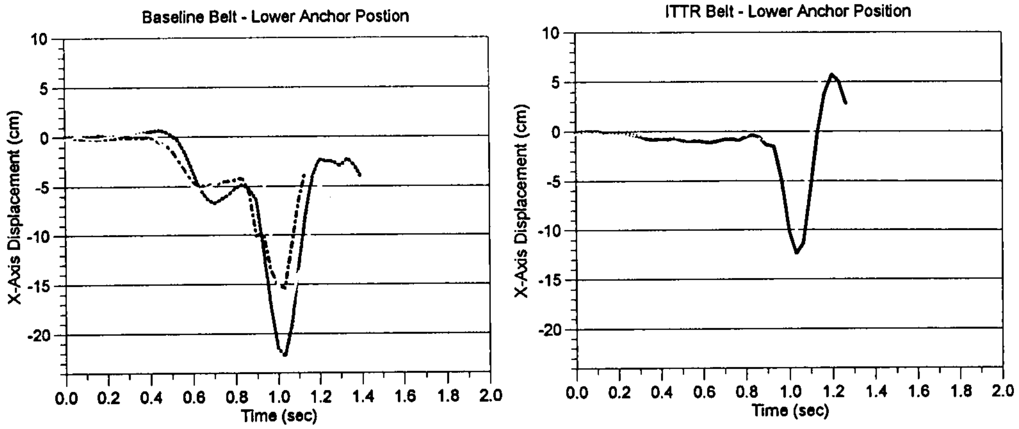

Figure 7. X-axis excursion in lower d-ring adjustment position.

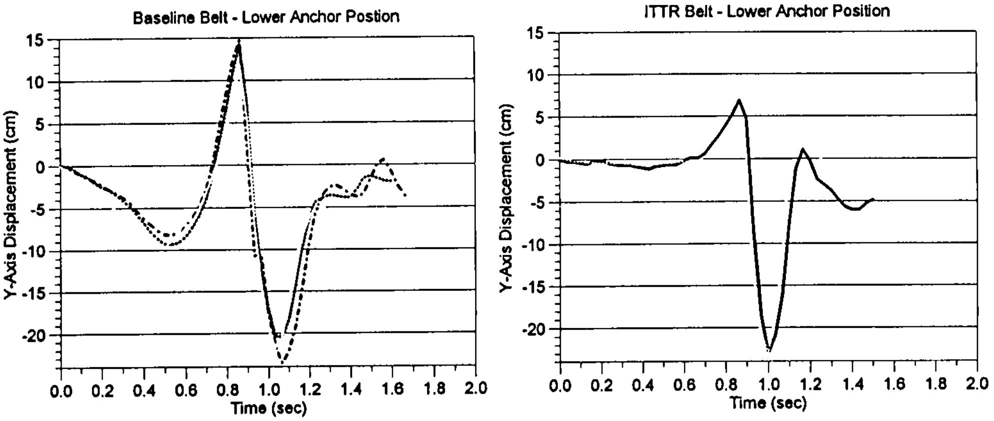

Figure 8. Y-axis excursion in lower d-ring adjustment position.

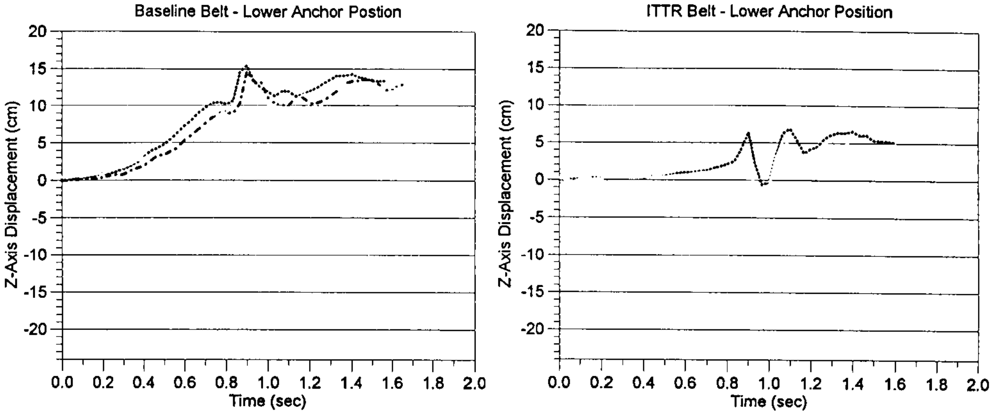

Figure 9. Z-axis excursion in lower d-ring adjustment position.

which means the dummy moved inboard as the platform rotated (Figure 5). As the platform rotated beyond 90° of rotation, the rotational forces began pulling the dummy outboard and a sharp peak occurred (0.9 seconds). At the same time, the platform impacted the shock tower and the platform decelerated. The dummy momentum continued in the same path and moved to the inboard side against the restraint. The ITTR again effectively restricted motion up to the impact with the shock tower at 180° of rotation. However, the maximum inboard motion was as severe as the baseline restraint after impact with the shock tower.

Vertical head excursion was measured in the Z-direction and results are shown in Figure 6 for the lower D-ring adjustment position. Maximum excursion was greatly reduced (as shown in Table 6) using the ITTR. When looking at the excursion trace (Figure 6) a sudden dip in vertical excursion after the initial peak is shown. This was attributable to the side-to-side motion which effectively reduced the vertical head excursion.

Head excursion in the lower D-ring adjustment position were qualitatively similar to those in the upper D-ring adjustment position. The baseline restraint and ITTR had lower excursion numbers in the upper D-ring adjustment position for all three directions. As discussed with the tabular data, this change in excursion is attributable to the shoulder belt height and angle change as the anchorage is raised or lowered. The angle on the shoulder and height on the shoulder determine how well it holds the upper torso in position. In this case, the upper or mid D-ring adjustment position was most effective in preventing head excursion.

SUMMARY AND CONCLUSIONS

A test program was conducted to determine the effectiveness of D-ring adjustment and an improved restraining device on preventing occupant excursion in a rollover crash. A typical 3-point lap and shoulder belt system and an inflatable tubular torso restraint (ITTR) were tested in a rollover restraints tester (RRT). Each restraint was placed on a 50th percentile male dummy and testing conducted at a single roll rate with varying D-ring adjustment positions. Each test simulated what was approximately a 260° per second rollover with the roof impacting the ground after 180° of roll. Occupant excursion and dummy injury measurements were recorded. Two or three tests were conducted under each condition. The following conclusions were drawn from this study:

1. 1The maximum dynamic vertical head excursion was almost three times the static dummy vertical excursion measurements made with the dummy upside down in the restraint.

2. The fit of the shoulder belt (D-ring adjustment position) on the 50th percentile male appeared to affect occupant excursion in dynamic testing. Raising the D-ring decreased the dummy head X-, Y- and Z-direction excursion in both restraints.

3. The ITTR effectively restrained the Z-direction (vertical) and X-direction excursion of the dummy. A reduction of approximately 60 to 75 percent was realized when compared to the baseline 3-point restraint. Y-direction excursion was not reduced from the baseline results.

Consequently, in this limited series of tests, it appears that occupant excursion can be reduced in rollover crashes with appropriate countermeasures, such as the ITTR. Reduced excursion would help prevent partial ejection and impact with vehicle interior components. The potential of holding the occupant upright in the seat while the roof collapses into the survival space, may be a negative consequence of such a system. However, it is expected that improved roof crush resistence would also be an integral part of the rollover crashworthiness of a vehicle, in conjunction with an improved restraint system.

FUTURE WORK

Additional testing is planned to address questions raised in this study. Testing with the 5th percentile female and 95th percentile male would aid in determining the role that the D-ring adjustment has in improving occupant restraint. It appears that D-ring adjustment could be an important factor in determining the effectiveness of restraints in preventing excursion in rollovers. Additional testing is also planned to examine a stiffer impact to determine how sensitive occupant motion is to roof stiffness.

REFERENCES

4. Traffic Safety Facts 1996 - Occupant Protection. National Center for Statistics & Analysis, 400 seventh street, S.W., Washington D.C.

5. Rains, Glen and Joseph Kanianthra. "Determination of the Significance of Roof Crush on Head and Neck Injury to Passenger Vehicle Occupants in Rollover Crashes," SAE 950655, Warrendale PA, 15096-0001.

6. Arndt et al. "Evaluation of Experimental Restraints in Rollover Conditions," SAE 952712, Warrendale PA, 15096-0001.

7. Arndt et al. "The development of a Method for Determining Effective Slack in Motor Vehicle Restraint Systems for Rollover Protection," SAE 970781, Warrendale PA, 15096-0001.

8. Cooper et al. "Head Excursion of Seat Belted Cadaver, Volunteers and Hybrid III ATD in an Dynamic/Static Rollover Fixture , SAE 973347, Warrendale PA, 15096-0001.

9. Summers, Stephen, Glen Rains, and Don Willke, "Current Research in Rollover and Occupant Retention", 15th International ESV Conference Proceedings, Melbourne Australia, p 760-765.

Technical Session 9

Biomechanics - Dummy Development and Computer Modeling

Chairperson: Keith Seyer, Federal Office of Road Safety, Australia

DESIGN AND DEVELOPMENT OF AN ADVANCED LOWER EXTREMITY: ALEX II

Alena V. Hagedorn
Transportation Research Center Inc.
Howard B. Pritz
National Highway Traffic Safety Administration
Michael S. Beebe
Applied Safety Technology Corporation
United States
Paper Number 98-S9-O-01

INTRODUCTION

ALEX II represents the second generation Advanced Lower Extremity which began with the National Highway Safety Traffic Administration's (NHTSA) original version (ALEX I, hereafter referred to as ALEX) several years ago. Current efforts have been undertaken in order to make design improvements in the ALEX leg. Many of the aspects of the original ALEX have been maintained, but additional biomechanics specifications for the foot and ankle have since become available and have thus been integrated into the new ALEX II design.

The most significant aspect of the new ALEX II design lies in its flexibility to achieve any desired torque-angle ankle characteristic with relative ease. This means that as future biomechanics data regarding ankle response continues to become available, the ankle can be easily "tuned" to the desired response. This is significant since the ALEX II will not require full redesign should future data provide, or future researchers require, a different ankle response characteristic. This paper emphasizes the flexibility of the ALEX II design in this respect. The importance of the ALEX II design lies in the *technique* used to achieve ankle moment-angle response, rather than the *actual* moment-angle characteristic responses achieved, since specifications for the ankle response may well change in the future.

DESIGN REQUIREMENTS

Design specifications were determined from biomechanics data collected primarily at Renault and/or the University of Virginia. A detailed explanation of the data collection techniques and determination of these specifications are given in Crandall, et al., (1) and Portier, et al., (2). Results of the study conducted by Crandall et al., indicated that the ankle response in both flexion and inversion/eversion modes from both volunteer and cadaver subjects was continuous, with steadily increasing moment as angle increased. Figure 1 (Portier (2)) displays the continuous ankle response from cadavers and various dummy legs. This continuous specification was not reflected in any current foot/ankle designs as Figure 1 illustrates. In the ALEX II therefore, this phenomenon was treated with particular importance and, along with *flexibility* for tuning the ankle response, became the primary focus of the ankle design process.

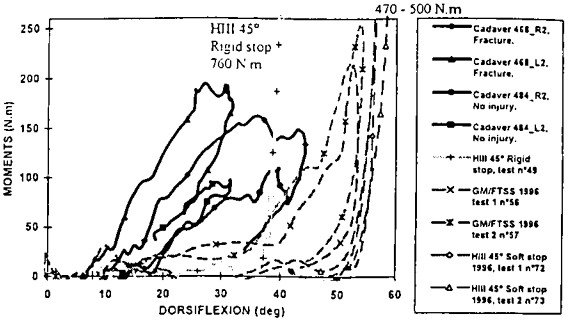

Figure 1. Dynamic dorsiflexion response using Renault impact setup for cadavers and various dummy legs (Portier et al. (2)).

Range of Motion

Many features of the original ALEX were maintained in the new ALEX II design. These include ankle rotation measurement at the ankle about the x (inversion/eversion) and y (plantarflexion/dorsiflexion) axes. In addition, the ALEX II is capable of measuring rotation about the z axis (internal/external rotation). Further, ALEX II offers a more biofidelic range of motion than ALEX in nearly all of these aspects (Table 1). Like ALEX, ALEX II utilizes separate axes for plantarflexion/dorsiflexion and inversion/eversion movement.

Table 1.
Range of motion comparison between ALEX and ALEX II

Range of Motion	Original ALEX	ALEX II	ALEX II Critical Moments at Max Angle ROM
Plantarflexion	38°	55°	25 Nm
Dorsiflexion	43°	45°	140 - 325 Nm
Inversion	19°	32.5°	27 Nm
Eversion	19°	32.5°	29 Nm
Internal Rotation	Not Available	22.5°	Not Available
External Rotation	Not Available	22.5°	Not Available

Achilles Tendon

In addition to the continuous moment-angle requirement of the ALEX II, an "Achilles tendon" element was incorporated into the design. The purpose of the Achilles element was to more realistically represent the compression forces in the tibia. Also, recent research into the importance of the Achilles tendon indicates that the tendon is capable of generating high forces during a panic braking scenario (Manning (3)). Although the ALEX II Achilles tendon was designed utilizing passive data, active tendon response might then be simulated in future studies with the ALEX II by pre-loading the brake pedal utilizing the Achilles.

Center of Rotation Heights

The centers of rotation for flexion, as well as inversion/eversion as recommended by Crandall et al.(1) is given in Table 2. The pivot location for the ALEX II was based on these findings.

Table 2.
Center of Rotation Heights from the Bottom of the Foot (Crandall (1))

Center of Rotation	Joint Height (mm)
Dorsiflexion Plantarflexion	76 +/- 8
Inversion Eversion	71 +/- 12

Center of Pressure and Foot Compression

ALEX II incorporates biofidelic center of pressure and foot compression characteristics as specified in the 45° Hybrid III foot. The ALEX II has an increased distance (compared to ALEX I) from the center of ankle to heel distance. The distance was increased from 19.0 mm to 28.2 mm (anatomic average was 28.2 +/- 6.35mm). This recommendation to increase center of ankle to heel distance from 19.0 mm to 28.2 mm was based on pressure point of the heel using pressure sensitive FUJI film paper on six volunteers (Crandall (1)). The ankle to heel distance of 28 +/- 6 mm is also currently specified for the Hybrid III 45° foot. The ALEX II design also has the 28 mm ankle to heel distance.

The center of pressure location at the ball of the foot for the new Hybrid III 45° foot was determined as 123 +/- 6 mm from the ball of the foot to the ankle joint. The ALEX II design also incorporates a distance of 123 +/- 6 mm from the ball of the foot to the ankle joint.

Dorsiflexion Characteristics

The dorsiflexion requirement (Figure 2) was derived (Kuppa (4)) from data collected by Portier, et al. (2) from dynamic cadaver test data. As stated previously, Figure 1 illustrates the continuous response characteristic of the ankle which became the primary focus of the design study. It should be noted that the test setup used by Renault to collect the data in Figure 1 utilized a spring-damper linear impactor system. In addition, the cadaver was supine with femur extended vertically and tibia horizontal for the impacts. This

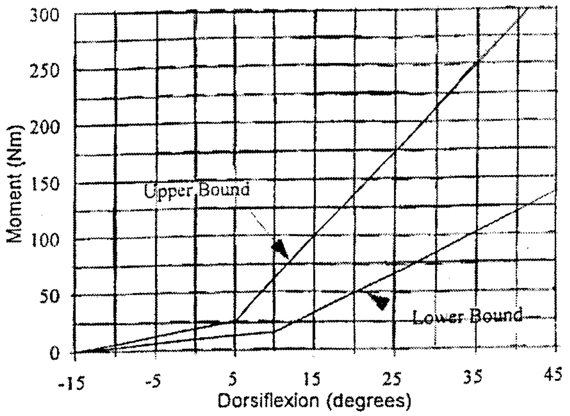

Figure 2. Dynamic moment-angle characteristic specification corridor (Kuppa (4)) for ALEX II leg based on Renault (Portier (2)) cadaver data seen in Figure 1.

meant that the impact at the ball of the foot created not only a dorsiflexion response at the ankle, but also rotation at the knee and hip joints. These corridors are specific to the particular test setup at Renault and comparisons pertain *only* in similar test conditions.

Plantarflexion Characteristics

Quasi-static tests were conducted by Paranteau (5) to determine the moment angle characteristics of the ankle joint using human cadaver lower legs excised at the distal tibia-fibula. There was no passive response from musculature in these tests since the muscles of the anterior crural compartment (which resist plantarflexion) had been severed. Therefore, the moment angle curves represent only the response at the ankle joint.

UVA conducted quasi-static volunteer tests to determine plantarflexion moment-angle curves. The test setup was the same as that used for the volunteer dorsiflexion tests. The volunteers were told to relax their muscles during the test. This data shows much higher rotational stiffness in plantarflexion than Paranteau's data. This could be due to passive and active muscle response of the volunteers in the UVA tests. UVA tests do suggest that there is zero moment up to 25° of plantarflexion. The design specifications for ALEX II shown in Figure 3 for plantarflexion utilize Paranteau's test data with a zero level up to 25°.

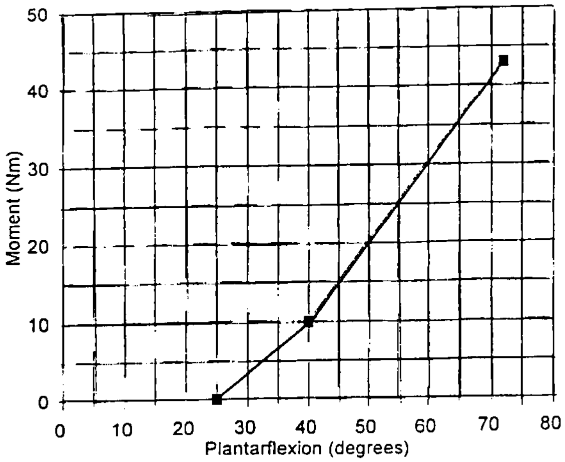

Figure 3. Joint response in plantarflexion design specification for the ALEX II utilizing Paranteau (5) data.

Inversion Characteristics

Quasi-static moment-angle responses in inversion were obtained from tests conducted at Renault using cadaveric subjects. Figure 4 (Crandall (1)) shows quasi-static inversion data from cadaveric subjects from which the target specification for ALEX II was derived (Figure 5).

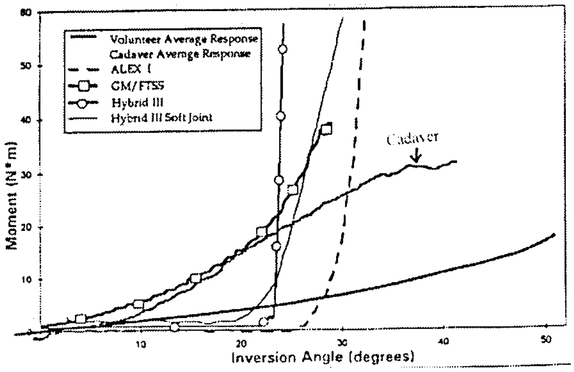

Figure 4. Quasi-static average moment-angle responses from volunteers, cadavers, and various dummy legs in inversion (Crandall (1)).

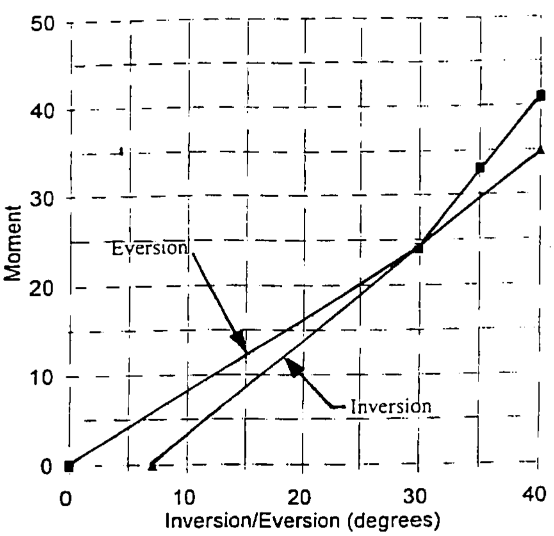

Figure 5. Quasi-static moment-angle specifications for the ALEX II leg in inversion and eversion.

Eversion Characteristics

Quasi-static moment-angle responses in eversion were obtained from tests conducted at Renault using cadaveric subjects and at UVA using volunteers (Figure 6, Crandall(1)). The results from both labs are very similar. The moment-angle curve in eversion from UVA was used for the ALEX II design (Figure 5).

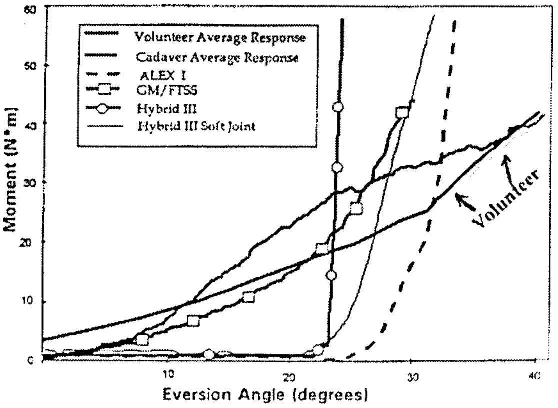

Figure 6. Quasi-static average moment-angle responses from volunteers, cadavers, and various dummy legs in eversion (Crandall (1)).

IMPLEMENTATION DESIGN

Figures 7 and 8 show the design of the ALEX II and illustrate the various features implemented in the ALEX II leg. The location of ALEX II sensors are noted in the figures. Figure 9 is a photograph of the leg. The ALEX II leg is capable of measuring 22 channels of data. These measurements are shown in Table 3. The ALEX II total weight was 5.29 kg. Subassembly weights are given in Table 4.

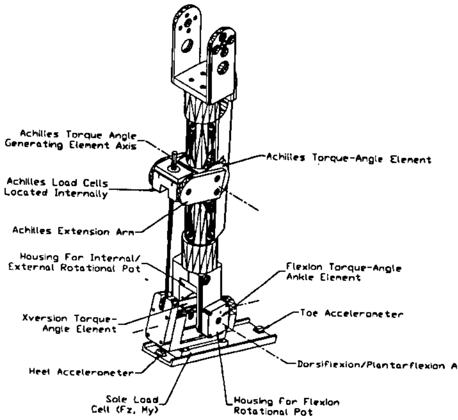
Achilles Torque Angle Generating Element Axis
Achilles Torque-Angle Element
Achilles Load Cells Located Internally
Achilles Extension Arm
Housing For Internal/ External Rotational Pot
Flexion Torque-Angle Ankle Element
Xversion Torque-Angle Element
Toe Accelerometer
Dorsiflexion/Plantarflexion Axis
Heel Accelerometer
Sole Load Cell (Fz, My)
Housing For Flexion Rotational Pot

Figure 7. ALEX II leg (oblique view) shown with Achilles tendon and various features.

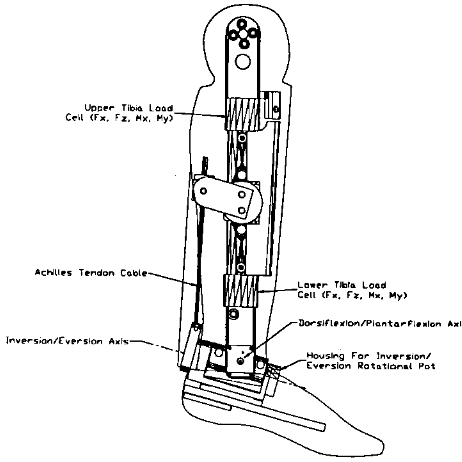
Upper Tibia Load Cell (Fx, Fz, Mx, My)
Achilles Tendon Cable
Lower Tibia Load Cell (Fx, Fz, Mx, My)
Dorsiflexion/Plantarflexion Axis
Inversion/Eversion Axis
Housing For Inversion/ Eversion Rotational Pot

Figure 8. ALEX II leg (side view) shown with Achilles tendon and various features.

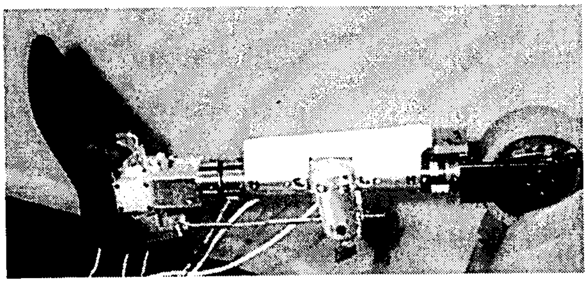

Figure 9. Photo of ALEX II.

Table 3.
ALEX II data channels.

ALEX II Area of Measurement	**Measurement (Ang = Angle, F = Force, M = Moment, A = Acceleration)**
Ankle	Ang_x Ang_y Ang_z
Femur	F_x F_y F_z M_x M_y M_z
Upper Tibia	F_x F_z M_x M_y
Lower Tibia	F_x F_z M_x M_y
Toe	A_z
Heel	A_z
Achilles Tendon	F_z
Sole of Foot*	F_z M_y

* Not yet available. Provisions are made in the design to include these load cells upon availability.

Table 4.
Weight characteristics of the ALEX II leg

Component	**Weight (kg)**
Lower leg including foot	3.99
Foot only	1.24
Total lower leg weight	5.23

The proximal and distal ends of the tibia for the original ALEX, as well as Hybrid III, provided axial and shear loads at an angle to the anatomical axis. Therefore, the ALEX II design implements a straight tibia shaft with the location of the knee and ankle attachments moved accordingly. In the current Hybrid III leg, a compressive force introduces a moment due to angles at the proximal and distal ends of the tibia. A straight tibia would eliminate these moment artifacts. The ALEX II design incorporates an oblong shaped and tapered tibia bone in order to place the anterior tibia bone in the same position as the Hybrid III relative to the anterior tibia flesh while eliminating the angles at the proximal and distal ends of the tibia shaft. The Hybrid III knee casting design was maintained since the knee slider mechanism has been recently improved by Applied Safety Technology Corporation (ASTC (6)) with a ball slider mechanism, currently available for the Hybrid III.

The ALEX II design allows ankle rotation and measurement about all 3 axes (X, Y, and Z) and includes more biofidelic ranges of motion and stops (Table 1). Bumpers with characteristics similar to the Hybrid III ankle bumpers are utilized at the joint stops to prevent metal-to-metal contact. The ankle angles are critical measurements since the ankle design is specified by a moment-angle characteristic. It is therefore not only necessary to determine moment characteristics, but also at *what angle* these moments occur. The rotation measurements are made by three Tocos (7) (model GF12)) rotary potentiometers. These devices are small potentiometers which are installed on the ALEX II heel (X rotation measurement), at the medial malleolus (Y rotation measurement), and distal to the lower tibia load cell (Z rotation) (Figures 7 and 8).

The ankle rotation was achieved by a separate axes joint design with orthogonal axes. The moment-angle specification for the ankle indicates continuous loading with increasing resistance for all ankle motions (Figure 1). The mechanism which achieves this response is described below. The ALEX II was designed with the flexibility to permit *any* desired moment angle characteristic to be achieved, should these specifications be revised in the future as new data becomes available.

Continuous Torque

Ankle Joints - Various methods were investigated to achieve the required torque-angle characteristics of the design specifications. Since the specifications required a continuous torque-angle response with a progressively increasing torque, an isolation damper device was utilized. The design began with an off-the-shelf isolation damper manufactured by Rosta Company (8) which could then be easily modified to meet *any* desired torque-angle characteristic. This particular type of damper assembly is commonly used on small cars and trailers outside the United States as a vibration dampening suspension mount. This device (shown schematically in Figure 10) consists of a rigid external housing into which four cylindrical rubber elements and a square center shaft are inserted. When the center shaft is rotated, the cylindrical elements compress and generate a continuous torque-angle response. The rubber elements can easily be "tuned" in a number of ways to elicit any desired torque-angle response. For example, changing the length of the rubber cylinder elements, the durometer or type of rubber, the shape of the elements, or shape of the center shaft all affect the response. Therefore, this method of generating the desired specification is appealing since the ankle can be "tuned" as desired as new biomechanics data becomes available.

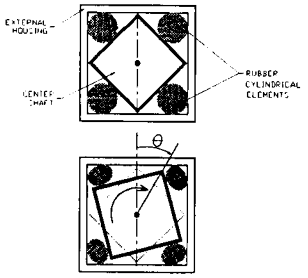

Figure 10. Cross section of torque-angle element (Rosta (8)) used in ALEX II ankle and Achilles tendon. Top Figure illustrates zero torque-angle. Bottom Figure shows compression of rubber elements to generate torque when a rotation is applied to the center shaft.

Figure 11 shows various torque-angle elements which were "tuned" to exhibit several responses by changing the length of the rubber cylindrical elements. These curves illustrate the ability of the design to achieve any number of desired responses by changing the rubber elements. The design is extremely flexible in that respect.

The torque-angle method described above was utilized at both the ankle and the Achilles tendon. For the ankle, two torque-angle elements were positioned perpendicularly (Figures 7 and 8) for generating the desired responses in both dorsiflexion/plantarflexion and inversion/eversion modes. At the ankle, the center shaft of the torque-angle element was rotated at a 15° initial position in plantarflexion to simulate the "natural" position of the foot, the point at which torque on the ankle is zero.

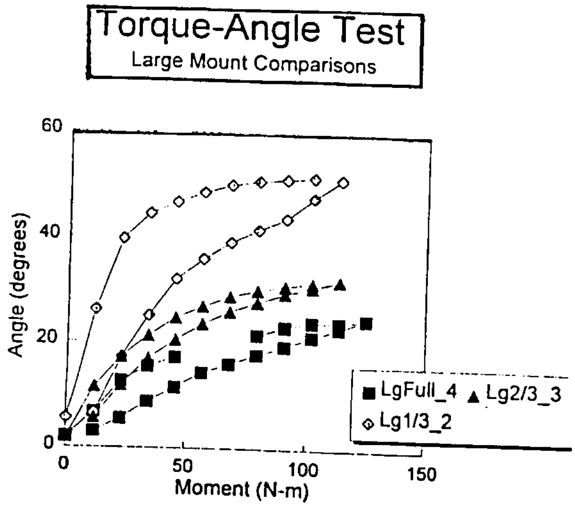

Figure 11. Moment-angle responses of several modified isolation damper elements. Devices were modified by varying the length of the rubber cylindrical elements seen in Figure 10. Responses indicate the flexibility of the design to easily achieve any desired moment-angle characteristic.

Figure 12 shows results from a dynamic test with the moment generating element installed in the ALEX II leg at the Achilles tendon and at the ankle. The corridors shown represent design corridors based on data collected by Portier et.al. (2). However, these design corridors were derived from the Renault test setup described by Portier et.al. (2) which utilized a spring-damper linear impactor system. In addition, the cadaver was supine with femur extended vertically and tibia horizontal for the impacts. This meant that the impact at the ball of the foot created not only a dorsiflexion response at the ankle, but also rotation at the knee and hip joints.

Since it was not possible to achieve the same test setup and test the ALEX II leg in that particular configuration prior to publication of this paper, another type of dynamic test was conducted. In that setup (Figure 13) the ALEX II tibia was rigidly mounted in a horizontal position proximal to the upper tibia load cell (no knee and hip were utilized). A linear pendulum with a representation of a pedal was initially positioned against the ball of the foot. The foot was then impacted from rest to achieve a dorsiflexion response. Since the two test configurations differ, the corridors cannot be *directly* applied to this impact test. However, these results *do* illustrate the ability of the ALEX II to perform dynamically. Since the ALEX II design is extremely flexible with respect to the moment

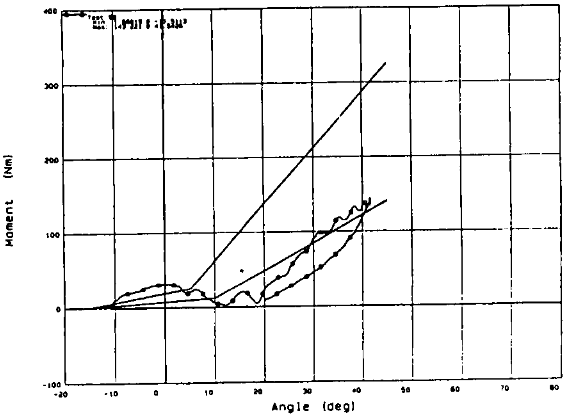

Figure 12. Dynamic dorsiflexion response of the ALEX II achieved from the rigidly mounted tibia test setup. Design corridors indicate the Renault test specification corridor (Figure 2). Although the two tests differ in setup and the corridor cannot be *directly* compared to the data, the rigid-mount test provides an indication of the ability of the ALEX II leg to perform dynamically.

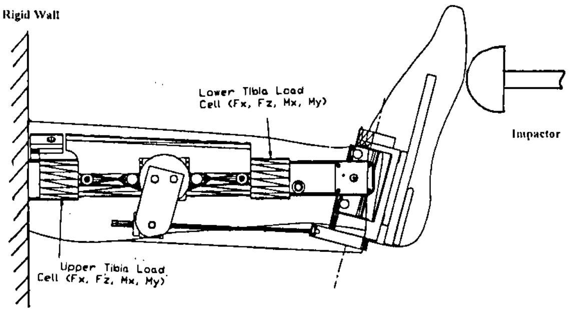
Rigid Wall
Lower Tibia Load Cell (Fx, Fz, Mx, My)
Impactor
Upper Tibia Load Cell (Fx, Fz, Mx, My)

Figure 13. Setup for dynamically testing the ALEX II in dorsiflexion by rigidly mounting the tibia. Results for this type of test are indicated in Figure 12.

generating device in the ankle, the ALEX II can be easily "tuned" to fall within the corridor shown in Figures 2 and 12 when the Renault test setup is eventually available for test; at that time, a *direct* comparison can be made between ALEX II response and design specifications.

Inversion/eversion torque-angle response was generated quasi-statically, rather than dynamically, by the perpendicular torque-angle element at the ankle only, without influence of the Achilles tendon cable. The ALEX II results for inversion/eversion are illustrated in Figure 14. Since the moment generating element for inversion/eversion for the ALEX II is symmetrical, these results represent *both* inversion and

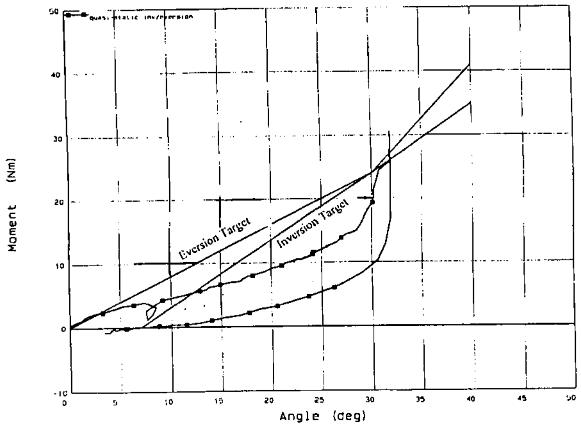

Figure 14. Quasi-static inversion/eversion results for the ALEX II compared to target specifications. ALEX II responds the same in inversion and eversion due to symmetry of the joint.

eversion response. Again, the ALEX II design could very simply be "tuned" by modifying the size, shape or stiffness of the rubber cylindrical elements (Figure 10) should the current ALEX II response need to be adjusted.

Achilles Tendon - Early versions of the ALEX II had the full moment response built entirely into the ankle joint. However, for more realistic Fz loads, this was later changed to incorporate a tendon and the torque at the ankle joint was softened. Choice as to the presence of the Achilles or incorporating the moment characteristics entirely into the ankle depends on the accuracy of tibia compression loads desired, since the Achilles tendon increases such loads and changes moment in the tibia. Since the Tibia Index calculation utilizes the resultant moment and compressive (Fz) force, the Tibia Index calculation would require revision due to the presence of the Achilles tendon. At a system level however, the response of the foot and ankle would be the same; the stiffness between the foot and leg remains unchanged in either of the two design configurations, with or without an Achilles tendon.

The current ALEX II has been designed with an "Achilles tendon" element. This element consists of a steel cable (7x19, 3mm diameter) with swedge welds at each end. An "eyebolt-like" element was swedge-welded to the distal end of the Achilles cable; the cable was attached to heel with a bolt through this hole. This prevents the tendon from binding during flexion events. The proximal end contains a threaded portion to allow for lengthening or shortening the Achilles tendon so that the initial position of the foot can be changed if desired. The Achilles cable was approximately 20 cm in length. It was attached to the tibia approximately 20.8 cm distal to the center of rotation of the knee joint (21 cm proximal to the center of rotation of the dorsiflexion axis). A Sensotec (9) "button" load cell (model LFH-7I/280-10) was utilized to measure Achilles tendon forces.

The torque-angle method described above was also utilized at the Achilles tendon. For the Achilles tendon, a torque-angle element was inserted into the tibia near the upper portion of the tibia shaft below the lower tibia load cell (Figures 7 and 8). In order to generate torque-angle from the Achilles cable, a small extension "arm" attached to the center shaft of the torque-angle element was utilized. The proximal end of the Achilles cable was fixed to the end of the arm while the distal end of the cable was attached to the back of the heel. The resulting design allowed the cable to rotate the torque-generating element thus placing the cable in tension during dorsiflexion and generating an increasing resistance. In addition to torque generated through the Achilles element, moment was also produced at the ankle joint as explained above. Conversely, during plantarflexion, the Achilles cable remained slack and torque was generated only by the torque-angle element at the ankle joint.

CONCLUSIONS

ALEX II Design Summary

The following is a summary of the major features incorporated into the ALEX II design.

- Ankle rotation and measurement about all 3 axes (X, Y, and Z)
- More biofidelic ranges of motion and stops:
    - 45° dorsiflexion
    - 55° plantarflexion
    - 32.5° inversion
    - 32.5° eversion
    - 22.5° internal rotation
    - 22.5° external rotation
- Continuous loading with increasing resistance for all ankle motions
- Separate joints with orthogonal axes
- Optional "Achilles tendon" element
- Ankle height for dorsiflexion/plantarflexion: 76 +/- 8mm from bottom of foot
- Ankle height for inversion/eversion: 71 +/- 12mm from bottom of foot
- Ankle to heel distance: 28 mm
- Ankle to ball of foot distance: 123 mm
- Weight of lower leg including foot: 5.23 kg
- Weight of foot: 1.24 kg
- Weight of tibia (lower leg, excluding foot): 3.99 kg
- Utilize current (Hybrid III 45° foot) center of pressure and foot compression data in foot design
- Removal of proximal and distal tibia angles so that tibia load cells are on the center line between the knee and ankle pivots
- Ball knee slider

ALEX II Data Channel Summary

The ALEX II leg design utilizes the following data channels:

- Femur forces and moments
- Upper and lower tibia forces and moments (Fx, Mx, My, Fz)
- Ankle angle for all three axes
- Toe and Heel acceleration (z)
- "Achilles tendon" load
- Provisions for a load cell to measure force and moment of the sole of the foot (Fz, My)

SUMMARY

The ALEX II foot and ankle represents the next generation Advanced Lower Extremity. It incorporates various new design aspects based on newly obtained biomechanics data. Among the most significant changes in the design is the inclusion of an Achilles tendon device. In addition, major efforts in the design process were focused on the implementation of a continuous moment-angle response device at both the ankle joint and Achilles tendon element. These elements have been shown to be easily tuned and have been designed to give any desired response characteristics in plantarflexion/dorsiflexion and inversion/eversion. The technique utilized to achieve the continuous torque-angle characteristic of the ankle was emphasized, rather than adherence of the results to specific design corridors. This aspect of the design means that the ALEX II can be easily modified to achieve *any* desired response as future data becomes available. Further development of the ALEX II leg would include fine "tuning"the responses for current and future biomechanics data. This would entail validation of the dorsiflexion response in a Renault-type fixture which was utilized for specification of the dorsiflexion ankle response. Additional future studies might also entail the possibility of utilizing the Achilles tendon element to simulate active braking.

REFERENCES

1. Crandall, J.R., Portier, L., Petit, P., Hall, G.W., Bass, C.R., Klopp, G.S., Hurwitz, S., Pilkey, W.d., Trosseille, X., Tarriere, C., and Lassau, J.P., "Biomechanical Response and Physical Properties of the Leg, Foot, and Ankle," Proceedings of the 40th Stapp Car Crash Conference, Paper #962424, 1996.
2. Portier, L., Petit, P.,Domont, A.,Trosseille, X., Le Coz, J.Y., Tarriere, C.,and Lassau, J.P., "Dynamic Biomechanical Dorsiflexion Responses and Tolerances of the Ankle Joint Complex,"Proceedings of the 41st Stapp Car Crash Conference, Paper #973330, 1997.
3. Manning, P., Wallace, A., Roberts, A.K., Owen, C.J., and Lowne, R.W., "The Position and Movement of the Foot in Emergency Manoeuvres and the Influence of Tension in the Achilles Tendon," Proceedings of the 41st Stapp Car Crash Conference, Paper# 973329, 1997.
4. Kuppa, Shashi, Conrad Technologies Inc., Washington, D.C. per personal communication.
5. Parenteau, C.S., and Viano, D.C., "A New Method to Determine the Biomechanical Properties of Human and Dummy Joints," IRCOBI, 1995.
6. Applied Safety Technology Corporation (ASTC), Milan, OH.
7. Tocos America Inc., Schaumburg, IL.
8. Rosta Company, Switzerland.
9. Sensotec Inc., Columbus, OH.

OPTIMISATION OF VEHICLE PASSIVE SAFETY FOR OCCUPANTS WITH VARYING ANTHROPOMETRY

R. Happee, R. van Haaster
TNO Crash-Safety Research Centre
The Netherlands
L. Michaelsen, R. Hoffmann
EASi Engineering GmbH
Germany
Paper Number 98-S9-O-03

ABSTRACT

A method has been developed to generate models representing subjects of varying anthropometry. This method has been applied to crash-dummy models, and will in the future also be applied to human body models. The first step of the method is to generate a set of target anthropometry parameters from a relevant population. The second step is to scale an existing model towards the desired anthropometry. Different scaling factors are being applied for the different body parts and dimensions. These factors are used to derive body dimensions, mass and inertia properties, joint resistance and contact resistance parameters. For this study on adult subjects it has been assumed that material properties are invariant with subject size. Quasi-static simulations were performed to confirm that the resulting stiffness of complete body parts obey the scaling rules applied to the model components.

The design of a vehicle has been evaluated with respect to passive safety for a wide range of occupant sizes. Starting point was a set of validated frontal impact simulations including Hybrid III dummies. These simulations were repeated with occupant models of varying size and weight. The model setup for the frontal impact simulation was similar the model used in the study of Michaelsen, 1997. The frontal impact simulations have shown a wide range of results for the different types of occupant. Due to different seat positions and body proportions the injury parameters exceed the range of results found for standard dummies.

INTRODUCTION

In the area of vehicle crash-safety design limited attention is being paid to variations of body size. For adults, current regulations only prescribe testing with dummies representing a "50th percentile male". For frontal impact two other versions are available of the Hybrid III dummy (Mertz et al., 1989). These dummies represent respectively a small female (5th percentile) and a large male (95th percentile). A small female dummy for side impact has recently been introduced (Daniel et al., 1995). Due to the time and cost involved in design and production of new physical dummies the number of available dummy sizes will remain limited. The current dummy sizes do represent variations in length but do not cover variations in corpulence and other body proportions. Mathematical human body models developed for ergonomic design do describe such variations in body proportions (Fig 1).

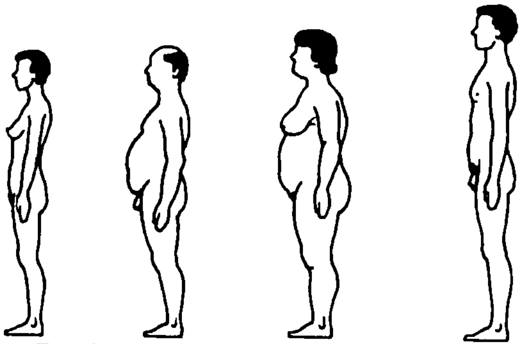

Fig. 1. Variability in Bodyproportion and -height (Pictures from Flügel, 1986)

These models are based on extensive anthropometric measurements on various populations (e.g. Flügel, 1986; Geuß, 1984; Ramsis, 1998). The current paper describes a method to generate models representing subjects of varying anthropometry. Crash dummy models with varying body size and body proportions are generated using scaling techniques. These models are used to evaluate occupant protection in frontal impact.

METHODS

Occupant model scaling

A method has been developed to generate models representing subjects of varying anthropometry (MADYMO, 1998). This method has been applied to crash-dummy models, and will in the future also be applied to human body models. The first step of the method is to generate a set of target anthropometry parameters from a relevant population. The second step is to scale an existing model towards the desired anthropometry.

Scaling procedures have been used widely in the field of crash safety. The design of the Hybrid III small female and large male dummies is partly based on scaling (Mertz et al. 1989). Available biofidelity requirements for adults have been used to estimate requirements for children. Scaling was applied for the design of the TNO P1½ dummy (see Thunnissen et al., 1994), the TNO Q3 dummy (van Ratingen, 1997), and child Hybrid III and CRABI dummies (Irwin and Mertz, 1997).

Scaling is relatively simple if all length dimensions scale with the same factor. Such simple scaling is called *geometric scaling*. In our study a more advanced scaling method is applied. Different scaling factors are specified for x, y, and z dimensions. Furthermore different scaling factors are applied for different body parts. Thus the model geometry can be adapted freely to the desired anthropometry parameters.

Input for the scaling is a set of target anthropometry parameters (see Table 1). The corresponding parameters have also been evaluated for the standard models which are to be scaled. Initial scaling factors are simply derived as the ratio of target length divided by standard length. Thus various scaling factors are derived for different body parts and for x, y and z dimensions. The resulting scaling factors are then applied to the standard model. Finally the mass and the main dimensions of the resulting model are checked. The mass is only an indirect result of the scaling process and therefore normally deviates slightly from the specifications. Therefore a second phase of the scaling, the so-called correction is performed. The model is simulated repeatedly to optimise the prediction of mass, erect standing height, seated height and shoulder width. In this correction phase only the geometry scaling factors are optimised. No variation of the assumed body tissue density is performed. The orientations of the segments will not be changed, which means that the models will have the same (initial) posture as the standard model, used as starting-point.

Table 1. Anthropometry parameters used for generation of scaled dummy models.

Anthropomety parameter	Remarks
weight	
standing height	without shoes
seated height	
head length	
head breadth	
head to chin height	
neck circumference	derived using ramsis skin points
shoulder breadth	
chest depth	
chest breadth	
waist depth	derived using ramsis skin points
waist breadth	derived using ramsis skin points
buttock depth	derived using ramsis skin points
hip breadth,standing	
shoulder to elbow length	
forearm-hand length	
knee height,seated	without shoes
ankle height,outside	without shoes
foot breadth	without shoes

In addition to the geometry, all other model parameters are scaled, so there is scaling of:

- Geometry
- Sensor locations
- Reference length for the V*C criterion
- Mass and Moments of Inertia
- All joint characteristics (stiffness, friction, damping and hysteresis)
- Ellipsoids and contact characteristics
- All other force models

The scaling rules applied are largely equivalent to those used for scaling and normalization (Mertz et al. 1989, van Ratingen, 1997, Irwin and Mertz, 1997). Here it should be noted that we applied scaling to model parameters where others mostly scale "response corridors" (see Thunnissen et al., 1994 for discussion). Scaling is performed assuming that material properties are invariant with subject size. Biomechanically this seems to be an acceptable approach for adult subjects. For scaling towards children, or to simulate elderly persons the variation of material properties should be included. The assumption of equal density leads to analytical scaling rules for mass, centre of gravity and rotational inertia. For the scaling of stiffness and damping the assumption of identical material parameters leads to simple scaling rules. For instance when scaling the force deflection behaviour of an ellipsoid, deflection scales with the representative length and force scales with surface and thereby with length to the second power. Quasi-static simulations were performed to confirm that the resulting stiffness of complete body parts obey the scaling rules applied to the parameters of model components.

Occupant population

Models were generated representing typologies from the Ramsis anthropometric database (Flügel, 1986; Geuß, 1984; Ramsis, 1998). Table 2 lists the selected options. The parameter *proportion* describes the relative length of torso and legs. All models were based on the 1984 German population, age group 18-70 year. The selected occupant population is summarized in Table 3. Here models number 0-12 represent standard typologies whereas numbers 13 and 14 represent extreme body sizes generated with the Ramsis Body Builder (Ramsis, 1998). For the extreme male models a maximal length has been obtained by defining 99th percentile for age group 18-29 year in reference year 2010. Maximal corpulence was selected as 99th percentile. For the extreme females a minimal length was obtained by defining 1th percentile for age group 18-70 year in reference year 1984. For the population from Table 2, target anthropometric parameters from Table 1 were generated. Most of these parameters were standard output, but some parameters had to be reconstructed using "skin point" positions in the default posture. These parameters were applied to scale the dummy models. For all male models the 50th percentile male Hybrid III model was scaled whereas for all female models the 5th percentile female model was scaled. For a number of scaled dummy models the geometry was verified by comparison to the Ramsis skin and joint positions. Figure 2 illustrates that for the external dimensions a generally good correspondence was obtained but the dummy models have a somewhat reduced shoulder height.

Table 2. Standard typologies selected for model generation.

parameter	selected options		
gender	male	female	
length (standing)	very short	medium	very tall
corpulence	slim waist	medium waist	large waist
proportion	short torso	medium torso	long torso

Table 3. Population defined.

number	length	corpulence/ waist	torso	length [m]		mass [kg]	
				male	female	male	female
0	medium	medium	medium	1.7425	1.6227	75.697	62.575
1	v.short	slim	short	1.6264	1.5249	54.959	48.036
2	v.short	slim	long	1.6049	1.5213	57.645	48.082
3	medium	slim	short	1.75	1.6337	62.82	54.002
4	medium	slim	long	1.737	1.6123	64.129	53.932
5	v.tall	slim	short	1.8713	1.7302	70.491	60.011
6	v.tall	slim	long	1.8472	1.7149	71.643	59.951
7	v.short	large	short	1.6272	1.5251	81.46	71.788
8	v.short	large	long	1.6131	1.515	83.392	73.861
9	medium	large	short	1.7515	1.627	89.125	76.929
10	medium	large	long	1.7256	1.6124	89.371	77.695
11	v.tall	large	short	1.8551	1.7277	92.415	80.704
12	v.tall	large	long	1.8557	1.7186	94.828	81.813
13m	xx.tall	medium	medium	1.98	---	89.003	---
14m	xx.tall	xx.large	medium	1.98	---	102.769	---
13f	xx.short	medium	medium	---	1.4774	---	55.513
14f	xx.short	slim	medium	---	1.478	---	41.681
standard MADYMO Hybrid III dummy models							
P5	v. small				1.52		48
P50	medium			1.72		77	
P95	v. tall			1.85		101	

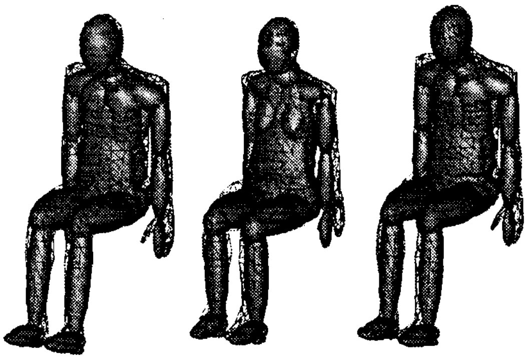

Fig. 2. Comparison of scaled dummy models (ellipsoids) to Ramsis surface (mesh).

FRONTAL IMPACT SIMULATION

Simulation model setup

The frontal impact simulations were done with MADYMO V5.2. The driver side model represents an European middle class car. The restraint system contains a driver airbag of 60ltr. and a belt with a retractor loadlimiter (loadlevel: 4kN). The simulation model was also equipped with a deformable steering column (loadlevel: 5kN, max. deformation: 80mm).

The airbag was optimized for an unbelted 50th%ile Hybrid III Dummy in a FMVSS 208 crashtest. The frontal impact simulations were done with belted occupants. The occupants were positioned in such a way, that they could reach the pedals and the steering wheel. The pelvis angle was set to 25°. Due to the different body sizes the H-point positions of the scaled dummies differ up to 280mm.

For the frontal impact simulations the following 3 different crashpulses were used:

- NCAP
- Offset 55km/h
- 50km/h 0°

Fig. 3 shows the very small/thick and the very tall/slim male occupant in the carmodel.

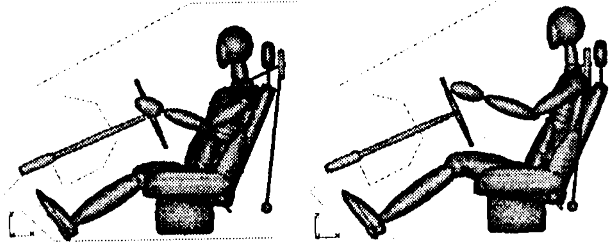

Fig. 3. Very small/thick/long torso male (left) and very tall/slim/long torso male occupant (right)

Occupant simulation results

The following consideration of the simulation results focusses on the stiff (NCAP), medium (50km/h 0°), and smooth (Offset 55km/h) crashpulse.

The kinematics of a very tall/slim male occupant with long torso is shown in Fig. 4.

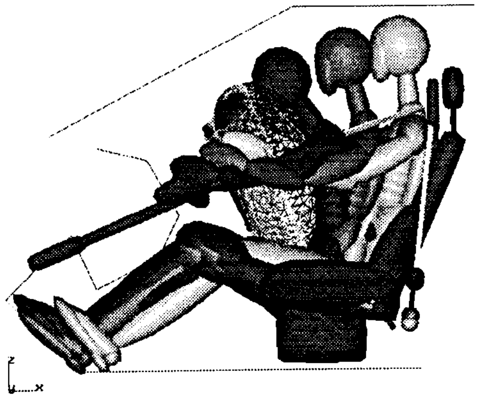

Fig. 4. Kinematics of a very tall/slim/long torso male occupant (time states: 0, 60, 80, 120ms)

The injury parameters of the occupant simulation have shown a large bandwidth of results. The following figures show the deviation of the injury parameters in percent relative to the 50th%ile male Hybrid III model. That means, that the results of the 50th%ile male are set to 0% deviation. The results of the three standard dummies are marked with little boxes in the following figures.

Fig. 5 shows the 3ms-head acceleration versus the H-Point position relative to the vehicle for the NCAP-Crashpulse. The results of the scaled dummies exceed the bandwidth of the three standard dummies results. Some higher 3ms-head accelerations (>60%) are caused by contact between head and upper steering rim. This occurs for large occupants, where the head moves over the airbag and impacts on the steering rim. The extreme small/slim occupants are sitting very close to the steering wheel, which causes „mild OOP“ for the NCAP crashpulse. Apparently identical H-Point positions can cause a wide range of results.

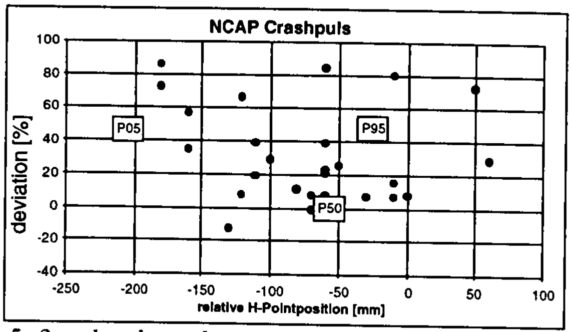

Fig. 5. 3ms-head acceleration against the relative H-Point-position for the NCAP crashpulse

The same observations for the range of results can be made for the 3ms-chest acceleration (Fig. 6) and the chest deflection (Fig. 7). Here the chest deflection is given relative to a scaled reference length representing chest depth.

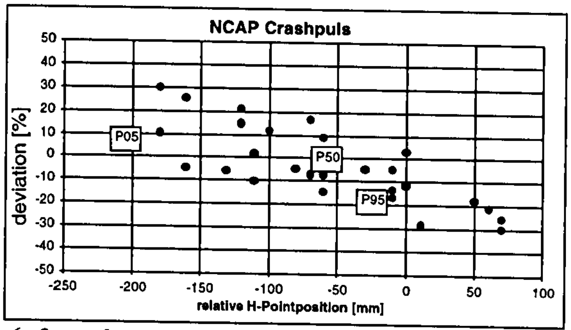

Fig. 6. 3ms-chest acceleration against the relative H-Point-position for the NCAP crashpulse

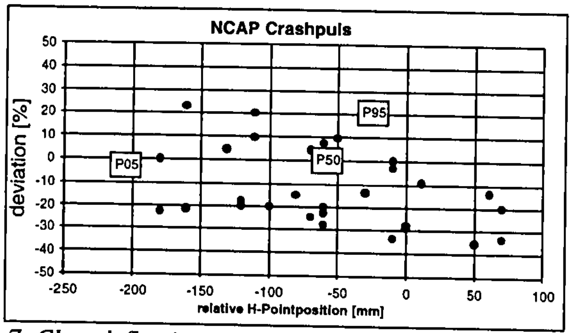

Fig. 7. Chestdeflection against the relative H-Point-position for the NCAP crashpulse

The relationship between the 3ms-chest acceleration and the weight of the occupant can be seen in Fig. 8. The higher weight causes a lower chest acceleration for the NCAP crashpulse.

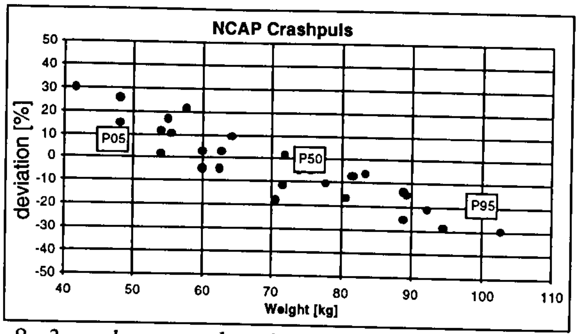

Fig. 8. 3ms-chest acceleration against the weight for the NCAP crashpulse

The other crashpulses have shown similar results as for the NCAP crashpulse. The following figures show the 3ms-chest acceleration for the Offset 55km/h (Fig. 9) and the 50km/h 0° crashpulse (Fig. 10).

Fig. 9 shows the „smooth" Crashpulse (Offset 55km/h), where the 3ms-chest acceleration hardly correlates with body weight. This is due to the smaller influence of the airbag in this crash type. The belt takes most of the occupant energy in this case.

The results for the „medium" crashpulse in Fig. 10 also show a strong correlation between the 3ms-chest acceleration and the weight of the occupants.

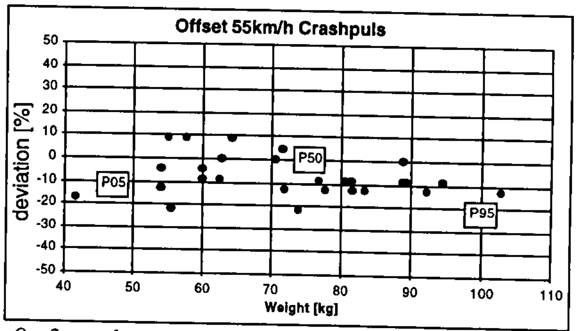

Fig. 9. 3ms-chest acceleration against the weight for the Offset 55km/h crashpulse

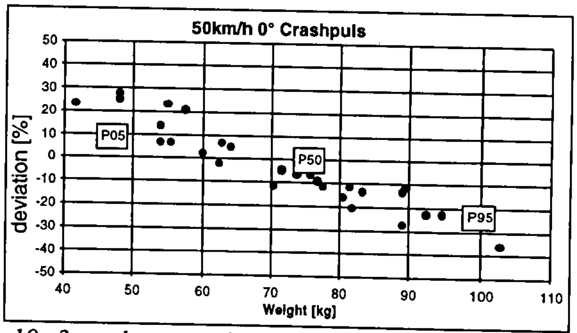

Fig. 10. 3ms-chest acceleration against the weight for the 50km/h 0° crashpulse

DISCUSSION

Scaleable crash-dummy models can be used for the design of safer vehicles and restraint systems. With such models the safety of vehicles can be evaluated for subjects with an anthropometry not represented by available dummies. This is relevant, in particular for the design of "smart restraint systems". For accident reconstructions it is considered important to have a model that describes the anthropometry of the subject involved with sufficient accuracy. In many cases the size and weight of accident subjects deviates considerably from any available dummy. Here sometimes models with an extreme anthropometry are required.

The scaled dummy models are based on scaling methods similar to those used in the design of small and large dummies. We thereby feel that the scaled models have a biofidelity comparable to these small and large dummies. A next step will be to apply the scaling methods for human body modelling. Only a validation on biological specimens of varying anthropometry can really validate such scaling methods. Here it is expected that for the simulation of children or elderly persons variation of properties of biological tissues will have to be considered.

The frontal impact simulations with the new scaled dummy models have shown, that the current standard dummies (5th%ile, 50th%ile, 95th%ile) provide only a limited representation of the real world occupant population. The range of results for the scaled dummies is significantly larger than for the standard dummies. This is partly due to the variation of corpulence and proportion (torso/leg length) which is not considered with standard dummies. This is also partly due to the larger range considered for length and mass. The population studied includes body masses of 42-103 kg where Hybrid III dummies range from 48-101 kg. The population studied includes lengths ranging from 1.48-1.98 m where Hybrid III ranges from 1.52 to only 1.85 m (see Table 1). The results also have shown, that the injury parameters could be largely different for occupants on the same seat position. This has to be taken into account for the development of adaptive restraint systems.

The robustness of restraint systems can be evaluated and improved with the scaled dummy models. The current simulation models have CPU of only 3 minutes on a SGI Origin200 workstation. This made it feasible to analyze 34 occupant sizes for different crash conditions in a limited time. A next step will be to *optimize* a design for different occupants sizes. Here it is presumably recommended to optimize a somewhat more limited population and number of crash conditions.

REFERENCES

Daniel et al. (1995). Technical specifications of the SID-IIs Dummy. SAE paper 952735.

Flügel B., Greil H., Sommer K. (1986). Anthropologischer Atlas: Alters- und Geschlechtsvariabilität des Menschen: Grundlagen und Daten.

Geuβ H. (1994). Entwicklung eines anthropometrischen Meβsystems für das CAD-Menschmodel Ramsis. PhD thesis, München University.

Irwin, A.L., Mertz H.J. (1997). Biomechanical bases for the Crabi and Hybrid III child dummies. SAE 973317, STAPP-1997.

MADYMO (1998). MADYMO scaleable dummy databases, version 5.3.1.

Mertz H.J., Irwin A.L., Melvin J.W., Stalnaker R.L., Beebe M.S. (1989). Size weight and biomechanical impact response requirements for adult size small female and large male dummies. SAE-890756.

Michaelsen L. and Hoffmann R. (1997). Real world development of adaptive restraint systems through the use of anthropometrically scaled occupant simulation models. (in German). VDI Berichte 1354. Tagung Berlin 30-31 Oct. 1997.

Ratingen M.R., Twisk D., Schrooten M., Beusenberg M.C., Barnes A., Platten G., (1997). Biomechanically based design and performance targets for a 3-year old child crash dummy for frontal and side impact. SAE 973316. Child Occupant Protection Symposium 1997.

Ramsis (1998). Body Builder Users Guide version 1.1, Tecmath human modelling, Kaiserslautern, Germany.

Thunnissen, J.G.M., Happee R., Eummelen P., Beusenberg M.C. (1994). "Scaling of adult to Child Responses applied to the thorax", IRCOBI Conference, Lyon, September 21-23, 1994.

DEVELOPMENT AND APPLICATION OF A SIDE AIRBAG COMPUTER MODEL USING THE CVS/ATB MULTI-BODY DYNAMICS PROGRAM

Edwin Sieveka
Jeff Crandall
Stefan Duma
Walter Pilkey
University of Virginia
Paper Number 98-S9-O-05

ABSTRACT

A new computer model for studying side airbag and occupant interactions was developed for the CVS/ATB multi-body dynamics program. This model employs standard CVS/ATB segment ellipsoids to represent the airbag. Bag stiffness is represented by a standard force vs. penetration contact function, however, the CVS/ATB program code was modified to allow the stiffness function to be multiplied by an additional, time dependent scaling function. This permits simple simulation of bag inflation and deflation without direct modeling of hydrodynamic bag parameters. The 5th and 50th percentile occupant models were originally obtained from the GEBOD program. These models were modified to incorporate clavicle segments. The additional shoulder freedom, permitted by extensive clavicle motion, results in significant kinematic differences between H3-type dummies and cadavers when performing side airbag tests. In the computer simulations, dummy cases are represented with a locked clavicle joint, while for cadaver cases the clavicle is permitted to move relative to the torso. This model has been exercised for a variety of potential occupant seating positions and has proven effective in distinguishing differences in load and kinematics. This in turn has helped guide the choices made for laboratory experiments such that testing efficiency is maximized.

INTRODUCTION

As part of the University of Virginia's Automobile Safety Laboratory (ASL) study of Honda side-impact airbags, models were developed for use in the CVS/ATB multi-body dynamics program. In contrast to other recent modeling efforts which make extensive use of finite elements [1,2], the models described in this paper are multi-body only and run on current Pentium PCs in one or two minutes. These models, of 5th percentile female and 50th percentile male occupants in various positions, were used to efficiently obtain qualitative information about the kinematics that could result from each airbag interaction, as well as to estimate the relative load levels expected in the occupant's arm. This information was helpful in refining the laboratory test matrix to achieve greater efficiency and cost-effectiveness by identifying the worst cases. Computer runs were performed to show the effects of occupant size, position, and clavicle flexibility. The latter distinguished between the response anticipated for Hybrid III dummies versus relaxed humans. Most of the runs simulated the laboratory's static deployment configuration, but several runs were also made which exercised the model in a full-motion, door-intrusion event. All simulations were made with an airbag that approximated Honda's medium-energy bag.

MODEL DESCRIPTION

Occupant Compartment Dimensions

The occupant compartment in the CVS/ATB model was constructed with measurements from a drawing of the seat and airbag system supplied by Honda, and from direct measurements of a 1997 Honda Accord. The seat drawing was used to position the airbag correctly relative to the seat and to size the airbag accurately. The Accord measurements were used to ensure that the seat was properly positioned relative to the inside and the top of the door, and relative to the arm-rest. The oblique and side views of the final model geometry, including a 5th percentile female occupant, are shown in Fig. 1.

Airbag Model

The CVS/ATB airbag model was adapted from an earlier driver-bag model [3]. The bag geometry was approximated by a combination of 5 CVS/ATB ellipsoids, comprising a primary bag and 4 secondary bags. The initial position and shape is shown in Fig. 1. To simulate inflation, the bag begins behind the seat and is forced along a track (slip-joint) by a forcing function that is based on the pressure time-history from Honda tests and from the observation of a high-speed film of a bag deployment test. The time-history curve is shown in Fig. 2.

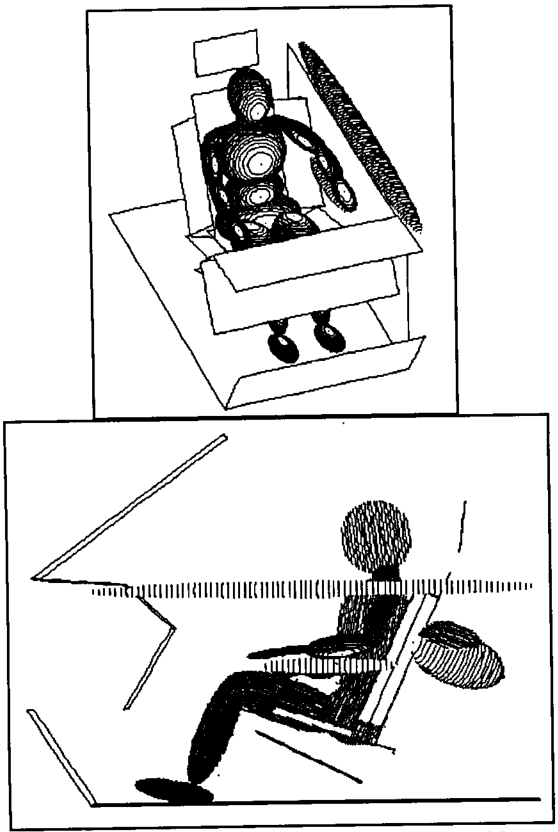

Figure 1. Model geometry: oblique and side views.

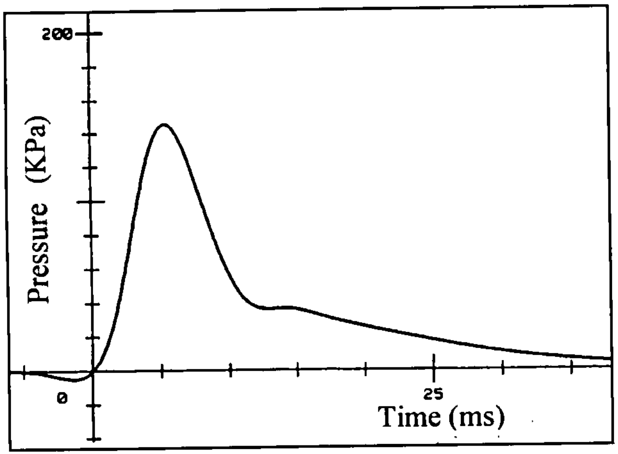

Figure 2. Bag pressure time-history.

The forcing function was modeled as a 1/4 sine from the moment of punchout (at about 5 ms) until 10 ms. In this short time interval, the bag is almost totally deployed; hence, in the model, the bag must move from behind the seat to its deployed position (about 32 cm) in about 5 ms. This combination of time, travel distance, and force function shape, along with the weight of the bag, allows the peak magnitude of the force function to be determined.

For a 1/4 sine wave impulse of duration T, the maximum acceleration, A, versus the distance traveled, D, is given by:

$$A = (\pi^2 * D) / (4 * T^2) .$$

If D=32 cm and T=.005 sec, then

$$A = 3.158 * 10^6 \text{ cm/sec}^2 \text{ or } 3222 \text{ G's} .$$

For the airbag, which weighs about 1.25 N, the peak force required is 4028 N. In tuning the model, a maximum force closer to 5000 N was needed to compensate for the loss of energy associated with the door impact.

A stiff spring, which is initially slack, defines the end of the track and stops the deployment of the bag. Equilibrium between this spring and the post-deployment forcing function keeps the bag in position. The slip-joint connecting the primary bag to the track also allows rotational motion via a superposed ball-joint. This permits the bag to rotate as it encounters the door and to assume the correct post-deployment orientation.

The four secondary bags are deployed in a slightly different manner. Each is connected to the primary bag by a pair of springs. One spring is initially slack and functions as the stop, or tether, spring. The other spring is pre-loaded and drives the deployment. The slip-joints connecting the primary and secondary bags are initially locked at a value just above the pre-load value in the deployment spring. The forcing function in this case is used as a trigger to unlock the slip joints. After that, the secondary bags move out from the primary bag until equilibrium is reached between the deployment spring and the tether spring. This method ensures that a force applied to one of the secondary bags is transmitted to the whole bag system. If external forcing functions were used to deploy the secondary bags, there would be no load transmitted to the primary bag when the secondary bags were loaded. The fully-deployed bag shape is shown in Fig. 3.

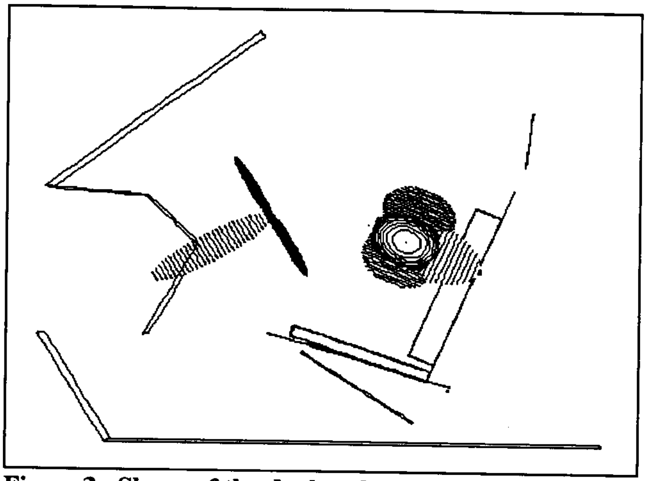

Figure 3. Shape of the deployed airbag.

The actual bag stiffness as seen by the occupant's arm has been estimated by tuning the arm reaction to that observed in test films. The interaction forces between the bag and the door were inferred in this manner also.

Near the end of this phase of the project, UVA's version of CVS/ATB was modified to permit the deflation of the airbag to be approximated. This involved changing the program code so that any force/deformation function can be multiplied by a time-dependent scaling function. In this way, the force/deformation function used for airbag stiffness could be made to soften with time. This was needed in order to obtain more realistic results for simulations involving intrusion. These simulations involve extended contact between the occupant and the airbag, and using an airbag that did not deflate caused the forces loading the occupant to be over-predicted. Intrusion study results are described in detail in a later section.

Occupant Arm Model

The left arm in the occupant models was enhanced to provide an estimate of the loads experienced at the centers of the upper arm and forearm segments. These segments were each split into two separate segments connected by locked joints. CVS/ATB reports the forces and torques that it applies at these joints to satisfy the locked constraint. These values can be compared directly to load cell measurements.

To maintain smooth contact with the airbag, a single ellipsoid was used to give shape to each of the upper arm and forearm segment pairs. This ellipsoid was attached to the segment containing the original, single-segment c.g.. This design introduces the fewest possibilities for artifactual results when computing arm-to-airbag contact. Note how in an early simulation, the airbag gets "stuck" when the upper arm's shape is represented by two ellipsoids (Fig. 4).

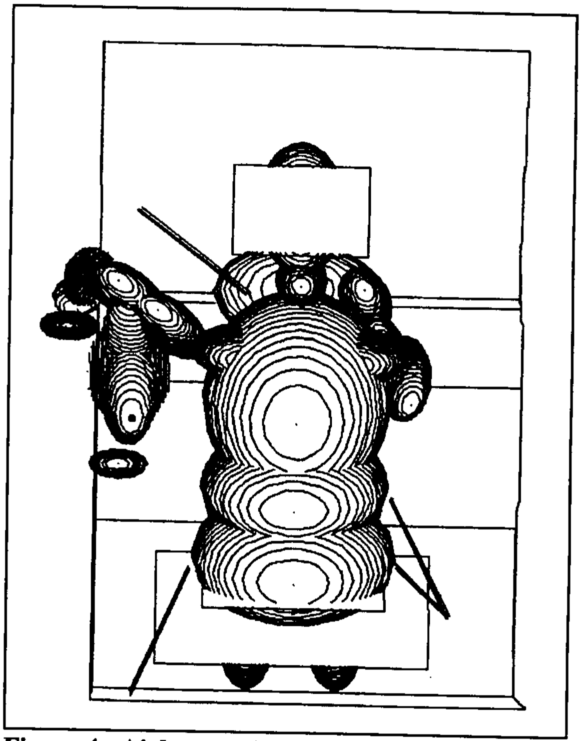

Figure 4. Airbag getting “stuck” between upper arm ellipsoids.

PARAMETER STUDIES

Multi-Position Study

The first study conducted with the new side airbag model was one to determine the relative severity of possible sitting positions with regard to the airbag/arm interaction. Initially, five positions were defined as:

1. Normal sitting position with forearm flat on the armrest (8),
2. Normal sitting position with forearm flat on the top of the door (6),
3. Occupant reclining against door with upper arm and forearm on armrest (9),
4. Forearm flat against door and upper arm directly in airbag's path (11),
5. Occupant leaning against door with upper arm between seat and door (5).

These positions are shown in Fig. 5. The arm positions after 32 ms are shown in Fig. 6.

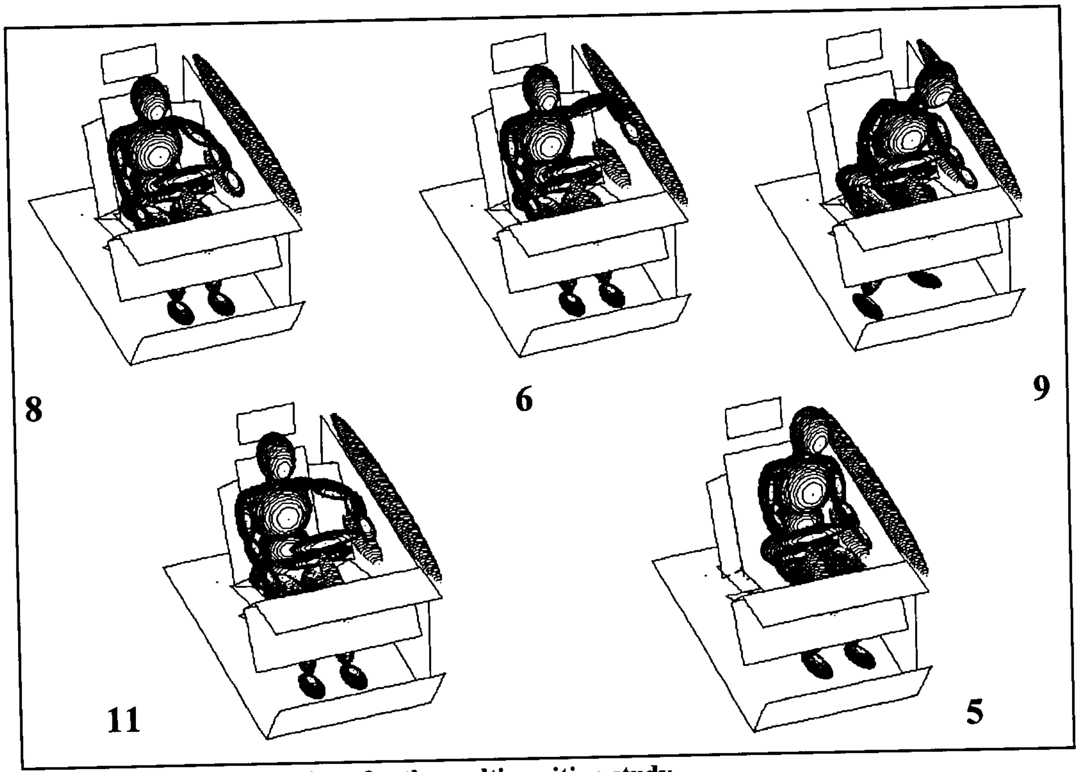

Figure 5. Occupant positions for the multi-position study.

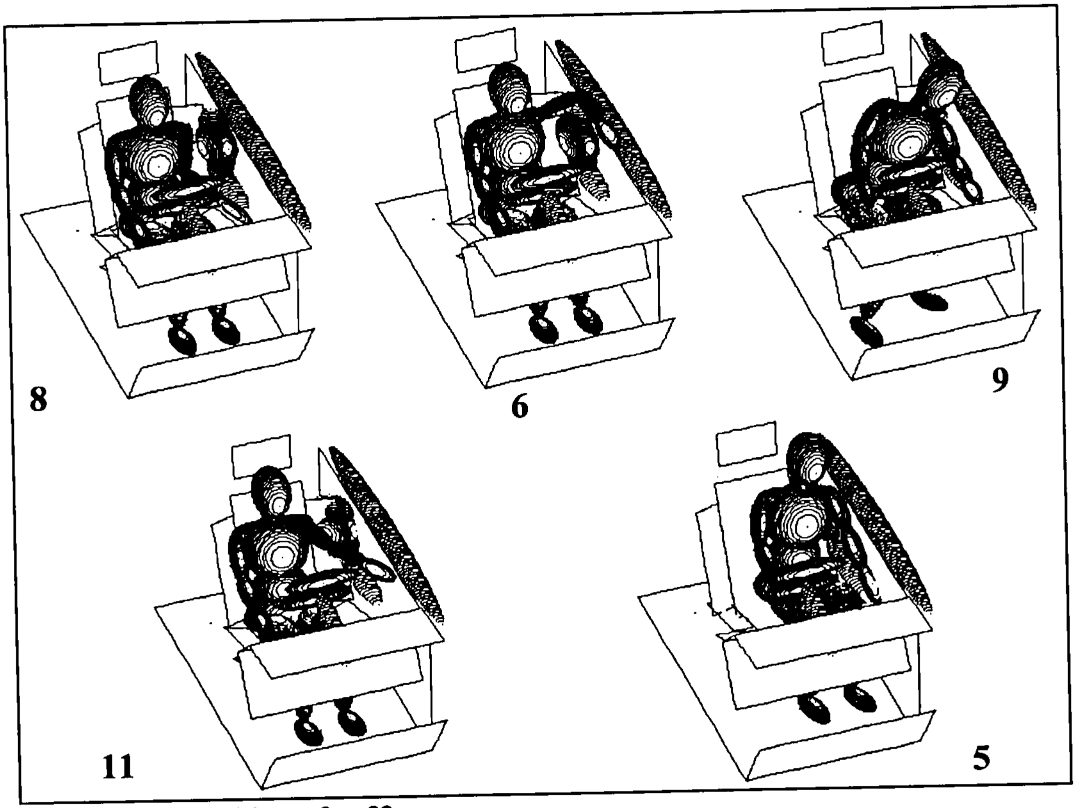

Figure 6. Arm positions after 32 ms.

A 5th percentile female occupant was used for all of the runs in this first series. The numbers denote the ASL's test configuration number. These numbers will be used to refer to each case in the subsequent discussion. Figure 7 shows the mid-humerus X-Y resultant moment for all of the above cases and Fig. 8 shows the elbow X-Y resultant moment for the four worst cases.

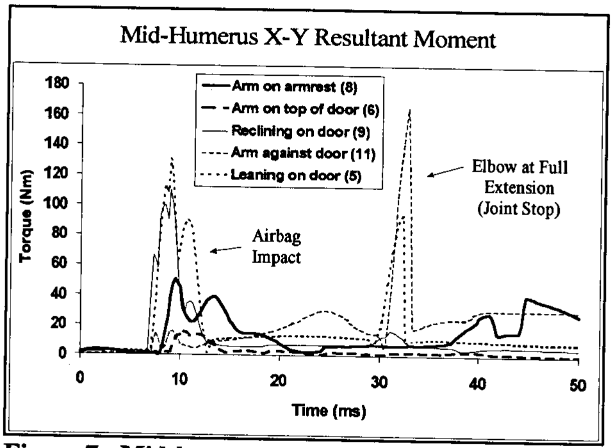

Figure 7. Mid-humerus X-Y resultant moment.

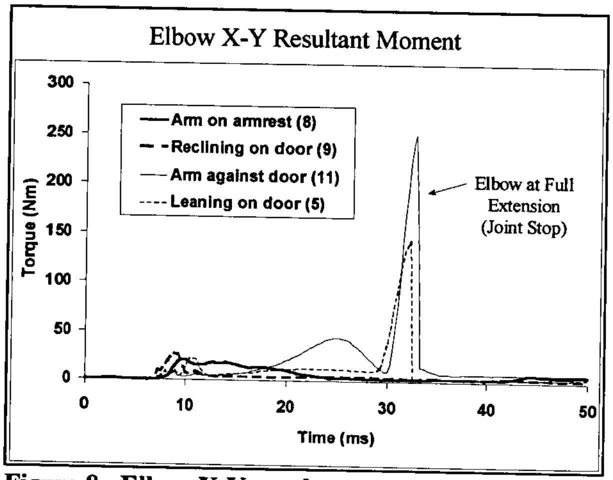

Figure 8. Elbow X-Y resultant moment.

Case 5 clearly stands out as the worst overall since it involves a large mid-humerus moment during airbag contact as well as a sharp spike in the elbow moment due to hyper-extension 20 ms later. The normal armrest position in Case 8 produces intermediate results, while Case 6 with the arm on top of the door involves relatively little airbag interaction. Of considerable interest are the results from Case 11. In this case, the airbag loads the arm near the elbow joint. This produces a very small mid-humerus torque during the airbag contact phase. However, the upper arm experiences rapid rotational acceleration which results in a large spike as the elbow hyper-extends into the joint stop. This spike is, in fact, the largest from all of these initial simulations. Case 11 demonstrates how the greatest loads may result from secondary effects which occur after the primary airbag contact.

Based on these results, a new position was defined which was intended to be a worst case. In this position, described as the Modified 8 position, the occupant was translated sideways until the shoulder was at the edge of the seat and the elbow was just touching the door, but not pressed tightly against it. The occupant was also raised slightly so that the upper arm could lie in the plane of the seat back with the forearm flat against the armrest. This differs from position 5 in that there is less contact, hence friction, between the arm and the door, and because the exposure of the upper arm to the deploying airbag is maximized. The kinematics from this simulation are shown in Fig. 9 and the moment plots in Fig. 10. Due to its severity, this position was added to the ASL test matrix.

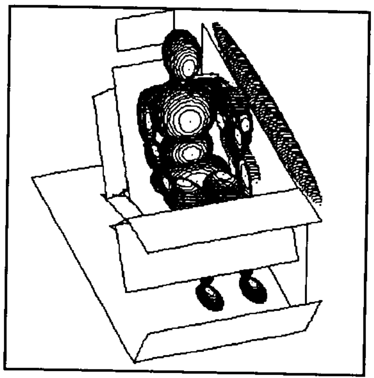

Figure 9. Modified position 8.

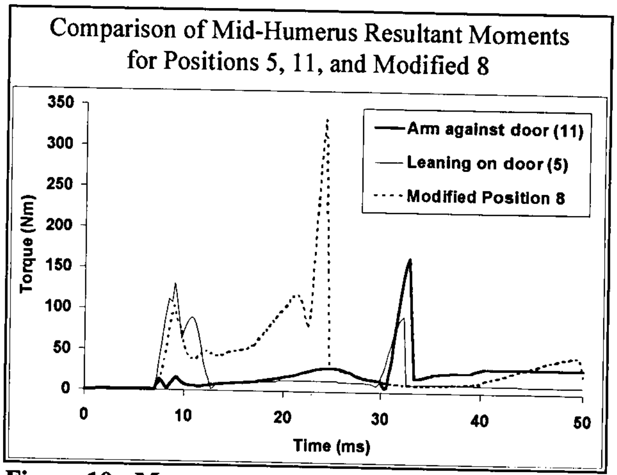

Figure 10. Moment comparisons of positions 5, 11, and modified 8.

Joint Friction Study

Joints on the Hybrid III (H3) dummies are normally adjusted so that the arms will fall from a horizontal position with approximately constant angular velocity. Thus the torque generated by joint friction is almost in equilibrium with the torque created by gravity. This is often referred to as 1-G joint friction. Humans on the other hand, have almost zero joint friction. Since friction at the elbow and shoulder joints can influence the arm's response to the airbag, it is important to know if the normal H3 joint friction will have a significant effect. To answer this question, Position 8 simulations were run with 1 G and 0.01 G friction at the shoulder and elbow. The plots in Fig. 11 show that, at normal H3 levels, joint friction has a negligible effect on arm response.

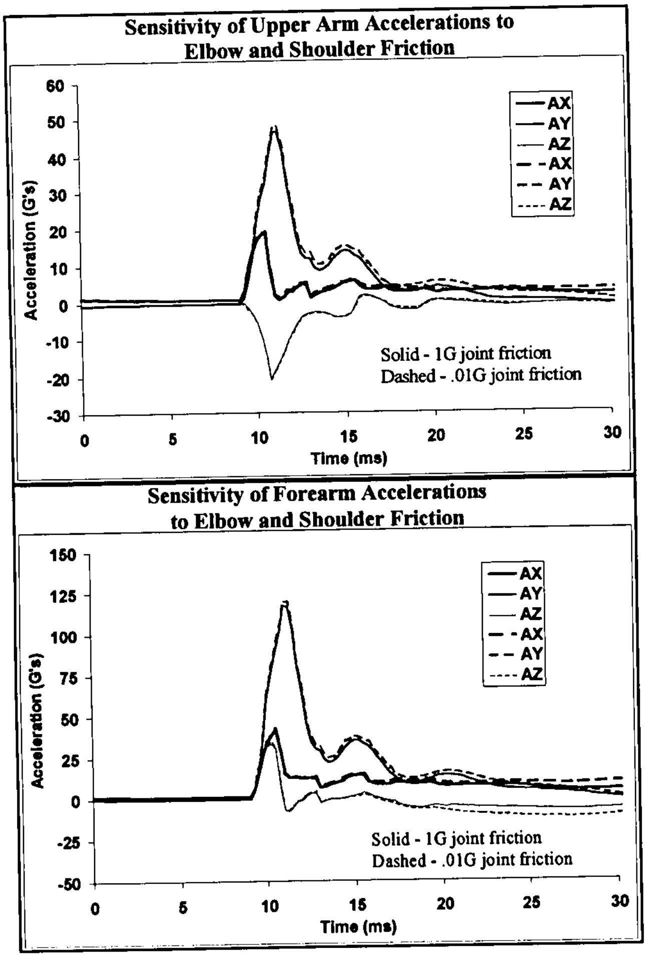

Figure 11. Influence of joint friction on arm accelerations for arm-on-armrest (position 8).

Clavicle Effect Study

The occupant models provided by the CVS/ATB GEBOD database program do not contain segments representing the clavicles. For the H3-type dummies, this is not a bad approximation because the dummy clavicles are very stiff and have a very limited range of motion. For a human, however, the clavicle accounts for most of the fore-aft motion of the shoulder joint complex, and for about 1/3 of the range-of-motion when a person is standing and the arm is raised straight up over the head. This additional compliance at the shoulder joint should produce noticeable differences between dummies and humans. In order to examine this effect prior to laboratory testing, the occupant models in the side airbag study were modified to include clavicle segments. These segments were kept locked for dummy-like simulations and were unlocked for human-like simulations. In the latter case, the clavicle joint was allowed to move with only a viscous constraint force until it neared the estimated range of motion. At that point, an angle-dependent spring torque was applied.

The three most severe cases from the initial study, 5, 9, and 11, were rerun with the free clavicle. Results from this study show consistent differences for the locked and free clavicle joints. In all cases, the calculated arm loads were reduced when the extra degrees of freedom were added at the clavicle joint. Thus, arm loads measured with the dummy can be considered a worst-case since they should consistently over-predict the loads that would be experienced by a human in the same situation. These simulation results are summarized by the plots in Fig. 12.

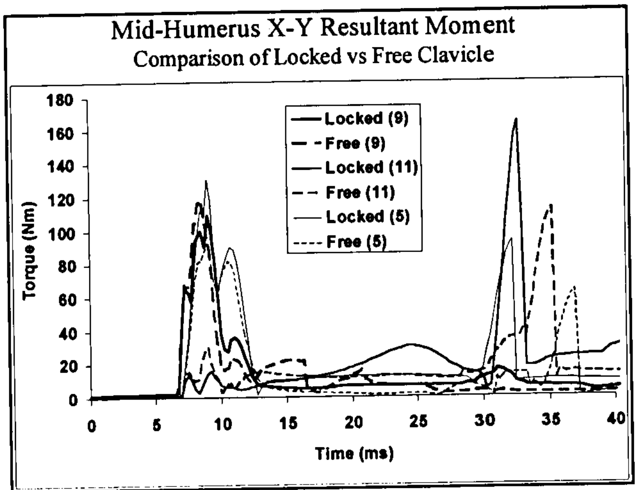

Figure 12. Results from the clavicle effect study.

Male vs. Female Study

Male and female occupants will interact differently with the airbag because of arm weight and because stature differences produce subtle changes in arm orientation for what are, nominally, the same sitting positions. To examine how these differences might affect test results, simulations of the 50th percentile male were performed for the original and modified position 8 cases. Kinematic results at 48 ms are shown in Figs. 13 and 14. The results for mid-humerus moment and elbow resultant force are plotted in Fig. 15 along with the 5th percentile female data..

The differences seen in both the plots and pictures are considerable, but do not always indicate a male-to-female difference. In the Modified 8 simulations the fact that the male's arm is knocked sideways while the female's is pushed in a more forward direction may have more to do with position subtleties than with arm weight. It does seem likely, however, that the larger initial peak in the male's mid-humerus moment curve is associated with his arm's larger inertia, which makes it harder for the airbag to bump it out of the way.

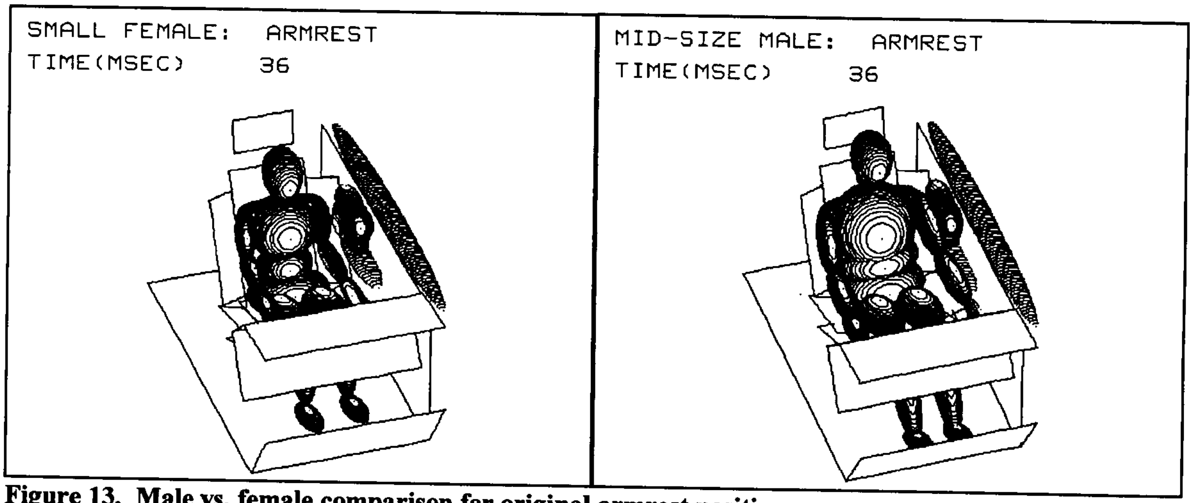
SMALL FEMALE: ARMREST
TIME(MSEC) 36
MID-SIZE MALE: ARMREST
TIME(MSEC) 36

Figure 13. Male vs. female comparison for original armrest position.

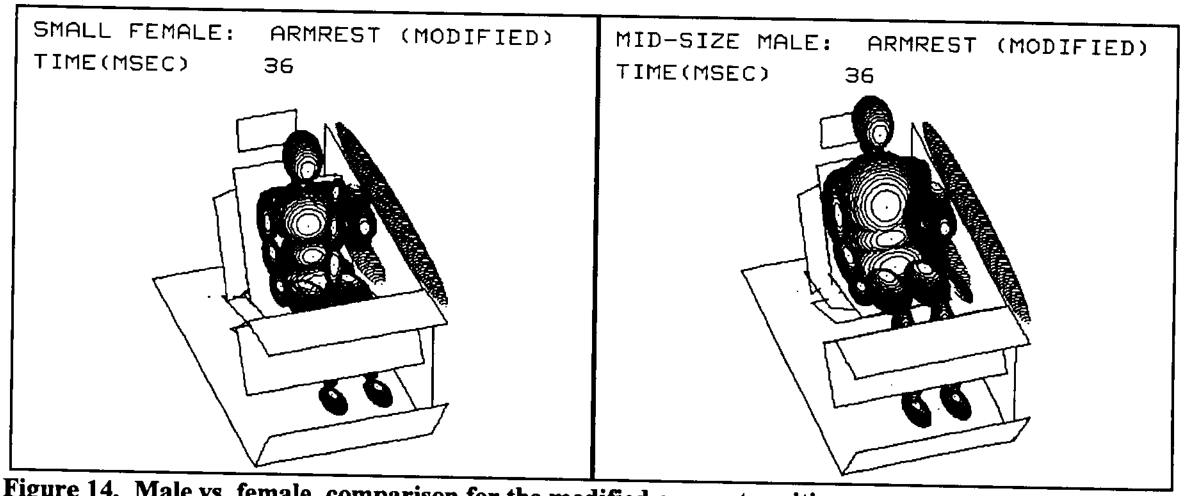
SMALL FEMALE: ARMREST (MODIFIED)
TIME(MSEC) 36
MID-SIZE MALE: ARMREST (MODIFIED)
TIME(MSEC) 36

Figure 14. Male vs. female comparison for the modified armrest position.

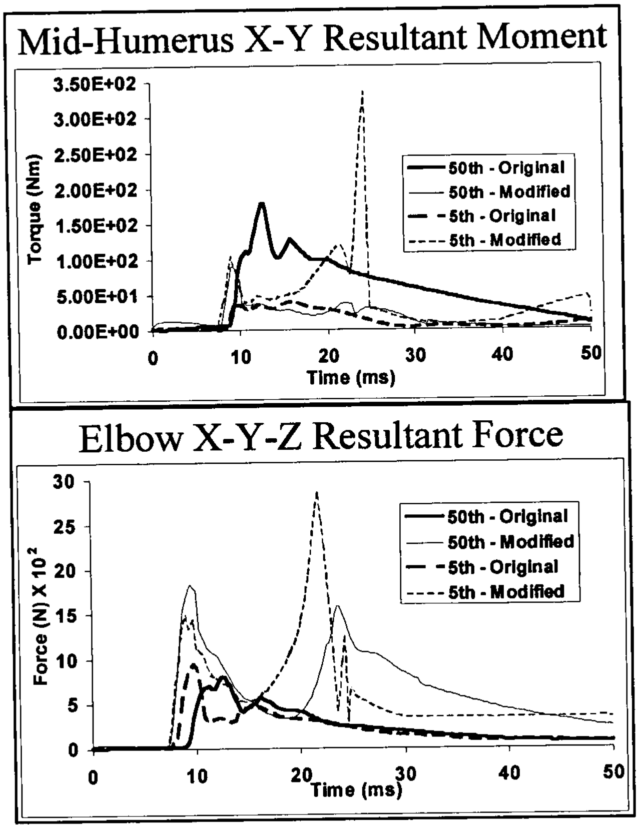

Figure 15. Results from the male vs. female study.

Intrusion Study

The static deployment simulations represent situations that could occur if the side airbag were to deploy accidentally. In these cases, the spacing between the seat and the door remains fixed. In actual side impacts, however, door intrusion is of fundamental importance. To study the influence of intrusion, the static deployment files were modified to include vehicle and door motion time-histories which were supplied by Honda for a 25 kph side impact test. In this test, direct contact between the door and the seat is minimal, so the seat motion is assumed to be the same as that of the vehicle. The displacement time-histories are show in Fig. 16. Airbag inflator firing occurs at 13 ms.

Runs were made initially for the 5th percentile female in the 8 and modified 8 positions. However, in the case of the modified 8 position, the airbag remains trapped behind the occupant and cannot effect the impact between the occupant and the door (see Fig. 17). Therefore, the modified 8 position was dropped from the intrusion study. It was eventually replaced with an arms-at-the-side, or SID position.

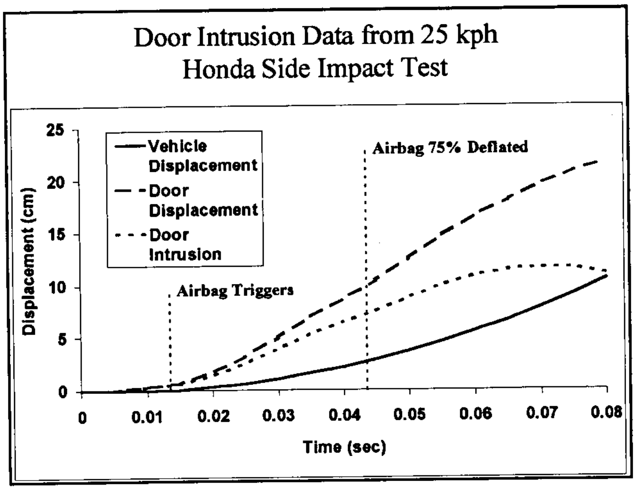

Figure 16. Side-impact test displacement time-histories.

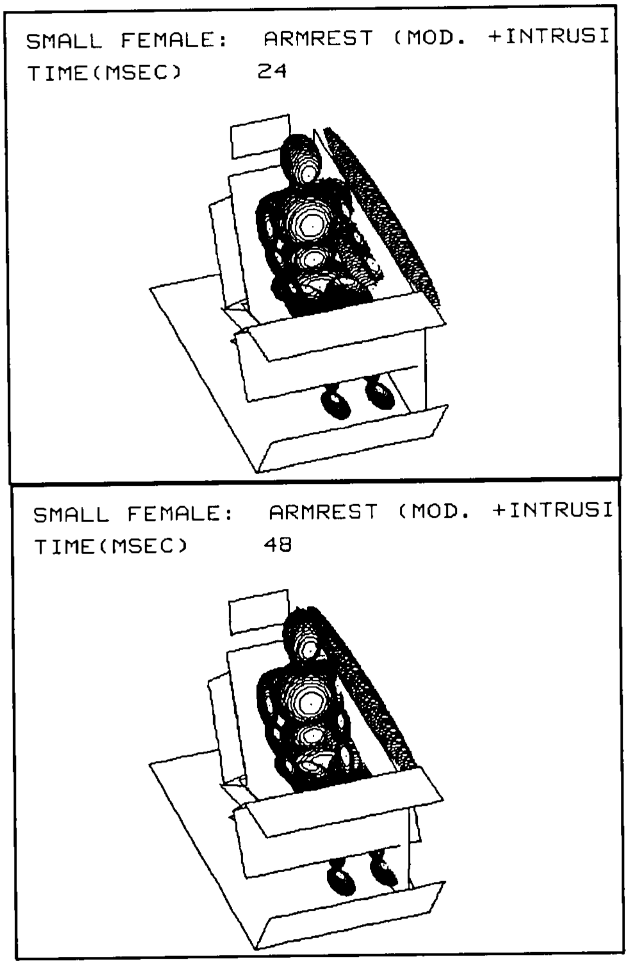
SMALL FEMALE: ARMREST (MOD. +INTRUSI
TIME(MSEC) 24
SMALL FEMALE: ARMREST (MOD. +INTRUSI
TIME(MSEC) 48

Figure 17. Modified position 8: airbag behavior with an intruding door.

Next, position 8 runs were made with the original, non-deflating airbag and with no airbag. The bag effectiveness was measured by plotting the chest c.g. acceleration (Fig. 18). Note that the results for the airbag are slightly worse than for no bag. This suggests that a non-deflating bag is no longer sufficient when the relatively long contact times of a actual side impact are present. The non-deflating bag was acceptable for the static deployment simulations since contact times were brief, and the significant interaction between the occupant and the bag occurred while the bag was fully inflated.

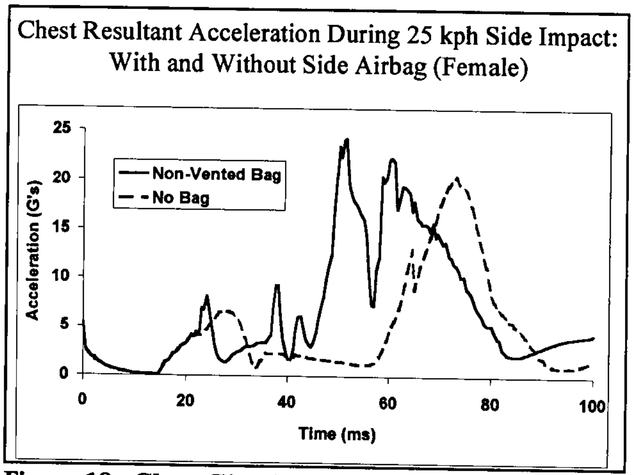

Figure 18. Chest G's with no airbag and with a non-deflating airbag.

As described earlier, the CVS/ATB code was modified to permit the airbag's deflation to be simulated with a time-dependent scaling function multiplied by the airbag's contact force/deformation function. The scaling function is shown in Fig. 19. It is based on the Honda inflator pressure curve (see Fig. 2) which shows the pressure falling to zero about 50 ms after triggering. The plot in Fig. 20 shows the results after the position 8 intrusion case was rerun with bag deflation. The improvement is small, but the results with the bag are now definitely better than without.

One reason for the bag's limited effect in the previous simulation is the timing of the primary door impact. It occurs late enough in the crash that the airbag has already deflated significantly and can offer little additional cushioning. To study this further, two more simulations were set up with 5th and 50th percentile occupants in the SID position. A 50th percentile, no-airbag case was also run. The SID position places the upper arm in a direct line between the door and the chest, which effectively reduces the chest-to-door spacing. The greater size of the male occupant further reduces the spacing. The results of the SID position simulations are shown in Fig. 21. In the case of the female, the influence of the airbag is still small, but for the male the result is dramatic; the chest G's for the male occupant with a side airbag are lower by almost a factor of three. This increased effectiveness is caused by the smaller initial door spacing, which results in the primary door contact occurring while the airbag is still pressurized. These results strongly suggest that the optimization of bag size, bag pressure, inflator trigger time, and venting rate will be critical for effective bag performance.

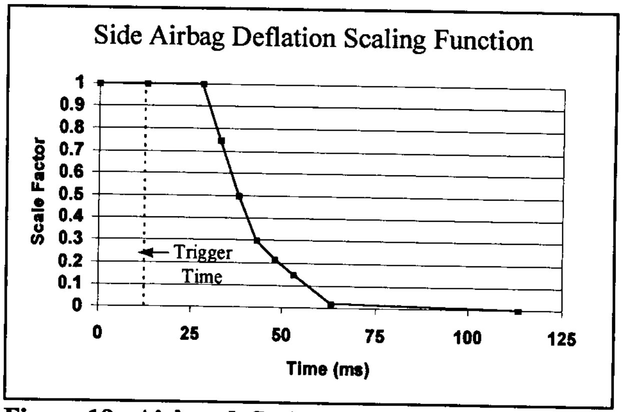

Figure 19. Airbag deflation scaling function.

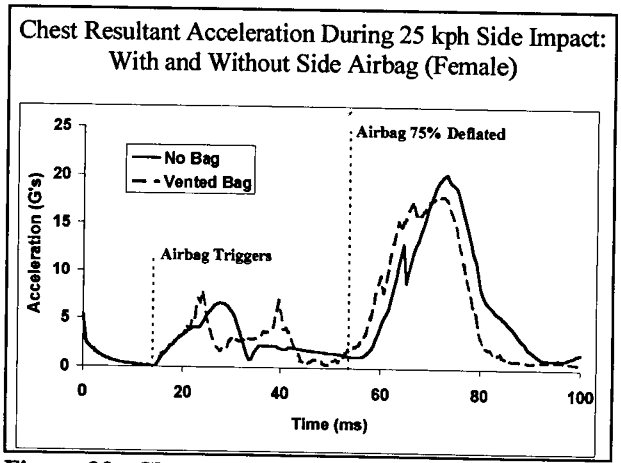

Figure 20. Chest G results with a deflating airbag.

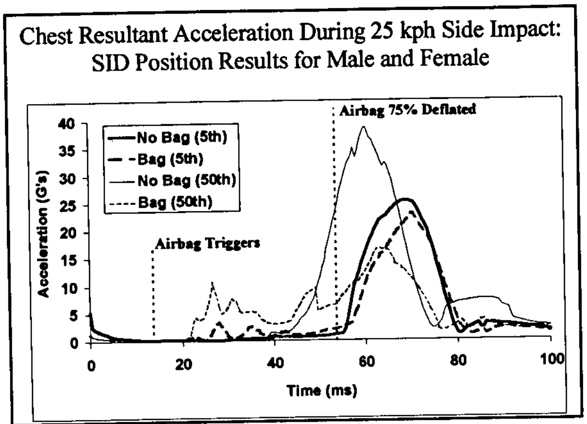

Figure 21. Chest acceleration results for SID position occupants.

CONCLUSIONS

A series of CVS/ATB models were created, each of which incorporated a model of the Honda Type-A airbag. These models included 5th percentile female and 50th percentile male occupants in a variety of positions producing different degrees of upper arm exposure to the deploying airbag. Most of the cases simulate static deployment tests in which the occupant and compartment are initially at rest, but several cases were also set up to model a side impact test with door intrusion.

Occupant Position

From five proposed positions, two were shown to produce significantly higher arm loads. In one of these positions, the upper arm was nearly horizontal, with the elbow against the door and the center-of-gravity (c.g.) of the upper arm in the path of the deploying bag. In the other position, the occupant was leaning sideways, with the shoulder against the door and the forearm on the armrest. After examining these positions, a new position was defined that was intended to be a worst-case in which the occupant was translated sideways until the shoulder was at the edge of the seat. The forearm was placed on the armrest and the occupant was raised slightly so that the upper arm c.g. was directly in the airbag's path. The simulation results for this position did show that it captured the worst elements of the other two positions and confirmed that it should be used in the laboratory test matrix.

Clavicle Motion

Another area of study involved the influence of clavicle motion on mid-humerus measurements. The simulation results show that a moveable clavicle does influence the torque measured at the mid-humerus point, but that it always lowers peak values. Thus, if dummy measurements are used to evaluate airbag performance, they will over-predict upper arm loading. This, in turn, means that if dummy tests show that an airbag is operating within safe limits, there should be an additional margin of safety for an actual human.

Joint Friction

The issue of joint friction is also of concern when comparing dummy and cadaver test results. The simulation results show that the difference between zero friction joints and 1-G friction joints is negligible for airbag interaction studies. Therefore, no special adjustment of the dummy is required.

Occupant Size

There is a considerable size difference between the 5th percentile female occupant and the 50th percentile male occupant. The simulations show that, for the same seating position, the difference in body size and weight will produce different arm loads and kinematics as a result of airbag contact. In general, due to greater inertia, the male occupant will register higher peak loads in the humerus since a heavier arm is harder for the airbag to move. The female, on the other hand, will experience higher arm accelerations and higher secondary loads when the elbow and shoulder reach the limits of their range of motion.

Intrusion

The simulation project was completed with several intrusion cases to study bag performance under realistic side impact conditions. Vehicle and door motions were based on a 25 kph test conducted by Honda. Door intrusion for this test was about 11 cm with minor structural deformation of the seat. In this situation, it was found that for normally seated occupants, the airbag had little effect since it deflated before significant occupant and door contact occurred. However, if the initial occupant-to-door spacing was reduced, the airbag could lower peak chest acceleration significantly.

ACKNOWLEDGMENTS

The authors would like to thank Honda R&D Co., LTD. of Japan and Honda R&D North America, Inc. for funding and supporting this work.

REFERENCES

1. Deng, Y.; Tzeng, B.; "Side Impact Countermeasure Study Using a Hybrid Modeling Technique," SAE Paper No. 962413, 1996

2. Vaidyaraman, S.; Khandelwal, H.; Lee, C.; Xu, J.; Nayef, A.; "State-of-the-Art Side Airbag Modeling and Its Application in Occupant Safety in Lateral Collisions," SAE Paper No. 980915, *SAE Winter Congress*, Detroit, MI, 1998.

3. Sieveka, E. M.; Duma, S. M.; Pellettiere, J.; Crandall, J. R.; Bass, C. R.; Pilkey, W. D.; "Multi-Body Model of Upper Extremity-Airbag Interaction with Deploying Airbag," SAE Paper No. 970398, *SAE Winter Congress*, Detroit, MI, 1997.

DEVELOPMENT OF A HYBRID III LOWER LEG COMPUTER MODEL

Jamie A. Buchanan
Terry McKie
Andrew R. Hall
MIRA
John Green
Rover Group
Alan Thomas
Jaguar Cars
Djamal Midoun
Ford Motor Company
United Kingdom
Paper Number 98-S9-O-07

ABSTRACT

With the introduction of the lower leg injury criteria in the new European Frontal Impact Legislation, the leg kinematics and loading mechanisms must be considered at an early stage in vehicle development programmes. Finite Element codes such as LS-DYNA3D are used increasingly to model occupant/structure interactions for vehicle design, from concept to the final restraint system optimisation. A fully validated Hybrid III lower leg model is consequently an essential tool in the vehicle design process. However, due to the complex nature of the materials and geometry of the lower leg and footwell, development of such a model presents a number of problems.

In the collaborative LLIMP project (Lower Leg Injuries and Methods of Prevention vehicle design project), MIRA, with the project sponsors, Jaguar, Ford and Rover, has developed a Finite Element computer model of the Hybrid III lower leg which can be attached to a full Hybrid III Finite Element dummy model. The model has been used to support vehicle design as well as evaluating the effects of footwell intrusion and occupant position on lower leg injury criteria. The paper presents the development of the lower leg model, which includes the use of lower leg component tests and HyGe sled tests to validate the material models, contact characteristics and load levels. HyGe sled tests have been simulated to which lower leg kinematics, loading mechanisms and injury criteria have been correlated.

INTRODUCTION

In recent years there has been a significant reduction in the number of fatalities and life threatening injuries sustained by occupants in car accidents. This can be accounted for by the development and inclusion of safety features, such as air bags and seatbelt pre-tensioners, as well as improvements in the crashworthiness of vehicle structures.

However, with increased accident survivability there has been an increase in the effect on the lower legs. While lower leg injuries are not life threatening, serious fractures in the foot and ankle can cause permanent disability.

The development of a Finite Element model of the Hybrid III leg has been necessitated by the increased interest in reducing injury of the lower extremities. A numerical model would provide an essential tool to assist in the understanding of the complex leg kinematics and loading mechanisms experienced by the occupant in the crash event.

It is intended that the model is used as a development tool, for evaluation of lower leg kinematics and loading mechanisms under different footwell intrusion profiles and occupant positions. The model would also provide useful information in the early stages of vehicle development to mitigate injury and enable causes of injury to be designed out.

In the initial stages of the LLIMP project, analysis of crash test results highlighted the importance of evaluating the lower leg kinematics in order to understand the complex loading mechanisms, [1]. Therefore the computer model was required to accurately represent the kinematics, contributing to an accurate representation of the loading mechanisms in the leg.

OVERVIEW OF OCCUPANT SIMULATION TOOLS

Currently engineers have a number of simulation tools available to them, and with hardware developments, these tools are becoming ever more sophisticated. In codes such as LS-DYNA3D it is possible to run in excess of one million degrees of freedom structural models including occupant, restraint system and the vehicle structure.

In the past, when considering the lower legs, analysis has been limited by the information that could be extracted from the models. Rigid body occupant models, (Figure 1), represent general kinematics effectively but are often unable to extract injury data and simulate complex loading mechanisms. Contact representation is often inaccurate due to poor dummy surface representation with ellipsoid models and local stiffness imprecisions in the vehicle structure, occupant or occupant's clothing and shoes.

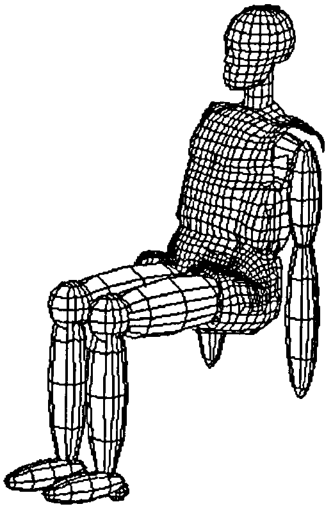

Figure 1: Rigid occupant model.

Finite Element Analysis with codes such as LS-DYNA3D has a major advantage over other simulation tools in the way it is possible to model the occupant and it's environment in detail to represent the complex interaction between the structure and occupant, [2,3].

MODEL DEVELOPMENT

Methodology

The lower leg model needed to be closely representative of the Hybrid III test device to accurately simulate the complex 3D motion, and assist in validation of the proposed five phases of quasi static and dynamic loading experienced by the leg over the duration of an impact, [1].

The model of the leg needed to be geometrically accurate to provide a detailed surface representation ensuring timing and mechanisms of contact are indicative of those seen in test. Inertial properties of individual components are also realistically represented due to the accurate geometry, and material densities used in the leg model.

Material characteristics in the Hybrid III leg Finite Element model account for nonlinearities of the foam materials, and hysteretic behaviour where relevant.

Each load cell in the leg is individually represented with a translational or rotational spring to provide a means for output of forces and bending moments experienced by the leg.

Extra accelerometer output is provided by accelerometers on the leg model adjacent to the knee and ankle and in the heel and toe. These are used to assist in the understanding of leg kinematics, [1].

To create a robust leg model that can be used with confidence, a development methodology was devised to incorporate a variety of tests, designed to provide supporting data for the model creation. There were two main test categories used in the development of the Finite Element leg model:

- Component tests; these were used to develop material models and validate load cell models.
- HyGe sled tests; these were used to validate the model as a complete system, including legs and rigid torso representation.

Model Construction

To accurately simulate lower leg kinematics and complex loading mechanisms, it was essential that the inertia and mass distribution through the model was representative of the Hybrid III test device. To this end, the foam covering and steel skeleton of the Femur, Tibia and Foot were modelled to be geometrically accurate using solid hexahedral and wedge elements, (Figures 2 and 3). Table 1 summarises the mass contribution from components in the legs and compares with Hybrid III mass information, [4].

'Flesh' foam surrounding the Tibia and Femur are represented with foam material models in LS-DYNA3D. Soft foam materials are susceptible to hourglass and contact problems due to the large strains involved. Therefore care was taken in the selection and correlation of materials to create a robust model, able to withstand high energy impacts without causing solution instabilities.

Instrumentation in the dummy leg was represented in the model to enable a direct comparison to be made between test and Finite Element analysis results. Accelerometers in the leg and foot are represented to give acceleration output in local co-ordinate systems. F_x and F_z load cell outputs are obtained from the model using translational springs. M_x and M_y are extracted from rotational springs at the load cell locations. Each of the springs used to output load cell data has an equivalent translational or rotational dashpot damper, damping out high frequency interference through the leg.

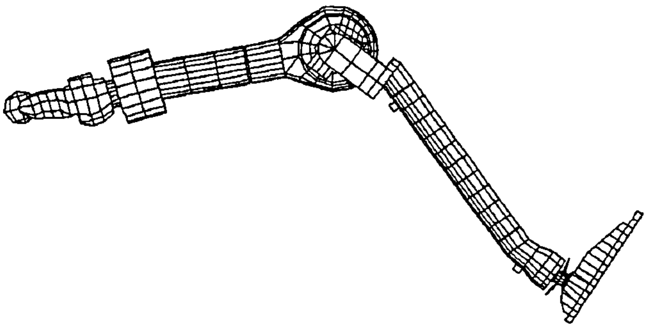

Figure 2: Skeletal leg model.

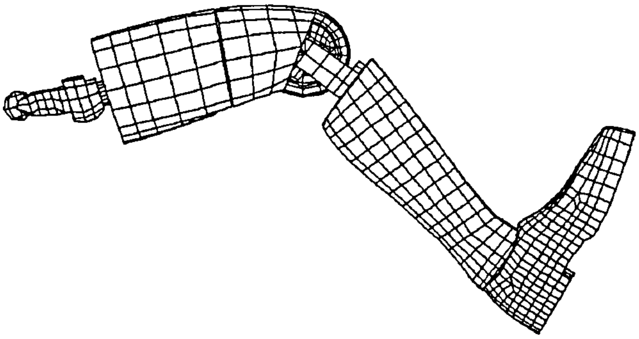

Figure 3: Complete leg model.

The complex interaction between the foot and shoe provide a significant obstacle to overcome. A limited understanding of the behaviour of contact between the foot and shoe was gained via component tests. Details of the component tests follow.

Table 1: Mass Properties of the Hybrid III Leg.

	Hybrid III (kg)	DYNA3D model (kg)
Foot	1.25	1.3
Lower Leg	3.28	3.3
Upper Leg	6.22	6.2

To date, the joints in occupant models have generally been represented using spherical joints, and their stiffness and rotation limits governed by nonlinear rotational springs. The magnitude of joint stiffness is highly variable from test to test, and throughout the duration of a test is dependent on the mechanism of loading through the joint. This is especially important when we consider the ankle joint in the lock up state. Throughout the lock up state the mechanism of locking can change between longitudinal and lateral lock up, depending on external factors, such as footrest and pedal design. The loading mechanism on the ankle joint also causes large variability in the ankle's rotational stiffness. This provides a significant obstacle when creating the DYNA3D model. Because of the high energy and short duration associated with impacts it is valid at this stage in the model development to assume that the ankle joint stiffness will have negligible effect on the loads measured in the legs. Although the ankle in the model has no rotational stiffness, the lock up state of the ankle is enabled by the accurate representation of the foot skeleton and lower Tibia, (Figures 4 and 5). The curvature of the ankle stop is represented both laterally and longitudinally to allow the nominal 45° stop angles in dorsiflection, and 30° stop angle in inversion and eversion.

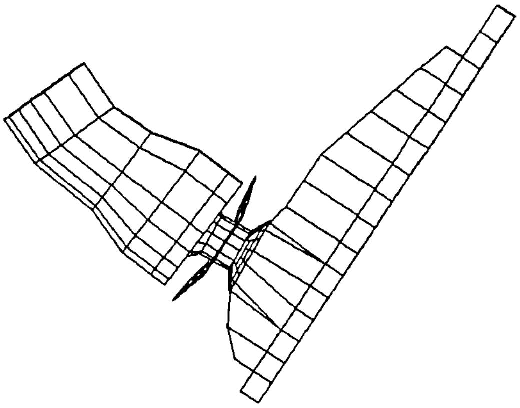

Figure 4: Accurate ankle joint representation.

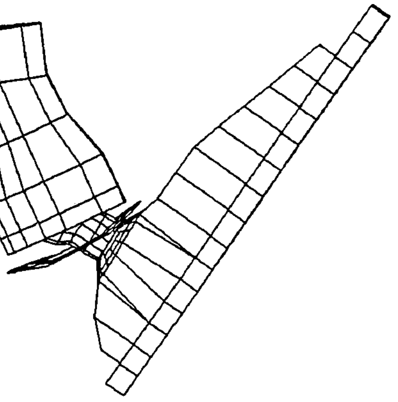

Figure 5: Ankle joint in lock up state.

Accurate geometrical representation was also considered important in the knee where there is both rotational and translational components of the joint dynamics. The rotation was governed in the model with a geometric joint definition, only allowing rotation about a single axis. The knee slider is controlled using a nonlinear translational spring.

Model Correlation

To correlate a Finite Element model with the complexity of the Hybrid III leg it is necessary to break the model into smaller sub-systems and correlate these models to physical component tests. Using this approach minimises the complexity of the problem and provides a method to highlight areas of the computer model that require attention. Once the sub-systems are understood they are assembled to form the complete structure. Finally the complete system is correlated to test. This modelling philosophy was considered to be essential to the development of a robust model of the Hybrid III leg.

The lower leg physical component testing consisted of three types of drop test. Each of the tests was repeated several times, and at different speeds to allow for experimental inaccuracies and rate dependency in the leg and foot foam. After each test, components were given time to recover before being re-tested. This was considered to be especially important when testing viscous foam materials.

Foot Drop Tests

Drop tests were used to develop the foam material model for the Hybrid III foot, (Figure 6). Twelve drop tests were carried out, including tests on both the left and right foot. Three velocities were used to enable the assessment of rate effects in the foam. The ankle was fixed rigidly for each test to minimise boundary effects. An aluminium headform impactor of mass 6.8kg was dropped onto the heel. An accelerometer was fixed to the impactor to measure acceleration in the direction of impact. This output was integrated to give the velocity and displacement of the impactor.

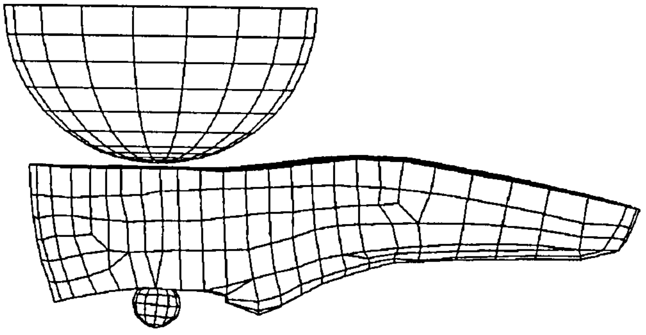

Figure 6: Foot drop tests performed at 1.5m/s, 2.5m/s and 3.5m/s.

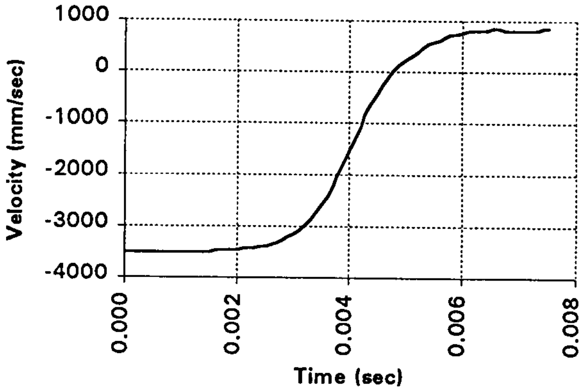

Figure 7: Impactor velocity highlighting energy absorption properties in the foot foam.

A significant feature of the foam in the foot is highlighted by the velocity trace, (Figure 7). The impact velocity is approximately 4.5 times the magnitude of the rebound velocity, suggesting that energy is absorbed by the foam. Therefore the choice of foam model needed to account for significant energy absorption. The large amount of hysterisis in the foam was overcome by using the Fu Chang foam model and including a high value of Young's relaxation modulus, [5]. LS-DYNA3D's implementation of the Fu Chang foam model can account for rate dependency in the material. Rate effects are included by supplying a number of stress strain relationships at given strain rates. This feature of the material model was not used in the development of the foot foam model, as the strain rate was not considered important over the range of impact velocities that the foot experiences. The implemented stress strain characteristic was considered valid for the strain rates encountered in this work.

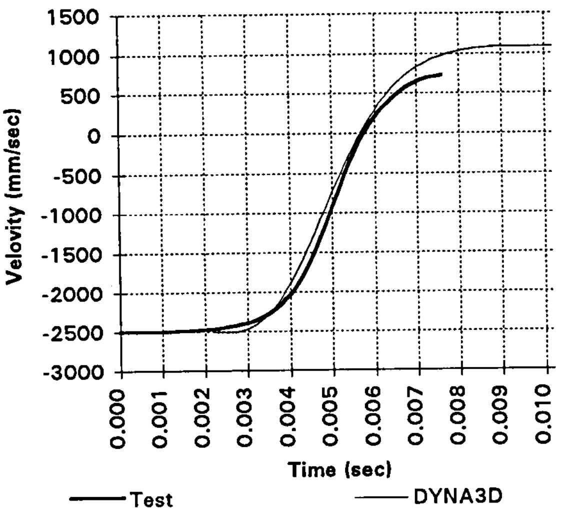

Figure 8: Impactor velocity comparing computer simulation to physical test.

The impactor accelerations and velocities from the Finite Element model correlated well to results from the physical test, (Figure 8). The energy absorption characteristic of the foot was considered to be the most important feature to represent. Without this, problems would be introduced with elastic impacts causing unrepresentative lower leg kinematics when the leg model was assembled as a complete system.

Shoe Drop Tests

To investigate the behaviour of the shoe the boundary conditions were identical to those used in the drop tests used for the foot investigation, (Figure 9).

Comparing acceleration traces of drop tests performed with and without the shoe displays an unexpected result, (Figure 10). Knowing that the sole of the shoe is stiffer than the foam of the foot, it was expected that the impactor should decelerate at a faster rate when dropped onto the foot with shoe. This was not the behaviour exhibited in test, suggesting that the interaction between the shoe and foot is an important feature of the overall foot/shoe system adding additional complexity to the creation of a computer model.

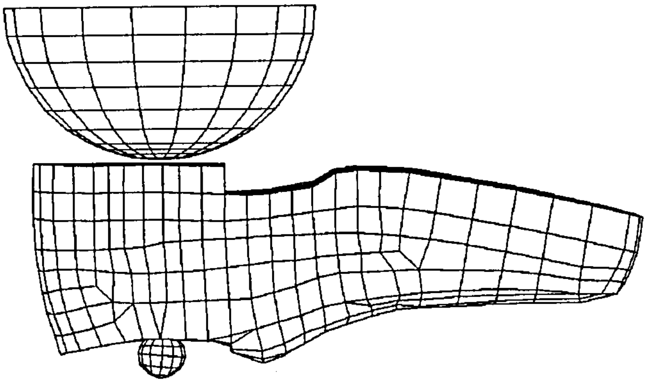

Figure 9: Shoe drop tests performed at 1.5m/s, 2.5m/s and 3.5m/s.

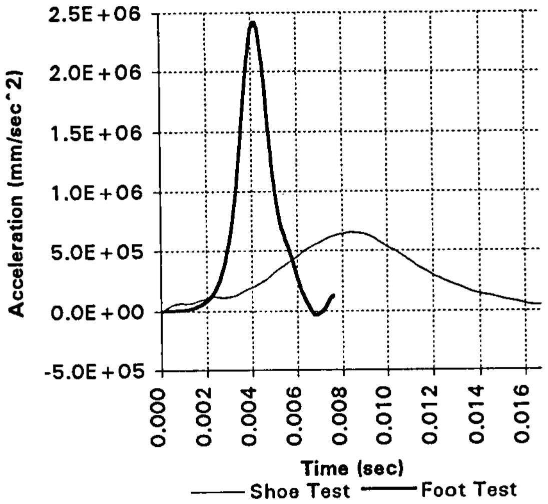

Figure 10: Comparison of impactor acceleration traces between drop tests performed with and without the shoe.

Lower Leg Impact Tests

Validation of the behaviour and output of the load cells in the lower leg was approached using a series of 24 drop tests. Three boundary condition combinations were tested at varying impact speed to provide data for correlating the bending moments and forces in the model to those measured in test. Each test was repeated twice to allow for experimental variability.

The 3.6kg impactor was designed specifically for these leg tests. It's impact face was rectangular with smoothed edges to reduce the risk of damaging the leg. The impact locations are shown in Figure 11. The knee joint was pinned to allow rotation only about the local y axis. Constraints were applied to the ankle to allow rotation about the y axis and translation in the z axis.

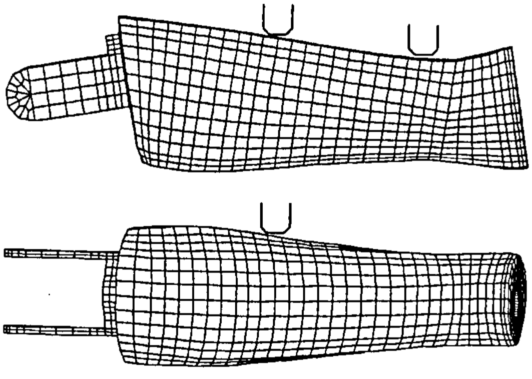

Figure 11: Lower leg impact tests - impact locations for Tibia front and side tests.

Upper and lower tibia M_y, M_x, F_y and F_x were investigated using data from impacts to the front face of the Tibia.

Output from the load cells in the Finite Element model was seen to be significantly linked to the characteristics of the foam surrounding the skeleton of the lower leg. Therefore correlation of the load cells was achieved by considering the properties of the foam. Impacts with the Tibia were seen to absorb less energy than those with the foot, so a less 'expensive' urethane material model was chosen to model the foam, requiring less CPU time to solve.

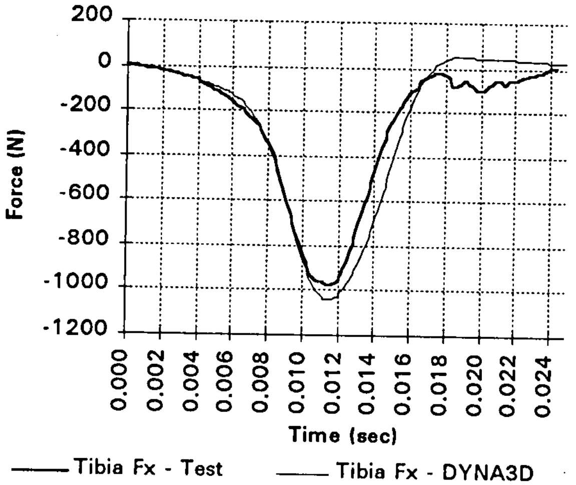

Figure 12: F_x in test and model for lower leg component tests.

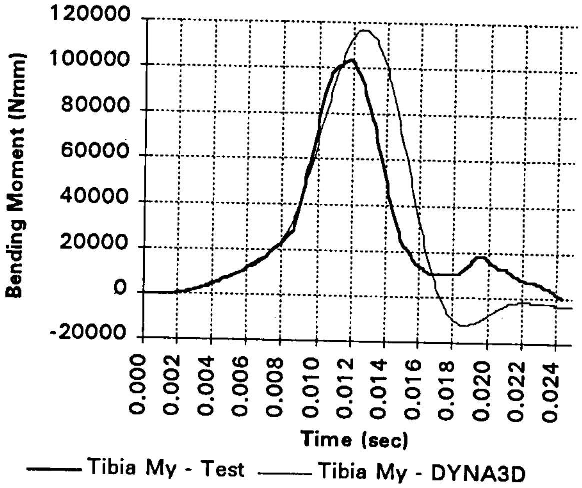

Figure 13: My in test and model for lower leg component tests.

HyGe Sled Tests

To correlate the complete occupant system, with the finite element legs attached to a rigid upper body, a series of four HyGe tests were devised. The tests were designed to have boundary conditions that would translate into a DYNA3D model with minimum complication, reducing sources of error and the number of unknown variables.

The test matrix incorporated two frontal impact pulses; one representative of a medium car, the other representative of a larger vehicle. The only other significant differences between tests were in the footwell, which consisted of two rigid planes with adjustable gradient, so each plane could be positioned at either 30° or 60° to the horizontal. Restraints were kept to a minimum, with only a length of low strain webbing to represent the belt system. No seatbelt retractor was included but the webbing had ample slack to allow enough forward excursion of the pelvis to permit the Tibia to reach a vertical position. Feet were positioned so that initially they were not in intimate contact with the footwell.

To gain confidence in the performance of the Finite Element leg model, the modelling of HyGe tests was split into two distinct phases. The first phase considered a rigid ellipsoid occupant. The second phase used the modified model with Finite Element representations of the legs. In both phases the HyGe sled was represented in the model by rigid planes fixed in space, (Figure 14).

Using the rigid occupant enabled the general occupant kinematics to be considered, and the occupant environment variables to be tuned without additional complication due to inclusion of the new legs. Once a good correlation of head, chest and pelvis acceleration had been achieved, the exercise could be repeated, but with emphasis on the performance of lower leg kinematics and loading in the model.

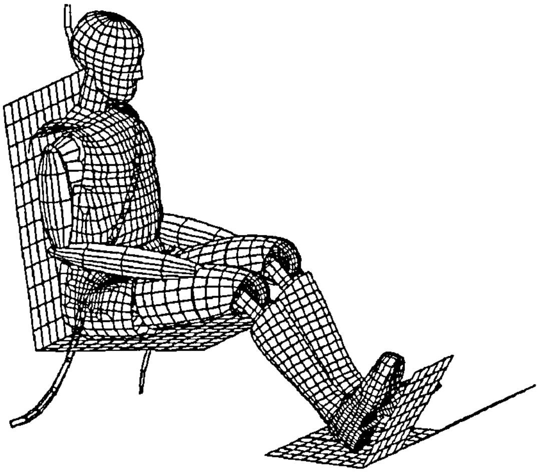

Figure 14: HyGe test used in correlation phase.

The correlation results for the chest and pelvis accelerations for the rigid ellipsoid model are shown in Figures 15 and 16. These results continue to be valid, with only minor differences when the ellipsoid legs are replaced with the FE representations. The global kinematics of upper body parts of the ellipsoid model are good, but closer inspection reveals that the dynamics of the feet and lower legs are unsatisfactory. This is due to the unrepresentative ellipsoid surface definition and lack of simulation of local stiffness variation in the occupant model.

Both the global and lower leg kinematics in the second phase modelling of the HyGe tests were very good. This lead to accurate output from load cell models that correlated well to test data. M_y and F_z all show the main peaks and troughs throughout loading. A sample of the correlation plots between test and analysis results for load data in the leg is shown in Figures 17 and 18. A sequence showing how the leg model behaves in the HyGe test is shown in Figure 19.

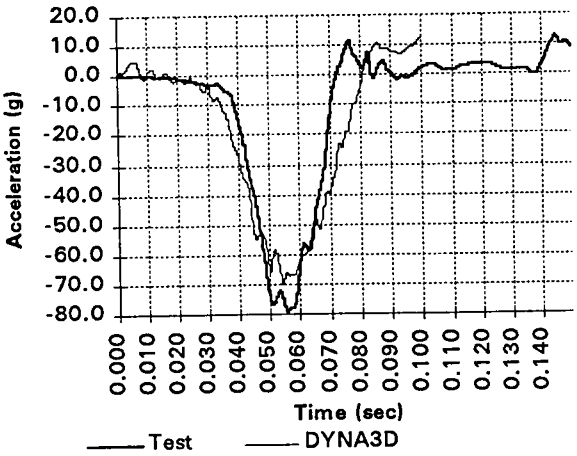

Figure 15: Chest acceleration of occupant in HyGe test.

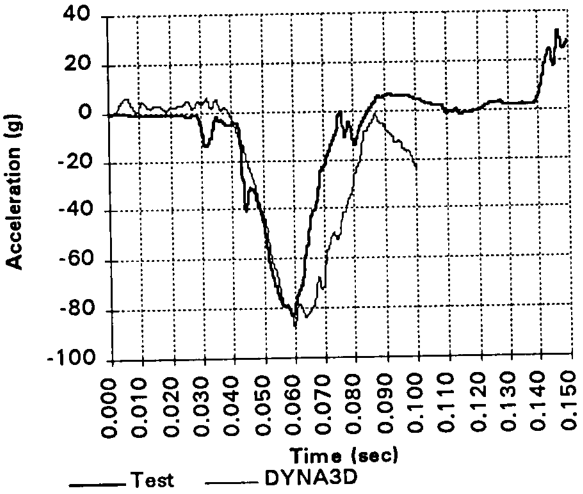

Figure 16: Pelvis acceleration of occupant in HyGe test.

Achieving good correlation between the model and HyGe tests, has given confidence in the numerical model. It can represent two dimensional behaviour, but boundary conditions in the tests did not allow for effects such as feet sliding off pedals or interaction between the legs and knee bolsters or facia. These effects add a further dimension to the behaviour of the legs, with the ankle joint moving into inversion or eversion. The loading mechanisms caused by these three dimensional effects are not yet fully understood, so it is not yet possible to validate these effects in the model. It is hoped however, that the model will assist in the understanding of three dimensional behaviour, in order to enable correlation to full scale crash tests.

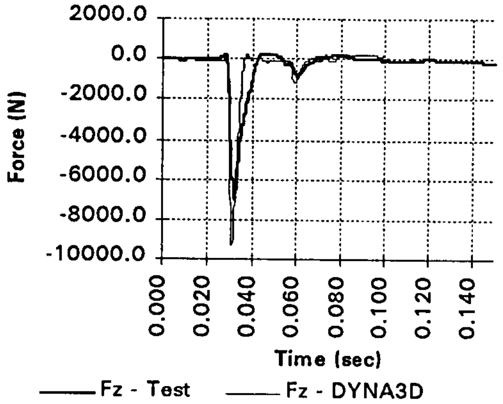

Figure 17: Right lower Tibia F_z force in HyGe test.

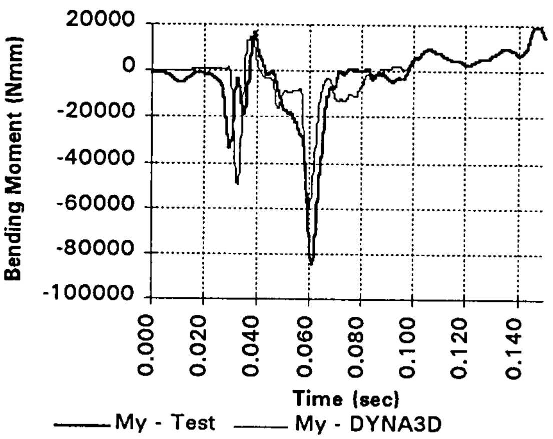

Figure 18: Right lower Tibia M_y bending moment in HyGe test.

CONCLUSIONS

The model is a useful tool that can be used to consider the two dimensional leg behaviour. The development of the Hybrid III lower leg has highlighted the need for a better understanding of three dimensional occupant lower leg behaviour.

Through the intensive correlation exercises performed on the leg components and complete occupant model we can be confident that the model provides accurate loading and kinematic data to assist in the early stages of vehicle design and development to mitigate injury.

The Finite Element model has helped considerably in the advancement in understanding of the two dimensional behaviour of the Hybrid III lower leg. The phases of loading and kinematics that the leg experiences during impact can be represented realistically with a good degree of correlation to test results. This has enabled the investigation of parameters in the footwell region that effect injury in the lower leg, [6]. There are still considerable obstacles in accurately representing the three dimensional behaviour of the legs, with effects such as feet sliding off pedals and nonlinear intrusion profiles being difficult to simulate.

FURTHER WORK

MIRA through the MISTIQUE project, (MIRA Intrusion Simulation Technique), have developed a test rig to be used in conjunction with the HyGe reverse accelerator. The MISTIQUE rig simulates footwell intrusion using rotating and translating planes. On completion, it is hoped that the lower leg computer model and MISTIQUE rig will work in partnership to aid the understanding and development of footwell design to mitigate lower leg injury. In the first instance the test rig will supply more data to further increase confidence in the Finite Element model and bridge the gap between HyGe test and complete vehicle frontal crash tests.

The leg model is currently being used in vehicle design to look at effects on the occupant due to intrusion. The model will be used from early stages in vehicle development programmes to reduce occupant injury, and increase awareness of the factors contributing to leg injury.

REFERENCES

1. A R Payne *et al.*, *'The Effect of Hybrid III Lower Leg Kinematics on Loading Mechanisms and Injury Criteria'*, ESV 98-S1-0-16, June 1998.
2. S Moss *et al.*, *'Development of an Advanced Finite Element Model Database of the Hybrid III Crash Test Dummy Family'*, 1st European LS-DYNA3D Conference, March 1997.
3. P Thomas *et al.*, *'Investigation of Lower Leg Injuries in Front Impact Crashes'*, OASYS LS-DYNA3D User Conference, 1995.
4. S H Backaitis, *'Hybrid III: The First Human-Like Crash Test Dummy'*, SAE International, 1994.
5. J. Hallquist *et al.*, *'LS-DYNA User's Manual'*, version 940, February 1997.
6. A R Payne *et al.*, *'Parametric Study on the Effect of the Footwell Geometry, Dynamic Intrusion and Occupant Location on Hybrid III Lower Leg Injury Criteria'*, ESV 98-S1-P-05, June 1998.

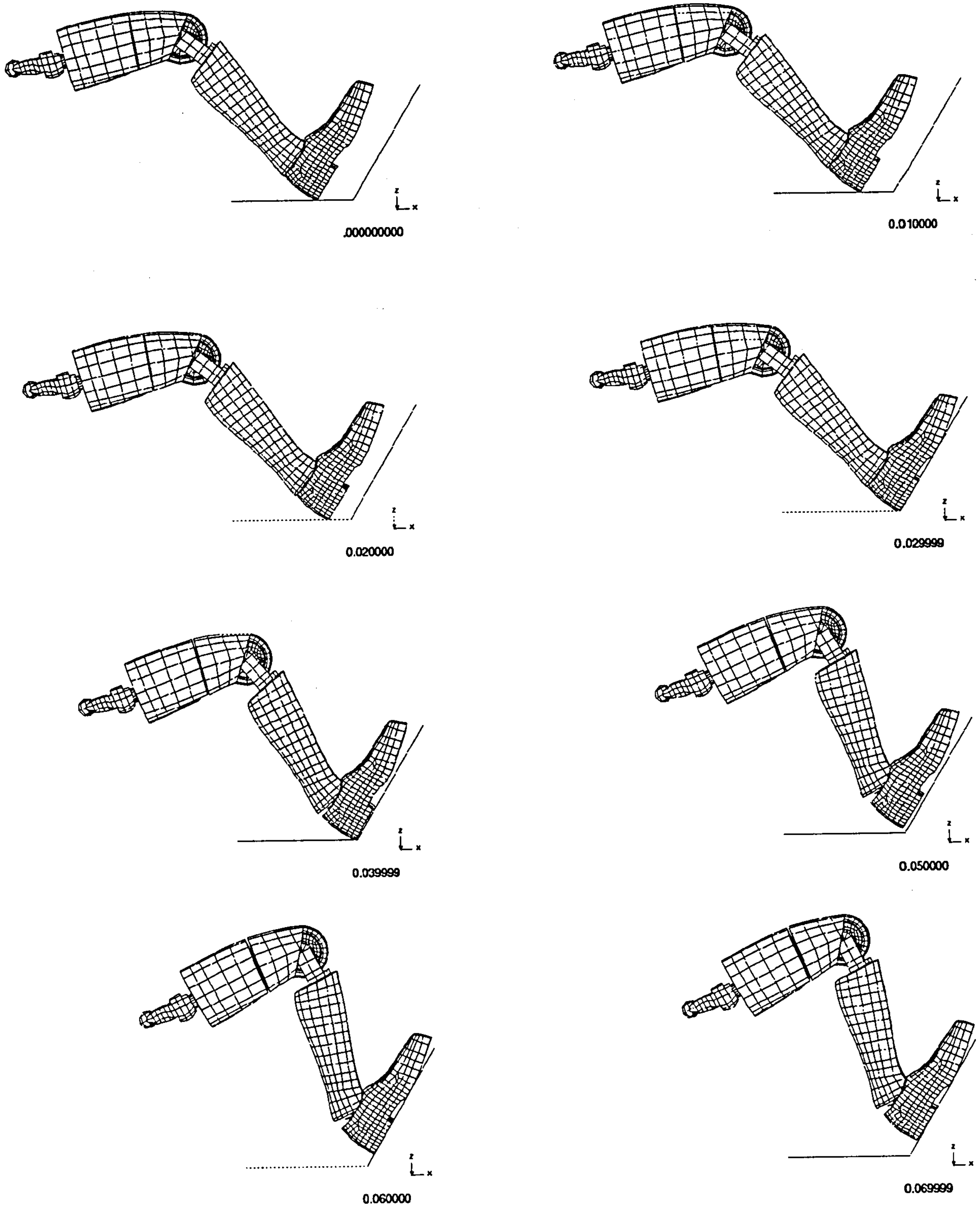
.000000000
0.010000
0.020000
0.029999
0.039999
0.050000
0.060000
0.069999
z
x

Figure 19: Event sequence for the right leg in HyGe test used for model validation work.

EVALUATION OF THOR DUMMY PROTOTYPE PERFORMANCE IN HYGE SLED TESTS

Masahiro Ito, Koshiro Ono
Japan Automobile Research Institute (JARI)
Yoshihisa Kanno
Japan Automobile Manufacturers Association (JAMA)
Japan
Mark Haffner
National Highway Traffic Safety Administration
Nagarajan Rangarajan, Tariq Shams
GESAC, Inc.
United States
Paper Number 98-S9-O-09

ABSTRACT

The THOR-50M dummy being developed as the next generation dummy for frontal impacts was leased out by NHTSA. This was mounted on a white body of a compact passenger car, and analyzed mainly were motions under relatively severe impact conditions using a HYGE sled at JARI. The characteristics of the THOR dummy were obtained by comparing the results with those of the HyIII dummy evaluated at 30 mph speed under three test conditions: an airbag only, a 3P seat belt only, and a 3P seat belt with an airbag system.

INTRODUCTION

R & D activities on advanced dummies were initiated in the USA in 1985 for further enhancement/improvement of conventional HyIII-50M (Hybrid III-50 Percentile Adult Male Dummy). As a result, TAD-50M (Trauma Assessment Device - 50 Percentile Adult Male Dummy) and THOR (Test Device for Human Occupant Restraint - 50 Percentile Adult Male Dummy) have been prototyped so far. One of the aims of the THOR development program is the international standardization of advanced dummies. JAMA/JARI decided to participate actively in the R & D work on the THOR dummy as an international evaluator for NHTSA1). We set the following objectives for the development/enhancement of advanced dummies in order to make proper proposals by conducting tests and evaluations of the dummy performance.

1) Identification of problems related with the HyIII dummy
2) Collection of basic data to ensure conformity with the dummy design requirements
3) Timely feedback of improvement measures, etc. for the development of advanced dummies, based on the information collected in 2) above
4) Contribution to the development of "easier to use dummies"

This paper describes our evaluation results of prototype THOR head, neck, chest, hip and thigh assemblies leased from NHTSA. THOR's impact responses were compared with those of the HyIII dummy in relatively severe HYGE sled tests.

TEST METHOD

The THOR dummy was seated in a white body of a compact passenger car of mass production mounted on a HYGE sled, and tested for the evaluation of impact responses. The HyIII dummy was also tested under the same impact conditions for the comparison of responses.

Table 1 shows the list of the test conditions and Figure 1 shows the sled pulse. Each dummy was seated in either the driver seat or front passenger seat, and tested at the sled velocity corresponding to the vehicle impact speed of 30 mph. The dummy restraint condition was varied - with an airbag only, a 3P seat belt only, or the combination of an airbag and a 3P seat belt. Data recorded in this study were the acceleration, displacement, load, moment and angle of each region of dummy, airbag deployment timing, sled acceleration, etc.

Table 1.
Test Conditions

Test No.	Restraint System	Impact Vel.	Setting Position	Dummy
DT30AB	3P Belt with Airbag	30mph	Driver	THOR
DT30A	Airbag			
PT30AB	3P Belt with Airbag		Passenger	
PT30B1	3P Belt			
PT30B2				
DH30AB	3P Belt with Airbag		Driver	HyIII
DH30A	Airbag			
PH30AB	3P Belt with Airbag		Passenger	
PH30AB2				
PH30B2	3P Belt			

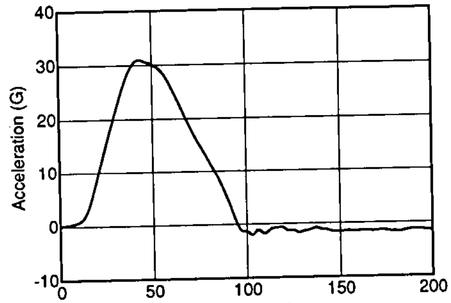

Figure 1. Sled acceleration for THOR and HyIII comparative HYGE sled tests

TEST RESULTS

Impacts were applied to the THOR and HyIII dummies by means of HYGE sled, and their responses were measured under the different restraint conditions. The practical applicability of the THOR dummy, items to be studied in future, have also been evaluated. Tables 2 and 3 show the responses of the dummies.

Table 2.
Summary of HYGE Sled Tests (Driver Side)

Configuration	30mph			
	3P Belt with Airbag		Airbag	
Test Number	No.1	No.2	No.3	No.4
	DT30AB	DH30AB	DT30A	DH30A
Dummy	THOR	HyIII	THOR	HyIII
HIC 36	277	559	419	300
HIC 15	199	330	242	204
Max. Head Resultant (G)	48	61	67	61
Max. Chest Resultant (G)	67	69	71	55
Max. Pelvis Resultant (G)	75	76	71	66
Lap Belt Force (kN)	8.06	11.03		
Shoulder Belt Force (kN)	10.6	10.63		
Max. Chest Deflection (mm)				
HyIII Sternum	——	-48	——	-55
THOR Right Sternum X	-44	——	-66.9	——
Left Sternum X	-43.6	——	-61.3	——
Right Lower Cage X	-59.3	——	-11.5	——
Left Lower Cage X	14.7	——	-14	——
Max. Lower Abdomen Deflection (mm)				
THOR Right X	-24	——	7.5	——
Left X	-16.9	——	7.4	——

Table 3.
Summary of HYGE Sled Tests (Passenger Side)

Configuration	30mph					
	3P Belt with Airbag			3P Belt		
Test Number	No.1	No.2	No.3	No.4	No.5	No.6
	PT30AB	PH30AB	PH30AB2	PT30B1	PT30B2	PH30B2
Dummy	THOR	HyIII	HyIII	THOR	THOR	HyIII
HIC 36	641	858	808	904	664	1045
HIC 15	324	399	419	502	330	541
Max. Head Resultant (G)	65	62	64	84	63	72
Max. Chest Resultant (G)	90	64	62	92	81	68
Max. Pelvis Resultant (G)	74	68	68	75	75	72
Lap Belt Force (kN)	10.39	11.23	12.06	11.01	10.13	12.59
Shoulder Belt Force (kN)	11.89	9.96	9.91	11.5	11.25	10.37
Max. Chest Deflection (mm)						
HyIII Sternum	——	-50.3	-48.8	——	——	-44.9
THOR Right Sternum X	-44.3	——	——	-56	-24.7	——
Left Sternum X	-48.7	——	——	-42.4	-58	——
Right Lower Cage X	17.6	——	——	10	14.8	——
Left Lower Cage X	-58.6	——	——	-61.9	-55.2	——
Max. Lower Abdomen Deflection (mm)						
THOR Right X	-13.8	——	——	-12.2	-16.7	——
Left X	-23.4	——	——	-22.6	-26.8	——

HIC - The HIC 36 values of THOR dummy were in the range of 277 to 904 in this test series, while those of the HyIII dummy tested for comparison were in the range of 300 to 1045. Although the number of tests conducted was limited, the relationship between the THOR and HyIII dummies in terms of HIC values is shown in Figure 2 by dummy restraint conditions. The HIC values of THOR are approximately 70 to 80 % of those of HyIII, similar to the tendency found between the TAD and HyIII dummies tested in 1995[2].

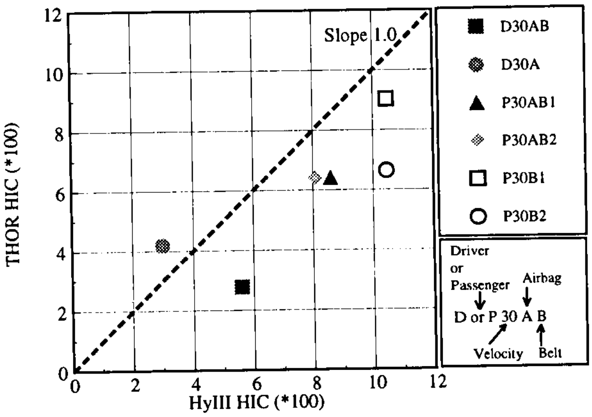

Figure 2. HIC Correlation between THOR and HyIII

Head Acceleration and Head Displacement - The relationship between the head X acceleration and the displacement was calculated by integrating the value of acceleration against the sled twice (the X-component of head C.G. acceleration and of sled acceleration was used). The comparison between the two dummies is shown in Figure 3 for each type of restraint. The values of displacement are greater for the THOR in each case though the initial rise tends to lag behind that of HyIII. In case of the comparison

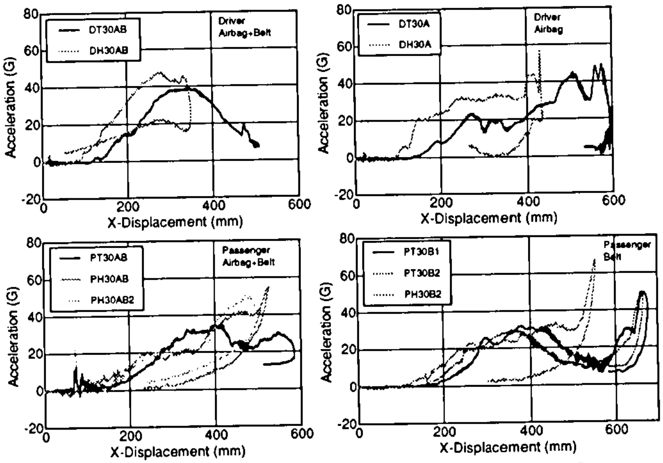

Figure 3. Relationship between head motion and head acceleration

at the front passenger seat, the deceleration rate of each dummy dropped once before reaching the peak value, but this tendency was more obvious for the THOR dummy. In case of a 3-point seat belt alone in particular, the displacement was 200 mm or so and the acceleration was reduced by 20 G in that period. It is deduced that this phenomenon was caused by the difference in neck stiffness, since it occurred around 75 to 100 ms (see Figure 4).

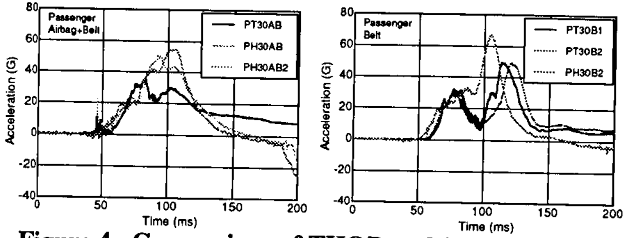

Figure 4. Comparison of THOR and HyIII head acceleration

Neck Bending Moment - The THOR head-neck assembly as tested at JARI permitted measurement of forces and moments transmitted at the occipital condyle joint representation, but the prototype tested was not instrumented to measure moment contributions from the neck cable elements[3), 4)], installed to make the neck bending characteristics similar to those of humans (Figure 5). Therefore, the THOR neck moment around the Y-axis is much smaller and the rise of moment is also slower than those of the HyIII, as shown in Figure 6 (passenger seat with the seat belt restraint). Therefore, all moments applied to the upper portion of neck could not be compared directly with those of HyIII.

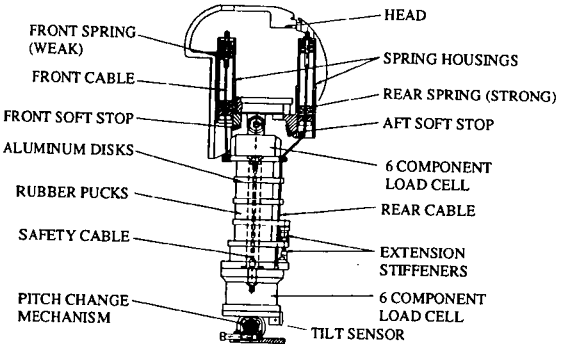

Figure 5. THOR Neck structure

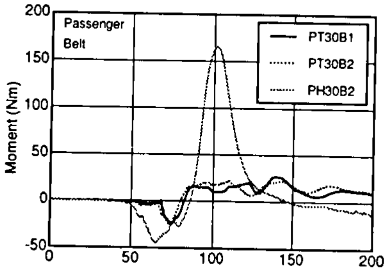

Figure 6. Comparison of neck moment between THOR and HyIII

Chest Acceleration and Displacement - The chest displacement in the X direction was calculated by integrating the acceleration against the sled twice (the X-component of chest C.G. acceleration and of sled acceleration was used), and the relationship between the chest acceleration and the displacement was determined. Comparisons of waveforms between the two dummies restrained under the same condition are shown in Figure 7. The THOR shows greater displacements in every case as in the case of head, and the rise of acceleration also tends to occur later for THOR. This is probably due to the softer chest of the THOR as compared to the HyIII chest, as in the case of TAD tested before[2)]. After the tests, evidence of metal-to-metal contact was found on the plate located at the bottom of the lower flex joint. A peak in the waveform caused by metal-to-metal contact is observed in the THOR dummy chest acceleration where the dummy is seat in the front passenger seat (Figure 8).

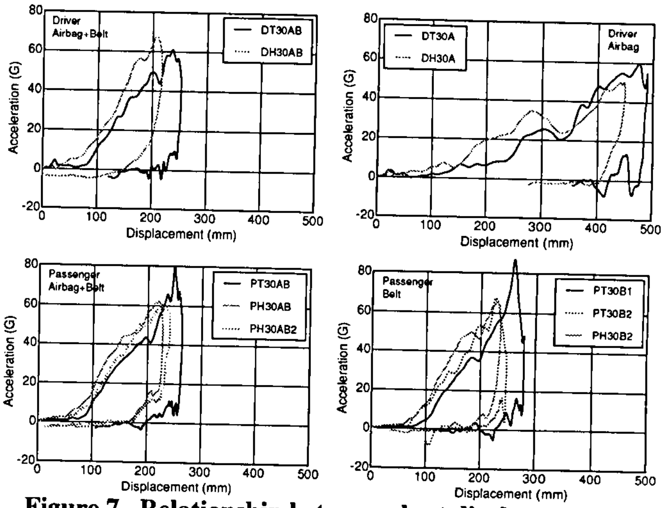

Figure 7. Relationship between chest displacement and chest acceleration

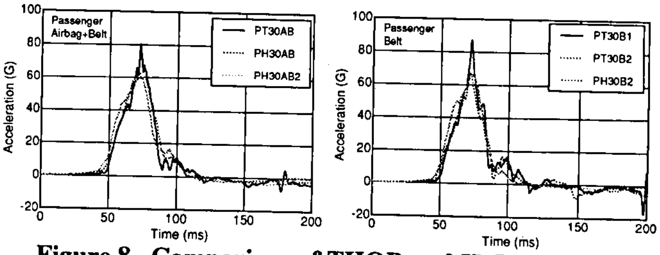

Figure 8. Comparison of THOR and HyIII chest acceleration

Chest deflection - Figure 9 shows the THOR chest and abdomen deflection coordinate system. Figure 10 shows the chest displacements for each dummy location and the

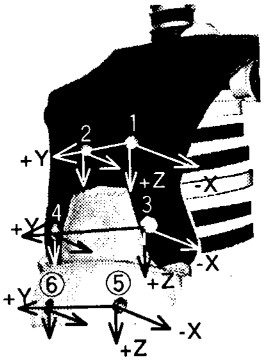

Chest deflection measurement system
CRUX : Compact Rotary Unit
① Upper left
② Upper right
③ Lower left
④ Lower right

Lower abdominal deflection measurement system
DGSP : Double Gimballed Stringpot
⑤ Left
⑥ Right

Figure 9. The chest and abdomen deflection coordinate system of THOR

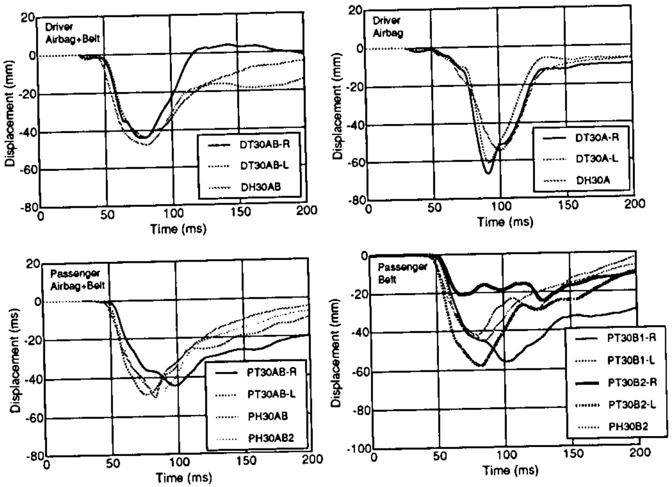

Figure 10. Comparison of THOR and HyIII chest deflection

type of restraint.

1) Comparisons between THOR and HyIII - Direct comparison of chest deflection between the two dummies could not be done due to differences in location and number of displacement gauges used in the dummies. However, deflections on right and left sides around the sternum in the X direction (longitudinal direction) were compared between the two dummies.

2) On driver seat - THOR upper ribcage displacement rises more rapidly to peak value than does HyIII chest displacement for the case of airbag only restraint. A sternal velocity comparison should show significant difference between the designs for this case. The differences between the left and right sides of THOR sternal displacement are difficult to find with the airbag alone. In the case where both the airbag and seat belt were used, hardly any difference was found in the tendency before reaching the peak, then the displacement of HyIII dummy became roughly the same as the average value of the displacements on the left and right sides of sternum.

3) On front passenger seat - Although some difference is found in the peak value with the seat belt only, the waveform on the left side of THOR sternum and the tendency of HyIII are relatively similar. On the right side of sternum, however, the waveform of THOR shows a different tendency despite being under the same restraint system. Some difference is also found in the peak value on the left side of sternum. With the combination of seat belt and air bag, the waveforms of both dummies on the left side of sternum tend to become similar, while those on the right side show different tendencies.

Comparison of Displacement by Restraint System for THOR - Figures 11 and 12 show the three-dimensional displacements measured on left and right sides of sternum and lower ribs, for the different dummy seating locations.

1) Airbag only - Only one case is available as an example of test results on the driver side, but it is found that the displacement is relatively simple in comparison to the displacement with the seat belt restraint. That is, the displacements concentrate in the X (longitudinal) direction toward the upper chest near sternum, without much

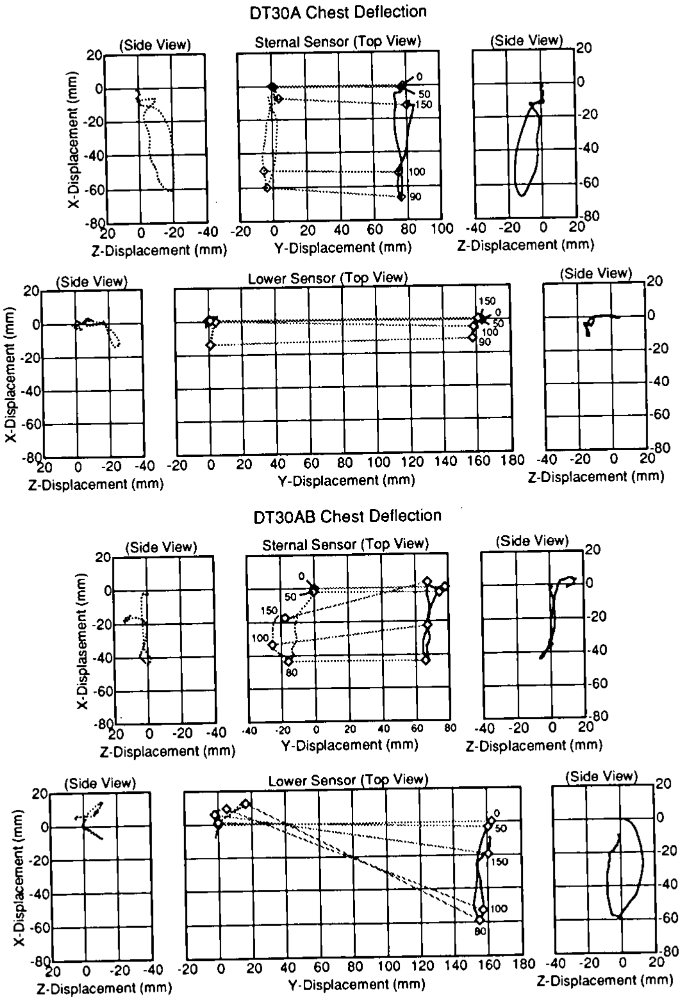

Figure 11. Three-dimensional chest deflection (THOR Driver side)

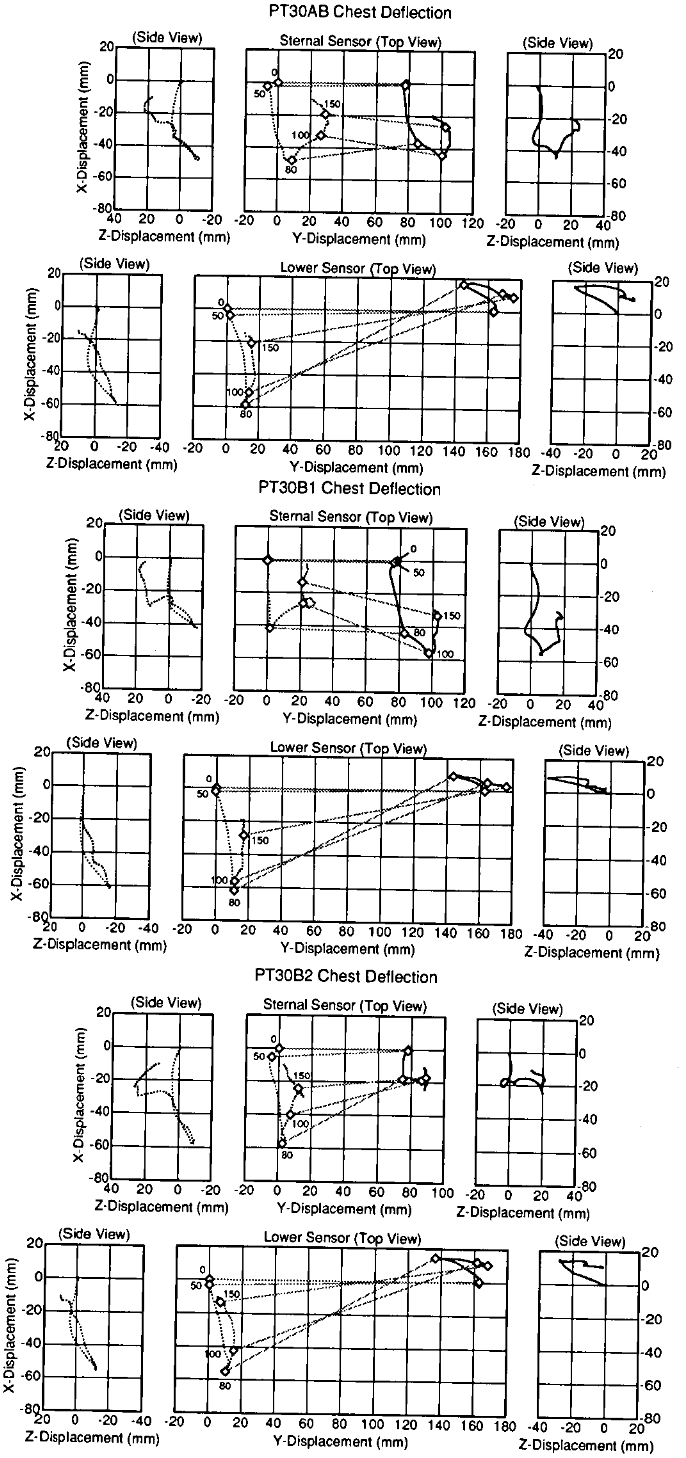

Figure 12. Three-dimensional chest deflection (THOR Passenger side)

difference between right and left sides, with the displacement becoming larger than that with the seat belt only. Around the lower ribs, the effect of airbag is reduced and the displacements in the X direction and the Y direction (lateral direction) are very small. In the Z direction, the displacement is equivalent to, or somewhat greater than that with the seat belt only.

2) Seat belt only, and seat belt + airbag - The X displacement is the greatest for both right and left sides of sternum, but the Y-axial displacement is also large toward the D-ring of the shoulder belt for both right and left sides of sternum. The Z displacement undergoes a somewhat complex process. Initially the ribs tends to stay level and then moves in the negative direction, and finally toward the positive direction. Around the lower ribs, displacements on the opposite side of buckle occur in such a manner that the chest expands toward the X with displacements in Y and Z directions becoming greater than the X displacement. On the buckle side, the X displacement becomes the greatest, with relatively small displacements in the Y and Z directions. On the driver side, however, the Z displacement is somewhat different from that on the passenger side, due to the difference in interference with the airbag.

Deflection of Abdomen - In case of THOR, abdomen displacements can be measured at three locations of abdomen - at the upper center, the lower right and left sides[3), 5)]. In this report, displacements at the lower right and left sides of abdomen will be described. Figures 13 and 14 show the three-dimensional displacements for each dummy location. The displacement observed on the XY plane shows a similar tendency to that of the lower rib displacement. In case where the dummy is restrained by both the seat belt and airbag, the displacement in the X direction on the buckle side is greater than that on the opposite side of buckle. However, the displacement that has caused the expansion in the X direction on the opposite side of buckle observed at the lower ribs is not found in this case. The expansion observed due to the force of inertia in the case with the airbag only, though the general tendency of displacement is similar to that of lower ribs.

Observation of displacements on the XZ plane reveals that the Z-displacement at the lower abdomen becomes

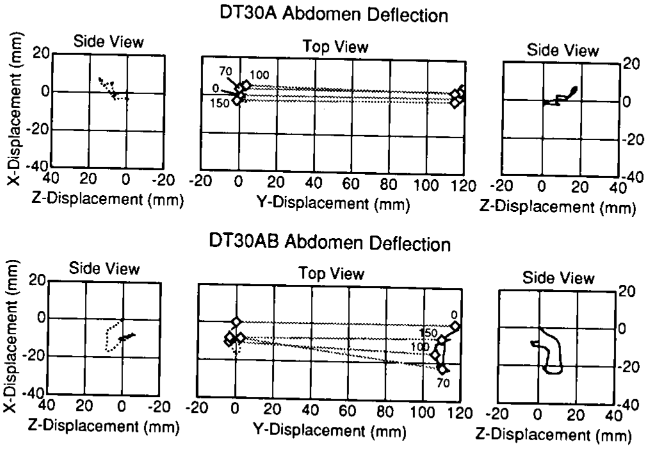

Figure 13. Three-dimensional abdomen deflection (THOR Driver side)

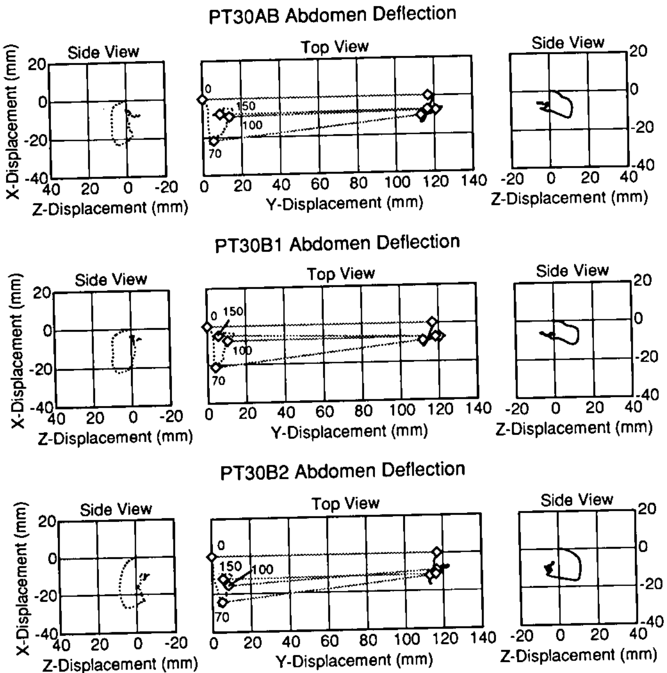

Figure 14. Three-dimensional abdomen deflection (THOR Passenger side)

positive with time in most cases, contrary to the upward (negative) displacement observed at the lower ribs. The tendency towards positive displacement is also found with the airbag only. Therefore, it is presumed that the difference in dummy posture upon impact also constitutes a factor of such displacements in addition to the effect of seat belt.

Dummy Trajectories - Figure 15 shows trajectories of heads, shoulders and knees of the THOR and HyIII dummies, for each dummy location and the kind of restraint system.

1) Comparison with airbag restraint - Comparison of head trajectories on the driver side with those with the airbag only shows that the head of HyIII starts going down sharply from 80 ms, while the head of THOR continues a linear motion as shown in Figure 16. The pelvis forward trajectory of HyIII is longer than that of THOR, and the pelvis slips down from the front end of seat cushion as the displacement attain maximum value. The pelvis forward trajectory of THOR is shorter than HyIII, and the change in pelvis position is also smaller. As shown in Figure 17, the upper torso of THOR is bent forward, while the upper torso of HyIII is not bent but the pelvis is submarined. This is presumably due to differences in shape of pelvis and the manner thighs are attached to the pelvis.

2) Comparison with seat belt restraint - Comparison of head trajectories on the front passenger side with the seat belt only shows that the head of THOR makes a larger circular motion than that of HyIII as shown in Figure 18. There are also differences between the two dummies in terms of chest deflection and neck bending angle. Namely, the upper torso of THOR with a less stiff chest is bent forward more than that of HyIII, and the head of THOR contacts the upper portion of thighs as the neck is bent forward furthermore, which is not found in the HyIII dummy. The shoulder trajectory, on the other hand, is longer for HyIII which makes a larger circular motion than THOR which moves roughly linearly. This is presumably due to the effects of differences in chest stiffness and the trajectories of the upper extremities caused by the difference in shoulder structure.

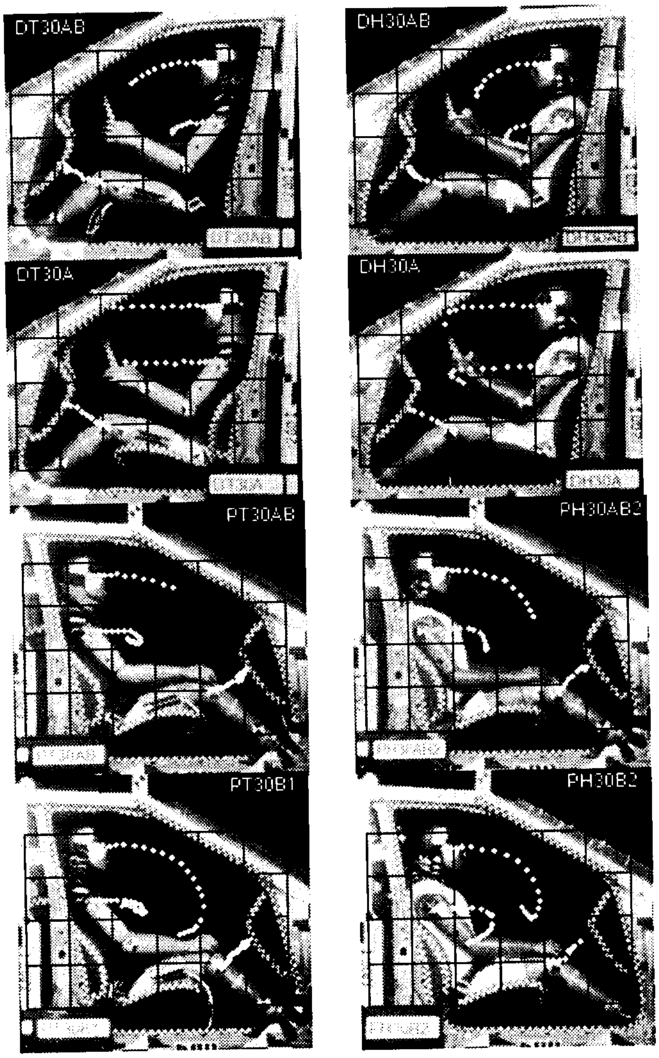

Figure 15. Dummy trajectories

COMPARISON OF THOR AND HyIII BIOFIDELITY

Characteristic features of the THOR and its differences from the HyIII have been evaluated through a series of experiments conducted under this study, which will be described below. If those features and differences are

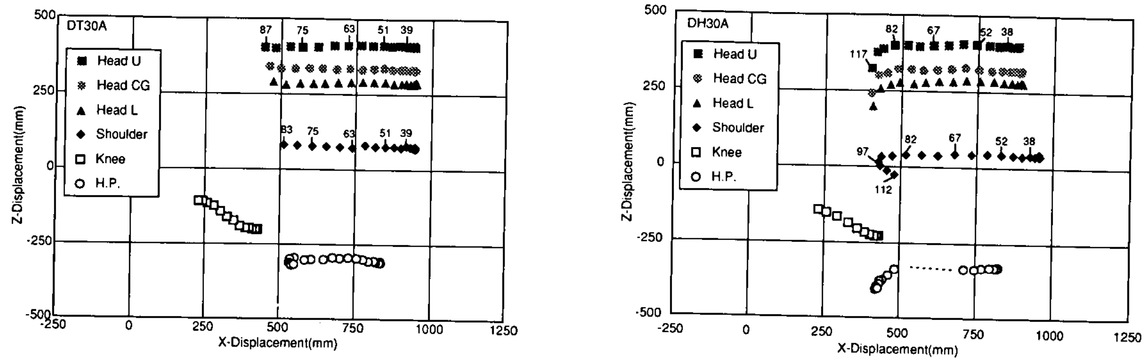

Figure 16. Comparison of trajectories between THOR and HyIII (Driver, Airbag only)

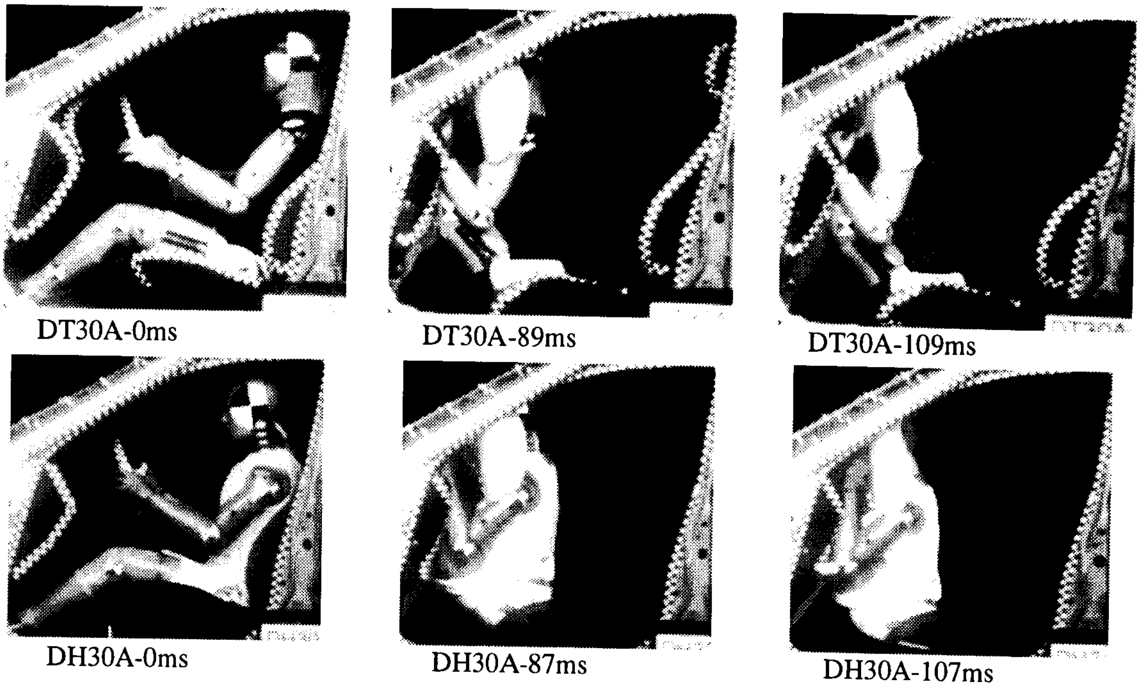
DT30A-0ms
DT30A-89ms
DT30A-109ms
DH30A-0ms
DH30A-87ms
DH30A-107ms

Figure 17. Comparison of dummy posture between THOR and HyIII (Driver, Airbag only)

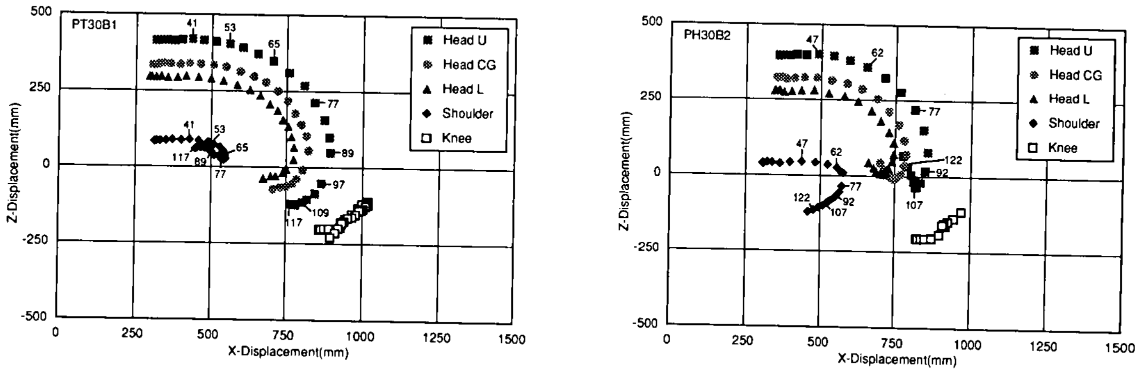

Figure 18. Comparison of trajectories between THOR and HyIII (Passenger, 3P seat belt only)

reflecting human characteristics with a higher accuracy, the utility of THOR as an evaluation tool will be enhanced.

1) The neck structure of the THOR is softer than that of the HyIII, resulting in a large bending motion of the lower region upon impact.
2) Difference in shoulder trajectory between THOR and HyIII - presumably due to the difference in structure - and the difference in trajectories of upper extremities caused by the above were particularly significant where only the seat belt was used.
3) The value of lower rib displacement was negative on the buckle side, while that on the opposite side was positive with the seat belt. Such rib displacements had been also observed in the tests conducted on the TAD in past[2].
4) In case where only the airbag was used as the restraint system, the lower abdomen expanded outward due to the force of inertia where the abdomen did not interfere with the airbag, resulted in a positive value on the displacement gauge.
5) The upper torso of THOR tended to bend forward more than that of HyIII upon impact, due to differences in shape of the pelvis and segmentation of the pelvis and femur in the two dummies.

APPLICABILITY OF MEASURED DATA TO INJURY ASSESSMENT

Some differences from the HyIII have been observed in the THOR in terms of regions that have become possible to measure and the measured values as described below. Clear determination of the correlation between the measured data and human injuries will be necessary.

1) Difference in HIC value is also observed between the THOR and HyIII, presumably due to the addition of articulation to the spine and the difference in structure of the neck. The HIC values of THOR are approximately 0.7 to 0.8 times of those of HyIII.
2) Significant difference is found in neck moment between the two dummies. This may be caused by the difference in neck structure and also because all data required to calculate neck moment for THOR were not available.
3) Chest vertical and lateral displacements can be measured with the THOR, same as the case with the TAD, which allows the determination of local displacements.
4) Displacement at the center of the upper abdomen and those on right and left sides of the lower abdomen can be measured with the THOR, which allows more accurate determination of interferences with the seat belt and/or airbag.

CONCLUSIONS

In keeping with the joint international R & D efforts by NHTSA, a prototype THOR dummy was leased to JARI/JAMA. We have measured THOR impact responses under the conditions used for the evaluation of occupant protection performance of Japanese mass production vehicles. We have also tested the HyIII dummy at the same time for comparison. The evaluation results of the THOR dummy obtained by the comparison are as follows.

1) The HIC of THOR dummy tends to show smaller values than those of the HyIII dummy, due to the differences in structures of the neck, chest and spine. Some difference in the head acceleration waveform is also found. It will be necessary to check on such differences in comparison to human characteristics.
2) The upper torso of the THOR shows more flexible motions than the HyIII dummy, due to the differences in structures of the neck, chest and spine. Some difference in trajectories of upper extremities is also found.
3) The THOR dummy chest acceleration waveform shows a slower rise than that of the HyIII dummy. Their peak values, however, are similar except for some case where there was metal-to-metal contact near the chest C.G. accelerometer housing.
4) Measured data of chest displacements cannot be compared directly between the two dummies. It appears, however, that both of them show similar tendencies according to the test data taken separately with each restraint system. The practical applicability as an evaluation tool also seems to have improved, as the displacements can be measured three-dimensionally at four points - at upper/lower and right/left regions of THOR dummy - and the influences of individual restraint systems on those regions can be also determined.
5) There is more information on displacements of abdomen as in the case of chest displacement. However, it will be necessary to further study factors that may influence additional displacement measurement.
6) We observed several differences between the response of the HyIII and the THOR dummy in our tests. These may have been caused by difference in design of the two dummies. It will be necessary to compare the response of THOR with cadaver under similar loading conditions in order to evaluate its biofidelity.

After the completion of our tests, improvement of spine structure to eliminate the metal contact, addition of neck and face load gauges, etc. have been done for the THOR dummy, and the evaluation tests are still going on. Therefore, it is expected that the THOR dummy will become a more practical and useful advanced dummy by utilizing the outcomes of the efforts mentioned above.

We have been unable to evaluate the durability and handling ease of the dummy sufficiently under this study, because of the relatively short dummy lease-out period.

ACKNOWLEDGMENT

The THOR dummy was designed by General Engineering and Systems Analysis Company (GESAC) under a contract entrusted by the National Highway Traffic Safety Administration (NHTSA) of the US Department of Transportation. The evaluation tests have been conducted by Japan Automobile Research Institute (JARI) with the financial aid provided by Japan Automobile Manufacturers Association (JAMA).

The authors wish to express their sincere appreciation to the members of the Advanced Frontal Dummy Working Group (JAMA) for their contributions to the establishment of the test program and the analysis of the test data.

REFERENCES

1) UNCONFIRMED MINUTES, SAE TASK GROUP ON FRONTAL IMPACT DUMMY ENHANCEMENTS of the SAE HUMAN BIOMECHANICS AND SIMULATION STANDARDS COMMITTEE, June, 1997.

2) Ono, Hayano, Ito, Matsuoka, "Evaluation of TAD-50M Dummy Prototype Performance in HYGE Sled Tests". 15th ESV Conference, May, 1996.

3) UNCONFIRMED MINUTES of the SAE Task Group on Frontal Impact Dummy Enhancements, of the Mechanical Human Simulation Subcommittee of the Human Biomechanics and Simulation Standards Committee, June, 1996.

4) UNCONFIRMED MINUTES of the SAE Task Group on Frontal Impact Dummy Enhancements, of the Mechanical Human Simulation Subcommittee of the Human Biomechanics and Simulation Standards Committee, Oct. 1996.

5) Rangarajan, Shams, White, Zhao, Beach, Haffner, Eppinger, Digges, "Design and Evaluation of an Instrumented Abdomen for the NHTSA Advanced Dummy". 15th ESV Conference, May, 1996.

DEVELOPING EXPERIMENTAL CERVICAL DUMMY MODELS FOR TESTING LOW-SPEED REAR-END COLLISIONS

Noboru Shimamoto
Masatoshi Tanaka
Daihatsu Motor Company, Ltd.
Sadami Tsutsumi
Hiroaki Yoshida
Yoichi Miyajima
Kyoto University
Japan

Paper Number 98-S9-O-10

ABSTRACT

In recent years, many studies have been made in the biomechanical and other fields on, "whiplash" or cervical vertical sprain which is on type of injury sustained by vehicle occupants in low-speed rear-end collisions.

This paper describes a cervical analysis of whiplash occurring in the lower rear-end collision. In particular, it describes the use of a more humanized biomechanical cervical model to analyze cervical behavior in low rear-end collisions. The results of tests with this model were verified on the TRID-II Neck* and the Hybrid-III Neck models.

INTRODUCTION

The percentage of accidents resulting from collisions in recent years, accounts for 27.5 percent of all vehicle accidents in Japan(Figure 1.).Though the death rate is low in these type of accidents, the minor injury rate is very high (Figure 2.). About 90 percent of these minor injuries are neck injuries and the so-called " Whiplash injury " which is prone to occur in these low-speed rear-end collision makes up a large share of these injuries.

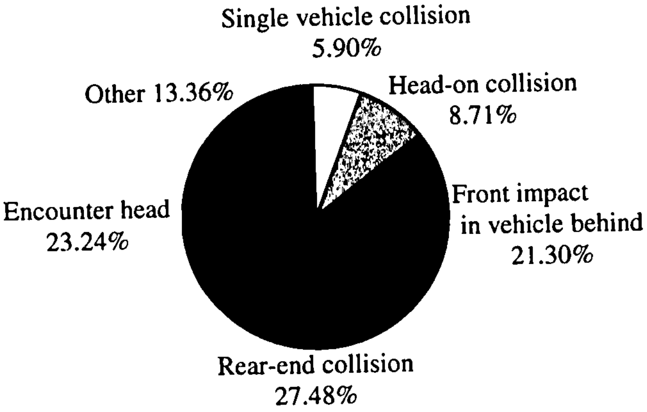

Figure 1. Accident typical other crew several ratioes.

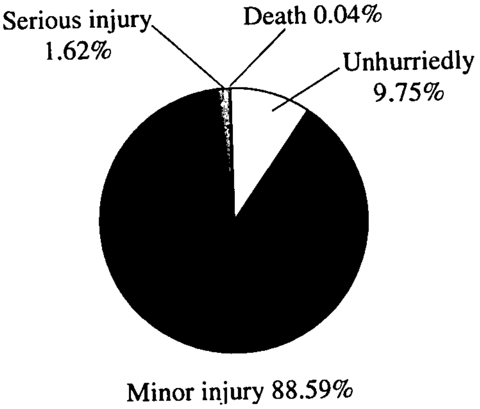

Figure 2. Injury level ratio of a rear-end collision driver.

A look at the totals for occurrence rate of neck injuries and barrier conversion speed (Figure 3.) shows that 70 percent of all people sustained their neck injuries at a barrier conversion speed (Delta V =) of approximately 8 kilometers per hour.

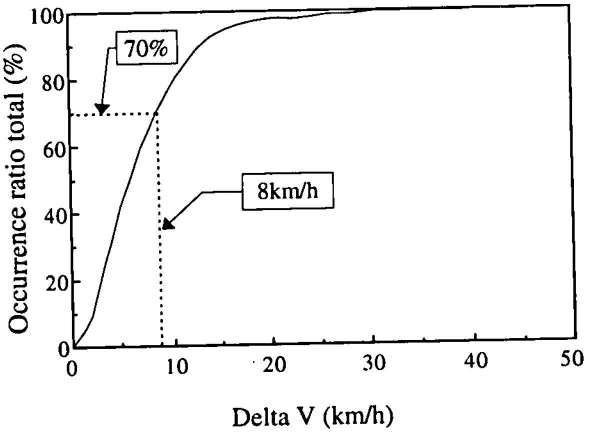

Figure 3. Neck injury accumulated occurrence rate of a rear-end collision

---

* Dummy neck model for the rear-end collision as TNO company develops use.
(TRID = TNO Rear Impact Dummy)

With this as a background we commenced our study of whiplash injury occurring in rear-end collisions.

While making studies using a biomechanical cervical model that more closely approximates the human form. We also investigated the mechanism that causes whiplash and made comparisons with the TRID-II Neck and Hybrid-III Neck model.

NECK MODEL CONFIGURATIONS

Biomechanical Cervical Model

The neck of the human body (Figure 4.) is composed of cervical vertebrae, ligaments, intervertebral disks, muscles and the other items. The speed of muscular response to stimulation is approximately 150 to 250ms. We decided we could exclude taking into account other phenomena that exert effects on muscles. This model is therefore comprised of three elements : cervical vertebrae, ligaments and intervertebral disks. An integrated, polymerized artificial material with biomechanical properties that closely resembled the matching parts in the human body was used.

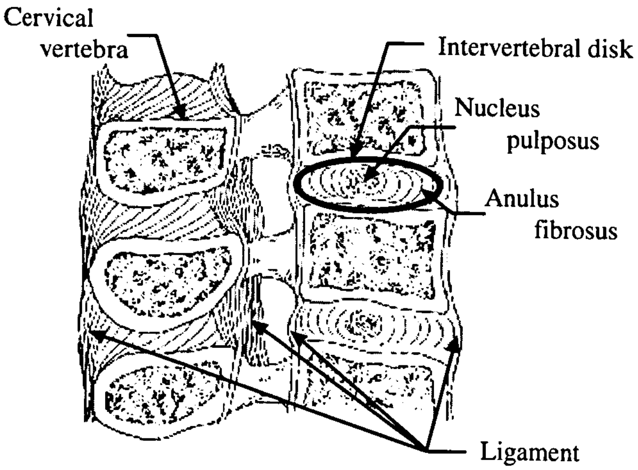

Figure 4. Structure of a human body neck

Substituting The Cervical Vertebrae

A copy of the cervical vertebrae were made from polyurethane based on a medical model of the cervical vertebrae*.

Substituting The Ligaments

Three-dimensional textiles** were used for the ligaments. These were comprised of multifilament and cotton thread using coupling thread (multifilament etc.,) having the correct rigidity forming a three- dimensional structure both lightweight yet having good elasticity.

Substituting The Intervertebral Disks

Silicon rubber was utilized.

Other Items

The cervical ligaments were covered with colorless silicon rubber*** in view of the soft tissue structures around the ligamentous neck. The colorless, transparent rubber allowed observation of movements of the biomechanical cervical model.

Figure 5 shows the biomechanical cervical model. The first cervical vertebra was eliminated in the Hybrid-III dummy that was actually used.

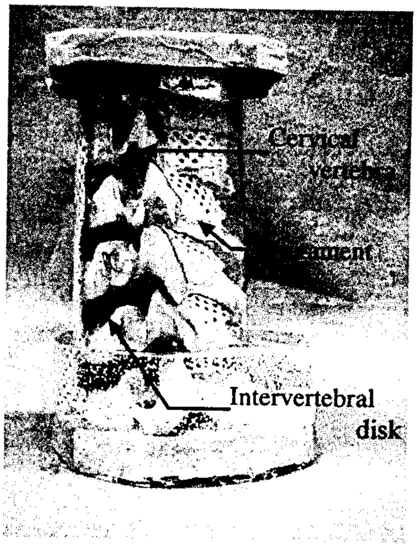

Figure 5. A new biomechanical neck model in rear-end collision

Hybrid- III Neck Model

The Hybrid-III dummy was developed based on experimental data from volunteers and cadavers. The neck structure is composed of five pieces of aluminum plate with hard rubber connecting them between the plates.

This neck model was designed for use in frontal impact tests at high speed so use of this model in low-speed impact tests needs further consideration.

TRID-II Neck Model

The TRID-II neck model was developed by TNO. This neck structure is composed of seven pieces: two upper and lower aluminum plates and five plastic plates. Integrates soft rubber disks were placed between each plate as a substitute for the intervertebral disks.

This neck model is only for use in rear-end collisions at low-speed of 25 kilometers per hour or less and more closely simulates the human body compared to the Hybrid-III neck model.

---

[*] Cervical vertical model for a medical science, Synthes Ltd.

[**] Cubic-eye HA6003, Yunitika Co., Ltd.

[***] RTV Rubber KE1603, Shin-Etsu Chemical Co.,Ltd.

NECK MODEL COMPARATIVE VERIFICATION TESTS

Pendulum Test

Several pendulum tests were carried out as part of the conventional dummy certification tests including evaluations as to whether the biomechanical cervical dummy was adequate and cervical sections of each dummy model were also compared. Measurement items included the neck angle rotation and the neck bending movement.

Test Results and Discussions

In order to evaluate whether the biomechanical cervical dummy was adequate, the neck rotation angle and neck bending movement were collated and compared with previous documents[*] and the evaluation then carried out. (Figure .6)

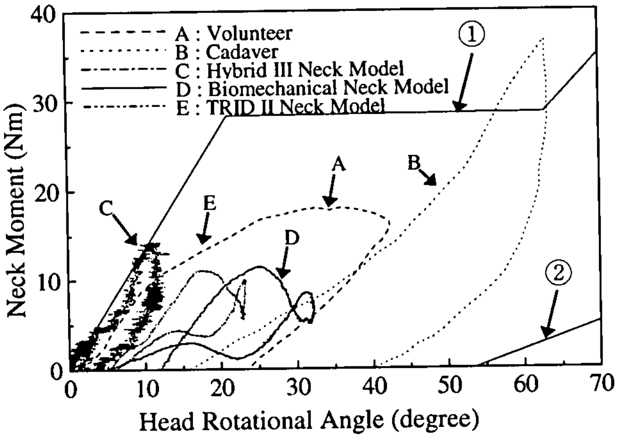

Figure 6. Neck extension torque vs angle responses

The cadaver test data is from results at a collision speed of 16 kilometers per hour and the volunteer test data is from results at 5 to 7 kilometers per hour. The dummy and biomechanical cervical model test data is from results at 5 kilometers per hour. The lines ① and ② in Figure. 6, are test results obtained from the cadaver and volunteer tests. The dummy test results must fall within this area.

Cadaver

Cadaver muscle tissue has no stiffness in the muscular tissue so the bending moment first occurs after a certain increase in the rotation angle.

Volunteer

Muscle tissue in volunteers has stiffness since the test subject contracts his muscles in anticipation of the impact.

Hybrid-III neck model

The Hybrid-III neck model was mainly designed for use in frontal impact tests and thus is too stiff for use in low-speed rear-end collision tests.

TRID-II neck model

The TRID-II neck model has a structure similar to that of the human neck so it more flexible than the Hybrid-III and has properties similar to the biomechanical cervical model.

Biomechanical cervical model

The head rotation angle of the biomechanical cervical model is greater that the other models in spite of a smaller bending movement. Therefore, the biomechanical cervical model is less stiff than the Hybrid-III neck model.

Based on the above results we concluded that the biomechanical cervical model had more flexibility when compared against the other dummy models. Whiplash damage also occurs when the subject does not anticipate a collision so muscle strain or contraction was not considered a significant factor here. In other words, our biomechanical cervical model simulates well the status of a driver who is not anticipating a collision.

Sled test

In the next step of the testing, sled tests were carried out using three neck models and neck action when not subjected to impacts was analyzed.

A driver seat was affixed to the sled as shown in Figure 7. A Hybrid III 50th percentile dummy was used and restrained with a seat belt. The different neck models were installed and test items such as dummy action and the load on the dummy neck at that time were measured. Test results are shown in Table 1.

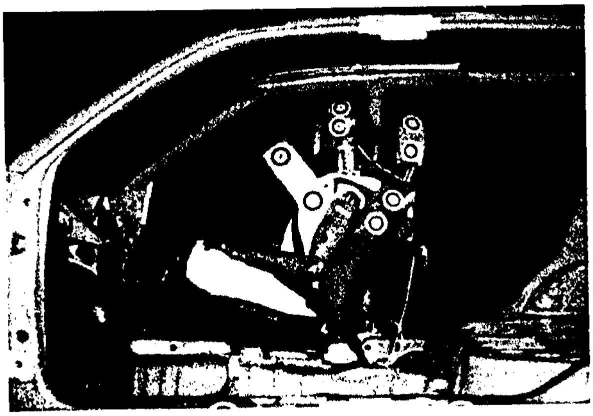

Figure 7. Sled test

---

[*] Meltz,H.and Patrick,L.,Strength and Response of the Human Neck, SAE Paper No.710855 (1971)

Table 1. Test condition

Velocity	8 km/h
Seat	Front Drivers Seat
Headrest	It is existing
Dummy Model	Hybrid III 50th percentile dummy

Results and discussions

The head and chest time acceleration curves and head rotation angle obtained at a speed of 8 kilometers per hour are shown respectively in Figure 8, Figure 9, Figure 10.

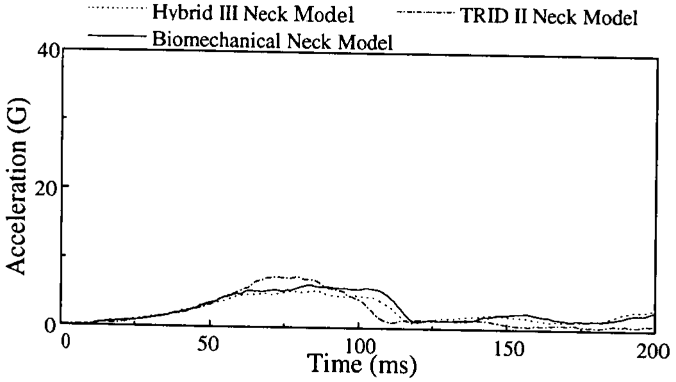

Figure 8. Chest acceleration

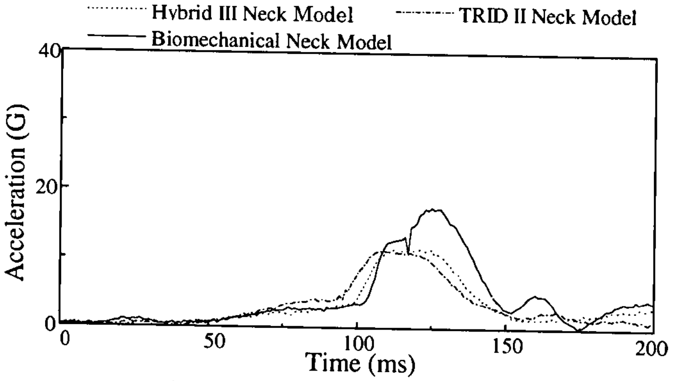

Figure 9.Head(C.G.) acceleration

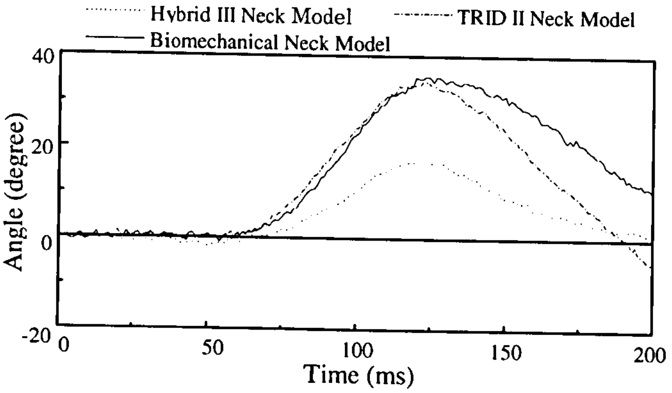

Figure 10. Head rotational angle

The chest time acceleration curve the same for both the Hybrid-III, TRID-II, and biomechanical cervical models after a reaction force from the back of the seat and returning forward after a maximum extension at approximately 100ms. In contrast, all head acceleration curves showed the same tendency up until the first 100 milliseconds after which a drastic difference appeared in the biomechanical model 110 milliseconds after the dummy head contacted the headrest. Also, on checking the head rotation angle versus the chest position in Figure 10, the biomechanical model and TRID-II models exhibited a large rotation angle while the Hybrid-III model showed almost no rotation. The biomechanical model had a larger rotation angle 120 milliseconds after contacting the headrest.

We can therefore conclude from the above results that:

(1) The Hybrid-III dummy head did not rotate much due to high neck stiffness after contact with the head restraint. The neck and head returned smoothly forward back to initial position as the chest was moved by the reaction force from the seat.

(2) Neck stiffness in the TRID-II model was lower than that in the Hybrid-III. However, after contacting the head restraint, the neck and head smoothly returned to initial condition due to the reaction force from the seat.

(3) The biomechanical cervical model on the other hand, rotates after contacting the head restraint but the chest is pressed back by the reaction force from the seat. Since the chest moves forward at this time while the head still remains in a rearward position, an offset occurs in the relative forward motions of the head and chest.

Consequently we believe that this so-called "neck offset phenomenon (Figure 11.)" occurs between the cervical vertebrae due to a deviation or offset between the forward and rearward forces. This phenomenon was not encountered in the neck sections of the Hybrid-III Neck and TRID-II Neck models. (Figure 12., 13.). We also think that this phenomenon is responsible for causing "whiplash" or neck injury.

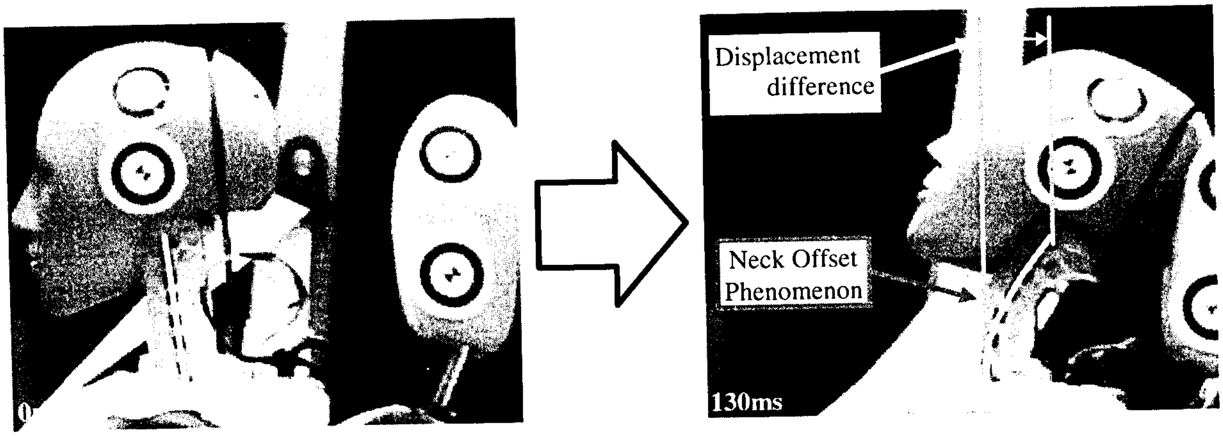
0
Displacement difference
Neck Offset Phenomenon
130ms

Figure 11. Biomechanical Cervical Model

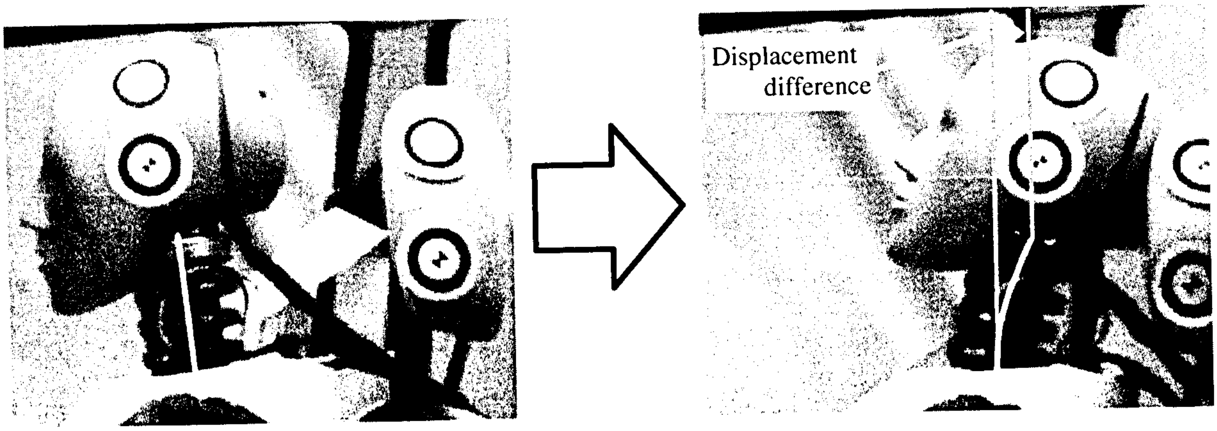
Displacement difference

Figure 12. Hybrid- III Neck Model

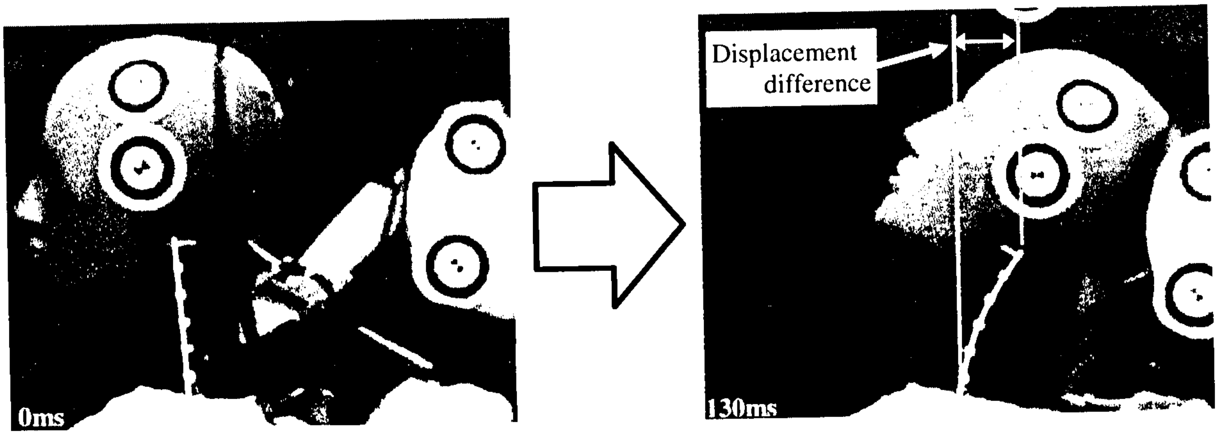
0ms
Displacement difference
130ms

Figure 13. TRID-II Neck Model

CONCLUSION

In this study, the Hybrid-III neck model, TRID-II neck model and the biomechanical cervical model were subjected to the sled test and their performance analyzed. We found the following upon analyzing the results.

(1) Neither cervical flexion or deviation or offset in the cervical vertebrae structure could be found in the TRID-II neck in the current analysis performed in the low speed region.

(2) The biomechanical cervical model however revealed cervical phenomenon which did not appear in the Hybrid-III dummy test. We think that this phenomenon occurs between the second, third and fourth cervical vertebrae, initiating a large shearing force which presses on spinal nerves and blood vessels causing injuries.

(3) The Hybrid-III neck model had too much stiffness to allow a detailed analysis of neck behavior in low-speed rear-end collisions.

We conclude from this study that the biomechanical cervical mode holds great promise as a tool for exposing the mechanism that causes neck injury and further research and development of this model will yield even greater results in the future.

REFERENCES

(1) Japan Automobile Research Institute, Inc., "Research of a traffic accident", (1992)

(2) Japan Automobile Research Institute, Inc., "Research of a traffic accident", p85 (1986)

(3) Richard S.Snell, "Snell Clinical Anatomy", Medical Science International Inc., in Japanese, p718 (1983)

(4) Hiroshi Ouchi et al, "Partial charge anatomy", Kanahara Publication, in Japanese, p27-33 p181-185 (1950)

(5) Yoshihito Ikada, "Biomaterial first step", Academic society publication center, in Japanese, p76 (1993)

(6) J.Chazal et al, "Biomechanical Properties of Spinal Ligaments and a Histological Study of the Supraspinal Ligament in Traction", J.Biomechanical, Vol.18, No.3, p167-176 (1985)

(7) Kotohito Yoshimura, "Physiologically human body", Kougakkann, in Japanese, p165 (1981)

(8) Michio Inokai, "Exercise physiological first step", Anjyusyoin, in Japanese, p128-129 (1963)

(9) Meltz,H.and Patrick,L., "Strength and Response of the Human Neck", SAE Paper No.710855 (1971)

(10) Sadami Tsutsumi, Hiroaki Yoshida, Yoichi Miyajima, "Impact Analyses of Whiplash Neck Behaviors in Rear-End Collisions", JSME Paper No.96-1088 (1997)

DYNAMIC RESPONSE AND INJURY MECHANISM IN THE HUMAN FOOT AND ANKLE AND AN ANALYSIS OF DUMMY BIOFIDELITY

Paul Manning
Angus Wallace
The University of Nottingham

Clare Owen
Adrian Roberts
Charles Oakley
Richard Lowne
The Transport Research Laboratory
United Kingdom
Paper Number: 98-S9-O-11

ABSTRACT

Lower leg injuries are the most frequent severe injury (AIS/3) to car occupants resulting from frontal impacts. Consequently it is important to be able to detect and quantify the risk of these injuries from car impact tests. The need for a more biofidelic instrumented lower leg and the development of well-founded injury criteria has been clearly identified. At present there are insufficient biomechanical data available to aid the design and construction of such a dummy leg or to define injury risk criteria.

Three phases of a research programme are reported. In phase one, a driving simulator trial was carried out using 24 subjects to investigate the positioning and bracing of the driver's lower leg prior to an emergency-braking event. In the second phase of the work, low energy impact tests have been carried out on post mortem human surrogate (PMHS) legs and volunteers. Comparative tests were performed on existing Hybrid III and GM/FTSS dummy feet/ankles. A new method to generate an Achilles force is reported which has been used to enable studies to be carried out into the effect of bracing by plantar flexion, such as emergency braking. Dynamic tests were based on the EEVC foot certification test procedure. The programme included tests to produce inversion and eversion. Additional toe impact tests were performed to assess lower leg behaviour with pre-impact bracing, allowing for future comparisons with the ALEx leg.

Difficulties inherent in the interpretation of PMHS testing are reviewed and comparisons between tests on PMHS subjects and human volunteers are presented.

The final part of the paper reports the findings of an in-depth retrospective accident analysis based on data in the UK Co-operative Crash Injury Study database. Accidents in which the front seat occupant had sustained a lower leg injury of AIS/2 in a frontal collision were examined along with the associated hospital notes and X-rays. The injuries are ranked in terms of frequency, severity and impairment in order to determine which lower leg injuries that are a priority for prevention.

INTRODUCTION

Historically, regulatory tests have been aimed at reducing the incidence of serious injuries to the body regions where there is a high risk of a fatal outcome. Thus protection criteria for the head and chest have been foremost in the early regulations. Significant improvements have been seen in the protection afforded against fatal injuries to these body regions and more attention is now being paid to the serious and debilitating injuries that contribute markedly to the societal costs of road accidents. For this reason, a requirement for injury protection to the leg and ankle was included in the EU Directive on Frontal Impact [1]. The ankle joint of the Hybrid III dummy was modified to include a soft bump stop at the ends of the articulation range to allow the measurements of the injury criteria to be made more reliably. This was regarded as a first step in the improvement of the protection for leg, foot and ankle injuries.

There have been a number of studies of lower extremity injuries. The long-term consequences of lower extremity fractures have been investigated by Luchter [2]. He analysed the outcome of lower extremity injuries resulting from police reported tow-away motor vehicle crashes in the US in 1993. Lower extremity injuries accounted for 17 percent of the total cost of these collisions but accounted for 41 percent of the life years lost as a result of injury. Miller, Martin and Crandall [3] stated that in police reported highway collisions in the US in 1993, lower limb injuries cost an estimated $21.5 billion in passenger vehicle occupant injury costs.

In France, Salmi et al [4], in a population based cohort study to look at long term post traumatic disablement, concluded that lower extremity injuries are one of the most frequent sources of injury-related hospitalisation and that they result in substantial long term morbidity.

From Australia, Fildes et al [5] have reported that lower limb injury occurs in about 40% of passenger car crashes that result in injury. Three quarters of all fractures occurred below 64 km/h. No simple relationship was apparent between intrusion and fracture of the lower limb and the authors state that it is possible that foot and ankle injuries can occur simply from the excessive loading that comes with bracing.

The increasing need to focus on non-life threatening car crash injuries has resulted in renewed interest in car crash dummy design and a number of research projects have focused on comparative tests on Post Mortem Human Surrogates (PMHS). A further development has been the realisation that PMHS specimens in themselves are not completely biofidelic and that they lack the properties of a physiologically active human being. In particular they lack any active muscle tension that would resist movement in a live human being [6-10].

In 1996, Crandall et al [11] reported a series of sled tests using PMHS specimens and the Hybrid III dummy. They concluded that the Hybrid III records greater axial tibial loads and ankle dorsiflexion than the PMHS in comparable conditions. In 1995 Schueler et al [12] reported a series of 60 dummy tests and 24 PMHS specimen tests using a co-axial impactor. They concluded that improved dummy lower legs were required for more reliable injury prediction. They recommended that improvements were needed in the following areas:

1. The kinematics of the foot and the knee joint.
2. The mass distribution and relationship of bony and muscular structures.
3. The location of measuring devices as close to the injury point as possible.

The Hybrid III Leg, Foot and Ankle

The standard Hybrid III dummy is based on a fiftieth percentile male. Within the dummy the pivot point of the knee is designed to be 49 cm from the ground and with the tibial plateau 44 cm from the sole of the foot with the ankle in the neutral position. The foot measures 26 cm in length and 10 cm in breadth. The lower leg assembly weighs 5.7 Kg. The foot and ankle assembly of the Hybrid III comprises a ball and socket type joint that is intended to simulate the movements of both the ankle and subtalar joints (Figure 1). Initial contact of the ankle shaft and ankle bumper occurs at 36° of dorsiflexion movement and is fully compressed at 45° of movement in this direction and 35° of plantar flexion. Eversion/inversion initial contact occurs at 20° of movement with a maximum 23° of rotation being achieved in each direction. [13]

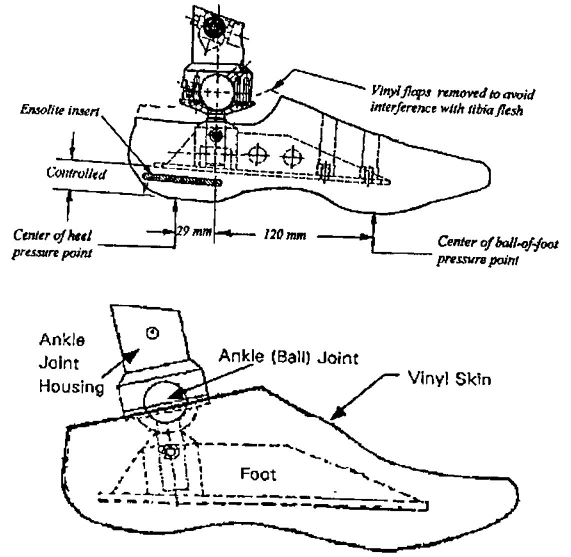
Vinyl flaps removed to avoid interference with tibia flesh
Ensolite insert
Controlled
Center of heel pressure point
29 mm
120 mm
Center of ball-of-foot pressure point
Ankle Joint Housing
Ankle (Ball) Joint
Vinyl Skin
Foot

Figure 1 - The Hybrid III Foot Assembly

The GM/FTSS Advanced Foot and Ankle

The GM/FTSS foot has been designed and manufactured to attach to the distal end of the Hybrid III lower leg assembly. In the GM/FTSS foot the ankle joint is represented by a hinge joint, and the subtalar joint by the inclusion of a further ball and socket joint below the ankle hinge (Figure 2). A compliant and continuous joint stop has been included that allows 60° of plantar flexion and 45° of dorsiflexion. In addition 30° of eversion and 35° of inversion are possible. A further joint is positioned in the midfoot position to represent movement within the foot arch, mid-tarsal and metatarsal joints. As with the Hybrid III foot, no instrumentation is included in the foot and ankle assembly.

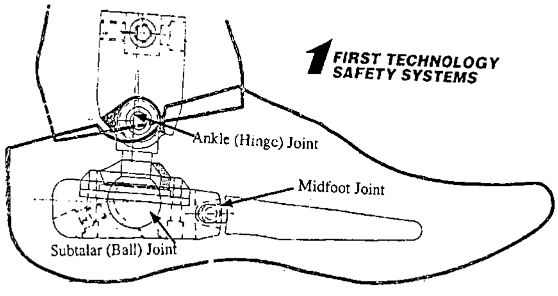

Figure 2 - The GM/FTSS Foot Assembly

Centres of Rotation

The centres of rotation of the hind foot joints for PMHS and dummy joints have been studied by several institutes including Crandall et al [9]. In their PMHS tests they report the centre of rotation for dorsiflexion at a distance of 76 ± 8 mm from the sole of the foot and 61 ± 6 mm from the posterior face of the heel. The centre of rotation in inversion and eversion was 71 ± 12 mm from the sole of the foot and 3 ±12 mm from the long axis of the leg. The Hybrid III foot and ankle moves in the planes of dorsiflexion and plantar flexion and inversion and eversion at the centre of its ball joint 82.6 mm from the sole of the foot. In the GM/FTSS foot the centre for dorsiflexion & plantar flexion has been calculated at 58 mm from the sole of the foot. The centre for inversion and eversion coincides with the position of the simulated sub-talar joint at 39 mm from the sole of the foot (Figure 3).

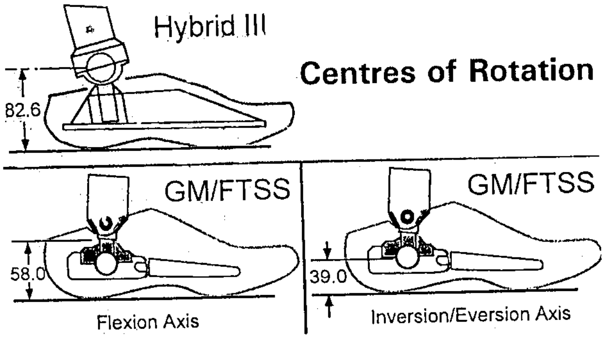

Figure 3 – Centres of Rotation for Dummies

The normal ranges of motion for male subjects aged 30-40 years were reported in 1982 by Roaas and Anderson [14]. In this study which was conducted using simple goniometers they reported the following results for the ankle joint. Dorsiflexion 5 to 40°, mean 15.3°; Plantar flexion 10 to 55°, mean 39.6°; Eversion 15 to 50°, mean 27.7°; Inversion 15 to 50 °, mean 27.7°. In PMHS specimens, movement to a greater degree, which would be beyond the pain threshold in a normal human, is possible without apparent damage.

Mass and Moments of Inertia

A number of laboratories have studied mass and moments of inertia differences for the lower leg [9], and measurement for comparison have been made in the tests reported in this paper. They are compared with other published data in the results section of this paper.

Summary of Tests to Date

In summarising their collected work, comparing the dummies to PMHS specimens, Crandall et al [9] conclude that the GM/FTSS and other new generation feet (ALEx II and Hybrid III with bump stop) show improvements in many parameters that give them a biofidelic advantage over the original Hybrid III. They highlighted important differences in geometry and consequently stability and response to load. In their work on the dynamic response to load, they highlight the importance of active and passive musculature in determining the axial and rotational responses of the lower leg. The gastrocnemius muscle group was shown to influence both the moment angle joint characteristics as well as the loading in the tibia and fibula during dorsiflexion.

In his thesis Portier [15] summarises both his own work and the collected data of other centres and makes some important conclusions with respect to the physical properties of the lower leg. His results showed substantial differences in centres of pressure, centres of rotation, inertial properties and axial stiffness.

In further work reported at Stapp 1997, Portier et al. [15] reported on the results of further sled tests. They supported the consensus view that the GM/FTSS foot was more biofidelic than the Hybrid III, but highlighted deficiencies in the moment rotation relationship. They firmly conclude that passive and active muscle tension should be included in future dummies to obtain improved ratios between the shear and compressive forces in the ankle joint.

This paper reports work carried out within the LLIMP project (Lower Limb Injuries, Methods of Prevention) which has been performed through the collaboration between the Transport Research Laboratory, the University of Nottingham and the Vehicle Safety Research Centre of the Institute of Consumer Ergonomics. This group has bought together doctors and engineers with a specialist interest in car crash injury prevention.

The first section of the paper reports the details of a series of driving simulation tests designed to assess the kinematics of the lower leg during emergency manoeuvres when driving and to evaluate the forces of braking generated at the same time. This is followed by a report of the biofidelity study comprising a series of low energy impact tests with PMHS specimens (through-knee amputations, above knee amputations and specimens with an applied plantar flexing force). These tests were then repeated with volunteers and with two different dummy feet to assess biofidelity.

Lastly the results of a recent, in-depth, accident analysis are given. This analysis focuses not only on the extent of the problem of lower leg injuries in the UK, but more importantly addresses fracture mechanisms and injury impairment scoring through an analysis conducted jointly by the Vehicle Safety Research Centre and the Department of Orthopaedics at the University of Nottingham.

This paper concludes with an overview of further work in this field currently being performed by the LLIMP collaborative group in the United Kingdom.

DRIVING SIMULATOR TRIALS

This study was designed to evaluate the kinematics of the driver's lower leg during braking, in a simulated emergency, whilst at the same time measuring the applied brake pedal force. The aim of this part of the study was to provide information on the position and extent of muscular bracing in the lower leg during emergency braking. These are thought to influence the potential risk and mechanism of lower leg injury in car crashes.

A driving simulator with realistic three-dimensional graphics (Silicon Graphics) has been developed at TRL (Figure 4). The simulator is based around a full-scale car (Rover 400, right hand drive configuration). The simulator was fitted with two hidden infrared cameras to record foot movements. A pressure transducer in the vehicle brake line was used to record applied brake pedal pressure. One of the cameras provided a view of the drivers' feet from underneath the drivers' seat and the second a lateral view from under the dashboard. Use of a driving simulator allows safe exposure to realistic driving scenarios, including emergencies.

To enhance the kinematic analysis, which included video recording, subjects were also fitted with a goniometer (Penny and Giles) to their right ankle to record both ankle joint and sub-talar joint movement.

Subjects

This study was conducted in two phases, each using twelve subjects, six male and six female. In both phases, all subjects had prior experience of driving the simulator. Each subject was led to believe that the driving task was speed control. Before each test each subject's sex, age, height and build were recorded. At the conclusion of each test, the subjects were questioned to ascertain how realistic they considered the simulation to be.

Test Configurations

In phase 1, two 'static' emergency events, a "military tank" obstructing the road and a fallen tree across the road, were introduced into a thirty-minute driving simulation. The location of the tank and the fallen tree were on a bend in the road, and over the brow of a hill respectively. In the second phase of the trial, the simulation was enhanced to include more traffic on the road during general driving, and the first static event was replaced with a dynamic emergency event. This took the form of a vehicle on the other side of the road overtaking into the path of the driver in the driving simulator. The event was designed such that the likelihood of the driver swerving to avoid the oncoming vehicle rather than braking was minimised. After the second emergency event in both phases of the trial, the simulation was terminated and the subject informed of the true purpose of the trial.

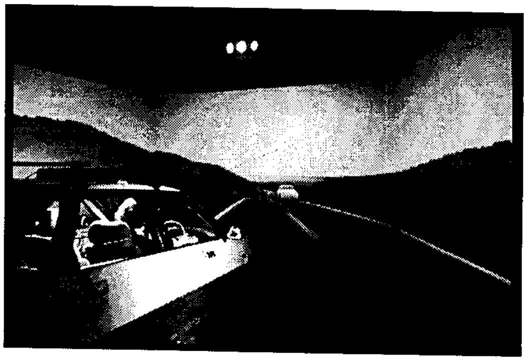

Figure 4 – The TRL driving simulator

Table 1 shows a summary of the physical data collected for each subject in the trial, and an indication as to the realism of the simulation as experienced by the subject. The recorded maximum braking force for both emergency events and the degree of plantar flexion of the right foot during the first emergency event is also presented in Table 1.

In both phases of the trial, a visual inspection of the video recordings showed that most of the subjects drove with their heel longitudinally in line with the brake pedal or longitudinally in line with a point between the brake pedal and accelerator. The foot was rotated clockwise and slightly plantar flexed to allow depression of the accelerator. Only four subjects drove with their heel in-line with the accelerator while driving. When responding to the emergency event, two different movements were used to depress the brake pedal. The first was lifting the foot off the floor and stamping on the brake pedal, the second involved rotating the whole foot onto the brake pedal and plantar flexing the foot with the heel still in contact with the floor. In addition it was observed that, although the heel was in contact with the floor as braking was initiated, in just less than 50 percent of all cases, heel to floor contact was lost as the brake pedal force was increased.

Table 1.
Simulator Trial Data for Phases 1 and 2

Subject No.	Sex	Age	Height (m)	Realistic Driving?	Max. Braking Force (N) (Event 1)	Max. Braking Force (N) (Event 2)	Plantar flexion (°)	Heel in contact during braking?	
								Ev1	Ev2
Phase 1									
1	F	20-30	1.65	No	820	821	43	Yes	Yes
2*	M	20-30	1.84	Yes	-	143	-	No	No
3	F	40-50	1.73	Yes	716	587	6	Yes	Yes
4**	F	40-50	1.69	No	807	-	1	No	No
5	F	40-50	1.58	-	817	927	17	No	No
6	M	40-50	1.94	Yes	1474	1003	14	Yes	Yes
7*	M	40-50	1.73	Yes	775	884	-	-	Yes
8	M	20-30	1.76	Yes	735	466	26	No	No
9	F	40-50	1.73	Yes	1474	862	16	No	No
10	F	20-30	1.64	Yes	620	928	15	Yes	Yes
11	M	40-50	1.7	Yes	331^{+}	252	23^{+}	Yes^{+}	Yes
12	M	20-30	1.72	Yes	636	431	21	No	No
Phase 2									
13	F	40-50	1.69	No	124	593	-5	No	No
14	F	40-50	1.68	Yes	401	554	9	No	No
15	F	20-30	1.72	Yes	249	108	14	No	No
16	M	40-50	1.83	Yes	119^{+}	84^{+}	-12^{+}	Yes^{+}	Yes^{+}
17*	M	20-30	1.82	No	-	108	-	-	Yes
18	F	20-30	1.71	Yes	214	88	6	Yes	Yes
19	F	20-30	1.67	Yes	404	200^{+}	44	No	No^{+}
20	M	20-30	1.84	No	1207	339	23	Yes	No
21	M	20-30	1.84	No	181	552	14	Yes	Yes
22**	M	40-50	1.85	No	550	-	12	No	-
23	F	40-50	1.7	Yes	482	1171	-2	Yes	Yes
24	M	20-30	1.76	Yes	1150	561	18	Yes	Yes

* - No data acquired for event 1 due to instrumentation problems
** - No data acquired for event 2 due to instrumentation problems
$^{+}$ - Data not included in analysis because speed prior to braking was less than 35mph

Combined Phase 1 & Phase 2 Results

For the purposes of this study the results of both phases of the trial have been combined. The mean peak brake force was determined to be 630N (standard deviation, σ 366N), with the ankle joint at a mean angle of 15° (σ 13°) of plantar flexion at the point of the applied peak brake force.

All the subjects in the trial used the ball of their foot to apply force to the brake pedal. The ball of the foot is represented on radiographs as the first metatarsal head. Analysis of the radiographs obtained from the PMHS specimens used for biomechanical testing in the LLIMP project indicated a 12:5 ratio in the distance between the first metatarsal head, the ankle joint centre and the insertion of the Achilles tendon. If the ankle joint is considered to act as a single axis hinge for the purpose of this estimate and it is assumed that all of the plantar flexing force is generated through the Achilles tendon, it is possible to calculate the mean plantar flexing force in the lower leg plantar flexing muscle group. Based on this assumption it was calculated that approximately 1.5kN (σ 900N) acting at the Achilles attachment would be required to recreate the mean maximum braking force seen in the two phases of the trial.

If males and females are considered separately for the two phases of the trial, the mean peak brake applied force was 636N (σ 389N) for males and 626N (σ356N) for females. For the purposes of this study, statistical significance is taken at the fifth percent level, thus this result is not statistically significant (p=0.932). There was also no significant difference in the mean angle of plantar flexion between males (18°) and females (14°) (p=0.464).

In comparing the combined results of phase 1 and 2 for event 1 and event 2, the data show that for event 1 the mean peak applied brake force was 692N (σ 397N) compared with 569N (σ 331N) for event 2, which was not statistically significant (p=0.295). The difference in the mean speed before event 1 (47mph σ 6.6mph) and event 2 (47.51mph σ 6.01mph) was also found to be not significant (p=0.846).

There was no significant difference (p=0.394) between the mean height of the subjects whose heel was in contact with the floor during braking (1.76m σ 9.12x10^{-2} m) and those subjects who lifted their heel during braking (1.72m σ 7.65x10^{-2} m).

In analysing the post-trial questionnaires, there was no significant difference (p=0.513) in the mean applied brake pedal force for subjects who thought that the driving simulation was realistic (643N σ 384N) and those who did not think that it was realistic (555 σ 347N).

A linear correlation calculation was carried out in order to determine whether there was a relationship between the subject's height and peak force applied to the brake pedal or the angle of plantar flexion. In both tests, no significant correlation was found with r=-0.003, p=0.99 for brake force and r=-0.089, p=0.752 for angle of plantar flexion. No significant correlation was found between the applied brake force and the angle of plantar flexion (r=0.231, p=0.342). An examination of the relationship between the speed prior to braking and the maximum applied brake pedal force showed a weak correlation (r=0.289, p=0.071).

Discussion of Simulator Trials

The work that has been reported here indicates that the driving simulator developed at TRL can be effectively used to evoke an emergency braking response. Our study indicated that the mean peak force applied to the brake pedal with the ball of the foot was 630N and that the right foot is plantar flexed by approximately 15° when the maximum braking force is achieved. It is not known at what point in time during an accident the ankle or foot is injured. If an injury is pedal induced and occurs during braking, as suggested by a recent accident analysis [16], then these results indicate that it would be preferable to study ankle injury with the foot in an initial plantar flexed position. The observation that for 50 percent of the drivers, the heel left the floor during the braking actions suggests that in accident investigations, firm evidence of foot position should be sought when ascertaining the mechanism of a lower leg injury. However, it is recognised that this would be extremely difficult to achieve in practice. In a similar way, biomechanical evaluations of fracture mechanisms should encompass both initial heel to floor contact and heel to floor separation. This study indicates that in future legislative crash testing the initial position of the lower leg should be better specified, particularly if the risk of lower leg injury is to be assessed.

The mean forefoot force of 630N reported in this study is significantly greater than the force used by other researchers [7] in their work to ascertain the effect of bracing on the lower leg. The simulator trial results indicate that in simulated realistic emergency situations, drivers can apply a force to the brake pedal far in excess of that required to obtain maximum braking power for their vehicles. The recent accident analysis of Taylor et al. [16] identified cases where drivers had deformed the brake pedal due to severe braking.

BIOFIDELITY TESTS

Introduction

With an increasing and ever more complex range of dummy components available for testing there is a need to be able to quantify how biofidelic each component is and how realistic the data obtained in impact testing are compared to that for a live human subject. Impact testing to injury levels cannot be undertaken on live human subjects, so conventionally PMHS specimens are used as a compromise to provide reference data. At the same time, repeated crash testing in real cars is expensive and resources are limited. There is therefore a strong desire to ensure that any data obtained in such tests are as realistic as possible.

The aim of any biofidelity research must allow for realistic modifications to dummies that will provide useful data as opposed to an attempt to recreate a surrogate so complex and diverse in its design that it becomes practical only as research tool and inappropriate for legislative testing.

Extensive work in the USA [17] has proved that, if the results of cadaveric biomechanical testing are to be repeatable and biofidelic, they can only be performed on fresh frozen specimens. Fresh frozen is a term commonly used to imply that the specimen is frozen fresh soon after retrieval and thawed at a later date prior to testing. All major international laboratories performing biomechanical studies now use fresh frozen cadavers. For the purposes of this study, fresh frozen cadaveric material has been used throughout.

Ethical approval for this study was granted by the relevant organisations in the UK.

PMHS specimen testing usually involves small numbers, most often taken from a relatively elderly population. In order that some comparison of results from different laboratories may be made, the collection of relevant anthropometric data and other physical properties is essential. In this study, a new method for normalisation of results to the fiftieth percentile using finite element modelling is described.

The tests were a series of simple sub-injury tests based around the dummy foot certification procedure [1]. Tests to examine the biofidelity of dummies in dynamic inversion and eversion impacts were introduced, in addition to the standard heel and toe impacts. While it is recognised that the currently available dummy lower legs are not all designed to incorporate a biofidelic inversion/eversion response, it is well known that these movements are involved in the mechanisms of lower leg injury [18]. It is assumed that a dummy ankle that behaves correctly in inversion/eversion would transmit loads to the leg via a more accurate load pathway to the tibia.

In the light of so many recent papers [15] highlighting the importance of the difference between the response to impact seen in a live individual and that in a flaccid cadaver, this study also reports on results of an impact analysis with volunteers. The tests in this part of the study were also conducted according to the EEVC new dummy foot certification procedure [1]. The energy delivered in each case was known to be of a sub-injury level from the results of the tests with the PMHS specimens. The results of further tests using pre-tensed or braced PMHS specimens are also reported in this paper.

No PMHS could ever be instrumented in such a way that natural muscle tension could be reproduced in all of the muscle groups acting across the knee, ankle, subtalar and other foot joints. It is also accepted that it is impossible to get a volunteer to relax and not actively contract his/her lower leg musculature when confronted with a simulated impact.

The biofidelity tests aim to provide comparative data that can be used to assess dummy leg performance compared to actual human lower leg behaviour. Full instrumentation of live human lower legs is impossible and most evaluations are made using data obtained from PMHS specimens. It is however, possible to study the kinematic response and impactor response of a live subject to a sub-injury impact.

Methods for PMHS Specimen Testing

Storage of PMHS Specimens - All specimens were initially frozen at -80°C and subsequently stored at -26°C. Each specimen was allowed to thaw for over 24 hours prior to instrumentation and subsequent testing.

Pre-Test Radiological Imaging - Standard lower leg radiographs were taken prior to the testing: An orthopaedic surgeon reviewed all radiographs for pre-existing anomalies, prior to testing. All specimens were analysed for Bone Mineral Density (BMD) using a DXA scanner.

Specimens - The specimens were all retrieved as above knee amputations, however for most tests in this study they were disarticulated through the tibio-femoral (knee) joint, and then cut cleanly at a consistently identifiable landmark just below the knee. A further additional series of tests was carried out on an above knee specimen to allow a direct comparison to be made between the two specimen types.

The PMHS specimens were all worked to allow a normal range of articulation.

Basic Physical Measurements - The following basic physical measurements were taken from the PMHS:

1. Mass of lower leg and mass of foot.
2. Dimensions:
   a) Lower leg length (tibial plateau to sole of foot with ankle at 90°)
   b) Foot length (end of first toe - dorsal edge of heel)
3. Volume of lower leg and foot.
4. Centre of Gravity.
5. Heel flesh depth at the ball and heel of the foot.
6. Moment of inertia about the y-axis for the leg and the y and z-axis for the foot. These were measured using a two-wire torsion tray based rig.

Potting Procedure - For the below knee specimens, the upper 5 cm of soft tissue were removed from the PMHS specimen by sharp dissection. To preserve the proximal tibia/fibula joint, the upper end of the fibula was secured to the tibia by means of a length of 5mm studding passed through a 6mm-drilled hole. The specimens were potted in standard polyester-based filler.

Tibial Load Cell - A Denton™ five axis load cell, which was a modification of the load cell used in the Hybrid III dummy, measured forces in three directions (F_x, F_y, F_z) as well as two bending moments (M_x and M_y). For this data to be comparable across all PMHS specimen tests the load cell had to be mounted not only in the correct orientation, but also maintaining the exact alignment of the tibial shaft in all planes. A special installation technique was developed which allowed exact alignment of the load cell whilst maintaining the integrity of the fibula without employing an external fixator (Figure 5). The full details of this technique are given in Appendix 1.

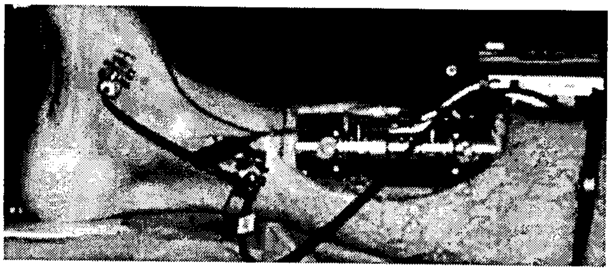

Figure 5 - Instrumented PMHS Specimen

Acoustic Transducer – An acoustic transducer was attached to a metatarsal with the object of detecting failures during the test (see end of Appendix 1).

Shoe Representation - Each PMHS was fitted with a representative sole of a shoe, which was secured by Ethibond sutures. The sole was made of industrial black Velbex Flexible 6290 plasticised PVC sheet, 3mm thick.

Physical Properties of the Instrumented Leg – The physical properties of the whole-instrumented PMHS specimen (PMHS, clevis clamp, tibial load cell, acoustic transducers and shoe representation) were measured according to the list above, excluding the volume measurements.

Pendulum Rig - A simple rigid pendulum impactor rig was used to perform the dynamic tests for this study. The design of this rig was based on the EEVC new dummy foot certification procedure [1] (Figure 6). It consisted of a horizontal cylinder of radius 25±1mm and a lightweight support arm. The cylinder had a mass of 1.25±0.02kg including instrumentation and the arm has a mass of 285±5g. The pendulum was supported by a scaffold structure, which had been adapted to allow the adjustments needed to position PMHS specimens of differing lengths on the rig.

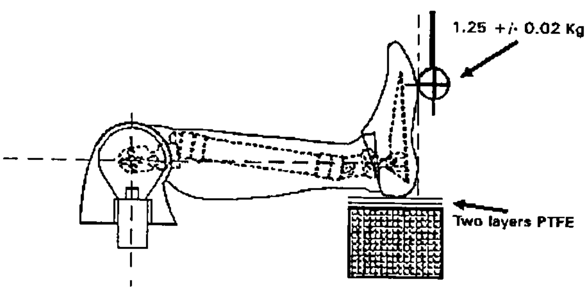

Figure 6 - Pendulum Rig Configuration

Pendulum Accelerometer - One single axis piezo-resistive accelerometer was mounted on the pendulum.

High Speed Film - Two 16mm high-speed cine cameras (lateral and overhead perspectives) operating at 400 frames per second, were used to provide a visual record of the tests.

Testing Specification

All testing for this study was designed around a derivation of the EEVC 'Tibia and Foot Certification Tests for use with the Hybrid III dummy in the EEVC Offset Deformable Front Impact Test Procedure' [1]. For the purposes of foot tests the procedure requires that (in the case of a dummy) the line joining the knee clevis joint and the ankle attachment is horizontal ± 3°, with the heel resting on two layers of low friction material. The underside (sole) of the foot should be vertical ± 3°

PMHS Specimen Orientation on the Rig - The proximal end of the specimen was attached to the back plate of the pendulum rig, using a clevis load cell. For heel and toe impacts the foot was orientated such that the second metatarsal pointed vertically upwards, with the ankle at 90° (neutral position). For inversion and eversion impacts the specimen was orientated such that the foot was resting on its medial or lateral side respectively, with the ankle remaining in the neutral position. The back plate was rigidly secured to prevent movement during impact. The specimen was orientated on the rig such that the line between the ankle joint (mid-malleolar point) and the knee joint was horizontal. This was checked by the alignment of the tibial load cell.

Lower Foot (Heel) Impact Test - The height at which the cylinder impacted the foot (as measured from the base of the heel) was calculated according to the relevant dummy test defined in the EEVC foot certification procedure. The EEVC foot certification procedure defines a height of 62mm for a total foot length of 265mm. Laterally, the centre of the cylinder was aligned with the axis of the second metatarsal. The heel impact tests were performed at 2m/sec and 4m/sec. At these impact velocities, the energy delivered is normally below the injury threshold.

Upper Foot (Toe) Impact Test - The EEVC foot certification procedure defines a height of 185mm for a total foot length of 265mm.

The toe impact tests were performed at 2m/sec, 4m/sec and 6m/sec. At these impact velocities, the energy delivered is normally below the injury threshold.

Inversion Impacts - The specimen was orientated and mounted lying on its lateral side. As above, the specimen was mounted such that the longitudinal axis was horizontal and the foot was in the neutral position. The cylinder was aligned such that it impacted the medial side of the foot, causing it to invert during impact. The height at which the cylinder impacts the foot was defined by impacting the first metatarsal head.

The eversion impact tests were performed at 2m/sec and 4m/sec. At these impact velocities, the energy delivered is normally below the injury threshold.

Eversion Impacts - The specimen was orientated and mounted lying on its medial side. As above, the specimen was mounted such that the longitudinal axis was horizontal and the foot was in the neutral position. The cylinder was aligned such that it impacted the lateral side of the foot, causing it to evert during impact. The height at which the cylinder impacted the foot was set so that it impacted the fifth metatarsal head

The inversion impact tests were performed at 2m/sec and 4m/sec. At these impact velocities, the energy delivered is normally below the injury threshold.

Test Order - The test order was changed for each specimen. This was to ensure that there was no bias in the results, due to possible changes in the articulation of the ankle, sub-talar and mid-foot joints with repeated testing.

Test Termination Conditions - All eight tests were performed unless a physical examination by an orthopaedic surgeon or the acoustic data suggested that an injury might have occurred during testing.

Post Test Procedures

After testing, the standard lower leg radiographs referred to above were re-taken. The radiographs were examined in detail by both an orthopaedic surgeon and a consultant radiologist. In addition to a clinical examination, each specimen was dissected at the conclusion of testing to exclude soft tissue and bony injuries. The physical properties of the foot were measured, after dis-articulation, for the normalisation process.

Methods - Dummy Comparative Tests

The Hybrid III lower leg fitted with the 45° articulating ankle and soft bump stop and the Hybrid III lower leg fitted with the GM/FTSS ankle and foot were used for these tests. The testing protocol was designed to mimic the tests carried out on the PMHS specimens exactly and to adhere to the guidelines of the EEVC dummy foot certification procedure [1] (Figure 7). For each dummy type and for each test configuration three identical tests were carried out. A recovery period of 30 minutes was allowed between each test as specified in the EEVC procedure.

Shoe Representation - In a similar fashion to the PMHS testing each dummy foot was fitted with a representative sole of a shoe.

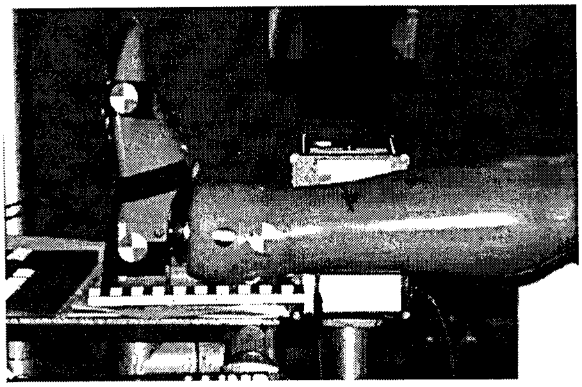

Figure 7 - Dummy Test Configuration

Methods - Volunteer Tests

Pendulum Rig - The same pendulum rig as used for the PMHS tests was used for six different volunteers. This rig was adapted to allow the volunteer to be comfortably reclined with their right lower leg in the position defined in the EEVC dummy foot certification procedure.

Instrumentation - For the tests with volunteers the instrumentation used was the pendulum accelerometer (as for PMHS and dummy tests) and a goniometer fitted to the volunteer's leg to measure the degree of dorsiflexion/ plantar flexion of the foot/ankle in response to the pendulum impact.

As with the PMHS and dummy tests, a shoe representation was fitted on to the sole of the foot and high speed cine cameras were used to film the impact.

Test Specification - The tests with volunteers were conducted both with the volunteer unaware of the impending impact to their foot and conversely with the volunteer fully aware of the impending impact. In the case of the volunteer being fully aware of the test, he/she was told to brace and resist the impacting pendulum. The volunteers were only exposed to the toe impacts and not the heel, inversion or eversion tests.

The volunteers were made unaware of the impending impact by wearing headphones and by being blindfolded for the duration of the testing session.

Volunteer Leg Orientation on Rig - The volunteers were positioned on a surgical couch with their foot in a similar position to that of the dummy leg in a dummy test. Two sheets of low friction (PTFE sheet) were placed under the heel. The volunteer's leg was orientated such that the foot pointed vertically upwards for the impacts, and such that the line between the ankle and the knee joint was horizontal.

The height at which the pendulum impacted the foot was calculated according to the relevant dummy test defined in the EEVC foot certification procedure. The toe impact tests were performed at 2m/sec, 4m/sec and 6m/sec, as for the PMHS tests (Figure 8).

Test Termination Conditions - All the required tests were performed unless the volunteer requested that the testing should stop.

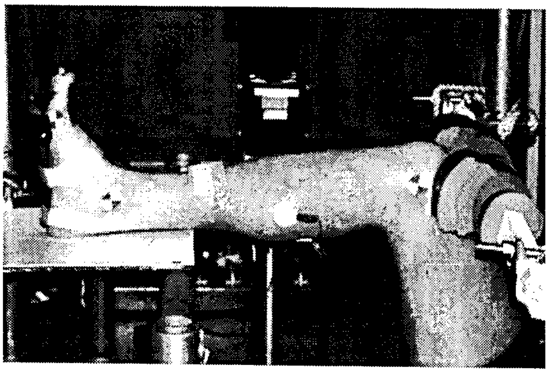

Figure 8 - Volunteer Test Configuration

Methods - Braced PMHS Specimen Testing

The Loading Cylinder - There have been attempts to load the Achilles tendon in human surrogate testing but the majority of these have failed to date due to an inability to adequately grip the tendon. In 1997 the authors have reported a series of tests [6] where a small hydraulic cylinder and clevis clamp had been successfully used. This method has been used again to apply a plantar flexing/bracing load in these tests.

This technique involved the replacement of the muscle group with a custom built tensioning device based on a hydraulic cylinder (Figure 9).

This cylinder is capable of developing loads of up to 4kN and is hydraulically driven through an air/oil intensifier, which is supplied by an air compressor. Control is achieved via fine pressure control valves on inlet and exhaust. One end of the cylinder is attached to the back plate via a turnbuckle (which allows for gross tension adjustments prior to testing).

The attachment to the back plate is adjustable so that the cylinder will pull in line with the long axis of the tibia thus preventing the introduction of artificial bending moments. The piston end is attached to the Achilles tendon and was clamped in a clevis bracket, on the end of the piston rod (Figure 10). The length of stroke of the cylinder was 70mm.

A load cell was located in line with the cylinder to measure the load applied and a further load cell was positioned in line with the stirrup to measure the force applied at the forefoot.

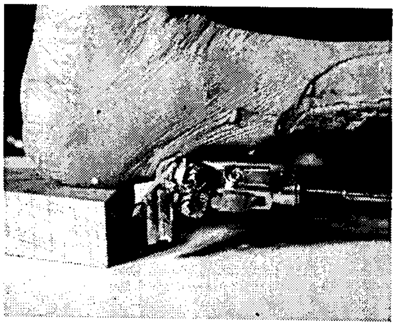

Figure 10 - Achilles Tendon Clamp

Instrumentation of Specimens - The specimens were prepared according to the method described in reference [6]

Active tension applied to the Achilles tendon resulted in plantar flexion of the unsupported foot. In order to restrict this motion the foot had to be externally supported. This was achieved by the use of a stirrup around the forefoot. The Achilles loading cylinder is schematically shown below the tibia and fibula (Figure 11). The general position of the tibia load cell is also illustrated. The Achilles loads chosen for this work were based on previous published work [9] and the results of the simulator trials described in this paper.

The chosen loading conditions were:

1. The loading cylinder in place, but with no tension applied to the Achilles tendon.

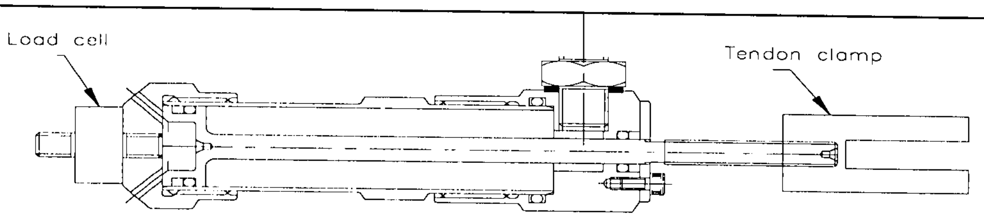

Figure 9 - The Achilles Tension Cylinder

2. Approximately 960N of tension (an estimate of the natural tension within the tendon in a live subject) applied to the Achilles tendon.
3. An "active" tension applied to the Achilles tendon based on the results of the simulator trials

The force in the tendon was increased until the desired active force was reached. When the tension was being increased the state of the tendon and clamping system was visually monitored to ensure that no tendon slippage through the fixing clamps occurred. The impact was initiated as soon as the tension remained stable. The foot was allowed to dorsiflex since the piston was held at a constant pressure with a large volume of air in the intensifier. (The 'passive' resistance of the piston and fluid is approximately 25N. With the intensifier activated the passive resistance increases to approximately 120-150N).

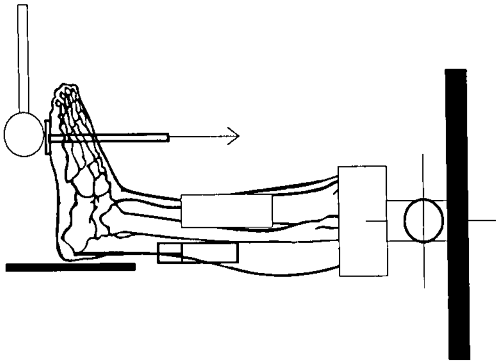

Figure 11 – Schematic of PMHS Specimen with Achilles Loading Cylinder In-Situ

Testing Specification -The PMHS specimens with an applied Achilles force were subjected to the toe impact tests from the EEVC certification procedure. The specimens were mounted and orientated as detailed above in the methods for the PMHS specimens. Impact tests were conducted at 4 and 6 m/sec. At these impact velocities, the energy delivered is normally below the injury threshold.

Test Order - The test order was kept the same for each specimen. The 'passive' 960N tests were performed first, then 'active' tension tests with 1800N or more, and finally the tests with no Achilles force.

Biofidelity Results

Overall, 78 tests were performed on 7 'through knee' amputation PMHS specimens, 7 tests were performed with an 'above knee' amputation specimen, 32 tests were performed with 6 volunteers and 60 comparable tests were performed on the two different dummy feet. The data from the important results are presented in this section and are discussed later in the paper.

Physical Properties of PHMS Specimens - The physical property data collected from the PMHS specimens used in this study are presented in Table 2 with comparisons to data collected in other institutes and for the dummy components.

High-Speed Film Analysis – A kinematic analysis from the high-speed films was carried out for all toe impacts on PMHS specimens, volunteers and the dummies. The films were analysed for dorsiflexion and time to peak dorsiflexion. The same two people analysed every PMHS, dummy and volunteer test to achieve consistency in the analysis. The dorsiflexion illustrated for each test type is the actual dorsiflexion corrected to a neutral starting point in each case. The high-speed film analysis is presented graphically, and on each graph, a one standard deviation corridor has been added.

PMHS Specimens - Figure 12 illustrates dorsiflexion for 'through knee amputation' specimens showing up to 34° of movement at 6 m/sec. Figure 13 illustrates the 'above knee amputated' specimen with up to 25° of movement. (Dotted lines show 61 standard deviation)

Volunteers - The results from tests with the volunteers are shown in Figures 14 and 15. Figure 14 illustrates the results where volunteers were unaware of the impending impact with up to 28° of movement at 6 m/sec shown. Figure 15 shows the results with the volunteer aware of the impending impact. In these tests the greatest range of movement was observed at 4 m/sec and was recorded to be 16° of dorsiflexion.

Dummies - Figure 16 illustrates the curves for the toe impact tests using the Hybrid III foot/ankle with up to 45° of movement shown and the GM/FTSS foot/ankle with up to 39° of movement shown.

Figure 17 shows an overlay of the results, where movement at the ankle can be compared for the volunteers, dummies and the PMHS specimens.

Instrumentation Output – The output from the pendulum accelerometer and the response of the leg, as measured by the tibia load cell, are presented as a series of overlay graphs in Figures 18-35. The graphs show the mean response of the PMHS specimens, GM/FTSS, Hybrid III and, where appropriate, the volunteers overlaid on the same axes. The graphs have been time-shifted and aligned on the principal peak in each case. Each curve is a plot of the mean response, which has been derived from the results of all the individual similar tests. Figures 18-23 show the pendulum acceleration, tibia force (Fz) and tibia bending moment (My) for the toe impact tests at 4m/sec and 6m/sec. Figures 24 & 25 show pendulum acceleration and tibia force (Fz) for heel impacts at 4m/sec. Figures 26-31 show pendulum acceleration, tibia force (Fz) and tibia bending moment (Mx) for inversion and eversion impacts at 4m/sec.

The graphs in Figures 32-35 show the mean peak values for pendulum acceleration, tibia force (Fz), bending moment (My) and dorsiflexion for the toe impacts, overlaid for comparison. In these graphs the parameters presented graphically are for toe impacts only.

A table of peaks of the relevant parameters for each test configuration is given in Appendix 2.

Table 2.
Basic Physical Properties

Parameter	**This Study**	**Crandall et al.**	**Hybrid III**	**GM/FTSS**
Age	66.75 σ 6.9			
Leg Length (mm)	454 σ 35	470 σ 41	442	442
Leg Volume (Litres)	2.629 σ 0.73			
Leg Mass (kg)	2.92 σ 0.75	3.19 σ 0.33	3.6	3.2
Foot Length (mm)	243 σ 11	244 σ 1.5	265	265
Foot Volume (Litres)	0.70 σ 0.15			
Foot Mass (kg)	0.75 σ 0.14	0.99 σ 0.12	1.48	1.11
Heel Flesh (mm)	16.86 σ 3.94			
Ball Foot Flesh (mm)	7.92 σ 0.689			
MoI Leg	0.07695 σ 0.02764			
MoI Instrumented leg	0.16468 σ 0.06154			
MoI Foot yy (kg/m²)	0.00343 σ 0.00074	0.00474	0.0064	0.00409
MoI Foot zz (kg/m²)	0.00342 σ 0.00076	0.00076	0.006325	0.0043

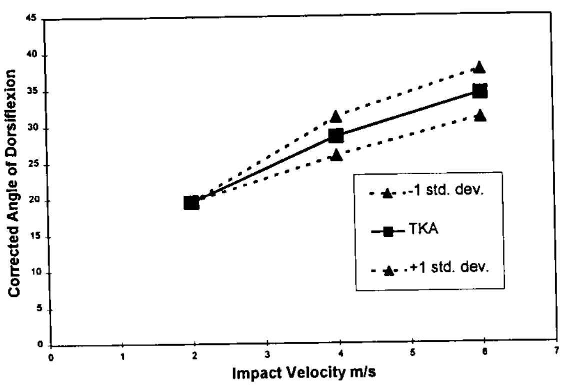

Figure 12 - Toe Impacts 'Through Knee Amputation'

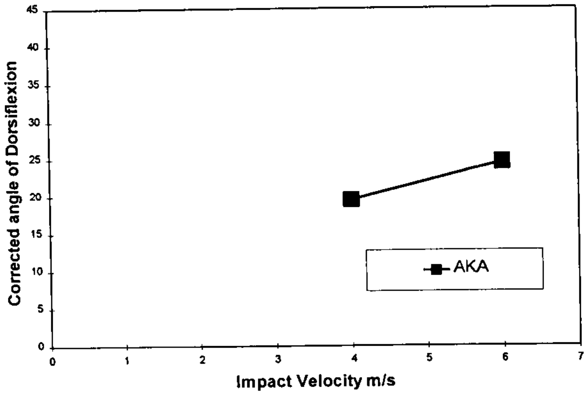

Figure 13 - Toe Impacts 'Above Knee Amputation'

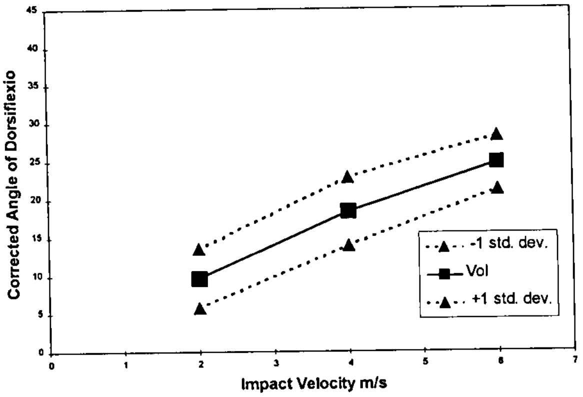

Figure 14 - Toe - Impacts Unaware Volunteers

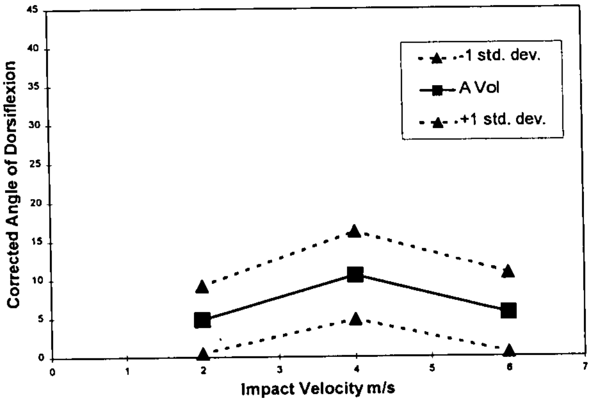

Figure 15 - Toe Impacts Aware Volunteers

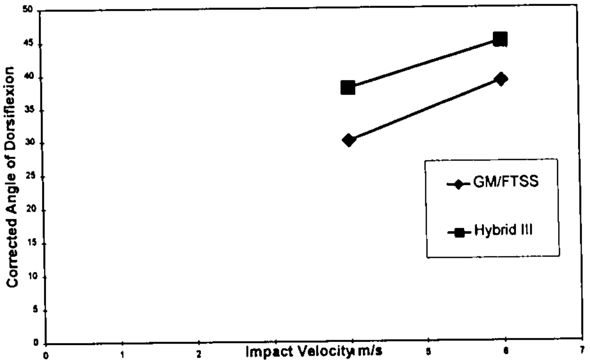

Figure 16 - Dummy Toe Impacts Dummies

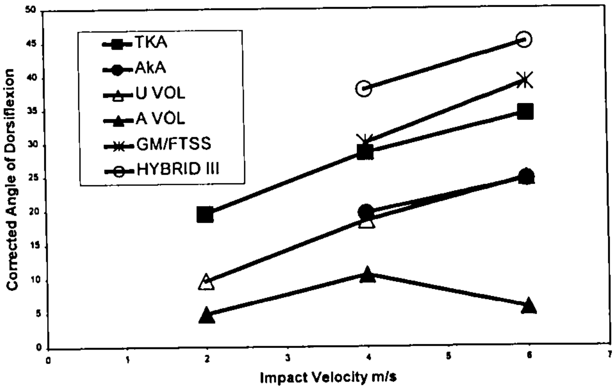

Figure 17 - Toe Impacts - All

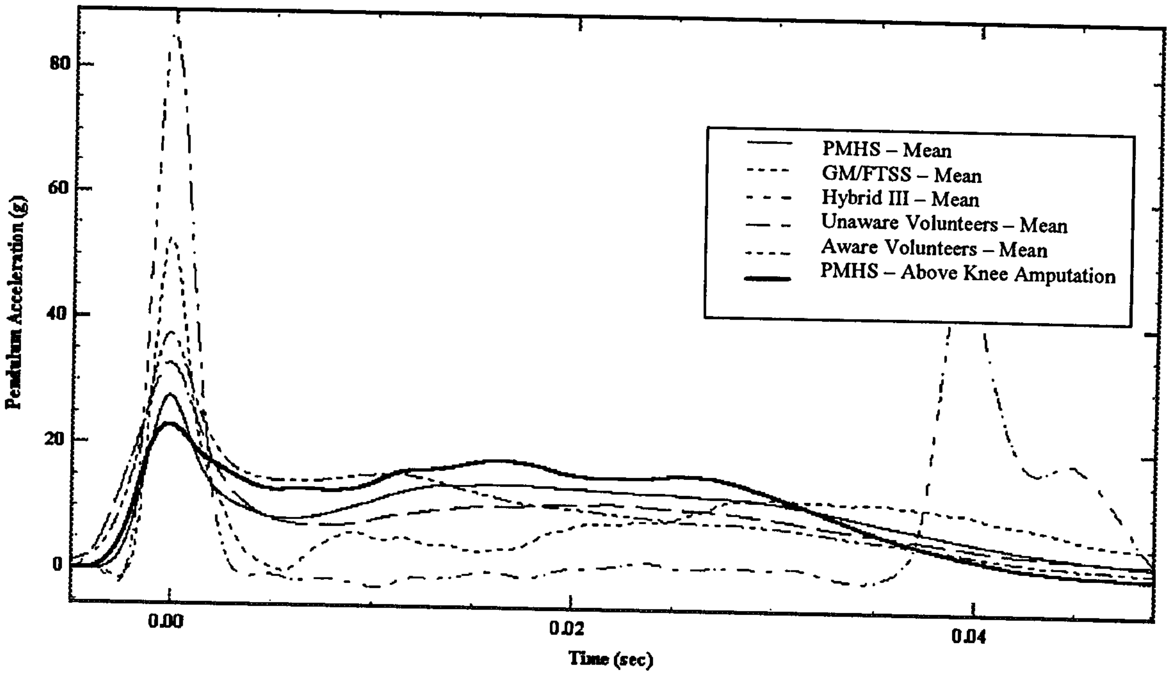

Figure 18 - Pendulum Acceleration at 4m/sec - Toe Impacts

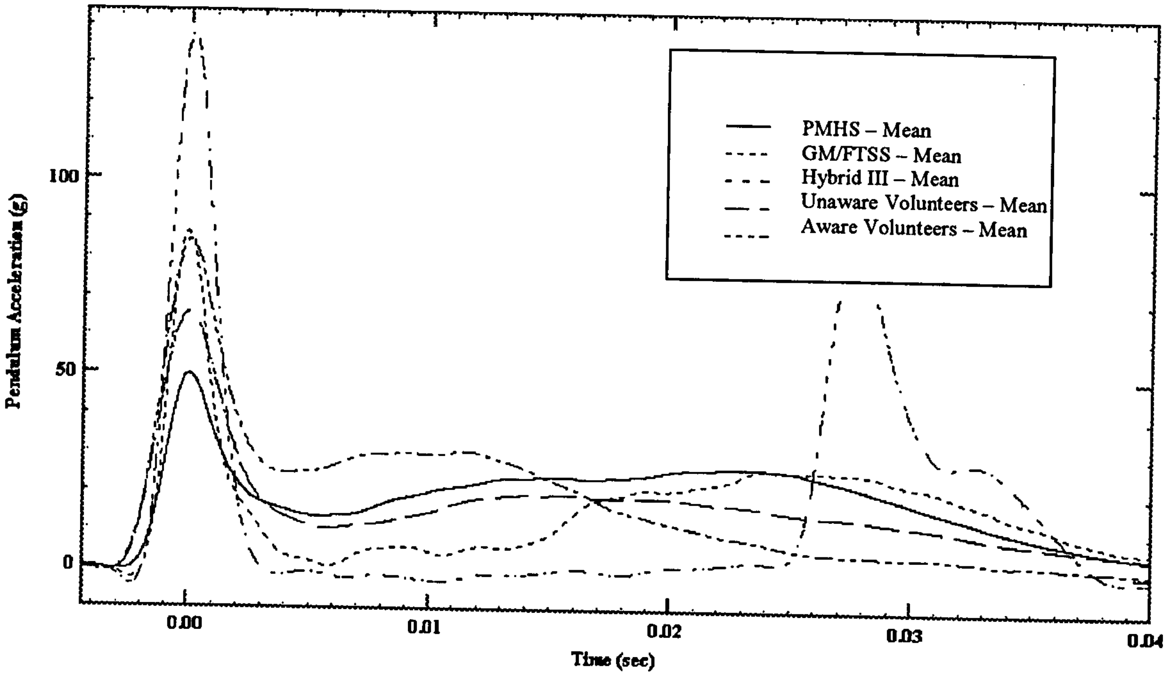

Figure 19 - Pendulum Acceleration at 6m/sec - Toe Impacts

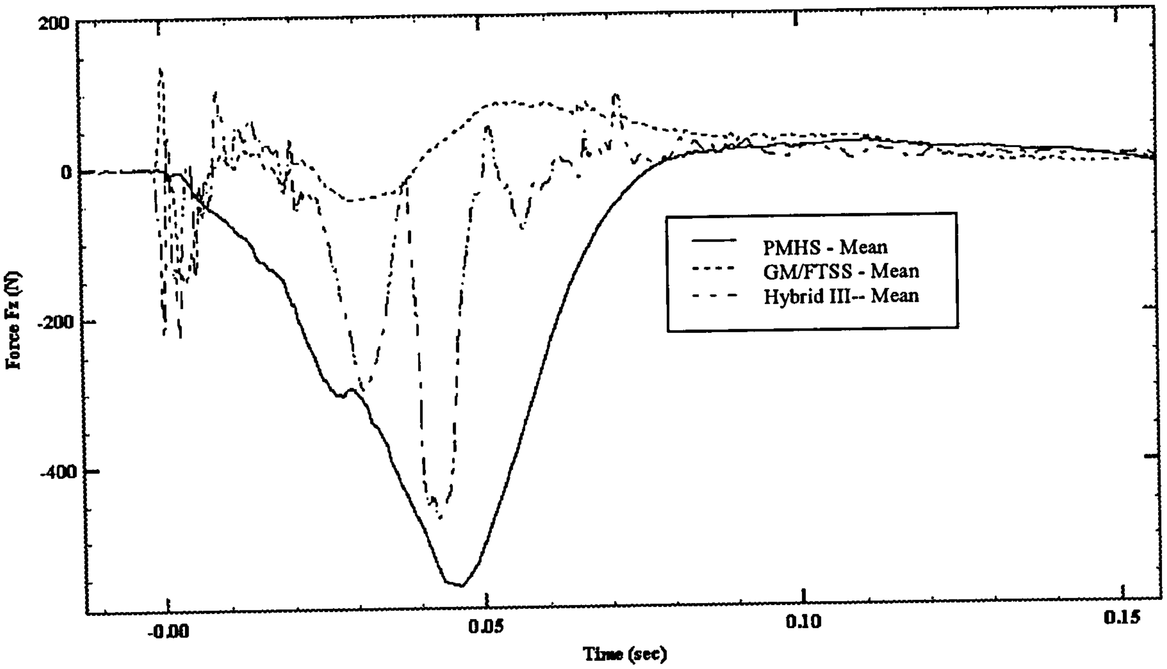

Figure 20 – Tibial Force Fz at 4m/sec - Toe Impacts

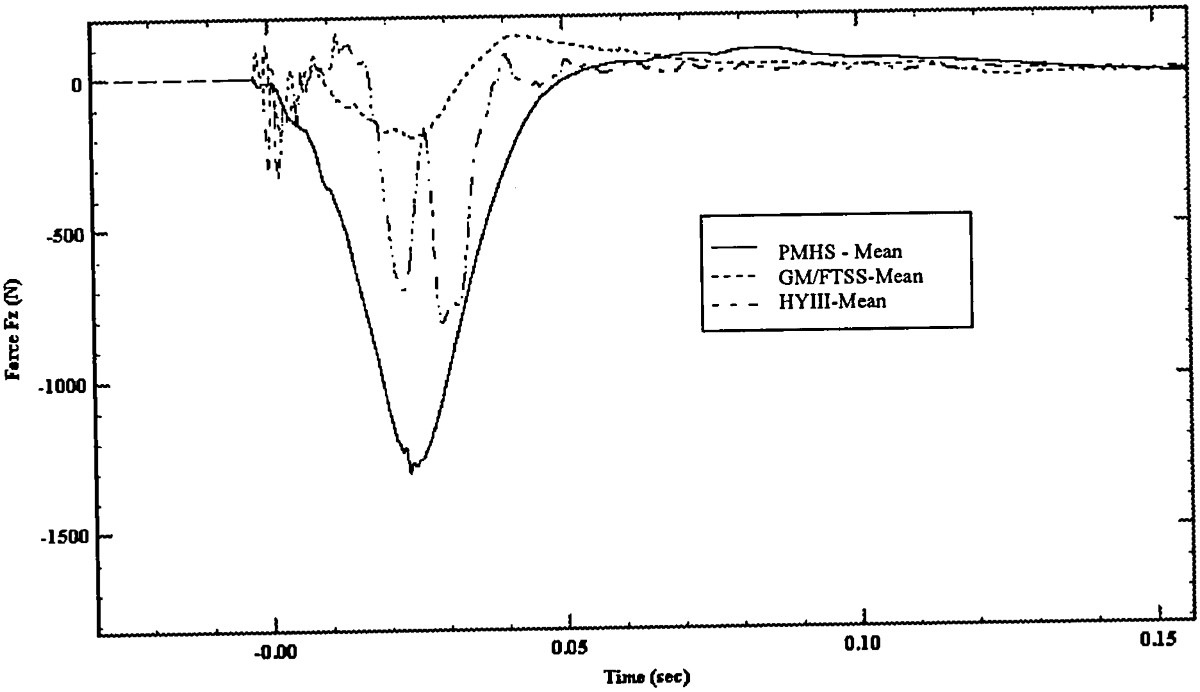

Figure 21 – Tibial Force Fz at 6 m/sec - Toe Impacts

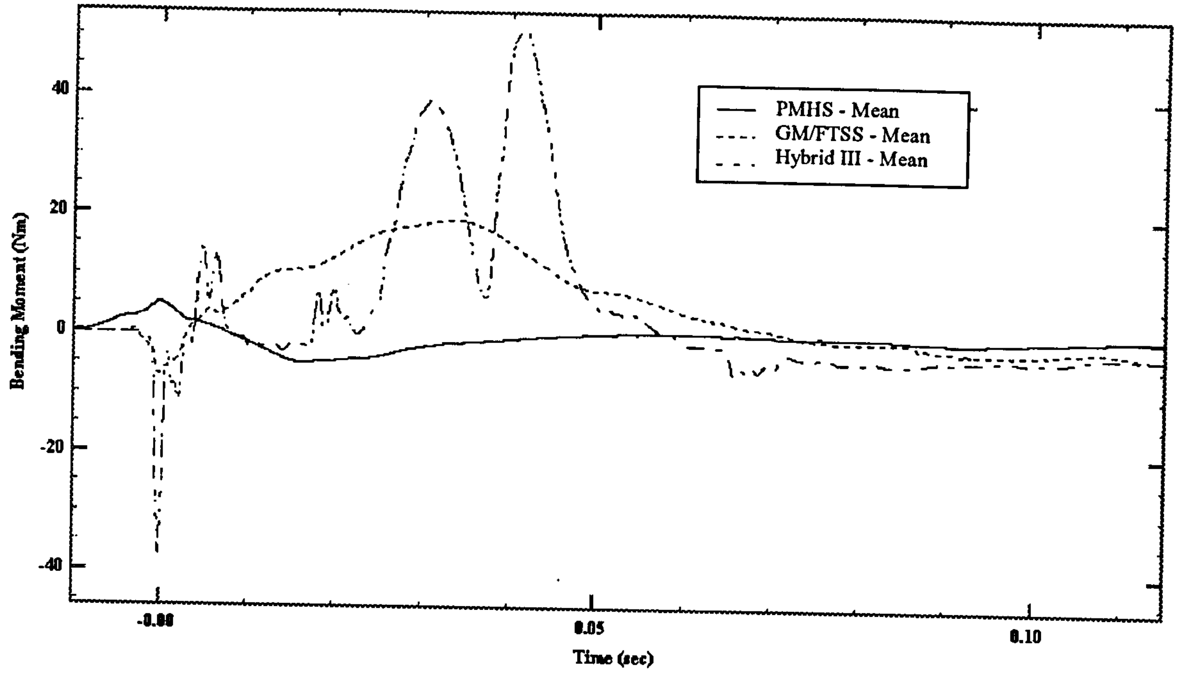

Figure 22 – Tibial Bending Moment My at 4 m/sec - Toe Impacts

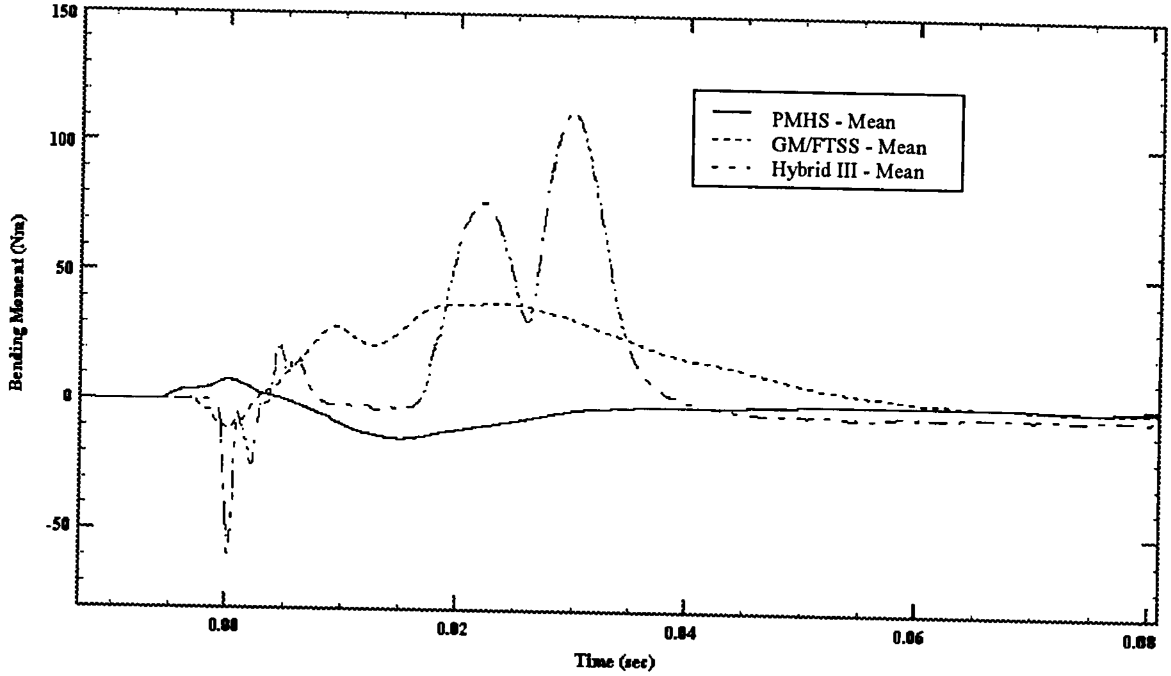

Figure 23 – Tibial Bending Moment My at 6 m/sec - Toe Impacts

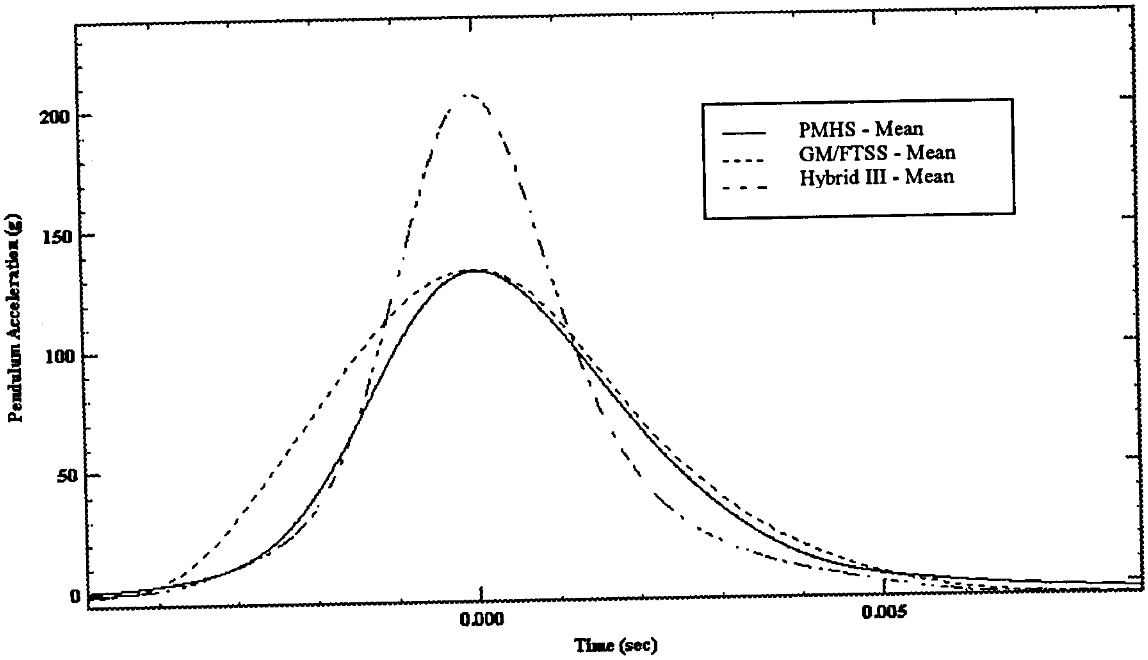

Figure 24 – Tibial Pendulum Acceleration at 4 m/sec, Heel Impacts

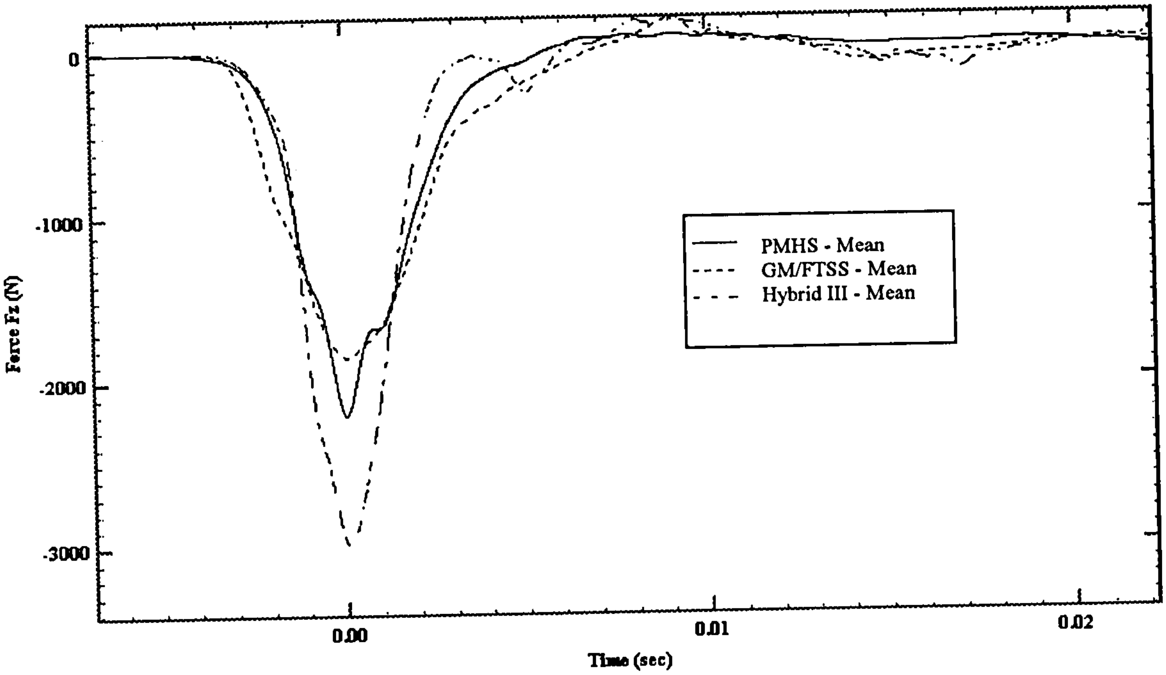

Figure 25 – Tibial Force Fz at 4 m/sec, Heel Impacts

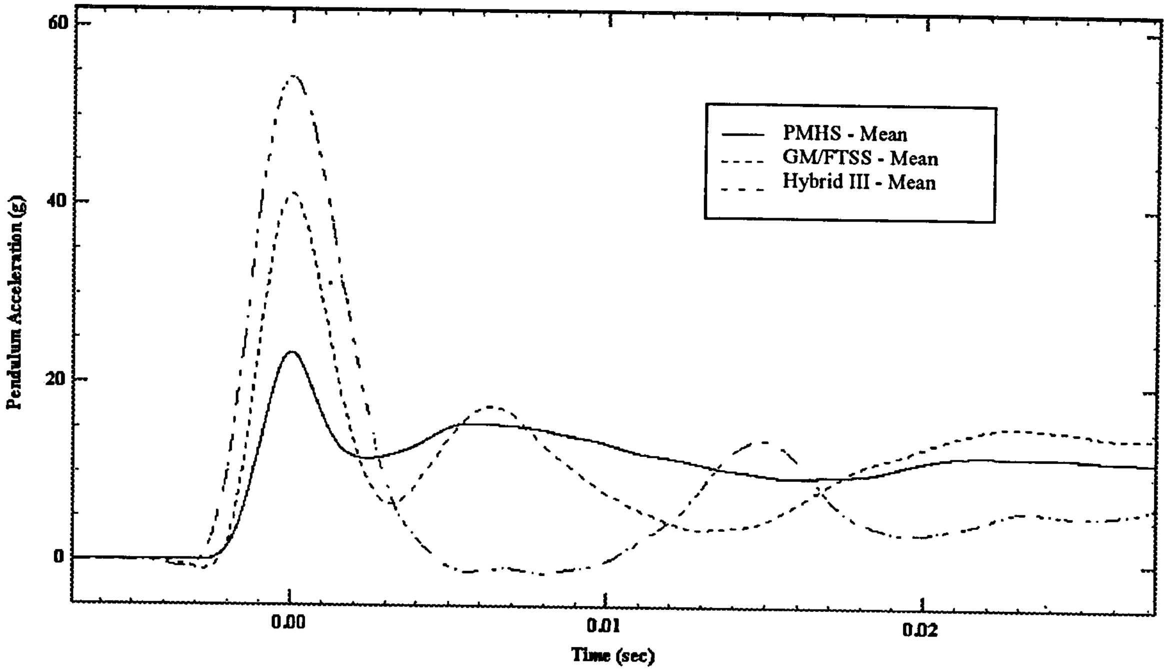

Figure 26 - Pendulum Acceleration at 4 m/sec, Inversion Impacts

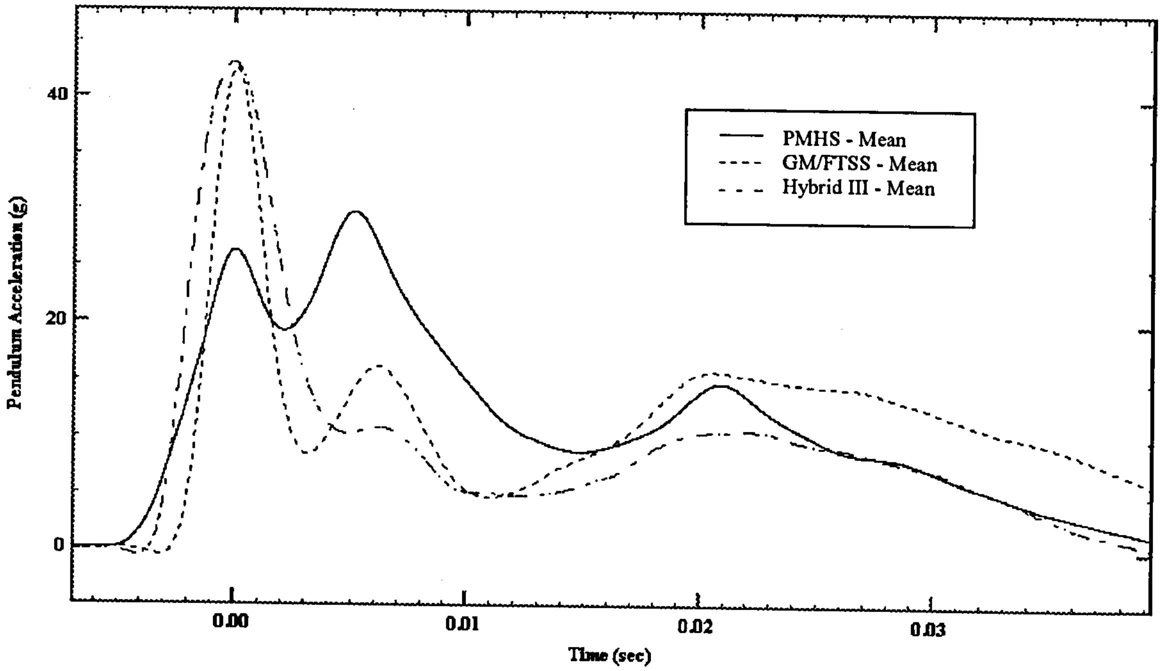

Figure 27 - Pendulum Acceleration at 4 m/sec, Eversion Impacts

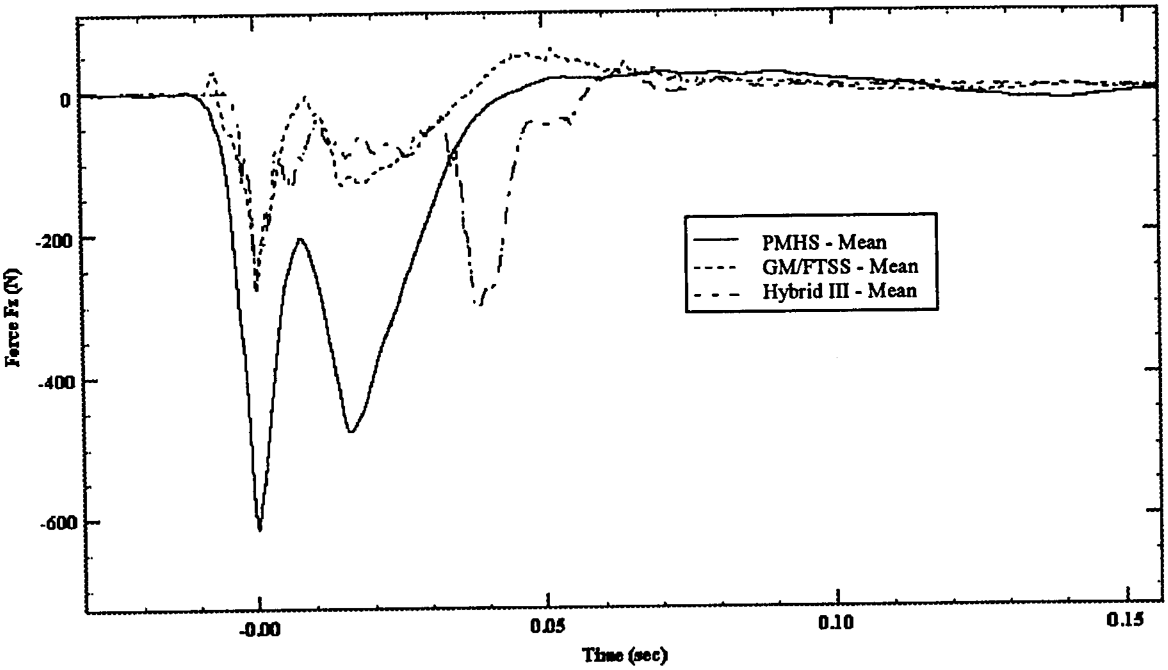

Figure 28 – Tibial Force Fz at 4 m/sec Eversion Impacts

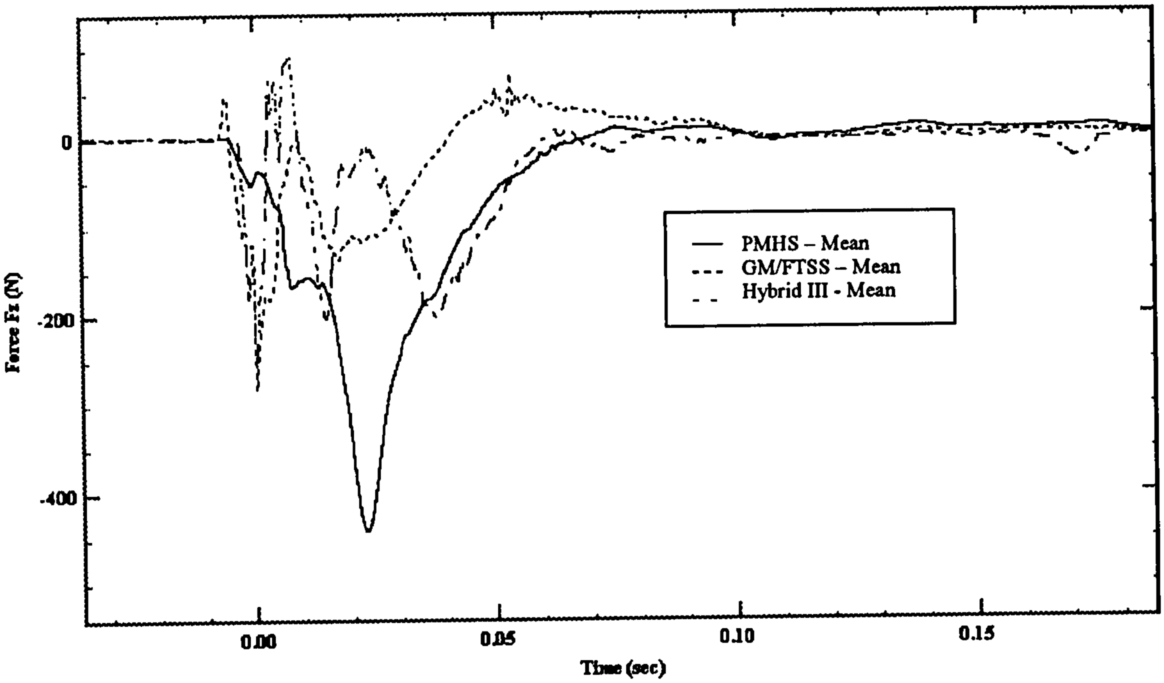

Figure 29 – Tibial Force Fz at 4 m/sec Inversion Impacts

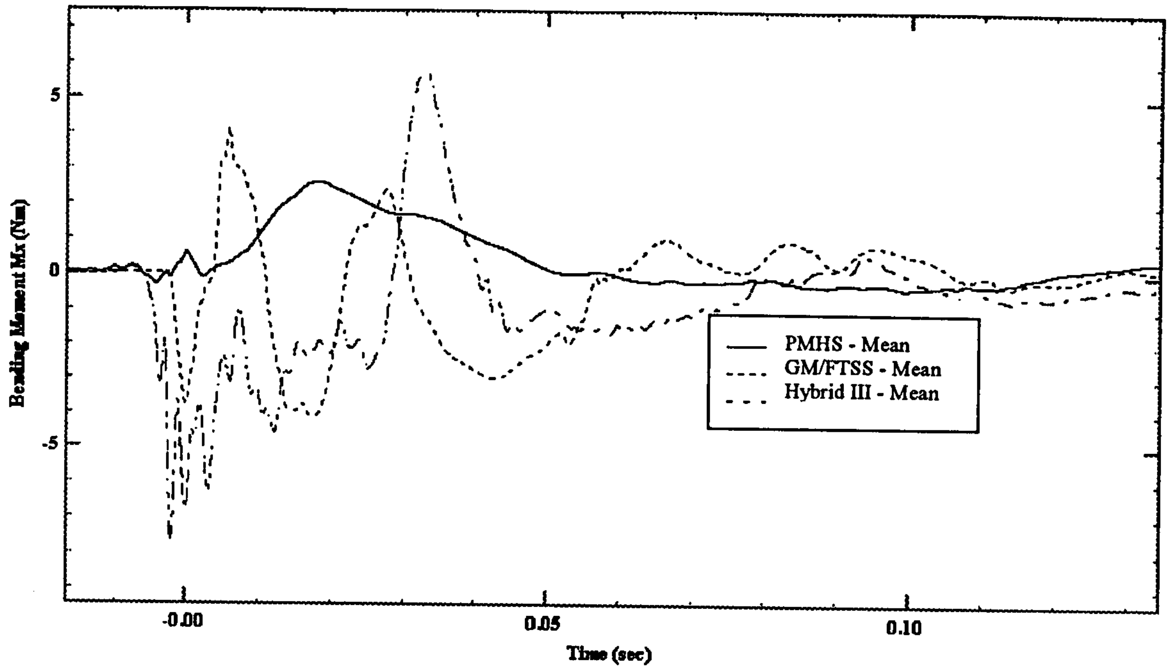

Figure 30 – Tibial Bending Moment Mx at 4 m/sec - Eversion Impacts

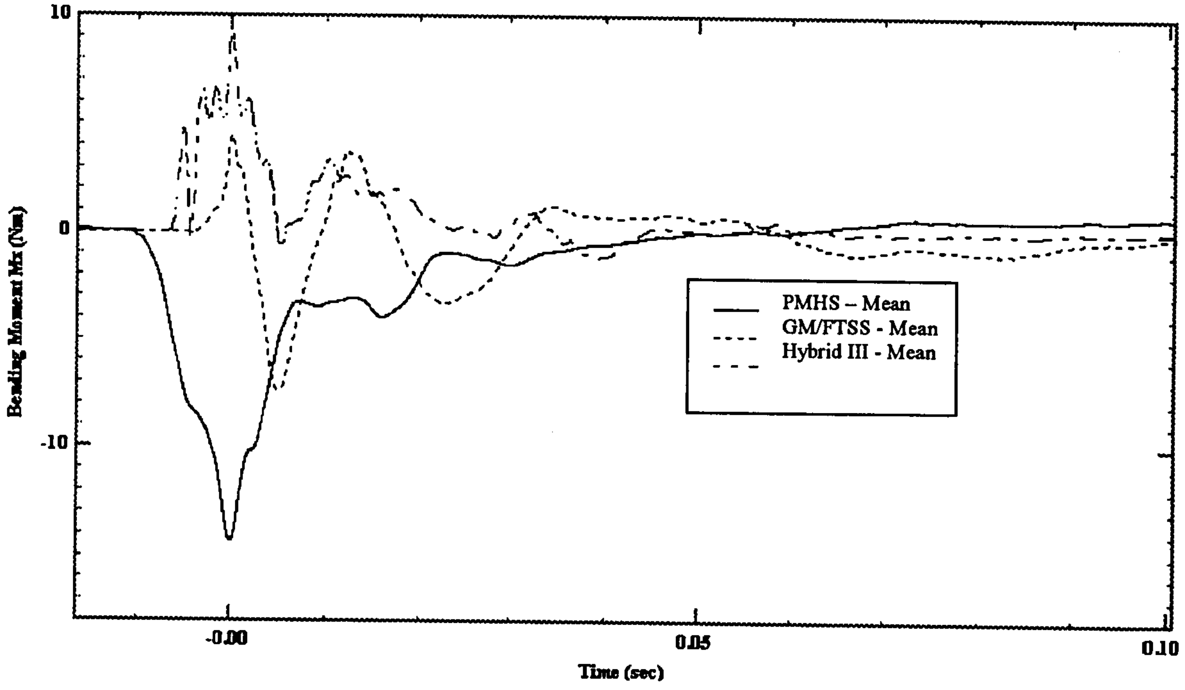

Figure 31 – Tibial Bending Moment Mx at 4 m/sec - Inversion Impacts

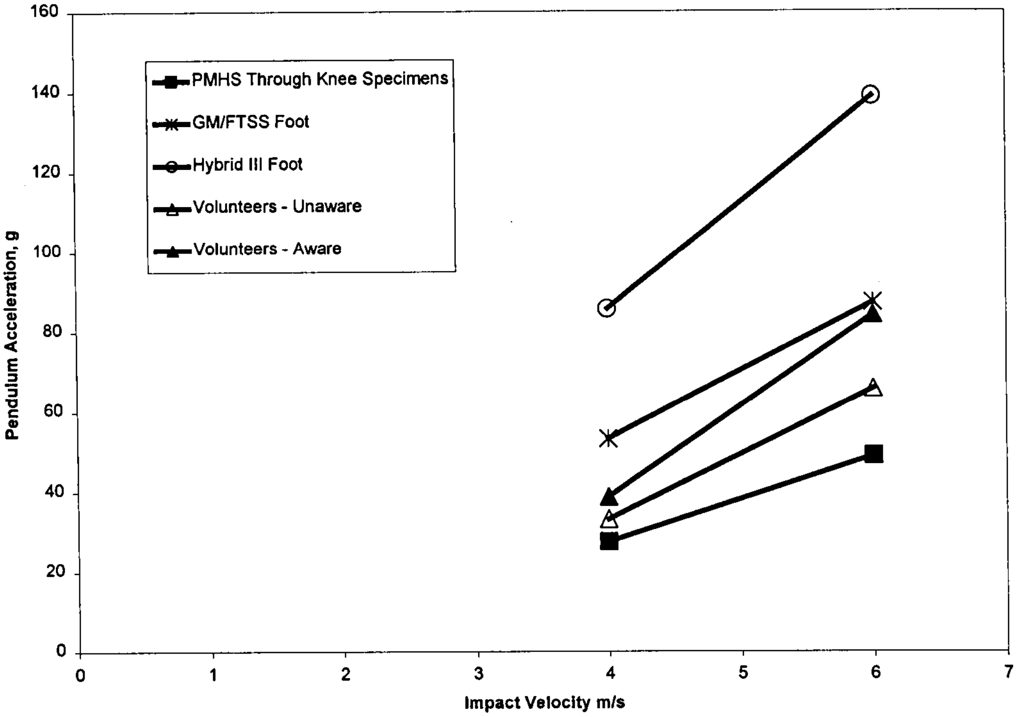

Figure 32 – Mean Peak Responses for Toe Impacts – Pendulum Acceleration

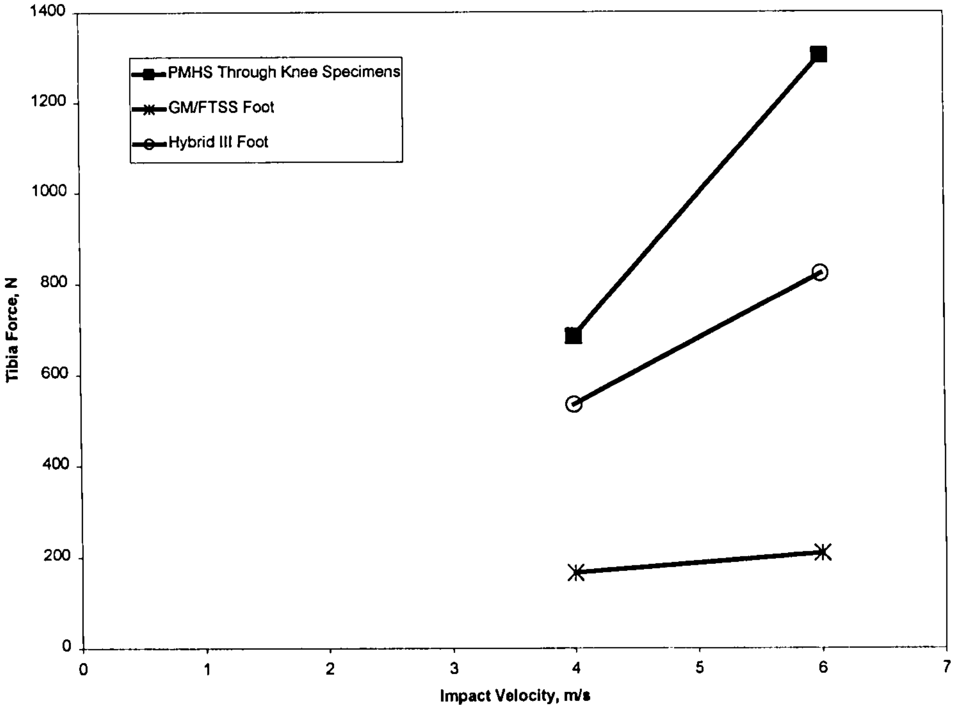

Figure 33 – Mean Peak Responses for Toe Impacts – Tibia Force Fz

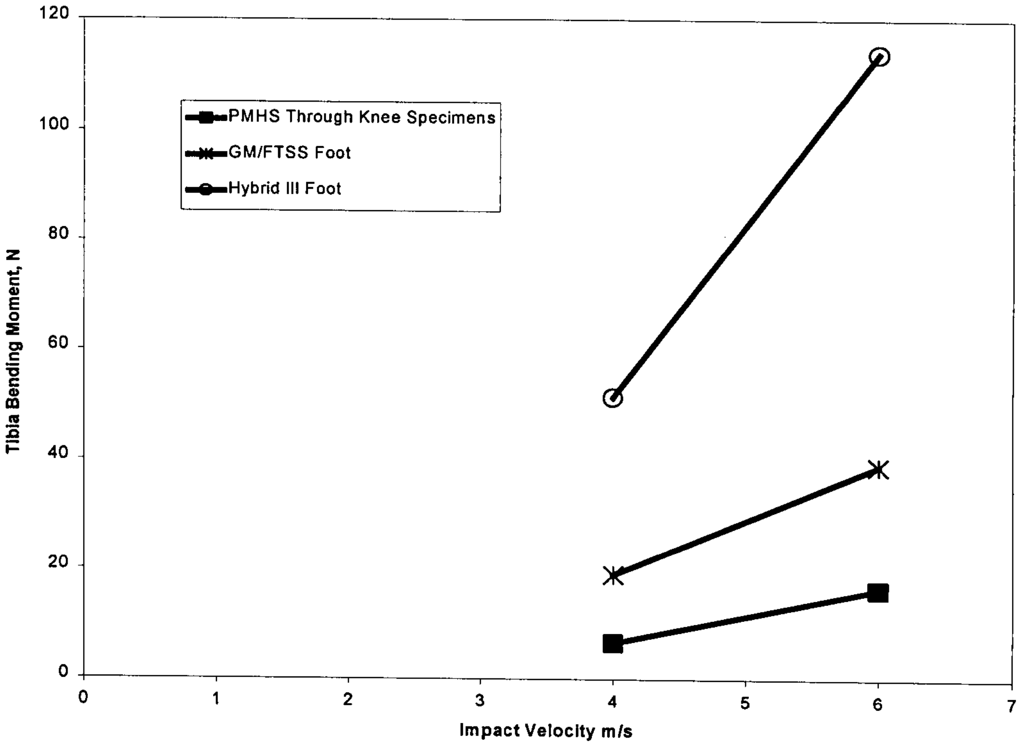

Figure 34 – Mean Peak Responses for Toe Impacts – Tibia Bending Moment My

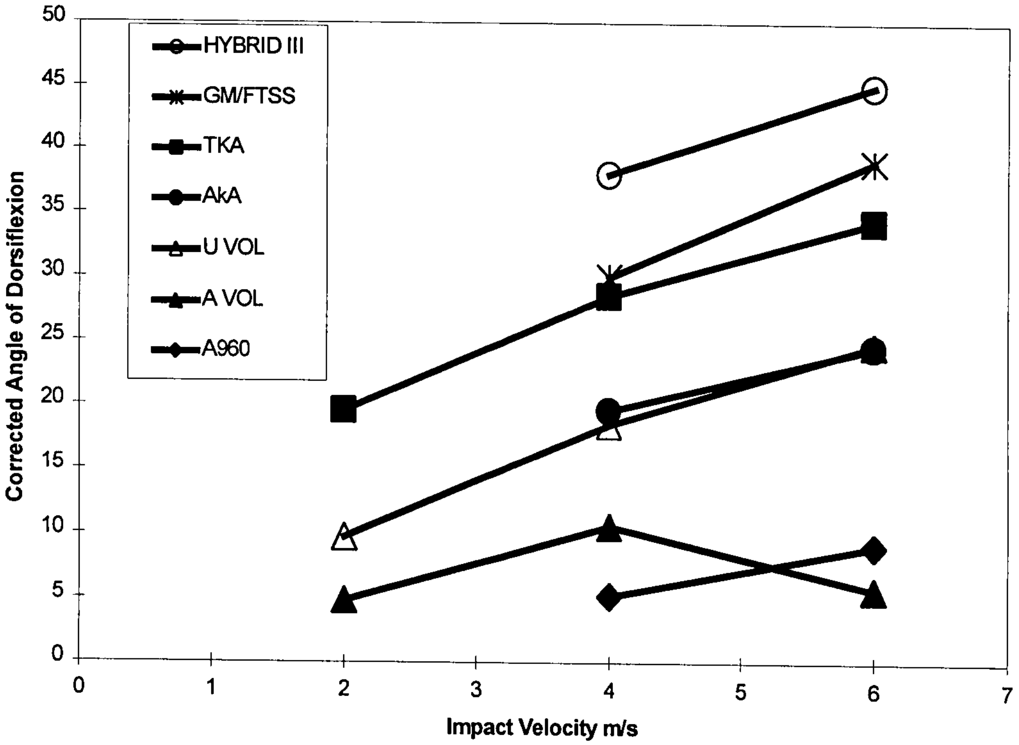

Figure 35 – Mean Peak Responses for Toe Impacts – Dorsiflexion

Normalisation

The results of any PMHS specimen tests will vary somewhat due to differences in mass, dimensions and physiologically related parameters. To achieve an estimation of a mean response from a PMHS specimen in this study, a process of normalisation to the 50th percentile was attempted.

The approach taken for this work was to adapt a simple FE skeletal leg model in order to simulate the test conditions. Each PMHS specimen test was then modelled so that a comparison could be made to a similar test on a fiftieth percentile specimen. By comparing the results of the two models a function could be developed that could be applied to the actual test results, in order to normalise them to the fiftieth percentile.

The model comprised a rigid body representation of the leg and foot bones, with accurate geometry and four joints: hip, knee, ankle and sub-talar joints. Each of these joints was represented by simple rotation about a fixed axis or a fixed point, in the case of the spherical hip joint. The joints were each assigned an appropriate stiffness characteristic.

The model included, a tibial load cell, a spring/damper system to represent the plantar flexing muscle groups and the Achilles tendon. Flesh was added to the sole of the foot with similar properties to those of 'Confor foam'.

After the model had been prepared and having verified it against a number of individual tests, the PMHS specimen data was normalised as follows. Tests with each PMHS were modelled, in terms of their geometry, test conditions (impactor velocity, position and orientation), mass and tibial load cell location. The responses from the model (F_Z, M_y, M_X and pendulum acceleration) were then obtained. A fiftieth percentile specimen was then modelled in the same test conditions. For each specimen tested, the results of the PMHS model were compared with the corresponding fiftieth percentile model. By noting the relationship of peak values between the two sets of model results, scaling factors were calculated to bring the test specimen model results to those of the fiftieth percentile model. These scaling factors were then applied to the actual test results to obtain normalised data.

Normalisation Results and Discussion

The normalisation procedure was designed to factor the results of the toe and heel impact tests to represent those of the fiftieth percentile. However, the initial output from the process indicated that the results were not converging as expected. Some examples of the effect of the procedure described are shown in Figures 36-38.

Figure36 shows a relatively successful normalisation of the pendulum acceleration magnitude from a toe impact test. The scatter in the results has been significantly reduced as intended. Figure 37 indicates some degree of normalisation on time scale for a similar test. However, in some cases such as that shown in Figure 38, the normalisation process did not appear to have any effect on the scatter of the results.

The premise for normalisation of results in the fashion described is that the results are related to the properties of the PMHS specimen in some way. For instance, it might be assumed that the tibia bending moment is proportional to a combination of bone dimensions, masses and the properties of the flesh, underneath the pendulum impact point. Thus by including these parameters in the normalisation process, their effect can be taken into account and the results aligned. However, if there were no such relationship, it would not be possible to normalise the results. A regression analysis was carried out between the results and the normalisation parameters. While some correlations did result from the analysis, relationships that were expected to be strong (such as that between pendulum acceleration and foot mass) did not occur but other relationships had unexpectedly high correlations. Thus the results remained inconclusive.

Other factors may have influenced the success of the technique as well. The model may have been over-sensitive to a particular parameter and therefore the response of the model would have been unrealistically influenced by this one parameter. This issue was addressed through a sensitivity study on the model. The results of which showed the model to be not unduly sensitive to any one parameter. The normalisation process would also fail, if the test results were being influenced by a parameter that was not taken into account in the normalisation process, such as joint stiffness. The parameters that were included in the procedure had been chosen as being those thought most likely to influence the results, but with the proviso that it was possible to measure them on the PMHS specimens. Some potentially influential factors such as joint stiffness were not included.

It would be surprising if there were no relationship at all between the results and the PMHS specimen properties. However, this relationship may be non-linear and variable and hence it may have been over-optimistic to expect to be able to remove the variability from the results.

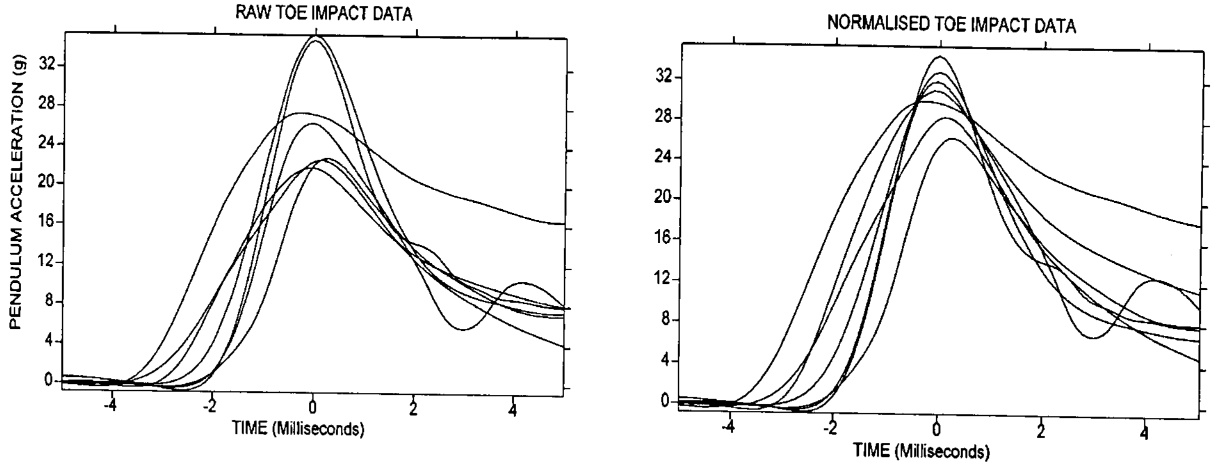

Figure 36 – Normalisation of Peaks with Respect to Magnitude for Toe Impact Pendulum Acceleration at 4m/sec

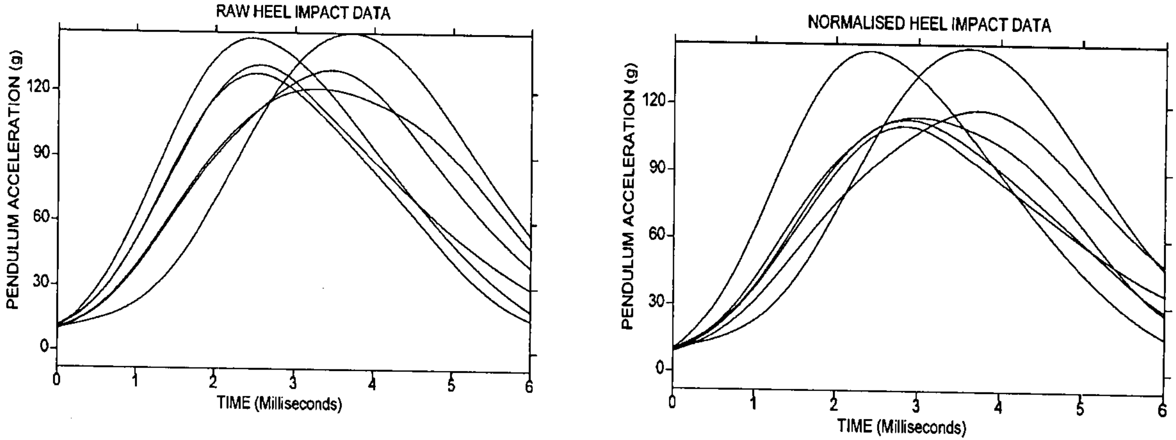

Figure 37 – Normalisation of Peaks with Respect to Time for Toe Impact Pendulum Acceleration at 6m/sec

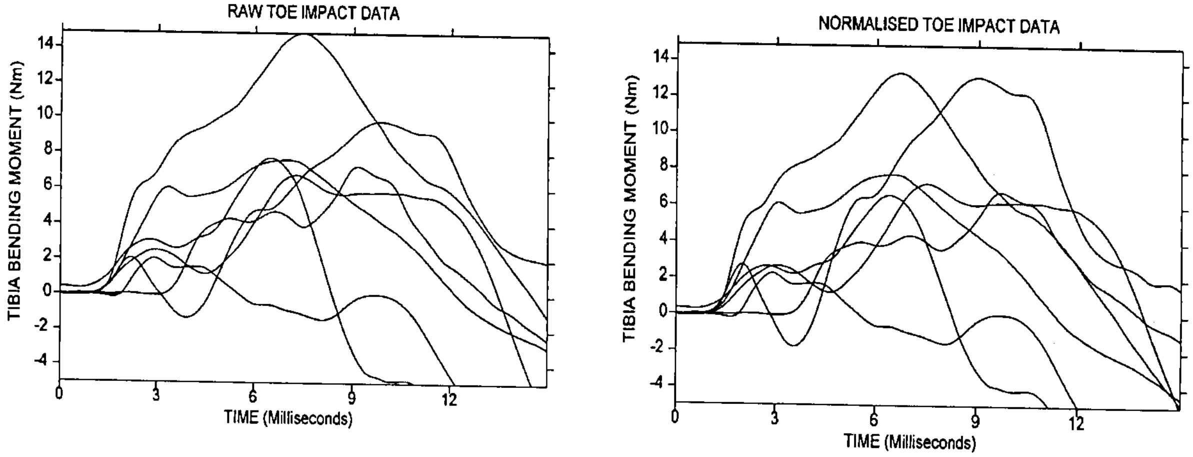

Figure 38 – An Example Showing the Normalisation Resulting in a Limited Effect on the Scatter of Results

Influence of Achilles Tension

The data for tests with an applied Achilles tension is presented here as a peak value analysis. This has enabled paired-t test comparisons to be made as the same specimens were used both with and without an applied tension. Only toe impacts were performed with the Achilles loading cylinder in-situ.

Axial Loading Fz - Table 3 shows the test conditions for which there were significant differences in Fz. A Through Knee Amputation is referred to as TKA, a specimen with the Cylinder In-Situ is referred to as CIS, with the force applied following, e.g. CIS - 960N. The difference between CIS-0 and CIS->1800 is significant only at the 10% level.

Table 3.
Significant Differences in F_z

Test Conditions	Mean Difference	P Value
TKA : CIS-960	1735N	0.001
TKA : CIS->1800	3234N	0.039
CIS-0 : CIS-960	1507N	0.007
CIS-0 : CIS->1800	2313N	0.064

Tibial Bending Moment - There were no apparent significant differences in the peak tibial (M_y) bending moment recorded for any of the comparative tests.

Ankle Dorsiflexion - Table 4 shows the test conditions for which there was a significant difference in the degree of dorsiflexion.

Table 4.
Significant Differences in Dorsiflexion

Test Conditions	Mean Difference	P Value
TKA : CIS-960	24°	0.001
CIS-0 : CIS-960	14°	0.045

Mean Impactor Force - Table 5 shows the test conditions for which there were significant differences in mean impactor force.

Table 5.
Significant Differences in Mean Impactor Force

Test Conditions	Mean Difference	P Value
TKA : CIS-960	244N	0.001
CIS-0 : CIS960	311N	0.016

Biofidelity Testing Discussion

The data presented in Table 2, comparing the basic physical parameters of the specimens used in the testing shows that the specimens used are comparable to those used in other institutes. It is recognised that a population with a mean age of 67 years will not reflect the driving population at large, particularly with respect to bone mineral density. The effect of ageing on bone quality has been well studied and it is recognised that an elderly population will tend to have weaker bones. It is for this reason that the data on bone mineral density has been collected. It is hoped that the continued collection of data with such experiments will allow for a definitive reference range to be established.

In further work, planned within this project, it is hoped to be able to normalise the results of any individual PMHS test and to correct the tolerances established for injury to mean population bone mineral density data.

The data for moments of inertia differ more between institutes and it is probable that this reflects differences in measuring techniques, as differences in dummy feet measurements have been observed compared to published results.

Over 170 different tests are reported in this paper all designed essentially to establish appropriate biofidelity requirements and to compare the performance of the two dummy designs with various human surrogates. Repeated PMHS testing was used in this study at a sub-injury level. In every case an orthopaedic surgeon examined the specimen after the conclusion of each test. Careful attention was paid to the ligamentous structures around the ankle joint. Testing with any one specimen was halted immediately that any injury became apparent, however minor.

Toe Impacts – Figures 12 – 23 illustrate the response of the foot to toe impacts.

Dorsiflexion - The kinematic analysis of the high speed films illustrated in Figure 17 allows a direct comparison between the different specimen types for ankle articulation in impact to be made. An increasing trend of humanlike behaviour can be observed from the Hybrid III foot, to the GM/FTSS foot, then the through knee PMHS specimens, the above knee specimen, unaware volunteers and finally the aware volunteers. It can be observed that the mean GM/FTSS results lie close to the upper one standard deviation limit for the through knee PMHS tests (Figures 12 & 16). In a similar way, the responses of the unaware volunteers are comparable to those of the above knee amputated specimen (Figures 13 & 14). When a tension of 960N was applied to the Achilles tendon of a PMHS specimen, the response is similar to that of an aware volunteer (Figure 35). Although the GM/FTSS is close to the flaccid through knee amputation PMHS results, both dummies show a higher dorsiflexion response than volunteers, the above knee PMHS specimen and the PMHS specimen with a passive (960N) force applied to the Achilles tendon.

The degree of dorsiflexion will to a certain degree be influenced by the stiffness of the ankle joint. In reality, and as the results of the simulator trial have indicated, there is likely to be an active tension in the lower leg plantar flexing muscle group, which will influence the kinematics of the foot. The impactor tests have shown that the application of tension through the Achilles tendon results in a decrease in the amount of dorsiflexion observed for a given impact energy. The unaware volunteers exhibit less dorsiflexion than the flaccid PMHS specimens and the dummy feet. It is very difficult to assess accurately the amount of muscle activity and its influence in human volunteers. It is possible that there may have been some degree of involuntary bracing even in the 'unaware' state. The aware volunteer dorsiflexion results showed some correlation with the PMHS that had 960N of applied force in the Achilles tendon. In PMHS specimens with 960N applied, less motion was seen compared to unaware volunteers. It has been suggested that 960N may be too high as a representation of passive muscle tension. This may be so if all of the force transmitted to the foot is applied through the Achilles tendon, which is not representative of the real-life situation.

Ankle stiffness and the tension in the lower leg plantar flexing muscle group influence peak dorsiflexion under impact to the toe. The stiffness of the ankle joint will determine, in part, the bending moment and force transmitted to the tibia. If these are to be recorded accurately in a dummy tibia then these data illustrate the importance of incorporating a biofidelic ankle in a car crash dummy.

Pendulum Acceleration - The profile of the response curves of the dummies, volunteers and PMHS are quite similar. The Hybrid III dummy exhibits a second peak in the response which is characteristic of the foot design (Figures 18 & 19). The first peak results from the pendulum contacting the foot, the second peak arises from the fact that the design of the foot/ankle allows the foot to rotate relatively freely until it impacts the tibia. This response has improved over previous design with the addition of the bump stop and the increase in the joint articulation to 45 degrees.

The response of the GM/FTSS foot was closer to the volunteers and the PMHS results. The difference was not significant when comparing with volunteers, but it was for PMHS specimens ($p>0.01$ for GM/FTSS v. volunteers and $p<0.001$ for GM/FTSS v. PMHS). The Hybrid III results were further away from the volunteers and PMHS results. These differences were significant, except for the comparison with aware volunteers at 4m/sec ($p=0.009$). The difference between the pendulum acceleration observed with the two dummies was also significant ($p<0.001$).

The proposed design of the ALEx II leg incorporates a simulated Achilles tendon, which when tensed will enhance ankle stiffness in a biofidelic manner. It is hoped that the response seen in testing will be closer to the results seen with PMHS specimens and volunteers. At the same time the bending moment imparted to the tibia by the ankle will hopefully remain unchanged. The success of the GM/FTSS foot in simulating the response of the PMHS specimens is due to its rubber bump stop which is incorporated within its ankle hinge.

Tibial Force Fz – Although the peak Hybrid III response was closer to the PMHS results than the GM/FTSS response, the difference between the PMHS response and that seen by the two dummies is striking, when the graphs of Fz for toe impacts are examined (Figures 20 & 21). At 4 m/sec, the difference between the PMHS specimens and the GM/FTSS leg is statistically significant ($p>0.005$), although between the PMHS and the Hybrid III it is not. The difference between the two dummy types is also significant at the fifth percent level ($p<0.001$). The low value seen with the GM/FTSS foot can be attributed in part to the rubber component of the joint. At 6 m/sec a similar pattern of behaviour is seen, however the difference is significant with both dummies, when compared to the PMHS specimen.

The accident analysis that is reported later in this paper, has highlighted axial loading as a significant cause of injury for the most disabling of ankle fractures (pilon, calcaneal and talar neck). It would seem that the advantage of the GM/FTSS foot, with its stiffer ankle, is offset by an adversely recorded peak axial load. If the risk of serious injury is to be assessed, then the ability of future dummy feet designs, to measure accurately Fz biomechanically, will be paramount. The new proposed design for ALEx II will hopefully address these issues by imparting enhanced ankle stiffness without affecting the actual ankle joint.

A series of tests in the same experimental configuration, but with an added Achilles loading of 960N applied, have been reported previously. [6] It has been demonstrated that the observed axial load is significantly increased by the application of a bracing force through the Achilles tendon. Thus while the Fz response observed in flaccid PMHS specimens is significantly different from current dummy designs. it is speculated that the theoretical response in tensed volunteers would be even further removed. One of the fundamental differences in the geometry of the human leg, compared with the design of the Hybrid III, is that the tibia is offset at an angle between the knee and ankle joints. This aspect of the dummy design will also be an important factor in the interpretation of the load cell data.

Bending Moment My - When bending moments for toe impacts are considered, the time history curves (illustrated in Figure 22 & 23) show that PMHS specimens recorded a lower bending moment (My) than the Hybrid III leg with either the Hybrid III foot or GM/FTSS foot attached. A double peak was seen with the Hybrid III foot and this was again due to the design of the ankle complex, which allows the foot to move relatively freely after the first impact until the foot hits the rubber bump stop. In the GM/FTSS foot a plateau effect is observed corresponding to the continuous resistance at the ankle joint of this dummy. These data suggest that neither dummy records bending moments, in a biofidelic fashion. This is in part due to the offset of the tibia in the dummy leg which will generate a bending moment when an applied compressive axial load (Fz) is applied. These results bring into question the reliance which can be made on tibial bending moment data for injury prediction in car crash tests with current dummy designs.

Heel Impacts – Figure 24 & 25 illustrate pendulum acceleration and tibial force for the heel impact tests on the PMHS and dummies. No heel impact tests were performed on volunteers nor to the PMHS specimens with imposed Achilles tendon force.

Pendulum Acceleration - Heel impacts were performed at 4m/sec on both PMHS and the two dummy designs. It can be seen that the pendulum acceleration response of the GM/FTSS foot is very similar to that of the mean PMHS response. The mean peak for both is approximately 130g. The mean peak for the Hybrid III foot is much higher at 206g and significantly different ($p<0.001$).

Tibia Fz - The second parameter analysed for heel impacts was tibia compressive force (Fz). In the dummy there are rigid connections between the foot/ankle/leg components whereas in the cadaver there is firstly the flesh and structure of the sole of the foot and then cartilage on both sides of the sub-talar and ankle joint all of which have energy absorbing properties. The tibia Fz response of the GM/FTSS foot is much closer to that of the PMHS specimens than the Hybrid III. The Hybrid III is significantly different ($p<0.001$) from the PMHS specimens, as is the difference between the two dummy types. Thus the foot design and rubber bump-stop incorporated in the GM/FTSS foot would appear to be more biofidelic in this test configuration than those used in the Hybrid III design.

Inversion/Eversion Impacts - There have to date been very few biomechanical tests designed specifically to assess inversion and eversion responses of the foot to impact. The simplified testing reported here was conducted as a derivation of the toe and heel impacts. The foot for all the tests was rested unconstrained on either its lateral or medial side. As such the foot was free to dorsiflex or plantar flex in each case. In the majority of these tests the foot was seen to dorsiflex in addition to either inverting or everting. This was considered to be more representative of human like behaviour, as it is known that with the human ankle fixed in a right-angle position, significantly less inversion or eversion is possible.

The graphs (Figures 26 & 27) illustrating pendulum acceleration for inversion and eversion impacts indicate a smaller magnitude of the response with PMHS specimens, compared to the two dummy designs. In inversion the difference between the mean peak response of the PMHS specimens and either of the dummies is statistically significant (PMHS v GM/FTSS $p=0.005$, PMHS v Hybrid III, $p<0.001$). In eversion, the peak responses of the two dummies are very similar but are higher than the PMHS response. This difference however, was not significant.

The mean difference between the two different dummy designs is also significant. When the impact tests are studied visually the lower centre of rotation of the GM/FTSS foot (illustrated in Figure 3) appears to give the foot a more human like movement. These data suggest that this movement is too stiff to give a similar response to the PMHS specimens. This testing has not been undertaken on volunteers and it is probable that with active muscle tension the response would be closer to that seen with the GM/FTSS foot.

The graphs illustrating the measured tibial force for inversion and eversion indicate a higher magnitude of the response recorded with the PMHS specimens when compared to the two different dummy designs. In inversion the differences between the mean peak tibia forces are not significant. The later peak seen in the PMHS specimens is possibly explained by the lack of a rigid connection between the foot and the leg and the need to move the ankle to tighten up the collateral ligaments before force can be conducted axially up the tibia. In eversion the mean peak tibia forces for the two dummies are similar however the usual double peak is seen with the Hybrid III foot corresponding to the foot hitting the bump stop in dorsiflexion. The mean peak force for the PMHS specimens (657N) is significantly higher than the dummies ($p=0.28$).

The graphs illustrating the Mx bending moment are more difficult to explain. In inversion the response of the PMHS is lower in magnitude than that of either of the dummies. This is to be expected with the sub-talar and ankle joint ligaments stretching to allow a more gradual transmission of force to bend the tibia. In eversion the PMHS appear to experience a much greater force. It is possible that this is an artefact of the way in which the eversion impacts were generated. It would be desirable to repeat these tests with a pure eversion force applied to a foot that was constrained to prevent dorsiflexion.

Tests with an Applied Achilles Force - Using the method described, it has been possible to generate forces up to 3300N in the Achilles tendon. Ferris et al [19], have been able to obtain the same magnitude of force within the Achilles tendon without failure using modified cryo-clamps. Other researchers have attempted to induce ankle torsion by direct application of torque through pins inserted into the calcaneus [7], but have been hampered by fractures of the calcaneus. At the University of Virginia pre-impact bracing has been induced by applying axial force through the lower leg [8]. The method described here produces bracing in a more biofidelic manner, by simulating a natural mechanism. It will allow the further evaluation of pedal induced injuries in the absence of heel to floor contact.

Ferris et al. [19] have reported that in studies on live subjects, the Achilles tendon contributes only 66 percent of the plantar flexing force at heel rise, the remainder being attributed to, five other muscles in the lower leg. In the PMHS test methodology described here, the whole plantar flexing force was generated through just the Achilles tendon, this may account for the high incidence of tendon rupture seen in this study. It is recognised that Achilles tendon strength decreases with age [20]. The specimens were taken from an elderly population and it is acknowledged that this will have had an effect.

This study reports a statistically (paired-t test) significant increase in axial loading and decrease in movement of the foot when a plantar flexing force is generated. The results support those of Petit et al. [7] who observed, in testing, an increased injury threshold for a dorsi flexing impact with an applied Achilles force.(47±17Nm with applied force, 33±17Nm without). Our results are also in agreement with Klopp et al. [8] who report an increase in axial loading three times the magnitude of the applied bracing force. By comparison, in this study the mean difference in the peak axial load was approximately twice the applied Achilles load. This supports the view of other researchers that a plantar flexing force in the Achilles tendon has more than a simple additive effect [8].

The significant increases in mean impactor force with an applied plantar flexing force, reported in this study, suggest that, in future biofidelity assessments of dummies, some account of bracing should be considered.

The finding that axial loading is increased by a magnitude significantly higher than the applied Achilles tension implies that, in bracing, car occupants could be at higher risk of these disabling fractures.

In this work specimens amputated through the knee were used with both heads of the gastrocnemius being detached. It has, however, been reported that the gastrocnemius does not contribute significant resistance when the knee is bent, as is usually the case when driving a car [9].

The method developed to apply an active plantar flexing force in PMHS specimens is being further developed. It is anticipated that the use of an active plantar flexing force will be required in future work particularly to generate pilon fractures.

ACCIDENT ANALYSIS

There have been many recent analyses addressing lower leg injuries in frontal car trauma. The following accident analysis is unusual in that an emphasis has been placed on the review of the clinical notes by an orthopaedic surgeon, in order to attempt deduce more accurately the mechanism of injury. Injuries have been ranked according to their frequency, severity and impairment in order to determine which injuries are a priority for prevention.

A retrospective, case by case accident analysis has been conducted to determine the incidence and mechanisms of lower extremity injuries to front seat occupants, and to determine which injuries are a priority for prevention. This has been based on their potential for causing long term impairment and disability. This study is the largest in-depth analysis of lower extremity injuries to be conducted in the UK. The accident data were taken from the CCIS database with in addition; the hospital medical notes and x-rays being obtained. This enabled a detailed examination of the injuries and associated vehicle damage for each case.

The specific objectives of this study were to:

1. Identify the lower limb fractures and serious soft tissue injuries sustained by front seat occupants in frontal crashes.
2. Identify the source of injury from each vehicle.
3. Detail the precise mechanism of injury (i.e. the load path and the direction of forces transmitted to the lower limb).
4. Judge which injuries are priorities for prevention with respect to their high incidence or their potential for causing severe and long-term disability.
5. Recommend methods of reproducing the injuries observed in 'real world situations in a laboratory.

Data for 114 front seat occupants, with a total of 194 lower leg injuries were obtained for this analysis.

Injury Severity

Most accident investigators use the Abbreviated Injury Scale (AIS) to code injuries to car occupants.

However, this scale categorises injures primarily on the basis of 'threat to life. It does not indicate the mechanism of injury or the likelihood of that injury being a cause of long term disability. An injury scale developed by the American Orthopaedic Foot and Ankle Society (AOFAS) was considered more useful in this respect and has been used in this study. An outline of the severity and impairment scoring system is shown in Table 5.

Table 5.
The AOFAS Severity and Impairment Codes for Foot and Ankle Injuries

Score	Severity of Injury	Expected Functional Outcome
0	No injury	No Impairment No residual signs or symptoms associated with the injury
1	Minimal Injury	Minimal Impairment Able to do all desired activities, may be slightly limited at impact activities, occasional discomfort
2	Mild Injury	Mild Impairment Unable to do impact activities, some limitations at work. Can't do a job requiring constant standing, walking or climbing
3	Moderate Injury	Moderate Impairment Walking is limited. Can do most activities but unable to walk for long periods. May use cane for support occasionally
4	Severe Injury	Severe Impairment Able to walk about living quarters. Usually can weight-bear but often needs walking aid (cane). Needs to sit most of time at work. Regularly uses medication to control pain.
5	Very Severe Injury	Very Severe Impairment Can barely get around living quarters with out walking aids. Must use walking aids or wheel chair outside of house. Only able to work in limited jobs requiring no standing, walking or climbing.
6	Currently Un-treatable	Total Impairment Unable to weight bear must use walking aid or wheel chair at all times. Unable to perform any type of work activities and/or household chores. Pain very poorly controlled

Lower Limb Injury Accident Analysis - Methods

The cases for the retrospective study were taken from the existing Co-operative Crash Injury Study (CCIS) database. This database contains data collected by professional accident investigators, who study accidents that occur in specific sampling areas within the UK. A detailed examination of vehicle damage is made, and compared with the occupants' medical data from hospital records, occupant questionnaires and post-mortem reports, as appropriate. The accidents were sampled such that fatal and serious crashes were investigated, where possible. Thus the database was biased towards accidents that are more serious.

The data contained within the CCIS database lacked the necessary detail to determine the mechanisms and source of injuries to the lower extremities of front seat occupants. In order to determine this information, a more in-depth systematic case-by-case analysis of the CCIS cases was undertaken which included reference to the original hospital medical notes and X-rays.

For this study, the cases selected were frontal impacts, i.e. the principal direction of force was between 11 and 1 o'clock (any accidents involving a rollover or multiple impact were excluded). The front seat occupant had to have sustained an Abbreviated Injury Score (AIS) of two or more to the lower extremity.

Retrospective Study Injury Types

The injuries found from the retrospective investigation were first broken down according to frequency of occurrence (Table 6). The most frequently injured regions were the ankle (18.6%), femoral shaft (18.6%), and fractures of the talus (8%), tibial shaft (7%) and forefoot (7%). Here, 'ankle' refers to the articulation between the talus, tibia and fibula. Therefore fractures of the ankle include malleolar fractures and fractures of the distal tibia weight bearing area (pilon fractures).

Table 6.
Frequency of AIS 2+ Injuries to the Lower Extremity by Anatomical Site for Subjects in the Retrospective Study

Injury Region/type	Frequency	%
Ankle Fractures	36	18.6
Femoral shaft	36	18.6
Patella	20	10.3
Talus	16	8.2
Forefoot	13	6.7
Tibial shaft	13	6.7
Tibial plateau	11	5.7
Supra-condylar	7	3.6
Hip dislocation	6	3.1
Acetabulum	6	3.1
Phalanges	6	3.1
Midfoot	6	3.1
Calcaneus	6	3.1
Lisfranc's joint	5	2.6
Femoral neck	3	1.5
Knee ligament	2	1.0
Pelvis	2	1.0
Total	194	100

Below Knee Injuries

This study focused on below knee injuries, which constitute over one half of the total lower limb injuries shown in Table 6. These were defined as AIS 2+ injuries to the tibial plateau and below. For ease of reference, these will be referred to as below knee injuries, although the tibial plateau constitutes part of the knee. 112 'below knee' injuries to 78 occupants (65 drivers and 13 front seat passengers) were analysed. The ankle was the most frequently injured site. One third of these ankle injuries were pilon fractures (Table 7). By frequency alone, injuries to the ankle (32%), talus (14%), tibial shaft and forefoot (both 12%) and tibial plateau (10%) would appear to be the most important injuries. However, this does not take into account that many of these injuries are of low severity and are associated with a good outcome, and also that several injuries that occur relatively infrequently account for a large proportion of the most disabling injuries.

Table 7.
Injury Frequencies by Site for All Below Knee Injuries.

Injury	Frequency	%
Ankle Malleolus	23	20.5
Talus	16	14.2
Ankle Pilon #	13	11.6
Tibial Shaft	13	11.6
Forefoot	13	11.6
Tibial Plateau	11	9.8
Midfoot	6	5.4
Phalanges	6	5.4
Calcaneus	6	5.4
Lisfranc's Joint	5	4.5
Total	112	100

The primary injury mechanism for each of these injuries was deduced from analysis of the X-rays of each injury. The breakdown of mechanism of injury for each site is contained in Tables 8-11.

Table 8.
Primary Mechanism of Fracture for Injuries to the Tibia and Ankle

Injury Site	Mechanism	Frequency
Tibial Plateau #	Axial Load + Varus/Valgus	7
	Axial Load + Rotation	1
	Axial Load + Combination	3
Tibial Shaft #	Bending	5
	Bending + Compression	6
	4-Point Bending	2
Ankle Pilon #	Combined (Axial Load)	13
Ankle Malleolus #	Abduction	11
	Adduction	8
	External Rotation	4

The majority of tibial plateau fractures were attributed to either a varus or a valgus force applied to the tibia (i.e. a force tending to rotate the tibia about the knee either towards [varus] or away from [valgus] the midline). This resulted in a unilateral tibial plateau fracture pattern. More complex loading mechanisms, implying greater axial compression and rotation were responsible for the bilateral plateau fractures.

The majority of tibial shaft fractures were attributable to a bending mechanism. A greater degree of axial compression of the tibia was implied by fragmentation at the fracture site.

Fractures of the ankle that involved only the malleoli were caused by rotation of the talus within the ankle mortise, as the foot was rotated about the tibia. Although common, these injuries are relatively straightforward to treat and are associated with a good outcome.

Fractures to the main weight bearing area of the distal tibia (pilon fractures) were caused principally by axial loads (i.e. loads in the direction of the long axis of the tibia) with secondary rotations of the foot ankle complex. In contrast to malleolar fractures, pilon fractures are very difficult to treat and often lead to poor outcome for the patient (Table 8).

The most important fractures of the hind-foot, fractures of the talar neck and intra-articular calcaneal fractures, are caused by axial loads (i.e. loads parallel to the long-axis of the tibia). Hind-foot injuries caused by inversion or eversion of the foot would not be expected to cause long-term disability, unlike fractures of the talar neck and calcaneus (caused by axial loading) which often leave the patient severely disabled (Table 9).

Table 9.
Principal Mechanisms of Injury to the Talus and Calcaneus

Injury Site	Mechanism	Frequency
Talar Neck #	Axial load and Dorsiflexion	9
Talar Avulsion #	Inversion/Eversion of Foot	3
	Dorsiflexion and Inversion	4
Intra-articular Calcaneus #	Axial Load	5
Calcaneus Avulsion #	Inversion/Eversion of Foot	1

Fractures to the mid-foot and the Lisfranc's joint were caused by indirect loading to these structures and excessive bending in abduction, adduction and plantar flexion (Table 10).

Table 10.
Principal Mechanisms of Injury to the Mid-foot and Lisfranc's Joint

Injury Site	Mechanism	Frequency
Mid-foot #	Medial Stress	1
	Lateral Stress	5
Lisfranc's Joint #	Plantar-flexion / Abduction/Adduction	5

In contrast, injuries to the forefoot region are usually a result of direct trauma to the fractured area (Table 11). Often damage is localised to a small area (e.g. one or two metatarsal necks only) suggesting a small area of concentrated load.

Table 11.
Principle Mechanisms of Injury to the Forefoot (Metatarsals and Phalanges)

Injury Site	Mechanism	Frequency
Forefoot #	Direct Blow	11
	Bending	2
Phalanges #	Crush/Direct Blow	4
	Axial Load + Varus or Valgus	2

From this analysis, it would appear that the most important mechanism of loading of the foot and ankle is from forces whose principal vector is along the axis of the tibia. Although injuries caused by rotations of the foot and ankle account for a large number of injuries, these are not likely to cause the more severe injuries seen to front seat car occupants.

Below-Knee Primary Injury Sources

For each injury detailed above, a primary contact source was deduced from inspection of the vehicle and the type and mechanism of injury. This was defined as the Primary Injury Source. Table 12 details the different primary injury source for each injury type. Several categories have been amalgamated for ease of analysis (e.g. firewall and wheel-well intrusion are coded separately on the database but combined in Table 12.

Intrusion was correlated with the primary injury mechanism in almost half of injuries below the knee. Intrusion also played a significant role in the 19 cases where entrapment between floor and facia occurred. In these cases, it was judged that, because the leg had become trapped, as evident by contacts identified on the facia, the injury was not simply correlated with intrusion. The entrapment would be likely to increase the risk of injury or to increase the severity of injuries that may have occurred in the presence of intrusion alone.

Table 12.
Primary Injury Source for Below-Knee Injuries

	A	B	C	D	E	F
Tibial Plateau #	5				3	3
Tibial Shaft #	8				3	2
Pilon #	3	1			9	
Malleolus #		2	8		10	3
Talus #	2	2	1		11	
Calcaneus #	1				5	
Midfoot #				1	5	
Lisfranc's #		2		1	2	
Forefoot #		10			3	
Phalanges #		2		2	2	
Total	19	19	9	4	53	8

A = Entrapment between floor and facia
B = Foot-pedal contact
C = Rolled off pedal
D = Foot trapped under pedal
E = Intrusion of footwell
F = Floor contact

For pilon fractures, malleolus fractures, talus fractures, fractures of the calcaneus and midfoot region, intrusion was again correlated with primary injury mechanism. Intrusion was also implicated in fractures of the tibial shaft and tibial plateau but in addition, there was evidence of the knee becoming trapped by the facia in over 50 percent of these fractures.

Injuries attributable to contact with a foot pedal or the foot rolling off a pedal accounted for 25 percent of below knee injuries. The 'foot roll-off pedal' injuries were almost exclusively ankle-malleolus fractures and this mechanism accounted for 8 of the 23 (34%) malleolar fractures. It was concluded that for these injuries, the foot was on the pedal (usually the brake pedal) at the time of impact and then rolled off one side of the pedal due to the crash pulse, leading to ankle fractures..

The majority of forefoot injuries attributed to foot pedal contact were fractures of the distal metatarsals. From careful consideration of the vehicle inspection notes and accident circumstances, it was concluded that the foot was on the pedal at the time of impact and that the fractures seen in these cases were consistent with concentrated loading over a small area of the foot (e.g. fracture of two metatarsals only).

Injury Severity and Impairment

When only the frequency of the different below knee injuries is considered, fractures of the ankle (malleolar and pilon fracture types) are the found to be the most important fractures to prevent, followed by fractures of the talus (all types), forefoot and tibia (shaft and plateau). In order to prioritise the injuries, the severity of each injury and its potential for causing long term disability needs to be evaluated. This analysis was performed using the injury severity and impairment scales defined by the American Orthopaedic Foot and Ankle Society Trauma Committee (AOFAS). Table 13 shows the AOFAS injury severity score by anatomical site for all below knee injuries.

Table 13.
AOFAS Injury Severity Score by Site for Below Knee AIS 2+ Injuries

Injury Site	Injury Severity Score (AOFAS Scale)					
	1	2	3	4	5	6
Tibial Shaft #				4	7	2
Malleolus #	10	5	5	3		
Pilon #			1	5		7
Talus #	1	1	8	1	4	1
Calcaneus #			1		5	
Mid-foot #			6			
Lisfranc's #					5	
Forefoot #		2	7	4		
Phalanges #		2	4			
Totals	11	10	32	17	21	10

Of the most severe below knee injuries (i.e. those that are most difficult to treat), the most important injuries in descending rank were:

1 Pilon fractures
2 Tibial shaft fractures
3 Fractures of the Calcaneus
4 Fractures of the Talus (Talar Neck fractures)
5 Lisfranc's Joint injuries

However, this analysis fails to take into account the likely outcome from such injuries. An analysis can be carried out in which the impairment scores, as determined by the AOFAS scale, can examined by injury site (Table 14).

Table 14.
AOFAS Injury Impairment Score by Site for Below Knee AIS 2+ Injuries

Injury Site	Impairment Score (AOFAS Scale)					
	0	1	2	3	4	5
Tibial Shaft #		3	8	2		
Malleolus #	10	6	7			
Pilon #			6		7	
Talus #		8	2	5	1	
Calcaneus #				5		1
Mid-foot #		2	2	2		
Lisfranc's #				5		
Forefoot #		8	5			
Phalanges #		6				

If the likely long-term impairment from each injury is considered then the most important injuries become:

1. Pilon Fractures
2. Fractures of the Talar Neck
3. Fractures of the Calcaneus
4. Lisfranc's Joint Injuries
5. Fractures of the Tibia
6. Malleolar Fractures

Comparison of Driver and Passenger Injuries

There were 93 individual injuries to drivers and 19 injuries to front seat passengers. With such a small sample of front seat passenger injuries, it is difficult to draw any firm conclusions. An interesting point to note is that for both talus fractures and pilon fractures, the driver's right leg is seen to be at risk of injury (although in neither case was this relationship seen to be statistically significant). This may reflect that intrusion of the foot-well region is usually highest on the vehicle outboard because of the locality of the wheel-well. However, it should also be remembered that the right leg is used for braking.

Apart from these general observations, there is insufficient data to allow any firm conclusions to be drawn regarding the mechanisms of injury to front seat passenger legs, feet and ankles. The spectrum of injuries is broad with only small numbers in each category of primary injury source and so it was not possible to make any further observations.

Accident Analysis Discussion

The primary focus of future impact biomechanics experiments should be:

1. Pilon fractures
2. Fractures of the Calcaneus
3. Fractures of the Neck of the Talus

For these three injuries, the principal mechanism of is axial loading. Injuries related to foot pedal roll-off were common but would not be expected to cause significant long-term disability or impairment. The application of a protection criterion, relating to this phenomenon, would be somewhat difficult in full-scale impact testing due to the unpredictable nature of the roll-off process.

It was concluded that intrusion was the most important method of loading the tibia, foot and ankle. However, it was not possible to demonstrate the relationship between increasing levels of intrusion and increasing risk of severe and impairing injuries.

It is recommended that the loading mechanisms in the laboratory-based experiments should be a simplification of the loading mechanisms that occur in 'real world' car crashes in which occupants sustain lower limb injuries, in order that the mechanisms can be studied in a more defined manner.

SUMMARY

In the driving simulator trials, the mean brake pedal force in an emergency event was 630N. At the same time a mean plantar flexion of the foot of 15° was recorded. Half of the drivers lifted their heel from the floor pan during the braking action.

In live humans, it is known that the braking force will be generated by a combination of extension at the knee joint and tension applied through all the plantar flexing muscles (Achilles, soleus, flexor hallucis longus etc). In the biomechanical tests reported here, it was only possible to use the Achilles tendon to regenerate the plantar flexing force. Anatomical measurements, made during the study, were used and a mean required force in the Achilles tendon of 1.5kN was calculated. The results reported here and previous reports [6-8], have shown that the application of such a force will significantly enhance peak axial loading.

The accident analysis, summarised at the end of this paper and previous reports [18, 21], have indicated the importance of axial loading in the three most disabling injuries at the ankle (pilon, calcaneal and talar neck). It seems probable that, while bracing hard may help an occupant remain in the seat during an impact, it will at the same time significantly increase the risk of a disabling lower leg injury.

It is not known at what point foot and ankle injuries occur during an impact. If drivers are usually braking prior to the accident, as suggested by previous work, [18] and the simulator trial, it would appear desirable to conduct biomechanical tests with the foot in an initial plantar flexed position with a loading force applied. The indicated 1.5kN of active lower leg muscle force calculated here is larger than the passive forces used in previous biomechanical studies (450N [22] 960N [6]). This figure is a good indicator of the forces that should be considered for future biomechanical studies to reproduce a realistic situation. It also seems essential that biomechanical evaluations of fracture mechanisms should encompass both initial heel floor contact and no contact between the heel and the floor in the experimental set up.

Currently the Hybrid III is used almost universally for legislative car crash testing, and the test procedure specifies that the dummy foot should be placed on the vehicle accelerator at the start of the test. This study indicated that, in frontal collisions, most drivers were braking at the time of the impact. The position of the feet in future car crash testing needs careful consideration, if the next generation of dummies are to be used to accurately measure the risk of lower leg injury.

In a similar way the application of a braking force needs careful consideration, although there would clearly be difficulties in achieving this controllably under crash test conditions. The proposed design for ALEx II incorporates a passive Achilles tension that will apply a consistent force to the ankle joint without a large increase in bending moment at the end of the tibia. This will allow more biofidelic movement at the ankle joint and at the same time, a partial addition to axial loading. A higher, active force would have to be applied to the simulated tendon if plantar flexing forces, such as those recorded in this work, were to be generated.

The biofidelity tests carried out for this work have examined the response of the foot and ankle to sub-injury simple pendulum impact tests, based around the EEVC foot certification procedure. Tests were performed on both PMHS specimens as well as live human volunteers. For live volunteers the foot response with the lower leg muscles both tensed and relaxed was tested. The response of the foot to both heel and toe impacts was studied. For the PMHS specimens and for the dummy, attempts to assess the dynamic response of the foot in inversion and eversion were made. An attempt was also made to normalise the results of both the PMHS specimen tests and the volunteer tests in order to align the results with that of the fiftieth percentile. The normalisation procedure reduced the scatter for some of the test results, but was not sufficiently well developed nor validated at this stage to allow a comparison of normalised results to be made. The reason that this failed was probably due to the fact that it was not possible to measure all potentially influential factors prior to testing. For future work, extra measurements will be made to improve the normalisation procedure e.g. ankle joint stiffness. The results presented are thus the unnormalised data from the PMHS specimens and volunteers compared with the dummy results.

Two designs dummy feet and ankle were tested, the Hybrid III with the 'soft-stop' 45° ankle and the GM/FTSS foot, attached to the Hybrid III leg. The GM/FTSS foot and ankle responses were closer to those of the PMHS specimens and human volunteers (where measured) for the mean peak dorsiflexion angle, pendulum acceleration and tibial bending moment than those obtained for the Hybrid III. Conversely for the mean peak tibia force, the Hybrid III results were closer to those of the PMHS specimens than the GM/FTSS foot, although the difference were statistically significant for both. The tests using heel impacts have shown that the data recorded using the GM/FTSS foot is very similar to the data obtained with PMHS specimens. The data obtained with the Hybrid III foot differs significantly. Neither dummy foot appears to be superior, regarding the biofidelity to inversion or eversion. Both generate a higher acceleration response on the pendulum but result in a lower peak tibial axial force when compared with the PMHS test results.

Most people involved in frontal impacts will be aware of the impending accident. Therefore, it could be considered that the most appropriate condition that the dummy response should simulate, would be that of the aware volunteers.

Due to the reduction in fatalities of occupants in car accidents, injuries to the lower leg are being increasingly recognised as a source of both severe and long term impairing injuries. Dummy design has been aimed at addressing injury assessment for body regions where there is a high risk of fatality if injury occurs. The shift in emphasis to other body regions calls for the refinement in both the design and injury criteria of the current dummy used for assessment of vehicle performance in frontal impact, the Hybrid III.

The accident analysis of lower leg injuries in the UK population showed that, if frequency alone is considered, the ankle is the most common fracture site (32%), followed by fractures of the talus (14%), forefoot and tibia (both 12%) and tibial plateau (10%). However, if severity and impairment are taken into consideration this ranking changes and the order for prevention is pilon, calcaneal and talar neck fractures. The primary source of injury was attributed to intrusion of the footwell.

Future Work - The next phase of this work will focus on recreating the lower leg injuries, seen in car accidents in the laboratory. The aim will be to recreate the loading patterns and intrusion seen in the foot well and use cadaver legs and dummy legs to compare the results. This research should lead to a clearer understanding of the mechanism of injury and aid the development of future dummies such that new injury criteria can be developed.

CONCLUSIONS

1. In simulated frontal impacts, drivers were found to apply a mean peak force of 630N to the brake pedal with the ball of the foot.
2. The equivalent force that would be needed in the Achilles tendon to generate this applied braking force was calculated to be 1.5kN
3. In just under half of the emergency braking events, the subject's heel was not in contact with the floor pan at the point of applied peak brake force.
4. The mean ankle articulation at the time of peak brake force application was found to be 15° of plantar flexion
5. Dynamic responses of PMHS and volunteers' lower legs to sub-injury pendulum foot impacts have been obtained to provide biomechanical reference data for dummy response evaluation.
6. A technique has been developed to generate forces of up to 3.3kN in the Achilles tendon of the PMHS prior to impact.
7. The application of Achilles tendon force significantly increases the tibia axial force and decreases the dorsiflexion angular response to impacts to the PMHS toe area.
8. For the aware volunteers, the dorsiflexion angular displacement was reduced and the impactor response increased in comparison with unaware volunteers.
9. Neither of the two dummy feet and ankles evaluated gave the same responses as the PMHS or volunteers for all the parameters measured. The GM/FTSS foot was closest for most conditions with good biofidelity for heel impacts. The Hybrid III foot was nearer to the PMHS for tibia axial force for toe impacts but the differences were significant.
10. The Hybrid III dummy leg would have to be redesigned to align the axis of the tibia with the ankle and knee joints if an artificial generation of tibia bending moments from an applied tibia compressive force is to be avoided.
11. The three most important lower leg injuries found in accidents, taking into account frequency, severity and outcome, are pilon, calcaneal and talar neck fractures.
12. The most likely cause of these most important lower leg injuries is considered to be axial force.
13. For future legislative crash testing, the initial position of the dummy lower limb and the representation of active muscle tension in the lower leg should be considered, particularly if the risk of lower leg injury is to be assessed in a biofidelic manner.

ACKNOWLEDGEMENTS

The work described in this report forms part of a biomechanics research project funded by the UK Department of the Environment, Transport and the Regions. The authors wish to acknowledge the valuable contributions of Mr Peter Thomas of the Vehicle Safety Research Centre, Mr Andrew Taylor and Mr Mark Parry of the University of Nottingham.

REFERENCES

1. Union, E., *DIRECTIVE 96/79/EC OF THE EUROPEAN PARLIAMENT AND THE COUNCIL ON THE PROTECTION OF OCCUPANTS OF MOTOR VEHICLES IN THE EVENT OF A FRONTAL IMPACT.* The Official Journal of the European Communities, 1996. 40(21): p. 1-7.
2. Luchter, S., *Long Term Consequences of Lower Extremity Injuries*, , National Highway Traffic Safety Administration.
3. Miller, T.R., P.G. Martin, and J.R. Crandall., *Costs of Lower Limb Injuries in Highway Crashes.* International Conference on Pelvic and Lower Extremities. 1995. Washington, DC, USA., 1995.
4. Salmi, R., et.al., *Impairments, Disabilities and Handicaps Five Years After Isolated Lower Extremity Injuries: A Population-Based Study.*

International Conference on Pelvic and Lower Extremity Injuries. 1995. Washington, DC USA., 1995.

5. Fildes, B., *et al.*, *Lower Limb Injury in Frontal Crashes*, , Monash University Accident Research Centre: Victoria.
6. Manning, P., *et al. The Position and Movement of the Foot in Emergency Manoeuvres and the Influence of Tension in the Achilles Tendon.* in *41st Annual Stapp Car crash Conference.* 1997. Florida (USA): SAE.
7. Petit, P., *et al. Quasistatic Characterization of the Human Foot-Ankle Joints in Simulated Tensed State and Updated Accidentological Data.* in *1996 International IRCOBI Conference on The Biomechanics of Impact.* 1996. Dublin, Ireland: IRCOBI.
8. Klopp, G.S., *et al. Simulation of Muscle Tensing in Pre-Impact Bracing.* in *IRCOBI.* 1995. Brunnen, Switzerland: IRCOBI.
9. Crandall, J., *et al. Biomechanical Response and Physical Properties of the Leg, Foot and Ankle.* in *40th Stapp Car Crash Conference.* 1996. Albuquerque, New Mexico: SAE.
10. Portier, L.e.a., *Dynamic Biomechanical Dorsiflexion Responses and Tolerances of the Ankle Joint Complex.* 41st Stapp Car Crash Conference. 1997. Orlando, Florida, USA: SAE., 1997.
11. Crandall, J.R., *et al. Sled Tests with Toepan Intrusion Using Post-Mortem Human Surrogates and the Hybrid III Dummy.* in *1996 International IRCOBI Conference on The Biomechanics of Impact.* 1996. Dublin Ireland.
12. Schueler, F., *et al. Injuries of the Lower Legs - Foot, Ankle Joint, Tibia; Mechanisms, Tolerance Limits, Injury-Criteria Evaluation of a Recent Biomechanic Experiment-Series.* in *IRCOBI.* 1995.
13. Systems, F.T.S., *New FTSS 45 Degree Foot.* Newsline, 1996. V(II): p.1-8., 1996.
14. Roaas, A. and G.B.J. Andersson, *Normal Range of Motion of the Hip, Knee and Ankle Joints in Male Subjects, 30-40 Years of Age.* Acta orthop scand, 1982(53): p. 205-208.
15. Portier, L., *Securite Automobile et Protection des Members Inferieurs.* Genie Biologique et Medical. 1997 Universite de Paris: Paris p. 243., 1997.
16. Taylor, A., *et al.*, *Lower Limb Injuries to Car Occupants, An In Depth Analysis*, . 1997, The University of Nottingham: Nottingham.
17. Crandall, J., *The Preservation of Human Surrogates for Biomechanical Studies*, in *Faculty of Engineering and Applied Science.* 1994, University of Virginia: Charlottesville. p. 271.
18. Morris, A., *et al. Mechanisms of Fractures in Ankle and Hind-Foot Injuries to Front Car Seat Occupants - An In-Depth Accident Data Analysis.* in *41st Annual Stapp Car Crash Conference.* 1997. Florida (USA): SAE.
19. Ferris, L., *et al.*, *Influence of Extrinsic Plantar Flexors on Forefoot Loading During Heel Rise.* Foot and Ankle International, 1995. **16**(8): p. 464-473.
20. Simonsen, E., H. Klitgaard, and F. Bojsen-Moller, *The influence of strength training, swin training and ageing on the Achilles tendon and m. soleus of the rat.* Journal of Sports Sciences, 1995. **13**: p. 291-295.
21. Taylor, A., *et al. Mechanisms of Lower Extremity Injuries to Front Seat Car Occupants - An In-Depth Analysis.* in *International IRCOBI Conference on the Biomechanics of Impact.* 1997. Hannover (Germany): IRCOBI.
22. Peter, R.E., *et al.*, *Biomechanical Effects of Internal Fixation of the Distal Tibiofibular Syndesmotic Joint: Comparison of Two Fixation Techniques.* J Orthop Trauma, 1994. **8**(3): p. 215-220.

© Copyright TRL Limited 1998. This paper has been produced by the Transport Laboratory, as part of the contract placed by the UK Department of the Environment, Transport and the Regions. Any views expressed are not necessarily those of the Department. Extracts from the text (excluding photographs) may be reproduced except for commercial purposes, provided the source is acknowledged.

APPENDIX 1 – TIBIAL LOADCELL INSERTION

The method of insertion of the tibial load cell was developed specifically for this project, a 12x5cm area of skin and superficial tissue were removed from the anterior surface of the leg at a point defined by the subcutaneous surface of the tibia 6cm above the ankle joint. The area of tibia thus exposed was then stripped of the periosteum by a periosteal elevator. The 12-cm section of the tibia was then freed from all surrounding tissues by gentle sharp dissection around its circumference. Particular attention was paid to preserving the soft tissue integrity around the posterior aspect of the tibia. The fibula shaft was vulnerable to fracture and great care was taken to preserve its integrity. The intra-osseous membrane was only divided for the 12cms and care is taken to preserve the structure both proximally and distally at the syndesmosis.

The PMHS specimen was held with the leg in its anatomical position such that the foot rests at 90° to the tibial shaft with the 2nd toe pointing vertically upwards. The two posterior end sections of the drilling jig (Figure A1) were passed around the tibia along with securing ties. The anterior section of the jig was positioned to join with the two posterior sections and secured. The whole drilling jig was then manipulated and adjusted around the tibia using four adjusting screws to ensure that the orientation was correct in all planes, both radially and axially. The drilling jig was marked with the central longitudinal axis, to assist with this task. Locating holes were drilled through the tibia through which four fixing pins were placed, two at right angles to each other at each end (Figure A2). Care was exercised when drilling through the tibia to minimise the risk of mal-alignment, as the hole was drilled obliquely into the surface of the tibia. The tibia was also marked for cutting through the jig. The tibia was divided and the removed section kept for further physical property analysis. A fine cutting ring was then placed over the ends of the tibia and fixing pins reinserted to maintain its position. The sawn end of the tibia was then ground down to exactly the right length (Figure A3).

The cut tibial ends were prepared, over a 25mm length from the cut edge, with a degreasing agent. The potting cups were then placed on the tibial ends and realigned with the fixing pins to maintain their position and a dummy tibial load cell was inserted to maintain the alignment of the leg (and stop any relative movement due to dehydration or degradation) (Figure A4). Potting media is pressure injected into the cups via two 6mm holes (Figures A5) drills to maintain position. The completed tibial load cell assembly is shown in Figure A6.

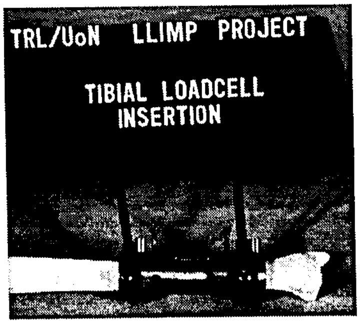

Figure A1 - Cutting Jig In-Situ on Tibia

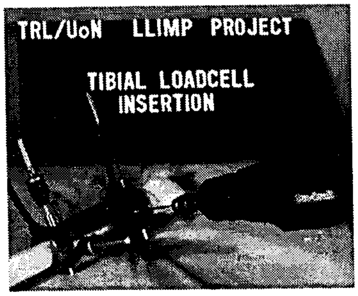

Figure A2 - Guide Wire Drilling

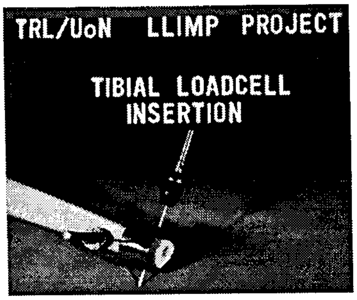

Figure A3 - Cutting Jig and Guide Wires

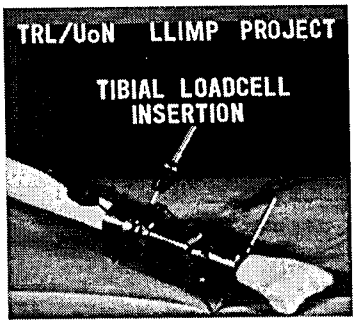

Figure A4 - Dummy Load Cell In-Situ

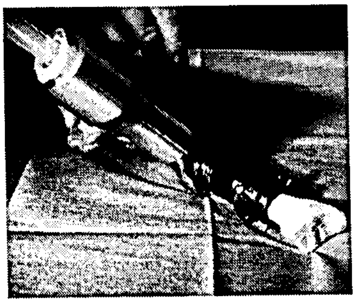

Figure A5 - Pressure Injection

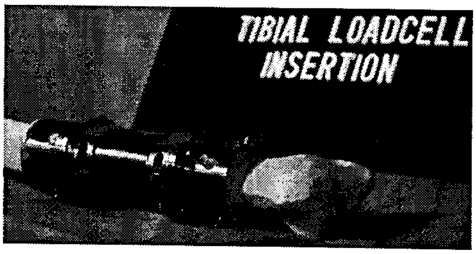

Figure A6 - Completed Assembly

Acoustic Transducers - It was hypothesised that a failure, whether bone fracture or ligament rupture could produce an acoustic 'event' i.e. a high frequency signature. These data could be used to determine the environment and forces that exist at the time of any defined injury. For the purpose of these tests a simple 'acoustic' guitar pick up, one located on the surface of the second metatarsal and the other on the tibia was used to measure any acoustic signals which might be generated due to an injury event. In the tests reported in this paper no failures were detected

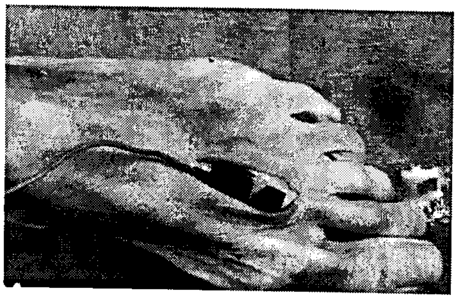

Figure A7 - Acoustic Transducer on Second Metatarsal

APPENDIX 2 – PEAK RESPONSES FOR INDIVIDUAL TESTS FOR PMHS, DUMMIES AND VOLUNTEERS

	Peak Pendulum Acceleration (g)				
Specimen	Heel Impact 4m/sec	Toe Impact 4m/sec	Toe impact 6m/sec	Eversion Impact 4m/sec	Inversion Impact 4m/sec
TRL001R	Not tested	21.3	43.75	Not tested	Not tested
TRL001L	132.78	21.7	41.37	28.17	21.59
TRL004R	117.83	34.82	62.25	31.51	26.79
TRL004L	146.28	33.94	51.01	25.89	35.95
TRL007R	130.74	27.96	46.57	52.57	31.71
TRL007L	122.11	26.41	44.91	32.02	21.17
TRL005L	146.22	26.92	53.04	29.77	27.38
*TRL005R	140.09	22.88	41.48	33.14	26.89
GM/FTSS – Test 1	132.56	51	87.69	58.02	39.86
GM/FTSS – Test 2	133.77	54.37	86.2	36.43	42.56
GM/FTSS – Test 3	127.91	54.46	87.96	53.36	41.34
Hybrid III – Test 1	213.29	86.06	139.41	43.15	54.87
Hybrid III – Test 2	206.43	85.36	141.11	47.59	55.08
Hybrid III – Test 3	201.18	No data	136.13	38.64	53.43
Volunteer 1 - Unaware	Not tested	26.05	47.42	Not tested	Not tested
Volunteer 2 - Unaware		32.64	76.19		
Volunteer 3- Unaware		23.96	64.35		
Volunteer 4 - Unaware		46.81	61.97		
Volunteer 5 - Unaware		36.83	78.48		
Volunteer 1 - Tensed		No data	57.64		
Volunteer 2 - Tensed		29.17	94.97		
Volunteer 3 - Tensed		29.49	No data		
Volunteer 4 - Tensed		56.03	95.69		
Volunteer 5 - Tensed		40.46	88.44		

*Above knee Amputation

	Peak Tibial Force Fz (N)				
Specimen	**Heel Impact 4m/sec**	**Toe Impact 4m/sec**	**Toe impact 6m/sec**	**Eversion Impact 4m/sec**	**Inversion Impact 4m/sec**
TRL001R	Not tested	-861	-1676	Not tested	Not tested
TRL001L	-2329	-1112	-1839	-764	-265
TRL004R	-2179	-532	-1181	-832	-404
TRL004L	-2640	-600	-1109	-455	-391
TRL007R	-1834	-428	-1003	-916	-335
TRL007L	-2047	-541	-1009	-326	-331
TRL005L	-2199	-709	-1304	-651	-577
*TRL005R	-2219	-851	-1575	-543	-645
GM/FTSS – Test 1	-1861	-153	-198	-284	-293
GM/FTSS – Test 2	-1894	-158	-189	-221	-308
GM/FTSS – Test 3	-1819	-182	-233	-323	-255
Hybrid III – Test 1	-2999	-495	-860	-328	-256
Hybrid III – Test 2	-3094	-572	-821	-361	-246
Hybrid III – Test 3	-2878	No data	-785	-269	-258

*** Above knee Amputation**

	Peak Tibia Bending Moment, My (Nm)		Peak Tibia Bending Moment, Mx (Nm)	
Specimen	**Toe Impact 4m/sec**	**Toe Impact 6m/sec**	**Eversion Impact 4m/sec**	**Inversion Impact 4m/sec**
TRL001R	5.86	9.85	Not tested	Not tested
TRL001L	6.95	-19.2	-9.91	-7.71
TRL004R	9.44	14.83	-15.86	6.08
TRL004L	-7.23	-14.27	6.7	6.08
TRL007R	-6.3	-17.95	-26.2	5.23
TRL007L	-9.43	-20.57	-8.38	-5.39
TRL005L	-11.9	-21.99	13.01	3.83
*TRL005R	5.82	-10.74	-5.91	-9.45
GM/FTSS – Test 1	19.14	39.22	-7.07	6.07
GM/FTSS – Test 2	19.98	38.19	-9.92	-4.68
GM/FTSS – Test 3	17.99	39.35	8.3	-4.7
Hybrid III – Test 1	51.11	115.85	10.81	-9.25
Hybrid III – Test 2	51.73	114.01	-8.8	-8.54
Hybrid III – Test 3	No data	111.79	10.79	-7.98

*** Above knee Amputation**

DESIGN AND PERFORMANCE OF THE THOR ADVANCED FRONTAL CRASH TEST DUMMY THORAX AND ABDOMEN ASSEMBLIES

N. Rangarajan
R. White, Jr.
T. Shams
D. Beach
J. Fullerton
GESAC, Incorporated
M.P. Haffner
R.E. Eppinger
H. Pritz
National Highway Traffic Safety Administration
D. Rhule
Transportation Research Center, Incorporated
D. Dalmotas
Transport Canada
E. Fournier
Biokinetics and Associates, Incorporated
United States

Paper Number 98-S9-O-12

ABSTRACT

In May 1994, GESAC was awarded a contract to design an advanced frontal crash test dummy which has been named THOR. This paper describes the results of an intensive two-year effort to develop the design criteria, design, and test the thorax and abdomen of THOR and its associated instrumentation.

The paper will describe refinement of thoracic anthropometry, design of a realistic belt to shoulder interface, refinements in rib bonding procedures leading to greatly improved durability, design of a posture adjustment system, development of a new 3-D chest deflection measurement system capable of tracking chest compressive velocities up to 10 m/s, new upper and lower abdomen designs which permit continuous measurement of abdominal penetration by restraint and vehicle components, and other design features which have resulted in a more modular, serviceable design.

The paper will also present and summarize the extensive component and sled tests conducted both in the United States and in Canada, for the purpose of evaluating and documenting THOR thorax and abdomen performance against program goals.

INTRODUCTION

Since the early 1980s the NHTSA has supported the development of an advanced frontal crash test dummy with improved biofidelity under frontal impact conditions and with expanded injury assessment capabilities. The program consisted of first developing anthropometric specifications for a family of adult dummies in the automotive seating environment [Robbins,1983], followed by detailed analyses of available human impact response data in conjunction with a study of patterns of motor vehicle injuries [Melvin, 1985]. The primary purpose of these efforts was to provide a sound technical basis for the dummy design and development efforts to follow. Using the new specifications, the University of Michigan Transportation Research Institute (UMTRI) developed a new torso system that was integrated with the standard Hybrid III head, neck, and extremity components and was known as the 50th percentile male Trauma Assessment Device (TAD-50M) and described by Schneider [1992].

In 1994, NHTSA funded GESAC, Inc to begin a

---

[1] Currently with Acentech in Cambridge, MA.

major effort whose scope, in addition to the refinement of the torso design, also encompassed development of advanced representations of the head and face, neck, abdomen, pelvis, and femur. Improvements to various instrumentation systems were also to be investigated, and incorporation of additional sensors accomplished, so that the correlation of dummy responses to estimates of human injury potential could be achieved with greater confidence.

A systematic evaluation of design requirements for the body regions was first accomplished which included a review of the design elements incorporated in TAD-50M. The design of THOR resulted in improvements to all the dummy components except the arms (which remain Hybrid III stock pending conclusion of arm development efforts ongoing within the automotive industry). In particular the design criteria for the thorax was based on the recommendations of Schneider [1989], and the design criteria for the abdomen based on the recommendations of Rouhana [1989].

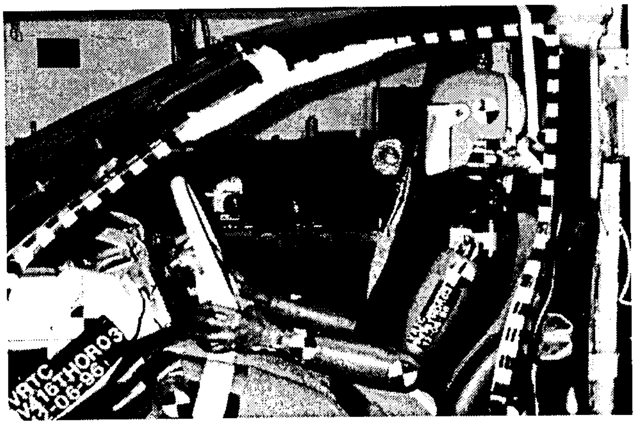

Figure 1. THOR in seated sled test environment

This paper will detail the design features and performance of the THOR thorax and abdomen assemblies. Figure 1 shows the new advanced frontal crash test dummy which has been named THOR (Test Device for Human Occupant Restraint), after the Norse god of thunder, strength, and healing art. Figure 2 presents an assembly drawing of THOR indicating its primary new features. Currently, two dummies have been fabricated and they have been undergoing extensive testing at a number of laboratories under various test conditions.

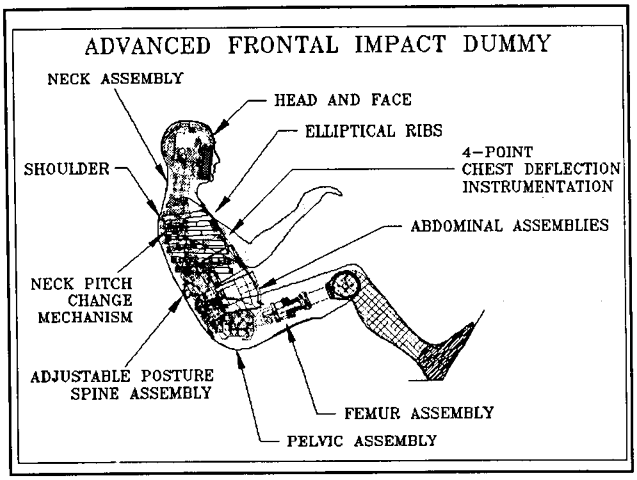
ADVANCED FRONTAL IMPACT DUMMY
NECK ASSEMBLY
HEAD AND FACE
ELLIPTICAL RIBS
SHOULDER
4-POINT CHEST DEFLECTION INSTRUMENTATION
ABDOMINAL ASSEMBLIES
NECK PITCH CHANGE MECHANISM
ADJUSTABLE POSTURE SPINE ASSEMBLY
FEMUR ASSEMBLY
PELVIC ASSEMBLY

Figure 2. Principal features of THOR

DESIGN

Design of THOR Thorax

The THOR thorax includes improvements to the previous design developed for TAD-50M and addresses some of the problems encountered with its performance.

- Improved ribcage anthropometry and stiffness: Though the width and depth of the ribcage in TAD-50M generally reflected the dimensions of the human ribcage, the cross-section was still box-shaped, whereas the human shape is more elliptical. The ribs in THOR have been designed with an elliptical cross-section, but with the same width and depth as the TAD-50M ribs. Apart from improving the anthropometry of the ribcage, modeling and testing on single ribs indicated that the geometry reduced the stiffness of the ribs, in localized loading, by about 15%, which improves agreement with quasi-static stiffness obtained with humans.

- Improved rib fabrication procedure: A problem pointed out by several test laboratories in previous testing with the TAD-50M was the occasional debonding of the damping material from the steel. The new procedure includes thorough surface treatment of the metal and a controlled curing process after application of the adhesive. Testing at a number of different laboratories has indicated that the new procedure is working successfully, and debonding has been markedly reduced.

- New thorax instrumentation: A new two-bar linkage instrumentation system (shown in Figure 3) was developed to meet the more demanding performance requirements for measuring chest compression under out-of-position airbag exposures. The chest deflection measurement in TAD-50M was limited to measurement of compressive velocities below 7 m/s, too slow to measure the higher rates involved in impulsive loading from out-of-position airbags.

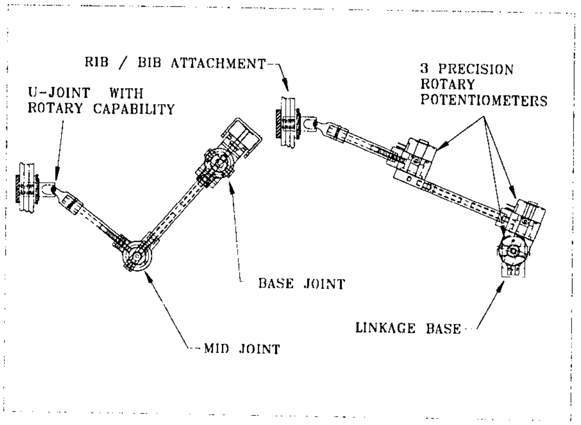
RIB / BIB ATTACHMENT
U-JOINT WITH ROTARY CAPABILITY
3 PRECISION ROTARY POTENTIOMETERS
BASE JOINT
LINKAGE BASE
MID JOINT

Figure 3. CRUX unit for measuring chest deflection in Thor.

Each linkage, called a CRUX, consists of two rigid links in which the relative motion between the links and the base attachment points are measured by precision rotary potentiometers. Once the system has been initially calibrated, recalibration between tests is not required. These transducer systems are attached to ribs 3 and 6 at each side of the centerline, at the rib attachment points to the bib. Extensive testing of these units has demonstrated their reliability, ruggedness and accuracy. The signals from the rotary potentiometers are processed in a dedicated algorithm to yield x, y, and z deflections of the four anterior rib attachments. The measurement system has been evaluated in several out-of-position airbag tests and has performed properly. The results from out-of-position tests done at VRTC are described later in this paper.

Design of Spine

The thoracic spine in THOR is divided into two sections connected through a deformable element at the location of T7/T8. This element was introduced in TAD-50M to provide an additional degree of flexibility to the Hybrid III spine which was considered too rigid [Melvin, 1985a]. Two new modifications have been made in the THOR spine design:

- The thoracic load cell has been moved from the lower lumbar part of the spine to the T12/L1 location. This change was undertaken to place the load cell at the location where the majority of automotive thoracolumbar spine injuries have been observed.
- A pitch change mechanism has been incorporated just below the thoracic spine. This allows the user to adjust the orientation of the pelvis relative to the thoracic spine and permits the dummy to assume various intial seated postures.

Posture adjustment in THOR - Under subcontract to GESAC, Reynolds at Michigan State University [1996] conducted a study of human posture in automotive seated position and defined spinal geometries for four postures. These positions are namely, erect, normal, slouched, and super slouched. The data from this study were analyzed and relative angles between the thoracic spine, lumbar spine and pelvis were estimated for the four positions. It was determined that a single posture adjustment mechanism placed a little above the T12/L1 joint could provide the range of movement that allowed a good fit to the above four postures. The different postures can be realized in THOR by means of a pitch change mechanism. The mechanism is a radial toothed circular section in which two matching segments are adjustable relative to one another. This mechanism permits pitch changes to be made in 3 degree increments. A similar pitch change mechanism has been placed under the lower neck load cell to allow the pitch angle of the head and neck to be changed. Using this mechanism, the head can be maintained in a horizontal orientation for different postures of the thoracic and lumbar spines.

Assembly of the spine components has also been simplified so that the spine and thorax subassemblies can be removed as individual units for service. Figure 4 presents a sketch of the THOR spine assembly with the location of the load cell and pitch change mechanism noted. Figure 5 presents the relative angles between the various spinal sections for the four primary orientations, from erect to super slouched (it can also assume positions in-between these).

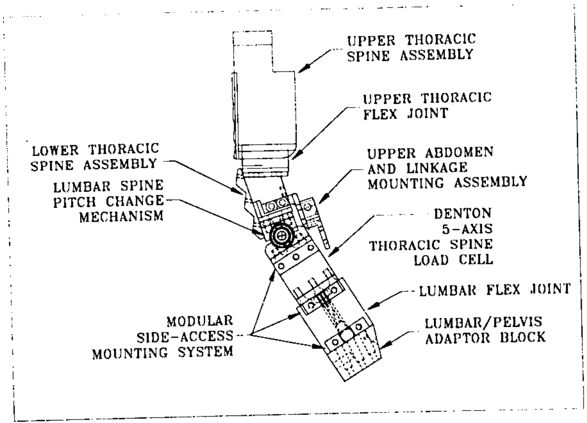
UPPER THORACIC SPINE ASSEMBLY
UPPER THORACIC FLEX JOINT
LOWER THORACIC SPINE ASSEMBLY
UPPER ABDOMEN AND LINKAGE MOUNTING ASSEMBLY
LUMBAR SPINE PITCH CHANGE MECHANISM
DENTON 5-AXIS THORACIC SPINE LOAD CELL
LUMBAR FLEX JOINT
MODULAR SIDE-ACCESS MOUNTING SYSTEM
LUMBAR/PELVIS ADAPTOR BLOCK

Figure 4. View of spinal assembly in Thor.

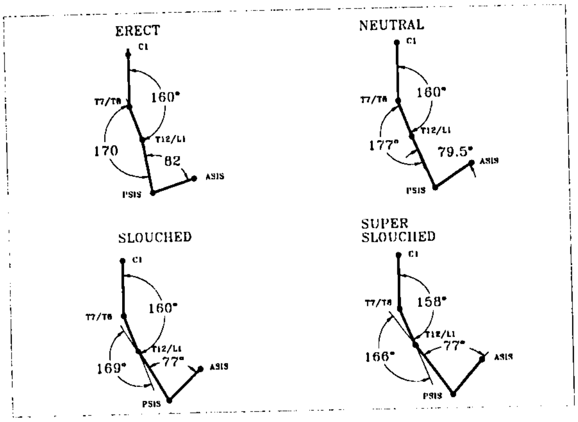
ERECT
C1
T7/T8
160°
T12/L1
170
82
ASIS
PSIS
NEUTRAL
C1
T7/T8
160°
T12/L1
177°
79.5°
ASIS
PSIS
SLOUCHED
C1
160°
T7/T8
T12/L1
169°
77°
ASIS
PSIS
SUPER SLOUCHED
C1
T7/T8
158°
T12/L1
77°
166°
ASIS
PSIS

Figure 5. Four seating postures based on Reynolds' data.

Design of Shoulder Complex

Figure 6 presents a drawing of the shoulder complex that is incorporated into THOR. The clavicle is designed to approximately represent the human structure and to couple loads applied to it to the sternum and ribs. This was meant to provided more realistic interaction of the shoulder belt with the torso. The clavicle was designed to prevent the shoulder belt from being snagged in the support structure when the shoulder belt was oriented in an outboard position. The shoulder structure is designed to permit controlled fore and aft motions. Further, an elevation/depression degree of freedom was added to provide more realistic interaction of the shoulder belt with the shoulder complex.

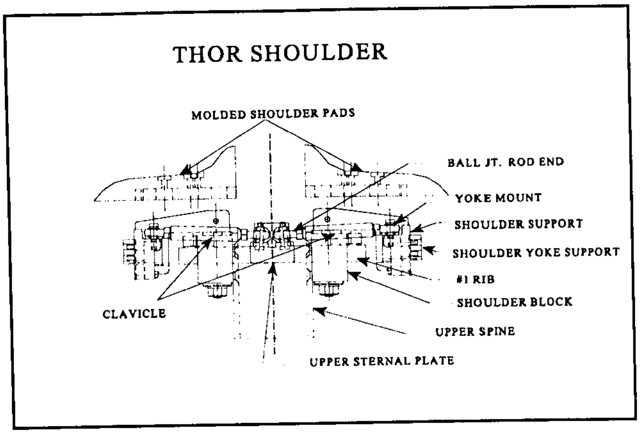
THOR SHOULDER
MOLDED SHOULDER PADS
BALL JT. ROD END
YOKE MOUNT
SHOULDER SUPPORT
SHOULDER YOKE SUPPORT
#1 RIB
SHOULDER BLOCK
CLAVICLE
UPPER SPINE
UPPER STERNAL PLATE

Figure 6. Thor shoulder assembly.

Design of Abdomen

The abdomen design developed for THOR consists of an upper and a lower unit. The upper unit is attached to the thorax through ribs 5, 6, and 7 and the lower unit fills the space between the lower ribs and the pelvis. A cross-sectional drawing of the upper abdomen unit is shown in Figure 7.

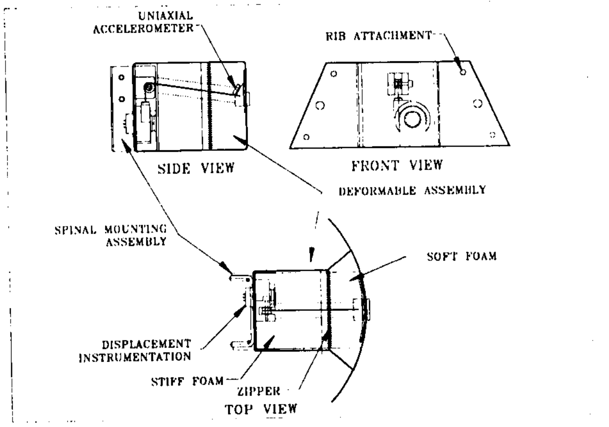
UNIAXIAL ACCELEROMETER
RIB ATTACHMENT
SIDE VIEW
FRONT VIEW
DEFORMABLE ASSEMBLY
SPINAL MOUNTING ASSEMBLY
SOFT FOAM
DISPLACEMENT INSTRUMENTATION
STIFF FOAM
ZIPPER
TOP VIEW

Figure 7. Upper abdominal assembly.

The front of the abdomen is attached to the ribs and the rear is attached to the spine through a structural bracket. The interior of the abdomen is layered with foam of two different compressive stiffnesses; soft foam is placed in the front, backed by a stiffer foam in the rear. The foam is enclosed with a cloth cover that has a zipper to provide maintenance access. The upper abdomen unit is instrumented with a uniaxial accelerometer behind the anterior surface to sense possible impulsive air bag loading in the X direction, and a high-speed string pot to measure the deflection in the X direction.

The lower abdomen assembly is shown in Figure 8. The cloth-covered bag is similar in construction to the upper bag in that it is of layered foam construction. Instrumentation consists of bilateral advanced DGSP (double-gimballed string pot) assemblies and precision potentiometers that maintain permanent calibration. Three-dimensional deflections of the DGSP attachment points at the front of the bag are calculated via a dedicated algorithm, utilizing potentiometer outputs. It is noted that the signals obtained from this instrumentation assembly during impact loading are sufficiently smooth that differentiation of the calculated displacements to velocity is feasible. Overload protection is provided to protect the instrumentation if compression of the abdomen exceeds approximately 4.5 inches.

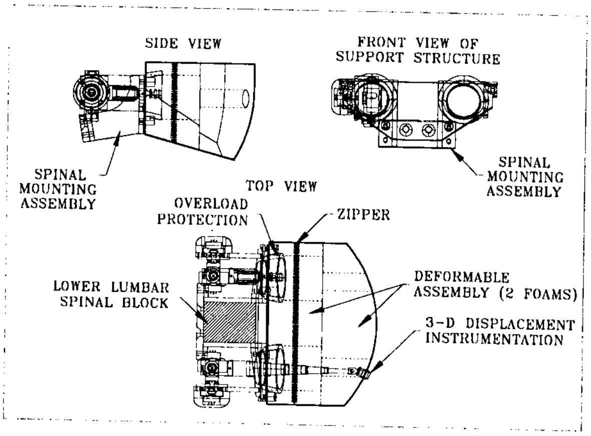
SIDE VIEW
FRONT VIEW OF SUPPORT STRUCTURE
SPINAL MOUNTING ASSEMBLY
SPINAL MOUNTING ASSEMBLY
TOP VIEW
OVERLOAD PROTECTION
ZIPPER
LOWER LUMBAR SPINAL BLOCK
DEFORMABLE ASSEMBLY (2 FOAMS)
3-D DISPLACEMENT INSTRUMENTATION

Figure 8. Lower abdominal assembly.

Because a gap can be created between the upper and lower abdomen units when the initial posture of the dummy is changed, a pie shaped insert has been placed in a pocket at the top of the lower abdomen unit to fill the gap between the two abdomen units. Tests have shown that this insert adequately prevents a striking object from penetrating this area during impact loading. Both the upper and lower abdomen assemblies have been designed as modular units so that with the removal of a few bolts at the spine attachment, the entire unit including instrumentation may be easily removed.

The abdomen assemblies have been extensively tested, and have been shown to maintain geometric and structural integrity under repeated impact loading and provide repeatable response.

TESTING

Two THOR prototypes were initially built. The first series of evaluation sled tests were conducted under the sponsorship of the Road and Safety Directorate of Transport Canada at the facilities of Defence and Civil Institute of Environmental Medicine (DCIEM) in Toronto. The second prototype was sent to the Vehicle Research and Test Center (VRTC) in East Liberty, Ohio for a series of component tests and full scale sled tests. It was the purpose of the test series to elicit suggestions regarding the performance of the dummy. The results from these tests and suggestions from the labs were reviewed and appropriate design changes made.

Testing at DCIEM in Canada

Full scale testing of THOR was performed at DCIEM on their HyGe accelerator sled using a crash pulse typical for a passenger vehicle, with a delta-V of 56 km/h and peak deceleration in the range of 20-25 G. A mock-up of the driver's side compartment of a standard size vehicle was mounted on the sled. This consisted of a rigid seat, dashboard, steering wheel, windshield and toepan. The seat and seat back was padded with polyethylene foam covered with a tweed seat cover.

A total of seven sled tests was performed. The dummy was restrained with independent lap and shoulder belts. The restraints were varied by changing the locations of the seat belt anchorages, the slack in the belt, and the contact location of the shoulder belt with the shoulder. A two point shoulder belt was used in one of the tests. Table 1 provides a summary of the seven tests performed in Canada. It describes the restraint system used and the basic configuration of the dummy.

The test data and film were used to evaluate the durabiltiy and general performance of the dummy. Instrumentation problems led to the loss of some data channels. Table 2 shows the maximum (absolute) values for the principal accelerometer channels and the shoulder belt loads. The maximums have been obtained from an inspection of the plots of the selected channels for the time interval 0 to .150 sec. The time at which the maximum values were attained are indicated below the value (also in seconds). For all the tests, the principal loading phase occurred in this interval. During this analysis, the unloading phase was not included.

Table 1. Summary of Canadian tests

Test #	Lap	Shoulder	Knee Bols	Toepan	Posture	Description
2585	taut	taut	yes	yes	erect	normal setup
2586	taut	taut	yes	yes	erect	shoulder belt placed near shoulder joint
2587	taut	taut	yes	yes	erect	repeat #2585
2588	v.slack	v.slack	no	yes	erect	almost unrestrained
2589	no	taut	yes	yes	erect	2 pt shoulder belt only
2590	slack,hi taut	no	no	no	slouched	attempt to induce submarining
2591	v.slack	v.slack	no	yes	erect	repeat #2588

Table 2. Maximum values of selected channels

Tests	Head-X (G)	Head-Z (G)	Chest-X (G)	Chest-Z (G)	Pelv-X (G)	Pelv-Z (G)	Shld(top) (N)
2585	-30	-70	-40	5	-40	*	10700
	0.08	0.07	0.05	0.05	0.04	*	0.05
2586	-28	-60	-40	12	-45	-	
	0.08	0.08	.065	0.07	0.06	-	
2587	-55	-65	-40	-10	-40	7	9800
	0.12	0.08	0.06	0.07	0.06	0.04	0.08
2588	-30	-30	-25	10	-15	5	7100
	0.10	0.08	0.07	0.07	0.06	0.04	.075
2589	-35	-20	-15	5	-20	5	13800
	0.09	0.08	0.07	0.07	0.07	0.04	.075
2590	-150	-55	-60	-35	-55	5	10900
	0.09	0.08	0.07	.075	0.07	0.04	0.07
2591	-60	-40	-50	10	-50	7	8500
	0.14	0.10	0.07	0.10	.075	0.04	0.07

In some tests (e.g. #2587, 2591) the higher head X-acceleration was due to a chin-chest contact. The very high value seen in Test #2590 was due to a steering wheel contact. From an initial review of the behavior during unloading, there appears to be a secondary and positive peak at around 250 msec. From the films, this appears to correlate with impact with the seat back. It is not clear whether there is some contribution from the rear stop at the bottom of the head when it contacts the neck.

There is some variation in the chest and pelvis accelerations, though they also seem to fall within a physically reasonable range. One sees that for the first very slack belt test (Test #2588), the chest and pelvis accelerations are low, as are the lap and shoulder belt loads. But for the repeat of the test (Test # 2591), the chest and pelvis accelerations were appreciably higher. In the latter test, contact with the windshield occurred after the shoulder belt was torn by the metal neck guard.

One of the items of interest in this first series of tests with Thor was the performance of the deflection transducers in the chest and abdomen. The maximum deflections in the X direction (perpendicular to the ribcage) ranged from 40 to 70 mm. A significant amount of deflection in the Y direction was also measured by the lower right CRUX unit. The CRUX units responded in a smooth fashion, but since the initial angular positions of the pots were not obtained, a detailed analysis of the deflection results was not possible.

Testing at Vehicle Research and Test Center, Ohio

A comprehensive set of component tests were performed at VRTC, followed by a series of sled tests and two out-of-position airbag tests.

Table 3. Component Tests at VRTC

Component	Location	Description	Impactor/ indentor
Thorax	mid-sternum	quasi-static compression	3" disk or 6" square
Thorax	CRUX locations	quasi-static compression	3" disk or 6" square
Thorax	mid-sternum	Kroell type impact	15 cm disk
Thorax	3rd rib	oblique impact	15 cm disk
Thorax	left & right lower ribcage	oblique impact	15 cm disk
Abdomen	upper	quasi-static compression	3" disk or 6" square
Abdomen	lower	rod impact	2.5 x 30 cm rod
Abdomen	lower	steering wheel impact	-
Femur	left & right knee	pendulum impact	4.6 kg; 3 cm disk
Neck	frontal & lateral	head/neck sled test	-

Table 4. Sled Tests at VRTC

Location	Belt	Airbag	Description
Driver	3-pt	yes	frontal impact
Driver	no	yes	frontal
Driver	yes	no	oblique 15 deg impact
Passenger	yes	no	frontal
Passenger	yes	no	frontal, with lap belt high on abdomen
Driver	yes	no	frontal
Driver	yes	no	D-ring moved outboard and forward
Driver	yes	no	seat 2" from full forward

Table 5. Out-of-Position Airbag Tests at VRTC

Location	Belt	Airbag	Description
Driver	no	yes	out-of-position, ISO 1
Driver	no	yes	out-of-position, ISO 2

Component Tests - The results of the Kroell tests performed at VRTC for 4.3 m/s and 6.7 m/s are shown in Figures 9 and 10 respectively and compared with the standard Kroell corridors at these speeds. The results from impact tests performed at GESAC, are also shown. The results for the 4.3 m/s impact show a somewhat stiffer response than the earlier GESAC results, while the results for 6.7 m/s are similar. The stiffer response seen in the 4.3 m/s impact may have been due to the presence of the central string pot, which was later removed.

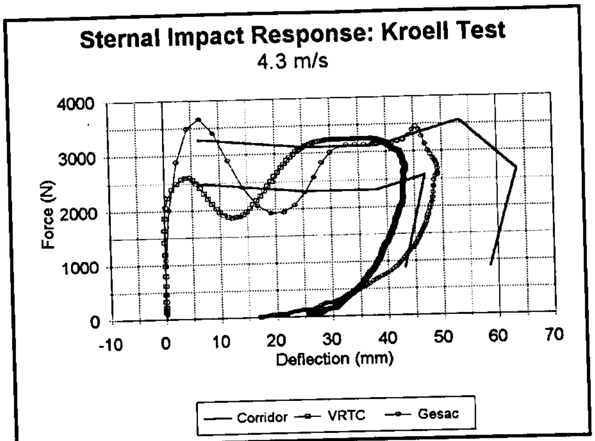

Figure 9. Kroell test results from VRTC and GESAC for 4.3 m/s impact

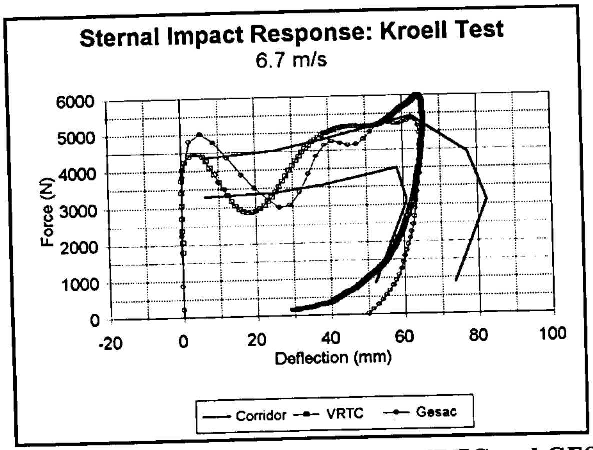

Figure 10. Kroell test results from VRTC and GESAC for 6.7 m/s impact

The lower abdomen response to a 25 mm rod impact at about 6 m/s is shown in Figure 11 and compared against the response corridor. The response corridor for force vs external deflection for rod impact at low speed (average impact speed of 6.1 m/s) has been defined by Cavanaugh [1986]. The external deflection was measured with a LVDT, and when compared with the corridor shows that the deflections are within the corridor for deflections somewhat greater than 75 mm which was the design range. Internal deflections within the lower abdomen are measured by the two DGSPs, and measurements made at both VRTC and GESAC are shown in Figure 12. The internal deflections from the VRTC testing show a slightly stiffer response than the internal deflections measured at GESAC. At VRTC, the pelvic skin in the area of the lower abdomen had been reinforced by several layers of duct tape which may have resulted in the increased stiffness.

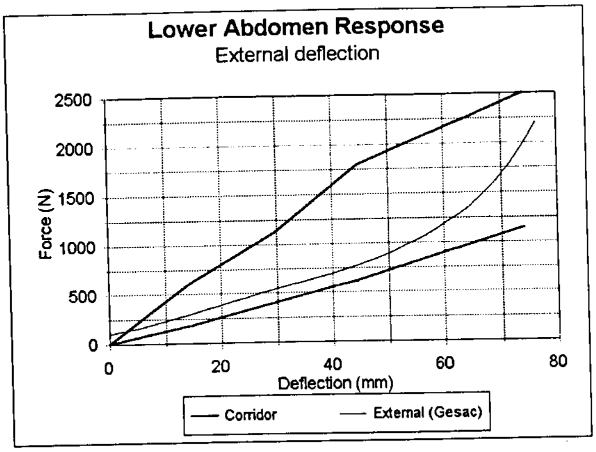

Figure 11. External deflections from 25 mm rod impact to lower abdomen at 6 m/s

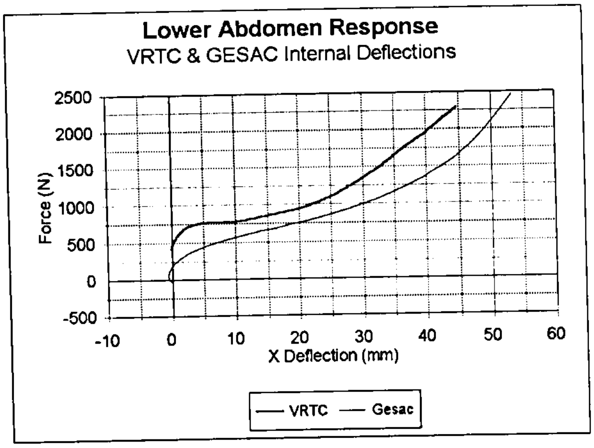

Figure 12. Internal deflections from 25 mm rod impact to lower abdomen.

Sled Tests - The crash pulse used in the VRTC sled tests corresponded to an impact speed of 56 kph (35 mph) with a peak deceleration of about 33 G. The pulse is shown in Figure 13.

During the first series of tests, the results for the airbag and 3-pt belt restraint condition were compared to those obtained for the corresponding tests with a Hybrid III dummy. There was fairly good agreement in total head and chest accelerations, in magnitude and duration. The total chest deflections, as measured by the CRUXes showed a slightly smaller deflection in Thor than in Hybrid III. Figures 14 and 15 show the comparison of head and chest resultant accelerations for Hybrid III and Thor.

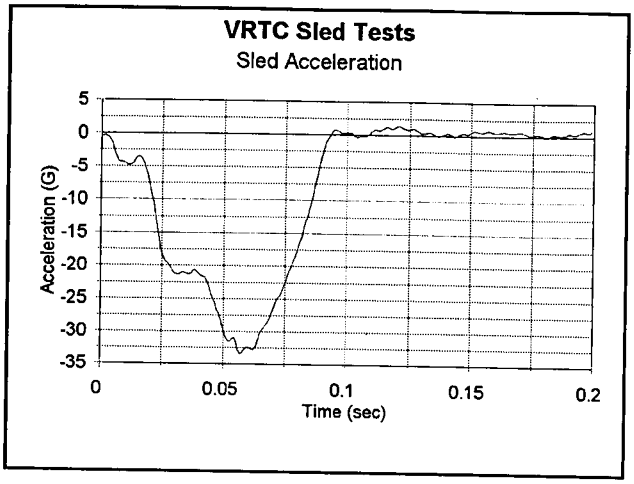

Figure 13. Typical sled pulse used in VRTC tests.

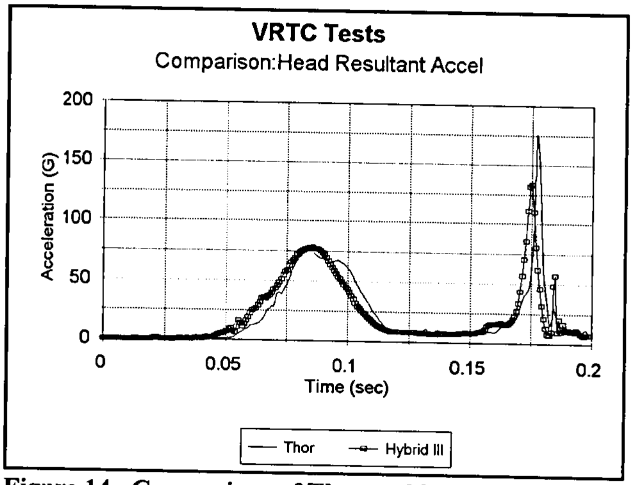

Figure 14. Comparison of Thor and Hybrid III resultant head acceleration.

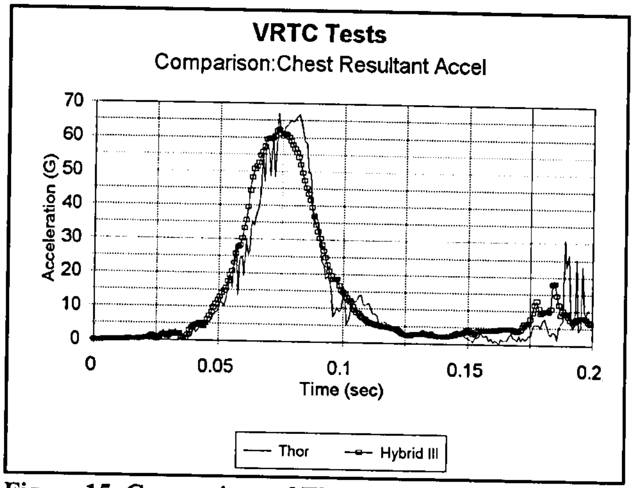

Figure 15. Comparison of Thor and Hybrid III resultant chest acceleration.

Figure 16 shows the comparison for the upper ribcage deflections.

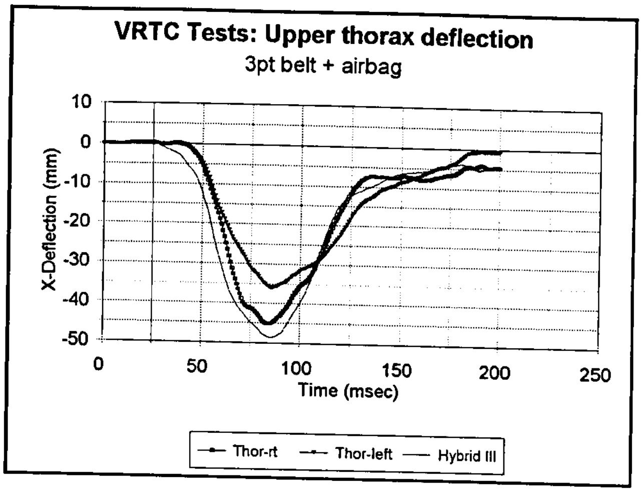

Figure 16. Comparison of Thor and Hybrid III chest deflections.

It is seen that there is some asymmetry between the right and left CRUX units, as might be expected in a restraint environment where the 3-pt belt influences the overall symmetry of the airbag loading. Also the Hybrid III deflection appears to be closer to the right side CRUX measurement.

Figures 17-19 show the chest deflections measured by the CRUX units for three different restraint conditions. Figure 17 and 18 show the responses for a bag and 3-pt belt restraint and an airbag only restraint respectively with a frontal deceleration pulse. Figure 19 shows the response for a 3-pt belt only condition with an oblique deceleration pulse . The deflections are shown in the horizontal plane (relative to the lower thoracic spine coordinate system), with the X displacement representing A-P motion and Y displacement representing right-left motion. The figures for the tests with belts show the characteristic asymmetry associated with 3-pt belts. The bag only test also shows some asymmetry. The video indicates a small degree of rotation during the unloading phase of the bag which likely explains the asymmetry. The 3-pt belt and airbag case also shows some small expansion of the lower left CRUX. This is not seen in the 3-pt only case, presumably since it is associated with significant rotation of the torso (generated from the obliquely applied crash pulse) .

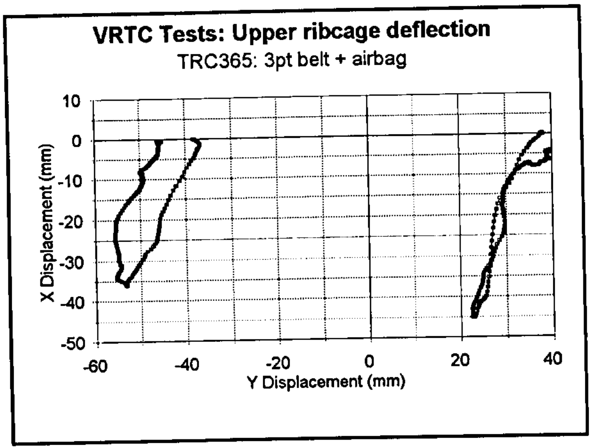

Figure 17. Upper chest deflections for airbag and 3-pt belt restraint.

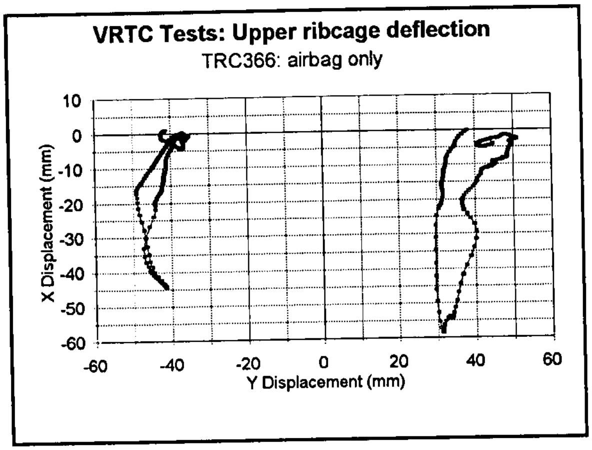

Figure 18. Upper chest deflections for airbag only restraint.

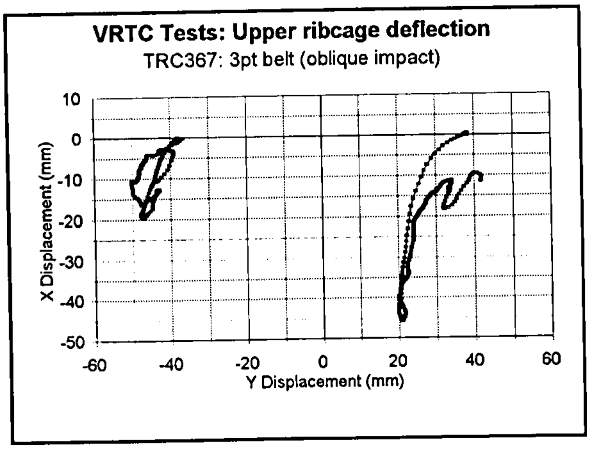

Figure 19. Upper chest deflections for 3-pt belt only restraint.

Figures 20 and 21 compares the responses of the right and left DGSPs (for the X-direction displacement) to two 3-pt belt tests. The belts were situated for a passenger, and in the first test, the lap belt was placed at its normal position on the iliac spine. For the second test, the lap belt was placed higher to allow for maximum abdominal penetration. The responses indicate that an additional 15 mm of penetration occurred with the second setup for the right side, and additional 5 mm penetration for the left side.

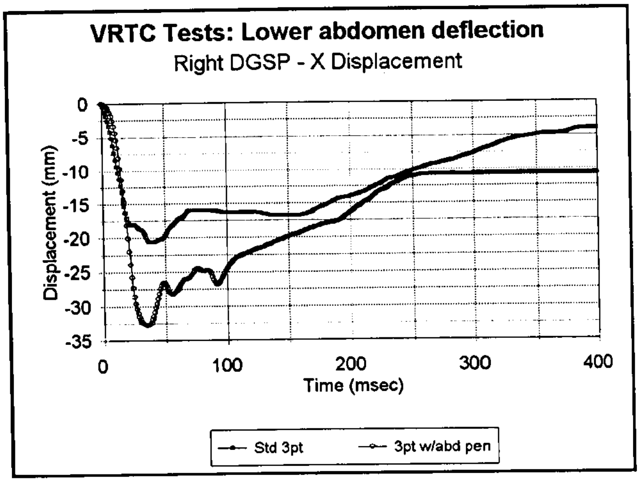

Figure 20. Lower abdomen penetration (by lap belt) as measured by the right DGSP.

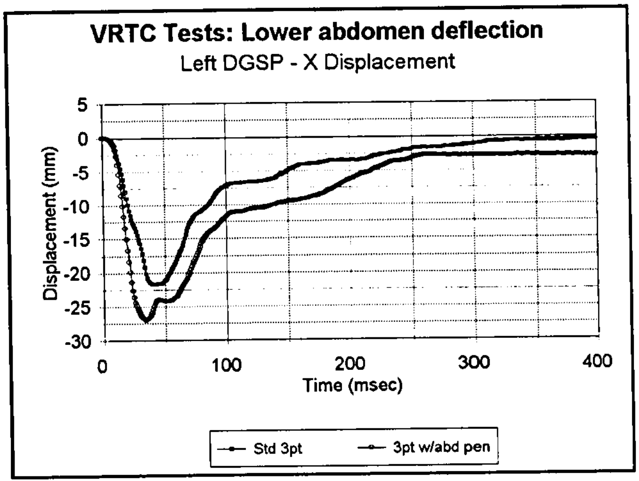

Figure 21. Lower abdomen penetration (by lap belt) as measured by the left DGSP.

Another test situation of interest was the out-of-position airbag test with THOR being put in both standard ISO configurations. The chest on module configuration with the associated high rate of chest compression allowed us to gauge how the new CRUX system performed in this condition. Figure 22 shows the comparison of the rate of compression measured by the left and right CRUXes (by computing the derivative of the displacement) and the corresponding measurement from the sternal accelerometer (by integrating the acceleration).

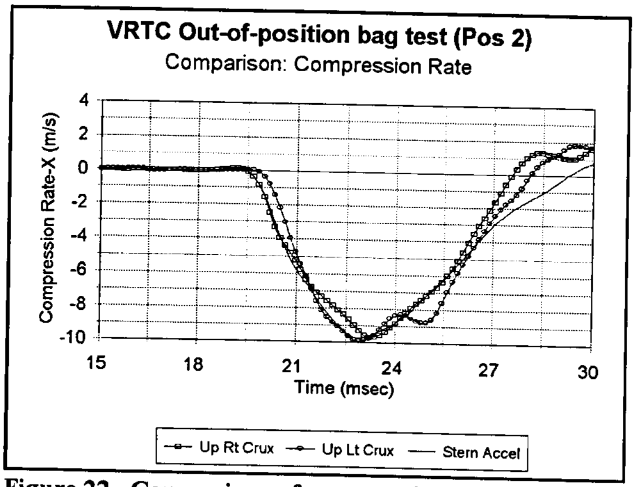

Figure 22. Comparison of compression rate from CRUX and accelerometer for OOP test.

It shows that there is good agreement between the CRUXes and the accelerometer during the main loading period (the plot shows only the significant loading duration). In this test, the maximum deflection rate reached about 9.5 m/s and the tests showed that the CRUX units successfully measured deflection rates of this magnitude. Figure 23 shows the actual X-Y deflections seen by the CRUXes, showing the symmetric displacement pattern associated with airbag loading.

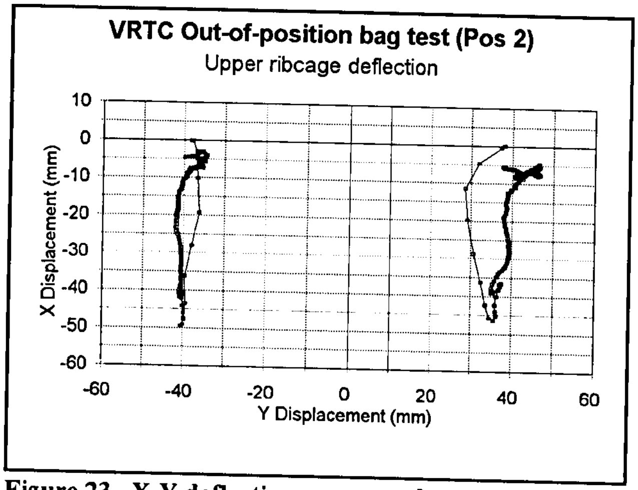

Figure 23. X-Y deflections measured at upper chest during OOP test.

Design Modifications

Based on the results of the tests conducted in Canada and VRTC and feedback from the laboratory staff, a number of design revisions to THOR were made to address some problems of durability and to make improvements to the appearance and performance of the dummy. The principal revisions are described below.

- Molded urethane pads more closely resembling the human shoulder contour replaced the steel flanges on the shoulder. The steel flanges, originally installed to avoid the belt from sliding across the shoulder and loading the neck, tore the shoulder belt in two of the Canadian tests.
- The mid-sternal string pot was removed after it was seen to be making contact with the ribcage. The string pot was probably responsible for increasing the stiffness of the ribcage, which was noticed in the Kroell tests at VRTC.
- The CRUX units were redesigned to avoid any interference between the units and the ribs and upper abdomen. The procedure for processing the CRUX data was improved to avoid measurement problems that had been initially encountered.
- The size and shape of the lower abdomen was slightly modified to allow for better integration with the upper abdomen and interaction with the lap belt.
- A new pelvis skin was created to reduce damage seen in the tests with the original pelvis skin that had been attached with Velcro fasteners. Improvements were also made in the jacket design to reduce burns and tears.
- Strain relief was added to all wires to minimize the likelihood of wires breaking during the motion of the dummy.

DISCUSSION

The first two prototypes of THOR, the new advanced frontal crash test dummy, have been tested at DCIEM in Canada and at VRTC in Ohio. The results from these tests have been evaluated along with comments from the laboratories. The tests in Canada were used to make a preliminary evaluation of the motion of THOR in a 3-pt belt and 2-pt belt environment; to check the new deflection measurement systems in the chest and abdomen; and to assess the durability of the various dummy components. The tests at VRTC were more comprehensive in nature, with both component and full sled tests being performed. The component tests were meant to evaluate the biomechanical response of several dummy parts, such as the thorax, abdomen, femur, and neck. One of the sled tests was performed to provide a comparison with Hybrid III for the case of an airbag and

3-pt belt restraint.

The results from the two series of tests were very helpful in suggesting a number design revisions to improve the performance of the dummy. These revisions have been carried out, and the redesigned prototype has been subsequently tested at a number of additional research laboratories.

CONCLUSIONS

The first two series of tests with the new THOR dummy, in Canada and at VRTC, allowed us to evaluate its performance in a number of different environments. The following could be concluded from this evaluation:

- The dummy was quite robust and the principal components held up well under 56 kph deceleration pulses and peak decelerations greater than 30G. This was true in oblique testing with this pulse. Smaller components such as foam inserts and parts of the skin received some damage, problems which have been addressed in the revised design.
- The CRUX units worked well and were able to provide 3-D deflection information at the four sites on the ribcage. The deflection patterns produced could distinguish differing restraint systems. In the tests, the deflections at the four locations distinguished between airbag only, belt only, and bag and belt combinations.
- Out-of-position airbag tests indicated that the CRUX units were able to operate properly at sternal compression rates of above 9 m/s.
- The DGSPs used for measuring abdominal deflections provided smooth time history data for abdomen penetrations. The penetrations were found to be sensitive to lap belt location.
- In one test, where comparison was made with Hybrid III response, the head, chest, and pelvis accelerations were found to be similar in magnitude and shape. The upper chest deflections were comparable, though the Hybrid III showed a slightly greater deflection at the sternum.

ACKNOWLEDGMENT

The efforts reported in this paper were supported by the National Highway Traffic Safety Administration of the U.S. Department of Transportation under contract DTNH22-94-C-07010. We are grateful to the NHTSA staff for their technical guidance and support. We are also grateful to Transport Canada for supporting the initial round of testing at DCIEM in Canada, and to Biokinetics, Inc for providing very helpful technical and logistical support. We are grateful to VRTC for providing excellent support and critical feedback during testing at VRTC. The sled tests at VRTC were performed at the Transportation Research Center, Inc (TRC).

REFERENCES

Cavanaugh, J., Nyquist, G.W., Goldberg, S.J., King, A.I. 1986. "Lower Abdomen Impact Tolerance," Proceedings of the 30th Stapp Car Crash Conference.

Melvin, J.W., et.al. 1988. “Advanced Anthropometric Test Device (AATD) Development Program. Phase I Reports: Concept Definition. Tasks A-F.” University of Michigan Transportation Research Institute, DOT-HS-807-224.

Nusholtz, G.S., P.S. Kaiker, D.F. Huelke, and B.R. Suggitt. 1985. Thoraco-Abdominal Response to Steering Wheel Impacts. Proceedings of 29th Stapp Car Crash Conference. 221-267.

Reynolds, H. 1996. "Pelvic and Lumbar Posture in a Trauma Assessment Device," Ergonomics Research Laboratory, Michigan State University.

Robbins, D. 1985. "Development of Anthropometrically Based Design Specifications for an Advanced Adult Anthropometric Dummy Family. Volume 2: Anthropometric Specifications for Mid-Sized Male Dummy", DOT-HS-806-716 & 717.

Rouhana, S.W. 1993. Biomechanics of Abdominal Trauma. In Accidental Injury - Biomechanics and Prevention. Ed. Nahum, A.M. and J.W. Melvin. Springer-Verlag. 391-428.

Schneider, L., King, A., and Beebe, M., 1990. "Design Requirements and Specifications: Thorax-Abdomen Development Task," Interim Report, Trauma Assessment Device Development Program, DOT-HS-807-511.

Schneider, L.W., Ricci, L.L., Salloum, M.J., Beebe, M.S., King, A.I., Rouhana, S.W., Neathery, R.F. 1994. "Design and Development of an Advanced ATD Thorax System for Frontal Crash Environments, Volume 1: Primary Concept Development," DOT-HS- 808-138.

PROSPECTS FOR ELECTRONIC COMPLIANCE WITH BELT FIT REQUIREMENTS

Y. Ian Noy
Vittoria Battista
Transport Canada
Canada
Paper Number 98-S9-O-13

ABSTRACT

The effectiveness of seat belts depends largely on the extent to which their geometric design matches the occupants' anatomical characteristics. Transport Canada research into seat belt fit requirements culminated in the design of a Belt Fit Test Device (BTD), a full-scale model representing 50th percentile Canadian adult and based on the H-Point Machine. The purpose of this study was to determine the feasibility of developing an electronic representation of the BTD that could be used by manufacturers for restraint system design and certification. The project was not fully realized due to difficulties in obtaining suitable 3-D digital representations of automobile seats. However, the study demonstrated that seat belt design can be accurately assessed for proper fit using computer models.

INTRODUCTION

The effectiveness of seat belts depends largely on the extent to which their geometric design matches the occupants' anatomical characteristics. The Belt-Fit Test Device (BTD) is a device used for the measurement and assessment of static seat belt geometry of automobile seat belts (Gibson et al., 1994, Tylko et al., 1993, Tylko et al., 1994). The device was conceived and developed to address abdominal and upper body injuries that may result from a mismatch between belt geometry and the occupants' anthropometric characteristics. In essence, the BTD comprises an SAE 3-dimensional H-Point Machine with the addition of special torso and lap forms that are designed to represent the 50th percentile Canadian adult male. The surfaces of the lap and torso forms are marked with scales to permit quantifying belt position. When positioned on an automobile seat, the device indicates whether the lap and shoulder belts fall within specified bounds relative to anatomical landmarks. Four criteria establish acceptable position limits with respect to the clavicle, sternum and lap scales. Belts which meet these criteria should adequately restrain the occupant in a crash, without causing serious injuries to soft tissue and organs from belt forces.

The BTD test was intended to complement other occupant protection requirements such as peak head acceleration and chest deflection. The current requirements of the Canadian Motor Vehicle Safety Standard (CMVSS) 208, which specify the permissible angle of the lap belt and stipulate the location of the upper anchorage of the shoulder belt, do not ensure that the lap and shoulder belts are correctly positioned (Dalmotas and Welbourne, 1991). Although the original intention was to introduce new seat belt fit requirements as part of the 1997 CMVSS 208 amendment*, the automotive industry requested that further research be conducted before its use was mandated. In response, a government-industry Joint Working Group on Abdominal Injury Reduction was formed to explore alternative approaches to minimizing the risk of belt-induced injury. The Joint Working Group was to make its recommendations by March 1998, but the research program was recently extended to explore the potential of developing a computer-based version of the BTD for electronic compliance, building on previous research to develop and validate the electronic BTD.

The development of an electronic version of the BTD was already underway at Transport Canada. Once the design of the BTD was finalized, research interests shifted to investigating the extent to which the BTD criteria accommodate the full range of the occupant sizes. The new focus was the development of an electronic representation of the BTD and the application of new computer human modeling techniques to extend the capabilities of the physical device.

Electronic compliance refers to the application of computer-based procedures to verify that hardware meets specified requirements. It promotes 'compliance by design' and, for certain standards, it may replace costly physical tests. The BTD test is an ideal first candidate for electronic compliance since the belt fit requirements relate to simple geometric properties of the restraint system and the test is static in nature.

This paper reviews the development of the electronic BTD and discusses its potential usefulness for electronic compliance with belt fit requirements.

---

* A series of studies established the efficacy of the BTD as a reliable and accurate indicator of proper seat belt fit. According to the results of vehicle tests, the use of the BTD would require only minor changes to the current location of lap belt anchorages; however, it could impose greater restrictions on the location of shoulder belt anchorages.

BACKGROUND

Development of the Belt Fit Test Device (BTD)

The development of the BTD began in the mid-seventies in an effort to minimize the incidence of lacerations and rupture of vital organs due to lap belt intrusion (Gibson et al., 1994). A review of the literature and analysis of collision data identified geometric and anthropometric criteria for the correct positioning of the lap belt relative to the anterior superior iliac spines (ASIS). It was further determined that the shoulder belt should rest on the middle third of the collar bone, and that it should cross the sternum near the centre of the chest.

A need was identified for a reliable test of pelvic and thoracic belt fit in any vehicle. To ensure compatibility with existing automotive engineering practices, it was decided that the device would be based on the standard SAE H-Point Machine. Three-dimensional lap and torso forms were constructed from anthropometric data obtained from a sample of Canadian adults. Participants for this effort were selected on the basis of their height and weight to reflect the 50th percentile values reported in a 1981 Fitness Canada survey. The height and weight screening criteria were 164.9 cm and 66.7 kg respectively. Details of the development of the lap and torso forms can be found in (Gibson et al., 1994).

The proposed quality of fit requirements include four independent criteria which establish belt position limits with respect to the clavicle, sternum, and inboard and outboard lap scales. The minimum acceptable scores are outlined in Table 1. The clavicle and torso scores represent the intersection of the lower edge of the shoulder belt with the clavicle and torso scales, respectively. The inboard and outboard lap scores are taken with reference to the upper edge of the lap belt.

For further information about the development and use of the BTD, the reader is referred to Gibson et al. (1994) and Tylko et al. (1994).

Table 1.
BTD Criteria

Measurement Criteria
1. Lap Form: $x > 1.5$ on inboard and outboard scales
2. Clavicle: $7 < x < 13$
3. Sternum: $12 < x < 22$
4. Belt contact at each of the clavicle and lap scales

Development Of The Electronic BTD

The development of the electronic BTD is described in Noy et al. (1997). The main purpose of this effort was to determine the validity of BTD criteria in assessing the correct positioning of lap and shoulder belts for a wide range of occupant sizes. Additional advantages included improved repeatability and simplification of restraint testing and facilitation of compliance by design. The objectives of this program were to develop and validate an electronic version of the BTD and to determine the need to replace the BTD with computer-based human models representing a wider distribution of the occupant population.

In brief, the first stage involved creating an electronic version of the H-Point machine and adding the three-dimensional free-form surfaces representing the lap and torso shape of the 50th percentile Canadian adult male.

To simulate the seat belt, a computerized flexible seat belt model was created. As a first approximation, the position of the seat belt in three-dimensional space was defined as the shortest curve lying on the surface of the lap and torso forms and constrained by the anchor points*. The belt was mathematically represented as a set of three spline curves lying on a surface with two tangent directionally constrained forces at each end. The three splines corresponded to the two edges and the middle of the belt. The shapes of these spline curves were defined by the two forces at each end, the shape of the surface and by various anchor points. Assuming no friction forces between the surface of the body and the belt, the true definition of spline curves was used for the part of the belt that lay over the body surface. The segment between the extreme contact points on the body and the anchor point was a straight line. The portion of the belt on the surface of the body was defined as the intersection between a plane containing the spline curve and the surface of the body.

Validation Of Electronic BTD

Two validation studies were performed. The initial validation of the electronic BTD was performed by comparing coordinate values of specific landmarks generated electronically with the actual BTD coordinates. The physical BTD was installed on two different seats (one having a soft cushion and the other a firm cushion) and seat belt fit measurements were taken in accordance with the procedures outlined in the Operations Manual for the BTD (Transport Canada 1993).

---

* The anchor point here is defined as the end of the flexible portion of the belt.

Since initial validation indicated good correspondence between computed and measured BTD coordinates of seat belt reference points, a more complete validation was undertaken. Actual BTD scores were obtained from ten vehicles. Seat belt anchor points and the H-point were digitized.

The electronic BTD was positioned in the seat by aligning its H-point with the corresponding digitized coordinate obtained with the actual BTD*. While this procedure was necessitated by the lack of appropriate seating algorithms, it does not detract from the usefulness of the electronic BTD since the H-point** can be readily obtained from vehicle manufacturers.

Electronic BTD scores were generated and compared with actual BTD scores. The results for the ten vehicles comparing the actual and the electronic BTD data are presented in Figures 1-4 for the inboard and outboard lap, clavicle and sternum scores, respectively. The horizontal reference lines on these figures represent the test pass/fail criteria levels.

In total, 40 BTD scores were computed using the electronic BTD and compared with actual BTD values. In 30 of the 40 comparisons, the discrepancy between measured and computed values was less than one centimetre. When BTD scores were expressed in terms of test performance using the pass/fail criteria indicated in Table 1, 36 of the 40 comparisons were in agreement. The four instances for which computed and measured performance differed, were associated mostly with the torso form.

In terms of overall belt system performance, the electronic and actual BTD results were in agreement for seven out of the ten vehicles tested. One vehicle, the 1989 Toyota Tercel, failed the electronic BTD evaluation (both on clavicle and sternum scales) but passed with the actual device. It should be noted, however, that the clavicle and sternum scores were extremely close to criteria levels. The second vehicle, a 1985 Chevrolet Jimmy, failed the electronic BTD (outboard lap score) but passed when using the actual device. The third vehicle, a 1995 Ford Windstar, failed on the electronic sternum score.

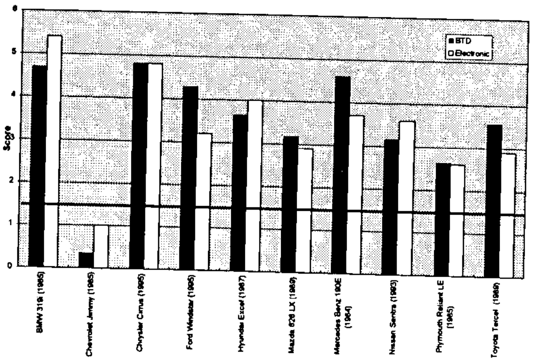

Figure 1. Lap Inboard.

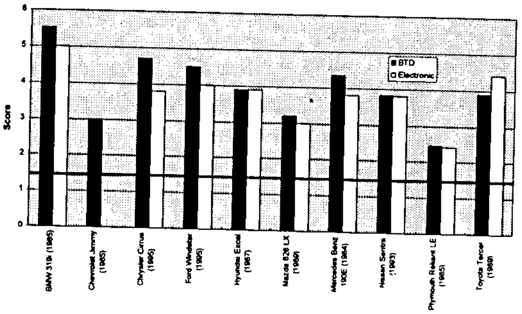

Figure 2. Lap Outboard.

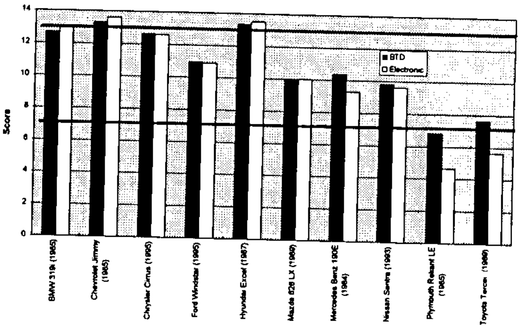

Figure 3. Clavicle.

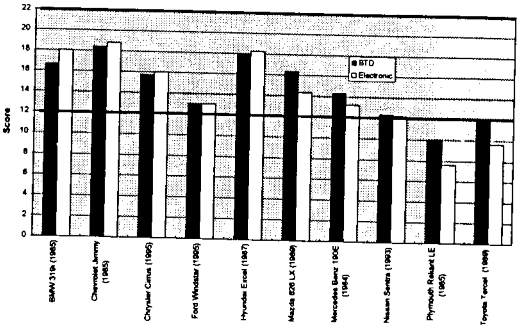

Figure 4. Sternum.

---

* The resting position of a mannequin when placed on a seat depends upon numerous factors including seat cushion and seat back angles, the distribution of weight on regions of the buttocks and back, the deformation properties of the cushion, the shape of the cushion, the type of upholstery material used, belt contact points, etc. There are no algorithms available, at present, that can be used to determine the position of the H-point as a function of known seat and mannequin characteristics.

** The H-point is equivalent to the seating reference point (SRP).

This study indicated the need to refine the seat belt algorithm to address more complex seat and restraint systems (double retractors, various types of belt hardware, seat squab angles, different seat designs, etc.).

PURPOSE OF THE PRESENT STUDY

The present study was undertaken to explore further the feasibility of developing an electronic BTD that would be suitable to verify compliance with belt fit requirements. Two specific objectives were established; (1) to refine the electronic BTD and seat belt algorithm, and (2) to demonstrate test feasibility by assessing a small sample of actual production vehicles using digital data provided by vehicle manufacturers. These two objectives are elaborated further below.

Due to the unavailability of seat data necessary to address the second objective, as explained below, the scope of this study was limited to refining and validating the model and seat belt algorithm.

Improvements to the Electronic BTD and the Seat Belt Algorithm

A number of improvements were made to both the electronic BTD and the seat belt algorithm. For example, the number of cross-sections representing the geometry of the torso and the lap forms was increased by a factor of ten. This was considered essential for the lap form due to its highly variable contours. With the improved algorithm, the number of cross-sections was about 100 for each form, resulting in substantial improvement in the accuracy of the collision detection algorithm, used to locate the belt on the form in three-dimensional space.

The simple spline equation which was used in the earlier version to define the belt routing was modified by inclusion of tensile force calculations at each end of the belt. This modification was implemented to ensure that the part of the belt lying on the torso is deformed according to the geometrical shape of the form. Assuming no friction between the form and the belt, a mathematical model of the belt can be represented as series parallel splines lying on a surface with two tangent directional constrained forces at each end. Again, three splines were created to represent the belt, one at the middle and one at each edge of the belt. The belt routing was defined by the intersection of the three cutting plane with the cross-section of the form. Each intersection point between the plane and cross-section represented a point on the belt in contact with the form. The belt was constructed from the intersection points using interconnectivity algorithms.

The electronic BTD was modified to allow users to input the seat pan angle as a user-defined variable. In previous studies, seat squab angle was found to affect belt fit scores but was not adequately accounted for in the model. The ability to input manufacturer-specified or empirically-derived seat squab angle was expected to reduce potential errors due to variations in seat design.

The electronic BTD was also modified to allow users to input certain seat geometric data such as seat height, seat width, physical length of the buckle hardware, SRP and H-point location.

As implemented within *Safework*™ *, the electronic BTD has an improved graphical user interface, permitting users to assess the effects of changing anchor points and other seat properties on belt fit.

Feasibility Electronic Compliance

The second objective of the study was to demonstrate the procedure for assessing restraint systems using the electronic BTD (and improved seat belt algorithm) completely within a computer-aided-design environment. In order to accomplish this, it was necessary to obtain from manufacturers digital 3-D surface drawings of seats that could be imported into the CAD environment and manipulated as objects. The only other data required to assess belt fit were the coordinates of the seat belt anchor points, the SRP and a seat squab reference point.

Despite best efforts, it was not possible to obtain the necessary data to accomplish this objective. For a variety of reasons, manufacturers were unable to provide digital representations of seats that can be used in the way envisioned. Few manufacturers require digital definition of seat surfaces. Seat manufacturers, on the other hand, may have such data, but they are not necessarily available to vehicle manufacturers.

The feasibility of electronic compliance relies on the availability of appropriate digital data. Further efforts in this area will require a concerted effort on the part of the industry to obtain and provide the requisite data.

Ideally, the input variables to the seat belt algorithm should include only characteristics that can be readily obtained from the manufacturers, such as seat belt type, specifications for associated hardware (belt buckle, plastic sleeves, etc.) and coordinates of anchorage locations. The seat belt algorithm would use these characteristics to determine the natural routing of the belt, taking into account the buckle characteristics and the interaction between webbing and mannequin as well as seat contact points.

---

* *Safework*™ is a computer application developed by Genicom Consultants for human modeling applications such as the design, evaluation and re-design of workstations from a human engineering point of view.

METHODOLOGY

Two vehicles were selected for the study, a 1998 GM Cavalier and a 1998 Dodge Caravan. The BTD was placed in each vehicle, and coordinates of the seat belt anchor points and H-point were digitized using a Faro Arm. In addition, the seat geometry and surface elements were digitized so that a digital representation could be imported into the CAD environment.

RESULTS

Figure 5 shows the electronic BTD as it was implemented within *Safework*™. The snapshot illustrates the dialogue box used for entering the coordinates of belt anchor points, the SRP and seat squab angle.

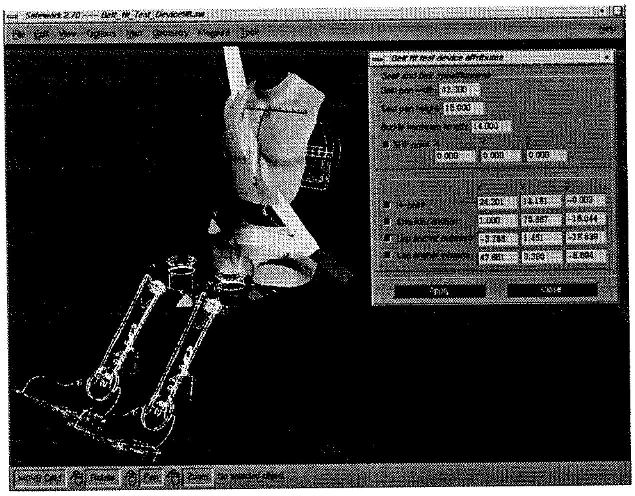

Figure 5. The Electronic BTD as implemented in *Safework*™

Figure 6 is a computer screen snapshot showing the electronic representation of the BTD in the GM Cavalier. The spline curves representing the lap and torso forms are clearly visible in this view; the seat details, unfortunately, cannot be seen. Figure 7 is a snapshot showing a close-up of the shoulder belt of the Cavalier over part of the torso form. The belt fit scores can be read directly from the clavicle and sternum scales and they can be generated electronically .

The data comparing actual and electronic BTD scores are presented in Tables 2 and 3 for the GM Cavalier and the Dodge Caravan, respectively. Test failure is indicated in the table by the underlined scores.

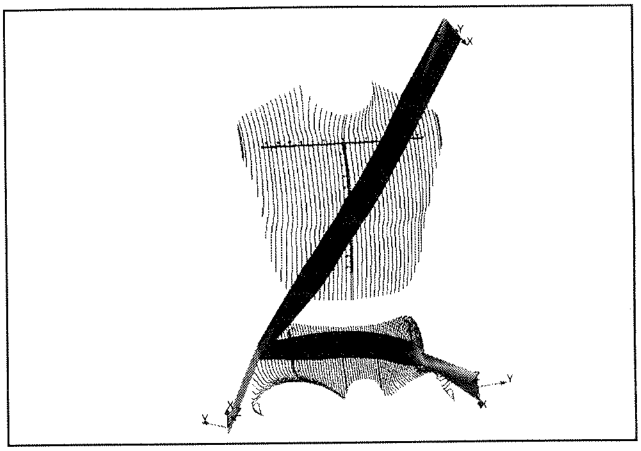

Figure 6. The GM Cavalier

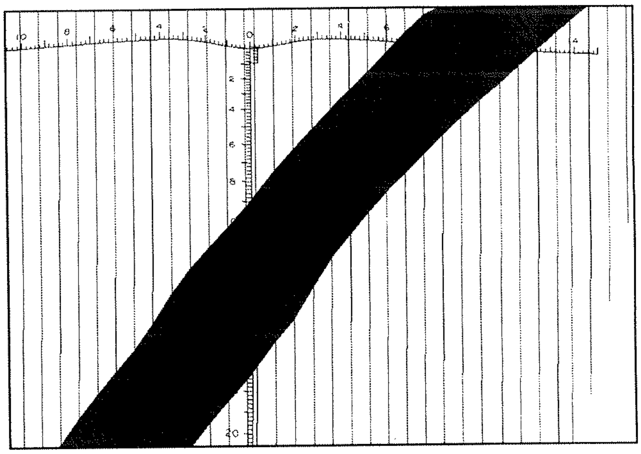

Figure 7. Close-up of the Cavalier Shoulder Belt

Table 2.
Validation 1998 Cavalier

Scale	Actual BTD	Electronic BTD
Clavicle	12.6	12.4
Sternum	17.5	17.1
Lap Inboard	2.2	1.3
Lap Outboard	3.9	3.8

Table 3.
Validation 1998 Dodge Caravan

Scale	Actual BTD	Electronic BTD
Clavicle	11.2	11.1
Sternum	13.8	13.9
Lap Inboard	4.8	4.0
Lap Outboard	4.2	4.2

DISCUSSION

The data presented in Tables 2 and 3 indicate that the differences between the electronic and actual BTD scores were all within one centimetre. In one instance, there was disagreement between predicted and observed pass/fail outcomes. The 1998 Cavalier failed the inboard lap criterion using the electronic BTD but passed using the actual device. It should be noted, however, that the electronic score was within 2 mm of the criterion value of 1.5 cm. The actual score was 2.2 cm, within 7 mm of being acceptable.

The results confirm the potential for the electronic BTD to replace the actual device. There was good correspondence between electronic and actual scores for a popular model passenger car and a minivan.

CONCLUSIONS

The computer-based model of the BTD was refined and validated. The results of the validation study demonstrated good concordance with scores obtained with the actual device. However, as a result of the difficulties in obtaining digital 3-D seat data, it was not possible to adequately test the concept of electronic compliance. The feasibility of electronic compliance relies on the availability of appropriate digital data. Further collaborative efforts in this area will explore the potential for industry to acquire and provide the requisite data.

ACKNOWLEDGEMENTS

The authors thank Genicom Consultants for their assistance in this project.

REFERENCES

Dalmotas, D.J. and Welbourne, E.R., "Improving the Protection of Front Seat Occupants in Frontal Crashes", Proceedings of the 13th International Technical Conference on Experimental Safety Vehicles, Nov. 4-7, 1991, Paris, France.

Gibson, T., Tylko S., and Shewchenko, N., “The Belt-Fit Test Device: A Description of its Development and Function as an Evaluative Tool”, Biokinetics & Associates, Document R93-05, June 1994.

Noy, I., Battista, V. and Carrier, R., “Development of an Electronic Belt Fit Test Device”, SAE Anthropmetric Dummies and Crash Instrumentation Sensors SP-1261, Paper 971137, February 1997.

Transport Canada, “Operational Manual For The Belt Deployment Test Device”, Road Safety, January 1993.

Tylko, S. and Gibson, T.,” Belt Fit Test Device Fleet Measurement”, Biokinetics & Associates, Document R94-02, May 1994.

Tylko, S., Gibson, T., Descôteaux and Fournier, E., “ A Demonstration of the Capabilities of the Belt-Fit Test Device”, Biokinetics & Associates, Document R93-06, June 1994.

Tylko, S., Gibson, T., and Shewchenko, N. "Towards the Development of a Seat Belt Fit Compliance Procedure Based on the Belt-Fit Test Device (BTD)", contract report to Transport Canada, Ottawa, January 1993, BAL report R92-11B.

A HIGH-SPEED SENSOR FOR MEASURING CHEST DEFLECTION IN CRASH TEST DUMMIES

Stephen W. Rouhana
Safety Research Department
General Motors Global Research and Development Operations
Ali M. Elhagediab
Jeffrey J. Chapp
Aerotek Lab Support
United States

Paper Number 98-S9-O-15

ABSTRACT

Chest deflection measurement is critical for the assessment of thoracic injury since the two most widely accepted criteria for chest injury (chest deflection and the viscous response) are based on deflection. One major issue with the measurement of chest deflection in crash test dummies has been the inability to accurately track motion of the chest at very high deflection speeds (above 10 m/s under certain circumstances). This limitation has increased the difficulty in evaluating some deployable safety devices, most notably airbags. When there is no interaction with the dummy, airbags deploy at velocities of 50 to 150 m/s. When there is interaction with the dummy, such as occurs in out-of-position tests with the chest in contact with the airbag module, airbags can deform the chest at deflection rates of 10 to 18 m/s.

Our main research goal was to develop a new sensor to measure chest deflection at all speeds of interest in the automotive environment (quasi-static to 18 m/s). The device developed, called the I/R-TRACC system (InfraRed - Telescoping Rod for Assessment of Chest Compression), uses two infrared LEDs inside of a telescoping rod. One LED is used as the emitter and the other is used as the receiver of the infrared light. The output of this device is a linear function of chest compression. The data presented in this paper shows that the IR-TRACC system appears to have met the design requirements set forth at the beginning of the project and should be suitable for any crash test dummy designed to measure chest deflection, including frontal and side impact dummies.

INTRODUCTION

Over the years since anthropomorphic test devices (ATDs) or crash test dummies first became available, many different devices have been developed or adapted to them for the measurement of chest deflection. Measurement of chest deflection is critical for the assessment of thoracic injury since the two most widely accepted criteria for injury are based on deflection. Those criteria are deflection itself (which is evaluated in FMVSS 208) and the viscous response (deflection times velocity of the deflection).

Each of these sensors for measurement of deflection has had limitations, which have prevented their use in some crash test evaluations using ATDs. One major issue has been the inability to accurately track motion of the chest at very high deflection speeds (above 10 m/s under certain circumstances). This limitation has increased the difficulty in evaluating some deployable safety devices, most notably airbags. When there is no interaction with the dummy airbags deploy at velocities of 50 to 150 m/s. When there is interaction with the dummy, such as occurs in out-of-position tests with the chest in contact with the airbag module, airbags can deform the chest at deflection rates of 10 to 18 m/s.

Another issue relative to chest deflection measurement has been electrical or mechanical noise associated with the measuring instrumentation or sensor. Noise in the deflection time history can prevent assessment of the viscous response because of the differentiation needed in the calculation. Differentiation of a noisy signal typically leads to an unusable result. Filtering may be helpful to some extent; however, experience has shown that the degree of filtering typically necessary to smooth a noisy signal for the viscous response calculation is unacceptable because of the significant loss of data that results.

Our main research goal was to develop a new sensor to measure chest deflection at all speeds of interest in the automotive environment (quasi-static to 18 m/s). A secondary goal included addressing other problem areas of previous devices (e.g., Hybrid III ball/slider disconnect in severe belt loading) with the new sensor to be developed.

The device we developed, called the **I/R -TRACC** system (**I**nfra**R**ed - **T**elescoping **R**od for **A**ssessment of **C**hest **C**ompression), has several different modes of operation using various combinations of infrared LEDs and phototransistors inside of a telescoping rod. As will be shown for the LED-to-LED Mode, this system appears to have met the design requirements set forth at the beginning of the project. Although the original intent of this program was to develop a transducer to replace the sensor in the Hybrid III frontal impact dummy, the I/R TRACC system should be suitable for any crash test dummy designed to measure chest deflection, including frontal and side impact dummies.

Previously Developed Chest Deflection Instrumentation

Since two of the accepted injury criteria for assessing chest injury rely on measurement of chest deflection (chest compression and viscous response), many attempts have been made to develop deflection-measuring systems. Examples of some of the published work follow. More detail will be provided relative to the Hybrid III chest deflection transducer because that is a regulated dummy and was the initial focus of our work. In addition, we will provide more detail on the method used in the NHTSA's Advanced ATD because our method builds on that work as originally conceived and first implemented by Schneider et al. [1][1].

In the 1973 design of the dummy called "Repeatable Pete", McElhaney, et al. [2] used a space linkage, which was movable in three dimensions and had rotary potentiometers attached at the pivots. The output of the potentiometers was added differentially to make the output "proportional to the horizontal motion of the chest attachment point and independent of the other components of [the] motion".

When the Hybrid III dummy was introduced in 1976 it utilized an "articulated arm" chest deflection transducer [3,4]. This transducer consists of a rotary potentiometer mounted on the thoracic spine and connected by an aluminum rod to a ball and Delrin slider mechanism on the sternum [Figure 1]. As the chest wall moves relative to the spine, the ball moves up or down the slider track and changes the output of the potentiometer in proportion to the relative distance between the chest and spine. The original device was capable of measuring deflections up to 90 mm.

Over the years a number of issues have arisen regarding the measurement made using the articulated arm of Hybrid III. These include:

- loss of data because of ball-slider decoupling in out-of-position airbag tests and high severity belted crash tests,
- lack of three dimensional understanding of chest motion,
- difficulty differentiating signal due to electrical noise,
- limited displacement measurement, especially in smaller dummies, and
- lack of understanding as to the exact point on the chest to which the deflection measurement corresponds [5,6,7,8].

In spite of these limitations, and despite a number of attempts to replace it, no device has been found with performance superior to the Hybrid III chest deflection transducer.

Stalnaker et al. [9] used a magnetic pickup over a moving rod that had slots machined in it to measure lateral chest deflection in a Part 572 (Hybrid II) dummy which had been modified for use in lateral impacts.

Several research groups have utilized strain gauges bonded to the ribs to determine chest compression in dummies. Wiechel et al. [5] showed that, in a Hybrid III dummy, the peak strain measured at the point of maximum strain was linearly proportional to the peak chest deflection as measured by the chest deflection transducer. Grosch [10] and Grosch et al. [11] used strain gauges to determine rib deflections in a Hybrid II dummy.

While not developed for use in ATDs, Eppinger [12] used strain gauges in the development of the EPIDM (External Peripheral Instrument for Deformation

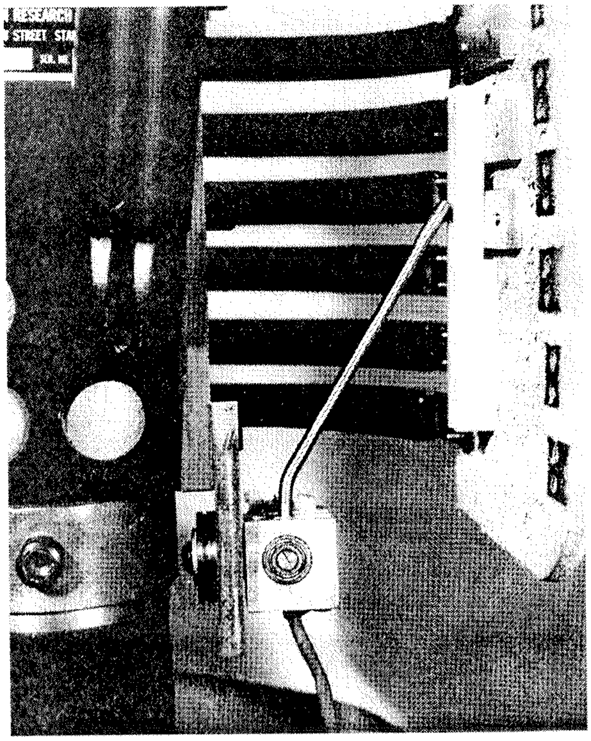

Figure 1. Hybrid III Articulated Arm Chest Deflection Transducer (from [3]).

---

[1] Numbers in square brackets denote references found at the end of the paper.

Measurement), commonly called the "Chest Band". This device measures contours of the complete periphery of an object as it deforms in time. It consists of a 0.015" thick steel band that is 0.5" wide and 46" long. Strain gauges, forming four active arm bridges, are affixed at precise locations along the band. The larger the number of gauges, the better the resolution of the contour.

An optical transducer was used by Fayon et al. [13] in the development of the APROD dummy thorax and subsequently in the EuroSID dummy [14]. This method consisted of a reflecting graticule attached to the piston within the chest and a photo-optical sensor that counts each time a graticule mark passes.

Lau et al. [15] chose a linear position transducer (LVDT) in a modified EuroSID thorax in the work leading to the development of the BioSID. Subsequently, the SAE Side Impact Task Group chose high tension string potentiometers for measurement of deflection in the BioSID [16]. String potentiometers are made by winding a cable around a spool, which is connected, to a spring that continually exerts tension on the cable to reel it in. The spool is connected to a rotary potentiometer which changes resistance, and hence voltage output, as a function of its rotation.

High-tension string potentiometers have also been considered for frontal impact dummies. The main drawback to a string potentiometer, however, can be observed in very high speed loading situations, such as when the dummy chest is in direct contact with an airbag module. As deployment begins, the string potentiometer cannot follow the rapid chest motion and lags behind. While it may provide an accurate assessment of peak deflection, in this situation the string potentiometer does not give an accurate time-history and is therefore unsuitable for determining the viscous response.

Another optical position sensing system was developed by Ogata et al. [7] for the Hybrid III mid-sized male dummy. This system performs binocular triangulation using two pairs of position sensing detector cameras and two pairs of flashing LEDs.

In the development of the Advanced ATD under contract from the NHTSA, Schneider et al. [1] developed a double-gimballed string potentiometer (DGSP) in a telescoping joystick. A Chest Deflection Task Force of the SAE Human Biomechanics and Simulation Standards Committee working with the UMTRI group first considered a triangulation method using three string potentiometers attached to each point at which deflection measurement was desired. After eliminating that method, the DGSP was chosen by UMTRI. The double-gimballing allowed the DGSP transducers to track up/down and lateral motion using rotary potentiometers attached to the pivots. The string potentiometer down the center of the telescoping joystick allowed tracking the in/out motion of the anterior chest wall relative to the spine.

As described earlier, the main drawback to the string potentiometer is its lack of response in ultra-high speed loading situations such as those that occur with ATDs out-of-position and in contact with airbags as deployment begins.

Finally, several attempts have been made to determine chest deflection by taking the difference between a twice-integrated output of accelerometers on the sternum and spine of an ATD [8,17]. This method has not met with success principally because of two factors. First, integration techniques introduce constants into the resulting output, which are difficult to remove. Second, motion of the ribcage is not typically constrained to rectilinear motion. The ribs and sternum often bend causing rotation of the accelerometers in addition to any rectilinear motion. This makes interpretation of the data very difficult.

The I/R -TRACC System (InfraRed Telescoping Rod for Assessment of Compression)

The I/R-TRACC system, as proposed, consists of two infrared light emitting diodes (LEDs) "facing" each other from the two ends of a stainless steel, double-gimballed telescoping rod as described below [Figures 2a and 2b]. We arrived at this configuration after a development program that examined a number of different configurations. These configurations consist of various combinations of light emitting diodes and an infrared phototransistor sensor mounted within the telescoping rod. This paper reports data from the four most promising implementations of the I/R-TRACC system. Each configuration has strengths and weaknesses as will be outlined in the paper. While we propose using only the LED-to-LED Mode, under some circumstances one of the other implementations might also be satisfactory as will be discussed. Therefore, with some exceptions only the results from the LED-to-LED Mode system will be presented in the main paper. The results for the other systems will be presented in Appendix III. Those results are useful in understanding the limitations and design philosophy of the device. The exceptions will be for some data from the other implementations which will be presented as exemplars for discussion purposes.

The different implementations of the IR-TRACC system are:

1. **Transmission Mode** – an infrared LED at the base or larger diameter end of the telescoping rod transmits light to a phototransistor at the smaller diameter end of the rod (Figure 3).

2. **Reflection Mode** – an infrared LED transmits light through half the fibers in a bifurcated fiberoptic

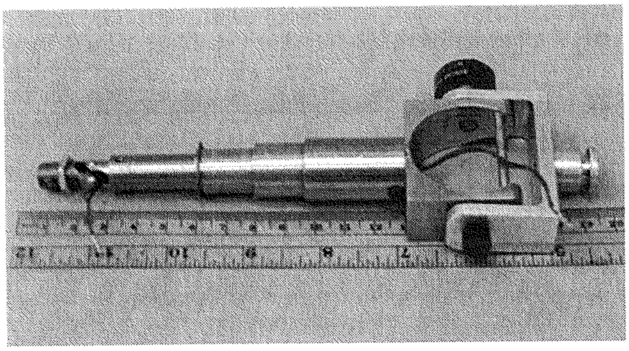

Figure 2a. IR-TRACC System for a Hybrid III - 6 Year Old Child dummy, fully extended.

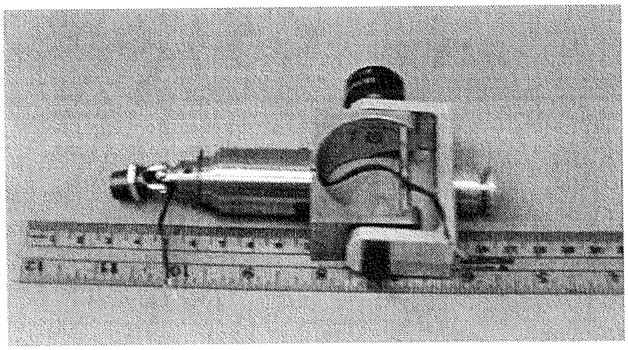

Figure 2b. IR-TRACC System for a Hybrid III - 6 Year Old Child dummy, fully compressed.

cable at the small end of the rod. Upon exiting the aperture of the fiber optic cable inside the rod, the light travels down the rod and impinges on retro-reflective tape bonded to the base. The light is reflected from the base in a perpendicular direction and travels back to the aperture of the fiberoptic cable. There the light enters the cable and travels via the other half of the fibers to a phototransistor where it is detected. The fiberoptic cable, LED and phototransistor assembly is bonded with epoxy to the inside of the smallest diameter segment of the telescoping rod (Figure 4).

3. **Ruggedized Transmission Mode** – similar to Transmission Mode, except that the lens of the phototransistor is removed and the case is filled with a clear epoxy to prevent the active element from dislodging during the large accelerations of the impact tests.
4. **LED-to-LED Mode** – two infrared LEDs are located at opposite ends of the rod. One LED is used as the emitter and the other is used as the receiver of the infrared light.

In I/R-TRACC modes 1, 2 and 3 only one leg of the phototransistor is actually used so that, in practice, the phototransistor is used as a photodiode. The output from this photodiode is input to an operational amplifier (Op Amp) which has a gain of about 22 and is part of a circuit to be described later. This amplified output voltage is then monitored as a function of time. The pertinent specifications for the components used in the Transmission, Reflection and LED-to-LED Mode systems are given in Tables 1, 2 and 3, respectively.

Principle of Operation of the Transmission and Reflection Modes

A simple summary of the principle of operation is presented here, with a more thorough discussion in Appendix I. Figure 5 illustrates schematically how the system operates. The principle of operation of the system is photo-optical. The LED emits light in the infrared region of the spectrum which exits through a plastic lens that is part of the housing. The rays of light from the LED diverge in a conical pattern with a beam divergence angle of ± 10° as they leave the source. The irradiance of the light as shown in the manufacturer's product data sheet obeys an inverse square law [18]. That is, the irradiance at a plane through which the beam passes is proportional to the inverse of the square of the distance from that plane to the LED. Therefore, as the LED is moved closer to the photodiode the irradiance increases as in Equation 1.

$$E_e \propto \frac{1}{d^2} \qquad (1.)$$

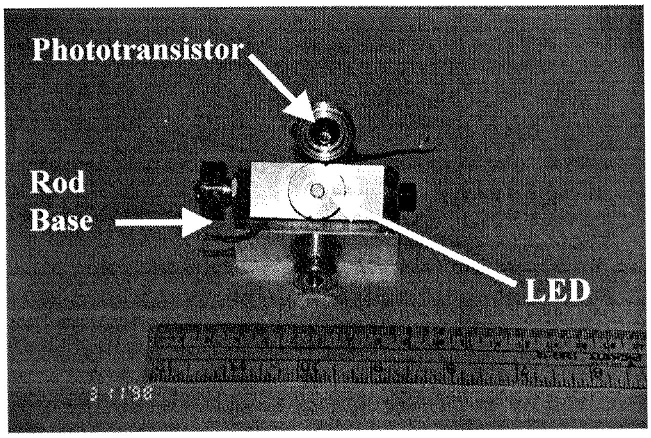

Figure 3. Transmission Mode system with telescoping rod collapsed and opened up to show the internal sensor and LED.

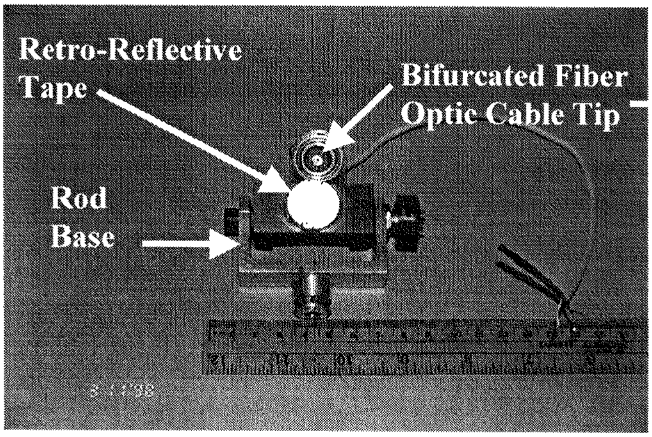

Figure 4. Reflection Mode system with telescoping rod collapsed and opened up to show the aperture of the bifurcated fiber optic cable and the retro-reflective tape. The inset shows the bifurcation of the fiber optic cable. The LED is connected to one of the apertures on the right and the phototransistor sensor is connected to the other aperture.

where,

$\mathbf{E_e}$ = irradiance (W/m^2) and

d = the distance between the LED and phototransistor.

As shown in the appendix, the output voltage measured after the signal is amplified is given by:

$$V_{out} \propto E_e \qquad (2.)$$

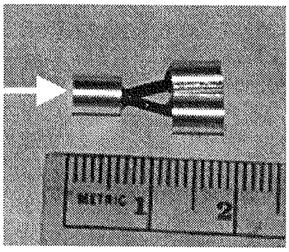

Since the irradiance is proportional to the inverse square of the distance between the LED and phototransistor, then, the voltage is also proportional to the inverse of the distance squared.

$$V_{out} \propto \frac{1}{d^2} \qquad (3.)$$

Thus, the distance between the phototransistor and LED is obtained by taking the inverse square root of the phototransistor output voltage as shown in Equation 4.

$$d \propto \sqrt{\frac{1}{V_{out}}} \qquad (4.)$$

For comparison, it is helpful to note that the output voltage that the circuit measures in Transmission and Reflection Modes is a function of the current across the photodiode section of the phototransistor. This photocurrent is governed by the amount of light reaching the phototransistor.

Table 1.
Transmission & Ruggedized Transmission Mode Components

LED		Phototransistor	
Manufacturer	Optek	Manufacturer	Honeywell
Model	OP295C	Model	SD-5443-003
Wavelength	890 ± 80 nm	Wavelength	890 nm
Beam Angle	± 10 degrees	Acceptance Angle	18 degrees
Irradiance at Aperture	22 mW/cm^2	Rise/Fall Time	15 µs

Table 2.
Reflection Mode Components

LED		Phototransistor	
Manufacturer	Honeywell	Manufacturer	Honeywell
Model	HFE-4000-014	Model	HFD-3002-002
Wavelength	850 ± 50 nm	Wavelength	850 nm
Beam Angle	Collimated	Acceptance Angle	85 degrees
Fiber Coupled Power	25 µW	Rise/Fall Time	10 ns

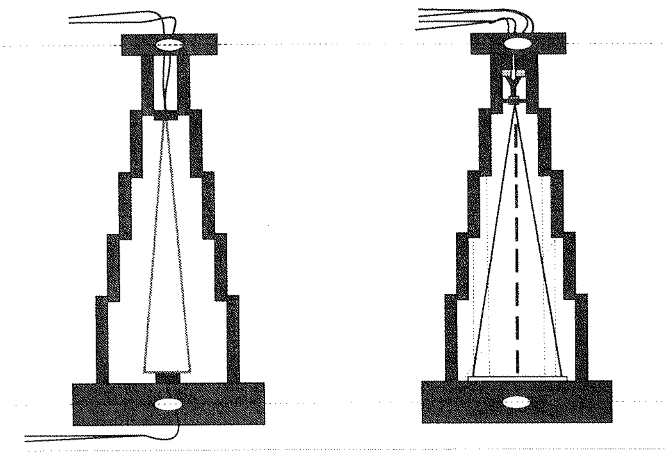

Figure 5. Schematic of Transmission (left) and Reflection (right) Modes of operation.

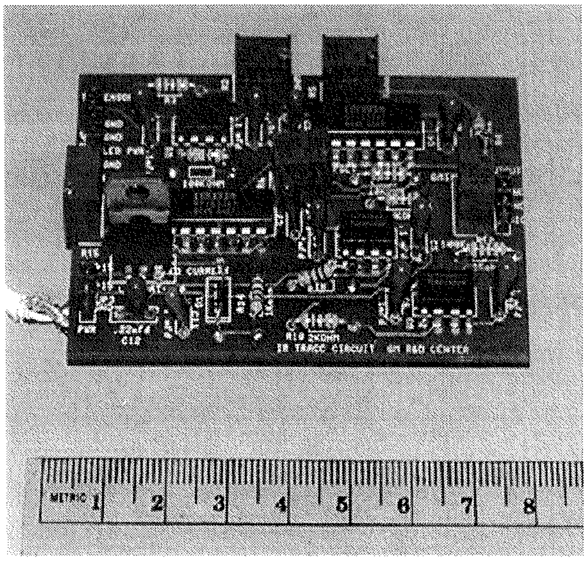

Figure 6. IR-TRACC printed circuit board for Transmission and Reflection Modes.

Linearization of Output from the Transmission and Reflection Mode IR-TRACC Systems

The theoretical discussion in Appendix I serves as the basis for making the output of the photodiode section of the phototransistor a linear function of the distance between the phototransistor and IR LED. This "linearization" of the output, requires either post-processing software or a hardware circuit. The Transmission and Reflection Mode I/R-TRACC systems send the output through two circuit stages which invert the output and take its square root to convert the voltage to a linear function of the distance between the LED and photodiode. Figure 6 shows the circuit board developed for this linearizing circuit. The 2 inch by 3 inch PC board houses all of the components necessary to make the output voltage a linear function of the deflection. Since the board is small and is rugged (it contains only solid state components) it should be suitable for mounting inside the dummy.

Principle of Operation of the LED-to-LED Mode

Again, a simple summary of the principle of operation is presented here, with a more thorough discussion in Appendix II. Due to the photoelectric effect, any semiconductor material will generate a photocurrent on absorption of incident radiation [19]. In an LED, a semiconductor element is used to generate light and therefore, can also absorb light (in principle acting like a photodiode). As shown in Appendix II, the photocurrent in a photodiode is proportional to the exponential of the voltage across the diode [20]. Then, it follows, that the voltage across the diode is proportional to the natural log of the photocurrent. The photocurrent is also proportional to the irradiance of the light impinging upon it. Then, the voltage across the photodiode is also proportional to the natural log of the irradiance as shown in Equation 5.

$$V_D \propto \ln(E_e) \tag{5.}$$

But, the irradiance is proportional to the inverse distance squared between the two LEDs. So, the voltage across the photodiode is proportional to the natural log of the inverse square of the distance between the LEDs as in Equation 6.

$$V_D \propto \ln\left(\frac{1}{d^2}\right) \tag{6.}$$

Then, the output voltage across the sensor LED should be proportional to the natural log of the reciprocal

Table 3.
LED-to-LED Mode Components

LED	
Manufacturer	Optek
Model	OP295C
Wavelength	890 ± 80 nm
Beam Angle	± 10 degrees
Irradiance at Aperture	22 mW/cm^2

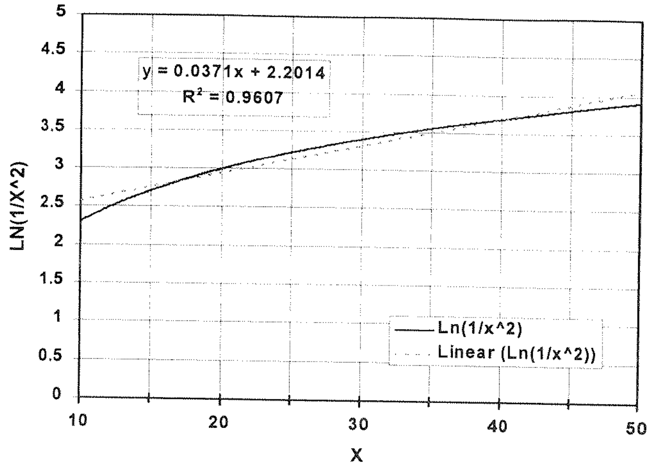

Figure 7. Natural log of a general inverse square function (solid line) and linear regression of that function (dashed line).

squared distance between the LEDs. In practice, however, as shown in Figure 7, the natural log of an inverse square function is nearly linear over a broad range (r^2 = 0.96). For this reason the linearization circuit developed for the other modes of operation is not necessary with the LED-to-LED mode of operation. While it is conceivable to build a circuit like that developed for the other modes of operation, the measured direct output appears to be linear in the range of operation of the IR-TRACC (r^2=0.99).

In contrast to the other modes of operation, in LED-to-LED Mode the output voltage is directly related to the voltage across the sensor diode (LED). Therefore, for simplicity, in this mode the voltage measured across the sensor LED is input directly into a buffer and amplifier circuit with a gain of approximately 100.

METHODS

The data presented in this paper was obtained from tests at various deflection rates using two different methods. Tests were done quasi-statically (QS), and at approximately 2 m/s and 5 m/s, on an MTS™ hydraulic test system. The main purpose of these tests was to assess the repeatability of the IR-TRACC system under nominally identical test conditions. The quasi-static tests also served as the determinants of the calibration factors for the various systems. Higher speed tests were done using a pneumatic impactor or air cannon. These tests were done at approximately 4 m/s, 10 m/s and 18 m/s.

MTS Tests - The larger diameter end of the rod was attached to a rigid plate which was mounted to the MTS table such that the axis of the rod was vertical and coaxial with the MTS piston. (Figure 8) The smaller diameter end of the rod was attached through a mounting block and a load cell to the piston of the MTS at its centerline. For the LED-to-LED Mode, the output from the sensor was connected to the buffer/amplifier circuit as previously described. For the other modes, the output from the phototransistor was connected to the input stage of an IR-TRACC PC board. The output from either the buffer/amplifier circuit or the IR-TRACC circuit was then connected to the data acquisition system.

Pneumatic Impactor Tests - The main purpose of these tests was to assess the ability of the rod to track deflections at higher rates of speed and to see how durable and repeatable the rod was under more dynamic conditions.

In these tests the rod was mounted horizontally in an aluminum channel section as shown in Figure 9. The channel section was in contact with a foam cushion to reduce the stopping acceleration of the IR-TRACC unit. A foam pad was also placed in front of the IR-TRACC to reduce initial accelerations from metal to metal contact with the impactor and to distribute the loading over a broader area similar to the chest of an ATD. A contact foil was used on the face of the impactor to initiate data acquisition and high-speed video data capture. Targets were installed on the base of the rod and at the top of the rod to enable accurate tracking. A scale factor strip (not shown) was suspended over the centerline of the rod to enable accurate comparison of motion in the same plane as the LEDs.

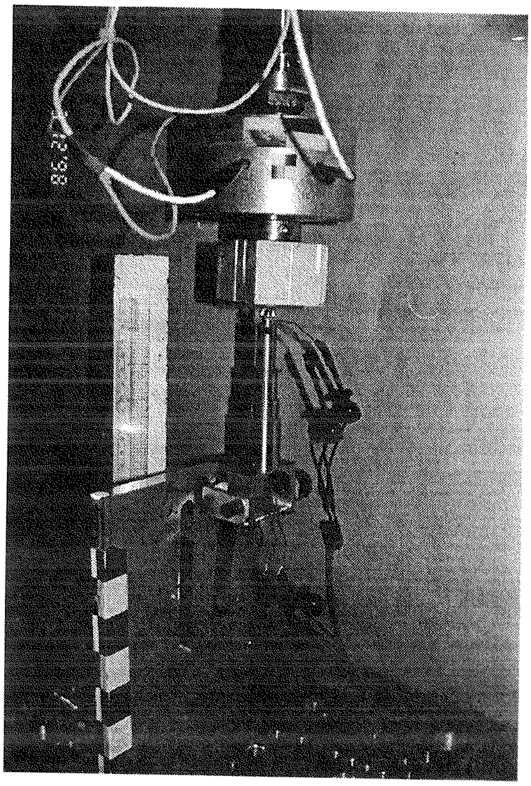

Figure 8. MTS test setup.

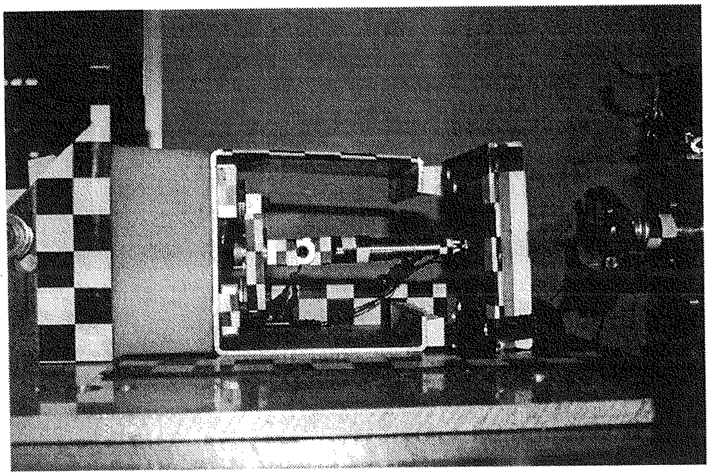

Figure 9. Pneumatic impactor test setup.

General Conditions

The Transmission, Ruggedized Transmission and Reflection Mode quasi-static deflection data were sampled at 500 samples/second. The 2.7 m/s and 5.5 m/s deflection data were sampled at 10000 samples/second, then anti-alias filtered at 2 kHz and digitally filtered using an SAE Channel Class 600 filter. All data for LED-to-LED Mode were sampled at 10000 samples/second and digitally filtered using an SAE Channel Class 600 filter.

Measurement Standards

- Deflection of the IR-TRACC in the MTS tests was compared to the displacement given by the standard MTS controller LVDT. The IR-TRACC sensor was calibrated to obtain a known voltage-displacement relationship immediately prior to each test. The data was scaled using that calibration factor.
- Deflection of the IR-TRACC in the air cannon tests was compared to motion data obtained from high-speed video taken at 9000 frames/second using a Kodak Ektapro™ HS Model 4540 with a 28-105 mm macro zoom lens and tracked by a Kodak Image Express™ system.

RESULTS

When this project began, the focus was on developing a rod for use with the mid-sized male Hybrid III. During the course of the work it became apparent that the need was even more acute for the smaller members of the Hybrid III family and so the focus of the project was shifted to the 6 year old Hybrid III. The data presented in this paper is for a rod with an overall length of 100 mm (3.94 inches), a size that is appropriate for use in the 6 year old. The maximum distance that this rod can collapse is 57.7 mm (2.27 inches), but the maximum calibrated displacement for this rod is approximately 42 mm (1.65 inches).

We experimented with rods of different lengths and under certain circumstances were able to make this system work for rods up to 200 mm (8 inches) in length with displacements of up to 150 mm (6 inches).

As shown in Table 4, for LED-to-LED mode of the IR-TRACC system, five tests were performed at each speed on the MTS. On the pneumatic impactor, we ran five tests at 4 m/s, and inadvertently ran six tests at 10 m/s and four tests at 18 m/s.

As will be explained below, the LED-to-LED Mode is the recommended system for the IR-TRACC. Therefore, all graphs for Transmission, Reflection and Ruggedized Transmission Mode tests are given in Appendix III. Only representative tests will be shown in the main text to illustrate the technical issues the tests uncovered.

Table 4.
Test Matrix

Device & Speed	Trans Mode	Rug Tran Mode	Refl Mode	LED/LED Mode
MTS				
QS	4	3	5	5
2.5 m/s	4	3	5	5
5.5 m/s	4	3	5	5
Impactor				
4 m/s	▨	▨	▨	5
10 m/s	▨	▨	▨	6
18 m/s	▨	▨	▨	4

MTS Test Results

Deflection-time histories from all LED-to-LED Mode MTS tests are shown in Figure 10. Deflections measured using the IR-TRACC sensor are overlaid on the displacements measured by the MTS LVDT. This figure provides a qualitative look at the accuracy of the IR-TRACC system. The generally good agreement of the deflection-time histories is obvious.

To obtain a quantitative view of the accuracy of the IR-TRACC system, the maximum difference and the standard deviation of the IR-TRACC deflection data with respect to the LVDT data was calculated for each MTS test. With the LVDT displacement data as the comparison the maximum differences were 1.80 mm, 2.31 mm, and 3.35 mm for the quasistatic, 2 m/s and 4 m/s tests, respectively. The standard deviations ranged from ± 0.6 to ± 0.9 mm.

To determine scale factors and to obtain a quantitative view of the linearity of the IR-TRACC system, the IR-TRACC output voltage was cross-plotted against the MTS displacements for each test at each speed as shown in Figure 11. A linear regression was fit through the cross-plot with the equation and correlation coefficient (r^2 value) shown on each graph. For clarity, the actual trend line is only shown on one graph. This figure shows the excellent linearity between the IR-TRACC system and the MTS. Note that all r^2 values exceed 0.99.

Dynamic Pneumatic Impactor Test Results

In Figures 12a, 12b and 12c the time-history of each LED-to-LED Mode IR-TRACC deflection is overlaid onto the corresponding high-speed video tracked displacement for each pneumatic impactor test, at each speed. This figure provides a qualitative look at the accuracy of the IR-TRACC system at high-speed.

It was difficult to synchronize the video and IR-TRACC data because of the different data sampling rates for the two devices and because of different triggering schemes for the video and our data acquisition system. Therefore, the time scales were shifted manually to match

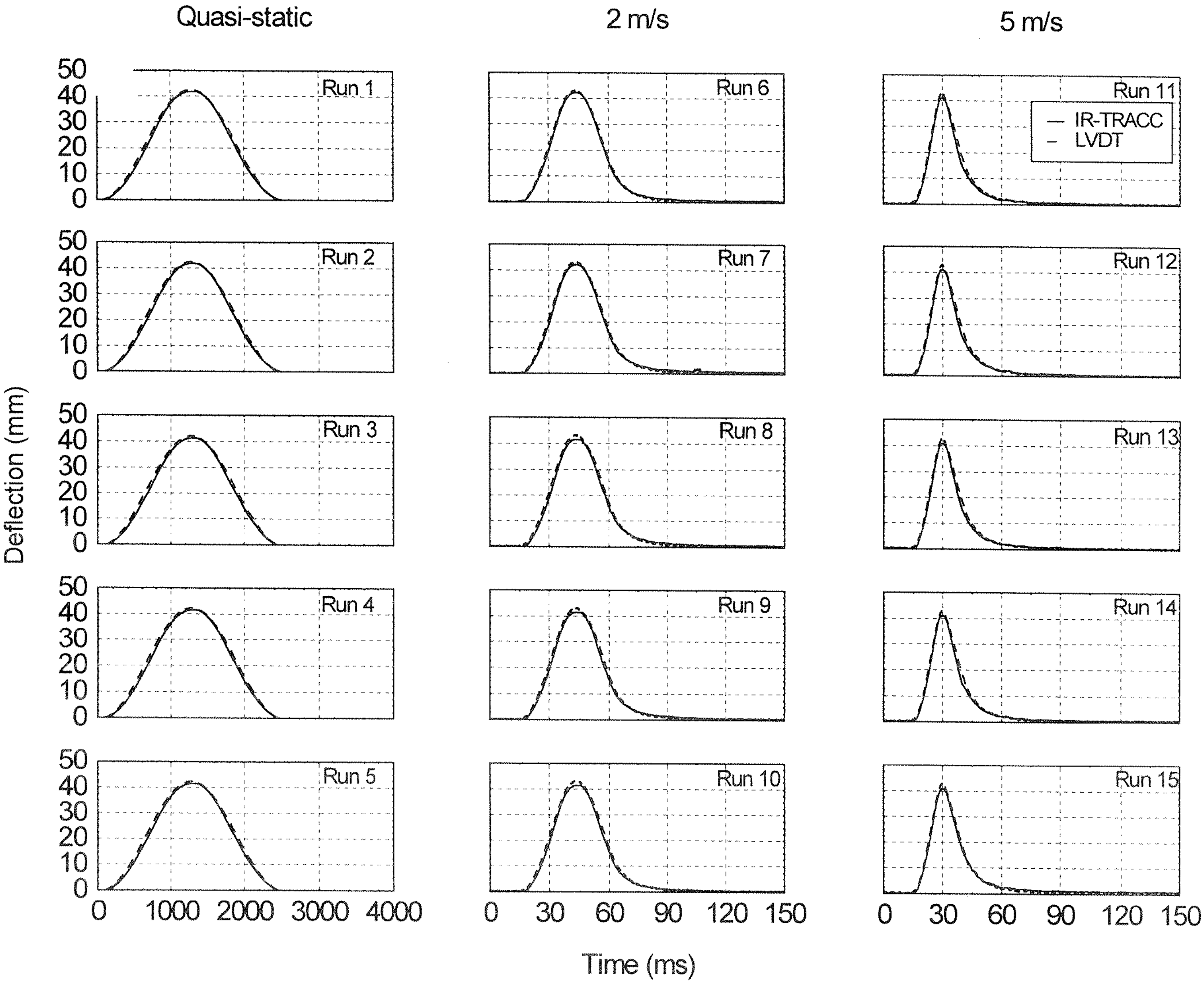

Figure 10. Deflection-time histories for LED-to-LED Mode IR-TRACC sensor (solid line) overlaid on deflections from LVDT on MTS (dashed line).

the initial rise from the baseline.

A more quantitative view of the system was obtained by calculating the difference between the peak deflection measured by the IR-TRACC and that calculated from the video data for each test. The average maximum difference between the IR-TRACC and the video data was 0.59 mm, 1.57 mm and 1.06 mm for the 4 m/s, 10 m/s and 20 m/s tests, respectively. It is important to note that these numbers simply reflect the **difference** between the measurements taken from the video and those of the IR-TRACC system. They do **not** represent the error because the video is not an absolute standard. In fact, they may be more representative of the error inherent in 2-D video tracking and not the error in the IR-TRACC system. The origins of these differences in the data will be discussed later.

Differentiation

One of the primary reasons that a new method of chest deflection has been sought is so that the deflection-time histories could be differentiated to obtain velocity-time and the viscous response as a function of time. Therefore, each IR-TRACC deflection time-history was filtered at SAE channel class 600 and then digitally differentiated. The velocity-time histories for each of the MTS tests with the LED-to-LED Mode sensor are shown in Figure 13. These curves show that the differentiated data appears to be well behaved enough for typical automotive use.

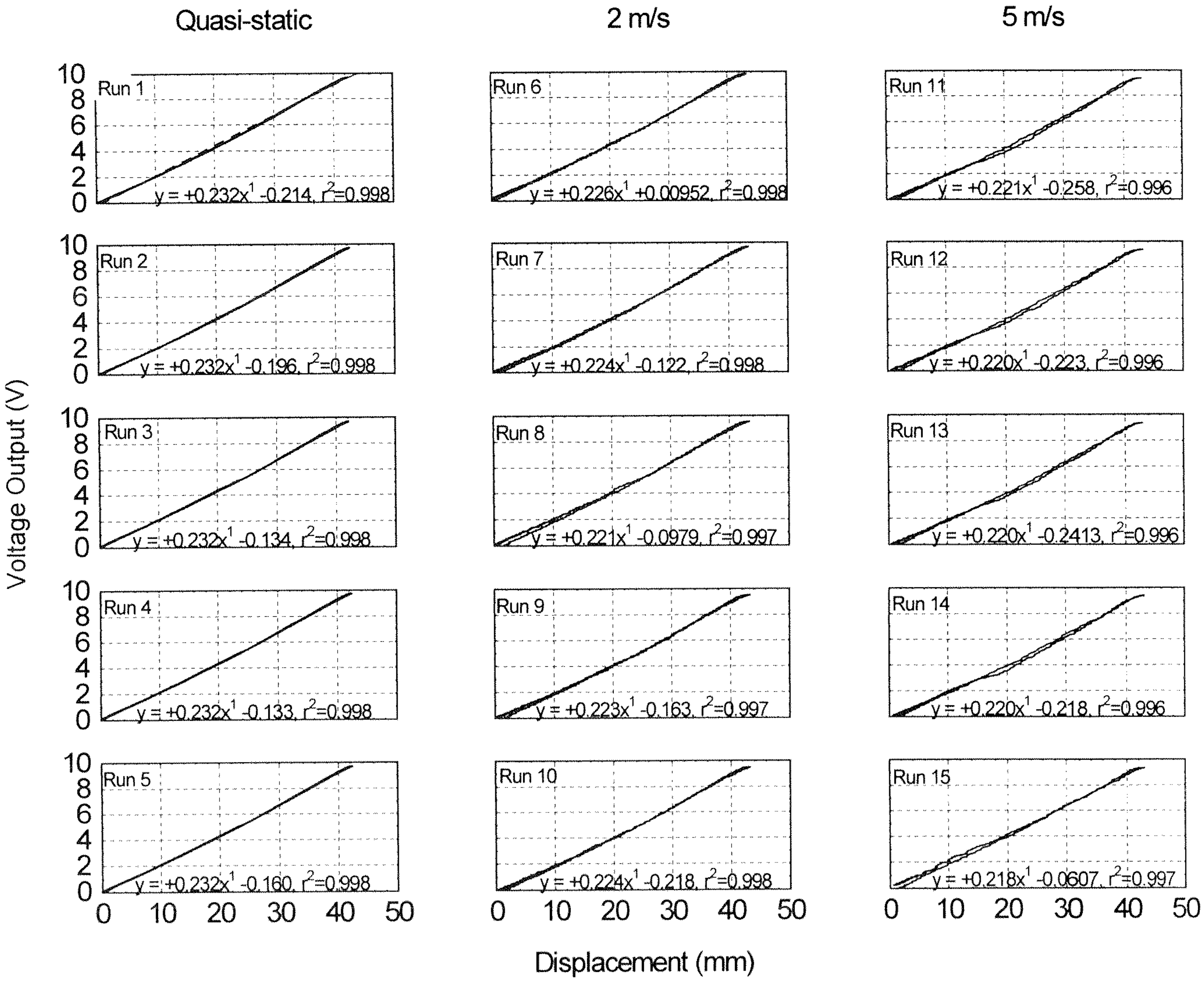

Figure 11. Cross-plots of the amplified IR-TRACC output voltage and MTS displacement from the LVDT to obtain scale factor for the sensor in LED-to-LED Mode tests.

The time scales on one representative graph from Figures 12a and 12b and all of the graphs from Figure 12c (the 18 m/s tests) have been expanded in Figures 14, 15 and 16a-d, respectively. This expansion was done to allow a closer examination and comparison of the deflections, velocities and viscous responses.

All of the signals are clearly differentiable. The large velocity swings have mechanical reasons, which will be discussed below. The agreement between the IR-TRACC and the high-speed video appears to be acceptable even up to 20 m/s.

V*C Calculation

As a further check on the data, the viscous response (V*C) was calculated for the IR-TRACC data. Representative curves are shown in Figure 17 for MTS tests at the three different speeds. The data is clearly well behaved. We also calculated the viscous response for the pneumatic impactor tests as shown in Figure 14, 15 and 16.

The reader will note that there was some very small jitter (less than 2% of the peak deflection) after the impact on two MTS tests (see Figures 10 and 13, runs 7 and 10). When differentiated this small jitter was amplified so that the resulting apparent velocity was greater than the MTS velocity. This highlights the need for a clean signal for V*C calculations. Obviously in this case, since there is no deflection occurring at the time of that spike, the calculation of $(V^*C)_{max}$ would yield zero, but $V_{max}{}^*C_{max}$ (a form of the viscous response which is calculated using the peaks instead of the time-varying functions) would be misleading. We believe that these spikes were most likely caused by contact slap. The wires connecting the LEDs to the instrumentation were spring clamped and taped together, not soldered. As a result the rapid cable deceleration on contact with the MTS worktable could have caused the spikes. Obviously, in the final design for in-dummy use, all cables and attachments will be ruggedized.

As a more quantitative look at the viscous response data, we compared the peak viscous response calculated from the IR-TRACC data with that calculated from the video data. The average percent difference between the IR-TRACC and the video data was 10.4%, 14.2% and 12.5% for the 4 m/s, 10 m/s and 20 m/s tests, respectively. As mentioned previously, it is important to note that these numbers only reflect the **difference** between the measurements taken from the video and those of the IR-TRACC system. They do **not** represent percent error because the video is not an absolute standard. Again, they may be more representative of the error inherent in 2-D video tracking and not the error in the IR-TRACC system. The origins of these differences in the data will be discussed later.

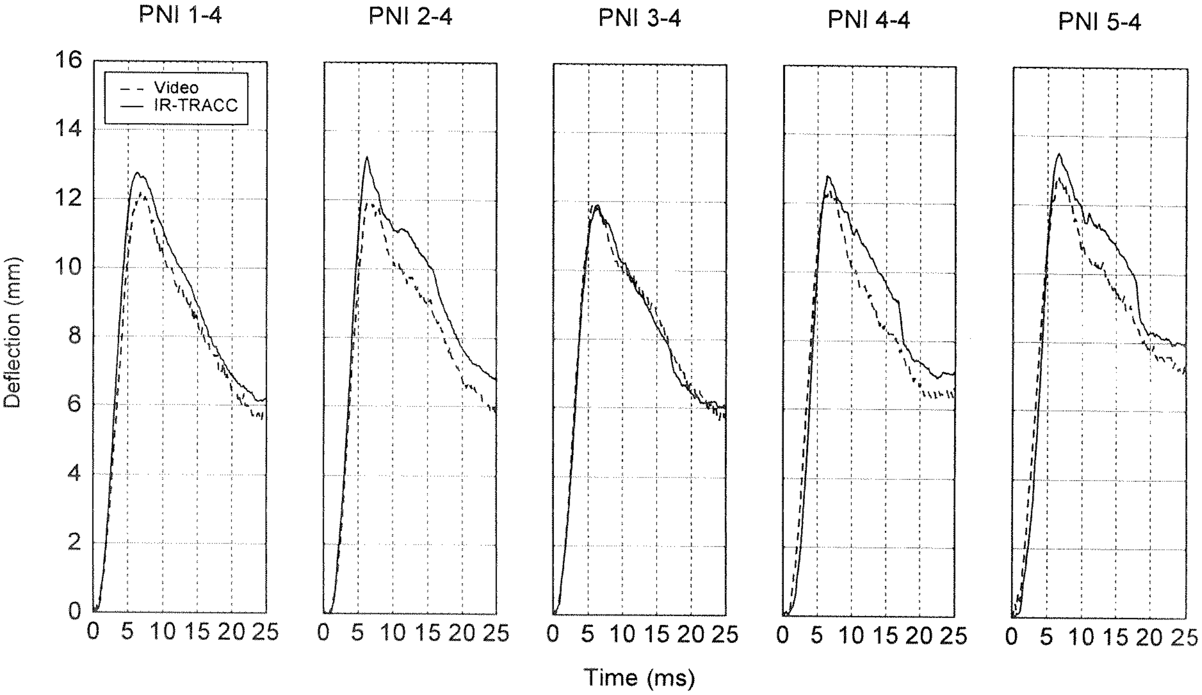

Figure 12a. IR-TRACC deflection-time histories from 4 m/s pneumatic impactor tests overlaid on displacement-time histories from high-speed video images tracked at 9000 frames/second.

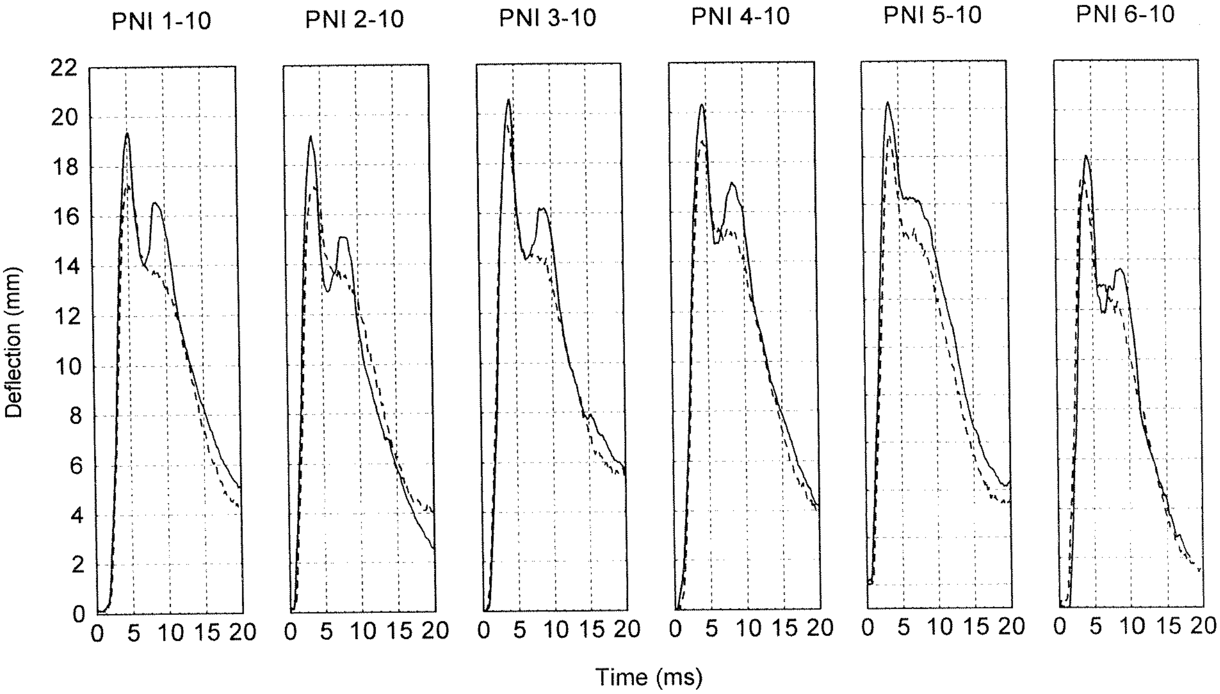

Figure 12b. IR-TRACC deflection-time histories from 10 m/s pneumatic impactor tests overlaid on displacement-time histories from high-speed video images tracked at 9000 frames/second.

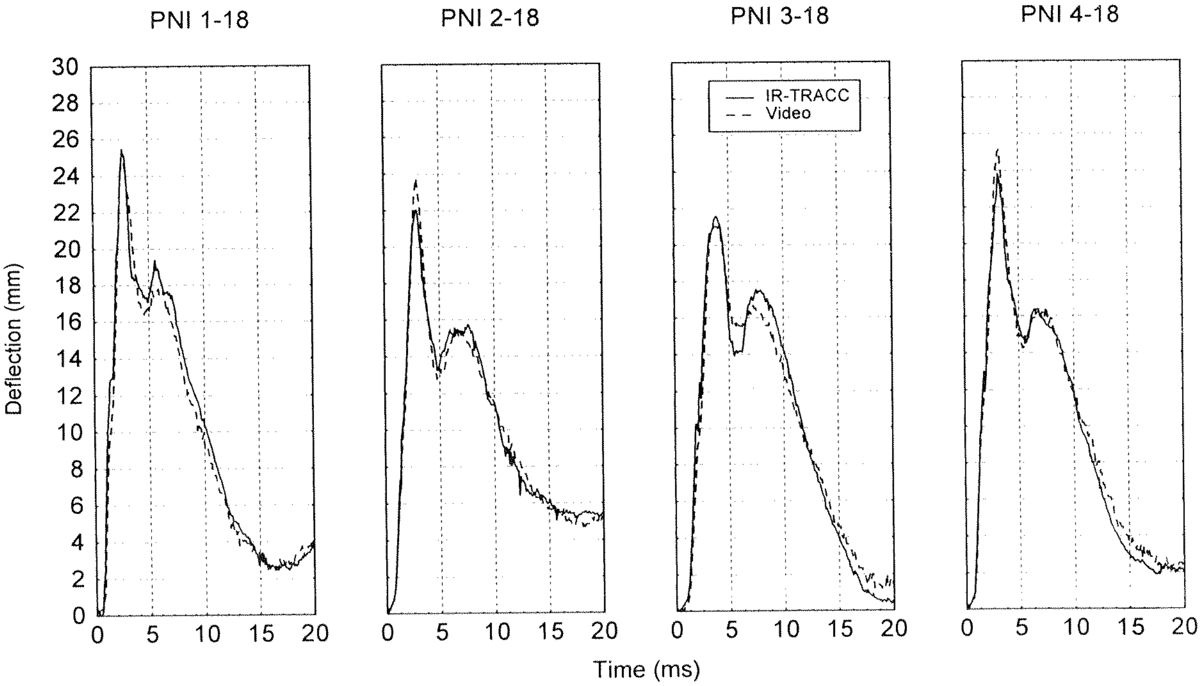

Figure 12c. IR-TRACC deflection-time histories from 18 m/s pneumatic impactor tests overlaid on displacement-time histories from high-speed video images tracked at 9000 frames/second.

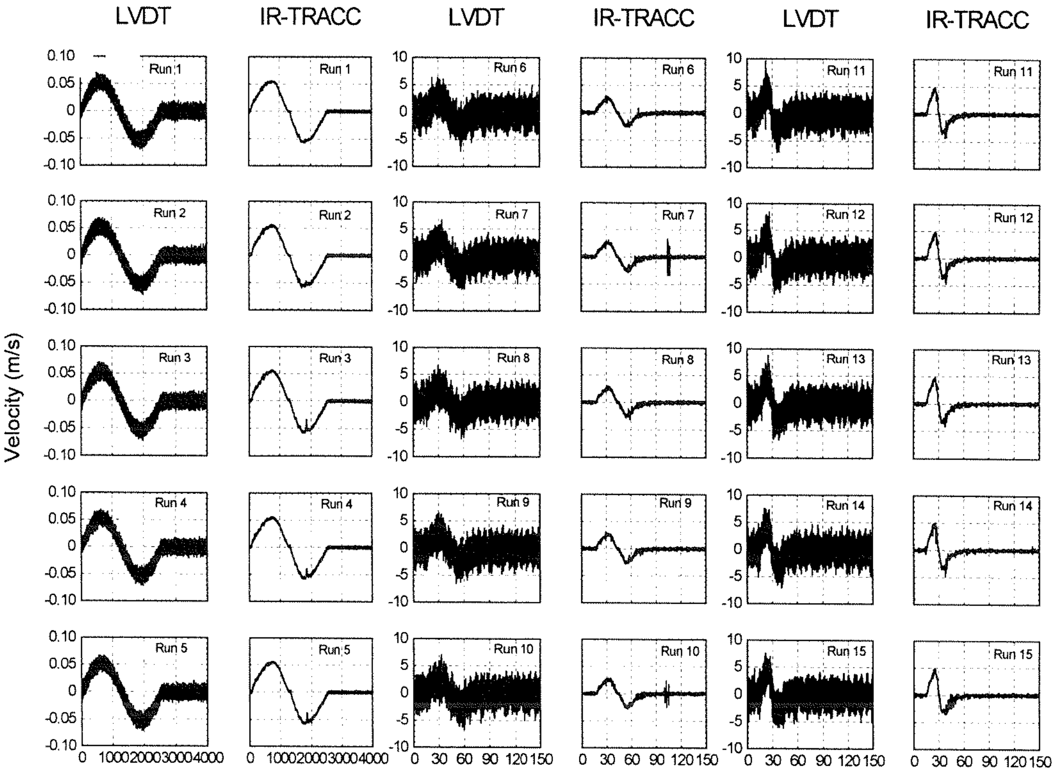

Figure 13. MTS/LVDT and IR-TRACC velocities from differentiated displacement-time histories for each test at each speed on the MTS. Both displacement-time histories were filtered at SAE Channel Class 600. The first, third and fifth columns are MTS/LVDT data. The second, fourth and sixth are IR-TRACC sensor data.

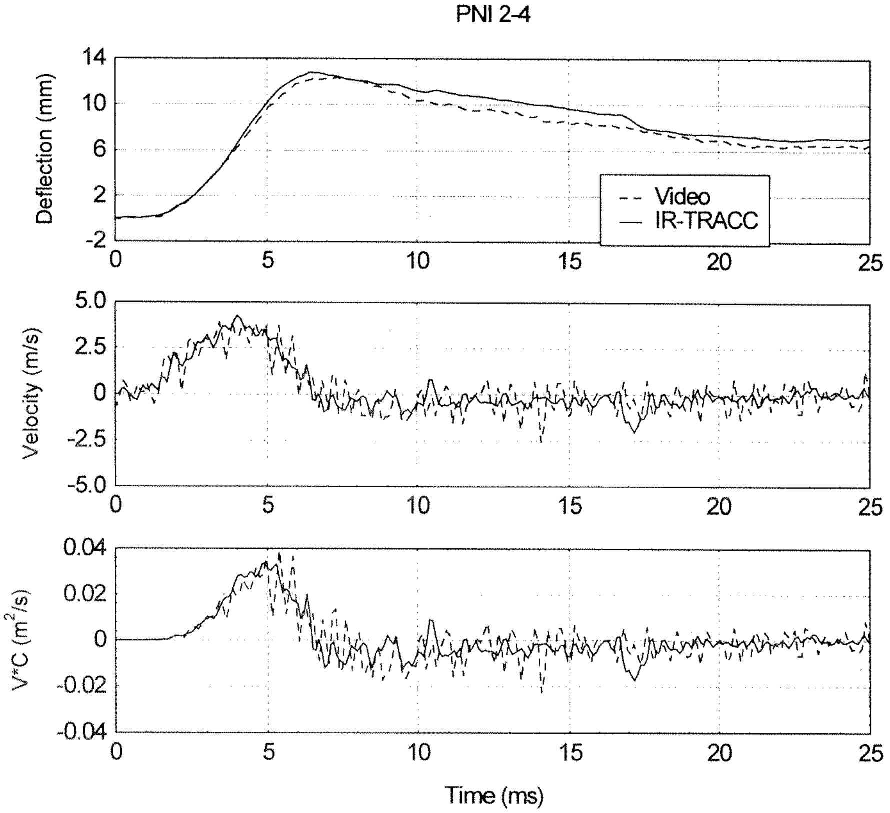

Figure 14. Expanded displacement-time history for IR-TRACC in approximately 4 m/s pneumatic impactor test overlaid on displacement-time history from high-speed video tracking at 9000 frames/second.

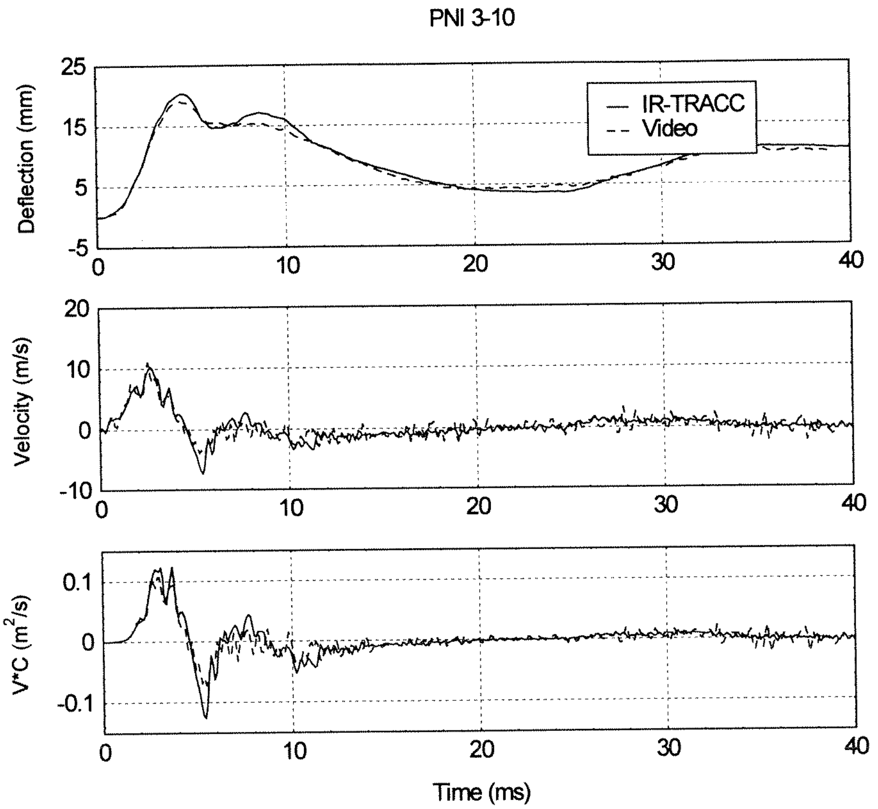

Figure 15. Expanded displacement-time history for IR-TRACC in approximately 10 m/s pneumatic impactor test overlaid on displacement-time history from high-speed video tracking at 9000 frames/second.

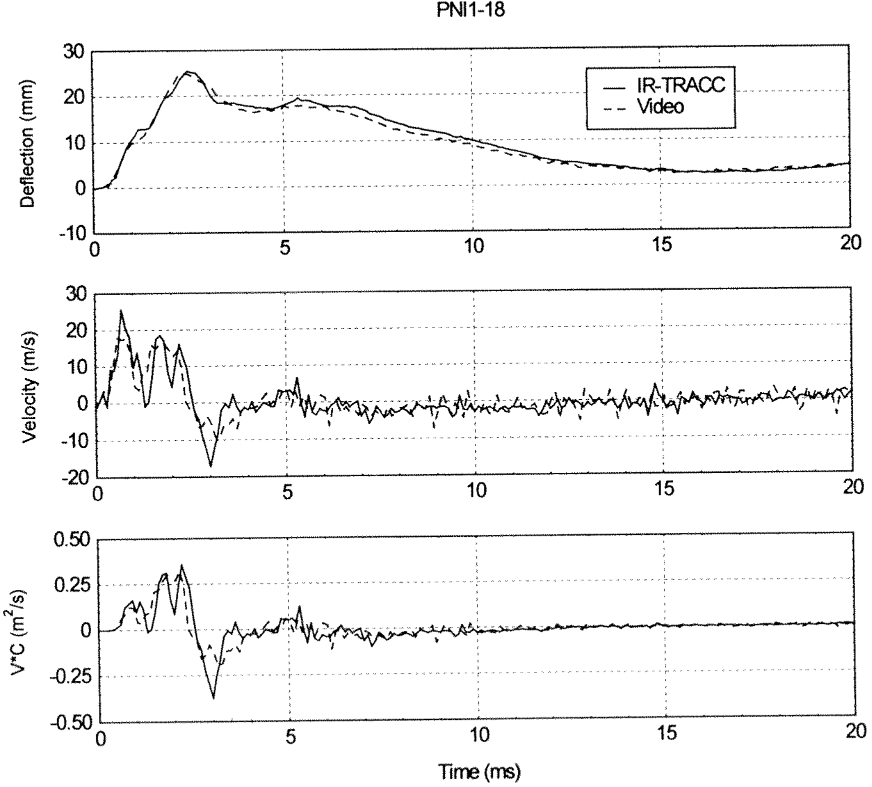

Figure 16a. Expanded displacement-time history for IR-TRACC in approximately 18 m/s pneumatic impactor test overlaid on displacement-time history from high-speed video tracking at 9000 frames/second.

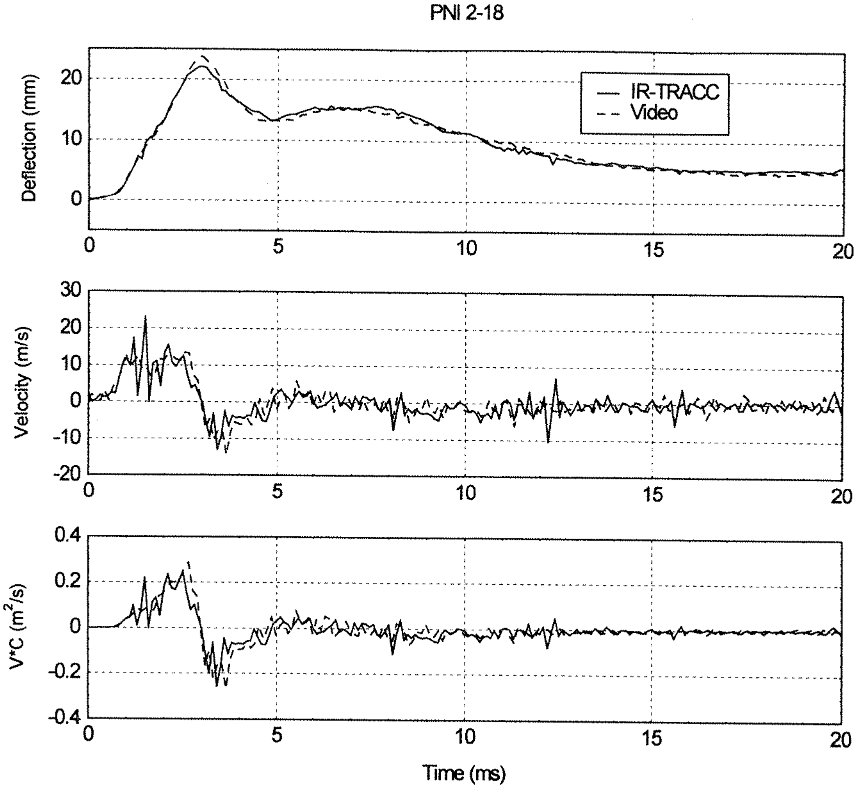

Figure 16b. Expanded displacement-time history for IR-TRACC in approximately 18 m/s pneumatic impactor test overlaid on displacement-time history from high-speed video tracking at 9000 frames/second.

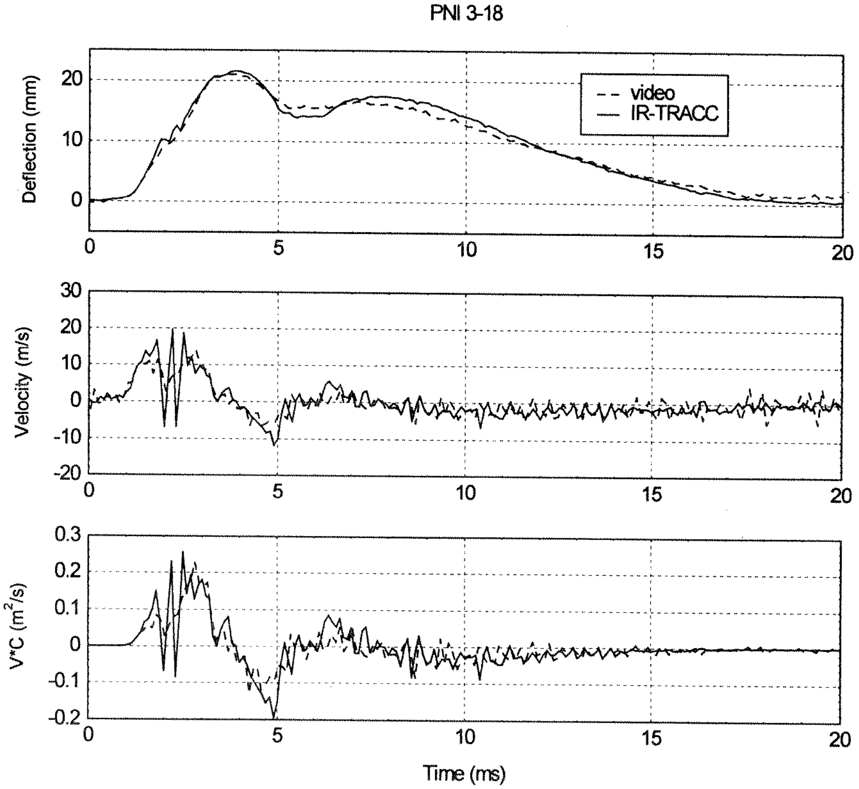

Figure 16c. Expanded displacement-time history for IR-TRACC in approximately 18 m/s pneumatic impactor test overlaid on displacement-time history from high-speed video tracking at 9000 frames/second.

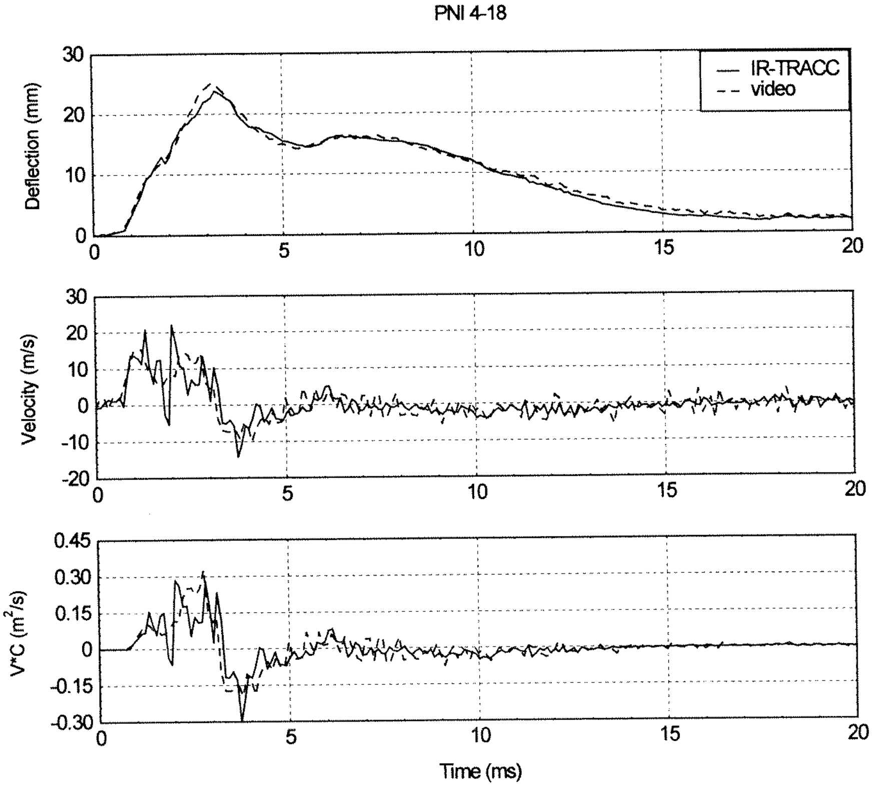

Figure 16d. Expanded displacement-time history for IR-TRACC in approximately 18 m/s pneumatic impactor test overlaid on displacement-time history from high-speed video tracking at 9000 frames/second.

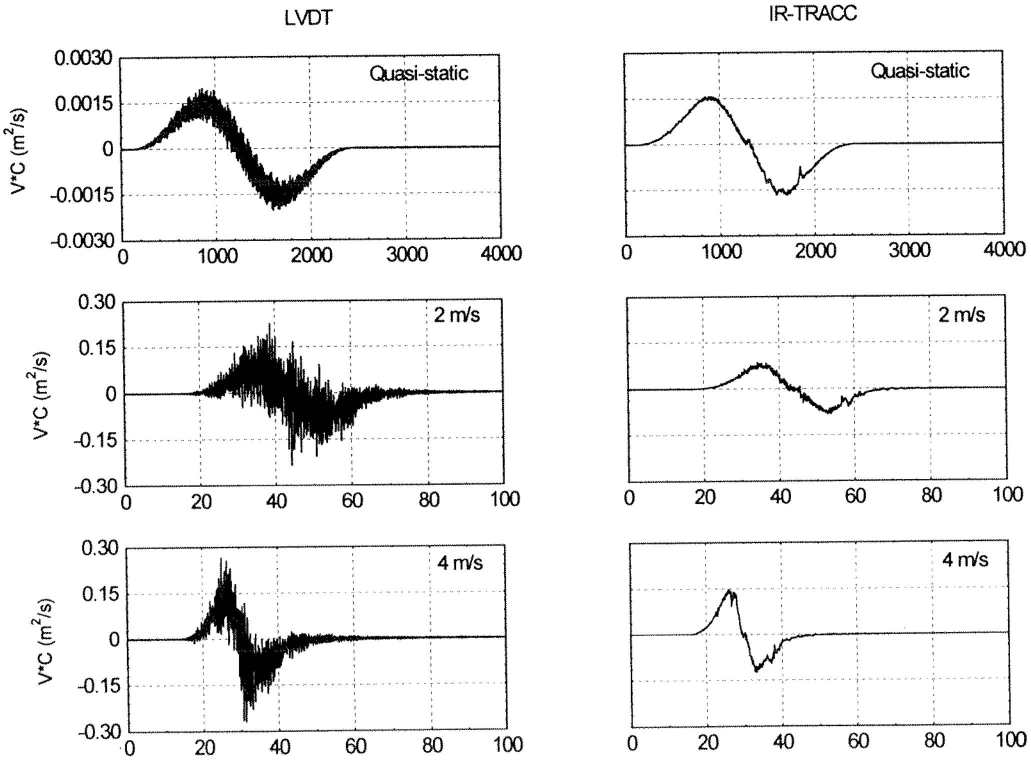

Figure 17. Viscous response calculated from IR-TRACC and MTS/LVDT for one MTS test at each speed in LED-to-LED Mode.

DISCUSSION

A major advantage of this system over those previously attempted is its ability to track motion under very rigorous conditions (pneumatic impactor at speeds in excess of 18 m/s). In addition, its output is linear with displacement allowing for easy calibration. And, the output can be coupled with the output from the gimballed rotary potentiometers to give a complete 3-dimensional motion description for the point on the chest to which it is attached. Nevertheless, testing of these prototype parts led to observation of some issues which must be addressed by whatever company decides to manufacture the IR-TRACC system. Some of the strengths and weaknesses of the system are discussed below.

Linearity of the System

The linearity of the LED-to-LED Mode IR-TRACC system is shown for a typical test in Figure 11. The indicated versus actual displacement for the current articulated arm chest deflection transducer in the Hybrid III dummy is shown in Figure 18 (data scaled from [3]). The IR-TRACC is clearly as good as the current chest potentiometer in linearity. The error associated with the articulated arm chest deflection transducer was stated as a 1.53% "mechanical error".

There is a physical limitation of all IR-TRACC systems at small separations. The inverse square law begins to break down when the sensor and LED move too close together. The reason for this change is that as the source LED approaches the sensor LED or phototransistor, the source LED no longer resembles a point source. That is, the LED emission semiconductor has a finite area that becomes more and more apparent to the sensor as their separation distance decreases. The point source then becomes a distributed source with a divergence that is not as well-characterized using the inverse square law.

To reduce the chance for errors due to non-linearity, several design factors should be considered. First, the LEDs can be recessed to the extent possible to prevent them from ever getting too close. Second, the length of the rod for a given dummy should exceed the distance for which a deflection measurement is desired. This may be a packaging challenge for the child dummies, but for the larger dummies such as the small female through large male, it should not be an issue.

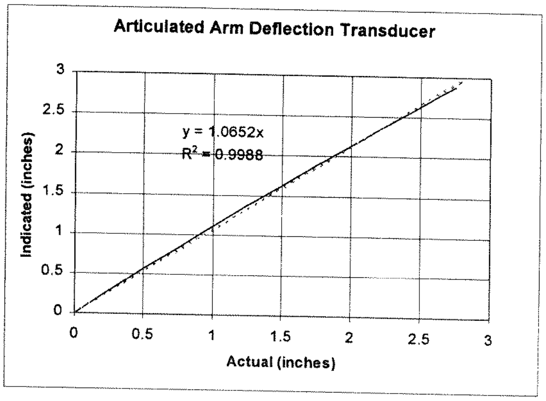

Figure 18. Hybrid III articulated arm calibration curve

Sensitivity

While under normal conditions sensitivity in a test instrument is good, results from an instrument which is more sensitive than its predecessors can cause some confusion until the users gain experience with it. This is evidenced in the IR-TRACC system as seen in Figures 16a-d. In the early phase of loading under the pneumatic impacts, there appears to be a small unloading of the sensor such that the displacement actually decreases by around 1 mm before increasing again. This motion was especially clear in the velocity-time history (middle graphs). It is only slightly apparent in the video data as a change in slope.

Given the unexpected result, we attempted to understand whether that rearward motion was real. To do this we reviewed the high-speed video motion at the time of the supposed rearward motion of the sensor. We concluded that the motion was real for one of two reasons, and possibly for both reasons.

The first hypothesis is that the nature of the loading caused the rearward motion. As shown in Figure 9, the pneumatic impactor did not strike the loading plate at its center of mass. As a result, what we observed in the high-speed video was that the top of the loading plate tilted away from the impactor before the entire plate started to move. Then, when the top of the loading plate struck the channel piece to which the base of the sensor was attached, some rearward rotation relative to the bottom of the plate appears to have begun. This contact occurred at exactly the time of the rearward motion in the displacement-time curves. Then, the realigning of the loading plate appears to have allowed rearward motion of the sensor.

The second hypothesis is that the small amount of play in the linkage of the rod noted earlier might have allowed for a vibration upon impact of the loading plate which could have been on the same order of magnitude as that observed.

The video system did not track this motion as precisely as the IR-TRACC for two main reasons which we believe were cumulative. First, the video data was sampled less frequently (9,000 frames/second vs. 10,000 samples/second for IR-TRACC). Second, the Image Express analysis resolution in our setup was approximately 0.25 mm.

Therefore, we believe that what the IR-TRACC recorded was a real mechanical event (not electrical noise).

If that is the case it highlights a difficulty with calculating the viscous response with a more accurate instrument than before. While we don't expect this type of motion in a dummy chest, this system will track motion that previously may have been unnoticed. Yet, the velocity associated with such small displacement changes is probably not important for assessment of injury risk unless the velocity approaches the blast regime. Therefore, at a minimum, the viscous response determined in crash tests with this instrument should be examined in the context of the displacement-time history recorded. If there are large velocities caused by small displacement changes, the viscous response information should be examined carefully.

Durability of Rods

All of the Transmission, Ruggedized and LED-to-LED Mode tests described in this paper were run with a single telescoping rod (Reflection Mode tests were performed with a different rod). This single rod was subjected to more than 150 tests including MTS, calibration pendulum and pneumatic impactor. For each series of tests using a new configuration, the photoelectric components of the rod were removed and replaced with the new sensors within the same mechanical system. Even with the gimballing on both ends of the rod, the higher speed MTS tests and the pneumatic impactor tests were especially severe. The 20 m/s pneumatic impactor tests were more severe than any tests ever expected in a dummy chest.

Given this environment, it is not surprising that two durability issues surfaced during the testing. The first issue was the durability of the gimbals used at the small end of the rod. The initial design used a welded ball configuration (Figure 19) which gave excellent range of motion to this joint at lower speeds. However, it could not withstand the harsh acceleration environment of the pneumatic impactor. After several tests on the pneumatic impactor the welds broke and the connection failed. This gimbal was modified to a ball joint which proved to be very durable for the remainder of the tests (Figure 20).

A second durability issue was with the rod itself. The rod performed flawlessly for more than 120 tests. After those, during one MTS test series, the linkages at the end of the rod were locked to reduce mechanical play. We noted that the rod started to bind after these tests, probably because we had reduced the degrees of freedom of the rod during the MTS stroke which may have caused the rod to bend under the large forces of the MTS piston. Despite the binding of the rod, we were able to conduct an additional 30 tests on the MTS in the LED-to-LED Mode.

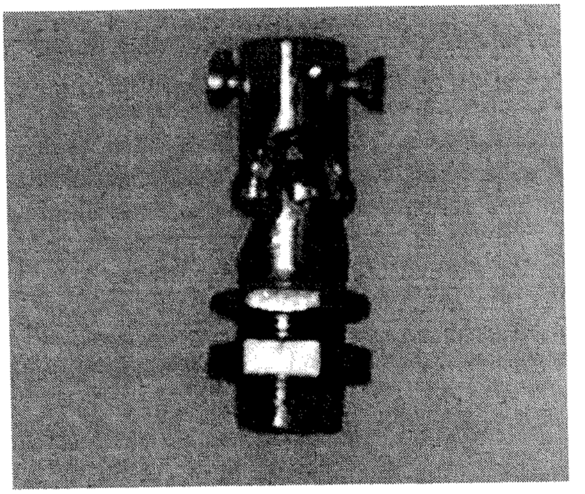

Figure 19. Welded ball gimball used in Transmission Mode tests.

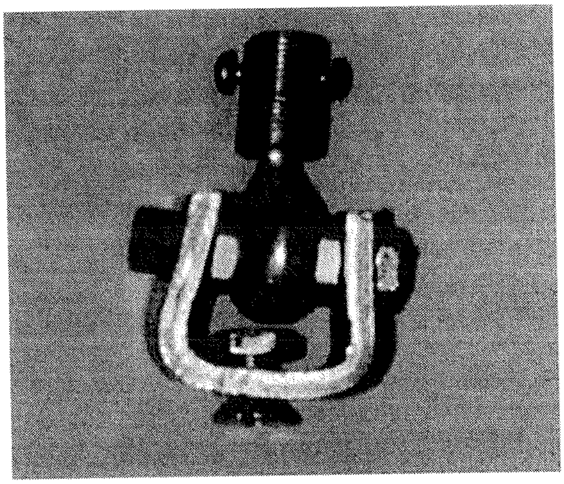

Figure 20. Ball joint gimball used in LED-to-LED Mode tests.

The ball joint linkage at the smaller end of the rod had a small amount of axial play in it when loaded. Because of this play in the rod, during the last 30 LED-to-LED tests when the rod would bind, the linkage would be loaded more heavily and would "give" slightly. The combination of these two factors (binding and "give") led to small differences (≤ 1 mm) between the maximum deflections recorded by the IR-TRACC system when compared to the MTS and high-speed video (see 5 m/s tests in Figure 10). These differences were more apparent at the higher test speeds. In a production system, more precise machining should eliminate the free axial play in the rod linkage. In addition, since this test environment was more rigorous than any expected in the dummy chest, the binding of the rod should not be an issue.

While the mechanical rod components did have some durability issues, the solid state LEDs proved to be quite rugged. In fact, in all of the bench testing, both on the MTS and with the pneumatic impactor, the LEDs never failed, even under severe impacts that caused the steel rod to fail. The reason for this can be seen in the construction of the LEDs. In a typical LED the photodiode is covered by a firm silicone gel and then completely encapsulated in a rigid plastic molding that also serves as a lens. The plastic also encapsulates the small wires inside the LED which prevents them from breaking or being exposed to any differential motion during large accelerations.

In contrast, the Transmission and Reflection Mode phototransistors are simply bonded to the can that contains them. When these systems were tested on the MTS and pneumatic impactor, acceleration-induced anomalies appeared in the deflection-time histories as seen for a Reflection Mode sensor in Figure 21 (the "blips" on the rising portion of the curve). In one test, the active sensor element completely debonded from the case and was connected only by the wire making the electrical connection to one of the leads. This type of behavior would make the data from these sensors unsuitable for differentiation and calculation of the viscous response.

Because of this acceleration sensitivity, work on the Transmission and Reflection Modes was stopped and a search was made for commercially available ruggedized sensors. No ruggedized sensor with high enough sensitivity could be found. Therefore, we attempted to ruggedize the sensors ourselves. To do this we removed the lens from the phototransistor can and filled the can with clear epoxy. While the epoxy did remove the acceleration sensitivity of the sensor, it changed the optics to such an extent that the results were less linear with distance (Figure 22). Although this was a less than desirable result, it did highlight the fact that if a commercially available ruggedized sensor can be obtained, the durability issue with the Transmission and Reflection Mode sensors will be eliminated.

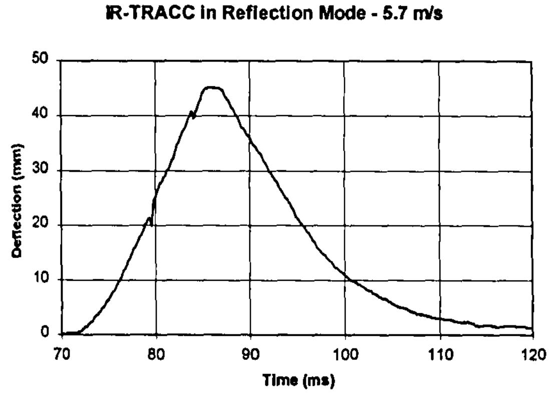

Figure 21. Example of an acceleration-induced anomaly in Reflection Mode.

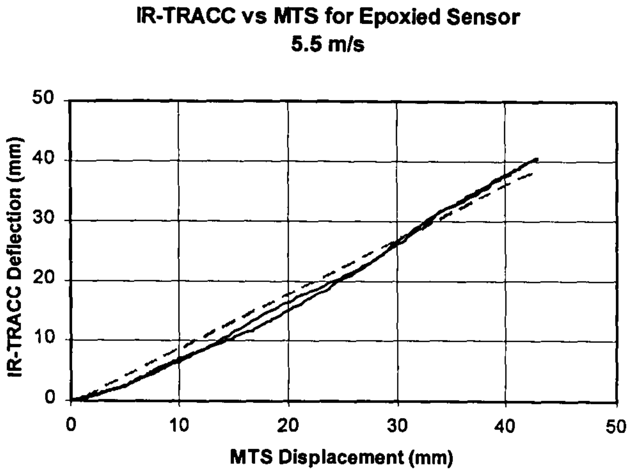

Figure 22. Example of linearity in Ruggedized Transmission Mode (dashed line is trend line).

Reflections

One of the earliest issues to arise with the IR-TRACC system, when the work was focusing on longer rods, was reflection of the infrared light from the sides of the telescoping rod. These reflections were apparent as a non-linearity in the deflection-time history data. The main cause of the reflections was the beam divergence of the LED in the telescoping rod. If the beam divergence angle is large enough and the rod is long enough, because the diameter of the rod must be kept small, the beam will strike the wall of the rod and reflect off. This reflected light will then add to the light that the sensor "sees" by inverse square law behavior and will confuse the output from the sensor. That is, during chest compression the light initially detected by the phototransistor is a combination of the inverse square law intensity and the reflected intensity. As the rod collapses, however, there will be a point at which the beam becomes narrow enough to eliminate the reflections. At that point there would be a change in the detected intensity which would be evidenced as an anomaly in the time-history data. For a short enough rod, there should be no reflections.

In Transmission Mode, the reflection problem was greatly reduced by interchanging the locations of the LED and phototransistor. The reason this worked is believed to be because when the LED is at the wider end of the rod, the light travels toward a diameter which decreases as discrete step functions as it passes through the different segments of the rod. The reflected light is most likely at too large an angle to be reflected into the continually narrowing segments of the rod and the light that strikes the ends of the segments is reflected back away from the sensor.

This information about intra-rod reflections highlights one of the design criteria for the IR-TRACC system. The LED beam divergence angle with respect to the length of the rod should be optimized to the size of the sensor. The sensor may not work as well if the beam is too narrow or too wide.

The reflection problem was also nearly eliminated using the Reflection Mode. The main reason is probably due to the collimating effect of the custom-designed fiber optic cable. This effect tends to reduce the beam divergence at the aperture of the cable relative to the divergence at the LED. Then, the light that exits towards the retro-reflective tape is more focused than without the fiber optic cable.

There was no sign of reflection-induced anomalies in the data for the LED-to-LED Mode IR-TRACC system.

Effect of Lateral Play in the Rod ("Wiggle")

Another issue, which was apparent in the early designs of the IR-TRACC, is what has been called lateral play or "wiggle". Wiggle is a phenomenon that occurs when the rod is moved side-to-side rather than in a telescoping fashion. That is, if one were to hold onto the base of the rod and the tip of the rod and move them laterally in opposite directions, ideally there should be no output from the sensor. In the Transmission Mode sensor design, however, there was some output due to wiggle. The wiggle was greatly reduced in the Reflection and in the LED-to-LED Modes relative to the Transmission Mode. Figure 23 shows the deflection output caused solely by lateral motion of the 6 year old size rod without any telescoping for the Transmission, Reflection and LED-to-LED Modes, respectively. As seen in the figure, the maximum error introduced by wiggle is approximately ±1.0 mm in Transmission Mode, ±0.2 mm in Reflection Mode, and ±0.3 mm in LED-to-LED Mode.

The causes of the wiggle problem appear to be: first,

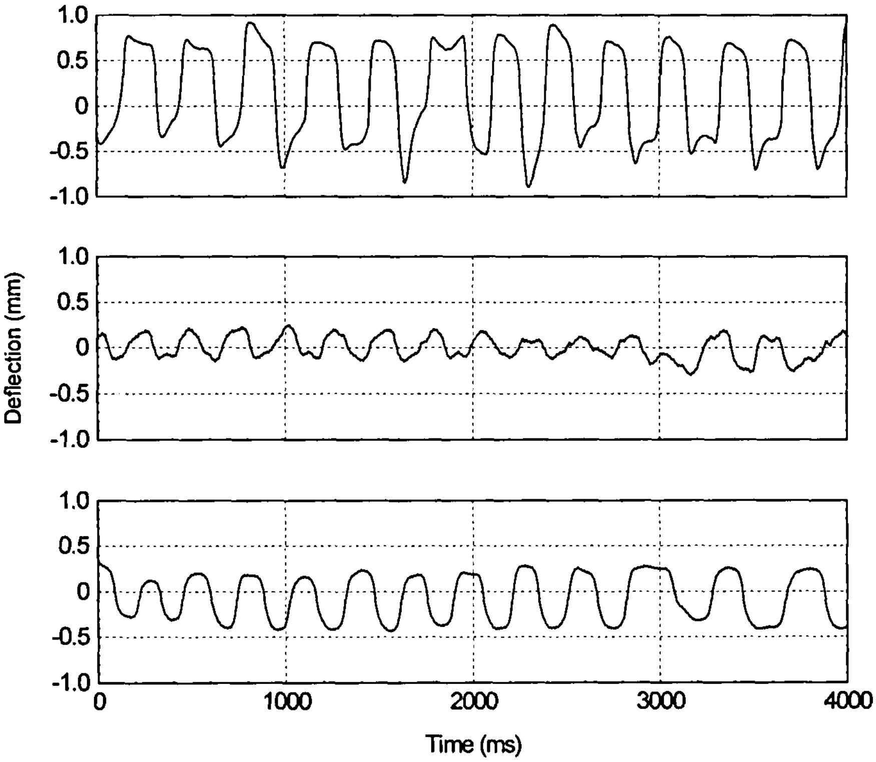

Figure 23. "Wiggle" test of IR-TRACC telescoping rod for: Transmission Mode (top graph), Reflection Mode (middle graph) and LED-to-LED Mode (bottom graph). Note that for the LED-to-LED Mode, the magnitude of the sensitivity to "wiggle" is less than approximately ± 0.3 mm.

the need for clearance between the sections of the telescoping rod in order to facilitate motion; and second, the lack of uniformity in the beam intensity in some LEDs. The clearance between segments of the rod is a necessity. The original design, however, used more small segments and fewer large segments. The resulting overlap between segments was very small and the rod was very susceptible to wiggling. The current LEDs being utilized appear to have sufficient intensity uniformity to reduce the concern over wiggle-induced output.

Thermal Changes in LEDs

Light Emitting Diodes are known to be sensitive to thermal changes. We attempted to see if this would affect the LED-to-LED Mode of the IR-TRACC by running two sets of experiments. In the first experiments, we ran three tests sequentially in which the ambient temperature was held constant and we recorded the output of the IR-TRACC system. Then we repeated the tests with a rack of sled lights one meter away with 4 kW of lights turned on. The results of these tests are shown in Figure 24. Two conclusions were drawn from these experiments. First, when the lights are off (no added heat) the IR-TRACC is very stable. Second, when the rod is exposed to the lights, the sensitivity changes, but the sensitivity remains a linear function of distance as can be seen by the virtually identical slopes, but increasingly negative y-intercepts.

The second set of experiments was done to assess the effectiveness of the dummy chest skin in thermally shielding the IR-TRACC system. This was done by again exposing the rod to 4 kW of sled lights at a distance of one meter. Again we ran a test of no heat added to examine baseline stability, which again was excellent (Figure 25, top graph). Then with no chest skin on the dummy, the lights were turned on for 40 seconds and temperature and output monitored. As seen in the middle graph of Figure 25, the IR-TRACC output did increase with temperature, but in a linear fashion and with a slope of approximately 0.06 mm/second.

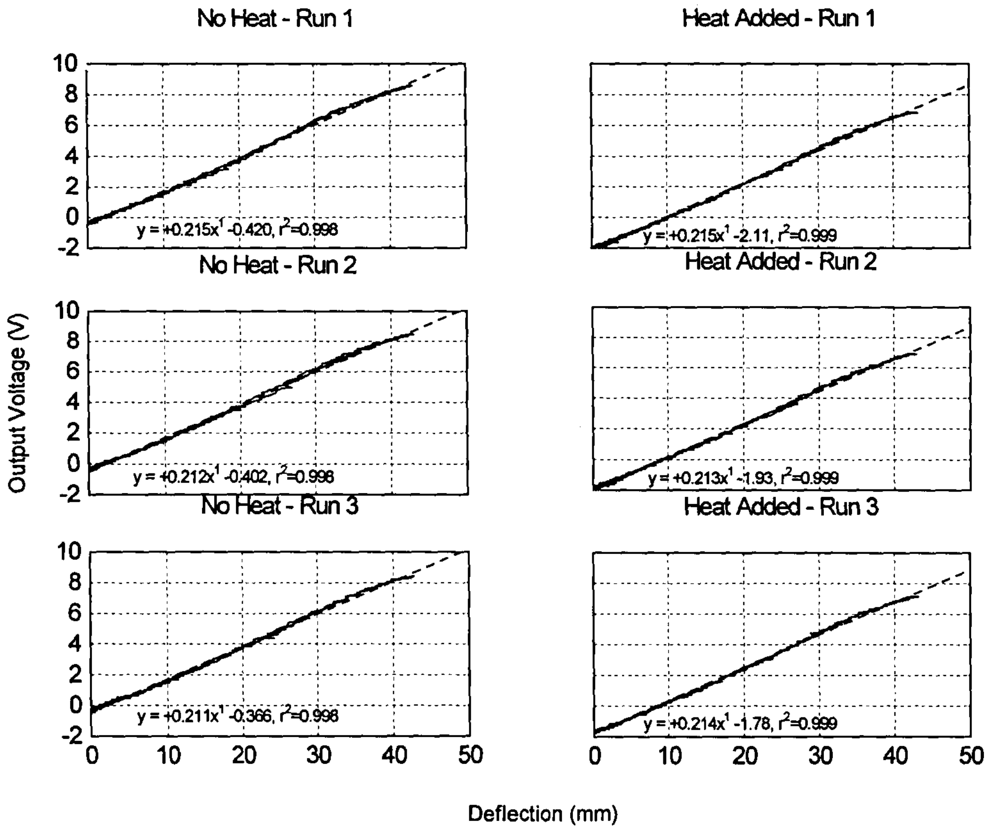

Figure 24. Cross-plots of output voltage from IR-TRACC in LED-to-LED Mode during quasi-static tests on the MTS with application of heating by 4 kW of sled lights (right column of graphs) and without any heat added (left column of graphs). Tests were done sequentially, 3 with no heat first, followed by 3 with heat. Note that the y-intercept changes with the addition of heat, but the slope of the line (i.e., the sensitivity of the transducer) does not.

In practice, sled lights are only on for around 5 seconds, and the IR-TRACC rod will be in the dummy chest under simulated flesh and clothing. This should help to insulate the sensors for the short time periods of a typical sled test. Our next test showed this to be true (Figure 25, bottom graph). With the dummy chest skin and lights on (i.e., heat on), the increase in IR-TRACC output as a function of time was reduced by approximately two orders of magnitude to 0.008 mm/second. For a typical sled test then, the effect of the heat from sled lights would be a maximum error of approximately 0.035 mm.

Our "bake" test showed that the IR-TRACC system should be virtually insensitive to temperature changes during routine sled testing. But, although the sensitivity of the transducer changes, the behavior is still a linear function of distance with no notable change in slope (Figure 24). Therefore, if a test environment is to be used which is outside the normal range of laboratory temperatures, the sensor only needs to be zeroed and calibrated at that temperature and it will still function as designed.

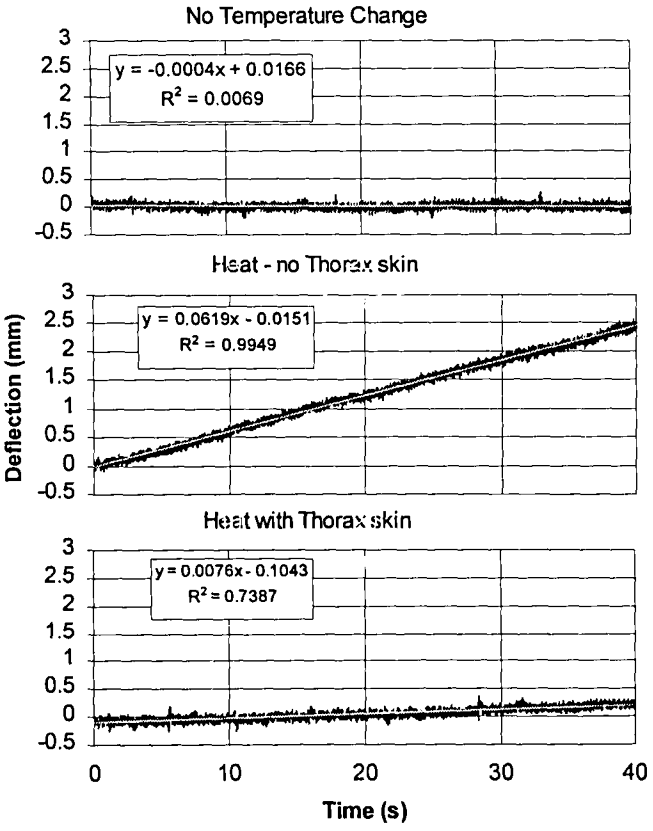

Figure 25. IR-TRACC sensor in dummy with no lights, no temperature change and no motion (top graph). IR-TRACC sensor inside dummy with no chest jacket, 4kW of light at a distance of one meter and no motion (middle graph). IR-TRACC sensor inside dummy with chest jacket, 4 kW of light at a distance of one meter and no motion (bottom graph).

If automatic temperature compensation is desired, a blinded, reversed-polarity compensating LED could be put in parallel with the sensing LED. Then, since it could not be affected by light, any output changes by the LED would be due to temperature alone. Assuming identical thermal sensitivities, the reversal of polarity would then allow thermally induced output from the compensating LED to exactly null out any thermally induced output from the sensing LED.

Accuracy of the System

Several attempts were made to understand the accuracy of the IR-TRACC system. This was difficult to achieve because there was no objective standard with which to compare. We decided to use the LVDT for the MTS tests and ultra high-speed video for the pneumatic impactor tests.

As shown in the Results section, the maximum difference between the IR-TRACC measured deflections and the LVDT measured displacements from the MTS tests was 3.35 mm. The standard deviation ranged from ± 0.6 to ± 0.9 mm. We believe that the major factor contributing to this difference is the previously mentioned axial play in the rod. This play could account for about 1 mm of the difference. Then in a system with a better linkage the maximum error should be less than 2 mm.

The results for the pneumatic impactor tests were similar. In those tests however, the axial play of the rod was eliminated from the data comparison by choosing a target location on the segment of the rod that housed the LED. Whereas the LVDT was compared to the motion of the rod and its linkages, the video data was only compared to the motion of the rod. In this way, the confounding factor of the axial play in the ball joint linkage was eliminated.

The maximum difference in peak displacement between the IR-TRACC and video data was 2.15 mm. The average difference in peak displacement from all of the pneumatic impactor tests was 1.08 mm. It is likely that there were several factors responsible for these differences. Most notably, the video system had a tracking error of approximately 1 mm because our targets were small and good illumination was difficult to achieve. In addition, there was some out-of-plane motion of the entire system noted in review of the videos. This motion was greatest in magnitude during the unloading phase of the event and likely explains the visual differences in the tails of the deflection-time curves from the pneumatic impactor tests. Finally, there may have been some contribution to the difference from the wiggle effect.

In summary, the maximum error attributable to the IR-TRACC device itself appears to be on the order of 1-2 mm. With a maximum chest deflection in a Hybrid III six year old dummy of approximately 42 mm, this represents a maximum error of between 2.4 % to 4.8%

Dummy Modifications to Accommodate the IR-TRACC System

Figure 26 shows the modifications made to the spine of a Hybrid III six-year old child dummy by First Technology Safety Systems to accommodate the IR-TRACC system. Clearly, the bracket for the articulated arm chest deflection transducer is no longer necessary. Installation of the IR-TRACC in the thoracic spine box requires removal of a section of the spine box. The double-gimballing of the rod allows mounting to be accomplished through a simple pin joint.

Applicability

While this work began with frontal impact dummies in mind, the utility of the device we developed does not appear to be restricted to frontal impact. Therefore, it may have broad applicability in side impact dummies and other dummies which will inevitably be created as technology improves.

FUTURE WORK

Implementation in an ATD

Development to-date has consisted of obtaining reasonable output from the system within the telescoping rod. Plans for the future are to incorporate this device into Hybrid III dummies of various sizes for continued testing and into the second generation advanced dummy from the NHTSA (THOR). Since the string potentiometer in the DGSP is much bulkier than the LEDs used here, the fit and range of motion in the Hybrid III and THOR should be improved over that in the original Advanced dummy.

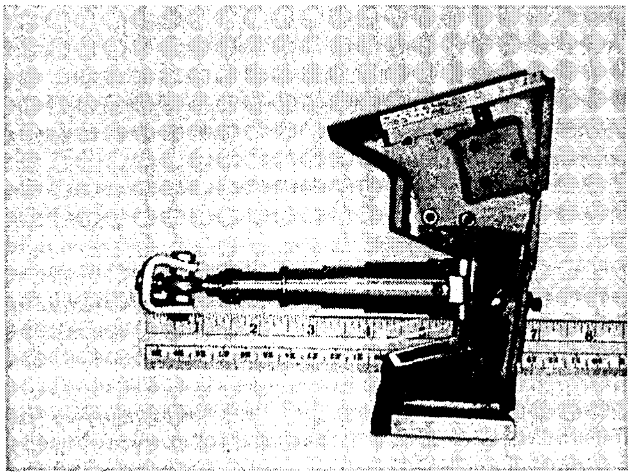

Figure 26. Modified spine box of Hybrid III six year old child dummy.

Multiple Units in a Single Chest

Backaitis and St.-Laurent [6] performed a series of experiments aimed at elucidating the relationship between Hybrid III dummy-measured chest deflection and actual human volunteer chest deflection in similar loading situations. They pointed out that the Hybrid III chest deflection gauge underestimated the amount of deflection when the loading surface was angled and not acting in the sagittal plane of the dummy and when the surface area of the impact probe was small. An approach similar to that taken by Schneider et al. [1] which used multiple measurement locations would eliminate this issue. While the current articulated arm deflection transducer would not be easy to adapt to such a scenario, the IR-TRACC should be easily adapted to measure deflection at multiple locations.

Therefore, after testing with a single IR/TRACC in the Hybrid III mid-sized male dummy's chest, installation of multiple units will be attempted.

SUMMARY AND CONCLUSIONS

This research has led to the development of a new method for measuring chest deflection in automotive crash test dummies. Data presented in this paper shows that the IR-TRACC system allows measurement of chest deflection at speeds in excess of 18 m/s. Data obtained with this system also meets the design goal of providing a differentiable signal for viscous response calculations. The maximum error in the system is on the order of 1 to 2 mm, or 2.4% to 4.8% of full scale for a Hybrid III six year old child dummy chest.

The system is easy to use and calibrate and requires no special data acquisition. The concept development is essentially complete and has been applied to a Hybrid III 6-year old child dummy. A round robin test series will be initiated as soon as practical, through the SAE Chest Deflection Task Force of the Human Biomechanics and Simulation Standards Committee. Then utilizing the experience gained in that series, work will begin to scale the device for use in other size dummies to allow all families of frontal and side impact dummies to benefit from this improved method of measuring chest deflection.

REFERENCES

1. Schneider, L.W., Haffner, M.P., Eppinger, R.H., Salloum, M.J., Beebe, M.S., Rouhana, S.W, King, A.I., Hardy, W.N., and Neathery, R.F.: "Development of an Advanced ATD Thorax System for Improved Injury Assessment in Frontal Crash Environments", Proceedings of the 36th Stapp Car Crash Conference, SAE Technical Paper Number 922520, 1992. pp. 129-156.

2. McElhaney, J.H., Mate, P.I., and Roberts, V.L.: "A New Crash Test Device – Repeatable Pete", Proceedings of the 17th Stapp Car Crash Conference, SAE Technical Paper Number 730983, 1973. pp. 467-507.

3. Woley, P.F.: "Development of an Articulated Arm Chest Deflection Transducer", GM Environmental Activities Staff Publication Number A-3340, 1976.

4. Foster, J.K., Kortge, J.O., and Wolanin, M.J.: "Hybrid III – A Biomechanically-Based Crash Test Dummy", Proceedings of the 21st Stapp Car Crash Conference, SAE Technical Paper Number 770938, 1977. pp. 975-1014.

5. Wiechel, J.F., Bell, S., Pritz, H., Guenther, D.: "Enhancement of the Hybrid III Dummy Thorax", Proceedings of the 29th Stapp Car Crash Conference, SAE Technical Paper Number 851732, 1985. pp. 147-158.

6. Backaitis, S.H., and St-Laurent, A.: "Chest Deflection Characteristics of Volunteers and Hybrid III Dummies", Proceedings of the 30th Stapp Car Crash Conference, SAE Technical Paper Number 861884, 1986. pp. 157-166.

7. Ogata, K., Chiba, M., Kawai, H., Asakura, F.: "Development of a Sternum Displacement Sensing System for Hybrid III Dummy", Proceedings of the Thirteenth International Technical Conference on Experimental Safety Vehicles, SAE Technical Paper Number 916124, 1991. pp. 947-956.

8. Minutes of the SAE Chest Deflection Task Force of the Human Biomechanics and Simulation Standards Committee, 1995-1996.

9. Stalnaker, R.L., Tarrière, C., Fayon, A., Walfisch, G., Balthazard, M., Masset, J., Got, C., and Patel, A.: "Modification of Part 572 Dummy for Lateral Impact According to Biomechanical Data", Proceedings of the 23rd Stapp Car Crash Conference, SAE Technical Paper Number 791031, 1979. pp. 843-872.

10. Grosch, L.: "Chest injury Criteria for Combined Restraint Systems", 1985 Government/Industry Meeting, SAE Technical Paper Number 851247, 1985.

11. Grosch, L., Katz, E., Kassing, L., Marwitz, H., and Zeidler, F.: "New Measurement Methods to Assess the Improved Protection Potential of Airbag Systems", in SAE Publication SP-690: *Restraint Technologies – Front Seat Occupant Protection*, SAE Technical Paper Number 870333, 1987. pp 161-166.

12. Eppinger, R.H.: "On the Development of a Deformation Measurement System and Its Application Toward Developing Mechanically Based Injury Indices", Proceedings of the 33rd Stapp Car Crash Conference, SAE Technical Paper Number 892426, 1989. pp. 21-28.

13. Fayon, A., Tarrière, C., Walfisch, G., Duprey, M., and Balthazard, H.: "Development and Performance of the APR Dummy (APROD)", Proceedings of the Eighth International Technical Conference on Experimental Safety Vehicles, Wolfsburg, SAE Technical Paper Number 806041, 1980. pp. 451-462.

14. Nielson, L., Lowne, R., Tarrière, C., Bendjellal, F., Gillet, D., Maltha, J., Cesari, D., Bouquet, R.: "The EUROSID Side Impact Dummy", Proceedings of the Tenth International Technical Conference on Experimental Safety Vehicles, Oxford, SAE Technical Paper Number 856029, 1985. pp. 153-165.

15. Lau, I.V., Viano, D.C., Culver, C.C., and Jedrzejczak, E.A.: "Design of a Modified Chest for EUROSID Providing Biofidelity for Injury Assessment", in Side Impact: Injury Causation and Occupant Protection, SP-769, SAE Technical Paper Number 890991, 1989. pp. 163-171.

16. Beebe, M.S.: "What is Biosid?", SAE Technical Paper Number 900377, 1990.

17. ISO/TC22/SC12/WG3: "Measurement of Deflection with Integration of Accelerations", Document N303, 1994.

18. Chappell, A. (ed.): "Optoelectronics – Theory and Practice", McGraw-Hill Book Company, New York, 1978.

19. Nunley, W. and Bechtel, J.S.: "Infrared Optoelectronics – Devices and Applications", Marcel Dekker, Inc., New York, 1987.

20. Schilling, D.L., Belove, C., Apelewicz, T., Saccardi, R.J.: "Electronic Circuits – Discrete and Integrated", McGraw-Hill Book Company, New York, 1989.

ACKNOWLEDGEMENTS

This report was prepared by General Motors pursuant to an agreement between GM and the U.S. Department of Transportation.

Many people helped out in the performance of this work. We would like to acknowledge the technical contributions of: Joseph McCleary of the GM R&D Safety Research Department, Anthony Walbridge of Aerotek Lab Support on contract at the GM R&D Safety Research Department, Michael Salloum of First Technology Safety Systems, Larry Oberdier and Michel Sultan of the GM R&D Electrical and Electronics Department, David Roessler of the GM R&D Physics and Physical Chemistry Department and WKM Associates.

APPENDIX I

– Principle of Operation in Transmission Mode

The following discussion is meant to give a more detailed description than the main text, but a still simplified understanding of the principles of operation. The details are considerably more complex than what is presented and are beyond the scope of this work. The reader may review the references cited for additional detail.

Figure 5 illustrates schematically how the system operates. The principle of operation of the system is photo-optical. The LED emits light in the infrared region of the spectrum which exits through a plastic lens that is part of the housing. The rays of light from the LED diverge in a conical pattern with a beam divergence angle of ± 10° as they leave the source. The irradiance of the light as shown in the manufacturer's product data sheet obeys an inverse square law [18]. That is, the irradiance at a plane through which the beam passes is proportional to the inverse of the square of the distance from that plane to the LED. So as the LED is moved closer to the photodiode, or as the distance, **d**, between them decreases, the irradiance, $\mathbf{E_e}$, increases as in Equation I.1.

$$\mathbf{E_e \propto 1/d^2} \qquad \text{(I.1.)}$$

Phototransistors obtain their base current from the photocurrent generated in their collector-base photodiode section. The photocurrent of a non-amplifying junction photocell (the photodiode section of a phototransistor) is proportional to the incident radiant power as in Equation 2 [18].

$$\mathbf{I_D = s(\lambda) * \Phi_e} \qquad \text{(I.2.)}$$

where,

I_D = the photocurrent (in amperes) through the transistor (also across the diode)

Φ_e = the incident radiant power (in watts)

$s(\lambda)$ = absolute spectral photosensitivity for wavelength λ which is a constant for monochromatic light.

But,

$$\mathbf{\Phi_e = E_e * A_E} \qquad \text{(I.3.)}$$

where,

E_e = irradiance (W/m^2) and

A_E = receiver area (m^2) which is also a constant for a given phototransistor.

Combining equations I.2 and I.3 yields:

$$\mathbf{I_D = s(\lambda) * A_E * E_e} \qquad \text{(I.4.)}$$

The spectral emission as a function of wavelength for the infrared LEDs used was a relatively sharp distribution. Then, to a first order of approximation the light can be considered monochromatic. Therefore,

$$\mathbf{I_D \;\alpha\; constant * E_e} \qquad \text{(I.5.)}$$

Thus, the photocurrent is linearly related to the irradiance on the phototransistor.

A diagram showing the amplification circuit for the phototransistor is shown in Figure AI.1. Analysis of the circuit can be performed assuming that the phototransistor behaves like a variable resistor (R_1). Then, the current through the photodiode is related by Ohm's Law to the voltage across it and its resistance.

$$\mathbf{V_D = I_D * R_1} \qquad \text{(I.6.)}$$

So,

$$\mathbf{R_1 = V_D / I_D} \qquad \text{(I.7.)}$$

The output voltage measured after the signal is amplified is given by:

$$\mathbf{V_{out} = -(R_2 / R_1) * V_D} \qquad \text{(I.8.)}$$

Thus combining equations I.6, I.7 and I.8 yields:

$$V_{out} = (R_2 * V_D) / (V_D\ / I_D) \qquad \text{(I.9.)}$$

$$V_{out} = R_2 * I_D \qquad \text{(I.10.)}$$

Putting Equations I.5 and I.10 together yields:

$$V_{out}\ \alpha\ E_e \qquad \text{(I.11.)}$$

Since the irradiance decreases as the inverse square of the distance between the LED and phototransistor, and all other parameters in Equations I.10 and I.11 are constant, then the output voltage is proportional to the inverse of the distance squared.

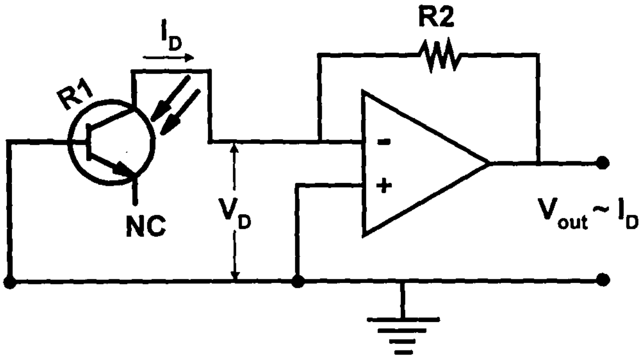

Figure AI.1. Phototransistor amplification circuit.

$$V_{out}\ \alpha\ (1/d^2) \qquad \text{(I.12.)}$$

Then, the distance between the phototransistor and LED is obtained by taking the inverse square root of the output voltage as measured from the amplifier stage of the circuit as shown in Equation I.13.

$$d\ \alpha\ \sqrt{(1/V_{out})} \qquad \text{(I.13.)}$$

APPENDIX II

- Principle of Operation in LED-to-LED Mode

The photocurrent from the photodiode is related to the voltage output by [20]:

$$I_D = I_0(e^{qV_D/mkT} - 1) \qquad \text{(II.1.)}$$

where,
I_0 = reverse saturation current (A)
q = electron charge (1.6×10^{-19} C)
V_D = voltage across the diode (V)
m = an empirical constant between 1 and 2
k = Boltzmann's constant (1.38×10^{-23} J/K)
T = absolute temperature (K).

But, to a first order of approximation this reduces to:

$$I_D \approx a\, e^{bV_D} \qquad \text{(II.2.)}$$

a,b = constants

This implies that:

$$V_D \propto \ln(I_D) \qquad \text{(II.3.}$$

As in Appendix I, the photocurrent, I_D, is directly proportional to the irradiance, E_e. This means that

$$V_D \propto \ln(E_e) \qquad \text{(II.4.)}$$

But, from Equation I.1,

$$E_e \propto 1/d^2 \qquad \text{(II.5.)}$$

Therefore,

$$V_D \propto \ln(1/d^2) \qquad \text{(II.6.)}$$

So, the output voltage of the LED-to-LED Mode system is directly proportional to the natural logarithm of the inverse squared distance between the LEDs. This is mathematically approximated as a linear function of distance as shown in Figure 7 in the text. Therefore, the output from the sensor LED is simply amplified as in the circuit shown in Figure AII.1.

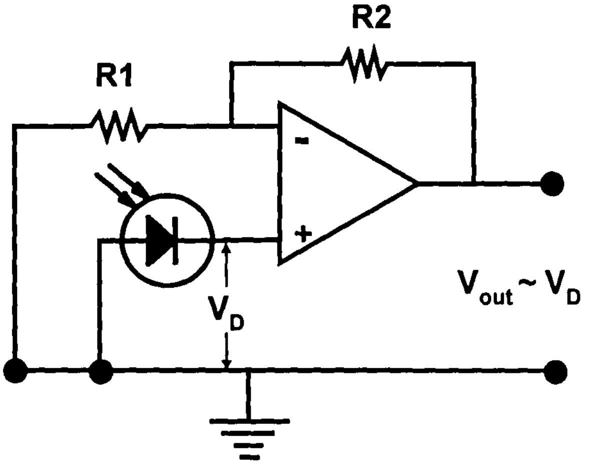

Figure AII.1. LED-to-LED Mode buffer amplifier circuit.

APPENDIX III

- Data For Transmission, Ruggedized Transmission and Reflection Modes

Graphs of all IR-TRACC deflections, for **LED-to-LED Mode** tests at each speed are shown in the main text since that is the system we recommend for use.

Deflection-time histories of all IR-TRACC deflections for **Transmission Mode** tests, overlaid on the MTS displacements at each speed, are shown in Figure AIII.1. A more quantitative measure of the agreement between the IR-TRACC and the LVDT is obtained by cross-plotting the deflections as shown in Figure AIII.2.

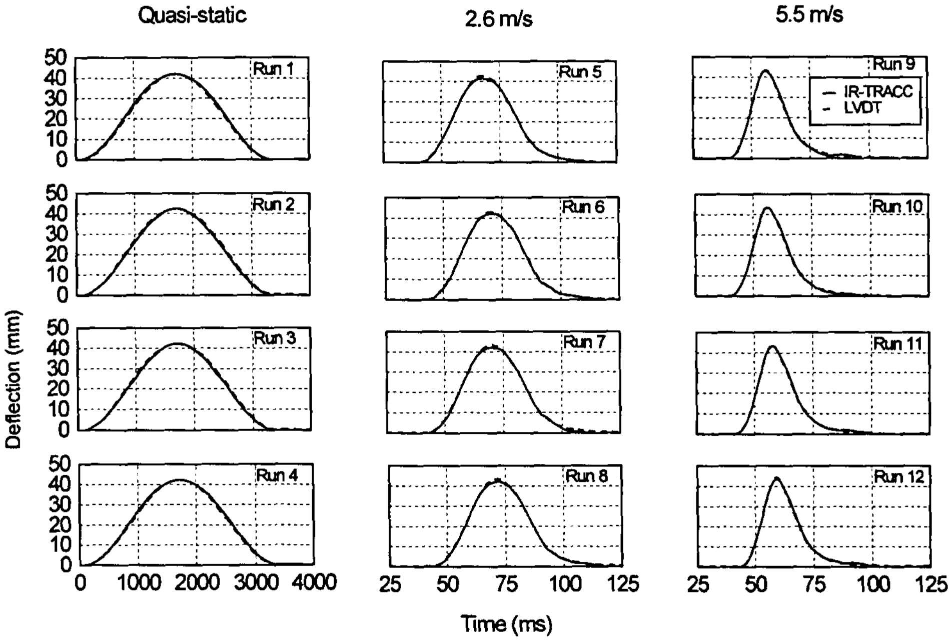

Figure AIII.1. Deflection-time histories for MTS tests of the Transmission Mode IR-TRACC for tests at each speed with the IR-TRACC (solid line) overlaid on the LVDT (dashed line).

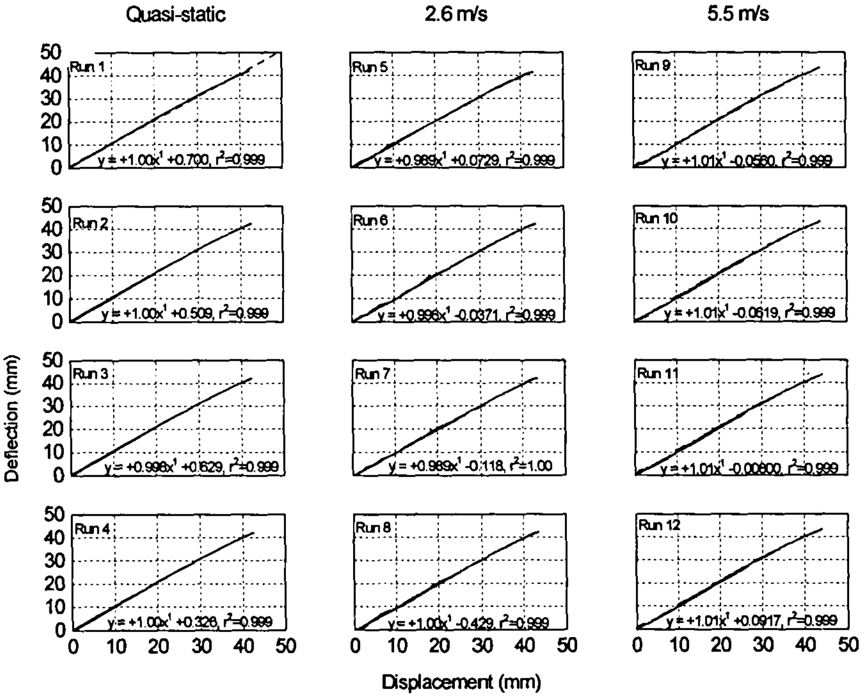

Figure AIII.2. Cross-plots of deflection-time histories for the IR-TRACC sensor and the MTS/LVDT in MTS tests of the Transmission Mode IR-TRACC for tests at each speed.

Deflection-time histories of all IR-TRACC deflections for **Reflection Mode** tests, overlaid on the MTS displacements at each speed, are shown in Figure AIII.3. Again, a more quantitative measure of the agreement between the IR-TRACC and the LVDT is obtained by cross-plotting the deflections as shown in Figure AIII.4.

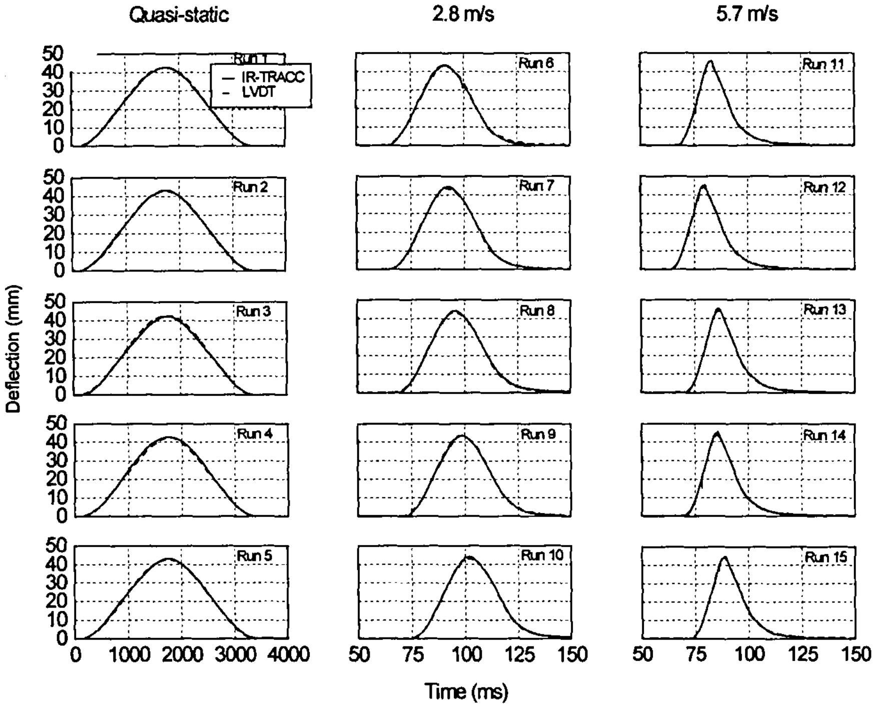

Figure AIII.3. Deflection-time histories for MTS tests of the Reflection Mode IR-TRACC for tests at each speed with the IR-TRACC (solid line) overlaid on the LVDT (dashed line).

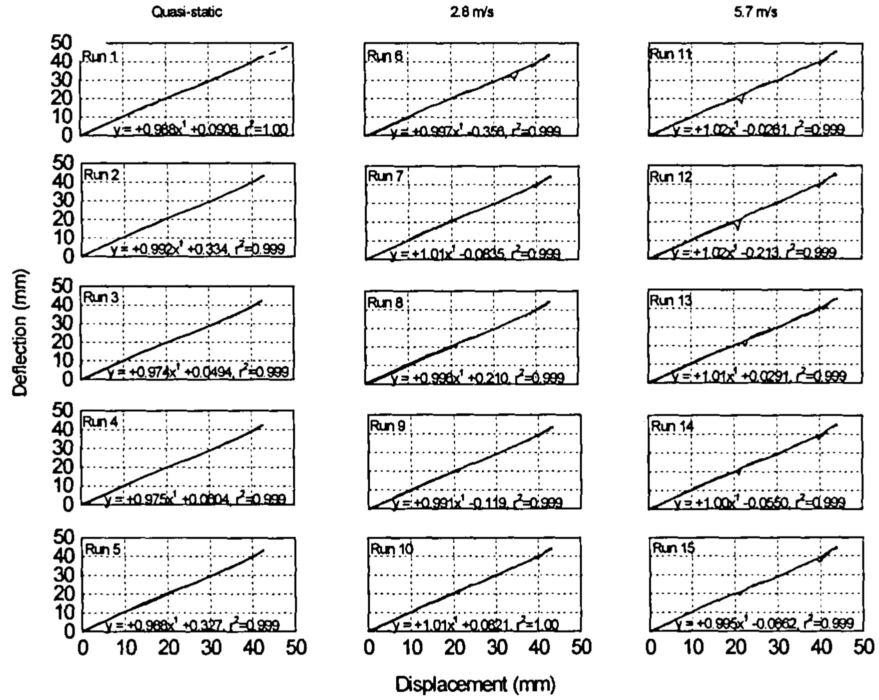

Figure AIII.4. Cross-plots of deflection-time histories for the IR-TRACC sensor and the MTS/LVDT in MTS tests of Reflection Mode IR-TRACC for tests at each speed.

Deflection-time histories of all IR-TRACC deflections for **Ruggedized Transmission Mode** tests, overlaid on the MTS displacements at each speed, are shown in Figure AIII.5. Again, a more quantitative measure of the agreement between the IR-TRACC and the LVDT is obtained by cross-plotting the deflections as shown in Figure AIII.6.

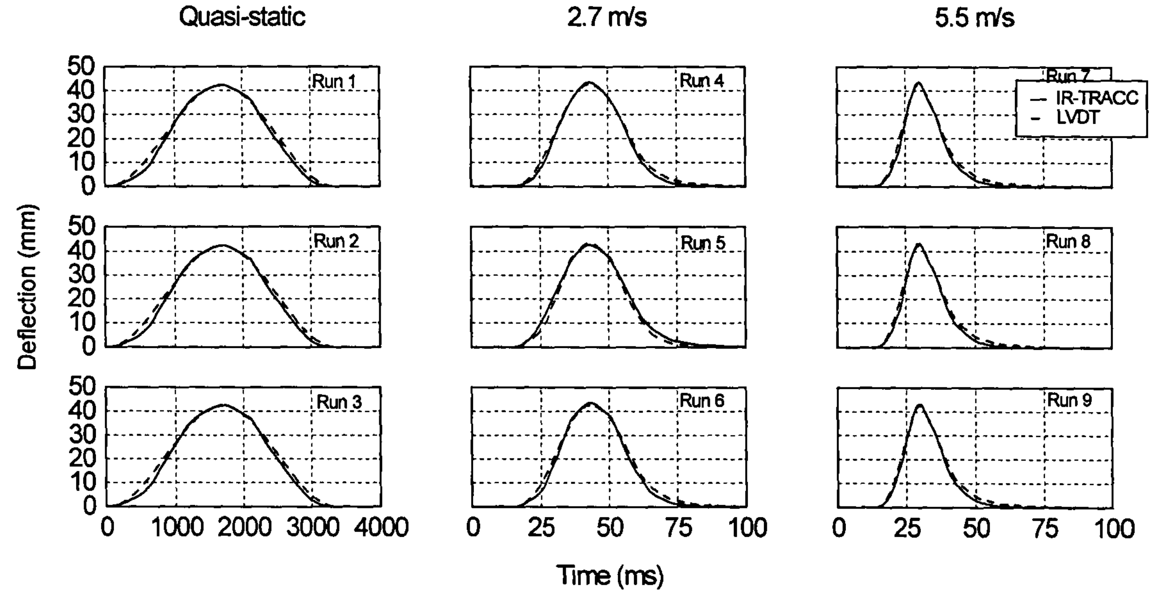

Figure AIII.5. Deflection-time histories for MTS tests of the Transmission Mode IR-TRACC for tests at each speed with the IR-TRACC (solid line) overlaid on the LVDT (dashed line).

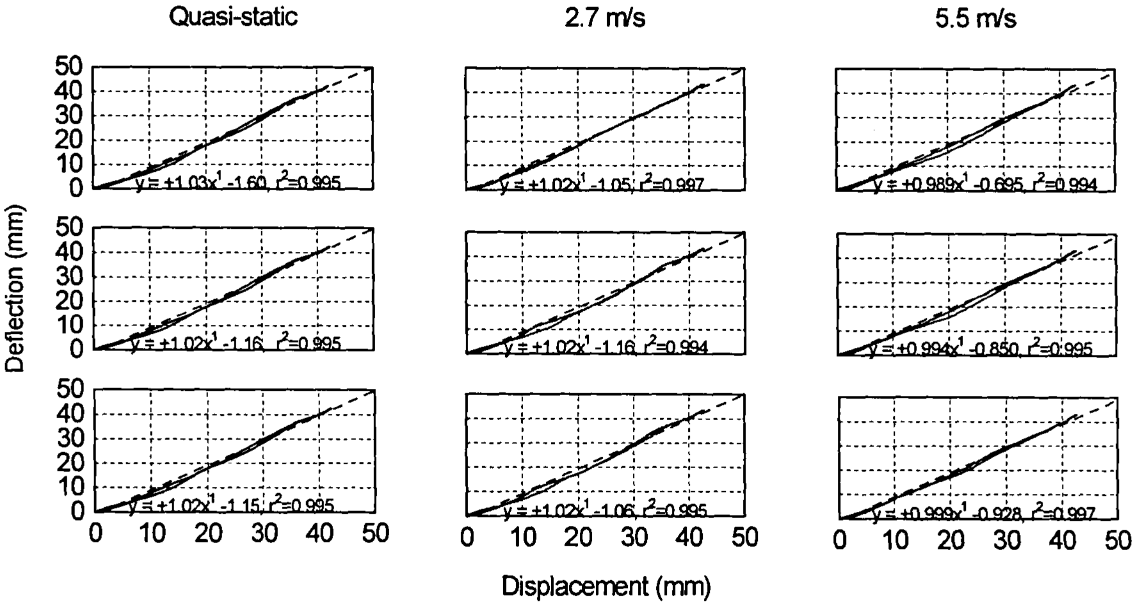

Figure AIII.6. Cross-plots of deflection-time histories for the IR-TRACC sensor and the MTS/LVDT in MTS tests of Ruggedized Transmission Mode IR-TRACC for tests at each speed.

INJURIES TO PREGNANT OCCUPANTS IN AUTOMOTIVE CRASHES

Kathleen DeSantis Klinich
Lawrence W. Schneider
Jamie L. Moore
University of Michigan Transportation Research Institute
Mark D. Pearlman
University of Michigan Health Systems
United States
Paper Number 98-SP-P-17

ABSTRACT

Injuries unique to pregnant occupants involved in motor-vehicle crashes include placental abruption, uterine rupture or laceration, and direct fetal injury. The mechanisms and characteristics of these injuries are discussed using examples from a literature review and from recent investigations of crashes involving pregnant occupants. In addition, a review of the relationship between the pregnant driver and automotive restraints and the steering wheel illustrates how injury potential may differ from the non-pregnant occupant.

AUTOMOTIVE TRAUMA IN PREGNANCY

Introduction

Firm statistics on fetal loss resulting from automotive trauma are not available because fetal death certificates do not record recent maternal involvement in crashes as a potential cause of death. In addition, since miscarriage occurs in 10-20% of all pregnancies in the early part of pregnancy, only deaths to fetuses over 20 weeks gestational age are legally defined and recorded. However, based on the frequencies of pregnancies and crash involvement of the general population, it has been estimated that between 1500 and 5000 fetal losses occur each year in the United States as a result of maternal involvement in automotive crashes (Pearlman 1997). Additional uncounted adverse fetal outcomes occur as well, as many children grow up disabled as a result of injuries sustained in utero. Even if a fetus survives, complications arising from early emergency delivery of a premature fetus (such as low birth weight and neonatal respiratory distress syndrome) can lead to long-term negative consequences for the child.

Pregnant Anatomy

Figure 1 illustrates the general anatomy of a pregnant abdomen (Pritchard et al. 1985). The uterus is a muscular organ that grows in capacity from 5 mL to 5 to 10 L over the course of pregnancy. Its wall thickness at seven months is about 2 cm, and at term (40 weeks) it is about 1 cm. The size of the uterus depends more on the size of the fetus than the size of the mother. Since most women generally have babies who weigh 2.7 to 3.6 kg (6 to 8 pounds), uterine size is not expected to vary significantly with the stature or weight of the mother. The uterus is attached at its base to the cervix which leads to the vagina, but is otherwise unattached in the abdominal cavity. As the uterus grows, it pushes the other abdominal organs rearward and upward. The base of the uterus is in close proximity to the lumbar spine.

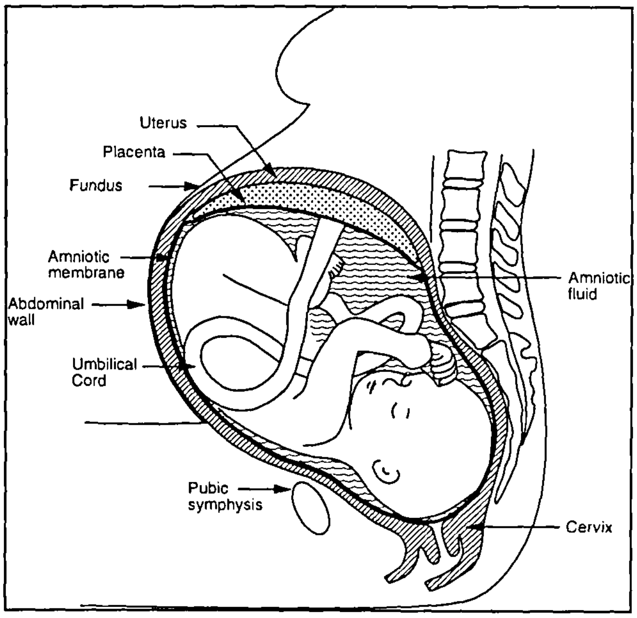

Figure 1. Pregnant anatomy

The placenta is a vascular organ within the uterus that exchanges oxygen, nutrients, and waste between the mother and fetus. Commonly called the "afterbirth," it separates from the uterus and delivers spontaneously after the fetus is born. Eighty percent of placentas are located near the top (fundus) of the uterus by the third trimester. It is roughly circular in shape, and measures 2 to 2.5 cm in thickness in the last trimester of pregnancy. It covers roughly one-fourth of the internal surface area of the uterus throughout pregnancy. The placenta attaches to the uterus by microvilli, which are finger-like projections (diameter of ~ 50 micrometers) that grow into the superficial covering of the uterine wall (decidual layer). The interface between the uterus and placenta is considered to be weaker than either of the two tissues.

The amniotic membrane lines the inner surfaces of the uterus and placenta and contains the fetus and the amniotic fluid. The umbilical cord runs from the placenta through the wall of the membrane to the fetus. As the fetus grows, the relative proportion of the uterine volume filled with amniotic fluid decreases. By the last trimester, the fetus is positioned with its head down in over 95% of pregnancies.

Pregnant Occupants in the Automotive Environment

A research program targeted toward increasing understanding of automotive trauma in pregnancy and developing a second-generation pregnant abdomen for the small female crash dummy is currently underway. As part of this larger program, an anthropometric study of the pregnant automotive occupant is being conducted. Pregnant women in five different stature groups are being tested in laboratory simulations of vehicle interiors. Two seat heights are being used, one representing a mid-size sedan (H30=270 mm) and the other typical of a minivan or light truck (H30=360 mm). Belt anchorage locations are also varied. Subjects are measured in the 3rd, 5th, 7th, and 9th months of pregnancy to study how selected seat position, belt fit, and proximity to the steering wheel change with advancing pregnancy.

Data for fifteen subjects in four different stature groups are currently available. Table 1 shows the group number, mean stature at the initial test session, and number of subjects tested to date. Each subject was tested in four configurations at each visit: two at each seat height with different belt locations.

Table 1.
Subject Information

Group	Mean Stature (mm)	Number of Subjects
2	1580	3
3	1627	5
4	1664	2
5	1708	5

Abdomen-to-wheel clearance is the minimum distance between the bottom of the steering-wheel rim and the subject's midline abdomen contour. Figures 2 and 3 show the abdomen-to-wheel clearance averaged by subject group for each test session. Each point is the average of twice the number of subjects in each group, because each subject was tested twice at each seat height. Different belt conditions are not expected to affect abdomen-to-wheel clearance. Figure 2 illustrates the data for the mid-seat-height test configurations, while Figure 3 shows the data for the high-seat-height test conditions. As expected, all groups show decreasing abdomen-to-wheel clearance with increasing gestational age. The shortest subjects (Group 2) had the least clearance in each test session, while the tallest subjects (Group 5) had the most clearance. Groups 3 and 4 had similar levels of clearance in each test session. The tallest subjects (Group 5) show approximately 100 mm more clearance than the shortest subjects (Group 2) at each test session and at each seat height. Clearances are similar for the two different seat-height configurations.

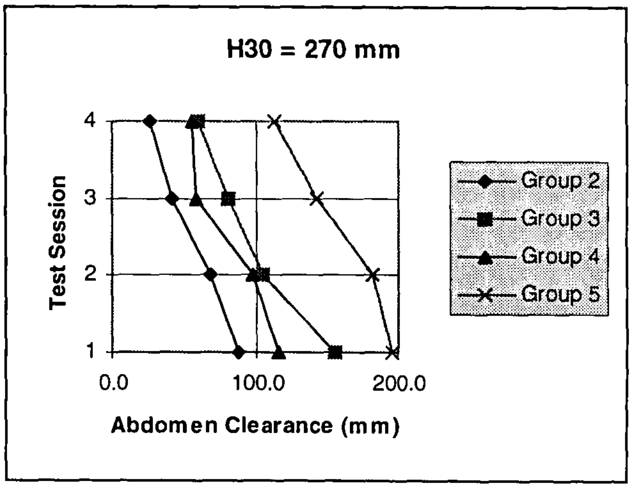

Figure 2. Abdomen-to-wheel-rim clearance averaged by subject group for each test session at mid-seat-height test conditions.

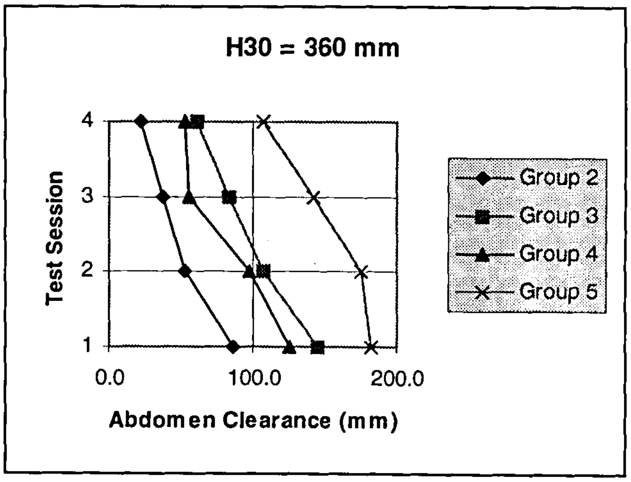

Figure 3. Abdomen-to-wheel-rim clearance averaged by subject group for each test session at high-seat-height test conditions.

Figure 4 shows a stick-figure representation of the average posture and anthropometry of Group-2 subjects for each test session at mid-seat height conditions. The subjects did not move further away from the steering wheel as pregnancy progressed because of the need to comfortably operate the pedals.

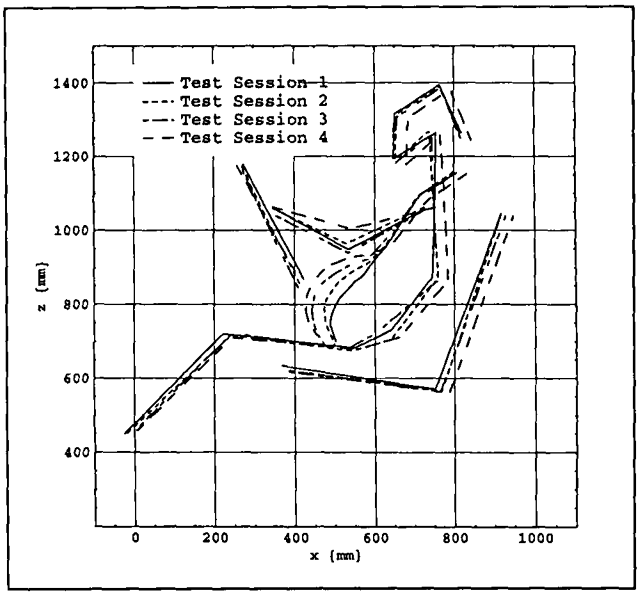

Figure 4. Average posture of Group-2 subjects for each test session at mid-seat-height conditions.

The position of the lap belt relative to the uterus was also measured during testing. Subjects were instructed to position the lap belt below the prominence of their pregnant abdomen, as recommended by the American College of Obstetricians and Gynecologists (ACOG 1991). Ideally, the top of the belt should be at or below the anterior superior iliac spines (ASIS), so the bony structures are loaded during impact rather than the soft tissues. Figure 5 shows a front view of the centerline of a lap belt for one subject. The geometric shape connects the fundus (top of uterus), left ASIS, pubic symphysis, and right ASIS. This subject, who was in her 37th week of pregnancy, positioned the belt so the centerline was very close to the ASIS points.

The side view of the lap belt relative to the pregnant abdomen in Figure 6 illustrates the challenges posed by pregnant anatomy to automotive safety engineers. This subject positioned the belt correctly, and it crossed very close to the left and right ASIS as desired. However, in the midline plane, the lap belt crosses over the protruding pregnant abdomen directly over the uterus. In a crash, the uterus would be loaded before the bony structures. For non-pregnant occupants, a correctly positioned lap belt loads the pelvis through the ASIS rather than the soft tissues of the abdomen.

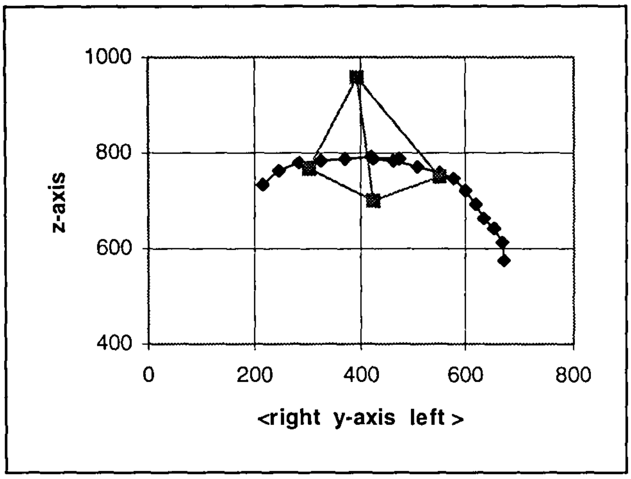

Figure 5. Front view of lap belt centerline (diamonds) relative to fundus, ASIS, and pubic symphysis (squares).

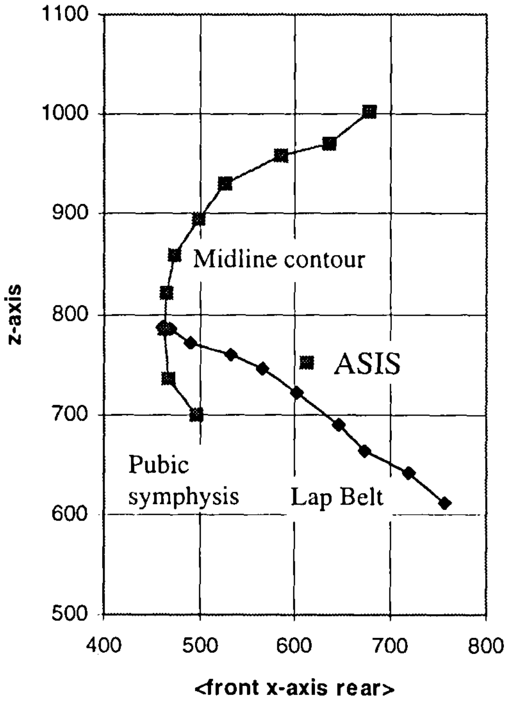

Figure 6. Side view of lap belt centerline (diamonds) showing its intersection with the midline contour (squares) of the pregnant abdomen.

INJURIES UNIQUE TO PREGNANT WOMEN IN CAR CRASHES

Overview

Table A.1 in the Appendix provides information on 120 automotive crashes involving pregnant occupants. Most of the cases (93) are taken from the medical and automotive safety literature. The main criteria for inclusion in this review was availability of information on restraint usage by the pregnant occupant and the pregnant occupant being at least 20 weeks pregnant. Since most medical case studies focus on the injuries and treatment and not the crash event, information regarding the impact direction is often unavailable. In addition, the estimate of the crash severity is usually not calculated and is derived from the occupant's or physicians' estimates. The cases from the literature are usually reported because they involve an unusual or serious injury and are not intended to be representative of situations experienced by most pregnant occupants.

The remaining 27 cases in Table A.1 are from UMTRI's ongoing accident investigation study of crashes involving pregnant occupants. Fourteen cases (designated GMP-0XX) are classified as major investigations, while 13 cases (designated GMP-2XX) are considered minor investigations. An investigation is usually considered minor if the vehicle or medical records are not available for inspection or review. However, even in these cases, the vehicle damage information is generally more complete than most of the cases reported in the medical literature. The UMTRI case set is expected to be more representative, as it includes a wider range of outcomes.

The first column in Table A.1 lists a case number for reference in this paper. The second column lists the occupant position in the vehicle, impact direction, and impact severity if the data are available. Some sources from the literature only reported the occupant as being a passenger and did not indicate whether the location was the front or rear seat. The type of crash is classified as front, side, rear, rollover, or multiple impact. Information on whether the crash was a "near" or "far"-side impact is usually not available. Crash severity is based on the following divisions: minor is less than 24 km/h (15 mph) change in velocity, moderate is 24 to 48 km/h (15 to 30 mph), and severe is greater than 48 km/h (30 mph). The values reported for major UMTRI cases are based on input of vehicle crush measurements into crash-reconstruction programs such as SMASH, and are therefore more accurate. The remaining crash-severity estimates were made by the occupants or physicians and probably relate more to the speed of travel before the crash rather than actual change in velocity. In the majority of cases in Table A.1, no estimate of crash severity is made.

The third column in Table A.1 lists the restraint conditions for the pregnant occupant. Some of the sources reported use of a belt restraint, but did not clarify whether a lap belt or 3-point belt was used, or if the belt was positioned properly; these cases are listed only as "restrained." If the pregnant occupant reported wearing the lap belt portion of the belt across the bulge of her pregnant abdomen (crossing near the umbilicus) rather than below it, belt use is documented as improper. The fourth column gives gestational age in weeks, with 40 weeks considered full term. In the text of this paper, gestational ages are grouped into four-week increments and referred to as the 5th month (20-23 weeks), 6th month (24-27 weeks), 7th month (28-31 weeks), 8th month (32-35 weeks), or 9th month (36 weeks or more) of pregnancy.

Maternal injuries are given in the fifth column and are described in two ways. The first term describes the overall severity of injuries that are not related to pregnancy. The categories are none, minor, moderate, and major. These descriptions are estimates of the maximum AIS scores (ignoring uterine or placenta injuries), with minor corresponding to MAIS 1 or 2, moderate, MAIS 3 or 4, and major, MAIS 5 or 6. The remainder of the maternal injury description describes the injuries to the uterus and placenta. Pelvic fractures are specifically noted in the maternal injury column as they are suspected to increase the probability of injury to the pregnant abdomen and fetus. Maternal death is indicated by italic type.

The sixth column describes the fetal outcome, specifically listing any direct injuries or complications. Fetal survival is indicated by italic type.

The final column lists the source of the case data. For cases from the literature, the source lists the authors and year of publication, plus a case number if the source presented more than one case. For UMTRI cases, the case number and year of the crash are given.

Figure 7 documents the distribution of crash types from Table A.1. The majority of crashes are frontal impacts (61%, n=74), followed by side impacts (25%, n=30). The breakdown of crash severity is shown in Figure 8, with over half of the cases not reporting any estimate of crash severity. The distribution of occupant position is shown in Figure 9, with most cases involving drivers (55%, n=66).

Figure 10 shows the distribution of restraint use of the pregnant occupants for the cases in Table A.1. About half (49%, n=59) were unrestrained. Only a few cases (3%, n=4) were confirmed to have improper belt use, with the lap belt positioned across, rather than under, the pregnant abdomen. Since the case dates range back to the 1960's, about 6% (n=7) used a lap belt only, often because it was all that was available. The gestational ages of the pregnant occupants appear in Figure 11, with most cases in the last trimester, particularly the last month.

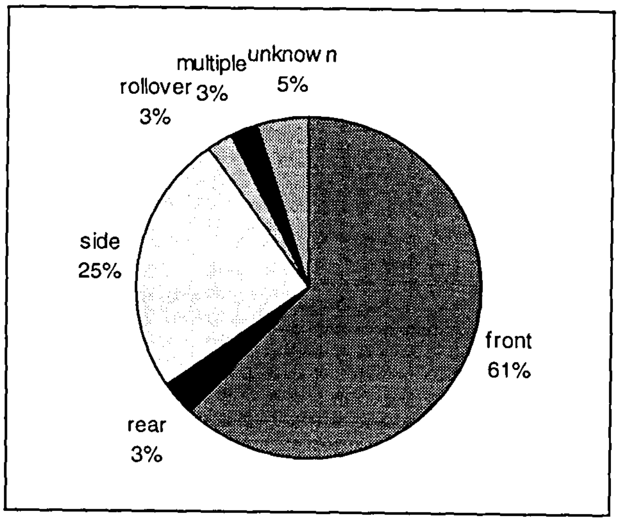

Figure 7. Distribution of impact type for cases in Table A.1.

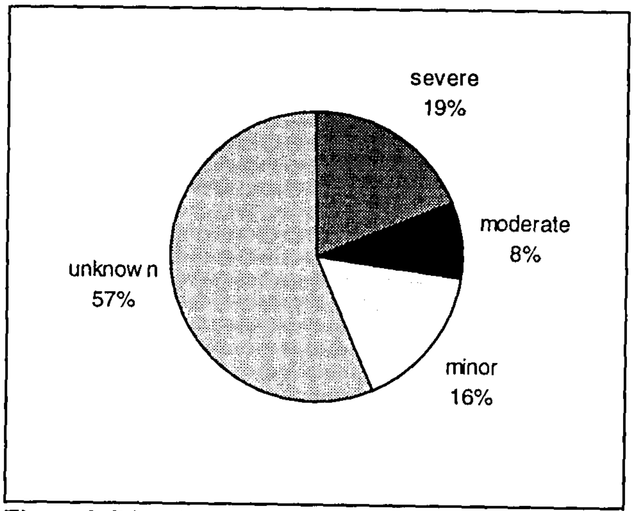

Figure 8. Distribution of estimated impact severity for cases in Table A.1.

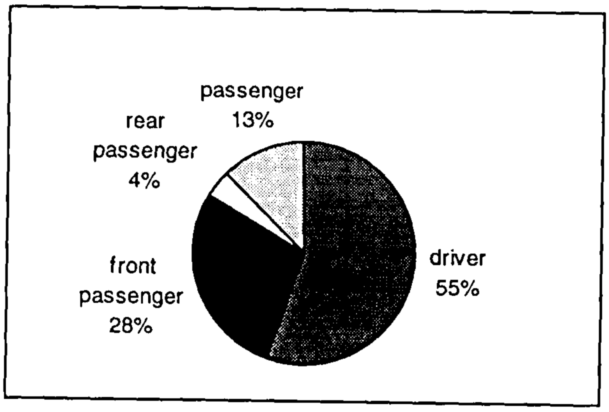

Figure 9. Distribution of seating position of pregnant occupant for cases in Table A.1.

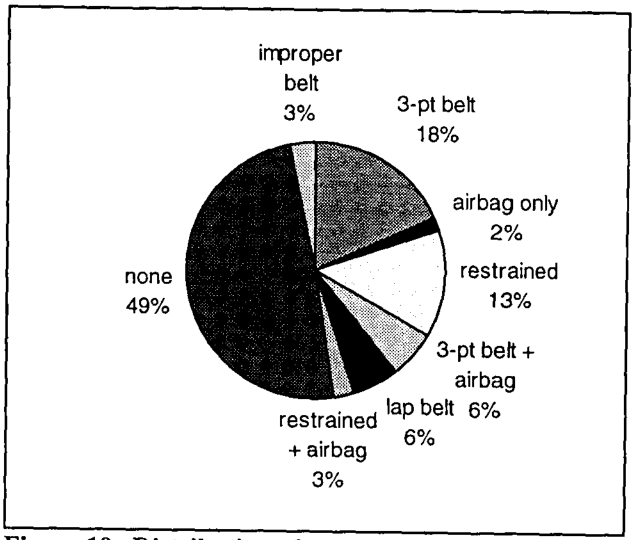

Figure 10. Distribution of restraint use by pregnant occupant for cases in Table A.1.

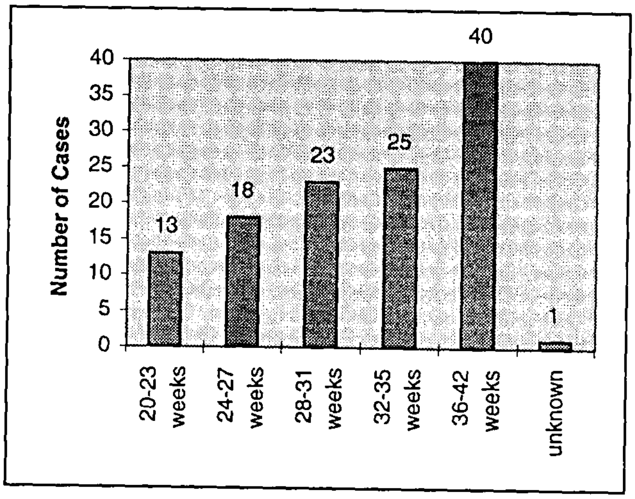

Figure 11. Distribution of gestational age for cases in Table A.1.

The chart in Figure 12 indicates the types of pregnancy-related injuries sustained by the pregnant occupants in Table A.1. The most frequent outcome is placenta injury only; none of the fetuses in these cases survived. There are six instances of placenta injury plus additional complications, with all of these fetuses surviving. Seventeen cases had placenta and direct fetal injuries. Eighteen cases had completely positive outcomes, although two of these mothers sustained pelvic fractures. Five cases involved only complications, and all of these fetuses survived. In eight cases, the fetus was stillborn and no direct injuries to the fetus or reproductive organs were found. However, five of these cases involved maternal death, so there are really just three stillborn cases

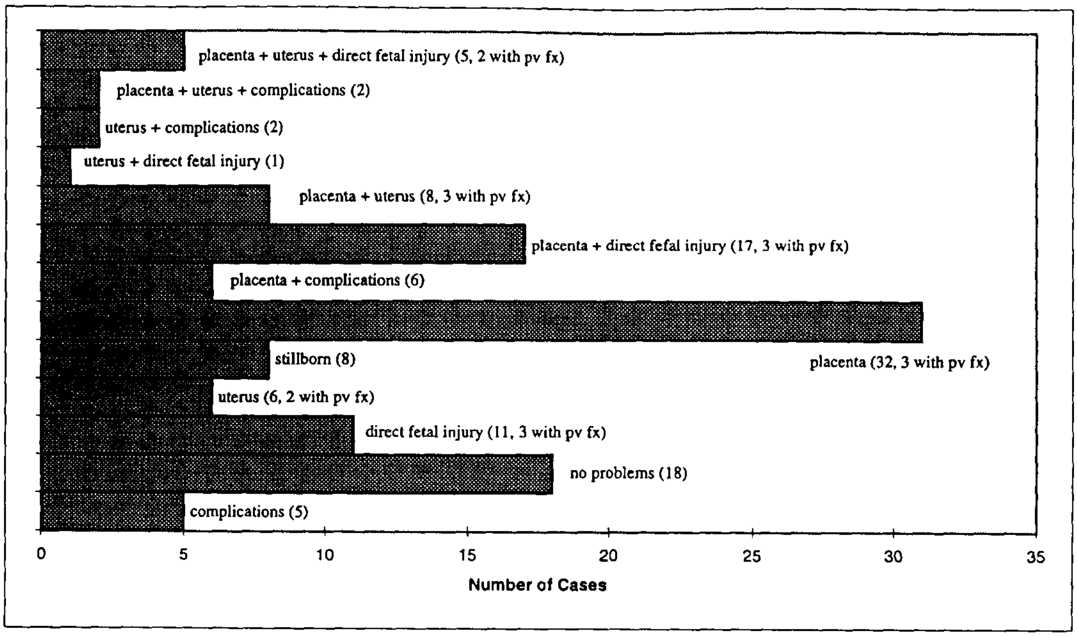

Figure 12. Distribution of injury patterns.

without additional explanation. Eight cases involve injuries to both the uterus and placenta. In one of these cases, the fetus survived although it experienced complications. Three other of these cases also involved pelvic fracture. The other most common injury patterns are direct fetal injury (11 cases, 3 with pelvic fracture), and uterine injury only (6 cases, two with pelvic fracture). In one of the uterine injury cases, the fetus survived with complications. The remaining bars show the less frequent combinations of placenta, uterine, direct fetal, and pelvic fracture injuries.

Of the 120 cases in Table A.1, nine involve both maternal and fetal death. While the mother survived in the other 111 cases, the fetus did not survive in 74 cases.

The remainder of this paper discusses each type of pregnancy injury and outcome in more detail, and highlights the characteristics of the crashes and injury patterns.

Placental Abruption

Placental abruption is the most common cause of fetal loss in automotive crashes. It occurs in 1 to 5% of minor severity crashes during pregnancy and from 20 to 50% of severe crashes during pregnancy. The injury occurs when the placenta detaches from the uterine wall, disrupting the supply of oxygen and nutrients to the fetus. Partial abruptions can also occur, with the possibility of the pregnancy continuing successfully depending on the degree of placental separation from the uterus. The interface between the placenta and the uterus is considered to be weaker than either the uterus or the placenta, and therefore usually fails before either the uterus or placenta fails.

Pearlman et al. (1990) have noted that the likelihood of placental abruption is independent of the placenta location on the uterus (Pearlman et al. 1990). This may imply that there are several mechanisms of placental abruption, with the particular cause depending on the placental location relative to the loading location and nature of the loading. For example, some placental abruptions may result from high-velocity, low-mass airbag loading, or from compression between the mother's body and the steering wheel, belt, or instrument panel. Abruption may also result from acceleration differentials between the placenta and uterus. Thus, mechanisms of placental abruption may include inertial loading, direct loading by the fetus, and excessive shear or tensile strain.

The first 69 cases in Table A.1 involve some injury to the placenta or the placenta/uterine interface. Of these cases, thirty-nine of the pregnant occupants were drivers, fourteen were front passengers, five were rear passengers, and eleven were passengers of unknown seating position. Most of the impacts were frontal (46), twelve were side, three were rollovers, two each were rear or multiple impacts, and four impact types were not reported. Many of the cases did not estimate impact severity (49), while twelve were severe and four each were estimated to be minor or moderate impacts.

Forty-two cases (1-42) involve complete abruption and fifteen cases (43-57) involve partial abruptions. In eight cases (58-65), lacerations of the placenta occurred, and in the four remaining cases (66-69), the placenta was damaged but not separated or lacerated. Only two cases (16 and 33) resulted in both fetal and maternal death. When the mother survived, the fetus died in 56 cases. Twenty-two of the cases with placental injury also had direct fetal injury, fifteen cases also involve uterine laceration or rupture, and nine of these pregnant occupants sustained pelvic fractures.

In the majority of cases with placental abruption, the pregnant occupant was unrestrained (48 out of 69). One pregnant occupant sustaining a placental abruption was restrained by both a 3-point belt and a deploying airbag, eight were documented as properly using a 3-point belt, and twelve were listed as restrained without further specification. Five women used a lap belt only, and three wore the belt improperly with the lap belt portion positioned across the bulge of their abdomens. While these results show that placental injuries can occur to properly belted pregnant occupants, they also show that avoiding belt use during pregnancy may significantly increase the risk of placental abruption and subsequent fetal loss in a crash.

This compilation of case data also suggests that placental abruption may be more likely to occur later in the term of pregnancy. Five cases of placental injury involve women in their 5th month of pregnancy, 10 in the 6th, 13 in the 7th, 20 in the 8th, and 21 in the 9th month. The pregnant occupants were most likely to have a minor injury in addition to their placental injury (41 cases). Sixteen pregnant occupants sustained moderate injuries, two suffered major injuries, and ten sustained no injuries other that the placental injury. These findings agree with clinical experience in which women with serious pregnancy injuries often appear, at initial exam, to have sustained minor or no other injuries (Pearlman 1990).

Uterine Injury

Uterine rupture and lacerations are rare during pregnancy, occurring in less than 1% of pregnant trauma cases (Pearlman 1990). Injury to the uterus in automotive accidents occurs almost exclusively during pregnancy (compared to any other time) because it is much larger, extends outside the pelvic cavity, and is filled with fluid. While uterine rupture is very rare, the likelihood of fetal death with such an injury is near 100%.

Uterine injury is often reported in the literature as resulting from direct loading from the seat belt. While this may occur, it can also occur to unbelted women who are directly loaded by the steering wheel or instrument panel. Some cases report uterine damage directly beneath the area of seatbelt loading. For example, in case GMP-006 (Case 10), the pregnant driver sustained two lacerations approximately 50 mm apart extending across the lower uterus, corresponding to the width of the seat belt. Other cases (75 and 78) report the site of uterine rupture as being opposite the site of loading, suggesting a "contrecoup" type of injury mechanism.

Twenty-four cases in Table A.1 involve uterine injuries. In eleven of the cases, the pregnant occupant was the driver. Fourteen of the crashes were frontal impacts, seven were side, one was rear, one involved multiple impacts, and one involved unknown crash conditions. Of the seven side impacts, only one pregnant occupant may have been properly restrained (one had the lap belt improperly positioned and five were unrestrained). The impact severity is only estimated for five of the twenty-four uterine injury cases, so no conclusions can be drawn about the frequency of uterine injury and the severity of crashes.

Three different types of uterine injuries are reported: one complete transection (70), thirteen ruptures (1-8, 74-78) and ten lacerations (9-12, 43-44, 58, 71-73). All but three of these experienced fetal loss, and all three of these cases (10, 44, 71) involved fetal complications. Seven of the laceration cases and eight of the rupture cases involved at least a partial placental abruption. Seven of the uterine injury cases also involved direct fetal injury, and six uterine injuries were accompanied by pelvic fractures. (The proportion of cases with uterine injury in Table A.1 is higher than seen clinically, because the literature cases are more likely to report unusual injuries.)

In the twenty-four cases with uterine injury, only four of the pregnant occupants were properly restrained by a three-point belt, and one driver was also restrained by an airbag. Two additional cases reported restraint use, but did not report the type of belt or whether it was positioned properly. Half of the occupants with uterine injury were unbelted. For all the cases in Table A.1, the four cases where improper belt use was confirmed (lap belt portion placed across the dome of the abdomen) all resulted in uterine injury. In the last two cases with uterine injury, the occupants used only a lap belt.

Distribution of gestational ages of pregnant women with uterine injury is fairly uniform, with five occupants each in the 5th, 6th, and 8th months, six in the 7th month, and three in the 9th month. None of the pregnant occupants with uterine injury sustained major injuries, six sustained other moderate injuries, seventeen suffered other minor injuries, and one received no other injuries. This distribution of maternal injuries confirms the trend noted in the literature that pregnant women often sustain a uterine injury that is usually life-threatening to the fetus, while sustaining only minor injuries to themselves.

Direct Fetal Injury

Direct fetal injury (DFI) is also quite rare, occurring in less than 10% of automotive crashes involving pregnant occupants (Pearlman 1990). In the first three months of pregnancy, the uterus is still completely surrounded by the pelvis and is considered an abdominal organ. After the first three months, the uterus protrudes out from the abdomen, but the structure of the pregnant abdomen protects the fetus by encasing it in amniotic fluid which acts as a shock absorber to isolate the fetus. The fetus sometimes sustains injury from direct loading of the abdomen when the protective cavity is compromised by pelvic fractures or uterine rupture. The most frequently injured fetal body region is the head, because it is the largest part of the fetal body and offers the "biggest target." It is thought that skull fracture most often occurs when the fetal head is loaded against the bony structures of the maternal pelvis or spine by a belt, steering wheel, or instrument panel.

Judging from the thirty-four cases involving direct fetal injury in Table A.1, it appears that crashes with minor, moderate, or severe impact severities can all result in direct fetal injuries, although data on the crash severity are limited. Nineteen of the cases involved drivers as the maternal occupant. Nineteen were frontal impacts, ten were side, two were rear, and the remaining three were multiple or unknown types of impacts.

The cases with direct fetal injury in Table A.1 are numbers 1-3, 9, 13-16, 43, 45-53, 65-68, 70, and 79-90. As mentioned previously, the cases taken from the literature tend to focus on more unusual injuries, so the proportion of cases with direct fetal injury in Table A.1 is greater than that seen clinically. Twenty-two cases involve head injuries only, four involve both the head and thorax injuries, six involve thorax/abdomen injury only, and one injury each is documented for the spine and upper extremity. Of the sixteen cases in Table A.1 in which the mother sustained a pelvic fracture, eight of the fetuses sustained direct injuries to the head. Twenty-two of the direct fetal injury cases also involved placenta injuries, suggesting that accident conditions severe enough to result in direct fetal injury often result in placental damage as well. Six occupants sustained uterine injuries with direct fetal injury. Five fetuses with direct injuries survived, with three requiring emergency cesarean section (c/s) deliveries.

Most of the occupants with direct injuries to the fetus were not properly restrained. Nineteen were unbelted, four used a lap belt only, and three had the lap belt improperly positioned across the bulge of the abdomen. Five occupants were wearing the 3-point belt properly, and the remaining three occupants were reported to be using belt restraints, although the type of belt and placement are not reported.

The frequency of direct fetal injury for this sample is slightly skewed toward later gestational ages. Only two DFI cases occurred in the 5th month, six occurred in the 6th month, eight each in the 7th and 8th months, and ten in the 9th month. Intuitively this makes sense, as the fetus is a bigger target as gestational age increases, and the amniotic fluid takes up a relatively smaller proportion of the uterus volume as pregnancy progresses. Direct fetal injuries occur regardless of the injury severity sustained by the mother, with eight of these cases having no maternal injury, sixteen having minor maternal injuries, eight having moderate injuries, and two having major injuries.

Other Negative Outcomes

Some pregnant automotive crash victims suffer negative pregnancy complications whether or not they sustain any placenta, uterus, or direct fetal injuries. One common occurrence is a premature delivery, in which the infant often has a low birth weight and can suffer from neonatal respiratory distress syndrome because its lungs are not fully developed. Both of these factors can lead to health problems and disabilities throughout the child's life.

Even if a fetus is very close to full term, maternal involvement in a crash can lead to an emergency cesarean delivery, which poses higher risks to the mother and neonate. Contractions often begin after an accident, sometimes requiring drug intervention to prevent early delivery. Crashes involving pregnant occupants occasionally result in stillborn births without any visible injury responsible for the loss.

In the sixteen negative outcome cases, nine of the pregnant occupants were drivers. Nine crashes were frontal impacts, two were side, three were rear, and two were unknown. Seven of these crashes were rated as severe, one as moderate, and three as minor in crash severity, with no crash-severity rating available for the remaining five cases.

Table A.1 contains seven cases (90-93, 97, 99,100) in which the crash resulted in a negative pregnancy outcome without any placenta, uterus, or direct fetal injuries. There are also nine cases with placenta or uterine injury (10, 17-19, 44, 54-56, 71) where the fetus survived but experienced some of the additional negative outcomes described above. In three cases, the fetus was stillborn after the crash, although there were no placenta, uterus, or fetal injuries responsible for the loss. In three other cases, the pregnant occupant started having contractions after the crash although no intervention was needed. In one of these cases, the neonate was born months after the crash and diagnosed with brain damage attributed to the crash. In the remaining case, the neonate suffered from hydrocephalus that may have resulted from the crash at 28 weeks gestation. The nine cases with placenta or uterine damage required emergency cesarean delivery of premature infants. Five of these infants suffered from seizures or newborn respiratory distress syndrome.

In these sixteen negative outcome cases, eleven mothers were not using belt restraints. Two used a 3-point belt and airbag, one used a 3-point belt only, and in one case with an unspecified type of belt restraint, the airbag deployed. One pregnant occupant used only a lap belt.

The gestational ages of the cases with negative outcomes is almost evenly distributed over the last three months of pregnancy, with 5 each in the 7th, 8th, and 9th months and one case in the 6th month. Four of the mothers sustained no other injuries, ten had minor injuries only, and two had moderate levels of injury.

Positive Outcomes

Eighteen of the cases in the Table A.1 (103-120) had good fetal outcomes with no complications. The majority of these cases are from the UMTRI study, as the medical literature usually reports only complicated cases. All of the mothers and fetuses in these cases survived.

Twelve of the pregnant occupants were drivers, while the remaining six were front-seat passengers. Ten impacts were frontal, six were side, one was a rear impact, and one impact type was not recorded. Crash severity is available for all of these cases, with thirteen being minor, four moderate, and one severe.

The most obvious difference between the positive-outcome cases and the other cases in Table A.1 is the restraint usage of the maternal occupant: 17 out of 18 of the occupants in the positive outcome cases used a restraint. Seven of these used a 3-point belt, seven used a 3-point belt and the airbag deployed, and two were unbelted but the airbag deployed.

These cases are weighted towards the last month of pregnancy, with ten cases in the 9th month of pregnancy, three in the 5th month, two in the 8th month, and one each in the 6th, 7th, and unknown months. Twelve of the mothers sustained minor injuries, three had none, and three suffered moderate injuries. Two of the mothers had pelvic fractures.

DISCUSSSION

The preceding descriptions of injuries sustained by pregnant women in crashes highlights the conditions under which different injuries occur. To provide an overview, histograms of the distributions of the independent variables impact type, impact severity, seating position, restraint use, and gestational age were developed for all cases in Table A.1, and for subsets of the cases based on injury type or outcome. The different proportions in each distribution were grouped according to the different levels of each independent variable for plotting in Figures 13 through 17. The number of cases in each injury or outcome appears in Table 2. The sum of the numbers of cases in all the different groups does not equal the total number of cases in Table A.1 because cases with more than one injury are included more than once (i.e., a case with both uterus and placenta injuries is counted in both categories).

Table 2.
Number of Cases in Each Outcome

Outcome	Number of Cases
All Cases	120
Placenta	69
Uterus	24
Direct Fetal	34
Negative Outcomes	16
Positive Outcomes	18

The distributions of impact type in Figure 13 show that, in general, the distributions for each outcome are similar to the overall distribution. The negative outcome cases had higher proportions of rear and unknown impacts. The cases with placenta injuries had a slightly lower proportion of side impacts and a slightly higher proportion of front impacts.

Figure 14 shows distributions of estimated impact severity. The negative outcome cases had higher proportions of major and minor impacts and had fewer unknown crash severities. The positive outcome cases had the highest proportions of minor and moderate severity crashes, and had no unknown impact severities.

The distributions of pregnant occupant seating position are found in Figure 15. Most of the outcomes have a seating-position distribution similar to the overall distribution. The uterine injuries have the highest proportion of front passengers and the lowest proportion of drivers. The placenta injury cases have the lowest proportion of front passengers and the highest proportion of rear passengers.

Figure 16 illustrates the distributions of restraint use by pregnant occupants. Cases with positive outcomes have the highest percentage of 3-point belt use and 3-point belt plus airbag use, and the lowest percentage of no restraint use. Placenta injuries and negative outcomes have relatively high proportions of not using restraints. Uterine injuries have the highest proportion of improper belt use.

The distribution of gestational age for the different outcomes is found in Figure 17. The positive outcome cases had the highest proportion of cases in the 9th month of pregnancy. Since a birth resulting from a crash would not be considered premature in the ninth month, this may contribute to this shift in proportion. Uterus injury cases

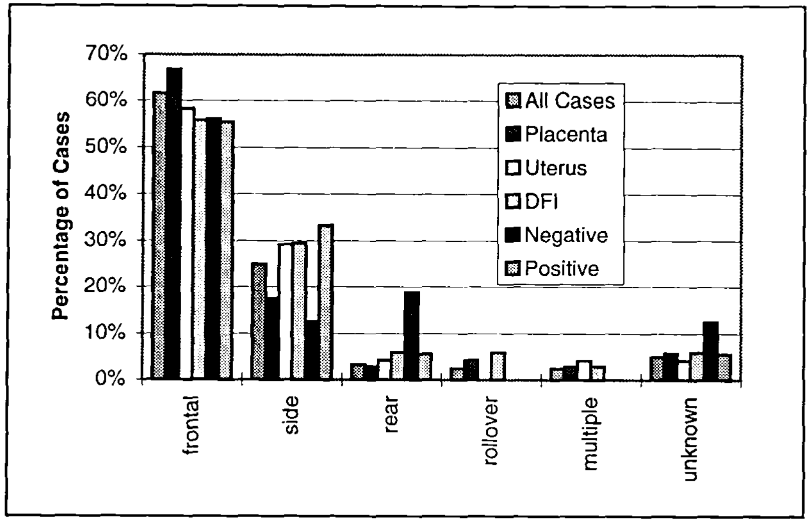

Figure 13. Distributions of impact type for all cases in Table A.1 and by injury or outcome, grouped by impact type.

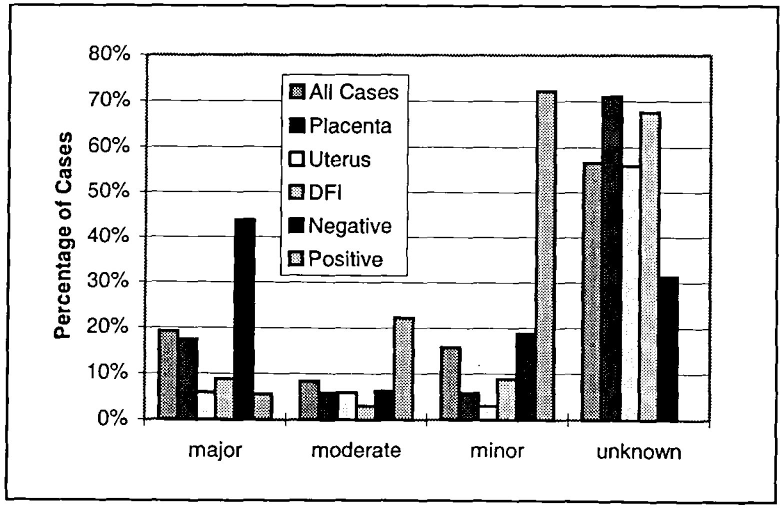

Figure 14. Distributions of impact severity for all cases in Table A.1 and by injury or outcome, grouped by impact severity.

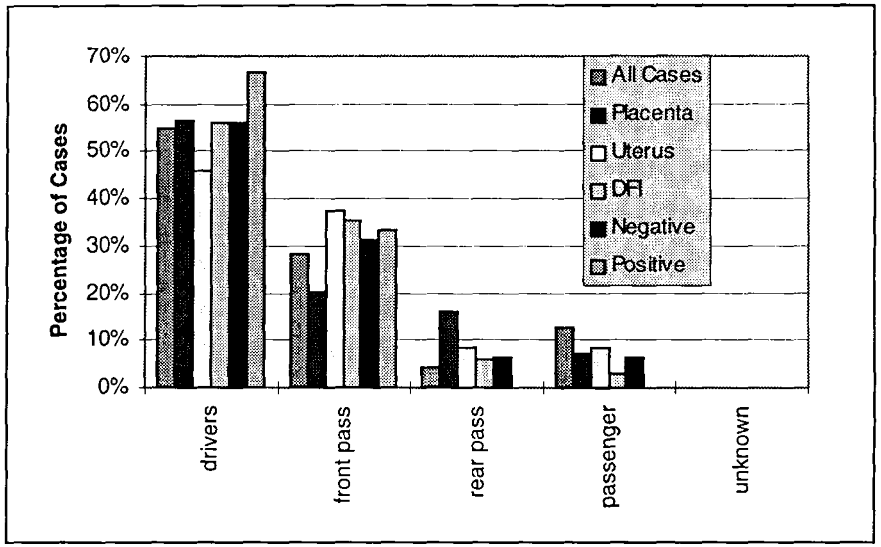

Figure 15. Distributions of pregnant occupant seating position for all cases in Table A.1 and by injury or outcome, grouped by seating position.

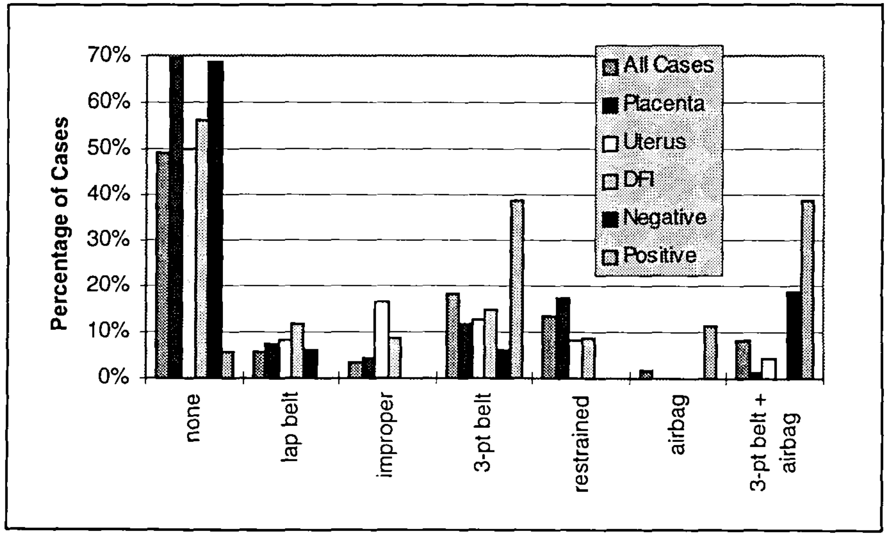

Figure 16. Distributions of pregnant occupant restraint use for all cases in Table A.1 and by injury or outcome, grouped by restraint use.

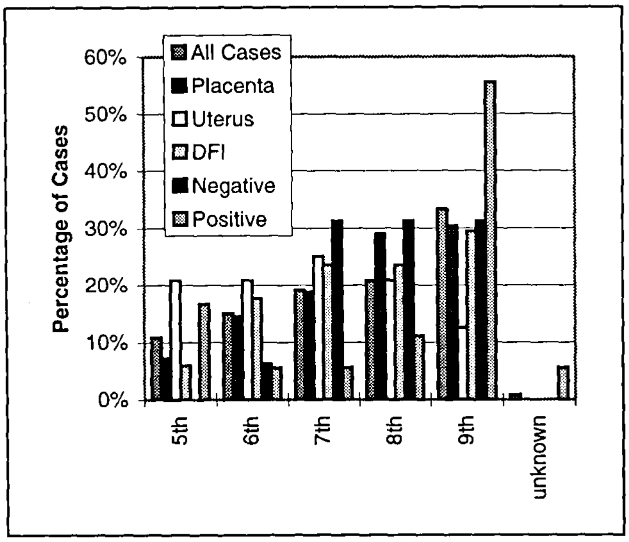

Figure 17. Distributions of gestational age for all cases in Table A.1 and by injury or outcome, grouped by gestational age.

were the most evenly distributed, and had the highest proportions in the 5th and 6th months of pregnancy. The proportion of placenta injuries seems to increase with gestational age, as do direct fetal injuries. Negative outcomes primarily occur in the last trimester of pregnancy.

CONCLUSIONS

A review of injuries specific to pregnant motor vehicle occupants illustrates the following points regarding pregnant occupants involved in automotive crashes.

- All nine cases involving maternal death resulted in fetal death, and eight of these women were unbelted. Thus, the most basic way to protect the fetus is to protect the mother through proper use of belt restraints.
- While placental, uterine, and fetal injuries may occur with properly belted occupants, the majority of the cases involving these injuries are to unrestrained occupants.
- The distinguishing characteristic of the cases with completely positive fetal outcomes was proper restraint use by the mother.
- 65% of the cases with direct fetal injury also involved placental injury, as did 63% of the cases with uterine injury. Thus, reducing the likelihood of placental abruption is likely to reduce the probability of uterine and direct fetal injury as well.
- All pregnant women involved in crashes, even minor ones, should immediately seek medical attention. In most cases with fetal loss, the mother sustained only minor or no other injuries other than placental, uterine, or fetal damage.
- The anatomy of pregnant women while seated in automotive posture poses a unique challenge to restraint designers because of difficulty positioning the lap belt and close proximity to the steering wheel and airbag module.

The information presented in this paper will be used to guide the development of the second-generation pregnant crash dummy. A key goal of the next-generation design is to assess the likelihood of placental abruption, the leading cause of fetal death in crashes.

ACKNOWLEDGMENTS

The work covered by this report was financed by GM pursuant to an agreement between GM and the U.S. Department of Transportation. The authors gratefully appreciate their support.

REFERENCES

ACOG Technical Bulletin #161 (1993). Trauma During Pregnancy, *International Journal of Gynecology and Obstetrics*, 40:165-170.

Agran, P. F., Dunkle, D. E., Winn, D. G., Kent, D. (1986). Fetal Death in Motor Vehicle Collisions. *30th Annual AAAM Proceedings,* 285-294.

Astarita, D. C., Feldman, B. (1997). Seat Belt Placement Resulting in Uterine Rupture. *Journal of Trauma*, 42(4):738-740.

Bowdler, N., Faix, R. G., Elkins, T. (1987). Fetal Skull Fracture and Brain Injury After a Maternal Automobile Accident: A Case Report. *Journal of Reproductive Medicine*, 32(5):375-378.

Chetcuti, P., Levene, M. I. (1987). Seat Belts: A Potential Hazard to the Fetus. *Journal of Perinatal Medicine*, 15(2):207-209.

Civil, I. D., Talucci, R. C., Schwab, C. W. (1988). Placental Laceration and Fetal Death as a Result of Blunt Abdominal Trauma. *Journal of Trauma*, 28(5):708-710.

Connor, E., Curran, J. (1976). In Utero Traumatic Intra-Abdominal Deceleration Injury to the Fetus--A Case Report. *American Journal of Obstetrics and Gynecology*, 125(4):567-569.

Cumming, D. C., Wren, F. D. (1978). Fetal Skull Fracture From an Apparently Trivial Motor Vehicle Accident. *American Journal of Obstetrics and Gynecology*, 132(3):342-343.

Dash, N., Lupetin, A. R. (1991). Uterine Rupture Secondary to Trauma: CT Findings. *Journal of Computer Assisted Tomography*, 15(2):329-331.

Dittrich, K. C. (1996). Rupture of the Gravid Uterus Secondary to Motor Vehicle Trauma. *Journal of Emergency Medicine*, 14(2):177-180.

Evard, J. R., Sturner, W. Q., Murray, E. J. (1989). Fetal Skull Fracture from an Automobile Accident. *American Journal of Forensic Medicine and Pathology*, 10(3):232-234.

Fakhoury, G. W., Gibson, J. R. M. (1986). Seat Belt Hazards in Pregnancy: Case Report. *British Journal of Obstetrics and Gynaecology*, 93(4):395-396.

Ford, R. M., Picker, R. H. (1989). Fetal Head Injury Following Motor Vehicle Accident; An Unusual Case of Intrauterine Death. *Australian and New Zealand Journal of Obstetrics and Gynecology*, 29(1):72-73.

Fries, M. H., Hankins, G. D.V. (1989). Motor Vehicle Accident Associated with Minimal Maternal Trauma but Subsequent Fetal Demise. *Annals of Emergency Medicine*, 18(3):301-304.

Galle, P. C., Anderson, S. G. (1979). A Case of Automobile Trauma During Pregnancy. *Obstetrics and Gynecology*, 54(4):467-468.

Griffiths, M., Hillman, G., Userwood, M. (1991). Seat Belt Injury in Pregnancy Resulting in Fetal Death. A Need for Education? Case Reports. *British Journal of Obstetrics and Gynaecology*, 98(3):320-321.

Handel, C. K. (1978). Case Report of Uterine Rupture After an Automobile Accident. *Journal of Reproductive Medicine*, 20(2):90-92.

Harrison, S. D., Nghiem, H. V., Shy, K. (1995). Uterine Rupture with Fetal Death Following Blunt Trauma. *American Journal of Roentgenology*, 165(6):1452.

Hartl, R., Ko, K. (1996). In Utero Skull Fracture: Case Report. *Journal of Trauma*, 41(3):549-552.

Heitzman, E. R., Markarian, B. (1970). Vaginal Bleeding After Trauma in Pregnant Woman. *New York State Journal of Medicine*, 70(18):2338-2340.

Kettel, L. M., Branch, D. W., Scott, J. R. (1988). Occult Placental Abruption After Maternal Trauma. *Obstetrics and Gynecology*, 71(3 pt 2):449-453.

Knuppel, R. A., Salvatore, D. L., Agarwal, R., et al. (1994). Documented Fetal Brain Damage Resulting From a Motor Vehicle Accident. *Journal of Ultrasound in Medicine*, 13(5):402-404.

Landers, D. F., Newland, M., Penney, L. L. (1989). Multiple Uterine Rupture and Crushing Injury of the Fetal Skull After Blunt Maternal Trauma: A Case Report. *Journal of Reproductive Medicine*, 34(12):988-993.

Lavin, J. P., Miodovnik, M. (1981). Delayed Abruption After Maternal Trauma as a Result of an Automobile Accident. *Journal of Reproductive Medicine*, 26(12):621-624.

Levin, R. D., Edson, M. (1994). A Pregnant Pause: Blunt Urologic Trauma in a Young Woman. *Urology*, 44(5):764-767.

Matthews, C. D. (1975). Incorrectly Used Seat Belt Associated with Uterine Rupture Following Vehicular Collision. *American Journal of Obstetrics and Gynecology*, 121(8):1115-1116.

Matthews, G., Hammersley, B. (1997). A Case of Maternal Pelvic Trauma Following a Road Traffic Accident, Associated with Fetal Intracranial Haemorrhage. *Journal of Accident and Emergency Medicine*, 14(2):115-7.

McCormick, D.R. (1968). Seat Belt Injury: Case of Complete Transection of Pregnant Uterus. *Journal of the American Osteopathic Association*, 67(10):1139-1141.

Nichols, M. M., Weedn, V. W. (1986). Placental Laceration and Stillbirth Following Motor Vehicle Accident: with Legal Ramifications. *Texas Medicine*, 82(3):26-28.

Parkinson, E. B. (1964). Perinatal Loss Due to External Trauma To The Uterus. *American Journal of Obstetrics and Gynecology*, 90(1):30-33.

Pearlman, M. D., (1997). Motor Vehicle Crashes, Pregnancy Loss, and Preterm Labor, *International Journal of Gynaecology and Obstetrics*, 57(2):127-132.

Pearlman, M. D., Tintinalli, J. E., Lorenz, R. P. (1990). Blunt Trauma During Pregnancy. *New England Journal of Medicine*, 323(23):1609-1613.

Pearlman, M. D., Tintinalli, J. E., Lorenz, R. P, et al., (1988). Trauma in Pregnancy. *Annals of Emergency Medicine*, 17(8):829-834.

Pepperell, R. J., Rubinstein, E., MacIsaac, I. A. (1977). Motor-Car Accidents During Pregnancy. *Medical Journal of Australia*, 1(7):203-205.

Poulson, Jr., A. M., Gabert, H. A. (1973). Fetal Death Secondary to Nonpenetrating Trauma to the Gravid Uterus. *American Journal of Obstetrics and Gynecology*, 116(4):580-582.

Pritchard, J. A., MacDonald, P. C., Gant, N. F. (1985). *Williams Obstetrics*, Seventeenth Edition. Appleton-Cnetruy-Crofts, Norwalk.

Punnonen, R. (1974). Traumatic Premature Separation of Placenta. *Annales Chirurgiae et Gynaecologiae Fenniae*, 63(6):487-488.

Raney, E. H. (1970). Fetal Death Secondary to Non-Penetrating Trauma to the Gravid Uterus.

American Journal of Obstetrics and Gynecology, 106(2):313-314.

Ravangard, F., Porter, C. V. (1980). Traumatic Laceration of the Placenta. *West Virginia Medical Journal*, 76(6):125-129.

Rothenberger, D. A., Horringan, T. P., Sturm, J. T. (1981). Neonatal Death Following In Utero Traumatic Splenic Rupture. *Journal of Pediatric Surgery*, 16(5):754-755.

Rowe, T. F., Lafayette, S., Cox, S. (1996). An Unusual Fetal Complication of Traumatic Uterine Rupture. *Journal of Emergency Medicine*, 14(2):173-176.

Rubovits, F. E. (1964). Traumatic Rupture of the Pregnant Uterus From "Seat Belt" Injury. *American Journal of Obstetrics and Gynecology*, 90(6):828-829.

Sherer, D. M., Abramowicz, J. S., Babkowski, R., et al. (1993). Extensive Fetal Intrathoracic Injuries Sustained in a Motor Vehicle Accident. *American Journal of Perinatology*, 10(10):414-416.

Siddal-Allum, J. N., Hughes, J. H., Kaler, S., Reginald, P. W. (1991). Splenic Rupture in Utero Following a Road Traffic Accident: Case Report. *British Journal of Obstetrics and Gynaecology*, 98(3):318-319.

Sims, C. J., Boardman, C. H., Fuller, S. J. (1996). Airbag Deployment Following a Motor Vehicle Accident in Pregnancy. *Obstetrics and Gynecology*, 88(4 pt 2):726.

Smith, A. J., LeMire III, W. A., Hurd, W. W., and Pearlman, M. (1994). Repair of the Traumatically Ruptured Gravid Uterus. *Journal of Reproductive Medicine*, 39(10):825-828.

Stafford, P. A., Biddinger, P. W., Zumwalt, R. E. (1988). Lethal Intrauterine Fetal Trauma. *Obstetrics and Gynecology*, 159(2):485-589.

Stuart, G. C. E., Harding P. G. R., Davies, E. M. (1980). Blunt Abdominal Trauma in Pregnancy. *Canadian Medical Association Journal*, 122(8):901-905.

Svendsen, E., Morild, I. (1988). Fetal Strangulation Following Uterine Rupture. *American Journal of Forensic Medicine and Pathology*, 9(1):54-57.

Van Enk, A., Van Zwam, W. (1994). Uterine Rupture: A Seat Belt Hazard. *Acta Obstetricia et Gynecologica Scandinavcia*, 73(5):432-433.

Weinstein, E. C., Pallais, V. (1968). Rupture of the Pregnant Uterus From Blunt Trauma. *Journal of Trauma*, 8(6):1111-1112.

Whitehouse, D. B. (1972). Hazard to Fetus from Safety Harness. *British Medical Journal*, 1(798):510.

APPENDIX A

TABLE A.1 SUMMARY OF AUTOMOTIVE CRASHES INVOLVING PREGNANT OCCUPANTS

No.	Occupant Position Impact Direction Impact Severity	Restraint	Gest Age (wk)	Maternal Injuries (italics indicate maternal fatality)	Fetal Outcome (italics indicate fetal survival)	Case Source
1	driver side impact	improper 3-pt belt	28	minor, placental abruption, uterine rupture	brain hemorrhages	Handel (1978)
2	driver front impact	none	34	moderate, pelvic fx, placental abruption, uterine rupture	skull fracture	Landers et al. (1989)
3	front passenger front impact	lap belt	22	minor, placental abruption, uterine rupture	decapitation	Rowe et al. (1996)
4	passenger side impact	none	37	minor, placental abruption, uterine rupture	stillborn	Pepperell et al. Case 13 (1977)
5	driver front impact moderate crash	none	34	minor, placental abruption, uterine rupture	stillborn	Agran et al. Case 6 (1986)
6	driver side impact	none	24	minor, pelvic fx, placental abruption, uterine rupture	stillborn	Dash & Leptin (1991)
7	rear passenger front impact severe crash	none	30	moderate, pelvic fx, placental abruption, uterine rupture	stillborn	Dittrich (1996)

TABLE A.1 SUMMARY OF AUTOMOTIVE CRASHES INVOLVING PREGNANT OCCUPANTS

No.	Occupant Position Impact Direction Impact Severity	Restraint	Gest Age (wk)	Maternal Injuries (italics indicate maternal fatality)	Fetal Outcome (italics indicate fetal survival)	Case Source
8	driver front impact moderate crash	3-pt belt	22	minor, placental abruption, uterine rupture	stillborn	Harrison et al. (1996)
9	rear passenger	improper lap belt	27	minor, placental abruption, uterine laceration	brain hemorrhage, transected aorta & spine, lacerated liver & kidney	Astarita & Feldman (1997)
10	driver front impact minor crash	3-pt belt + airbag	35	minor, placental abruption, uterine laceration	*premature birth, respiratory distress*	UMTRI GMP-006 (1997)
11	front passenger front crash	improper 3-pt belt	25	minor, placental abruption, uterine laceration	stillborn	Matthews (1975)
12	front passenger front crash	none	32	moderate, placental abruption, uterine laceration	stillborn	Smith et al. Case 1 (1994)
13	driver side impact	restrained	26	minor, placental abruption	skull fracture	Pepperell et al. Case 6 (1977)
14	passenger rollover	restrained	28	minor, placental abruption	rib fracture, liver rupture	Pepperell et al. Case 19 (1977)
15	driver front impact	none	35	moderate, placental abruption & laceration	skull fracture	Agran et al. Case 7 (1986)
16	driver front impact	none	34	*major, placental abruption*	skull fracture	Pepperell et al. Case 24 (1977)
17	driver front impact severe crash	none	28	minor, placental abruption	*emergency C/S, premature, respiratory distress*	Lavin and Miodovnik (1981)
18	rear passenger rear impact severe crash	none	34	minor, placental abruption	*premature*	UMTRI GMP-207A (1996)
19	front passenger rear impact severe crash	none	32	minor, placental abruption	*premature, possible head injury*	UMTRI GMP-207B (1996)
20	driver front impact severe crash	3-pt belt	34	minor, placental abruption	stillborn	Whitehouse (1974)
21	driver front impact	restrained	37	minor, placental abruption	stillborn	Pepperell et al. Case 4 (1977)
22	driver front impact	restrained	27	minor, placental abruption	stillborn	Pepperell et al. Case 5 (1977)
23	driver side impact	restrained	28	none, placental abruption	stillborn	Pepperell et al. Case 7 (1977)
24	driver side impact	restrained	29	minor, placental abruption	stillborn	Pepperell et al. Case 8 (1977)
25	passenger front impact	none	36	minor, placental abruption	stillborn	Pepperell et al. Case 10 (1977)
26	passenger front impact	none	26	moderate, placental abruption	stillborn	Pepperell et al. Case 11 (1977)
27	passenger front impact	restrained	32	none, placental abruption	stillborn	Pepperell et al. Case 15 (1977)

TABLE A.1 SUMMARY OF AUTOMOTIVE CRASHES INVOLVING PREGNANT OCCUPANTS

No.	Occupant Position Impact Direction Impact Severity	Restraint	Gest Age (wk)	Maternal Injuries (italics indicate maternal fatality)	Fetal Outcome (italics indicate fetal survival)	Case Source
28	passenger side impact	restrained	36	moderate, placental abruption	stillborn	Pepperell et al. Case 16 (1977)
29	passenger side impact	restrained	30	minor, placental abruption	stillborn	Pepperell et al. Case 17 (1977)
30	passenger front impact	restrained	34	minor, placental abruption	stillborn	Pepperell et al. Case 18 (1977)
31	passenger front impact	restrained	34	minor, placental abruption	stillborn	Pepperell et al. Case 20 (1977)
32	passenger front impact	restrained	37	minor, placental abruption	stillborn	Pepperell et al. Case 21 (1977)
33	passenger side impact	none	34	*major, pelvic fx, placental abruption*	stillborn	Pepperell et al. Case 25 (1977)
34	rear passenger rollover severe crash	none	23	moderate, placental abruption	stillborn	Agran et al. Case 2 (1986)
35	driver front impact moderate crash	none	23	minor, placental abruption	stillborn	Agran et al. Case 3 (1986)
36	driver front impact severe crash	none	26	minor, placental abruption	stillborn	Agran et al. Case 4 (1986)
37	driver front impact	none	30	minor, placental abruption	stillborn	Agran et al. Case 5 (1986)
38	driver front impact moderate crash	none	38	minor, placental abruption	stillborn	Agran et al. Case 8 (1986)
39	driver front impact	none	39	minor, placental abruption	stillborn	Agran et al. Case 9 (1986)
40	driver multiple impact	3-pt belt	32	moderate, pelvic fx, placental abruption	stillborn	Pearlman et al. (1988)
41	driver front impact severe crash	3-pt belt	40	moderate, placental abruption	stillborn	UMTRI GMP-101 (1997)
42	driver front impact	3-pt belt	24	none, placental abruption	stillborn	UMTRI GMP-208 (1994)
43	front passenger side impact	none	31	minor, pelvic fx, partial placental abruption, uterine laceration	skull fracture, scalp laceration	Poulson & Gabert (1973)
44	driver front impact	none	29	moderate, partial placental abruption, uterine laceration	*emergency C/S, premature*	Kettel et al. Case 2 (1988)
45	front passenger front impact	lap belt	28	minor, partial placental abruption	brain hemorrhages	Raney (1970)
46	front passenger side impact	none	37	moderate, pelvic fx, partial placental abruption	*emergency C/S, skull fracture, brain hemorrhages, apnea*	Bowdler et al. (1987)
47	front passenger front impact	none	33	minor, partial placental abruption	brain hemorrhages	Stafford et al. Case 4 (1988)

TABLE A.1 SUMMARY OF AUTOMOTIVE CRASHES INVOLVING PREGNANT OCCUPANTS

No.	Occupant Position Impact Direction Impact Severity	Restraint	Gest Age (wk)	Maternal Injuries (italics indicate maternal fatality)	Fetal Outcome (italics indicate fetal survival)	Case Source
48	front passenger multiple impact	3-pt belt	34	none, pelvic fx, partial placental abruption	skull fracture, brain contusions and lacerations	Stafford et al. Case 5 (1988)
49	driver front impact	none	27	minor, partial placental abruption	brain hemorrhages	Stafford et al. Case 8 (1988)
50	rear passenger rollover	none	41	minor, partial placental abruption	*emergency C/S, skull fracture*	Hartl and Ko (1996)
51	driver front	none	36	none, partial placental abruption	chest hemorrhages	Stafford et al. Case 2 (1988)
52	driver front impact minor crash	none	39	none, partial placental abruption	lacerated spleen	Rothenberger et al. (1981)
53	driver front impact	none	39	moderate, partial placental abruption	liver, adrenal, and kidney contusions, seizures	Connor & Curran (1976)
54	driver front impact minor crash	none	36	none, partial placental abruption	*emergency C/S, premature*	Punnonan (1974)
55	front passenger front impact severe crash	lap belt	37	none, partial placental abruption	*emergency C/S, seizures, renal failure*	Chetcuti and Levene (1987)
56	front passenger	none	34	none, partial placental abruption	*emergency C/S, premature*	Kettel et al. Case 3 (1988)
57	driver front impact	none	41	minor, partial placental abruption	stillborn	Nichols & Weedn (1986)
58	driver side impact	none	24	moderate, placental laceration, uterine laceration	stillborn	Weinstein & Pallais (1968)
59	driver front impact	none	39	none, placental laceration	stillborn	Pepperell et al. Case 2 (1977)
60	front passenger front impact	none	36	minor, placental laceration	stillborn	Ravangard & Porter (1980)
61	driver front impact severe crash	lap belt	34	moderate, placental laceration	stillborn	Stuart et al. Case 1 (1980)
62	driver front impact severe crash	none	28	minor, placental laceration	stillborn	Stuart et al. Case 2 (1980)
63	driver front impact severe crash	none	37	moderate, placental laceration	stillborn	Civil et al. (1988)
64	driver front impact	none	21	minor, placental laceration	stillborn	Stafford et al. Case 3 (1988)
65	front passenger	3-pt belt	36	moderate, placental laceration	head contusions	Griffiths et al. (1991)
66	driver front impact minor crash	none	37	minor, placental damage	skull fracture, brain hemorrhage	Cumming & Wren (1978)

TABLE A.1 SUMMARY OF AUTOMOTIVE CRASHES INVOLVING PREGNANT OCCUPANTS

No.	Occupant Position Impact Direction Impact Severity	Restraint	Gest Age (wk)	Maternal Injuries (italics indicate maternal fatality)	Fetal Outcome (italics indicate fetal survival)	Case Source
67	driver front impact	lap belt	33	minor, placental damage	skull fracture, brain hemorrhage	Stafford et al. Case 6 (1988)
68	driver front impact	none	32	minor, pelvic fx, placental damage	brain hemorrhages	Stafford et al. Case 7 (1988)
69	front passenger	3-pt belt	31	minor, placental damage	stillborn	Griffiths et al. (1991)
70	front passenger front impact	improper lap belt	20	none, uterine transection	transection	McCormick (1968)
71	driver rear impact	none	39	minor, uterine laceration	*emergency delivery, seizures, respiratory distress*	Galle & Anderson (1979)
72	driver front impact	none	20	minor, pelvic fx, uterine laceration	stillborn	Heitzman & Markarian (1970)
73	front passenger side impact	none	37	minor, pelvic fx, uterine laceration	stillborn	Smith et al. Case 2 (1994)
74	front passenger front impact	3-pt belt	30	minor, uterine rupture	strangled by cord	Svendsen & Morild (1988)
75	front passenger front impact severe crash	lap belt	24	minor, uterine rupture	stilllborn	Rubovits (1964)
76	driver front impact	restrained	22	minor, uterine rupture	stillborn	Pepperell et al. Case 9 (1977)
77	passenger side impact	restrained	30	minor, uterine rupture	stillborn	Pepperell et al. Case 14 (1977)
78	front passenger multiple impact	3-pt belt	32	moderate, uterine rupture	stillborn	Van Enk & Van Zwam (1994)
79	driver front impact	none	36	none	splenic rupture	Siddall-allum et al. (1991)
80	front passenger side impact	lap belt	24	minor	*spinal cord damage/paraplegia*	Weyerts et al. (1992)
81	front passenger side impact moderate crash	none	28	*major*	arm fracture	UMTRI GMP-002 (1996)
82	front passenger front impact severe crash	3-pt belt	30	minor	head, thorax, and abdomen hemorrhages	Fakhoury & Gibson (1986)
83	driver front impact severe crash	3-pt belt	27	none	cerebral hemorrhage, hepatic hemorrhage, hemoperitoneum	Fries & Hankins (1989)
84	driver side impact	none	27	pelvic fx	skull fracture, brain hemorrhages, thoracic hemorrhages	Sherer et al. (1993)
85	driver front impact	none	30	none	skull fracture	Pepperell et al. Case 3 (1977)
86	driver side impact severe crash	none	32	*moderate, pelvic fx*	skull fracture	Evrard et al. (1989)
87	driver front impact	restrained	30	moderate	brain hematomas	Ford & Picker (1989)

TABLE A.1 SUMMARY OF AUTOMOTIVE CRASHES INVOLVING PREGNANT OCCUPANTS

No.	Occupant Position Impact Direction Impact Severity	Restraint	Gest Age (wk)	Maternal Injuries (italics indicate maternal fatality)	Fetal Outcome (italics indicate fetal survival)	Case Source
88	front passenger side impact minor crash	none	37	minor	*brain hemorrhage, apnea, seizures*	UMTRI GMP-001 (1996)
89	driver side impact	3-pt belt	39	moderate, pelvic fx	*emergency C/S, brain contusion, seizures*	Matthews & Hammersly (1997)
90	driver front impact severe crash	none	25	minor	*contractions stopped w/o intervention, brain damage*	Knuppel et al. (1994)
91	front passenger front impact severe crash	none	28	minor	*hydrocephalus, possibly from crash*	UMTRI GMP-013 (1997)
92	driver minor crash	restrained + airbag	33	minor	*contractions stopped without intervention*	Sims et al. Case 3 (1996)
93	front passenger front impact moderate crash	3-pt belt + airbag	31	minor	*contractions stopped without intervention*	UMTRI GMP-009 (1997)
94	front passenger front impact	none	38	minor	amniotic membrane rupture	Parkinson Case 3 (1964)
95	front passenger front impact severe crash	none	24	*major*	stillborn	Agran et al. Case 1 (1986)
96	driver side impact severe crash	none	23	*major*	stillborn	UMTRI GMP-205 (1997)
97	driver front impact severe crash	3-pt belt	28	minor	stillborn	UMTRI GMP-206 (1995)
98	front passenger side impact severe crash	3-pt belt	22	*major*	stillborn	UMTRI GMP-212 (1997)
99	driver side impact	none	36	none	stillborn	Pepperell et al. Case 1 (1977)
100	passenger side impact	none	38	moderate	stillborn	Pepperell et al. Case 12 (1977)
101	passenger front impact	none	38	*major*	stillborn	Pepperell et al. Case 23 (1977)
102	passenger front impact	none	26	*major*	stillborn	Pepperell et al. Case 26 (1977)
103	front passenger front impact minor crash	none	39	moderate	*no complications*	UMTRI GMP-003 (1996)
104	driver side impact moderate crash	3-pt belt	20	minor, pelvic fx	*no complications*	UMTRI GMP-004 (1997)
105	driver front impact minor crash	airbag	23	minor	*no complications*	UMTRI GMP-005 (1997)

TABLE A.1 SUMMARY OF AUTOMOTIVE CRASHES INVOLVING PREGNANT OCCUPANTS

No.	Occupant Position Impact Direction Impact Severity	Restraint	Gest Age (wk)	Maternal Injuries (italics indicate maternal fatality)	Fetal Outcome (italics indicate fetal survival)	Case Source
106	driver side impact minor crash	3-pt belt	35	minor	*no complications*	UMTRI GMP-007 (1997)
107	front passenger front impact minor crash	3-pt belt	36	minor	*no complications*	UMTRI GMP-008 (1997)
108	driver side impact minor crash	3-pt belt + airbag	22	minor	*no complications*	UMTRI GMP-011 (1997)
109	front passenger side impact minor crash	3-pt belt	31	minor	*no complications*	UMTRI GMP-012 (1997)
110	driver front impact minor crash	3-pt belt + airbag	26	minor	*no complications*	UMTRI GMP-014 (1997)
111	driver front impact minor crash	3-pt belt + airbag	38	minor	*no complications*	UMTRI GMP-201 (1997)
112	driver front impact minor crash	airbag	38	moderate	*no complications*	UMTRI GMP-202 (1996)
113	front passenger front impact moderate crash	3-pt belt	38	minor	*no complications*	UMTRI GMP-203 (1996)
114	front passenger front impact minor crash	3-pt belt + airbag	36	minor	*no complications*	UMTRI GMP-204 (1996)
115	driver side impact minor crash	3-pt belt	40	none	*no complications*	UMTRI GMP-209 (1997)
116	driver rear impact minor crash	3-pt belt	37	minor	*no complications*	UMTRI GMP-210 (1997)
117	driver front impact moderate crash	3-pt belt + airbag	39	moderate	*no complications*	UMTRI GMP-211 (1997)
118	front passenger severe crash	restrained	?	none, pelvic fx	*no complications*	Levin & Edson (1994)
119	driver side impact minor crash	restrained + airbag	39	none	*no complications*	Sims et al. Case 1 (1996)
120	driver front impact moderate crash	restrained + airbag	35	minor	*no complications*	Sims et al. Case 2 (1996)

MORPHOMETRIC STUDY OF THE HUMAN PELVIS

Benoît BESNAULT
François LAVASTE
Laboratory of Biomechanics, ENSAM
Hervé GUILLEMOT
CEESAR, European Center of Safety and Risk Analysis
Stéphane ROBIN
Jean-Yves LE COZ
Laboratory of Accidentology and Biomechanics, PSA Peugeot-Citroën Renault
France
Paper Number 98-S9-P-18

ABSTRACT

Finite element model analysis and numerical simulations are more and more used in the field of automobile safety. The models of anthropomorphic dummies are already developed. The following work, which is carried out both by the Laboratory of Biomechanics LBM (ENSAM) and the Laboratory of Accidentology and Biomechanics LAB (Nanterre), consists in a geometrical study of the human pelvis. This analysis, based on the Reynolds' data, is performed to determine significant parameters for each class of pelvis. A statistical study has been performed with Student and Snedecor tests, to analyse the means and the variances of the characters. These parameters, exclusively computed distances, could be used to distort a mesh with an interpolation technique (kriging).

INTRODUCTION

Finite element model analysis and numerical simulations are more and more used in the field of the automobile safety. The models of anthropomorphic dummies were already developed, but the behaviour of the human being in car accidents needs now a new approach, consisting in the development of a human FE model. The biomechanical aspects were previously studied through cadaver tests, this FE model will increase our biomechanical knowledge, particularly for the evaluation of new safety devices in vehicle environment.

This work, which is carried out both by the Laboratory of Biomechanics LBM (ENSAM) and the Laboratory of Accidentology and Biomechanics LAB (Nanterre), consists first in an anatomical reconstruction of a human being, in a seated position. The next step consists in the validation of each segment, as well as a whole body evaluation. But the multiple human parameters, age, gender or geometry, results in a wide range of responses from cadavers tests used for the validation.

Thus this paper is focused on the pelvic bone and its geometry. A statistical analysis based on Reynolds' data [6], is performed to extract significant parameters, for each class of pelvis.

These parameters could be used to distort an existing mesh of the pelvic bone.

ANALYSIS OF THE REYNOLDS' DATA

H.M. Reynolds [6] published a morphometric study of the pelvis of the United States' population.

The Classification was done on the factor H.E.S. basis (Health and Examination Survey) resulting from a study made by the U.S. Public Health Service between 1961 and 1964. This factor stipulates that a relationship between the size and the weight of a subject exists.

The assumption made by Reynolds and based on criterion H.E.S., was that the size and the weight of the pelvis vary like the stature.

The pelvis measured by Reynolds result from the "collection" of Hamann-Todd skeletons of the Cleveland Museum of Natural History (3000 pelvis) collected between 1919 and 1939. The weight, the size and the age of each subject have been indexed.

Reynolds defined 3 pelvis sizes for the 2 genders, according to the size and the weight, by adding a corrective factor to the weight considered as too weak (Figure 1).

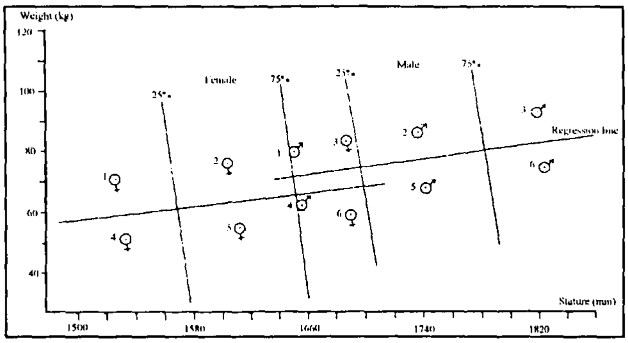

Figure 1 : Distribution of the population (after Reynolds)

He retained for its study only 3 groups :

- Small Female (SF)
- Medium Male (MM)
- Large Male (LM)

The pattern of the measured settlement is thus the following : Small female 24% - Medium male 52% - Large male 24%.

The pelvis population being able to be measured consists of 165 pelvis. Within sight of the 3 groups chosen, only 88 pelvis will be measured, divided into Small female (28), Medium male (34), Large male (26).

The reference axis system of measurement (Figure 2) is an anatomical reference system, which corresponds to the pelvis position of the subject in standing position.

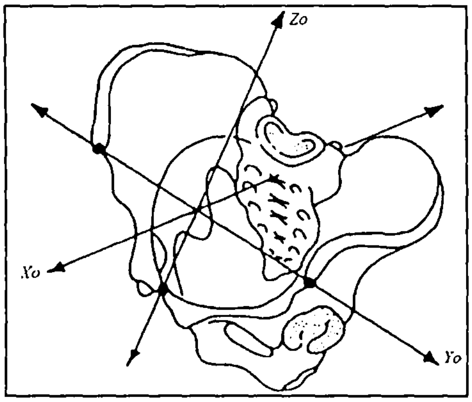

Figure 2 : Reference axis system R_0 of measurement

Reynolds thus measured 105 points per pelvis, by considering a symmetrical pelvis. The measured points (on the right half-pelvis) are represented on the following pictures (Figures 3-4-5-6-7).

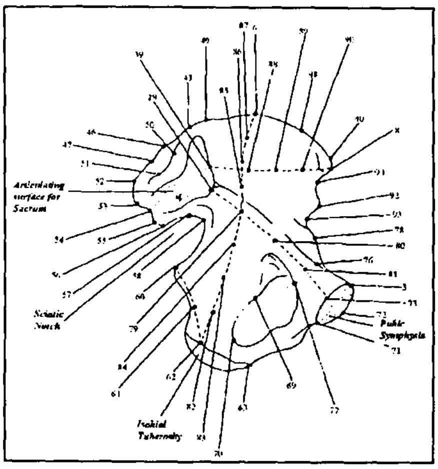
Articulating surface for Sacrum
Sciatic Notch
Ischial Tuberosity
Pubic Symphysis

Figure 3 : Data points for the iliac wing (after Reynolds)

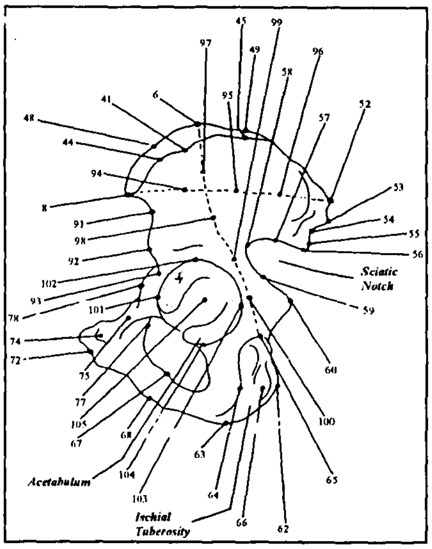
Sciatic Notch
Acetabulum
Ischial Tuberosity

Figure 4 : Data points for the iliac wing (after Reynolds)

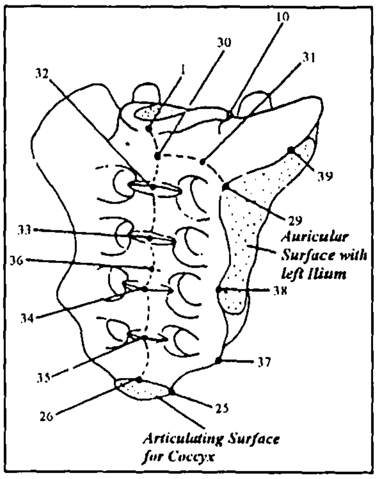
10
30
31
32
1
39
29
Auricular Surface with left Ilium
33
36
38
34
37
35
25
26
Articulating Surface for Coccyx

Figure 5 : Data points for the sacrum (after Reynolds)

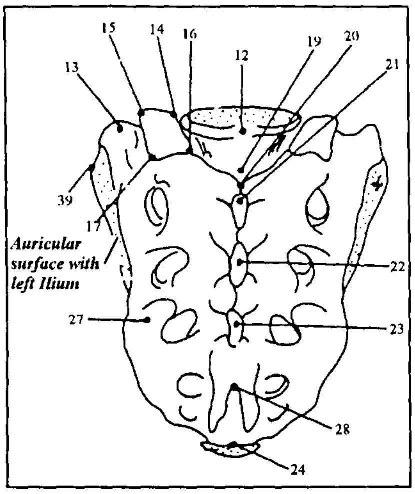

Figure 6 : Data points for the sacrum (after Reynolds)

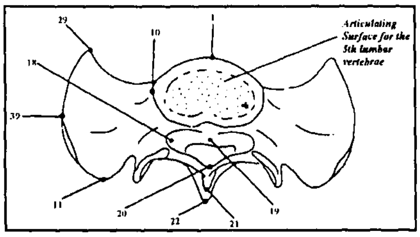

Figure 7 : Data points for the sacrum (after Reynolds)

In Reynolds' publication, the average values, the standard deviation and the number of measurements associated with each coordinate, are given.

The first 9 measured points are used to locate the pelvis skew system.

The number of measurements and the standard deviation are variable according to the measured coordinate. The palpation variation of some points, whose definition is not precise enough, generates a great uncertainty (Points in the medium of the iliac wings, edges of the iliac wings).

Statistical calculations are made on small samples, the number of measurements being at the utmost of 34.

To be able to apply statistical tests, the studied characters must follow a normal law distribution and their variances must be equal. The characters' normality is an assumption made by Reynolds since he carries out calculations of average and standard deviation (Gaussian law). This is the case in biology where the characters result from the addition of multiple independent effects, that follow laws close to the normal one. The differential factor acts much more on the average value than on the variability.

METHOD

Notations used :

- For the sample :	Number of individuals	n
	Standard deviation	s
	Mean	m
- For the population :	Number of individuals	N
	Standard deviation	σ
	Mean	$\bar{x}$

For each Reynolds' group and each coordinate, we initially calculate the average of the total population, the standard deviation on the average and the total.

Then we calculate the minima and maxima values of the average, and the minima and maxima values of the character, by considering that the average of the population x and the sample m are identical.

These values are calculated by considering only 68% of the population, which corresponds to the calculation of the minima and maxima values with ± ?.

Calculation of the standard deviation on the average :

$$v(\bar{x}) = \sqrt{\frac{1}{n-1}}.s$$

Calculation of the total standard deviation :

$$\sigma = \sqrt{\frac{n}{n-1}}.s$$

Comparison statistical tests on the points are carried out to determine characteristic points of the structure.

Since the test of comparison is only possible if the compared characters have identical standard deviations, a statistical test must also be applied to the variances.

COMPARISON OF THE VARIANCES

To check the variances' equality, those of the two characters are compared.

For sample A and B :

- Number of individuals	n_A	n_B
- Standard deviation	σ_A	σ_B
- Mean	m_A	m_B
- Estimated variance		

$$s_A = \sqrt{\frac{n_A}{n_A-1}}.\sigma_A \qquad s_B = \sqrt{\frac{n_B}{n_B-1}}.\sigma_B$$

The test of Snedecor F is applied.

The ratio F is calculated : $F = \frac{s_A^2}{s_B^2}$

from where $$F = \frac{(n_B - 1).n_A.\sigma_A^2}{(n_A - 1).n_B.\sigma_B^2}$$

The value F is compared to the Fs from the table " point 2,5% " [7] at intersection of column (n_A-1) and line (n_B-1). If F is lower than Fs, the two variances do not differ significantly (to 5%). This percentage is the one used as reference in medical and biological tests.

COMPARISON OF THE AVERAGES

The comparison of the averages is based on calculation of the parameter t, and is valid if the variances of the characters are closely related (test of Snedecor F).

We will compare the samples two by two. Three comparisons should be made, between the small female and the medium man, between the small female and the large man and between the medium man and the large man. The comparison will be carried out between small samples (n<30), or between a small sample and a big one (n>30). Calculations will be in any case identical in both cases.

The variable t is calculated : $$t = \frac{m_A - m_B}{\sqrt{\frac{s_A^2}{n_A} + \frac{s_B^2}{n_B}}}$$

For this calculation, s^2 is the common likely variance of the two samples :

$$s = \sqrt{\frac{(n_A - 1).s_A^2 + (n_B - 1).s_B^2}{n_A + n_B - 2}}$$

If |t| is lower than t from the table [7] for a degree of freedom equal to (n_A+n_B-2) and a risk of 5% (value retained by the biologists), the difference between the two characters tested is not significant. In the contrary case, it is significant.

COMPARISON OF THE POINTS

The populations are compared two by two, according to the three coordinates by differentiating them X, Y then Z.

In order to have a significant coordinate, the variances should not differ significantly from more than 5% and the t test should be significant for the three comparisons.

Thus all the significant coordinates are deduced from the 105 Reynolds' points.

Moreover, we study the variation of the coordinates to determine its monotony (increase or decrease on three groups SF-MM-LM), and then to deduce the really significant points.

Only 13 coordinates are therefore significant on the 315 raised by Reynolds. We observe an increase of the coordinate values, therefore a total increase in pelvis dimensions is related to the size of the subject (for example, width of the sacrum).

Only few points are significant for this classification, measurements of distances would have been more significant to classify the pelvis.

We then become interested in the distances resulting from the points measured by Reynolds.

COMPARISON OF THE DISTANCES

Anatomical Distances - Distances which, from an anatomical point of view, appear representative of general dimensions and the pelvis morphology, are calculated. 28 distances are thus calculated for each of Reynolds' pelvis. These distances are used in obstetrics before a childbirth.

The calculated distances are for example :

- Diameter of acetabulum
- Width of the pelvic operture
- Biischial distance (between right and left tuberosities)
- Distance between iliac crests
- Pelvis width
- Distance between the two posterior superior iliac spines
- Height of the pelvis (between the top of the iliac crest and the ischial tuberosity)
- Angle of pubic arch
- Axis of foramen obturator
- Width of the sacrum
- Height of the sacrum
- Distances between the pubic symphysis and the sacral vertebrae (which characterize the curve of the sacrum).

None of them appear significant to differentiate the pelvis. We can notice that some distances are more important for the female than for the male :

- Biischial distance
- Width of the pelvic operture
- Angle of pubic arch

The pelvis morphology of the male is thus completely different from the female's one, which assures us in our search for significant parameters, to get different finite element models.

To determine significant distances differentiating the pelvis groups, only a calculation of all the distances between all the points of a pelvis (measured and symmetrical) enables us to extract the most significant one and therefore the parameters.

Significant Distances - Afterwards we consider a complete pelvis instead of a half one. The pelvis are always regarded as symmetrical. Each pelvis thus consists of 210 points on the whole, with redundant points. The number of calculated distances for one pelvis is thus higher than 21000, and these distances are associated with their standard deviation and a number of measurements.

Standard deviation of a point - To determine the standard deviation relating to a point, the maximum standard deviation on the 3 coordinates is considered. As a matter of fact, the point is included statistically in an ellipsoid of semi-axes (σ_X; σ_Y; σ_Z) (Figure 8) , by considering 68 % of the population.

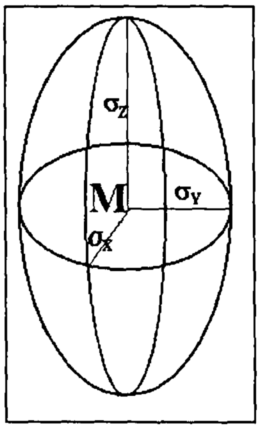

Figure 8 : Standard deviation ellipsoid around a point

By only taking account of the maximum standard deviation on the 3 coordinates, the point is included statistically in a sphere of $2\sigma_{max}$ diameter (Figure 9). The number of measurements associated with the point is the one which is associated with the maximum standard deviation.

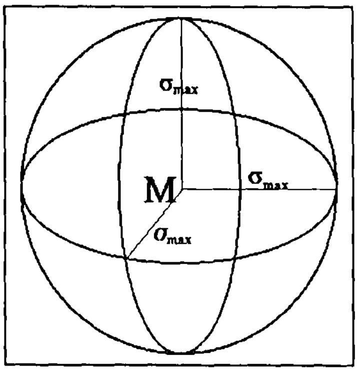

Figure 9 : Standard deviation sphere around a point

Distance between 2 points - The calculation of the average distances between the points is easy.

We consider 2 points M_1 and M_2 and the associated variation-types $?_1$ and $?_2$. The average distance between these two points is : $dist = \left\|\overline{M_1 M_2}\right\|$

The standard deviation connected with this distance is :

$$\sigma_{dist} = \sqrt{\sigma_1^2 + \sigma_2^2}$$

The number of associated distances is equal to the lowest number of measurements on the coordinates of the 2 points.

In this way, we obtain all the distances, the standard deviation and the number of distances associated, for the 3 Reynolds' pelvis classes.

Using the same statistical tests as those applied to the points, we deduce from them the characteristic distances for tests with 5% and monotonous variations (Distances Small Female < Distances Medium Male < Distances Large Male).

So we obtain 490 significant distances to differentiate the 3 different pelvis groups.

Among them, some are not reliable. Indeed, some points cannot be taken into account. They are on the symmetry plane of the pelvis, others are already on the right half-pelvis. Others still have high degree of uncertainty of palpation, the localisation of the point is not very reliable taking into account its geometrical definition.

The number of distances is now reduced to 378, then to 264 by removing the redundant distances. These distances must be individually studied to evaluate their relevance and facility of measurement.

The selection criteria for the distances are the following

- Palpation facility of the extreme points
- Distances concerning the points of the general reference marks
- Distances concerning the anatomically recognised points
- Distances along the axes, but also omnidirectional to get the complete morphological differences.

So we obtain 138 significantly different distances to classify the pelvis according to the 3 Reynolds' groups.

PELVIS CLASSIFICATION

Geometry Acquisition - The purpose of this geometrical study is to obtain a pelvis data base resulting from French human beings and the classification of the pelvis according to the Reynolds' groups.

The used measurement protocol is based on the palpation of isolated pelvis, resulting from the given body. The measured points are a result of the Reynolds' study and are adapted so as to be compared with his results. The reference system of measurement (Figure 10), related to the assembly of setting and maintenance in position of the pelvis, is not identical to the Reynolds' one but differs only by a rotation around the Y axis and a translation.

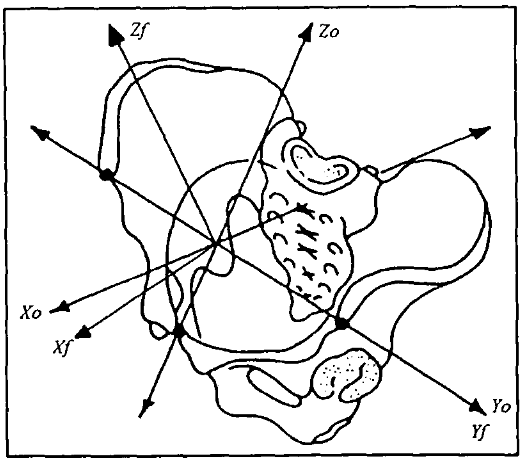

Figure 10 : Reference axis system of Reynolds R_0 & Guillemot's R_f measurement

The Fastrak's measurement device is an electromagnetic system composed of a pen and 3 motionless magnetic reels. The movement of the pen induces a modification of the magnetic field in the reels, which makes it possible to calculate the coordinates of the pen point compared to a reference mark related to the reels. The assembly of measurement consists of Plexiglas and plastic elements to avoid any interference with this magnetic system.

The weight and volume are also measured for each pelvis.

The data base currently consists of 25 pelvis.

Pelvis Comparison - We consider the points which take into account the significant distances such as principal nodes. There are 53 nodes, whereas there are 189 measured and symmetrized points, therefore 28% of the totality of the points. On these principal nodes, we build a structure for the 3 pelvis groups (SF-MM-LM) and we compare visually to the measured pelvis. We can observe on the following picture the comparison of this structure for the MM geometry with 50th percentile male FE model (Figure 11).

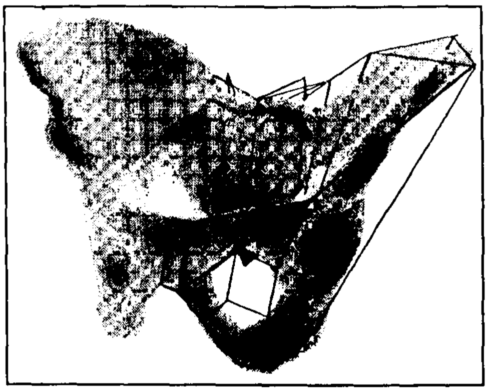

Figure 11 : Comparison between MM geometry and 50th percentile FE model

To have a more precise idea of the group of measured pelvis, we calculate, using our measurements, the significant distances. Then we compare them with those calculated with the Reynolds' pelvis. We give an impact to the calculated distance according to his nearness with the standard pelvis (Figures 12-13).

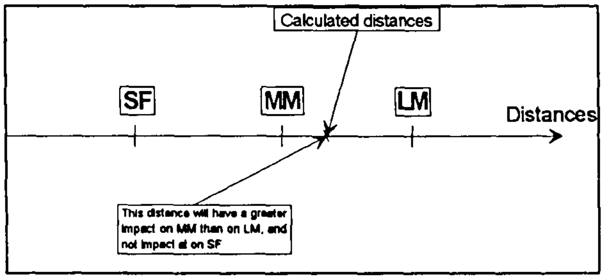
Calculated distances
SF
MM
LM
Distances
This distance will have a greater impact on MM than on LM, and not impact at on SF

Figure 12 : Impact distribution

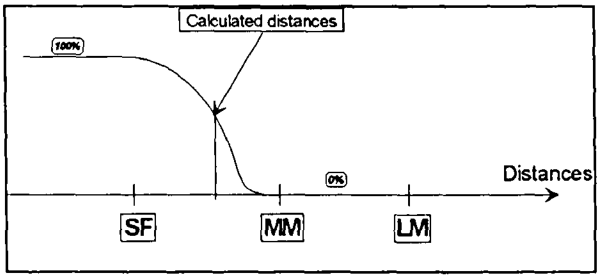

Figure 13 : Impact calculation

We add the relative impact of each group, the pelvis belongs to the group whose impact is the most significant. This procedure is automated to be carried out with each new pelvis.

We determined the significant distances on an unspecified pelvis, these distances are thus the parameters of the pelvis.

We extracted from them the principal points, they will be used for the deformation of an existing mesh for the adaptation to other geometries.

MESH DEFORMATION

Technique Used - To adapt as much as possible the FE model geometry to different morphologies, we chose to deform the existing mesh by the kriging technique. This technique enables us to obtain a personalied mesh while reducing the development time, and to adapt the 50th percentile pelvis mesh to the 5th and 95th percentile morphologies.

The kriging is a interpolation technique of statistical origin applied for the first time in 1951 by D.C. Krige to estimate the resources of a gold mine. Its formalism dates from the sixties and results from G. Matheron's works.

This technique generalises the least squares method by making it possible for the model to go through the measurement points (control points).

Automatic procedures has been developed, by using MATLAB, to allow the fast application of the algorithm of kriging.

Pelvis Kriging - The control points of the structure are the end points of the significant distances. They are regarded as remarkable and were thus selected. Their number is 57 for the complete pelvis, whose FE mesh comprises 1219 nodes, it is thus 5% compared to the totality of the model.

The deformations carried out enable us to obtain meshes adapted to various geometries. The results are visible on the following picture (Figure 14). We can note that the kriging give not aberrant deformations on the pelvis, which indicates a judicious choice of the control points. The geometry of the meshes presents morphological differences noted during our measurements on fresh pelvis.

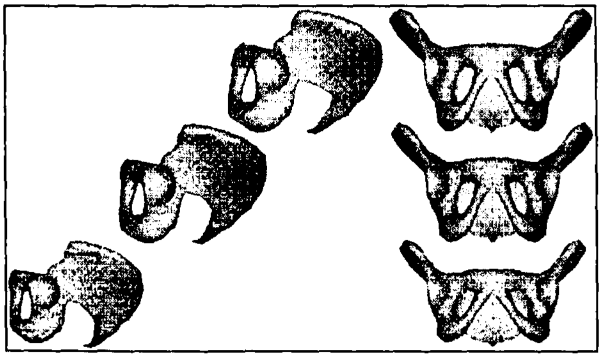

Figure 14 : 3 kriging pelvis models

CONCLUSION

It is still necessary to validate this deformation procedure, by evaluation of the generated error on surface, and to see the geometry influence during a FE simulation. This validation is in hand and lets predict good results.

Each dynamic test of H. Guillemot [9-10] on fresh pelvic bones was preceded by a points measurement, and could thus be simulated by taking into account of the geometry in order to gain a better appreciation of the fracture phenomenon.

Moreover this kriging technique opens the way towards the mesh of a 5th percentile female and a 95th percentile male without using homothetic deformations, prejudicial from a morphological point of view, but this technique requires the use of judiciously selected control points, which are difficult to find on the whole human body.

This work forms part of a vast program aiming at obtaining a human being FE model to predict the injuries, but also with different morphologies.

REFERENCES

1. Trochu, F. : A contouring program based on dual kriging interpolation, Engineering with computers, pp 160-177, 1993

2. De Silvio, E. : Surface modelling at Serra do Madeira mine in Pitinga, Amazo, Mine planning and equipment selection, Balkema - Rotterdam, 1994

3. Lele, S. : Inner produkt matrices, kriging, and non-parametric estimation of variogram, Mathematical geology, 27(5), pp 673-692, 1995

4. Knoters, M., Brus, D.J. and Oude Voshaar, J.H. : A comparison of kriging, co-kriging and kriging combined with regression for spatial interpolation of horizon depth with censored observations, Geoderma , 67, pp 227-246, 1995

5. Asli, M. and Marcotte, D. : Comparison of approaches to spatial estimation in a bivariate context, Mathematical geology, 27(5), pp 641-658, 1995

6. Reynolds, H., Snow, C. and Young, J. : Spatial geometry of the human pelvis, FAA Civil Aeromedical Institute, Oklahoma City

7. Schwartz, D. : Méthodes statistiques à l'usage des médecins et des biologistes, Médecine - Sciences, Flammarion

8. Guillemot, H. : Pelvic fracture under side impact loading condition, International conference on pelvic and lower extremity injuries, Washington, 1995

9. Guillemot, H. : Pelvic injuries in side impact collisions : an accidental analysis and dynamic tests on isolated pelvic bones, 41th Stapp CAR Crash Conference, 1997

10. Guillemot, H. : Etude biomécanique du bassin en choc latéral automobile, Thèse de docteur en biomécanique, ENSAM Paris, Nov. 1997

GEOMETRICAL CHARACTERISATION OF A SEATED OCCUPANT

Laurent Chabert
Equipements et Composants pour l'Industrie Automobile
Slah Ghannouchi
Laboratoire d'Anatomie, Faculté de Médecine de Sousse
Claude Cavallero
Laboratoire de Biomécanique Appliquée, Faculté de Médecine Nord, Université de la Méditerranée
France
Paper Number 98-S9-P-19

ABSTRACT

This paper presents the results from a project based on an anatomical study to improve the knowledge of the human anatomy for a belted car occupant.

The four phases for data collection consists of :

- the selection of a cadaver placed in a car seat.
- the realisation of a set of physical cross sections
- anatomical identification of organs seen on each section
- computer analysis and visualisation of organs.

General methods, from physical sections to 3D computer generated reconstruction were presented in [Chabert96].

The purpose of this present paper is to provide a geometrical description of a human body in the seat belt posture.

Many skeletal landmarks are viewed with reference to the H point, in the vehicle coordinate system. The pelvis and thoracic bones are seen with the seat belt below. The geometry of the spine is described by the 3D position of the centres of each vertebral body. The curvature, which is given by the angles between each vertebral axis along the spine is compared to an X-ray study performed on living volunteers. The anatomic results, which refer to a male PMHS closed to the 50° percentile, should be interesting in the fields of ergonomics, anthropometric dummy design and biomechanics.

INTRODUCTION

Human Anatomy descriptions are done according to a conventional position, which results from teaching inherent needs. New techniques in medical imaging and data-processing tools development allowed the rise of human three-dimensional representation in this position [Ackerman95]. However there are no data-bank available for the Anatomy human in seated position.

How can a study of the sitting position be conceive, which may go until the creation of a data-bank? The most adapted methodology can be neither the dissection, neither conventional radiology, nor even the nuclear magnetic imaging (CT-scan and MRI are currently unsuitable to perform examinations on people in seated positions).

The aim of our study is to provide elements for the anatomical study of human body seated on an automobile seat, this work is based on an anatomical analysis of PMHS placed in driving configuration on a usual automobile seat. The approach is based on the serial sectioning technique that has often been used in Anatomy. The elements seen on each section are placed in an initial reference frame for a geometrical description of the occupant. With a validating aim, a study by radiography on volunteer subjects in sitting position on an automobile seat was undertaken.

METHODOLOGY

Choice of the PMHS

The subject used has morphological characteristics closed to the 50th male percentile for the two parameters : body mass and height (stature of 174 centimetres for a weight of 75kg). The body was treated by Winckler conservation technique [Winckler74], which restores a muscular flexibility and maintains a good articular mobility. A complete radiological examination was carried out in order to detect any pathology.

Seated position

We use a driver's cockpit obtained from a mid sized European mass-produced vehicle. This model car includes a seat with floor mountings, a steering column and wheel, control pedals and a restraint system. The seat, provided with a head-rest, is a standard piece which has longitudinal and backrest inclination adjustments. The seat is placed in configuration to use of a tester corresponding to the PMHS morphotype (50th percentile in our case). The subject's positioning on the seat is a very delicate stage and must be carried out with a lot of attention. Indeed, the only criteria to obtain a realistic position is the manipulators appreciation. After some adjustments on seat position, the subject is placed in driving configuration, with horizontal viewing direction, hands on the steering wheel, feet on the control pedals. This stage of the experiment cannot be validate by radiological examination because of the metal elements belonging to the cockpit's and seat's structures.

We especially respect spinal column vertical alignment in the median plane of the seat and the symmetry of the position taken by the pelvis by checking the tops of the iliac crests which must be aligned on same horizontal plane. The backward inclination of the pelvis is estimated by identification of three points accessible by palpation : the left and right ASIS and the pubic symphysis. The subject is installed with a 40° backward pelvis inclination. Lastly, the pelvis is longitudinally placed on the seat cushion, in order to obtain thigh-leg and trunk-vertical intersegmental angles in the interval of least discomfort reported by anthropometric investigations [Rebiffé84].

At the level of the upper body part, hands are attached on the steering wheel in a 10.10 o'clock driving position. The lack of muscular activity in the neck forces us to support the subject's head. It is tilted to obtain a horizontal vision axis ; a 60 millimetre distance is maintained between the back of the head and the head rest. It is noted that the shoulders are slightly taken off of the seat backrest.

Figure 1 shows the result of this positioning, with visualisation of the examination reference frame.

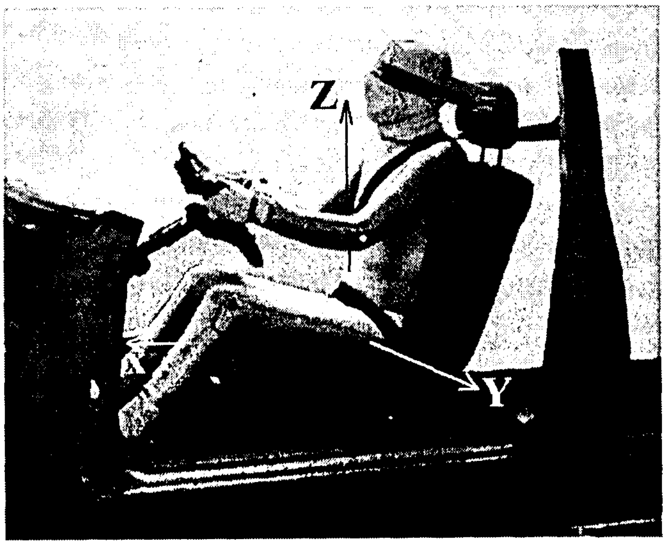

Figure 1. PMHS position in the seat.

The described position is then referenced in the cockpit by measurements of skin landmarks which coordinates will be used to replace the digital representation in the initial reference system. The co-ordinates system related to the vehicle is composed of the XOY plane which is horizontal, parallel to the vehicle support plan, XOZ which is vertical and defines the longitudinal median plane of the vehicle and YOZ which is vertical and contains the two wheels axis in front of the vehicle.

The reference frame visualised on Figure 1 corresponds to the vehicle reference system where the origin was translated in the subject's sagittal plane, between the external edges of the right and left trochanters, approximating the localisation of the H points.

Some anatomical reference points (accessible by palpation) are raised in the described reference frame.

The last stage, which completes the positioning procedure is related to the freezing step. In order to definitively fix the subject's attitude and in order to carry out serial sections, the PMHS and the seat are placed in cold room at a temperature of -23 degrees until complete freezing. This solid state will be preserved until the term of the experimentation.

Realisation of the sections

Sections are produced according to the sagittal direction (reference XOZ frame). This plane preserves in sitting position all the characteristics of the anatomy described in a conventional way of the man upright. Indeed, the sagittal plane of the individual upright crosses, in his median part, of many anatomical points such as the vertex, the spinal processes of all vertebrae, the point of the sternum or the pubic symphysis. During the passage in seated posture, only relative antero-posterior movements of body parts are involved ; the osseous points previously enumerated remain in the same median plane.

The sagittal plane is moreover very interesting for a visualisation of spinal column curvatures.

The sections are serial, with a ten millimetres interval. At the end of a complete cleaning of the surface to be analysed, a picture of the section is taken. The slides representing each section are projected on a translucent table where an anatomical diagram is carried out. This stage which consists in identifying each elementary component belonging to a section (anatomical elements and associated reference points) is necessary and is concluded by an anatomist.

RESULTS

While superimposing data coming from various sections, we bring back the entire visible elements on each section of our reference frame. The superimposition of bidimensional data allows a visualisation of some bony and skin elements (Figure 2). These numerical elements are subjected to quantitative examinations such as the measurement of angles between all the vertebrae.

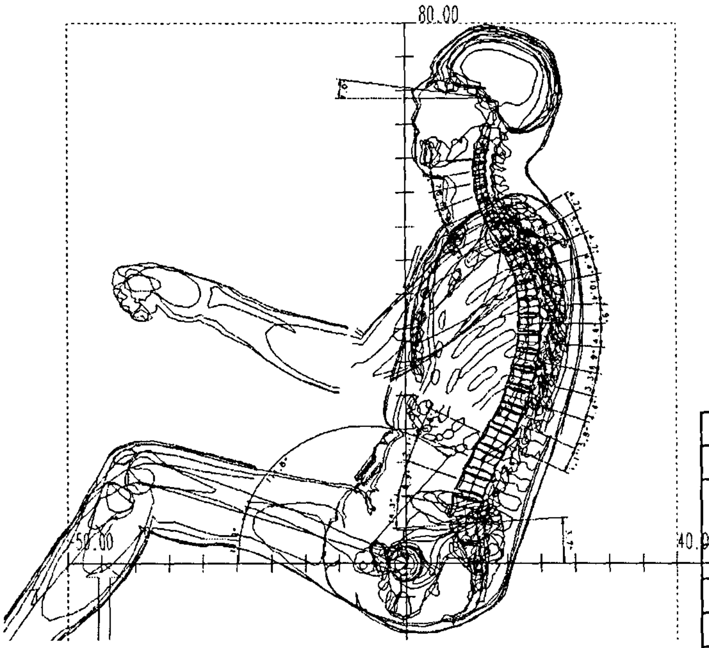

Figure 2. Contours in the XOZ plane
Only subject's right half (from the sagittal .plan) are showed, in order to facilitate the visualisation..

Characterisation of the skeleton

Pelvis

We choose two points to define the inclination of the pelvis : the first one located on the right ASIS and the second one on the former part of the pubic symphysis. The angle (measured in the XZ plane) between the line connecting these two points and the vertical characterises the pelvis slope ; this angle is equal to 41°. In natural position, prone upright, this angle is very close to 0° [Peterson88].

Angle pelvis/femur

The theoretical H-point (Hth) corresponds the femoral head centre. Let us indicate by "thigh axis" the line which contains Hth and a Knee point corresponding to the centre of lateral the condyle. The thigh axis is tilted of 17° from the horizontal axis. The angle between the pelvis and the femur (ASIS/Symphysis/Knee) is equal to 115°.

Chest slope

The chest's axis is given by Hip and shoulder and points (the last one is given by the centre of humerus head). The chest is tilted of 73.5° from the horizontal axis.

Lumbar-femur angle

We noticed first of all that the four vertebrae L1 L2 L3 L4 are almost in straightness : the former walls of L1 L2 L3 and L4 are practically aligned on the same line. The lumbar curvature appears primarily by two important angles : first between L5-S1 and second between L4-L5, other lumbar vertebrae are in straightness. The angle (measured in the XZ plane) between L1-L4 and the thigh axis is equal to 96°; a reference value, which corresponds in a state of balance, is of 135° (reported by [Keegan53]).

Complementary measures

According to Figure 2, several coordinates of skeletal points are listed below :

	X	Z
H	0.0	0.0
Superior side of the right Trochanter	1.5	1.9
Pubic Symphysis	5.2	2.9
Right ASIS	-0.8	9.5
Iliac Crest	-8.3	10.3
Coccyx tip	-7	-8.7
Ischion tip	0.5	-8.2
Shoulder (center of the Humeral head)	1-4.4	48.5
Acromion	-15.9	53.5
C1 (top of the odontoïde process)	-12.4	64.7
Vertex	-12.6	79.2
Infraorbital	-6.2	69.7
Suprasternal	-7.1	48.7
Ear	-12.7	68.9

Table 1. Measures of skeletal points
(X direction is forward)

Description of the vertebral column

Each vertebral body is compared to a quadrilateral geometry : the four points selected to represent the vertebral body are the former and posterior edges of the higher and the lower plates of each vertebra. The geometrical centre of the quadrilateral thus defined indicates the centre of the vertebral body.

The vertebral axis corresponds to the bisector of the two segments representing the higher and lower plates of each vertebral body (figure 3). The co-ordinates of the vertebral centres in the reference frame centred out of H and the angles between the vertebral axes are as following (table 2).

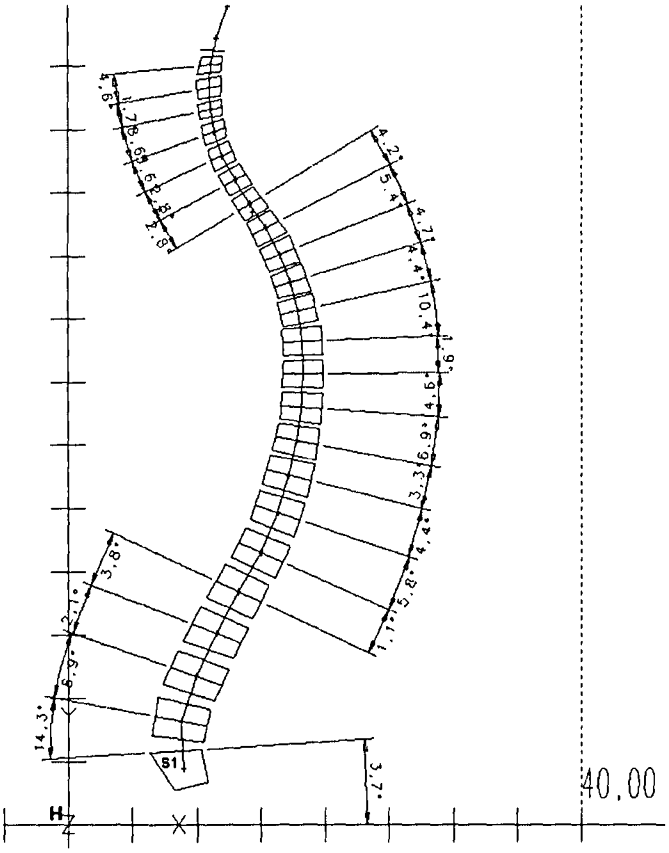

Figure 3. position of the spinal column location of the vertebral bodies and cartography of the angles between the vertebral axes

Vertebrae body	X	Y			angle
S1	8.9	4.5		S1/Horiz.	3.5
L5	8.8	8.2		L5/S1	14.5
L4	9.9	11.8		L4/L5	9
L3	11.5	15.1		L3/L4	2
L2	13.2	18.5		L2/L3	4
L1	15	21.5		L1/L2	-1
T12	16.3	24.7		T12/L1	-6
T11	17.2	27.6		T11/T12	-4.5
T10	17.8	30.3		T10/T11	-3.5
T9	18.2	33		T9/T10	-7
T8	18.3	35.6		T8/T9	-4.5
T7	18.2	38.2		T7/T8	-2
T6	17.9	40.6		T6/T7	-10.5
T5	17.3	42.9		T5/T6	-4.5
T4	16.5	45.1		T4/T5	-4.5
T3	15.4	47.2		T3/T4	-5.5
T2	14.1	49.1		T2/T3	-4
T1	13	51		T1/T2	3
C7	11.9	52.9		C7/T1	3
C6	11.4	54.8		C6/C7	5.5
C5	11.1	56.6		C5/C6	8.5
C4	11	58.3		C4/C5	1.5
C3	11.1	60.1		C3/C4	4.5
C2/C1	12.4	64.7			

Table 2. XZ Position of vertebrae and angles between vertebral axes

POSITION CHECKING

Several works based on subjects radiographs in sitting position have already been reported in [Colombini85], [Biot84], [Nyquist76]. The results presented include dispersions which are related on one hand to individual characteristics and on the other hand with the specific position adopted by each subject. Experimental protocol difficulty led the authors to limit the number of radiographs to provide only the description of the lower part of the spinal column in sitting position. Also, the seat used is always a cast solid radio-transparent matter part such as wood or plaster.

We have used the first results of a study performed by the Laboratory of Anatomy of Sousse and the radiology department of the Hospital of Sousse (Tunisia). This data where used to compare with the previously presented above.

Methodology

20 voluntary subjects, of different ages and morphologies were submitted to two successive radiographs under profile incidence ; the first carried out

on upright subject (standard radiography), the second carried out on same subject sitting in an automobile standard seat.

The sample is composed of 9 women and 11 men, the average age is 29 years (with a 19 years minimum and a 53 years maximum). Freedom was left on the subject in the choice of the various parameters of adjustments. The medical radiograph was carried out when the individual obtained the optimal configuration of comfort which corresponds to its position of usual automobile behaviour (figure 4). A receiving plate was inclined with the backrest to remain in the subject axis to provide a skeleton visualisation in the pelvic, thoracic and cervical areas (figure 4).

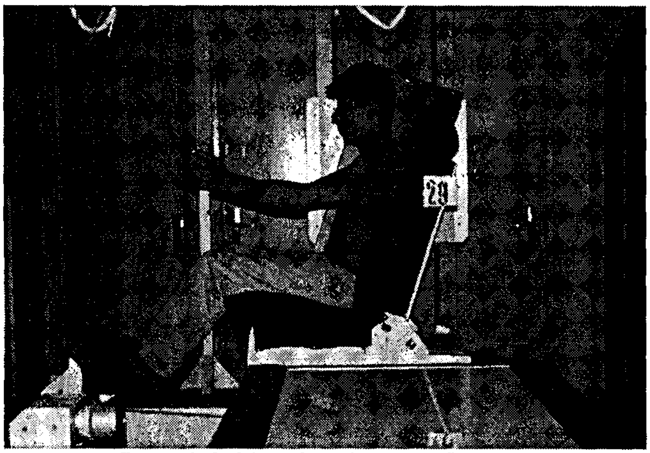

figure 4. Subject in driving configuration

Results

The vertebral bodies of the lumbar column are geometrically schematised. It makes possible to define vertebral axes. These axes allow us to measure the relative slopes of the vertebrae in the sagittal plane. The simultaneous visualisation of the angles describing the spinal column of an individual upright can be directly compared with measured obtained in seated posture (figure 5).

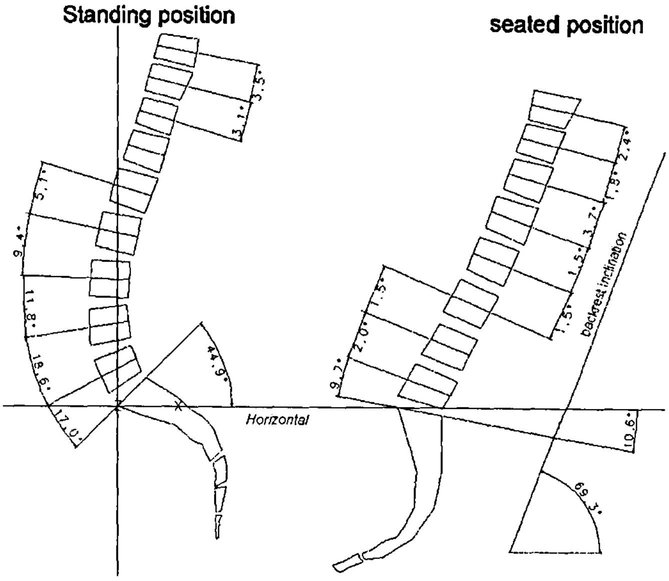

Figure 5. Schematic representation of the vertebral bodies (sacrum and vertebral axes)

In order to quantify curvature modifications, the geometrical magnitudes that we successively measured for the individuals in upright position in automobile configuration are as follow (figure 6) :

* S1/Horizontal angle characterising the orientation of the higher plate of the sacrum compared to the horizontal line.

* cartography of angles between vertebrae axis from T10 to L5, which provides seven angles : T10-T11, T11-T12, T12-L1, L1-L2, L2-L3, L3-L4 and L4-L5.

* angle L5-S1 which is measured between the higher plate of S1 and L5 vertebrae axis.

* lordotic angle L1-S1, defined as the difference in slope measured between the vertebral axis of L1 and the higher plate of S1. This angle generally characterises the lumbar lordosis of an individual upright. Let us notice that "lordotic angle L1-S1" is usually devoted to represent the angle between the higher plate of L1 and the higher plate of S1. Our quantity L1-S1 introduces little difference with the traditional angle described in the literature since we retained, for each vertebra, a transverse axis which is tilted compared to the higher plate.

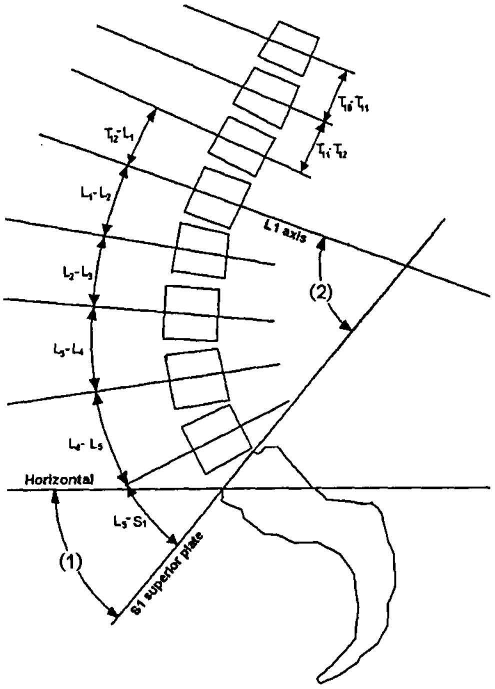

Figure 6. Angular measures
(1) sacrum orientation
(2) Lordotic angle L1-S1.

Case #	L1/S1	S1/H
1	6,8	-15,8
2	10,2	-10,6
3	9,9	-27,9
4	48,2	21,7
5	-10,2	-33,5
6	27	-1,7
7	2,4	-25,1
8	19,2	-3,3
9	11,2	-10,8
10	-0,7	-23,4
11	3,9	-15,0
12	17,9	-16,0
13	28,4	5,1
14	0,6	-20,9
15	12,5	-12,7
16	-10,9	-24,4
17	4,3	-27,0
18	20,8	-12,4
19	7,6	-20,5
20	8,2	-16,8
Mean	10,9	-14,6
Men	11,6	-13,2
Women	9,9	-16,2

Table 3. individual angles in seated position, the values are graphically displayed in the next figure.

Comparison

The PMHS lordotic angle L1-S1 is equal to 28,5°and the slope of S1 higher plate on the Horizontal plane is equal to 3,5°.

On the diagram which shows the L1-S1 lordotic angle distribution according to the inclination angle of the sacrum on the horizontal plane (figure 7), the PMHS shows a behaviour similar to the observations obtained on voluntary individuals. The pelvis position and the lumbar curve state are completely compatible with data coming from voluntary individuals. The subject position seems to be representative of a realistic position.

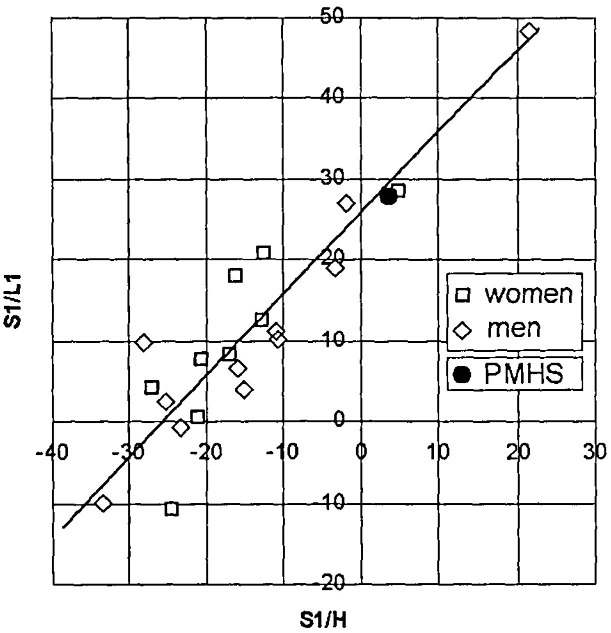

Figure 7. Lordotic angle L1-S1 function of the orientation of the sacrum (for volunteers and PMHS in seated posture)

CONCLUSION

Approaches aiming to provide descriptions of cars occupants posture were based on anthropometric approaches [Robbins83] or on analysis by radiographs [Biot84], [Nyquist76].

The technique of the serial sections is very reliable to apprehend the anatomy of human being. If radiography is easy to use, it suffers of problems involved in the 2D projection which generates uncertainties during the identification. The subject presented here was submitted to sections according to a sagittal datum-line, which is appropriate for a visualisation under side incidence. The data description in XZ plane is immediate. On the other hand, the elements location along the third axis of co-ordinates is not as easy. It requires an identification by level of section. The techniques of three-dimensional rebuilding make possible to take into account the third co-ordinate of space and provide a synthetic vision of initial objects. Complementary results, which provide a description in a reference frame to three dimensions are presented in [Chabert96].

This approach makes possible to consider applications in the fields of safety and comfort. Moreover among the research of less discomfort conditions in the sitting position, this approach makes possible to understand some anatomical adaptation mechanisms of the skeleton in this specific position. Moreover, in the world of safety, these results provide basic elements for anthropometry in the design of test dummies, but also for safety systems development installed around the subject, in the posture we described.

REFERENCES

Ackerman MJ, 1995
"Accessing the Visible Human project". D-Lib Magazine, National Library of Medicine, October 1995.

Biot B, Fauchet R, De Mauroy JC, Josselin L, 1984
"Etude radiologique de la statique du rachls en position assise". Le siège dans les véhicules de transport, Journées d'étude ONSER.

Chabert L, Ghannouchi S, Cavallero C, Bonnoit J, 1996
"Anatomical Study and three-dimensional Reconstruction of the Belted Human Body in Seated Position". 15th ESV conference. Melbourne.

Colombini D, Occipinti E, 1985
"Sitting posture : Analys of lumbar stresses with upper limbs supported". Ergonomics 29.9.85.

Keegan JJ, Omaha MD, 1953
"Alterations ofthe lumbar curve related to posture and seating". J. Bone Joint Surgery, (Amer.) vol 35, No3, pp589-603.

Nyquist G.W, Patrick L.M, 1976
"Lumbar and pelvic orientations of the vehicle seated volunteers". 21th STAPP Car Crash Conference.

Peterson Kendall F, Kendall McCreary E, 1988
"Les muscles. Bilan et étude fonctionnelle".
Maloine editeur, Paris 1988, 325p.

Rebiffé R, Guillien J, 1984
"La prise en compte des variations inter-individuelles dans la conception du siège et son adaptation au poste de conduite". Le siège dans les véhicules de transport, Journées d'étude ONSER.

Robins DH, Schneider LW, Pflug M, Haffner M, 1983
"Seated posture of vehicule occupants". 27th Stapp Car Crash Conference.

Winckler G, 1974
" Manuel d'anatomie topographique et fonctionnelle". Masson SA Editeurs, Paris.

FINITE ELEMENT MODELLING OF BLUNT OR NON-CONTACT HEAD INJURIES

A. R. Lawson
MIRA
M. M. Sadeghi
Cranfield Impact Centre
United Kingdom
Paper Number 98-S9-P-26

ABSTRACT

At present the injury that the human head is subjected to is predicted by the Head Injury Criterion (HIC). This criterion is inadequate as it is not based upon a thorough understanding of the underlying head injury mechanisms.

The important blunt or non-contact head injury mechanisms are diffuse axonal injury, bridging vein disruption and surface contact contusions. They are the result of the relative motion of the brain and skull.

Tissue failure criteria are developed for these injury mechanisms so that head injury tolerance curves can be developed.

Validated finite element models are used to determine the biomechanics of head injury and develop head injury tolerance curves.

The severity of head injury is related to the magnitude, direction and pulse duration of both translational and rotational head acceleration.

This paper represents a summary of research conducted as part of the authors Phd.

INTRODUCTION

Head injuries not only represent a serious trauma for those involved but are also responsible for a significant societal burden. These have been the driving forces behind continued research. This attempts to develop a better understanding of the biomechanics of head injury and develop criteria which can be used to develop improved safety devices and systems.

At present the injury that the human head is subjected to is predicted by the Head Injury Criterion (HIC). This is a single function which takes into account resultant translational head accelerations (a) and pulse duration (t_2-t_1), see equation 1.

It is a quantitative index used in the prediction of the severity of head injury in automotive

$$HIC = \left[\frac{1}{(t_2 - t_1)} \int_{t_1}^{t_2} a\,dt \right]^{2.5} (t_2 - t_1) \text{-----}\text{--} (1)$$

and other instances where human injury is important in design considerations. A value of 1000 is considered to represent an acceptable level of risk for head injury. It is estimated that a HIC of 1000 represents an 8.5% risk of death from head injury. This equation developed from earlier attempts to use mathematical functions to approximate the Wayne State Tolerance Curve (WSTC) [32]. The WSTC is a head injury tolerance curve which is based upon the assumption that linear skull fracture is linked to brain damage. Cadaver experiments were used to evaluate the acceleration tolerance for pulse durations up to 6ms. Other information from cadaver and animal experiments and human volunteer studies were used to evaluate the tolerance data for longer pulse durations.

The assumption that skull fracture and brain injury are directly linked has been challenged for a number of years. Recent pathological studies have found that brain damage is not necessarily linked to skull fracture [30]. The criterion neglects the effect of rotational acceleration on the severity of brain injury although rotational acceleration of the head has been found to cause brain injuries. Studies have also demonstrated that HIC deviates from the WSTC at pulse durations above 15ms.

The Head Injury Criterion has been effective in reducing the risk of head injuries by reducing the resulting levels of translational accelerations experienced by the head. To reduce the risk even further there is a need for ever more sophisticated safety systems and products. This requires a better understanding of the biomechanics of head injury and the use of improved head injury criteria. Validated head injury finite element models are valuable tools in investigating the injuries that result from linear and rotational head accelerations.

To predict the severity of head injuries it is essential to understand the underlying head injury mechanisms. This research project will examine blunt or non-contact closed head injuries. These injuries are the least understood and are becoming increasingly problematic in modern vehicular accidents with improved safety systems. The injury mechanisms examined are diffuse axonal injury, bridging vein disruption and surface contact contusions.

The economic cost of motor vehicle crashes is approximately $150 billion per year in the US and European Communities. The direct and indirect cost of head injuries in the US is estimated at $25 billion per year [24]. The 40000 fatalities and 5.2 million non fatally injured patients that occur due to vehicle crashes each year is a significant contributor to this figure.

Injuries to the brain and spinal cord are the major causes of serious disability and fatality. Traumatic brain injuries account for 68% of all trauma-related fatalities, 34% of all injuries and 50% of all injuries in vehicular crashes. Diffuse axonal injury is associated with mechanical disruption of axons in the central nervous system. Diffuse axonal injury is responsible for more than one-third of all head injury deaths, and is the greatest cause of severely disabled and vegetative survivors. 55% mortality, 3% vegetative survival and 9% severe deficit is the experience of patients 1 month after injury. Bridging vein disruption is responsible for some of the intracranial haemorrhages that produce haematomas. Subdural haematoma is one of these and has a 30% incidence with 60% mortality rate in the severely injured. Surface contact contusions are caused by the brain impacting the inner surface of the skull. They have an incidence of 89% in brains examined at post-mortem [5]. A computerised tomography (CT) scan study showed that they have a 31% rate of incidence in head injuries admitted to hospital [32]. The clinical outcome associated with contusions is difficult to assess although the affected region dictates the function that will be impaired. Mortality rates are thought to range from 25-60% [5].

The societal cost of injuries, the relative importance of head injuries, the limitations of the Head Injury Criterion and the increased demand for safer motor vehicles explains the extensive attention that head injury research has received from medical and biomechanical researchers over recent years. The relatively high incidence and mortality of diffuse axonal injury, bridging vein disruption and surface contact contusions in head injuries justifies the scope of this research project. Biomechanics of human injury is a difficult activity as it relies on a series of hypotheses which are sometimes difficult to categorically prove or disprove.

HEAD INJURY MECHANISMS

Three major factors influence the intracranial injuries sustained when the head is subjected to a rapid change in motion. They are related to the relative motion of the brain and the skull [6] and have been demonstrated through experimentation [10]. The degree of relative motion is limited by various anatomical entities. These are the meningeal partitions, bridging veins, subarachnoid (pacchionian) granulations and the brain skull interface which contains a interstitial fluid layer [6].

The meningeal partitions include the falx cerebri and tentorium cerebelli, see Figure 1. The falx cerebri is situated between the cerebral hemispheres and the tentorium cerebelli is situated between the cerebral hemispheres and the cerebellum. The falx cerebri mostly restricts cerebral hemisphere motion when the head is accelerated in the coronal plane. The tentorium cerebelli mostly restricts cerebral hemisphere motion when the head is accelerated in the sagittal plane.

The bridging veins drain blood from the brain into the dural sinus, see Figure 2. The majority of the bridging veins are located on the saggital midline. The arachnoid granulations drain cerebrospinal fluid from the subarachnoid space into the dural sinus, also shown in Figure 2. The subarachnoid granulations are located on the cerebral vertex.

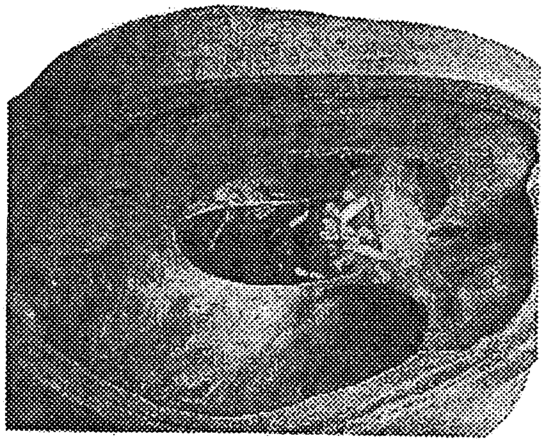

Figure 1 : Meningeal Partitions - Cranial Cavity with the Brain Removed.

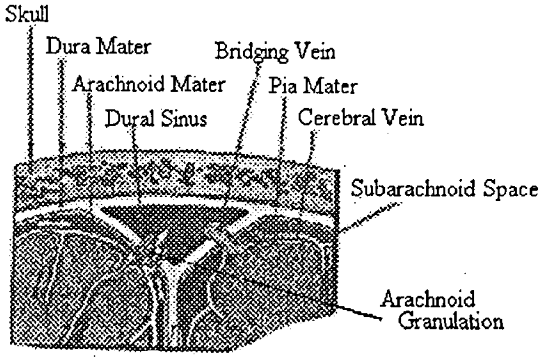

Figure 2 : Drainage of Blood and Cerebrospinal Fluid into Dural Sinus.

The cerebrospinal fluid system involves the production of cerebrospinal fluid in the ventricles which flow into the subarachnoid space. This is then drained into the dural sinus via the subarachnoid granulations once a certain pressure is reached. This maintains a certain pressure as well as continuously renewing the fluid. The fluid within the ventricles acts as a strain release. The fluid contained in the subarachnoid space of the brain/skull interface, which can decouple, damps the brain's response [6].

The first major factor that influences intracranial injuries is the distribution of shear waves throughout the central nervous system; the second is the disruption of bridging veins at the brain skull interface, and the third is the contact of the brain surface with the irregular skull.

Brain tissue has a relatively low shear modulus and therefore has a low resistance to shear waves and high strains result. Axon tracts, as well as other elements of the neurone, see Figure 3, are sensitive to strain. When the central nervous system is subjected to strain, diffuse axonal injury occurs. This is the widespread microscopic damage of the axons due to the resulting brain tissue shear strain.

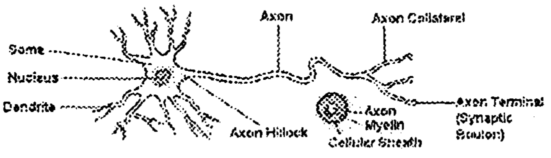

Figure 3 : Typical Neurone.

Observations of diffuse axonal injury were pioneered by Strich during the 1960's [19]. They were found to be prevalent in long duration, gradual onset accelerations as found in many modern vehicle accidents. The strain is severe at changes in geometry and material properties [19]; this includes the white/grey matter and brain tissue/ventricle interfaces, brain periphery, areas around the dural partitions, cerebral hemispheres below the slender stalk of the midbrain [19], the spinal cord, and its interaction with the foramen magnum. The levels of strain are also heavily dependent upon the applied axis of rotation. Coronal rotation produces the most severe strain levels, mainly due to the influence of the falx.

Axon damage is a combination of structural alteration and dysfunction. Much of the pioneering work was carried out by Thibault over the last few decades [9]. Total structural failure occurs at strains above 25% and dysfunction by calcium absorption at strains above 20%. It has been discovered that up to 5% of the applied elongation can be used in taking up the slack of the axons' natural orientation.

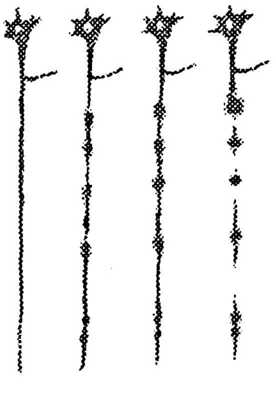

Figure 4 : Axon Damage Sequel.

The mechanism of axon damage is not fully understood. The current thoughts are that when the axons are subjected to shearing and tearing, they form retraction balls produced by the extrusion of axoplasm, forming large retraction swellings, see Figure 4. The common understanding of retraction ball formation is due to the work of Ramon and Cajal in 1928 who investigated sections of damaged central nervous system elements [22]. The continuum of axon damage is time dependent and the exact mechanisms are not that important unless they can be reversed or prevented by treatment.

Another possible consequence of the brain tissue strain is that the intracerebral blood vessels of the brain's blood supply system could be damaged. This would lead to intracerebral haemorrhages.

The relative motion of the brain in the cranial vault causes the sagittal bridging veins that pass blood from the brain into the venous system to be subjected to strain [9]. The positions of the sagittal bridging veins have been investigated, see Figure 5, and their damage is a sign of serious closed head injury.

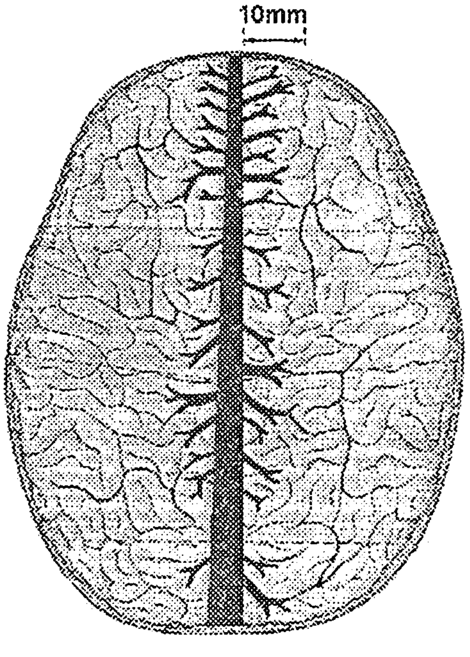

Figure 5 : The Location of Bridging Veins.

Sagittal plane rotations are the most injurious to the sagittal bridging veins. This is due to the majority of the bridging veins being situated in the parasagittal region. Dorsal bridging veins are the most easily injured, according to experiments conducted by Lindenberg [15]. This is due to the lack of brain tethering and the orientation of the bridging veins in this region.

Bridging vein strain results in a reduction in diameter and so hypoxic and ischaemic problems arise; strains above 15% result in significant effects. Their breaking strength varies from 1.5 - 14 Mpa and they can withstand an ultimate strain in excess of 100% [9]. Experiments conducted by Lee [14] showed that bridging veins have a characteristic load-stretch curve, see Figure 6. It suggests that the bridging veins start to neck at a stretch ratio of 1.5 and total structural failure occurs at a stretch ratio of 2 [14].

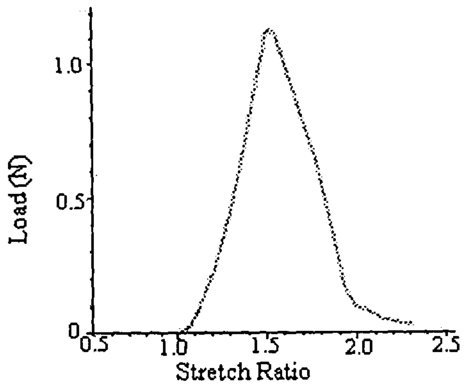

Figure 6 : Load v Stretch Characteristic of Bridging Veins.

The failure of the bridging veins results in a variety of haemorrhages including subdural and subarachnoid. It is important to realise that the clinical signs may take some time to manifest themselves. This is particularly the case when the venous system is concerned, where the blood pressure is relatively low and haematomas, for example, take time to form.

The relative motion of the brain within the cranial vault causes the brain to impact with irregularities of the inner surface [11]. These cause contusions at the impact site due to damage of blood vessels in the superficial brain layers or direct deformation of brain tissue [3]. Strains of between 20 and 40% cause the brain tissue to retain the effects of indentation [3].

The contusions found at sites remote from the impact site are most likely the result of the same injury mechanism as the contusions found at the impact site. The relative movement of the brain causes contact with skull irregularities and dural partitions, and is most likely due to the complex head motions that occur in real accidents [22]. This is in agreement with a novel theory that complex modal responses cause contusions of the brain on the irregularities of the skull [34]. The fact that contrecoup injuries occur in similar frontotemporal regions regardless of impact site strengthens this theory.

TISSUE FAILURE CRITERIA

It is important to have a way of linking the parameters determined in the head injury finite element models to the severity of injury. Tissue failure criteria have been developed for this purpose. The parameter used to predict the severity of injury is dependent upon the injury mechanism.

The severity of diffuse axonal injury is linked to the level of strain to which the axons are subjected [17]. Animal studies, isolated tissue tests, physical models and numerical techniques [17, 35], have been used to determine the most suitable measure of the strain tolerance of axons. The research conducted in these studies determined that shear strain is the best indicator of the severity of diffuse axonal injury. Shear strains under 5% represent no injury, 5 - 10% represent mild injury, 10 - 15% represent moderate injury and strains above 15% represent severe injury.

The brainstem and corpus callosum regions are common areas of diffuse axonal injury [7]. If diffuse axonal injury occurs in these regions, the clinical outcome is usually serious. The shear strain in the corpus callosum and brainstem regions of the head injury finite element models will be used to predict the severity of diffuse axonal injury. This is directly linked to the subsequent clinical outcome. This information is also used to develop the head injury tolerance curves for diffuse axonal injury.

Bridging vein disruption can cause a continuum of injuries ranging from hypoxic and ischaemic problems, starting at relatively low elongations through severe necking, to structural failure leading to severe haemorrhaging. An elongation of 50% produces necking and an elongation of 100% produces structural failure [14]. The mean length of bridging veins is 6mm and therefore 50% and 100% elongations are equivalent to 3mm and 6mm respectively [14]. The mean length of the bridging veins is used to develop the tissue failure criteria.

Surface contact contusions result from the brain impacting skull irregularities and dural partitions. The clinical outcome of this type of injury is dependent upon the area that is involved.

A compressive strain of above 20% will result in a contusion [3]. The site of the contusions is used in the validation process, where predicted injury sites are compared to the pathological findings. Tolerance curves are not developed for surface contact contusions as they have a limited link with the degree of clinical outcome and it would be difficult to grade the predicted contusion injury.

MODEL DEVELOPMENT

The directional dependence of the injury mechanisms justifies the use of two dimensional models. The mechanisms of injury are dependent upon the applied acceleration direction. Sagittal and coronal models are developed as these directions of acceleration are critical in producing diffuse axonal injury and bridging vein disruption. A horizontal model would only be useful in predicting superficial contusions. It would require increased anatomical detail and would be of little benefit in terms of determining the biomechanics of head injury. A fine mesh is required when the models are used to analyse severe head trauma. Coarse meshes would be unable to handle the high brain and membrane deformations. The finer brain mesh will enable a better representation of the ventricular cerebrospinal fluid which has been found to affect the developed strain field. It will also better represent the various contacts and subsequent deformation patterns of the brain and membranes. These affect the motion of the brain with respect to the skull and the developed strain fields. The relatively stiff behaviour of the free edges of the partitioning membrane structure enables the use of stabilising springs in the two dimensional analysis models to be used to achieve the same behaviour.

The skull is assumed rigid and the bridging veins are assumed to have a negligible effect on the response of the brain. The ventricular cerebrospinal fluid is considered an elastic compressible fluid. This is related to the fact that the fluid system allows flow between ventricles, which causes the fluid to act in a compressible manner. The partitioning membranes affect the motion of the brain during trauma and therefore elastic representations of the falx and tentorium are included. They are restrained using stabilising springs, which ensure that they deform in the same way as the three dimensional structure. The brain is modelled as a viscoelastic incompressible material, see equation 2.

$$G(t) = Gx + (Go - Gx)e^{-\beta t} \text{ ------------ } (2)$$

The brain mesh does not include the sulci, as they would be difficult to deal with and they do not have a significant effect on the brain's global movements. The general shape of the brain is maintained and the major longitudinal fissure, lateral sulcus and cerebellum are included as these significantly affect brain motion and developed strain field of the brain. The coronal slice passes through the corpus callosum region of the brain, which is a major indicator of the severity of diffuse axonal injury. It also includes the temporal lobes which have a significant effect on the brain's response. The sagittal slice passes through the midline plane and includes the brainstem, spinal cord, cerebellum and bridging veins. The brainstem is a major indicator of the severity of diffuse axonal injury and the bridging vein response is a major indicator of bridging vein disruption and associated haemorrhages. The spinal cord is included, as its response affects the strain field in the brainstem. The cerebellum is included, as it has a significant effect on the brain's response.

The brain mesh includes a representation of the white and grey matters. This is done because they have different material properties and this will affect the developed strain field. The white and grey matter material property parameters are developed by modifying existing data [25] to include established material differences [29]. The brain/skull interface is made up of membrane layers with an interstitial fluid layer, which is assumed to decouple under certain levels of applied acceleration, see Figure 7.

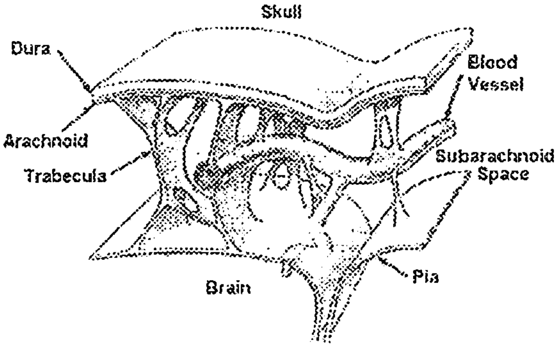

Figure 7 : Meningeal Layers.

The dura is attached to the skull and the pia is attached to the brain. The arachnoid lies between these two membranes and is held to the pia by a variety of trabecula. The gap which is formed is termed the subarachnoid space and is filled with cerebrospinal fluid. This fluid protects the brain during trauma by acting as a structural damper. The arachnoid and dura are free to slide past each other. The models have to take these interfaces into account as they have a significant effect on the behaviour of the brain during trauma. The arachnoid/dura interface can decouple if sufficient mechanical input is applied to the head during trauma. The models assume that the brain/skull interface decouples under any level of loading. Both coupled and decoupled interfaces cannot be included in the same model and as the injuries are caused due to decoupling, the interface is modelled in that way. This does mean that the models will predict more severe injuries in minor head trauma. It will also produce unrealistic field parameter values in some regions of the brain where the coupling effect is significant. However, this will have a negligible effect on the critical regions of the brain such as the corpus callosum and brainstem.

In the models, the damping produced by the subarachnoid cerebrospinal fluid is included by having a representation of the fluid layer using LS-Dyna3D elastic fluid elements, which have zero shear modulus, between the brain and skull elements, see figure 8.

The brain contacts the fluid elements (contact 1) before contacting the skull elements (contact 2), therefore reducing the relative velocity and motion of the brain with respect to the skull resulting in less severe injuries. The contact force is related to the penetration that is calculated between time-steps. The fluid elements are attached to the skull to stabilise their behaviour and prevent numerical instabilities.

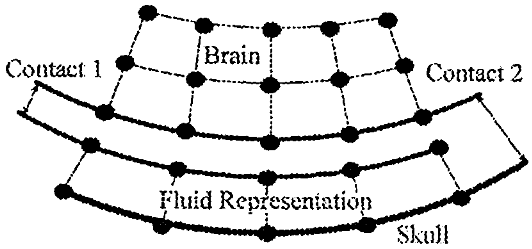

Figure 8 : Brain/Skull Interface

As the brain moves relative to the skull, membrane contacts on membrane as the arachnoid slides on the dura. The contact between the brain and the skull in the models is considered to be that of arachnoid and dura. The elements that represent the subarachnoid cerebrospinal fluid are stabilised using spring elements to prevent instabilities occurring during the simulations. These have a negligible effect on the response of the brain and are valuable tools in ensuring that the simulations reach the termination time successfully.

The cerebrospinal fluid circulates around the central nervous system. The cerebrospinal fluid is produced in the ventricles of the brain and passes through other ventricles into the subarachnoid space. Cerebrospinal fluid is produced all the time and as the pressure builds, older cerebrospinal fluid is removed. It is passed into the venous sinuses via subarachnoid granulations which act as one way pressure relief valves. These are located at the top of the parasagittal region. Through post-mortem examinations [28], it was found that these granulations restrict the relative motion of the brain and the skull. This is inagreement with forensic neuropathological findings [6]. A spring representation of these is included in the models. The stiffness is evaluated by considering them to be dura matter. The models have these granulations attaching the brain to the skull. In reality they attach the arachnoid matter to the dura matter of the superior sagittal sinus. During the analysis higher local strains can occur in this region due to this simplification.

The subarachnoid granulations and the brain/skull interface are the important details that limit motion of the brain with respect to the skull.

The falx and tentorium membranes that are included in the models are restrained using stabilising springs. These are used to ensure that the two dimensional representations behave in the same way as the three dimensional structure when they are loaded. The springs are attached to the membranes at one end and to an artificial structure at the other. The artificial structure is used to anchor the stabilising springs, so that only movements of the membranes cause changes in length of the spring elements.

Dentate ligaments restrain the spinal cord from moving along its length [27]. This restraint limits the relative motion of the brain and also significantly affects the strain field that develops in the brainstem. The sagittal model includes a rigid spring approximation of the dentate ligaments at the position of the first dentate ligament. The springs are fixed to the elements which represent the spinal cord at one end and to an artificial structure at the other. This artificial structure is used to represent the denticular ligament's rigid anchorage points.

The pia matter that covers the brain restricts the motion of the temporal lobes with respect to the cerebral hemispheres. A spring element representation of this pia matter is applied between the cerebral hemispheres and the temporal lobes. This ensures that the coronal model accurately predicts the brain's response.

The two dimensional coronal and sagittal models are shown in Figures 9&10. The figures clearly show the various entities modelled. The material property parameters are obtained and adapted from published literature, see Table 1.

The head complex input either comes through the neck or by direct impact, depending upon the type of trauma. The skull then transfers this input into the intracranial contents. Brain motion is caused by the movement of the skull and membranes. The rigid body skull is given prescribed velocity pulses about the centre of mass of the head to achieve both the desired acceleration and realistic skull kinematics.

The field parameters in particular elements which are critical to the prediction of the severity of the injury mechanisms are chosen for analysis. These are used in the validation cases and also to determine the biomechanics of head injury and develop improved head injury tolerance curves. The maximum shear strain of the central elements of the corpus callosum and brainstem regions are used to predict the severity of diffuse axonal injury. The elongation of the spring elements is used to indicate the severity of bridging vein disruption in various regions of the brain/skull interface. The maximum principal strain of the surface elements of the brain are monitored to determine the severity of surface contact contusions.

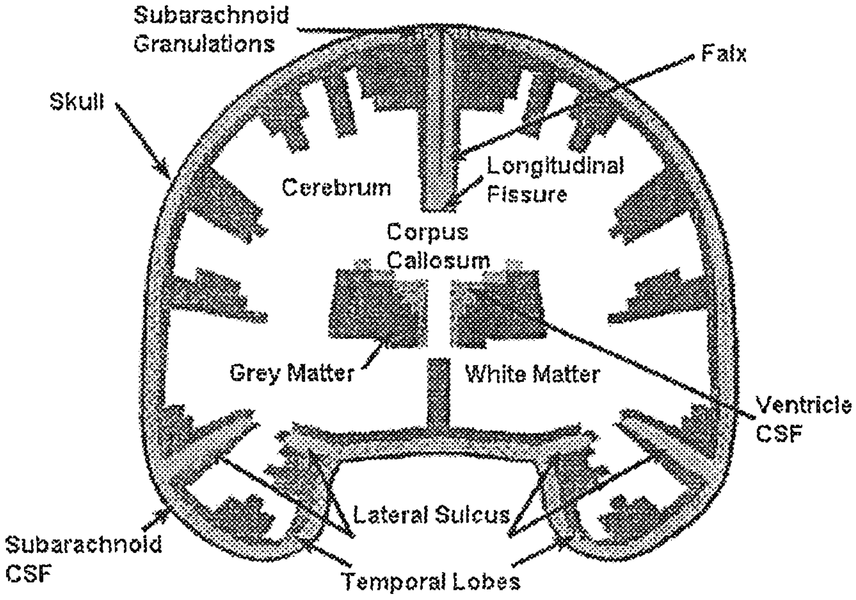
Subarachnoid Granulations
Falx
Skull
Cerebrum
Longitudinal Fissure
Corpus Callosum
Grey Matter
White Matter
Ventricle CSF
Lateral Sulcus
Subarachnoid CSF
Temporal Lobes

Figure 9 : Two Dimensional Coronal Model.

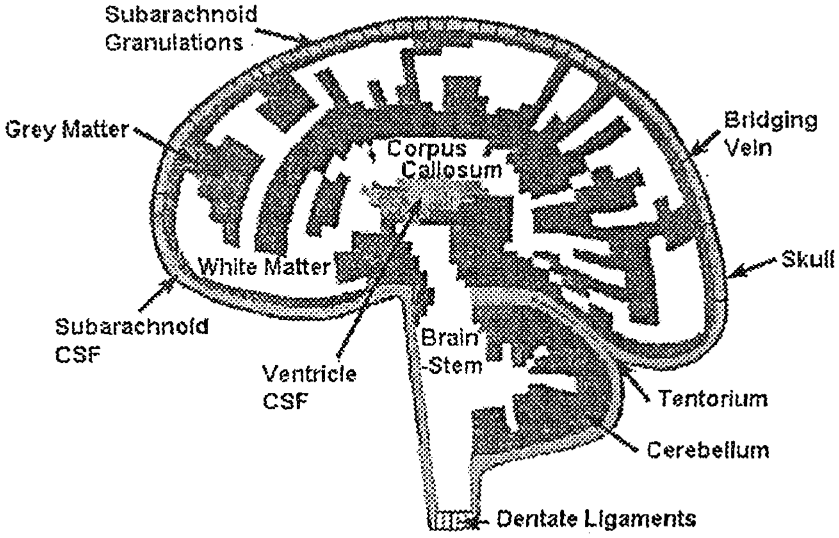
Subarachnoid Granulations
Grey Matter
Corpus Callosum
Bridging Vein
Skull
White Matter
Subarachnoid CSF
Ventricle CSF
Brain -Stem
Tentorium
Cerebellum
Dentate Ligaments

Figure 10 : Two Dimensional Sagittal Model.

Table 1 : Material Property Parameters.

Reference	Structure	Density (kg/m^3)	E (N/m^2)	Poisson Ratio	Go (N/m^2)	Gx (N/m^2)	B (/s)	K (N/m^2)
25	Dura	1133	31.5E06	0.45				
23	Brain							
&	White Matter	1040			5.48E05	1.74E05	35	2.19E09
29	Gray Matter	1040			5.08E05	1.62E05	35	2.19E09
23	CSF							
&	Ventricular	1000						1.11E07
14	Subarachnoid	1000						4.45E05
12	Skull	1410	4.46E09	0.21				
35	Pia Matter	1133	11.5E06	0.45				

VALIDATION

Validation of the head injury finite element models is critical if they are to be used as engineering and medical tools. The validation process involves the use of pathological observations, cadaver experiments, accident reconstructions and volunteer data. Each of these sources of validation data has its limitations. This paper includes the qualitative post mortem validation. The complete validation process can be found in the authors Phd [13]. Cadaver experiments demonstrate brain/skull interface decoupling. Accident reconstructions show that the models can predict real world injury data and volunteer studies show that the models can predict no or minor injury.

There have been many studies regarding the observations made at post-mortems. These studies discuss the patterns of injuries that occur in real life head trauma. This information is used to qualitatively validate the injuries predicted by the head injury finite element models.

The saggital and coronal head injury finite element models demonstrate the degree of relative motion of the brain and the skull that occurs, see Figures 11 and 12. The coronal model also shows the motion of the temporal lobes that is induced, see Figure 12. This motion would produce the superficial contusions seen at post-mortem in the frontotemporal region. These occur regardless of the impact site and are due to the skull irregularities that exist in this region [6,7].

The relative motion of the brain would not produce contusions in the occipital lobes where the skull is smooth. This is in agreement with post-mortem observations where the occipital lobes are rarely contused in frontal impacts [6]. The degree of relative motion would also explain the occurrence of contusions at the impact site [6] where the brain impacts the inner surface of the skull. The motion of the temporal lobes causes high strains to be induced in the temporal lobe at the impact site as well as the other temporal lobe. This is in agreement with post-mortem observations that indicate contusions in both temporal lobes after lateral impacts [6]. The relative motion of the brain produces high strains in the corpus callosum, brainstem and parasaggital regions of the brain as well as regions adjacent to the ventricles. These regions are areas of diffuse axonal injury and lesions that are found at post-mortem [7]. The relative motion of the brain causes the bridging veins to be elongated, see Figure 11. This explains the subarachnoid haemorrhages that are often present on one or both sides of the brain [7]. The subarachnoid haemorrhage can be caused by distant bridging vein disruptions and can be confused for coup and contrecoup lesions at post-mortem [7]. This can lead to confusion when determining the mechanism of injury particularly with respect to coup and contrecoup.

The relative motion of the brain and the skull, the complex motion of the temporal lobes and the pattern of strain induced in the brain predicted by the models, explain the injuries found at post-mortem. They explain the classic triad of diffuse axonal injury involving focal lesions in the corpus callosum and brainstem and microscopical evidence of diffuse damage to axons [1]. They also explains the contusion patterns that are seen in the frontotemporal and parasagittal regions of the brain plus the disruption of bridging veins.

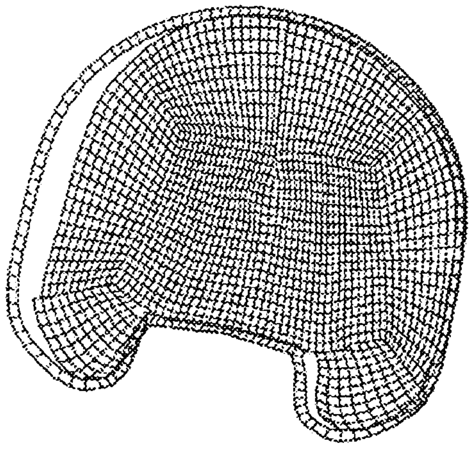

Figure 11 : Coronal Model.

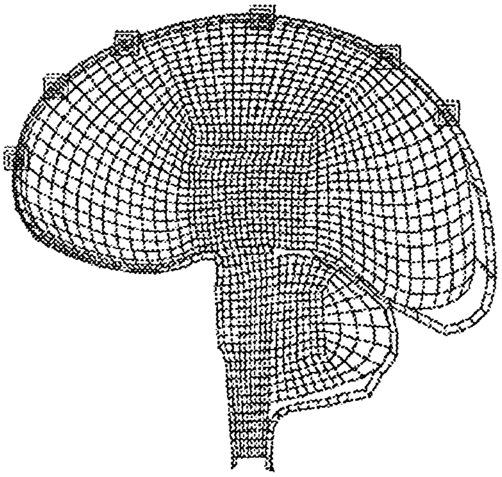

Figure 12 : Sagittal Model.

BIOMECHANICS AND HEAD INJURY TOLERANCE CURVES

The validated head injury finite element models are used to determine the biomechanics of head injury and develop head injury tolerance curves. Simulations are carried out to determine whether the biomechanics of head injury due to applied accelerations are as hypothesised. Head injury tolerance curves have been developed for diffuse axonal injury and bridging vein disruption [13]. They are developed using the tissue failure criteria discussed earlier.

The head injury finite element models show that the motion of the brain with respect to the skull is responsible for the head injury mechanisms as hypothesised. The three head injury mechanisms are produced by different consequences of the motion of the brain relative to the skull.

In the coronal model, the relative motion of the two cerebral hemispheres induces relatively high shear strains in the corpus callosum. In the sagittal model the motion of the cerebral hemispheres is resisted by the brainstem, causing relatively high shear strains to be induced. The level of shear strain is dependent upon the severity and direction of the applied acceleration and the applied pulse duration. This dependency is illustrated in the head injury tolerance curves [13]. The shear strain pattern then spreads throughout the brain tissue as the events progress.

The models provide viable hypotheses of the mechanisms behind the classic triad of diffuse axonal injury. The relatively high shear strains are responsible for the focal lesions found in the corpus callosum and brainstem regions. The lower level shear strains which spread throughout the brain are responsible for the microscopical evidence found in the axons of the white matter.

The sagittal model shows that when the head is accelerated, the brain moves relative to the skull. This relative motion elongates the spring elements which represent the bridging veins passing between the brain and dural sinus, which is attached to the skull. The level of elongation is dependent upon the severity and direction of the applied acceleration and the applied pulse duration. This dependency is illustrated in the head injury tolerance curves.

The sagittal model provides a viable hypothesis of the mechanism of bridging vein disruption found at post-mortem.

The relative motion of the brain predicted by the coronal model produces relatively high compressive strains in the temporal region of the brain. The relative motion predicted by the sagittal model would result in high compressive strains in the frontal region of the brain, if the model included the irregular features of the skull in that region. The model does not include such irregular features, as the resulting element deformations would have caused numerical instabilities.

The models provide a viable hypothesis of the mechanisms behind the frontotemporal contusions that are found at post-mortem. The relative motion of the brain and the skull also explains contusions found at other sites, including the impact region.

Figures 13 and 14 contain a summary of the head injury tolerance curves, which represent moderate injury, determined during the study [13] and the tolerance curves contained within the literature.

The Head Injury Criterion (HIC) is the accepted means of determining the severity of head injuries due to acceleration. Figure 13 contains the translational head injury tolerance curves determined during this study and the tolerance curve which represents a HIC of 1000. This is the value used by the automotive industry as representing an acceptable level of risk of head injury. It makes no allowance for the severity of rotational acceleration. The comparison shows that the HIC equals 1000 curve underestimates the risk of injury at shorter pulse durations and overestimates the risk of injury at longer pulse durations. This has implications when HIC is used to influence the design of motor vehicles in relation to head injuries.

Figure 14 contains the rotational head injury tolerance curves determined in this study and the tolerance curves contained within the literature.

Lowenhielm et al [16] developed this tolerance curve using cadaver experiments and mathematical modelling. Ryan et al [26] used the reconstruction of pedestrian accidents and mathematical modelling to determine the tolerance curve. Both these tolerance curves ignored the important influence of translational acceleration that was present. Both Thibault et al [33] and Ommaya et al [20] used animal experiments as the basis for the tolerance curves. The anatomy of the human head is different from that of even the closest primate. The injury mechanisms are related to the brain's response and the differences in anatomy would produce different responses. These differences are not overcome with the use of simple scaling laws. Bycroft et al [4] used a simplified mathematical model to examine angular accelerations. Stalnaker et al [31] used head injury finite element models to determine a rotational acceleration limit for recoverable diffuse axonal injury. These models were incapable of simulating

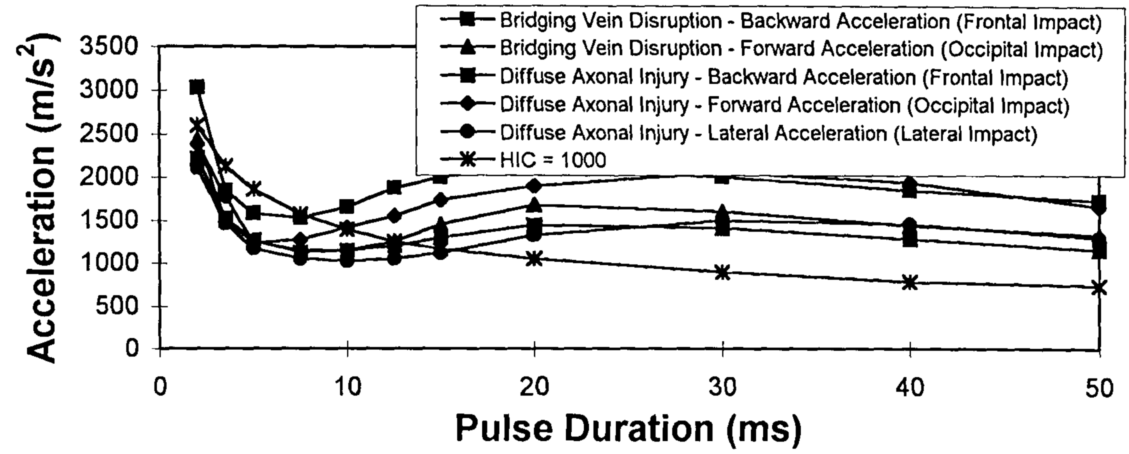

Figure 13 : Translational Acceleration Head Injury Tolerance Curves

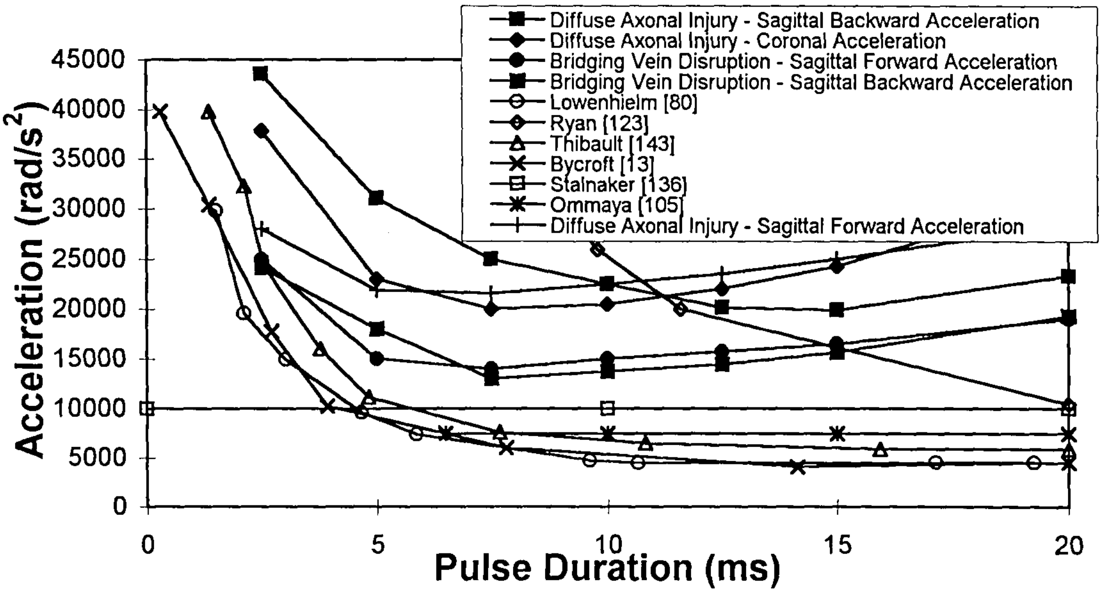

Figure 14 : Rotational Acceleration Head Injury Tolerance Curves.

the complex brain kinematics that occur during rotational accelerations of the head.

All the tolerance curves except that of Ryan et al [26] have limits for concussion or irrecoverable injury that are significantly lower than the acceleration pulses experienced by boxers. These are regularly in excess of 5000 rad/s^2 and can reach 13600 rad/s^2 [21]. These tolerance curves are obviously far too conservative. The tolerance curve of Ryan et al [26] ignored the important influence of translational acceleration. The tolerance curve cannot be relied upon because the translational acceleration is an unknown input which has a significant effect on injury severity.

The head injury models have been successful in determining the biomechanics of head injury and developing improved head injury tolerance curves. The severity of the three head injury mechanisms is related to the consequences of the relative motion of the brain and the skull. The head injury tolerance curves provide a valuable tool for engineering safety system design.

Other head injury finite element models [18,24,35] have concluded that translational acceleration has a minimal effect on the severity of injury. This is due to the modelling assumption used for the brain/skull interface, such that models did not predict realistic motion of the brain with respect to the skull. The models in this study showed that translational and rotational accelerations are key in determining the severity of head injury. This was achieved because of the unique method of modelling the brain/skull interface, allowing the more realistic prediction of levels of relative motion. The different combinations of translation and rotation in terms of applied direction are important in determining the severity of injury. It is the complex head kinematics that must be considered when trying to predict the severity of head injury. Consider the combination of two tolerable acceleration pulses applied to the coronal model. A translational pulse of 1025 m/s^2 with a 10ms pulse duration produces a corpus callosum maximum shear strain of 10%. A rotational acceleration pulse of 20500 rad/s^2 with a 10ms pulse duration also produces a corpus callosum maximum shear strain of 10%. Combining these two acceleration pulses produces a range of corpus callosum maximum shear strains of 6.0% to 13.0% dependent upon the combination of directions used.

The head injury tolerance curves developed in this study show that HIC is not an accurate predictor of the severity of head injury. It doesn't consider the injury mechanism, direction of applied acceleration pulse or rotational acceleration. These have been shown to have an influence on the severity of head injury. The models also suggest that HIC underestimates the severity of injury at short pulse durations and overestimates the severity of injury at long pulse durations.

DISCUSSION AND CONCLUSIONS

The coronal and sagittal models provide a viable hypothesis behind the classic triad of diffuse axonal injury, bridging vein disruption and frontotemporal contusions found at post-mortem. The relatively high shear strains that are produced in the corpus callosum and brainstem regions are responsible for the corresponding lesions. The high shear strains in the corpus callosum region are caused by the relative motion of the two cerebral hemispheres as a result of the relative motion of the brain and the skull. The high shear strains in the brainstem region are caused by the motion of the cerebral hemispheres being resisted by the brainstem, during the relative motion of the brain and the skull. The lower level shear strains, which spread throughout the brain, are responsible for the microscopical evidence found in the axons of the white matter. The elongation of the spring elements which represent the bridging veins are responsible for the bridging vein disruption. The high compressive strains in the temporal regions of the brain are responsible for the corresponding contusions. The relative motion of the frontal region of the brain is responsible for the corresponding contusions.

Diffuse axonal injury and bridging vein disruption tolerance curves have been developed for translational and rotational acceleration in the coronal and sagittal planes [13]. These tie in with existing head tolerance data and represent an improvement on existing head injury tolerance curves. They demonstrate the directional and injury mechanism dependency of head injuries. The use of a single simple function such as the Head Injury Criterion (HIC) is not sufficient in predicting the severity of head injury. It doesn't consider the injury mechanism, direction of applied acceleration pulse or rotational acceleration. These have been shown to have an influence on the severity of head injury. The models also suggest that HIC underestimates the severity of injury at short pulse durations and overestimates the severity of injury at long pulse durations.

Translational and rotational accelerations both have a role to play in the severity of the relative motion of the brain and the skull and therefore the resulting injury severity. These are the first head injury finite element models that have shown that both translational and rotational accelerations are responsible for the severity of injury. The use of HIC has shown that translational acceleration is responsible for injuries. Reducing the severity of translational acceleration through HIC has led to a reduction in injuries. The many combinations of translational and rotational accelerations that occur in head trauma are critical to the resulting head injury severity. It is therefore necessary to determine the complex kinematics of the head during head trauma if a reliable estimate is to be made of the severity of injury.

Further research will aim to develop a three dimensional model with an improved representation of the brain/skull interface. This interface representation will aim to explicitly represent the fluid and decoupling process.

RFERENCES

1. Adams, J. H., Graham, D. I. Murray, G. & Jennet, B. "Diffuse Axonal Injury due to Non-Missile Head Injury in Humans : An Analysis of 45 Cases." Ann. Neurol., Vol. 12, Pages 557-563, 1982.

2. Andrews, B. "Microsurgical Anatomy of the Venous Drainage into the Superior Sinus." Journal of Neurosurgery, Vol. 24, No. 4, Pages 514-520, 1989.

3. Atluri, S.N., Kobayashi, A.S. & Cheng, J.S. "Brain Tissue Fragility - A Finite Strain Analysis by a Hybrid Finite Element Method." Journal of Applied Mechanics. June 1975.

4. Bycroft, G.N. "Mathematical Modelling of a Head Subject to an Angular Acceleration." Transactions of the American Society of Mechanical Engineers, Journal of Biomechanical Engineering, Series K, Pages 487-497, 1973.

5. Cooper, P.R. "Post-Traumatic Intracranial Mass Lesions." Head Injury, Pages 65-82, 1982 Edited by P.R. Cooper, Williams and Wilkins, Baltimore/London.

6. Courville, C.B. "Forensic Neuropathology - II : Mechanisms of Craniocerebral injury and their Medicolegal Significance." Journal of Forensic Science, Vol. 7, No. 1, Pages 1-28, 1962.

7. Doyle, D. & Sturrock, K. "Head Protection : Motor Cyclists, Sports and Industry." AGARD/NATO Specialist Meeting on "Impact Head Injury : Responses, Mechanisms, Tolerance, Treatment and Countermeasures." Paper 16, 7-9th November, 1996, Mescalero, New Mexico, USA.

8. Gennarelli, T.A., Champion, H.R. & Copers, W.S. "Importance of Mortality from Head Injury in Immediate Survivors of Vehicular Injuries." IRCOBI, 1992, Pages 167-178.

9. Goldsmith, W. "Meaningful Concepts of Head Injury Criteria." 1989. Department of Mechanical Engineering, University of California, Berkeley, CA 94720 USA.

10. Gosch, H.H., Gooding, E. & Schneider, R.C. "The Lexan Calvarium for the Study of Cerebral Responses to Acute Trauma." Journal of Trauma, Vol 10, No. 5, 1970.

11. Gurdjian, E.S., Lissner, H.R. & Patrick, L.M. "Concussion - Mechanisms and Pathology." 7th Stapp Car Crash Conference, 1963.

12. Hosey, R.R. "A Homeomorphic F.E. Model Impact, Head and Neck Injury." PhD Dissertation, Tulane University, 1981.

13. Lawson, A.R. "Finite Element Modelling of blunt or Non-Contact Head Injuries." PhD Dissertation, Cranfield University, September 1997.

14. Lee, M.C. & Haut, R.C. "Insensitivity of Tensile Failure Properties of Human Bridging Veins to Strain Rate: Implications in Biomechanics of Subdural Hematoma." Journal of Biomechanics, Vol. 22, No. 6/7, Pages 537-542, 1989.

15. Lindenberg, R. "Trauma of Meninges and Brain." Pages 1705-1765 In "Pathology of the Nervous System." Minckler, J. New York McGraw-Hill, 1971.

16. Lowenhielm, P. "Tolerance Levels for Bridging Vein Disruption Calculated with a Mathematical Model." University of Lund, Lund, Sweden, 1977.

17. Margulies, S.S. & Thibault, L.E. "A Proposed Tolerance Criterion for Diffuse Axonal Injury in Man." Journal of Biomechanics, Vol. 25, No. 8, Pages 917-923, 1992.

18. Mendis, K.K. "Finite Element Modeling of the Brain to Establish Diffuse Axonal Injury Criteria." PhD Dissertation, The Ohio State University, 1992.

19.Ommaya, A.K. "Biomechanics of Head Injuries : Experimental Aspects." Pages 245-269, 1984 In "The Biomechanics of Trauma." Nahum, A. & Melvin, A.

20.Ommaya, A.K., Yarnell, P., Hirsch, A.E. & Harris, E.H. "Scaling of Experimental Data on Cerebral Concussion in Sub-Human Primates to Concussion Threshold for Man." Society of Automotive Engineers Paper Number : 670906.

21. Pincemaille, Y., Trosseille, X., Mack, P. et al "Some New Data Related to Human Tolerance Obtained fron Volunteer Boxers." Society of Automotive Engineers Paper Number : 892435. 1989.

22. Povlishock, J.T., Kontos H.A. & Ellis, E.F. "Current Thoughts on Experimental Head Injury." In Head Injury : Basic and Clinical Aspects. New York, Raven Press, 1982.

23. Ruan, J.S. "Finite Element Modeling of Direct Head Impact." Society of Automotive Engineers Paper Number : 933114. 1993.

24. Ruan, J.S. "Impact Biomechanics of Head Injury by Mathematical Modelling." PhD Dissertation, Wayne State University, 1994.

25. Ruan, J.S., Khalil, T.B. & King A.I. "Human Head Dynamic Response to Side Impact by Finite Element Modelling." Journal of Biomechanical Engineering, Vol. 113, 1991.

26. Ryan, G.A. & Vilenius, A.T.S. "Field and Analytical Observations of Impact Brain Injury in Fatally Injured Pedestrians." Journal of Neurotrauma, Vol. 12, No. 4, 1995.

27. Saltman, H.F. & Blackwood, W. "An Atomical Study of the Role of the Dentate Ligament in the Cervical Spinal Cord." Journal of Neurosurgery, Volume 24, Pages 43-46, 1966.

28. Sheppard, N. & Lawson, A.R. Postmortem Examinations, Pathology Department, Gloucester Royal Hospital, 1996.

29. Shuck, L.Z. & Advani, S.H. "Rheological Response of Human Brain Tissue in Shear." Journal of Basic Engineering, December, 1972.

30. Simpson, D.A., Ryan, G.A., Piax, B.R. et al "Brain Injuries in Car Occupants : A Correlation of Impact Data with Neuropathological Findings." IRCOBI, Pages 89-100, 1991.

31. Stalnaker, R.L., Mendis, K.K.. & Rojanavanich, V. "The Unified Head Injury Theory." PD-Vol. 47-2, Engineering Systems Design and Analysis, Vol. 2, ASME, 1992.

32. Tarriere, C. "Investigation of Brain Injuries Using the C.T. Scanner." Head and Neck Injury Criteria : A Consensus Workshop., Pages 39-49, 1981. Edited by Ommaya, A.K. US Department of Transportation, National Highway Traffic Safety Administration, Washington DC.

33. Thibault, L.E., Gennarelli, T.A., Margulies, S.S., Marcus, J. & Eppinger, R. "The Strain Dependent Pathophysiological Consequences of Inertial Loading on the Central Nervous System." 1989. University of Pennsylvania, Philadelphia, Pennsylvania 19104, USA.

34. Willinger, R., Kopp, C.M. & Cesari, D. "New Concept of Contrecoup Lesion Mechanism : Modal Analysis of a F.E.M. of the Head." 1991 INRETS-LCB, Case 24, Bron, France.

35. Zhou, C. "Finite Element Modeling of the Impact Response of an Inhomogeneous Brain." PhD Dissertation, Wayne State University, 1995.

FIDELITY OF ANTHROPOMETRIC TEST DUMMY NECKS IN ROLLOVER ACCIDENTS

Brian Herbst
Stephen Forrest
David Chng
Liability Research Group
SAFE, LLC
Anthony Sances, Jr.
Biomechanics Institute
United States
Paper Number 98-S9-W-20

ABSTRACT

Rollover accidents pose a serious cost to society, while they account for 10% of all passenger car accidents they cause about 20% of Harm (Harm is defined as the sum of all injured people each weighted in proportion to the outcome, as represented by the cost of the person's most severe injury). This is primarily due to serious head and neck injuries resulting in permanent disability or death. The literature regarding neck injury in rollovers can be divided into two groups, one that attributes neck injury to significant roof crush and the vertical excursion due to the vehicle belt system. The other who subscribes to the "diving injury" and "torso augmentation" theory and conclude that roof crush is inconsequential. The Hybrid-III test dummy has been used in rollover and drop tests to support this conclusion.

This paper will show that the Hybrid-III head and neck complex is significantly stiffer and less flexible than the human neck. This lack of biofidelity means that the Hybrid-III neck cannot provide meaningful data in rollover environments.

INTRODUCTION

The human spine is a complex mechanical structure composed of bony vertebrae, ligaments and intervertebral discs. Its primary function is to protect the spinal cord and nerve roots while carrying loads and allowing physical motion. Inherent in the spinal structure are natural curvatures throughout the spine in each of the major spinal sections: cervical, thoracic, lumbar and sacral. The spine's curvature provides flexibility and shock absorption.

The Hybrid-III neck is designed to mimic the cervical portion of the human spine and has a rigid attachment to the torso and the head. The neck is a one piece column made of butyl elastomers separated with aluminum discs. Through the center of this column runs a single steel cable. There is no inherent curvature to the Hybrid-III neck column.

The Hybrid-III dummy is the most widely accepted dummy for automotive crash testing in the world. Its response resembles that of a human more closely than any previous anthropometric test dummy (ATD) before it. The Hybrid-III neck was designed to meet flexion and extension criteria established by Mertz[1] in a series of sled tests involving volunteer and cadaveric subjects. Other neck response modes were secondary considerations in the development of this neck. The neck response corridors are a relation between the moment about the occipital condyles and the angular position of the head relative to the torso. These requirements are not adequate to properly reproduce human motions. Mertz et. al. [2]and Melvin et al.[3] have suggested neck requirements that relate to the head trajectory as well. Further refinements in response requirements and neck design are required in order to achieve more biofidelic and useful test dummies.

LITERATURE

The Hybrid-III was designed to perform primarily in frontal impacts. However, the Hybrid-III head and neck complex displays significant differences from human volunteers even in this mode. Seemann, et al. [4] conducted tests at the Naval Biodynamics Lab that studied the responses of human volunteers and the Hybrid-III in various deceleration directions. Comparing the head trajectories for the two test groups, it became apparent that the downward travel and timing of the human head in 15g frontal sled tests differed dramatically from Hybrid-III. The human head traveled farther downward and over a longer period of time, while the Hybrid-III head rebounded faster after translating downward a smaller distance. It was noted that the Hybrid-III head vertical displacement was less than half the displacement of one volunteer. Similarly, when subjected to 12g vertical accelerations, the Hybrid-III neck was too stiff. Seemann concluded that the Hybrid-III neck is too stiff and is not biofidelic in flexion.

Early studies to determine the strength of the human cervical column were conducted with vertical drops and conducted by Nusholtz and Huelke[5] who dropped intact cadavers both constrained and unconstrained from drop heights up to 1.8 meters. Various cervical fractures were observed, however those with potential spinal cord injury involved fractures of vertebral bodies C-4 and C-5, fracture of dens and subluxation of lower cervical elements. This study indicates that 1.1 to 1.8 meter drop heights are required to produce serious cervical injury.

Vertical drop studies of intact cadavers by Yoganandan and Sances[6] were conducted with restrained upper cervical columns and unrestrained preparations. The force of impacts on the head was recorded along with force from gauges implanted in the cervical vertebral spaces and accelerometers along the spine. Photo targets at various vertebral bodies and the occipital were also used. The cervical fractures resulting in probable clinical injury included anterior subluxation of C-5 and C-6 with locked facets, Jefferson fracture of C-1, a C-3 fracture and a C-2 vertebral body lamina fracture. These injuries occurred at drop heights between 0.91 and 1.5 m. Cervical compression of 2 to 4 cm were observed. A force of 2600 N was recorded in the cervical column gauge with a C3 fracture. This supports the drop height range required for cervical injury discussed by Nusholtz and Huelke[5].

McElhaney[7] studied injuries from swimming pool accidents and attempted to replicate the drop heights for cervical injury from trajectory and velocity profiles of test subjects. He extrapolated cervical injuries from his simulations ranging from 3.3 m/s to 7 m/s for edge of pool dives. This study was however conditioned upon the history of the accidents and based on the analogy of injuries in swimming pools in contrast to non-aquatic situations.

Pintar[8] produced clinical type cervical injuries in the vertically oriented human cadaver head/neck preparation with the head stabilized with a spring in the posterior area and dead weights in the anterior area. The study described the need for preflexion (the removal of the resting lordosis) to create vertebral compression injuries. The preparations were impacted with a high speed piston at the top of the head with the cervical column aligned vertically and forces recorded in the region of T-1. Fractures produced were of compression or compression-flexion type and also included partial subluxation of C-5 on C-6. Burst fractures and anterior wedge body fractures were produced. This study included parallel investigations with the Hybrid-III head and neck. The Hybrid-III head and neck complex transmits 3 times as much force from the head to the distal point at T-1. Approximately 80 to 90 percent of the force applied to the head of the Hybrid-III was measured at the distal plate at T-1, while forces in the region of 25 to 30 percent of those applied to the head of the human preparation from the piston were measured in the distal force plate at the T-1. These experiments indicate that the Hybrid-III transmits force markedly different than the human/neck complex because of its stiffness. The quasi-static biomechanical comparison of the axial compressive characteristics of the human cadaveric neck and the Hybrid-III conducted by Yoganandan and Sances[9] indicate that the Hybrid-III neck is 3 to 5 times stiffer at loading rates up to 0.25 m/s.

Subsequent studies conducted by Pintar and Yoganandan[10] determined the dynamic characteristics of the human cervical column based on twenty cadaveric specimen loadings under axial compression. The corridors indicate an initial soft response of the human head/neck preparation which commences to stiffen following approximately 10 to 15 millimeters of deformation reaching an average stiffness of approximately 555 N/mm at speeds of 2.5 to 8 m/s with a mean force of 3326 N at failure. Recent studies by Sances and Voo[11] found that the Hybrid-III head/neck preparation was at least 2 times stiffer compared to the human under dynamic axial compressive loading. Dynamic forces and curves in the Hybrid-III necks in comparison to the cadavers of Pintar are shown in Figure 1. Typically the stiffness of the Hybrid-III was 958 N/mm at 2 m/s, 1111 N/mm at 4 m/s and 2160 N/mm at 7.6 m/s.

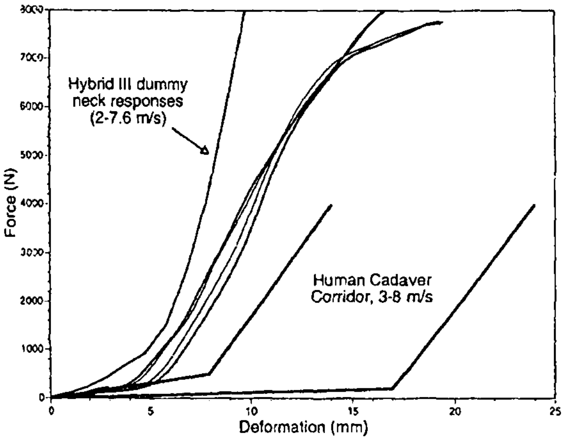

Figure 1. Dynamic loading of Hybrid-III and human cadaveric necks

A recent study by Nightingale and McElhaney[12] showed fractures of the cervical column of the human cadaver with a 32 pound weight attached to the torso with vertical drops of the head/neck complex onto a force plate. The experiments demonstrated cervical fractures at impact speeds of approximately 3.2 m/s. However, this study does not account for the flexibility of the thoracic spine which will decrease the overall stiffness of the preparation. Larger drop heights will be expected to receive similar cervical fractures due to substantial thoracic telescoping and decrease in overall stiffness of the spine. Marked thoracic bending was also observed in high speed photographs of subjects dropped vertically.

In another investigation, McElhaney, et al. (1983)[13] conducted tests on Rhesus monkeys and unembalmed cadaver cervical spines. They concluded that there is a significant deformation rate dependence and that small eccentricities (±1cm.) in the load axis could change the buckling mode from posterior to anterior. A 1 cm. difference in alignment created flexion, compression or extension injuries. McElhaney[14] in 1988 reported that the Hybrid-III dummy neck was significantly stiffer than the human cadaveric cervical spine which had quasi-static bending loads applied. The study also included compression flexion, tension flexion and compression lateral bending. The bending stiffness was significantly influenced by direction of the bending moment and the type of end restraint. These experiments indicate that when the loading is eccentric (as it almost always is), the primary deformation mode is bending.

Myers, et al.[15] reported the Hybrid-III neck is substantially stiffer than the human cadaver with various end conditions. Myers concluded that the risk of cervical injury may be strongly dependent on the degree of head restraint imposed by the contact surface. He suggests that injury environments should be designed to minimize this constraint. In the absence of significant constraint, the stiffness of the structure was low, the spine was able to flex significantly and no injuries were observed.

Myers concluded that the Hybrid-III neckform was 10 to 50 fold stiffer than the human cadaver cervical spine depending on the imposed end condition (10 times for fully constrained; 12 times for rotationally constrained, 50 times for unconstrained). Myers further concludes that the availability of a high biofidelity head-neck for compression would be a great benefit to the design and evaluation of safety equipment. Also, since the imposed end condition reliably alters the failure mechanism of the cervical spine, safety equipment and injury environments should be designed to minimize the degree of imposed constraint on the head.

The risk of cervical injury can be avoided if the loading is not transmitted to the cervical spine secondary to escape of the head from the loading surface. This was observed in the vertical drop studies by Yoganandan and Sances and others.[16, 17] The studies of Pintar and Nightingale have determined an approximate tolerance level for the human spine in the region of approximately 4 kN in compression. For vertical drops the combined effects of the head-neck plus torso tissues will undoubtedly reduce the transmitted force to the cervical spinal column when the additional displacement of the thoracic column is included in the tested preparation. Consequently, one would expect substantially greater drop heights for injury similar to those observed by Nusholtz[18] and Yoganandan[19] for an intact preparation. In rollovers there is a high probability of bilateral locked facets which usually occurs in the absence of bony damage and produces serious reductions in the spinal canal with concomitant spinal cord trauma. These injuries most likely occur secondary to force imposed upon the region of the head posterior to the vertex during flexion of the head-neck complex. Flexion of the head is a likely protective mechanism invoked by an occupant during a rollover event.

One can demonstrate that the intact human can substantially increase the head to roof clearance by flexing the head-neck complex and/or rotating the torso. This increase in head to roof clearance has substantial potential for injury reduction. (See Figure 2)

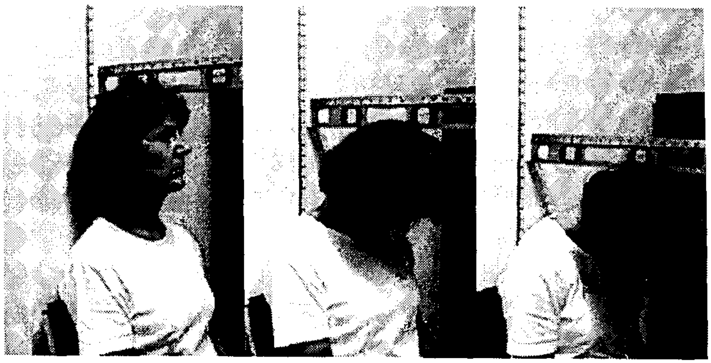

Figure 2.

Cadaveric studies should be weighted because of the disproportionate strength of the older cervical elements. Yamada[20] has shown that a 40 to 50 percent decrease in the strength of vertebral bodies in the geriatric population compared to a 26 year old. Also ligaments decrease in strength with age. Therefore greater drop heights would be required for fractures of vertebral bodies preparation in the younger population than the 60-80 year old preparations often used for cadaveric studies.

Early human studies by Ewing and Thomas[21] have demonstrated that the head lags the body in frontal or rear collisions. The Hybrid-III does not exhibit this behavior. Various studies have been done to show that head lag occurs with human studies during rear sled impacts. Cadaveric preparations of the head and neck complex demonstrated that the head lag produced an S-curve in the cervical column for either frontal or rear impacts. This characteristic is not replicated by the Hybrid-III head and neck complex.

A concerted effort is being made by the department of Transportation to develop an improved dummy neck in concert with others because of the lack of biofidelity of the Hybrid-III neck both in flexion/extension and axially. The National Highway Traffic Safety Administration (NHTSA) has set out to develop a more biofidelic frontal impact dummy. NHTSA[22] concluded, after conducted tests at its Vehicle Research and Test Center, that the Hybrid-III neck was stiff when compared with the Naval Biodynamics Laboratory volunteer data. The most important missing characteristic was the lack of head lag exhibited by the volunteers when the neck went into flexion. The location and timing of the head motion relative to the vehicle interior is important to vehicle impacts. Their solution for a new neck was to create a neck that was less stiff than the Hybrid-III and a spring/cable exterior to the neck was needed to produce the proper head lag. Researchers added design goals to included biofidelity in frontal and lateral flexion, extension and axial compression. One prototype was designed and tested by GESAC. Also a computer simulation using DYNAMAN was created for testing and development . The prototype neck's axial stiffness was 400 N/mm versus 560N/mm for the Hybrid-III and 159N/mm for cadavers.

In order to understand the effectiveness of head restraints, TNO Crash-Safety Centre[23] has started to develop the Rear Impact Dummy (RID). TNO determined current crash test dummies are not biofidelic for low severity rear impacts.

A lack of biofidelity of the Hybrid-III is attributed to excessive high resistance to bending of the neck and the torso in low severity impacts. Minimum requirements for the RID neck are an accurate representation of the human head rotations and neck bending, otherwise the head might impact the headrest in a different location or even will have no contact with the headrest or interior at all. Since the Hybrid-III lower spine is rigid, any new retrofitted neck must incorporate the flexibility of the thoracic spine as well as the cervical portion it physically represents. The Hybrid-III neck was concluded to be too stiff for the low severity rear impact environment since a majority of occupants do not anticipate rear impacts and therefore have not tensed their neck muscles. TNO has developed two prototype necks that retrofit to the Hybrid-III that appear to be first steps toward developing a true rear impact dummy.

DeSantis [24] discusses the development of a prototype multi-directional neck (MDN) by Transportation Research Center under contract to NHTSA which targets biofidelic motion in both frontal and lateral impacts. The MDN is designed with two ball-and-socket joints which connect the head and thorax with a rigid link. The neck is designed to retrofit onto the Hybrid-III and the Advanced Dummy. A series of tests were conducted on the prototype neck and compared to the Hybrid-III neck and the volunteer data from the Naval Biodynamics Laboratory. It is apparent that from this papers that, especially at low speeds, that the Hybrid-III neck remains on the stiffer side of the corridors and sometimes outside of them relative to human motion. The MDN neck demonstrated improved biofidelity in both frontal and lateral impacts when compared to volunteer data.

REAL WORLD INJURY PATTERN

As part of the work done by the Liability Research Group, we have studied the injuries received by occupants in motor vehicle accidents. Over a period of 6 years, 1992 to 1998, we have studied in depth, 124 cases of serious rollover incidents. Of these, 57 people suffered major neck injuries. In this sample, the medical examinations revealed 29 flexion type injuries, 11 combination flexion-compression injuries, 3 compression injuries, 1 rotation type injury and the remaining 13 cases no determination was made (some due to lack of comprehensive autopsy). The majority of these cases, 40 of 44 cases (91%), exhibited a flexion type or flexion-compression injury pattern,. The dummy studies conducted by Moffatt, et al.[25], [26] are inconsistent with this real world injury data.

One explanation for this discrepancy lies in the lack of biofidelity of the Hybrid-III neck in a rollover accident mode. In a rollover accident, a human neck will usually rotate itself into a non-aligned arrangement to relieve pressure. Injury occurs when the head and neck is pushed beyond its limits or in rare cases when the cervical spine is aligned without the natural curvature and compressed by approximately 15-25 mm. For the Hybrid-III neck, the force is transmitted straight through the neck and the neck load cells record high axial loads with small deflections and prior to any significant bending.

Friedman et al.[27] performed a set of experiments that showed that with a pre-flexed head in contact with a rigid roof, the human volunteer was uninjured at drop heights of 15 cm. A Hybrid-III neck would likely have registered injurious loads. Friedman and Friedman[28] have conducted a series of drop tests where a Hybrid-III dummy in an inverted rollcaged vehicle recorded injurious levels of load in the neck (similar to the studies conducted by Moffatt et. al) while a human volunteer, in the identical environment, was unhurt.

CONCLUSIONS

The aforementioned studies and continued evolution of dummy necks presents clear evidence that the Hybrid-III neck does not provide adequate biofidelity. Despite the overwhelming evidence, a recent publication interprets the works of other authors and suggests that the Hybrid-III is biofidelic.[29] Under compressive loading, the Hybrid-III neck compares closest to the human neck only once the human spine has the lordosis removed, the load path is within 1 cm of the spine's vertical axis and with the spine constrained. Even in these conditions, it remains many times stiffer than the human spine. The human spine's stiffness and load bearing characteristics change dramatically when natural or induced spinal curvature is included, the load path is off center more than 1 cm or the flexibilty of the thoracic spine is considered. The Hybrid-III neck becomes more than an order of magnitude stiffer than human spine under these conditions.

A properly biofidelic neck must represent, as accurately as possible, a human neck in all directions. This will insure accurate motion and loading to the dummy. Due to excessive stiffness in all directions, the Hybrid-III neck cannot provide meaningful data in environments in which accelerations and loadings come from multiple directions such as those seen in rollovers. Previous studies[30, 31] have used the Hybrid-III neck to draw the conclusion that in rollovers, roof strength is not casual to neck injury. Injury rates occurring in these rollover tests were two orders of magnitude more frequent than that seen in the real world accidents. This can be directly attributed to the lack of biofidelity of the Hybrid-III neck, and its tendency to over-represent axial compression injuries. We believe that if the Malibu studies were conducted with a biofidelic neck, the results would support a relationship between roof crush and injury. Recent drop tests[28] have reinforced that the Hybrid-III dummy overpredicts injury in humans.

Important considerations for future dummy necks are:

- reproducing head trajectories comparable to humans;
- incorporate geometry representative of the human curvatures and structure;
- representation of the thoracic spine characteristics;
- replicate rate sensitivity, load transmission, stiffness and bending characteristics.

REFERENCES

[1] Mertz, H.J., Patrick, L.M. *Strength and Response of the Human Neck*, SAE 710855, 1971.

[2] Mertz, H.J., Neathery, R.F. and Culver, C.C. *Performance Requirements and Characteristics of Mechanical Necks*, Human Impact Response, 1973.

[3] Melvin, J.W., McElhaney, J.H., Roberts, V.L., *Evaluation of Dummy Neck Performance,* Human Impact Response, 1973.

[4] Seemann, M.R., Muzzy III, W.H., Lustick, L.S. *Comparison of Human and Hybrid-III Head and Neck Dynamic Response*, SAE 861892, 1986.

[5] Nusholtz G.S., Huelke D.E., Lux P., Alem P., Montalvo F. *Cervical Spine Injury Mechanisms.* Proceedings of the 27th Stapp Car Crash Conference, Society of Automotive Engineers, Warrendale, PA, 1983, pp. 179-198.

[6] Yoganandan N., Sances A. Jr., Maiman D., Myklebust J., Pech P., Larson S. *Experimental Spinal Injuries with Vertical Impact.* Spine, 11(9): 855-860.

[7] McElhaney J., Snyder R., States J., Gabrielsen M. *Biomechanical Analysis of Swimming Pool Neck Injuries.* SAE/SP-79/438, 1979.

[8] Pintar F.A., Sances A. Jr., Yoganandan N., et al. *Biodynamics of the Total Human Cadaver Cervical Spine.* Proceedings of the 34th Stapp Car Crash Conference, Orlando, FL, 1990, pp. 55-72.

[9] Yoganandan N., Sances A. Jr., Pintar F.A. *Biomechanical Evaluation of the Axial Compressive Responses of the Human Cadaveric and Manikin Necks.* Journal of Biomechanical Engineering, III (3): 250-255, 1989.

[10] Pintar F.A., Yoganandan N., Voo L.M., Cusick J.F., Maiman D.J., Sances A. Jr. *Dynamic Characteristics of the Human Cervical Spine.* SAE Transactions 104 (6): 3087-3094, 1995.

[11] Sances A. Jr., Voo L.M. *Biofidelity of the Hybrid III Neck for Spinal Trauma Assessment.* ASME Advanced Bioengineering. BED-Vol. 36: 249-250, 1997.

[12] Nightingale R., McElhaney J., Camacho D., Kleinberger M., Winkelstein B., Myers B. *The Dynamic Responses of the Cervical Spine: Buckling, End Conditions, and Tolerance in Compressive Impacts.* SAE 41st Stapp Car Crash Conference, 1997 Proceedings, SAE 973344.

[13] McElhaney, J.H., Paver, Jacqueline,G.P., McCrackin, H.J., Maxwell, G.M., *Cervical Spine Compression Responses,* SAE 831615, 1983.

[14] McElhaney J.H., Doherty B.J., Paver J.G., Myers B.S., et al: *Combined Bending and Axial Loading Responses of the Human Cervical Spine.* Proceedings of the 32nd Stapp Car Crash Conference, Atlanta, GA, 1988, pp 21-28.

[15] Myers B.S., McElhaney J.H., Richardson W.J., et al: *The Influence of End Condition on Human Cervical Spine Injury Mechanism.* Proceedings of the 35th Stapp Car Crash Conference, San Diego, CA, 1991, pp 391-399.

[16] Yoganandan N., Sances A. Jr., Maiman D., Myklebust J., Pech P., Larson S. *Experimental Spinal Injuries with Vertical Impact.* Spine, 11(9): 855-860.

[17] Nightingale R., McElhaney J., Camacho D., Kleinberger M., Winkelstein B., Myers B. *The Dynamic Responses of the Cervical Spine: Buckling, End Conditions, and Tolerance in Compressive Impacts.* SAE 41st Stapp Car Crash Conference, 1997 Proceedings, SAE 973344.

[18] Nusholtz G.S., Huelke D.E., Lux P., Alem P., Montalvo F. *Cervical Spine Injury Mechanisms.* Proceedings of the 27th Stapp Car Crash Conference, Society of Automotive Engineers, Warrendale, PA, 1983, pp. 179-198.

[19] Yoganandan N., Sances A. Jr., Maiman D., Myklebust J., Pech P., Larson S. *Experimental Spinal Injuries with Vertical Impact.* Spine, 11(9): 855-860.

[20] Yamada H. *Strength of Biological Materials.* Williams Wilkins, July 1969, p. 297.

[21] Ewing C.L., Thomas D., Lustick L., Muzzy W.H., et al. *The Effect of Duration, Rate of Onset and Peak Sled Acceleration on the Dynamic Response of the Human Head and Neck.* Proceedings of the 20th Stapp Car Crash Conference, Dearborn, MI, Society of Automotive Engineers, Inc., 1976.

[22] White, R.P. Jr., Zhao, Y., Rangarajan, N., Haffner, M., Eppinger, R., Kleinberger, M. *Development of an Instrumented Biofidelic Neck for the NHTSA Advanced Frontal Test Dummy.* ESV, 96-S10-W-19, 1996.

[23] Thunnissen, J.G.M., Van Ratingen, M.R., Janseen, E.G. *A Dummy Neck for Low Severity Rear Impacts.* ESV, 96-S10-O-12, 1996.

[24] DeSantis, Kathleen, *Development of an Improved Multi-Directional Neck Prototype.* SAE 912918, 1991.

[25] Moffatt, E., Orlowski, K.F., Stocke, J.E., Bahling, G.S., Bundorf, R.T., and Kaspzyk. *Rollover and Drop Tests - The Influence of Roof Strength on Injury Mechanics Using Belted Dummies.* SAE 902314, 1990.

[26] Orlowski, K.F., Bundorf, R.T., Moffatt, E.A. *Rollover Crash Tests- The Influence of Roof Strength on Injury Mechanics.* SAE 851734, 1985.

[27] Friedman, D. and Chng, D. *Human Subject Experiments in Occupant Response to Rollover with Reduced Headroom.* SAE 980212, 1998.

[28] Friedman, K. and Friedman, D. *Upper Interior Head, Face and Neck Injury Experiments.* ESV 1998, Paper Number 98-S8-P-11.

[29] Piziali, R., Hopper, R., Girvan, D. and Merala, R. *Injury Causation in Rollover Accidents and the Biofidelity of Hybrid III Data in Rollover Tests.* SAE 980362, 1998.

[30] Moffatt, E., Orlowski, K.F., Stocke, J.E., Bahling, G.S., Bundorf, R.T., and Kaspzyk. *Rollover and Drop Tests - The Influence of Roof Strength on Injury Mechanics Using Belted Dummies.* SAE 902314, 1990.

[31] Orlowski, K.F., Bundorf, R.T., Moffatt, E.A. *Rollover Crash Tests- The Influence of Roof Strength on Injury Mechanics.* SAE 851734, 1985.

THE LOAD PATH FROM UPPER LEGS TO CHEST IN THE HYBRID III DUMMY; EXPERIMENTS AND SIMULATIONS

R. Happee, A.R. Kant
TNO Crash-Safety Research Centre
The Netherlands
E. Abramoski, J. Feustel
Ford Motor Company, MI
USA
Paper Number 98-S9-W-24

ABSTRACT

It has been shown that the design of the Hybrid III dummy's hip joint can cause abnormally high spikes in the chest accelerations. These spikes are generated when the pelvis rotation is suddenly stopped by the bottoming out of the hip joint. This creates large lumbar shear and tension forces which act to resist forward movement of the dummy's chest. This problem has partly been resolved by the introduction of "modified femurs". However, even with modified femurs, high peaks have still been observed in chest accelerations of some front barrier crashes.

In order to analyze the load path from upper legs to chest, dynamic experiments have been performed on the hip joint (with modified femurs and with standard femurs), on the isolated lumbar spine and on a partial dummy consisting of upper legs, torso, neck and head. These tests have been used to significantly improve an existing model of the dummy.

In the hip joint, a considerable rate-dependency was found and the adjustment of hip friction was found to be an important factor. For different lumbar spines from the same manufacturer, major differences in response were found. These differences between dummy parts are a concern for reproducibility of full dummy tests.

A sensitivity analysis showed that such dummy related factors lead to variations in the order of 2-8% for peak chest acceleration and chest deflection, but lead to much larger variations in lumbar loads.

INTRODUCTION

Uncharacteristic high thoracic spine accelerations have been noted by several vehicle manufacturers when driver and passenger air bag restraints were used in combination with the unbelted 50th percentile Hybrid III dummy. These peaks were shown to be caused by bottoming out of the hip joint. This problem is mostly referred to as "hip lock" or hip joint interference. As this response of the dummy was not considered biofidelic, modified femurs have been designed. Several evaluations showed that this modification reduced the signs of hip lock (Abramoski et al., 1994; Abramoski et al., 1995; SAE 950660; Nusholtz et al., 1995; Klinich et al., 1995; Kanno et al., 1996). Well validated mathematical models of the Hybrid III dummy failed to reproduce these peaks in the thoracic spine acceleration. Furthermore the lumbar spine loads were not accurately predicted. Apparently the load path from upper legs to chest was not well captured. In order to clarify the mechanics of this load path the following series of experiments was performed.

1) Dynamic tests on the isolated lumbar spine
2) Dynamic hip flexion tests
3) Dynamic tests on a partial dummy including hip joints, upper torso, neck and head

These tests have been used to improve an existing model of the dummy. With this improved Hybrid III model, full scale tests have been analyzed in order to further clarify the role of different dummy components in the load path from legs to spine. Major variations in resistance were found between different lumbar spines, and it was found that hip friction is generally not set as prescribed. To evaluate these sources of variability on injury numbers a sensitivity analysis was performed on realistic applications of the Hybrid III dummy.

LUMBAR SPINE TESTING & MODELLING

In a previous test programme the relations between rotations (bending & torsion) and displacements (compression & elongation and shear), and moments and forces were determined in a quasi-static manner (MADYMO, 1994). Damping coefficients were then estimated on the basis of pendulum test results. Below more extensive dynamic tests on the lumbar spine are described.

Lumbar spine bending and shear

Dynamic lumbar spine tests were performed where the lumbar spine was rigidly connected to a sled. A sled acceleration with the appropriate pulse shape was induced with a Monterey setup. On the lumbar spine a Hybrid III spine box was attached including a spine load cell. Ribs and neck bracket were removed. The spine box yields an inertial loading to the lumbar spine. By attaching one or more load masses to the spine box this inertial loading was manipulated. Three loading assemblies were used:

- shear assembly; an assembly with a CG below the spine box was designed such that mainly shear was induced in the lumbar spine.
- bending assembly; a mass was attached on top of the spine box which resulted in strong bending and limited shear in the lumbar spine.
- torsion assembly; a mass was attached lateral (to the right) of the spine box such that a combination of torsion, bending and shear was induced in the lumbar spine.

For all conditions, two or three loading severities were applied with one lumbar spine which further will be referred to as *specimen 1*. The shear and bending tests with the highest loading severities have been repeated with another lumbar spine (*specimen 2*).

Repeatability and reproducibility - For repeated tests with specimen 1 only minor differences were observed. Film results showed a good repeatability for displacements and rotations. The response of specimen 2 differed notably from specimen 1. Furthermore the repeated tests with specimen 2 showed rather large differences. Both for the shear and the bending condition, specimen 2 gave reduced spine deformations as compared to specimen 1. These results indicate that the reproducibility of different spines is poor. Repeatability is good for specimen 1 with which all test conditions were studied and repeatability is not good for specimen 2. Given the differences found it seemed worthwhile to test more specimens. Additional tests on three lumbar spines were conducted using the most severe loading conditions of the bending and shear test configurations. Test specimens were chosen to have spines at the low, mid and high range of the part specification tolerance of 75 to 85 durometer. The spines tested had measured durometers of 77, 81, and 84. As part of this study the spine cable tension was also varied +/- 15% from the nominal specification of 12 in-lbs. Since there is no performance specification for the Hybrid III dummy lumbar spine, these two variables essentially are the only controlled parameters that could affect its performance (the spine geometry is also defined but because it is made out of polyacrylate it does not completely return to its initial geometry after it has been deformed). Each test configuration was done two times resulting in a total number of 36 tests. The results show that the spine stiffness can vary significantly, even among certified lumbar spines. A strong relationship was found between the lumbar spine durometer and the bending stiffness as is evident by looking at Figure 1. The higher the durometer of the lumbar spine, the higher the measured loads and the lower the spine box rotation. There was no relationship evident between the spine cable tension and the spine stiffness. It should also be mentioned that the measurements of the spine durometer were done by a person familiar with taking this measurement from First Technology Safety Systems. The same lumbar spines were remeasured by the same person 3 months later and were found to be within +/- 1 durometer from the original measurement. But when other people measured the durometer, they got significantly different values (by as much as 6). This indicates that specifying a durometer specification may not be appropriate since it appears to be very user dependent. This is primarily due to the lumbar spine not having a flat surface from which the durometer could be measured.

Lumbar spine axial compression

The response of the lumbar spine in axial loading is particularly relevant for aircraft seat testing. Therefore dynamic tests were performed for axial compression. These were performed with a Zwick-Rel dynamic testing machine at various loading rates.

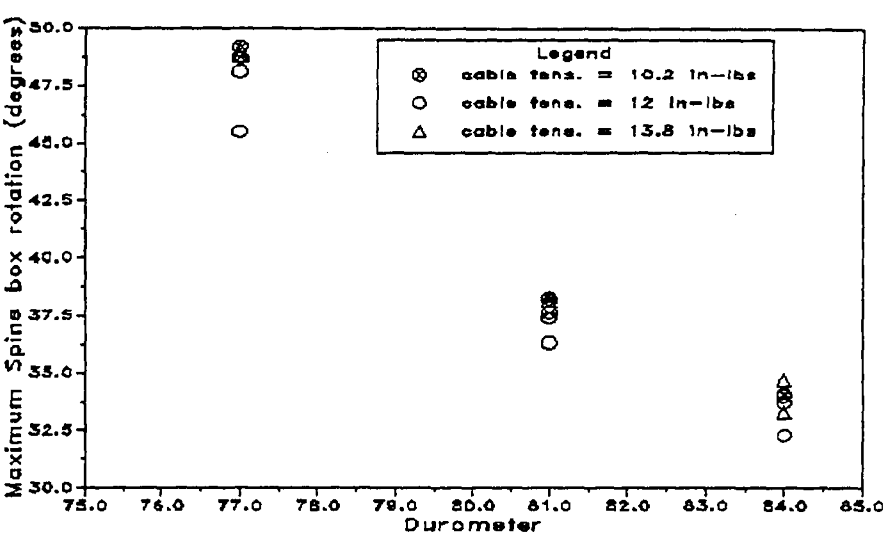

Figure 1: Spine box rotation vs. spine durometer from the lumbar spine bending tests.

Lumbar spine modelling

The dynamic lumbar spine tests described above have been used to improve the existing lumbar spine model (MADYMO, 1994). The model was optimized, such that the differences between the simulations and the experimental results were minimized. Some parts of the optimization were performed manually. The most complicated parts of the optimization were performed automatically (MADYMO, 1997). The automated optimization has the following advantages:

- several parameters can be optimized together; the program deals with the interaction between the parameters and finds an optimal set of parameters,
- different signals from one test, and even from different tests can be combined into one objective function

In several steps the model was optimized. The existing model was based on extensive quasi-static tests and a limited set of dynamic experiments. Therefore it was expected that mainly the damping parameters of the model should be adapted. Some information on the rate dependent behaviour of the Hybrid III lumbar spine can be found in Begeman et al. (1994). Here it was concluded that the shear resistance of the lumbar spine is strongly rate dependent. These effects were already apparent at the applied maximum loading rates of 50 mm/s whereas shear rates up to 2.8 m/s were found in the component tests now used for modelling. In the existing model the spine cables were modelled as a very high joint stiffness for elongation. An improved prediction was obtained by modelling the cables separately as a Kelvin element. As stated above the results for specimen 2 differed strongly from specimen 1. The model was optimized for specimen 1. Finally the model was optimized also for specimen 2. This optimization had the following results. The bending resistance of specimen 2 was found to be 1.4 times that of specimen 1. The shear resistance was estimated to be practically the same for both specimens. This confirms that specimen 2 has a much higher resistance in bending as compared to specimen 1.

HIP JOINT TESTING AND MODELLING

Dynamic component tests have been performed on the hip joint. The goal of these experiments was to determine the dynamic resistance of the hip joint. The modified femurs are designed to prevent the occurrence of interference in the hip joints. Hip lock occurs when the dummy's upper femur bottoms out and makes metal to metal contact with the pelvis bone. A distinction is made between "hard" hip lock and "cushioned hip lock" (Klinich et al., 1995). Hard hip lock can occur in the standard femur and cushioned hip lock can occur in the modified femurs. Two pelvis/femur assemblies have been tested. The first assembly is a standard 50th percentile Hybrid III pelvis with standard femurs. The second assembly is a new pelvis with modified femurs. These two assemblies are respectively abbreviated as "standard femurs" and "modified femurs".

The pelvis was held "rigidly" at the lumbar spine attachment with the upper legs directed upwards and the lower legs removed. Both legs were tested at the same time in order to study differences in behaviour between the left and the right hip. It is known that the left and right hips behave differently because the pelvis is not left/right symmetric (Klinich et al., 1995; Abramoski et al., 1994).

The modified femurs were tested at two loading severities and at different loading rates. The highest severity tested induced "cushioned hip lock". The low severity tests were also repeated with standard femurs and did not result in hip lock. Accelerations in x, y and z directions were recorded at the sled, the pelvis and the knees. The hip flexion angles were calculated from string pot measurement. The flexion angles calculated from the string pots were verified using high speed video. It was concluded that the string pots were able to follow the dynamics of the knees accurately.

Hip friction

Calibration procedures describe that "Limb joints are set at 1 G, barely restraining the weight of the limb when it is extended horizontally" (CFR part 572 subpart E). Calculations assuming a horizontal upper and lower leg were performed. Thus the static hip joint friction was estimated to be about 56.1 Nm. However, in our experience a friction much below 56.1 Nm is often applied in real dummies. Simulations of various full dummy tests indicated a hip friction in the order of 12.8 Nm which was further adopted for the model. This will be treated further in the discussion.

Friction has been implemented for the hip joints with the COULOMB FRICTION model. Both a constant friction and an additional load dependent friction were specified.

Hip stiffness and damping

Hip flexion requirements were specified by the SAE Large Male and Small Female Dummy Task Group (SAE 950660). Calibration specification tests were carried out for the modified femurs which were used in the dynamic hip flexion tests. It was found that the left femur did meet the specifications and that the right femur was right on the limit of 46 degrees at 340 Nm. The torque-angle result for the left leg calibration was applied in the model. Additional damping was implemented as being dependent on the rotation angle. The dynamic component tests were used to optimize the model. Optimization methods were used to systematically determine parameters providing a best fit for several output variables of different experiments. The hip joint model was optimized using test data of the left joint. It was found that the model based on the left hip is sufficiently accurate for the right hip. The hip model was updated using test data of the modified femurs. Moderate loading of standard femurs was also simulated with the new hip model. From these simulations it was concluded that the new model provides a reasonable prediction for moderate loading of standard femurs.

DYNAMIC TESTS ON HIP JOINTS, TORSO, NECK AND HEAD

Tests with a partial dummy have been executed to study the behaviour of the combined hip/lumbar spine section of the dummy. In such tests, lumbar spine deformation is not only resisted by the lumbar spine itself but also by contact interactions of the rib cage, the abdomen and the lower torso (Heinz, 1993). In all tests the arms were removed. Head and neck were included in these experiments. In all forward loading tests, the lower legs were removed and the knees were mounted on the sled. The pelvis was supported by a rigid horizontal plane. The knee-slider, and knee rotation mechanism were included in the tests. So, the dummy could move forward slightly, and rotate freely around the knee axis. In the rearward loading tests, the upper legs were replaced by rigid supports, and the pelvis was also supported at the back.

Four forward loading tests, were performed with a belt restraining the upper torso. The belt was attached to the base of the neck. The belt was chosen such that it approximates the restraining effect of an airbag. Before performing the experiments, several simulations were run to select the appropriate belt characteristics. This belt limits the rotation of the torso, but the films show that even with this belt, the ribs came close to the upper legs.

Two experiments were also performed without the abdomen. The abdomen reduces the recorded lumbar spine bending torques (MY) by around 10%. This is logical since there is load sharing between lumbar spine and contacts; part of the total bending torque is generated by the abdomen. In other signals smaller effects were found. Even in the lumbar My the differences observed are not very large. However, also when the abdomen is removed, contact interactions still occur between ribs, jacket, pelvis and legs. The experiments do not show directly how large this influence is. Only tests with the abdomen present have been used below for model validation and improvement.

Optimization of the model

The experiments were used to optimize a model representing contacts between ribs, jacket, abdomen and pelvis. These contacts will further be mentioned as "abdomen contacts". A notable effect of these contacts was found for tests with large forward bending of the torso. With these contacts present in the model an improved prediction was obtained of the lumbar spine loads. Upper and lower spine bending torques were reduced up to 35%. These contacts also affected chest kinematics and accelerations.

FULL DUMMY TESTS

Several tests with the complete dummy were analyzed to validate the complete dummy model, and to analyze the load path from legs to femurs. A relatively simple sled test with a rigid seat and with separate shoulder and lap belt has been used for validation. Test and simulation are described as an example in the MADYMO database manual (MADYMO, 1997). Results obtained with the new model results were almost identical to those presented in the manuals for the existing model. The actual tests were performed with standard femurs. However, the updated model based on modified femurs was applied. For this condition, only minor hip rotations were observed. This illustrates that for these conditions, the updated model is also suitable to simulate tests with standard femurs.

Barrier tests with a driver airbag, unbelted were simulated. Kinematics are shown in Fig. 2 and phasing of important experimental signals is given in Fig. 3. Around 40 ms knee bolster contact induces axial femur loads and pelvis acceleration (Fig 3, upper). Around 70 ms maximal lumbar forces and chest accelerations are observed (Fig 3, middle). Validation results are shown in Fig. 4.

SENSITIVITY ANALYSIS

Above concerns were raised about factors in the Hybrid III dummy which will negatively affect the reproducibility and repeatibility of tests. A sensitivity analysis was performed to quantify these effects (Table 1). This analysis was performed for the following configurations

1. *driver airbag unbelted*: this test with validation results is described above.
2. *depowered driver airbag*: The driver airbag unbelted model was modified to simulate the recently adopted AAMA proposal for FMVSS 208. This includes changing the barrier crash pulse to a half sine (17.2g-125ms) pulse and using a less forceful inflatable restraint.
3. *aircraft drop test 30 deg nose down 16 m/s*. This test was performed in accordance with MIL-S-58095 and the body was effectively restrained by a five-point harnass belt.

The following variations of the Hybrid III model were analysed:

1. *softer hip lock* was simulated by applying a hip flexion stiffness based on modified femurs but with a reduced stiffness beyond 340 Nm. Instead of the highly non-linear bottoming out function now a linear stiffness was taken. It should be noted that this model also matches the calibration specs for 340 Nm.
2. *hip friction of 56.1 Nm*: the friction of 12.8 Nm from the standard database was increased to 56.1 Nm.
3. *double lumbar resistance*: the resistance of the lumbar spine model was doubled to simulate a variation comparable to the maximal expected component variations.
4. *no spine cable*: the KELVIN element representing the spine cable was removed from the model. This variation was performed mainly to assess the effect of the spine cable on lumbar tensile forces.
5. *rib-pelvis contacts removed*: this variation was performed to assess the contribution of the contact interactions between ribs, abdomen and pelvis.

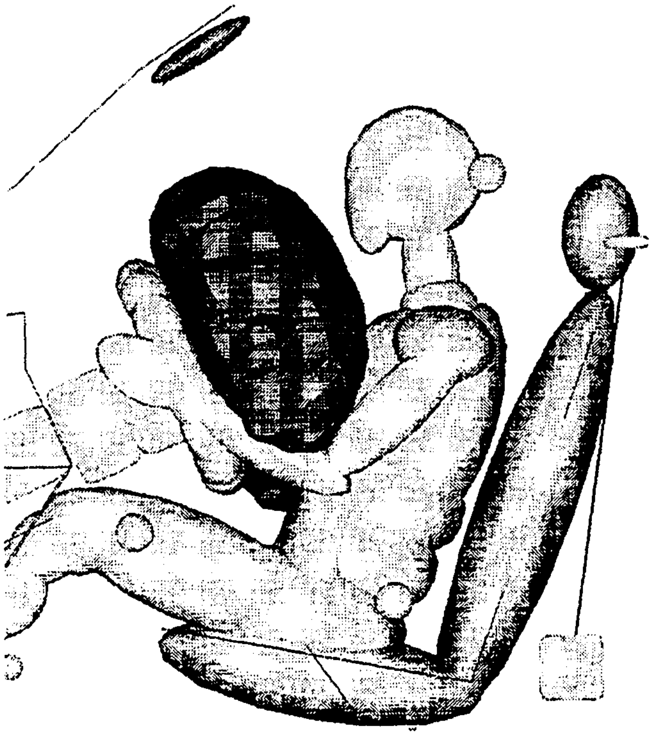

Figure 2. Kinematics of model driver airbag unbelted at 40 ms.

Table 1.

Sensitivity analysis; each block represents a loading condition. For each condition first results are given for the experiment and for the improved dummy model. Then the relative effect of several model variations is given with respect to the standard model. Effects below 1% are omitted (-)

condition model variation	peak chest acc (3 ms) [m/s2]	peak chest deflection [m]	peak lower lumbar Fz [N]	peak lower lumbar My [Nm]	peak femur axial force Fz [N]
driver airbag unbelted					
experiment	720	0.048	-6600 tension	-190	8400
standard model	707.7	.05342	-5630	-382	9529
softer hip lock	-5.6%	-	-4.8%	-12%	-
hip friction 56.1 Nm	-5.7%	-	-8.5%	-7.2%	-9.7%
lumbar resistance*2	-5.9%	-3.7%	-11.7%	+30%	-
no spine cable	-5.8%	+1.2%	-8.5%	-10%	-
no abdomen contact	-	-	-	+0.5%	-
depowered driver airbag unbelted					
experiment	-	-	-	-	-
standard model	357.5	0.03232	+2588 compressive	-210.7	8351
softer hip lock	-	-	-	-	-
hip friction 56.1 Nm	-6.7%	-7.8%	-	+6.6%	-2.4%
lumbar resistance*2	-3.1%	+2.1%	+2.1%	+20%	-1.4%
no spine cable	-	-	+3.6%	+1.3%	-
no abdomen contact	-	-	-	+1.8%	-
aircraft drop test 30 deg nose down					
experiment					
standard model	336.6	0.0178	+6637 compressive	-452	2553
softer hip lock	-	-	-	-	-
hip friction 56.1 Nm	-5.9%	-6.2%	+2.1%	-13%	+8.5%
lumbar resistance*2	+37%	+2.6%	+110%	+59%	-2.0%
no spine cable	-	-	-	-	-
no abdomen contact	-3.9%	-1.5%	-28%	-16%	-

DISCUSSION

Dynamic tests have been performed on lumbar spines, on hip joints with standard and modified femurs and on partial dummies. These tests have been used to improve an existing model.

In the hip joint, a considerable rate-dependency was found. For component tests below hip lock level, limited differences were observed between the old and the new femurs. This is in agreement with full dummy evaluations described in the literature (Klinich et al., 1995; Nusholtz et al., 1995). The current specification for hip resistance surely reduces variability induced by the condition of the dummy (SAE950660). Some variation may still be found above the calibration level. Table 1 indicates that such a variation could affect chest G's in the order of 6% for conditions with cushioned hip lock. The standard calibration requirement for hip friction results in a value of about 56.1 Nm. Only 12.8 Nm was implemented in the model since in our experience a friction much below 56.1 Nm is often applied in real dummies. The sensitivity analysis indicated a considerable influence of hip friction on the dummy response. Given the influence of hip friction it is recommended that this variable is well controlled in experiments. This would improve reproducibility of tests and would facilitate modelling.

Major differences in response were found for different lumbar spines. These were shown to relate to durometer testing (see Fig. 1). However lumbar durometer measurements are found to be very user dependent. Alternatively a dynamic bending calibration could be specified for the lumbar spine. This would help in reducing test variability. In component tests and in the sensitivity analysis only minor effects of the spine cable were found. Tests and simulations on the partial dummy showed significant effects of contacts between ribs, abdomen and pelvis. These contacts add to the bending resistance of the lumbar spine, and thereby affect the lumbar spine loads. The sensitivity analysis showed that this effect was particularly relevant in the aircraft test.

CONCLUSIONS

Testing on hips, lumbar spines and partial dummies provided insight in the load path from legs to upper torso and was used to improve an existing model of the dummy. Major variations in bending resistance were observed for the lumbar spine, and concerns were raised about the adjustment of hip friction. The sensitivity analysis showed that such dummy related factors lead to variations in the order of 2-8% for peak chest acceleration and chest deflection, but lead to much larger variations in lumbar loads.

REFERENCES

Abramoski, E., Warmann, K., Feustel, J., Nilkar, S. and Nagrant, N.J. (1994). *High chest accelerations in the Hybrid III dummy due to interference in the hip joint.* 38th Stapp Car Crash Conference, Fort Lauderdale, Florida, November 1994, SAE-942224.

Abramoski E., Warman K., Feustel J., Wilson P., Wagner B., Nilkar S. (1995). An evaluation of the SAE Recommended design changes to the Hybrid III dummy hip joint. SAE-950665.

Begeman P.C., Visarius H., Nolte L.P., Prasad P. (1994). Viscoelastic shear responses of the cadaver and Hybrid III lumbar spine. STAPP Conference, 1994, SAE paper 942205.

Berge S., Planath-Skogsmo I. (1995). Interaction of the Hybrid III femur and pelvis - a mechanical analysis. SAE 950664.

Heinz M. (1993). Some aspects of the lumbar spine joint of the 50th percentile Hybrid III - dummy database. MADYMO Users Meeting 1993.

Klinich, K., Beebe, M.S. and Backaitis, S.H. (1995). *Evaluation of a proposed Hybrid III hip modification.* SAE-952730.

Kanno Y., Masuda M., Matsuoaka F., (1996). Evaluations of the recommended new parts for the Hybrid III dummy - neck shield and hip joint. SAE-960450.

MADYMO (1994). MADYMO version 5.1, Database manual 3D, Chapter 2: The 50th percentile sitting Hybrid III dummy.

MADYMO (1997). MADYMO version 5.3, Madymizer manual.

Nusholtz, G., et al. (1995). *Analysis of the pelvis-chest interactions in Hybrid III.* Society of Automotive Engineers, 1995, SAE-950663.

SAE-950660. Large male, small female, and 6-year-old dummies task group (1995). *Hip flexion requirements for adult dummies.* Society of Automotive Engineers, 1995, SAE-950660.

Figure 3. Experimental signals of test driver airbag unbelted

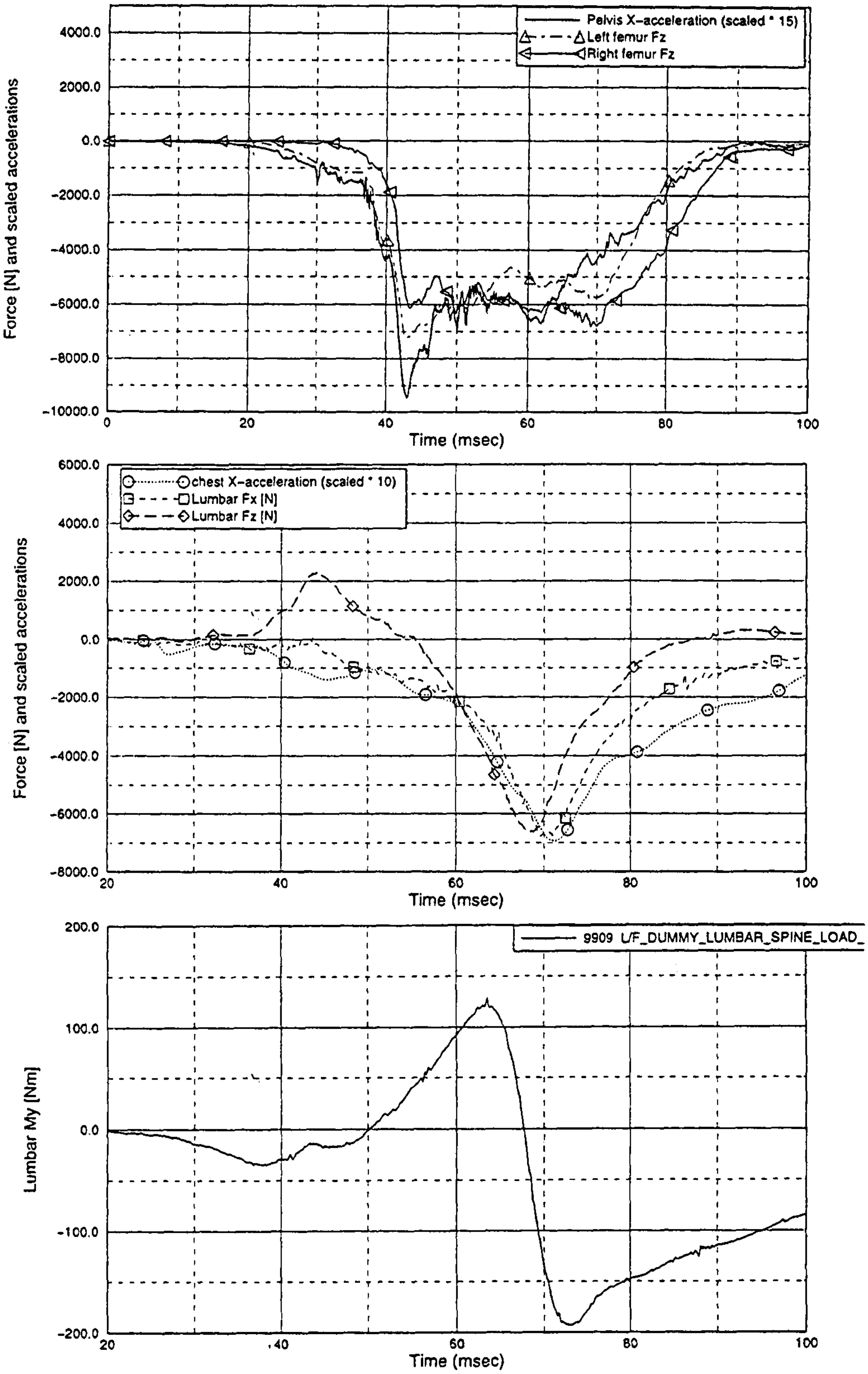

Figure 4. Validation results of test driver airbag unbelted

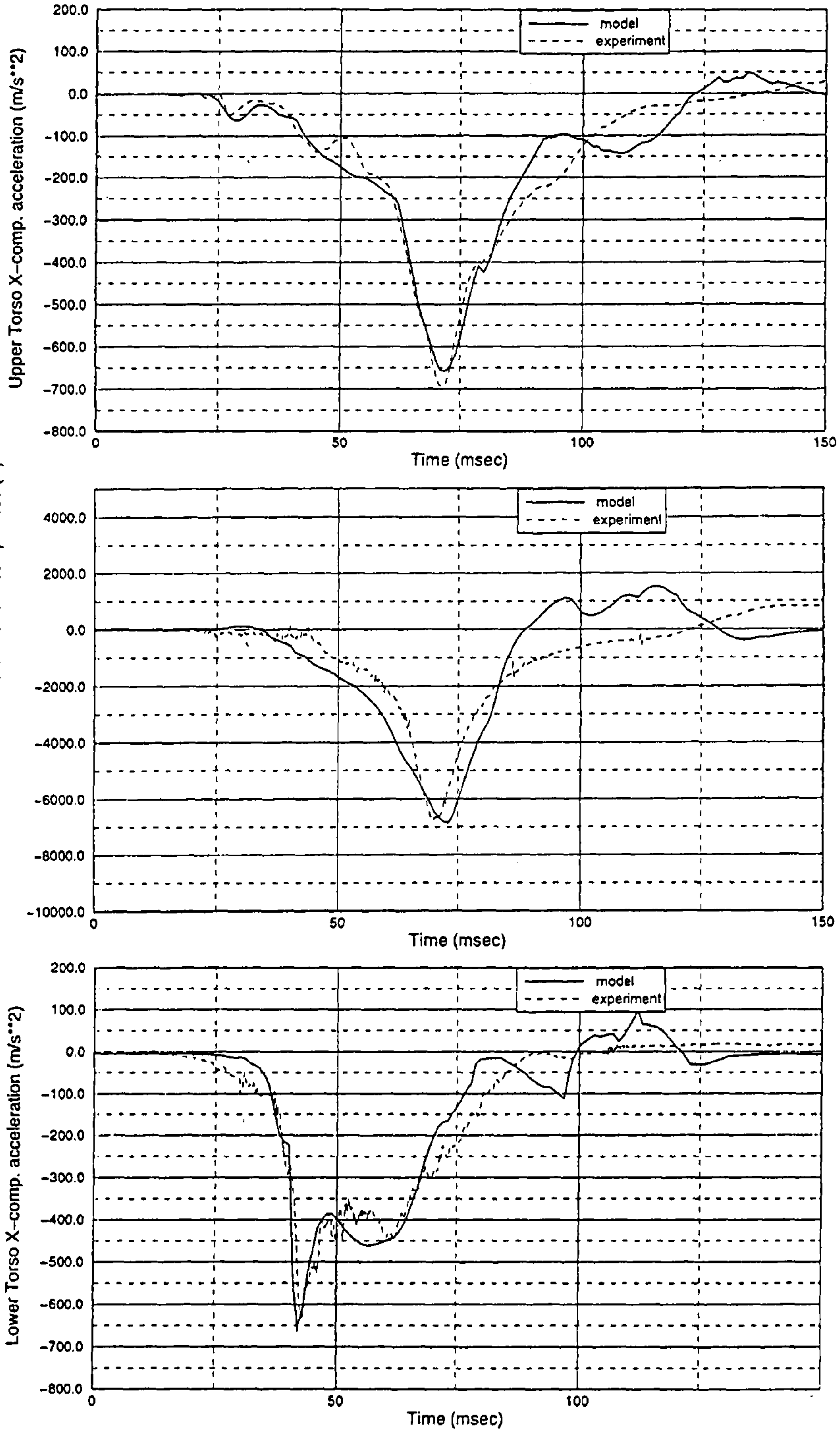

A SUMMARY OF THE WORK OF THE SAE ATD CHEST DEFLECTION TASK TEAM

John B. Athey
Joseph S. Balser
General Motors Corporation
United States of America
Paper Number 98-S9-W-27

ABSTRACT

This paper focuses on the work of the SAE ATD Chest Deflection Task Team, chaired by Mr. Joseph Balser. Data are presented, and discussed, on the most promising methods that were tried, as well as an examination of these methods.

An abbreviated version of their mission statement summarizes their work, "The ATD (Anthropomorphic Test Dummy) Chest Deflection Task Team will focus on the development and validation of a new transducer or transducers that will accurately measure ATD rib deflections and velocities in three axes when the ATD is exposed to belt and/or air bag testing. The first phase of work will be to improve and commonize deflection transducer hardware being used today. Phase two will be to develop and validate an advanced ATD chest deflection transducer that will effectively produce valid measurements at up to 18 meters per second at SAE filter class 600."

INTRODUCTION

The first meeting of the SAE ATD Chest Deflection Task Team, chaired by Mr. Joseph Balser, took place on September 13, 1995. This task team continued the work of the USCAR OSRP ATD Chest Deflection Task Team which first met on May 9, 1995, which was also chaired by Mr. Balser. The primary work of the SAE task team is not finished. The goal of this paper is to present the work that has been accomplished as of this writing, and to offer advice to users of ATD's as to how the work that this task team has accomplished can best be put to use. A secondary goal is to give some general direction that others can take in developing methods of making this very difficult measurement within the crash test environment.

DESIGN GOALS

At the first meeting of this task team chairman Balser had the task team define the goals of any new chest deflection transducers that they would be developing for use in ATD's. The task team used the term goals rather than requirements since some of the desired traits may be unattainable, or compromises may be necessary between two or more goals. The design goals that were agreed on for any transducers by the task team are listed below:

1. Accurately measure or compute rib deflections and velocities in the range of 0 to 18 meters per second, at SAE CFC 600, in the Hybrid-III 5th percentile ATD, with the plan to use the same basic device in all adult Hybrid-III ATD's.
2. Should be small, allowing multiple rib deflection transducers to be installed in the same ATD.
3. Must be easy to use and be compatible with standard data systems of either the onboard or off-board versions if transducers are to be used in high production testing facilities.
4. Ease and accuracy of calibration must be a major consideration.
5. Cost per channel must be considered.
6. Ease of installation and test setup must be highly considered.
7. Durability is a major consideration.

Most of the design goals were based on the combined experience of the task team. The exception to this was the first item which stipulates that rib velocities of up to 18 m/s must be able to be measured or calculated at SAE CFC 600. Dr. Rouhana suggested this number to the task team. He stated that he has seen driver air bags with membrane velocities of 100 miles per hour. Under certain conditions this can translate to a sternum velocity of about 8 m/s. Since passenger bags can have membrane velocities of approximately 200 miles per hour the task team agreed that it would be reasonable to infer a potential sternum velocity of 16 m/s with such an air bag. The task team agreed with Dr. Rouhana's recommendation. The additional 2 m/s (which yielded the 18 m/s value) was added to allow for some excess capacity.

MEASURING CHEST DEFLECTION

Traditional Methods of Measurement

Generally, frontal chest deflection measurements have been made using a rotary potentiometer. When rib deflection has been measured on side impact ATD's, a linear potentiometer or string potentiometer has typically been used. The problems of making the measurement with potentiometers are illustrated in Figures 1 and 2.

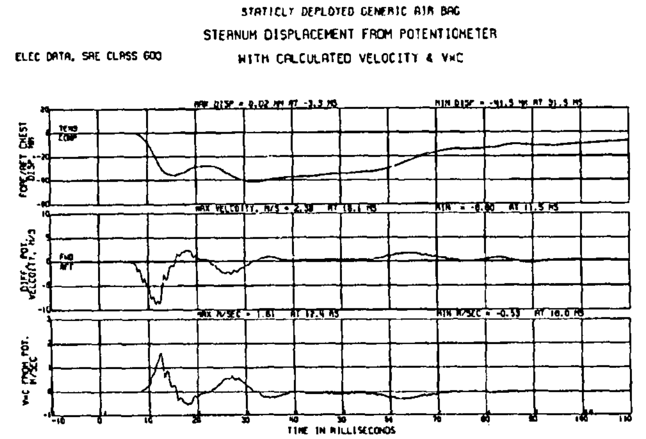

Figure 1. Data from a rotary potentiometer as used on a Hybrid III 5th percentile female.

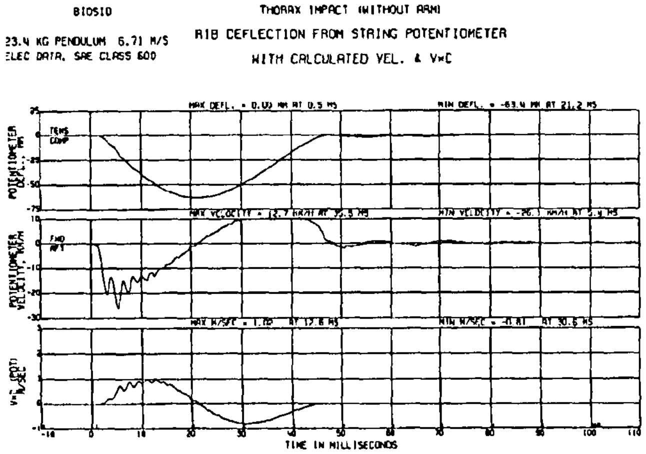

Figure 2. Data from a string potentiometer as used on a BIOSID.

Figure 1 shows three data traces, all from a Hybrid III 5th percentile female chest deflection transducer utilizing a rotary potentiometer. All three data traces are filtered at SAE CFC 600. The top trace is the chest deflection measurement. The second trace is the relative sternum velocity which was calculated by differentiating the deflection. The bottom trace is the Viscous Injury Criteria which basically is the deflection (top trace) multiplied by the velocity (middle trace) divided by a constant (this will be covered in detail later in this paper). As can be seen in all but the deflection (top) trace, there is an excessive amount of noise in the data.

The data from linear potentiometers generally display a similar type of noise, and they are frequently bothered by the vibrations which are in the crash test environment. Their data typically looks similar to that of the rotary potentiometer's data as described in the previous paragraph.

String potentiometers are often used to measure lateral rib deflection in side impact ATD's. String potentiometers have the problem of not being able to respond quickly enough to rapid increases in velocity, although they are not as sensitive to vibration. A sample of the data, at SAE CFC 600, from a string potentiometer is shown in Figure 2. Again, the top trace is the deflection, the second trace is the velocity (obtained by differentiating the deflection), and the bottom trace is the V*C data. The oscillations that can be seen in the velocity and V*C data are caused by small amounts of slack occurring in the string during periods of high rib acceleration when the potentiometer can not keep up with the rapid change in velocity.

The noise seen on these velocity traces could be smoothed out by filtering with a SAE CFC 60 filter. However, this filtering would also attenuate the peak velocity and distort the wave shape which are undesirable results. With the desire to produce meaningful velocity data at SAE CFC 600 it became necessary to find a method of making this measurement that would produce less noise.

Other Possible Methods of Measuring Chest Deflection

During the work of this task team, a number of different ideas and methods were mentioned and in some cases explored and tried. If desired, the reader may obtain information on these ideas by reviewing the minutes of the task team's work.

VISCOUS INJURY CRITERIA

In its simplest terms, for frontal ATD's, Viscous Injury Criteria (V*C) is determined by multiplying the sternum velocity by the sternum deflection. This product is then multiplied by the constant 1.3 and divided by the equivalent human chest depth. For side impact ATD's, the V*C is determined by multiplying the rib velocity by the rib deflection. This product is then divided by one-half of the equivalent thorax width.

Previously V*C was calculated with data filtered at 60 Hz (SAE CFC 60). When it was determined that air bags generate high thoracic velocities, it became necessary to make V*C calculations at 600 Hz (SAE CFC 600). Generally, in order to minimize the risk of thoracic injury, a maximum V*C value of up to 1.0 is allowed. As will be shown, at SAE CFC 600, there are significant difficulties to be overcome before meaningful data can be provided.

A Basic Method of Calculating Viscous Injury Criteria

This method utilizes only the chest deflection potentiometer data filtered at CFC 600 and is typical of methods that are widely used independent of the ATD type. The constant used in the following V*C calculation is specific to the Hybrid III 50th percentile ATD.

1. Filter the chest deflection data at SAE CFC 600.
2. Differentiate the data (this yields velocity). Convert to meters per second (m/s) if necessary.
3. If necessary, convert the filtered chest deflection data, from step 1, to meters (m).
4. Multiply the velocity (m/s) by the deflection (m).
5. Multiply this product by 1.3 and divide by the constant 0.229 meters (the chest depth). This result is the V*C data. Only the positive peak value is typically of interest.

Justification of SAE CFC 600 V*C Data

While it is beyond the scope of this paper to fully explain the justification of increasing the channel filter class to 600 for Viscous Injury Criteria data it can be seen from the data in Figures 3, 4 & 5 that there is a significant change in the amplitude, as well as the wave shape, of the data at 60, 180 and 600 Hz. The plots in Figure 3 are all of V*C data from a standard rotary potentiometer in a Hybrid III 5th percentile female; they are at SAE CFC 600, 180 & 60 from top to bottom.

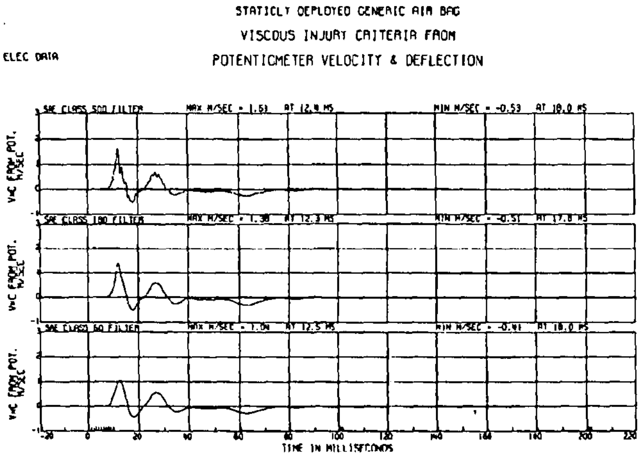

Figure 3. Viscous Injury Criteria data from a rotary potentiometer that has been filtered at SAE CFC 600, 180 & 60.

The ATD used on this test also had upper, mid and lower sternum, as well as corresponding upper, mid and lower spine accelerometers installed in the longitudinal axis. The three traces in Figure 4 are data from the upper sternum and upper spine accelerometers which were used to measure V*C. The use of accelerometers for measuring V*C will be covered later in this paper. The accelerometer data are used here to illustrate that even when V*C data are produced without noise, there is still a high enough frequency content to justify using SAE CFC 600 filters for the Viscous Injury Criteria data. Although on this test there is little change in the data at SAE CFC 180 and 600, other tests have demonstrated that larger differences exist as the sternum velocity increases -- such as in out of position air bag testing. Also, the three traces in Figure 5 show that the relative sternum velocity data from these accelerometers, which are used to produce the V*C data, show a significant difference in wave shape at SAE CFC 180 and 600. This indicates that there is a faster rise time in the velocity data than the SAE CFC 180 filter can capture.

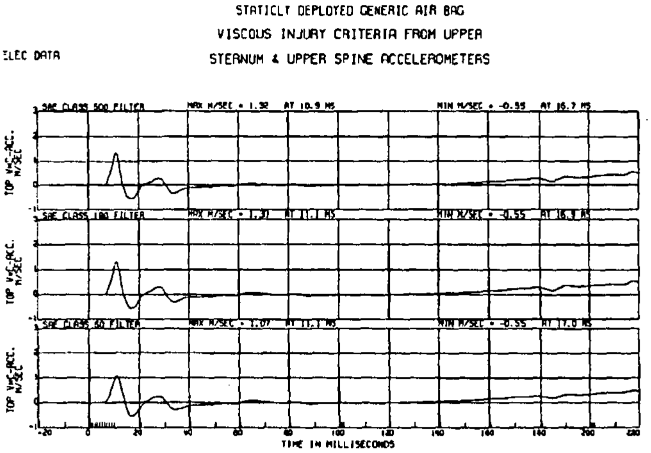

Figure 4. Viscous Injury Criteria data as calculated from integrated accelerometer data at SAE CFC 600, 180 & 60.

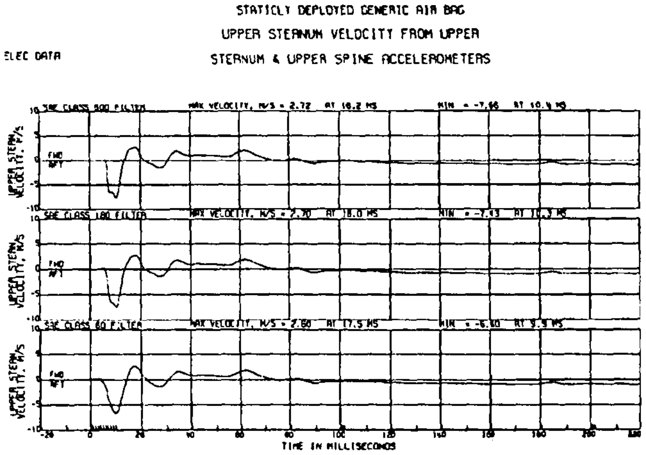

Figure 5. Relative sternum velocity as calculated from the first integral of the difference in sternum and spine acceleration at SAE CFC 600, 180 & 60.

RECOMMENDED METHODS OF MEASURING VISCOUS INJURY CRITERIA

This paper will focus on the most promising methods that have been evaluated up this point. Many of the methods that were not pursued further may be potentially workable, but the task team had limited resources and funding available so they focused their resources in the areas that they had expertise in and that they believed showed the most promise.

Dr. Steven W. Rouhana is writing and presenting a paper for this ESV Conference titled, "A High Speed Sensor for Measuring Chest Deflection in Crash Test Dummies." Since his paper completely describes a sensor that he and his team developed, his work will not be explored in this paper. All readers of this paper are encouraged to read his paper (paper number 98-S9-O-15).

The Standard Potentiometer Method

This method has been used in the Hybrid III 50th percentile male since the ATD was introduced in 1975. A rotary potentiometer is mounted on a bracket to the upper lumbar area of the ATD, and a shaft connects the potentiometer to the sternum. This transducer and hardware are shown in drawing #78051-317 in the Hybrid III drawing package. The task team explored numerous ways of minimizing the noise in the data that is typically inherent with this method. The suggested enhancements are listed below:

1. Eliminating excessive clearance and binding between the ball and slider of the chest deflection transducer assembly.
2. Using a Hall Effect Potentiometer instead of a resistive element potentiometer.
3. Using sealed instrumentation grade bearings.
4. Eliminating stress on the bearings.

Eliminating Excessive Clearance and Binding - Although the noise generated by the mechanical linkage from the potentiometer to the sternum is not repeatable it was shown that the level of noise can be decreased by making certain that there is a good fit between the slider and the ball. It is not uncommon for the ball to bind in certain areas of its travel in the slider or for the clearance between the ball and slider to be sufficient in some areas as to allow actual rattling.

The easiest method for checking the fit of these items is to hold the slider in one hand and the transducer arm and ball assembly in the other hand while the ball is within the track of the slider. By moving the ball slowly through the slider one can feel any areas where there is excessive friction or excessive clearance. Generally, if there is excessive friction or clearance it is best to replace the slider with a new part, although the ball should also be inspected for any flat spots, burrs or foreign materials on its surface. In some instances, such as a nick on the slider, it may be possible to locate and correct the problem when there is excessive friction on a portion of its travel.

Hall Effect Potentiometers - In some instances data could be shown where there was less noise on the velocity data when a Hall Effect Potentiometer was used than with a resistive potentiometer. However, this was not always true. It appears that when the data were improved by replacing the resistive potentiometer with a Hall Effect Potentiometer that the resistive potentiometer had exceeded its useful life. Although the deflection data from it were still acceptable, the differentiated deflection data (velocity) had become noisy.

One of the primary advantages of using Hall Effect Potentiometers is that there are no wiper contacts that can lift off the resistive element or become oxidized causing intermittent contact. A new high quality resistive potentiometer, with an infinite resolution resistive element will generally give data comparable to that of Hall Effect Potentiometers. Eventually the data from a resistive element potentiometer will normally degrade and become more noisy over time.

Instrumentation Grade Sealed Bearings - The standard bearings for the chest deflection transducer assembly are neither sealed nor of instrumentation grade. One of the task team members had considerable success with improving the data by replacing the standard bearings with high quality instrumentation grade sealed bearings. The task team member explained that over a period of time particulate matter can accumulate on the bearing surfaces which creates enough friction where the roughness can be felt when the bearing is turned by hand. This will show up as significant spikes in velocity data (differentiated deflection). By using sealed instrumentation grade bearings the data will be improved and also should not deteriorate since particulate matter will not be able to get into the bearing to damage the machined surfaces. The reason for using instrumentation grade bearings is due to the tighter tolerances that they are machined to which eliminates clearances than may lead to mechanical noise and data noise.

Eliminating Bearing Stress - It was also mentioned that the data had been improved in some instances by mounting the bearings within a custom made transducer bracket with RTV adhesive/sealant. This would eliminate any stresses placed on the bearing by manufacturing tolerances causing the bearings to not be accurately aligned. It was believed that this may no longer be necessary since manufacturing methods have been improved over the last two decades when this ATD was initially designed. However, since the transducer bracket is not typically replaced this is a significant issue to be aware of when searching for the cause of noise in the data.

Summarizing the Potentiometer Method - One of the main advantages of this method is that the technology has been in place for decades without significant change and in general it works quite well. If 60 Hz data was adequate, there would be no need to improve on this method. By utilizing the above steps as a guide, significant steps can be made in improving the data provided by the standard hardware at SAE CFC 600.

The Accelerometer Method

This method uses the data from accelerometers to calculate both the velocity and deflection. Depending on the test conditions, this method can work anywhere from extremely well to very poorly. Some of the issues can be improved, but others appear to be permanent issues that make this method less than ideal for many situations. However, there are enough advantages to this method to make it a valuable tool for the additional information that it provides.

The primary advantage of the accelerometer method is that the data it produces are extremely smooth and free of noise. Samples of these data (at SAE CFC 600) were shown previously in Figures 4 and 5. The disadvantage of this method is that the deflection (second integral of the acceleration) drifts further and further from the zero level as the test progresses from time zero. This can also be seen in the velocity (first integral of the acceleration) data, although to a much lesser extent. The drifting of the deflection and velocity data will also cause drifting of the V*C data when it is calculated using this method.

The traces shown in Figure 6 demonstrate this problem toward the right side of the plot; as the test progresses the traces are moving further from zero rather than approaching zero which is typically what is really happening. The data shown in Figures 4, 5 & 6 are from an out-of-position test with a staticly deployed airbag. Sled testing will usually produce data that has this problem to a greater extent, occasionally the drifting problem in the second interval (relative deflection) of the accelerometer data is so severe that the real peak sternum deflection can not be located or determined from it. This is likely only when the maximum deflection is very small or when the peak deflection occurs more than approximately 50 ms after time zero (this is typically the case on standard sled & barrier tests -- not out-of-position tests).

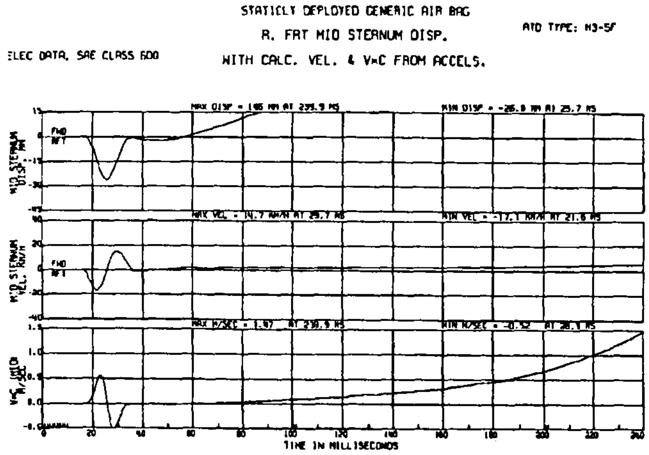

Figure 6. Mid Sternum deflection, velocity and V*C all calculated using accelerometers.

There are many factors that contribute to the drifting problem that cannot be easily controlled. Frequently either the ATD undergoes rotation during the test or the sternum is deflected inward at an angle. Either of these will cause the accelerometer to move differently than what its single channel of data can indicate. To overcome this would require numerous additional data channels and complex processing. Some other causes of drifting are the hysteresis of the accelerometer beam and the zero level noise integration. Although the problem of the deflection and, to a lesser extent, the velocity data drifting cannot be readily eliminated, there are steps that can lessen the drifting. The following steps will help to minimize this problem:

1. Use a full scale value that is not drastically higher than the maximum acceleration that is likely to be observed when the data system (for the accelerometers) is being calibrated. This will increase the resolution of the data and help minimize the drifting. This step is widely recognized as good laboratory practice.
2. Do not start the integration process of the accelerometer data until the chest potentiometer begins showing chest deflection. This will cut down on the total time that the accelerometer's data need to be integrated which will lessen the drifting problem. This can be especially useful on sled or full scale testing; it will be less helpful on out-of-position testing.
3. If possible, reset the integrals to zero at known points. At some point while the data is still being collected the sternum will have returned to its initial relative velocity of zero. For example, the potentiometer data shown in Figure 7 (2nd trace from the top) indicate that the ribs settled to a final zero velocity by approximately 100 milliseconds after time zero. This can be deduced by noting that at this point the deflection is no longer changing; if the deflection is

not changing, the relative sternum velocity is zero. The time that the relative sternum velocity returns to zero can also be determined from the differentiated potentiometer deflection. If the processing software allows the integration to be set to zero at both the beginning and ending points (using 100 milliseconds as the ending point in this example) the accuracy of the data in between these areas can be dramatically improved. This would cause the other data shown in Figure 7 to not drift off of the plot as they do now.

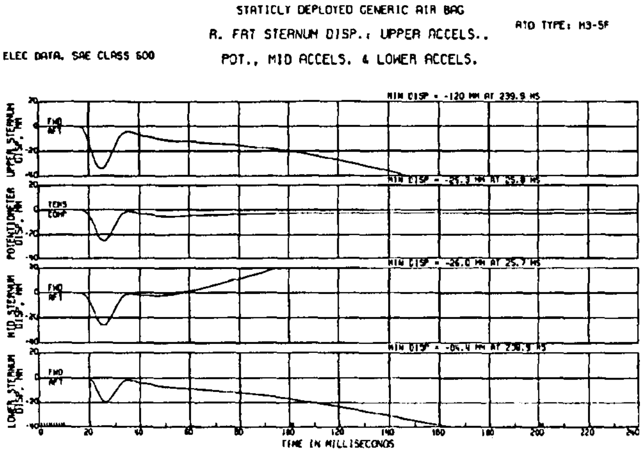

Figure 7. Sternum deflection from upper accelerometers, potentiometer, mid and lower accelerometers.

Summarizing the Accelerometer Method - Due to the inherent drifting that exists in this method, it is recommended that this method be used to supplement (not replace) the deflection data that is available from the potentiometer. At the time of this writing, the Hybrid III 5th percentile, 3 & 6-year-old child ATD's come with the accelerometer mounts necessary to install accelerometers to record this information. The user needs to instrument the ATD, record and process the data accordingly. The user does need to be aware of the drifting problems that occur and examine the data carefully. This method is capable of providing far more information than is available from only the potentiometer; most notably the relative velocity, deflection and the V*C of the top and bottom of the sternum.

The Combination Method

This method uses the velocity as calculated from the first integral of the acceleration and the deflection as measured by the potentiometer for calculating V*C. The V*C data from this method tend not to drift away significantly from zero due to the deflection from the potentiometer being used in the calculation. Any drifting that does occur will be caused by the integrated accelerometer velocity, and this is not usually significant enough to be troublesome. It is highly recommended that this method be used for side impact ATD's provided the ATD is capable of measuring the lateral acceleration of each rib and the lateral spine acceleration at each point opposite the rib. This method is also recommended for frontal ATD's, but only for the mid sternum -- not the upper and lower sternum.

The problem with using this method for the upper and lower sternum of frontal ATD's is that the deflection is not being measured from the same location as the velocity. This can cause misleading V*C information. Figure 8 shows the V*C calculated at SAE CFC 600 using the accelerometers only (traces 1, 3 & 4), and the potentiometer only (trace 2). Figure 9 shows the V*C calculated using the combination method. Traces 1, 3 & 4 were calculated using the upper, middle and lower sternum relative acceleration respectively for velocity and the potentiometer for deflection. The 2nd trace was calculated using the average of the upper and mid sternum relative acceleration with the potentiometer used for deflection. The average of these two locations was used because this is equivalent to the approximate location of the point that the standard chest deflection transducer measures when the ribs are compressed significantly. As the data demonstrate the V*C, using the combination method, disagrees substantially with the accelerometer data in this instance. The reason for this can be seen by looking carefully at the data in Figures 10 & 11. Figure 10 shows the relative sternum deflection as calculated by the sternum and spine accelerometers (traces 1, 3 & 4), as well as the sternum deflection measured by the potentiometer (2nd trace). Figure 11 shows the relative sternum velocity as calculated from the sternum and spine accelerometer data (traces 1, 3 & 4), and the sternum velocity as calculated by the potentiometer data (2nd trace). As can be seen from Figure 10, the upper sternum compresses to a greater magnitude, and it reaches its peak deflection sooner than the lower sternum. As can be seen from Figure 11, the upper sternum compresses with a higher relative velocity than the lower sternum, and it reaches its peak velocity sooner than the lower sternum.

The reason the data in Figures 8 & 9 are different can be seen by looking carefully at the data in Figures 10 & 11. For the combination method, the relative sternum deflection data of the potentiometer (2nd trace from the top in Figure 10) is multiplied by the relative sternum velocity data (Figure 11) to yield the V*C data as shown in Figure 9 (after multiplying by a constant). The peak velocity and its time for the upper, mid and lower relative sternum velocity are shown in Table 1. The relative sternum deflection (from the potentiometer) is multiplied for the combination method with the relative sternum velocity (from integrated acceleration) for the upper, mid and lower sternum. The purpose of including the peak values and times as listed in Table 1 is to clarify what is happening. The same deflection data is used for each sternum location in the combination method. The time of the peak deflection in relation to the time of peak velocity of each sternum location that it is multiplied with needs to be emphasized as an indication of how the different sternum locations are moving in relation to each other at different times.

Table 1.

Peak Velocities & times for Figure 10 (traces 1, 3 & 4)

Location	Peak Relative Velocity	Time of Peak Vel.
Upper Sternum	23.5 km per hour	20.6 milliseconds
Mid Sternum	17.1 km per hour	21.6 milliseconds
Lower Sternum	15.5 km per hour	23.2 milliseconds

The peak sternum deflection was 25.3 millimeters at 25.8 milliseconds as measured by the potentiometer. As we move down the sternum the time of the peak velocity approaches the time of peak deflection (as measured by the potentiometer), this causes the resulting V*C number to be higher. The peak velocity of the lower sternum took place at 23.2 ms. This is only 2.6 ms before the peak deflection. As can be seen from the deflection trace (Figure 10, second trace from the top), the deflection is approximately 20 mm at this time (23.2 ms). The upper sternum reaches its peak velocity of 23.5 km per hour at 20.6 ms. This is 5.2 ms before the peak deflection. When the upper sternum is at its peak velocity the deflection that it is being multiplied by is less than 10 mm. For this test, the combination method caused the V*C to be low for the upper sternum and high for the lower sternum. This is shown by the data in Figure 9 (combination method) as compared to the data in Figure 8 (traces 1, 3 & 4 calculated using the accelerometer method; trace 2 calculated using the potentiometer method).

As has been shown, the combination method caused the V*C to increase as we went from the top of the sternum to the bottom of the sternum. The potentiometer makes its deflection measurement near the center of the sternum. The measuring point rises as the ribs are compressed, and the measuring point will also change if the rib cage is forced up or down by the restraint system. The upward and downward motion of the rib cage is limited in the latest version of the Hybrid III 5th, 3 and 6-year-old ATD's, but can still occur to a limited extent. Each measured location on the sternum reached its maximum velocity prior to the time that the same location reached its maximum deflection (this is always the case since at maximum relative deflection the relative velocity is zero). The higher portions of the sternum reached each of their peak deflections and velocities before the lower portions (this can vary with different test conditions). These issues will cause erroneous V*C calculations to be produced when the combination method is used for frontal ATD's if it is used at all sternum locations (top, middle and bottom). When the lower sternum relative velocity

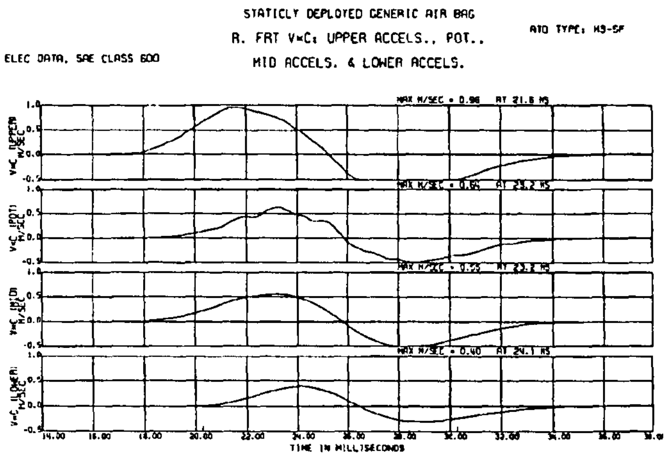

Figure 8. V*C from upper accelerometers, potentiometer, mid & lower accelerometers.

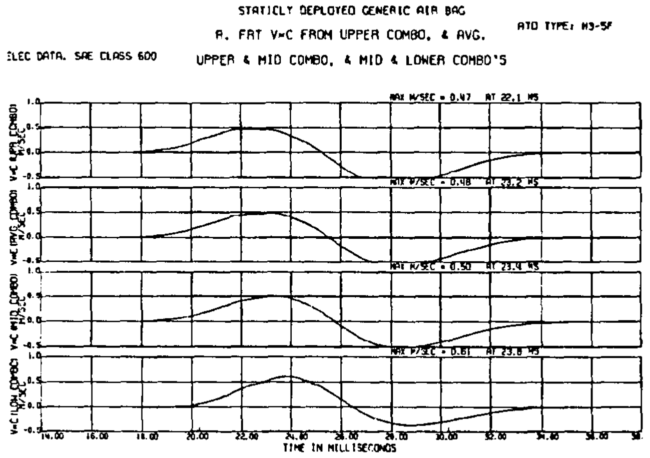

Figure 9. V*C from upper sternum combination method, average upper & mid sternum combination method, mid and lower sternum combination method.

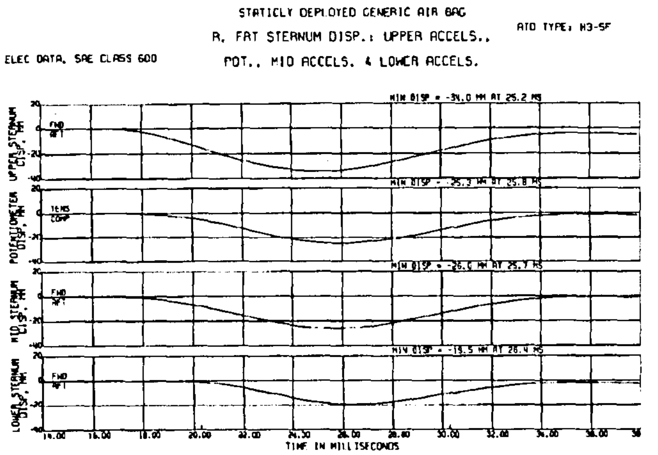

Figure 10. Relative sternum deflection from the upper accelerometers, potentiometer, mid & lower accelerometers.

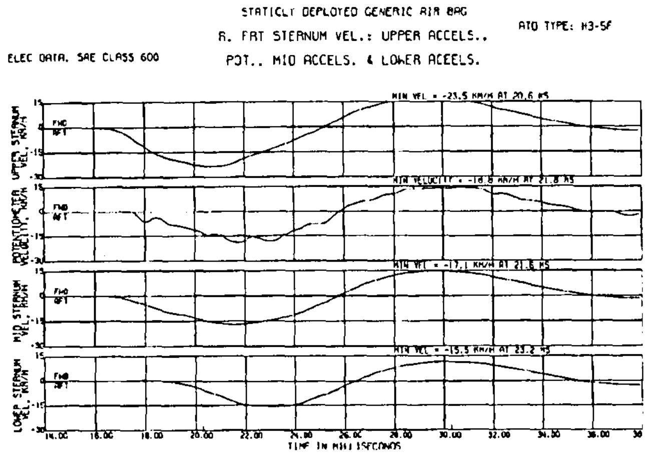

Figure 11. Relative sternum velocity from upper accelerometers, potentiometer, mid & lower accelerometers.

was multiplied by the potentiometer deflection the resulting V*C is higher because the peak velocity (even though it is lower) took place later in time, at which point the deflection is higher -- the end result is that the lower sternum V*C is shown to be incorrectly higher when calculated by the combination method on this test.

However, if the combination method is used on the mid sternum location only, the results obtained are comparable to the V*C calculation from the potentiometer if one visually averages out the noise of the potentiometer's data at SAE CFC 600. This can be seen by comparing the third trace of Figure 9 (V*C Mid Combo) with the second trace of Figure 8 (V*C Pot). The potentiometer's data is higher than it should be because of the fairly high frequency noise content in its data (note that the time base on this plot is stretched out to 2 milliseconds per division). The combination method provides reasonably accurate data only for the center portion of the sternum; it does not provide useful data for the top or bottom of the sternum. For ATD's without the mid sternum accelerometer, the combination method can be used by first averaging the upper and lower sternum acceleration, and subtracting the average of the upper and lower spine acceleration to determine the relative mid sternum acceleration. The relative mid sternum acceleration can then be integrated to obtain the relative mid sternum velocity.

It needs to be acknowledged that there is a ten percent difference between the V*C result from the combination method (0.50) and the result from the accelerometer method (0.55). Much of the reason that the V*C number from the combination method is lower is from the phase shift as discussed previously in this section. This will cause differences because the potentiometer does not measure the sternum deflection at the same point on the sternum though out the test.

When drifting of the data are excessive the data provided by this method can be improved by utilizing the same three items methods mentioned in the Accelerometer Method section.

Summarizing the Combination Method - The combination method is not recommended for all sternum locations for frontal ATD's because of the erroneous V*C data that it produces. This is caused by the deflection (from the potentiometer) being measured at a different location than the velocity (calculated by integrating the accelerometer data). For frontal ATD's it is recommended that the combination method be used to determine the mid-sternum V*C only. The results from this should be comparable to the V*C determined from the potentiometer if the noise on the potentiometer's data is visually averaged. It should also be comparable to the mid sternum data from the accelerometer method (in this test there was a 10% difference).

The combination method is being recommended as the preferred method for side impact ATD's provided that the relative rib acceleration can be determined. On side impact ATD's, determining the relative rib acceleration requires two lateral accelerometers per rib. One accelerometer to measure lateral rib acceleration, and one accelerometer to measure the spine acceleration at a point opposite of the rib accelerometer. The relative rib acceleration is determined by subtracting the spine acceleration from the rib acceleration. The combination method works well for side impact ATD's because, unlike the frontal ATD's, the accelerometer and the potentiometer are both taking their data from virtually the same location.

CONSTANTS USED FOR CALCULATING V*C

The following tables (2 & 3) show the constants that were mentioned in the previous sections for calculating V*C. The constants have the unit of "meters" in the denominator with the numerator having no unit. Since this is confusing it is left out of the "constant" column. For frontal ATD's the constant is obtained by dividing 1.3 by the corresponding human percentile chest depth. For side impact ATD's the constant is obtained by dividing 1.0 by 1/2 of the corresponding human percentile thorax width. Most people typically do not include the units (meter per second) when discussing V*C data but just mention the peak positive value reached without units.

Table 2.

V*C Calculation Constants for Frontal ATD's

ATD Type	Human Chest Depth	Constant
Hybrid III 3-year-old	0.122 meters	10.656
Hybrid III 6-year-old	0.143 meters	9.091
Hybrid III 5th percentile	0.187 meters	6.952
Hybrid III 50th percentile	0.229 meters	5.677
Hybrid III 95th percentile	0.254 meters	5.118

Table 3.

V*C Calculation Constants for Side Impact ATD's

Side Impact ATD Type	1/2 Chest Width	Constant
SID-IIs (5th percentile)	0.138 meters	7.246
BIOSID (50th percentile)	0.175 meters	5.714
EUROSID-1 (50th percentile)	0.140 meters	7.143

RECOMMENDATIONS

This paper has discussed, in detail, three methods. The recommended methods are shown in Table 4 for making the velocity and deflection measurements and in Table 5 for the V*C measurements.

Table 4.

Recommended Measurement Methods

Measurement	ATD Type	Method
Deflection	All	Potentiometer
Deflection	Frontal*	2nd Integral of Accel.
Velocity	Frontal**	Differentiated Pot.
Velocity	All	1st Integral of Accel.

* It is recommended that this deflection measurement be made on frontal ATD's in order to provide additional measurement locations (upper, mid & lower sternum), to the single deflection measurement made from the potentiometer.

** It is recommended that this velocity measurement be made on frontal ATD's to use as a supplement to the velocity measurements made from the accelerometers.

Table 5.

Recommended V*C Measurement Methods

ATD Type	Method
Frontal	Potentiometer *
Frontal	Accelerometer *
Frontal	Combination *
Side Impact	Combination

* It is recommended that all three methods be used on frontal ATD's so that they can be used as a supplement to each other as described previously. In some instances the accelerometer method may drift too much on some sled and barrier test to be of significant value. In these instances, the combination and potentiometer method must be relied on. The accelerometer method is of most use for out-of-position testing.

The Potentiometer Method

This is the oldest method. It is recommended that the data from this method always be recorded for the deflection data and differentiated to provide velocity data even though it is likely to be somewhat noisy. By providing this data there is more information to check either the accelerometer or the combination method for their accuracy. As has been mentioned earlier in this paper, even when there is excessive noise in the data, one can usually read through the noise to obtain a realistic approximation of the true velocity value. The deflection data that it gives is accurate and doesn't drift and is seldom noisy. The velocity data that this method provides is noisy, but does not drift. This makes it useful for correctly interpreting the data provided from the other methods.

Recommended Processing Procedure for the Potentiometer Method - Since there are so many possibilities of the order that many of the processing steps can be performed in while still meeting the requirements of J211, it was believed advantageous to specify one method of processing so that all people involved would be handling the data the same way. The suggested method is outlined below:

1. Filter the chest deflection data at SAE CFC 600. The units should be in millimeters.
2. Differentiate the filtered chest deflection to get the sternum velocity. The velocity should have the units of meters per second.
3. Multiply the chest deflection by .001 to convert the deflection from millimeters to meters.
4. Multiply the sternum velocity by the deflection. The result will be data that have meters squared per second as the unit.
5. Obtain the final V*C result by multiplying this data by the appropriate constant for the ATD type. The constant is the number 1.3 (1.0 for side impact ATD's) divided by the depth of the chest of the corresponding percentile human (or 1/2 of the human thorax width for side impact ATD's) measured in meters. This constant has meters as its unit in the denominator. After multiplying the constant and the result in step 4 you have the V*C (Viscous Injury Criteria) values with meters per second as the unit. Only the positive peak value is typically of interest.

This method of processing the data meets all of the requirements of J211; most notably not filtering digitally more than once, and filtering before any nonlinear operations.

The Accelerometer Method

This method is recommended for frontal ATD's, and is especially useful for out-of-position testing. The user must use caution when examining the data. The data from the accelerometers will not usually be valid for the entire duration of the test, but will typically be valid (with only a small error) through the time of peak deflection. The data should be compared to the potentiometer's data to confirm that it made sense and that it compliments rather than contradicts the potentiometer's data.

Recommended Processing Procedure for the Accelerometer Method -
Since there are so many possibilities of the order that many of the processing steps can be performed in while still meeting the requirements of J211, it was believed advantageous to specify one method of processing so that all people involved would be handling the data the same way. The suggested method is outlined below:

1. Subtract the spine acceleration from the sternum acceleration. This gives the acceleration of the sternum relative to the spine. This is the same acceleration that the chest deflection transducer would see. Filter this result at SAE CFC 600.
2. Integrate the result to get the relative sternum velocity. This is the same velocity that the chest deflection transducer would see. The velocity should have the units of meters per second.
3. Integrate the relative sternum velocity to get the relative sternum deflection. This is the same deflection that the chest deflection transducer measures. The deflection should have the units of millimeters.
4. Multiply the deflection by 0.001 to convert the calculated deflection from millimeters to meters. This may be different depending on what constants you use when doing your integration.
5. Multiply the relative sternum deflection (in meters) by the relative sternum velocity (in meters per second). The result will be data that has meters squared per second as the unit.
6. Obtain the final V*C result by multiplying this data by the appropriate constant for the ATD type. This constant is the number 1.3 (1.0 for side impact ATD's) divided by the depth of the chest of the ATD (or 1/2 of the thorax width for side impact ATD's) measured in meters. This constant has meters as its unit in the denominator. After multiplying the constant and the result in step 5 you have the V*C (Viscous Injury Criteria) number with meters per second as the unit. Only the positive peak value is typically of interest.

This method of processing the data meets all of the requirements of J211; most notably not filtering digitally more than once, and filtering before any nonlinear operations.

The Combination Method

On frontal ATD's, this method is recommended only for the mid sternum. This is the preferred method for side impact ATD's. Although the possibility still exists for an occasional test where the velocity data will drift off excessively causing the V*C data to show an ever increasing or decreasing number as the test progresses. This is the exception and is not likely to be a problem until well after the region of interest in the test data.

On side impact ATD's, the combination method can only be used when the rib acceleration relative to the spine can be determined. This requires an accelerometer on the spine opposite from the one on the rib.

Recommended Processing Procedure for the Combination Method - Since there are so many possibilities of the order that many of the processing steps can be performed in while still meeting the requirements of J211, it was believed advantageous to specify one method of processing so that all people involved would be handling the data the same way. The suggested method is outlined below:

1. Subtract the spine acceleration from the sternum acceleration. This gives the acceleration of the sternum relative to the spine. This is the same relative acceleration that the chest deflection transducer would see. Filter this result at SAE CFC 600.
2. Integrate the result to get the relative sternum velocity. This is the same relative velocity that the chest deflection transducer would see. The velocity should have the units of meters per second.
3. Filter the chest potentiometer deflection data at SAE CFC 600. The units should be in millimeters.
4. Multiply the filtered deflection by 0.001 to convert the measured deflection from millimeters to meters.
5. Multiply the sternum deflection (in meters) by the sternum velocity (in meters per second). The result will be data that has meters squared per second as the unit.
6. Obtain the final V*C result by multiplying these values by the appropriate constant for the ATD type. The constant is the number 1.3 (1.0 for side impact ATD's) divided by the depth of the chest of the corresponding percentile human (or 1/2 of the human thorax width for side impact ATD's) measured in meters. This constant has meters as its unit in the denominator. After multiplying the constant and the results in step 5 you have the V*C (Viscous Injury Criteria) values with meters per second as the unit. Only the positive peak value is typically of interest.

This method of processing the data meets all of the requirements of J211; most notably not filtering digitally more than once, and filtering before any nonlinear operations.

CONCLUSION

The work of this task team is not completed. The task team hoped to develop a single transducer that could provide both deflection and velocity data that could be used for determining V*C. As of yet they have not developed this transducer. Chairman Balser plans to resume the task team work when more data is available or a new technology is developed that shows promise of making this measurement in an improved fashion beyond what is currently available.

ACKNOWLEDGMENTS

Chairman Balser would like to thank all the members of the task team for their participation in their work which was summarized in this paper. The only data published in this paper was produced within General Motors. Many other individuals and companies submitted data and information that appears in the SAE published minutes of this task team. All members of the task team expended valuable time, energy and input into the yet uncompleted, but valuable work of this task team.

Technical Session 10

Pedestrian, Child Restraints, and Motorcycle Safety

Chairperson: Yoshiyuki Mizuno, Japan Automobile Standards Internationalization Center, Japan

The International Harmonized Research Activities (IHRA) Status Report of the Pedestrian Safety Working Group was presented at the onset of this Session during the 16th ESV Conference. This Report begins Technical Session 10.

INTERNATIONAL HARMONIZED RESEARCH ACTIVITIES (IHRA) STATUS REPORT OF THE PEDESTRIAN SAFETY WORKING GROUP

Yoshiyuki Mizuno
Japan Automobile Standards Internationalization Center
Japan

The ESV/IHRA Project was introduced at the ESV held in Melbourne, May 1996. Also at the Meeting, the leading country for each project was announced, whereby Japan was assigned the leading country for the research item of PEDESTRIAN SAFETY. Japan, in response, requested ESV member countries to select their experts in pedestrian safety, and has been carrying out the assigned work with the selected experts assuming the central research role. Below is a summary of these activities.

1. Task Assigned to IHRA/Pedestrian Safety

The task of IHRA/Pedestrian Safety is to propose harmonized test procedures and its requirements which will contribute to a reduction of pedestrian injuries and fatalities in accidents between passenger cars and pedestrians (adults and children) while reflecting the latest accident data of ESV member countries.

2. Target Timing

The above proposal shall be reported to the 17th ESV Meeting scheduled for 2001.

3. Method of Realization

The experts selected from ESV member countries hold meetings to discuss, formulate and finalize test procedures and its requirements through consensus among the experts.

4. Research Resources

The experts from ESV member countries basically utilize the useful results of past studies, and when additional studies are necessary, they define the areas requiring the additional studies which shall be apportioned to ESV member countries.

5. Research Steps

(1) Selection of experts.
(2) Formulation of a research master plan.
(3) Execution of accident survey in ESV member countries.
(4) Comprehensive analysis based on the accident data of ESV member countries.
(5) Ranking of priorities for the development of test procedures in accordance with the results of comprehensive analysis.
(6) Identification of useful research results (biomechanics, test procedures, testing tools, etc.) and research items requiring additional research efforts, prioritization of work, and apportionment of work to ESV member countries.
(7) Development of test procedures and its requirements.
(8) Evaluation of the developed test procedures and its requirements, including cost evaluation.
(9) Finalization of the test procedures and its requirements.

At present, IHRA/Pedestrian Safety is in Step 5.

6. IHRA/Pedestrian Safety Experts Meeting

1997.7.15-16	1st Experts Meeting Tokyo, Japan
1998.3.3-5	2nd Experts Meeting Washington D.C.,USA
1998.9.16-18	3rd Experts Meeting Europe

7. Matters Decided at Experts Meetings

- Experts Meetings shall be held twice a year, in principle.
- A research master plan was formulated.
- It is not possible to develop test procedures using pedestrian dummies by the 2001 target year, due to a long time needed to develop such dummies. Consequently, the component test employed by ISO and EEVC shall be employed.
- Analysis was conducted on the basis of the first accident analysis data provided by the U.S., Europe and Japan. In results:
  Higher priorities -
    a. Head / bonnet (adults and children)
    b. Leg / bumper.

The above a. and b. were decided to be the combinations for which test procedures shall be developed.

- Notable characteristics of recent accidents:
  a. A decrease in pelvis / bonnet accidents due to changes in the vehicle body shape.
  b. An increase in the incidents of the adult's head colliding into the windshield glass.
- Accident data shall be rearranged using a unified format.
- An action list for future Meetings shall be produced, specifying subject matters for discussion, assigned countries, and related remarks.
- Although infrastructure and education are important in the reduction of accidents, the Expert Group shall only briefly touch upon these subjects in its final report, citing existing reports.
- The IHRA/Steering Committee has recommended the definition of passenger vehicles as those with a seating capacity of not more than 9 occupants and GVW of not more than 4,500 kg. The Expert Group shall finalize its research, analyzing accident data in accordance with this definition.
- This research shall be incorporated into the project schedule in order to verify the technical compatibility of the automobile on the whole within the test procedures to be proposed and to avoid disharmony between these test procedures and other regulations.

8. Scheduled Activities

- Reexamination of accident analysis reports.
- Identification of the most accident-prone juvenile age group for the development of an impactor for children.
- Production of biomechanical injury risk curves.
  - Deciding of the cover ratio for vehicle collision speeds.
  - Deciding of an injury level target for the reduction of injuries and fatalities
- Identification, prioritization and apportionment of research work.
- Development of test procedures for two combinations: head / bonnet (adults and children) and leg / bumper.
- Discussion on possibilities of utilizing a computer simulation model.

9. IHRA/Pedestrian Safety Experts Member List

Name	Title	Country
Mr. Yoshiyuki Mizuno	Chairperson	JAPAN
Mr. Hiroshi Ishimaru	Secretariat	JAPAN
Mr. Manual Bartolo	Expert	USA
Dr. Francoise Brun-Cassan	Expert	EU
Mrs. Maria Dabrowska-Loranc	Expert	POLAND
Dr. Hirotoshi Ishikawa	Expert	JAPAN
Mr. Norbert Jahn	Expert	EU
Mr. E.G. Janssen	Expert	EU
Mr. Graham Lawrence	Expert	EU
Dr. Jack McLean	Expert	AUSTRALIA
Mr. Akira Sasaki	Expert	JAPAN
Dr. Roger Saul	Expert	USA

INJURY PATTERN OF PEDESTRIANS HIT BY CARS OF RECENT DESIGN

Jean-Yves Foret-Bruno
Gerard Raverjon
Jean-Yves Le Coz
Accidentology and Biomechanics Laboratory
PSA Peugeot-Citroën-Renault
France
Paper Number 98-S10-O-02

AIMS OF THIS STUDY

The present studies treating the passive protection of pedestrians struck by passenger cars are based on accident study files dating back 10 to 15 years.

However, the design of these cars has considerably changed since these enquiries and it may be supposed that the new profile of cars which characterise the present-day parc have an influence on the kinematics of the pedestrians, and also, clearly, on the frequency of lesions to the different parts of the body.

The aim of this new study is therefore :

- to obtain a more up-to-date picture of the real-world crashes by analyzing collisions which involved cars designed recently (marketed after 1989),
- to compare this survey to the similar one conducted by the LAB at the end of the 1970's to assess the injury risk evolution.

PROPORTION OF PEDESTRIANS STRUCK BY CARS

Before analysing in greater detail only those accidents where cars strike pedestrians, it is useful to identify the proportion of pedestrians struck by other vehicles (motorcycles, vans, trucks).

The figure 1, drawn from the figures of the SETRA (French National file of personal injury crashes) shows that the percentage of pedestrians struck only by cars is between 74 and 80% according to the severity.

80% of the cases concern lightly and seriously injured cases and 74% are fatalities. Concerning the latter, it may be observed that the proportion of trucks is very high : 20%.

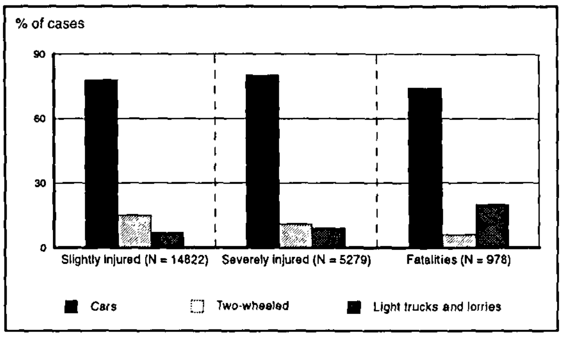

Figure 1. Percentage of cars as striking party in pedestrian collisions according to overall injury severity.

CHARACTERISTICS OF THIS PEDESTRIAN ACCIDENT FILE

File Used for this Study

Concerning only the cases of cars against pedestrians, the accidents analysed are taken from the accident reports of the National Gendarmerie for which the selection criteria were as follows :

- cars marketed after 1989,
- accidents happening between 1994 and 1995,
- accidents where original photos of the car were available, clearly an essential element for such an analysis,
- accidents where the medical files of the pedestrians were available.

The number of reports considered in this period was 594, and 529 of them were in fact taken into account for this analysis.

It is necessary to note that the selection of accidents occuring on the Gendarmerie network, for which photographs were available, clearly implies a sample of pedestrian accidents where the mortality is superior to the national average.

Here, this mortality is four times higher to that observed in the whole of France. The advantage of such a file is evidently to be able to show rapidly, and in relatively few cases, the most representative serious lesions according to the speed and the zones struck by the car.

So, for each accident, the following parameters were studied :

- the calculated impact speeds according to : the braking marks, the stopping distances and the projection of the pedestrians, the interview with the parties involved (driver,witness,etc..)
- the zones impacted by the various body areas, notably the head.

Representativity of this File

Apart from the very high severity of this file, it is important to check that it is representative of all the accidents happening in France :

- firstly concerning the distribution of the size/classes of cars impacting,
- then the distribution of victims and fatalities by age category.

This table 1 compares the distribution of size/classes of cars of this accident file to those of two different sources :

- vehicles against pedestrians in 1995 (source SETRA),
- sale of cars in France after 1989 (source manufacturers).

Table 1.
Breakdown (%) of Striking Cars to Size/Class

N = 529	Studied sample %	Comparison with other sources	
		Car-to-pedestrian (%) France 95 (DOT)	French car sales after 1989 (%)
LOWER CLASS (Clio, 106, Twingo, Corsa, Punto, ...)*	**47**	45	43
LOWER AVERAGE CLASS (ZX, Escort, 306, Golf, Astra,...)*	**32**	24	27
UPPER AVERAGE CLASS (Xantia, Laguna, Mondéo, Primera, Audi, ...)*	**13**	20	20
UPPER CLASS (Safrane, Espace, BMW, Volvo 850, Saab, ...)*	**8**	11	10

It may be verified here that the cars taken into account in this selection are not fundamentally different in size from the reality of accidents in France.

We observe five to six points more pedestrians struck by cars of lower average class compensated by seven points more of upper average class.

The cars most representative of the classes are :

- the CLIO and 106 for the lower class,
- ZX, 306 and ESCORT for the lower averages,
- XANTIA,LAGUNA and MONDEO for the upper averages,
- SAFRANE, ESPACE and BMW for the upper classes,

If we now compare by age class the proportions of pedestrians struck by these cars selected from the Police files to those of all pedestrians struck by cars in France in 1995, we can observe a certain similarity, i.e. a few less pedestrians aged between 18 and 50 in our sample compensated by a few more aged pedestrians (figure 2).

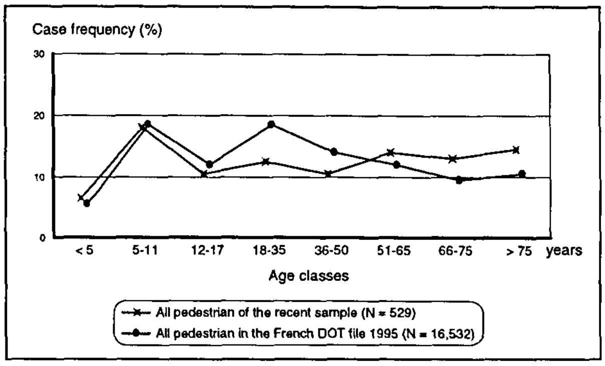

Figure 2. Breakdown of pedestrian involvement according to age classes

For the fatalities, the distributions by age class are essentially the same in our sample and for all the pedestrians killed in France (figure 3).

This file of 529 pedestrians struck by the cars is therefore representative of the severe accidents which will happen in France at the start of the years 2000s, in a parc principally composed of these cars.

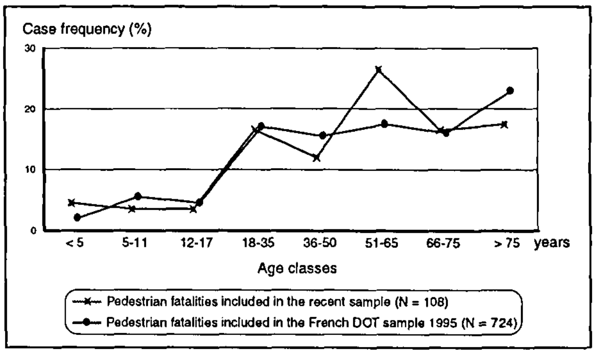

Figure 3. Breakdown of fatally injured pedestrian according to age classes

Frequency of Pedestrians Struck by the Front Face of Car

We will now study in greater detail the way in which these 529 pedestrians were struck by the car. It may be seen in figure 4 that , in many cases, the pedestrians are not directly struck by the front face of the car, but are hit by the wings or by the wing mirrors without direct impact of the bumper against the lower limbs.

So, for these 529 pedestrians distributed here according to the gravity described earlier, 134 were not touched by the front face of the car, i.e. 25%. For those lightly or seriously injured, they amount to about 30%, and to only 11% for those killed.

The number of pedestrians thus taken into account in this study is 395.

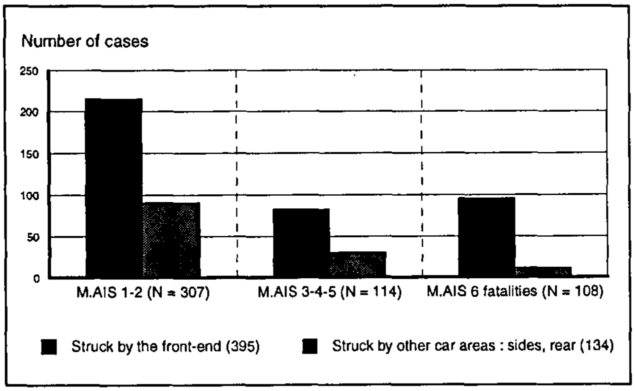

Figure 4. Total number and overall injury severity of pedestrians struck by the car front-end.

RESULTS FOR THESE 395 PEDESTRIANS STRUCK BY THE FRONT FACE

Gravity According to the Impact Speeds and the Age Classes

We have defined three age classes in the following : children under the age of twelve years, « young » adults between twelve and forty nine, and the pedestrians aged more than fifty years old.

Figure 5 shows that for these three different age classes, important differences in impact tolerance exist at the same vehicle impact speed.

Therefore the gravity, i.e. the percentage of dead and seriously injured (MAIS 3+) amongst those involved, increases with the speed for each age class, which is logical, but for a given impact speed the children are more tolerant up to 45 k.p.h..

The most aged evidently present the highest risks for the same category of speed.

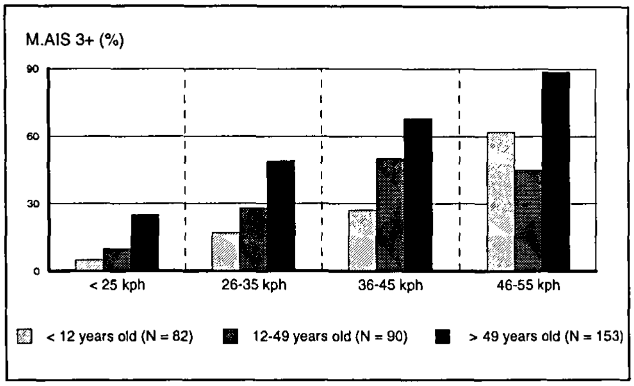

Figure 5. Percentage of severely and fatally injured pedestrians according to striking car speed and age classes.

Zones Struck by the Head for Serious and Fatal Lesions

For this corporal zone which is the site of 80 to 85% of the fatal lesions, it is worthwhile to state the hypotheses which were used to attribute head lesions, either to impact with the vehicle, either with the ground.

Evidently, if no impact with the car has been recorded, the head lesion is attributed to the ground impact.

If a head impact on the car is found, the gravity of this impact of the head is systematically attributed to the car, and not to the ground at the moment of falling. Beaving in mind the results of other accidentology studies, we may suppose that this hypothesis is the most likely to be true for serious and fatal (AIS3+) injuries.

For head lesions of level AIS 1 and 2, it is certainly difficult to decide the car or ground responsability for a simple loss of consciousness or a cut to the head.

In any case, these hypotheses maximise the car as the source of serious or fatal lesions to the head, as well as for light and moderate lesions.

Therefore, where only serious and fatal (AIS3+) lesions to the head are concerned, and for all pedestrians, the frequencies of the zones impacted on the car, all speeds included, are as follows (figure 6) :

- 17% of cases by impact on the hood and the upper fenders,
- 28% against the zone where the windscreen meets the hood (the scuttle),
- 25% against the windscreen supports (A pillars).

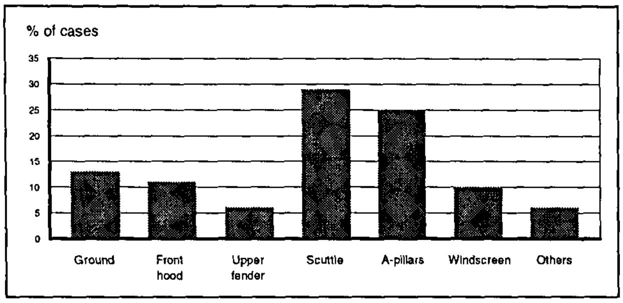

Figure 6. Breakdown (%) of pedestrian head AIS3+ injuries according to car contact locations.

It may be seen that the proportion of serious lesions attributable to the windscreen are not frequent (10%) and are observed exclusively for the most aged pedestrians.

The proportion of serious and fatal lesions avising from ground contact is less than 15%, as is shown by most of the former accidentology studies.

If we calculate, for each zone of the car as defined earlier, the gravity rate, i.e. the percentage of serious and fatal lesions (gravity rate) from all impacts detected, we can see, on figure 7, a risk which increases as a function of the average " stiffnesses " of the zones impacted, the most A pillars followed by the scuttle.

The gravity rates of the impacts against the windscreen and the ground are here the lowest.

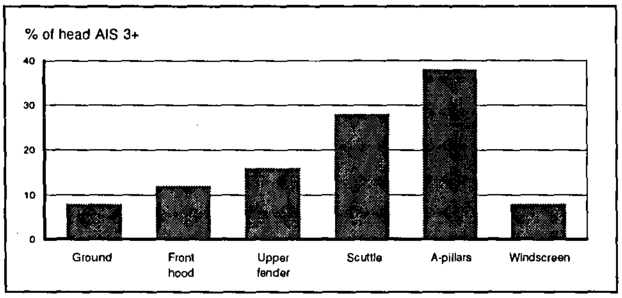

Figure 7. Percentage of severe and fatal head injuries according to car contact locations.

Frequency of Moderate to Fatal Lesions (AIS 2+) According to the Age of the Pedestrians (figure 8)

We will now study, by body areas, the percentage of pedestrians presenting moderate to fatal lesions (AIS 2 and more) amongst all the pedestrians struck, for two age classes : under twelve and over twelve years old.

It should be underlined here that this file is considerably more severe than the national average and that this frequency of lesion is fortunately not that observed in France for all pedestrians.

We have defined different anatomical territories in this table, which are :

- the head and the neck,
- the trunk, comprising the thorax, the abdomen and the dorsal-lumbar column,
- the upper limbs,
- the pelvis including the head of the femur and the neck of the femur,
- the femur not including the condyl and the head of the femur,
- the knee including the joint, knee ligaments, tibial plate and femural condyl,
- the tibia and the fibula,
- the foot and the ankle including the articulations and malleolus.

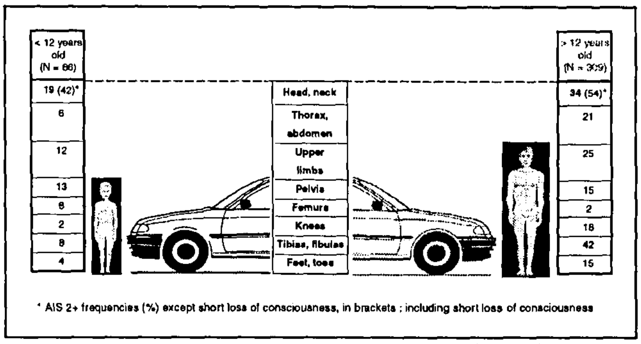

Figure 8. Pedestrian non-minor injuries (AIS2+) frequency (%) versus age.

It may be seen, for all speeds, that the lesional frequencies are very different. These differences are due, in part, to the greater tolerance of the children, but also to the frequently much more severe impacts sustained by the adults, notably those less than fifty years old.

For these two age classes, the head and the lower limbs are the most exposed territories.

For the head, 19% of AIS 2+ lesions for the children are noted, against 34% for the other age class without counting the isolated brief or initial losses of consciousness. If they are counted, the frequencies are therefore 42 and 54%.

Concerning the lower limbs in the wide sense, the principle zones of lesions are very different.

The pelvis is priority for the child (13%), then comes the femur and the tibia with 8%.

The tibia zone for the adults is by far the territory most often concerned (42%), followed by the knee (18%) and the pelvis (15%).

These lesions of the knee, are in half of the cases fractures of the tibial plates, the other half being lesions of the ligaments.

The fractures of the pelvis, we will see later, are very much linked to the age where adults are concerned.

The fractures of the femur for the adults are very rare here (2%).

If we were only interested in the fatal lesions, the head is by far the most exposed territory with 85% of the cases with fatal lesions whatever the age.

Distribution of those Involved According to the Pedestrian Severity and the Speed

It was interesting to know the distribution of impact speeds according to the pedestrian injury severities.

This figure 9 allows us to see the populations implicated according to the different speed classes and for each level of severity.

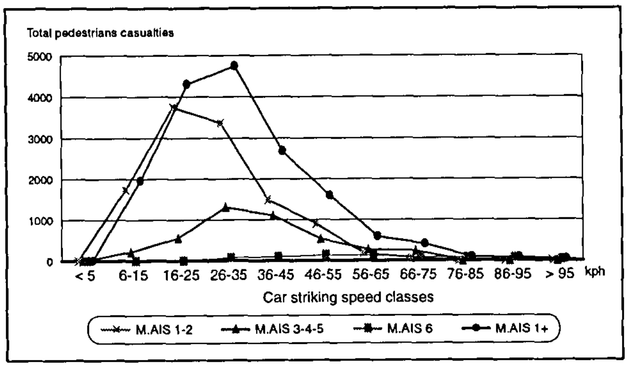

Figure 9. Breakdown of pedestrian casualties according to overall injury severity and striking car speed.

These distributions are deduced from the severities given by the SETRA, and grouped according to the speeds calculated in our study.

The distributions for the 16458 pedestrians struck (MAIS 1+) by the cars have been defined as follows :

- the lightly and moderately injured of the SETRA correspond to the MAIS 1-2,
- the seriously and very seriously injured to the MAIS 3-4-5,
- those killed at the MAIS 6.

It may so be observed that the average of the impact speeds for all the pedestrians involved is 25 k.p.h., and 35 k.p.h. for the seriously injured, while the vast majority of those killed are situated at very high speeds.

Number of Pedestrians Presenting Serious Head Lesions as a Function of the Zones Impacted

We will now examine, for the two age classes defined earlier, the number of serious lesions and fatal head lesions attributable to the engine hood and to the hood surroundings, to the zone where the hood meets the windshield, and to the windshield pillars.

Now, to have a more precise idea of what happens on a national level, we make a projection of the different results found earlier in the sub-sample of 529 pedestrians, to all of the pedestrians killed or seriously injured in France in 1995.

Firstly, the pedestrians killed in 1995 numbered 1021, and 987 in 1996.

We may see that 93% of those killed are over twelve years old (952) taking all striking vehicles into account (figure 10). Then we find the number of pedestrians :

- struck by the cars,about 74%,
- struck by the front face of the cars, close to 90%,
- struck by the front face of the cars and presenting serious or mortal lesions to the head, 85%.

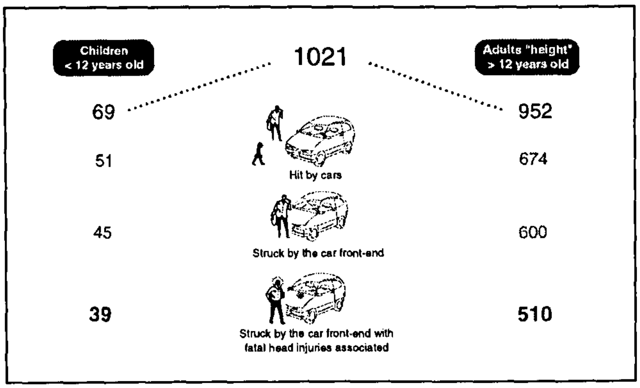
Children
< 12 years old
1021
Adults "height"
> 12 years old
69
952
51
Hit by cars
674
45
Struck by the car front-end
600
39
Struck by the car front-end with fatal head injuries associated
510

Figure 10. Pedestrians fatalities in France 1995

Overall, for one hundred pedestrians killed, a little over 50% were struck by the front face of the car and presented fatal lesions to the head.

Now, for these fatal head lesions, we can see the different zones impacted by the head (figure 11).

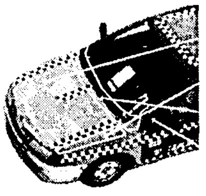

	< 12 years old	> 12 years old
Total number of casualties	39	510
Front hood	18	5
Upper fenders	13	5
Scuttle	6	178
A-pillars	0	178
Other areas (incl. windscreen, ground)	2	144

Figure 11. Breakdown of fatal pedestrian « head -vehicle » contact locations.

The total number of fatal impacts against the hood and upper fenders is 41 from a total of 1021 pedestrians, i.e. 4%, including all speeds and principally for the children.

As for the adults, they strike principally the scuttle and the A pillars (180, or about 18% of all the pedestrians killed for each zone).

In the same manner, for the 5500 seriously injured pedestrians in France in 1995, we make the same distribution.... Here, close to 20% of the seriously injured are less than twelve years old, taking all vehicles into account (figure 12).

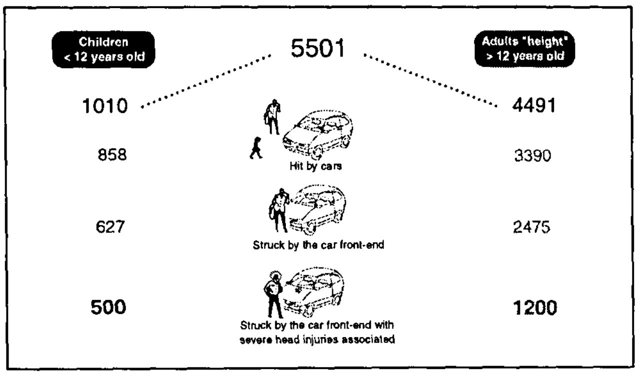

Figure 12. Severely injured pedestrians in France 1995.

The proportions of pedestrians struck by the front face of the cars and presenting serious injuries to the head are 50% for those less than twelve years old and of the order of only 25% for those over twelve.

This may be quite simply explained by the greater frequency of serious lesions to the lower limbs in adults, often isolated lesions when compared to children.

The results (figure 13) concerning the serious impacts of the head against the hood are of the same order as for those killed, 6% of all the seriously injured and practically exclusively for the children (324 from a total of 5500).

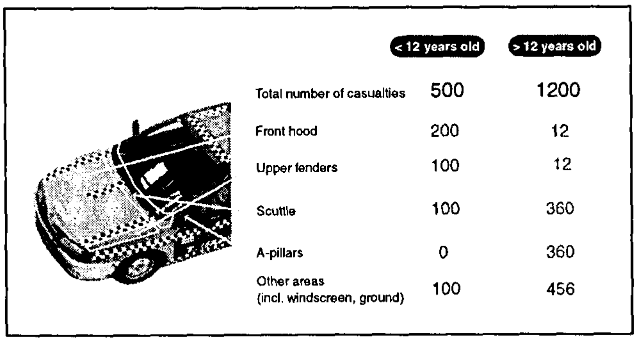

	< 12 years old	> 12 years old
Total number of casualties	500	1200
Front hood	200	12
Upper fenders	100	12
Scuttle	100	360
A-pillars	0	360
Other areas (incl. windscreen, ground)	100	456

Figure 13. Breakdown of severe pedestrian « head -vehicle » contact locations.

As for the scuttle, this represents 8% of the serious injuries (total of 460 lesions), for all speeds, it should once again be mentioned.

COMPARISON OF THE GRAVITY AND FATALITY RATES BETWEEN THIS FILE AND THE 1980 LAB FILE

Having studied these accidents of pedestrians struck by the front face of cars of recent design, it was interesting to check if the risk of lesions had changed compared to an older file.

To do this, we have used the accidentology file of the LAB which comprises 282 pedestrians struck by the front faces of car; the study was made between 1974 and 1983, and is also of a severity close to that analysed before with a mortality rate around four times superior to the national average for these years.

To be able to make these comparisons of gravity between the different corporal territories for the three age classes as defined at the beginning of the presentation, it was essential that for a given age class, the distributions implied by class of speed should be identical. These corrections were made systematically wherever needed. We should specify that the same methods for evaluating the impact speeds against the pedestrians were used for the two files.

Comparisons of Gravity Rates Between the two Files

Globally, concerning the seriously injured and killed (MAIS 3+), we observe a lesser aggressivity of these new cars for identical impact violence and for all three age classes (figure 14).

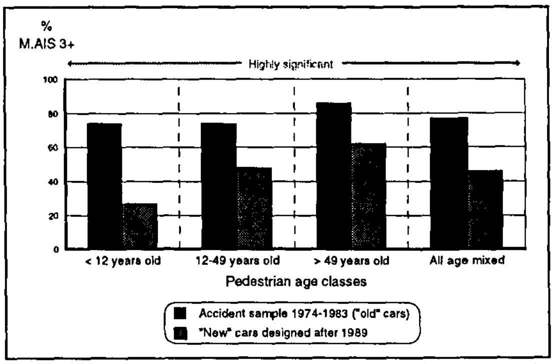

Figure 14. Comparison of frequency (%) of pedestrian sustaining MAIS3+ between old and new striking cars according to age classes.

These reductions of gravity rate are statistically very significant (test of the chi2) for the three age classes and of course for all the pedestrians (40% reduction). A more important reduction of gravity is noted among the youngest persons.

Comparisons of Fatality Rates Between the two Files

The comparison of fatality rates (% killed of those involved) does not show a significant difference for all the pedestrians, however for the most aged class we note a significant reduction of mortality rate (figure 15).

In fact, this efficiency seen for the new cars, and only for the most aged concerning mortality rate, may very certainly be explained by a reduction of the number of lesions of level AIS 2+ and AIS 3+ observed at many body areas, an association of lesions which, we know, may often imply a unfavourable vital prognostic for an aged injured person.

For the other age classes, the fatal lesions being practically all situated on the head, it is difficult to imagine a notable reduction in mortality rate only by modifications to the profile of the cars.

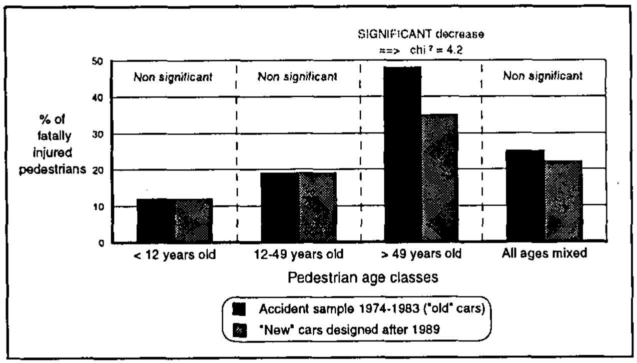

Figure 15. Comparison of frequency (%) of fatally injured pedestrian between old and new striking cars according to age classes.

Comparisons of Gravity Rates Between the two Files According to the Body Areas

In fact, these important reductions of the gravity rate MAIS3+ of almost 40% (as well as 15% for the MAIS2+) for the pedestrians struck by the cars of recent design are attributable to the reduction in frequency of level AIS2+ lesions in almost all the body areas, as may be verified on figure 16: the head, the trunk, the pelvis, the femur and the tibia are less frequently injured, only the knee lesions are not reduced. These observed reductions are statistically significant for all the territories (except the knee, of course) as well as the "trunk" zone which includes the thorax, the abdomen and the dorsal lumbar column.

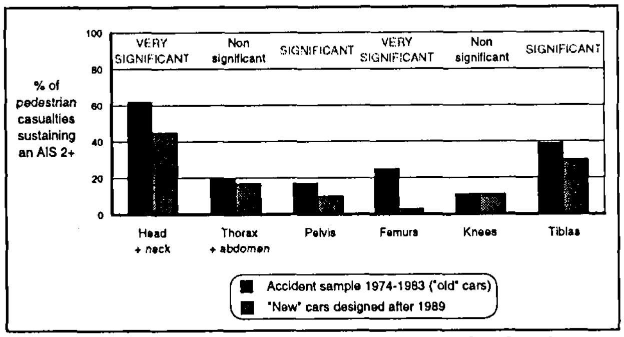

Figure 16. Comparison of percentages of pedestrian AIS2+ occurrence between old and new striking car designs by body area.

The reduction of gravity rate for the head/neck zone, all ages included, is 25% and is statistically very significant (chi²= 18). They are also significant for the youngest age classes (figure 17).

We may suppose that the profile of the newer cars has contributed to reducing the gravity rate of these impacts both for the adults as well as the children :

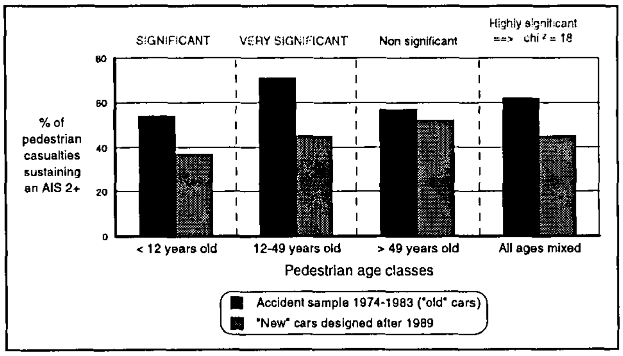

Figure 17. Comparison of percentages of non-minor (AIS2+) head injuries occurrence between old and new striking car designs by age classes.

- the more " profiled " hoods which reduce the direct impacts of the heads of the youngest children against the anterior panel of the hood, observed on the older cars.

- the more " enveloping " hoods which protect, for certain cars, the upper fenders as well as the more agressive windshield wiper pivots and the windshield bay.

- the more " laid-back " A pillars than before, for better car aerodynamics, which can have an influence also on the frequency and the severity of impact of the adults for a given impact speed.

We may also suppose that the glued-in place laminated windscreens on recent cars, compared to the toughened windscreens or the non-glued laminated windscreens, offer a better " shock absorbtion " of the head, so limiting the secondary impacts against the rigid elements of the passenger compartment.

The reduction of gravity rate for the trunk zone, for all ages, is 15%, but it is not significant for any age class.

Three territories merit a special attention.

The pelvis (figure 18) where overall there is a significant risk reduction (from 17 to 10%), but this is attributable only to the reduction in risk for the " young " adults, who go from 21 to 0%. No lesions were recorded in a population of 100 adults struck, compared to 22 lesion cases in the earlier file for a population of 106.

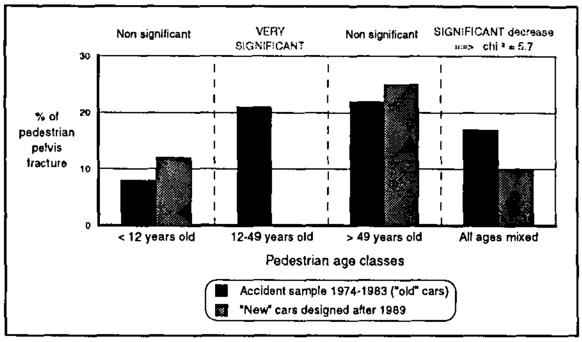

Figure 18. Comparison of percentages of pedestrian pelvis fracture occurrence between old and new striking car designs by age classes.

For the older pedestrians, where 90% of these lesions are observed between 60 and 80 years old (50% for the over 70s), the risk is not modified. The increase observed is not statistically significant.

It is known that the fractures of the hip joint happen easily when aged people fall an the ground. May we ask ourselves if these lesions are attributable to falls on the ground or on the hood which is now much less aggressive for those more tolerant.

We note an increase in risk for the children (but not significant), the bumpers and the " nose " of the hood are to blame for most of the cases, particulary for the youngest amongst them (8 out of 9 are less than years old).

The risk of fracture for the femur (figure 19) has, against these new cars, been reduced in a spectacular fashion, as we observe a 85% risk reduction for all ages (statistically very significant reduction for the three age classes).

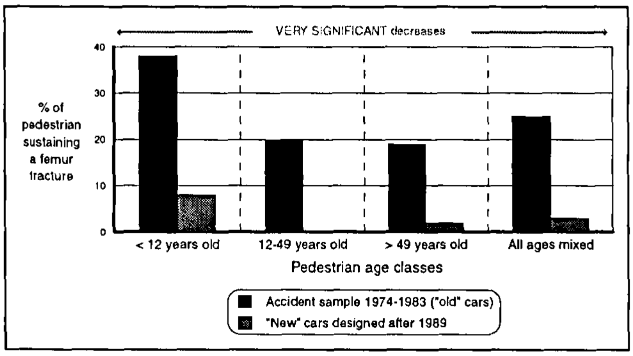

Figure 19. Comparison of percentages of pedestrian sustaining a femur fracture between old and new striking car designs by age classes.

The risks are zero for the young adults and extremely low for the older (2 cases for ages 70 and 84). We recall that the pelvic zone includes the lesions to the hip joint and the top of the femur.

For the children, the risk is now very low as it goes from 38 to 8%.

For the tibia (figure 20) the risks are reduced from 10 to 40% according to the age. For all ages, the 23% reduction observed is significant. For each age class, we note a reduction in risk but only that of the most aged is significant.

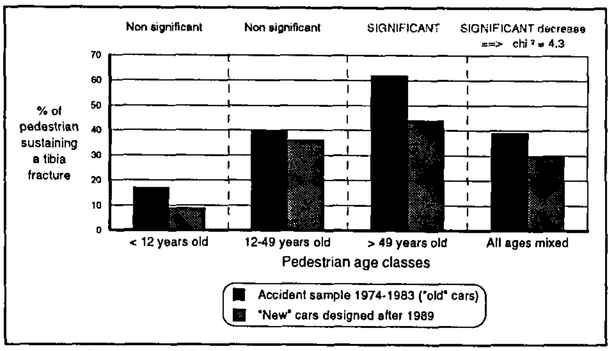

Figure 20. Comparison of percentages of pedestrian sustaining a tibia fracture occurrence between old and new striking car designs by age classes.

In fact, the more detailed analysis of the types of fractures in this corporal territory for the two samples is edifying, as may be seen on table 2.

For all pedestrians presenting fractures in this territory, the proportion of open fractures to one or both legs, attributable to the bumpers, goes therefore from 44% for the old cars to 9% for the new cars.

Table 2
Comparison of Percentages of Pedestrian Tibia Fracture Occurrence Versus the Old and New LAB Samples

		Old LAB sample 74-83 (93 injuries)	New LAB sample 1995 (86 injuries)
CLOSED fracture(s)	1 leg	54 %	84 %
	2 legs	2 %	7 %
OPENED fracture(s)	1 leg	31 %	6 %
	2 legs	13 %	3 %

The fractures of two legs goes also from 15 to 10%. This leads us to believe that the modifications to the bumpers have greatly contributed to reducing the gravity of these lesions.

This significant reduction of gravity rates for most of the body areas of pedestrians struck by cars of recent design therefore influences the overall gravity rate for all ages as well as the mortality rate for the most aged category.

CONCLUSIONS

This new accidentology study of pedestrians struck by cars shows :

- the positive effect of the design of new cars on the gravity rate of lesions compared to an older parc on which most of present-day accidentology studies are based,
- an extremely important reduction of fractures of the femur for all pedestrians, 85% less than with the older parc,
- the pelvis is no longer a preoccupation for young adults when the new parc is concerned,
- the problems bear essentially on the lesions of the head and the lower limbs,
- the only remaining pelvic lesions are mainly observed on aged pedestrians, between sixty and eighty years old, for whom more detailed studies would be needed to know if these lesions are due to falls on the ground or on the hood,
- lesions of the tibia/ fibula are clearly reduced (23%) and are also above all less serious (clear reductions in open fractures are often observed to the two legs),
- for adults, the majority of serious and fatal impacts to the head occur in the scuttle and A pillars.
- on the other hand, when only children are concerned, most of the serious head blows are located on the hood zone.

ACKNOWLEDGEMENTS :

The valuable aid of the management of the National Gendarmerie is acknowledged in collecting the various accident reports, so allowing this accidentology study to be carried out in the best conditions. We must inderline here the quality of the photographs and the description of the impacts mentioned in these reports by the different Gendarmerie brigades, who we thank most warmly. Without such a high quality of compilation, this study could clearly not have been done.

PEDESTRIAN SAFETY TESTING USING THE EEVC PEDESTRIAN IMPACTORS

Graham J L Lawrence
Brian J Hardy
Transport Research Laboratory
United Kingdom
Paper Number 98-S10-O-03

ABSTRACT

An European Experimental Vehicles Committee (EEVC) working group has developed a set of test procedures for evaluating the safety performance of cars when they strike pedestrians. These are being considered for possible legislative use in an European Directive. The Transport Research Laboratory (TRL) has played a major part in this working group, including the study of accidents and injuries, and development of the test procedures. It has developed the upper legform to bonnet leading edge impactor and test procedure, and has made substantial contributions to the development of the legform impactor used to test the bumper area.

TRL has also performed a large number of tests to cars, using the headform impactors to test the bonnet area, as well as using the upper legform and legform impactors. Many of these tests were performed as part of a New Car Assessment Programme. The experience gained in testing with the impactors has led to a number of minor refinements to the test procedures.

This paper reports some results from these tests, and demonstrates the current level of pedestrian protection. Test locations that offer relatively high levels of protection indicate that solutions to the problem of achieving better pedestrian safety are often readily available, low cost, and could be applied over a higher proportion of the car surface.

INTRODUCTION

In European countries unprotected road users account for a significant proportion of road accident casualties. In 1995 there were just less than seven and a half thousand pedestrians killed and approximately eighty thousand seriously injured on the roads of the European Union. Accident data show that approximately sixty percent of pedestrian casualties were struck by the fronts of cars. In a typical frontal accident at moderate speeds, the impact of the bumper and bonnet leading edge causes the pedestrian to wrap over the front of the car with their head striking the bonnet top, windscreen or windscreen frame. They then slide forward onto the road as the car slows under the action of braking. Pedestrian accident studies have shown that the most frequent causes of serious injuries were impacts of the legs with the bumper, the upper legs, pelvis or abdomen with the leading edge of the bonnet and wings, and the head and chest with the top surface of the bonnet and wings, scuttle, windscreen frame and ground. To help reduce this undesirably high pedestrian casualty rate, the UK Department of Transport (now the "Department of the Environment, Transport and the Regions") funded the Transport Research Laboratory to carry out research into the possibility of reducing pedestrian injuries by making cars less aggressive in accidents. This work by TRL has made a major contribution to the development of the EEVC pedestrian protection test procedures (some of the EEVC pedestrian working group research was partially funded by the European Commission). These procedures have now been incorporated in the European Commission's draft proposal for a European Parliament and Council Directive (1). The test procedures comprise three sub-system impact tests to assess a car's performance. Separate impactors are used to represent the pedestrian in each main phase of impact. The three impactor types are: a bumper impactor representing the adult lower limb to indicate lateral knee joint shear displacement, bending angle and tibia acceleration, a bonnet leading edge impactor representing the upper leg to record bending moments and forces, and child and adult head impactors to record head accelerations. Each impactor is propelled into the car and the output from the impactor instrumentation is used to establish whether the energy absorbing characteristics of the car are acceptable.

Within the EEVC Working Group, BASt was responsible for developing the head impact procedure and the prototype head impactors, TRL was responsible for developing the upper legform to bonnet leading edge test method and the "research" upper legform impactor, and INRETS was responsible for developing the legform to bumper test procedure and the "research" legform impactor.

The design of the headform impactors was refined by TNO to produce a "production version". TNO are currently considering further minor changes to the headforms to improve the accelerometer mounting and durability.

The design of the upper legform impactor, developed by TRL, has been refined to produce a "production version" suitable for use as a regulatory tool.

TRL have also developed a prototype legform impactor which is a development of the INRETS research legform but modified for use as a regulatory tool.

This paper provides a brief description of the test methods and the work to improve the prototype TRL legform and upper legform impactors. Observations made by TRL and others following experience with using the test methods are reviewed. Finally, the results of testing current cars are summarised and the significance of these test results are discussed.

THE EEVC PEDESTRIAN TEST PROCEDURES

To gain the maximum benefit, all the parts of the vehicle likely to strike pedestrians should be as "pedestrian friendly" as possible. The impact location on a car of a pedestrian's main body regions is dependent on the pedestrian's build and stature, stance and motion, as well as the vehicle's shape and impact speed. Because of this and the wide range of real life accident circumstances, the whole surface of the car front can potentially strike a pedestrian.

Sub-systems test methods, as a regulatory tool, have many benefits over using pedestrian dummies for both the car industry and approval authorities. If pedestrian dummies were used for legislative tests it would be very difficult to predict and control the impact locations of body parts to test selected danger points accurately, particularly the head. Also a range of pedestrian dummies of different stature would be required to test all areas likely to be hit in real life. A test with a single size (eg fiftieth percentile) dummy would not be sufficient for pedestrian protection. It would also be particularly difficult to achieve repeatable results using pedestrian dummies. Separate sub-system tests, using impactors to represent parts of a pedestrian's body, do not suffer from these problems, are much cheaper in terms of hardware, the impact conditions are known and can be designed for, and they can be used in vehicle development to test sub-assemblies of the car. However, for a sub-system test to represent part of a complete pedestrian impact, a detailed knowledge of pedestrian impact conditions is required; this knowledge was available within the EEVC working group. The mandate for the EEVC working group was to develop sub-system tests that:

a) represented a pedestrian accident at 40 km/h and assessed the level of pedestrian protection provided by the car.
b) restricted the test area for the head impact tests to include only the bonnet top, wing tops, scuttle and base of the windscreen.

The speed was chosen because studies had shown that protection effective at this speed was practical and would produce significant reductions in the severity of pedestrian injuries, whilst requiring reasonable levels of energy absorbing and crush depths from the car structure. Its is assumed that protection effective at 40 km/h would also be effective in accidents at speed below 40 km/h and provide some injury reductions in accidents at higher speeds.

The test area was limited to these areas because research had demonstrated that it was practical to provide protection in these areas. However, the windscreen, A pillars and upper frame contribute considerably to the vehicle's overall strength. Although research has shown that it was possible to make some improvements to these parts, the practicality of this had not been proven. Present types of windscreen glass were generally considered to be acceptable for pedestrian head impacts in accidents at speeds up to 40 km/h, apart from the edges which are supported by the surround.

Accident studies (2) (3) have shown that, at speeds of up to 40 km/h, adult pedestrians are more at risk of being seriously injured than child pedestrians from the impact of the bumper and bonnet leading edge (apart from those children so small as to be hit directly on the head by the bonnet leading edge). The legform to bumper impactor and the upper legform to bonnet leading edge impactor have both been designed to represent the contact between the leg of an adult male pedestrian and the front of a car travelling at 40 km/h. For the bonnet top, both child and adult pedestrians are at risk of suffering serious head injuries and therefore the bonnet top test requirement is for a child headform test to the front section of the bonnet and an adult headform test to the rear of the bonnet. The development of these test procedures are reported in more detail in the EEVC WG 10 report (4).

Legform impactor to bumper test

The impactor that has been developed for the bumper sub-systems test was chosen to represent an adult leg being impacted from the side. The design philosophy of this impactor and test method was to reproduce the significant interactions between a pedestrian's leg and the car front whilst taking measurements that could be related to the risk of injury to the knee joint and the fracture of the leg bones. The legform impactor consists of "femur" and "tibia" sections joined by a mechanical knee. The shapes of the sections have been simplified but have physical properties (length, mass, centre of gravity and moment of inertia) equivalent to the leg of a 50th percentile male. The tibia section includes the mass of a foot. The knee joint has stiffnesses in both shear and bending that are similar to a human knee loaded sideways, as specified by EEVC WG10. The impactor has a 25 mm layer of heavy energy absorbing foam flesh covered with a 6 mm thick neoprene skin.

The test method requires the legform impactor to be propelled to strike the car front in free-flight at 40 km/h. The legform, with the deformable knee joint, will respond in a similar way to a human leg (without broken bones) when impacted by something having the shape and stiffness of the car front. The knee instrumentation reports knee bending angle and shear displacement whilst the accelerometer measures the tibia acceleration. The acceptance criteria for the knee joint are intended to prevent serious ligament damage in both bending and shear. Also, the additional criterion on acceleration would require a deforming structure that limits the contact force, and thereby reduces the risk of tibia injuries.

The upper legform to bonnet leading edge test

In pedestrian accidents the first contact is normally with the pedestrian, side on, and is between the lower leg and the bumper. This contact starts to sweep the pedestrian's legs from under him or her. For the adult the next contact is normally between the upper leg and / or pelvis and the bonnet leading edge. However, the first contact between the bumper and lower legs will affect the nature of this second contact with the bonnet leading edge, particularly the upper leg angle and impact velocity. The extent to which the bumper contact affects the bonnet leading edge impact is very dependent on the vehicle geometry.

When the bonnet leading edge strikes a pedestrian, it generates forces in the pedestrian's body. The contact with the upper leg accelerates the impacted part of the leg and this in turn reacts against the mass and inertia of the pedestrian's body above and below the contact point. This action causes bending of the femur and forces in the joints at each end of the femur, particularly at the hip joint and can result in femur fractures or pelvis fractures. The effective mass seen by the car bonnet is a combination of the mass of the struck part plus some of the mass of the pedestrian's body parts above and below the contact and its value is also effected by vehicle geometry.

For the sub-system test it was necessary to establish the relationship between vehicle geometry and upper leg impact angle, velocity and effective mass. This information was obtained both experimentally and mathematically by simulating impacts between a pedestrian dummy and a range of car shapes (5) (6). In these studies the energy absorbing properties of the cars were selected to be of the correct order needed to provide pedestrian protection. These relationships have been incorporated into the test method in the form of parameter look-up graphs.

The design philosophy of this impactor and test method was to reproduce the significant interactions between a pedestrian's upper leg and the bonnet leading edge whilst taking measurements that can be related to the risk of femur and pelvic fractures. The upper legform impactor is propelled into a stationary car so as to represent a pedestrian's accident at an initial car impact speed of 40 km/h. A diagram of the current impactor is shown in Figure 1. The impactor consists of a front member, which represents an adult femur (though it was intentionally made shorter than an adult femur), supported at top and bottom, via load transducers, to a vertical rear member, which is in turn mounted on the end of the guidance system through a torque limiting joint. The front member is equipped with

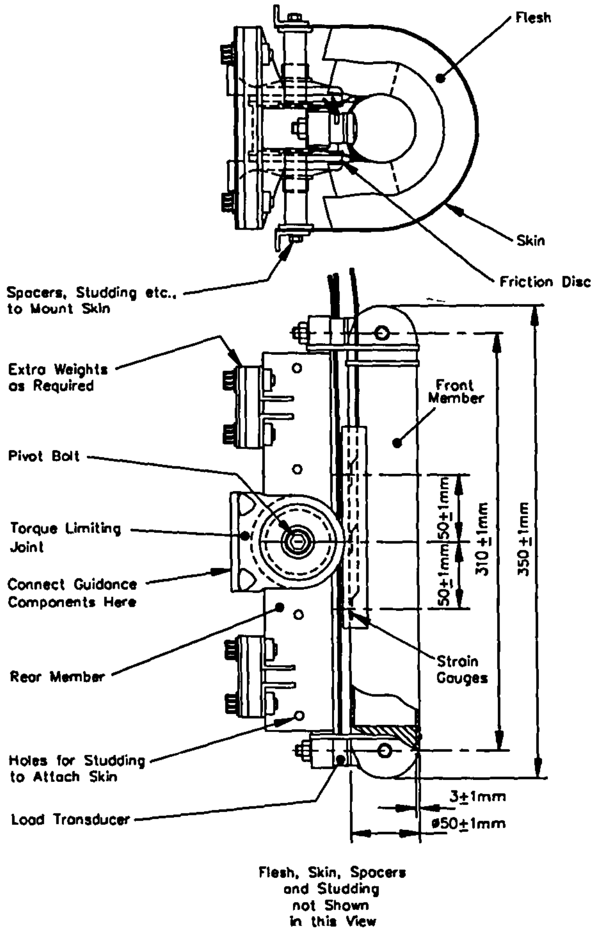
Flesh
Skin
Friction Disc
Spacers, Studding etc., to Mount Skin
Extra Weights as Required
Front Member
Pivot Bolt
Torque Limiting Joint
Connect Guidance Components Here
50±1mm
50±1mm
310±1mm
350±1mm
Rear Member
Strain Gauges
Holes for Studding to Attach Skin
Load Transducer
3±1mm
ø50±1mm
Flesh, Skin, Spacers and Studding not Shown in this View

Figure 1. Upper legform impactor

strain gauges to measure bending and is covered by a 50 mm thick layer of heavy energy absorbing foam to represent the flesh covering a pedestrian's upper leg.

On impact with the bonnet leading edge of a car, the femur tube can react against its top and bottom supports in a similar way to a pedestrian's femur reacting against the pelvis and lower leg. The femur tube is free to bend in the middle, under the influence of the contact forces from the bonnet leading edge, again like the pedestrian's femur.

For each car and each impact location on the car, the car's shape (bonnet leading edge height and bumper lead) will be different, therefore different impact conditions are required for each test. The impactor's angle, mass and velocity values, appropriate for the shape of the car under test, are found from the parameter look-up graphs in the test procedure or, more practically, by a computer program available from TRL. The provision to attach weights to the impactor was to allow the mass to be adjusted to match the effective mass of the pedestrian's upper leg which is appropriate for the shape of the car being tested. The angle and velocity of the propulsion system can also be adjusted to appropriate values for the shape of the car being tested.

Analysis of tests with adult pedestrian dummies showed that, for most car shapes, the angle of the upper leg changed little during the most severe part of the impact with the bonnet leading edge. This is due to the restraining effect of the inertia of the pedestrian's body parts above and below the impact and the short duration of this phase. It was also observed that any rolling of the pedestrian's upper leg that took place during the main bonnet leading edge impact had little effect on the direction of force generated in the car's bonnet leading edge. To reproduce this restraint simply, the upper legform impactor is attached to a linear guide throughout the impact with the car.

The impactor has been used to reproduce well documented pedestrian accidents. These tests confirmed that the impactor and test method faithfully reproduced vehicle damage in accidents with adult pedestrians of average build.

The torque limiting joint was provided to protect the guidance system from damage when testing cars with very poor pedestrian protection. It was not intended to move in tests on cars with acceptable levels of pedestrian protection, and the minimum torque setting specified will not be exceeded in tests with cars that meet the current proposed acceptance criteria.

The acceptance criteria for the upper legform impactor are intended to prevent fractures of the femur and pelvis. However, the current acceptance values are provisional and are almost certain to be significantly raised in the near future making the requirements less demanding while retaining the same targets for protection levels. This is discussed further in the section on the upper legform acceptance criteria.

The headform to bonnet top test

Accident data have shown that the body region most frequently suffering life threatening injuries is the head in both child and adult pedestrian accidents. Adult head impacts points were most frequently towards the rearward part of the top of the bonnet and wings, the windscreen frame and the windscreen. The head impacts of young children were more frequently to the frontal part of the top of the bonnet and wings.

Therefore, two assessments have been included in this sub-systems test. One is based on an impactor representing a child headform to evaluate the forward section of the bonnet and wings and the second based on an adult headform to assess the rear of the bonnet, wings and the scuttle. The child headform is propelled to strike the car in free-flight at 40 km/h at an angle of 50° to the horizontal and the adult headform to strike the car in free-flight at 40 km/h at an angle of 65° to the horizontal.

Both of the headforms that have been developed for these tests are of spherical shape (to give more repeatable results), with a 7.5 mm thick silicone outer flesh. The headforms are equipped with tri-axial accelerometers. The acceptance criterion (Head Injury Criterion of 1000) is intended to prevent serious, life threatening, head injuries.

DEVELOPMENT OF IMPACTORS AND TEST METHODS, AND PROBLEMS IN USE

TRL and others have been using the impactors for several years, and the experience thus obtained has also led to a number of minor refinements of the test procedures, such as improved tolerances and, in some places, a greater clarity of wording. This experience has also led to a number of minor improvements being made to the impactors. The modifications to the legform and upper legform impactors are to improve their reliability, repeatability and ease of use.

Development of the TRL legform impactor

Since the first reporting of the EEVC pedestrian impact test procedures (7), TRL has produced a prototype legform impactor and revised the legform static certification corridors. These revised corridors were included in the EC draft Directive. A total of 13 of these prototype impactors have been manufactured by TRL and are in use in both test houses and car manufacturers' test departments.

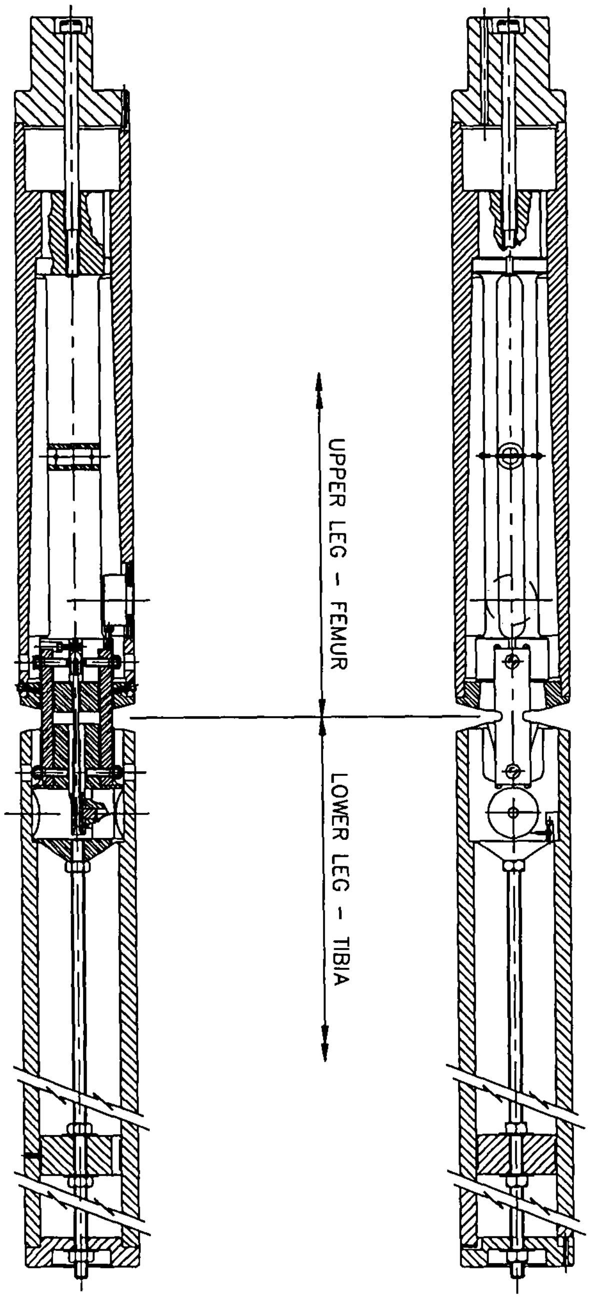

Figure 2. TRL legform impactor

The knee of the TRL prototype impactor contains an elastic spring to produce the shear stiffness together with disposable deformable steel ligaments to provide the bending stiffness. The instrumentation system independently measures the knee shear displacement and bending rotation. The current legform design is shown in Figure 2.

The TRL legform impactor is currently subject to small improvements. In the current prototype there is an undesirable vibration of the knee shear spring leg mass system. The two sections of the legform are connected by the knee shear-spring and the knee shear and acceleration outputs are adversely affected by the natural frequency of vibration of this spring / mass system. The need for a damped shear-spring leg-mass system was considered when the impactor was first developed. However, it was decided to develop and assess firstly an impactor without damping. This assessment has shown that the impactor meets the EEVC requirements and it has proved robust in use but it exhibits this undesirable vibration during dynamic tests. Therefore, a damping system is being added to resolve this outstanding problem, in a further phase of impactor development.

Currently, TRL have made and assessed an experimental damped legform which incorporates a readily available hydraulic damper. This damper met the damping requirement but was not ideal for building into the legform because it was larger than necessary and therefore vulnerable to damage. Testing of this experimental damped legform has shown that the damper has resolved the vibration problem without adversely affecting the knee joint's shear performance. The next phase of development to produce a tailor-made damper unit of minimal size is now in hand, and a damped legform impactor (see Figure 3) will then be made and tested.

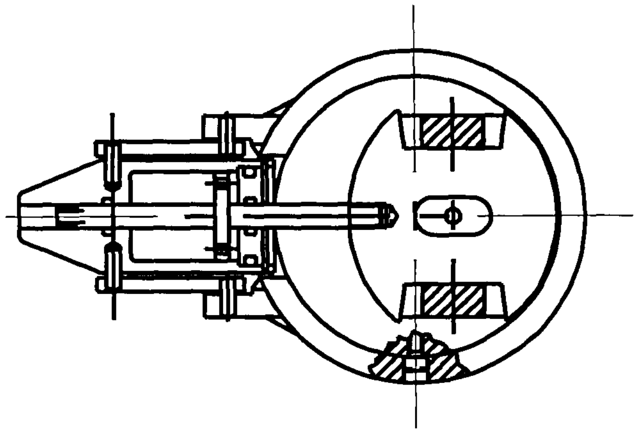

Figure 3. Section through damped legform

Development of an improved dynamic certification test for the legform impactor The current dynamic certification method, developed by TNO, makes use of a pendulum system originally designed to certify the necks of test dummies. This certification method has a number of disadvantages in practice. As the legform is attached to the pendulum its trajectory and impact configuration is not typical of a car impact and the knee shear displacement is too close to the full-scale displacement limit.

To overcome these problems, TRL is proposing a new certification method. The details of this certification method are shown in Figure 4.

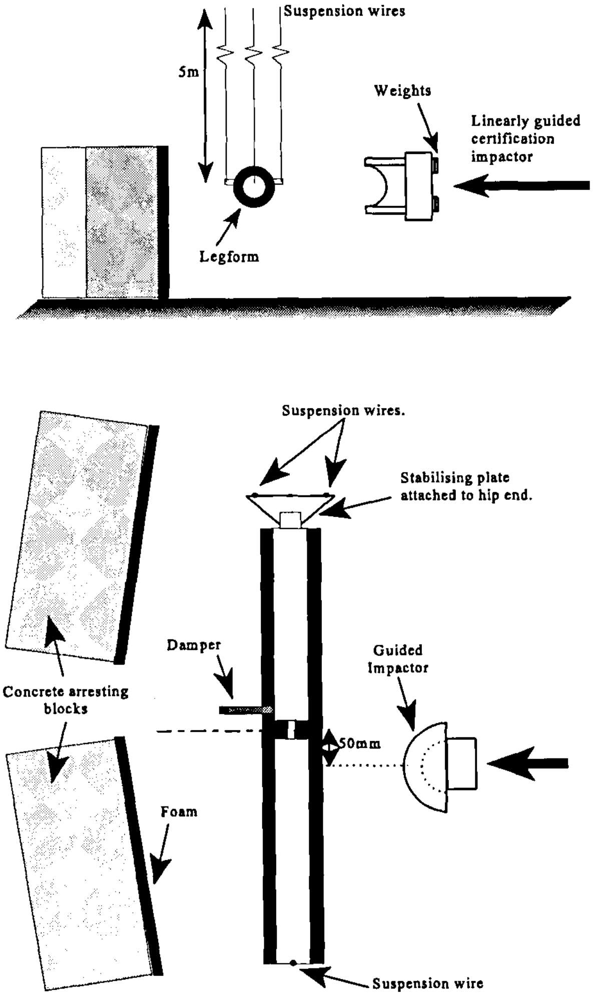
Suspension wires
5m
Weights
Linearly guided certification impactor
Legform
Suspension wires.
Stabilising plate attached to hip end.
Damper
Guided Impactor
Concrete arresting blocks
50mm
Foam
Suspension wire

Figure 4. New legform certification method

Testing of the damped experimental legform to this new certification method has shown that it appears to be satisfactory, generating the required levels of knee bending and shear, and giving repeatable results. It is not intended to finalise this certification test method until the final version of the legform impactor with the damped knee shear system is available and the effects of acceptable variations in impactor performance (knee bending stiffness, foam flesh etc) have been further investigated. It should also be noted that the experimental damped legform had no corrections for the added mass of the damper and this will have had a small effect on its performance in the new dynamic certification test.

Problems found in using the legform impactor

Experience with the legform impactor and test method, both at TRL and within industry, have given rise to several observations. These points are reviewed below together with the proposed modifications, if appropriate:

Vibrations Vibrations have been observed in dynamic tests and the legform requires a damper for the knee shear-spring leg-mass system. As described above TRL are developing such a system.

Certification The dynamic certification method is in conflict with the knee shear displacement stops. TRL have developed an improved dynamic certification method which has resolved this problem and is described above.

Bending ligament specification It has been suggested (8) that the effects of the range of knee bending ligament stiffnesses permitted within the corridor, would have a large effect on impactor performance. However, the energy required to bend the knee joint, to the bending acceptance level of 15 degrees, is only about 12% of the total kinetic energy of the legform. Because of this, the distribution of force along the impactor face, rather than knee bending stiffness, should predominate in controlling the knee bending angle. The effect of the bending corridor's width on the ligament bending energy, compared with the impactor's kinetic energy, is less than plus or minus 2% which seems very unlikely to effect test results significantly. In practice, it would be impossible to manufacture a ligament which followed either extreme of the bending stiffness corridor, particularly at the start; this would reduce the effects of the corridor's width still further.

Initial tests using the dynamic certification method to investigate the effect of ligament stiffness have suggested that the corridor would have a maximum effect of about plus or minus 14% on the certification bending angle. This test, with a concentrated load applied close to the knee, is far more likely to be affected by different ligament stiffness than a car test with the distributed load of a car bumper system. Further full scale tests on a car which has passed the legform requirement will be performed, using ligaments at the practical extremes of the bending stiffness corridor, to determine the effects of the permitted range of ligament stiffnesses, within the corridor, on test results.

It is also suggested that there is insufficient testing of bending ligaments to confirm their compliance statistically. The current requirement in the test method is to certify one pair of bending ligaments in the static test and one pair in the dynamic test, and then use the impactor, for a maximum of 20 tests, with ligaments from the same batch of manufacture. However, as well as this it is obviously the responsibility of the ligament manufacturer to establish methods of quality control to ensure compliance. For TRL's own quality control system, large sheets of steel are purchased from which about 1500 pairs of ligaments can be made. Sample ligaments are then made and tested using the static bending certification test to establish an appropriate ligament waist size for the material properties of that sheet of material. Ligaments are then manufactured from that sheet in batches of 50 pairs, with statistical control methods being used to ensure conformity of ligament dimensions. The tolerances of the ligament dimensions have been set at an appropriate level to ensure that their effects on ligament stiffness are small and well within the corridor width. At least one pair from each batch is then tested by TRL in the static bending certification test and the results are monitored to ensure consistency and identify any changes in material properties as the sheet of raw material is consumed.

Methods of further controlling and shaping the ligament bending properties are being investigated since the performance of the steel in plastic bending is different from sheet to sheet of raw material and does not necessarily match the slope of the corridor. However, even if better control of the ligament stiffness is developed no change of the existing static bending certification corridor is anticipated at present.

Shear displacement anomalies Positive or negative peak shear displacements have been observed under nominally identical test conditions. Typical car tests produce shear displacements first in one direction and then in the reverse direction. These positive and negative displacements are often of very similar magnitude, therefore it is not surprising to see this effect. However, the effects of the vibration of the un-damped shear-spring leg-mass system could often contribute to this effect; the damped version should improve the repeatability of shear displacements.

Mechanical shear displacement limits There is concern that the mechanical limits of the shear spring are only about 15% in excess of the acceptance criteria, giving little overload information. The mechanical stops were intended to give a 20% overload capacity and TRL are investigating improvements to give that intended displacement. The shear spring system, and the impactor's dimensions and specification make it difficult, if not impossible, to increase the overload capacity above 20% within the current design. This overload capacity is considered to be sufficient for using the impactor for its primary purpose as a legislative test tool. It should be noted that it is most probable that a bumper system that meets the bending and acceleration requirements will also meet the shear requirements. The current impactor already has a large overload capacity for these two measurements, which will probably provide sufficient feed-back for manufacturers to develop bumper systems to meet the requirement. The value of an overload capacity as a development tool is recognised and the possibility of producing a different version of the impactor (or a kit of parts), with a larger shear overload capacity, for the purpose of developing bumper systems will be investigated if there was sufficient demand for it.

Flesh properties It has been suggested that the neoprene skin and Confor™ foam flesh are not sufficiently well specified nor chosen with biofidelity in mind. The type and dimensions of these materials are specified in the test method and their dynamic performance is controlled and specified by the dynamic certification performance requirements. Like test dummies, the pedestrian impactors have problems with flesh. For durability and practicality reasons the majority of the weight is concentrated in the metal parts or "bones" of the test devices and not in the flesh as in a human. However, the pedestrian legform impactor makes use of Confor™ foam which is more like human flesh than the foam flesh used in test dummies because it is both significantly heavier and more capable of absorbing impact energy. The vehicle crush depth and energy absorption required to meet the legform criteria is much larger than the available flesh crush depth and energy absorption capabilities in both humans and the legform impactor. Consequently the influence of the impactor and human flesh is relatively insignificant to the response. Also the flesh on the leg will have little, if any, influence on the strength of the bone and knee. Therefore, the biofidelity of the flesh is not considered critical.

Development of the TRL upper legform impactor

The original research version of the upper legform impactor, used to develop the test method, was described by Lawrence, et al (9). It has since been refined to produce a "production version", although it has not been changed in principle since its conception.

This production version was most recently modified (in January 1996) to remove an unwanted load path through the foam flesh to the back of the impactor. After this revision of the flesh and skin system a series of impact tests was performed to confirm that the load transducers accurately reported the impactor force. For this the impactor impulse, derived from the measurement of impactor acceleration and mass behind the load transducers, was compared with the impulse derived from the force time histories, and the results are shown in Table 1. These results confirm that the load transducers were accurately reporting the impactor force, with the impulse derived from both methods agreeing to within 1% in all tests. Measurements of impulse rather than force were used for this comparison because instantaneous values of force derived from acceleration and mass are likely to suffer from the inherent noise found in the accelerometer time histories of mechanical systems.

The amended design is now considered to be satisfactory for this aspect.

Table 1. Results of upper legform impulse tests into a foam covered concrete block (current impactor design with revised flesh system)

Test No	Impact Orientation	Impulse A # (Ns)	Impulse B ✣ (Ns)	Ratio of A/B (%)
1	normal*	111.5	111.3	99.8
2	normal*	112.1	111.4	99.3
3	normal*	112.0	111.8	99.8
4	normal*	165.6	165.7	100.1
5	normal*	163.3	161.8	99.1
6	simulated bonnet leading edge†	134.4	134.5	100.1
7	simulated bonnet leading edge†	136.0	137.2	100.9
8	simulated bonnet leading edge ‡	135.4	135.1	99.8
9	simulated bonnet leading edge‡	135.8	136.0	100.1

** impactor front member normal to face of test block*

† centre of impactor front member, to simulated bonnet leading edge

‡ impactor front member contact at level of inner skin spacer, to simulated bonnet leading edge

# calculated from: Mass behind load transducers x Velocity change (by integration of acceleration)

✣ calculated from integration of load transducers outputs

Acceptance criteria for the upper legform impactor The current acceptance values for the upper legform to bonnet leading edge test were based on published biomechanical data and the reconstruction of pedestrian accidents with the upper legform impactor (9). The accident reconstructions were carried out as part of the development of the test method using the first research version of the upper legform impactor. These reconstructions demonstrated the large variation in human injury thresholds which are always found in biomechanical studies, making it difficult to select suitable acceptance values. It was concluded that these data were insufficient to select well justified acceptance criteria and the current values have therefore always been regarded as provisional. Improvements to the impactor (improvements to the flesh etc) since these first reconstructions have resulted in the impactor producing larger outputs, making these provisional criteria less appropriate. To provide further data on which to select the acceptance criteria, one additional accident reconstruction programme has been completed and a second one started. Other research institutes are also carrying out accident reconstruction programmes, which will be combined with the TRL results to produce revised acceptance criteria. The initial results from these programmes indicate that the criteria are likely to be increased significantly. The results of this work are expected to be reported before the end of 1998.

Test impact energy requirement for the upper legform impactor The current test energy parameter look-up graphs were based on computer simulations, with the results adjusted to reflect the energy required to replicate vehicle damage in accident reconstructions. As a cars become more streamlined, the severity of the bonnet leading edge impact declines and this is reflected in the test energy look-up graph. However, accident reconstructions with newer, more streamlined cars have suggested that the damage caused in the upper legform test may be more severe than that found in accidents at the same speed. This effect may be partially or completely due to the comparatively stiff bumpers of modern cars which reduce the severity of the bonnet leading edge impact at the expense of a more severe impact to the knee and lower leg. Recent accident data have shown an increase in the proportion of knee and lower leg injuries as the proportion of upper leg and pelvis injuries has declined (10). Computer simulations are being performed to examine in more detail the effects of car shape on the upper leg to car bonnet deformation energy and the effects on this energy of modifying the bumper and bonnet leading edge stiffnesses to make them safe for pedestrian impacts.

Problems found in using the upper legform impactor

Experience with the upper legform impactor and test method, both at TRL and within industry, have given rise to several observations. These points are reviewed below together with modifications proposed, where appropriate:

Look-up graphs Manual interpolation of test parameters from the parameter look-up graphs in the regulation can lead to inconsistency in selecting test conditions. A software program to calculate these values has been produced. This program contains an identical data set to that used to draw the parameter look-up graphs and removes the possibility of human error in reading off test conditions. This program has been readily available to all since 1992.

Contact point First contact is not always to the bonnet leading edge reference line. The bonnet leading edge reference line is part of a simplified method of determining a car's shape to set the test conditions. For most vehicle shapes first contact will be very close to the bonnet reference line, however, it was never intended for first contact to coincide precisely with this line.

Impactor durability The impactor body can be damaged in moderate to severe overload conditions. The impactor has been designed to withstand loads in excess of 2.5 times the acceptance criteria. It has been used in tests to steel bull bars and has withstood forces and bending moments in excess of 4 times the acceptance criteria without damage. Only one impactor has been returned to TRL with damage to the body. Although the records of the test house concerned showed that the impactor had not been overloaded, testing at TRL proved that it had in fact been inadvertently subjected to loads in excess of 6 times the acceptance criteria.

Flesh specification The rubber skin and Confor™ foam flesh are not closely specified nor chosen with biofidelity in mind. This observation is similar to that for the legform impactor discussed above. It is considered that the specification in the test method is sufficient. The biofidelity of the flesh is not critical and its performance has been taken into account in determining the acceptance criteria.

Off- road vehicles For some large off-road and multi-purpose vehicles, the test method requires an upper legform test at heights higher that the thigh of pedestrians of normal stature. The upper legform test becomes less appropriate for bonnet leading edge heights in excess of 1000 mm. For these tall fronted vehicles an abdomen impactor or even a chest impactor might be more appropriate. However, these vehicles form a very small proportion of the fleet so it was decided not to develop these impactors. Instead, the vehicles are required to pass an upper legform test because design changes to meet this requirement would result in an improvement from current practice and would reduce injuries, as the upper legform requirements are considered to be roughly similar (but less demanding) to those for protection of the abdomen or chest.

Available crush depth For large vehicles the combination of test energy and current acceptance criteria requires impractically large vehicle crush depths. It must be accepted that these vehicles are particularly likely to cause serious injuries from bonnet leading edge contacts. The acceptance criteria are currently under review and are likely to be increased, which will reduce crush depth requirements pro-rata. However, if this adjustment proves to be insufficient to reduce the crush requirement to more practical levels, it may be necessary to consider capping the energy requirement to limit the required crush depth.

Duplication of testing Both the legform impactor and the upper legform impactor strike the bonnet leading edge, causing duplication. The knee and lower leg injuries occur before the upper leg impact with the bonnet leading edge is complete. However, the position and stiffness of the bonnet leading edge will affect the risk of knee injury. The femur section of the full legform impactor is suitable for reproducing the early stages of the impact with the bonnet leading edge with regard to knee and lower leg injuries. Because the legform has no upper body mass nor instrumentation to record the risk of upper leg injury, it is not suitable for reproducing or assessing the safety of the complete upper leg impact with the bonnet leading edge. Therefore, the two test tools are complementary and are both required.

REPEATABILITY OF THE TEST METHODS

It is clearly important for the test procedures to be repeatable. Four potential causes of a possible lack of repeatability in the tests results can be identified:

a) differences in the test-to-test impact conditions due variations in the propulsion system's performance.

b) differences in the test-to-test performance of the impactors due to variations in the flesh and ligaments etc.

c) real differences in the test-to-test performance of the car, replacement car panels and fitting tolerances.

d) differences, between test houses, with the equipment and data recording systems used.

Repeatability of the legform impactor

The repeatability of the first prototype legform impactor was assessed by TRL by testing a simulated car designed to deform in a repeatable way. The results are shown in Table 2 and show a maximum coefficient of variation of only 4.6%. The repeatability of the experimental damped legform has also been established by carrying out repeated dynamic certification tests using the proposed TRL certification method. Repeatability tests on cars were not carried out with this impactor because the large damper unit used in this experimental model was considered to be too vulnerable to damage from rebound impacts. Table 3 shows the results of these repeatability tests using the new certification test, and these also show low coefficients of variation.

Table 2. Results of first prototype legform repeatability tests into a simulated repeatable car

Test no.	Knee angle (deg.)	Knee shear disp. (mm)	Max. accl. (g)	Impact velocity (ms^{-1})
1	24.32	1.82	140.5	11.31
2	24.91	1.70	143.3	11.29
3	27.52	1.68	146.6	11.29
4	24.47	1.78	147.9	11.27
5	25.53	1.72	151.1	11.33
Coefficient of Variation (%)	4.6	3.0	2.5	0.4

Table 3. Results of repeated dynamic certification tests (new TRL certification method) to the experimental damped legform impactor

Test no.	Knee angle (deg.)	Knee shear disp. (mm)	Max. accl. (g)	Certification impactor velocity (ms^{-1})
1	10.94	6.25	232	7.53
2	10.90	6.18	226	7.58
3	10.54	5.85	210	7.45
4	10.27	5.93	207	7.40
5	10.57	5.88	211	7.42
6	10.79	5.91	214	7.47
7	10.76	5.98	214	7.47
Coefficient of Variation (%)	2.2	2.6	4.3	0.8

Repeatability of the upper legform impactor

The repeatability of the impactor was assessed by a series of impact tests to the certification tube, which represents a car with repeatable characteristics. The results of these tests are shown in Table 4, and show a maximum coefficient of variation of only 1.7%.

Table 4. Results of upper legform repeatability tests into the certification tube *

Test No.	Impact velocity (ms^{-1})	Temperature (°C)	Bending (Nm)			Force (kN)	
			Upper	Centre	Lower	Top	Bottom
1	7.95	18	175	205	183	1.26	1.32
2	7.92	18	173	204	182	1.28	1.31
3	7.97	18	170	202	181	1.24	1.30
4	7.97	18	176	208	184	1.29	1.33
5	8.00	18	171	201	178	1.25	1.26
6	8.00	18	173	204	181	1.29	1.29
Coefficient of Variation (%)			1.2	1.1	1.0	1.5	1.7

* *new foam from the same batch used for each test*

Discussion of the repeatability of the test methods

These repeatability tests show that, under tightly controlled conditions, both the legform and the upper legform tests are highly repeatable.

Variations in impact velocity (cause a) above), are likely to affect the results. It may prove necessary to restrict the tolerance to plus or minus 2%.

Variations in impactor performance (cause b) above) will, of course, lead to greater variation when using flesh and ligaments from different batches. The dynamic certification requirements will limit the potential effect of the former, and tight control of the manufacturing process the effect of the latter.

Variations in the car (cause c) above), are real and should not be considered a failing of the test methods. Tight control of the manufacturing process could reduce this source of variation.

Cause d) above covers a number of areas, mainly propulsion systems, impactors, instrumentation and analysis and this aspect is not unique to the pedestrian test procedures. Currently many test houses are using existing propulsion systems which have been adapted for pedestrian testing. Impactors in use at different test houses are expected to behave similarly and the certification requirements will prevent significant differences arising.

TEST RESULTS OF CURRENT CARS

To date, a total of 34 cars have been subjected to pedestrian tests as part of the European New Car Assessment Programme (EuroNCAP). The main difference between the EuroNCAP assessment and the draft EC pedestrian requirement is that, for EuroNCAP, the number of headform tests per car has been reduced from nine to six for both the child and adult headforms.

Tests meeting performance requirements

The results of these EuroNCAP pedestrian tests are summarised in Table 5. As explained above the acceptance levels for the upper legform are subject to review once the accident reconstructions have been completed. For interest, the results have been analysed also for the current best estimate of this revised value, based on the limited accident reconstruction results available to date.

Table 5. Summary of pedestrian test results from the EuroNCAP programme (34 cars) - number of test locations passing the EEVC WG10 test requirements

Impactor type	Number of tests	Number of tests passing	Proportion of tests passing (%)
Child headform	204	72	35
Adult headform	183 #	12	6.6
Upper legform	102	0	0
Upper legform †	102	7	6.9
Legform	101	8	7.9

† *using TRL's current best estimate of the revised acceptance criteria for the upper legform test*

# *For the 7 small cars the number of adult headform tests was reduced to 3 per car because the adult head test area was small.*

The results of the EuroNCAP pedestrian tests have provided considerable data on the performance of current cars. The examination of these data, in Table 5, shows that a number of the test sites are meeting the pedestrian requirements. For each test method the passes are distributed amongst the car models tested, however, some models have a higher rate of passes. Further examination of the EuroNCAP data also shows that, for the bumper, one car met the requirement at all three test points and a further two cars met the requirement at two out of the three test points.

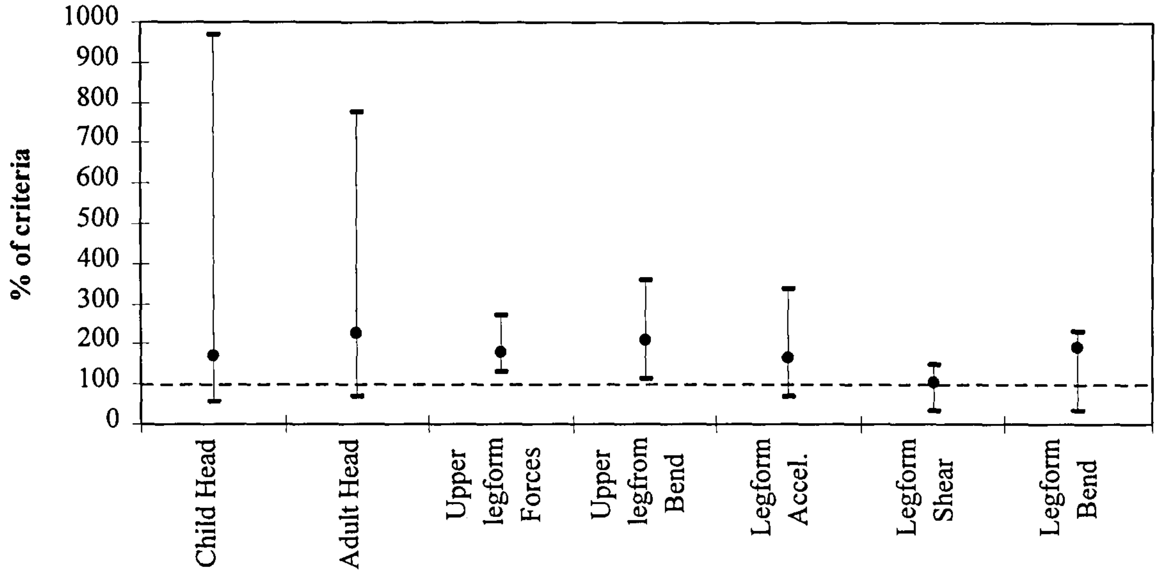

Figure 5. **Comparison of spans and means from EuroNCAP pedestrian tests, as per cent of criteria**

For the legform knee shear and bending, the built in mechanical limits impose an artificial ceiling on the upper end of the range of measurements.
The upper legform criteria are currently under review.

For the upper legform no cars met the current criteria at any point but, using TRL's current best estimate of the revised acceptance criteria, one car met the requirement at two of the three test points tested and five other cars met the requirement at one of the three points tested. For the child headform test, eight cars met the requirement in four out of the six points tested and a further eight cars met the requirement in three out of the six points tested. For the adult headform, two cars passed the requirement in three out of six tests.

The EuroNCAP pedestrian tests data are presented to show the mean and span for each impactor type in Figure 5 above.

Tests within 25 per cent of the performance requirement

The number of test sites passing or which are close to passing the requirements is also of interest. As current cars have not been designed to meet the requirements, this will provide a more appropriate indication as to how cars might have performed if they had been designed with a moderate attention to pedestrian safety. Table 6 shows the number of tests below a value set at an arbitrary 25% above the acceptance criteria.

Table 6. Summary of pedestrian test results from the EuroNCAP programme (34 cars) - number of test locations passing or within 25% of the EEVC WG10 test requirements

Impactor type	Number of tests	Number of tests passing or within 25%	Proportion of tests passing or within 25% (%)
Child headform	204	103	50
Adult headform	183 #	37	20
Upper legform	102	1	1.0
Upper legform †	102	31	30
Legform	101	16	16

† *using TRL's current best estimate of the revised acceptance criteria for the upper legform test*
# *For the 7 small cars the number of adult headform tests was reduced because the adult head test area was small.*

The results of the EuroNCAP pedestrian tests in Table 6, show that many test sites met or were close to meeting the pedestrian requirements. Car models with large areas meeting or close to meeting the requirement have been found from the EuroNCAP data. This examination shows that for the legform test three cars were within 25% or better at all three test points and a further two cars had two test points within 25% or better. For the upper legform, using TRL's best estimate of the revised acceptance criteria, four cars were within 25% or better at all three test points and a further six cars had two out of three tests that were within 25% or better. For the child headform test eighteen cars had at least four out of the six tests within 25% or better. Of these five cars had five out of the six tests within 25% or better. For the adult headform six cars had three tests within 25% or better and one of these had five out of six tests within 25% or better.

These test results must be seen in the context of the tests being performed on cars which have been designed in the absence of any dynamic pedestrian test requirement, and only the requirement to avoid sharp forward facing edges to meet the exterior projections requirements. The low proportion of passes is then not surprising. The relatively large proportion (about one third) of test locations already passing the child headform test is very encouraging.

The results indicate that significant improvements in pedestrian safety are in some areas achievable, at low cost, by copying current best practice from other cars or other areas of a car. For instance, in many cases hard under-bonnet components could be moved or replaced by softer materials. In some cases it could be as simple as changing the length of a mounting stud. It has to be accepted, however, that, for some areas, compliance will be more difficult and costly.

CONCLUSIONS

1. Experience with using the pedestrian test impactors has shown that the test procedure is both practical and repeatable. Nevertheless, it has led to modifications to the test devices to improve their performance.

2. An improved, prototype legform impactor has been developed which has deformable ligaments solely for knee bending, and an elastic spring for knee shear displacement. The instrumentation now measures these outputs independently. Modified legform bending and shear certification corridors have been introduced in the EC draft Directive.

3. A new and improved legform dynamic certification procedure has been developed.

4. A prototype damped version of the legform has been tested which has demonstrated that this will remove the unwanted resonance of the shear spring.

5. Changes have been made to the upper legform impactor to remove an unwanted load path. Tests have been carried out to verify that the load outputs now read correctly.

6. Further accident reconstructions are being carried out with the upper legform impactor. It is likely that these will lead to a significant increase in the upper legform acceptance levels.

7. Pedestrian test results from the EuroNCAP programme show that a third of child headform tests passed, though less than ten percent of tests passed with the other impactors. However, many more tests were within 25 percent of the pass criteria.

ACKNOWLEDGMENTS

This paper has been produced by the Transport Research Laboratory, as part of a contract placed by the Department of the Environment, Transport and the Regions. Any views expressed are not necessarily those of the Department.

REFERENCES

1. EUROPEAN COMMISSION (1996). Draft proposal for a European Parliament and Council Directive relating to the protection of pedestrians and other road users in the event of a collision with a motor vehicle. *Document reference III/5021/96 EN, 7 February 1996.* Brussels: European Commission.

2. OTTE, D (1988). Influence of vehicle front geometry on injuries to pedestrians involved in accidents. *Study of accident research at Medical University of Hanover under contract to BASt, 1988.*

3. ASHTON, SJ and GM MACKAY (1979). Some characteristics of the population who suffer trauma as pedestrians when hit by cars and some resulting implications. *Proceedings of 4th International IRCOBI Conference on the Biomechanics of Trauma, Goeteborg, Sweden, 5-7 September, 1979.* Lyon: International Research Committee on Biokinetics of Impacts Secretariat.

4. EEVC COMMITTEE (1994). EEVC Working Group 10 report. Proposals for methods to evaluate pedestrian protection for cars.

5. LAWRENCE, GJL (1990). The influence of car shape on pedestrian impact energies and its application to sub-system tests. *Proceedings Twelfth International Technical Conference on Experimental Safety Vehicles, Gothenburg, Sweden, May 1989.* USA: US Department of Transportation. pp 1253-1265.

6. JANSSEN, EG and JJ NIEBOER (1990). Protection of vulnerable road users in the event of a collision with a passenger car, part I - Computer simulations. *TNO report No: 75405002/I December 1, 1990.* Delft, The Netherlands: TNO Crash-Safety Research Centre.

7. HARRIS, J (1993). Proposals for test methods to evaluate pedestrian protection for cars. *Proceedings Thirteenth International Technical Conference on Experimental Safety Vehicles, Paris, France, November 1991.* USA: US Department of Transportation. pp 293-302.

8. SCHUSTER, PJ and B STAINES (1998). Determination of bumper styling and engineering parameters to reduce pedestrian leg injuries. *SAE paper 980361, presented at the SAE Congress, Detroit, 1998.* Warrendale, USA: Society of Automotive Engineers.

9. LAWRENCE, GJL, BJ HARDY and J HARRIS (1993). Bonnet leading edge sub-systems test for cars to assess protection for pedestrians. *Proceedings Thirteenth International Technical Conference on Experimental Safety Vehicles, Paris, France, November 1991.* USA: US Department of Transportation. pp 402-413.

10. HARDY, BJ (1998). Analysis of pedestrian accidents, using police fatal accident files and SHIPS data. *TRL Report 282* (to be published in 1998). Crowthorne, UK: Transport Research Laboratory.

© Copyright TRL Limited 1998. Extracts from the text may be reproduced, except for commercial purposes, provided the source is acknowledged.

A TECHNICAL EVALUATION OF THE EEVC PROPOSAL ON PEDESTRIAN PROTECTION TEST METHODOLOGY

John Green
Rover Group
United Kingdom
(on behalf of ACEA Pedestrian Task Force)
Paper Number 98-S10-O-04

ABSTRACT

Following the publication in November 1994 of the EEVC WG10 proposal for methods to evaluate pedestrian protection for passenger cars and the subsequent adoption of those recommendations into a European Commission draft proposal, ACEA (European Automotive Manufacturers Association) initiated a project to perform a technical evaluation of those test methodologies. The proposed methodology consists of sub-system tests of a child and an adult headform to the bonnet surface, an upper leg impact to the bonnet leading edge, and a leg impact to the bumper and front structure of the vehicle.

The programme of work undertaken by ACEA was performed at two European test laboratories and consisted of 269 tests with the four impactors. The tests were performed on seven vehicles selected to represent the variety of vehicles currently on the European roads. Subsequent additional testing has also been performed to add to the experience gained in this initial test programme.

This paper reports the work performed within this test programme plus the subsequent test work performed to date. It details the test results of typical vehicles on the road today, evaluates the test methodology in terms of repeatability and reproducibility. The experience gained in performing the tests is reported and conclusions are drawn relating to the practicality of performing these tests and the technical feasibility of applying the proposed requirements to future vehicles.

INTRODUCTION

An ACEA project was set up in 1995 to perform a technical evaluation of the proposed pedestrian protection test procedure which had been developed by EEVC WG10, and to assess the practicality of the procedures in a vehicle development environment. The objectives of this programme were to evaluate the test methods, to establish the performance of current vehicles and to assess the technical feasibility of the proposed legislation for European vehicles.

The ACEA programme consisted of a total of 269 tests with the four pedestrian impactors and at two laboratories, with seven different vehicles. The seven vehicles which were initially selected for this programme, were chosen to represent the European vehicle parc, as regards mainly their size, design and engine configuration. An eighth vehicle, on which an additional 18 tests were performed, was later added to obtain improved repeatability data for the upper leg and leg impactors. The vehicles selected were the Citroën XM, Fiat Punto, Range Rover, Renault Twingo, Renault Espace, Rover 100, Volvo 940, and VW Golf.

For each of the four subsystems, the test programme consisted of:

- An evaluation of each of the vehicles according to the proposed test procedure;
- A study of the repeatability of the test procedure;
- A study of the reproducibility of the test procedure;

OVERVIEW OF TEST METHOD AND PROGRAMME

The programme of vehicle tests was performed according to the EEVC WG 10 pedestrian protection test procedure which was adopted as a draft proposal by the EC DG III. The test proposal consists of a series of sub-system impact tests to the front end structure of a vehicle with instrumented impactors designed to represent the adult head, child head, upper leg, and leg of a pedestrian.

According to the proposal, the vehicle bonnet is struck by a child or an adult headform depending on the impact position on the bonnet. Both headforms strike the vehicle at 40 km/h (11.1 m/s) and are in free flight before contacting the bonnet. The child headform, weighing 2.5 kg, is fired at 40 degrees to the vertical, whilst the adult headform, weighing 4.8 kg, is fired at 25 degrees to the vertical. A triaxial accelerometer mounted at the centre of the headform measures accelerations from which a Head Injury Criteria can be calculated. Where the impact zones permitted, twelve head impact tests were performed on each vehicle split equally between child headforms and adult headforms, and between those locations expected to give better results and those expected to give worse results. On vehicles with shorter bonnets some adult headform tests were omitted. Further, one vehicle was selected on which repeatability tests were performed.

The bonnet leading edge of the vehicle is struck by a linearly guided upper legform impactor. The impact conditions (energy, velocity, and angle) are dependent on each vehicles' geometry and, for any vehicle, can vary from the centre of a vehicle to its edges. The impact energy for a vehicle could theoretically be between 200 J and just under 1000 J, the velocity between 20 km/h and 40 km/h, and the impact angle between 10 and 47 degrees to the horizontal. Values for the tested vehicles were in the ranges: 312-949 J, 22.7-40 km/h, and 19.1-43.3 degrees, which represents a good spread acroos the range of test conditions. The impactor is instrumented to measure impact force on each end of the impactor front member, and the bending moment near the centre of the front member of the impactor. Three upper leg impact tests were performed on each vehicle at different positions. Again, one vehicle was selected for repeatability tests.

The bumper and front structure of the vehicle are struck by a legform impactor which has an articulated knee joint. The impactor, weighing 13.4 kg, strikes the vehicle front at 40 km/h and is in free flight on contact. The leg is instrumented to measure accelerations in the tibia, shear displacement in the knee joint and the bending angle in the knee joint. Three leg impact tests were performed on each vehicle at different positions followed by repeatability tests on one selected vehicle.

Once these tests were completed additional tests were performed at a second test laboratory on the vehicles selected at the first laboratory for repeatability tests. Three head impact tests were performed at 6 bonnet positions and three upper leg and three leg impact tests were performed at each of the three impact positions used previously. This gave both repeatability data from two test laboratories and permitted the reproducibility between the test laboratories using different test rigs to be calculated. An eighth vehicle was also later tested at the second laboratory with three upper leg and three leg impact tests at each of three locations on the bonnet leading edge and bumper to more appropriate repeatability data.

The upper leg impactor was also tested against a flat rigid plate at reduced impact speeds in order to investigate the bending moment which can be induced purely by the uniform compression of the Confor™ foam.

ANALYSIS OF RESULTS

Headform Tests

The cars were tested with the child and adult headform impactors, insofar as the impact area for adults on the bonnet was large enough. This was not the case with two cars, for which no adult point could be tested, and, to a certain extent, with a third car, for which only four adult impact points could be tested instead of six. Impact points were carefully selcted to get both good and bad results for both the child and the adult headforms.

The results of the tests are illustrated in Figure 1 for all the vehicles and all the impact locations. Despite 50 % of the locations being chosen with the expectation of being better locations, only 22.9 % of all the points tested could meet the requirement of a HIC less than 1000; this corresponds to 16 points out of a total of 70 points tested (9 for the child headform out of 42 tests and 7 for the adult headform out of 28 tests). As a whole, the results showed that none of the tested vehicles is able to meet the required HIC value for all of the impact locations.

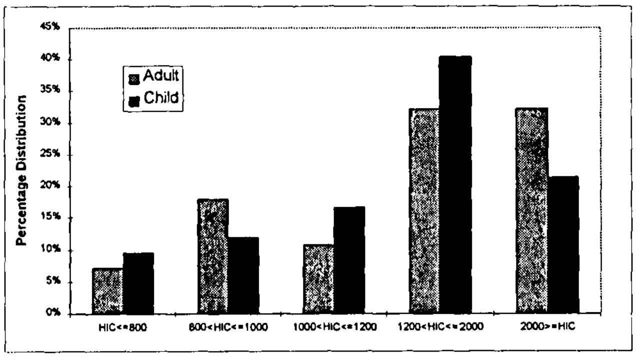

Figure 1. Percentage Distribution of Head HIC levels for Adult and Child Headforms.

One vehicle was selected in order to investigate the repeatability of the procedure. Two additional tests were performed on six of the original twelve locations. On examination of these results it was observed that the repeatability improved as the HIC level reduced (Figure 2). This was assumed to be due to the absence of contact with underbonnet hard points which increases the test sensitivity. As a result, the repeatability is reported only for those three impact locations giving results around the EEVC limits.

The repeatability[*] of the tests at LAB 1 ranged from -4.9 % to 4.7 %, whilst at LAB 2 the repeatability was from -4.3 % to 3.7 %.

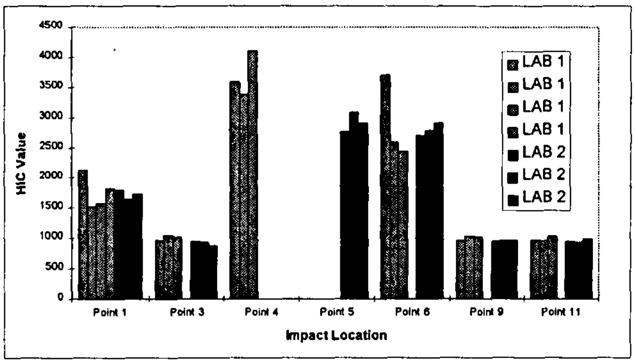

Figure 2. Repeatability and Reproducibility results for Head Impact Tests.

The reproducibility[**] between the two laboratories, where the results were around the EEVC limits, was ± 4.9 %. This gives a total scatter of all comparable tests in the range of -9.0 % to 9.1 %.

Upper Legform Tests

The vehicles were tested along their bonnet leading edge (BLE). In each third of the BLE one target point is associated to two geometric distances (bonnet leading edge height and bumper lead) which define the test conditions (velocity, energy and impact angle) of the upper legform impactor, in accordance with the requirements of the EEVC proposal. Each vehicle was tested at:

- the centre line
- the centre of the left-hand headlight
- the inside corner of the right-hand headlight

A new piece of Confor™ foam was used for each test because it was believed that the properties of the foam would degrade with each impact. The tests were conducted using Confor™ foam cut according to the new dimensions specified by TRL which avoids a load path to the back of the impactor through the foam.

The results of these tests are given in Figure 3 for all vehicles. No vehicle met the requirements either for the total load or for the bending moment in any of the 21 tests. The measured values were up to three times higher than the proposed EEVC limits (4 kN - total load, 220 Nm - bending moment).

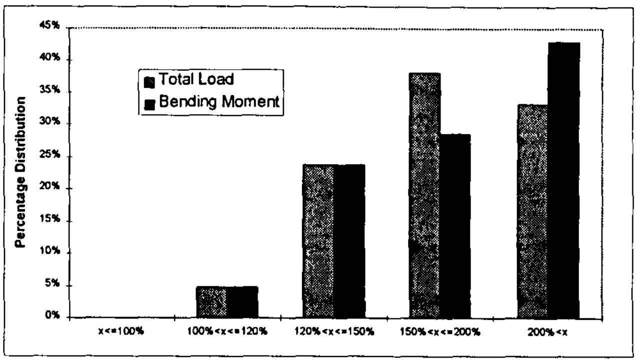

Figure 3. Percentage Distribution of Upper Leg Load and Bending Moment Relative to the Proposed Limits.

One vehicle was chosen for two additional tests to show the accuracy of repeatability. The values measured for the total loads scattered in the range of -11.9 % to 16.2 % and for maximum bending moments in the range of -11.1 % to 14.1 % at LAB 1. For LAB 2, the values measured for the total loads were scattered in the range of -10.3 % to 7.2 % and for the maximum bending moments in the range of -10.3 % to 7.8 %.

Having found that with the head impact the repeatability alters as the limits are approached, additional tests were performed with an eighth vehicle which was believed to have a better performance. Tests on the eighth vehicle at LAB 2 resulted in total load being scattered in the range of -4.4% to 7.7% and bending moments in the range of -4.3% to 4.5%.

The reproducibility (Figure 4) between LAB 1 and LAB 2 was up to ± 7.8 % for both loads and moments. The total scattering for comparable test results from LAB 1 and LAB 2 was in the range of -16.5 % to 15.3 % for both, loads and moments.

Legform Tests

The tests were performed at three points across the front of the car. In accordance with the prescribed procedure, these were selected to provide the most severe conditions, and the centreline. Typically the bumper mounting, towing bracket, or front longitudinal provided the 'worst case' targets.

---

[*] Repeatability is calculated as the percentage of deviation of a single test from the average of the tests for an impact location at a single laboratory.

[**] Reproducibility is calculated as the percentage of deviation of the test lab average from the mean value of both test lab averages.

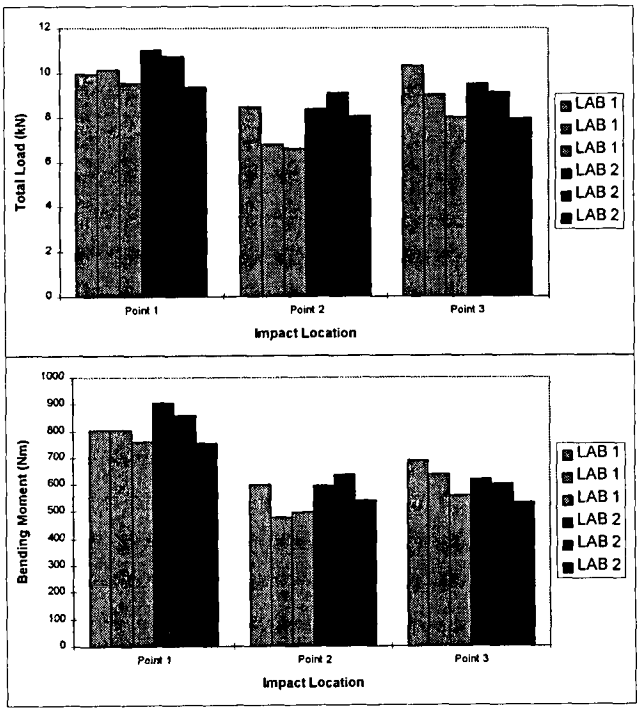

Figure 4. Repeatability and Reproducibility Results for Total Load in Upper Leg Impacts.

The summarised results for all vehicles are presented in Figure 5. It was seen that no vehicle met the EEVC Criteria for the legform completely. The tibia acceleration values exceeded the 150 g limit in 17 of the 21 cases. The peak bending angle limit of 15° was exceeded in all but two cases, one recording 14.8° at a location bolt, and another 11.3° at the corner of the mounting. 15 of the 21 tests had a bending angle peak value above 28.5°; the design maximum mechanical limit of the knee joint is around 30°, and all these results probably involve physical limits of the knee being reached; values could be higher if more articulation was possible.

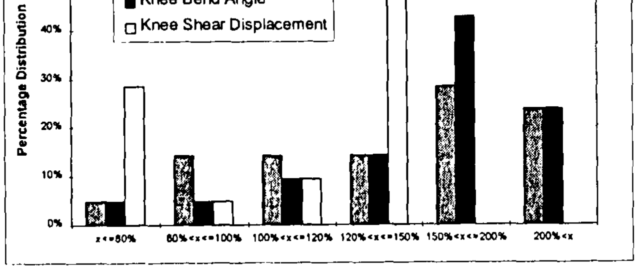

Figure 5. Percentage Distribution of Leg Injury Parameters Relative to the Proposed Limits.

In contrast, the peak shear displacement was satisfied in 6 cases, three on one vehicle, two on another. However, the highest twleve results all exceeded 7 mm displacement and were all most likely affected by the mechanical limit.

The result for any vehicle is dependent on shape, stiffness, and height of the major bumper elements and of the nearby structure above the bumper. The ligaments absorb little of the initial kinetic energy by bending meaning that both sections of the legform must be physically stopped by the vehicle structure in a controlled manner.

At LAB 1, a vehicle was selected for repeat tests at a reduced impact speed of 35 km/h in the expectation that the results would be less affected by the mechanical shear and bend limits. Even at these reduced speeds the bending mechanical limit was reached on each test and therefore repeatability data for knee bending cannot be calculated.

Repeatability tests at LAB 1 (based on two tests per point) gave ± 3.5 % for tibia acceleration and ± 12.7 % for knee shear. The same vehicle was used for repeatability tests (based on three tests per point) at LAB 2 and gave a range of 12.3 % to - 12.6 % for tibia acceleration and a range of 50 % to - 26 % for knee shear.

Similar to the upper leg testing, an eighth vehicle, which was believed to have a better performance, was tested at LAB 2. In all the tests on this vehicle the mechanical limits were not reached. For the tibia acceleration the repeatability was -11.1% to 10.8%, for knee bend it was -21.4% to 12.3%, and for knee shear it was -10.5% to 7.5%. Though these results are better, they are far from the level of repeatability one would expect from a legislative test requirement.

Reproducibility between the two laboratories (Figure 6.) is up to 15.7 % for tibia acceleration and up to 42 % for knee shear displacement. The overall range of scatter is 25.6 % to - 19.4 % for tibia acceleration and 79.8 % to - 46.1 % for knee shear displacement.

Additional Testing

Upper legform impact tests against a rigid plate at 4, 5, and 6 m/s gave an apparently linear relationship between impact speed and measured impact force. The relationship indicated that an impact generating the proposed force limit of 4 kN would require an impact speed of 4.48 m/s, and that the bending moment created due to compression of the foam would be 205 Nm. Though the impactor was created to encourage designs with greater radii of curvature, even with an infinite radius the inherent design of the impactor creates a bending moment close to the proposed criteria of 220 Nm, unless there is significant deformation.

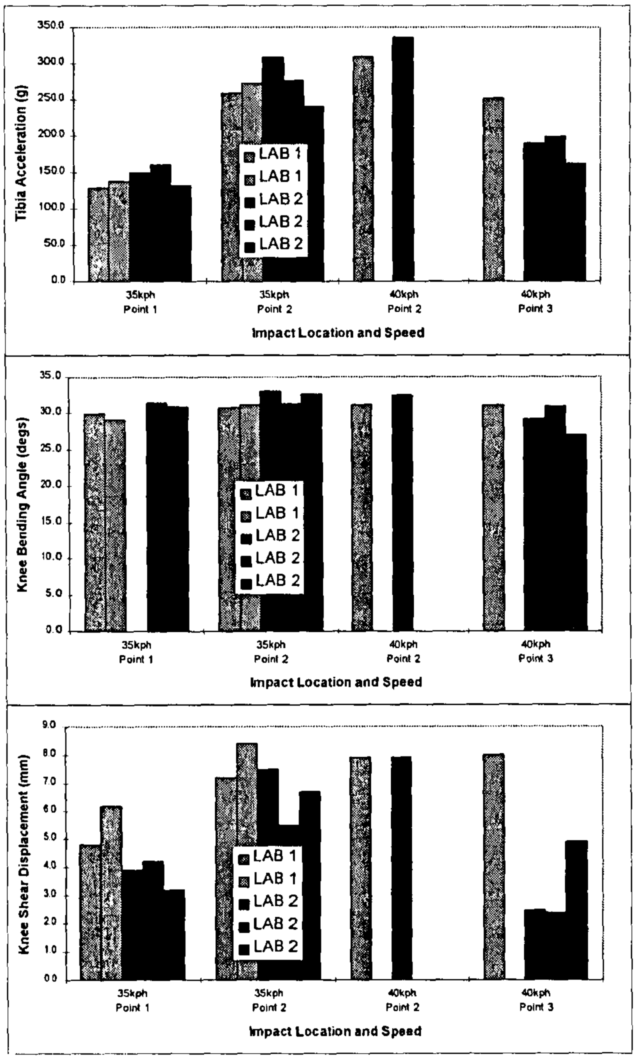

Figure 6. Repeatability and Reproducibility Results for Lower Leg Impact Tests

The geometry of some vehicles, particularly off-road vehicles, necessitates performing an upper legform impact and a child head impact at the same location. A mock-up vehicle front end was constructed using layers of foam with a covering of a single sheet of 0.7 mm thick steel such as would be able to achieve the upper legform criteria. An impact test with the upper legform was performed at the conditions typical of an off-road vehicle which has the maximum impact energy. The mock-up was very close to achieving upper legform compliance. But, when a child headform impact was performed a HIC of 1863 was calculated indicating that the two impact test requirements could be incompatible.

TEST EXPERIENCE AND COMMENTS

Headform Tests

The calibration corridor of 225 to 275 g for adult headform and 210 to 260 g for the child headform could cause large deviations on HIC. On the other hand, the measured deceleration of the headform appeared to be quite sensitive to the fixation of the skin and a variation in decelerations of 100 g were measured during the calibration procedure in one test house.

A minimum time between impacts, including the certification tests, should be established to ensure that the skin has fully recovered before the next test.

The impact velocity required is 11.1 m/s ± 0.5 m/s; the 0.5 m/s tolerance (equivalent to ± 9 % of energy) could cause large deviations in the HIC values; this will increase the amount of scattering in repeatability tests. It is proposed that this tolerance should be reduced.

Upper Legform Tests

A main problem was the abnormal bending of the main body of the impactor after only 50 impacts although the load cells never exceeded their maximum load limit of 18 kN.

The shape of some vehicle front ends caused the impactor to contact another point on the bonnet before contacting the target point. This caused the impactor to rotate upwards or downwards. The proposal does not ensure that the first point struck is always the target point.

The allowed velocity deviation of about ± 5 % could cause increased scattering in repeatability tests and should be reduced.

Pre-loading of the Confor™ foam caused by fitting the rubber skin could influence the results of the impactor. Further investigation of this phenomenon is required.

Legform Tests

Examination of traces showed that a vibration at about 80 Hz was present, and this is noticeable in the acceleration and shear outputs at about 5-10 g and 1 mm amplitude respectively. Relative to the proposed criteria this vibration would limit confidence in the repeatability of test results, and could change 'passes' into 'fails', or vice versa. Further modifications to the legform are being investigated at TRL to damp out the shear vibration, and so the results and any conclusions for this impactor have to be regarded as provisional.

Detailed analysis of the results is hampered by nearly all tests reaching the mechanical stops at an angle around 30° or a shear around 7.5 mm. Such tests will provide very little in terms of design guidance, as it changes the kinematics of the leg, and could render the acceleration result meaningless. The legform needs to be designed such that there is an increased overload capability without influencing the kinematics, particularly for the knee shear displacement, in order to be a valid vehicle development tool.

One repeatability test at 40 km/h suffered from breakage of the ligament retaining bolts after the maximum possible angle had been reached and excess energy remained, but this was late enough not to affect tibia 'g' values. The bolt problem has been encountered at TRL too, however in a vehicle which complies with the proposed requirements this problem should not reoccur.

In the repeat tests, the maximum shear displacements were sometimes positive, sometimes negative. The shape of the trace always followed a set pattern and the highest absolute value is used in the analysis of the results. There is still a very large variation in the absolute values for nominally identical tests. For shear displacements, the unpredictable change of peak time and direction between impacts indicates a potentially unrepeatable situation which is not a satisfactory basis for a legislative proposal.

The tibia accelerations can vary by 20 % for nominally identical conditions. It was noted later that there was a 10 mm difference in some bumper reference line positions between the two laboratories. If this was due to damage not apparent on visual inspection, it is likely that the performance could also be affected. A further study of repair/replacement conditions is required; visual inspection may not be adequate.

The legform was calibrated to the quasistatic procedures specified but not to the dynamic calibration requirements specified in the draft proposal as these were known to be invalid. The necessity for a dynamic test which recreates the vehicles impact conditions without reaching the mechanical limits is clear. Further, the requirements for re-calibration in the proposal also need clarification.

CONCLUSIONS

This extensive series of testing of vehicles representative of the European vehicle parc has indicated that most, if not all, vehicles would be severely affected by the introduction of the proposed pedestrian requirements. Though about a quarter of head impact locations achieved compliance there would be significant challenges in meeting the requirements for all impact locations. Upper leg and leg impact performance was far from achieving the proposed requirements and would involve major redesign and repackaging of vehicle front ends. It may be that conflicts will exist between the front end requirements to protect pedestrians and the other crashworthiness requirements for vehicle front ends.

The head impact test appears to be the most robust with acceptable repeatability and reproducibility in testing compliant locations. This is not the case for the upper leg impact test where the repeatability and reproducibility can be slightly larger than would be recommended as regulatory tool. Significant concerns must be expressed regarding the leg impact test where even tests that give acceptable results experienced unacceptably poor repeatability.

Some details of the proposed requirements need clarification or amendment, and some further investigation of the impactors is required. In particular, the impact speed tolerance should be reduced and the calibration requirements and methods reviewed. The legform impactor suffers from oscillations in it's shear displacement measurement which need to be damped. It is further limited as a development tool by the lack of overload designed into the knee shear with the mechanical limit being only around 1.5mm greater than the proposed requirement.

Designing vehicles to provide pedestrian protection is a further step towards reducing the fatalities and injuries on the road, however the tools and requirements used to guide the design of vehicles must be robust and repeatable to be used in a development environment.

ACKNOWLEDGEMENTS

ACEA TF.P members who contributed to this test programme are:

F Brun-Cassan (Pilot of TF.P), PSA
F Bauer, BMW
J Green, Rover
B Hallweger, BMW
P Massaia, Fiat
H Myrholt, Volvo
O Ries, VW
J Sameus, Volvo
A Thomas, Jaguar

REFERENCES

EEVC WG10, "Proposals for methods to evaluate pedestrian protection for passenger cars". Final Report. November 1994

EC DG III, "Draft proposal for a European Parliament and Council Directive relating to the protection of pedestrians and other road users in the event of a collision with a motor vehicle and amending Directive 70/156/EEC". February 1996

VALIDATION OF PEDESTRIAN UPPER LEGFORM IMPACT TEST - RECONSTRUCTION OF PEDESTRIAN ACCIDENTS

Yasuhiro Matsui
Hirotoshi Ishikawa
Japan Automobile Research Institute
Akira Sasaki
Japan Automobile Manufacturers Association, Incorporated
Japan

Paper Number 98-S10-O-05

ABSTRACT

EEVC/WG10 proposed three component pedestrian subsystem tests. Euro-NCAP pedestrian tests have been conducted according to these procedures. The results from Euro-NCAP indicate that the upper legform impact test has the most difficulty fulfilling the current injury criteria. However, the number of severe injuries from impact against the bonnet leading edge has been decreasing recently.

The objective of this research is to validate the test conditions and injury criteria of the EEVC upper legform impact test from accident analyses, impact tests with production cars and accident reconstruction tests.

The top four factors affecting the injury risk of the femur/pelvis were the bonnet leading edge height, the pedestrian age, the vehicle registration year, and the bumper lead. The fracture of lower leg also affected the significance of the upper leg injury.

The Weibull cumulative frequency curve was obtained as a biomechanical injury risk curve from accident reconstruction tests. At the 50 percentile injury risk level, 7.5 kN for impact force and 510 Nm for bending moment were obtained. The current injury criteria of 4 kN for impact force and 220 Nm for bending moment are too severe.

It is necessary to reconsider the injury criteria and test conditions of the EEVC pedestrian upper legform impact test.

INTRODUCTION

Pedestrians are vulnerable road users. Pedestrian casualties are still a major concern in traffic accident safety in European countries, the USA, Australia and Japan. European Experimental Vehicles Committee (EEVC), National Highway Traffic Safety Administration (NHTSA), International Standard Organization (ISO), and International Harmonized Research Activity (IHRA) have been conducting research to propose a pedestrian test procedure reflecting real-world pedestrian accidents.

The EEVC/WG10[1] proposed three component subsystem tests, the headform impact against the bonnet, the upper legform impact against the bonnet leading edge and the legform impact against the bumper, as shown in Figure 1.

Recently, pedestrian impact tests with production cars have been conducted in Euro-NCAP tests according to the current EEVC subsystem test method. The results from the Euro-NCAP tests indicate that none of the cars tested fulfills the current requirements of the three EEVC subsystem tests. The upper legform impact test seems to have the most difficulty fulfilling the requirement among the three tests. However, recent accident analyses indicate that the priority of the upper legform impact test seems to be the lowest in the three EEVC subsystem tests.

Accordingly, we conducted pedestrian accident analyses, impact tests with production cars and accident reconstruction tests to validate the EEVC upper legform impact test. This report summarizes the results of the accident analysis and the impact tests and proposes new injury criteria for the upper legform impact test.

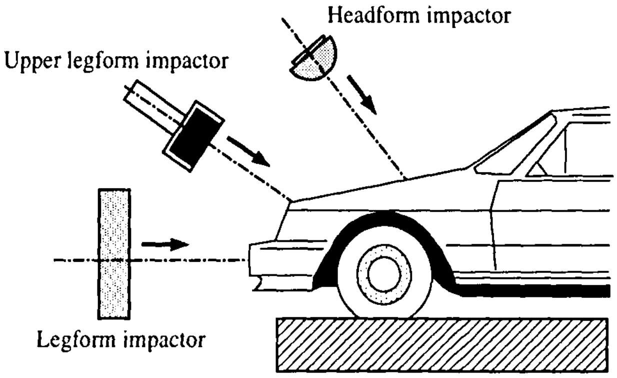

Figure 1. EEVC subsystem tests.

PEDESTRIAN ACCIDENT DATA ANALYSIS

Current Situation of Pedestrian Accident

Pedestrians are often involved in traffic accidents. In Japan in 1997, pedestrian fatalities (persons who died within 24 hours) represented 27 % (2,643 persons) of the total fatalities (9,640 persons) in traffic accidents(2).

In fatal pedestrian accidents the most severely injured parts of the body are the head/face/neck (64%) and the chest (12%); in nonfatal accidents they are the leg (40%) and the head/face/neck (32%), as shown in Figure 2.

In more than 50% of the fatal and nonfatal pedestrian accidents, pedestrians are hit by passenger cars(3). Constitution ratios of the body region with AIS 2+ have changed drastically during last ten years as shown in Figure 3. In particular, femur injuries decreased from 17% to 4% and knee injuries, from 10% to 1%. During the same period, chest injuries increased from 3% to 11% and lower leg injuries, from 19% to 36%.

Constitution ratios of car parts causing AIS 2+ injury have also changed during the last ten years as shown in Figure 4 in which others include front spoiler, license plate, and front grill. The ratio of the car parts, such as front bumper and others, related to the lower leg injuries increased from 45% to 55%. The ratio of the car parts, such as windshield, frame, and A pillar, related to head injuries also increased from 13% to 21%. In contrast, the ratio of the leading edge of bonnet and wing related to femur/pelvis injuries decreased from 17% to 8%. The ratio of top surface of bonnet and wing decreased from 26% to 16%.

When we consider the current situation of pedestrian accidents, the highest priority should be head protection followed by lower leg protection. The upper legform impact test related to the femur/pelvis injury is the lowest priority among the EEVC pedestrian subsystem tests.

In-depth Analysis on Femur/Pelvis Injuries

The JARI pedestrian accident data base was used to analyze femur/pelvis injuries caused by the leading edge of the bonnet or wing. The data base consists of 121 pedestrian accident cases from 1987 to 1988. A total of 54 cases with contact mark or residual deformation on the leading edge was selected. All pedestrians were adults (16 years and older) and children taller than 150 cm.

Injuries Selected

The selected 54 cases consisted of 30% for AIS 2+, 35% for AIS 1 and 35% for no injury as shown in Figure 5. For AIS 2+ injury, 81 % of the cases involved femur, pelvis or lumbar vertebra fractures as shown in Table 1.

Cumulative frequencies of the impact velocity were obtained for the two different injury severities as shown in Figure 6. There is no significant difference between the two curves. The difference is only 5 km/h at the 50 percentile. The impact velocity does not seem to be major factor in causing femur/pelvis injuries.

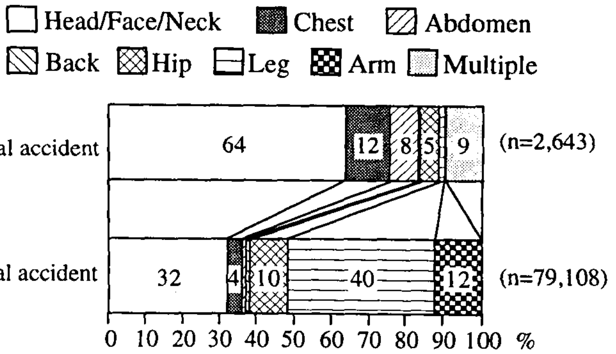

Figure 2. Body regions with most severely injured. (1997 in Japan (2))

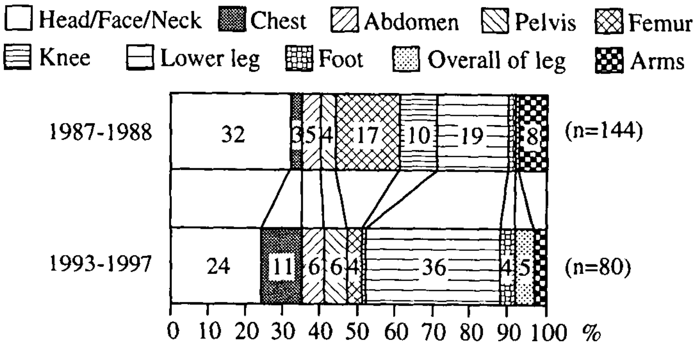

Figure 3. Body regions with AIS 2+ injury in passenger car (4).

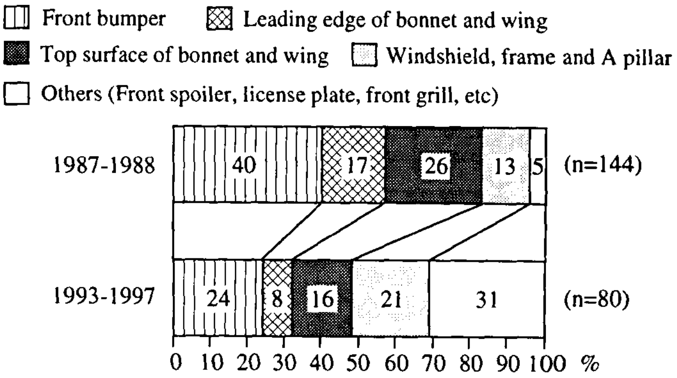

Figure 4. Car parts causing AIS 2+ injury (4).

Influence of Vehicle

The contact locations of the leading edge of bonnet and wing are divided into five areas as shown in Figure 7. Pedestrians tend to impact at the front left side (18 cases) rather than at the front right side (12 cases) as shown in

Figure 8. Note that in Japan vehicles run on the left side and drivers sit on the right side. This results may be opposite in most of the European countries and the USA.

The possibility of contacting the leading edge of the wing was relatively high in spite of its small area.

Accident cases with AIS 2+ distributions of the contact location were similar to the previous results as shown in Figure 9.

The risk of severe injuries of AIS 2+ was higher in the area of the wing (A) than in the bonnet area (B and C) as shown in Figure 10.

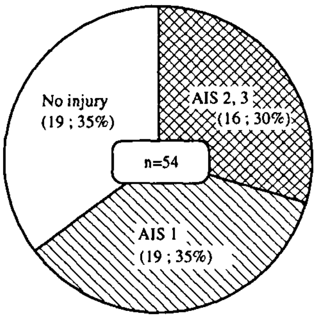

Figure 5. Constitution ratio of injuries caused by leading edge of bonnet or wing.

Table 1.
Description of AIS 2+ Injuries for Femur/pelvis

Injury (n=16)		case	%
Fracture of	Femur and pelvis	2	13
	Femur	5	31
	Pelvis	4	25
	Pelvis with abdominal injury	1	6
	Lumbar vertebra	1	6
Abdominal injury		3	19

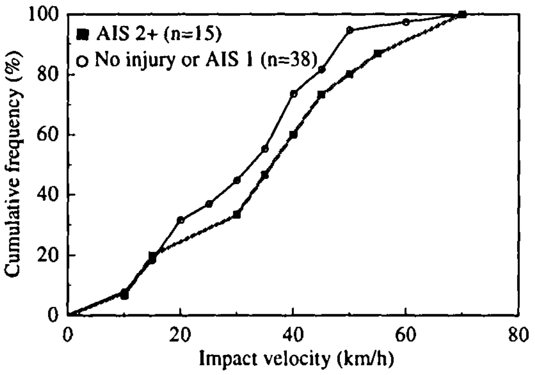

Figure 6. Cumulative frequency of impact velocity.

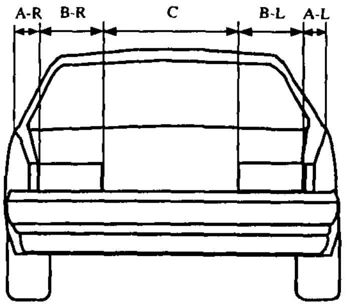

Figure 7. Definition of contact locations.

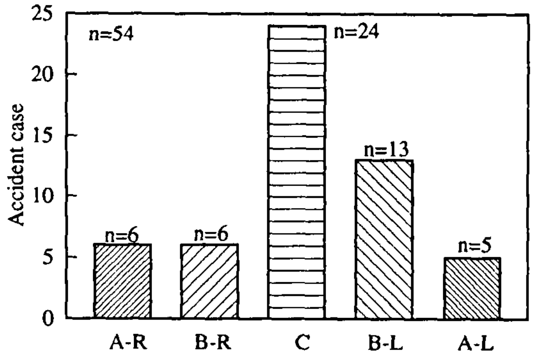

Figure 8. Distribution of pedestrian contact.

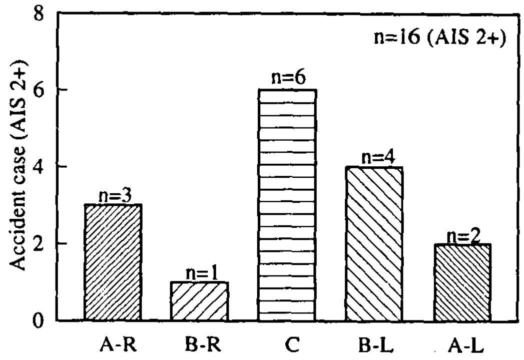

Figure 9. Distribution of pedestrian contact with AIS 2+ injury.

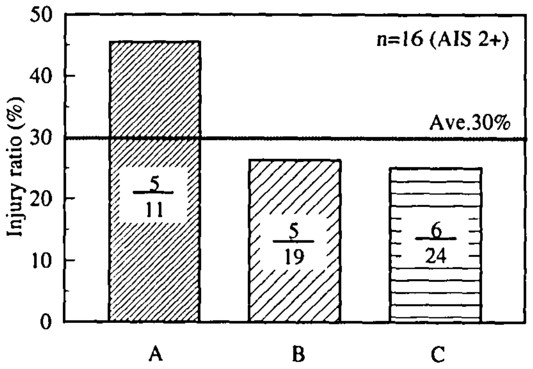

Figure 10. Injury ratio of AIS 2+ by contact location.

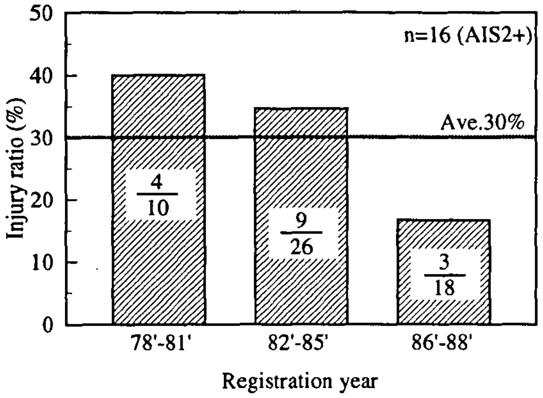

Figure 11. Injury ratio of AIS 2+ by vehicle registered year.

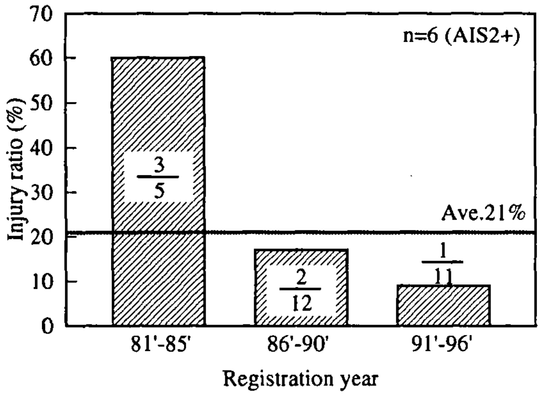

Figure 12. Injury ratio of AIS 2+ by vehicle registered year referred from ITARDA data [5].

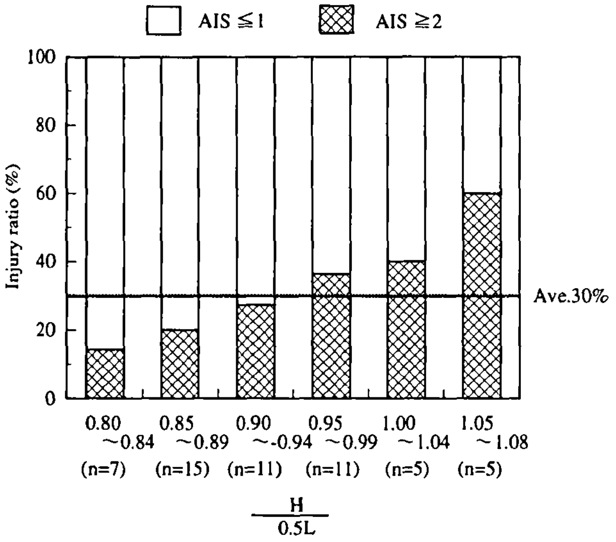

Figure 13. Injury ratio versus normalized bonnet leading edge height.

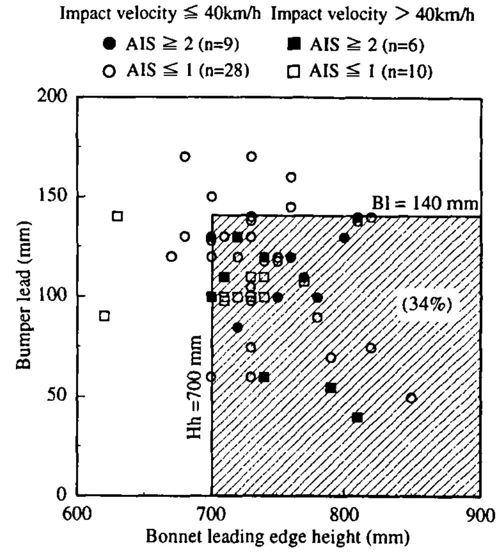

( ) : Injury ratio of AIS 2+

Figure 14. Distributions of all injuries by bonnet leading edge height and bumper lead.

Older vehicles had a higher risk of AIS 2+ compared to newer vehicles as shown in Figure 11. The registration year is almost comparable to model year.

When we referred to the latest pedestrian accident data [5], new model indicated a lower risk of AIS 2+ as shown in Figure 12.

For majority of adult pedestrians, the impact of the bonnet leading edge will be directly on the femur [6]. The effective height of the bonnet leading edge or wing may differ according to the pedestrian height. Consequently the injury risk by the normalized bonnet leading edge height (H / 0.5L) was obtained as shown in Figure 13. The normalized height was the ratio of the bonnet leading edge height (H) to the pedestrian hip joint height (0.5L). The hip joint height was assumed to be 50 % of the pedestrian stature (L). The injury ratio of AIS 2+ increased with the increase of the normalized bonnet leading edge height.

Distributions of All Injuries

The impact condition of the upper legform impact test are dependent on the bonnet leading edge height and the bumper lead. Figure 14 shows the distributions of all injuries by the bonnet leading edge height and the bumper lead. AIS 2+ injuries were located within the area of over 700 mm of the bonnet leading edge height and less than 140 mm of the bumper lead.

The normalized bonnet leading edge height (H / 0.5L) and the bumper lead affected the injury ratio of AIS 2+ as shown in Figure 15. The injury ratio was highest in the area of over 0.92 of the normalized bonnet leading edge height and less than 115 mm of the bumper lead. Each boundary line was determined considering about 50 percentile.

The pedestrian age and the vehicle registration year

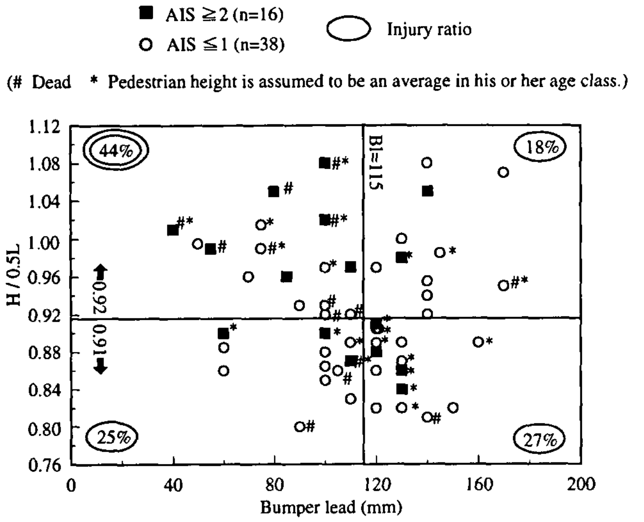

Figure 15. Distributions of all injuries by normalized bonnet leading edge height and bumper lead.

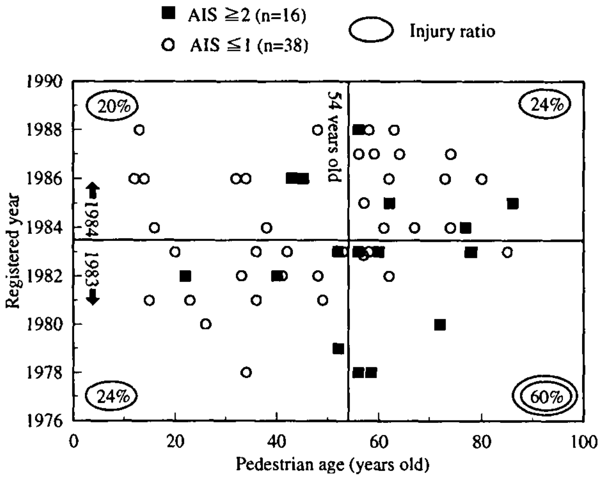

Figure 16. Distributions of all injuries by vehicle registration year and pedestrian age.

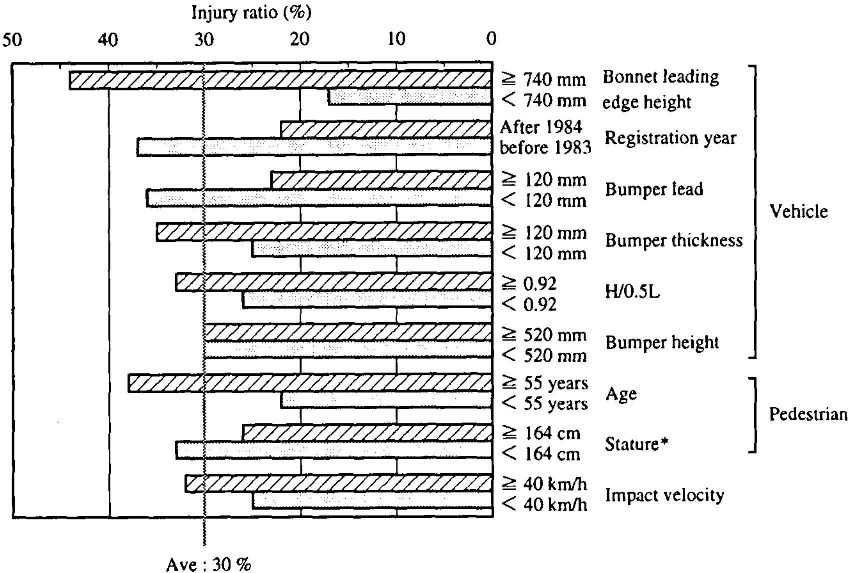

∴ Specific values are defined by considering the cumulative frequency of about 50 percentile.
* : 39 % of pedestrian stature is assumed to be an average in his or her age group.

Figure 17. Injury ratio by vehicle and pedestrian parameters.

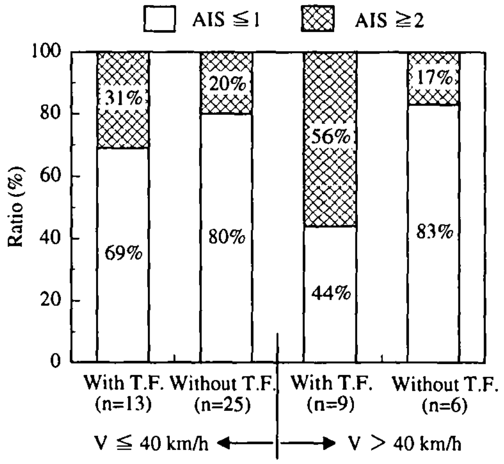

∴ T.F. : Tibia/fibula fracture

Figure 18. Constitution of femur/pelvis injury.

affected the injury ratio of AIS 2+ as shown in Figure 16. The injury ratio was highest for persons more than 54 years old and vehicles registered before 1983. The each boundary line was about 50 percentile.

The vehicle and pedestrian factors affecting the injury ratio of AIS 2+ are summarized in Figure 17. The top four factors affecting the injury risk of femur and pelvis were the bonnet leading edge height, the pedestrian age, the vehicle registration year and the bumper lead. The test condition of the upper legform impact test is determined from the bonnet leading edge height and bumper lead only. There seems to be other important factors to be considered in determining the test condition.

Influence of Lower Leg Fracture

In order to understand the influence of existence of tibia/fibula fractures on the injury severity of femur/pelvis, we conducted the following analyses.

For the two impact velocity groups and the two lower leg severity groups, the injury ratio of AIS 2+ femur/pelvis injury was obtained as shown in Figure 18. The severity of the upper leg injury has something to do with the severity of the lower leg injury. The upper leg injury severity may decrease if there is no fracture in the lower leg. This means that a pedestrian-friendly bumper could reduce the upper leg injuries.

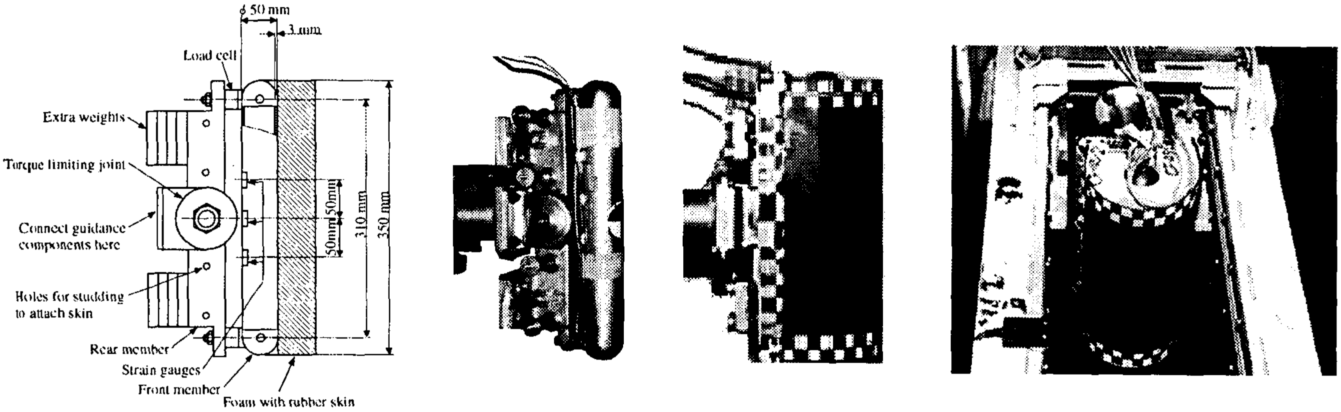
ϕ 50 mm
3 mm
Load cell
Extra weights
Torque limiting joint
Connect guidance components here
Holes for studding to attach skin
Rear member
Strain gauges
Front member
Foam with rubber skin
50mm
50mm
310 mm
350 mm

Schematic **Side view** **Covered foam and skin** **Installed on propulsion system**

Figure 19. Upper legform impactor.

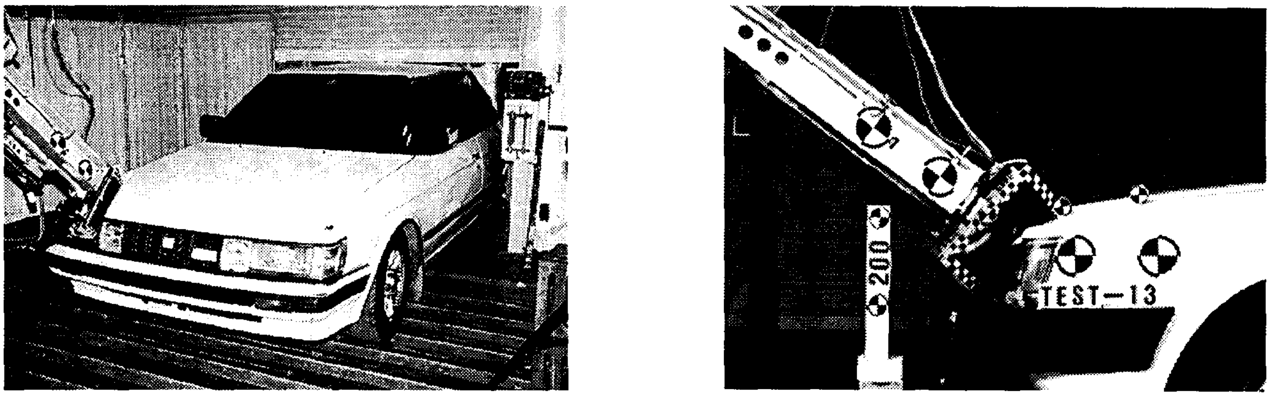

Figure 20. Upper legform to bonnet leading edge test.

EEVC UPPER LEGFORM IMPACT TEST

Pedestrian impact tests with production cars have been conducted according to the current EEVC method of the upper legform impact test in order to understand the reliability of this test procedure.

Methodology

EEVC/WG10 proposed a subsystem upper legform impact test method(1)(7)(8). The aim of the upper legform to bonnet leading edge test is to evaluate the aggressiveness of the leading edge of the bonnet in causing femur/pelvis fractures.

Figure 19 shows the impactor developed by TRL. The impactor consists of a foam covered tube with three strain gauges (front member) and two load cells in between the front member and the rear member. Figure 20 shows the upper legform impact test. The vehicle with two 75 kg occupants is used to represent an impact at 40 km/h. The bonnet leading edge reference line is defined as shown in Figure 21. Figure 22 shows the impact condition. The impact velocity and the impact angle are determined with reference to Figures 23 and 24. The impactor mass (M) is calculated from Equation (1) with the impact velocity (V) and the energy (E). The energy is derived from Figure 25.

$$M = \frac{2E}{V^2} \qquad (1)$$

The upper legform impactor has been modified recently by TRL as shown in Figure 26. The initial design (type A) had inner and outer foam components (③ , ④) and screws ⑦ intruding directly into the foam components. The type A caused a problem in measuring the impact force. The problem was considered to be an interaction between the foam components and screws. TRL then modified the type A and developed type B in which adapters ⑨ are inserted to prevent the interaction between the screws and the foam components. However, we found the type B still presents a problem in measuring the impact force.

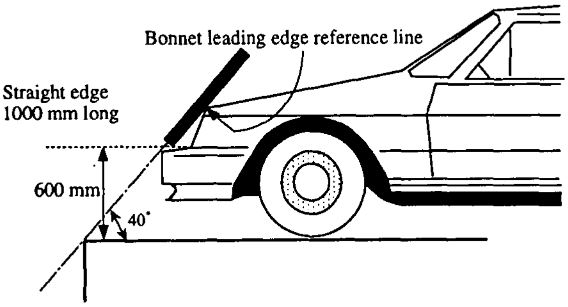

Figure 21. Bonnet leading edge reference line.

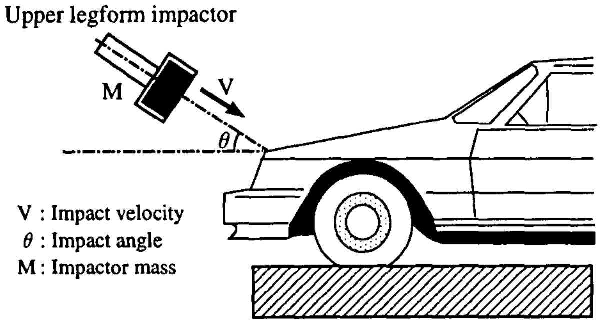

V : Impact velocity
θ : Impact angle
M : Impactor mass

Figure 22. Impact condition.

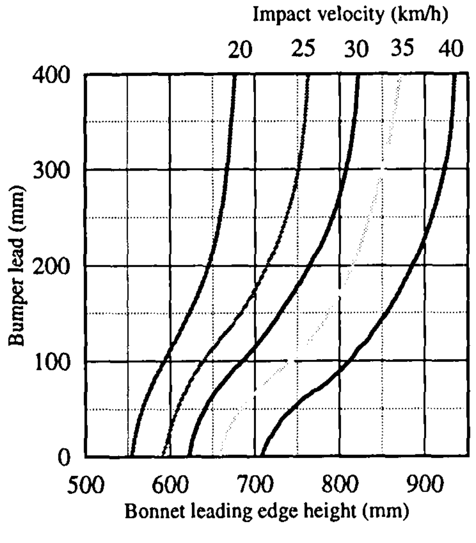

Notes:

1. Interpolate horizontally between curves.
2. With configurations below 20km/h - test at 20km/h.
3. With configurations above 40km/h - test at 40km/h.
4. With negative bumper leads - test as for zero bumper lead.
5. With bumper leads above 400 mm - test as for 400mm.

Figure 23. Impact velocity with respect to vehicle shape.

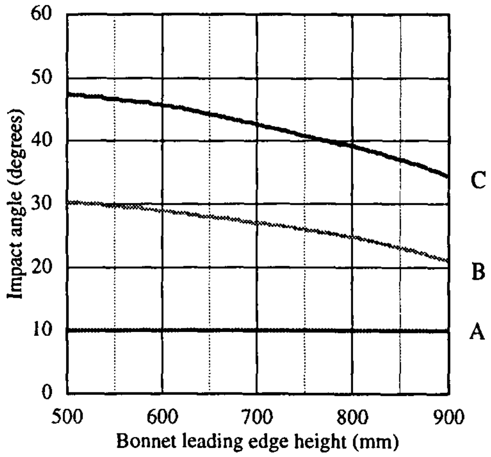

A ≦ 0 mm bumper lead
B = 50 mm bumper lead
C ≧ 150 mm bumper lead

Notes:

1. Interpolate horizontally between curves.
2. With negative bumper leads - test as for zero bumper lead.
3. With bumper leads above 150 mm - test as for 150mm.
4. With bonnet heights above 900 mm - test as for 900mm.

Figure 24. Impact angle with respect to vehicle shape.

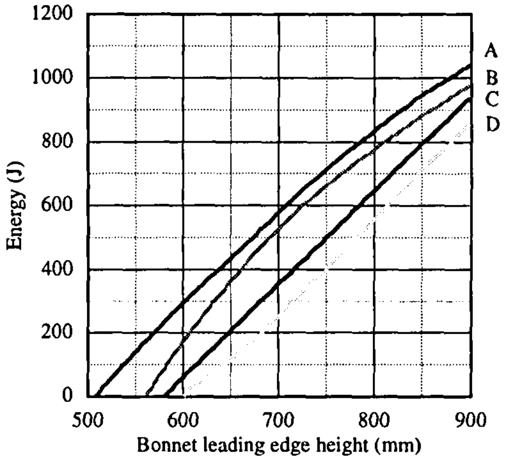

A ≦ 0 mm bumper lead
B = 100 mm bumper lead
C = 225 mm bumper lead
D ≧ 350 mm bumper lead

Notes:

1. Interpolate horizontally between curves.
2. With negative bumper leads - test as for zero bumper lead.
3. With bumper leads above 350 mm - test as for 350mm.
4. With bonnet heights above 900 mm - test as for 900mm.

Figure 25. Impact energy with respect to vehicle shape.

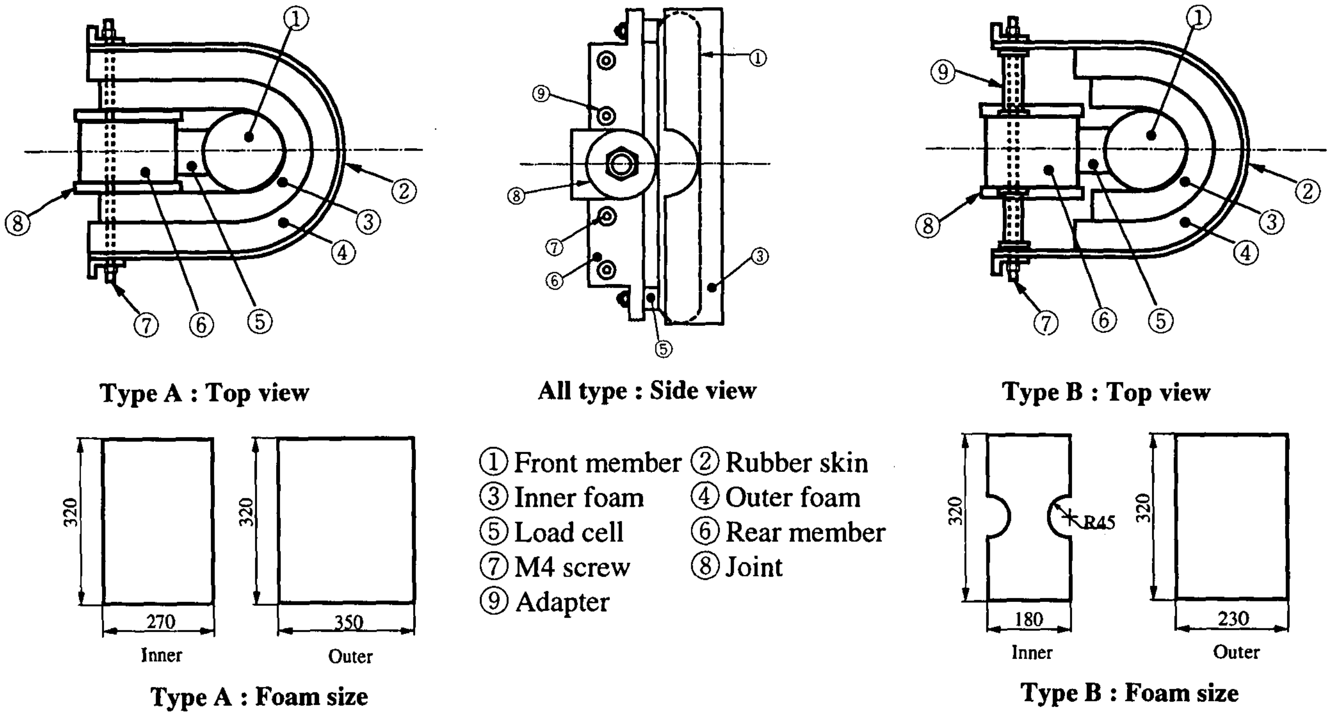

Type A : Top view

All type : Side view

Type B : Top view

① Front member ② Rubber skin
③ Inner foam ④ Outer foam
⑤ Load cell ⑥ Rear member
⑦ M4 screw ⑧ Joint
⑨ Adapter

Type A : Foam size

Type B : Foam size

Figure 26. Modification of upper legform impactor.

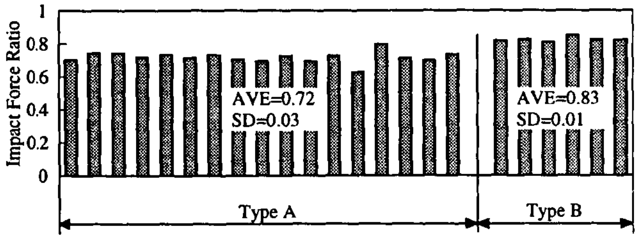

Figure 27. Impact force ratio in EEVC upper legform impact tests.

In measuring the impact force, load cells were recommended to be Kistler type 9021A piezo-electric [9]. Figure 27 shows the ratio of the peak impact force from the load cell to the inertia force calculated by the rear member mass and its acceleration. Theoretically the impact force ratio should be one. However the type A and type B do not reach the ratio of one. We use strain gauge load cells in order to improve the accuracy in measuring the impact force.

Test Results Using Production Cars

We conducted the upper legform impact test using 15 production cars. The current injury criteria is a total force of 4 kN and a bending moment of 220 Nm. Figure 28 shows the results from 19 tests comparing to the injury criteria. None of the test results met the requirement.

When we review the pedestrian accident data, the number of severe femur/pelvis injuries caused by the bonnet leading edge is smaller than that of other severe injuries caused by the bonnet or bumper. In contrast, the results from the three EEVC component tests with production cars indicated that the upper legform impact test had the most difficulty fulfilling the requirements of the current injury criteria. When we consider the priority of the pedestrian test procedure, the upper legform impact test should be the lowest

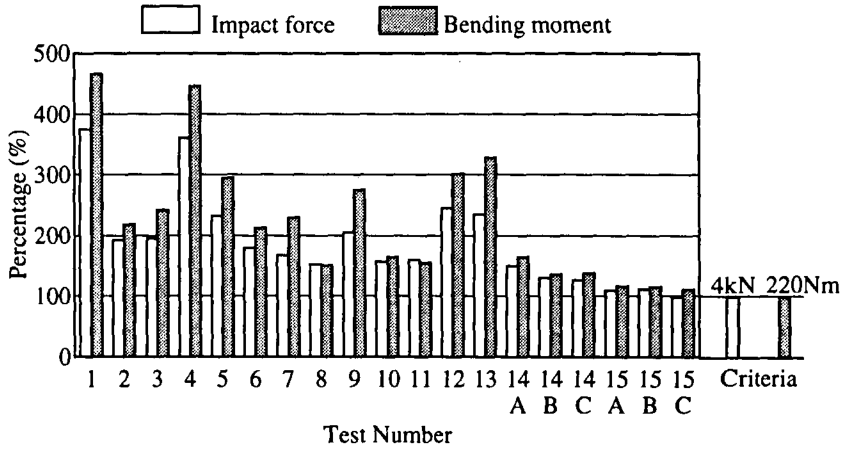

Figure 28. Results of EEVC upper legform impact tests.

among the three subsystem tests. The current injury criteria of the upper legform impact test does not reflect real world-pedestrian accidents. The current injury criteria were derived from the three accident reconstruction tests for AIS 3 cases by TRL(6).

Accordingly, we conducted accident reconstruction tests to validate the EEVC upper legform impact test and its injury criteria.

ACCIDENT RECONSTRUCTION TEST

The objective of this test is to validate the current injury criteria of the upper legform impact test proposed by EEVC/WG10(8). Using the upper legform impactor we reconstructed the vehicle damage and physical values related to pedestrian injuries induced by the leading edge of bonnet or wing.

Accident Data Selected

We selected 16 accident cases in which pedestrians were adults and a child with 150 cm stature from the JARI pedestrian accident data base. Table 2 lists the selected accident cases. The vehicle impact velocity is 40 ± 10 km/h for 15 cases and 25 km/h for 1 case. To evaluate physical value of different injury severities, AIS 2+ injury cases (6 cases) and no injury or AIS 1 injury cases (10 cases) were selected. The definition of injured part is shown in Figure 29.

Table 2.
Selected Accident Cases

Case	Car							Pedestrian						
	Impact velocity (km/h)	Model year	Frontal shape			Hoodedge damage		Sex	Age	Stature (cm)	Weight (kg)	Impact direction***	Injury of upper leg	
			B/L (mm)	Bh (mm)	H (mm)	Damage location*	凹 (mm)						AIS	Injury description
1	40	1983	85	570	780	B-L	0	F	78	-	-	F	3	Femur fracture
2	50	1985	30	560	810	A-R	5	M	62	-	-	L	3	Femur fracture
3	35	1982	120	510	770	C	20	M	22	168	58	L	2	Kidney damage
4	30	1979	130	480	800	C	50	M	52	-	-	R	2	Pelvic fracture
5	40	1986	155	490	705	C	20	F	80	-	-	L	1	Thigh contusion
6	25	1983	110	500	700	C	5	F	20	163	45	R	1	Thigh contusion
7	30	1983	140	520	730	A-L	10	M	58	158	52	B	1	Waist contusion
8	45	1982	105	525	690	B-L	30	M	33	160	63	F	1	Thigh contusion
9	30	1986	110	501	733	C	15	F	12	150	43	L	1	Waist contusion
10	35	1984	104	495	695	A-L	10	F	77	150	50	L	3 2	Femur fracture Pelvic fracture
11	35	1987	98	510	701	C	7	M	59	170	80	L	0	No injury
12	40	1984	160	492	759	C	10	M	38	175	70	R	0	No injury
13	40	1984	135	470	680	C	5	F	16	-	-	B	0	No injury
14	40	1986	113	506	734	B-L	10**	M	56	-	-	R	0	No injury
15	45	1986	146	444	657	B-L	10	M	45	-	-	L	2	Pelvic fracture
16	45	1984	114	498	698	C	10	F	67	-	-	B	0	No injury

* : See Figure 7.
** : The residual deformation is estimated from photograph.
*** : F ; Front, B ; Back, R ; Right, L ; Left

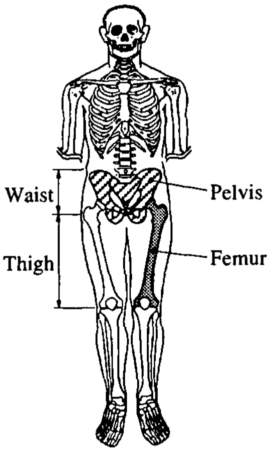

Figure 29. Definition of injury part.

Methodology

Two methods were used to conduct the reconstruction tests. One was essentially based on the EEVC (EEVC method) and the other, on the computer simulation (Simulation method).

In the EEVC method, the impact angle, impactor mass, and impact velocity were derived from the look-up graphs (See Figures 23, 24 and 25) according to the bonnet leading edge height and the bumper lead. When the accident impact speed was not 40 km/h, the impact velocity was compensated considering the speed ratio of the reported accident impact speed to 40 km/h.

In the Simulation method, the impact conditions were calculated using a validated car-pedestrian impact model (10). The impact angle was calculated from the impact force vector when the impact force became maximum. The impact velocity was the relative velocity between the pedestrian and vehicle when they start to contact. Impact energy was obtained by integrating the impact force by the displacement of femur/pelvis until the impact force became maximum. The impactor mass can be calculated from the impact velocity and the impact energy by means of Equation (1). However, the impactor mass was fixed to be 20 kg in some test cases in order to understand the influence of impactor mass onto the physical values to be measured. In these cases, the impact velocity from the computer simulation was not used, and the impact velocity was adjusted by considering the mass ratio of the impactor under the given impact energy.

We conducted phase 1 reconstruction tests (accident cases 1 to 8) and phase 2 reconstruction tests (accident cases 9 to 16). In the phase 1 tests, only the EEVC method was used. In the phase 2 tests, both the EEVC method and the Simulation methods were used. A new bonnet was used in each test.

Results

A total of 12 accident cases was successfully reconstructed, but four cases were not. Table 3 summarizes the test conditions and results of all our reconstruction tests (32 tests). Typical cases in which there was good agreement, acceptable agreement, or disagreement are shown in Appendix A.

Using the EEVC method, only five out of 16 accident cases (31%) were reconstructed with good agreement as shown in Table 3. Case number 9 to 16 were reconstructed according to the EEVC and Simulation methods. By using the Simulation method, we reconstructed four out of 8 accident cases (50%) with good agreement. The EEVC upper legform impact test method still seems to be incomplete and needs further improvement to reflect real-world pedestrian accidents.

Through the reconstruction tests using the fixed impactor mass of 20 kg, we found that the impact energy was most important to reproduce the damage pattern of vehicle with the upper legform impactor. Impactor mass can be fixed. Impact velocity can be defined from the impact energy and the constant impactor mass without using an impact velocity look-up graph.

In order to understand the relationship between measured physical values and injury severity, 12 test cases or the best cases are selected from the accident reconstruction tests as shown in Table 4. Six cases are for AIS 2+, one case for AIS 1, and five cases for no injury.

To clarify the current injury criteria (4 kN, 220 Nm) relative to the injury severity, we plotted measured impact forces and bending moments with injury severity as shown in Figure 30. The test results clearly indicate that the current injury criteria means a 0 % possibility causing AIS 2+ injuries.

Figures 31 shows the cumulative frequency of impact forces and bending moments for two different injury severities (AIS 2+ and no injury or AIS 1). It should be noted that the measured impact forces and bending moments in AIS 2+ injuries are lower than those in no injury or AIS 1 injuries because a femur/pelvis fracture may affect the impact forces and bending moments. A femur/pelvis fracture mechanism was not incorporated when designing the upper legform impactor.

Table 5 summarizes the impact forces and the bending moments, in which some reference values are listed for minimum, maximum, average ± standard deviation, 20 percentile and 50 percentile. The EEVC current injury criteria were derived from an average value for AIS 3 accident cases (6). The average impact forces and bending moments in AIS 2+ injuries are about twice as high as the current injury criteria.

Table 3.
Test Conditions and Results (32 Tests for 16 Accident Cases)

Accident			Reconstruction test										
	Car		Conditions					Results					Agreement
Case	Impact velocity (km/h)	[ll] (mm)	Ped.-car impact vel.** (km/h)	Upper legform impactor Velocity (km/h)	Angle (degree)	Energy (J)	Mass (kg)	Hoodedge damage [ll](mm)	Force (kN)	Bending moment Upper (Nm)	Middle (Nm)	Lower (Nm)	of the hoodedge damage****
1	40	0	25 [E]	20.8 {23.1}	29.5	232	13.9	1	7.4	386	542	525	○+
			40 [E]	38.3 {36.9}	29.5	787	13.9	20	14.4	741	981	916	×
2	50	5	20 [E]	19.1 {20.0}	18.0	187	13.3	5	5.2	333	395	375	○+
			25 [E]	24.4 {25.0}	18.0	305	13.3	11	6.9	479	545	459	△
			35 [E]	35.3 {35.0}	18.0	639	13.3	27	10.1	558	722	672	×
			40 [E]	40.1 {40.0}	18.0	825	13.3	35	15.0	849	1026	915	×
3	35	20	40 [E]	35.3 {35.5}	29.5	663	13.8	20	8.2	473	605	556	○+
4	30	50	40 [E]	38.0 {36.9}	35.0	774	13.9	36	7.7	479	467	321	△+
			35 [E]	32.9 {32.3}	35.0	580	13.9	32	6.8	456	455	309	△
5	40	20	40 [E]	25.9 {26.7}	41.5	424	16.4	21	6.8	348	384	311	×
			40 [E]	25.7 {26.7}	41.5	418	16.4	20	6.3	304	363	309	×
6	25	5	40 [E]	30.8 {30.5}	35.5	509	13.9	20	6.1	307	331	269	×
7	30	10	40 [E]	31.1 {30.5}	39.5	560	15.0	45	9.3	537	650	536	×
8	45	30	40 [E]	31.1 {30.5}	35.0	489	13.1	20	6.7	382	505	471	×
9	30	15	30 [S]	23.8 {23.4}	10.6	437	20.0	15	7.4	366	444	396	○+
			30 [E]	25.8 {24.9}	34.7	475	18.5	10	8.4	457	546	486	×
10	35	10	30 [S]	22.1 {21.2}	19.9	377	20.0	13	9.4	418	560	556	○+
			25 [S]	17.5 {17.7}	16.8***	236	20.0	11	5.8	213	278	286	△
			35 [E]	25.3 {26.7}	35.0	388	15.7	15	9.4	534	618	530	△
11	35	7	35 [E]	28.5 {27.6}	33.9	486	15.5	10	9.4	550	662	588	○+
			35 [S]	25.5 {26.8}	17.3	502	20.0	9	10.9	509	674	654	△
12	40	10	35 [S]	27.1 {27.5}	35.6	567	20.0	10	10.2	561	677	595	○+
			40 [E]	29.4 {31.8}	39.8	504	15.1	9	9.8	566	663	569	○
13	40	5	30 [S]	20.2 {18.9}	54.2	231	14.7	7	5.1	265	306	263	○+
			40 [E]	26.9 {26.0}	40.3	433	15.5	13	6.4	286	341	311	×
14	40	10*	40 [E]	31.1 {33.1}	35.1	520	13.9	9	9.4	567	721	672	△+
			30 [S]	23.0 {23.67}	14.2	408	20.0	5	10.8	515	698	679	×
15	45	10	45 [E]	26.3 {25.9}	42.7	363	13.6	13	6.6	326	429	404	△+
			45 [E]	28.4 {25.9}	42.7	423	13.6	13	6.3	334	438	412	△
			50 [S]	30.0 {30.9}	29.5	358	10.3	6	6.3	258	369	378	×
16	45	10	45 [E]	33.0 {33.7}	36.4	529	12.6	12	7.7	371	445	400	△+
			40 [S]	25.9 {24.0}	62.8	518	20.0	25	6.6	321	334	265	△

* : The residual deformation is estimated from photograph.

** : [E] ; EEVC method, [S] ; Simulation method.

*** : The impact angle should be 24.3 °.

**** : ○ ; Good agreement, △ ; Acceptable agreement, × ; Disagreement.

: + ; Best case in the accident reconstructions.

Table 4.
Summary of Accident Reconstruction Tests (12 Accident Cases)

#	Case	Pedestrian						Car				Reconstruction test results					Agreement of the hoodedge damage
		Injury induced by hoodedge		Sex	Age	Height, L (cm)	Weight (kg)	Impact velocity (km/h)	Frontal shape			Ped. - car impact velocity (km/h)	Force (kN)	Bending moment			
		AIS	Injury description						B/L (mm)	Bh (mm)	H (mm)			Upper (Nm)	Middle (Nm)	Lower (Nm)	
1	1	3	Femur fracture	F	78	-	-	40	85	570	780	25 [E]	7.4	386	542	525	○
2	2	3	Femur fracture	M	62	-	-	50	30	560	810	20 [E]	5.2	333	395	375	○
3	10	3	Femur / pelvic fracture	F	77	150	50	35	104	495	695	30 [S]	9.4	418	560	556	○
4	3	2	Kidney damage	M	22	168	58	35	120	510	770	40 [E]	8.2	473	605	556	○
5	4	2	Pelvic fracture	M	52	-	-	30	130	480	800	40 [E]	7.7	479	467	321	△
6	15	2	Pelvic fracture	M	45	-	-	45	146	444	657	45 [E]	6.6	326	429	404	△
7	9	1	Waist contusion	F	12	150	43	30	110	501	733	30 [S]	7.4	366	444	396	○
8	11	0	No injury	M	59	170	80	35	98	510	701	35 [E]	9.4	550	662	588	○
9	12	0	No injury	M	38	175	70	40	160	492	759	35 [S]	10.2	561	677	595	○
10	13	0	No injury	F	16	-	-	40	135	470	680	30 [S]	5.1	265	306	263	○
11	14	0	No injury	M	56	-	-	40	113	506	734	40 [E]	9.4	567	721	672	△
12	16	0	No injury	F	67	-	-	45	114	498	698	45 [E]	7.7	371	445	400	△

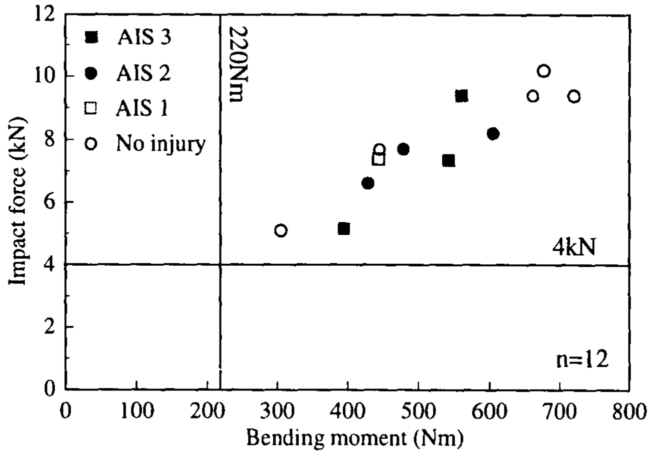

Figure 30. Impact force and bending moment with injury severity from accident reconstructions.

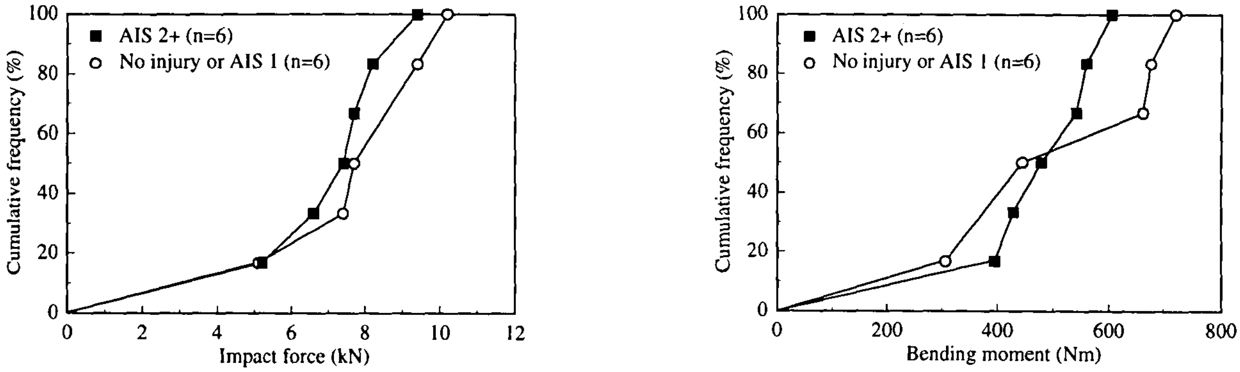

(1) Impact force (2) Bending moment

Figure 31. Cumulative frequency of physical value.

Table 5.
Summary of Impact Force and Bending Moment (12 Accident Cases)

Injury severity	cases	Measured impact force (kN)				
		Min.	Max.	Ave. ±SD	20 percentile	50 percentile
AIS 2+	6	5.2	9.4	7.4 ±1.3	5.5	7.4
No injury and AIS 1	6	5.1	10.2	8.2 ±1.7	5.6	7.7
Injury severity	cases	Measured bending moment (Nm)				
		Min.	Max.	Ave.	20 percentile	50 percentile
AIS 2+	6	395	605	502 ±74	402	479
No injury and AIS 1	6	306	721	543 ±152	334	445

∴ 20 percentile and 50 percentile are obtained from the cumulative frequency curve (Figures 47 and 48).

DISCUSSION

The impact force and the bending moment related to each AIS level may also be presented as an injury risk curve as shown in Figure 32. The solid lines are on the average values in each AIS level. These lines show that the impact force and the bending moment tend to decrease with the increase of AIS. The measured impact forces and bending moments did not correlate to the significance of AIS severity (See Appendix B).

On the contrary, in case of the head injury criteria (HIC), HIC values increase according to the significance of AIS severity (11). If the upper legform impact test is appropriate to reconstruct the femur/pelvis injuries, the measured impact force and bending moment could increase with the increase of AIS.

This contradiction may raise questions of whether the current upper legform impact test reflects the real world pedestrian accidents.

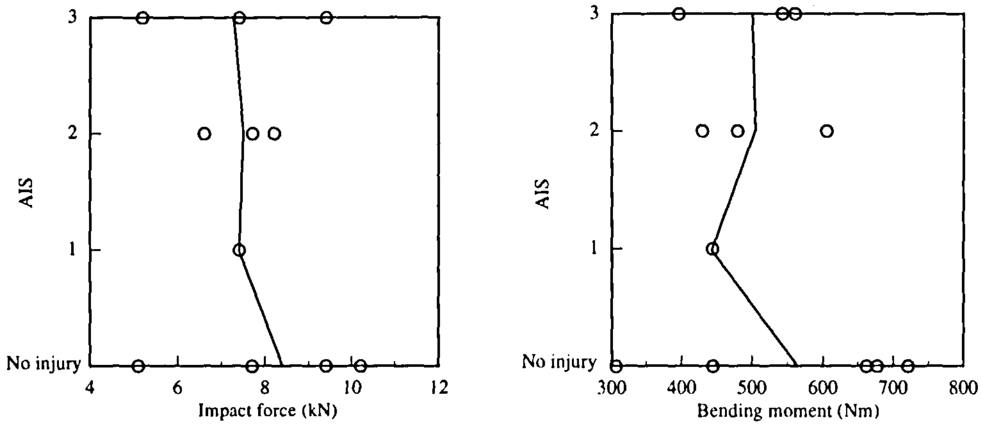

(1) Impact force **(2) Bending moment**

Figure 32. Physical value versus injury severity.

A biomechanical injury risk curve describing the relationship between the injury level and its corresponding physical value is necessary to propose the injury criteria for the upper legform impact test. To establish the injury criteria for femur/pelvis AIS 2+ injuries, we made a Weibull cumulative frequency curve from the accident reconstruction tests as shown in Figure 33. The Weibull curve with one variable and three parameters is defined as follows;

$$W(z;\alpha,\beta,\gamma) = 1 - e^{-\left(\frac{z-\gamma}{\alpha}\right)^{\beta}} \quad (2)$$

Where
Z is independent variable,
α is the scale parameter,
β is the shape parameter, and
γ is the location parameter.

The scale and shape parameters were chosen based on the impact force and bending moment causing the AIS 2+ injury. The location parameter was decided to be 4 kN and 220 Nm with 0 % probability of causing an AIS 2+ injury (See Figure 30).

Head Injury Criteria (HIC) 1000 means about a 20 % probability of death (12). A femur/pelvis fracture is not commonly a life threatening injury. Accordingly, the probability of the femur/pelvis AIS 2+ injury can be raised to 50 %. For a 50 % femur/pelvis injury risk with AIS 2+, the impact force is 7.5 kN and the bending moment is 510 Nm. For a 20 % risk, the impact force is 6.3 kN and the bending moment is 417 Nm.

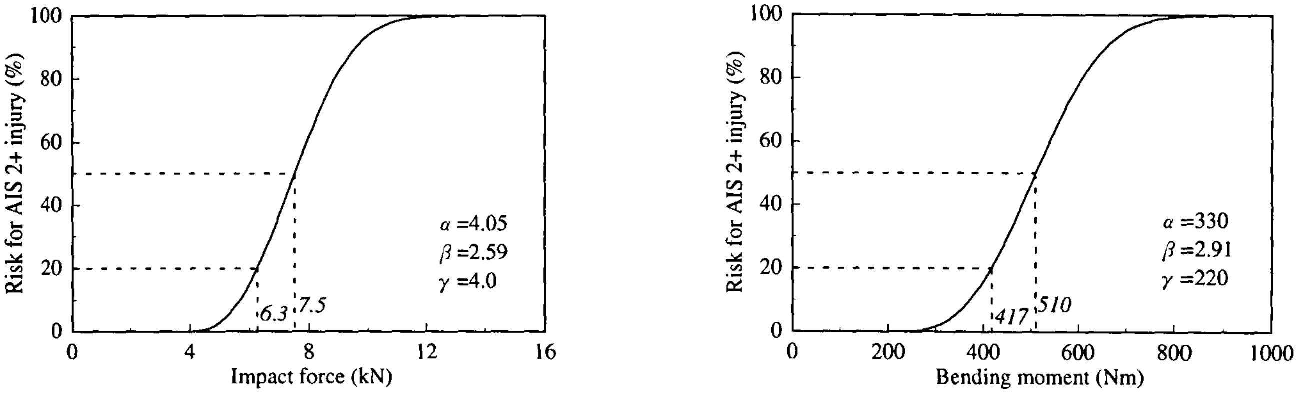

(1) Impact force **(2) Bending moment**

Figure 33. Weibull injury risk curve.

CONCLUSIONS

Pedestrian accident analysis and accident reconstruction test were conducted to validate the EEVC pedestrian upper legform impact test. Conclusions are summarized below.

(1) The pedestrian accident data indicated the related injury of femur and pelvis with AIS 2+ caused by the leading edge of the bonnet and wing decreased by 50 % during the last ten years.

(2) Recent accident analyses indicate that the priority of the upper legform impact test seems to be the lowest in the three EEVC subsystem tests. However, the upper legform impact test had the most difficulty fulfilling the requirement of the current injury criteria among the three EEVC pedestrian tests.

(3) In pedestrian accident, the top four factors affecting the injury of femur and pelvis were the bonnet leading edge height, the pedestrian age, the vehicle registration year, and the bumper lead.

(4) The upper leg injury severity may decrease if there is no fracture in the lower leg. This means that a pedestrian-friendly bumper will reduce the upper leg injuries.

(5) The biomechanical injury risk curve for the upper legform impact test was obtained from the accident reconstruction tests using the Weibull cumulative frequency curve. For the 50 percentile injury risk of femur and pelvis with AIS 2+, the impact force is 7.5 kN and the bending moment is 510 Nm.

(6) Physical values used as injury criteria should correlate to the significance of injury severity. However, the measured impact force and bending moment did not increase with the significance of AIS severity. This contradiction raises questions of whether the current injury criteria and method of the upper legform impact test are valid.

(7) Impact energy was most important to reconstruct the damage pattern of vehicle with the upper legform impactor. Constant mass can be used for the impactor. Impact velocity can be defined from the impact energy and the constant impactor mass without using an impact velocity look-up graph.

REFERENCES

(1) European Experimental Vehicles Committee, Proposals for Methods to Evaluate Pedestrian Protection for Passenger Cars, EEVC Working Group 10 Report, 1994.

(2) The National Police Agency, Statistics of Traffic (in Japanese), 1998.

(3) Kajzer J., Schroeder G., Ishikawa H., Matsui Y., Bosh U., Shearing and bending Effects at the Knee Joint at High Speed Lateral Loading, 41st STAPP, 1997.

(4) IHRA/Pedestrian Safety Experts Meeting, 1998.

(5) Institute for Traffic Accident Research and Data Analysis, Accident Report (in Japanese), 1998.

(6) Lawrence G., Hardy B., Harris J., Bonnet Leading Edge Subsystem Test for Cars to Assess Protection for Pedestrians, 13th ESV, 1991.

(7) European Commission, Draft Proposal for a European Parliament and Council Directive relating to the Protection of Pedestrians and Other Road Users in the Event of a Collision with a Motor Vehicle and Amending Directive 70/156/EEC, 3/5021/96 EN, 1996.

(8) Janssen E., EEVC Test Methods to Evaluate Pedestrian Protection Afforded by Passengers Cars, 15th ESV, 1996.

(9) Hardy B., Notes on the Use of the TRL Prototype Pedestrian Bonnet Leading Edge Impactor, Version 1.1 TRL document, 1993.

(10) Konosu A., Ishikawa H., Sasaki A., A Study on Pedestrian Impact Test Procedure by Computer Simulation, 16th ESV, 1998.

(11) Ishikawa H., Accident Reconstruction of Pedestrian Head Injuries, Toyota Human Life Support Biomechanics Symposium, Nagoya University Symposion, pp41-pp46, July 15-16, 1997.

(12) Monk M., Injury Severity and Measured Response for Pedestrian Head Impacts, DOT HS 807 476, 1989.

APPENDIX A

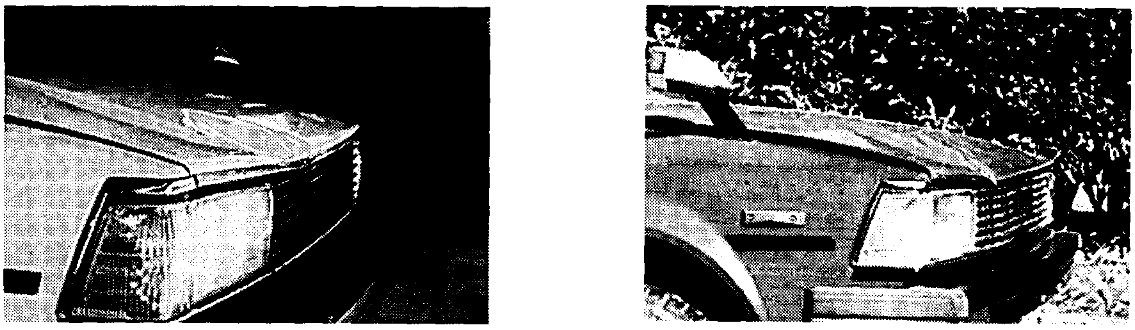

Accident

Residual deformation : 20 mm
Ped-car impact vel. : 35 km/h

Test

Residual deformation : 20 mm
Ped-car impact vel : 40 km/h [E]
Impact angle : 29.5 deg.

Figure A-1. Good agreement case (case number 3).

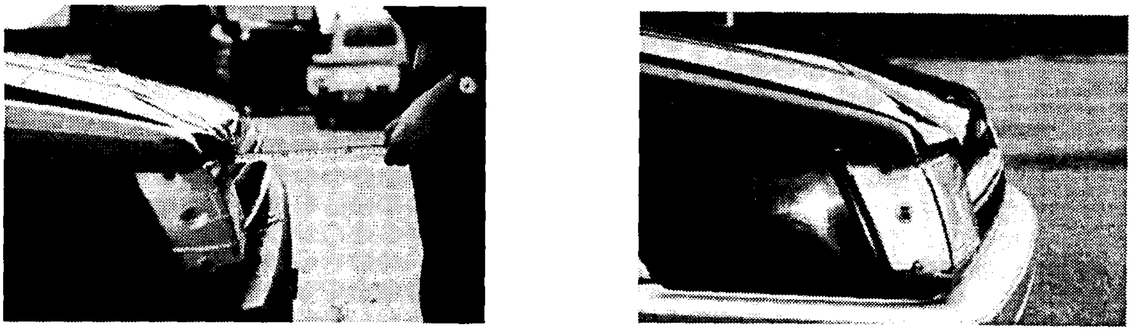

Accident

Residual deformation : 10 mm
Ped-car impact vel : 45 km/h

Test

Residual deformation : 12 mm
Ped-car impact vel : 45 km/h [E]
Impact angle : 36.4 deg.

Figure A-2. Acceptable agreement case (case number 16).

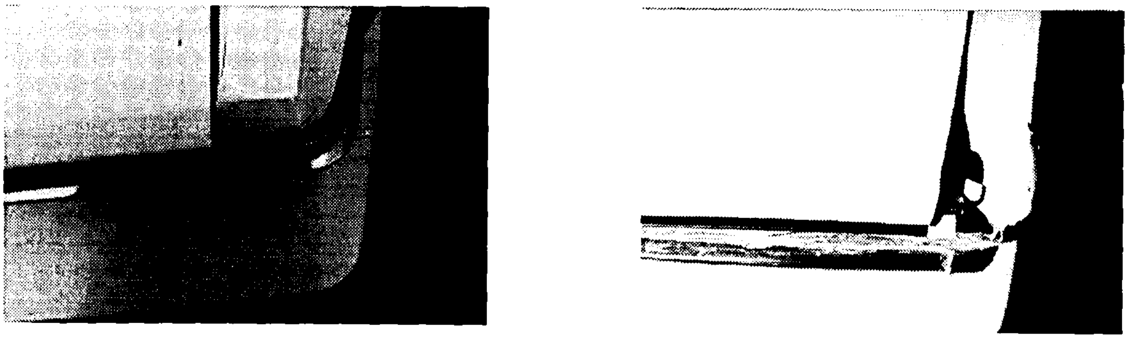

Accident

Residual deformation : 10 mm
Ped-car impact vel : 30 km/h

Test

Residual deformation : 45 mm
Ped-car impact vel : 40 km/h [E]
Impact angle : 39.5 deg.

Figure A-3. Disagreement case (case number 7).

APPENDIX B

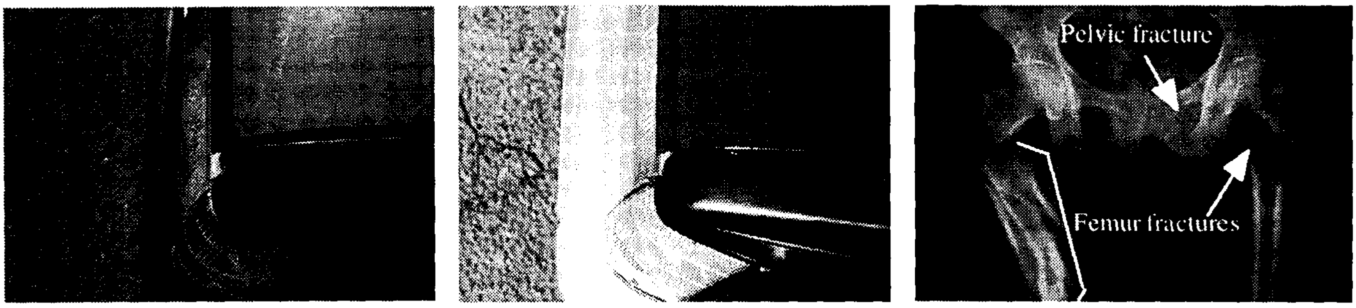
Pelvic fracture
Femur fractures

Accident

Test

Femur/pelvis fractures in an accident

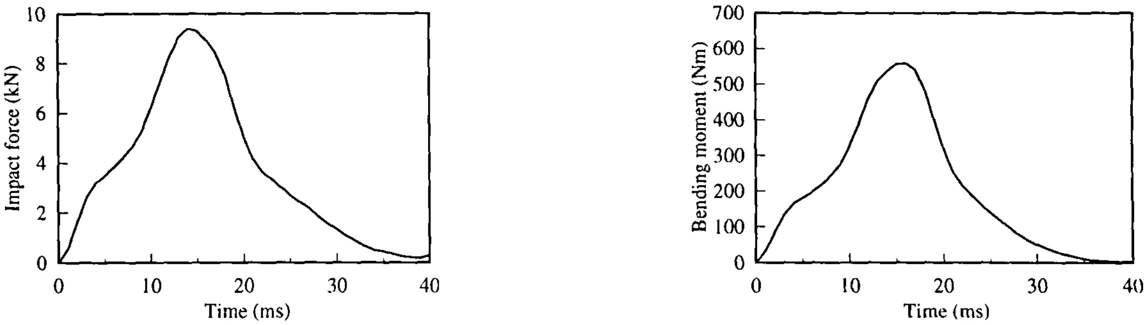

Impact force

Bending moment

Figure B-1. AIS 2+ injury (fracture of femur and pelvis) case in good agreement (case number 10).

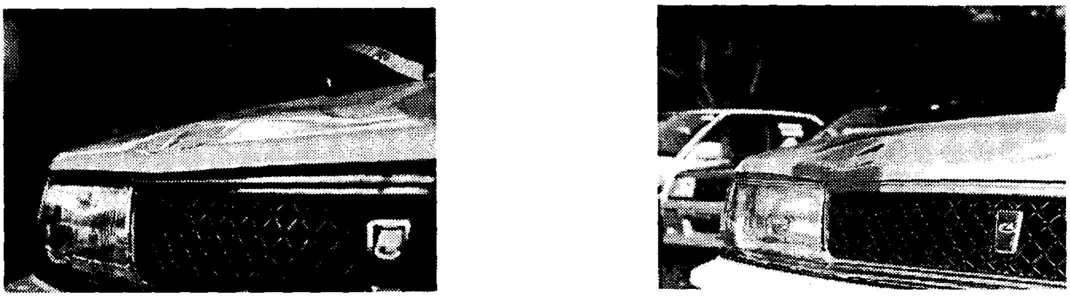

Accident

Test

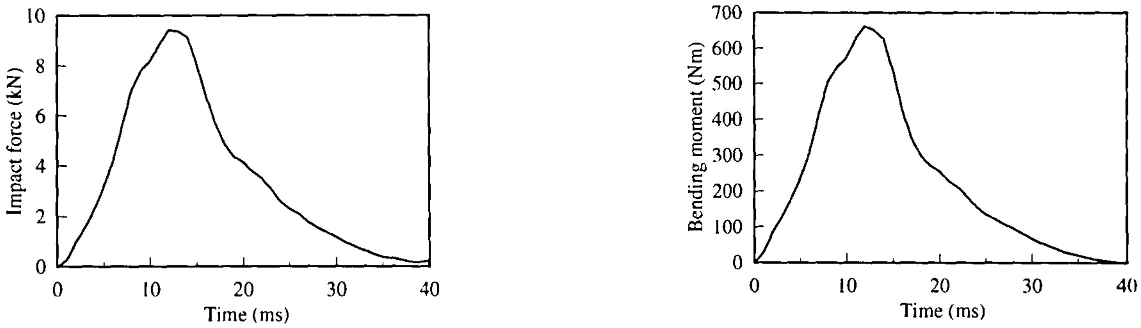

Impact force

Bending moment

Figure B-2. No injury case in good agreement (case number 11).

DEVELOPMENT OF A NON-FRANGIBLE PEDESTRIAN LEGFORM IMPACTOR

James R. Marous
David B. Reynolds
Wright State University
Douglas C. Longhitano
The Ohio State University
Roger A. Saul
National Highway Traffic Safety Administration
United States

Paper Number 98-S10-O-06

ABSTRACT

Standards to test the aggressiveness of vehicle front end geometry and its relation to pedestrian lower leg and knee injuries have been proposed by the International Standards Organization (ISO). These standards call for the use of a legform impactor designed to meet prescribed performance and physical criteria developed to represent a typical adult lower extremity.

The current effort focuses on developing a legform impactor subsystem to comply with the ISO standards. It is also the intention of this project to eliminate the necessity of using plastically deformable elements. This system is constructed with non-frangible knee elements and cylindrical segments representing the tibial and femoral components. Dynamic deformation of the legform subsystem is separated into isolated bending and shearing responses which can be directly measured. Bending is controlled by a clutch type mechanism which can be easily adjusted for calibration and certification purposes. The shearing characteristics of the legform are defined by viscoelastic elements which allow medial/lateral translation of the lower leg segment relative to the upper leg.

Bench testing has proven that this mechanism is a viable alternative to the current legform impactor designs which use frangible knee elements. Details concerning the design development, calibration results and practical testing are included in this paper.

INTRODUCTION

Approximately 5400 pedestrians were fatally injured by motor vehicles in the United States in 1996. On average, a pedestrian is killed in a traffic crash every 97 minutes (NHTSA, 1996). Head and thorax injuries were the major causes of pedestrian fatalities, however, lower extremity injuries accounted for most of the non-fatal injuries.

Injuries to the lower extremities and specifically to the knee are generally not life-threatening but often present long term consequences with the possibility of permanent disability. The long-term mobility of the victim is often significantly affected causing not only an emotional burden on the victim, but a monetary burden on society as a whole (Cesari, et al., 1994).

Pedestrians are generally struck when crossing a road with an impact direction close to the perpendicular of the vehicles motion axis. These pedestrian crashes generally occur in urban areas where the vehicle speed at impact is relatively low, most times below 48 km/h (29.83 mph) (Tanner, 1992).

BACKGROUND

The frequency of lower leg injuries due to contact from with the vehicle bumper, and the resulting long term impairment constituted the basis for experimental research dealing with the response of the human knee during lateral impact. Parameters as to physical dimensions and biofidelic performance characteristics were then generated (Kajzer, 1991). These characteristics were adopted by ISO and used as the basis for a legform impactor test device.

This test device is an impactor subsystem, the legform will be propelled into a stationary vehicle, not vise-versa (ISO, 1997). The impactor must simulate the biofidelic nature of a human leg while being constructed soundly enough to endure multiple impacts to a vehicle.

ISO Standard

The ISO standard for the legform impactor includes physical dimensions, inertial parameters and force-time histories for both bending and shearing at the knee joint (Table 1 and Figure 1). Also included in the ISO standard are certification procedures and a procedure for practical testing of the legform impactor on vehicles.

Table 1.
ISO Legform Impactor Parameters

Parameter	ISO Standard
Lower Leg Length	493±5 mm
Lower Leg Center of Gravity	233±10 mm
Lower Leg Mass	4.8±0.1 Kg
Lower Leg Moment of Inertia	0.120±0.001 Kg-m^2
Lower Leg Outside Diameter	120±10 mm
Upper Leg Length	428±10 mm
Upper Leg Center of Gravity	218±10 mm
Upper Leg Mass	8.6±0.1 Kg
Upper Leg Moment of Inertia	0.127±0.001 Kg-m^2
Upper Leg Outside Diameter	120±10 mm
Legform Total Mass	13.4±0.1 Kg
Flesh Thickness	30±5 mm

Internationally, several programs have developed impactor subsystems (Lawrence and Thornton, 1996, Cesari, 1994, Ishikawa, et al., Tanner, 1992). However, all of these systems share a common characteristic of using frangible knee elements in their design. These frangible knee elements are designed to permanently deform during each impact test.

The use of plastically deformable elements causes a concern about the response variation between pairs of knee ligaments. It is not possible to experimentally validate the performance characteristics of each specific set of ligaments used in testing (Tanner, 1992). Calibration and certification must be done using random samples from each batch of the deformable knee ligaments produced. This causes concern about production and material viability within each batch of deformable knee elements.

Legform Impactor Certification

In order to qualify for ISO acceptance, the legform impactor must conform to the prescribed ISO biofidelic performance corridors as illustrated earlier.

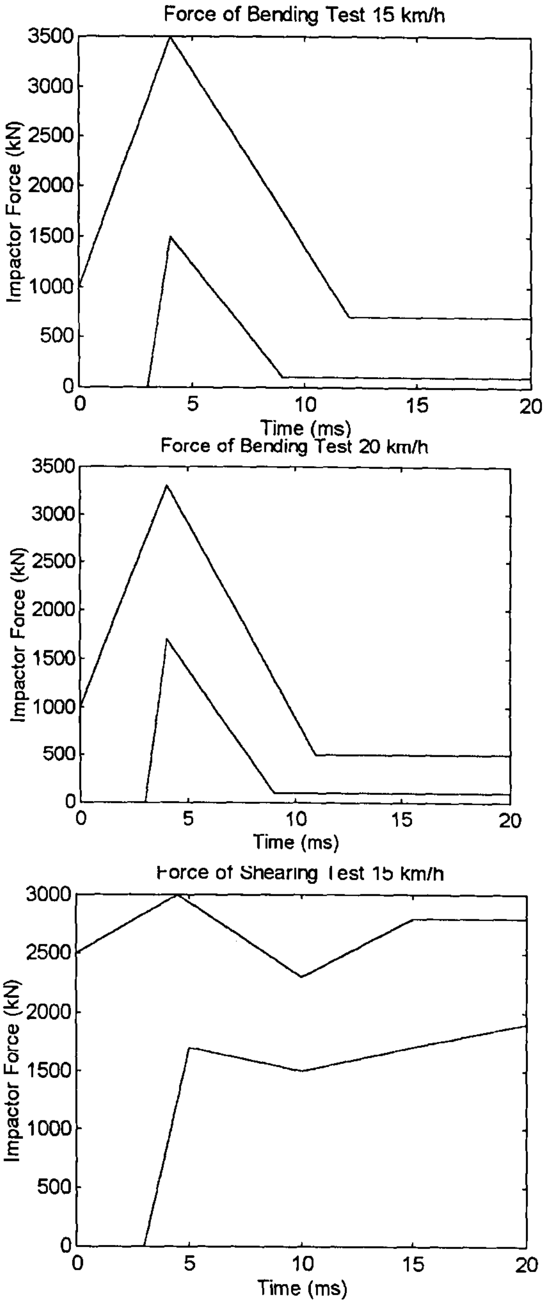

Figure 1. Three ISO biofidelity response corridors corresponding to (top to bottom) two bending tests at 15 and 20 kph and one shearing test at 15 kph.

The ISO standard precisely describes the conditions for the certification tests, including details of the testing configuration and methods. A test fixture was fabricated which allowed both bending and shearing certification tests to be performed on the same fixture. This test fixture is illustrated in Figures 2 and 3.

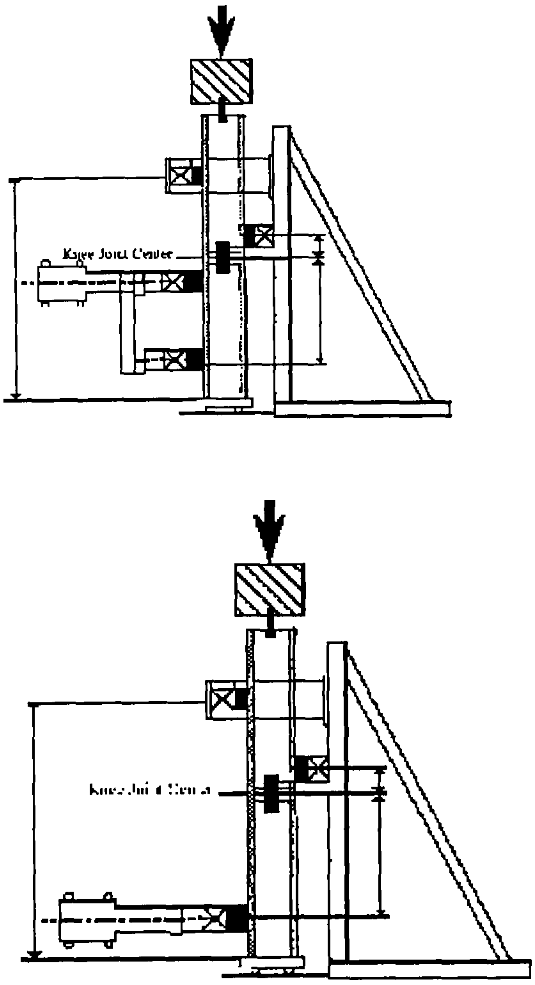

Figure 2. ISO certification test fixtures for shearing (top) and bending (bottom).

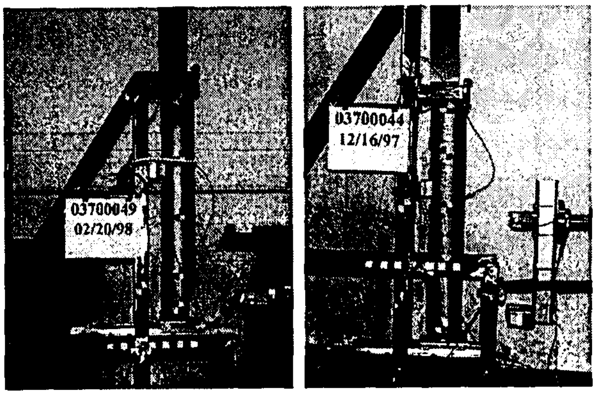

Figure 3. NHTSA certification test fixtures for bending (left) and shearing (right).

NHTSA PROTOTYPE DEVELOPMENT

In order to overcome the problems inherent in calibration and consistency of frangible knee elements, NHTSA has pursued the development of a legform impactor system constructed without the use of frangible elements. Based on this premise, work began on an initial prototype in 1996 (Longhitano, 1997). In this prototype, shearing and bending responses were separated, but constrained about the same axis (Figure 4).

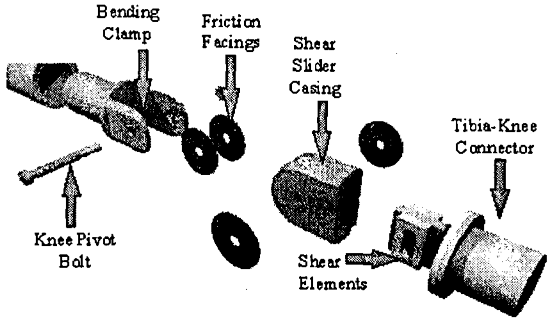

Figure 4. NHTSA prototype pedestrian legform impactor.

The bending response of the knee was defined by a clutch-type knee mechanism constructed of parallel friction plates compressed by a clamp and center pivot bolt. Variation in the torque of the bolt caused a corresponding change in the clamping force between the friction plates. The level of clamping force defined the bending response of the legform during impact event.

Elastic shear elements located in the center of the shear slider casing controlled shear in the medial/lateral direction. These shear elements were constructed from a viscoelastic damping material and sized to give performance within the ISO biofidelic corridor. The elements were designed to elastically deflect 6 mm for an applied load of 4kN.

The initial prototype proved the viability of a legform impactor constructed with non-frangible elements, with the results of the bending tests falling reasonably well within the required ISO biofidelity corridors for both 15 and 20 kph tests. The shear elements however, were not robust enough to withstand the shearing certification test. In this prototype, the shear elements were bonded with an adhesive to a smooth surface, but the bonding strength of this method proved to be inadequate.

The physical and inertial properties of this prototype were not experimentally verified and compliance with the ISO standards for mass, center of gravity and mass moment of inertia was not established.

During practical tests on vehicles, the ISO standards require measurement of bending angle of the knee and shear displacement. The first prototype included direct measurement of each of these parameters. Bending angle was measured, by a rotary potentiometer, as the relative angle between the shear slider casing and the bending clamp. Shear displacement was measured using a miniature string potentiometer which indicated the relative displacement between the shear slider casing and the center post of the tibia cap. The instrumentation for this prototype was not sufficiently robust for repeated impact and thus was found to be inadequate for dynamic testing.

SECOND PROTOTYPE DEVELOPMENT

In construction of a second prototype legform impactor, three goals were set forth: 1) redesign of the shear elements to alleviate the failures found in the first prototype, 2) verification of inertial and physical properties, and 3) redesign of the system instrumentation to give reliable and accurate performance.

Shear Element Revisions

In the initial prototype, the shear elements were bonded to the interior of the shear slider casing and to the center post of the upper tibial cap, both smooth surfaces. The rapid impulse of the dynamic impact exceeded the bonding strength of the chosen adhesive. To overcome this problem, mechanical fixation of the shear elements has been added and the need for an adhesive eliminated. The shape of the elastic shear elements has been modified to include tabs which fit into slots added to the shear slider casing and knee center post (Figure 5).

Physical and Inertial Parameters

During the first prototype development, calculations were made to determine the physical dimensions of the legform impactor that would best meet the ISO standards for physical properties. Design parameters were evaluated in MATLAB software using custom written routines. Design parameters such as element lengths, widths and bore depths were altered in the computer algorithms until the values for the physical properties were within the specified ISO values. Using the MATLAB results, fabrication proceeded for the first prototype.

In the interest of sound design, it was decided that for the second prototype the physical properties of the legform impactor should be experimentally verified. The Human Effectiveness Branch of The Air Force Research Laboratory at Wright Patterson Air Force Base was contacted and agreed to donate the time and expertise for testing.

Using the U.S. Air Force Standard Automated Mass Properties (STAMP) Testing and Calibration Procedure, physical properties can be found experimentally with great accuracy and precision. Using a moment table and an inverted torsional pendulum, mass, centers of gravity and mass moments of inertia were all experimentally verified. The results of the testing and a comparison to the MATLAB results are given in Tables 2 and 3.

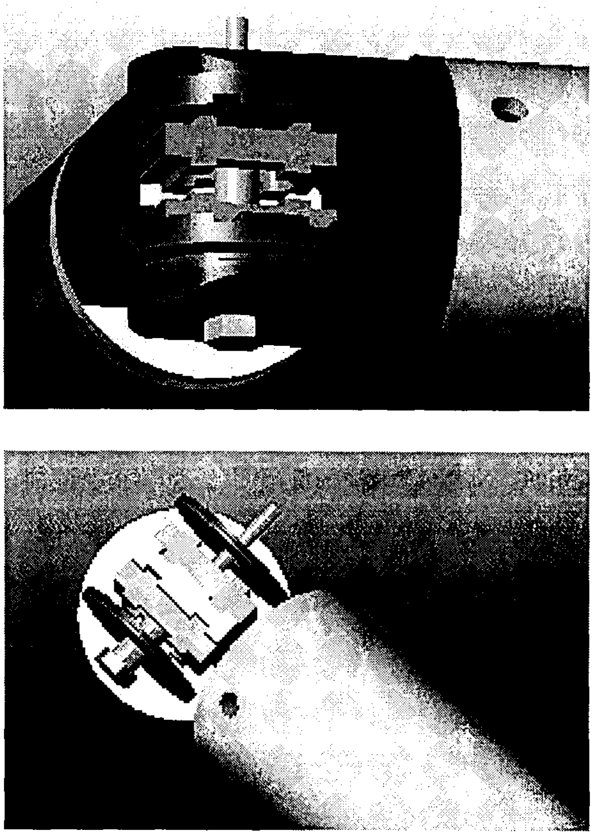

Figure 5. Two views showing the second prototype knee elements illustrating mechanical fixation of the elastic shear elements.

Table 2.

Upper Leg	ISO	MATLAB	Experimental
Mass	8.5 - 8.7 Kg	8.5491 Kg	7.34 Kg
Center of Gravity (From Knee Center)	208 - 228 mm	208.2 mm	209.6 mm
Mass Moment of Inertia	0.126 - 0.128 Kg-m^2	0.1273 Kg-m^2	0.1204 Kg-m^2

Table 3.

Lower Leg	ISO	MATLAB	Experimental
Mass	4.6 - 4.9 Kg	4.336 Kg	4.10 Kg
Center of Gravity (From Knee Center)	223 - 243 mm	241.6 mm	204.8 mm
Mass Moment of Inertia	0.119 - 0.121 Kg-m^2	0.0970 Kg-m^2	0.07876 Kg-m^2

Results show that the MATLAB calculations are in agreement with the ISO specifications for the upper leg segment. For the lower leg, the calculated mass and mass moment of inertia were below specified values. This was due to simplifications made in the MATLAB algorithm and will be corrected in future revisions.

The differences in the experimental and theoretical values for the lower leg are due to the lower cap of the lower leg having been constructed of Delrin and not steel. The lower cap was fabricated from Delrin to reduce the friction between the legform impactor and the certification fixture. If an increase in material density due to steel are factored into the experimental values for the lower leg, the properties are much closer to the prescribed values. The experimental values were also made without the flesh covering, which resulted in a decrease in mass, but had negligible influence on centers of gravity and mass moments of inertia.

Instrumentation Revisions

In the initial prototype, bending angle between the leg segments was measured by a rotary potentiometer. The potentiometer was configured to directly measure the rotation of one segment relative to the other. During testing, this method was found to be inadequate and was abandoned.

Measurement of shear displacement in the initial prototype involved the use of a miniature string potentiometer transducer mounted within the knee structure. Because of the repeated failures of the shear elements, the viability of this method was not verified.

For the second prototype, miniature string potentiometers were used for both the bending angle and shear displacement measurements. Data collected with the redesigned instrumentation system was found to be reliable and repeatable. Sample output is given in Figures 6 and 7.

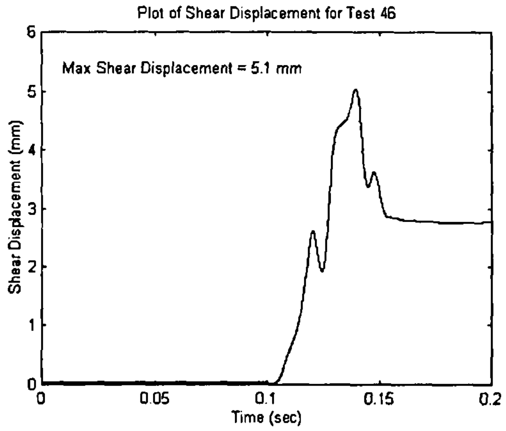

Figure 6. Sample output for shear displacement.

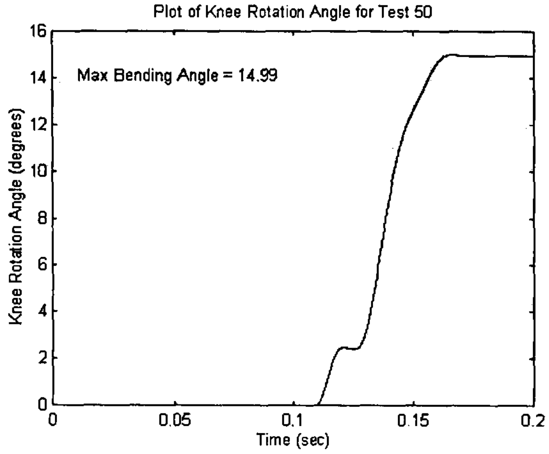

Figure 7. Sample output for knee rotation angle.

Certification of Second Prototype

Upon completion of the second prototype, certification of the prototype proceeded. Results of the bending and certification tests are given in Figures 8, 9 and 10.

The results of both bending tests are well within the ISO biofidelic corridor. The results of the shear tests are correct for magnitude of the force, but are only within the ISO corridor for the first 10 ms and fall rapidly after 10 ms.

One explanation of this discrepancy is the method used to measure the contact force during impact. For both bending tests, the contact force was measured using a load cell affixed to the end of the impactor ram. In the shear tests, force measurements were made indirectly using an accelerometer mounted on the lower leg segment. This indirect method of force measurement caused the discrepancy in the shear test. Further testing with a direct force measurement is needed before certification of the shear tests is established.

NHTSA VEHICLE IMPACT TESTS

The first phase of vehicle bumper tests was fabrication of a propulsion system to launch the legform impactor into the stationary vehicle (Figure 11). A system was fabricated using a hydraulic ram to accelerate the legform impactor. During propulsion, the legform impactor is supported at the center of gravity for both the upper and lower leg segment as well as at the center of knee rotation.

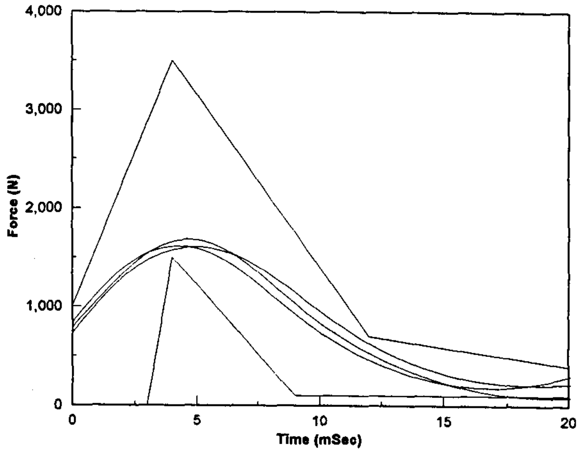

Figure 8. Certification results for the 15 kph bending test.

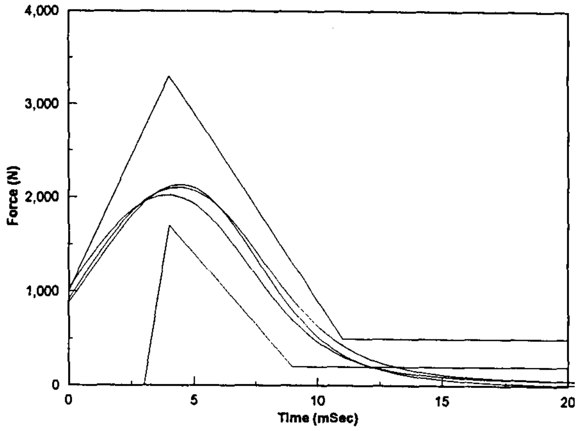

Figure 9. Certification results for the 20 kph bending test.

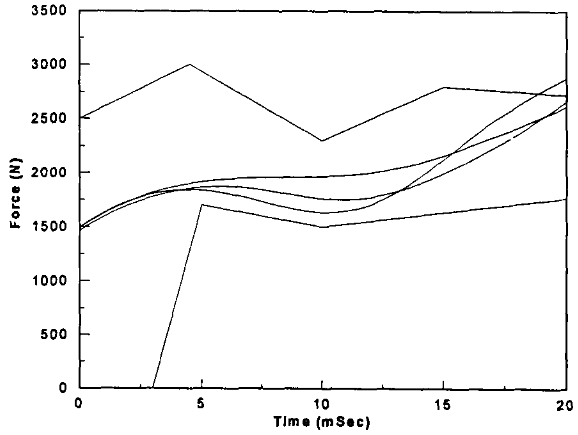

Figure 10. Certification results for the 15 kph shearing test.

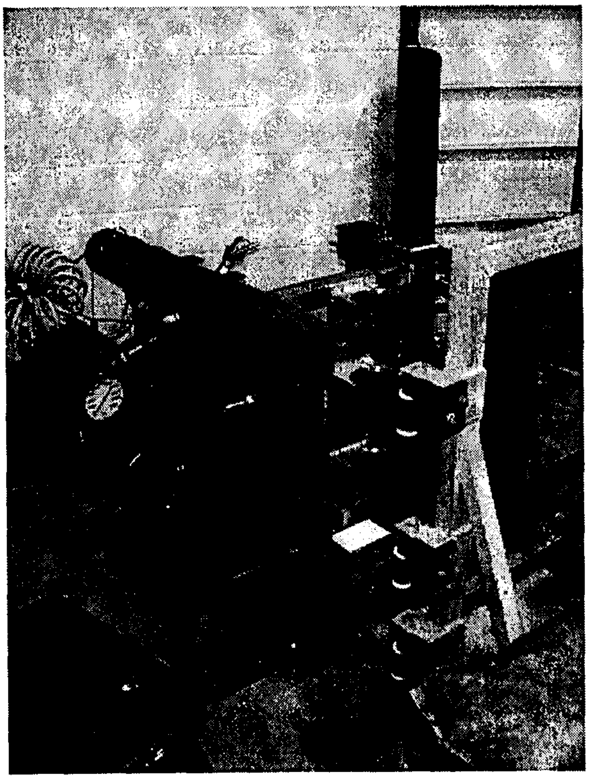

Figure 11. NHTSA legform propulsion system.

As stated in the ISO standards, the legform impactor must be in free flight at the time of impact with an angular velocity less than 50 deg/sec, and within 10 mm of ground level. Further tolerances for yaw, pitch and roll of the legform impactor at impactor are also stated in the ISO document.

Verification of the above parameters was made using motion analysis software and digital film of several test firings. Motion analysis verified that the legform impactor rotational velocity, vertical displacement and vertical tolerances were all acceptable as shown in Table 4.

Table 4.

Parameter	ISO	Experimental
Angular Velocity	< 50 deg/sec	30 deg/sec
Deviation From Vertical	± 6 deg	5.37 deg
Distance From Ground Reference Level	< 10 mm	4.56 mm
Yaw, Pitch and Roll	± 5 deg	< 1 deg

Testing of several vehicles is currently in process at VRTC. Sample output for a completed test are illustrated below. The test vehicle shown in Figures 12 through 16 is a 1993 Ford Explorer.

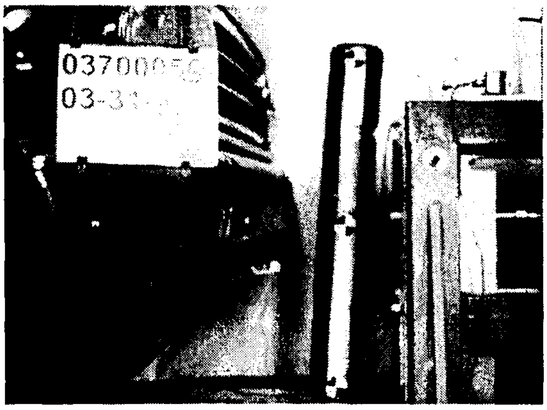

Figure 12. NHTSA legform impact immediately before impact to a 1993 Ford Explorer.

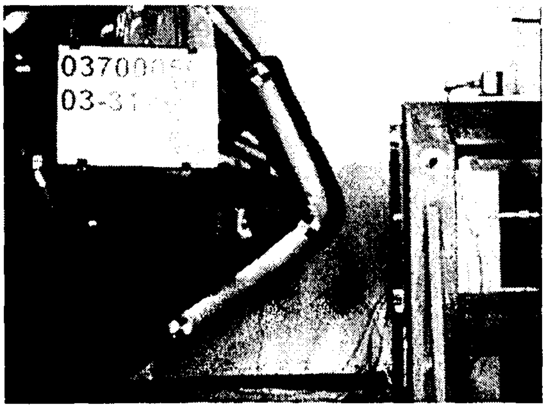

Figure 13. NHTSA legform impact immediately after impact to a 1993 Ford Explorer.

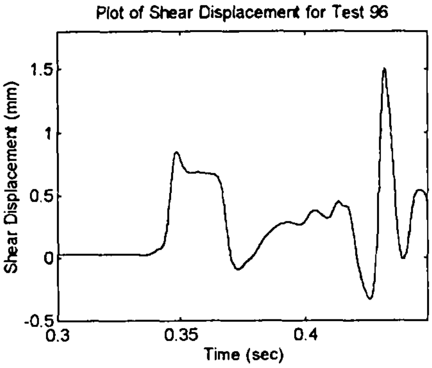

Figure 14. Sample output of shear displacement for test 96, a 1993 Ford Explorer.

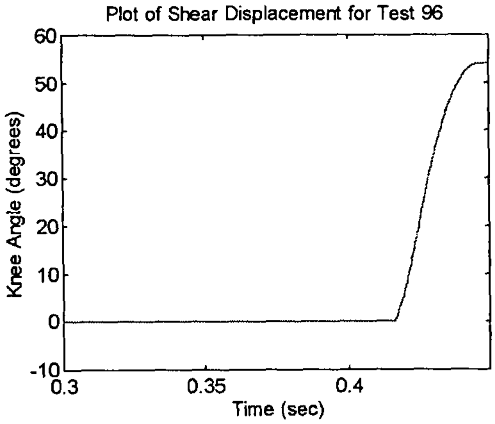

Figure 15. Sample output of knee rotation angle for test 96.

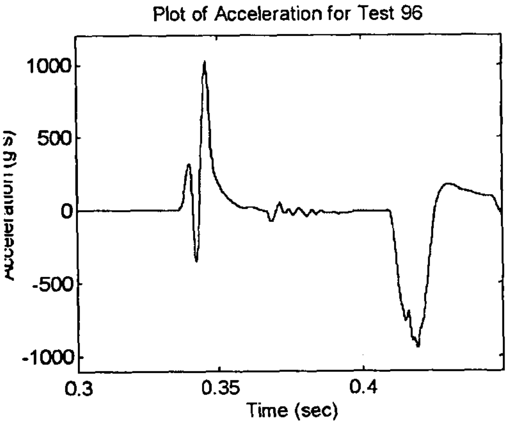

Figure 16. Sample output of leg acceleration for test 96.

Testing of the current system has shown that the system gives reliable, repeatable output and has been tested for durability in test impacts up to 32 mph (51.5 kph).

FINAL PROTOTYPE DEVELOPMENT

There are a number of items which should be addressed in the development of a final prototype:

1. The inertial and physical parameters outlined by the ISO standard must be achieved and verified.
2. The shear response of the legform must be validated using a load cell on the certification ram.
3. Flesh and skin components must be developed using materials that are not required to be replaced with each test.
4. Repeatability of the test device must be confirmed using the propulsion system and a stationary test fixture representing the front end of a vehicle.
5. Durability of the current system must be verified over a larger number of tests and varying testing conditions.
6. Legform impactor performance should be correlated with real-world injury data through a series of crash reconstructions with different impact velocities, vehicle profiles, and injury outcomes.
7. Feasibility, including cost, manpower and resources of a production version of the legform impactor must be explored.

CONCLUSIONS

This legform impactor developed by VRTC is the first known proposal of a pedestrian leg subsystem which is designed to adhere to the ISO standard which does not require the use of frangible elements. The bending response characteristics have been experimentally verified with respect to the biofidelity corridors for pure bending impacts at 15 kph and 20 kph. The shear slider response has demonstrated characteristics consistent with the ISO requirement, but final validation has not yet been achieved.

Repeated testing of these prototypes has demonstrated that the construction is robust. The system is capable of producing data for impacts much more severe than is outlined by ISO. Further design refinements are needed for a final design construction, but development of the legform impactor is near completion.

Finally, with the development of this legform it has been proven that the concept of using non-frangible elements is feasible.

REFERENCES

Cesari, Dominique, Bouquet, Robert, Caire, Yves , and Bermond, Francois. "Protection of Pedestrians Against Leg Injuries," Proceedings of the 14th International Technical Conference on Experimental Safety Vehicles: Munich: 1994.

Ishikawa, Hirotoshi, Janusz Kajzer, Ono, Koshiro, and Sakurai, Minoru. "Simulation of Car Impact to Pedestrian Lower Extremity," Japan Automobile Research Institute, Dept. of Injury Prevention, Chalmers University of Technology. Gotenborg, Sweden.

ISO/TC22/SC10/WG2. "Passenger Cars and Light Commercial Vehicles - Pedestrian Protection - Impact Test Method for Pedestrian Leg and Knee," Document Number N552, 1997.

Kajzer, Janusz. "Impact Biomechanics of the Knee," Chalmers University of Technology. Gotenborg, Sweden. 1991.

Lawrence, Graham J.L., and S. Thornton. "The Development and Evaluation of the TRL Legform Impactor," Unpublished Project Report PR/VE/189/96, Project Record S220C/VF, Transport Research Laboratory. Crowthorne, England: 1996.

Longhitano, Douglas. "Development of a Non-Frangible Pedestrian Legform Impactor," The Ohio State University. Columbus, OH: 1997.

Traffic Safety Facts – Pedestrians, NHTSA, 1996.

Tanner, Brian C., "Pedestrian Lower Leg Injury Mitigation Research," Progress Report, U.S. DOT, Vehicle Research and Test Center. East Liberty, Ohio: September 1992.

USE AND MISUSE OF CHILD RESTRAINT DEVICES IN MICHIGAN

David W. Eby
Lidia P. Kostyniuk
University of Michigan Transportation Research Institute
United States
Paper Number 98-S10-O-07

ABSTRACT

This paper provides an overview of a statewide survey of child restraint device (CRD) use and misuse in Michigan. The study found that about 75 percent of children under the age of four were in a CRD and that CRD use generally followed the safety belt use patterns of the drivers. The study also found that when a CRD was used, nearly 90 percent of the time an error was made in either how the CRD was placed in the vehicle or how the child was placed in the CRD. Patterns of misuse are discussed as well as some ideas for improving correct use.

INTRODUCTION

In 1996, 88,000 children under the age of five years were killed or injured in motor vehicle crashes in the United States (NHTSA, 1997). Use of a child restraint device (CRD) has been identified as an effective means for reducing death and injury in the youngest group of motor vehicle occupants. In order to encourage use of CRDs, most states have passed mandatory CRD use laws (Insurance Institute for Highway Safety, 1995). However, because of the difficulties in finding target-age children (those under four years of age) in high enough concentrations, no state had previously conducted a statewide survey of CRD use to determine the effectiveness of their law. Instead, states have limited their surveys to cities or regions. Thus the purpose of the present work was to determine a statewide CRD use rate for Michigan. At the same time, determining a statewide CRD use rate may not capture the entire CRD use picture. Nonstatewide studies have found that even when CRDs are used, misuse is high (e.g., Bolton & Dale, 1996; Decina & Knoebel, 1996; Margolis, Wagenaar & Molnar, 1992). Thus, a secondary objective was to determine frequency with which CRDs are misused and the patterns of this misuse.

METHODS

CRD use was determined by observing use in vehicles entering the facilities at 88 randomly selected day care and pediatric centers around the state of Michigan. In addition to CRD use, observers also recorded driver age category, sex, belt use, and several other variables. CRD misuse was determined by interviewing drivers of vehicles with a child in a CRD and by inspecting how the CRD was installed in the vehicle and how the child was secured in the seat at 28 randomly selected day care centers around Michigan. This part of the study was conducted as a pilot for use in designing a more detailed study of CRD misuse in Michigan.

RESULTS

Child Safety Seat Use Rates

The estimated child restraint device use rate for the state of Michigan was 74.5 ± 3.7 percent of all children under four years of age (i.e., target-age children) traveling in passenger cars, pickup trucks, sport utility vehicles, and van/minivans during the summer of 1997.

The estimated CRD use rate varied by driver belt use. When the driver was using a safety belt, target-aged children were in CRDs 80.8 percent of the time. If the driver was not belted, children were in CRDs only 51.8 percent of the time. While not surprising, this result suggests that continued efforts to increase safety belt use may also increase the frequency with which CRDs are used.

The analysis of CRD use by the sex of the person driving the vehicle in which the child was observed showed that women drivers (75.0 percent) tended to have target-age children in CRDs more often than men drivers (67.1 percent). Since surveys have consistently shown that safety belt use rates for women are generally about ten percentage points higher than men (see Kostyniuk, Molnar, & Eby, 1996 for a review of Michigan drivers), this sex difference observed in the present study may be related to the higher safety belt use of women. Further information on the CRD use results can be found elsewhere (Eby, Kostyniuk, & Christoff, 1997).

Child Restraint Device Misuse

Because this portion of the study was designed as a pilot test of CRD misuse data collection, a total of only 87 driver interviews and CRD inspections were conducted. While small, this number is sufficient to determine some statewide trends.

The large majority of drivers were female (86.2 percent), had at least some college education (80.4 percent), were married (89.7 percent), and believed that the CRD and child were correctly placed in the vehicle (96.6 percent). The majority of drivers (67.8 percent) acquired the CRD though self-purchase. Most drivers (71.3 percent) reported that they learned to install the CRD in the vehicle by reading manufacturer instructions, whereas none of the drivers used this information in learning how to secure the child in the CRD. Instead, most felt that placing the child in the CRD was "obvious" and either they or a family member (88.5 percent) simply figured it out on their own.

Overall the CRD misuse rate was 88.5 percent. This rate includes all vehicles in which at least one type of misuse was found in placing the child in the CRD or installing the CRD in the vehicle. This very high misuse rate is in agreement with the results of several other studies (e.g., Bolton & Dale, 1996; Decina & Knoebel, 1996; Margolis, Wagenaar, & Molnar, 1992).

The analysis of the specific errors people made with CRDs revealed several interesting patterns. First, errors, regardless of severity, were more common when placing the child in the seat than when installing the seat in the vehicle. This is, perhaps, not surprising since a large majority of drivers reported that they learned to put the child in the seat without using instructions from others or the CRD manufacturer. Many reported that placing the child in seat was "obvious." This finding suggests that educational efforts should strongly focus on the process of securing the child in the CRD, emphasizing that it may not be as self-evident as it appears. Second, certain kinds of misuse were common while others were infrequent. The most common problems were related to the tightness of fit; that is, securing the seat to the vehicle and strapping the child in the seat. Neither of these types of misuse could easily be corrected through verbal instruction. Rather, both would seem to require hands-on demonstration. Similarly, high misuse rates were found for items related to the safety belt locking clip and the harness positioning clip. Again, the proper use of both is difficult to convey through verbal means. With regard to infant seats, we found that the majority of parents left the infant-seat carrying handle inappropriately in an upright position. Finally, among the CRDs that we inspected none were placed inappropriately in the rear-facing position in a seat with an air bag. It appears that recent warning about this type of misuse have been effective. More detailed information on misuse patterns can be found in elsewhere (Eby, Kostyniuk, & Christoff, 1997).

ACKNOWLEDGMENTS

Carl Christoff, Michelle Hopp, Hans Joksch, Lisa Molnar, and Fredrick Streff assisted on this project. This work was sponsored by the Michigan Office of Highway Safety Planning (OHSP) The opinions, findings, and conclusions expressed here are those of the authors and not necessarily those of OHSP

REFERENCES

Bolton, S.L. & Dale, A. (1996). *Child Car Safety Seat Use/Misuse in Orange County.* Orange County, CA: County of Orange Health Care.

Decina, L.E. & Knoebel, K.Y. (1996). *Patterns of Misuse of Child Safety Seats.* Malvern, PA: Ketron Division of the Bionetics Corporation.

Eby, D.W., Kostyniuk, L.P., & Christoff, C. (1997). *Child Restraint Device Use and Misuse in Michigan* (Report No. UMTRI-97-36). Ann Arbor, MI: UMTRI

Insurance Institute for Highway Safety (1995). *Child Restraint, Belt Laws.* Arlington, VA: Insurance Institute for Highway Safety.

Kostyniuk, L.P., Molnar, L.J., & Eby, D.W. (1996).Are women taking more risks while driving? A look at Michigan drivers. *Proceedings of the Second National Conference on Women's Travel Issues.* Baltimore, MD.

Margolis, L.H., Wagenaar, A.C., & Molnar, L.J. (1992). Use and misuse of automobile child restraint devices. *American Journal of Disabilities of Children*, **146**, 361-366.

National Highway Traffic Safety Administration. (1997). *Traffic Safety Facts 1996.* (World Wide Web Document (http://www.nhtsa.dot.gov). Washington, D.C.: NHTSA

DEVELOPMENT OF A SLED SIDE IMPACT TEST FOR CHILD RESTRAINT SYSTEMS

I P Paton
A P Roy
Middlesex University
R Lowne
Transport Research Laboratory
United Kingdom

Paper No. 98-S10-O-09

ABSTRACT

Currently the majority of Child Restraint Systems (CRS) in the UK are approved to ECE Regulation 44 Amendment 03. This focuses on the crash performance of the CRS under frontal and rear impacts and does not include a sled side impact test.

Although standards from Australia and New Zealand have for some time contained such a test, they do not include an element reproducing the effects of intrusion. Intrusion is a major factor in serious and fatal injuries to children in CRS. This paper describes a research programme conducted to develop a simple side impact test which attempts to reproduce the effects of side structure intrusion on a CRS installed in a car on the struck side. A hinged door was mounted on the Middlesex University test sled, which, when opened contacted a CRS restrained on the ECE R 44 test seat mounted laterally on the sled. The door was opened under impact conditions when it struck an auxiliary impactor at the beginning of the sled deceleration phase. The chest and head response of ATDs restrained in current and prototype CRS was measured. These were compared with full car side impacts conducted at TRL. The results suggested that the peak response of the ATD was representative of the car/barrier impacts but the energy input to the CRS as a function of time needs more development.

INTRODUCTION

Analysis of accidents in which child occupants of vehicles were killed or seriously injured indicates that side impact incidents are potentially more serious in terms of occupant outcome than the more common frontal incident [1]. Adult belt retained CRS, widely sold and used in the UK, are presently all approved to the European standard ECE R44, currently to amendment 03. This standard, although comprehensive and exacting in most respects, does not incorporate a dynamic evaluation of CRS in a side impact scenario. It is only in certain antipodean countries that CRS are evaluated in such an impact type [2]. However even these tests do not reflect fully the dynamic effects observed during actual lateral car to car impacts, as they do not include the effects of the intruding structure.

OBJECTIVE

The objective of the work conducted in this study was to ascertain the practicability of developing a simple and reproducible side impact test with intruding side structure. The input to the child occupant is representative of that seen during typical vehicle to vehicle perpendicular side impact collisions. It is intended that the test be capable of being conducted on a single sled as described below, which is of a type used widely by organisations involved in the CRS industry in the UK. The research is being performed as a contribution to the development of an international standard for the side impact testing of child restraints through ISO.

DYNAMIC TEST FACILITY

Testing was conducted at the dynamic test facility of Middlesex University's Road Safety Engineering Laboratory*.

The dynamic impact test rig consists of a 'bungee' propelled, rail mounted sled which is decelerated by, in this instance the appropriate ECE R44 polyurethane deceleration tubes and olives. The facility was designed to be particularly suitable for routine dynamic testing of adult and child restraints and has been described in detail elsewhere [3]. Manikin head/chest (tri-axial) and sled (uni-axial) accelerations were routinely recorded and in addition, where appropriate, belt forces and loads imparted by a restraint system upon its fixings. Kinematic motion of both manikin and sled throughout the event were recorded using high speed video equipment. Standard data processing techniques were employed during the analysis.

IMPACT DIRECTION AND SEVERITY

ISO has concluded, from a review of accidents, that it would be appropriate for a test procedure to be developed that would represent a perpendicular car side impact of 50kph [1]. It was hence determined that the sled based test should represent the important conditions of such an impact, with the possibility for child occupant on either the struck or non struck sides. The basic parameters to which the sled test needed to conform were established by a series of full scale vehicle tests employing six vehicles in the average mass range described in [1], being struck by a trolley with a deformable front structure of mass 950kg similar to the struck vehicles.

---

*Impact sled now located at TRL.

The resulting post impact plastic deformation of the struck vehicles was established in the area of the rear seated child occupant by measurement, which showed a characteristic side impact deformation. The profile of the interior intrusion was found to be minimal at the 'C' pillar, and maximum near the 'B' pillar / front edge of the rear seat cushion, the surface of the rear door inner panel / trim remaining basically flat. The rear door essentially folded in around the rear door rebate in the latch area, (Figure 1). If the front seating position were to be simulated, the intrusion effect would be reversed, with again peak intrusion at the 'B' pillar, and minimal intrusion at the 'A' pillar.

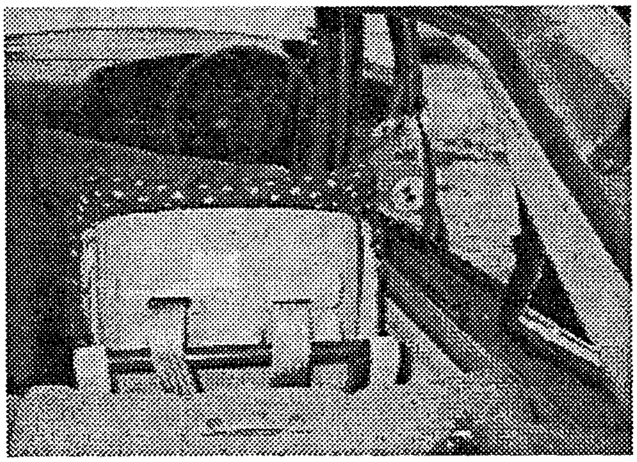

Figure 1 Deformation of vehicle side structure

In addition to accelerations experienced by the manikin at the head and chest, the lateral accelerations of the vehicle shell at the non struck 'B' pillar, and both the CRS and intruding door or side structure were recorded.

The following figures detail the derived angular velocity of the intruding rear door surface or side structure during the events, in addition to the lateral linear acceleration of the struck (initially stationary) target vehicles.

Based upon this range of data from the six test vehicles, corridors were established for both intrusion panel angular velocity and linear lateral acceleration of the struck vehicle against time. These corridors formed the foundation of the rig test requirements.

SLED TEST SET UP

The standard ECE R44 test seat was mounted longitudinally on the sled.

An intrusion panel was hinged on a structure at the front of the test seat (the hinges being perpendicular to the test seat cushion) which when fully 'open' latched into position (at 17.5°). The hinge line of the panel was in a position similar to the door rebate of the vehicle 'C' pillar with respect to the occupant.

Although it is not possible to reproduce totally the complex interactions of a full scale side impact on a single sled, this methodology attempts to generate the important separate dynamics of the intruding structure and the chassis acceleration in a standardised test for child restraints. The test sled with seat and anchors reproduces the dynamics of the undeformed struck car structure, while the intruding 'door' structure reproduces the dynamic intrusion.

Reproducing the events observed in the vehicle tests requires two basic tasks; firstly rapidly accelerating the intruding door structure into the seated occupant at an angular velocity commensurate with the data given in Figure 2, and secondly accelerating the seat bench from under the occupant in line with the lateral acceleration characteristics seen in the vehicles as seen in Figure 3.

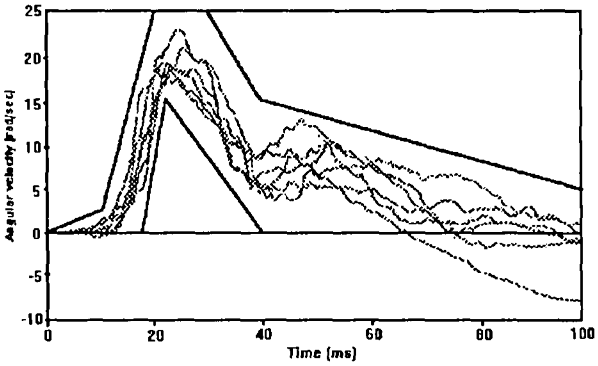

Figure 2 Angular velocity of a hinged plane simulating the vehicle side structure intrusion calculated from full scale impact tests

The timing of these two events is critical to reproduce the scenario of events seen in the vehicle tests.

With regard to manikin response, other factors must be considered, particularly stiffness of structures, seat and other contacting surfaces.

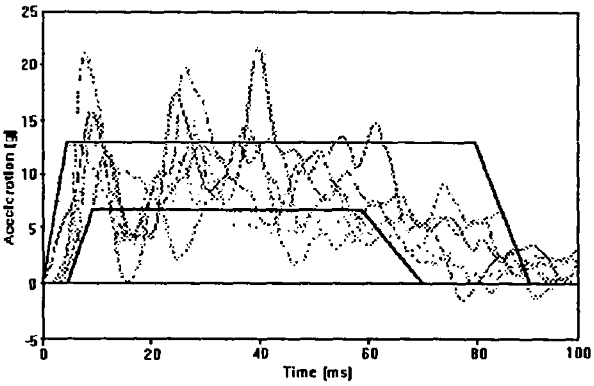

Figure 3 Lateral acceleration of target vehicle

Lateral acceleration of the sled from under the occupant can be achieved relatively simply by employing deceleration of the sled. The impact velocity of the sled was 25kph (6.9m/s), thus reproducing the post impact velocity of the target vehicle when impacted by a vehicle of similar mass travelling at 50kph.

It proved more difficult to achieve an angular velocity of the intrusion panel of at least 15 rad/sec relative to the sled. To open (and latch) the intrusion panel, a separate impactor with stiff rubber spring on its end was employed. The problem with a set-up of this type is that the deceleration of the sled over approximately 0.5m predominately takes place after the contact between intrusion panel and its impactor. Unfortunately the maximum linear travel of the panel is considerably less than 0.5m. This means that after impact with the panel, the impactor must be moved away to prevent the panel from being ripped off.

Initially a simple mechanical lever system affixed to the head of the sled was employed to push the impactor away. Results of those initial tests were reported in [1]. The system proved sufficient to demonstrate the principles, but the angular velocity of the intrusion panel was insufficient.

The second series of tests employed an alternative intrusion panel impactor. Instead of being affixed to the head of the sled, the impactor incorporating a stiff rubber spring at its contact end, was free to 'fly clear' after impact with the panel (see figure 4). A design of this type gave the benefit of allowing the impactor to strike the centre area of the panel - a situation that was effectively impossible with the previous mechanical design. By striking at the calculated point of percussion it was found possible to increase the angular velocity of the panel without overloading the hinges. The characteristics of the initial spring stiffness and the door panel and impactor masses were established by mathematical modelling to realise the desired panel acceleration and angular velocity.

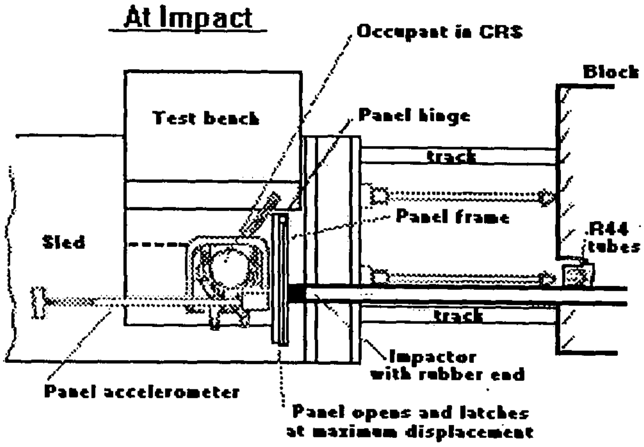

Figure 4 Final test set up (plan view)

PARAMETERS EVALUATED

In addition to the above mentioned parameters, manikin head, chest and CRS lateral accelerations were measured to allow comparison with the vehicle test results. The manikin employed in the comparative tests was a TNO P3, whilst in addition, a TNO P¾, was used in later CRS assessments [4].

DESCRIPTION OF CRS EVALUATED

For the comparative tests purposes, similar CRS were used in the sled and vehicle evaluations. At a later stage a range of alternative production belt retained and prototype CRS employing rigid fixings were evaluated. These later CRS were all based on the same moulded production types to facilitate comparison.

INITIAL COMPARATIVE TESTING

Having defined the door velocity profile and the sled deceleration, the mass and moment of inertia of the door were modified until close proximity of the results to the vehicle tests was obtained.

Figures 5 and 6 below show the initial comparative sled tests compared to the corridor defined by the full scale vehicle tests. It will be noted that in comparison with figure 2, the intrusion panel angular velocity traces only just reach the required minimum value. It will also be noted that the angular velocity of the door falls more rapidly than in the vehicle tests. Furthermore, the linear acceleration of the sled does not rise quite as rapidly as in the vehicle tests. Figure 7 shows the tabulated peak manikin response data obtained for the comparative tests.

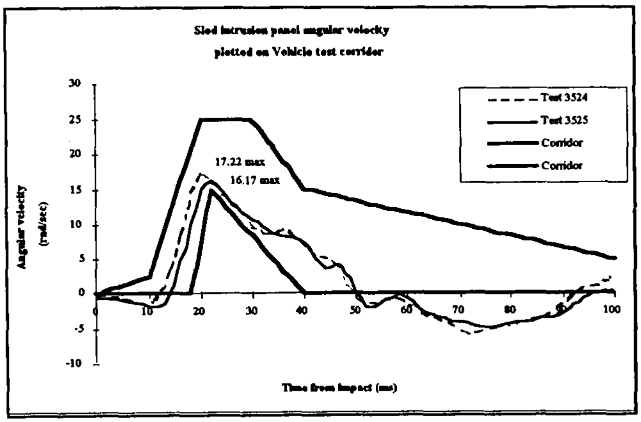

Figure 5 Angular velocity of intrusion panel

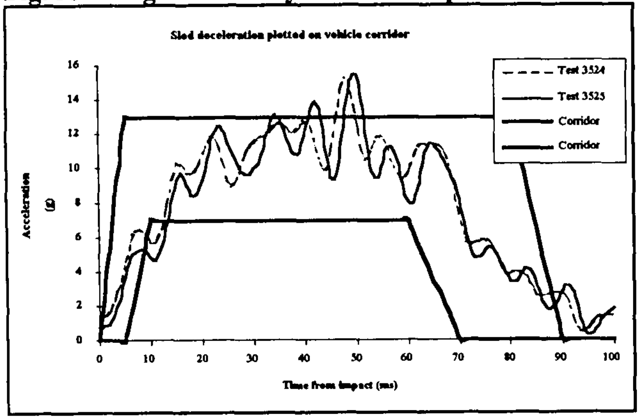

Figure 6 Linear sled acceleration

Figure 7 Manikin response in comparative tests

	Resultant 3ms chest acceleration [peak accel] (g)	Resultant 3ms head acceleration [peak accel] (g)	Lateral CRS acceleration [peak] (g)
Full scale vehicle test	56 [67]	42 [45]	118
Test 3524	65 [69]	61 [75]	103
Test 3525	66 [82]	61 [107]	85

It can be seen that the chest response in the sled tests is similar to that seen in the vehicle test whilst the head response is somewhat higher. This higher result is considered to be attributable to the higher position of the top of the hinged intrusion panel in the test in comparison with that in the particular model of vehicle used in the baseline test.

Even though the results have not been found to duplicate completely the vehicle test results, it was decided to proceed with an evaluation of a number of child restraint systems, both conventional and prototype, in direct comparison to the New Zealand side impact test NZS 5411, which it should be noted is conducted at a slightly higher velocity change of 32kph (8.9m/s).

	New Zealand test (8.9m/s impact)				Intrusion panel test (6.9m/s impact)			
	Test No	Chest resultant	Head resultant	head excursion	Test No	Chest resultant	Head resultant	lateral accel
CRS type		g	g	mm		g	g	g
Forward facing P3 manikin								
Conventional framed CRS					3524	65	61	103
L & D retained					3525	66	61	85
Conventional molded plastic CRS, L & D retained	3176	40	44	454	3535	52	46	85
Prototype CRS. Two rigid lower fixings + top tether	3198	26	35	320	3568	39*	30*	105*
Prototype CRS. Two lower straps + top tether	3177	32	35	527	3537	53	42	91
Rear facing P3/4 manikin								
Rigid molded plastic CRS, L & D retained	3239	31	39	600	3542	80	110	100
Molded polystyrene CRS, L & D retained					3541	105	107	108
Prototype CRS. Two rigid lower fixings + top tether	3237	27	25	387	3549	64	86	90
Prototype CRS. Two lower straps + top tether	3250	42	45	552	3554	66	85	103

* Door failed to latch. Results not comparable to other tests.

Figure 8 Intrusion panel tests vs non intrusion panel tests (ECE R44 03 belt anchor positions)

CRS EVALUATIONS

Figure 8 compares side impact tests, with intruding structure, with tests conducted to the existing side impact procedures without side structure.

The following observations can be made from the above results. Firstly with respect to the intruding structure test, it is evident that the size, mass and particularly the rigidity of attachment of the CRS is significant. The concern is particularly evident with the larger CRS employing rigid attachments, where insufficient energy is available to move or deform the seat sufficiently, a situation not evident in the vehicle tests. It can be seen that, although conducted at a lower velocity than the existing sled based side impact test, the effect of the manikin and CRS striking the intruded structure does, as expected, produce an increase in occupant deceleration levels. However, when reviewing the forward facing 15kg occupant, the increases are not large when compared with the lateral CRS acceleration levels. This can be attributed to the head and chest being in close proximity to the hinge about which the intruding panel rotates, and hence seeing contact at a much lower velocity, reflecting reality for the rear seat situation. The situation can be seen to be reversed when considering rear facing infants whose head is in close proximity to the vehicle 'B' pillar. In these cases, the head and chest acceleration levels, particularly in the case of less rigidly retained CRS are much higher. The lightest conventionally retained CRS demonstrates the highest levels of acceleration. It must at this point be noted that the manikins employed for these tests are relatively stiff, and have a limited neck structure. This effect has been observed in some full scale vehicle impacts performed in the EuroNCAP test programme[5].

This represents the impact conditions for a child restraint seated in the rear seating position of the vehicle. To represent the front seating position, the door should be hinged at the front edge to duplicate the intrusion pattern for the front seat. The relative effects on the rear and forward facing child restraints would then be expected to be reversed.

SUMMARY

It is apparent that the angular velocity of the intruding structure, although reaching the prescribed levels, is still low, and drops off rapidly. If Figures 2 and 5 are compared, it is apparent that a shortfall in kinetic energy exists in comparison to the full scale vehicle tests, particularly later in the intrusion panel travel.

Apart from modifications to the test to impart more energy to the intrusion panel later in the event, the remaining parameters that can affect impact severity and hence occupant response are panel mass and stiffness. These parameters need to be tuned to obtain the optimum desired CRS and manikin response levels equivalent to the full scale vehicle tests.

CONCLUSION

The concept of an intruding panel side impact test does offer potential advantages over current performance evaluations for existing CRS retained by adult belts in rear seating positions. However the test, as presently proposed, does not seem to impart sufficient energy to evaluate adequately the very rigidly retained CRS proposed in the near future (ISOFIX).

This test procedure will, however, offer an opportunity to assess more realistically the lateral impact performance of CRS, particularly rear facing infant carriers in the rear of vehicles where the child's head is positioned in close proximity to the area of maximum potential intrusion in a side impact. A modification to the test arrangements would be necessary to evaluate the performance in the front seating position.

The preliminary sled test findings relating to rear facing infant carriers detailed here, supported by observations made during the recent EuroNCAP tests, indicated a significant potential risk of head and chest injury in a side impact when positioned on the struck side in rear seating positions.

ACKNOWLEDGEMENTS

The authors wish to acknowledge the support of both Mr G T Savage and Mr C T Witherington for their assistance in the dynamic testing and subsequent data analysis at Middlesex University.

The bulk of the work described in this paper forms part of a Transport Research Laboratory research programme performed under a contract placed by the Department of the Environment, Transport and the Regions. Any views expressed in it are not necessarily those of the Department.

REFERENCES

[1] Langwieder K, Hell W, Lowne R, Huijskens C. Side impact to children in cars. Experience from international accident analysis and safety tests. 15th ESV conference Melbourne 1996

[2] New Zealand standard NZS 5411, Australian standard AS 1754.

[3] Hill K J, Roy A P. Simulation of the Effects of Vehicle Impacts on Restrained Child Occupants - Part A: A description of the KL/MP Test facility. Journal of the Society of Environmental Engineers 21st March 1982.

[4] TNO Research institute for road vehicles, Holland. P range of manikins developed for ECE R44 CRS approvals.

[5] Euro NCAP Family Car Crash Test Results (1997). Extracts published by *'What Car'* magazine.

TOWARDS IMPROVED INFANT RESTRAINT SYSTEM REQUIREMENTS

France Legault
Del Stewart
Transport Canada
Canada
Paper Number 98-S10-O-10

ABSTRACT

Observational surveys and analysis of motor vehicle collision data files have confirmed that some infants are transferred to the next category of restraint or taken out before they have "out-grown" their prescribed protective devices. Legislation, enforcement and education countermeasures are tools that have been used to increase proper restraint use among infants. The next phase of improving protection for infants is regulating aspects of the product to increase prolong proper use. The introduction of larger infant dummies in sled testing is one of the most important of these regulatory initiatives as it applies to infant restraints.

Canadian collision data files were analyzed and crash tests simulations (sled tests) were conducted. Convertible restraints were tested in the rear and forward facing configurations using 6-, 9-, 12- and 18-month and 3-year dummies. All parameters for the 12- and 18-month dummies were recorded for a more in-depth comparison of the performance of restraints when tested facing forward or rearward. Every convertible restraint tested in the rear facing configuration passed the CMVSS 213.1/FMVSS 213 criteria with the 6-, 9-, 12- and 18-month dummies. Some of the restraints passed the regulations' criteria with the 3-year old dummy although the dummy's legs interaction with the standard seat back was a challenge for proper installation. In all cases, the structural integrity of the restraint was intact.

Canadian child restraint use surveys were reviewed to determine the level of proper use and orientation of infant restraints. Likewise, accident data files were analyzed to determine the proportion of infants and children involved in motor vehicle collisions who occupy infant/child restraint devices. The injury severity levels were determined. These injuries were compared for restrained/unrestrained and ages of occupants, and if the restraint devices was used properly or not.

Analytical methods are employed to determine whether any significant effects on the restraint performance exist due to infant dummy size, restraint model or the interaction of the two. Also, similarities and differences in performance among the forward and rear facing configurations and various restraint models are measured and compared.

Infants and young toddlers, are provided with a higher level of safety when restrained in a rear facing infant restraint system as long as possible rather than not being restrained, being restrained in a forward facing restraint or restrained by a seat belt.

INTRODUCTION

In some countries it has long been recognized that restraining children in devices facing the rear of the vehicle offers optimum protection and a high degree of acceptability by users.[1] [2] [3] [4] [5] In other countries the use of restraints that face the rear of the vehicle have been met with mixed reactions by the users.[6] In Canada, currently close to 26 % of users of infant restraints designed to face the rear orient them in the wrong direction.[7] Because of snowy and wet weather conditions during the Canadian winter, it is anticipated that, at first, acceptance of rear facing restraints for older children may be limited to pre-walkers. However, with 50 % of one-year old children not yet walking[8] greater use of rear facing restraints for older infants would be anticipated over the years.

The heavy head of children in comparison to their total body mass[9] and their weak neck is best protected while being in a rear facing restraint by the continuous seat back. This is especially important in frontal collisions, the most frequent and severe direction of impact encountered in automotive crashes. In Canada, victims of frontal impacts account for 44 % of all collision victims[10]

Rear facing infant restraint systems have been available in North-America since the late-sixties.[11] A Canadian regulation governs their safety performance since 1972.[12] Recognizing the specific needs of infants, a regulation addressing the safety of rear facing infants was promulgated in Canada in 1982.[13] The main objective o this regulation is to ensure the safety of new-borns, while properly restrained in a rear facing device, until they weigh 9 kg. At the time the regulation came into force, the only available dummy to test such a device was the 50th percentile 6-month "bean bag" dummy.[14] The mass of this and other dummies used for testing in this program are listed in Table 1. In 1996 the use of the 9-month (3/4 TNO) dummy[15] was permitted in Canada.[16] This permitted the maximum usable mass for rear facing infant restraints to be increased to 10 kg.

Table 1.
Mass of dummies used in this test program

50th percentile dummies	mass (kg)	mass (lb.)
6- months	7.8	17.2
9- months	9	19.8
12- months	10.0	22.0
18- months	11.5	25.4
3- years	15.73	34.69

One of the dynamic criteria for rear facing infant restraints in Canada is that the head of the dummy does not pass a pair of orthogonal planes at the top-most part of the restraint at any time during the crash simulation. These planes are illustrated in Figure 1. The other criteria is that the angle of the seat back of the infant restraint with respect to the horizontal does not exceed 70 degrees from the vertical. This is graphically depicted in Figure 2.

The next category of restraints in Canada are designed to protect children whose mass is over 9 kg and less than 22 kg. The Hybrid II 3-year old[17] is the referenced surrogate to test these restraints in accordance with the regulation.[18] The criterion established for the simulated dynamic crash test is that at no time during the test should any part of the head of the dummy exceed a distance of 720 mm from a fixed reference point on the standard seat.[19] This criterion and the dummy with which the test is perform is equally applicable for forward facing or rear facing restraint systems for older children. Because the head of a 3-year old dummy in current convertible restraint designs is already beyond the permissible 720 mm limit, rear facing child restraints have not been sold in Canada.

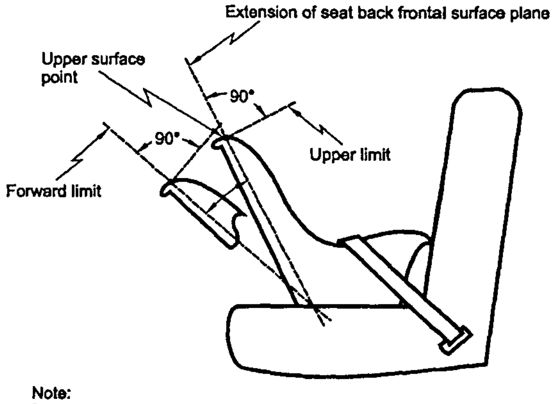

Note:
The illustrated limits move during dynamic testing.

Figure 1. Orthogonal planes limiting the movement of the head of the dummy during dynamic testing.

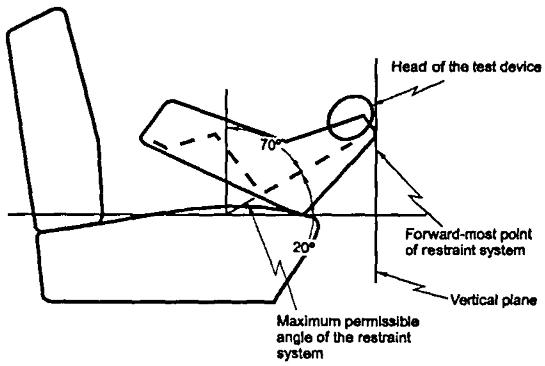
Head of the test device
70°
Forward-most point of restraint system
20°
Vertical plane
Maximum permissible angle of the restraint system

Figure 2. Maximum permissible seat back tip angle during dynamic testing

Regnonizing the benefits of protecting children in a rear facing orientation, consideration was given to solutions that would allow Canadian restraint users a safer alternative.[20] A test program was conducted using different makes of convertible restraint systems. A convertible restraint is one that is used in a reclined position and installed facing the rear of the vehicle for infants. The convertible restraint is then turned to face the front of the vehicle in a more upright position to restrain older children.

Convertible restraints of the same make and model were tested forward facing and rear facing. The head and chest accelerations, neck forces and moments and shoulder loads were compared for the forward and rear facing modes under experimentally controlled conditions. A comparison was made with previously reported data[21] of the forward configuration when the restraints were untethered.

It was expected that the head and chest accelerations, neck forces and moments would tend to have lower values in the rear facing configurations as compared to forward facing. No references on shoulder loads and threshold could be found in the literature. Only relative effects on shoulder loads could be analyzed. However, it was predicted that F_z would increase in the rear facing configuration as compared to forward facing, while F_x would decrease.

The testing was performed using some older generation dummies, the 6-month "bean bag" and the 3-year old Hybrid II dummies; one newer but uninstrumented 9-month (TNO ¾) and two state-of-the-art fully instrumented 12- and 18-month CRABI dummies.[22] [23] These dummies were selected since they surrogate children of physical development that most likely benefit from using rear facing restraint systems. The capacity of the CRABI dummies to measure upper and lower forces and triaxial moments in the neck allowed for the recording of new parameters. A literature search has not identified any studies measuring neck upper and lower forces and triaxial moments using these dummies in child restraints with tethers.

Four commercially available convertible restraint systems and the CanFIX[24] [25] were tested. All restraints tested had a similar T-shield type harness design system to minimize harness variability. T-shields are typical and commonly used in Canada.

The make of child restraint system was not expected to have any significant effects on the results within the parameters recorded. The performance of the CanFIX was expected to be slightly better relative to similar child restraint systems since the base was rigidly attached to the standard bench seat of the sled.

A major analytic objective of this research study was to determine whether any significant differences in performance among the infant restraint systems exist, particularly as these differences relate to any significant effects due to infant restraint type, dummy size and particularly restraint installation orientation (i.e., forward-facing or rear-facing).

Canadian field accident data were also analyzed to determine the crash involvement of restrained children, properly and improperly restrained, by injury severity.

ANALYSIS OF CANADIAN COLLISION DATA FILES

Data Source

Detailed national investigation data – known as 'Level II accident investigation case studies' – were analyzed in an attempt to shed some light on the nature of the child's restraint status and their injury severity. Level II accident investigations differ from Level I (police investigated and reported) in that they are Level II accident investigations differ from Level I investigations (police investigated and reported) in that they are conducted by specially trained accident investigators and reconstructionists and the breadth, detail and accuracy of information collected on the factors and characteristics present in the collision is significantly greater. Specifically, the Level II Accident Investigation Passenger Car Study (PCS) [26] that was used is an in-depth investigation of motor vehicle collisions in which at least one passenger car is involved and at least one occupant of the vehicles involved was either killed (fatal collision investigations) or injured (injury-producing collision investigations). The entire database contains 363 data elements (categorized within 27 separate files - each file represents a specific type of data collection form, e.g. vehicle, restraint use). An extensive range of collision, road user, road/infrastructure, vehicle, environment and temporal factors and characteristics associated with each accident investigation case study are described. The number of case studies in the databases totals 7,853. The survey was conducted between 1984 and 1992 inclusive by Transport Canada and a national network of ten university-based accident investigation teams located within eight provinces including British Columbia, Alberta, Saskatchewan, Manitoba, Ontario, Quebec, New Brunswick and Nova Scotia. A statistically representative survey design and sampling plan was designed by Transport Canada (and implemented by the accident investigation teams) to ensure 'random' and 'unbiased' selection of collisions for investigation. Due to financial limitations it was not possible to obtain sufficient personnel resources to conduct the survey on the entire road system networks in each province. As a result the geographic coverage of the survey was restricted to roads and highways that were within a 80 km radius of the university at which the accident investigation team is located.

These data bases were analyzed employing the methods and procedures developed by Stewart[27] to identify injury severity of children in fatal and injury producing collisions cross-classified by correctness of restraint installation, correctness of restraint system use, and the age of the child (six age groups were analyzed including 0-6 months, 6-9 months, 9-12 months, 12-18 months, 18-36 months and 36 to 60 months). Unfortunately, due to the detailed level of this information coupled with the relatively small number of case studies completed across Canada each year, the final cross-classified data base quickly reduces to only 129 children meeting the analysis criteria above. Therefore, all estimators reported here are subject to high variability, i.e., the errors associated with them are quite large - in the order of 40 % and higher in some instances.

Results of PCS Analysis

Among the 129 injured children in the PCS data files between the years 1984 to 1992 there are 41 fatalities and 88 injuries. A fatality is defined as any child who died within 30 days of injuries sustained in the motor vehicle collision. An injury is defined as visible signs of being hurt and an injury form being completed for the individual.

Examination of the results for the fatally injured children showed that for the age groups 0-6 months and 6-9 months all the children killed were in infant restraint systems that were both incorrectly installed and improperly used (i.e., the child was not properly restrained in the infant restraint seat). For the 12-18 month age group the results indicate that: 32.7 % of the fatally injured children were in a child restraint system that was improperly installed and improperly used; 36.6 % of the deceased children were in a child restraint system that was incorrectly installed, but the child was properly restrained in the system itself; and 30.6 % of this fatally injured age group were in child restraint systems that were correctly installed and properly used. The other age groups analyzed, namely 9-12 months, 18-36 months and 36-60 months were not represented in the fatally injured case studies over the years 1984 to 1992 inclusive.

A similar analysis of the children injured in the PCS data bases revealed that all of the 0-6 month old children injured in a collision accommodated infant restraint systems that were not correctly installed and who were not properly restrained in the infant restraint system itself. Among the 6-9 month old infants, 50 % of the injured children were improperly restrained in an infant seat that was also incorrectly installed. The other 50 % of these injured 6-9 month old infants were properly restrained in a system that was correctly installed as well. The analysis of the 9-12 month old infants showed that 92.2 % of the infants injured in collisions were improperly restrained in a system that was also incorrectly installed. The remaining 7.8 % of the injured infants were properly restrained in the restraint system itself, but unfortunately the restraint system was incorrectly installed in the vehicle. The other three age groups (12-18 months, 18-36 months and 36-60 months) were not represented in the injured PCS data bases.

Summary

Although it must be re-iterated that the results provided above are subject to high levels of error (due to the small sample sizes they comprise within the entire PCS data bases) the trend is quite evident.

A strong correlation between incorrect restraint installation, improper restraint use and the probability of sustaining an injury or fatality is quite apparent. It is therefore necessary to work towards improving protection for infants through mechanisms such as regulating aspects of the various restraint system products to increase both their correct installation and proper use.

SLED TEST METHODOLOGY

Test Set-Up

Laboratory tests were conducted on the HyGe sled at the Defence and Civil Institute of Environmental Medicine (DCIEM) at a δV of 48 km/hr. The pulse was 20 "g" for a duration varying between 11 and 48 milliseconds. The standard bench seat was in accordance with drawing package NHTSA SAS-100-1000. These conditions, specifications for atmospheric soaking and test preparation, are specified in Canadian test procedures for testing child restraint systems.[28] Contrary to European practice,[29] this test program was not conducted with a simulated dash, rather the restraints were allowed to travel forward uninterrupted. As opposed to Australia[30], rear facing restraints are not yet used in Canada with a tether. Therefore the rear facing tests have been performed without a tether whereas the forward facing restraints were tethered.

High-speed cameras were mounted on the test sled such that the films could be analyzed to determine dummy motion and maximum excursion.

Dummies

CRABI 12-month and 18-month fully instrumented anthropometric test devices were used in this test program. These dummies represent occupants in the targeted ages for increasing the maximum occupant mass in Canada. To compare with the current typical use and test methods, a "bean bag" 6-month and an un-instrumented 9-month old (TNO ¾) dummies were used. Finally, to assess the potential of reviewing the criteria for a larger mannequin to be used for rear facing testing, a Hybrid II 3-year instrumented with head and chest acceleration sensors was also used.

Both CRABI dummies were fully instrumented with sensors as summarized in Table 2.[31] These included force and moment transducers for the upper and lower neck and shoulder loads. The dummies were clothed as specified in the current test method[32] for child restraint systems with adjustments made for their respective sizes.

Table 2.
CRABI 12- and 18-month instrumentation

LOCATION	TYPE	AXIS	FULL SCALE	OUTPUT @ CAPACITY
Right/left shoulders	Denton model 2791	F_X	1 780 N	1.5 mV/V
		F_Z	1 780 N	1.5 mV/V
Upper and lower neck	Endevco model 7264-2000	F_X	890 N	1.8 mV/V
		F_Y	890 N	1.8 mV/V
		F_Z	2 225 N	0.8 mV/V
		M_X	56,5 N-m	2.5 mV/V
		M_Y	56,5 N-m	2.5 mV/V
		M_Z	33,9 N-m	1.3 mV/V
Head	Endevco 7264 A-2000	a_X	200 g	1.4 mV/V
		a_Y	200 g	1.4 mV/V
		a_Z	200 g	1.4 mV/V
Thorax	Endevco 7264 A-2000	a_X	200 g	1.4 mV/V
		a_Y	200 g	1.4 mV/V
		a_Z	200 g	1.4 mV/V

Only the CRABI 18-month dummy was available to test the CanFIX.

Restraints

Four restraints commercially available in Canada and the CanFIX concept restraint were selected for the tests. All restraints tested including the CanFIX had a similar T-shield type harness design system to minimize harness variability. The commercial restraints have not been identified in the paper by make and model but rather by letter codes, "T", "S", "C' and "U".

A new restraint was used for every test. The dummy was placed in the restraint according to the procedures recognized in the field.[33] [34] Similarly, every restraint was installed on the standard seat according to prescribed procedures of CMVSS/FMVSS (in references).

Repeatability Tests - Repeatability testing was performed within five different test conditions. Two tests were performed for each of the eight configurations. This information is reported in Table 3.

Table 3.
Repeatability Tests List

Restraint	Run Numbers	Repeatability Runs
"T"	2525 & 2566 2524 & 2537 2631 & 2632 2600 & 2607	√
"S"	2536 & 2570	√
"U"		no
"C"		no
CanFIX		no

Forward vs. Rear Facing Performance - As one of the objectives of this study is to determine the effect of restraining children rear facing as opposed to forward facing, every restraint in the test program was tested in both configurations with every one of the dummies.

Corrected Neck Values - The values recorded for upper and lower neck moments M_y' have been corrected to take into account the off-centre location of the sensors in the upper and lower neck of the CRABI 12- and 18-month old dummies.[35]

$$M_y' = M_y - 0.0058\, F_x \qquad (1.)$$

where M_y' is the corrected neck moment about the Y-axis
M_y is the recorded neck moment about the Y-axis
F_x is the recorded neck force along the X-axis

The neck moment values are reported in the corrected format.

Film and Analysis - Each test was recorded and the data were analyzed using the following equipment :

- Transducers on the sled were supplied with 10 V. DC from local sled-mounted power supplies. Outputs were fed to a sled-mounted, variable gain and offset amplifiers which converted the signals from differential to single-ended.
- Amplified signals were sent to active analog filters (via a low-noise multi-coaxial umbilical cable) which filters at SAE classes 180, 600 or 1000 Hz depending on the rate at which the signals were sampled (1500, 5000, or 8000 samples/sec).
- Filtered outputs were fed to a series of four National Instruments NB-MIO-16 multifunction boards containing 12-bit A/D converters which provided direct memory access to the RAM of a Macintosh II FX.
- Data were then transferred to disk, where custom-designed National Instruments Labview software was used to provide for digital filtering (at SAE class 60, 180, 600, or 1000 Hz),[36] and for scaling, further processing and plotting.

The video recordings were used to perform the kinematics analysis for each test and determine maximum head excursion. This information was recorded using:

- A Kodak EM Ektapro Motion Analyzer system.
- A Kodak High-gain imager (video camera).
- A Kodak EM Processor (model 1012) producing black & white motion pictures with X-Y electronic crosshair calculation capability.
- The frame rate was 500 frames per second.
- The shutter speed was 1/1000 sec.

RESULTS

The numeric results for every test in the program are listed in Appendix A, Table A-1. For the purposes of this paper, maximum values for head and chest excursion, chest acceleration, upper and lower neck F_x and F_z and corrected M_y and right and left shoulder loads are reported for the 12- and 18-month old mannequins. Original restraint back angle and maximum seat back angle with respect to the vertical are reported for the non-instrumented mannequins (6- and 9-month old and 3-year old).

The results are graphically presented in the Appendix "B" as Figures B-1 through B-12.

The acceptable limits for head excursion of 720 mm and chest acceleration of 60 g are those specified in CMVSS 213. For reference purposes, the 80 g acceptable level of head acceleration was adopted from the criteria for the 3-year old dummy level for built-in child restraint systems.[37]

Crash reconstructions have led researchers to establish injury threshold limits for the upper neck of different dummies.[38] [39] [40] Since the 12- and 18-month dummies used in the current study are relatively new, a literature search has not produced any studies that have established threshold levels for their neck. In such cases for the purpose of this analysis, thresholds from all previous studies have been included where appropriate in the graphs of Appendix "B". Table 4 summarizes the threshold values of previous studies.

Table 4.
Threshold limits - upper neck - studies

Researcher	Dummy used for reconstruction	Tensile axial force F_z (N)	Shear force F_x (N)	Forward bending moment M_y (N-m)
Planath et al., 1992	3-year old	1000	300	30
Trosseille and Tarrière, 1993	six-month old CRABI	1200	950	41
Janssen et al., 1993	9-month - adult Hybrid III values /scaling	850	800	41

For comparative purposes, whenever a threshold is associated with a parameter, a line is drawn at the threshold level in the graphs.

Effect Dummy Size on Seat Back Tip Angle

The initial seat back angle was, as expected, not greatly influenced by the size of the dummy. Restraint "C" demonstrated a difference where the initial angle increased with the size of the dummy because of leg interference with the seat back of the standard seat.

The maximum seat back angle has a tendency to increase as the size of the dummy increases. This was expected since a heavier dummy applies more load during the test on the seat back. This trend was not consistent with Restraint "C" but could be attributable to dummy leg interference with the standard seat back as described above.

In all cases the convertible restraint tested with larger dummies than specified in the current Canadian regulation passed the maximum seat back angle in the rear facing configuration.

The structural integrity of the restraints was not damaged during the test.

Effect of 12- Versus 18-Month Dummy

The following analysis is based on the more exhaustive data recorded using the 12- and 18- CRABI dummies.

Head Acceleration - The head acceleration data is presented graphically in Appendix "B", Figure B-1. In all cases the head acceleration is between 30 and 59 % lower than the accepted threshold of 80 g's. In every case, but Restraint "S" and Restraint "T" and the CanFIX tested with the 18-month dummy , the head acceleration was either lower or approximately equal, for rear facing compared to forward facing. In the absence of a simulated seat back or dash, all the head accelerations were inertial.

Chest Acceleration - Figure B-2 of Appendix "B" presents the results for chest acceleration recorded during this test program. In all cases, the chest acceleration was lower when a similar restraint was tested with the same dummy and placed rear facing as compared to forward facing. In all the cases tested, the chest acceleration was lower than the accepted threshold for child restraints.

Upper Neck Loads **(F_x and F_z)** - The data for upper neck loads F_x and F_z are presented respectively in figures B-3 and B-4 of Appendix "B". The lack of head contact with any external object and the similar restraining forces mean that the head would be restrained by the neck alone. In all cases, the upper neck load x-component, F_x was always lower for the rear facing than for the forward facing configuration. The rear facing values for F_x for Restraint "S", Restraint "U" tested with the 18-month and the CanFIX exceeded the threshold suggested by one study, whereas F_x exceeded the same threshold for every forward facing configurations.

For F_z in every case, but Restraint "T" tested with the 18-month and the CanFIX, the result was lower for the rear facing than the forward facing configuration. In fact for three of the eight tests with the commercial restraints, the forward facing value exceed the three thresholds suggested by various studies. None of the restraint in the rear facing installation exceeded the three thresholds with the exception of the CanFIX.

Upper Neck Moments (M_y) - Upper neck moments about the y-axis, M_y are reported in Figure B-5 of Appendix "B". In half of the test conditions, upper neck M_y was lower rear facing than forward facing. In the other half however the reverse was true. No definite trend could be identified from the data and more investigation may be required to be more conclusive. However, in all forward and rear facing cases, the values were below the suggested threshold limits thus confirming that it would not pose bending moment injuries to restraint older children rear facing.

Lower Neck Loads **(F_x and F_z)** - Data for lower neck loads in the x-direction, F_x are presented in Figure B-6 of Appendix "B". In all cases, the values were lower for rear facing conditions than for corresponding forward facing conditions. The graph for lower neck loads in the z-direction, F_z appears in Figure B-7 of Appendix "B". In this case, the trend is reversed in all but one case, Restraint "C" when tested with the 12-month dummy. This contradiction could not be explained from the testing and further investigation would be necessary to resolve it.

Lower Neck Moments (M_y) - Lower neck moments about the y-axis, M_y are graphically represented in Figure B-8 of Appendix "B". Although one data channel was lost, (Restraint "U" tested rear facing with the 12-month dummy) readings for all other tests indicate that M_y had considerably lower values for the rear facing tests as compared to the forward facing ones.

Neck Parameter Correlation - Correlation between upper and lower neck values were calculated for each test and are presented in Table 5a. It was expected that upper and lower neck values might have correlated with one another. This was the case for about half of the responses. The discrepancies between the expected performance of the dummies and the observed performance will require further research to explain.

Table 5a.
Correlation between upper and lower neck parameter for the same test

	12-month rear facing	12-month forward	18-month rear facing	18-month forward facing
Fx	-0.81	-0.86	-0.13	-0.47
Fz	0.93	0.55	0.98	0.47
My	-0.10	-0.16	-0.02	-0.91

Right and Left Shoulder Loads (**F_x and F_z**) - The right and left shoulder loads in x-direction, F_x were between four and ten times lower in the rear facing mode as compared to forward facing. This trend was reversed for the z-component of force but the difference was much less pronounced. The shoulder loads are plotted in Figures B-9, B-10, B-11 and B-12 of Appendix "B". Correlation between right and left shoulder loads were calculated for each test and are presented in Table 5b. The CanFIX were not included in this analysis. It was expected that left and right shoulder values would correlate with one another. This was the case in six out of the eight conditions.

Table 5b.
Correlation between the right and left shoulder for the same test

	12-month rear facing	12-month forward	18-month rear facing	18-month forward facing
Fx	0.45	0.97	0.72	0.89
Fz	0.93	0.77	0.94	0.36

Initial and Maximum Seat Back Tip Angles

The dynamic criteria for rear facing infant restraints that limits with the top-most part of the restraint was met in every rear-facing test even with dummies larger than which were intended. In the Canadian regulation the criterion limiting the angle of the seat back of the infant restraint with respect to the horizontal is 70 degrees from the vertical. It was met for every restraint. Graphs of seat back tip angles are presented in Appendix "C", figures C- 1 through C- 4.

RESTRAINT PERFORMANCE DIFFERENCES AND SIMILARITIES

In order to determine whether any significant differences in performance among the infant restraint systems exist, particularly as these differences relate to any significant effects due to infant restraint type, dummy size and infant restraint installation orientation (i.e., forward-facing or rear-facing) an analysis was undertaken.

Experimental Design

To accomplish this an experimental design appropriate for analyzing the test program data available had to be identified. In general, the test data lends itself to a broad class of factorial experiments composed of multifactors with repeated measures on the same elements used in the tests. Further adjustments in the analytical methods for these types of designs were made to accommodate missing test data (i.e., data was not available for all performance measures, factors and their levels from all tests carried out) which resulted in unequal cell frequencies in the design matrix. These adjustments were accounted for through the development of statistical models using 'unweighted-means' analysis methods.[41] [42] [43] [44] These procedures are more appropriate than least-squares solutions for the test data collected in this research due to the completed experimental design has unequal group sizes because of conditions that are unrelated to the treatments. That is, the unequal cell frequencies are not the result of pre-planned stratification on the levels of the factors, i.e., infant restraint type, dummy size or restraint orientation, being investigated.

The experimental design to use, therefore, for analyzing the sled test data is that of a p x q x r factorial experiment in which there are repeated observations on the last two factors q and r. A schematic representation is given as follows:

$$\begin{array}{ccccccccc}
 & & b_1 & & \cdots & & b_q & \\
 & c_1 & \cdots & c_r & \cdots & c_1 & \cdots & c_r \\
a_1 & G_1 & \cdots & G_1 & \cdots & G_1 & \cdots & G_1 \\
a_2 & G_2 & \cdots & G_2 & \cdots & G_2 & \cdots & G_2 \\
\cdot & \cdot & & \cdot & & \cdot & & \cdot \\
\cdot & \cdot & & \cdot & & \cdot & & \cdot \\
\cdot & \cdot & & \cdot & & \cdot & & \cdot \\
a_p & G_p & \cdots & G_p & \cdots & G_p & \cdots & G_p
\end{array}$$

There are n_{ijk} subjects in each group. Each subject is 'potentially' observed under all qr combinations of factors b and c but only under a single level of factor a. This basic design was used for investigating whether any significant differences in performance measures (i.e., head acceleration, chest acceleration, upper neck $\{F_x, F_z, M_y\}$, lower neck $\{F_x, F_y, M_y\}$, left shoulder $\{F_x, F_z, F_r\}$, and right shoulder $\{F_x, F_y, F_r\}$) exist and whether the differences are due to the three main factors - infant restraint type, dummy size and infant restraint installation orientation (i.e., forward-facing or rear-facing).

Analytical Methods and Procedures

To illustrate the analytical methods and procedures a detailed description of the head acceleration performance measure is described here. Table 6 shows the basic head acceleration test results data within the format of the p x q x r experimental design used for this analysis. The cell means for the design are given in Table 7. Due to the fact that an unequal number of observations are in each of the cells of the basic data matrix the harmonic mean of the cell frequencies must be computed and used to compute the SS (sum of squares) used in the Analysis of Variance for the various factors and their interaction effects. The formula for computing the harmonic mean is given in equation (2.).

$$\overline{n}_h = \frac{pqr}{\sum_i \sum_j \sum_k \left(\frac{1}{n_{ijk}} \right)} \qquad (2.)$$

For our head acceleration example here $\overline{n}_h = 1.230769$.

Next the within-cell information required in the analysis is given in Table 8. Using the above information the various definitions and numerical values of the computational symbols and relevant sums of squares needed for carrying out the analysis of variance are computed and they are given as follows:

n = 2 , p = 2 , q = 2, r = 4 , ΣΣΣn_{ijk} = 22 ,
G = 1032.1 , G' = 747.55 ,
(1') = [G'**2]/pqr = 34926.93766 ,
(2) = Σ(Xi**2) = 49018.85 ,
(3') = [Σ(Ai'**2)] /qr = 34963.08781 ,
(3) = [Σ(Ai**2)]/nqr = 48483.48455 ,
(4') = [Σ(Bj'**2)]/pr = 34944.68281 ,
(6') = [Σ(AB'ij**2)]/r = 34984.78313 ,
(6) = [Σ{(ABij**2)/ni}]/r = 48510.42933 ,
(7') = [Σ(AC'ik**2)]/q = 35200.50625 ,
(7) = [Σ{(ACik**2)/ni}]/q= 48718.5025 ,
(8') = [Σ(BC'jk**2)]/p = 35382.94125 ,
(9') = [Σ(ABC'ijk**2)] = 35444.9025 ,
(9) = [Σ{(ABCijk**2)/ni..}] = 48985.705 ,
(10) = [Σ{(Pm**2)/ni..}] = 48484.02458 (where ni.. is the total observations for Pm) ,
(11) = [Σ{(BPjm**2)/ni..}] = 48518.0125 (where ni.. is the total observations for BPjm) ,
(12) = [Σ{(CPkm**2)/ni..}] = 48782.57 (where ni.. is the total number of observations for CPkm).

The analysis of variance (ANOVA) for the unweighted means solution is given in Table 9. It must be noted that since all factors A, B and C are fixed the MS[w.cell] (shown in the Table) is the proper denominator to use for all significance tests.

Results

All statistical significance tests and decisions are based on a 95% level of statistical confidence. Only the head acceleration analyses are described in detail. The same type of analytical methods were designed and implemented for the other factors however, for the sake of brevity, and in the interest of focusing on the main findings only the results are discussed.

Head Acceleration - Examining Table 9 it is readily observed that the effects due to the size of the dummy have a significant impact on the head acceleration test results. Head acceleration responses are significantly higher for the 12-month old test dummy in comparison to the 18-month old dummy (i.e., the computed F[3,6] = 8.05 is larger than the tabulated $F_{.95}[3,6] = 4.76$). Also, the infant restraint orientation in the sled test (i.e., forward-facing versus rear-facing) has a significant effect on the head acceleration responses obtained with the larger head accelerations being experienced when the infant restraint is in a forward-facing position. The three-way interaction effects among the three factors being investigated was not significant implying that the variation in the head acceleration responses are not due to varying effects of the different levels of two of the factors on the third factor. Also, the two-way interaction effects of dummy size with restraint orientation and dummy size with infant restraint type are not significant. Therefore, the head accelerations are not dependent upon the joint effects of the dummy size and seat orientation or the dummy size and the restraint type. The most noteworthy finding was the significant interaction detected between the infant restraint orientation and the type of infant restraint. The head acceleration responses were significantly different - that is, the different infant

Table 6.
Basic Test Data Results for Dummy head accelerations (measured in g's)

		b 1				b 2				
Sub-jects										Total
		c1	c2	c3	c4	c1	c2	c3	c4	388.3
a1	1	52.5	51.6	46.4	51.7	47.4	56.2	36.6	45.9	146.5
	2	52.7	45.2			48.6				
a2	3	43.7	45.7	46.9	45.8	45.0	54.7	33.1	45.9	360.8
	4	45.7				48.1			42.7	136.5

where,

a1 = 12 month old dummy size
a2 = 18 month old dummy size
b1 = front facing infant restraint system orientation
b2 = rear facing infant restraint system orientation

c1 = Restraint "T"
c2 = Restraint "S"
c3 = Restraint "C"
c4 = Restraint "U"

Table 7.
Summary table of cell means (a', b', c') for the p x q x r factorial design

	b' 1				b' 2				
	c'1	c'2	c'3	c'4	c'1	c'2	c'3	c'4	Total
a'1	52.6	48.4	46.4	51.7	48	56.2	36.6	45.9	385.8
a'2	44.7	45.7	46.9	45.8	46.55	54.7	33.1	44.3	361.75
Total	97.3	94.1	93.3	97.5	94.55	110.9	69.7	90.2	747.55 = G'
Σ Bj'	382.2				365.35				
Σ Ck'	191.85	205	163	187.7					
AB'ij	199.1				186.7				
	183.1				178.65				
AC'ik	100.6	104.6	83	97.6					
	91.25	100.4	80	90.1					

Table 8.
Summary of the within-cell information required in the analysis

		b 1				b 2			
		c1	c2	c3	c4	c1	c2	c3	c4
a1	n_{ijk}	2	2	1	1	2	1	1	1
	$\Sigma(X_{ijk})$	105.2	96.8	46.4	51.7	96	56.2	36.6	45.9
	$\Sigma(X^*X)$	5533.54	4705.6	2152.96	2672.89	4608.72	3158.44	1339.56	2106.81
	SS_{ijk}	0.02	20.48	0	0	0.72	0	0	0
a2	n_{ijk}	2	1	1	1	2	1	1	2
	$\Sigma(X_{ijk})$	89.4	45.7	46.9	45.8	93.1	54.7	33.1	88.6
	$\Sigma(X^*X)$	3998.18	2088.49	2199.61	2097.64	4338.61	2992.09	1095.61	3930.1
	SS_{ijk}	2	0	0	0	4.805	0	0	5.12

The pooled within-cell variation is given by: SS[w.cell] = $\Sigma\Sigma\Sigma[SS_{ijk}]$ = 33.145
The degrees of freedom for the within-cell variation, df{w.cell} = $\Sigma\Sigma\Sigma[n_{ijk}] - pqr = 6$

Table 9.
Summary of the ANOVA

Source of Variation	Computational Formula	SS	df	MS	F
Between Subjects	(10) - (1')	13557.0869	3		
A	$\bar{n}$ [h]{(3') - (1')}	44.4925	1	44.4925	8.05
Subject w. groups[error (a)]	(10) - (3)	0.5400	2	0.2700	
Within Subjects	(2) - (10)	534.8254	28		
B	$\bar{n}$ [h]{(4') - (1')}	35.4903	1	35.4903	6.42
AB	$\bar{n}$ [h]{(6') - (3') - (4') + (1')}	4.8617	1	4.8617	0.88
B x Subject w. groups[error (b)]	(11) - (6) - (10) + (3)	7.0431	2	3.5215	
C	$\bar{n}$ [h]{(5') - (1')}	284.2959	3	94.7653	17.15
AC	$\bar{n}$ [h]{(7') - (3') - (5') + (1')}	7.9113	3	2.6371	0.47
C x Subject w. groups	(12) - (7) - (10) + (3)	63.5274	6	10.5879	
BC	$\bar{n}$ [h]{(8') - (4') - (5') + (1')}	255.0990	3	85.0330	15.39
ABC	$\bar{n}$ [h]{(9') - (6') - (7') - (8') + (3') + (4') + (5') - (1')}	18.9944	3	6.3314	1.14
BC x Subject w. groups[error (bc)]	(2) - (9) - (11) - (12) + (6) + (7) + (10) - (3)	-37.9656	6	-6.3276	
Within cell	(2) - (9)	33.145	6	5.5241	

restraint systems generate significantly different head accelerations depending upon the orientation of the restraint system (i.e.; forward-facing or rearward-facing).

Chest Acceleration - Unlike the head acceleration results the dummy size did not produce significantly different chest accelerations. On the other hand, the chest accelerations are significantly higher for infant restraint systems oriented in the forward-facing than in the rear-facing position. Significant differences in chest acceleration results were also found for the different infant restraint systems. All two-way interaction effects were also found to be statistically significant (i.e., dummy size and restraint orientation, dummy size and infant restraint type, and restraint orientation and infant restraint type). This means that the chest acceleration responses are significantly different for all three factors, with the differences being dependent upon the level of another factor present in the sled test. Finally, unlike the head acceleration results, the chest acceleration responses are not significantly affected by the joint three-way interaction of all three factors. In other words the chest acceleration responses are not significantly affected or dependent upon the level of any of the three factors present in a particular sled test.

Upper Neck Loads (F_x) - The results of these analyses revealed that only the infant restraint orientation (i.e., forward-facing versus rear-facing) has a significant effect on the upper neck load x-component. The rear-facing loads are statistically significantly lower than the forward-facing. Neither of the other two factors (i.e., dummy size or infant restraint type) had a significant effect on the variations in the F_x responses. Also, none of the two-way interactions among the three factors nor the three-way interaction has a significant impact upon the F_x responses in the sled tests.

Upper Neck Loads (F_z) - The upper neck loads in the z-direction are significantly affected by the infant restraint orientation and the type of infant restraint. The size of the dummy has no significant impact upon the F_z results obtained. The only significant interaction effect identified was the infant restraint orientation by infant restraint type – the F_z responses are significantly dependent upon the restraint type and its orientation.

Upper Neck Moments (M_y) - The results of the analyses performed on the upper neck moments (M_y) responses from the sled tests revealed that none of the factors, non of the two-way interactions of the factors, nor the three-way interaction of the three factors has a significant effect on the M_y responses observed. In other words, the M_y responses are not significantly different for different dummy size, infant restraint orientation, infant restraint type, interactions of any of the levels of the two factors, or the three-way interaction of the factors.

Lower Neck Loads (F_x) - The ANOVA findings revealed that only the infant restraint orientation was a significant factor affecting the lower neck F_x's in the sled tests. The dummy size and infant restraint type did not have an appreciable affect on the F_x responses. Also, non of the two-way or the three-way interactions among the three factors provided any significant ability to predict the lower neck F_x loads.

Lower Neck Loads (F_z) - Contrary to the results found for the lower neck F_x loads, the analyses of the z-direction lower neck loads (F_z) identified a number of significant factors affecting the responses. All of the factors (dummy size, infant restraint orientation and infant restraint type) are significant with respect to the lower neck F_z sled test responses. This means that the lower neck F_z results are dependent upon all three factors – the significant differences depend upon the dummy size, infant restraint orientation and infant restraint type. Among the three two-way and the three-way interaction effects only one interaction effect is found to be statistically significant – the interaction of the dummy size and the infant restraint orientation. This implies that the lower neck F_z loads are statistically different for different dummy size and infant restraint orientation. In other words, the response loads are dependent upon the size of the dummy and the orientation of the infant restraint.

Lower Neck Moments (M_y) – From the analysis of variance carried out on the lower neck moments only one of the factors has a significant effect on the responses observed from the sled tests – the infant restraint orientation. Neither of the other two factors (i.e., dummy size or infant restraint type) nor any of the three two-way or the three-way interactions is a significant factor in explaining the source of variation among the lower neck moments (M_y) responses. Therefore, only the orientation of the infant restraint system – forward-facing versus rear-facing – has a significant effect on the level of lower neck M_y response. The responses are significantly smaller for the rear-facing orientation.

Left Shoulder Loads (F_x) – As in the case of the lower neck moments (M_y) above, the only factor that has a significant impact on the level of left shoulder loads observed among the sled tests is the infant restraint orientation. The left shoulder F_x's are significantly smaller for the rear-facing orientation than the forward-facing position. Neither the dummy size or the infant restraint type have an appreciable effect on the left shoulder F_x loads, nor do any of the two-way or the three-way interactions among the factors.

Left Shoulder Loads (F_z) – The findings of the analyses conducted on the left shoulder loads in the z-direction revealed the same results as the lower neck moments and the left shoulder F_x loads. The only significant factor having the capacity to explain variations in the left should F_z loads of the sled tests being the infant restraint orientation. The major difference, however, is that the rear-facing restraint orientation generates significantly higher F_z responses than the forward-facing restraint position.

Right Shoulder Loads (F_x) – These results differed considerably from those found for the left shoulder F_x response loads. Only dummy size has a significant effect on the responses observed in the case of the left shoulder F_x loads, whereas all three factors (i.e., dummy size, infant restraint orientation and infant restraint type) have significant impacts on the levels of response for the right shoulder F_x loads observed in the sled tests. Further differences resulted with respect to interactions – none were found in the case of the left shoulder forces in the x-direction, but the interactions of dummy size and infant restraint type, infant restraint orientation and infant restraint type, and the three-way interaction of dummy size by infant restraint orientation by infant restraint type are all significant components for explaining the variation among the right shoulder F_x responses in the sled tests. One of the most significant observations to note is how small the right shoulder F_x forces are in the rear-facing infant restraint orientation compared to the forward-facing position.

Right Shoulder Loads (F_z) – Quite different results were found for the right shoulder loads in the z-direction than for the F_z left shoulder responses. All three factors are statistically significant with respect to explaining variations among the right shoulder F_z responses, but only the infant restraint orientation has a significant effect on the level of left shoulder F_z response observed in the sled tests. Also the interaction effect due to the dummy size and infant restraint orientation as well as that due to infant restraint orientation and infant restraint type have significant impacts on the right shoulder loads in the z-direction. In contrast, no interaction effects whatsoever among the three factors were detected among the left shoulder F_z responses.

RELIABILITY OF MEASUREMENTS

In any experimental design involving test procedures and measuring devices there is always potential for sources of error to occur thereby affecting the resultant measurements. It is important that the amount of measurement error is known so that the results can be properly interpreted and also for making improvements in subsequent studies. Stewart[45] developed and implemented methodology for assessing the reliability of emission gas response estimates measured in Transport Canada's Emission Test Program on Methanol Fuels. The following sections present modified methodology based on this work for quantifying the amounts of measurement error present in the sled tests involved in the present research study and the implementation of these methods to measure the reliability of the responses obtained for each of the response variables measured.

Methodology

Given that a particular unit of a population possesses a magnitude π of a specified characteristic. In the measurement of this characteristic with some measuring device the observed score may have the magnitude $\pi + \eta$, where η is the 'error of measurement' – all measurements have some amount of this type of error. The amount of error due to η is in part due to the measuring device itself and in part due to the conditions surrounding the actual measurement. Therefore, a measurement on unit i with measuring instrument j may be represented as

$$X_{ij} = \pi_i + \eta_{ij} \qquad (3.)$$

where,

X_{ij} **= observed measurement,**

π_i **= true magnitude of characteristic being measured,**

η_{ij} **= error of measurement.**

Upon repeated measurement with the same or comparable instruments, π_i is assumed to remain constant, whereas η_{ij} is assumed to vary. The mean of k such repeated measures may be represented as shown in equation (4.).

$$\left(\sum_j X_{ij}\right) \Big/ k = \overline{P}_i = \pi_i + \overline{\eta}_i . \qquad (4.)$$

A schematic representation of the data for a random sample of k measurements on the same or comparable measuring instruments is provided in Table 10.

Given that π_i remains constant for all measurements, the variance within unit i is due to error of measurement, and the pooled within-unit variance also estimates variance due to error of measurement. On the other hand, the variance in the $\overline{P}_i$'s is due in part to differences between the true magnitudes of the characteristic possessed by the η units and in part due to differences in the average error of measurement for each unit. The analysis of variance (ANOVA) and the expected values for the mean squares for data of this type are given in Table 10.

Table 10.
Estimation of Reliability

	Comparable Measurements								
Unit	**1**	**2**	**2**	**...**	**j**	**...**	**k**	**Total**	**Mean**
1	X_{11}	X_{12}	X_{13}	.	X_{1j}	.	X_{1k}	P_1	$\overline{P}_1$
2	X_{21}	X_{22}	X_{23}	.	X_{2j}	.	X_{2k}	P_2	$\overline{P}_2$
.	.	.	.	.	.	.	.	.	.
.	.	.	.	.	.	.	.	.	.
.	.	.	.	.	.	.	.	.	.
i	X_{i1}	X_{i2}	X_{i3}	.	X_{ij}	.	X_{ik}	P_i	$\overline{P}_i$
.	.	.	.	.	.	.	.	.	.
.	.	.	.	.	.	.	.	.	.
.	.	.	.	.	.	.	.	.	.
n	X_{n1}	X_{n2}	X_{n3}	.	X_{nj}	.	X_{nk}	P_n	$\overline{P}_n$
Total	$\overline{T}_1$	$\overline{T}_2$	$\overline{T}_3$	...	$\overline{T}_j$	...	$\overline{T}_k$	$\overline{G}$	

$MS_{b.units}$ is defined in equation (5.).

$$MS_{b.units} = k\sum\left(\overline{P}_i - \overline{G}\right)^2 \Big/ (n-1) \qquad (5.)$$

Table 11.
Analysis of Variance for Model in (3.)

Source of Variation	MS	E(MS)
Between units	$MS_{b.units}$	$\sigma^2_\eta + k\,\sigma^2_\pi$
Within units	$MS_{w.units}$	σ^2_η

and the variance of the P's given in equation (6.).

$$s^2_{\overline{P}} = \sum\left(\overline{P}_i - \overline{G}\right)^2 \Big/ (n-1) \qquad (6.)$$

Therefore, $$MS_{b.units} = k\ s^2_{\overline{P}}$$

In terms of (4.), the expected value of the variance of the P's is given by,

$$E\left(s^2_{\overline{P}}\right) = \sigma^2_{\overline{\eta}} + \sigma^2_{\pi}.$$

The quantity σ^2_{π}. is the variance of the true measures in the population of which the n units in the study represent a random sample. From the relationship between $MS_{b.units}$ and $s^2_{\overline{P}}$ we have,

$$E\left(MS_{b.units}\right) = k\sigma^2_{\overline{n}} + k\sigma^2_{\pi}$$

since $$k\sigma^2_{\overline{\eta}} = \sigma^2_{\eta}.$$

The reliability of $\overline{P}_i$, the mean of k measurements, is defined as

$$\rho_k = \frac{\sigma^2_\pi}{\sigma^2_\pi + \sigma^2_{\overline{\eta}}} = \frac{\sigma^2_\pi}{\sigma^2_\pi + \left(\sigma^2_\eta / k\right)} \qquad (7.)$$

This is interpreted as the reliability of the mean of k measurements is the variance due to true scores divided by the sum of the variance due to true scores and the variance due to the mean of the errors of measurement. If we define,

$$\theta = \sigma^2_\pi \Big/ \sigma^2_\eta ,$$

then the formulae for ρ_k may be written in the form

$$\rho_k = \frac{k\theta}{1 + k\theta} \qquad (8.)$$

Therefore, when k = 1, (8.) becomes,

$$\rho_1 = \frac{\theta}{1+\theta} = \frac{\sigma^2_\pi}{\sigma^2_\pi + \sigma^2_\eta} \qquad (9.)$$

which, by definition, is the reliability of a single measurement. Within the context of the variance-component model of the analysis of variance, (8.) represents the *intraclass* correlation.

Results

The above methodology was implemented to assess the reliability of the measurements taken on head accelerations, chest accelerations, upper neck loads (F_x, F_z) and moments (M_y), lower neck loads (F_x, F_z) and moments (M_y), left shoulder loads (F_x, F_z) and right shoulder loads (F_x, F_z). It must be noted that some cells of the three factor experimental design (dummy size, infant restraint orientation and infant restraint type) for which measurements on each of the above response variables were sought are not available. That is because some of the data on certain response variables was lost during the sled test. In some instances there were no responses obtained for a particular factor in a sled test. As a result, the reliability of measurement analyses presented here only includes the experimental design cells for each of the response variables above where there are two measurements (i.e., two sled test measurements were obtained). This is because reliability indicators can only be measured for response variables that have two or more comparable measurements. The results for all reliability tests carried out are provided in Table 12. The following summarizes the findings.

Head Acceleration - Two measurements available on the head acceleration response variable results in a reliability estimate of 0.700 (or 70 %). This is interpreted as two comparable measurements on head acceleration (i.e., two tests done for the same dummy size, infant restraint orientation and infant restraint type) results in an average measurement that is 70 % reliable, or in other words, an error of +/- 15 % of the average of two measurements on the head acceleration response variable will contain the true population head acceleration response value. As can also be seen from the table, if only one measurement is taken then the reliability of the head acceleration response drops considerably down to 53.8 %.

Chest Accelerations - The reliability of the chest acceleration responses is significantly higher than that of the head accelerations. Two measurements for the same dummy size, infant restraint orientation and infant restraint type results in an average chest acceleration response measurement that is 96.3 % reliable - an error of less than +/- 2 %. Even one sled test for each of the dummy sizes, infant restraint orientations and infant restraint types would produce responses that are 92.9 % reliable.

Upper Neck Loads (F_x) - The results for the upper neck loads in the x-direction are nearly identical to the chest acceleration findings. Two measurements per cell of the experimental design generates an average upper neck F_x response estimate that is 96.7 % reliable. If only one measurement were available per cell the reliability would still be 93.5 %.

Upper Neck Loads (F_z) - The upper neck loads in the z-direction are not nearly as reliable as those in the x-direction. The reliability of the mean of two measurements on F_z for a given dummy size, infant restraint orientation and infant restraint type in a sled test is 86.1 %. Therefore, the errors surrounding the mean of these two sled tests is +/- 7 %. One sled test measurement would only result in an upper neck F_z response measurement that is only 75.6 % reliable.

Upper Neck Moments (M_y) - The upper neck moments (M_y) are not reliable at all. Two comparable measurements on the same dummy size, infant restraint orientation and infant restraint type yields a mean estimate that is only 18.5% reliable. This means that the true population value of the upper neck moment (M_y) is somewhere within the range of the mean +/- 42 %. A single sled test would produce upper neck M_y's that are only 10.2 % reliable. Clearly, there is a need to improve the measurement devices and procedures for minimizing the error surrounding the upper neck moments (M_y) response variables. Otherwise, a very large number of sled tests is required to generate results that even begin to reflect the true population value of the upper neck M_y's.

Lower Neck Loads (F_x) - The reliability of these response variables are also quite low. Two measurements on the same dummy size, infant restraint orientation and infant restraint type only generates a mean value that has a 63.5 % reliability - the mean has error bounds of +/- 18 %. If only one measurement were taken per cell of the experimental design than the reliability of the lower neck F_x loads drops further to 46.5 %.

Lower Neck Loads (F_z) - The lower neck loads in the z-direction show responses that appear to be quite reliable. A 95.7 % level of reliability is attained with two measurements on the same dummy size, infant restraint orientation and infant restraint type. If only one measurement is taken the reliability is still in the order of 92 %.

Lower Neck Moments (M_y) - Very reliable results are indicated in the case of the lower neck moments

(M_y). An unprecedented 96.4 % reliability is attained with two measurements on the same dummy size, infant restraint orientation and infant restraint type. Even if only a single measurement is obtained per cell of the experimental design the lower neck moments (M_y) still enjoy a 93.1 % level of reliability.

Left Shoulder Loads (F_x) – The left shoulder loads in the x-direction are extremely reliable. Two measurements within the same cell of the experimental design matrix produce a mean estimator that has a 97.9 % reliability associated with it. This means that the true population value of the left shoulder F_x loads is contained within the mean +/- 1 %. A single measurement (i.e., only one sled test) for a given dummy size, infant restraint orientation and infant restraint type yields a response value that is 95.9 % reliable.

Left Shoulder Loads (F_z) – The left shoulder loads in the z-direction are no where near as reliable as those in the x-direction. Two sled tests on the same dummy size, infant restraint orientation and infant restraint type results in a mean estimator of left shoulder F_z that is 86.5 % reliable – the true population value is somewhere within the mean +/- 7 %. If only a single sled test is conducted for a particular dummy size, infant restraint orientation and infant restraint type then the level of reliability falls appreciably some to 76.3 %.

Right Shoulder Loads (F_x) – The right shoulder loads in the x-direction have the highest reliability of any of the response variables. Two measurements on the same dummy size, infant restraint orientation and infant restraint type result in a mean estimator that is 99.4 % reliable. In other words, the true population value of the right shoulder F_x load is found within the mean +/- 0.3 %. Even if only one sled test is performed the singe measurement has a 98.8 % level of reliability associated with it.

Right Shoulder Loads (F_z) – Although not quite as high as the right shoulder loads in the x-direction, the right shoulder loads in the z-direction are still extremely reliable. Two measurements on the same dummy size, infant restraint orientation and infant restraint type yield a mean that has a reliability of 96.5 % - or the true population value is within the range of the mean +/- 1.75 %. If only one sled test is performed for a particular dummy size, infant restraint orientation and infant restraint type the level of reliability of the resulting response variable is still high, at 93.3 %.

Table 12.
Reliability of Response Variable Measurements

Response Variable	Number of Comparable Measures	Reliability (%)
Head Accelerations	1	53.8
	2	70.0
Chest Accelerations	1	92.9
	2	96.3
Upper Neck Loads (F_x)	1	93.5
	2	96.7
Upper Neck Loads (F_z)	1	75.6
	2	86.1
Upper Neck Moments(M_y)	1	10.2
	2	18.5
Lower Neck Loads (F_x)	1	46.5
	2	63.5
Lower Neck Loads (F_z)	1	91.8
	2	95.7
Lower Neck Moments(M_y)	1	93.1
	2	96.4
Left Shoulder Loads (F_x)	1	95.9
	2	97.9
Left Shoulder Loads (F_z)	1	76.3
	2	86.5
Right Shoulder Loads (F_x)	1	98.8
	2	99.4
Right Shoulder Loads (F_z)	1	93.3
	2	96.5

From the results of the "reliability of measurements" analyses conducted the '22 sled test program' generated estimates on the response variables that are:

(i) at least 95% reliable for chest accelerations, upper neck loads in the x-direction, lower neck loads in the z-direction, lower neck moments (My), left shoulder loads in the x-direction, right should loads in the x-direction, and right shoulder loads in the z-direction, given two sled tests are performed on a particular dummy size, infant restraint orientation and infant restraint type; and

(ii) at least 95% reliable for left shoulder loads in the x-direction and right shoulder loads in the x-direction given one sled test was performed on a particular dummy size, infant restraint orientation and infant restraint type;

In general two sled tests carried out for a particular dummy size, infant restraint orientation and infant restraint type generates response estimates that are 95%

reliable for all variables with the exception of head accelerations, upper neck loads in the z-direction, upper neck moments (My), lower neck loads in the x-direction, and left shoulder loads in the z-direction. To improve the estimators for these response variables it is necessary to either improve the test method and procedures (to generate more controlled and accurate responses) or increase the number of tests to a sufficient number to attain a level of 95% reliability.

If the number of tests were increased to attain a 95% level of reliability for the response variables above that fell short of this criterion, then the number of tests required for each for a particular dummy size, infant restraint orientation and infant restraint type would be as follows:

Response Variable	# Tests Required
Head accelerations	12
Upper neck loads (F_z)	7
Upper neck moments (M_y)	168
Lower neck loads (F_x)	22
Left shoulder loads (F_z)	6

It must be noted, however, that the number of test results acquired for each response variable in this research was not two consistently. Some response variable results are entirely missing or only have one test result due to lost data in some of the 22 sled tests conducted. It is therefore expected that some of the reliability on the measurements for the above five response variables would be significantly improved if future programs ensured that all data is captured from each sled test.

CONCLUSIONS AND DISCUSSIONS

From this study, the following conclusions have been drawn:

- Infants and young toddlers, are provided with a higher level of safety when restrained in a rear facing infant restraint system as long as possible rather than not being restrained, being restrained in a forward facing restraint or restrained by a seat belt.

- The results of the ANOVA revealed that all response variables, with the exception of the upper neck moment (M_y) and the right shoulder (F_x) loads, were significantly affected by the orientation of the restraint. Furthermore, the responses are all smaller for the rear facing orientation than the forward facing ones.

- Even though the current Canadian criteria for infant restraints are in place for the 6- and a 9-dummies, convertible restraints that were tested rear facing with larger 12-, 18- and 3-year old dummies meet them.

- Generally, the head and chest acceleration, upper and lower neck loads and moments were lower for a comparable set of test conditions for the rear facing orientation as compared to forward facing. The exception to this was the lower neck loads, F_z where the opposite was observed.

- Generally the shoulder loads were produced considerably lower values for a comparable set of test conditions for the rear facing orientation as compared to forward facing for the x-component. The reverse was true in the z-direction but the difference was much less. However in the absence of any injury threshold criteria for child shoulders, it could not be determined if these higher loads in the z-direction would be injurious. However shoulder related injuries have not been reported by countries where children up to three and four years are restrained rear facing.

- In addition to permitting the use of larger dummies than currently specified, the next step in the process to ensure that rear-facing restraints are available more widely in Canada is to determine what benefits would be gained from specifying maximum head and chest acceleration, neck load and moments and shoulder load maximums in the regulations.

- In all cases, the structural integrity of the restraint was intact indicating that little redesign would be need of restraint manufacturers to adapt their restraints for larger children in the rear facing installation.

- A series of tests of North American convertible restraints on the standard bench seat with a simulated dash similar to that of ECE Reg. 44 should be envisaged since the larger restraints meant to restrain larger children may be more realistically tested in that manner.

- Although a better performer in the majority of cases, the CanFIX, a restraint rigidly attached at its base to the standard test bench, did not consistently perform better rear facing compared to forward facing. Further investigating the effect of rigidly attached restraint base may be necessary since the testing was performed with an early prototype of the CanFIX.

- Reconstructions with the 12- and 18-month dummies are required to establish threshold limits for the neck.

- Additional research in shoulder injuries to restrained children is required to.

- Although it must be re-iterated that the results provided for the field data are subject to high levels of error (due to the small sample sizes they comprise within the entire PCS data bases) the trend is quite evident. A strong correlation between incorrect restraint installation, improper restraint use and the probability of sustaining an injury or fatality is quite apparent. It is therefore necessary to work towards improving protection for infants through mechanisms such as regulating aspects of the various restraint system products to increase both their correct installation and proper use.

- From the results of the "reliability of measurements" analyses conducted the '22 sled test program' generated estimates on the response variables that are:
  (i) at least 95% reliable for chest accelerations, upper neck loads in the x-direction, lower neck loads in the z-direction, lower neck moments (My), left shoulder loads in the x-direction, right should loads in the x-direction, and right shoulder loads in the z-direction, given 2 sled tests are performed on a particular dummy size, infant restraint orientation and infant restraint type.
  (ii) at least 95% reliable for left shoulder loads in the x-direction and right shoulder loads in the x-direction given 1 sled test was performed on a particular dummy size, infant restraint orientation and infant restraint type.

- In general two sled tests carried out for a particular dummy size, infant restraint orientation and infant restraint type generate response estimates that are 95% reliable for all variables with the exception of head accelerations, upper neck loads in the z-direction, upper neck moments (M_y), lower neck loads in the x-direction, and left shoulder loads in the z-direction. To improve the estimators for these response variables it is necessary to either improve the test method and procedures (to generate more controlled and accurate responses) or increase the number of tests to a sufficient number to attain a level of 95% reliability.

ACKNOWLEDGMENTS:

The authors of this paper would like to acknowledge the following individuals for their contribution to this study:

Murray Dance, Barbara Baines, Nayan Banerjee, Janet Boufford, Éric Gagné and Elizabeth Morgan of Transport Canada; Don Day and Robert Miles of DCIEM; Richard Bélanger and Albert Godard of PMG Technologies; Graig Morgan of Denton, Dr Jean Amyotte, Paediatric Chiropractor and VRTC for the loan of the 12-month old CRABI dummy

DISCLAIMER

The responsibility for the results presented herein rests entirely with the authors. The conclusions drawn are those of the authors alone and do not necessarily reflect the views of Transport Canada.

REFRENCES

---

[1] Aldman, B. A.; *A Protective Seat for Children - Experiments with a Safety Seat for Children between One and Six*; Proceedings of the 8th Stapp Car Crash Conference, Detroit 1964; pp. 320-328
[2] Kamren, B.; Koch, M. V.; Kullgren, A.; Lie, A.; Tingvall, C.; Larsson, S.; Turbell, T.; *The Protective Effects of Rearward Facing CRS: An Overview of Possibilities and Problems Associated with Child Restraints for Children Aged 0 - 3 Years*; SAE 933093, SP-986, Child Occupant Protection, San Antonio, 1993
[3] Carlsson, G.; Norin, H.; Ysander, L.; "*Rearward-facing Child Seats - The Safest Car Restraint for Children*"; Accident Analysis and Prevention, vol. 23, Nos. 2/3, pp. 175-182, 1991
[4] Carlsson, G.; Norin, H.; Ysander, L.; "*Rearward-facing Child Seats - The Safest Car Restraint for Children*" - 33rd Proceedings of the Association for the Advancement of automotive Medicine, Baltimore, 1989
[5] Weber, K.; "*Rear-facing Restraint for Small Child Passengers - A Medical Alert*"; UMTRI Research Review, April-June 1995, vol. 25, no. 5
[6] Pincemaille, Y.; Brutel, G.; Le Coz, J. Y.; "Problems Related to the Acceptability of a New Concept of CRS in France: Rearward Facing Systems"; 38th Proceedings, Association for the Advancement of Automotive Medicine, Lyon, 1994
[7] "*Child Restraint Use in Canada*": 1997 Survey Data"; Transport Canada publication # CL9804, 1998
[8] Weber, M. L.; "*Dictonnaire thérapeutique pédiatrique*"; Presse de l'Université de Montréal, 1993

---

[9] Demirjian, A.; *"Anthropometry Report"*, Nutrition Canada, 1980

[10] *Canadian Traffic Accident Information Database*, 1991-1995 for British Columbia, N. W. T., Alberta, Saskatchewan, Manitoba, Ontario, New-Brunswick, P. E. I., Nova Scotia and Newfoundland,

[11] Feles, N.; *"Design and Development of the General Motors Infant Safety Carrier"*; SAE Paper 700042

[12] SOR/72-127, May 10, 1972; *"Children's Car Seats and Harness Regulations - Hazardous Products Act"* Consumer and Corporate Affairs

[13] CMVSS 213.1 - *Infant Seating and Restraint Systems*; SOR/82-569; SOR/84-374; Chapter M-10 Of the Revised Statutes of Canada, 1985; SOR/89-490; SOR/92-545; SOR/94-669; SOR/97-447 and SOR/98-160

[14] Sub-part D; Part 572, *"United States Code of Federal Regulations"*; Title 49, Ch. V

[15] Sub-part J; Part 572, *"United States Code of Federal Regulations"*; Title 49, Ch. V

[16] Canada Gazette, Part I; *"Order Respecting Requirements for Infant Restraint Systems that Are Designed for Use by Infants Whose Mass Is 10 Kilograms or Less"*; November 23, 1996

[17] Sub-part C Part 572, *"United States Code of Federal Regulations"*; Title 49, Ch. V

[18] CMVSS 213 - *Child Restraint Systems*; SOR/82-569 3; SOR/84-374; SOR/89-490; Chapter M-10 of the Revised Statutes of Canada, 1985; SOR/92-545; SOR/94-669; SOR/97-447; SOR/98-160

[19] NHTSA-SAS-100-1000

[20] Gardner, W. T.; Pedder, J. B. and Legault, F.; *"Potential Improvements to the Canadian Child Restraint Regulations"*, SAE Paper 933088, Child Occupant Protection, SAE Publication SP-986, San Antonio, 1993

[21] Legault, France; Gardner, William; Vincent, Alex; *"The effect of top tether strap configurations on child restraint performance"*; SAE Paper 973304, Child Occupant Protection II Conference, Orlando, 1997

[22] First Technology Safety Systems, CRABI Twelve-Month Old Infant Dummy, Anthropometric Dimensions and Segment Weights, Version 1.1

[23] First Technology Safety Systems, CRABI Eighteen-Month Old Infant Dummy, Anthropometric Dimensions and Segment Weights, Version 1.1

[24] Pedder, Jocelyn; Legault, France; Slacudean, George; Hillebrandt, David; Gardner, William; Labrecque, Mathieu; *"Development of the CanFIX Infant and Child Restraint/Vehicle Interface System"*; SAE paper 942221, P-279; 38th Stapp Car Crash Conference Proceedings, Fort Lauderdale, 1994

[25] Pedder, J, Gardner, W. T.; Legault, F; Salcudean, G; Hillebrandt, D.; *"Development of a CanFIX Interlock System for Child Restraints"*; Proceedings of the Canadian Multidisciplinary Road Safety Conference IX, Montréal, 1995

[26] *"Level II Accident Investigation Passenger Car Study (PCS), 1984 - 1992"*, Evaluation and Data Systems Division, Road Safety Directorate, Transport Canada.

[27] Stewart, Delbert E.; *"Documentation For All Phases of the Data Development and Analysis of the PCS System"*, Evaluation and Data Systems Division, Road Safety Directorate, Transport Canada, 1996.

[28] Canada Motor Vehicle Safety Test Method 213.1, Revised November 1, 1986

[29] *"Uniform Provisions Concerning the Approval of Restraining Devices for Child Occupants of Power-Driven Vehicles ("Child Restraint System")"*; ECE/Trans/505/Reg. 44

[30] Lumley, M.; "Child Restraint Tether Straps - A Simple Method of Increasing Safety of Children", SAE Paper 973305, P-316; Child Occupant Protection - 2nd Symposium, Orlando, 1997

[31] Robert A. Denton Specifications Sheets B-2791; B-2789; B-2554 and J-2791

[32] Canada Motor Vehicle Safety Test Method No. 213.1; *"Infant Restraint Systems"* issued April 1, 1982; revised October 1, 1997

[33] Ibid.

[34] Code of Federal Regulations, Transportation, Title 49, Part 400 to 999, revised as of October 1, 1996, Part 571.213, page 532

[35] Robert A. Denton Specifications Sheets B-2791; B-2789; B-2554 and J-2791

[36] SAE J211OCT88; *"Instrumentation for Impact Test"*

[37] CMVSS 213.4, *"Built-in Child Restraint Systems and Built-in Booster Cushions"*, SOR/94-669, effective April 25, 1995

[38] Planath, Ingrid; Rygaard, Camilla; Nilsson; *"Synthesis of Data Towards Neck Protection Criteria for Children"*, Proceedings of 1992 IRCOBI Conference, Verona 1992

[39] Janssen, E. G.; Huijskens, R.; Verschut, R. and Twist, D.; *"Cervical Spine Loads Induced in Restrained Child Dummies"*, SAE Paper 933102, Child Occupant Protection (SP-986)

[40] Trosseille, X. and Tarrière, C.; *"Neck Injury Criteria for Children from Real Crash Reconstructions"*, SAE Paper 933103, Child Occupant Protection (SP986), 1993

[41] Stewart, D.E.; *"DCIEM and Calspan Child Restraint System Test Programs : An Analysis of Test Data"*, TMSE 8602, Evaluation and Data Systems Division, Road Safety Directorate, Transport Canada, October, 1986.

[42] Stewart, D.E.; *"Maximum head Excursion in Front Impact : Child Restraints Tethered and Untethered*

(DCIEM Test Data)", TMSE 8203, Evaluation and Data Systems Division, Road Safety Directorate, Transport Canada, November, 1982.

[43] Stewart, D.E.: *"Maximum Head Excursion in Front Impact : Child Restraints Performance by Seat Configuration and Age of Dummy (Calspan Test Data)"*, TMSE 8201, Evaluation and Data Systems Division, Road Safety Directorate, Transport Canada, September, 1982.

[44] Stewart, D.E.; *"Infant Carrier Restraint Systems Experimental Design, Testing and Analyses"*, TMSE 8202, Evaluation and Data Systems Division, Road Safety Directorate, Transport Canada, October, 1982.

[45] Stewart, D.E.; *"EMISSION TEST PROGRAM : EVALUATION OF METHANOL FUELS – EXPERIMENTAL DESIGN CONSIDERATIONS"*, TMSE 8404, Evaluation and Data Systems Division, Road Safety Directorate, Transport Canada, July, 1984.

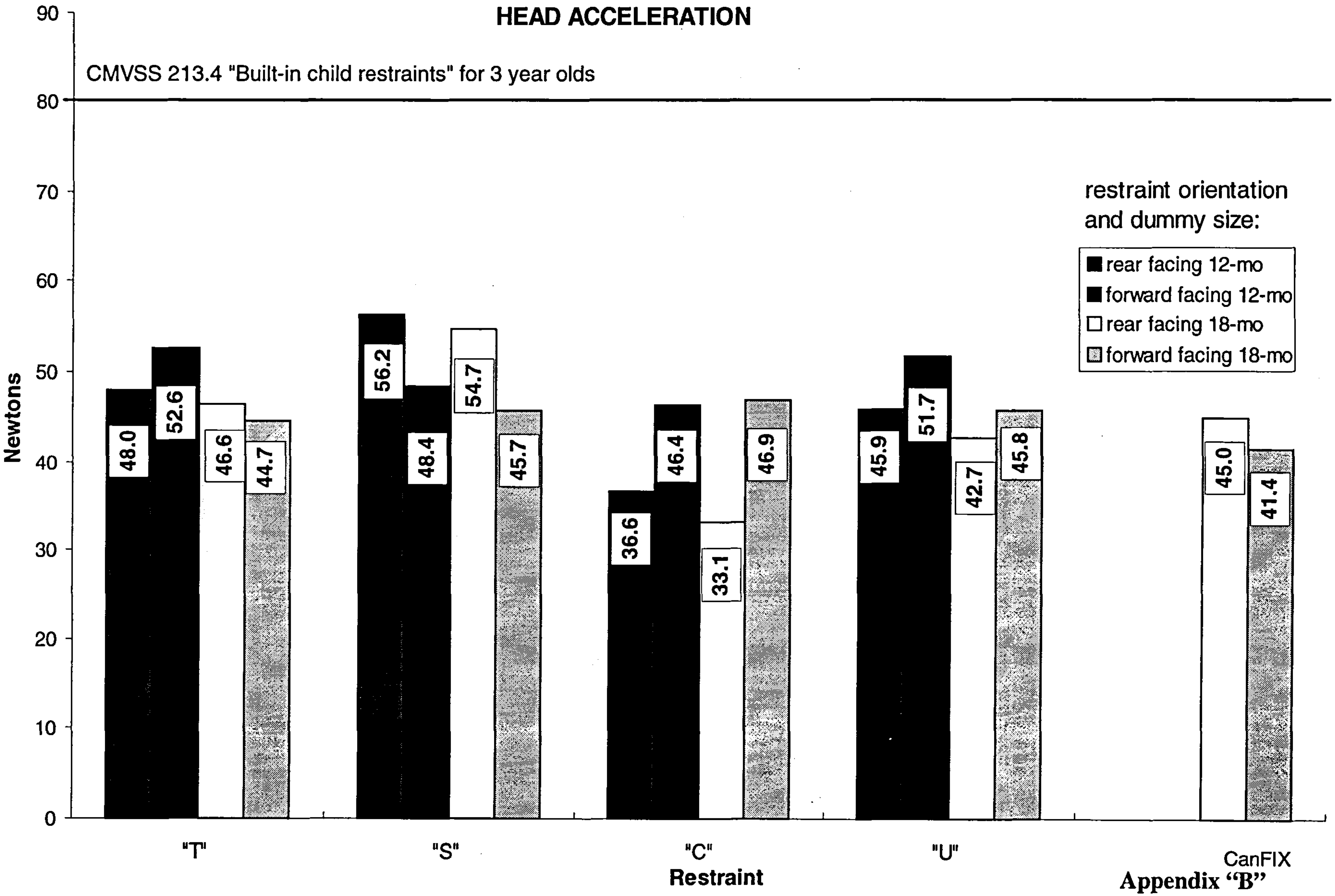

Appendix "B"

Figure "B-1"

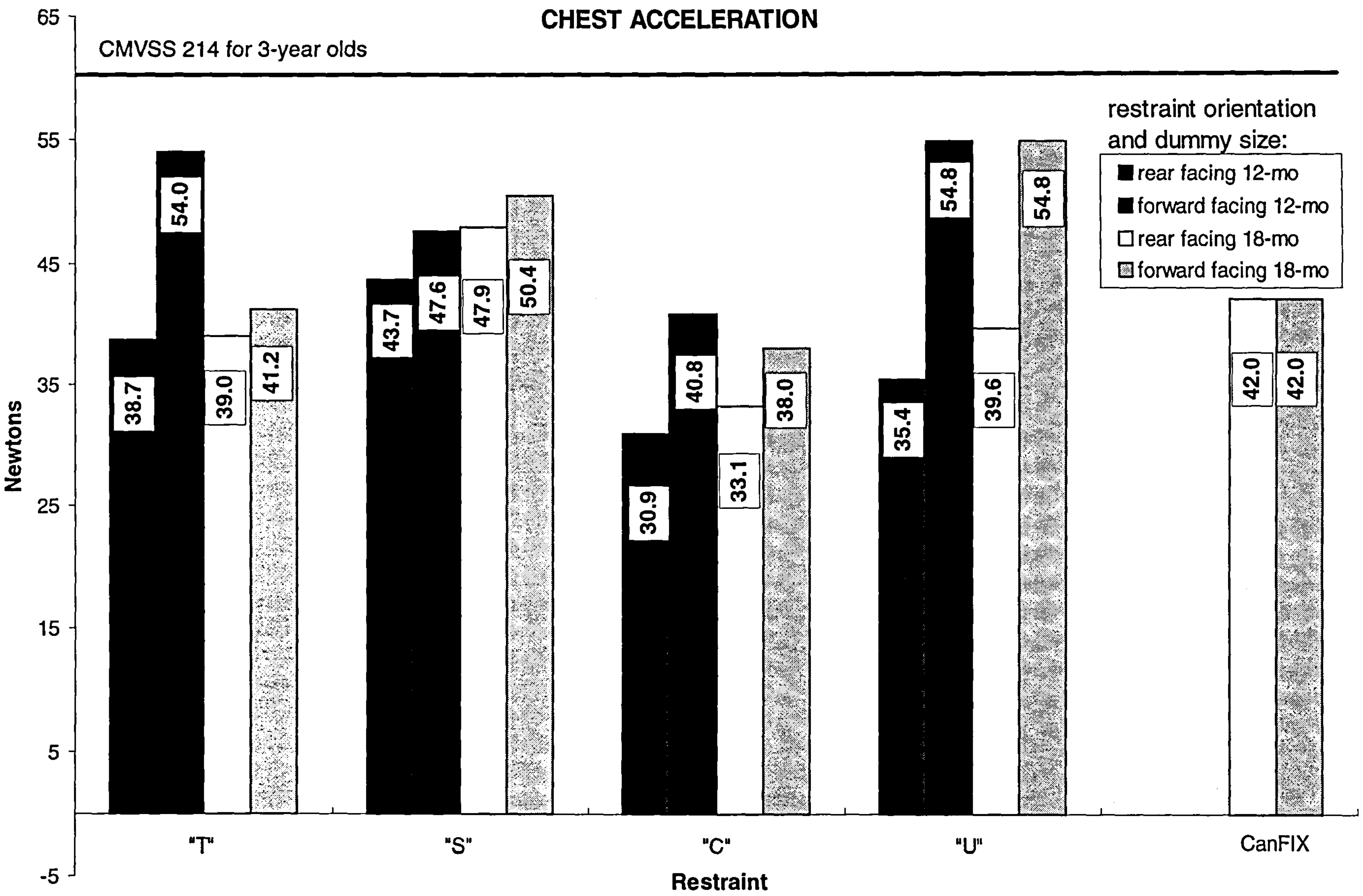

Appendix "B"

Figure "B-2"

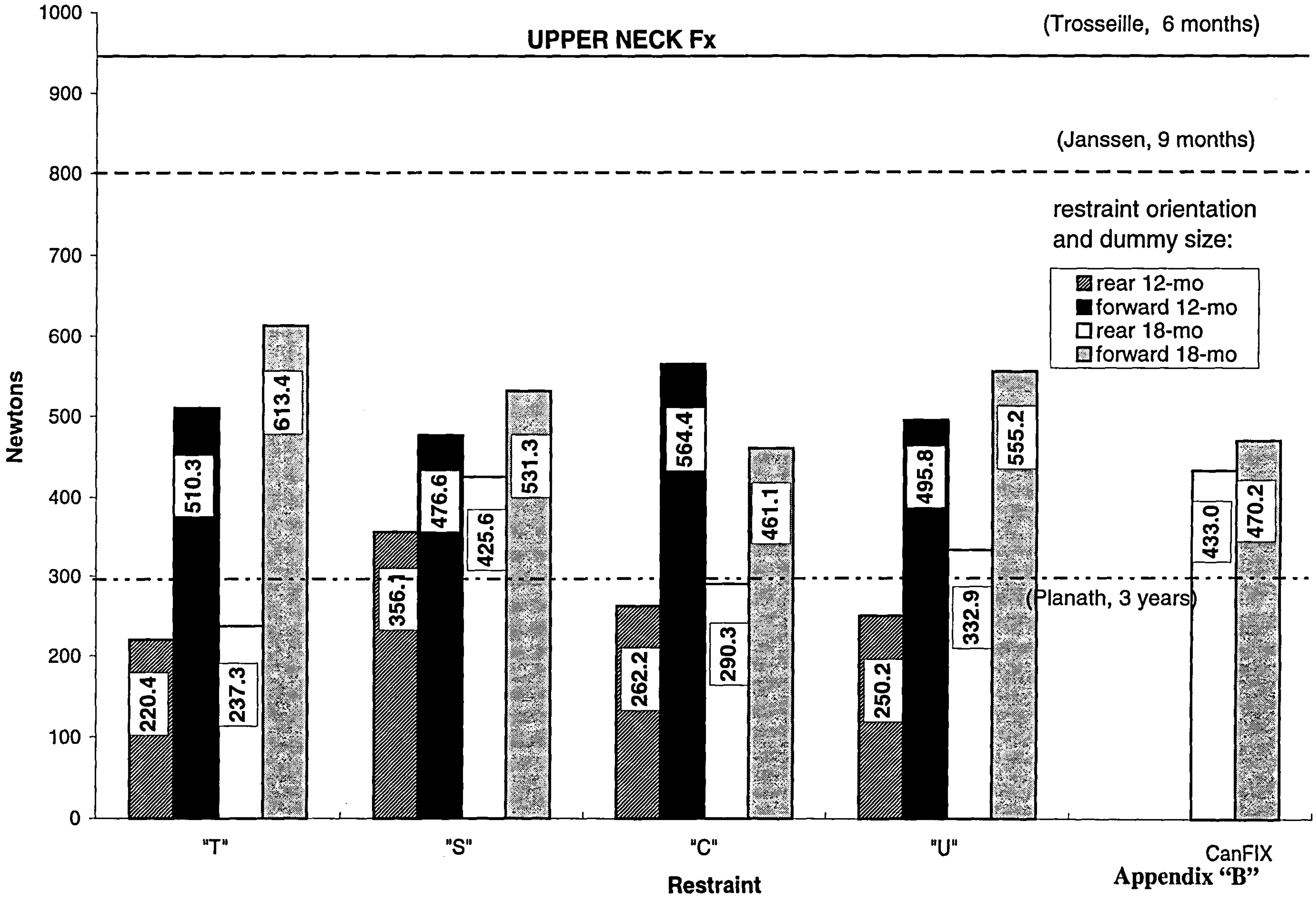

Appendix "B"

Figure "B-3"

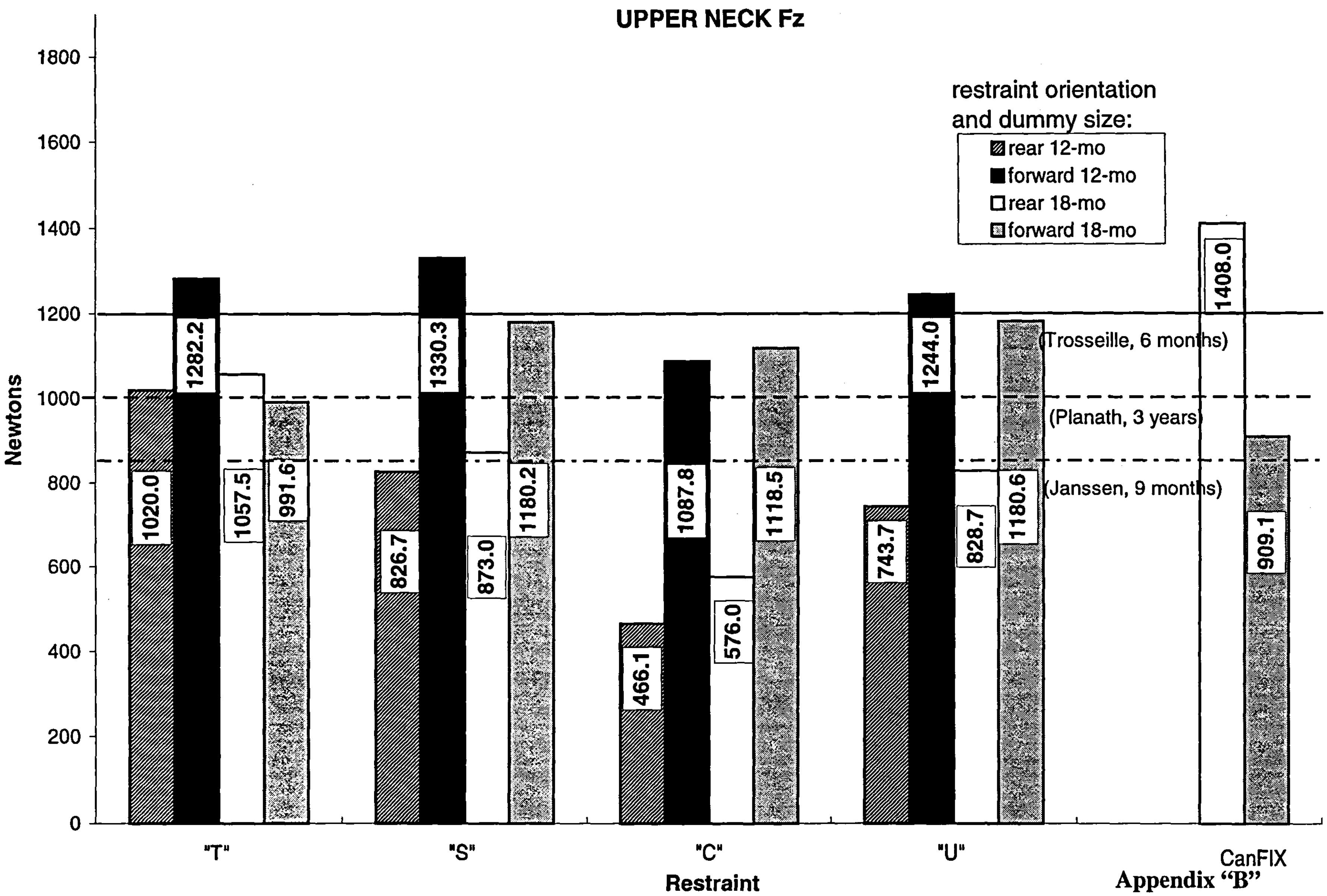

Appendix "B"

Figure "B-4"

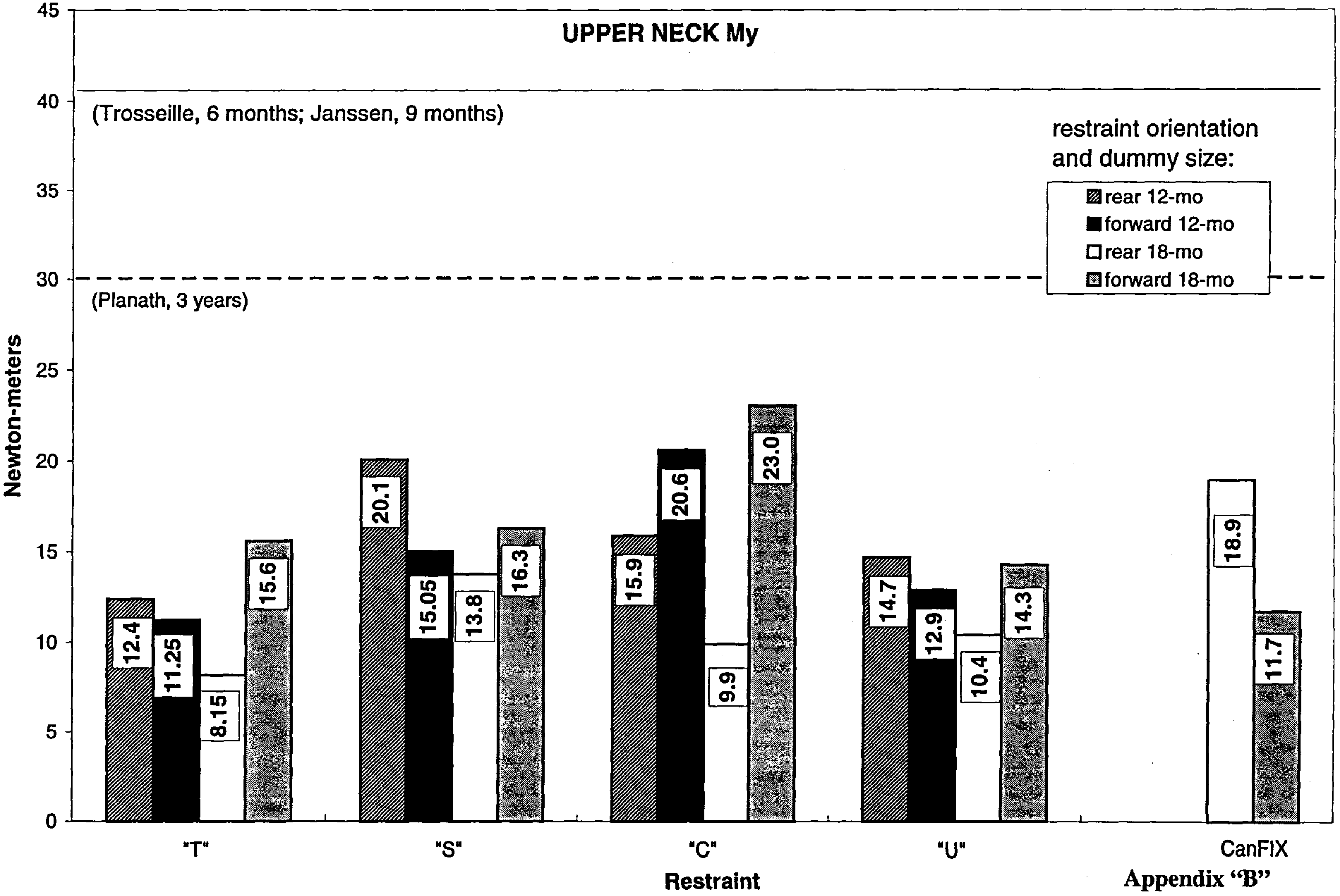

Appendix "B"

Figure "B-5"

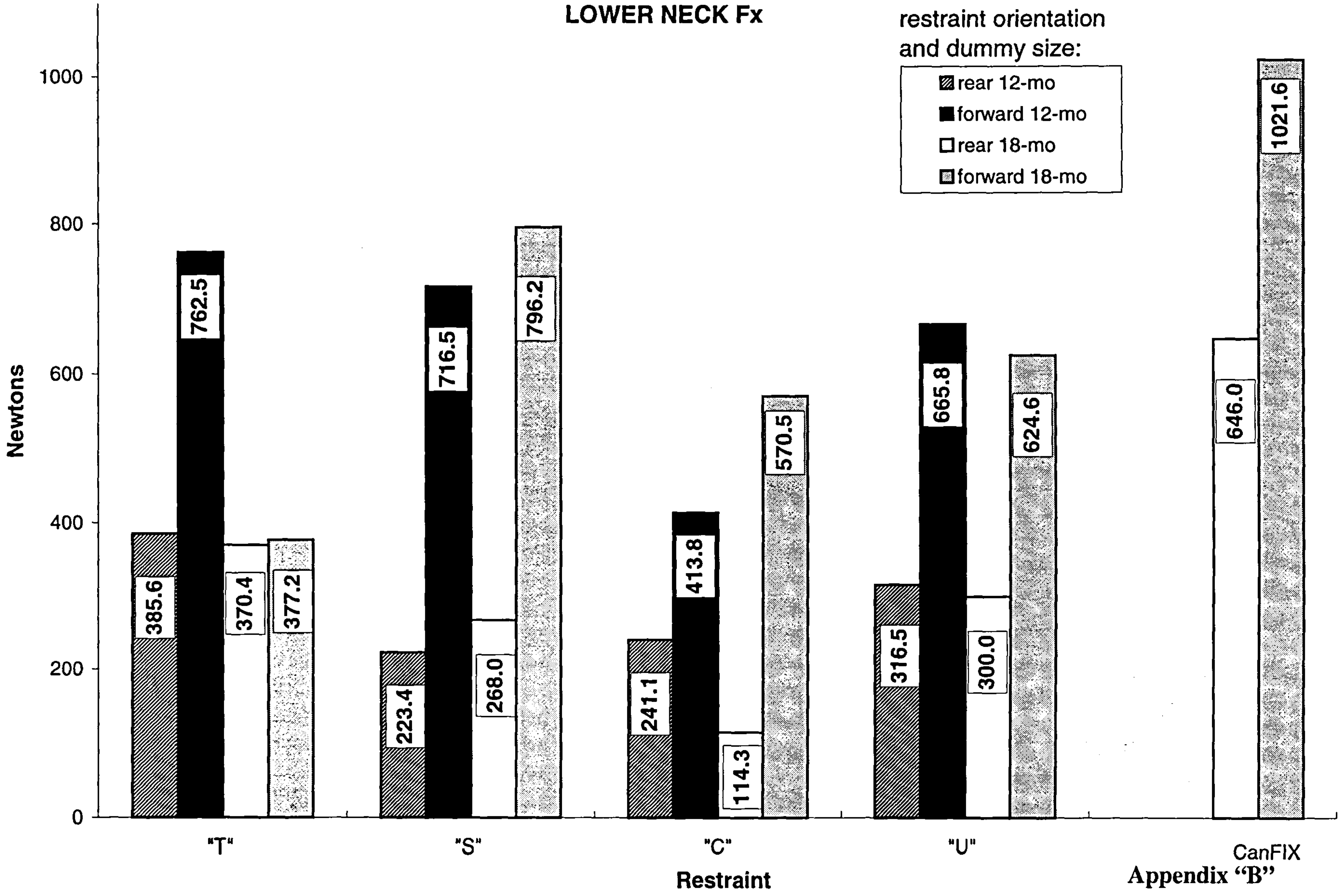

Appendix "B"

Figure "B-6"

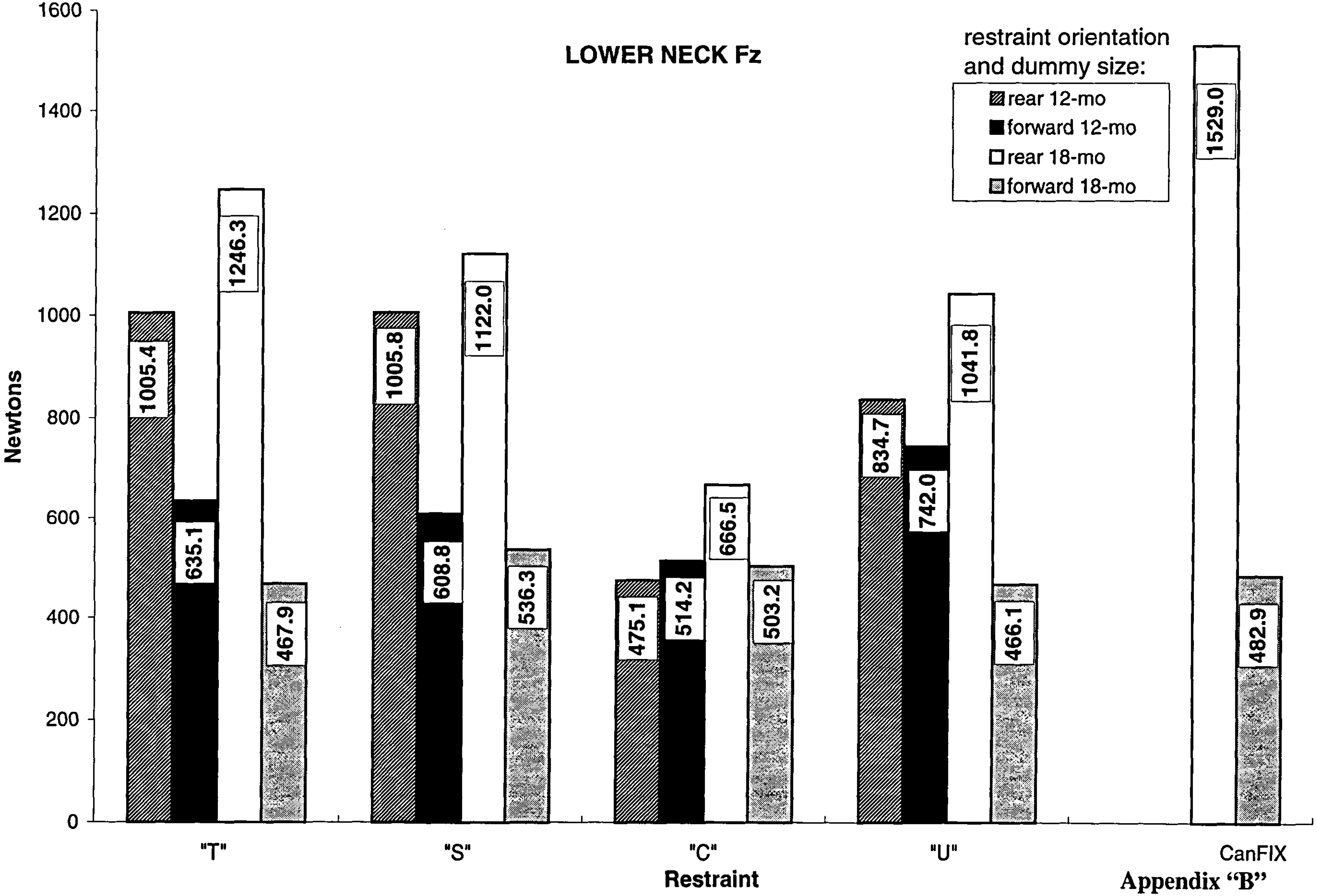

Appendix "B"

Figure "B-7"

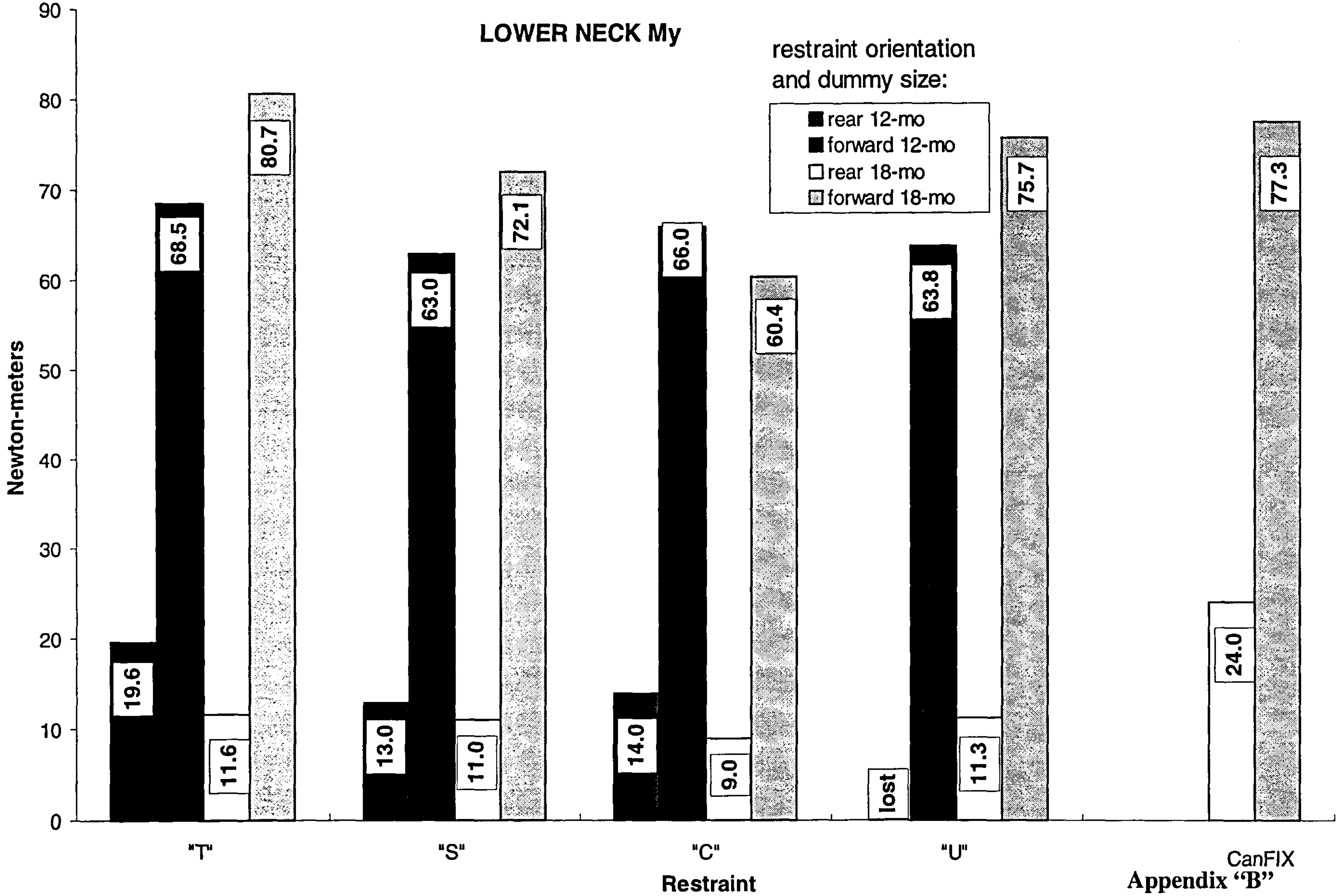

Appendix "B"

Figure "B-8"

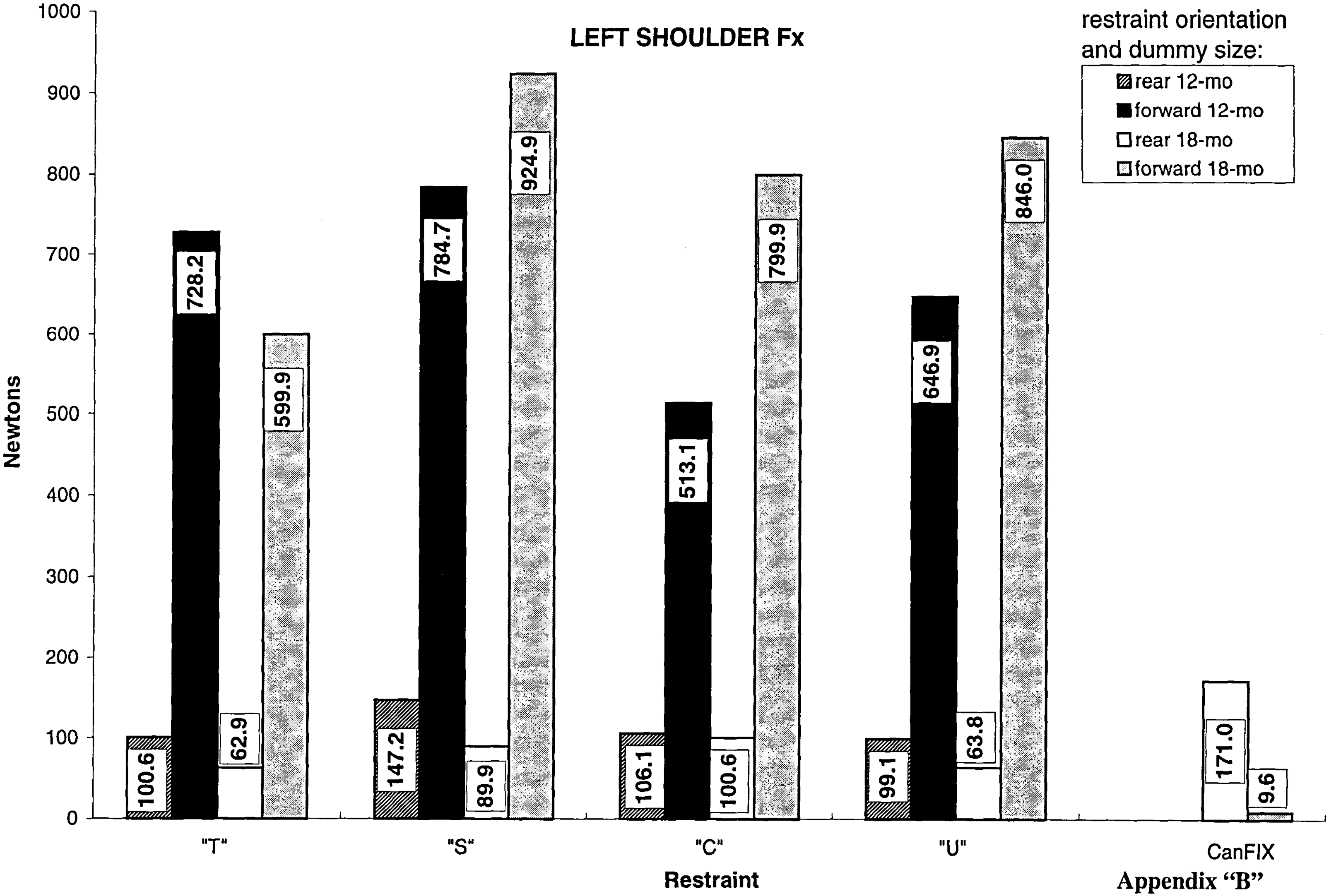

Appendix "B"

Figure "B-9"

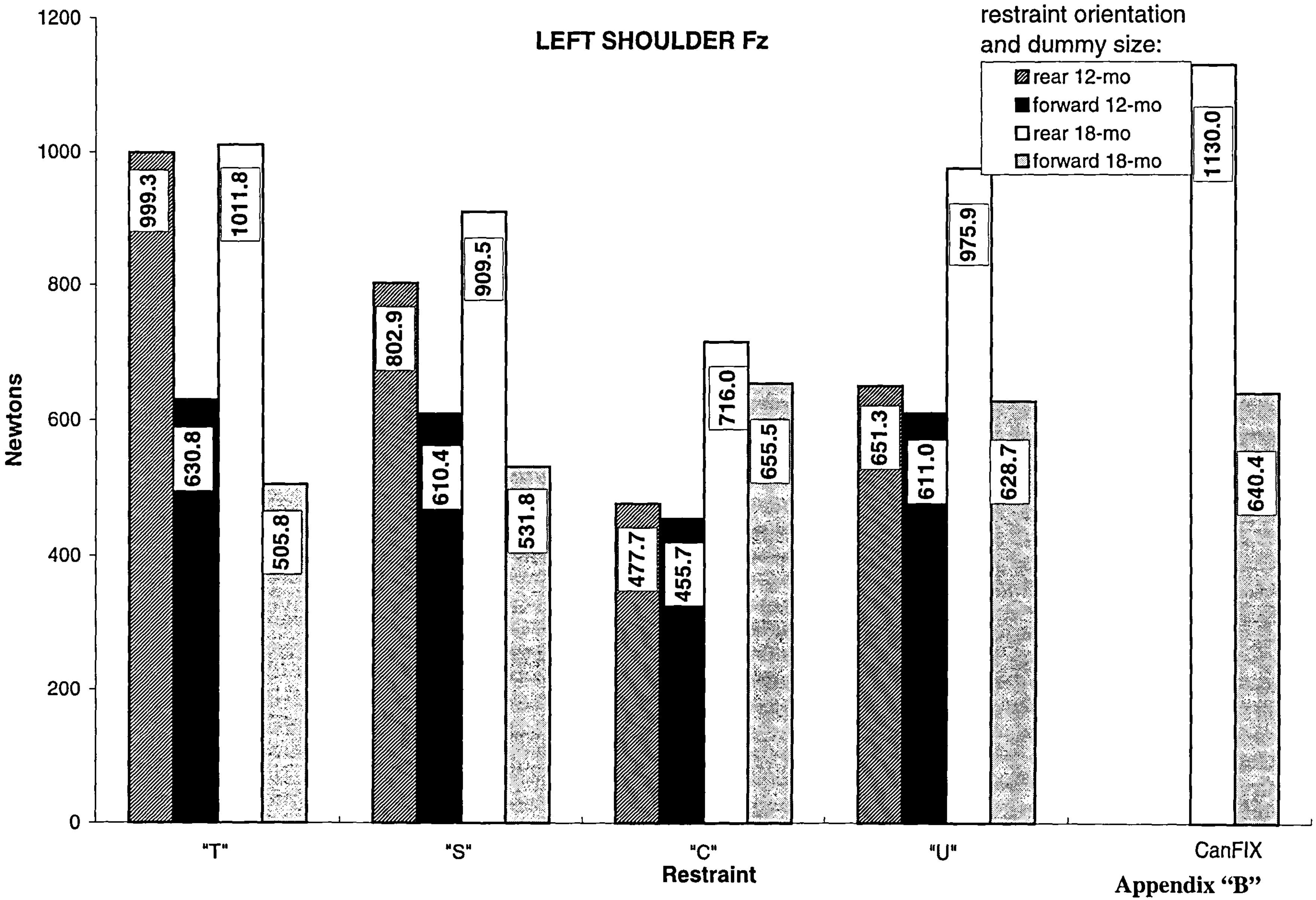

Appendix "B"

Figure "B-10"

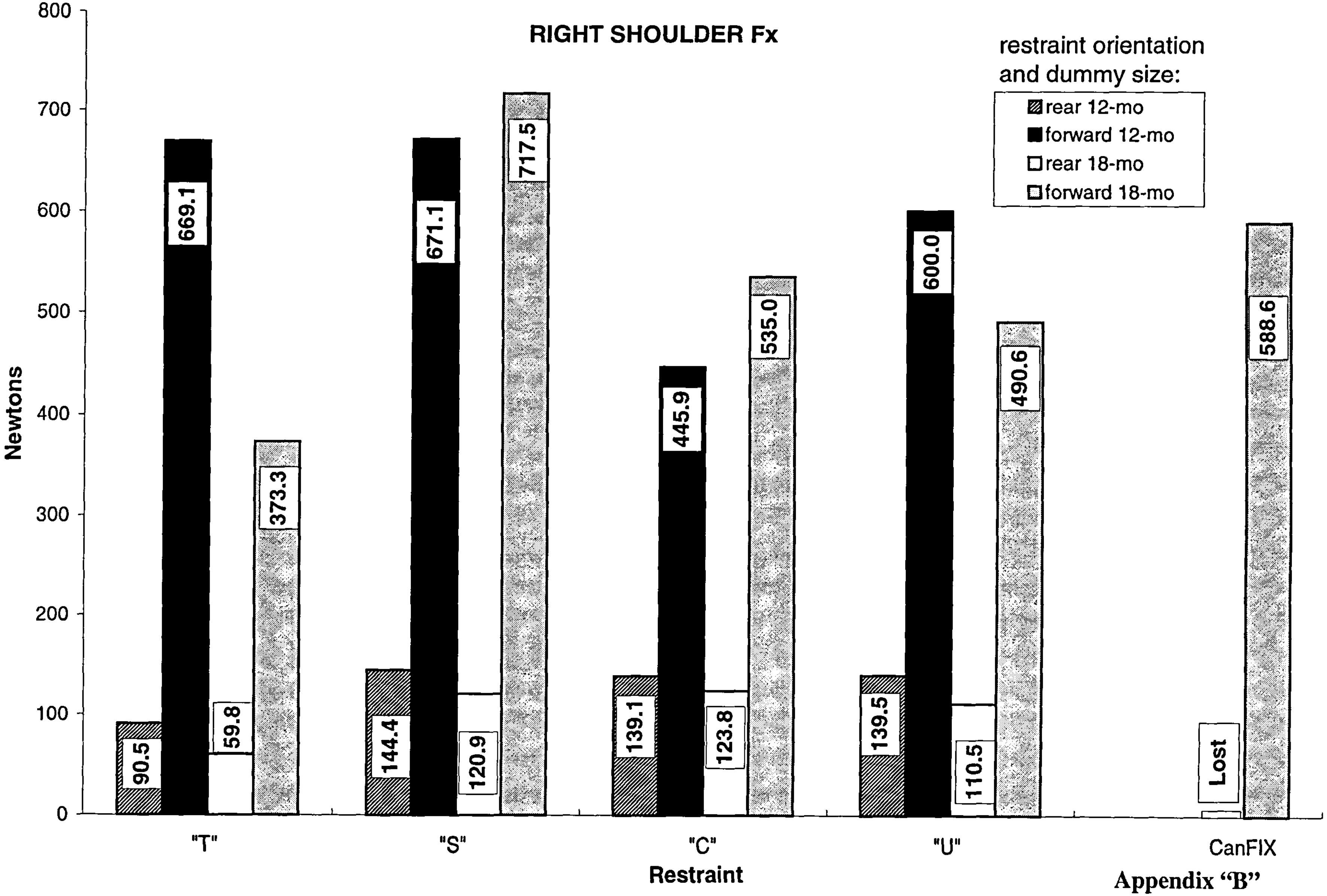

Appendix "B"

Figure "B-11"

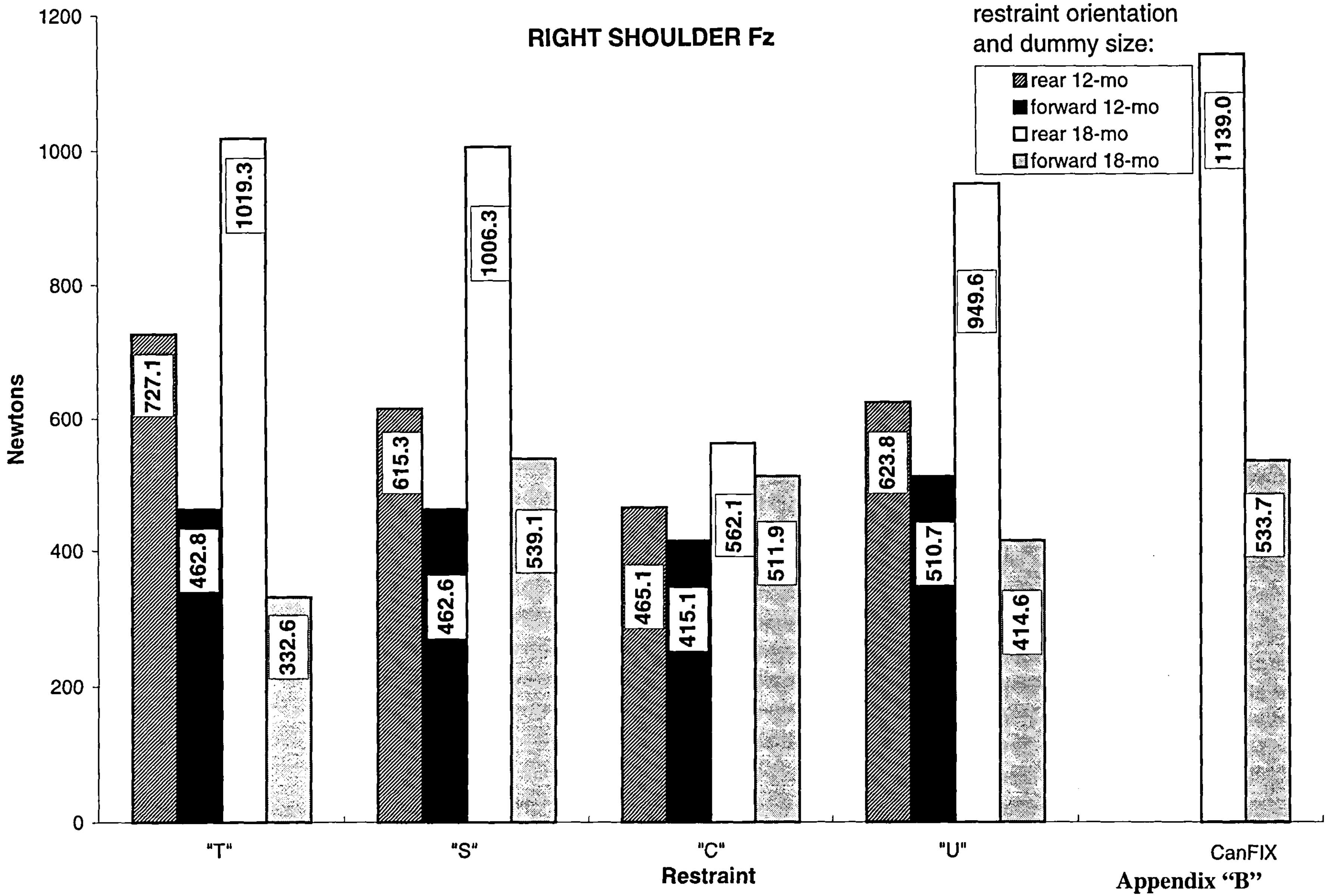

Appendix "B"

Figure "B-12"

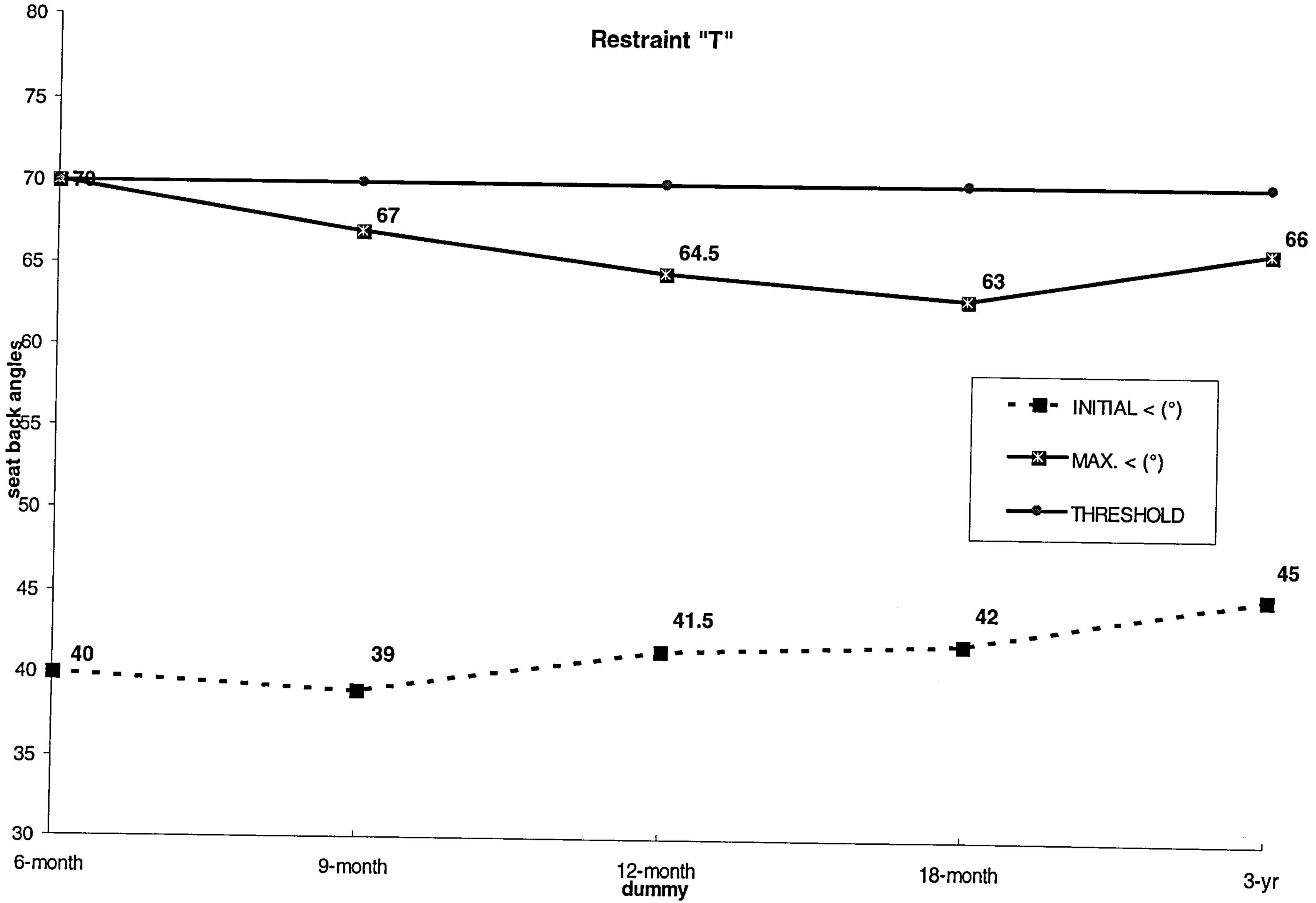

Appendix “C”

Figure “C-1”

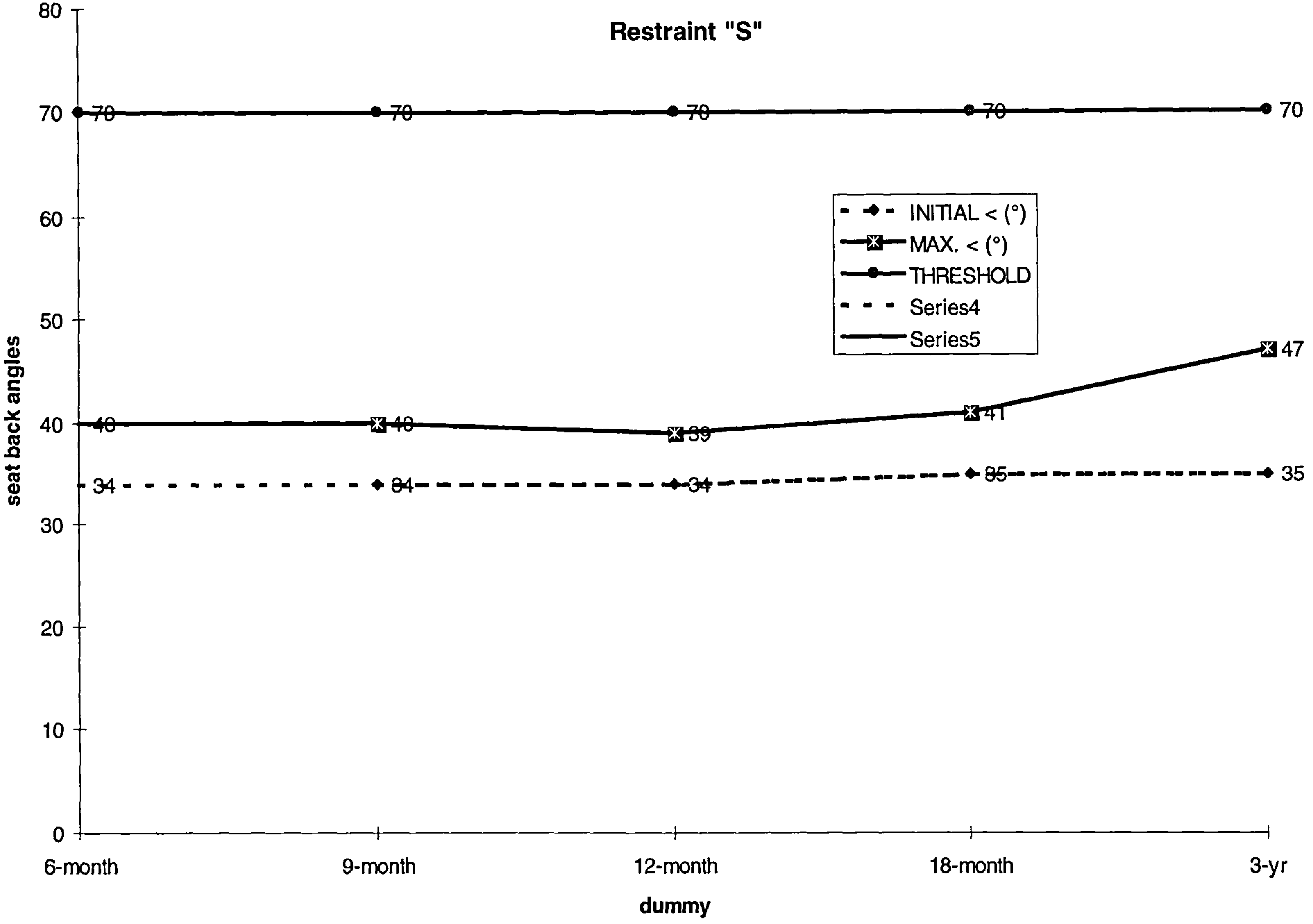

Appendix "C"

Figure "C-2"

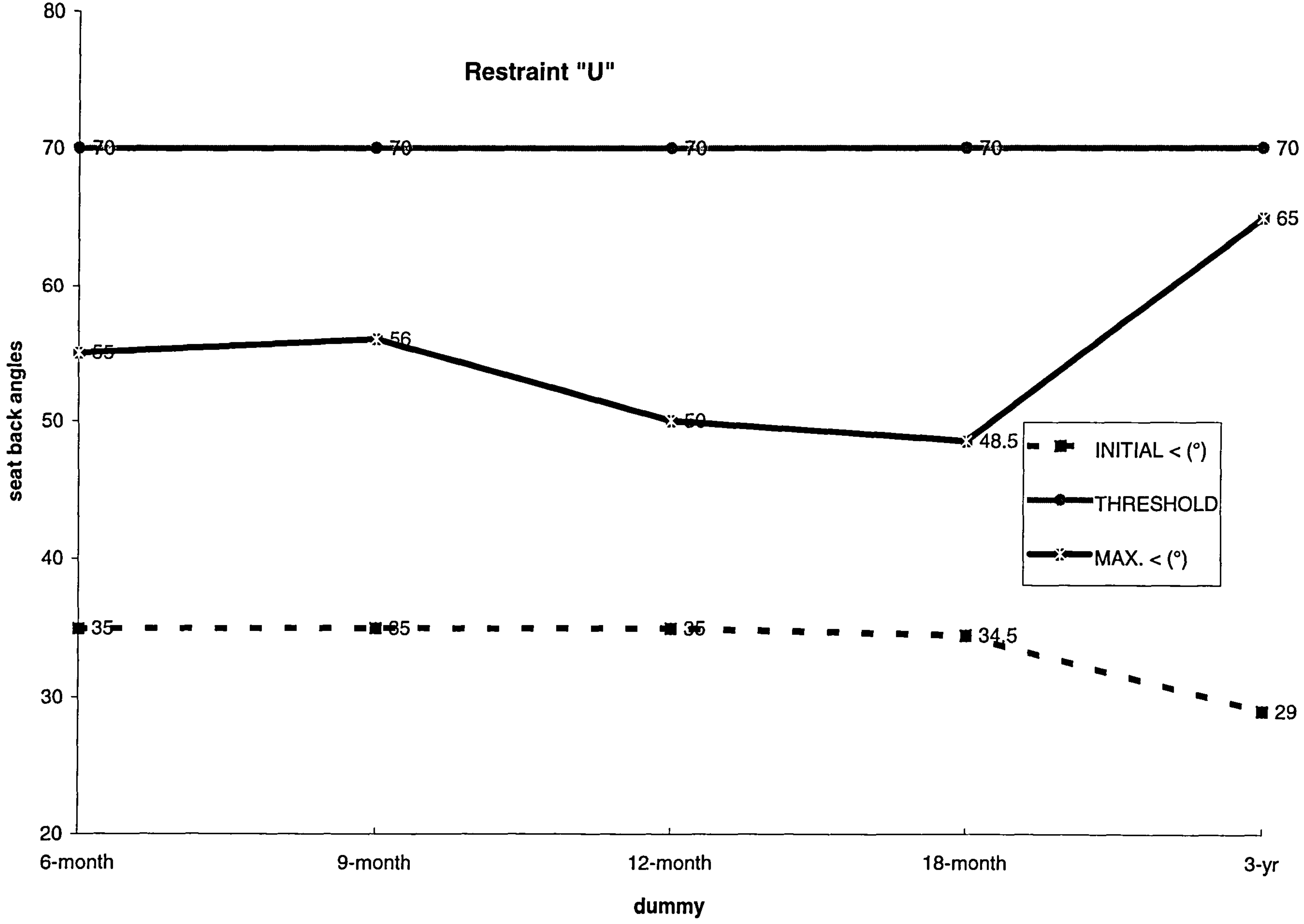

Appendix "C"

Figure "C-3"

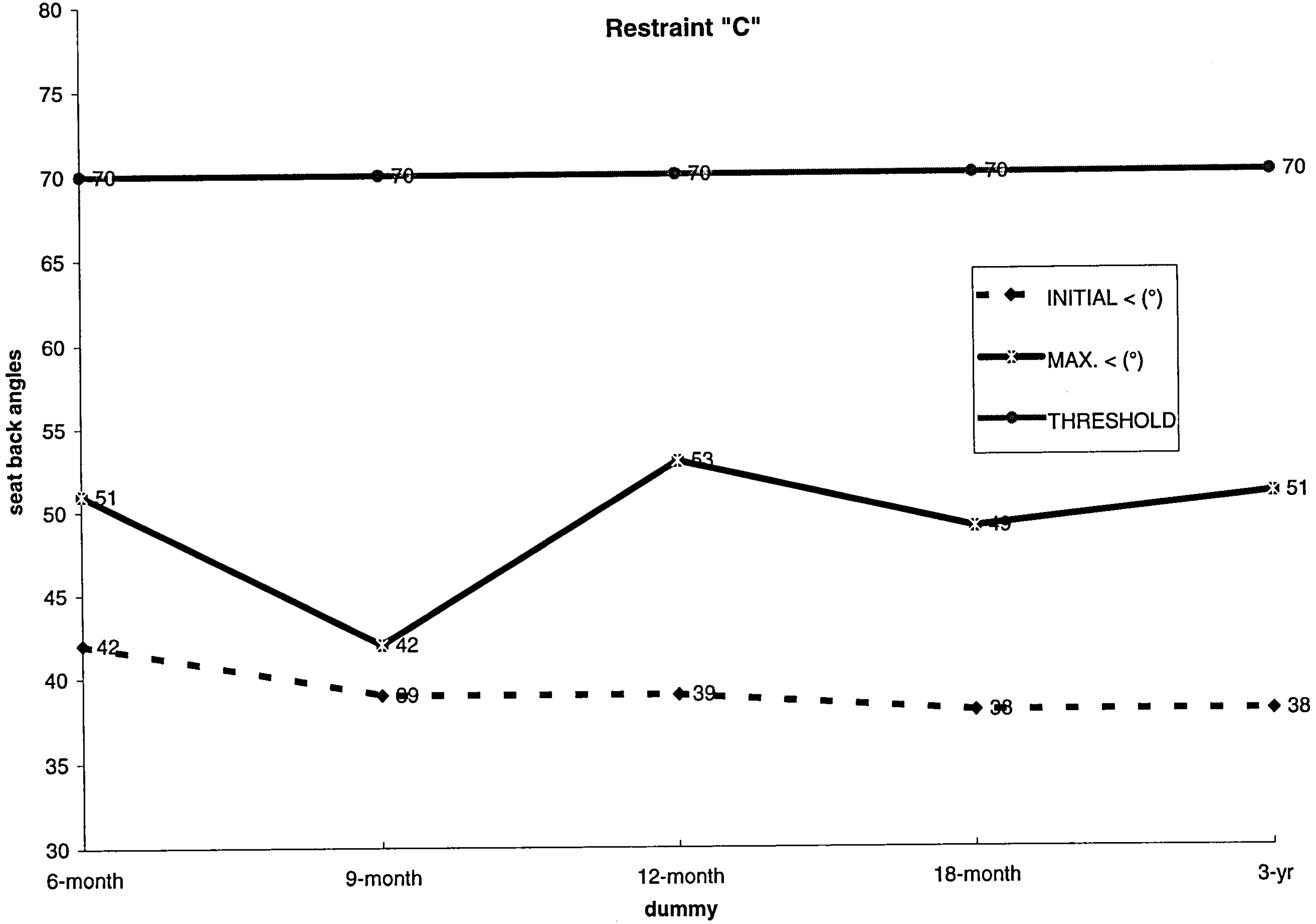

Appendix “C”

Figure “C-4”

ANALYSIS OF THE PASSIVE SAFETY OF MOTORCYCLES USING ACCIDENT INVESTIGATIONS AND CRASH TESTS

F. Alexander Berg
Heiko Bürkle
Frank Schmidts
Jörg Epple
DEKRA Automobil AG
Germany
Paper Number 98-S10-O-11

ABSTRACT

Based on information in DEKRA accident reconstruction expertises, 302 motorcycle accidents were analysed which occurred within the period 1989 to 1996 in Germany. Among them were 46 accidents involving motor scooters. The accident analysis results (e.g. distribution of accident types, motorcycle movement before crash, movement of the riders after the crash) are described and commented upon to supplement and update findings already published earlier in relation to actual accident occurrences involving motorcycles. In particular, there is a discussion of collision configurations and collision velocities together with the injuries of the rider (injured body parts, causes of the injuries). In addition, the collision configurations and collision velocities in accidents involving cars and motorcycles are compared with the crash test configurations described in ISO/DIS 13232.

In accordance with ISO/DIS 13232, four crash tests were carried out in which motorcycles collided with the side of cars. In two tests the car was stationary before the collision; in two other tests a collision of two moving vehicles was simulated. A Hybrid III pedestrian dummy (50 th percentile male) was used as the motorcycle rider.

In conclusion, against the background of actual accident occurrences and the test results, the current position with regard to the passive safety of motorcycles is described and pointers given toward possibilities for improvement.

INTRODUCTION

The current regulations of the Federal Republic of Germany define **motorized two-wheelers** as follows.

Kleinkraftrad: Mopeds and motor-assisted bicycles with an engine capacity not exceeding 50 cc and a maximum design speed not exceeding 50 km/h, bearing an identification mark, as well as „mopeds" and bicycles fitted with an auxiliary motor as defined by the former German Democratic Republic regulations, with up to 50 cc and up to 60 km/h.

Mofa 25: Bicycles fitted with an auxiliary motor (including „Leichtmofas") with an engine capacity not exceeding 50 cc and a maximum design speed not exceeding 25 km/h, bearing an identification mark.

Leichtkraftrad: Motorcycles/motor scooters with over 50 to 125 cc piston capacity and a power not exceeding 11 kW (as well as „Kleinkrafträder" with up to 50 cc and exceeding 40 km/h, provided that they were registered prior to 31 December 1983).

Kraftrad: Motorcycles with an engine capacity exceeding 80 cc.

Kraftroller: Motor scooters with an engine capacity with over 80 cc.

Motorrad: Two-wheeled **motorcycles** bearing an official registration number (**„Leichtkraftrad", „Kraftrad"** and **„Kraftroller"**).

German terms will be used partially with regard to explicit definitions in the following. **Figure 1** contains a long-term overview of the development of the relative frequency for the motorcyclists killed and severely injured in accidents inside and outside urban areas in the former German countries within the period 1956-1996. In **Figure 2** are the corresponding figures of registered motorcycles („Krafträder" and „Kraftroller") in the same period.

After beginning with a high level in the 50s, when the motorcycle has been a mass-transportation vehicle in Germany, the figures of killed and severely injured motorcyclists dropped by the middle of the 60s, remained constant until the beginning of the 70s and rose again clearly afterwards. New highest levels were reached in the years 1982/83: 959 killed outside urban areas (1982), 14 420 severely injured inside urban areas (1983) and 8 875 severely injured outside urban areas (1983). The number of motorcyclists killed inside urban areas did not follow this trend: 543 killed were registered in the year 1975 and 512 killed in 1983.

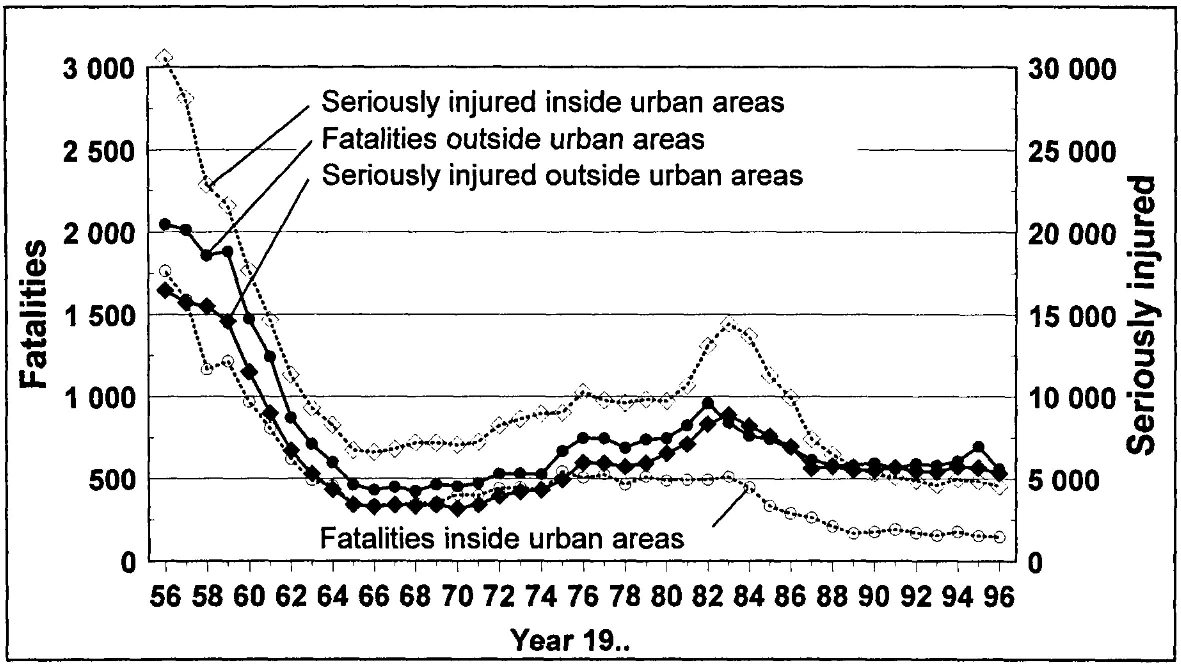

Figure 1. Absolute frequency of fatally injured or severely injured motorcycle riders in the former German countries within the period 1956 to 1996 (source: German Federal Ministry of Statistics)

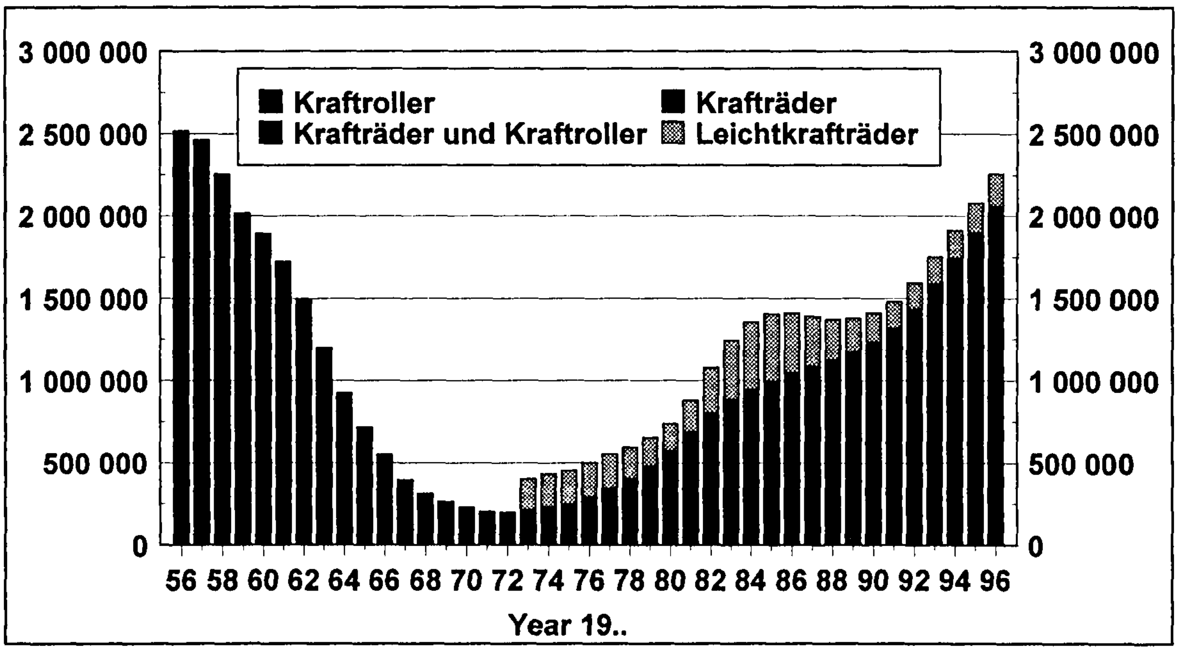

Figure 2. Absolute frequency of registered motorcycles („Krafträder" and „Kraftroller") in the former German countries within the period 1956 to 1996 (source: German Federal Ministry of Statistics)

The figures of killed and severely injured motorcyclists dropped again clearly until the end of the 80s. The development of the figures for motorcyclists killed inside and outside urban areas was approximately equal. In contrast, the number of severely injured decreased much more inside urban areas than outside. In the 90s the number of killed and severely injured motorcyclists remained virtually constant.

In comparison with the number of registered vehicles it can be observed, that the drop of killed and severely injured from 1982/83 until 1989/90 is reflected partially in the change in the number of registered „Leichtkrafträder". Because „Leichtkrafträder" are used predominantly by beginners and inside urban areas, the clear decrease of severely injured inside urban areas can be put down to the fall in the number of registered vehicles of this type. It is also remarkable that the clear increase of motorcycles beginning in the mid-80s does not follow a parallel increase of severely injured and killed motorcyclists.

Great increase rates were registered on the German market regarding the number of sold Motorroller, **Figure 3**. Very popular are hereby Motorroller with 50 cc piston capacity and 50 km/h maximum speed (as „Kleinkrafträder" not represented in Figure 2). From the 186 000 „Motorroller" sold in Germany in 1995, 166 000 belonged in the category 50-cc-„Roller". As well attractive are „Motorroller" with 125 cc piston capacity („Leichtkraftrad"), whose maximum engine power is 11 kW and a speed not allowed to exceed 80 km/h. These vehicles are permitted to be driven with a driving licence for passenger cars which was issued before April 1, 1980.

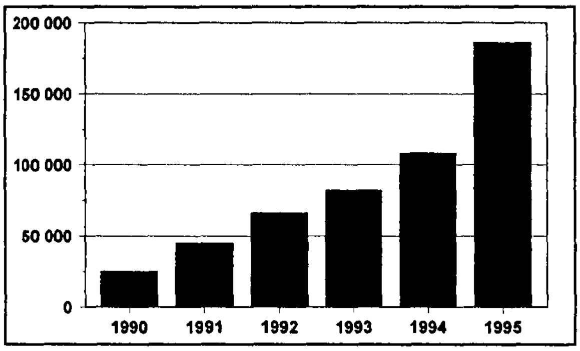

Figure 3. Motor scooters sold on the German market in the 90s (source: Verband der Fahrrad- und Motorrad-Industrie IVM)

Among the important changes in the legal regulations in Germany with regard to the traffic safety of motorized two-wheelers are:

August 1, 1980: Fine for riders of motorized two-wheelers (except „Mofas") who drive without using a helmet.

October 1, 1985: Compulsory wearing of a helmet and a fine for „Mofa" riders riding without a helmet.

April 1, 1986: Introduction of a graded motorcycle licence for motorcyclists.

October 1, 1988: Compulsory use of a dipped headlight for motorcyclists even during daytime.

Great significance is attached to the compulsory use of a helmet and to the graded motorcycle licence which, in spite of an increasing number of motorcycles, have helped to prevent a parallel increase in the number of motorcyclists killed and severely injured in accidents. In this context one must also take into account the improvements in protective clothing (helmet and suit).

Assessments of the technical evolution of the motorcycle itself show that active safety has been improved through further development of the chassis, tyres and the antilock brake system. The potential benefit of these measurements lies in the avoidance of accidents. However, technical improvements of the motorcycle in the field of passive safety, designed to lessen the effects of an accident (like the airbag in cars), can barely be registered at production motorcycles (LANGWIEDER et al., 1987, GRANDEL and BERG, 1994).

Considering that the active safety of motorcycles already displays a very high standard of evolution - similar to the protective clothing of the motorcyclists designed to ease the injuries - the passive safety of motorcycles is increasingly becoming the focus of interest. This should be seen in front of the goal of lowering the number of deaths in accidents from 45 000 in 1997 to 25 000 in 2010 within the European Community (SAFETY MONITOR, 1997). To reach this goal within the existing standards of vehicle safety, all potentials for further traffic system improvements must be examined and exploited if there is to be any prospect of success. The passive safety of the motorcycle has to be considered here in an appropriate way.

RESULTS OF AN ANALYSES OF 302 MOTORCYCLE ACCIDENTS IN GERMANY

By evaluation of accident-analytical DEKRA expertises 302 accidents, involving a total of 315 motorized two-wheelers with 358 riders, which occurred between 1989 and 1996 in Germany, were analysed (VON BRÜHL, 1994, MALL, 1995, DOBIASCH, 1997, BREHMER, 1998). Expertises of these type are written by DEKRA experts to resolve single accidents in traffic. These expertises can be used by the department of accident research for further scientific studies.

The distribution of the accident location of the 302 DEKRA cases is shown in **Figure 4** in comparison with the accident location of the 55 275 registered accidents with motorized two-wheelers revealed in the federal statistics for 1995. While the accidents occurring inside urban areas (68.4 %) are predominant in the federal statistics, those which occurred outside urban areas dominate the DEKRA cases with 56 %.

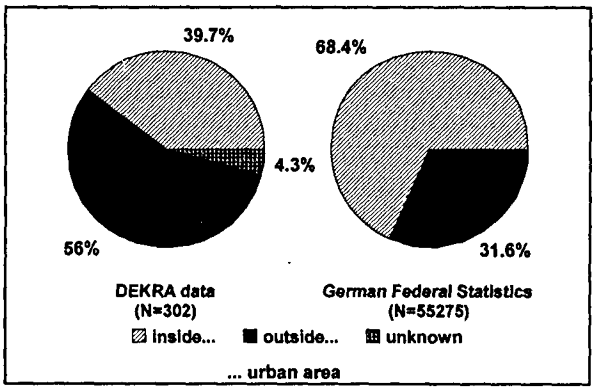

Figure 4. Location of the 302 accidents of motorized two-wheelers (years 1989 to 1996) in the DEKRA database compared with all such accidents in Germany (federal statistics, year 1995)

In **Figure 5** is a comparison of the injury severity between the accidents evaluated by DEKRA and the federal statistics. The DEKRA material contains more accidents with riders killed inside and outside urban areas than in the federal statistics. Corresponding to this the federal statistics contain more accidents inside and outside urban areas with slightly injured riders. Therefore the DEKRA cases are tending to be more severe.

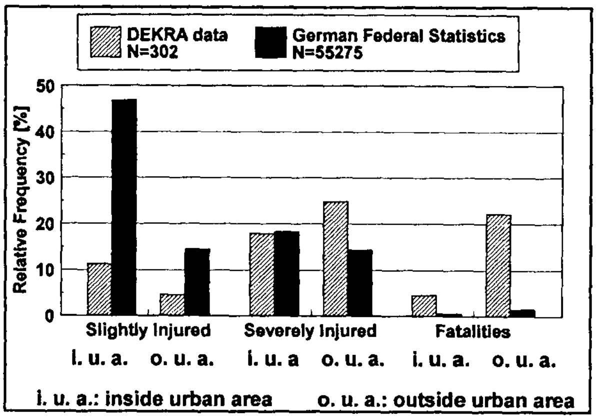

Figure 5. Severity distribution of the 302 accidents of motorized two-wheelers in the DEKRA database compared with all such accidents in Germany (federal statistics, year 1995)

Figure 6 contains further information about the types of motorized two-wheelers involved in the DEKRA cases. The classification of 297 out of 315 motorized two-wheelers was known. The „Sport-Motorräder“ were the most frequent among the „Krafträder“, followed by „Tourer“, „Sport-Tourer“, „Enduro“ and „Chopper“. The lighter vehicles with less than 80 cc piston capacity predominated in the „Roller“ category. „Mofas“ were seldom.

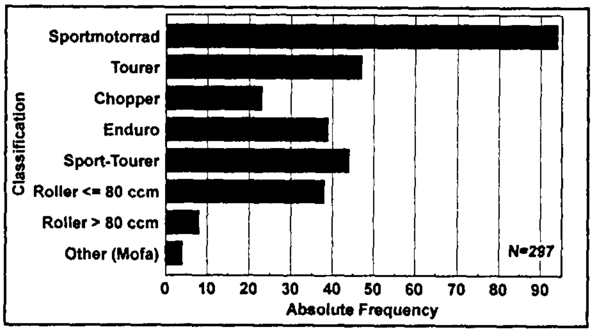

Figure 6. Distribution of the motorized-two-wheeler types in the DEKRA database

The following evaluations refer only to „Krafträder“ and „Roller“ (with no differentiation according to piston capacity). For these vehicles **Figure 7** shows the distribution of accident types of the corresponding 292 accidents. According to this, „Krafträder“ and „Roller“ are most frequently involved in accidents caused by turning into a road or crossing a road. Second frequently, both „Krafträder“ and „Roller“ were involved in accidents between vehicles moving along a carriageway and third frequently in accidents caused by turning off the road.

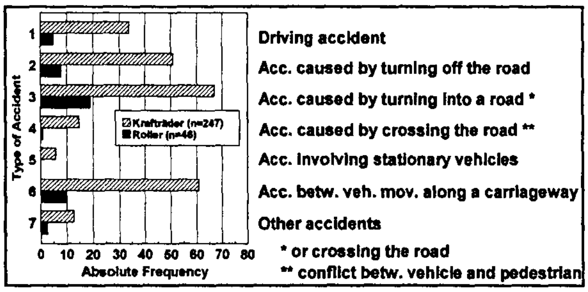

Figure 7. Distribution of the accident types of „Krafträder“ and „Roller“ in the DEKRA database

Figure 8 shows the absolute frequencies of the road category on which the „Krafträder“ and „Roller“ were moved at the time of the accident. Accidents on the „Autobahn“ were very rare. The „Krafträder“ mostly crashed on „Landesstraßen„ and „Bundesstraßen“ while the „Roller“ mostly crashed on „Ortsstraßen“.

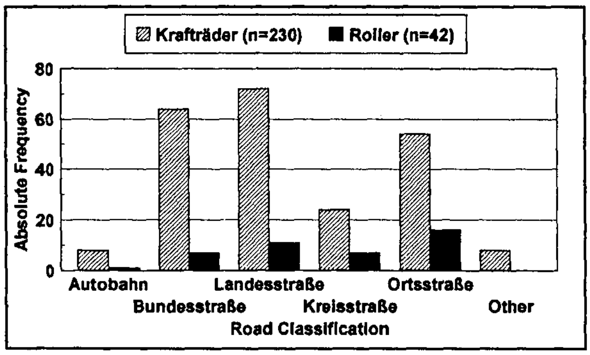

Figure 8. Road classification of accidents involving „Krafträder“ and „Roller“ from the DEKRA database

The most frequent opponent of the „Krafträder“ in the DEKRA cases was in 137 cases (63 %) a car and in 14 cases (6 %) a truck. Regarding the „Roller“ accidents, the car was again the most frequent opponent, with 31 cases. A corresponding evaluation of accidents with two participants featuring motorized two-wheelers and personal injury, as revealed in the federal statistics for the year 1995, shows a car as an opponent in 79 % of cases and a truck in 6 %.

The „Motorräder“ in the DEKRA cases were most frequently used by only one motorcyclist. Only 13 % of the „Krafträder“ and at least 15 % of the „Roller“ were being used by two riders at the time of the accident.

Figure 9 describes the movement of the „Krafträder“ and „Roller“ immediately before the accident. Most vehicles collided upright. Approximately 20 % of the „Krafträder“ and 18 % of the „Roller“ collided with the opponent while sliding on the side. Around 10 % of the „Krafträder“ collided moving in slant.

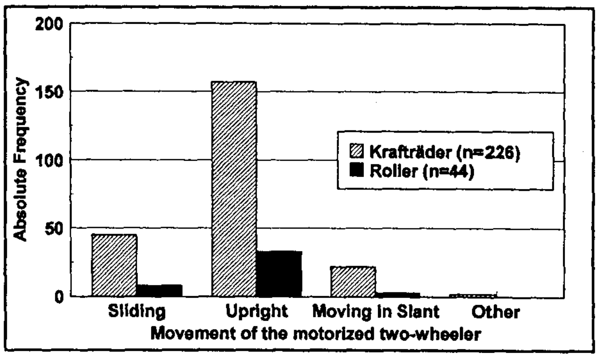

Figure 9. Classification of the movement of „Krafträder“ and „Roller“ immediately before the crash (DEKRA database)

The injury severity of 324 riders was known. The corresponding distribution of the killed, severely injured, slightly injured and uninjured riders is documented in **Figure 10**. The number of killed and severely injured riders on the „Roller ≤ 80 cc“ was equal while the number of slightly injured came close. Among the other types of motorized two-wheeler (except „Mofas“), the severely injured riders predominated.

From the frequencies shown in Figure 10 it is easy to determine the proportions of killed, severely injured and slightly injured riders corresponding to the two-wheeler types, **Figure 11**. These proportions reflect the corresponding risks. The passive safety of „Tourer“, „Chopper“ and „Enduro“ appears to be best because of the lowest proportion of killed riders. Because of their high proportion of killed riders the „Mofas“, „Roller > 80 cc“ and „Sportmotorräder“ do not appear to be favourable in terms of passive safety.

An in-depth assessment of the injury severity must also take into consideration the collision speed, **Figure 12**. The mean collision speed of every two-wheeler type with fatalities among the riders lies, as expected, above the mean collision speed in the accidents with severely injured riders. In analogy, the mean collision speed in accidents with slightly injured riders is lower than in those with severely injured riders. The mean collision speed in accidents with killed riders is highest among the „Sportmotorräder“, „Tourer“ and „Chopper“ at around 80 km/h.

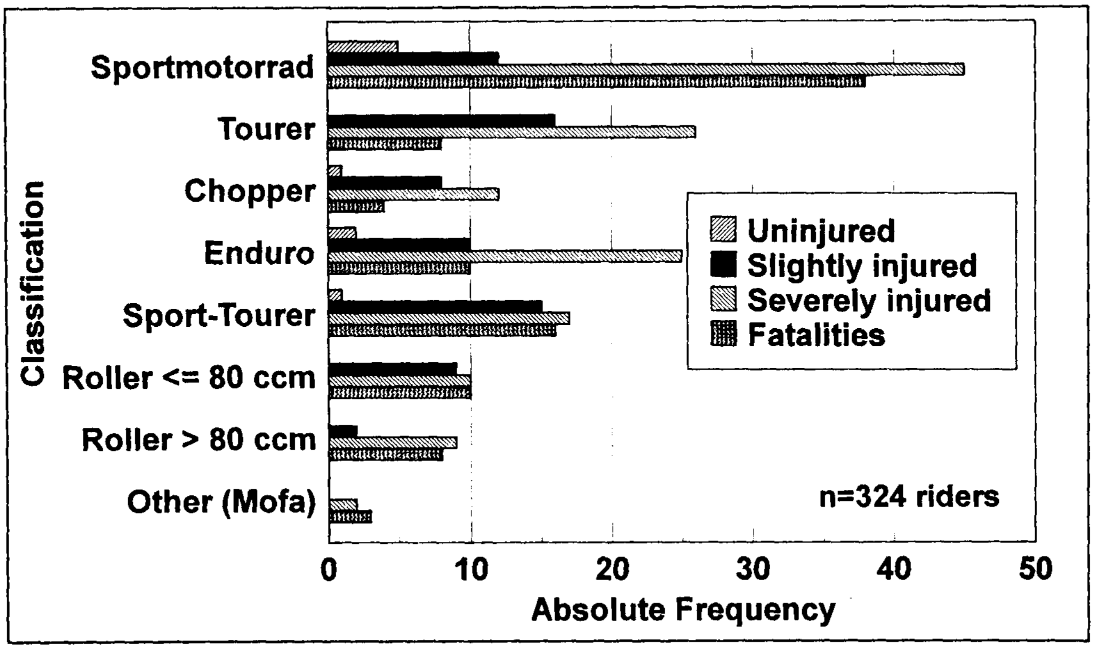

Figure 10. Injury severity in relation to the type of motorized two-wheeler

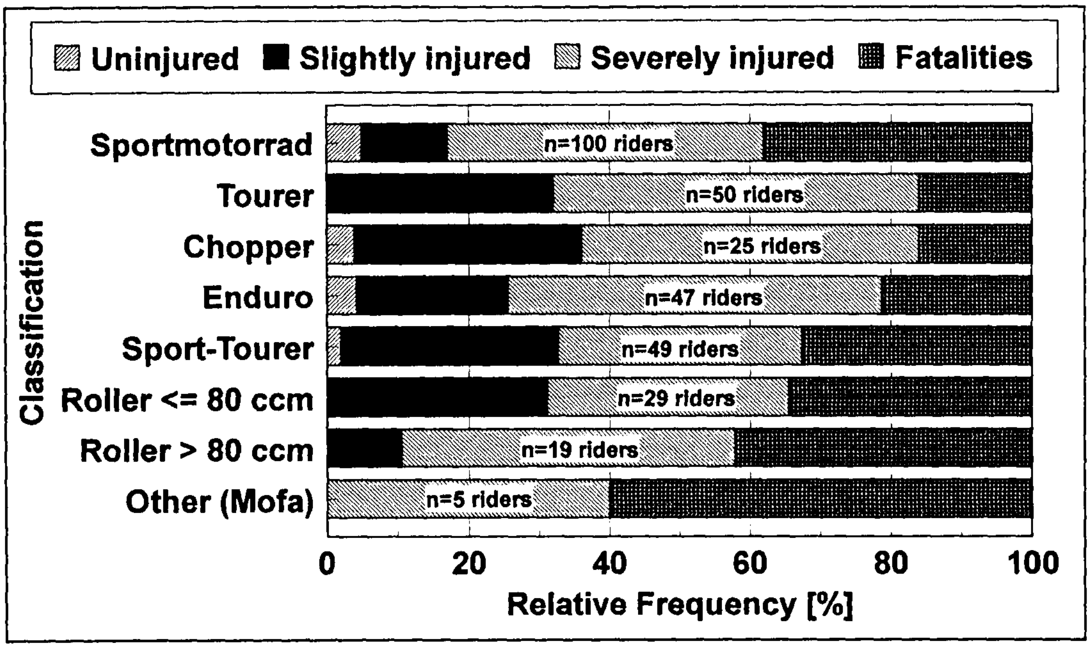

Figure 11. Proportion of killed, severely injured or slightly injured riders of the different types of motorized two-wheeler

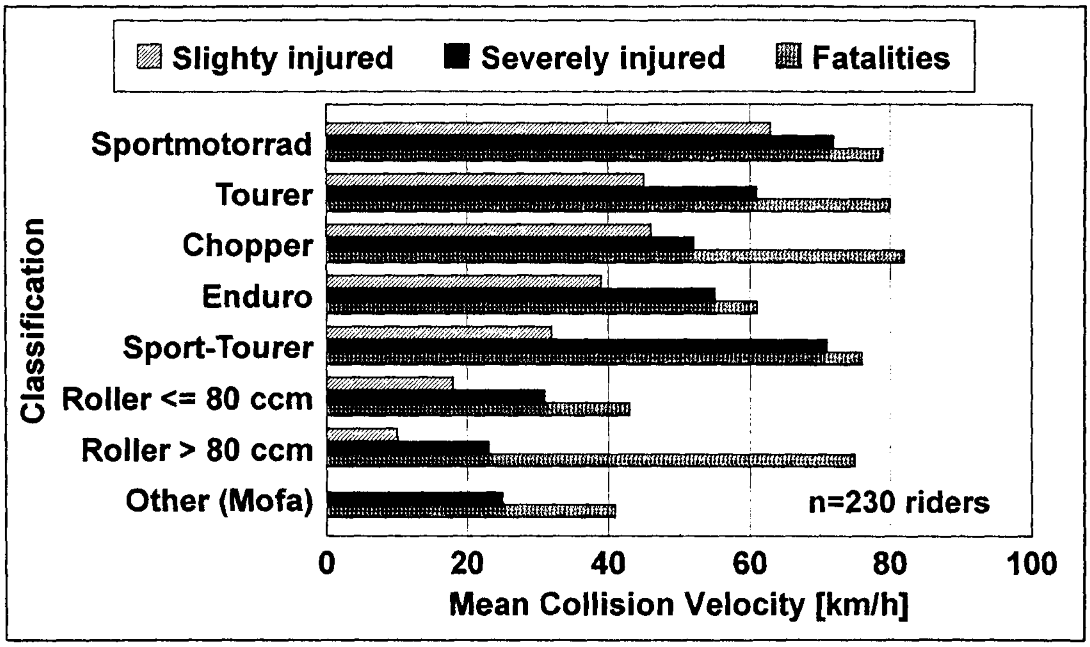

Figure 12. Mean collision velocity and injury severity in relation to the type of motorized two-wheeler

The mean collision speed for „Sport-Tourer“ with fatalities among the riders was 76 km/h and for „Roller > 80 cc“ 75 km/h. The killed riders on „Enduros“ had a mean collision speed of 61 km/h.

With a mean collision speed of 43 km/h the killed riders of the „Roller ≤ 80 cc“ category were moving significantly slower than the riders of the „Krafträder“ and „Roller > 80 cc“. The mean collision speed was lowest for „Mofa“ fatalities, at 41 km/h. On the one hand this corresponds with the lower engine power of these motorized two-wheelers, but on the other hand indicates illegal power-raising manipulations on the „Mofas“.

Different parameters are decisive in improving the passive safety of the different types of motorized two-wheeler. With regard to crash tests and the figures represented in Figure 12, the conclusion is clear that significantly clearly lower collision speeds are relevant for the „Roller ≤ 80 cc“ riders than for the „Motorräder“ riders.

In this context it must be remembered that the passive safety of two-wheeler riders also depends on their protective clothing and that the injury severity for the same mechanical loadings is influenced by the age and constitution of the riders.

Also relevant for the rider's injury type and severity is how they moved after the start of the collision and what they collided with in the further course of the accident.

Figure 13 contributes further results from the DEKRA survey. A collision between the riders of „Kraftrad“ and „Roller“ with the opponent was registered in most cases. Second frequently, the „Kraftrad“ riders slid on the road and the „Roller“ riders reached their final positions within a free flight. Third frequently, the „Roller“ riders slid on the road. Fourth frequently, the „Kraftrad“ riders had an impact with an obstacle (mostly on the roadside). This was rare for the „Roller“ riders. Also rare was for a „Kraftrad“ or „Roller“ rider to be run over by the opponent.

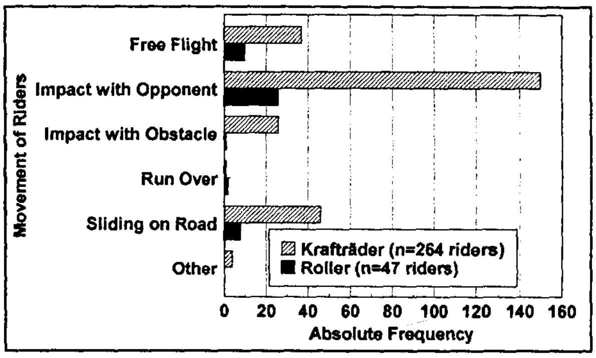

Figure 13. Movement of the riders of the motorized two-wheelers immediately after the crash

The cause of the rider injuries as established was in most cases the impact with the opponent, **Figure 14**. Only the „Krafträder“ riders injured themselves on the tank or the footrests of their own vehicle. The handle bar of the „Krafträder“ and „Roller“ was also an item which caused injuries. Injuries caused by the road surface could frequently be registered on the „Krafträder“ riders and as well on the „Roller“ riders.

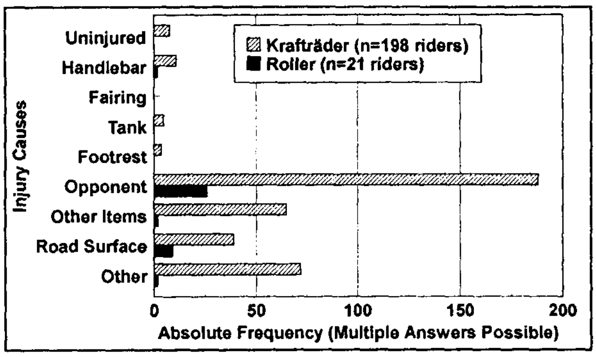

Figure 14. Injury causes of the riders of the motorized two-wheelers

An overview of the injured body parts is documented in the distribution shown in **Figure 15**. The „Krafträder“ and „Roller“ riders were mainly injured on the head. The riders are at considerable risk despite the use of a helmet.

With regard to „Roller“ riders, the knee is also at considerable risk, followed by the lower and upper leg. Furthermore the „Roller“ riders were also injured on the neck, foot/ankle, abdomen, back, pelvis/hip and lower arm. Injuries to the face, shoulder, upper arm, elbow and chest were not registered on „Roller“ riders.

Of importance for „Krafträder“ riders are injuries to the knee, hand/wrist, chest, neck, lower leg and foot/ankle. In any event, 6 „Krafträder“ riders survived the accident without injury.

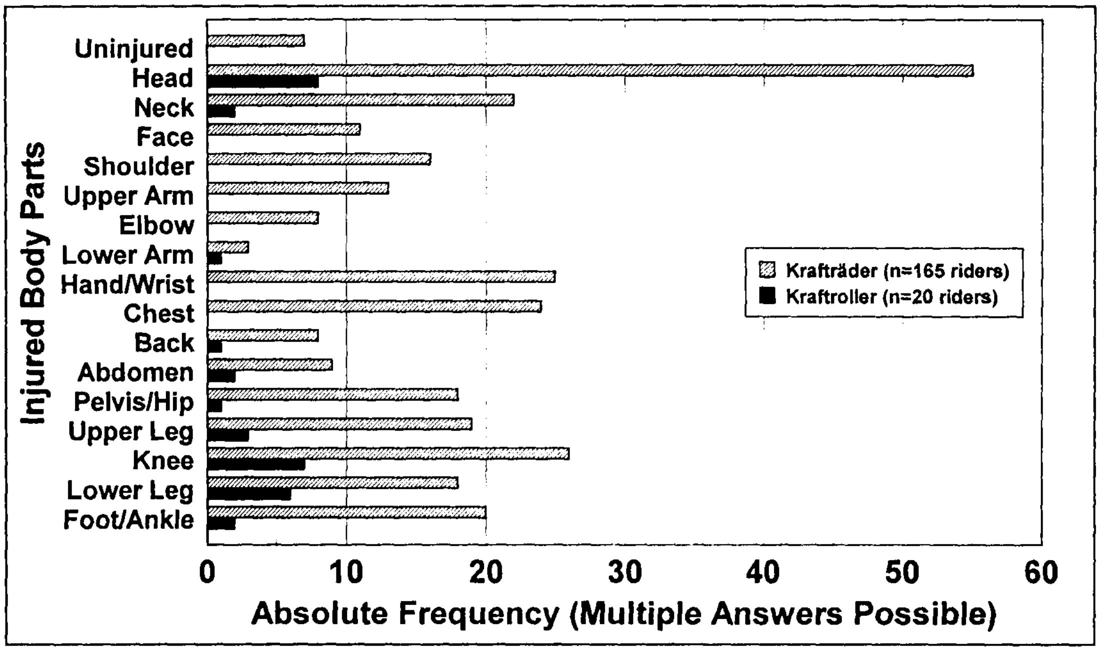

Figure 15. Injured body parts of the riders of the motorized two-wheelers

COLLISION SITUATIONS OF THE MOTORCYCLE ACCIDENTS IN THE DEKRA DATABASE COMPARED WITH ISO/DIS 13232

The standard ISO/DIS 13232 was the first world-wide created uniform requirements for standarized comparable crash tests in order to analyse the passive safety of motorized two-wheelers (VAN DRIESSCHE, 1994). This standard, developed by ISO/TC22/SC22/WG22, appeared in 1996 and is already taken into account by several producers of motorcycles and „Roller“.

501 motorcycle accidents from the USA (Los Angeles) and Germany (Hannover) were analysed in order to define the test matrix. 25 impact constellations were defined depending on the impact point on the car (figure 1), the impact point on the motorcycle (figure 2) and the impact angle (figure 3), **Figure 16**. Of these 25 constella-

tions, the six constellations 114, 143, 225, 412, 413 and 414 were selected for carrying out full-scale tests, **Figure 17**. For the remaining constellations the standard is suggesting numerical crash simulation.

The accident survey was studied with a subset of the motorcycle accidents from the DEKRA database (only accidents featuring a motorcycle/car collision) in accordance with the standard ISO/DIS 13232. The relative frequencies of the impact constellations from the DEKRA cases are shown in comparison with the relative frequencies as per ISO/DIS 13232, **Figure 18**.

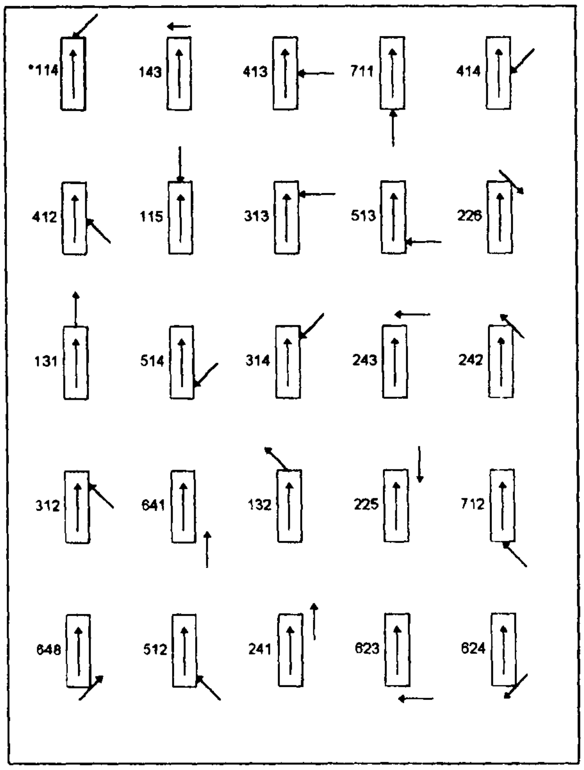

Figure 16 Motorcycle/car impact configurations defined in ISO/DIS 13232

In both data sources, ISO/DIS 13232 and DEKRA, the impact constellation 114 (oblique frontal impact of the motorcycle against the front of the car) is the most frequent, with 12.3 % and 13.0 % respectively. Impact constellation 143 (right-angled impact of the car front against the side of the motorcycle) is second most frequent according to ISO/DIS 13232 with 10.5 %, but only 3.3 % in the DEKRA material. According to ISO/DIS 13232 the impact constellation 413 (right-angled frontal impact of the motorcycle against the side of the car) is third most frequent with 10.0 %, similar to the DEKRA cases where it ranks second with 10.8 %. Impact constellation 226 (oblique impact of the car front against the motorcycle side) is represented with the same percentage (10.8 %) in the DEKRA cases, whereas in ISO/DIS 13232 this constellation is only of subordinate importance with 4 %.

In view of modest case numbers the impact constellations were not separated into „Krafträder“ and „Roller“. Against the background of possible differences between accident occurrences in Germany and in the USA - especially for severe accidents - the obvious priorities obtained from the data published in ISO/DIS 13232 should be further discussed.

The impact constellations suggested according to ISO/DIS 13232 for costly full-scale tests do not correspond in all cases with the rank order resulting from the evaluation of the material (suggested comparison of the rank order of the impact constellations 711 and 225 in Figure 16). Constellation 711 (impact with the motorcycle front against the back of the car) is third most frequent in the ISO/DIS 13232 data, but is not used for full-scale tests. Constellation 225 (glancing collision in opposite traffic) is used in full-scale crash tests although it ranks only 19th in ISO/DIS 13232.

The collision speeds defined in ISO/DIS 13232 must also be discussed. These measure 0 m/s, 6.7 m/s (about 24 km/h) and 9.8 m/s (about 35 km/h) for cars and 0 m/s and 13.4 m/s (about 48 km/h) for the motorcycle. Wherever two moving vehicles collide in a full-scale crash test, the motorcycle is always twice as fast as the car. This may depend on the speeds representable on the available crash facilities and is therefore justified with the demands of experimental practice. In comparison with the DEKRA data already available, 48 km/h appears to be too low for the motorcycle accidents and too high for the „Roller“ accidents.

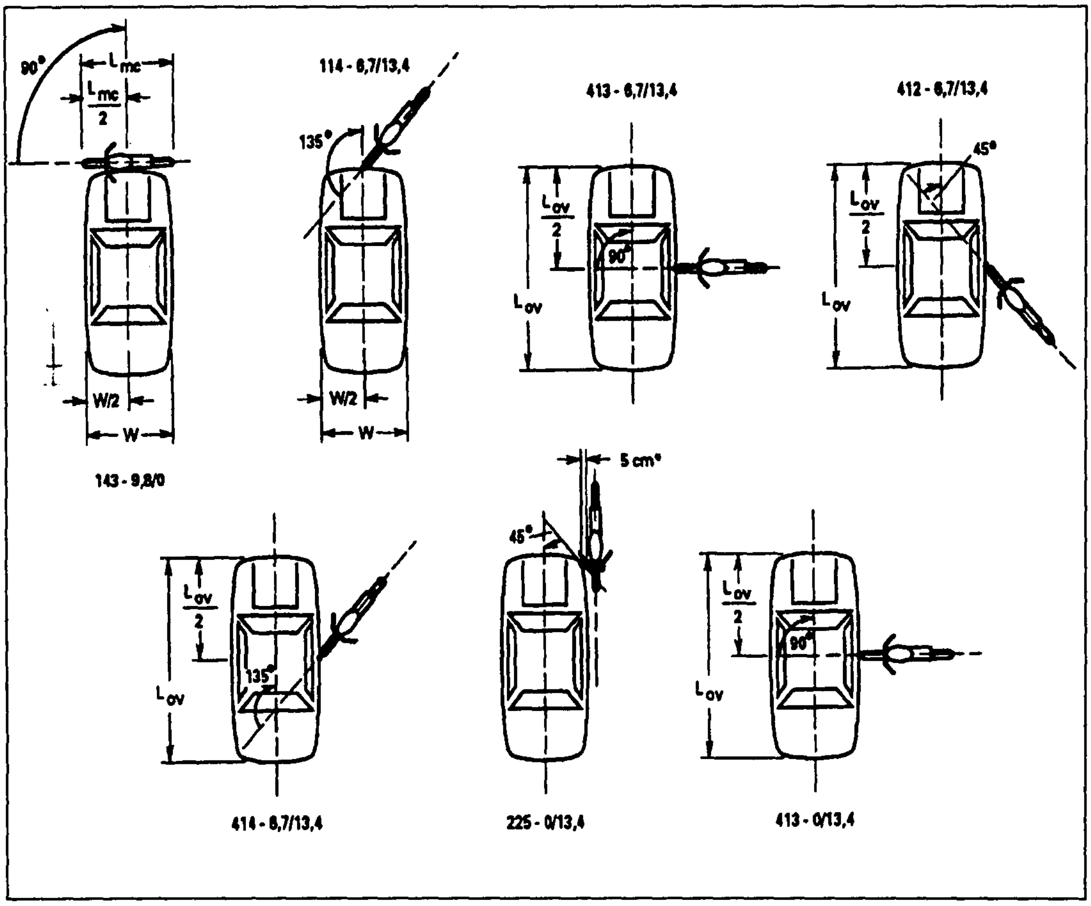
90°
L_mc
L_mc/2
W/2
W
143 - 9,8/0
114 - 6,7/13,4
135°
W/2
W
413 - 6,7/13,4
L_ov/2
L_ov
90°
412 - 6,7/13,4
45°
L_ov/2
L_ov
5 cm*
45°
L_ov/2
L_ov
135°
L_ov/2
L_ov
90°
414 - 6,7/13,4
225 - 0/13,4
413 - 0/13,4

Figure 17. Motorized two-wheeler/passenger car impact configurations defined for use in full-scale crash tests in ISO/DIS 13232

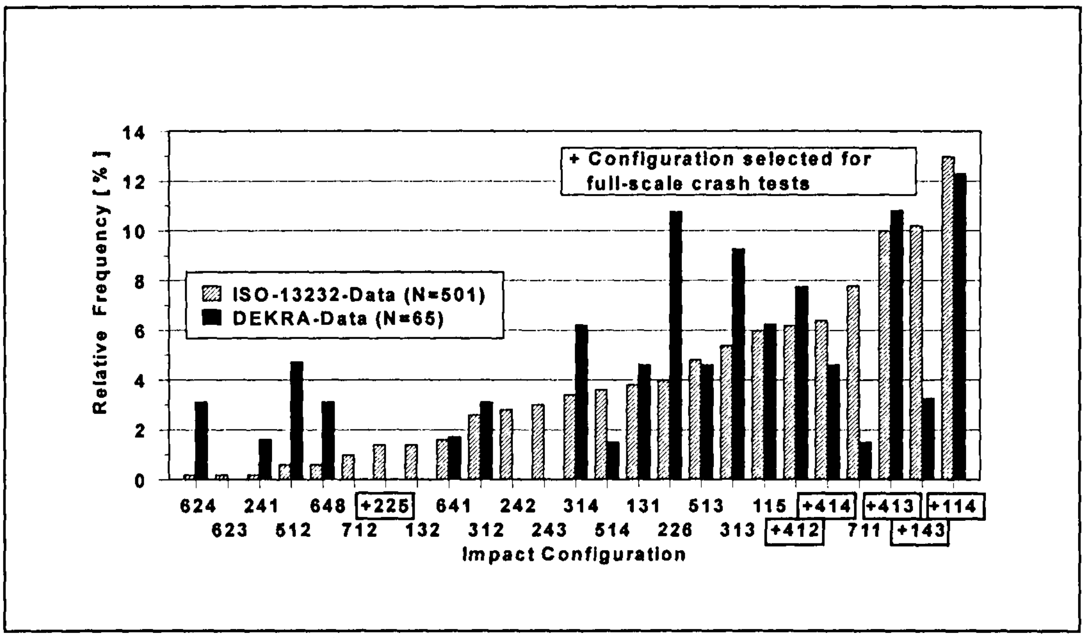

Figure 18. Relative frequencies of the motorized two-wheeler/passenger car impact configurations in the ISO/DIS-13232 database and in the DEKRA database

FULL-SCALE TESTS IN ACCORDANCE WITH ISO/DIS 13232

The DEKRA accident research department carried out four tests during the qualification period of the DEKRA crash centre for running instrumented full-scale crash tests as per ISO/DIS 13232. This was commissioned by vehicle producers with the object of making results available for publication. The impact constellations 414 and 413 were reproduced in these tests. In two tests the motorcycle collided with a stationary car and in two more tests a moving car was hit by a motorcycle.

Figure 19 gives an overview of the four full-scale crash tests which were carried out. It contains the collision speed of the vehicles and the impact configurations with their corresponding code numbers as per ISO/DIS 13232, as well as information concerning the head impact and the movement path of the rider.

Crash-numbers	Con-figuration	Head-Impact / Motion-course
SH 95.32 MuZ Skorpion Tour	414 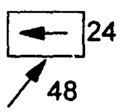	No head-impact at the car. Glances over tailgate
SH 95.33 Honda CB 450 N	(414) 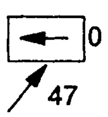	Head-impact at the roof edge. Glances over side
SH 96.20 MuZ Skorpion Tour	414 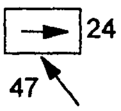	Head-impact at the side. Glances over side
SH 96.21 Suzuki GSX 400 E	413 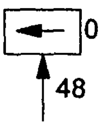	Head-impact at the side-window. Dive into cabin

Figure 19. Overview of the four full-scale motorcycle/passenger car crash tests carried out at the DEKRA crash centre in accordance to ISO/DIS 13232

The motorcycles were selected according to the sitting position and the size of the motorcycle. These parameters must be more or less identical in all tests in order to allow an interpretation of the test results. All four motorcycles were of the „Tourer" type. On this type the sitting position of the rider is relatively upright. The cars used as opponents were VW Golf I and Golf II. The rider was represented by a Hybrid III dummy (50th percentile male, standing doll). A rider dummy as suggested by ISO/DIS 13232 could not be used for reasons such as deadline and costs.

Figure 20 shows as an example the collision of two moving vehicles, whereby a MuZ Skorpion Tour impacted at 48 km/h against the B-pillar of a VW Golf I which was moving at 24 km/h. The movements of the rider were determined by evaluating the film. The loadings of the upper leg were available as a measurement. **Figure 21** shows the movement paths and the dummy loadings on head, chest and upper leg in an impact of a Honda CB 450 N motorcycle at 47 km/h with a stationary VW Golf I. The tests shown in Figure 20 and 21 correspond to configuration 414 as per ISO/DIS 13232.

In the collision of the MuZ Skorpion Tour and the moving VW Golf I (Figure 20), the dummy first hit the roof edge of the Golf with its left shoulder at time t = 124 ms after the start of the collision with the motorcycle's front wheel. From the beginning of the collision until this moment the motorcycle had gone a distance of about 70 cm referred to its centre of gravity. The Golf had gone a distance of about 80 cm in the same time frame because of its own speed. After the shoulder impact, the dummy slid over the tailgate of the Golf. No impact occurred between the rider's helmeted head and the body of the car. The loadings measured on the upper leg are somewhat high, at - 4.6 kN (push) respectively. 7.5 kN (pull), but are still clearly lower than the protection criterion of 10 kN.

The evaluation of the dummy movement with the same impact angle against a standing vehicle, Figure 21, shows that the dummy's head hits the roof edge of the Golf at t = 126 ms after the start of the collision. The stillstanding Golf massively hinders the movement of the dummy so that no further phase-out path remains. As a consequence only a small part of the impact energy of the dummy is transformed into a sliding movement. Nevertheless the loadings measured on head and chest are lower than their biomechanical limits (HIC = 1 000, a_{3ms}-Head = 80 g, a_{3ms}-Chest = 60 g, SI = 60 g). The loading on the left upper leg, at -10.3 kN (push), lies in the region of the corresponding protection criterion of 10 kN.

Figure 22 shows another test with two moved vehicles which was carried out with a collision angle of 135°. A MuZ Skorpion Tour at a speed of 47 km/h impacted with its front wheel on a VW Golf II moving with 24 km/h in the area of the B-pillar. The impact occurred in this test on the right side of the car. This test corresponds to constellation 414 as per ISO/DIS 13232 because of the symmetry and can therefore be compared directly with the tests shown in Figure 20 and 21.

Despite the same impact constellation with moving vehicles as in Figure 20, however in the test shown in Figure 22 an impact occurred between the helmeted dummy head and the Golf II body below the right side window. This is due to the strong upward movement of the motorcycle. The Golf covers a distance of about 1 m within the time period between the start of the collision and the head impact at t = 158 ms. With reference to its centre of gravity the motorcycle covers a distance of only about 10 cm in movement direction in the same time period. Therefore the collision location is not cleared by the Golf as it is in test SH 95.32. As the back of the motorcycle rises, the dummy receives a corresponding force which causes him to rotate about his transverse axis so that he impacts the Golf head first. In both upper legs of the dummy increased pulling forces of 7.5 and 10.0 kN were measured. The measured head loadings, at HIC = 108 and a_{3ms} = 33 g, are way down in the undercritical area. In contradiction to this, the chest loadings of SI = 1 042 and a_{3ms} = 90 g lie above the corresponding protection criteria. This loading results from the impact of the dummy's chest on the fork bridge of the motorcycle. In the further course of movement beginning at t = 158 ms the dummy slides over the rear side panel.

The fourth test, **Figure 23**, corresponds to configuration 413 as per ISO/DIS 13232. The Suzuki GSX 400 E motorcycle collides at 48 km/h perpendicular with the B-pillar of a standing VW Golf II car. In comparison to the other three tests, differences between collision angles of 90° and 135° become clear. No slipping occurs in the perpendicular impact and the dummy head brakes through the side window of the Golf II at t = 126 ms. He penetrates the passenger cell to a depth of about 30 cm by t = 200 ms. In the further course of movement the dummy sinks to the ground on the impacted side of the Golf. The value HIC = 319 determined from the loadings on the dummy head in fact lies far below the protection criterion of 1 000. However, the 3ms-deceleration value of 84 g lies in the region of the corresponding limit of 80 g. The chest loading of 32 g and an SI-value of 174 lie far below the corresponding protection criteria.

With knowledge of the movement paths and the measured dummy loadings of other similar tests, the results of which already have been published (BERG, 1988, GRANDEL and BERG, 1994, LANGWIEDER et al., 1987, GROSE, 1996), it is realistic to expect that on all four full-scale crash tests a motorcycle airbag installed in the area of the tank/steering head could have deployed in time. Therefore the movements of the riders could have been positively influenced and direct head and body impacts on the car body could have been intercepted. The forward-upward movement of the dummy supported by the airbag would have lifted the dummy head over the roof edge. So all in all, a more favourable movement path would have been initiated, leading to a flight with less injury risk or a glancing movement over the roof of the car in a real world accident.

Leg deflectors could also have contributed towards reducing the loadings on the upper and lower leg in all tests. Keeping the legs away from the handlebar of the motorcycle could also improve the effectiveness of the airbag. Thus the dummy's movement after the start of the collision could have been more flexible and in consequence less injury-prone.

t = 0 ms (start of impact) SH95.32

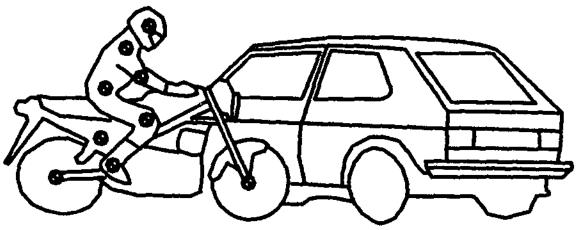

t = 0 ... 124 ms (impact of dummy shoulder)

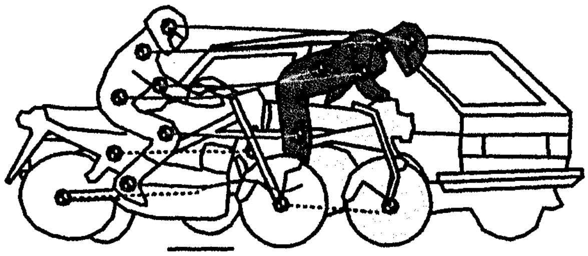

t = 124 ... 198 ms (dummy glances over tailgate)

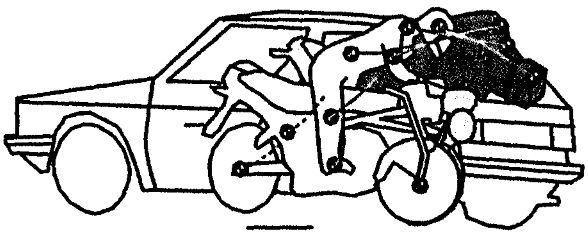

Head: a_{3ms} = --- HIC = ---

Chest: a_{3ms} = --- SI = ---

Pelvis: a_{3ms} = ---

Femur: F_{left} = -4.6 kN F_{right} = +7.5 kN

- nicht gemessen

Figure 20. Results of film evaluations of a full-scale crash test between moving motorcycle and moving passenger car and measured femur loadings of the dummy (Configuration 414 in ISO/DIS 13232)

t = 0 ms (start of impact) SH95.33

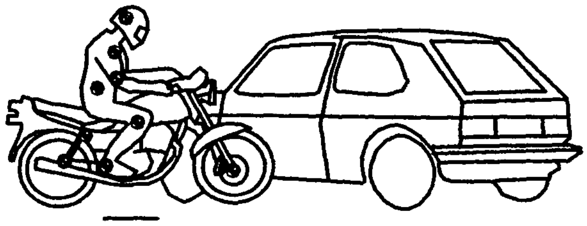

t = 0 ... 126 ms (impact of dummy head)

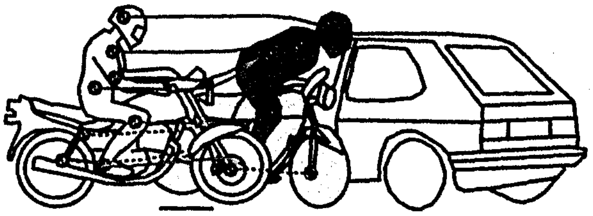

t = 126 ... 201 ms (dummy glances over side)

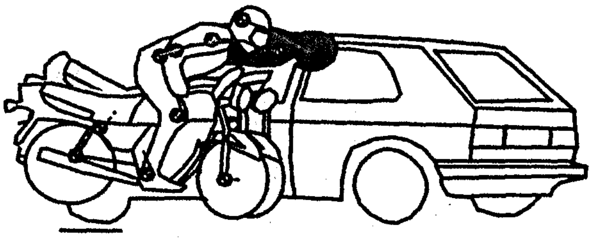

Head: a_{3ms} = 57 g, HIC = 157

Chest: a_{3ms} = 14 g SI = 52

Pelvis: a_{3ms} = ---

Femur: F_{left} = -10.3 kN F_{right} = +2.1 kN

- nicht gemessen

Figure 21. Results of film evaluations of a full-scale crash test between moving motorcycle and stationary passenger car and measured head, chest and femur loadings of the dummy (Configuration 414 in ISO/DIS 13232)

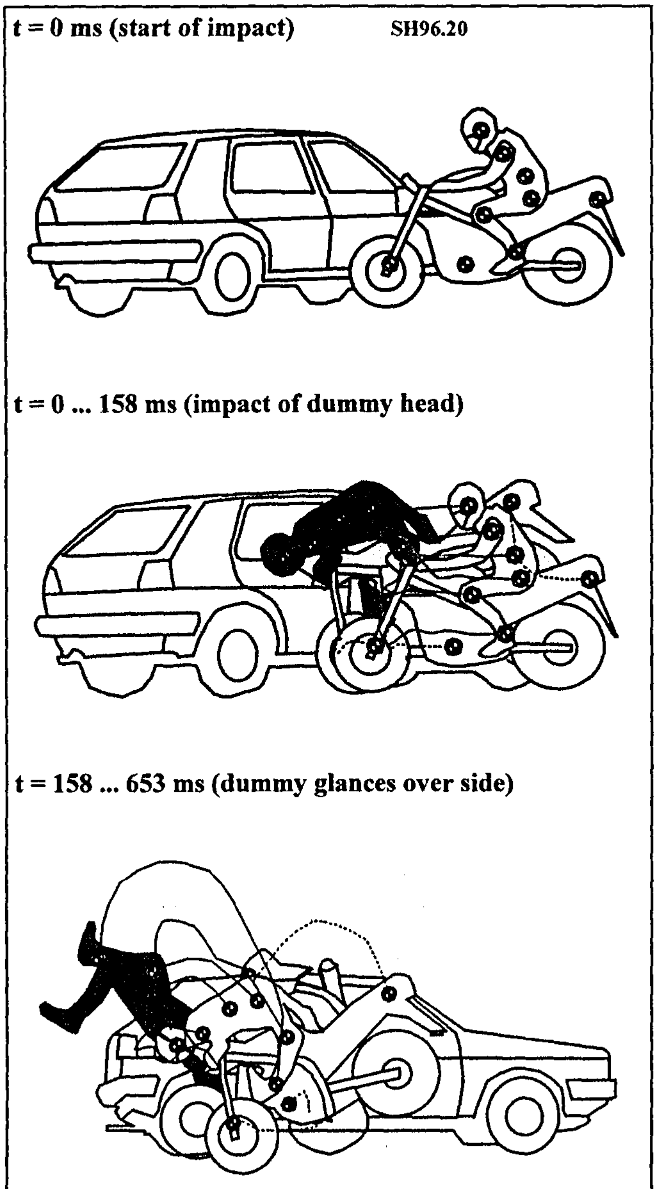

t = 0 ms (start of impact) SH96.20

t = 0 ... 158 ms (impact of dummy head)

t = 158 ... 653 ms (dummy glances over side)

Head: a_{3ms} = 33 g HIC = 108

Chest: a_{3ms} = 90 g SI = 1042

Pelvis: a_{3ms} = 25 g

Femur: F_{left} = +4.9 kN F_{right} = +10.0 kN

Figure 22. Results of film evaluation of a full-scale crash test between moving motorcycle and moving passenger car and measured loadings of the dummy (Configuration 414 in ISO/DIS 13232)

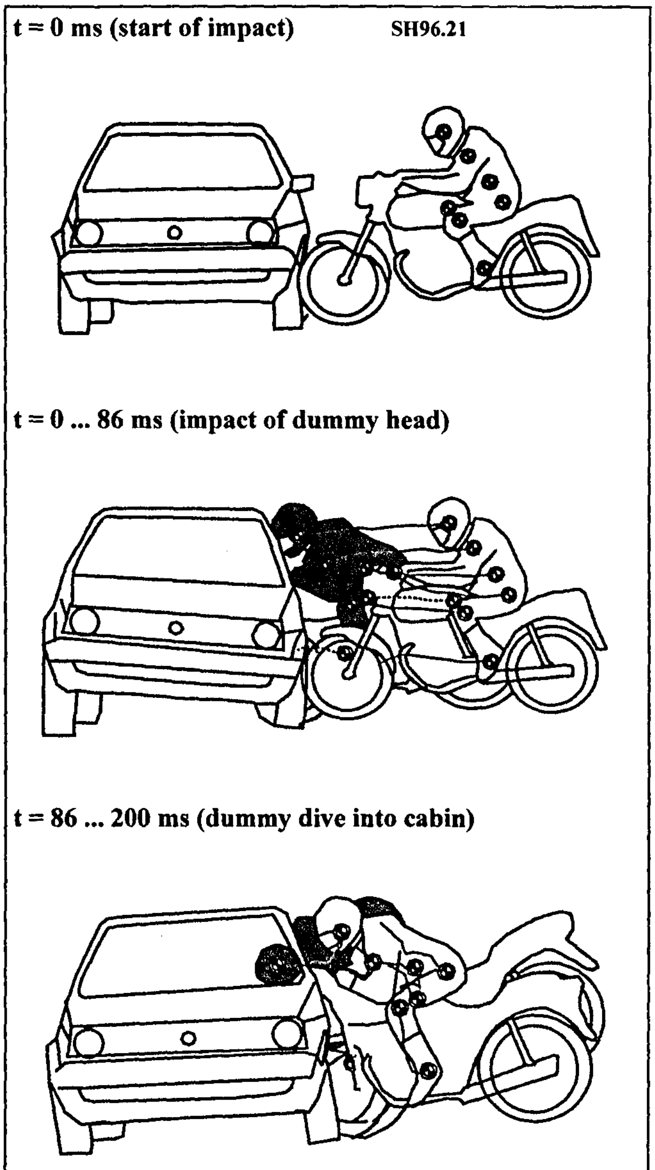

t = 0 ms (start of impact) SH96.21

t = 0 ... 86 ms (impact of dummy head)

t = 86 ... 200 ms (dummy dive into cabin)

Head: a_{3ms} = 84 g, HIC = 379

Chest: a_{3ms} = 32 g SI = 174

Pelvis: a_{3ms} = ---

Femur: F_{left} = +3.0 kN F_{right} = +4.6 kN

- nicht gemessen

Figure 23. Results of film evaluations of a full-scale crash test between moving motorcycle and stationary passenger car and measured head, chest and femur loadings of the dummy (Configuration 413 in ISO/DIS 13232)

CONCLUSIONS

1. The number of motorcycle riders killed and severely injured in accidents in Germany has remained almost constant in the 1990s to date. Simultaneously, in the category of motorcycles the number of registered „Krafträder“ (piston capacity of over 80 cc) has increased further while the number of „Leichtkrafträder“ (piston capacity 50 to 125 cc, engine power not exceeding 11 kW) has remained nearly constant. The number of „Roller“ (especially those with a piston capacity ≤ 80 cc) has also increased.

2. Evaluation of 302 accidents of motorized two-wheelers from the stock of the DEKRA accident research department, which occurred within the period 1989-1996 in Germany, shows that now as in the past the head and the lower extremities (foot/ankle, lower leg, knee, upper leg) are at particular risk. The „Kraftrad“ riders were also frequently injured on the face, shoulder and the upper extremities (hand/wrist, elbow, upper arm). This trend has not yet been confirmed with regard to „Roller“ riders.

3. The standard ISO/DIS 13232 for the first time created world-wide uniform requirements for standarized and comparable crash tests, and these are already being taken into consideration in the development of new vehicles by some producers of motorcycles and „Roller“. The impact constellations suggested in this standard should be further discussed against the background of real world accidents. For tests with a moving motorcycle, ISO/DIS 13232 always suggests a collision speed of 13.4 m/s (about 48 km/h). Evaluations carried out to date by the DEKRA accident research department in conjunction with the driving performance of the motorized two-wheelers indicate the use of higher speeds in crash tests for severe accidents with „Krafträder“ and suggest that lower speeds are relevant for crash tests with „Roller“.

4. Conducting crash tests with motorcycles with complete conformity with the standard ISO/DIS 13232 is difficult at present because of the high cost of motorcycle dummies. Therefore tests with a Hybrid III dummy (50th percentile male, standing doll) were carried out by the DEKRA accident research department for the qualification of the crash centre with a view to the impact constellations as per ISO/DIS 13232. The results of these tests indicate that crash tests featuring a frontal impact of the motorcycle with the side of the standing vehicle tend to lead to higher loadings on the dummy head than corresponding collisions with moving vehicles. The measured deceleration loadings on the helmeted dummy head still lay below the relevant protection criteria.

In one test where the motorcycle impacted a moving car, the measured deceleration loadings of the dummy's chest lay above the limit SI = 1000 and $a_{3ms} = 60$ g. Evaluation of the high-speed film showed that the reason was an impact of the dummy's chest against the fork bridge of the motorcycle.

In all tests performed the measured forces on the upper legs indicate an increased loading on these body parts.

On the one hand an airbag, which is being discussed in connection with terms such as concepts of a safety motorcycle and is already in use in prototype testing, could have had an impact-diminishing function by intercepting the head and the upper body. On the other hand a forward/upward movement of the dummy would have been initiated. This would have lifted the head over the area of danger and the dummy could have been diverted over the car. In conjunction with knee pads, the resulting movement of the dummy during the collision would have been more flexible and less injury-prone.

Hopefully the standard ISO/DIS 13232 can provide new impulses which will be useful in the further development of passive safety elements for suitable motorcycles, such as „Tourer" and „Enduro", up to their production launch.

REFERENCES

Berg F Alexander (1987): Unfallsimulationen mit Motorrädern und Personenkraftwagen. ATZ Automobiltechnische Zeitschrift 90 (1988) 5, pp. 269-270.

Brehmer Thomas (1998): Erhebung und Auswertung von Motorroller- und Motorrad-Unfalldaten. Diplom-arbeit. Fachhochschule Hamburg und DEKRA-Unfallforschung.

Von Brühl Marc (1994): Pilotstudie zur Erhebung und Auswertung von Motorrad-Unfalldaten. Diplomarbeit. Fachhochschule München, Fachbereich Maschinenbau und DEKRA-Unfallforschung.

Dobiasch Thomas (1997): Erhebung und Auswertung von Motorradunfällen. Diplomarbeit. Fachhochschule Kaiserslautern, DEKRA-Unfallforschung.

Van Driessche Hans (1994): Development of an ISO Standard for Motorcycle Research Impact Test Procedures. Procceedings of the Fourteenth International Technical Conference on the Enhanced Safety of Vehicles, Munich, Germany, May 23-26, 1994.

Grandel Jürgen, Berg F Alexander (1994): „Passive Sicherheit von Motorrädern". Verkehrsunfall und Fahrzeugtechnik 32, June 1994, pp. 152-156; September 1994 pp. 234-238 and Dezember 1994 pp. 324-332.

Grose Geoffrey, Patel Bipin, Okello John (1996): The Development of a Motorcycle Rider Airbag Restraint System. Procc. XXVI FISITA Congress, Praha, June 17 to 21, 1996.

Langwieder Klaus, Sporner Alexander and Polauke Joachim (1987): „Stand der passiven Sicherheit für Motorradfahrer und mögliche Entwicklungstendenzen". VDI-Berichte No. 657. pp. 29-52.

Mall Christian (1995): Erhebung und Auswertung von Motorrad-Unfalldaten. Diplomarbeit Fachhochschule Ulm und DEKRA-Unfallforschung.

SAFETY MONITOR (1997), ETSC News, Nr. 13, March 1997 Edition.

Statistisches Bundesamt (1997): Fachserie 8, Reihe 7, Verkehrsunfälle 1996. Verlag Metzler-Poeschel, Stuttgart.

NEW DEVELOPMENTS IN RETROSPECTIVE DATA BASES OF SERIOUS CAR CRASHES AND CAR COLLISIONS WITH PEDESTRIANS AND MOTORCYCLISTS. - THE RESEARCH ACTIVITIES OF THE GERMAN INSURERS (GDV)

Dieter Anselm
Klaus Langwieder
Alexander Sporner
GDV – Institute for Vehicle Safety
Germany

Paper Number 98-S10-O-12

ABSTRACT

The German Insurance Association (GDV) has continued and completed the accident research program „Vehicle Safety 90“.

Based on a data base of 15,000 car-to-car crashes, about 1,000 car crashes with serious injuries (MAIS3+) have been analyzed in depth. The results are presented, especially analysis regarding collision types and injury criteria. On the basis of a comprehensive injury description, using AIS, ISS and Scales showing long term disability, social economic cost factors are outlined which show the requirements of further injury reduction strategies.

Parallel to the research program „Vehicle Safety 90 – VS90“ two other data bases have been completed. Accident material of 600 motorcycle-to-car crashes shows both the accident circumstances as well as the crash characteristics and the injury pattern of motorcyclists.

A representative data base of 1,200 car-to-pedestrian accidents will be finished by mid 1998. The collision types and crash/injury characteristics are the focal areas of this research program.

These data bases are described in their structure and the accident parameters covered, the focal results concerning collision types, crash and injury data are outlined, which form the basis for continued analysis within GDV research.

Finally, proposals for data bases of the next research period „Vehicle Safety 2000“ will be made which should assist a continued and intensified international cooperation.

INTRODUCTION

Effective protective measures require a thorough knowledge of the accident scene.

This guiding principle of the German Insurers' accident research illustrates the aim of the Institute for Vehicle Safety in Munich.

The systematic research into all details of the accident sequence are presented on the following pages with the help of information from insurers' accident records, police reports and experts' opinions as well as some findings developed from them.

THE BASIS OF THE DATA

Accident research in Germany, and internationally, is divided up into three essential areas of analysis.

- The retrospective analysis of traffic accidents using accident records was the starting point for constructive accident research. The in-depth analysis at the scene of the accident, too, which also relates to data after the real-life accident, partially belongs to this area.
- Experimental simulations represent the second branch of accident research which involves applying the findings of automotive engineering and/or the testing of safety elements on and in the car.
- Mathematical simulation of accident sequences is regarded as the third aspect of accident research.

Without the retrospective preparatory work, however, the basis for experiments and for mathematical models would also be incomplete. In addition, the results of this work reflect the details of the real-life accident, and it is precisely here that it must be repeatedly pointed out that only the accident itself can furnish information on the consequences for the persons involved in it. It is particularly mathematically simulated results that offer at best a framework, which, however, is again and again broken through by real-life events.

The methods of collecting data

Data on accident sequences have been collected continuously by the German insurers since 1969.

This information on accidents is the basis of every data base. By means of coding into characters that the computer can understand a number of 100 to 350 data fields are made available per accident.

But where do these details of the accident come from?

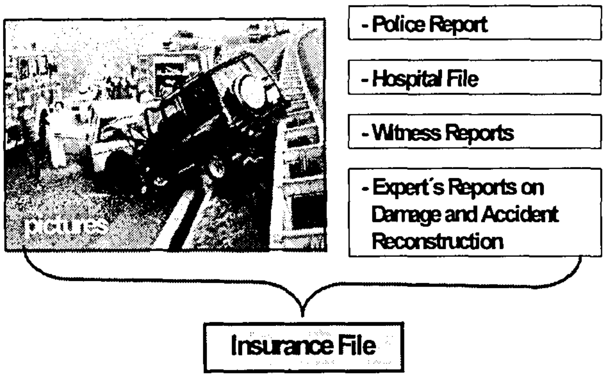

Fig. 1: Data sources for Insurance Files

Here the first decisive advantage of the German Insurers' accident research can be seen, namely access to all of the insurers' claims files relating to the accident.
In Germany the claims files of the insurers provide a valuable basis for accident research, as they contain extensive documentation which is compiled when claims are settled and is systematically expanded during retrospective examination by the Institute's engineers and medical experts.
In most cases an insurance file contains the accident sequence on the basis of the police report, as well as the expert's opinion on damage to the vehicle and the hospital report on injuries to the persons involved. In the case of serious accidents these data are supplemented by reconstructions of the accident sequence and an indication of the speeds.

Compared with collecting data at the scene of the accident, a significant advantage for the work can be recognized here, since nearly every information is available in one file and only has to be coded.
The disadvantage is in the delay between when the accident occurred and the evaluation, as before all the documents have come together in the file, about one year has passed. A further delay may result if some claims have still not been settled and the file is still in the hands of the court, especially in the case of serious accidents.

These disadvantages - on the one hand, in the case of retrospective accident research the delay in time and, on the other, in on-scene analysis the problem of combining all data sources - can, under certain circumstances, be eliminated in the foreseeable future if it turns out to be possible to harmonize the activities of the German insurers with the new efforts to extend the inquiry into the accident at the scene of the accident.
This approach to an interdisciplinary accident research could eliminate, at a stroke, the problems that will become more and more complex in the future.

In summary, if accident research should solve the more and more complicated question of traffic safety in future, there is no alternative to a multi-phased collection of accident data.

The limitations of data bases

The second step, after collecting the data, is to examine the plausibility of the data.
It is no secret that mistakes are made when information is transferred - firstly, when assessing, for example, a detail of the accident, and, secondly, by typing errors.

In most data bases these cases cannot be corrected, as it is no longer possible to access the original information.

In the case of the Institute for vehicle safety in Munich it is possible to specifically access the file once again and thus to integrate the missing information.

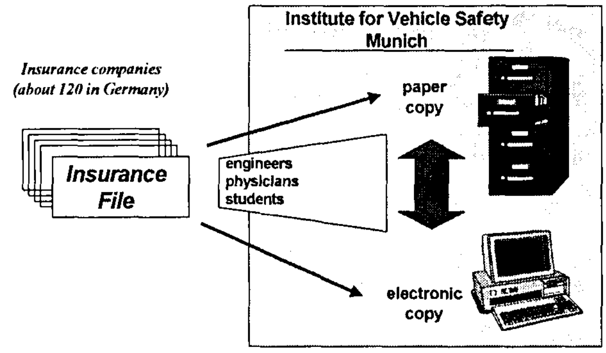
Institute for Vehicle Safety Munich
Insurance companies (about 120 in Germany)
Insurance File
engineers
physicians
students
paper copy
electronic copy

Fig. 2: data acquisition

But in the case of the new problems which crop up, for example, during the evaluation this kind of "redundant" data base has also proved successful. In this case the information can be specifically accessed a second time by looking into the physical file and the data base can be expanded.
This direct access to the records - also, for example, to copy special photos - is an important advantage of the independent accident research of the German Insurers.

In cases in which data from outside data sources are worked on, for example in the case of the official collection of accident data or of data bases that have been purchased, the user is faced with a series of numbers which supplies him with information in coded form. But it will never be possible to reconstruct whether the number of a data field really corresponds to the information about the accident.

Previous accident research of the Institute for Vehicle Safety

Beginning in 1969, there followed in 1974, 1980 and the last time in 1990 large scale analyses /1,2,3,4/ which founded the basis for the accident research of the Institute for Vehicle Safety, formerly known as "Büro für Kfz-Technik" in Munich.

The latest generation of this kind of data (VS90) contains 15,000 car/car accidents as well as 1,000 single-car accidents. The full report is available on request at the Institute for Vehicle Safety.

Apart from these large quantities of data, which on account of the information density are necessarily limited, in recent years special data bases have been built up which contain fewer accidents but more data.

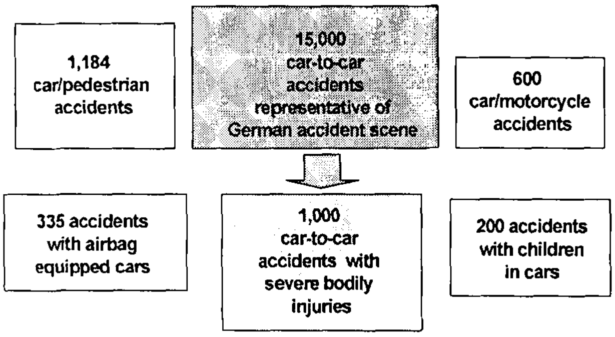
1,184 car/pedestrian accidents
15,000 car-to-car accidents representative of German accident scene
600 car/motorcycle accidents
335 accidents with airbag equipped cars
1,000 car-to-car accidents with severe bodily injuries
200 accidents with children in cars

Fig. 3: Data bases of the Institute of Vehicle Safety

Examples of this are 600 motorcycle to car accidents, 1184 car/pedestrian accidents, datasets of accidents in which injury severities exceeded MAIS 3, data about accidents involving children in cars/5,6,7/ and special accidents in which an airbag /8,9,10/ was deployed.

Accident studies of the risk behavior of young drivers or accidents on highways with fatalities also belong to this group of special evaluations /11/.
Medical information, too, for example, on the problems of cervical vertebral column (CVC) injuries, are stored by doctors in the Institute's data bases and are available for evaluation/12/.
All the studies mentioned are listed in the literature.

DATA BASES AND THE RESULTS

Car/car collisions - VS90

With the so-called "Vehicle Safety 90 - VS90" a representative data base of 15.000 accidents has been created. In this "basic analysis", about 100 accident parameters are defined and differentiated according to the factors "man, vehicle, environment"

The accidents considered reflected the accident scene in Germany of all accidents in which bodily injury occurred in one of the vehicles involved.

One of the basic results was the clear distinction of the collision-type as a function of accident severity

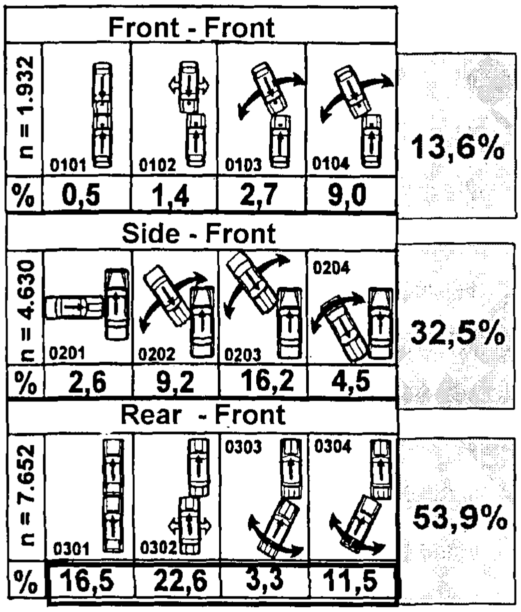
Front - Front
n = 1.932
0101
0102
0103
0104
%
0,5
1,4
2,7
9,0
13,6%
Side - Front
n = 4.630
0201
0202
0203
0204
%
2,6
9,2
16,2
4,5
32,5%
Rear - Front
n = 7.652
0301
0302
0303
0304
%
16,5
22,6
3,3
11,5
53,9%

Fig. 4: The distribution of collision-types in the German accident scene

Frontal collisions with 13.6% and side-collisions with 32.5% are also part of the material but as the entire accident scene is characterized by minor accidents, it is the rear-end collisions which are directly connected with the problems of CVC injuries, that dominate in this representative material.

CVC Injuries

In these accidents, injuries to the back of the neck (cervical vertebral column) are the most common type of injury. However, the importance of injuries to the cervical vertebral column is still underestimated, regarding their high social and economic costs.

Approximately 2 billion marks are spent in Germany every year on these injuries. Up to now there are no uniform strategies, either in the diagnosis or treatment of injuries to the cervical vertebral column.
In 12,200 of the total of 15,000 car/car accidents studied (81%), at least one of the occupants complained about CVC pain. CVC distortions (AIS 1) even if they are only declared therefore represent a mass problem in dealing with insurance claims.

61.3% of CVC injuries can be traced to a rear-end collision. The injuries to more than 1,000 people were examined in detail [13]. This analysis showed that the occupants of lightweight cars (up to 800 kg) were more likely to incur CVC injuries than the occupants of medium-heavy cars. Women in general suffered more frequently (79%) from minor CVC injuries than did men (55%) The biomechanical explanation for this tendency is that women have a weaker CVC muscular system.

The headrest is still a "forgotten safety system". Field research and observations have shown that in at least 40% of cars, and possibly as many as 73%, the headrest is incorrectly positioned, i.e. too low. The same conclusion was reached by a basic research project at the Allianz Zentrum für Technik [14].

Accidents with severe injuries – "RESIKO"

After the large scale study VS90 the files where again analyzed but now with the aim of concentrating on accidents in which severe or fatal injuries occurred. In addition, the data-density was raised to about three times more data fields than in the VS90.
This new study was called RE.SI.KO /15/ which stands for the German title "Retrospektive Sicherheitsanalyse von Pkw-Kollisionen mit Schwerverletzten"
In these accidents the shortcomings of passive safety systems are shown up. The limits of feasible safety have not yet been reached, only it will become more and more difficult to find improvements which are not already covered by existing safety elements such as the belt and the airbag.
RE.SI.KO. is aimed at resolving this problem and indicating further possibilities of improving safety.

Angled Front Collisions and Side-Collisions

As the severity of accidents increases, the collision types shift from the rear-end collision to the front and, in particular, to the angled front and side collision.

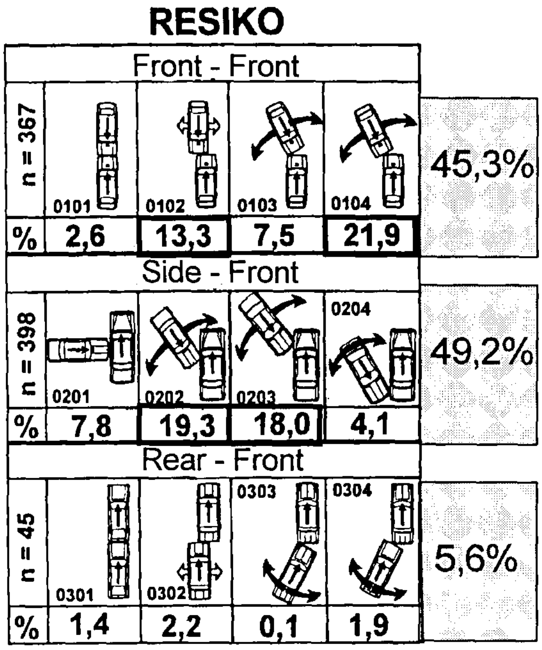

Fig. 5: Collision types in accidents with severe and fatal injuries

Frontal collisions with complete or partial overlap are the subject of constant discussion because of NCAP, EU-NCAP and, in Germany, the numerous crashtests of the motoring magazines.

In addition, our work in the future must address the problems of the angled frontal accidents as well as side collisions.

Angled frontal collisions indicate points of impact for the occupants, e.g. the A-pillar, which at the present time possess only limited passive safety elements. For this reason research activities are being focused on further work to optimize the side airbag or the interaction of frontal and side airbags and as well the design of padding in the vehicle's interior.

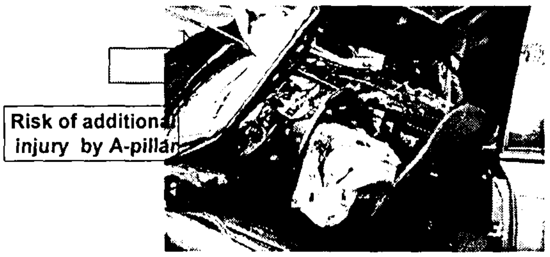

Fig. 6: Risk in angled front-collisions

Side collisions are a further main area on which to concentrate efforts to develop further passive safety.
This also becomes clear by means of a sophisticated presentation of the evaluation of accident severity according to the fundamental accident situations. It can then be seen that single car accidents and car-to-car accidents are mainly responsible for the high proportion of fatal injuries in cars.

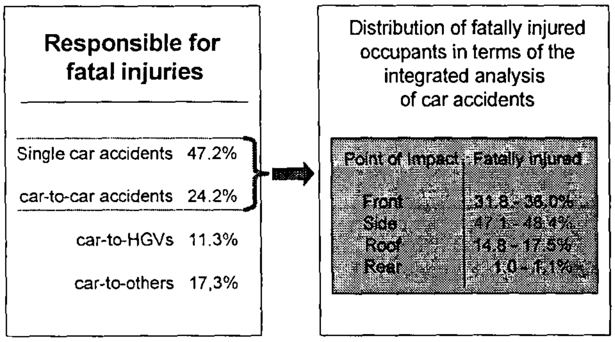

Responsible for fatal injuries

Single car accidents	47.2%
car-to-car accidents	24.2%
car-to-HGVs	11.3%
car-to-others	17,3%

Distribution of fatally injured occupants in terms of the integrated analysis of car accidents

Point of Impact	Fatally injured
Front	31.8 - 36.0%
Side	47.1 - 48.4%
Roof	14.8 - 17.5%
Rear	1.0 - 1.1%

Fig. 7: "Integrated Analysis of Car Accidents"

This so-called integrated evaluation is achieved by projecting the results of representative accident studies, based on a section of the overall accident database (e.g. car/car accidents), onto the overall national statistics.
The study also showed that it is not only sufficient to look at the impact on the driver's side but it is also necessary to concentrate on impact against the other side although sufficient safety space between the occupant and the opponent exists.

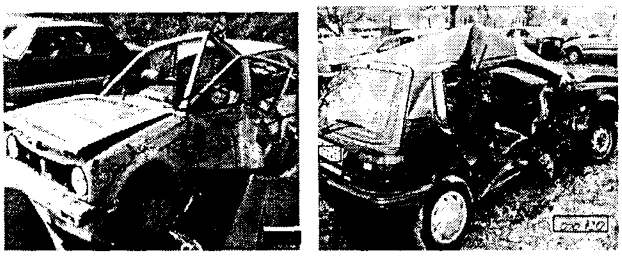

43% of all fatally injured drivers die due to an impact on the drivers side

As many as 17% of all killed drivers die due to an impact on the other side

Fig. 8: Side Collisions

The injury pattern of the occupant at the struck-side show that injuries to the thorax, with 12.1%, followed by head-injuries, with 8%, dominate the list of AIS 4+ injuries.
If looking at AIS 2+ injuries the injuries to the pelvis with 32.7%, are significant higher than in all other collision types.

At the non-struck-side the injuries concentrate on the head and thorax but also on neck injuries when only severe injuries are focused on.

Injuries to different body regions

The survey of the injury pattern was completed by an in-depth investigation of the different collision types and body regions. To clarify the difference between the frequency of injuries and the severity of injuries two samples where compared for each collision-type. One sample contained all AIS 2+ injuries the other all AIS 4+ injuries.

For all variations of collisions the head is still the most involved body region with 28.5%. The second position is represented by injuries to the thorax with 24.6%. As in this analysis all collision types are combined all other body regions like the lower arm (10.9%), pelvis (10.3%) show a relatively constant distribution.
This changes if the different collision types are focused.

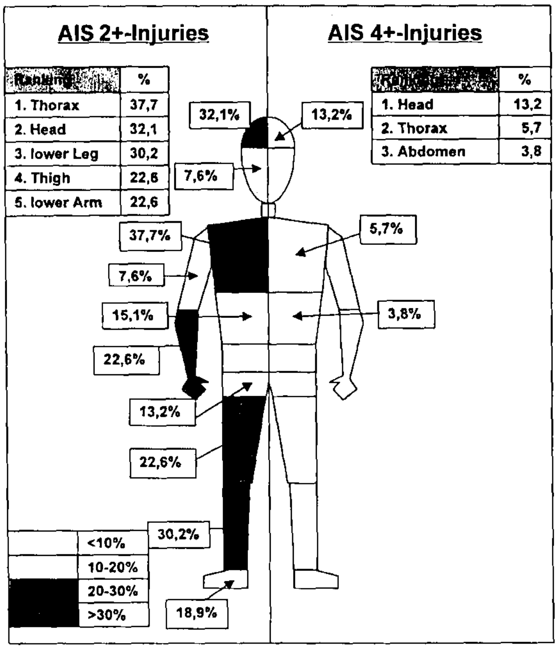

AIS 2+-Injuries

Ranking	%
1. Thorax	37,7
2. Head	32,1
3. lower Leg	30,2
4. Thigh	22,6
5. lower Arm	22,6

AIS 4+-Injuries

[illegible]	%
1. Head	13,2
2. Thorax	5,7
3. Abdomen	3,8

Fig.9: The distribution of injuries in frontal collisions with partial overlap

In frontal collisions with partial overlap it can be seen that nearly every body region has a higher risk than the average contribution.
As in these cases only occupants have been inspected who where belted and without an airbag the injury

contribution will change when accidents with airbags are included.

The following figure shows all frontal collisions. This result is taken from a special airbag investigation where the injuries of a certain accident severity is displayed once for drivers with belt and airbag and once for drivers who where belted only.

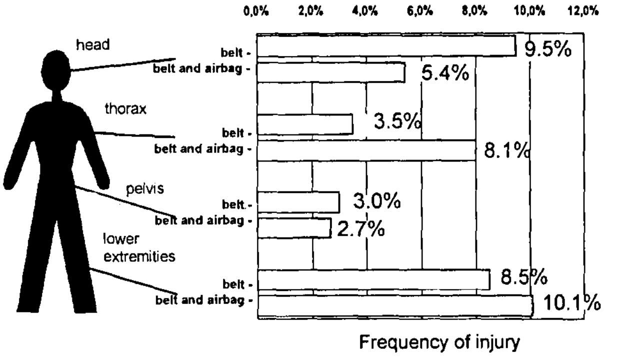

Fig. 10: Injury patterns for restrained drivers in frontal collisions of comparable accident severity

It clearly shows the reduction of injuries to the head but on the other hand an increase of injuries to the thorax. This increase of thorax injuries could be related to the higher age of the drivers in the airbag group but also to the lack of beltforce limiters.
The injuries to the lower extremities in this comparison become number one in ranking. This does not mean that the airbag has an influence on the frequency of these injuries but it shows that the injuries to the lower extremities become more obvious.

If the areas of the foot, lower leg and femur are combined there is a clear indication of a safety deficit. Optimizing the legroom and preventing the intrusion of parts of the engine into the passenger cell are two areas of research which hold out the promise of improvement.
An improved dummy design in the region of the lower extremities is necessary if the loading is to be researched realistically.

Injury costs

The RESIKO study also analyzed the injury costs depending on the type of collision. By means of the injury cost scale (ICS) it was possible to look at the average costs per body region.
The following results are calculated only for injured occupants. Calculations for killed persons have been incorporated.

For the entire accident material 1685 belted persons were inspected. The costs where calculated applying the definitions of the German "Berufsgenossenschaft" and set in relation to the appearance in all accidents and in special collision types.

One of the results concentrates on the injuries to the lower extremities. These injuries have been neglected in the past because of the dominance of the head injuries. Now, as the effect of the airbag is perceptible in decreasing head injuries, injuries to the lower extremities have to be studied greater in detail.
In figure 11 three different samples are compared. All accidents, all frontal collisions and only those frontal collisions where a partial overlap took place.
As it shows, the highest costs arise when the car is partially hit and that in those cases the costs double, especially for the lower extremities.

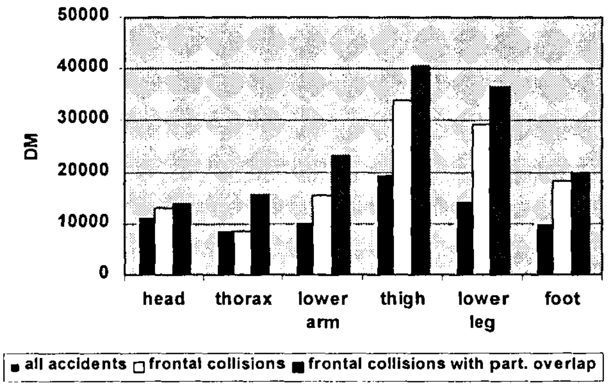

Fig. 11: Injury costs for different collision types

In future these injuries of the lower extremities will provide a lot of scientific potential to improve secondary safety in cars.

The problems of driving dynamics

Further results of the study of the accidents in which serious and fatal injuries occurred focus on problems of controlling the vehicle.
The material offers the possibility for analyzing both active and passive safety.
About 30% of all accidents between two cars resulting in fatalities take place at crossroads or junctions. The rest, about three-quarters of all fatal collisions, are the result of driver error on straight roads, in bends and when overtaking.

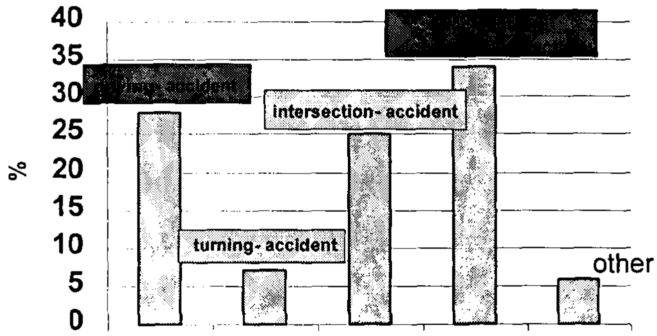

fig.12: Distribution of accident types in severe car-to-car collisions

The "driving accident", which is presented as the loss of control over the vehicle as a result of speeding in bends, faulty reactions by the driver and overestimating one's own driving ability, is ideally suitable as a field for developing new vehicle systems like driver assistance systems.

In Germany the development of such driving stabilization systems can be clearly observed.
Two findings can be derived from this.

Throughout the world there are no uniform tests to examine questions of active safety, and, the possibilities of improving active safety or driving dynamics like ABS, ESP and other driver assistance systems has to be intensively promoted. Activities have been started by the German VDA.

In accidents with serious bodily injury that have been studied this weak spot showed up quite clearly.
Besides the vehicle-specific improvements, however, the human being and the road also have to be included if accidents resulting from driving dynamics are to be overcome. Driver training, further instruction and appropriate ways of addressing driving errors have to be optimized.
Road instabilities, such as, for example, sunken road shoulders, are further parameters which, when a vehicle starts to swerve, counteract any rapid correction by the driver.
Before the potential of passive safety becomes effective, all the possibilities of active safety should be exhausted to avoid the accident in the first place.

CAR/MOTORCYCLE COLLISIONS

Besides the problems of car safety the data bases of the German automobile insurers also offers information on two wheeler accidents such as motorcycle and moped driver.
As an unprotected road-user the driver of a motorized two-wheel vehicle is exposed to higher risks. Numerous studies have dealt with this type of accident and the consequences.

The German Insurers' motorcycle data base first made it possible for a description of the accident according to the definition of the ISO standard 12232/13/ to be developed for this type of collision.

Collision type

The collision type, i.e. the way in which the two vehicles involved in the accident collide, constitutes the central starting point for assessing passive safety. It is precisely in the case of the motor cycle accident that so many trajectories arise depending on the collision type that a single examination can never describe all the possible injury patterns.
In the following comments the variations of collision types depending on the different ways they occurred and the consequences of the accidents for the motor cycle accident are described and evaluated.
The code prescribed in the ISO Standard is used as a definition of the collision type. The impact point on the accident opponent, on the motor cycle and the angle of the longitudinal axis result in a three-digit number.
These three digits can, when considered individually, also give the first indications of the critical points of the accident.
Fig. 13 shows the contact point on the accident opponent

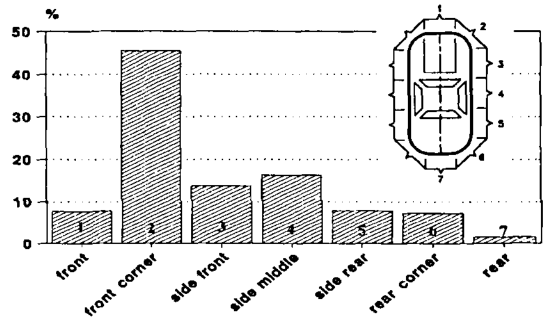

Fig. 13: Contact point on the car in collisions with motocycles

The front corner is obviously by far the most frequent point of contact on the car.

A distribution presented in the next Figure results from the contact points on the motor cycle.

As expected, the front of the motor cycle dominates with about 60%.

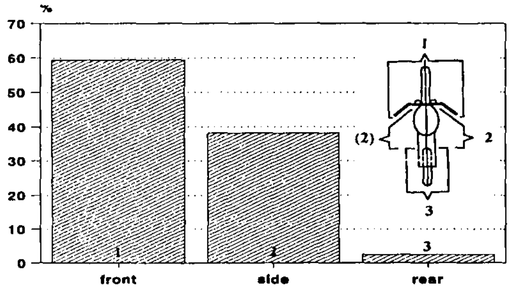

Fig.14: Contact point on the motor cycle in collisions with a car

Rear collisions, i.e. accidents in which the motor cycle is struck from behind, are rare.

The angle of the longitudinal axis of the vehicles involved is laid down as the third feature of the collision type. The distribution of the individual angle areas is shown in Fig. 15.

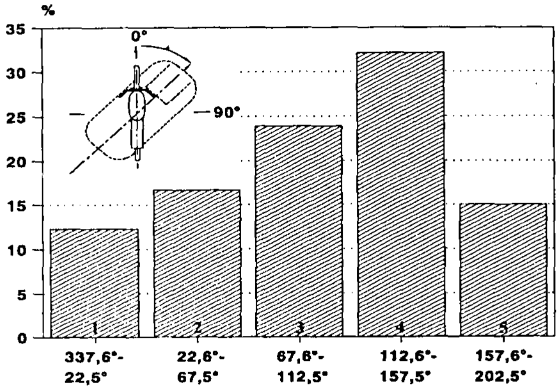

Fig. 15: Angles of the longitudinal axes to one another in car/motorcycle collisions

The opposing angled impact and the roughly perpendicular, about 90°-collision can be observed most frequently in the accidents.

Accident avoidance

What is new in this area is an analysis of the accidents in which a collision occurred between a car and a motorcycle, and only those cases were considered in which the motorcyclist was not responsible for the accident.

If the motorcyclist exceeds the critical speed in a bend or disregards the right of way, then this is an obvious error. It is quite different if the collision seems to take the motorcyclist by surprise. Unfortunately the proportion of these accidents is very high in Germany. Two-thirds of all collisions with a car fall into this group.

500 accidents of this kind were therefore stored in a new data base, and indications of how such accidents can, under certain circumstances, be recognized in advance and avoided were sought.

Cars ignoring the right of way at intersections was the most frequent accident type, namely 42%. This is followed by a car turning into a side street, motor cycle is overtaking and turning round by car.

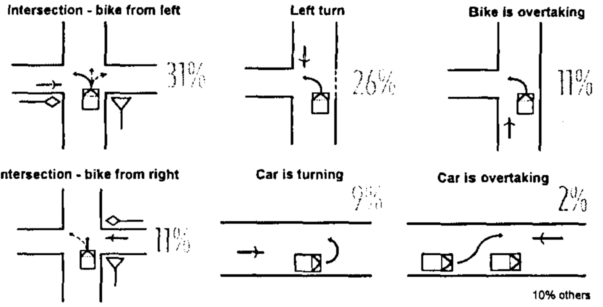

Fig 16: Accident types in collisions where the motorcycle driver was not guilty

For these main areas in the accident scene three rules of conduct were set up the aim of which is to make the motorcyclist sensitive to accident-prone situations.

Firstly, it is important not to take one's own right of way for granted. If under certain circumstances one risks a bump in the car, a motorcyclist suffers a more or less serious injury in almost all accidents. So the first rule is to distrust one's own right of way in unclear situations.

It is not always easy to recognize a one-track vehicle, i.e. there is a tendency to overlook a motorcyclist or in many cases his speed is wrongly estimated. He should therefore not simply assume that he has been noticed. Especially in situations in which car drivers do not react to an approaching motorcyclist such aids as the horn can attract attention.

This leads to the third rule, namely the motorcyclist should react in good time as soon as he has realized that the situation is unclear. In many cases it was observed that the motorcyclist had enough time to reduce his speed or to make himself noticed. But at a certain point it is too late, and the accident sequence can no longer be averted.

The findings of this motorcycle study were published in a brochure last year in cooperation with the Institute for Motorcycle Safety, and so far about 20,000 copies have been distributed. In addition, driving schools and private persons can order a video[1] on this subject.

CAR/PEDESTRIAN COLLISIONS

A data base on pedestrian accidents was completed in the spring of 1998. It comprises 1,185 collisions between a car and a pedestrian. Trifling accidents were left out, and only those accidents were entered in which the pedestrian at least required in-patient hospital treatment. Directly comparable data from official statistics are not available for these accidents.

This data base was created in two stages. After 348 accidents, the data was sifted, and then, after completion, compared with the entire database.
The background to this method of proceeding was to check the statistical stability from a certain number of cases beginning after about 350 accidents.
The data were collected at random and presented in the following table of the most important circumstances surrounding the accidents. The deviation of the individual collections is visible. Some parameters show good agreement. In the case of some information about, for example, the involvement of alcohol, the error span is 4% in total.

	348 cases %	1185 cases %	Diff.	%
Accident location				
Built-up areas	89,9	88,9	1,00	1,11
Crossing	25,3	20,1	5,20	20,55
Junction	17,5	21,6	-4,10	-23,43
Straight road	39,9	38,3	1,60	4,01
Weather				
Rain	21,8	20,9	0,90	4,13
Clear	49,2	46,8	2,40	4,88
Daylight	57,0	55,0	2,00	3,51
Traffic regulation				
none	56,3	53,3	3,00	5,33
Pedestrian crossing	20,8	20,1	0,70	3,37
Causes of accident - car				
speeding	18,3	18,4	-0,10	-0,55
Causes of accident - pedestrian				
Alcohol	14,2	10,1	4,10	28,87

Fig17.: Comparison of various datafields in different data sizes

Since, as already mentioned, there are no comparable groups of these accidents from the official statistics or from any study, the figures of the larger collection must be regarded as representative.
Case numbers of around 350 cases from this comparison cannot be considered adequately representative.

The results of the study will be published around the end of 1998. The following features can be identified in advance.

When an accident occurs between a car and a pedestrian it was the pedestrian's fault in one third of the cases.

The collision speeds of the cars are within a range in which improvements are still possible. In 58.4% of all pedestrian accidents the impact speed was below 30 kph. If the speeds are considered in cases in which the car driver was at fault, the proportion of this group was 65.6%.

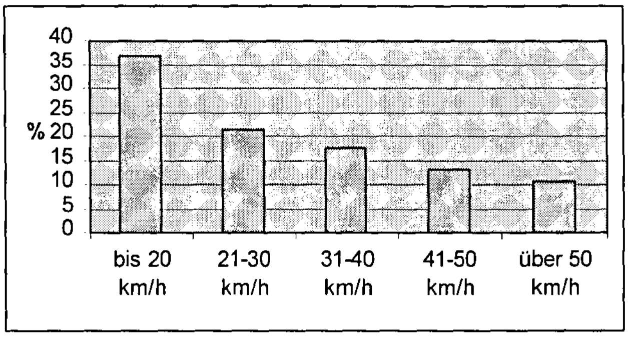

Fig. 18: Collision speed of the car in car-pedestrian accidents

With systematic measures it must be possible to optimize the vehicles front for this speed range.
This can be achieved by influencing the motion path and by avoiding hard vehicle parts in the area of contact.

The main body regions which are injured are the knee,/lower leg and head each with 19% occurrence. 50% of the killed pedestrians died due to a head injury.

Age groups at risk are children up to the age of 9 (18.8%) and pedestrians over 50 years old (49%).

In general, the problems of pedestrian accidents still provide an abundance of leads for further improving safety. The main areas of technical measures as well as training and educating adults have to be addressed.

---

[1] To order at GDV München

Summary - The aims of the German Insurers' accident research

The evaluation of data bases has become an indispensable part of accident research. But foreseeable developments show that gathering data is becoming more and more complicated, because, on the one hand, the quality of the data makes ever higher demands, but, on the other, it is becoming increasingly difficult to get at the data at all. Data protection and administrative problems are not diminishing.

The way out of this dilemma is to be found in the search for new ways of acquiring data.

Information only from insurance files will no longer meet the demand for more details of the accident.

On-the-spot accident research, in-depth analyses as well as closer cooperation with the police, fire brigade and authorities can help here.

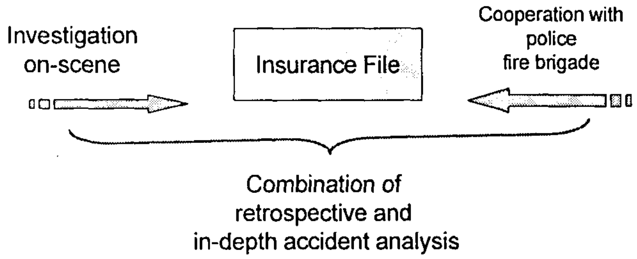
Investigation on-scene
Insurance File
Cooperation with police fire brigade
Combination of retrospective and in-depth accident analysis

Fig. 19: Future accident research

Thus the basis of the German Insurers can be realistically expanded and continued, and we face the challenges of the future with confidence.

REFERENCES

[1] HUK-Verband, "Innere Sicherheit im Auto", Hamburg, 1972

[2] HUK-Verband, "Fakten zu Unfallgeschehen und Fahrzeugsicherheit", Büro für Kfz-Technik, München, 1977

[3] K. Langwieder, "Retrospektive Erhebungen", HUK-Verband, Büro für Kfz-Technik (Nr. 8505), München, 1985

[4]. Verband der Schadenversicherer, „Vehicle Safety 90 - Analysis of Car Accidents, Foundations for Future Research Work“, Büro für Kfz-Technik, München, November 1994

[5] Th. Hummel, K. Langwieder, F. Finkbeiner, W. Hell, „Injury Risks, Misuse Rates and the Effect of Misuse Depending on the Kind of Child Restraints Systems“ Child Occupants Protection Conference, Orlando, Nov 1997

[6] K. Langwieder, W. Hell, R. Lowne, Cees G. Huijskens, „Side Impact to Children in Cars“ 15th International Technical Conference ESV, Melbourne, May 1996

[7] K. Langwieder, W. Hell, H. Willson, „Performance of Child Restraint Systems in Real-Life Lateral Collisions“ 40th STAPP Car Crash Conference, Albuquerque, Nov. 1996

[8] K. Langwieder, Th. Hummel, Chr. Müller, „Der Airbag im Reaunfall: Leistung und Schwächen – Erkenntnisse aus der Unfallforschung VDI-Tagung „Innovativer Insassenschutz im Pkw“, Berlin Okt. 1997

[9] K.Langwieder, „Airbags in Pkw – Weiter Optimierungsbedarf unter Kosten und Nutzenaspekten. Symposioum Autotechnik und Autoversicherung, Köln 1997

[10] K. Langwieder, Th. Hummel, Chr. Müller, „Experience with Airbag-Equipped Cars in Real-Life Accidents in Germany 15th International Technical Conference ESV, Melbourne May 1996

[11] K.Langwieder, „Junge Fahrer im Straßenverkehr – Risikoanalyse und Vorschläge zur Unfallprävention“, Mitgliederversammlung der Bundesvereinigung der Fahrlehrerverbände e.V. Juni 1995

[12] K. Langwieder, W. Hell, „Neck Injuries in Car Accidents – Causes, Problems and Solutions“ International Conference Active and Passive Safety, Capri 1996

[13] H. Münker, K. Langwieder, E. Chen, W. Hell, „HWS-Beschleunigungsverletzungen – eine Analyse von 15.000 Pkw/Pkw-Kollisionen“ NEUROORTHOPÄDIE, Bd. 6, Springer Verlag, Berlin

[14] C., Deutscher “Bewegungsablauf von Fahrzeuginsassen beim Heckaufprall“ Dissertation TU München 1993

[15] Institut für Fahrzeugsicherheit - RE.SI.KO. Gesamtverband der Deutschen Versicherungswirtschaft 1998 (will be published in July 98)

AN OVERALL EVALUATION OF UKDS MOTORCYCLIST LEG PROTECTORS BASED ON ISO 13232

Nicholas M. Rogers
International Motorcycle Manufacturers Association
Switzerland
John W. Zellner
Dynamic Research, Incorporated
United States
Paper Number 98-S10-O-13

ABSTRACT

The feasibility of devices intended to protect the legs of motorcyclists in impacts has been researched for three decades; this paper reviews the prior history and presents the latest results of an overall evaluation of a UK Draft Specification (UKDS) leg protector device, based on the standardized full scale test and simulation methods of ISO 13232. International Standard 13232 (1996) was developed and internationally approved for the purpose of providing common research methods for assessing the feasibility of protective devices which might be fitted to motorcycles and which are intended to reduce injuries to riders resulting from car impacts. A prototype UKDS device designed by the UK Transport Research Laboratory in 1990 was evaluated by means of 14 full scale crash tests with an instrumented MATD dummy; and 200 computer simulations representing 501 Los Angeles and Hannover accidents. The simulations were calibrated in detail against 32 instrumented laboratory tests and the 14 full scale tests. Results in terms of standardized injury analysis and risk/benefit analysis across the tests and simulated accident sample are presented, and conclusions and recommendations are discussed.

INTRODUCTION

Research on the feasibility of rider crash protection devices which might be fitted to motorcycles has occurred during the last 30 years in Great Britain, Japan, Germany and the United States. In general, this research has involved industry, government and private organizations; a variety of test methods, as reviewed by Rogers in Ref 1; and different rider protection strategies, for example those described by Sporner in Ref 2.

One example of such research during the 1980's was the leg protector work of the Transport and Road Research Laboratory (TRRL, now TRL) in the United Kingdom, culminating in 1987 in a proposed national and (later) international Draft Specification (UKDS, Ref 3) for motorcyclist leg protectors. Following publication of the UKDS, several leg protector designs intended to conform to it were evaluated in full scale tests by TRL, and by the motorcycle industry (Refs 4 to 6). One leg protector design was independently evaluated by TRL and by the industry, using different test methods (Ref 6); and this resulted in large differences in measurements and conclusions. Table 1 compares some of the different test methods used during this period of research.

In 1991, an International Leg Protector Seminar (Ref 7), and recommendation of experts in the crash protection field, led to the conclusion that an internationally accepted motorcyclist crash dummy and research methodology were the necessary next steps, before further objective and meaningful research could continue in the rider protection field.

In 1992, work on an International Standard on motorcycle crash research methodology was begun, and in 1996 this was finally approved as ISO 13232. The motorcycle industry then re-evaluated the UKDS leg protector device designed by TRL, this time using the ISO Standard, and this is the main topic of this paper.

This paper continues with a brief review of the history of leg protector research; the concurrent development of research methodologies, culminating in ISO 13232; application of the ISO 13232 to an overall evaluation of an example UKDS leg protector device; and the conclusions and recommendations reached regarding this type of device.

BACKGROUND

History of leg protector research

Since 1969, a number of industry and other organizations worldwide have studied a wide variety of motorcyclist leg protection devices with the aim of reducing injuries to riders during collisions.

A summary of leg protector research through 1990 is given by Rogers in Ref 1. This is described subsequently and summarized in Table 2.

Conventional crash bars - Early research in the late 1960s and early 1970s investigated commercially available accessory bars - generally loops of approximately 25 mm diameter steel tubes projecting to the side of the motorcycle. Bothwell, et al, (Ref 8) under contract to the US National Highway Traffic Safety Administration (NHTSA), found that these were too weak to protect legs during collisions and capsize situations.

Bothwell, et al (Ref 9) subsequently tested "revised heavy duty crash bars", constructed from 50 mm diameter tubes, which were able to endure 30 mi/h angled collisions. These retained leg space; however leg impacts to the bars were found to be potentially injurious.

Uto (Ref 10) of the Japan Automobile Manufacturers Association (JAMA) investigated "side protection devices", constructed of large diameter steel tubes with reinforcing braces. Using breakable dummy bones, it was found that: lower leg fractures could be reduced; however, upper leg fractures were changed from bending fractures to twisting fractures; and there was a greater tendency for the dummy to be ejected head first toward the opposing vehicle.

Livers (Ref 11) and Bartol, et al (Ref 12) under contract to the US NHTSA tested an "Experimental Safety Motorcycle Structure", similar in concept to the revised heavy duty crash bars and the side protection devices. It was found that upper and lower leg forces were reduced, but chest and head accelerations were generally greater, indicating an overall increase in potentially fatal injuries.

Modified reinforced leg protectors - Bothwell (Ref 13) next investigated a "reinforced leg shield fairing" which had thick knee pads covering the tubular structure. In an angled collision, the knee of the dummy impacted the knee pad, inducing a dummy somersaulting motion. This resulted in a large amount of dummy neck flexion, and lowered the head trajectory so that the head impacted the side of the opposing vehicle, again increasing the potential for fatal injury.

Chinn, et al (Ref 14) of TRL investigated a "hard leg protector", which was apparently the same concept as Bothwell's "reinforced leg shield fairing" (RLSF). Although few details were presented, the test results indicated decreased yaw motion during angled collisions with fixed barriers, and maintenance of leg space, similar to the RLSF. However, forward pitching of the dummy torso and lowering of the dummy head were observed, as with the RLSF.

Energy Absorbing Leg Protectors - Bartol, et al (Ref 12) also investigated a "crash bar with energy absorbing bucket seat", which - although intended to reduce head accelerations - in fact did not reduce dummy injuries in a measurable way.

Chinn, et al (Ref 14), based on work in his doctoral dissertation, investigated a "soft leg protector", and reported that this reduced the dummy's forward head velocity.

Tadokoro, et al (Ref 15) of JAMA proposed and tested a "crushable leg protector" (CLP) intended 1) to reduce motorcycle impact acceleration and thereby to reduce the ejection tendency of the dummy; and 2) to maintain a minimum amount of leg space (since excessive leg space was considered a cause of ejection). Tests indicated that this device reduced leg fractures, but dummy ejection and the associated increased head velocities were not solved by the CLP.

Energy Absorbing Leg Retention Leg Protectors - A further leg protector concept described by Chinn, et al (Refs 16 and 17) resembled a 1980 UK patent of Bothwell involving: external and internal (knee) energy absorbing regions; a rigid structure supporting these regions, and a fairing enclosure. Although Bothwell no longer considered this concept valid, Chinn of TRL continued work on it, adding a "leg lateral retention element" and a "breakaway" mount intended to prevent leg trap.

The TRL published research on leg protectors differed from other research in the UK, US and Japan, in that at all stages, the evolving concept showed promise (eg, Refs 16, 17, 18), and the negative effects reported by other researchers were not observed. The motorcycle industry considers that the most likely reason for this is the test methodology used by TRL in its research, which is summarized later.

In 1986, in view of the major divergence in results between TRL and other researchers, the motorcycle industry proposed to the United Nations Expert Group for General Vehicle Safety Provisions (UN/ECE/TRANS/WP29/GRSG) that improvement of test methodologies was the next logical step for finding clearer answers to rider leg protection.

UK Draft Specification (UKDS)

In July, 1987, despite the continuing differences in research results, the United Kingdom Department of Transport unexpectedly published a national Draft Specification for motorcycle leg protectors for comment. The UKDS was based on the TRRL work and was proposed as a regulation applicable to all motorcycles and mopeds. The UKDS involved:

- A primary impact element;
- A rigid support element;
- A knee protector element;
- Leg lateral retention;
- Detachment of the rigid support at high impact energies (optional in the original draft; mandatory in the revised drafts);
- Smooth outer contour (during and after impact).

These elements had specific geometric and mechanical requirements to be verified by laboratory testing.

Industry response to UKDS - The motorcycle industry responded to the publication of the UKDS in several ways, including:

- Two commissioned reports from independent experts (Refs 19, 20), which discussed the limitations of the TRL methodology, including the crushable "honeycomb" dummy leg, which could not accurately predict leg fractures;
- Preliminary full scale tests of a UKDS prototype device (Ref 21), which found that the device resulted in lower leg fracture and increased upper leg damage in all three impact configurations examined; and other harmful effects, including increased rider ejection, torso pitch and head impact with the car and road;
- A meeting with the UK Parliamentary Under Secretary of State for Roads and Traffic in 1988, at which it was agreed that: the UK Department of Transport would not proceed without consulting the motorcycle industry; industry would accelerate refinement of its evaluation methodology with a view to a fuller evaluation of the UKDS in tests during 1989; and TRL and industry experts would hold technical meetings to discuss their differing results;
- A presentation and discussion at the United Nations UN/ECE/TRANS/WP29/GRSG in May 1988, at which the delegates agreed to postpone discussion of a Draft Recommendation (based on the UKDS), until industry had completed further research;
- A large, in-depth series of crash tests of UKDS leg protectors in 1989 by the industry (Ref 5). These tests were the most comprehensive to date in terms of: the types of motorcycles and cars used; the leg protector designs and UKDS categories; the type of impact configurations considered; and the use of state-of-the-art test methodologies, including a new motorcycle impact dummy and performance indices. Test results indicated that UKDS leg protection devices could increase both leg and head injuries, as well as overall injury severity;
- A series of detailed technical meetings and discussions between TRL , the UK Department of Transport and the motorcycle industry. This resulted in nine main points of technical agreement between TRL and the industry (Ref 22). It also resulted in an agreement for TRL and the industry to independently evaluate a TRL-built UKDS leg protector for a medium sized Kawasaki GPZ 500 (subsequently further described);
- An International Leg Protector Seminar (Ref 7) at Chantilly in 1991, for the purpose of clarifying the technical issues, resulted in the recommendation of experts in the crash protection field that an internationally accepted motorcyclist crash dummy and research methodology were necessary first steps, before further objective and meaningful research could be pursued.

Development of Research Methodology

A wide range of test and evaluation methodologies have been used in the field of motorcyclist leg protection research, and, for example, Sakamoto (Ref 23) reviews the history of leg injury measurement methods. These included:

- Leg acceleration measurement;

- Leg lateral load measurement;

- Frangible (ie, breakable) surrogate leg bones;

- Leg "lateral impact energy" estimation, via crushable aluminum honeycomb material;

- Combinations of load measurement and frangible leg bones.

In addition, various crash dummies had been used in such research, as described by Zellner, et al (Ref 24), including:

- An early anthropomorphic manikin;

- Alderson CG-50 dummy and parachutist dummies;

- 50th percentile male anthropomorphic dummy;

- Modified Ito 3DGM-AM50-70 standing dummy;

- OPAT 50th percentile male manikin;

- Hybrid III/ Hybrid III combined standing dummies;

- A motorcyclist MATD-1 dummy (Ref 25).

In general, these dummies had different geometric, mass, stiffness and damping characteristics and corresponding impact responses; different levels of biofidelity; as well as different means for evaluating leg and other injuries. As a result, the same test done with different dummies would fundamentally produce different results.

A similar large diversity existed with regard to:

- Electronic and photo optic measurements;

- Injury indices;

- Full scale impact test procedures including the impact configurations used;

- Test documentation procedures.

Development of ISO 13232 - Recognizing the need for common tests and evaluation methods, the United Nations Expert Group for General Vehicle Safety Provisions (UN/ECE/TRANS/WP29/GRSG) decided in March 1992, at the suggestion of the International Motorcycle Manufacturers Association (IMMA) and in view of the Chantilly seminar recommendations, to ask the International Organization for Standardization (ISO), to establish a common research methodology for motorcycle crash testing.

GRSG's parent committee, UN Working Party 29, approved the plan but asked that the standard be completed before the end of 1995, which meant that a complete draft would be needed by Spring 1994.

In September 1992, the motorcycle subcommittee of ISO (ISO/TC22/SC22) established a new working group, WG22, to deal with "motorcycle research impact test procedures".

Six working group meetings were held between November 1992 and April 1994 involving some 25 experts and observers from the United Kingdom, Germany, France, the Netherlands, Belgium, Italy, the United States of America, Japan, Canada, and China, with input from both the motorcycle industry worldwide and technical experts in the crash research field (Ref 26). As official originator of the proposed ISO standard, IMMA provided to WG22 an initial working draft (WD), based on methods developed and used by the motorcycle industry in preceding years. In the process of preparing more detailed and complete drafts, WG22 based its work on the use of existing technology, consensus procedures, and data indicating method feasibility. The Standard was therefore a codification of methods which, for the most part, were available and in use. In addition, throughout the drafting process, liaison was maintained with the corresponding ISO car subcommittees.

In Summer 1994, a committee draft (CD) was balloted and approved within SC22. This was followed by balloting of a Draft International Standard (DIS); and final approval of the DIS by the ISO National Member Bodies in March 1996. ISO 13232 was finally approved and published in December 1996.

Review of ISO 13232 provisions - ISO 13232 consists of 8 interacting and mutually dependent parts:

- Part 1: Definitions
- Part 2: Definition of impact conditions in relation to accident data
- Part 3: Motorcyclist dummy
- Part 4: Measurements
- Part 5: Injury indices and risk/benefit analysis
- Part 6: Full scale impact test procedures

- Part 7: Computer simulation procedures
- Part 8: Test and simulation documentation

Application of these 8 parts enables:

- Quantitative measurement of the effect of the device on injury indices, for each body region, and summed across all body regions;
- A full scale test evaluation of the effects of a proposed device, based on seven pairs of full scale impact tests (ie, each pair comprising a motorcycle with and without the device fitted); and
- An overall evaluation of the predicted effects of the proposed device, across a sample of the accident population, based on a calibrated computer simulation, and 200 pairs of simulated impacts (with and without the device fitted).

A more detailed description of the provisions and rationale is given in Ref 26, and of the ISO motorcyclist dummy in Ref 24. In addition, specific rationale for the provisions is included in the Standard (Ref 32).

SUMMARY OF LATEST TESTS AND SIMULATIONS DONE

Beginning in 1994, IMMA conducted an overall evaluation of a UKDS leg protector prototype, in accordance with the test and analysis methods of ISO 13232 (based initially on the CD version and then subsequent versions). These tests and results are described in further detail in Ref 27. This involved the following test aspects:

UKDS leg protector - Photographs of the UKDS leg protector as designed and fitted to the test motorcycle by TRL are given in Figs 1 and 2. Table 3 describes the leg protector, and laboratory test data for it are described in Ref 6.

Motorcycle - The test motorcycle (MC) was a Kawasaki GPZ 500 with specifications given in Table 4.

Opposing Vehicle - The opposing vehicle was a production Toyota Corolla 4 door saloon, Japan domestic model, model year 1988 to 1990, inclusive, as specified in ISO 13232-6. Specifications are summarized in Table 5. Photographs of the opposing vehicle are given in Figs 3 and 4.

Impact configurations - The impact configurations (IC's) for the full scale tests were the seven IC's required by ISO 13232 for a full scale test evaluation of a proposed device, and illustrated in Fig 5, namely:

- IC1 : broadside
- IC2 : angled car front
- IC3 : T-bone, moving/moving
- IC4 : angled car side, similar direction
- IC5: angled car side, opposing direction
- IC6 : offset frontal
- IC7 : T-bone, stationary car

Summary of Test Results

Across the seven impact configurations tested and during the entire impact sequence (except as noted), and based on the analysis methods specified in ISO 13232-5, fitment of leg protectors resulted in the following changes:

- Head maximum GAMBIT (Generalized Acceleration Model for Brain Injury Trauma, Ref 32):
  - increased in 5 out of 7 cases;
  - decreased in 2 out of 7 cases;
- Head HIC (Head Injury Criterion, Ref 32):
  - increased in 4 out of 7 cases;
  - decreased in 3 out of 7 cases;
- Head AIS (Abbreviated Injury Scale, Ref 32):
  - increased in 3 out of 7 cases;
  - remained the same in 3 out of 7 cases;
  - decreased in 1 out of 7 cases;
- Risk of life threatening head injury:
  - increased in 1 out of 7 cases;
  - remained the same in 4 out of 7 cases;
  - decreased in 2 out of 7 cases;
- Neck shear injury index:
  - increased in 4 out of 7 cases;
  - decreased in 3 out of 7 cases;
- Neck tension injury index:
  - increased in 4 out of 7 cases;
  - decreased in 3 out of 7 cases;
- Neck compression injury index:
  - increased in 5 out of 7 cases;
  - decreased in 2 out of 7 cases;

- Neck flexion injury index:
  - increased in 3 out of 7 cases;
  - decreased in 4 out of 7 cases;
- Neck extension injury index:
  - increased in 2 out of 7 cases;
  - decreased in 5 out of 7 cases;
- Neck torsion injury index:
  - increased in 4 out of 7 cases;
  - decreased in 3 out of 7 cases;
- Chest AIS was zero in all cases;
- Abdomen AIS was zero in all cases;
- Femur AIS=3 fractures:
  - increased in 1 out of 7 cases;
  - remained the same in 5 out of 7 cases;
  - decreased in 1 out of 7 cases;
- There were no knee AIS=2 or 3 dislocations in any of the tests;
- Tibia AIS=2 fractures:
  - remained the same in 5 out of 7 cases;
  - decreased in 2 out of 7 cases;
- There were no tibia AIS=3 fractures in any of the tests;
- Helmet maximum vertical difference in trajectory (compared to the baseline trajectory)during the primary impact period was:
  - lower in 6 out of 7 cases;
  - undefined in 1 out of 7 cases;
- Percentage change in helmet velocity, at first helmet/OV contact was:
  - positive in 1 out of 7 cases;
  - negative in 4 out of 7 cases;
  - undefined in 2 cases;
- Permanent partial incapacity index:
  - increased in 1 out of 7 cases;
  - remained the same in 5 out of 7 cases;
  - decreased in 1 out of 7 cases;
- Probability of fatality:
  - increased in 4 out of 7 cases;
  - remained the same in 1 out of 7 cases;
  - decreased in 2 out of 7 cases.

Note that some of the indicated body region changes were at less than injurious levels, whilst others were at injurious levels, and this important difference should be considered when evaluating these results. ISO 13232 takes this into account by requiring the "normalized injury cost" - which includes changes for all body regions and injury severity levels - to be evaluated. In this regard, the:

-Normalized injury cost (NIC):
  - increased in 4 out of 7 cases;
  - remained the same in 1 out of 7 cases;
  - decreased in 2 out of 7 cases.

In the case of the neck, ISO 13232 does not yet quantify probable injury severities (as it does for other body regions), and the neck is not included in the normalized injury cost. However, it was observed in the test data that, of the six neck injury indices, the neck compression injury index tended to have the largest values in these tests (ie, be the closest to the levels for potential serious injury indicated in ISO 13232-5). Fitment of leg protectors increased the neck compression injury index in 5 out of 7 cases.

After taking into account the frequency of occurrence of each of the seven impact configurations, as listed in ISO 13232-2, the overall normalized injury cost summed across the seven configurations increased by 315%, as a result of fitment of UKDS leg protectors.

Discussion of Cause/Effect Relationships

The high speed films, electronic data and helmet trajectory and velocity data were examined in order to identify the causes of the leg protector harmful effects in the two cases in which such effects were most pronounced: the stationary T-bone (IC7) and angled car front (IC2) configurations.

In the stationary T-bone test, with the baseline motorcycle, the helmet contacted the top of the car with a head acceleration of 112 g and no head injury. With the leg protector motorcycle, the helmet trajectory was 123 mm (4.8 inches) lower than with the baseline motorcycle, and the helmet impacted the edge of the roof, resulting in a head acceleration of 193 g and an AIS 5 head injury. The lower helmet trajectory was the result of large restraint forces of the leg protector acting on the knees, which caused the torso to pitch downward about the hips.

In the angled car front configuration, a similar lower helmet trajectory (ie, 88 mm (3.5 inches) lower) occurred with leg protectors; and the resultant head acceleration was increased (from 42 g for baseline to 75 g with leg protectors) during primary impact. The leg protector acted to eliminate lower leg fracture by preventing initial car contact to the leg, thereby decreasing the tibia bending moment. However, impact of the left knee with the leg protector increased the femur compression force by 38 percent. More importantly, the femur forward bending moment was more than doubled by the leg protector, resulting in bending fracture of the femur. Examination of the high speed films and electronic data indicated that this was the result of the knee being forced into the deformable knee protection element, followed by an upward movement of the hip during the impact, resulting in very large forces and torques at the knee. This same "jamming" or "fixity" effect was observed in previous research (eg, Ref 5) and appears to be a fundamental deficiency of systems which concentrate all of the rider restraint forces on the knees, whilst the hip and upper body continue to move in other directions.

Computer Simulations and Results

Computer simulations were done involving the same UKDS leg protector device, motorcycle and opposing vehicle, in accordance with ISO 13232. This is described in further detail in Ref 28. The simulation preparation and analysis involved the following main steps:

- Modeling the leg protectors, motorcycle, dummy and opposing vehicle;
- Calibrating the models against instrumented laboratory and full scale impact tests;
- Using the calibrated model to simulate 200 motorcycle/car impact configurations - based on accidents in Los Angeles and Hannover described in ISO 13232 - with and without leg protectors;
- Analyzing the results for this larger sample of accidents in terms of injury benefits (ie, decreases of injuries resulting from fitment of the leg protectors); injury risks (ie, increases in injuries resulting from fitment of the leg protectors); and injury risk-to-benefit ratio.

Models of the leg protector, motorcycle, dummy and opposing vehicle were formulated in accordance with ISO 13232-7, and are summarized in Table 6. The models were implemented by means of the Articulated Total Body program (Ref 29).

Calibration of the models against 20 dynamic laboratory tests, 11 static laboratory tests and a motorcycle barrier test is described in Ref 28. The simulation data indicated close agreement with the test data.

The simulation was also calibrated and correlated with data from the 14 full scale impact tests previously described. This indicated that the level of the correlation between the simulations and the full scale tests was high, as follows:

- Head acceleration (g): $r^2 = 0.91$
- Percent correctly predicted:
  - Femur fractures/non fractures: 92.9%
  - Knee dislocations/non dislocations: 100.0%
  - Tibia dislocations/non dislocations: 92.9%

The calibrated simulation was then used to calculate dummy motions, forces and injuries in the 200 impact configurations - with and without leg protectors. As reported in Ref 28, the results indicated that the total injury risk (ie, total increase in injury cost resulting from leg protector fitment) *exceeded* the total injury benefit. The risk-to-benefit ratio was found to be 116%.

Further analysis described in Ref 28 indicated that this was the result of the increases in femur injuries (which are more costly) outweighing the decreases in tibia injuries, which occurred when leg protectors were fitted.

An injury risk-to-benefit ratio (or "harm"-to-benefit ratio) of 116% is also observed to be very much larger than corresponding ratios for, for example, car protective systems which are in use, such as seatbelts or head restraints. The latter are observed to have risk-to-benefit ratios in the range of 7 percent or less (eg, Refs 30, 31).

CONCLUSIONS AND RECOMMENDATIONS

The motorcycle industry has recently completed an overall evaluation of a UKDS leg protector device — designed and fitted by the UK's Transport Research Laboratory — using the test and analysis procedures specified in ISO 13232. The effects of leg protectors on rider injuries were assessed by means of seven pairs of full scale impact tests and 200 pairs of calibrated computer simulations.

As in previous research reported in 1988, 1989, 1991, 1994 and 1996, it was found that fitment of leg protectors resulted in a mixture of beneficial and harmful effects. In the full scale tests, upper and lower leg fractures were eliminated in the offset frontal configuration (which ISO 13232 indicates is the least frequently occurring among the seven standard impact configurations). However, fitment of UKDS leg protectors resulted in increased head injury severity in 3 out of 7 impact configurations; increased probability of fatality and normalized injury costs in 4 out of 7 impact configurations; and increased neck compression injury index in 5 out of 7 impact configurations. This was observed to be the result of forward and/or lateral torso pitch, caused by a robust restraint of the knee, by leg protectors.

With regard to injury cost, fitment of leg protectors increased the overall normalized injury cost of the seven full scale impact configurations specified by ISO 13232 by more than 300%.

Other harmful effects resulting from leg protector fitment include transfer of injury - from the lower leg to the upper leg - in the angled car front impact (the second most frequently occurring of the seven standard full scale impact configurations). This transfer of injury is a fundamental result of the way in which the knee is restrained, which applies large forces and torques sufficient to fracture the femur. Such femur fractures are more severe (and in some cases life threatening) than the lower leg fractures which leg protectors are intended to reduce.

Calibrated computer simulations of 200 pairs of impacts which occur in accidents - with and without leg protectors fitted - indicated that the total injury risks (ie, increases in injury costs resulting from leg protector fitment) exceeded the total injury benefits, with a risk-to-benefit ratio of 116%. This was observed to be much larger than risk-to-benefit ratios of 7% or less observed in car occupant protection systems, such as seatbelts or head restraints. The simulation results also indicated that leg protectors increased more costly upper leg injuries, whilst decreasing less costly lower leg injuries.

All of the foregoing results indicated that this concept of rider protection would produce a net harmful effect, which is undesirable and unacceptable in any device intended to improve safety. Based on these results and the previous research, this type of device should not be fitted to production motorcycles. For the same reasons, there appears to be no merit in the further development of this protection concept.

Research into the feasibility of other rider protection devices and concepts, and refinement of research methods, should continue.

ACKNOWLEDGMENT

The research reported herein was accomplished by the efforts of several organizations and individuals, including the members of IMMA, who supported and participated in the work; and members of the Japan Automobile Research Institute and Dynamic Research, Inc., who assisted in the conduct and analysis of the tests and simulations.

REFERENCES

1. Rogers, NM, "A Technical Evaluation of Motorcycle Leg Protectors," 13th International Technical Conference on Experimental Safety Vehicles, Paris, November 1991.

2. Sporner, A, Langwieder, K, Polauke, J, "Passive Safety for Motorcyclists - From Leg Protectors to the Airbag," Society of Automotive Engineers Paper 900756, February 1990.

3. Anon, Draft Specification: Leg Protection for Riders of Motorcycles, United Kingdom Department of Transport, 1987(Amended June 1988, February 1989).

4. Anon, TRRL Review of Research on Motorcycle Leg Protection - 1991, Transport and Road Research Laboratory, Crowthorne, United Kingdom, 1991.

5. Rogers, NM, "Further Crash Tests of Motorcycle Leg Protectors as Proposed in the UK Draft Specification," 13th International Technical Conference on Experimental Safety Vehicles, Paris, November 1991.

6. Rogers, NM, "Evaluation of TRL Designed Leg Protectors for a Medium Sport Motorcycle," 14th International Technical Conference on Enhanced Safety of Vehicles, Munich, May 1994.

7. Anon, Leg Protectors: Do They Work?, Proceedings of the International Seminar on Leg Protectors, at Chantilly, France, International Motorcycle Manufacturers Association, 1991.

8. Bothwell, PW, Knight, RE, Peterson, HC, Dynamics of Motorcycle Impact, Volume II, Motorcycle Crash Test Program, DOT-HS-5-01160, 1971.

9. Bothwell, PW, Peterson, HC, Dynamics of Motorcycle Impact, Volume II, Motorcycle Crash Test Program, DOT-HS-800-907, 1973.

10. Uto, T, Side Collision Test of Motorcycle Equipped with Side Protection Devices, Japan Automobile Manufacturers Association, 1975.

11. Livers, GD, An Analysis of Motorcycle Side Impact, DOT-HS-801-840, Final Report, 1976.

12. Bartol, JA, Livers, GD, Miennert, R, Near Term Safety Improvements for Motorcycles - Phase II, DOT-HS-801-653, 1975.

13. Bothwell, PW, Dynamics of Motorcycle Impact - Volume I, Motorcycle Crash Test Program, Interim Report, DOT-HS-126-3-632, 1975.

14. Chinn, BP, Macaulay, MA, "Leg Protection for Motorcycles," IRCOBI Conference on the Biomechanics of Impacts, 1984.

15. Tadokoro, H, Fukuda, S, Miyazaki, K, "A Study of Motorcycle Leg Protection," 10th International Technical Conference on Experimental Safety Vehicles, Oxford, May 1985.

16. Chinn, BP, Hopes, PD, Macaulay, MA, "Leg Protection for Riders of Motorcycles," 10th International Technical Conference on Experimental Safety Vehicles, Oxford, May 1985.

17. Chinn, BP, Hopes, PD, "Protecting Motorcyclists Legs," 11th International Technical Conference on Experimental Safety Vehicles, Washington, DC, May 1987.

18. Chinn, BP, Macaulay, MA, "Leg Protection for Motorcyclists," IRCOBI Conference on the Biomechanics of Impacts, 1986.

19. Anon, Comments on the UK Draft Specification for Leg Protection for Riders of Motorcycles, Dynamic Research Inc Technical Memorandum 88-2, Torrance California, January 1988.

20. Bothwell, PW, Bothwell, R, Motorcycle Leg Protectors - Response of the Motorcycle Association of Great Britain, Ltd to D.P. Legislative Proposals, Motorcycle Association of Great Britain, January 1988.

21. Sakamoto, S, Preliminary Evaluation of a Motorcycle Leg Protector Design as Proposed by the United Kingdom Department of Transport, Japan Automobile Manufacturers Association, June 1988.

22. Anon, Summary of Industry Position on Motorcycle Leg Protectors, International Motorcycle Manufacturers Association, Paris, 1990.

23. Sakamoto, S, "Research History of Motorcycle Leg Protection," Society of Automotive Engineers Paper 900755, February 1990.

24. Zellner, JW, Wiley, KD, Broen, NL, Newman JA, "A Standardized Motorcyclist Impact Dummy for Protective Device Research," 15th International Technical Conference on the Enhanced Safety of Vehicles, Melbourne, May 1996.

25. St-Laurent, A, Szabo, T, Shewchenko, N, Newman, J, "Design of a Motorcyclist Anthropometric Test Device," 12th International Technical Conference on Experimental Safety Vehicles, Goteborg, May 1989.

26. Van Driessche, H, "Development of an ISO Standard for Motorcycle Research Impact Test Procedures," 14th International Technical Conference on Enhanced Safety of Vehicles, Munich, May 1994. 1994.

27. Rogers, NM, "Application of ISO 13232 to Motorcyclist Protective Device Research," 15th International Technical Conference on the Enhanced Safety of Vehicles, Melbourne,.May 1996.

28. Kebschull, SA, Zellner, JW, Van Auken, M, "Injury Risk/Benefit Analysis of Motorcyclist Protective Devices Using Computer Simulation and ISO 13232," 16th International Technical Conference on the Enhanced Safety of Vehicles, Windsor, Ontario, June 1998.

29. Obergefell, LA, Fleck, JT, Kaleps, I, Gardner, TR, Articulated Total Body Model Enhancements, US Air Force AAMRL-TR-88-009, January 1988.

30. Malliaris, AC, Hitchcock, R, Hedlund, J, "A Search for Priorities in Crash Protection," Society of Automotive Engineers Paper 820242, 1982.

31. Huelke, DF, O'Day, J, "The Federal Motor Vehicle Safety Standards: Recommendations for Increased Occupant Safety," Fourth International Congress on Automotive Safety, July 1975.

32. Anon, International Standard ISO 13232: 1996(E), Motorcycles - Test and analysis procedures for research evaluation of rider crash protective devices fitted to motorcycles, Parts 1 to 8, International Standardization Organization, Geneva, December 1996.

Table 1
Comparison of Some of the Past Test Methods used in Leg Protector Research

Test Element	TRRL	IMMA
Dummy	Modified OPAT	Modified Hybrid III
Injury indicating dummy legs	Aluminum honeycomb on metal plates	Breakable composite bones
Dummy knees	1 axis	3 axis
Data acquisition system	External, via cable	Internal to dummy (to avoid motion distortion due to cable)
Dummy hand position	Taped to fuel tank	Grippable hands on handlebars
Opposing vehicle	GM Vauxhaul Ford Sierra various others	Toyota Crown Toyota Celica
Relative angle between motorcycle and car	various, at 30° increments	various, at 45° increments
Motorcycle wheels prior to release from trolley	Stationary	Rolling (for increased stability, accuracy, realism)

Table 2
Example Leg Protector Types
Examined Through 1987

Time Period	Proposed Device	Reference
1971	Accessor bars	8
1973	Revised heavy duty crash bars	9
1975	Side protection devices	10
1973-76	Experimental Safety Motorcycle (ESM) structure	11, 12
1975	Crash bar with energy absorbing bucket seat	11
1975-81	Reinforced leg shield fairing device	13
1984	Hard leg protector	14, 16
1984-87	Soft leg protector	14, 15, 16, 17
1985	Crushable leg protector	15

Table 3.
Leg Protector Description

Element		Material
PIE	External	Sheet metal
	Internal	Polyurethane
RSE		Sheet metal + solid bar with notch
KPE		Aluminum honeycomb

Table 4.
Specifications of Test Motorcycle

Size:	Medium
UKDS category:	3a
Manufacturer:	Kawasaki
Overall length:	2 125 mm
Overall width:	675 mm
Overall height:	1 165 mm
Weight - Motorcycle with LP:	189 kg (dry)

Table 5.
Specifications of Opposing Vehicle

Type:	Saloon
Manufacturer:	Toyota
Model:	Corolla
Model year:	1988 - 1990
Overall length:	4 200 mm
Overall width:	1 660 mm
Overall height:	1 340 mm
Weight:	1 100 kg ± 20 kg

Table 6.
General Description of Leg Protector, Motorcycle, Dummy, and Opposing Vehicle Models

Model	Number of :			
	Bodies	Joints	Ellipsoids	Planes
Leg protector (L + R)	2	2	4	10
Motorcycle	7	6	18	0
Dummy	30	29	28	0
Opposing Vehicle	7	6	26	4

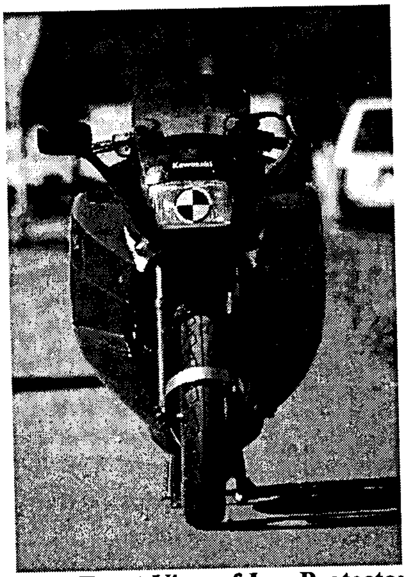

Figure 1. Front View of Leg Protector, Fitted to Test Motorcycle

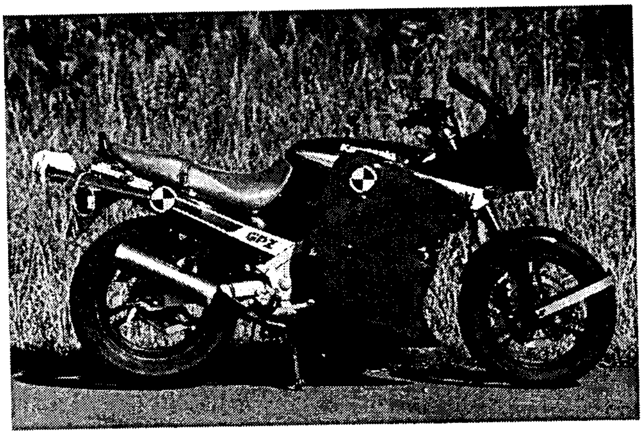

Figure 2. Side View of Leg Protector Fitted to Test Motorcycle

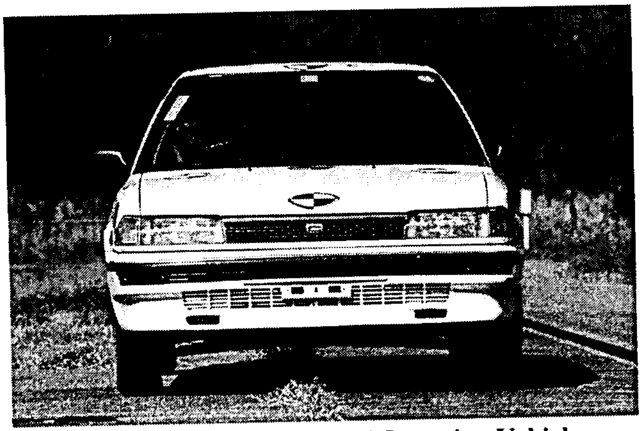

Figure 3. Front View of Opposing Vehicle

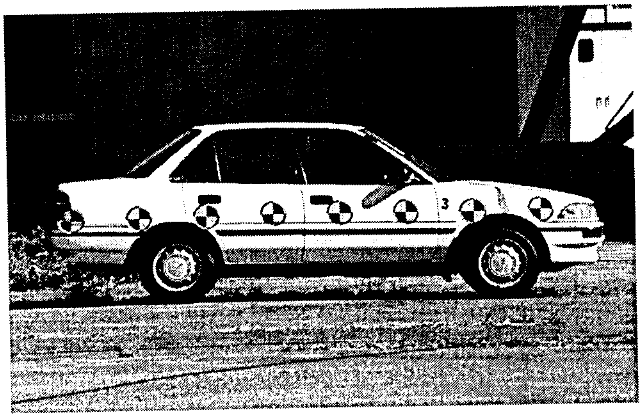

Figure 4. Side View of Opposing Vehicle

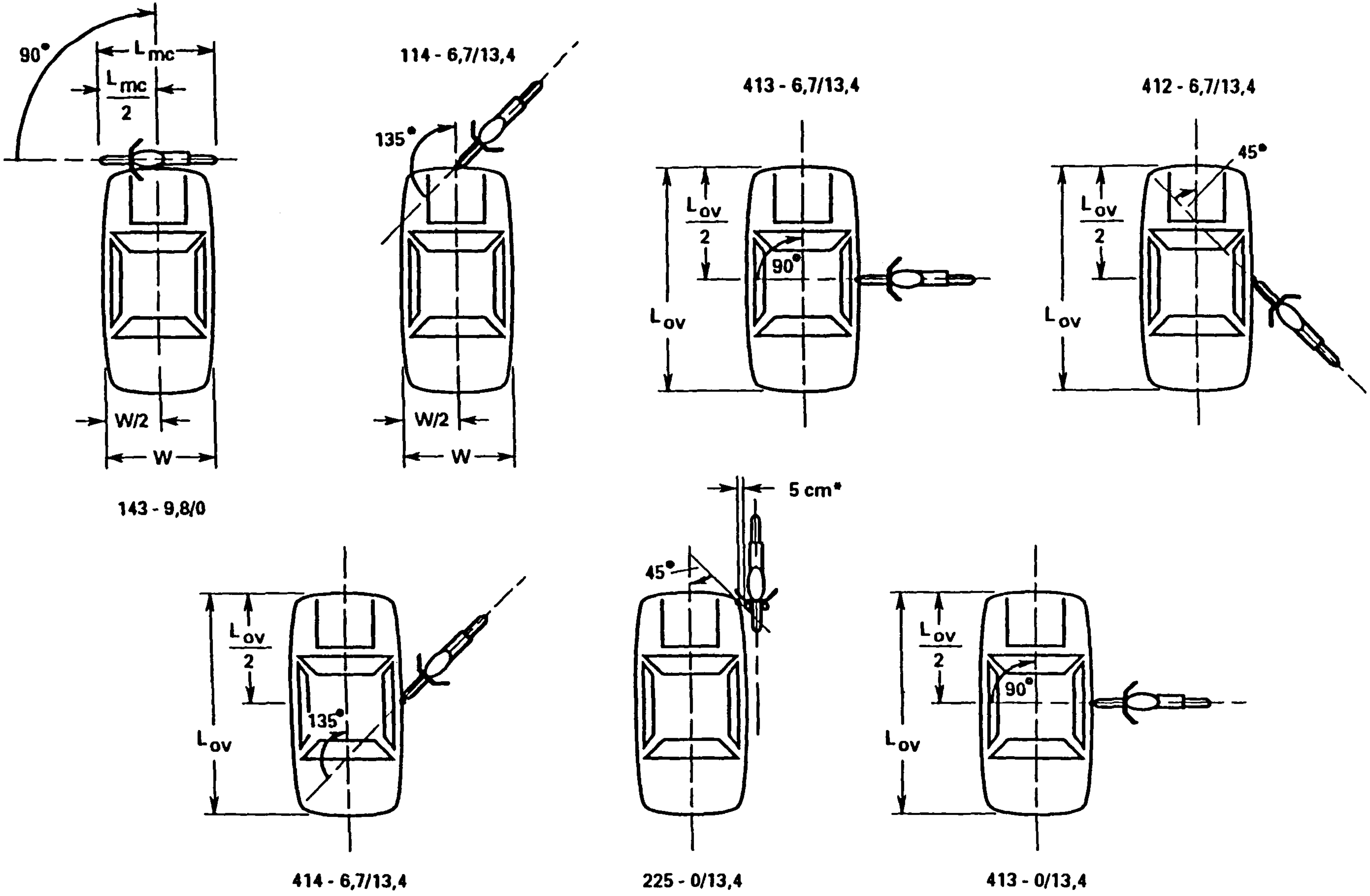
90°
L_{mc}
$\frac{L_{mc}}{2}$
W/2
W
143 - 9,8/0
114 - 6,7/13,4
135°
W/2
W
413 - 6,7/13,4
$\frac{L_{ov}}{2}$
L_{ov}
90°
412 - 6,7/13,4
45°
$\frac{L_{ov}}{2}$
L_{ov}
5 cm*
45°
$\frac{L_{ov}}{2}$
L_{ov}
135°
414 - 6,7/13,4
225 - 0/13,4
$\frac{L_{ov}}{2}$
L_{ov}
90°
413 - 0/13,4

* At first MC/OV contact

Figure 5. Target impact geometries at first MC/OV contact for seven full scale impact configurations.

EXPLORATORY STUDY OF AN AIRBAG CONCEPT FOR A LARGE TOURING MOTORCYCLE

Satoshi Iijima
Soichiro Hosono
Atsuo Ota
Takenori Yamamoto
Honda R&D Co., Ltd
Japan
Paper Number 98-S10-O-14

ABSTRACT

Honda began its research on motorcycle rider protection in the 1960's and since then has been active, along with other researchers in this field. One type of protection system - a motorcycle mounted airbag system - has been researched in various countries since the 1970's. Recently, Honda has focused its motorcycle airbag research on one particular concept aimed at: reducing rider ejection speed; minimizing sensitivity to motorcycle impact angle, and motorcycle or opposing vehicle shapes; application to motorcycles which have a mass much larger than the rider mass; realizing a practicable airbag size and location ; and consideration of both the running and impact motions of motorcycles.

Prototype devices intended to meet these objectives were refined by testing, and a prototype airbag system for a GL 1500 motorcycle was designed including special bag shape, inflator, cover and sensor system. The prototype system was evaluated using full scale impact tests and computer simulation procedures based on ISO 13232, across a range of car impact configuration, with a 50th percentile male MATD dummy. Results indicate some prototype airbag potential benefits and adverse effects. Factors not yet considered include: other sizes and positions of riders; small, medium and step-through motorcycles; other objects and opposing vehicles types; reliability and environmental exposure on motorcycles; and other factors.

INTRODUCTION

Since its founding 50 years ago, Honda has been actively researching new motorcycles and other vehicles, with safety as an important consideration.

Honda began its research on motorcycle rider protection in the 1960's (Ref 1), and since then has been active, including joint work with others in this field.

Recently, Honda focused on an airbag system as one candidate for a rider protection device, and conducted a basic study on the concept of motorcycle airbags . As a result, it was recognized that conceiving one airbag concept that would be functional for all motorcycle types would be extremely difficult. Subsequently, efforts were focused on an airbag system for a specific, large and heavy motorcycle - the GL 1500 - which was seen as an apparent airbag candidate because of its size, weight and configuration. This paper describes an exploratory study of an airbag system for one specific, large motorcycle - the GL 1500 - and in general this study is not considered to be applicable to other sizes, types or models of motorcycle.

A prototype airbag system for the GL 1500 was designed based on knowledge derived from basic studies. Research of the system components was done by means of static inflation tests, sled tests, and other preliminary tests and analysis. The sensor system aspects were considered by means of various running tests and preliminary crash tests. As a result of these basic studies, a prototype airbag system was fabricated.

As a next step a series of full scale crash tests and computer simulations was done, using the prototype airbag motorcycle and based on the full scale test and analysis procedures defined in ISO 13232. Additional full scale impact configurations were also added. Computer simulations across a wider range of motorcycle/car impacts was also done, also according to ISO 13232. This paper presents the results of these exploratory tests and simulations.

To evaluate the overall feasibility of an airbag system, many items should be studied, as described in Fig 1. The content of this paper would be only one portion of an overall feasibility study for a motorcycle airbag system for one type of motorcycle.

Riders

- Single
- Double
- Small
- Medium
- Large
- Out-of-position

Motorcycles

- Configuration, type
- Size
- Weight

Impacts

Opposing objects:

- Car types
- Other vehicles types
- Fixed objects
- Road (fall down)
- Speeds
- Angles
- Contact points

Non-Impacts

Resistance to:

- Road bumps, vibration
- Environmental exposure
- Maintenance/repair
- Use and misuse
- Theft
- Tampering
- Disposal

Consequences of Unintended Deployment:

Figure 1. Topics for consideration in motorcycle airbag feasibility research.

CONCEPT OF THE PROTOTYPE AIRBAG IN HONDA'S EXPLORATORY STUDY

An examination of statistics for motorcycle fatal accidents in Japan (Ref 2) indicate that (Fig 2):

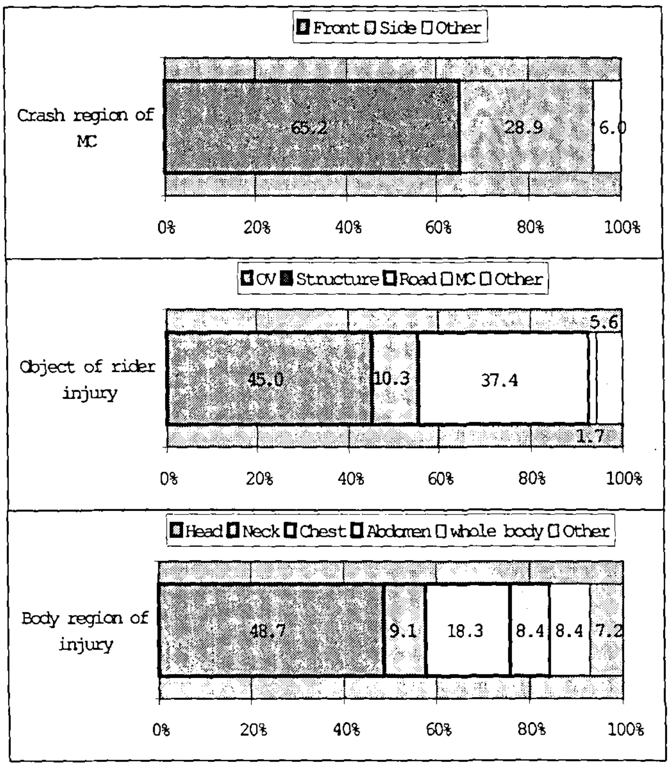

Figure 2. Data describing motorcycle fatal accidents in Japan (Ref 2)

- they are mostly (ie, about 65 percent) motorcycle frontal impacts;
- most rider impacts (ie, about 90 percent) are against objects other than the motorcycle;
- the most frequently and severely injured body region lies in the upper half of the body.

Based on this data, a typical fatal accident scenario involves: impact at the front of the motorcycle, the rider separating from the motorcycle, hitting an opposing vehicle or ground and receiving a fatal injury to the upper half of the body.

From this information, a concept involving non-ejection or energy reduction of the rider was conceived as one concept for rider protection. Subsequently, Honda has studied a motorcycle mounted airbag as one implementation of this concept.

Additional factors were also considered, including the following, based on past test experience and accident data:

- the airbag position and horizontal forces being supported by the motorcycle itself (eg, even in front-to-front impacts with passenger cars the airbag should function without the airbag needing to be in

contact with the opposing vehicle);
- maintaining airbag effectiveness as much as possible during various motorcycle crash motions, especially the yaw, pitch and roll motions which tend to occur during motorcycle crashes;
- not increasing the risk of fatality in higher speed impacts.

Test Motorcycle for Installation of the Prototype System

The GL 1500 motorcycle shown in Fig 3 was selected for this exploratory study. This motorcycle is the largest made by Honda and was selected for several reasons. In view of some of the potential technical challenges related to installation of airbags on motorcycles, selection of the GL 1500 tended to minimize these because of:

- its internal (under the seat) fuel tank, which allows an airbag module to be installed in the space in front of the rider, without affecting the fuel system;
- its upright riding position, which increases the space available in front of the rider for the airbag to inflate;
- relatively low center of gravity, large mass (370 kg with airbag system) and large inertia results in less motorcycle pitching, rolling, yawing or somersaulting during impact;
- its large full fairing may also contribute to reduced motorcycle pitching during impact.

Specifications of the GL 1500 motorcycle are given in Appendix 1.

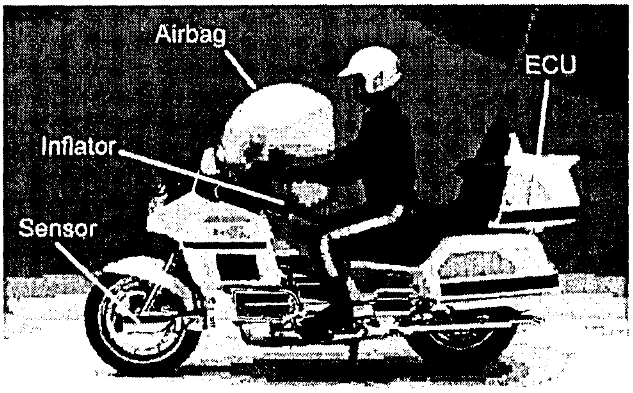

Figure 3. Prototype airbag system installed on the GL 1500 motorcycle.

Bag specifications and installation of the airbag on the motorcycle

The prototype airbag specifications indicated in Table 1 were set based on a series of basic tests, considering the goals of rider non-ejection, energy absorption and acceleration-reducing performance. Figures 4 and 5 illustrate the overall shape of the airbag and the internal tethers, which control bag shape.

Table 1.
Prototype Airbag Specifications

Volume:	120 liter (net, inflated)
Height x width x length:	630mm x 500mm x 615mm
Vent holes:	2 x 50mm diameter
Tethers: - Connecting rear and bottom sides - Connecting right and left sides	3; forms a concave "V" bag shape; see Fig 4, 5 1; to reduce bag/handlebar contact
Bag mounting:	1) to module box 2) to motorcycle frame beneath the seat, via 2 connecting belts

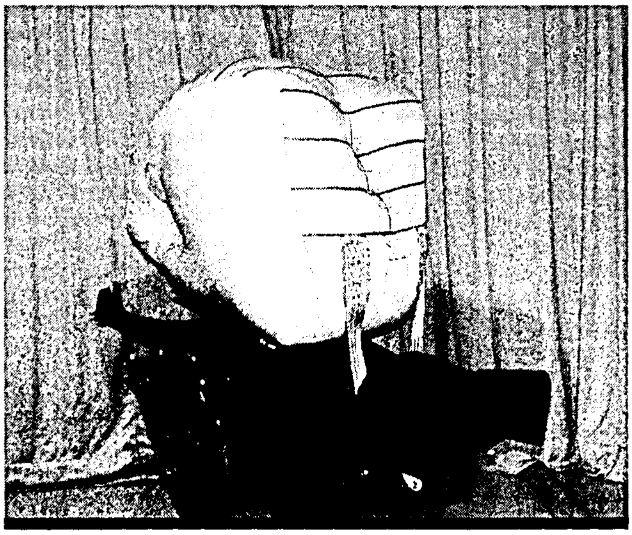

Figure 4. Photo showing shape of prototype airbag.

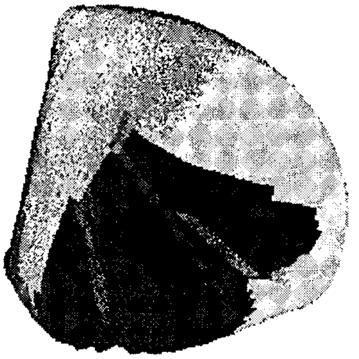

Figure 5. Schematic of airbag internal tethers.

The airbag specifications have taken into account the following considerations and test experience:

- Excessively small (or no) vent holes can result in undesirable dummy motions, such as rearward rebound or large lifting or sidewards deflection; excessively large vent holes result in less restraint and energy absorption;
- The "V" shaped planform assists in stabilizing the bag against small amounts of rider position offset or changes in motorcycle motion;
- The bag is subjected to large shear forces as the rider moves forward and over the bag. The connecting belts attached to the motorcycle beneath its seat act to resist these forces. This also allows more design freedom by not requiring the module position (ie, the main anchoring point) to be at the rearmost portion of the bag.

Inflator, cover and module box

Appropriate inflator characteristics were chosen mainly from static inflation tests. Figure 6 presents results of the static inflation tests. The horizontal axis shows time, and the vertical axis shows the inflated area as measured from a side view high speed camera. The results indicate that a maximum pressure of 300 kPa produced insufficient bag expansion; 350 kPa required excessive time to reach maximum expansion; and 450 kPa produced rapid and well-damped bag expansion.

Considerations were also given to the design of a module cover which would open at the beginning of airbag inflation; bag folding method; and specifications for the module box for containing the inflator and folded bag. Specifications for these are described in Table 2.

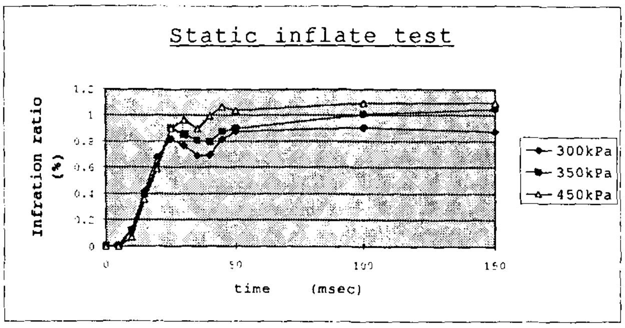

Figure 6. Time histories of inflated area (side view) as a function of maximum inflation pressure

Table 2.
Specifications of Airbag Module

Inflator:	Pyrotechic; passenger car type; 450 KPa maximum pressure; see Fig 7.
Module cover:	Thermo Plastic Elastomer (TPE) with shearing portion; passenger car type; aluminum plate hinge to allow full opening of cover; see Fig 8.
Bag folding pattern:	See Fig 9.
Module box:	Container for bag and inflator, with cover attachment; see Fig 10.
Airbag mounting:	See Fig 11.

These specifications include the following considerations and test experience factors:

- the inflation direction of the bag was desired to be forward and upward, not towards the rider;
- minimal attention was given to styling and detailed design aspects, at this exploratory stage.

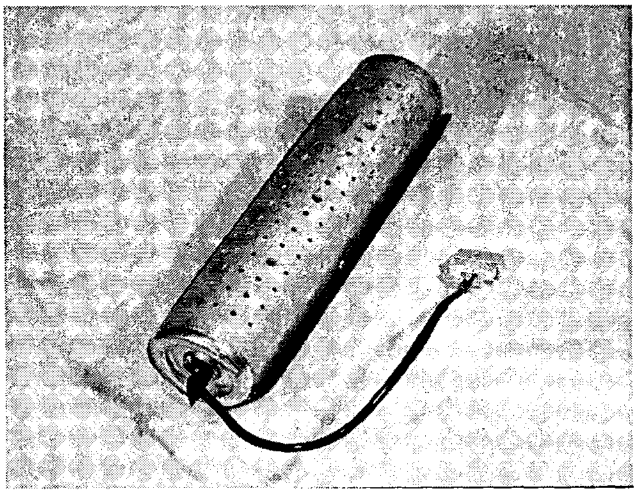
Figure 7. Photo of inflator unit

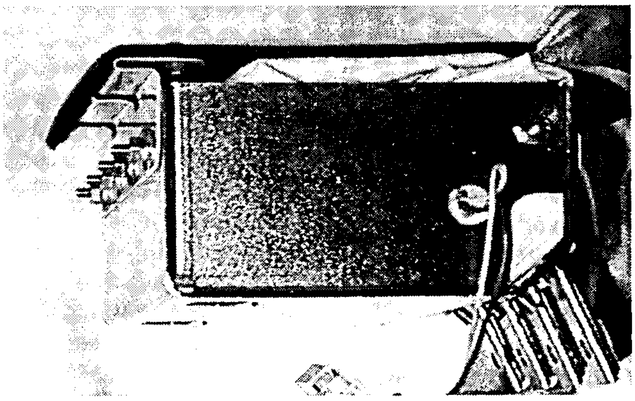
Figure 8. Photo of airbag module cover hinge.

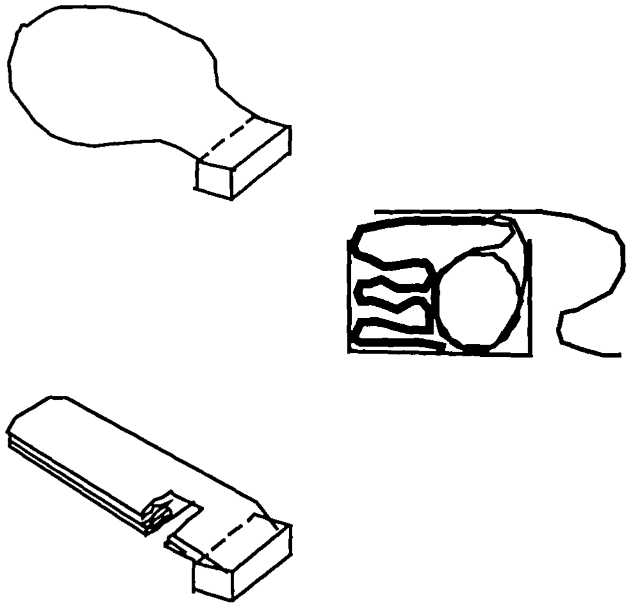
Figure 9. Folding pattern of bag.

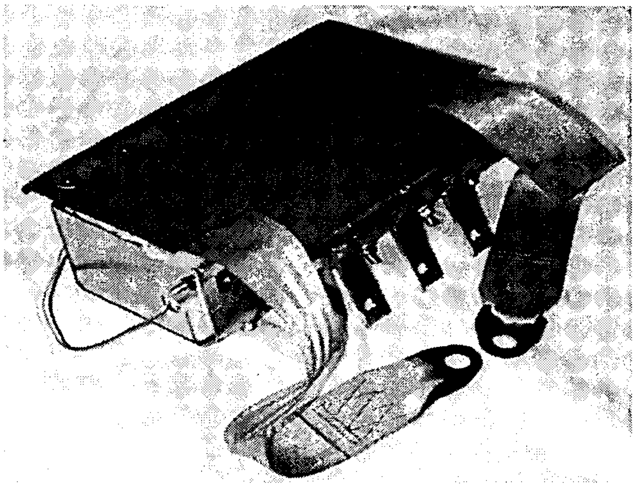
Figure 10. Module assembly.

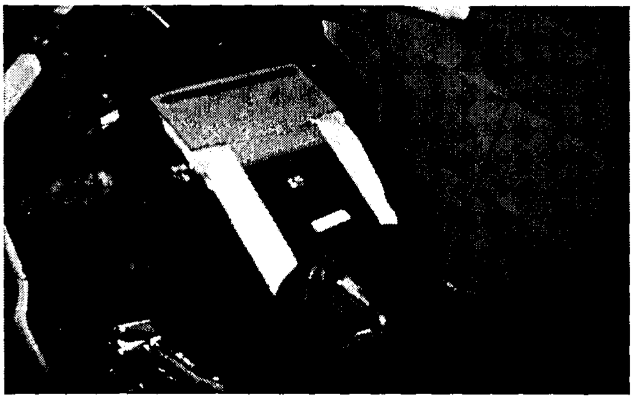
Figure 11. Airbag mounting on GL 1500.

Sensor System

The sensor system needs to quickly distinguish crash conditions from normal running conditions; and to send a signal to activate the inflator. Several sensing concepts (eg, crash acceleration; bending of the front fork; crush of the frontal structure; etc) were considered and from those, use of the acceleration at the front fork near the axle seemed to be the most useful. To implement this concept, several crash tests and running tests were done, and the specifications in Table 3 were derived.

The sensor system specifications were based on the following considerations:

- Accelerations at and to the rear of the steering head can be used to distinguish "normal" and "crash" conditions, but these signals contain delays which can be too long;

Table 3.
Sensor System Specifications.

Sensors:	Accelerometers; at front axle; perpendicular to front fork and front axle; see App 2, Fig 2-1.
Sensing units:	Left and right sides of front fork; signals calculated separately; earlier signal triggers the system; see App 2, Fig 2-2.
ECU:	See App 2, Fig 2-2.
Calculation method:	If sensed acceleration (rearward/downward) exceeds 9g, start "velocity change" calculation; if "velocity change" exceeds 2.4 m/s, send trigger signal; if "velocity change" does not exceed 2.4 m/s and acceleration becomes less than 9g stop "velocity change" calculation, and reset to zero; see Figs 12, 13.

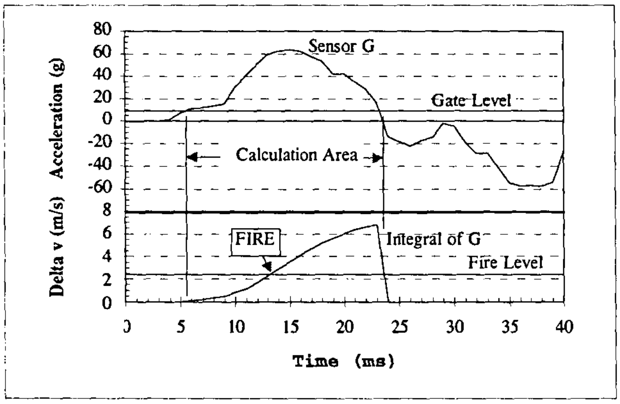

Figure 12. Acceleration and velocity change, crash test example

- two sensors near the front axle were used in the prototype system, however one sensor at the center of the front axle may be adequate for functional purposes.

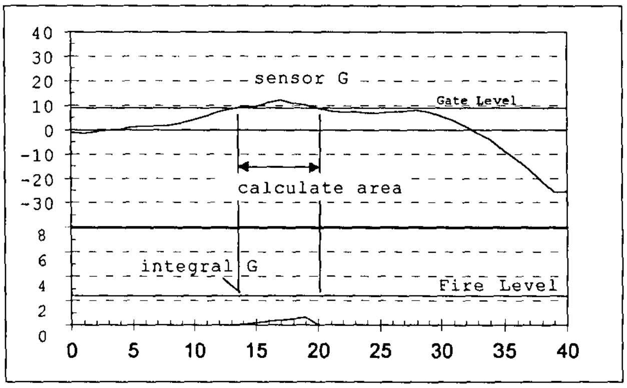

Figure 13. Acceleration and velocity change, running example

Figure 14 presents the change of velocity calculated with the method described in Table 3 using signals sensed during example running conditions and crash conditions. The running conditions included bumpy road running, and running over a curb. Many of the running conditions resulted in zero velocity change, since the acceleration did not reach the level which initiates calculation of the velocity change. A velocity change of 0.6 m/s was the maximum reached in these running tests, however, further research is needed to determine whether larger values may occur in other running situations.

In contrast, velocity changes in crash conditions were usually 2.9 m/s or greater in a 20 mi/h impact to a passenger car (eg, a Corolla), and 5.7 m/s or greater in a 30 mi/h impact. Therefore a velocity change of 2.4 m/s, initiated by a 9 g acceleration excedance, was able to distinguish running conditions from crash conditions, in this exploratory stage of research. The time required to make this judgment is approximately 10 to 21 ms, based upon the data in Fig 14.

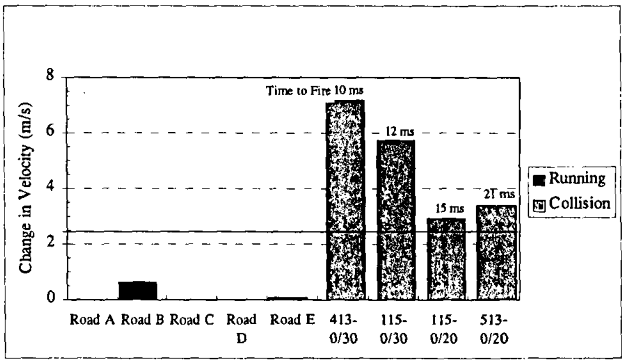

Figure 14. Velocity changes recorded in normal running and crash conditions, and judgment time required.

FULL SCALE CRASH TEST CONDUCTED WITH THE PROTOTYPE AIRBAG SYSTEM

Test Methods

Twenty full scale impact tests against passenger cars were conducted, based in general upon ISO 13232 - *Test and analysis procedures for research evaluation of rider crash protective devices fitted to motorcycles* (Ref 3). Six out of the seven full scale pairs[1] listed in ISO 13232 - each pair comprising a baseline motorcycle test and an airbag motorcycle test — were done, for twelve of the tests. Eight additional tests involving five other impact configurations were also done. These additional tests were for observing airbag effects considered relevant for this particular airbag concept, including the following items:

- high speed impact: 45 mi/h frontal impact of the motorcycle to the front and to the side of a stationary car;
- rider with passenger: 30 mi/h frontal impact of the motorcycle with rider and passenger to the front of a stationary car. The rider dummy was an instrumented ISO 13232 MATD 50th percentile male dummy, and the passenger dummy was an uninstrumented 50th percentile Hybrid III male dummy with sit/stand pelvis;
- Forward leaning posture: 30 mi/h frontal impact of the motorcycle to the front of a stationary car, with the dummy torso angle inclined forward 45 degrees from vertical.

Figure 15 illustrates the impact configurations used.

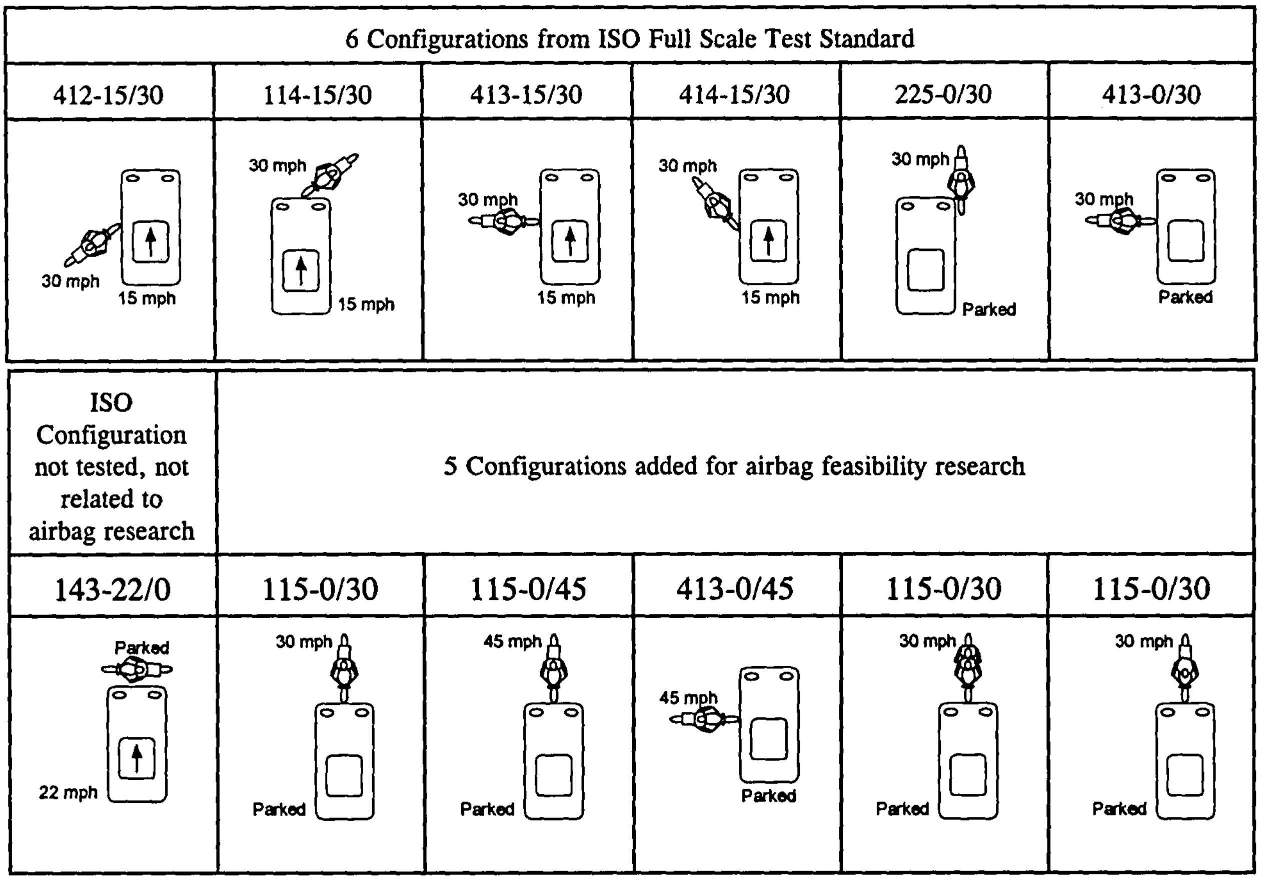
6 Configurations from ISO Full Scale Test Standard
412-15/30
30 mph
15 mph
114-15/30
30 mph
15 mph
413-15/30
30 mph
15 mph
414-15/30
30 mph
15 mph
225-0/30
30 mph
Parked
413-0/30
30 mph
Parked
ISO Configuration not tested, not related to airbag research
5 Configurations added for airbag feasibility research
143-22/0
Parked
22 mph
115-0/30
30 mph
Parked
115-0/45
45 mph
Parked
413-0/45
45 mph
Parked
115-0/30
30 mph
Parked
115-0/30
30 mph
Parked

Figure 15. Impact configurations used.

---

[1] The car-front-to-motorcycle-side ("broadside") impact configuration of ISO 13232 was not tested in this exploratory research, since it did not seem to have a direct relation to a frontal airbag device.

The rider dummy used for all tests was an ISO 13232 Motorcyclist Anthropometric Test Device (MATD). Measurement of injury indices for the head, neck, chest, abdomen, upper legs, knees and lower legs were made in accordance with ISO 13232.

The opposing vehicle for all tests was a Toyota Corolla, in accordance with ISO 13232. However, the US Corolla model was used rather than the Japan model, because of availability, and because inclusion of side protection beams in the US model was judged to be more representative of the worldwide trend.

ISO Impact Tolerances and Accuracies

Appendix 4 lists the relative and absolute tolerances in impact conditions prescribed by ISO 13232, and the conditions measured in these exploratory tests. Some excedance of some of the tolerances occurred in some of the tests, however because of the exploratory nature of these tests, these excedances were judged to be acceptable.

COMPUTER SIMULATION PROCEDURES

Computer simulation models of the GL 1500 with and without the prototype airbag, the US Toyota Corolla, and the MATD dummy were formulated and calibrated in accordance with the ISO 13232 simulation procedures.

The models had the following multi body segments and finite elements:

- GL1500	7 segments
- Airbag	614 finite elements
- Dummy	30 segments
- Toyota Corolla	7 segments

The airbag sensor location, orientation and logic described previously were also modelled.

The models were implemented with software which linked the US Air Force's Articulated Total Body multi body simulation with Livermore Software's LS-DYNA3D nonlinear finite element simulation.

Laboratory tests were done of the MATD dummy, the GL1500, the airbag and the US Corolla, and calibration of the simulation against test data from 32 laboratory tests was done in terms of force-deflection and force-time characteristics.

The simulation was also calibrated and correlated with data from the nine full scale test pairs which involved the GL1500 motorcycle with and without an airbag, for the primary impact period (ie, the first 500 ms of the impact sequence), according to ISO 13232. Figure 16 shows the correlation between the simulation and the full scale test data in terms of head maximum resultant linear acceleration. This indicates a correlation coefficient (r^2) of 0.88. Table 4 lists results for "percentage correct" injury predictions for the upper legs, knees, and lower legs, which indicated 94 percent or more agreement between simulation and test data.

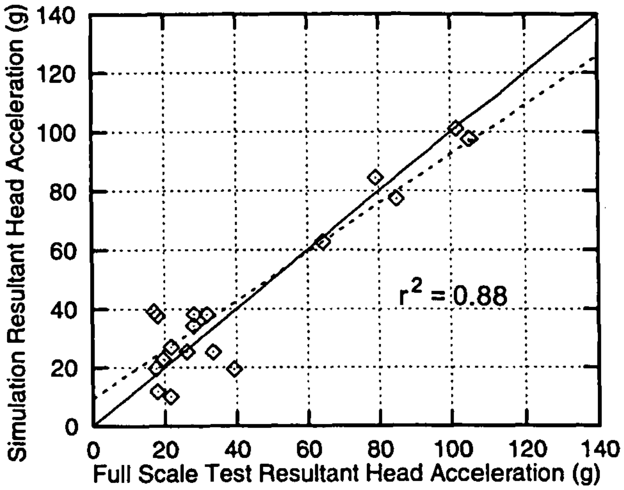

Figure 16. Correlation of head maximum resultant linear acceleration.

Figure 17 compares a top view image of the simulation to the corresponding image from the full scale test. Subjectively, there was close agreement in terms of motions, between the simulations and the 18 full scale tests.

The calibrated simulation was next used to simulate the 200 motorcycle/car impact configurations representing 501 real accidents in Los Angeles and Hannover (ie, some impact configurations had multiple occurrances), according to ISO 13232, for the primary impact period, and with and without the airbag fitted to the GL1500.

The time histories of the motions and forces from these simulations were then analyzed to determine dummy injury indices, according to ISO 13232.

INJURY ANALYSIS METHODS

The injury analysis methods used to analyze both the full scale test data and computer simulation data were those specified in ISO 13232. This includes calculation of injury assessment values and injury indices for the head, neck chest, abdomen, upper legs, knees and lower legs; and combining the information for all body regions to calculate

Table 4.
Leg Injury Correlation

Femurs		Full Scale Tests		Percent correct
		Fracture	No Fracture	94%
Simulations	Fracture	0	2	
	No Fracture	0	34	

Knees		Full Scale Tests		
		Fracture	No Fracture	97%
Simulations	Fracture	0	0	
	No Fracture	1	35	

Tibias		Full Scale Tests		
		Fracture	No Fracture	94%
Simulations	Fracture	0	2	
	No Fracture	0	34	

the Normalized Injury Cost (NIC) for each test (NIC = 0.0 corresponding to no injuries, and NIC = 1.0 corresponding to a fatal injury).

Example injury assessment values (IAV) and corresponding injury index (II) values, excerpted from ISO 13232, are listed in Table 5, for general reference.[1]

Two additional injury analysis procedures were used in addition to those of ISO 13232: a preliminary neck injury assessment; and additional injury risk/benefit calculations.

Preliminary Neck Injury Assessment - ISO 13232 includes a method to calculate Neck Injury Indices (NII), but includes no specific criteria or injury probability curves which relate the NII values to probability of different severities of neck injury, as ISO 13232 provides for other body regions.

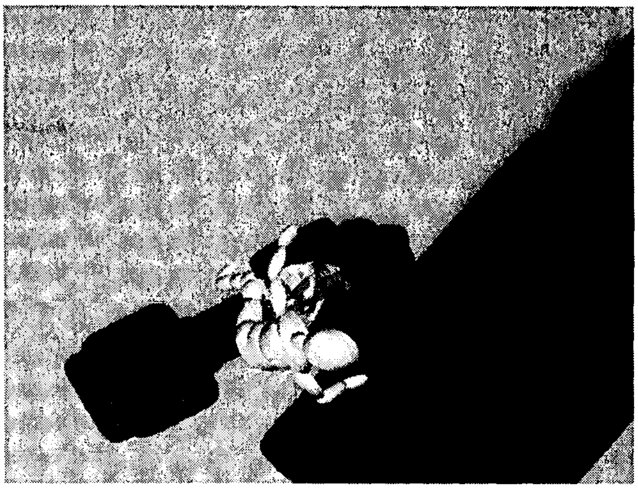

a) **Computer Simulaton**

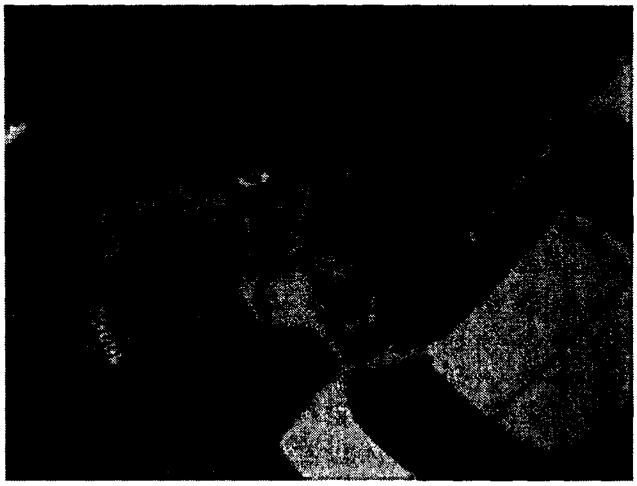

b) **Full Scale Test**

Figure 17. Example comparison of side view of simulation with full scale test, impact configuration 412-15/30, airbag.

The rationale for ISO 13232 (Part 5, Clause H.3.8) states in a general way that:

> "[NII] values near or above 1.0 are interpreted as likely neck fracture or dislocation; with significant likelihood of spinal cord damage, which at the C1/A0 location, has a fatal propensity."

It has been reported elsewhere (eg, Ref 6) that more research is needed: to improve the biofidelity of the dummy neck used in motorcycle impact research; and to clarify the probabilities of various types and severities of

---

[1] The IAV and II relationships defined in ISO 13232 are in many cases continuous, multivariable functions. The examples listed here are for approximate, example reference and are not definitive.

Table 5.
Example Injury Assessment Variable (IAV) Values and Corresponding Injury Index Values (II) from ISO 13232[1]

Body Region /IAV	Example IAV Value	Corresponding II Value
Head G (= normalized resultant of a_r and α_r)	0.85 (= 140g with simultaneous peak of 15.8 Kr/s^2)	P-AIS2
Neck		
Shear	5.0 kN, or	NII = 1.0 (P-AIS6 assumed)
Tension	5.0 kN, or	
Compression	4.0 kN, or	
Flexion	300 Nm, or	
Exension	90 Nm, or	
Torsion	40 Nm	
Chest		
Compression	24%, or	P-AIS1
Velocity-compression	0.2 m/s (with V>3 m/s)	P-AIS1
Abdominal Penetration	35 mm	P-AIS1
Femur Fracture	Non displaced	P-AIS3
Knee Dislocation	Partial	P-AIS2
Tibia Fracture	Non displaced	P-AIS2

neck injury, given measurements of the forces and moments acting upon a more biofidelic dummy neck.

In the interest of proceeding with exploratory airbag research, however, a conservative or worst case assumption regarding neck injury probability was made. Given the criticality of neck injury and the aforementioned uncertainties, it was assumed for purposes of this research that NII values greater than 1.0 would correspond to "certain, fatal neck injury." This assumption was then included in the injury analysis for both the full scale tests and the computer simulations.

Additional Injury Risk/Benefit Calculations - ISO 13232 describes a method which quantifies the percentages of the 200 impact configurations in which a given device is "beneficial", and in which a given device is "harmful," based on test and simulation results.

An amendment to ISO 13232 has been proposed (Ref 4) which would also calculate the total amount of benefit and harm (or "risk"), in addition to the percentages of cases which are beneficial and harmful. For purposes of assessing the amount of airbag benefit and harm in this exploratory study, this proposed amendment was considered to be useful. However, a slight modification of the equations in the proposed amendment, described in Appendix 3, is considered to better describe both the amount and the percentage of cases in which a device is beneficial or harmful. These modified equations were used in the analysis of the test and simulation data.

With regard to risk and benefit criteria, these have not been established or discussed for motor vehicles in general. However, for comparison purposes, the equations of Appendix 2 were applied to example car airbag data for the United States (Ref 5), and the results are summarized in Table 6.

Table 6.
Example Risk and Benefit Data for US Car Airbags, Fatals Only (Based on Ref 5)

Occupant Category	Lives		Risk/Benefit (%)
	Saved (Benefit)	Lost (Risk)	
All	2920[1]	94[2]	3
Drivers	2536	36	1
Adult Passengers	384	4	1
Passengers	384[1]	45[2]	12

Notes
1 Assumes zero child lives saved by airbags.
2 Excluding children in rear facing child safety seats.

The US car airbag data indicate that the estimated airbag risk-to-benefit ratio for drivers and for adult front passengers is about 1 percent. Airbag "benefit" data for children are not available; however if a worst case assumption is made that no child lives are saved by airbags, the resulting risk-to-benefit ratio for all front passengers - including children - is 12 percent (and less than this if there are some child lives saved by airbags).

So, it is observed that for car airbags, risk- to -benefit ratios for adults are about 1 percent, and for all front occupants are about 12 percent or less. It is also observed that designs and regulations for US car airbags are being modified in order to reduce the injury risks for front occupants (ie, in order to reduce the 12 percent statistic).

From this background it was considered on a preliminary basis that airbag risk-to-benefit ratios of 12 percent or more are relatively large and undesirable, and that ratios of 1 percent describe performance levels which currently occur for normal sized adult car occupants.

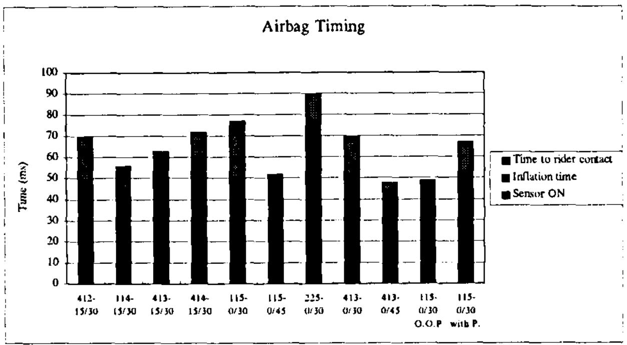

Figure 18. Airbag timing data from full scale tests.

RESULTS OF THE FULL SCALE TESTS OF THE PROTOTYPE AIRBAG SYSTEM

System Functionality

Figure 18 presents the time required for each of the important time periods of airbag functioning: the sensing time, the deployment time and the dummy time-to-contact, for the eleven full scale tests with airbags.

The sensing time is measured from first motorcycle/opposing vehicle contact until the trigger signal occurs. The deployment time is measured from the trigger signal until complete inflation. The dummy's time-to-contact is measured from first motorcycle/opposing vehicle contact until the dummy contacts the airbag. Time data were based on recordings in the ECU and on high speed film analysis.

Note that in the offset frontal impact configuration 225-0/30, although the acceleration and velocity change did not reach the criteria for airbag deployment, the airbag system was deployed. This was considered to be a case of "unintended deployment," probably caused by electromagnetic interference (EMI), for which there was no special electrical shielding provided in the prototype system.

For the 10 intended deployment tests, the dummy contacted the fully inflated airbag 2 to 26 ms after full inflation (average of 13 ms), except in the dummy leaning forward case. Sensing and inflation times were 8 to 14 ms and 34 to 46 ms respectively. So, overall, the system was considered to have functioned as intended with regard to timing for this series of tests.

In order to further evaluate the timing performance of the prototype system, further tests with conditions which are closer to "borderline" inflation conditions would be needed, such as crashes at lower speeds, or with lighter weight or less stiff opposing vehicles. Further study is needed with these and other conditions to determine whether the rider may contact the bag before full inflation, whether there are potential harmful effects and possible design changes to reduce or eliminate these.

Preliminary Results of Injury Evaluation

The effects of airbag deployment on injuries are summarized hereafter, based on dummy measurements from the full scale test pairs (with and without airbags), the ISO 13232 injury evaluation methods and the injury risk/benefit calculations of Appendix 3.

Results for each test pair and body region - Figure 19 presents the injury risks and benefits for each test pair, in terms of the change in AIS for each body region and NIC (across all body regions). The shaded portions indicate results for the period prior to 500 ms - the primary impact sequence - during which the main motorcycle, dummy and opposing vehicle interactions occur. The unshaded portions indicate results for the entire impact sequence, which includes dummy/ground contact and the dummy coming to rest.

Figure 19 indicates that:

- the main airbag effects (both risks and benefits) are to the head and neck, and are related to ground contact (ie, they do not occur during primary impact).
- in terms of NIC, the airbag is beneficial in 4 cases, harmful in 2 cases and has little or no effect in 3 cases.

Photographs of example airbag benefit and risk cases are shown in Figs 20 and 21, respectively.

The airbag benefit case of Figure 20 is for the high speed side of car impact (impact configuration 413-0/45). With the baseline motorcycle, the dummy's helmet contacts the car roof resulting in a fatal neck injury, whereas with the airbag motorcycle, dummy energy absorption occurs, and there is no helmet contact to the car roof. The only injury is an AIS 1 head injury on ground contact.

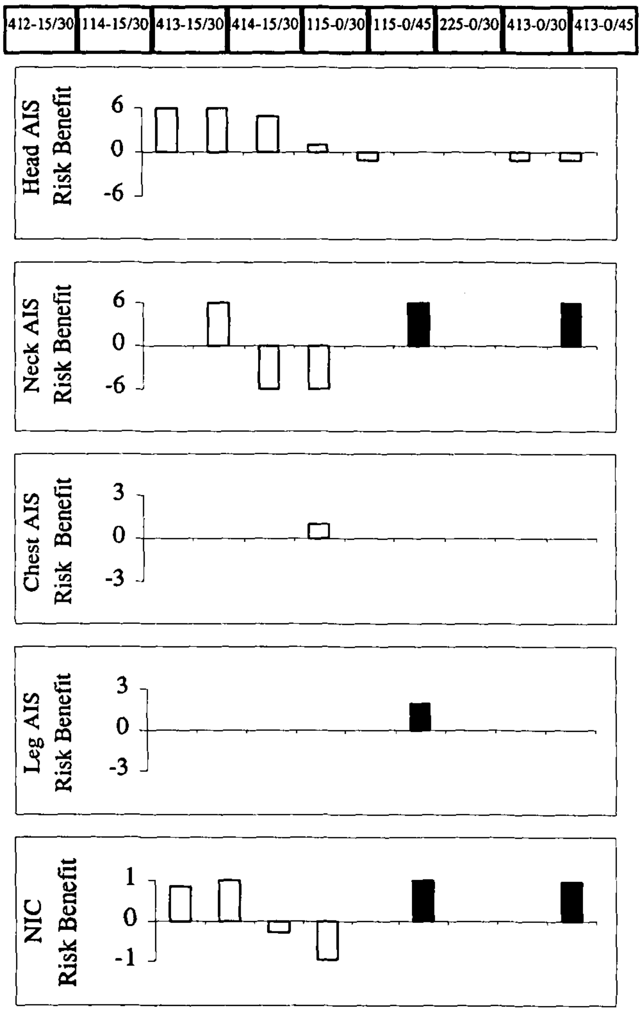

Figure 19. Airbag injury risks and benefits, by impact configuration and body region.

The airbag risk case of Fig 21 is for the angled car side impact (impact configuration 414-15/30). With the baseline motorcycle, the dummy is ejected and somersaults forward, contacting the ground with feet and pelvis (resulting in AIS 1 head and chest injuries for the entire impact sequence); whereas with the airbag motorcycle, dummy energy is absorbed, the dummy tends to stay on or near the motorcycle, and there is a fatal neck injury on ground contact as the motorcycle and dummy fall sidewards.

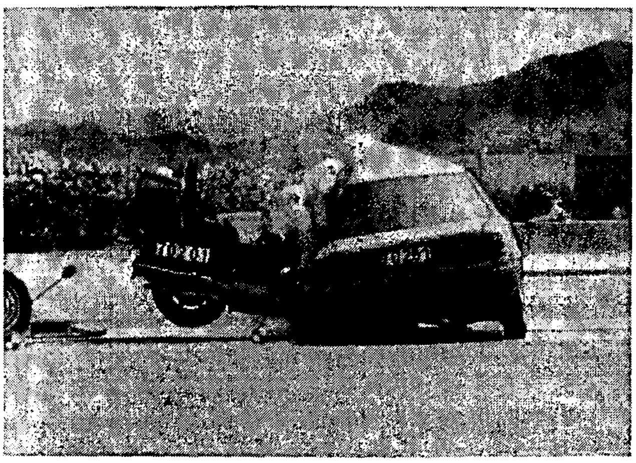

a) Baseline

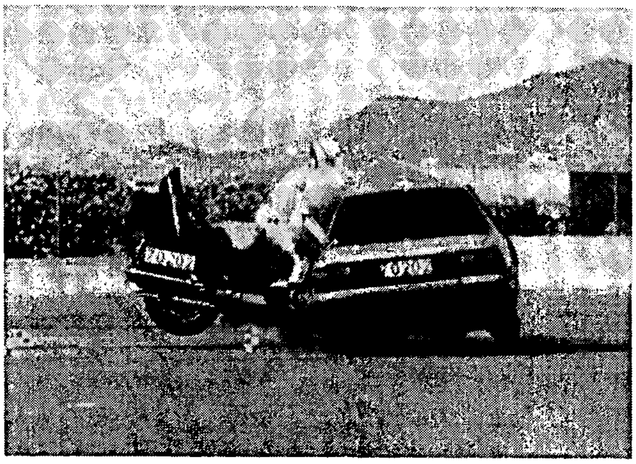

b) Airbag

Figure 20. Airbag benefit case (413-0/45)

Results for each body region, all test pairs - Figure 22 shows the benefit and risk by body region in terms of average change in AIS, across all impact configurations and for the entire impact sequence.

The main airbag effects - both benefits and risks - are to the head and neck. For the head and for these impact configurations, the injury benefits are much larger than the injury risks; whereas for the neck, the injury risks are relatively large in comparison to the injury benefits.

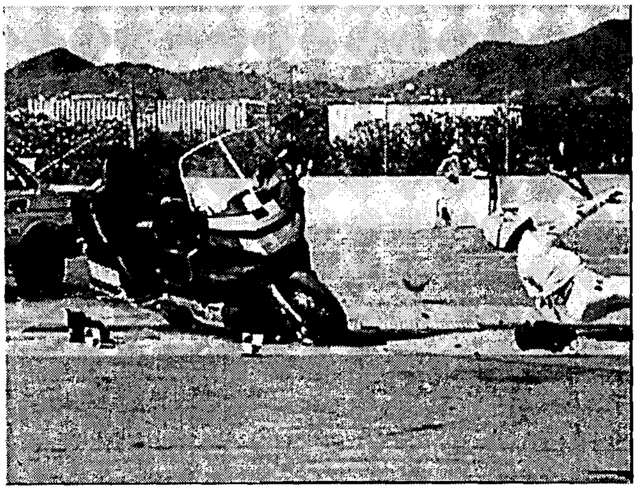

a) **Baseline**

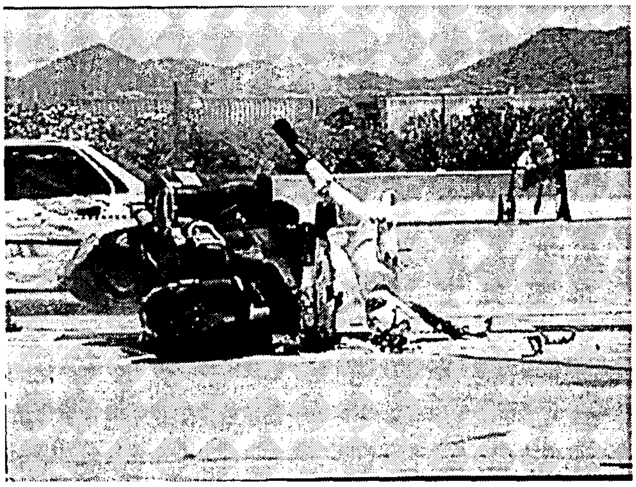

b) **Airbag**

Figure 21. Airbag risk case (414-15/30)

Total average benefit and risk, all test pairs - Figure 23 shows the total average injury benefit and risk in terms of average change in NIC across all test pairs, and accounting for frequency of occurrence of these impact configurations in accidents, according to Appendix 3.

The data - which are applicable to the subject motorcycle, airbag prototype, opposing vehicle and this set of impact configurations - indicate that the injury benefits are greater than the injury risks; but that the risks are substantial, with a risk-to-benefit ratio of 25 percent, in terms of Normalized Injury Cost. This is substantially more than the risk-to-benefit ratio of 1 percent for car airbags, noted previously.

Higher impact speed - Four of the previously described tests were for 45 mi/h motorcycle impact speeds to the front and side of a stationary car, in order to assess airbag effects at higher impact speeds.

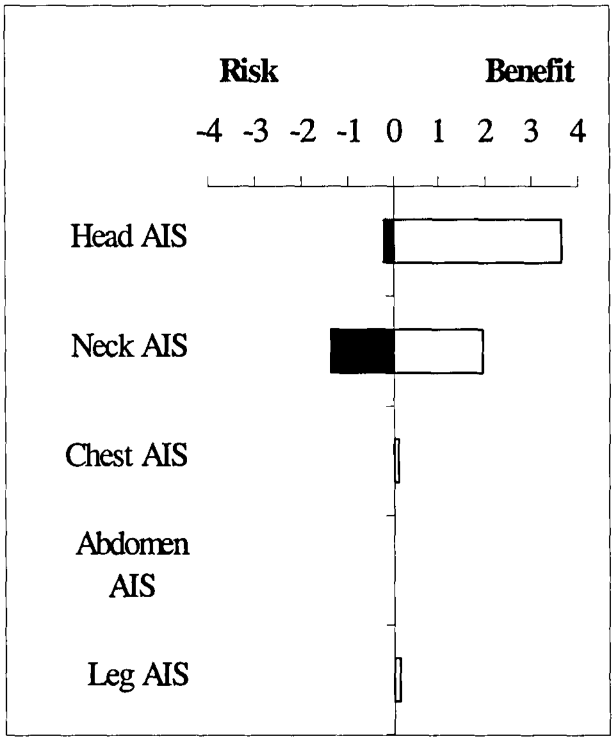

Figure 22. Airbag injury risks and benefits by body region, all test pairs, entire impact sequence.

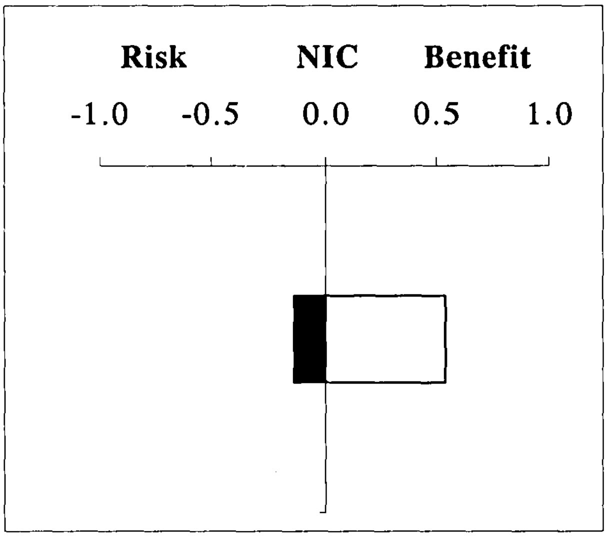

Figure 23. Total average benefits and risks, all tests

Effects of Other Test Variables

The functioning of the prototype airbag system was observed to be satisfactory in these 45 mi/h impacts, including the timing sequence. Although some increase in dummy/airbag forces were observed at higher speeds, these increases seemed to be limited by two other phenomena: the large motorcycle pitching motion in the impact to the front of the car; and the rupture of the prototype airbag in the impact to the side of the car.

In the car front impact, as illustrated in Figure 24, a complete forward pitchover of the motorcycle occurred during which the dummy slid over the top of the airbag, which may have limited the force from the airbag. The maximum bag internal pressure was 0.22 kg/cm^2, which is relatively low. Although head and neck forces were greater than those at 30 mi/h, the maximum chest compression was less than that at 30 mi/h.

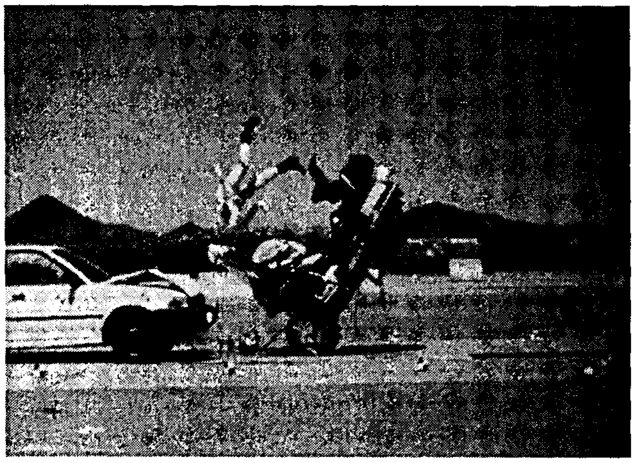

Figure 24. 45 mi/h impact tests, front of stationary car.

In the car side impact, as illustrated in Fig 20, a large amount of motorcycle pitching did not occur, due to the motorcycle fairing-to-car contact which was located well above the motorcycle center of gravity. Rupture of the bag occurred along the seam line in the 45 mi/h test, as shown in Fig 25. This may have acted to limit the amount of dummy/airbag force. The maximum bag internal pressure was 0.35 kg/cm^2.

Forward leaning posture - An impact to the front of a stationary car (impact configuration 115-0/30) with the dummy leaned 45 degrees forward (Fig 26) was conducted with only the airbag motorcycle, in order to investigate airbag-to-dummy contact effects in this riding position. When compared to the normal riding position test, the test

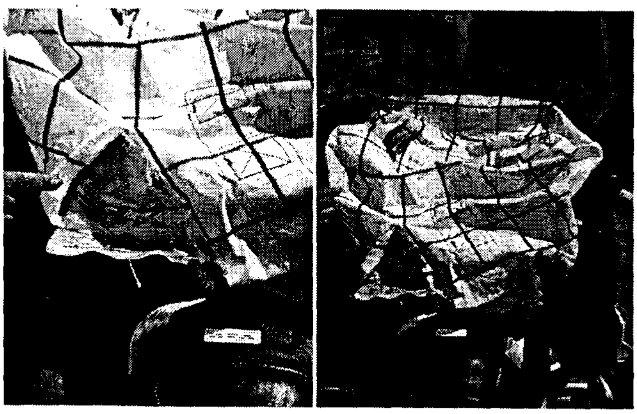

Figure 25. Photos of bag rupture which occurred during 45 mi/h impact to side of stationary car.

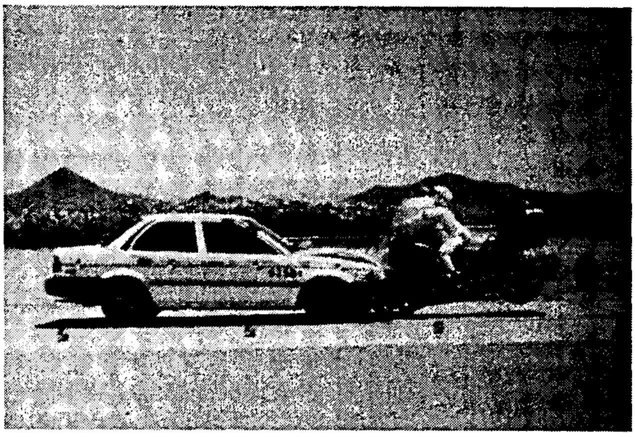

a) Forward leaning dummy

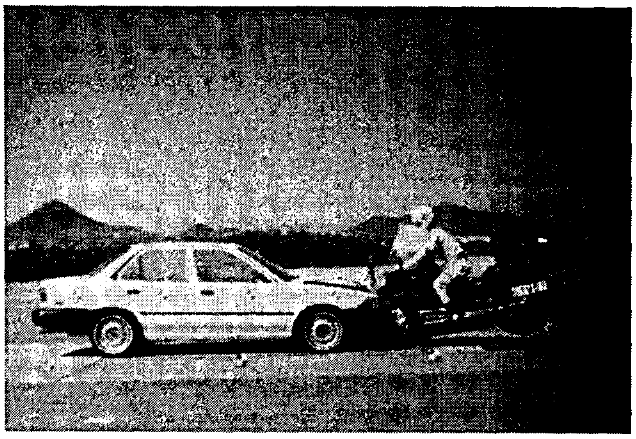

b) Normal position dummy

Figure 26. Impact test with forward leaning dummy.

data indicated no significant chest injury potential. The maximum bag internal pressure was 0.40 kg/cm^2. Dummy neck extension and moment increased but was well below the assumed fatal level. These and the other neck injury results should be further evaluated if and when further biomechanics research clarifies neck injury probability relationships.

With Rider and Passenger - This impact to the front of a stationary car (impact configuration 115-0/30), was also conducted with only the airbag motorcycle, in order to assess the effects of rider dummy/airbag contact forces when a passenger dummy was seated behind the rider dummy.

As illustrated in Fig 27, during the primary impact the rider dummy was caught between the airbag and the passenger dummy, resulting in a small, non injurious increase in the rider dummy chest compression. The maximum internal pressure of the bag was 0.31 kg/cm^2.

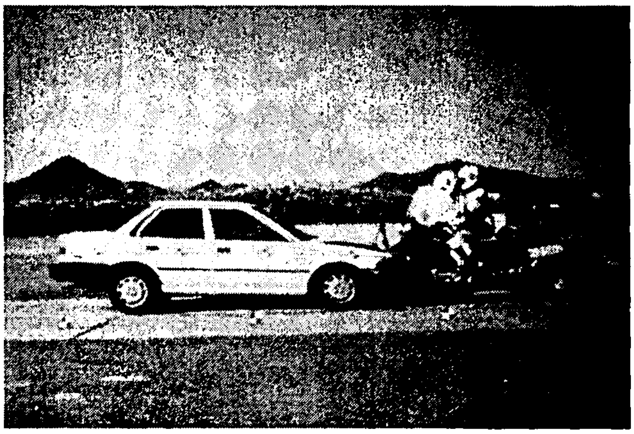

Figure 27. Impact test with rider and passenger.

COMPUTER SIMULATION RESULTS

Figure 28 presents the results from the calibrated computer simulations of 200 motorcycle/car impact configurations (ie, 200 pairs, with and without airbag) taking into account frequency of occurrence in terms of the "average change in AIS", due to the airbag, for five body regions (and for the primary impact period only). This indicates: relatively small injury benefits for the head and legs; substantial benefit for the neck; but also considerable injury risks for the neck and for the legs.

Further examination of the detailed simulation results indicated that the neck injury risks in many cases tended to be associated with neck hyper extension or hyper torsion, caused by contact with the airbag; and that the leg injury risks were associated with some increase in leg flail and associated impacts, when the upper body was restrained.

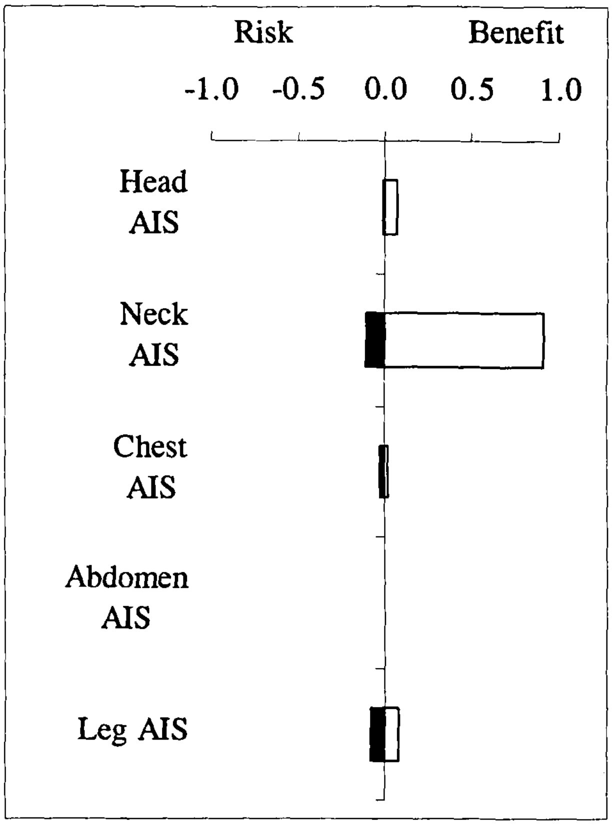

Figure 28. Average positive and negative changes in AIS, due to airbags, by body region, 200 impact configurations, primary impact period.

Figure 29 presents the overall average positive and negative changes (ie, injury benefits and risks) in terms of Normalized Injury Cost for the 200 simulations, taking into account frequency of occurrence, for the primary impact period. This indicates an injury benefit during primary impact, but also a considerable injury risk, with an injury risk-to-benefit ratio of 16 percent.

Figures 28 and 29 do not apply to the entire impact sequence, where, in the full scale tests, most of the airbag injury benefits and risks occurred. Based on the full scale test results, it would be expected that the simulation results for the entire impact sequence would be substantially different from those of Figs 28 and 29. Extending the simulation to cover the entire impact sequence would involve calibrating the simulation against the full scale data for this 3 second period, which would involve a relatively complex and substantial effort.

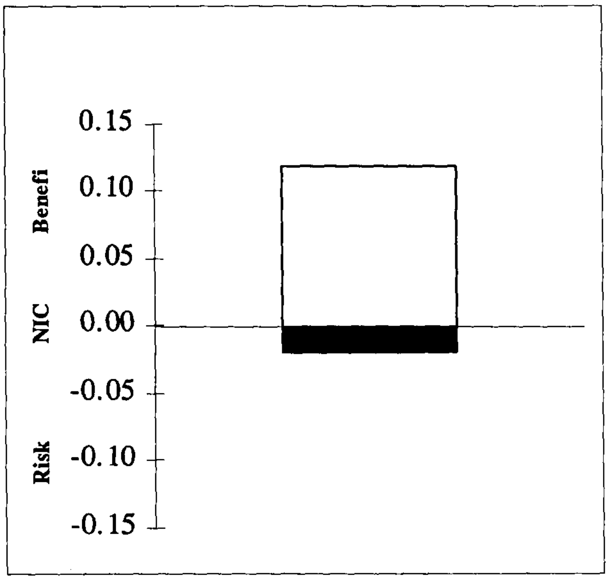

Figure 29. Average positive and negative changes in NIC, due to airbags, 200 impact configurations, primary impact period.

CONCLUSIONS AND RECOMMENDATIONS

A series of 20 exploratory full scale car impact tests and 400 calibrated computer simulations of car impacts were conducted to evaluate a prototype airbag system for a GL 1500 motorcycle.

The findings were that:

- In 10 out of the 11 tests with airbags, each airbag component functioned mechanically as expected (in one test there was an unintended deployment);
- Airbag deployment resulted in:
    - Decreased injuries (ie, decreased Normalized Injury Cost) in four out of nine test pairs (comparing motorcycles with and without airbags);
    - Increased injuries in two out of nine test pairs;
    - Little or no injury change in three out of nine tests pairs.
- Most of the changes in injury due to the airbag occurred at dummy/ground contact rather than during primary impact, as a result of changes in dummy motion with the airbag;
- Some uncertainty exists in the results related to neck injury probability, due to the current state of biomechanical knowledge;
- In the limited set of tests to examine particular airbag effects:
    - a forward leaning dummy posture resulted in increased neck forces during airbag contact but no change in injuries, compared to an upright dummy posture;
    - addition of a passenger resulted in increased chest deflection during airbag contact but no change in rider dummy injuries;
    - higher speed impacts resulted in increased chest compression but no change in chest injuries with the airbag, compared to lower speeds.
- Relatively large injury risk-to-benefit ratios were observed with the prototype airbag in comparison to car airbag risk-to-benefit ratios of 1 to 3 percent in accident data, ie:
    - a prototype airbag risk-to-benefit ratio of 25 percent in the nine test pairs;
    - a prototype airbag risk-to-benefit ratio of 16 percent in the 200 simulation pairs, for the primary impact period only.

In the future more research is needed to clarify:

- Evaluation methods, especially neck injury assessment and also a larger sample of ground contact injuries by means of computer simulation;
- Further study of impacts in which the airbag was found to be harmful, in order to identify possible remedies;
- Future study of many other crash and non-crash situations, and airbag injury benefits and risks in those situations;
- Exploration of the applicability of airbags to other sizes and types of motorcycles.

It is intended to continue to study these topics, with the goal of improving motorcycle rider passive safety.

REFERENCES

1. Inoue, T, Miura, K , et al, "Experimental Collision Test on Motorcycles with Passenger Cars," Paper No. 15 of the Safety Research Tour in the USA from the Viewpoint of Vehicle Dynamics, Society of Automotive Engineers of Japan, October 1969.

2. Anon, Traffic Accident Data, 1996, Institute for Traffic Accident Research and Data Analysis, Japan, 1998.
3. Anon, International Standard ISO 13232:1996(E), Motorcycles - Test and analysis procedures for research evaluation of rider crash protective devices fitted to motorcycles, Parts 1 to 8, International Standards Organization, Geneva, December 1996.
4. Kebschull, S, Zellner, J, Van Auken, M, "Proposed Amendment to ISO 13232, Part 5, 5.10.4, Risk/benefit Calculations," ISO/TC22/SC22/WG22 N236, May 1997.
5. Anon, Special Crash Investigation Report on Airbags, National Center for Statistics and Analysis, National Highway Traffic Safety Administration, US Department of Transportation, Washington, DC, March 1998.
6. Newman, J, Withnall, C, Gibson, T, Rogers, N, Zellner, J, "Performance Specifications for the Neck of a Motorcyclist Anthropometric Test Dummy," Fifteenth International Technical Conference on the Enhanced Safety of Vehicles, Melbourne, May 1996.

APPENDIX 1 - VEHICLE SPECIFICATIONS

Table 1-1.
Specifications of Test Motorcycle

Manufacturer:	Honda
Model:	GL1500 Interstate
Year:	1994-1996
Weight (empty, as tested, no airbag)	376 kg (average)
Weight (empty, as tested with airbag)	376 kg (average)
Length, overall:	2615 mm
Width, overall:	955 mm
Height, overall:	1495 mm
Wheelbase:	1690 mm
General size, weight:	Large, heavy
Type	Touring

Table 1-2.
Specifications of Opposing Vehicle

Manufacturer:	Toyota
Model:	Corrola, US
Year:	1989-1991
Weight (empty, as tested):	1100 kg (average)
Length, overall:	4200 mm
Width, overall:	1660 mm
Height, overall:	1360 mm
Wheelbase:	2430 mm
Type:	Sedan (Saloon)

APPENDIX 2 - AIRBAG SENSOR SPECIFICATIONS

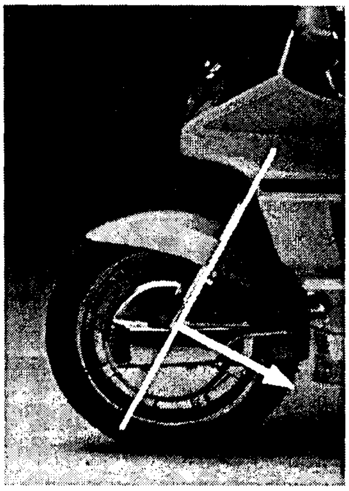

Figure 2-1. Front axle sensing location and direction

Table 2-1.
Sensor Specifications

Filter:	Low pass (243 Hz)
Type:	Piezo resistive
Range:	5884 m/s^2
Excitation:	5v DC
Current:	< 0.5 mA (peak)

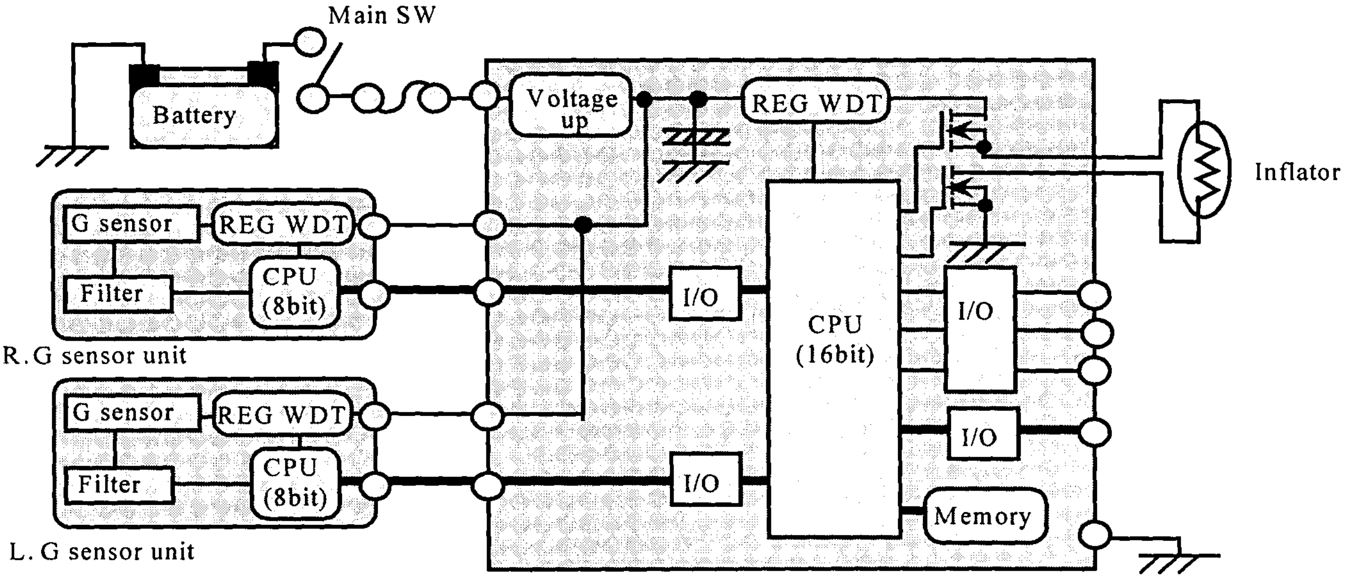

Figure 2-2. Schematic of sensor units and ECU.

APPENDIX 3 - RISK/BENEFIT CALCULATIONS

For purposes of this paper, the following definitions, adapted from Ref 4, were used:

benefit_j = average decrease in injury index j $= \frac{1}{N}\sum_{\ell=1}^{N_{ben}} (-\Delta x_{\ell,\,j} * FO_{\ell})$

risk_j = average increase in injury index j (a negative value which indicates an increase in the average injury value) $= \frac{1}{N}\sum_{k=1}^{N_{risk}} (-\Delta x_{k,\,j} * FO_{k})$

where:

N_{ben} = Number of configurations in which the protective device was beneficial (ie, resulted in a decrease in the injury index value) for a given injury index

N_{risk} = Number of configurations in which the protective device was harmful (ie, resulted in an increase in the injury index value) for a given injury index

Δx = Change in injury index value (protective device - baseline)

ℓ = Subscript for each impact configuration in which there was a decrease in the injury index value

k = Subscript for each impact configuration in which there was an increase in the injury index value

N = Total number of accidents (= 501 for ISO 13232, Part 2, Table B.1)

j = Subscript for each injury index

FO = Frequency of occurrence of a given impact configuration in accidents, based on ISO 13232, Part 2, Table B.1

Note that the injury indices analyzed in this paper include the AIS values for each body region; and the Normalized Injury Cost (NIC), which includes all the analyzed body regions and injury types.

In comparison with Ref 4, the foregoing formulation has the advantages of: being in the same units as the respective injury index; not being divided by the sum of the baseline injuries, which in some cases is zero; and quantifying the average change (rather than just the total change) of the injury index across all of the accidents.

APPENDIX 4 - ISO 13232 TOLERANCES AND TEST ACCURACIES

Impact Configurations (Test Pair)[1]	Absolute Tolerances						Relative Tolerances				
	RHA[2] 3	OVS 5	MCS 5	MCRA 5	CP varies[3]	DP 3[4]	RHA 3	OVS 5	MCS 5	MCRA 5	CP varies
412-15/30				X[5]		X		X	X	X	
114-15/30					XX						
413-15/30					XX						
414-15/30					X						X
115-0/30											
115-0/45[6]											
225-0/30											X
413-0/30											
413-0/45						X					
115-0/30 fwd lean					X						X
115-0/30 passenger											

Notes
1) Impact configuration codes as defined in ISO 13232-1.
2) RHA: Relative heading angle, degrees.
OVS: Opposing vehicle speed, percent.
MCS: Motorcycle speed, percent.
MCRA: Motorcycle roll angle, degrees.
CP: Contact point., cm
DP: Dummy position, pre-test and pre-impact, cm.
3) Tolerance varies, depending on impact configuration, generally between 3 and 15 cm.
4) Tolerance is taken to be 3 cm, according to proposed amendment to ISO 13232, per ISO/TC22/SC22/WG22 N207 and N242.
5) X : One test did not meet criterion.
XX : Both tests did not meet criterion.
6) Could not measure roll angle in one test.

SAFETY POTENTIAL OF FUTURE TWO-WHEEL CONCEPTS - A CHALLENGE

Ingo Kalliske
Christoph Albus
Federal Highway Research Institute
Paper Number 98-S10-O-15
Germany

ABSTRACT

Many big cities in Europe and elsewhere in the world have problems managing the traffic especially during rush hours. The improvement of the parking problematic and environmental protection as well are important aspects for the future traffic design of urban areas. To improve the traffic situation the development of new traffic concepts and alternative vehicles are required.

The BMW company has developed a new type of two-wheel vehicle. This two-wheeler constitutes a totally new concept. BMW implemented a lot of safety features, such as a structure made up of rollover bars and a crush element instead of a front protecting plate. Furthermore the driver can secure himself with two safety belts.

The paper contains a description of the novel two-wheel vehicle concept designed so far. BMW's concept and the safety features are also explained. The Federal Highway Research Institute (BASt) was given the task of assessing the concept as a whole with regard to the active and passive safety and the exemption of the obligation to wear a helmet. The expertise concluded, that the BMW two-wheeler concept has a very high safety standard. Some extracts of the expertise, in particular the investigations concerning the exemption of the obligation to wear a helmet are presented. Common legal requirements for the vehicle registration of vehicle concepts similar to the BMW two-wheeler in Germany have been formulated.

INTRODUCTION

Private transportation in 1994 made up 81% of total passenger transportation in Germany, with 44.56 million people being transported.

It is being attempted to shift private transportation out of the overcrowded centres and cities into the outskirts through transportation-related political measures. Many cities are hardly able to manage transportation at peak times because of the great increase in traffic, the borders in designing the flow of traffic as well as the limitations in building traffic ways. If you look at the average number of people in an automobile in city traffic (approx. 1.5 people per vehicle) you can see that a very unfavourable relationship between the number of transported people per automobile exists related to the required traffic space. Improvement through an increased utilisation of vehicles, for example through carpooling or alternative vehicle concepts in which vehicles require less traffic space would be possible solutions.

The last thought mentioned has been investigated for a long time now in regards to transposing special city vehicles to private means of transportation. An appropriate two-wheel vehicle for a new class of vehicles has been intensively discussed since the beginning of the 90s (SAMMER et al.), (HEINZE, 1991), (SIEVERT, 1997). This new type of two-wheel vehicle could represent a contribution to the solution of traffic problems in overcrowded areas. Aspects such as environmental protection as well as saving traffic and parking space play a big role in this. According to a study by SAMMER et al., there can be a 7% shifting expected in the portion of the road it takes up in such "new motorised two-wheel vehicle" in appropriate infrastructure conditions.

There is currently no precise definition of this possible new class of two-wheelers. Two and three-wheelers similar to motor-scooters with (partially) enclosed body structures or cabins are imaginable which can be used more as a means of transport fit for city and day-to-day traffic rather than as leisure time equipment. The literature locations named above as well as articles on the (functional) motorcycle of the future (ROUX et al, 1991), (WEIDELE, 1991) contain some possible characteristics as well as requirements of this new type of vehicle class:

- high user friendliness (for example automatic gears, easy handling, low-maintenance operation)
- comfort and weather protection
- high requirements for passive safety (if need be without a helmet or protective clothing)
- roof structure, closed cabin, leg protection
- stabilising aids in a standing position
- variable transport capacity.

The Honda model „Canopy", in which the construction is connected to the two-wheeler's back axle via a pivoting joint, as well as the „Bunny" model by TGB (SAMMER et al.), (MOTORRADKATALOG, 1996) can be named as examples of vehicles that point in this direction.

This concept has now been picked up by a large German two-wheeler manufacturer (Bayerische Motorenwerke - BMW AG) along with the C1 concept. This vehicle's idea was developed in 1991. In 1992 the C1 concept was presented within the framework of a talk at the VDI Motorcycle Conference with the title "Means of Transportation from the Future, Structural Interpretation of a Two-Wheel Safety Frame" (NURTSCH, 1993). That same year, BMW AG showed a conceptual study on C1 at the IFMA in order to investigate customer response. There it was shown that acceptance is heavily dependent on criteria such as maintaining individuality during transportation, extensive comfort as in an automobile (minimal weather-dependence, for example) and a high level of safety. Freedom from helmet laws has proven to be decisive for the vehicle's market acceptance.

The Federal Highway Research Institute (BASt) investigated the question of exemption of the obligation to wear a helmet for this two-wheeler and took on a thorough evaluation of active and passive safety. The documentation from 11 crash tests (see table 1) and additional computer simulations were available for this. Furthermore, various documents were evaluated, investigations and test drivings were carried out and meetings were held. Knowledge from discussions in the expert committee on Motor Vehicle Technology (FKT), special committee on "two-wheel vehicles" was brought in.

In addition, the BASt carried out a literature study and analysed crash tests run on the occasion of other projects.

The BASt conducted an inquiry at the Medical University of Hanover (Medizinische Hochschule Hannover - MHH) in order to get an evaluation of head injury risks from today's two-wheeler from the perspective of accident analysis. The carry-over of these results to the C1 two-wheeler remain unclear since this vehicle follows another concept (a buckled-up passenger, for example) which leads to different accident kinematics (no separation of driver and vehicle during the accident). Since these new types of two-wheel vehicles are not represented in today's traffic occurrences there are no accident data available. A possible similar group for comparison is formed by motor-scooters.

REAL WORLD ACCIDENT OF MOTORIZED TWO-WHEELER

In an evaluation of MHH within the BASt project "On the Spot Accident Surveys" relevant data from 1985 to 1995 about motorcycle (>80 ccm / n=776) and motor-scooter (<80 ccm and >80 ccm / n=89) accidents were compared (OTTE, 1996). The distribution regarding the frequency of the occurrences of certain collisions is shown in table 1.

A motor-scooter accident frequency rate of 88.9% in the city is higher than that of motorcycles (79.2%). The objects with which motor-scooters collided are less commonly automobiles and trucks in comparison to motorcycles, rather more often bicycles, pedestrians as well as objects.

The relative speed between the two-wheeler and the opposing vehicle is especially relevant for injury severity. Motor-scooters are less powerfully motorised than the motorcycles in the investigated collective. Accordingly, relative speeds in accidents with these vehicles are distinctly lower than in those with motorcycles. It can be seen that the proportion of head injuries and their severity increase along with increasing relative speed between the two-wheeler and the object with which it collided.

Table 1.
Collision types (OTTE, 1996)

	Type 1 Side-impact by car	Type 2 Frontal impact between car and two-wheeler	Type 3 90° side-impact by two-wheeler	Type 4 oblique impact from the side by two-wheeler	Type 5 Rear collision by two-wheeler	Type 6 Rear collision by car	Type 7 Solo accidents of the two-wheeler
	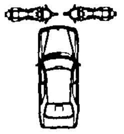	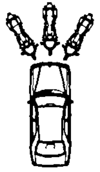	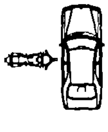	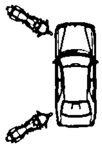	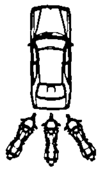	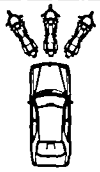	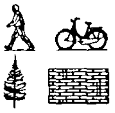
frequency at motor-scooter	5,1%	22,3%	7,0%	16,7%	5,2%	-	43,7%
frequency at motorcycle	4,2%	18,3%	5,9%	25,7%	11,2%	-	34,7%

If one compares the severity of head injuries in the different collision types for motorcycles and motor-scooters, the result is the ranking shown in table 2 for the most important collision types for each.

Table 2.
Representation of the three most important collision types regarding head injuries for accidents with motorcycles and motor-scooter (OTTE, 1996)

	Collision type	Frequency of head injuries with AIS 2+
Motorcycle:	Type 3	11,5%
	Type 7	9,2%
	Type 4	9,1%
Motor-scooter:	Type 4	6,8%
	Type 7	5,0%
	Type 2	2,0%

In all, head impacts are not of great consequence because of high helmet-wearing rates (approx. 90% of the accidents with AIS<2).

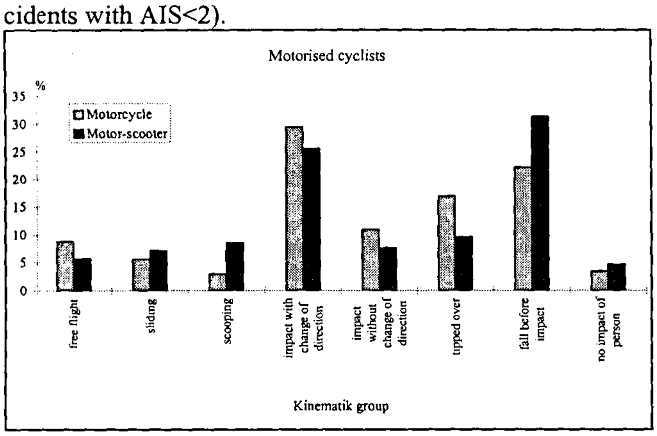

Figure 1: Cinematic groups and frequency distribution for motorcycles and motor-scooters (OTTE, 1996)

If one investigates head injuries concerning impact site it is shown that approx. 59% of head injuries occur through impact with the street. Impact with the opposing vehicle is the cause for 17% of motorcyclists' head injuries and 19% of motor-scooter drivers'. An analysis of head impact locations concerning the occurring degree of injury severity to the head shows that head impact against the colliding object count among those with the most severe consequences for motorcycle and motor-scooter drivers. The commonly occurring fall to the street leads, however, to predominantly minor injuries.

The cyclist's movement is based on studies up to now and presented according to the kinematic group definition (Figure 1). If one analyses head injuries regarding kinematic groups, the most head injuries occur in impacts with directional changes (approx. 25%-30%), in the two-wheeler's sideways movement on impact: falling over (approx. 10%-17%) as well as in isolated falling from the two-wheel vehicle (approx. 22%-31%).

THE TWO-WHEEL CONCEPT

BMW's newly developed two-wheel concept with the internal designation C1 is shown in figure 2.

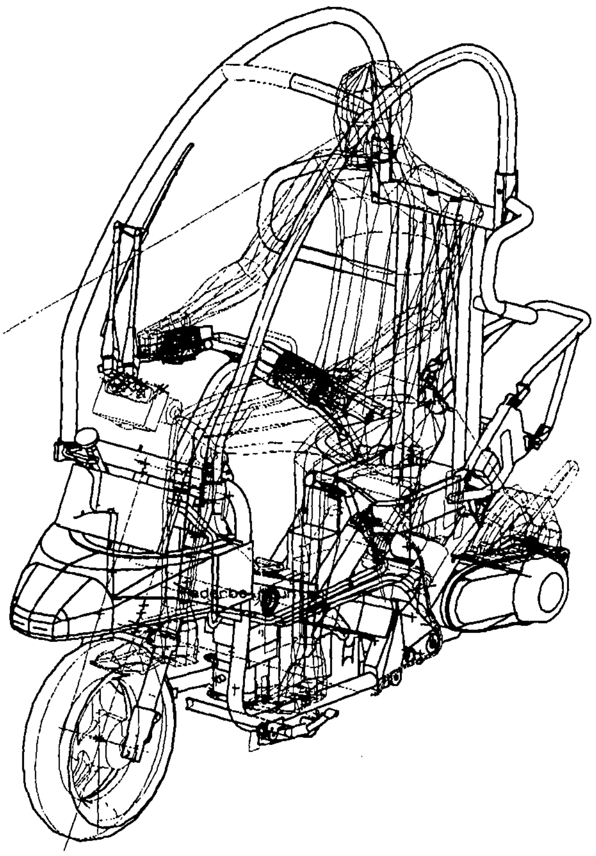

Figure 2: presentation of the principles of the C1 two-wheeler concept

The driver sits upright on this two-wheeler and is secured through a belt system. In order to assure survival space for the rider in case of a crash, a special frame structure with an integrated roll bar was developed. This, at the same time, offers extensive protection from weather influences. In addition the vehicle has a crumple zone in the front.

The C1 vehicle is, for the time being, constructed as a light motorcycle with one seat (EC definition). The two-wheeler should reach a maximum speed of approx. 100 km/h. It should be used above all at medium distances (20-50 km) in overcrowded centres. The conventional brake system will be offered with a specially equipped ABS. The handlebar is horizontal and adjustable in the vehicle's lengthwise direction.

The vehicle's special characteristics regarding passive safety are:

- The C1 vehicle is a two-wheeler with a safety frame structure made of aluminium (weight approx. 20 kg). The roll bars are integrated in these frames which also form the protective space for the rider.
- The roof frame structure was put through a roof crush resistance test derived from the test for passenger cells in automobile construction in the USA (FMVSS 216). In this test, the structure must remain with a maximum deformation of 127 mm against a semi-static pressure of at least 22 kN. In the C1 two-wheel a maximum pressure of 26 kN was measured with a given deformation of 127 mm. The roof frame structure should prevent injuries in alone accidents and/or secondary impacts.
- The two-wheeler is equipped with a restraining system that is composed of two separate belt systems, one three-point belt and one two-point shoulder belt. The three-point belt consists of a shoulder belt and a lap belt. The belt systems are installed so that the shoulder belts cross the chest of the rider. The belt anchoring and belt deflection points are fastened to the safety frame structure. According to the test specifications for belt anchors in passenger cars according to ECE-R14, the anchors of three-point belts with retractors (roll-up mechanism) and two point belts must be able to bear a tensile force of 13.5 kN over a period of at least 0.2 seconds. The three-point belt as well as the two-point belt each fulfils this requirement.
- The C1 two-wheeler has a safety seat. In the area at the front of the sitting area the seat was formed so that the riders are prevented from slipping through under the lap belt (submarining).
- There are safety bars attached to the left and right of the pelvic and shoulder areas which should extensively prevent the rider's upper body from leaving the area protected by the bar from the side as well as the intrusion of large vehicle parts and obstacles. These bars will be changed somewhat in the series vehicle in order to achieve a better protective effect. The newest version of the C1 is not equipped with a pelvic bar any more.
- Rather than a protective plate there is a deformable element (crash element) planned with which it is possible to reduce defined energy in a space of 300 mm. The crash element is especially designed for frontal impacts. If the crash element meets an obstacle or a collision opponent, the forces occurring during impact are induced with a relatively minimal vertical distance to the C1's centre of gravity as a result of the element's construction height. That leads to a minor lever-arm to the vehicle's centre of gravity. Through this, the tendency of the C1 two-wheel to lift itself with the rear end far from the road and, as a result, possibly to turn over is reduced.
- The front wheel suspension is realised through a „Telelever“ spring fork with pitch compensation. The „Telelever“ spring fork's special feature is that there is a support built in between the sliding tubes of the fork and the frame of the vehicle. At the attachment points the support is flexibly placed. The support causes stronger forces to be able to be absorbed through the spring fork. The „Telelever“ spring fork together with the crash element therefore determine the behaviour in frontal accidents since they are involved in reducing the collision energy.
- There is a windshield build into the roll bars in the driver's field of view. In the current design, a tempered safety glass was used for technical manufacturing reasons.

EVALUATION OF THE C1 TWO-WHEELER'S ACTIVE SAFETY

All technical vehicle measures which contribute to accident avoidance are understood under active safety. For two-wheelers it is especially important to look at the driver, vehicle and surrounding components as a complex, whole system rather than isolated since the driver actively and passively contributes to stabilisation through the coupling and because the two-wheeler reacts especially sensitively to interference from its surroundings. The whole system's performance ability regarding the task of accident avoidance is not only dependent on the assumptions of the driver, motorcycle and surroundings rather also on the interplay of these components.

Next to driving safety and driving behaviour, other important aspects of active safety are the operating and information concepts as well as the condition, perceptive, and system safety.

Special features of active safety and passive safety's objective conflicts in new types of two-wheel concepts

The characteristics and requirements of this new class of two-wheelers named in the introduction point to the fact that there are special aspects to be taken into consideration regarding active safety:

- driving behaviour at lower speeds
- wind influences in connection with the covering and vehicle's construction
- viewing conditions.

Next to constructive conditions, fixing the driver's upper body to the vehicle (seat belt, for example) as well as leg freedom of movement (weather protection, leg protection) play a role in stabilising the vehicle at low speeds. Objective conflicts can occur here in passive safety. Vehicle stabilisation problems at low speeds as well as in a standing position are increased through a constructively conditioned high position of centre of gravity. The appropriate support systems or support wheels may possibly be realised which, depending on the design, could lead to problems in driving behaviour at higher speeds. The foot space width or possible support device could have a negative effect on the ground clearance when banking of the vehicle.

Impairments through wind influences (side winds, whirlwinds) could develop from constructions designed for weather protection such as the covering, roof or closed cabin which influence driving stability.

The vehicle's frame posts and there padding have a negative influence on the field of vision. This especially plays a role if, during simultaneous wearing of a helmet, the field of vision is already restricted. Concerning the vehicle's "windshield", aspects such as windshield wipers and washers, ventilation against steaminess as well as scratching the shield play a role. The last point mentioned especially if plastic shields are used according to the current stand of technology. On the other hand, a plastic shield would be advantageous based on the height of the centre of gravity and passive safety.

The following points can be named as further aspects of active safety which possibly play a special role:

- By realising a high level of comfort and weather protection, positive effects on condition safety are to be expected.
- If starting were planned to be prevented through ignition interruption as an assurance of seatbelt use, dangerous situations could result from malfunctions during use when driving.
-
- Ability to recognise as well as identify a vehicle as a single-track vehicle is especially important in vehicles that will be used in city areas (SPORNER et al., 1993).

Assessment of the C1 two-wheeler's active safety

The judgement of the C1 concept's active safety is based on information from BMW AG as well as on impressions from test-drives.

When judging aspects of active safety it can be said that this, with the exception of the technical type approval regulations to be complied with, is only subjectively possible since the necessary criteria, test processes and limiting values do not exist. There were, in the past, estimates (see SCHMIEDER, 1991; SCHWEERS, 1991), but in general it can be assumed that active safety and especially a two-wheeler's driving behaviour cannot be evaluated through objective processes.

On principle, the presented C1 concept's active safety is positively judged. This can be explained especially in the following way:

- The special features that are carried by this new class of vehicle are well solved with the C1 concept and do not strike one as negative.
- The C1 concept has special equipment to increase active safety and customers are also given the opportunity to upgrade through special equipment such as ABS.
- According to statements from BMW AG and the responsible technical service, all technical vehicle type approval regulations have been complied with according to EC laws.

The vehicle can be well stabilised at lower speeds, is manoeuvrable and has no stability problems while driving at higher speeds. Relative to wind sensitivity and especially also with regard to side wind sensitivity, there is no negative behaviour present in the vehicle. According to statements from BMW AG tests have been made regarding this. There are, however, no measurements. There are no objective criteria known for judging side wind sensitivity. Through this vehicle's striking design and paint it can be assumed that good perceptibility has been achieved which is important for city traffic.

EVALUATION OF THE C1 TWO-WHEELER'S PASSIVE SAFETY

Since the C1 vehicle from BMW, as previously mentioned, can not be definitively assigned to any existing type of vehicle it is being tried to define certain accident sequences and accident phases (primary collisions, for example) in which driver strain can be evaluated. Based on the vehicle structure (safety frame structure, belt system, crash element above the front wheel, safety seat for example) the C1 vehicle is close to a comparison with a car in frontal impact. Since the balance of the driver-motorcycle system, consisting of C1 vehicle and seat, after the primary impact has a deciding influence on the accident's further progression, the C1 vehicle is to be compared with a motorcycle or a motor-scooter from this point on. For all other accident constellations, especially the side impact, driver strain evaluation and vehicle behaviour for the whole collision process will be drawn from a motor-scooter or motorcycle as a comparative vehicle.

Test results and their evaluation

BMW AG tested two ISO accident constellations (see table 3 and table 4), once each for the C1 vehicle and a conventional motor-scooter. In addition, one of the accident constellations was tested according to ISO for the C1 vehicle occupied with driver and pillion (see table 3).

The two-wheeler's oblique side impact (collision type 4 according to MHH, see table 1 as well as accident constellations 4 and 5 according to ISO, see table 4) which occurs very frequently in real world accidents was recently investigated by BMW AG in crash tests. The results have to be investigated. In addition to both accident constellations corresponding to ISO 13232, further tests were carried out according to BMW AG's own points which, however, based on the ISO and MHH constellations. For all planned test constellations according to ISO norm (ISO 13232, 1995) there were computer simulations carried out.

The results of the crash tests supplied by BMW AG as well as the computer simulations show that the respective load limits were fallen short of.

Table 3.
Survey of BMW AG's tests

Realised accident constellations by the BMW AG	Tested vehicles		
	C1 two-wheeler Solo	C1 two-wheeler With pillion	Motor-scooter Solo
90° side impact of the car	1		1
Two-wheeler's 90° side impact	1	1	1
Oblique 45° front impact between car and two-wheeler	1		
rear -end impact of the car (impact angle 0°)	1		
rear -end impact of the car (impact angle 30°)	1		
90° frontal impact against rigid barrier	1		
skidding test	1		
tipping the two-wheeler from a standing position	1		

Evaluation of crash test – after analysing the crash tests it can be expected that the C1 concept guarantees the rider a very high degree of passive safety. The measurements as well as the calculated values (HPC, for example) from the crash tests are predominantly low. They currently fall far below the admissible biomechanical load limits. A direct comparison of the C1 vehicle with a conventional motor-scooter in the same accident constellation resulted in mostly much lower strain for the C1 two-wheeler riders.

Table 4:
Accident constellations according to ISO

Constellation 1	Constellation 2	Constellation 3	Constellation 4	Constellation 5	Constellation 6	Constellation 7
v_{Pkw}=35 km/h	v_{Pkw}=24 km/h	v_{Pkw}=24 km/h	v_{Pkw}=24 km/h	v_{Pkw}=24 km/h	v_{Pkw}=0 km/h	v_{Pkw}=0 km/h
v_{Krad}=0 km/h	v_{Krad}=48 km/h	v_{Krad}=48 km/h	v_{Krad}=48 km/h	v_{Krad}=48 km/h	v_{Krad}=48 km/h	v_{Krad}=48 km/h
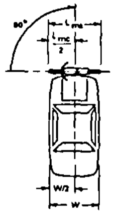	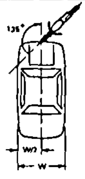	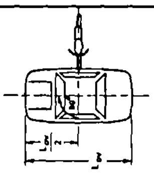	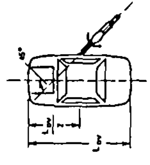	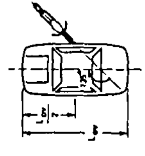	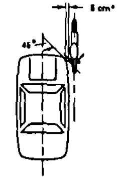	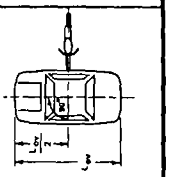

With this, in a real accident situation not only lower frequencies of injury can be expected but also lessened injury seriousness, to the head above all.

In a frontal collision the C1 vehicle's driver is bound to the vehicle by the safety belts. For this reason there is no collision of the driver with the opposing vehicle's parts (roof frame, for example). This results in low head acceleration and low HPC values for the C1 vehicle's riders. The neck momentum is reduced about 50% compared to the neck momentum of the driver of a conventional two-wheeler. The neck force is of the same order in both two-wheel concepts. It should be noted that the Dummy on the C1 vehicle and also the dummy on the commercial two-wheeler wore helmets. Through the helmet, the mass of the head area is increased. If assumed that the same deceleration is effective as they do on unhelmeted riders, the resulting forces and moments (with the same lever-arm) are larger for a helmeted rider. If the helmet-wearing law were dropped, we would expect more minimal neck strain to the C1 vehicle rider. The chest and hip strain of the C1 rider are higher than in the rider of the conventional two-wheeler (due to safety belt support); they lie, however, below the biomechanically acceptable load limit. In collisions between conventional two-wheeler and cars, a large part of the rider's kinetic energy is reduced through primary head impact, for example on the edge of the roof of the opposing vehicle, and through leg contact with the handlebars or parts of the covering and therefore only a very small strain results in the hip and chest areas. By belting the C1 rider the load occurring during impact is distributed more evenly on the upper body. No knowledge is present on the load in the abdomen. It is, however, assumed that the relationship of abdomen load (C1 rider as opposed to the rider of a conventional two-wheeler) is similar to the relationship of the strains in the hip and chest area. The lower extremities experience very low strains (only about 1/12 of the strain of the rider of a conventional two-wheeler).

In a side impact the C1 vehicle is scooped onto the car hitting it. The rotation leads to an impact between the upper portion of the C1's frame structure and the front of the car. Through the roll bar, the fixing of the rider by belts and the protective bar on the side the rider is extensively protected from direct contact with large parts of the opposing vehicle. In this way it will generally come to very low strain. Similar to the frontal impact, the C1 rider's neck momentum is lower in comparison to the neck momentum of the driver of a conventional two-wheeler (about 70%). The neck forces are about of the same order in both two-wheel concepts. Chest load in the C1 rider are higher than the conventional two-wheeler driver's chest load. They lie, however, underneath the biomechanical load limits applicable for car riders. In a 90° hit from the side the strain in the hip area was measured at 60.5 g. Legislation in the USA prescribes a hip load limit of less than 90 g or 130 g for a car collision from the side. Through the slightly higher sitting position of the C1 rider as compared to conventional two-wheeler there is no direct impact between the front of the car and the hips. After the first contact between the car and the C1 vehicle it is accelerated to the side. Since a connection free of relative movements between the C1 vehicle and the rider is not possible, the rider remains in its original place because of inertia. Since the protective bar in the seat area limits the rider's sideways freedom, in the collision sequence the hip impacts the protective bar which results in the slightly raised hip load. The test shows very low hip load in tests with conventional motor-scooters. These can be explained in that the driver and vehicle in the conventional two-wheeler in comparison with the C1 vehicle are not tightly bound to each other and that the driver scooped and the vehicle pushed away on impact. Here there is a more grazing impact between the front of the vehicle and the hip of the rider.

The primary impact in the lower extremity area has relatively minor consequences since the extremities can avoid the side of impact. In this way the risk of lengthy, cost intensive leg injuries occurring which additionally can often lead to a reduction of earning capacity is reduced. By the scooping the driver to the side, it often comes to a helmeted head-impact with parts of the opposing vehicle. In part, considerable head loads occur on the two-wheel passengers. In the C1 vehicle, the safety cage which is formed by the roll bar works against that. Through the C1 vehicle conception, driver and vehicle don't separate during the collision, that way loads in the upper extremities are possible (through jamming between the frame structure and the collision opponent). In general these dangers can be avoided through appropriate measures (for example, padding the roll bars and increasing the tube cross sections of the roll bar).

After the primary impact the post crash phase follows. It is characterised by the tipping over of the two-wheel vehicle, swerving motions and/or secondary impacts. If the C1 vehicle tips over head contact with the street could occur if the roll bar safety zone is not wide enough. If the rider were not helmeted it could lead to extensive injuries in the head area. In crash tests no head impact on the road was determined. Only minor head strains appeared there. In connection with this the transferability of the dummy's behaviour to human beings must be questioned. An estimate on this subject is presented in the section "Estimating the sideways head movement of a C1 rider" which takes into consideration that people are considerably more flexible than a test dummy. For objective evaluation of the C1's safety potential a test procedure was developed, in co-operation with BMW AG and BASt, that is presented in detail in APPENDIX II.

Swerving motions in the C1 vehicle can lead to the rider's extremities leaving the protective area of the C1 vehicle. Since these movements cannot be prevented through constructive measures, precautions are to be made that reduce the injuries (for example padding the roll bars and/or increasing the tube cross sections of the roll bar). No definitive statements can be made based on video recordings on the secondary impact of a swerving or skidding C1 vehicle. It is, however, assumed that a possible secondary impact only leads to small rider strains – smaller than a conventional two-wheeler – since the C1 vehicle has a very stiff frame structure. To evaluate the frame structure, a testing procedure was developed (roof crush resistance test) which is based on FMVSS 216 and is described in APPENDIX III.

It can come to strong structural frame distortions or impacts in all collision phases of which the possible effect is that the windshield will break in the rider's protective area. BMW AG is planning according to the current specs for the shield to be merely tempered safety glass which can, in case of breakage, disintegrate into very small pieces. If no closed helmet is worn, the resulting splinters could penetrate the driver's eyes and cause serious eye injuries. For this reason BASt recommends the use of shields that meet the requirements of the European Parliament's and the Council's regulation 97/24/EC from June 17, 1997, chapter 12: "Windshields, windshield wipers,..." according to which the fragments and splinters after the glass breaks should be of such type that the risk of injury is kept to a minimum.

Evaluation of simulation results – Computer simulations for head loads were carried out for all 7 accident constellations required according to ISO 13232. The calculations were done for the C1 two-wheeler for a rider without a helmet, for the C1 two-wheeler with a rider with helmet and a typical motor-scooter with a rider wear a helmet. The HPC, the head acceleration and the GAMBIT were determined. The probability of brain injuries resulting from linear acceleration and rotational acceleration is calculated with the GAMBIT.

The results show that the HPC, the head acceleration and the GAMBIT all show clearly smaller values for a helmeted rider on a C1 vehicle than for a typical motor-scooter with a helmeted rider. In test constellation 6 in which a grazing frontal impact between the two-wheeler and a car occurs, head loads for the C1 rider are larger than those for a common cyclist, but they are nevertheless lower than the biomechanical load limit. In all, the higher safety potential of the C1 vehicle compared to a typical two-wheeler is clear. A comparison of loads between helmeted and non-helmeted C1 drivers in tests according to ISO (ISO 13232, 1995) only shows small differences. Head acceleration in test constellation IV (oblique impact of the C1 vehicle with an angle of 45° into the side of a car) is clearly higher for the C1 driver with a helmet than for the C1 driver without a helmet. The differences in the strains for the C1 driver with helmet and the typical motor-scooter's driver with helmet are to be searched for in the different movement behaviours during the collision and in the post crash phase.

In a commercial motor-scooter, during impact the driver and the vehicle separate whereby high loads (HPC>1000 for example) probably develop through direct impacts with the object collided into or obstacles. The head loads resulting from the C1 two-wheel driver's simulations cannot be concluded for impacts with collision opponent, one's own vehicle or with obstacles.

Estimating the sideways head movement of a C1 rider– The test evaluations described above have shown that only small C1 rider loads occur in primary collisions. It seems, on the other hand, that the C1 two-wheeler's swerving movements are, as just mentioned, problematic. Since the crash films and simulation results only deliver little information for evaluating head movement in the swerving phase, high speed recordings of BASt's side crash tests were evaluated. In addition, an estimation of human head movement as opposed to a dummy as the rider of a C1 two-wheeler was undertaken. Side impact tests carry out in the BASt analysed here, a barrier with an impact speed of 50 km/h drove rectangular into the side of the vehicle to be tested. On the impact side the vehicles were occupied with EUROSID dummies. The evaluation showed that the dummy's head stuck out an average of approx. 40 mm over its pressed-in shoulder during the impact. With a safety bar width of 20 to 25 mm at shoulder height it could lead to the head leaving the C1 vehicle's protection space.

In the post crash phase, considerably lower side impact speeds occur than in the previously named tests. High speeds are to be expected if the two-wheeler falls from its upright driving position. In order to estimate the impact speeds of a head on the street it is assumed that the head's centre of gravity in an upright sitting position is located at a height of 1.3 m to 1.5 m. In order to make an estimate by approximation, the driver's and the C1 vehicle's inertial momentum are not considered. In this assumption the whole potential energy of the head is transformed into translational kinetic energy and the result is, according to the beginning height of the head's centre of gravity, the head's speeds upon impact onto the road of 5.1 m/s to 5.4 m/s (18.1 km/h to 19.4 km/h).

In a study on further development of a special dummy's neck (APROD) (HUE et al., 1982), investigations on the head-neck area's flexibility in dummies and in corpses during impacts on the side were carried out. The impact speed in these experiments was 22 km/h, corresponding to the approximate speed level of a C1 rider's head upon impact on the road after falling from a standing position. In the experiments the head bending angle (α) and the neck bending angle (β) were determined (see figure 3, APPENDIX I).

In order to carry out a rough calculation of the head's displacement to the side of an EUROSID dummy and human beings, the body dimensions required for calculation were taken from the EUROSID. The dimensions were taken over for the human being and are, together with the calculations of the results described in the following, put together in APPENDIX I. The head-neck system from the dummy as well as from the human being must also be displaced at least a half of a shoulder-width to the side in order for head contact with vehicle parts or obstacles near the shoulder to occur. Half of a shoulder-length is approx. 241 mm for an EUROSID. The calculation of sideways displacement of the head-neck system in an EUROSID, on the basis of test results for a dummy according to HUE et al., 1982 showed that this is displaced 217 mm at an impact speed of 22 km/h. If you continue the calculation on the basis of the test results for a person, it results in a sideways displacement of 274 mm in the head-neck system according to HUE et al., 1982. This shows people's higher flexibility as opposed to a dummy. The excess on the side of the head for the dummy is -24 mm (that means the head get not sideways beyond the shoulder) and 33 mm for the person (that means the head would be displaced sideways beyond the shoulder). These results show that tipping a C1 vehicle over occupied by a dummy produces no high loads, for example through impact on the street. Under the same testing conditions a human being would surely leave the C1 driver's protective space if it were only as wide as the driver's shoulders and it would result in contact with the road. Since the estimate of the sideways displacement of a person's head-neck system is just a rough calculation, BASt recommends constructing the protective space as well as the matching with the belt system so that even with a sideways displacement of the head of 50 mm beyond the side of the shoulder area no obstacle contact (the road for example) can occur.

To realise this request a test procedure was developed through co-operation between BMW AG and BASt. This procedure defined as a effectively requirement allows other constructive solutions in future developments. The detailed description of this test procedure can be found in APPENDIX II.

The buckling-up of the driver is a necessary condition for fulfilling this test procedure and for safe rider restraining. In order to prevent carelessness (forgetting, for example!) regarding buckling-up, a signal lamp was suggested according to BASt's opinion. This should be easily visible, shine with an appropriate intensity, and if necessary make the driver aware of the omitted buckling-up through blinking. From a behavioural science point of view a warning tone as a signal for an open belt is not agreed to since it unnecessarily causes noise stress and, as a result, could possibly have a negative influence on traffic. The light signal is not appropriate to prevent deliberate omission of seatbelt use.

GENERAL REQUIREMENTS OF THE C1 VEHICLES OR COMPARABLE VEHICLE CONCEPTS

Since the C1 vehicle is a new type of two-wheel concept the necessity arises of defining general requirements that the vehicles of this conceptional group should fulfil. In this section the requirements of passive safety for such vehicles especially regarding head protection will be presented from the BASt's point of view. These requirements were derived from the evaluation of the C1 two-wheeler concept. The concern is to define the general requirements so that a high safety standard for this type of vehicle can be reached through their fulfilment. In this way it should be possible to evaluate future developments from other vehicle manufacturers concerning their passive safety potential and to recognise products that do not meet the required safety levels and keep them away from the market. Because of the requirements presented here the Ministry for Transport (BMV) formulated an ordinance concerning exemption from the obligation to wear a helmet.

- The following accident constellations were recommended by the BASt for evaluating the passive safety of such two-wheel concepts:
  Accident constellations from ISO 13232 (see table 4):

  - Constellation 1: 90° side impact of the car
  - Constellation 2: oblique 45° front impact between two-wheeler and car
  - Constellation 4: two-wheeler's oblique (45°) impact into the car side from behind
  - Constellation 6: grazing frontal impact between car and two-wheeler
  - Constellation 7: 90° impact on the side by the two-wheeler against a standing car

  Constellation 3 is covered through constellations 4 and 7 and constellation 5 is comparable with constellation 2.

  In addition there are:

  - a sideways tipping test and
  - a roof crush resistance test

to be carried out. The respective test description and implementation is presented in APPENDIX II and APPENDIX III.

- In all of the previously described tests the load limit for rider head is HPC=1000 according to the requirements in the frontal and side impact tests for cars.
- The rider's extremities can leave the vehicle's safety area in the impact or swerving phases. In order to keep injuries to the extremities by being jammed in by one's own vehicle as minimal as possible, contact forces (surface pressures) are to be kept as minimal as possible. If the requirement of the regulation 97/24/EC of the European Parliament and the Council from June 17, 1997 on components and characteristics of two and three-wheeled motorised vehicles, chapter 3, cannot be fulfilled, padding is to be installed in the extremities' contact areas.
- The two-wheeler has to be equipped with an appropriate, state-of-the-art restraint system which meets the requirement of the regulation 97/24/EC of the European Parliament and the Council from June 17, 1997 on components and characteristics of two and three-wheeled motorised vehicles (chapter 11, Anchoring safety belts and safety belts on small three-wheeled motorcycles, three and four-wheeled vehicles with body constructions). The restraint system must safely restrain the rider in all phases of a possible accident and thereby protect him/her from contact with obstacles and/or parts of his/her own vehicle's structure.
- If the two-wheeler's protection area is foreseen with windows, they must meet the requirements of the regulation 97/24/EC of the European Parliament and the Council from June 17, 1997 on components and characteristics of two and three-wheeled motorised vehicles, chapter 12, appendix I, section 1.1. or 1.2..
- If a restraint system is foreseen for the vehicle's rider and it is to be manually operated, the installation of a signal lamp is required in order to prevent carelessness during use (forgetting, for example!). This lamp should be placed where it is easily visible, shine with appropriate intensity and meet the requirements of the EEC regulation 78/316, appendix III, figure 9. An informational sign must be within field of view of the prepared driver on which it is pointed out that the obligation to wear a helmet exists if the rider does not put on the belt system.

INVESTIGATIVE SUGGESTION FOR OBSERVING MARKET AND ACCIDENT EVENTS

It is possible that vehicles in this new class will reach a certain market share in the future and are to be found frequently, especially in city traffic. It must remain to be seen how this new class of vehicles will reflect in accident events since no experiences exist regarding this. For this reason it is being suggested to carry out an accompanying investigation regarding market development and accident events in the coming years parallel to the introduction of this new type of two-wheeler concept into the market. This investigation should be set up long term since market penetration at the beginning of the series' introduction will be very small. Information on market development can be expected from the vehicle manufacturers and importers. The accident event can take place through special evaluations at the Medical University of Hanover. According to a statement by BMW AG, the company will also investigate C1 accident behaviour in the future within the framework of its own accident inquiries of BMW vehicles in the Munich area.

LITERATURE

HEINZE, G.W.; KILL, H.H.:Chancen für das Motorrad im Verkehrssystem von morgen, Tagungsbericht - 4. Fachtagung - Motorrad, VDI Verlag, Düsseldorf 1991

HUE, B. et.al.: Injury Criteria in Lateral Collision, When an APROD Dummy is Used, 9 th International Technical Conference on Experimental Safety Vehicles, Kyoto, Japan, 1982

N.N.: Draft International Standard ISO/DIS 13232 (Teil 1-8), 1995

N.N: Motorradkatalog 1996, Ausgabe Nr. 27, Motor-Presse Verlag, Stuttgart, 1996

NURTSCH, B.; HELM, D.: C1, Verkehrsmittel der Zukunft, Strukturauslegung eines Zweiradsicherheitsrahmens, Tagungsbericht - 5. Fachtagung - Motorrad, VDI Verlag, Düsseldorf, 1993

OTTE, D.: Unfallanalytische Expertise zum BMW-C1-Projekt -Bewertung des Kopfverletzungsrisikos-, Dezember 1996

ROUX, P.L.; BLEZARD, P.N.: Das Motorrad der Zukunft, Tagungsbericht - 4. Fachtagung - Motorrad, VDI Verlag, Düsseldorf 1991

SAMMER, G.; WERNSPERGER,F.: Stadtverkehr der Zukunft (FP NMZ), Kurzfassung, Hrsg. IVM, Essen

SIEVERT, W.: Mobilität und das richtige Verkehrsmittel - Umweltschutz durch Typenvielfalt?, Zeitschrift „Polizei, Verkehr, Technik“, 2/1997

SPORNER, A.; LANGWIEDER, K.: Motorisierte 2- und 3-Radfahrzeuge als Individualverkehrsmittel der Zukunft, Tagungsbericht - 5. Fachtagung - Motorrad, VDI Verlag, Düsseldorf, 1993

WEIDELE, A.: Das Gebrauchsmotorrad der Zukunft - ein Denkansatz, Tagungsbericht - 4. Fachtagung - Motorrad, VDI Verlag, Düsseldorf 1991

APPENDIX 1 – ESTIMATION OF SIDEWAYS HEAD-NECK DISPLACEMENT

According to (HUE et al., 1982) the following head bending angles (α) and neck bending angles (β) were determined at an impact speed of 22 km/h:

	α	β
Dummy	61	48
Corpse	72	108

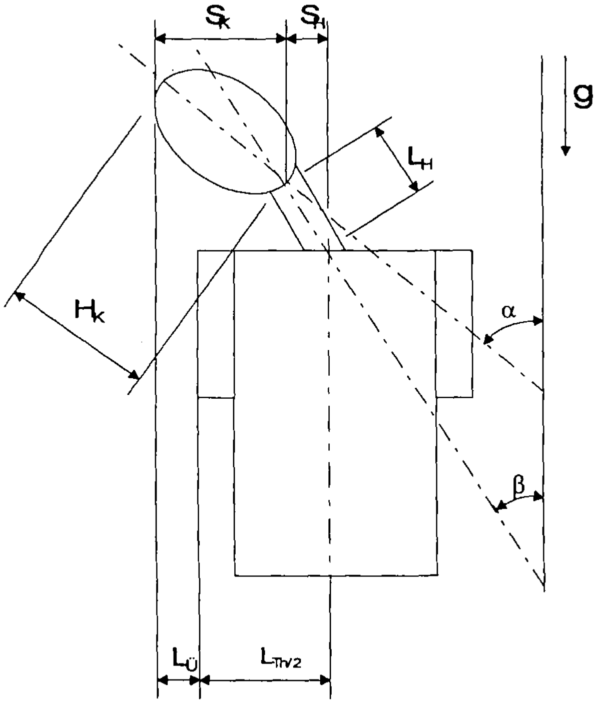

Figure 3: Geometric connections in the head-neck system during impact from the side and modified according to HUE et al., 1982

Values searched for:

sideways displacement of the neck: S_H
sideways displacement of the head: S_K
sideways displacement of the head-neck system: S_Σ
sideways excess of the head over the shoulder: $L_Ü$

For calculating of the required EUROSID dimensions:

Description	Formula sign	Dimension
Half width of the upper body in the shoulder area	$L_{Th/2}$	241mm
Neck length	L_H	146mm
Head height	H_K	143mm

The equations for calculating the desired S_H and S_K sizes can be derived from the angular relationships in figure 3's geometry.

Calculation S_H: $\sin\beta = \frac{S_H}{L_H} \Rightarrow S_H = \sin\beta \cdot L_H$

	Dummy	Human being
S_H	100 mm	145 mm

Calculation S_K : $\sin\alpha = \frac{S_K}{H_K} \Rightarrow S_K = \sin\alpha \cdot H_K$

	Dummy	Human being
S_K	117 mm	129 mm

The total sideways displacement of the head-neck system (S_Σ) can be calculated from the sum of the head's sideways displacement and the sideways neck displacement.

Calculation of S_Σ: $S_\Sigma = S_H + S_K$

	Dummy	Human being
S_Σ	217 mm	274 mm

The head excess on the side over the shoulder ($L_Ü$) results from the relationship of the half of the width of the upper body in the shoulder area (L_{TW2}) with the whole sideways displacement of the head-neck system (S_Σ).

Calculation of $L_Ü$: $L_Ü = S_\Sigma - S_{Th/2}$

	Dummy	Human being
$L_Ü$	-24,0 mm	33,0 mm

If you now imagine that the person hits the street sideways, for example, then negative side excess means that no contact with the road occurred. A positive $L_ü$ would mean the head touched the street.

APPENDIX II - SIDE TIPPING TEST

1. Area of use

In this test it is being investigated whether head contact between rider and road occurred while tipping the vehicle occupied with a driver.

2. Requirements

When the test-vehicle falls to the side, the EUROSID (corresponding to regulation 96/27/EC from May 20, 1996 on the protection of motorised vehicle passengers in a crash on the side) dummy's head speed must amount to 20 km/h + 2 km/h.

Thereby one of the points listed below must be fulfilled.

2.1. Distance from the head to the road

The distance between the head and the road may not touch the distance plate defined in 3.3.1.. There may not be any coloured markings visible on the head.

2.2. Protective devices for the head

Head load criteria HPC<1000 applies during use of protective devices for the head that prevent immediate contact with the ground.

3. Test set-up

3.1. Vehicle

Possibilities:

a) The testing vehicle either stands with both wheels on a horizontal, even, clean surface which is representative of a normal, dry, non-dirtied street surface (called "ground" in the following) or if need be on a raised platform set up parallel to this surface.

b) The vehicle will be hung up parallel to the ground with contact surface defined under 4.1..

The front wheel is found in the straight position. The wheels can be blocked through using or intervention in the brake system during the test.

If the handlebars project out from the contact surface it must be removed for the test or changed so that ground contact is avoided.

Adjustable seats and head-rests are be brought to their middle positions.

3.2. Dummy

An EUROSID dummy will be used as a test dummy. It is to be positioned in the middle of the longitudinal centre plane of the vehicle.

The legs are to be put down in the normal driving position.

The belt(s) are put on with the least possible belt slack.

The upper arms are adjusted at a 45° angle to the vertical upper body.

3.3. Measuring equipment

3.3.1. Determination of the head-ground distance

To determine the distance between head and contact level (according to 2.1.) a 75^{+2}_{-0} mm thick plate (distance plate) with appropriate dimensions placed on the ground so that before and during touching the vehicle's structure in the required contact level no contact with other body parts as the head and/or vehicle parts are possible.

The distance plate is coloured on the top part before the test.

When the head touches the plate, the coloured markings must build up paint marks.

3.3.2. Head load value determination

The head acceleration values from EUROSID are measured and evaluated (HPC, for example) in the test in 2.2..

3.3.3. Determination of maximum head speed

The process of determining head speed is not fixed yet. Possible procedures: the evaluation of a high-speed film recording or the integration of acceleration in the y-direction.

4. Test implementation

4.1. Process

A contact level will be defined as a touching surface for the vehicle's side and the ground for the testing procedure. The touch level resulting from the dynamics of the test according to 3.1.a) between the vehicle's side and a flat surface by which the head distance to the surface is the smallest is set as the contact level.

a) The vehicle tips from a standing position (vertical position) onto the foreseen side so that the contact level touched the ground.

b) The vehicle falls, aligned according to 3.1.b), to the ground from a height given through the requirement in 4.2.

4.2. Head speed

The maximum head speed in test procedures a) and b) should amount to 20 km/h +2 km/h.

In order to reach this speed it could be necessary in test 4.1.a), because of the design, to tip the vehicle from an elevated position (see 3.1.a)).

In test constellation 4.1.b) the necessary fall height corresponding to the impact speed of 20 km/h +2 km/h is to be determined.

5. Documentation

High speed film recordings from the head's impact area serve to document the sequence of movements.

APPENDIX III – ROOF CRUSH RESISTANCE TEST

1. Area of use

The procedure serves to check stiffness of roof frames and roof structures on single-track vehicles with belt systems for which an exemption from the obligation to wear a helmet is being striven.

2. Requirements

The maximum power that may appear during a 127 mm deformation distance is at least 22,2 kN during the roof crush resistance test of single-track vehicles with a belt system that are striving for exemption from the obligation to wear a helmet.

The energy absorbed during the roof structure's deformation must at least be 1.4 kJ. (This level meets a linear rise in power from 0 to 22.2 kN over a deformation distance of 127 mm – see figure 5) Very stiff roof constructions that collapse after very minimal deforming cannot fulfil these requirements.

3. Test set-up of the roof crush resistance test

3.1. Vehicle

The vehicle's frame with the roof structure is fixed on a flat, stable base plate so that it cannot be shifted during the test (see figure 4).

The vehicle's frame must be in a normal position relative to the base for this and supported so that a fixed point in the frame in the immediate vicinity of the vehicle's centre of gravity and the slant of the main frame remain nearly unchanged during the test (±10 mm, ±3°).

All supports must lie under a parallel level to the base plate through the H-point. For adjustable seats, the H-point from the lowest seat position applies.

Above this level there may be no additional reinforcement attached except for structural ones that are designed as supporting elements for the respective vehicle (for example: motor, bucket seat or body).

3.2. Pressure plate

With a flat, large enough plate (larger than the contact surface of the whole roof structure after deformation) the roof structure is pressed parallel to the base plate with constant speed (see figure 4).

4. Test implementation

The pressure plate is moved with a maximum speed of 0.013 m/s until a deformation of 127 mm. The maximum test time is 120 s.

5. Documentation

The force-travel-characteristic (vertical to the pressure plate) will be recorded for documentation of the force course (see figure 5).

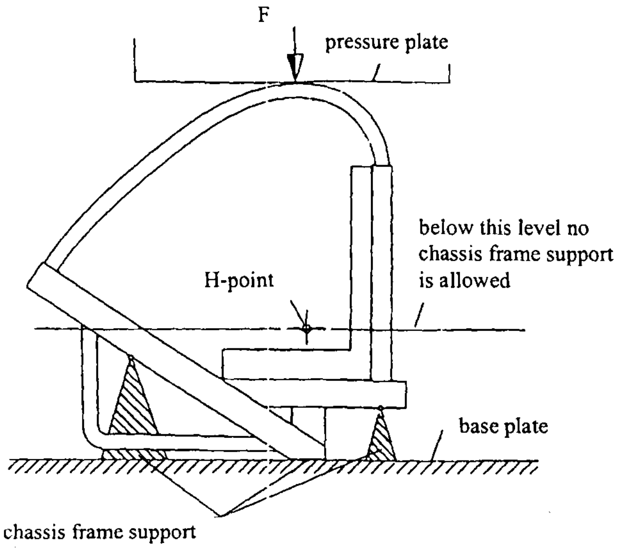
F
pressure plate
below this level no chassis frame support is allowed
H-point
base plate
chassis frame support

Figure 4: Test set-up

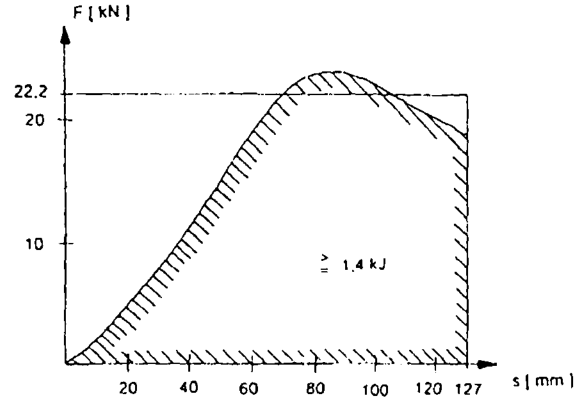

Figure 5: Force-travel diagram

THE PRACTICALITIES OF PEDESTRIAN PROTECTION

Keith C. Clemo
Robert G. Davies
Motor Industry Research Association
United Kingdom
Paper Number 98-S10-P-16

ABSTRACT:

In 1991, Working Group 10 of the European Experimental Vehicles Committee (EEVC) published a set of test requirements to address pedestrian impacts against car fronts. These consisted of component tests simulating impact by the lower leg and knee joint against the bumper, the upper leg and hip against the bonnet leading edge, and child and adult heads against the bonnet top. Since then, these requirements have been set out in a draft EC Directive, which may become part of the type-approval requirements for passenger cars sold in the European Union. The same test specification already forms part of the safety assessment of selected vehicles under the Euro-NCAP initiative. For both these reasons, manufacturers are paying close attention to the performance of their vehicles in these tests.

MIRA has carried out many tests to the EEVC WG10 specification, and experience to date shows that existing models fall well short of meeting these requirements. It appears that cars will need to undergo profound changes in design to meet the required standard. This paper details the engineering problems associated with achieving standards set out in the Directive in a variety of car types, and the other aspects of vehicle design which will be affected. Some possible design strategies are also outlined.

INTRODUCTION

During the late 1980's, the European Experimental Vehicles Committee (EEVC) was charged with drafting a set of vehicle performance criteria intended to minimise serious injuries to pedestrians in impacts at up to 40 km/h. The Committee reported in 1991 [1], proposing a set of component tests representing the three most important mechanisms of injury, that is:

- lower leg against bumper
- upper leg against bonnet edge
- head against bonnet and top of wing

A draft specification based on EEVC's work [2] has been drawn up and is currently being considered by the European Commission as part of the type-approval requirements for all new cars and light commercial vehicles sold in Europe, early in the next century.

As well as possibly becoming a mandatory requirements for cars, a similar test has already been incorporated into the European New Car Assessment Programme (EuroNCAP) [3]. This is similar to NCAP initiatives in the US and elsewhere, in that it does not impose fixed performance limits, but provides consumer information on the relative safety performance of selected models. Even though it does not impose a duty on manufacturers to comply with the requirements, its effect on sales is nevertheless a powerful incentive for them to improve the standing of their vehicles in the published performance league.

It is therefore clear that, whether or not these requirements are incorporated into legislation, they will constitute one of the major challenges to automotive designers in the near future.

TEST REQUIREMENTS

Lower Leg Test

The lower leg impact test addresses soft tissue injuries to the knee joint and fractures of the adjacent bones, caused as the leg is struck by the car bumper in the first stage of pedestrian impact. It consists of an impact against the bumper by a free-flight legform impactor. This is made of two rigid segments representing the upper and lower leg, which are connected by a deformable element representing the knee joint. This deformable element is replaced for each test. The rigid segments are covered by a layer of resilient elastomeric foam, representing the cushioning effect of the flesh in the human leg. The legform, with its axis initially vertical, is propelled horizontally into the bumper at 40 km/h, as shown in Figure 1. A minimum of three separate tests is proposed at different points within a zone bounded by the corners of the bumper, these points being selected by the test authority to represent the most severe impact conditions.

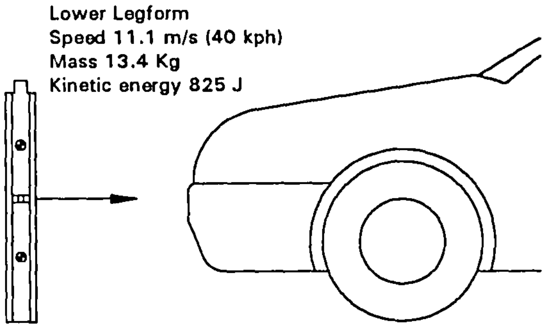

Figure 1: Lower Leg Impact Test

The legform is instrumented to record the relative dynamic shear and bending displacement of the segments during the impact, as well as the acceleration at the top of the lower leg segment.
The limits proposed by EEVC for these are as follows:

- Maximum dynamic knee shear displacement 6 mm
- Maximum dynamic bending displacement 15 degrees
- Maximum lower leg acceleration 150g

Upper Leg Test

The upper leg test addresses fracture of the femur and pelvis. It represents the second phase of the impact sequence, as the pedestrian is struck by the vehicle front after lower leg impact. In the test, the leading edge of the bonnet is struck by an impactor representing the upper leg, as shown in Figure 2. The impactor consists of a rigid mass, carrying a simply-supported beam in its impact face. The beam carries a layer of resilient elastomeric foam to simulate the leg flesh. The mass is constrained to move in a straight line during the impact, but is allowed to rotate in a vertical plane around a friction-loaded pivot. A minimum of three tests are proposed at different points along the bonnet leading edge between the corners of the vehicle, at points selected by the test authority to represent the most severe test conditions

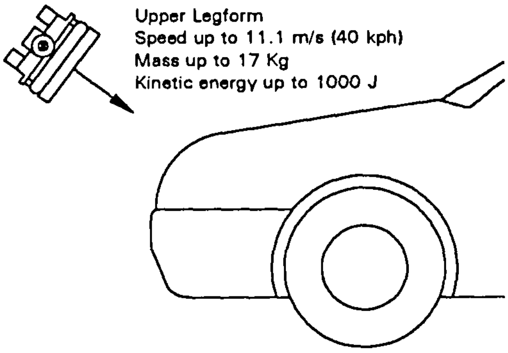

Figure 2: Upper Leg Impact Test

The impact direction relative to the ground, the mass of the impactor, and the impact velocity are all determined by the geometry of the front of the car, within the following ranges:

- Angle of impact, downwards at between 10 degrees and approximately 48 degrees to the horizontal, according to the bonnet leading edge height and the bumper lead dimensions
- Velocity, between 20 km/h and 40 km/h, according to the above dimensions
- Mass is selected to give a kinetic energy at impact between 200 J and 1050 J, according to the above dimensions and consistent with the impact velocity determined as above. Maximum 17 kg.

The effect of the vehicle dimensions on the test conditions is discussed in more detail later in this paper.

The impactor is instrumented to record the bending moment at three points along the front beam, and the compressive load at the beam's end supports. The limits proposed by EEVC for these are as follows:

- Maximum total force recorded at beam end supports 4 kN
- Maximum bending moment in beam 220 Nm

Head Impact Test

The head impact test addresses head injuries suffered as the pedestrian is pitched into the bonnet top following lower leg and/or upper leg impact. It consists of an impact at 40 km/h onto the upper surface of the car front with either of two free-flight impactors representing the head of a child or adult pedestrian, as shown in Figure 3. The child impactor has a mass of 2.5 kg and strikes points within a zone at the front of the bonnet, while the adult impactor has a mass of 4.8 kg and strikes points within a zone to the rear of the bonnet.

The front and rear boundaries of these two zones are determined according to the "wrap-around distance", that is the line described by the end of a string of given length, stretched vertically upwards from the road surface over the bumper and then longitudinally over the bonnet. For the child head impacts, the front edge of the zone lies at 1000 mm wrap-around distance and the rear edge at 1500 mm, whereas for the adult the front edge lies at 1500 mm and the rear 2100 mm. In any case, the impact zone is limited to areas forward of the windscreen lower edge. The impact direction is downwards in the vehicle's longitudinal plane, at 50 degrees to the horizontal for the child and at 65 degrees to the horizontal for the adult, reflecting the difference in stature between the two groups.

EEVC proposes a minimum of nine impacts with each impactor, at different points within the zone, again representing the most severe test conditions as judged by the test authority. For Euro-NCAP, six impacts are completed with each impactor.

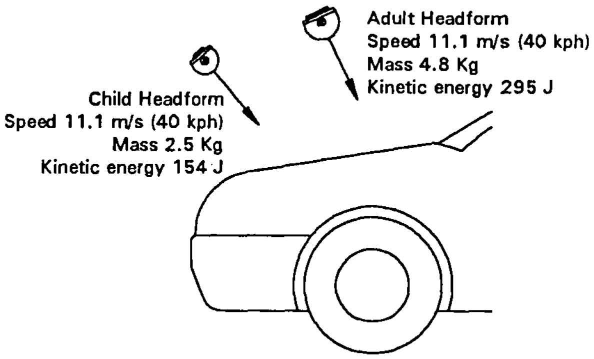

Figure 3: Headform Impact Tests

The headforms are instrumented to record the acceleration in three mutually-perpendicular axes. The injury criterion proposed by EEVC is that the Head Performance Criteria (HPC) should not exceed 1000. The HPC is determined by the following formula

$$\mathrm{HPC} = \left[\frac{1}{t_2-t_1}\int_{t_1}^{t_2} a\,dt\right]^{2.5} (t_2-t_1)\ \max$$

where a is the resultant acceleration of the headform as a multiple of "g", and t_1 and t_2 are any points in time (expressed in seconds) during the impact.

ENGINEERING REQUIREMENTS

In this section, the dynamics of the various impactors which are necessary to satisfy the various test criteria are considered, along with the magnitude and distribution of the impact forces which are needed to produce these dynamics. This in turn will lead to consideration of the engineering changes which may be needed in order to achieve compliance.

Lower Leg Impact Test

The draft specification imposes three sets of requirements for the bumper system design. Firstly, in order to limit the magnitude of the lower leg acceleration, as well as the inertia-based forces acting to bend and shear the knee element,. sufficient crush distance must be provided for the legform to decelerate on impact and sufficient energy-dissipation to limit the change of velocity, in other words to prevent spring-back.

Secondly, to limit the bending displacement of the knee, the distribution of force over the legform must be arranged to overcome the individual segments' tendency to pitch during the impact. This might be achieved by arranging for the impact force or forces to act closer to the segments centres of gravity, or by arranging some additional resistance near the extremities of the segment, to balance that applied close to the joint.

Thirdly, to limit the shear displacement of the knee, it is important to avoid a concentration of loading to one side of the joint. Either the force should be spread over the whole knee area, or else the separate forces above and below should be balanced.

The amount of crush space required to meet the first of these criteria can be estimated. A half-sine deceleration pulse for the lower leg from 40 km/h to zero (no recoil) with a peak of 150 g represents a deceleration distance of 66 mm [4]. Other pulse shapes, for example square-wave may result in slightly lower deceleration distance for a given velocity change, but these are difficult to achieve in practice. On the other hand, a half-sine is typical of the pulse shape which results from a round profile impactor penetrating a flat target surface and hence meeting an increasing resistive force.

Some of the deceleration distance may be accounted for by compression of the legform's foam covering. However, in practice it is unlikely that this could contribute much to the dynamics, since the foam readily compresses on impact.

Upper Leg Impact Test

The general requirements for the upper leg are similar to the above, in that sufficient intrusion distance must be allowed to limit the impact force (as measured in the total force at the beam supports), and contact forces must be distributed over the length of the beam so as to limit the bending moment at each location.

However, for this test, the effect of the vehicle geometry insofar as it affects the severity of the test conditions must also be considered. Generally speaking, increasing the bonnet leading edge height increases the impact speed and energy, whereas increasing bumper lead reduces them. The effect of these variables on impact angle cannot be quantified, since it may have a beneficial or detrimental effect, depending on the vehicle profile.

Given the link between vehicle geometry and test conditions, it is not possible to quantify the amount of impactor deceleration distance required for a general case as in the previous section. However, it is possible to derive some broad guidelines for typical examples of various types of vehicle. Taking a typical European small saloon car (see Table 1) with a bumper height of 575 mm, a bumper lead of 125 mm and a bonnet leading edge height of 775 mm, this would result in a 13.8 kg impactor mass and a speed of 9.58 m/s, corresponding to an energy of 633 J (see Table 2). Performing a similar calculation to that in the previous section, the minimum intrusion distance for a 4 kN total load at the impactor would be 203 mm [4].

Headform Impact Test

Although a more complex relationship exists between HPC and deceleration distance, it is possible again to calculate the deceleration distance needed to just achieve the limit. Taking a half-sine deceleration pulse shape as typical, a pulse with a peak of 123 g corresponds to an HPC of 1000, and this would experience a deceleration distance of 81mm from 40 km/h with zero recoil velocity [4]. The actual penetration of the headform into the panel would, of course, depend upon the angle of the impact, and this has been evaluated for typical examples of different classes of vehicles later in this paper (see Table 2).

EFFECT ON DIFFERENT CLASSES OF VEHICLE

In order to evaluate the effect of the proposed regulation on vehicle design, MIRA has conducted a design study [4] similar to that described above based on a selection of current models in each of the following vehicle classes:

- Small saloon car
- Medium saloon car
- Executive saloon
- 4x4
- Utility (people carrier and van)

Figure 4 illustrates typical configurations for each class of vehicle in the various tests, and in particular the available impact zone and angle of impact. Four points are immediately apparent from this diagram.

The first is the way in which the adult head impact zone has been restricted on the small saloon, through being limited to the area forward of the base of the windscreen. An even more extreme situation exists in the case of the utility vehicle; indeed, it is even possible that an adult head impact zone as currently defined may not exist on some cars, due to the 1500 mm wrap-around line falling behind the bottom edge of the windscreen.

The second is the apparent difficulty in achieving a satisfactory result in the lower leg test for 4x4 class vehicles, due to the bumper contacting the legform close to the top of the upper leg segment, with no support around the knee.

The third point is the coincidence of the upper leg impact zone and the child head impact zone on high-bonneted vehicles such as the 4 x 4 and utility classes. Given the relatively high energy of the upper leg test compared with the child headform, it is clear that there will be a conflict in designing to meet the requirements of these two tests. In other words, a bonnet which has a stiffness low enough to produce an acceptable child headform deceleration may not offer the stiffness necessary to satisfy the upper leg requirements without excessive intrusion.

The fourth point is similar to the above, but concerns the situation which exists in all vehicles at the boundary between the adult and child head impact zones, that is, along the 1500 mm "wrap-around" distance line. According to the draft specification, impacts by both types of impactor are possible along the boundary line between the zones, and therefore the area close to this line must be designed to satisfy both the adult and child criteria. Since the mass of the adult headform is roughly twice that of the child, the boundary zone must be designed with crush resistance which will satisfy the child head criteria, but with additional crush depth to absorb the additional energy of the adult headform. The result of this would be to approximately double the minimum crush zone depth to around 150 mm in this area.

Figure 5 superimposes typical crush zones on the outlines of vehicles in the various classes, based upon the minimum deceleration distances derived as above.

Table 1 summarises the results of the study in terms of typical critical dimensions and Table 2 in terms of the impact energy and required minimum deceleration distance of the impactor. This again shows that the typical shape of vehicles in the 4x4 class impose very severe test conditions in the upper leg test.

IMPLICATIONS FOR VEHICLE DESIGN

Having established the minimum thickness of crush zone needed to meet the requirements, the way the impact energy can be managed must be considered, in other words, how the vehicle surface and its underlying structure can be designed to control the resistance to penetration of the impactor, and so achieve an appropriate force or deceleration level. In most cases, it may not be possible to achieve or even

Table 1: Typical Dimensions by Vehicle Category [4]

Category	Front Shape	Bumper Height mm	Bumper Lead mm	Bonnet Edge Height mm	Bonnet Angle °
Small	3 box layout passenger car	575	125	775	14
Medium	3 box layout passenger car	525	125	750	12
Executive	3 box layout passenger car	550	125	775	11
4 x 4	2 box layout all terrain	650	175	1050	9
Utility	1 box layout van	575	175	850	29

Table 2: Energy Absorption and Crush by Vehicle Category [4]

	Small	Medium	Category Executive	4 x 4	Utility
Lower leg kinetic energy J	825	825	825	825	825
Lower leg minimum deformation mm	66	66	66	66	66
Upper leg kinetic energy J	633	573	675	941	824
Upper leg minimum deformation mm	203	184	216	308	265
Child head Kinetic Energy J	154	154	154	154	154
Child head minimum deformation mm	73	72	71	70	80
Adult head Kinetic Energy J	295	295	295	295	295
Adult head minimum deformation mm	80	79	79	78	81

approximate to the half-sine wave deceleration pulse on which the minimum thickness of the crush zone was based. In that case, there is no option other than to consider a deeper zone.

In nearly all present-day cars, there are hard components which lie just below the skin of the vehicle and have been positioned there by virtue of packaging constraints. These are, of course, the points which would be chosen for impact by the testing authority as representative of the most severe impact conditions. If the necessary crush space is to be created around these points, it will generally be necessary to either move the outer surface of the car outwards, or else change the shape of the underlying mechanical components so that they lie deeper below the surface. It is recognised that the major changes to powertrain and suspension systems which will be required to create this clearance without changing the outer profile of the vehicle will need considerable lead-time, and therefore it seems more likely that early vehicles designed to offer pedestrian protection will be rather more bulbous in shape than present-day cars.

Figure 6 outlines some of the practical changes which may have to be made to a typical small saloon car in order to meet the proposed specification. These are discussed in the next section, alongside some suggestions as to the engineering features which may be adopted to overcome the problems.

Table 3 details some of the individual features which may need to be redesigned to meet the requirements, and lists some of the potentially conflicting features which will need to be resolved with the new requirements.

POSSIBLE ENGINEERING SOLUTIONS

Front Bumper

This could be made deeper in profile to support the legform either side of the knee, and could be covered with a layer of energy-absorbing material to minimise the deceleration. By extending the bumper surface vertically downwards, or providing a secondary support bar vertically below the bumper, pitching of the lower leg segment may be reduced, and hence the bending at the knee joint. However, in such cases, care must be taken to avoid creating a feature which would exacerbate ankle injuries on impact. If a vertical surface is to be created, a grille or slats may need to be provided to maintain support for the leg across the cooling air aperture.

Headlamps

It is recognised that modern headlamp units are quite heavy and rigid, and it may be difficult to design sufficient energy-dissipation into them to satisfy the proposed upper-leg criteria. Such energy-dissipation might be incorporated into the headlamp unit mountings, but this may need to be accompanied by making the units lighter. An alternative solution may be to recess the units below the surface, perhaps in conjunction with a transparent cover to maintain a smooth aerodynamic profile.

Front Crossmember and Bonnet Latch

Most modern cars incorporate an upper crossmember positioned close to the bonnet leading edge. This serves to stiffen the vehicle front end structure and generally also supports the bonnet latch, as well as supporting the radiator, cooling fan and headlamps. Where space allows, this could be moved rearwards or downwards out of the crush zone, or else could be made in lighter material which would deform when struck by the upper legform. This may in turn require a change from a single bonnet latch to a twin latch arrangement, which might also allow a lighter bonnet structure (see below).

Wing Tops

High headform acceleration caused by direct contact with the hard seam at the junction of the inner and outer wings might be avoided by adopting a "wrap-over" style of bonnet, as fitted to many present 4 x 4 models. This would also help to eliminate a similar hazard in the form of the reinforcing members running along the sides of the bonnet.

Scuttle and Windscreen Lower Edge

Under the proposed directive, the rear edge of the head impact zone lies at the lower edge of the windscreen. It is possible that an impact point may be selected which lies exactly on this line, in which case the headform would effectively contact the glass.

Bonnet

In addition to the changes suggested above, there is likely to be further development needed to avoid hard headform impacts when striking bonnet reinforcements or underlying components in the engine compartment. One possible solution would be to design a sandwich-structure bonnet which uses an energy-dissipating core material such as foam or honeycomb below a thin metal skin. An alternative solution could be an active safety system such as an airbag, or pyrotechnic devices which raise the bonnet on impact sufficiently to provide the necessary deceleration zone. This in turn would require the development of an impact detection system which would trigger the device under the appropriate conditions.

In order to avoid hard head impact against the windscreen lower edge, the bonnet might be designed so that the rear edge overhangs the lower edge of the windscreen. This feature might also help to reduce the severity of head impacts against the wiper mechanism and scuttle.

Front Suspension System

In a typical McPherson strut front suspension system, the upper mounting point of the strut lies very close to the upper surface of the bonnet, and is a rigid part of the body structure. It will therefore constitute a difficult area from the point of view of head impact. Since the tops of the suspension towers invariably lie underneath the bonnet, an energy-dissipating bonnet which is adopted to protect hard points on the top of the engine may also be used to shield these zones in a similar way.

Engine Block

Depending upon the engine layout, there may be rigid parts which lie just below the bonnet skin. These could be the casings of engine auxiliaries such as alternators, power-steering pumps etc., or the drive belt pulleys for the same. Other parts may be suitable for manufacture in energy-dissipating materials, for example covers or inlet manifolds.

CONCLUSIONS

The provision of protection for pedestrians on impact seems set to be one of the dominant driving forces of automotive design for the European market over next few years. It is likely that this will be promoted as part of the type-approval requirements for cars and light commercial vehicles, as well as under the EuroNCAP scheme, and that the requirements will be very similar to the draft specification drawn up by the EEVC.

Achieving the test requirements will not be easy, and may demand a major re-appraisal of the design of many parts of the car front end, including the bumper, bodyshell, wings and bonnet in the short term and possibly the front suspension and powertrain in the long term. Certain classes of vehicle, notably off-roaders, may present particularly difficult problems for the designer, whereas other types may be easier to accommodate.

REFERENCES

1. HARRIS, J. (EEVC Working Group 10) "A Study of Test Methods to Evaluate Pedestrian Protection for Cars" ,13th International Conference on Experimental Safety Vehicles, Paris, Nov 91, Paper No 91-S3-O-06

2. European Commission Document III/5021/96/EN, "Proposal for a European Parliament and Council Directive Relating to the Protection of Pedestrians and Other Road Users in the Event of Collision with a Motor Vehicle", February 1996

3. WILLIAMS, D.A. : "European New Car Assessment Programme (Euro-NCAP) Frontal and Side Impact Testing Protocol" Transport Research Laboratory Project Report PR/SE/249/97

4. DAVIES, R. & CLEMO, K.: MIRA Project Report No 97-456502: "Study of Research into Pedestrian Protection, Costs and Benefits", 21/8/97 (Published by European Commission Directorate General III)

Table 3: Potential Design Conflicts

Feature	Conflict
Front bumper	Resistance to light collision damage Vulnerability to bird strike etc Aerodynamic drag Number plate mounting Airbag triggering pulse Cooling air flow Approach angles Auxiliary lamps Towing eyes
Headlamps	Positioning Mounting rigidity Aerodynamic drag Scuff resistance of lens / cover Wash / wipe system Distortion in bumper impact test
Radiator	Positioning Cooling airflow Fatigue strength of mountings Damage in bumper impact test
Bonnet	Rigidity Latch strength / vehicle security Vulnerability to bird strike etc Sit-on / lean-on damage Resistance to high engine compartment temperatures Access to front of engine compartment Damage in bumper impact test
Bonnet latch	Rigidity Resistance to slamming loads Positioning Adjustment (2-latch systems) Windscreen intrusion by bonnet
Front crossmember	Body torsional rigidity Frontal offset / angled crash performance Body fatigue
Bonnet hinges	Rigidity Resistance to wind loads Windscreen intrusion by bonnet
Windscreen	Lower edge mounting
Windscreen wipers	Mounting rigidity
Powertrain	Positioning Rigidity NVH Inlet air flow Belt drives Auxiliaries
Front suspension	Upper mounting rigidity Geometry
Front bulkhead	Upper crossmember rigidity Body torsional rigidity
Cabin	Forward field of view
Vehicle (general)	Cost of collision repair (Insurance Test)

Figure 4: Typical Test Configurations by Vehicle Category
(Models shown are for illustration only)

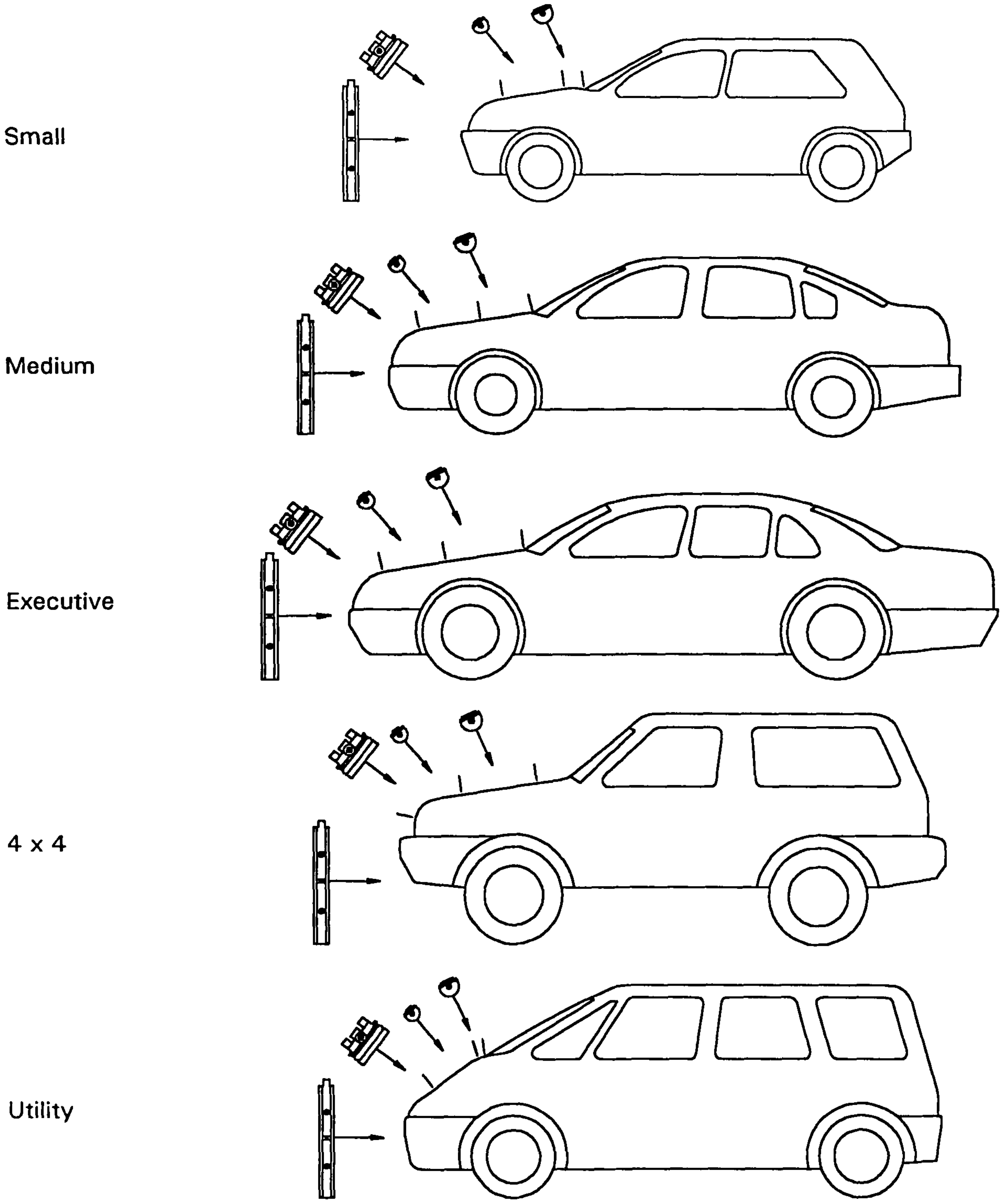
Small
Medium
Executive
4 x 4
Utility

Figure 5: Typical Crush Zones by Vehicle Category
(Models shown are for illustration only)

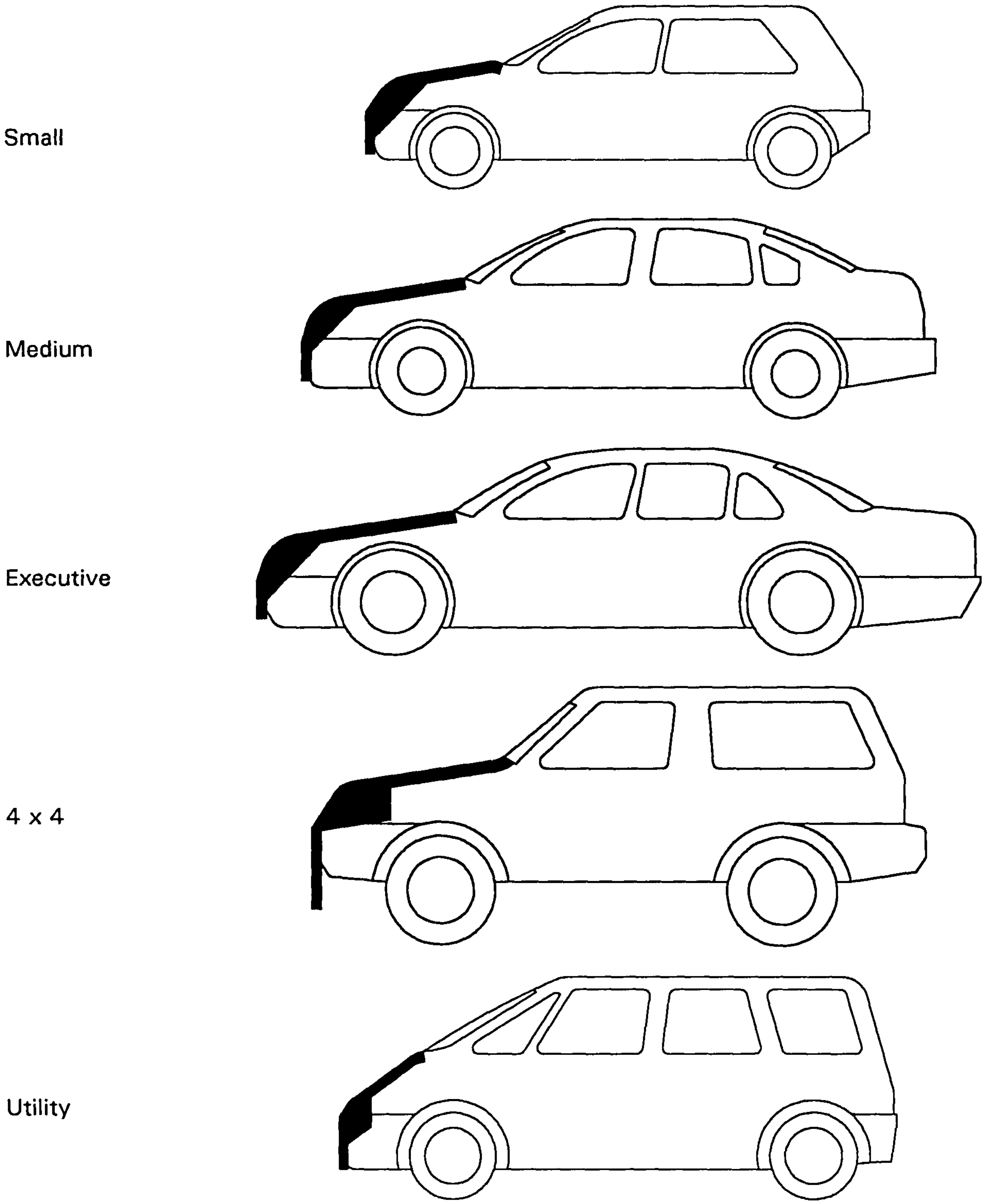
Small
Medium
Executive
4 x 4
Utility

Figure 6: Practical Vehicle Design Changes

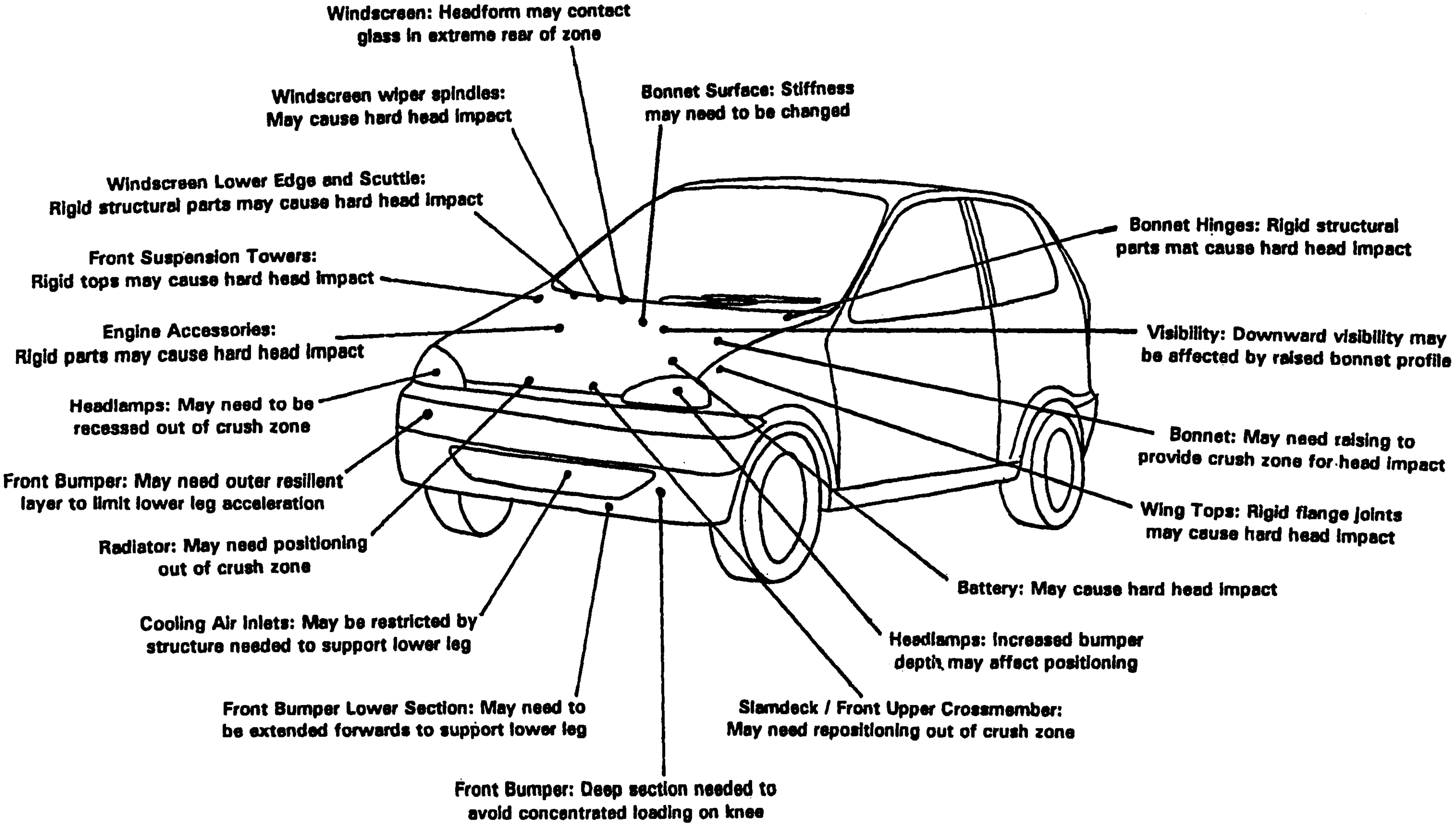
Windscreen: Headform may contact glass in extreme rear of zone
Windscreen wiper spindles: May cause hard head impact
Bonnet Surface: Stiffness may need to be changed
Windscreen Lower Edge and Scuttle: Rigid structural parts may cause hard head impact
Front Suspension Towers: Rigid tops may cause hard head impact
Bonnet Hinges: Rigid structural parts mat cause hard head impact
Engine Accessories: Rigid parts may cause hard head impact
Visibility: Downward visibility may be affected by raised bonnet profile
Headlamps: May need to be recessed out of crush zone
Bonnet: May need raising to provide crush zone for head impact
Front Bumper: May need outer resilient layer to limit lower leg acceleration
Wing Tops: Rigid flange joints may cause hard head impact
Radiator: May need positioning out of crush zone
Battery: May cause hard head impact
Cooling Air Inlets: May be restricted by structure needed to support lower leg
Headlamps: Increased bumper depth may affect positioning
Front Bumper Lower Section: May need to be extended forwards to support lower leg
Slamdeck / Front Upper Crossmember: May need repositioning out of crush zone
Front Bumper: Deep section needed to avoid concentrated loading on knee

CHILD RESTRAINT INFORMATION IN THE NATIONAL AUTOMOTIVE SAMPLING SYSTEM CRASHWORTHINESS DATA SYSTEM

Seymour D. Stern
National Highway Traffic Safety Administration
United States
Paper Number 98-S10-O-21

ABSTRACT

This paper will present a summary of child seat data in crashes. Use patterns between front and rear seats by child seat type are presented. Reductions in injury level is shown by the proper use of child seats.

INTRODUCTION

Since 1988, the National Automotive Sampling System (NASS) Crashworthiness Data System (CDS) has collected information on the use of child restraints in towed light vehicles involved in crashes. Nine years of child restraint data are available on 1,396 crashes involving 1,801 child restraints in 1,420 towed light vehicles. This represents approximately 705,000 crashes involving 810,000 child restraints in 723,000 towed light vehicles.

The children in child seats in the NASS CDS are 9 years old and under and weigh 29 kgs. or less. The total NASS CDS crash involved child population in this age/weight range over the years 1988-1996 is 3,738,000. Approximately 20% of these children are in child seats, 30% are restrained by a seat belt alone, and 50% have either no restraint use or the restraint use is unknown.

This paper presents a study of the involvement of child safety seats in towed light vehicles (car, light truck, or van) involved in a police reported crash. All of the analysis that follows is based solely upon this data. The presence of seats and how they are being used is only representative for the police reported tow away crashes indicated, not the vehicle-in-use population at large.

Information available for study includes the make and the type of seat (infant, toddler, booster, etc.); the proper and improper use of manual and automatic belts with the seats; the orientation of the child seats; and the presence of, addition of, and use or non-use of a harness, tether, or shield with the seat.

Child Seat Types In Use

The type of child seat is not known for a large number of vehicles because the seat cannot be viewed or the child seat owner cannot sufficiently describe it for a correct classification to be made.

Seats are classified as infant, toddler, convertible, and booster. An infant seat is designed to only face the rear of the vehicle and has a maximum capacity of 8-9 kgs. A toddler seat is designed to only face the front of the vehicle and to carry a child weighing approximately 9-23 kgs. A convertible seat is designed to face the front or rear of the vehicle and to carry a child ranging from birth to approximately 23 kgs. A booster seat is designed as a forward facing platform without a back.

The table below (Table 1) shows the distribution of child seat types used in this study. The 29% unknown rate is attributable to the factors mentioned previously.

Table 1.
Child Seat Type In The NASS CDS
1988-1996

Seat type	Nine Year Total Unweighted Count	Yearly Average Weighted Count	Yearly Average Weighted Percent
Infant	278	12211	13.6%
Toddler	355	18905	21.0%
Convertible	482	23044	25.6%
Booster	166	9291	10.3%
Other	9	330	0.4%
Unknown	511	26169	29.1%
Total	1801	89950	

Use of seat belts with child seats

The NASS CDS provides for the coding of proper and improper use of child seats. Unless the field researcher can view the child seat in the vehicle, the only source of information for the use of seatbelts with the child seat is from interviews conducted. This can be demonstrated by the 99% level of reported proper seat belt use with child seats. In the future we may be forced to drop the collection of this information.

Row placement of child seats

Most child seats can be found in the rear rows of the vehicle. This is a trend that can be seen to be gradually increasing from 59% in the rear seat row (1988-1990) to 66% (1994-1996) (Table 2).

Table 2.
Child Seat Distribution By Row
Yearly Average Weighted Count

	88-90	91-93	94-96	Total
Front	40%	41%	34%	38%
Rear	59%	59%	66%	62%

The first seat row of the vehicle is equally likely to contain a forward or rearward facing child seat (Table 3). However, rearward facing child seats are most likely to be found in the rear seat rows of the vehicle (71%) (Table 4).

Table 3.
Seat Row Distribution of Child Seats
Yearly Average Weighted Count

	Forward Facing	Rearward Facing	Unknown Orientation
First Row	42%	47%	11%
Second Row	8%	70%	22%

Table 4.
Child Seat Orientation By Row
Yearly Average Weighted Count

	First Row	Second Row
Forward Facing	76%	24%
Rearward Facing	29%	71%

The child seat type most likely to be in the first seat row is a convertible seat (28%), while the second seat row more likely contains a toddler or convertible seat (26%, 24%) (Table 5). However, when considering the use of the various types of seats, they have similar use patterns (40% in front, 60% in back), except toddler seats used 24% in the front seat and 76% in back (Table 6).

Table 5.
Seat Distribution of Child Seat Types
Yearly Average Weighted Count

Row	Infant	Toddler	Convert.	Booster	Unk
First	16%	14%	28%	11%	32%
Second	12%	26%	24%	10%	27%

Table 6.
Child Seat Type Distribution
Yearly Average Weighted Count

	First Row	Second Row
Infant	44%	56%
Toddler	24%	76%
Convertible	41%	59%
Booster	40%	60%

Harness, shield, and tether use

Child seats can come equipped with a harness, shield, tether, or some combination of these. NASS CDS field researchers note the presence and use of these features.

Harnesses are the feature most frequently present, except booster seats where shields predominate (Figure 1).

Shields are not present in about half the infant seats found in the crashes and are most often used with convertible seats (75%), while least used with booster seats (Figure 2).

Tethers are not very prevalent in the child seats found in the crashes. They were not present in more than 50% of the infant, convertible, and booster seats. When present, their use was low. The highest use rate was in convertible seats (31%) (Figure 3).

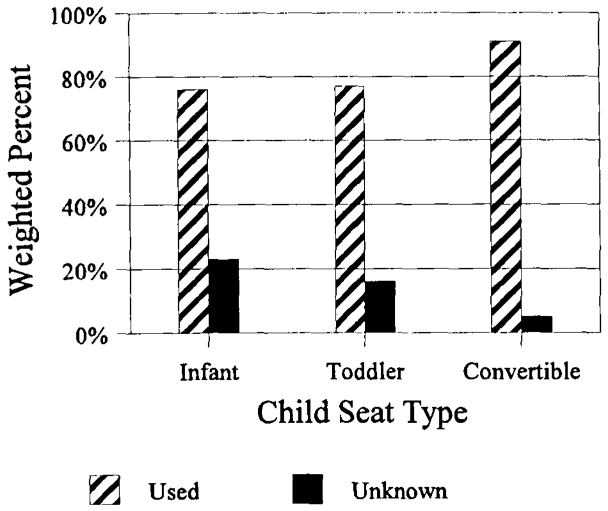

Figure 1. Child seat harness use, yearly average weighted percent.

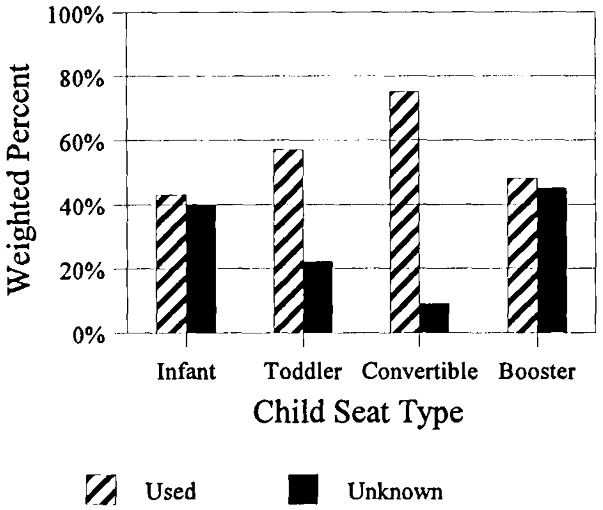

Figure 2. Child seat shield use, yearly average weighted percent.

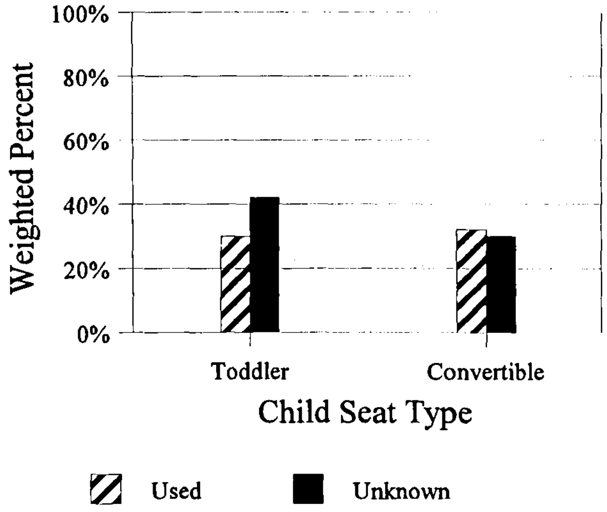

Figure 3. Child seat tether use, yearly average weighted percent.

Injury level by child seat feature used

When the available safety features of the child seat are used, there is a reduction in the maximum level of injury sustained by the child. All three features have an equivalent effect on maximum injury reduction. However, when the child is not using the harness that is available more severe injuries will result than if the shield or tether is not used (Tables 7,8,9).

Table 7.
Maximum Injury When Harness Used
Yearly Average Weighted Count

Harness Use	Max AIS 0	Max AIS 1+
Used	75%	25%
Not used	20%	80%

Table 8.
Maximum Injury When Shield Used
Yearly Average Weighted Count

Use	Max AIS 0	Max AIS 1+
Used	78%	22%
Not used	59%	41%

Table 9.
Maximum Injury When Tether Used
Yearly Average Weighted Count

Use	Max AIS 0	Max AIS 1+
Used	85%	15%
Not used	56%	44%

CONCLUSION

Information is available in the NASS CDS that indicates that not all features of child seats are used nor are the seats themselves placed properly in the rear seat of the vehicle. However, the data does show that their proper placement in the rear has improved from 1988-1996.

MOTORCYCLE HELMET TEST HEADFORM AND TEST APPARATUS COMPARISON

David R. Thom
Hugh H. Hurt, Jr.
Terry A. Smith
Head Protection Research Laboratory
United States

Paper Number 98-S10-P-29

ABSTRACT

Internationally, there are two types of headforms used for impact attenuation testing of motorcycle helmets. These two types of test headforms follow specifications established by the International Standards Organization (ISO), or the U.S. Department of Transportation (DOT). Both headforms are low resonance, rigid castings, but they differ in size, shape and weight. The headforms are supported by a rigid guide assembly that limits their motion to the vertical direction only. Different impact locations are obtained by adjustment of the headform on a spherical ball joint. Performance criteria are based on acceleration time history measurements from a uniaxial accelerometer located at the headform center of mass.

A second variation on the ISO headform is found in some European helmet standards that utilize an unrestrained headform instrumented with a triaxial accelerometer. These constrained headforms respond to impact with motion in many directions and performance criteria are based on the resultant of three axis acceleration time histories.

Impact attenuation tests were performed on 180 motorcycle helmets of three different designs and under environmental conditions specified by helmet performance standards. Selected tests were recorded on high-speed (1000 Hz) videotape for motion analysis. Test apparatus designs differ greatly and guided free-fall apparatus with restrained headforms produces consistently more rigorous tests than apparatus without headform guide or restraint. Significant differences were also found between DOT and ISO headforms for both peak acceleration and dwell time on flat anvil impacts when tested on the DOT-type monorail apparatus.

INTRODUCTION

Table 1 summarizes the impact attenuation test methods and failure criteria for major international standards. Current FMVSS No. 218 impact energy levels are realistic, with the flat anvil impacts corresponding to the 90th percentile of all traffic accident impacts (Hurt, Ouellet & Thom, 1981). Double impacts that exist as part of the standard tests are not typical of accident events, but the requirement is an acceptable procedure which provides a margin of safety for the consumer. While there is always the temptation to increase the impact energy level with the expectation of providing greater protection, any change that is without support by research may adversely affect accident performance. For example, if the impact energy of the standard test were increased, the typical design change would be an increase in liner density. These changes could provide the greater impact attenuation but may increase headform accelerations for impacts less than the standard test (Smith, 1997; Thom & Hurt, 1992, Mills & Gilchrist, 1991).

The scientific community generally concurs that some relationship exists between head impact acceleration, time duration and tolerance to head injury. However, the exact nature of this relationship has not been clearly defined. Many methods currently consolidate the relationship between headform acceleration and time duration, for example, Head Injury Criterion (HIC) and Gadd Severity Index (SI), yet all methods have been criticized regarding their application to head protection (Newman, 1975, 1982). Until an acceptable means of analysis is developed, time duration appears to be acceptable since it does have some basis in human tolerance (Ono, 1980). However, the most frequent impact attenuation failure of otherwise well-qualified helmets is to exceed the 200g dwell time limit.

Table 1 also lists the type, sizes and weights of the test headforms used by major international helmet performance standards. Note that the majority of these standards use ISO headforms as specified in standard EN960, 1995 or its predecessor standard, ISO/DIS 6220, 1983.

Considerable work has been done over the years comparing the test performance of the twin guide-wire test apparatus and the monorail apparatus (Henderson, 1975; Bishop, 1989). Both of these systems hold the

Table 1.
Summary of International Helmet Standards

Standard	Year	Drop Test Apparatus	Headforms	Headform Sizes	Drop Assembly Weight	Anvils	Impact Criteria	Number of Impacts	Failure Criteria
FMVSS No. 218	1988	Monorail	DOT	Small Medium Large	3.5 kg 5.0 kg 6.1 kg	Flat Hemi	Velocity: 6.0 m/s 5.2 m/s	Two @ each of 4 sites	< 400g 2.0 msec @ 200g 4.0 msec @ 150g
ANSI Z90.1	1992	Monorail or Guide-Wire	DOT or ISO	Small Medium Large or A,E,J,M	5.0 kg**	Flat Hemi	Velocity: Flat & Hemi: 1st 6.9 m/s 2nd 6.0 m/s	Two @ each of 4 sites	≤ 300g
AS 1698	1988	"Guided Fall"*	Magnesium AS 2512.1 (DOT)	A B C D	3.5 kg 4.0 kg 5.0 kg 6.0 kg	Flat Hemi	Drop Height: 1830 mm 1385 mm	Two @ each of 4 sites	≤ 300g 3.0 msec @ 200g 6.0 msec @ 150g
BS 6658	1985	"Guided Fall"*	ISO	A,E,J,M	5.0 kg	Type A Flat Hemi Type B Flat Hemi	Velocity: 1st 7.5 m/s 2nd 5.3 m/s 1st 7.0 m/s 2nd 5.0 m/s 1st 6.5 m/s 2nd 4.6 m/s 1st 6.0 m/s 2nd 4.3 m/s	Two (same anvil) @ each of 3 sites Two (same anvil) @ each of 3 sites	≤ 300g (Multi-part shells shall remain intact)
CAN3-D230	1985	"Guided Fall"*	ISO	A,E,J,M	5.0 kg	Flat Hemi	Velocity: 1st 5.1 m/s 2nd 7.2 m/s 1st 4.3 m/s 2nd 6.1 m/s	Two @ each of 4 sites	Low Energy: ≤ 200g High Energy: ≤ 300g
Snell M-95	1995	Monorail or Guide-Wire	ISO	A,E,J,M	≥ 5.0 kg, ≤ 6.5 kg	Flat Hemi Edge	Energy: Flat & Hemi 1st 150J 2nd 110J Edge 150J	Flat & Hemi: Two each @ 4 sites Edge: One impact @ one site	≤ 300g
ECE 22.4	1995	Unrestrained Headform with Tri-Axial Accelerometer	ISO	A E J M O	3.1 4.1 4.7 5.6 6.0	Flat Curb	Velocity: 7.5 m/s for both anvils	4 sites per helmet in sequence with 5th test @ 4 m/s or 8.5 m/s	Resultant ≤ 275g HIC ≤ 2400

* Apparatus not further specified

** Small & Large DOT headforms not currently available in 5 kg.

headform relatively rigid during the impact and utilize a single axis accelerometer. FMVSS No. 218 specifies the use of the monorail test apparatus.

The ECE 22 standard for motorcycle helmets requires the use of a completely different type of test system (ECE 22.4, 1995). This system carries an unrestrained headform equipped with a triaxial accelerometer in a headform support assembly. In contrast to both the twin guide-wire and the monorail, the ECE apparatus allows unrestrained motion of the test headform during the impact attenuation test. Search of the literature did not locate any record of side-by-side comparison of the monorail or twin guide-wire and the ECE basket type apparatus.

METHODS

Baseline Tests and Test Criteria

The research was based upon comprehensive baseline testing of a large number of helmets to the current FMVSS No. 218. The test program consisted of:

i. 72 helmets selected for three levels of expected performance
ii. three headform sizes
iii. all environmental conditions of the standard.

These tests were conducted on the monorail test apparatus shown in Figure 1.

Figure 1.
Monorail Test Apparatus with DOT Medium Headform and Flat Anvil

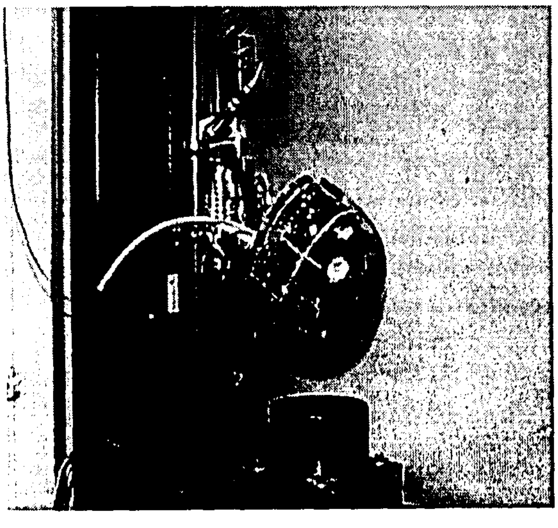

In order to provide test data for all combinations of impact anvil type and impact location, duplicate samples of all helmets were used. This "double" test provided impact tests against both anvil configurations (flat and hemispherical) at four locations on each helmet. Subsequent tests made for comparative purposes were assured of complete data for direct comparison.

Alternative Headforms

HPRL conducted comprehensive tests of identical 36 helmets using International Standards Organization (ISO) headforms). These tests were conducted on the monorail test apparatus. But this test series duplicated the baseline tests and used ISO headforms. Table 2 gives data for the comparison of the two types of headforms. Figure 2 shows the three types of headforms in equivalent sizes (ISO J and DOT Medium). The ISO headforms are most closely comparable by size rather than weight. While there is a much smaller, size "A" ISO headform, it is applicable to very small children who are not part of the motorcycle user population. There is an extra large (62 cm) ISO size “O” headform, but there is no comparable extra large DOT headform size.

Table 2.
Test Headform Comparison

Headform	Circumference	Weight
DOT Small	49 cm	3.5 kg
DOT Medium	56 cm	5.0 kg
DOT Large	60 cm	6.1 kg
ISO E	54 cm	4.1 kg
ISO J	57 cm	4.7 kg
ISO M	60 cm	5.6 kg

Figure 2.
Test Headforms (DOT Medium, ISO J)

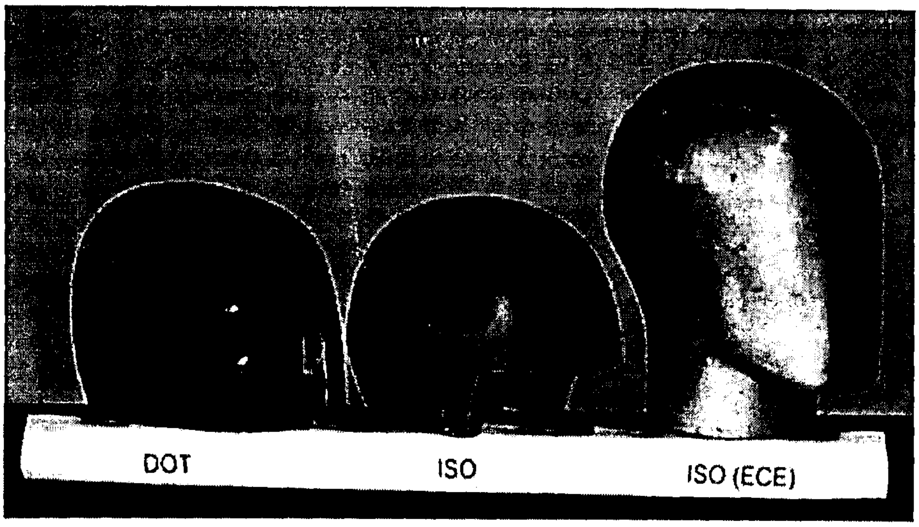

Alternative Test Apparatus

Selected tests of 36 equivalent helmets using the guided free-fall test apparatus as specified by ECE 22, etc. Because of the mechanics of this test, the ISO test headforms include the neck, however they have the same weights as the ISO headform impact assembly (see Figure 2).

The ECE-type test machinery and electronic instrumentation are considerably more complicated than those currently required by FMVSS No. 218. The ECE apparatus used in this work is shown in Figure 3. The helmeted headform is guided only until impact, then unrestrained rebound response is limited by the basket walls. Triaxial accelerometer instrumentation is required with the ECE test, and then the resultant of the three-axis peak acceleration is computed.

Alternative Impact Velocities

These tests were performed on an additional 36 helmets for direct comparison to the Baseline tests. These tests following the current FMVSS No. 218 specifications and used the same locations and anvils as the Baseline 1 tests. The only difference in the tests was increased impact velocity for the first of two impacts at each location. The results of this test series determined the impact velocities used for the following tests.

Figure 3.
ECE-Type Test Apparatus

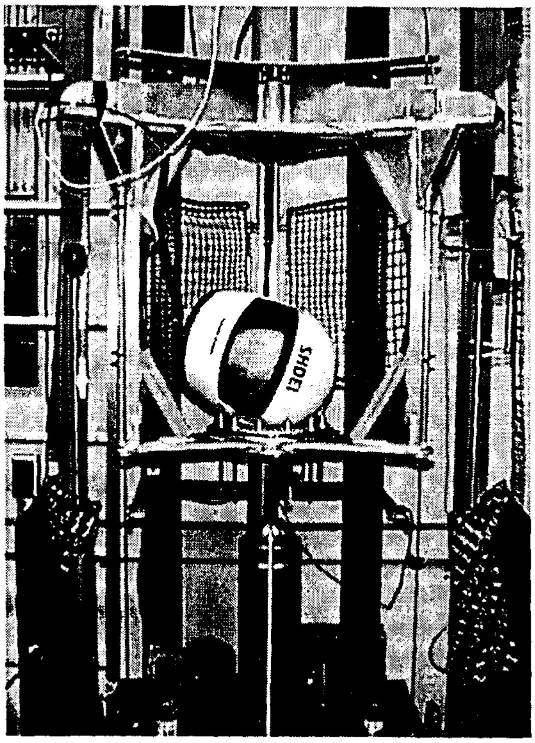

Selection of Impact Locations

HPRL performed preliminary tests to determine the effect of modifying full-facial coverage helmets by removal of the chinbar. Five full-facial coverage, polycarbonate shell helmets were tested on the flat anvil with varying degrees of modification as noted below. Helmets 1-4 were tested squarely on the sides and mid-sagittal at front and rear (0, 90, 180, 270 degrees).

- Helmet 1 No modification (1401 gm as tested).
- Helmet 2 Chinbar removed prior to any testing (1173 gm).
- Helmet 3 Lower portion of helmet removed, leaving the test area only intact (809 gm).
- Helmet 4 No modification for first three impacts (1401gm), chinbar removed to allow center of brow impact (1144 gm).
- Helmet 5 No modification, impacts at "corners" of helmet (50, 145, 210, 310 degrees—impact locations accessible without modification of helmet, 1399 gm).

Table 3 shows the results of these DOT flat anvil tests. The peak acceleration results vary within impact location by 0.8% to 7% for all tests but one (front impact #1, 11%) including the highly modified helmet No. 3. This variation is unremarkable and far less than the 20-24% difference shown between critical side and sub-critical "corner" impact locations.

In order to minimize any question of the effect of chinbar removal on overall results, the first three impact tests on each helmet were done with the helmets completely intact. The chinbar was then removed for the fourth and final test at the center of the brow.

High-Speed Video Analysis

A series of impact tests with the ECE test apparatus and monorail test apparatus were conducted using a Kodak Ektapro high speed video system which captured the entire helmet impact sequence at a rate of 1000 frames per second.

Test Helmet Construction

Representative helmets of those tested in this work were disassembled and their construction details are noted in Table 4.

Table 3.
Effect Of Impact Location On Peak Headform Acceleration

	Condition	**Location**	**Right #1**	**Right #2**	**Rear #1**	**Rear #2**	**Left #1**	**Left #2**	**Front #1**	**Front #2**
Helmet 1 ***	OEM	Peak g	212	252	219	253	201	246	**	**
		T@200g	1.0	2.6	0.9	2.7	0.1	2.7	**	**
Helmet 4 ***	OEM*	Peak g	208	252	217	250	215	245	178	222
		T@200g	0.9	2.6	0.8	2.9	0.4	2.7	0.0	1.8
Helmet 2	CB removed	Peak g	207	240	207	238	224	260	175	224
		T@200g	0.6	2.4	0.4	2.9	0.6	2.7	0.0	1.9
Helmet 3	Test Area	Peak g	200	227	207	242	205	243	186	224
		T@200g	0.1	2.1	0.6	2.0	0.7	2.2	0.0	1.9
		Location	**Right Front #1**	**Right Front #2**	**Left Front #1**	**Left Front # 2**	**Left Rear #1**	**Left Rear #2**	**Right Rear #1**	**Right Rear #2**
Helmet 5	OEM	Peak g	167	208	173	206	196	227	216	265
		T@200g	0.0	0.9	0.0	0.2	0.0	2.7	0.9	2.9

* Helmet intact for first 3 impacts, chinbar removed for last impact at brow
** No impact possible due to mechanical interference of monorail apparatus
*** Helmets and impacts identical for first 3 impacts

Table 4.
Test Helmet Construction

			HELMET SHELL		HELMET LINER			
Group	Coverage	Helmet Size	Shell Material	Shell Thickness (mm)	Liner Weight (gm)	Liner Volume (ml)	Density (Kg/cu.m..)	Nominal Thickness (mm)
A	Partial	XS	ABS	5.0	110	2450	45	30
A	Partial	M	ABS	5.0	131	2250	58	35
A	Partial	XL	ABS	5.0	113	2000	57	25
B	Full	XS	Polycarbonate	3.8	147	2900	51	30
B	Full Face	L	Polycarbonate	3.8	222	3700	60	35
B	Full Face	XL	Polycarbonate	3.8	183	3100	59	35
C	Full Face	XS	Fiberglass and Polyester Resin	3.8	136	4250	32	38
C	Full Face	M	Fiberglass and Polyester Resin	3.8	124	3500	35	36
C	Full Face	L	Fiberglass and Polyester Resin	3.8	121	3700	33	32

RESULTS

Peak Headform Acceleration by Test Groups

Table 5 lists the summary results and statistical significance of the peak headform accelerations for the test groups for the anvil configurations. All peak headform accelerations above 300g occurred for impacts at the center of the brow (front) location.

Test Headforms: DOT FMVSS No. 218 vs. International Standards Organization. These tests of DOT FMVSS No. 218 headforms (AV) and International Standards Organization (ISO) headforms (HF) are at the higher impact velocities specified in Table 6. The only variable between these tests is the headform type. For flat and hemispherical anvil tests combined, there was no statistically significant difference of peak headform accelerations (see Table 5). However, the flat anvil tests did show a statistically significant increase for the ISO headforms. The hemispherical anvil tests showed a slight decrease in mean peak headform acceleration that was not statistically significant.

Test Apparatus: Monorail vs. ECE-Type. Comparison of the ISO test headform (HF) group to the Alternative Apparatus (AA) group allows a direct comparison of test equipment, since both groups used ISO headforms and the higher impact velocities noted in Table 6. The result was a statistically significant 33g reduction of overall peak acceleration (see Table 5). This reduction is primarily due to decreased accelerations for the flat anvil tests, a difference of 52g. The hemispherical anvil test results involved much lower peak accelerations and were not statistically different.

Test Apparatus: Monorail Using DOT Headforms vs. ECE-Type. All peak accelerations shown in Table 5 were significantly lower on the ECE-Type apparatus. Unlike the apparatus comparison with ISO headforms (HF vs. AA), these tests showed similar reductions of peak acceleration, averaging 26g for both flat and hemispherical anvils.

Increased Impact Velocity. The current FMVSS No. 218 specifies impact velocity of 6.0 m/s for flat anvil impacts (both first and second impacts at each site) and 5.2 m/s for both hemispherical anvil impacts. The increased velocity test series used a flat anvil test velocity of 6.9 m/s for the first impact and retained the original 6.0 m/s for the second impact at each site. The hemispherical anvil test velocity was increased to 6.0 m/s for the first impact and retained the original 5.2 m/s for the second impact at each site. These velocities and the increased impact energies for the different test headforms are shown in Table 6.

Higher impact velocities showed statistically significant increases in peak acceleration for both flat and hemispherical anvils when compared to the baseline tests. There is a greatly increased incidence of failure of all impact attenuation criteria, with the mean value for headform acceleration increasing 34g (hemispherical anvil). The helmets also begin to show high peak accelerations in locations other than the brow at these higher impact velocities.

Dwell Time Differences by Test Groups. The various test groups were compared for the statistical differences between dwell times at 150 and 200g. Table 7 shows the summary of these comparisons.

Dwell Time at 150g. It is important to note that this criterion of helmet impact performance has never been a critical measure. In the current FMVSS No. 218, essentially any helmet which succeeds in qualifying to the 200g-2.0 msec. limit will also qualify to the 150g-4.0 msec. limit. In the 576 test impacts of the Baseline tests, there was only one exceedance of the 4.0 msec. limit. In subsequent tests with greater impact velocity, there were more frequent exceedance of the 4.0 msec. limit at 150g (see Table 8). These comparisons show statistically significant differences for several groups comparing velocity and test equipment.

Table 5.
Peak Headform Acceleration by Test Groups

Test Type	Test Group	Anvil	Mean Peak Acceleration	t-value	Significance
Baseline 1 (B1) vs. Baseline 2 (B2)	Baseline 1	Flat & Hemi	173	0.54	0.590
	Baseline 2	Flat & Hemi	170		
	Baseline 1	Flat	209	0.31	0.756
	Baseline 2	Flat	210		
	Baseline 1	Hemispherical	137	1.34	0.180
	Baseline 2	Hemispherical	130		
Baseline 1 (B1) vs. Increased Velocity (AV)	Baseline 1	Flat & Hemi	173	4.93	**0.000**
	Incr. Vel.	Flat & Hemi	201		
	Baseline 1	Flat	209	6.22	**0.000**
	Incr. Vel.	Flat	228		
	Baseline 1	Hemispherical	137	-3.84	**0.000**
	Incr. Vel.	Hemispherical	174		
ISO Headforms (HF) vs. DOT Headforms (AV)	ISO	Flat & Hemi	210	1.37	0.171
	DOT	Flat & Hemi	201		
	ISO	Flat	252	5.53	**0.000**
	DOT	Flat	228		
	ISO	Hemispherical	167	-0.59	0.556
	DOT	Hemispherical	173		
Monorail, ISO Headforms (HF) vs. Alternate Apparatus (AA)	Monorail	Flat & Hemi	210	5.12	**0.000**
	ECE	Flat & Hemi	177		
	Monorail	Flat	252	11.79	**0.000**
	ECE	Flat	200		
	Monorail	Hemispherical	167	1.27	0.205
	ECE	Hemispherical	154		
Monorail, DOT Headforms (AV) vs. Alternate Apparatus (AA)	Monorail	Flat & Hemi	201	-4.51	**0.000**
	ECE	Flat & Hemi	175		
	Monorail	Flat	228	-7.87	**0.000**
	ECE	Flat	200		
	Monorail	Hemispherical	173	-2.42	**0.016**
	ECE	Hemispherical	149		

Table 6.
Increased Impact Velocity and Energy

Headform (Weight)	Flat Anvil Velocity 1 (m/s)	Energy (Joules)	Flat Anvil Velocity 2 (m/s)	Energy (Joules)	Hemi Anvil Velocity 1 (m/s)	Energy (Joules)	Hemi Anvil Velocity 2 (m/s)	Energy (Joules)
DOT Small (3.5 kg.)	6.9	84	6.0	63	6.0	63	5.2	47
DOT Medium (5.0 kg.)	6.9	119	6.0	90	6.0	90	5.2	68
DOT Large (6.1 kg.)	6.9	145	6.0	110	6.0	110	5.2	82
ISO E (4.1 kg.)	6.9	98	6.0	74	6.0	74	5.2	55
ISO J (4.7 kg.)	6.9	112	6.0	85	6.0	85	5.2	64
ISO M (5.6 kg.)	6.9	133	6.0	101	6.0	101	5.2	76

Dwell time at 200g—Baseline Tests. The two baseline tests (B1, B2) show no overall difference when data for both flat and hemispherical anvils are combined for comparison. However, when the data for the two anvils are separated, there is a statistically significant difference between the hemispherical anvil test results, due to the increased vulnerability of the front (brow) to the more aggressive hemispherical anvil.

Dwell time at 200g—DOT vs. ISO Headforms. The ISO headforms overall produced a statistically significant increase in dwell time at 200g. In particular, this was due to the significant increase of dwell time on the flat anvil impacts. Hemispherical impacts were not significantly different.

Dwell time at 200g—Monorail vs. ECE-Type. The results show a statistically significant reduction in dwell time at 200g for the flat anvil tests. This is one of the most dramatic reductions in these tests, from a mean of 2.03 msec. for the monorail with ISO headforms to 0.594 msec. on the ECE apparatus. There was no statistically significant difference between results for the hemispherical anvil tests.

Dwell time at 200g—Monorail Using DOT Headforms vs. ECE-Type. As with the previous comparison of headform types with alternative test apparatus (HF vs. AA), there was a statistically significant decrease in the dwell times on flat anvil tests, but no statistically significant difference for the hemispherical anvil tests.

Summary of Test Criteria for All Test Groups. Table 8 summarizes the count and percentage of the total number of tests for any failures of test criteria for the seven test groups. Note that this summary table combines all helmet types and sizes, and counts each of the 1440 impact tests. Note that dwell times at 200g are included at several values: 2.0, 2.2, 2.4, 2.6, and 2.8 msec. The total number of impacts exceeding 2.0 msec @ 200g is 33 (5.7% of 576 impacts) for the Baseline tests. The number of impacts exceeding 2.2 msec @ 200g is 23 (4.0%): the majority (69.7%) of the impacts failing at 2.0 msec still fail at 2.2 msec.

Table 7.
Dwell Time Differences Between Test Groups

Test Type	Test Group	Anvil	Mean Time @ 150g	t value	Significance	Mean Time @ 200g	t value	Significance
Baseline 1 (B1) vs. Baseline 2 (B2)	Baseline 1	Flat & Hemi Combined	1.717	1.83	0.670	0.446	1.19	0.236
	Baseline 2	Flat & Hemi Combined	1.484			0.373		
	Baseline 1	Flat	3.208	5.23	**0.000**	0.855	1.06	0.292
	Baseline 2	Flat	2.759			0.747		
	Baseline 1	Hemispherical	0.225	0.29	0.773	0.037	2.51	**0.013**
	Baseline 2	Hemispherical	0.208			0.000		
Baseline 1 (B1) vs. Increased Velocity (AV)	Baseline 1	Flat & Hemi	1.717	-1.65	0.100	0.446	-5.35	**0.000**
	Increased Velocity	Flat & Hemi Combined	1.936			0.855		
	Baseline 1	Flat	3.208	-4.58	**0.000**	0.855	-6.46	**0.000**
	Increased Velocity	Flat	3.442			1.583		
	Baseline 1	Hemispherical	0.225	-2.77	**0.006**	0.037	-2.9	**0.004**
	Increased Velocity	Hemispherical	0.353			0.126		
Baseline 1 (B1) vs. Alternate Apparatus (AA)	Baseline 1	Flat & Hemi	1.716	-1.32	0.186	0.446	1.82	0.069
	ECE	Flat & Hemi Combined	1.549			0.340		
	Baseline 1	Flat	3.208	-5.20	**0.000**	0.855	2.64	**0.009**
	ECE	Flat	2.745			0.594		
	Baseline 1	Hemispherical	0.225	-1.84	0.066	0.037	1.82	0.069
	ECE	Hemispherical	0.353			0.085		
ISO Headforms (HF) vs. DOT Headforms (AV)	ISO	Flat & Hemi Combined	2.056	0.9	0.368	1.054	2.13	**0.034**
	DOT	Flat & Hemi Combined	1.936			0.855		
	ISO	Flat	3.509	-1.41	0.160	2.030	3.87	**0.000**
	DOT	Flat	3.442			1.583		
	ISO	Hemispherical	0.603	-1.91	0.058	0.078	-1.38	0.168
	DOT	Hemispherical	0.429			0.126		
Monorail, ISO Headforms (HF) vs. Alternative Apparatus(AA)	Monorail	Flat & Hemi Combined	2.056	-3.99	**0.000**	1.054	8.96	**0.000**
	ECE	Flat & Hemi Combined	1.549			0.340		
	Monorail	Flat	3.509	-8.79	**0.000**	2.030	14.12	**0.000**
	ECE	Flat	2.745			0.594		
	Monorail	Hemispherical	0.603	-2.84	**0.005**	0.078	-0.22	0.822
	ECE	Hemispherical	0.353			0.085		
Monorail, DOT Headforms (AV) vs. Alternative Apparatus(AA)	Monorail	Flat & Hemi Combined	1.935	-3.02	**0.003**	0.855	7.17	**0.000**
	ECE	Flat & Hemi Combined	1.549			0.340		
	Monorail	Flat	3.442	-7.95	**0.000**	1.583	9.35	**0.000**
	ECE	Flat	2.745			0.594		
	Monorail	Hemispherical	0.429	-0.95	0.343	0.126	1.18	0.238
	ECE	Hemispherical	0.353			0.085		

Dwell time at 200g—Baseline Tests. The two baseline tests (B1, B2) show no overall difference when data for both flat and hemispherical anvils are combined for comparison. However, when the data for the two anvils are separated, there is a statistically significant difference between the hemispherical anvil test results, due to the increased vulnerability of the front (brow) to the more aggressive hemispherical anvil.

Dwell time at 200g—DOT vs. ISO Headforms. The ISO headforms overall produced a statistically significant increase in dwell time at 200g. In particular, this was due to the significant increase of dwell time on the flat anvil impacts. Hemispherical impacts were not significantly different.

Dwell time at 200g—Monorail vs. ECE-Type. The results show a statistically significant reduction in dwell time at 200g for the flat anvil tests. This is one of the most dramatic reductions in these tests, from a mean of 2.03 msec. for the monorail with ISO headforms to 0.594 msec. on the ECE apparatus. There was no statistically significant difference between results for the hemispherical anvil tests.

Dwell time at 200g—Monorail Using DOT Headforms vs. ECE-Type. As with the previous comparison of headform types with alternative test apparatus (HF vs. AA), there was a statistically significant decrease in the dwell times on flat anvil tests, but no statistically significant difference for the hemispherical anvil tests.

Summary of Test Criteria for All Test Groups. Table 8 summarizes the count and percentage of the total number of tests for any failures of test criteria for the seven test groups. Note that this summary table combines all helmet brands and sizes, and counts each of the 1440 impact tests. Note that dwell times at 200g are included at several values: 2.0, 2.2, 2.4, 2.6, and 2.8 msec. Note that the data in Table 8 shows the results for all helmet types and sizes combined. The total number of impacts exceeding 2.0 msec @ 200g is 33 (5.7% of 576 impacts) for the Baseline tests. The number of impacts exceeding 2.2 msec @ 200g is 23 (4.0%): the majority (69.7%) of the impacts failing at 2.0 msec still fail at 2.2 msec.

Table 8.
Test Group by Failure Criteria
(N=1440)

	Baseline			ISO Headforms	Increased Velocity	Alternative Apparatus
Values greater than: count, (%)	B1 (n=288)	B2 (n=288)	B1 + B2 (n=576)	HF (n=288)	AV (n=288)	AA (n=288)
400g	3 (1.0)	3 (1.0)	6 (1.0)	6 (2.1)	11 (3.8)	4 (1.4)
300g	3 (1.0)	7 (2.4)	10 (1.7)	37 (12.8)	19 (6.6)	10 (3.5)
4.0 ms @ 150g	1 (0.3)	0	1 (0.15)	9 (3.1)	7 (2.4)	5 (1.7)
2.0 ms @ 200g	20 (6.9)	13 (4.5)	33 (5.7)	84 (29.2)	55 (19.1)	8 (2.8)
2.2 ms @ 200g	15 (5.2)	8 (2.8)	23 (4.0)	74 (25.7)	46 (16.0)	6 (2.1)
2.4 ms @ 200g	9 (3.1)	4 (1.4)	13 (2.3)	55 (19.1)	40 (13.9)	5 (1.7)
2.6 ms @ 200g	6 (2.1)	1 (0.3)	7 (1.2)	46 (16.0)	20 (6.9)	3 (1.0)
2.8 ms @ 200g	1 (0.3)	0	1 (0.15)	28 (9.7)	11 (3.8)	1 (0.3)

High Speed Video Analysis. A series of impact tests with the ECE test apparatus and monorail test apparatus were conducted using a Kodak Ektapro high speed video system which captured the entire helmet impact sequence at a rate of 1000 frames per second. Images were stored digitally and subsequently downloaded to a VHS video system at several different playback speeds.

The ECE test equipment consists of a full configuration (complete with neck) ISO test headform fitted with a tri-axial accelerometer at the center of gravity (See Figure 2). A helmet was placed on the test headform and the headform and helmet were oriented to make contact at the appropriate site and supported using a free fall support cage assembly. The headform, helmet and support cage assembly were raised to the appropriate drop height and released. The cage assembly proceeded to fall towards the impact anvil which then projects through a hole located in the bottom of the cage assembly (See Figure 3). This allows the cage assembly to clear the test anvil while the anvil makes direct contact with the helmet. Since the helmet was not fixed inside the cage assembly, it was free to move in any direction following the initial impact. Although there was very little motion during the primary impact into the test anvil, the secondary motion following the primary impact (i.e. the impact into the roof of the carriage assembly and the second impact onto the test anvil) caused a great deal of secondary damage to the helmet and the headform system. Additional tests in which there were secondary impacts may not indicate the true performance of the helmet, since the helmet could already have experienced some damage due to these secondary impacts. This characteristic may be unique to this particular design of ECE test apparatus; however, the potential of secondary helmet impacts does relate a problem with the ECE test procedures.

The amount of helmet and headform rotational motion observed during the ECE test procedures was obviously greater than the rotation observed during the monorail test procedures. This was because the center of gravity of the ISO test headform is not aligned with the point of impact on the test helmet. As a result of this offset, a moment was generated about the center of mass of the headform and helmet system, causing helmet rotation. The presence of rotation during the ECE test procedures indicates that some of the kinetic energy of the impact is directed into rotational kinetic energy rather than impact energy with the test anvil. A monorail test apparatus has a fixed and guided impact; therefore none of the kinetic energy of the impact is converted into post-impact rotational kinetic energy. Therefore, the amount of energy creating linear acceleration during an ECE test impact is less than for the monorail. This agreement of video and accelerometer data confirm that the ECE test is less severe than those tests conducted with the monorail.

DISCUSSION

The series of tests conducted for this project gives detailed test data for a small selection of the many helmet brands and models that are available in the market today. The selected helmet models are broadly representative of the categories currently available. Therefore, these tests provide depth of test data for the helmet models actually tested, and represent a limited selection of the wide variety of brands and models of helmets currently available. In this way, these tests correctly represent the helmets currently available to motorcyclists.

Helmets are constructed of an outer shell and energy-absorbing liner. There are two major areas for comparison: shell material type and thickness, and energy-absorbing liner thickness and density. Previous research has found that liner density has a dramatic effect on test performance (Mills & Gilchrist, 1991, Thom & Hurt, 1992). Note that the group C helmets which had the highest pass rate have the lowest density liners: 33 Kg per cubic meter (two pounds per cubic foot, see Table 4). This excellent performance is possible because of the combination of the strong and stiff shell and the soft, low-density liner. The group B helmets have considerably denser liners and showed consistently longer dwell times in all tests.

Test Headforms: DOT FMVSS No. 218 vs. ISO. A significant difference was observed between the DOT test headforms (AV) and the ISO test headforms (HF) when tested under identical conditions. The data indicated that the peak headform acceleration values for the flat anvil tests are higher when ISO test headforms were used in place of DOT test headforms. The difference was not sufficient to cause failures in well designed motorcycle helmets; however, it could cause marginally qualified helmets to fail a flat anvil test given the fact that ISO test headforms would result in higher peak headform accelerations. No significant differences were noted between headforms for the hemispherical anvil tests.

The adoption of the ISO test headforms would harmonize the DOT standard with other international motorcycle helmet standards which already use the ISO test headform. The anthropometric characteristics of the ISO test headforms are also considered to be more representative of the general population of human head shapes than the DOT test headforms (Gilchrist, et al., 1988).

Test Apparatus: Monorail vs. ECE-Type. The data presented in Table 6 indicated that there was a significant difference in peak headform acceleration and dwell time at 200g for the flat anvil tests. These differences were attributed largely to the differences in mass distribution of the test apparatus and the subsequent dynamics of the impact. Given the fact that the peak headform accelerations were consistently higher for the monorail tests, it may be assumed that these tests are more rigorous and represent a worst case scenario when compared to the same tests conducted using the ECE test apparatus. The ECE-type apparatus is considerably more complicated and yet it is a less severe test.

The ECE-22.4 standard sets limits of than 275g and a HIC value no greater than 2400. None of the other motorcycle helmet standards use HIC. The use of HIC has been both supported (Lockett, 1985) and criticized (Newman, 1975, 1982). It should be noted that HIC was developed for use with the Hybrid III headform in automotive crash testing, not any of the rigid alloy headforms used in motorcycle helmet testing.

As the comparison of test headforms and test apparatus show, there is little harmony in international motorcycle helmet standards. Comparisons of equipment or performance criteria must be carefully scrutinized in order to distinguish those few items that can be directly compared.

ACKNOWLEDGEMENT

This work was conducted for the United States Department of Transportation, National Highway Traffic Safety Administration under contract DTNH22-97-P-02001. The authors gratefully acknowledge the assistance of William J.J. Liu, Ph.D., the NHTSA Contract Manager and Christopher Lash of NHTSA Safety Assurance.

REFERENCES

American Standard Specifications for Protective Headgear for Vehicular Users. ASA Z90.1. New York: American Standards Association; 1966.

American National Standard Specifications for Protective Headgear for Vehicular Users. ANSI Z90.1. New York: American National Standards Institute; 1971.

American National Standard Supplement to Specifications for Protective Headgear for Vehicular Users. ANSI Z90.1a. New York: American National Standards Institute; 1973.

American National Standard Supplement to Specifications for Protective Headgear for Vehicular Users. ANSI Z90.1b. New York: American National Standards Institute; 1979.

American National Standard for Protective Headgear for Motor Vehicular Users. ANSI Z90.1. New York: American National Standards Institute; 1992.

Bishop, Patrick J., "A Comparison of Two Drop Test Protocols for Evaluating Helmet Performance: Monorail vs. Guidewire". ISO/TC83/SL5, 1988.

British Standard Specification for Protective Helmets for Vehicle Users. British Standards Institution. BS 6658; 1985.

EN960, Headforms for Use in the Testing of Protective Helmets, 1995.

Federal Motor Vehicle Safety Standard No. 218. 49 CFR 571.218, U.S. Department of Transportation, National Highway Traffic Safety Administration; 1974.

Federal Motor Vehicle Safety Standard No. 218. 49 CFR 571.218, U.S. Department of Transportation, National Highway Traffic Safety Administration; 1979.

Federal Motor Vehicle Safety Standard No. 218. 49 CFR 571.218, U.S. Department of Transportation, National Highway Traffic Safety Administration; 1988.

Gilchrist, A, Mills, N.J., Khan, T., "Survey of Head, Helmet and Headform Sizes Related to Motorcycle Helmet Design". Ergonomics 31, No. 10, 1988. pp. 1395-1412.

Henderson, G., “Correlation Anomalies Between Helmet Drop-Test Systems”. Jan. 15, 1975.

Hurt, H.H., Ouellet, J.V., Thom, D.R., “Motorcycle Accident Cause Factors and Identification of Countermeasures”. Vol. I: Technical Report, National Highway Traffic Safety Administration, U.S. Department of Transportation, NTIS PB81-206443, Final Report, January, 1981.

ISO/DIS 6220, “Headforms for use in the testing of protective helmets”. Draft International Standard, 1983.

Liu, W.J.J., “Analysis of Motorcycle Helmet Test Data for FMVSS No. 218”. Proceedings of the International Motorcycle Safety Conference, Motorcycle Safety Foundation, Vol. 3, 1980. pp. 1325-1345.

Lockett, F.J., “Biomechanics Justification for Empirical Head Tolerance Criteria”. Journal of Biomechanics, Vol. 18, No. 3, 1985. pp. 217-224.

Mills, N.J. & Gilchrist, A., “The Effectiveness of Foams in Bicycle and Motorcycle Helmets”. Accident Analysis and Prevention, Vol. 23, Nos. 2/3, 1991. pp. 153-163.

Newman, J.A., “On the Use of the Head Injury Criterion (HIC) in Protective Headgear Evaluation”. 19th Stapp Car Crash Conference, Society of Automotive Engineers 751162, 1975.

Newman, J.A., “The Influence of Time Duration as a Failure Criterion in Helmet Evaluation”. Society of Automotive Engineers 821008, 1982.

Ono, K. Kikuchi, A, Nakamura, N., “Human Head Tolerance to Sagittal Impact: Reliable Estimation Deduced from Experimental Head Injury Using Subhuman Primates and Human Cadaver Skulls”. Proceedings of the 24th Stapp Car Crash Conference, Society of Automotive Engineers, SAE 801303, 1980.

Smith. T.A., “The Effect of Liner Density Upon Acceleration and Local Contact Forces During Bicycle Helmet Impacts”. Ph.D. Dissertation, University of Southern California, Dec. 1997.

Snell Memorial Foundation, 1995 Standard for Protective Headgear for Use with Motorcycles and Other Automotive Vehicles. New York: Snell Memorial Foundation. M95; 1995.

Standard for Protective Headgear in Motor Vehicle Applications. Ontario: Canadian Standards Association. CAN3-D230; 1985.

Standards Association of Australia. Methods of Testing Protective Helmets. AS2512.1-1984, AS2512.2-1983, AS2512.3.1-1981, AS2512.5; 1986.

Thom, D.R. & Hurt, H.H. Jr., “Conflicts of Contemporary Motorcycle Helmet Standards”. 36th Proceedings of the Association for the Advancement of Automotive Medicine, 1992.

Thom, D.R., Hurt, H.H., Jr., Smith, T.A., Ouellet, J.V., “Feasibility Study of Upgrading FMVSS No. 218, Motorcycle Helmets”. DOT-NHTSA Final Report DTNH22-97-P-02001, September 1997.

TP-218-00, Laboratory Procedure for Motorcycle Helmet Testing, DOT-NHTSA, March 1974, revised 1984 (TP-218-02), 1992 (TP-218-03).

TESTING THE POSITIONAL STABILITY OF MOTORCYCLE HELMETS

Hugh H. Hurt, Jr.
David R. Thom
James V. Ouellet
Head Protection Research Laboratory
United States
Paper No. 98-S10-P-30

ABSTRACT

Traditional motorcycle helmet performance standards provide a test for the strength and stiffness of the retention system. While such tests assure adequate strength, they do not assure that the helmet will be retained in place on the motorcyclist's head, even when securely fastened. The reason is that the geometry of the retention system can allow the helmet to roll off when contact or inertial forces are generated in a collision. Different types and styles of motorcycle helmets were tested to determine the susceptibility to roll off, i.e. "positional stability" (Thom et. al., 1997).

Tests were performed using two commonly used, adult sizes of headforms corresponding to standards of the U.S. Department of Transportation (DOT) and the International Standards Organization (ISO). The test results were validated by comparison with essentially identical tests on a large number of human subjects. The results of the human subject tests show a meaningful relationship to the laboratory test which employs a 10kg mass dropped 60cm to jerk the helmet forward to roll off.

The geometry of the retention system has a powerful effect on the ability of the helmet to resist forward roll off, in both laboratory and human subject tests. Also, there is considerable difference in the retention characteristics between DOT and ISO headforms, with the DOT headform more closely correlating with human subject data.

INTRODUCTION

The retention of the motorcycle helmet in place on the head of the motorcyclist is absolutely necessary to provide the full capability for impact attenuation and injury prevention. When contemporary helmet standards develop high levels of impact energy absorption in the structure of the helmet shell and liner, all protection can be lost if the helmet is ejected, or significantly displaced during accident events. Accident research has shown that there is significant benefit of motorcycle helmets in reducing the frequency and severity of head injury. Accident research also has shown that the ejection of the helmet during accident events occurs frequently, and many causes have been investigated (Gilchrist & Mills, 1992, Hurt, et. al., 1981, 1993, 1996, 1997, Mills & Ward, 1985, Newman, 1979, Otte, 1986, 1991, Snively, 1978).

As a part of research to update the FMVSS No. 218 (Thom et. al., 1997, Hurt et. al., 1996) the various helmet standards were collected and reviewed. A summary of the various retention system tests is presented in Table 1, including the static and dynamic tests which are supposed to provide for retention of the helmet during accident events. Actual mechanical failures of retention components during accidents are extremely rare, and most helmet ejections occur without significant damage to the components of chin strap webbing, hangers, rivets, and buckles, or equivalent fastening devices (Hurt et al,1981, Otte and Felten, 1985). For this reason, the test for positional stability of any motorcycle helmet is a critical requirement for successful protection.

In general, the ejection or displacement of the helmet during motorcycle accident events is accountable by loose fastening of the chin strap and loose fitting of the helmet. This lack of secure fit and fastening or failure to fasten the system at all accounts for most of the ejections of helmets in accidents. However, there are cases where the helmet is properly fitted and the retention system has been securely fastened, but the helmet is ejected. Of course, some of such cases occur when severe facial impact causes fractures of the mandible then support for the chin strap is destroyed and any helmet can be ejected. In many other cases, the design of the retention system does not have correct geometry, then contact and inertial forces acting on the helmet cause the helmet to respond by rotation upon the head and then be ejected or significantly displaced.

Table 1.
Retention System Test Methods and Failure Criteria

Standard	Year	Helmet Mounting	Static		Dynamic				Failure Criteria			Positional Stability		
			Preload	Test Load	Preload	Test Mass	Drop Height	Number of Tests	Dynamic Extension	Residual Extension	Buckle Slip	Test Type	Test Mass & Drop	Limit
FMVSS No. 218	1988	Headform	223 N, 30 sec.	1335 N, 120 sec.				One		≤ 25mm		None		
ANSI Z90.1	1992	Headform or Base			23 kg	38 kg*	120 mm	One	< 30mm			None		
AS 1698	1988	Headform	225 N, 30 sec.	1110 N, 120 sec.				One		< 25mm		None		
BS 6658	1985	Headform & Helmet Base			7 kg (support assembly)	10 kg	750 mm	Two (Strap not tightened)	1st 32mm 2nd 25mm	16mm 8mm		Forward Roll-Off	10 kg - 0.75 m	Stay on Head-form
CAN3-D230	1985	Helmet Base			7 kg	10 kg	750 mm	Two (Strap not tightened)	1st 32mm 2nd 25mm		8 mm Total	None		
Snell M-95	1995	Headform			23 kg	38 kg*	120 mm	One	≤ 30mm			Forward & Rearward Roll-Off	4.0 kg - 0.6 m	Stay on Head-form
ASTM F1446 (draft)	1997											Forward & Rearward Roll-Off	4 kg-0.6 m or** 10 kg-0.6 m	Stay on Head-form
ECE 22.4	1995				15 kg	10 kg	750 mm		< 35mm	< 25mm ***		Forward Roll-Off	10 kg-0.5 m	< 30 degree angle change

* Preload removed "immediately prior" to test load.

** Drop mass and height to be specified by individual performance standards.

*** Measured 2 minutes after testing.

The most critical mobility of any helmet is rotation forward as if rolling off the head; backward rotation can happen but does not result in complete ejection or significant exposure of the head. When there is forward rotation of the helmet on the head, correct geometry of the helmet interior and retention system should cause tightening of the chin strap, thus resisting further displacement. If the chin strap anchor points are located far ahead of the center of helmet rotation, there is a tendency of the chin strap to loosen and rotation is not resisted, and the helmet may be ejected. Helmets with adverse design features, such as unfavorable locations for the chin strap anchor points, are known to have special vulnerability for ejection (Hurt, 1997, Mills & Ward, 1985, Otte & Felten, 1991)

The variations in helmet configurations affect the mobility of the helmet, with the partial coverage helmet being the most mobile and the full facial coverage helmet being the least mobile. As the helmet rotates forward on the head, the extent of coverage affects the resistance to that motion, with the obvious potential contact of the brow edge of the helmet with the nose and eyeglass frames (if worn). Denting of the EPS liner at the brow edge from contact with the nose and glass frame is typical evidence of the roll off motion. With the presence of the chin bar of the full facial coverage helmet, it is typical that contact of the chin bar with the motorcyclist's chin and sternum would limit the roll off motion. In this way, the full facial coverage helmet has an obstacle to the completion of roll off ejection. But the extra mobility of the partial coverage helmet may require special design considerations to resist roll off, e.g., a nape strap or Y-type chin strap harness. In these tests with human subjects, ejection rates for the partial coverage helmets ranged from 50 to 89% compared to 1 or 2% for full facial coverage helmets.

Fortunately, there is a tried and true method of preventing such roll off ejection by careful selection of the helmet, i.e., an "acceptance" test. It is recommended that when purchasing a helmet, the motorcyclist should try on the helmet, fasten the chin strap securely, then pull up on the posterior rim of the helmet. If the helmet displaces significantly or comes off, that helmet should be rejected and a different model, some other size, or a different manufacturer should be tried until such dangerous mobility does not occur. Of course, when the motorcyclist does not have the opportunity to make such a critical test, as for an occasional passenger, or a helmet already purchased without such test, roll off ejection in an accident is possible. Such a dangerous consequence clearly justifies a rigorous standard test of helmets to prevent such defective helmet designs from being offered to the unwary motorcyclist.

METHODOLOGY

During the study of updating the present FMVSS No. 218 (Hurt et. al., 1996), several methods of retention system testing were investigated (Thom et. al., 1997). In addition to the evaluation of testing for strength and stiffness, current methodology of testing for positional stability was investigated for possible incorporation into FMVSS No. 218. The specific elements to be included in the study were the most current roll off test methodologies, the effect of headform type, and correlation with human subjects.

The objective of the present research was to determine a minimum performance test of positional stability which could be adopted as a part of updating FMVSS No. 218. The suitable test procedure should provide reasonable simplicity and repeatability, and would correlate well with real world performance of helmets. It was decided to use the most current procedures developed by ASTM F08.53 committee (ASTM, 1995) to determine the positional stability of protective headgear. This method of testing was adopted by the Snell Memorial Foundation for the M95 motorcycle helmet standard. The test procedure involves placing the helmet on the test headform, which is supported at 45 degrees inclination from the vertical. A hook and strap are attached to the posterior rim of the helmet so that a forward roll off force can be applied there. A guide rod is attached to the strap and a sliding mass is allowed to drop along the guide rod, abruptly loading the helmet when the mass is arrested at the end of the guide rod. Figure 1 shows this apparatus with a test helmet in place. The current Snell test employs a 4kg mass dropped 60cm but the original ASTM draft standard employed a 10kg mass dropped 60cm for all motor sports helmets. This present investigation conducted tests with both 4kg and 10kg masses to determine the effect on various helmets.

An important reference standard for positional stability is the British Standards Institution standard BS 6658 (BSI, 1985), which uses a 10kg mass dropped 75cm. The BS 6658 utilizes a complex system of compliant surfaces on the headform, which is a complication thought to reduce repeatability of testing. The BS 6658 standard was not used in this study in favor of the less complicated ASTM F1446 draft.

Figure 1.
Roll-Off Test Apparatus

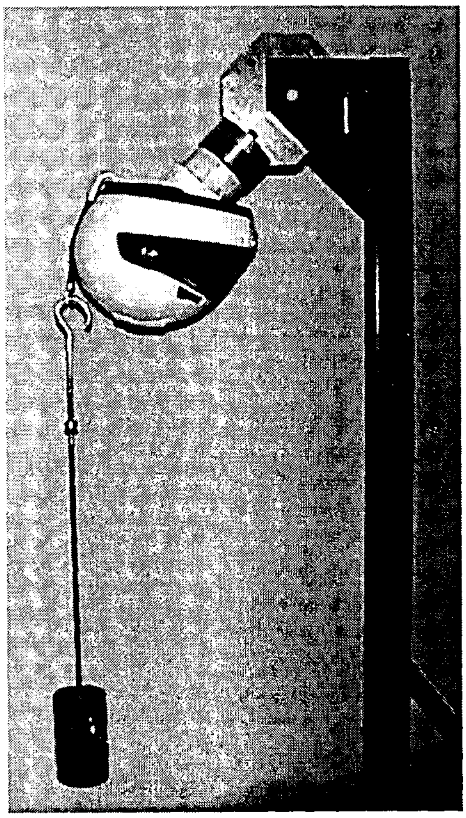

Using the ASTM F1446 draft procedure, six models of helmets were tested for positional stability. For each model set, all available sizes were obtained for testing, and since some models have more available sizes, the number of tests per set varies. Several helmets were tested on each size of headform, e.g., sizes XXS, XS and S typically would fit the DOT Small and ISO E size headforms, but would be too small for testing on the larger headforms. Of course, larger helmets were not tested on headforms that were clearly too small and inappropriate. For this laboratory testing, the roll off test results were collected according the following codes:

1. No movement
2. Some movement, definitely retained
3. Retention marginal, possibly ejected with greater force
4. Ejected with resistance
5. Ejected easily, minimal resistance
6. Retained on the 4kg mass test; ejected on the 10kg mass test

The results of the laboratory tests with DOT and ISO headforms are shown in Table 2.

In order to validate the findings of the laboratory roll off test, further tests were conducted with volunteer human subjects, and the results are shown in Table 3. Test procedures were carefully explained to each subject, and measurements were made of the head circumference in the horizontal plane (headband) and coronal plane (underneath the chin). Subjects were instructed to put on the helmet and fasten the chin strap so that it was in contact with the skin underneath the chin, but loose enough to slide one finger comfortably between the chin strap and the chin. Subjects were instructed to rotate the helmet rearward (to check for rearward stability) and then forward. Subjects were instructed to pull forward vigorously on the helmet, enough to cause discomfort but not to the point of causing pain. Some helmets would come off quite easily, others would come off only with discomfort. Since this test was controlled completely by the subject, each subject could monitor helmet movement, personal discomfort and sense how likely the helmet was to come of with additional force.

The helmets tested by the human subjects included two full facial coverage models, one full coverage model and three partial coverage models. Four to six sizes were available in each model. Subjects tried on two sizes of each model and were asked to determine the size which provided the "best fit" in each model when multiple sizes were tried. The test methodology required the first trial of the subject to use the helmet size most likely to be their "best fit", as correlated with the headband measurement. If the subject was unable to pull off that size helmet, the next larger size was tried because motorcyclists often use a helmet that is too large. Conversely, if the rider was able to pull off the "best fit" in a particular model, the next smaller size was tried to see if that could be pulled off as well. For this human subject testing, the roll off test results were collected according the following codes:

1. No movement
2. Some movement, definitely retained
3. Retention marginal, possibly ejected with greater force
4. Ejected with resistance
5. Ejected easily, minimal resistance

The results of the human subject tests are shown in Table 3. An important factor affecting the roll off resistance of a motorcycle helmet is the match between the exterior contour of the motorcyclist's head and the interior contour of the helmet. Ideally, every motorcyclist would be able to acquire a helmet that gives a comfortable and safe fit which limits the mobility on the head. However, the irregularities of shapes of the human head are numerous and a few motorcyclists will have difficulty in acquiring a helmet that has that "best fit" without some problems of contour match. The tendency is to accept a helmet that may be too large simply to avoid uncomfortable local contact areas, and this could affect retention performance. If the design of the helmet intentionally provides specific geometry to resist roll off, slight variations in helmet fit will not adversely affect the retention performance for those motorcyclists with heads that are difficult to fit. Finally, there will be a very few extreme head shapes which will defeat even the most careful designs, and that particular motorcyclist must use great caution in helmet selection, and should accept only a full facial coverage helmet which does well in the "acceptance" test.

DISCUSSION

The laboratory tests confirm the susceptibility to roll off ejection of the partial coverage helmet, in comparison with the full coverage and full facial coverage helmets. It is important to note that the six helmet models selected for these tests were not selected randomly from the total helmet population. Some helmet models were selected because of known performance from previous laboratory testing and accident research, in order to ensure a wide range of helmet responses in the proposed tests.

As expected, the full facial coverage helmets provide the most satisfactory performance for both laboratory and human subject testing, with ejection occurring in one or two percent of the tests. While the full facial models used in these tests are not a complete representation of all full facial helmets available, the results are indicative of significant resistance to roll off ejection simply by the greater coverage and presence of the chin bar. Because of such a physical obstacle to the roll off displacement, any securely fastened full facial coverage helmet which suffers roll off must have the retention system anchor points misplaced in obviously defective locations (Hurt, 1997, Mills & Ward, 1985, Otte & Felten, 1991).

Also as expected, the partial coverage helmets selected for these tests showed a high frequency of ejection for both laboratory and human subject tests, with some models failing almost all tests. The design of the retention system for these partial coverage helmets must incorporate special provisions to prevent such gross susceptibility, otherwise the motorcyclists using these helmets are at peril. The high ejection rates completely verify the need for a minimum performance roll off test for these helmets which are otherwise qualified to static and dynamic strength tests.

The laboratory tests show that the DOT headforms retain both full coverage and full facial coverage helmets better than the ISO headforms, but the ISO headforms retain the partial coverage helmets better than the DOT headforms. The small number of laboratory tests limits the significance of the headform effects, and there are inconsistencies in the results for DOT and ISO headforms. Resolution of these problems could be satisfied only with a larger number of laboratory tests, or simply the headform requirements of other areas of helmet testing. Significant differences are not determined at this point in this research.

The ASTM draft standard (ASTM, 1995) employs the ISO headforms but could be modified simply to specify the current DOT headforms. Either the DOT or ISO headforms could be specified for use since most manufacturers and test laboratories usually have both sets of headforms. The use of the DOT headforms would require further tests and validations since no such testing was done during the ASTM F08.53 Committee preparation of the draft procedure.

Table 2.
DOT and ISO Test Headform Forward Roll-Off Result Summary
(Human subject data included for comparison)

Headforms (All sizes combined)	Helmet (Count in category)	Retained, minimal movement	Retained, some movement	Retained, possibly ejected with greater force	Ejected with resistance	Ejected with minimal resistance	Retained in 4kg test, ejected on 10 kg test	No. Tests	Percent Ejected
DOT	Partial 1	0	1	0	2	1	3	7	86
ISO	Partial 1	1	1	0	0	0	7	9	78
Human	Partial 1	0	6	12	70	76	N/A	164	89
DOT	Partial 2	2	2	0	0	0	2	6	33
ISO	Partial 2	2	4	0	0	0	0	6	0
Human	Partial 2	8	55	22	27	15	N/A	127	33
DOT	Partial 3	1	1	0	0	1	1	4	50
ISO	Partial 3	1	1	0	0	1	1	4	50
Human	Partial 3	5	36	3	11	29	N/A	84	48
DOT	Full Coverage	0	4	0	1	0	4	9	56
ISO	Full Coverage	0	0	0	0	4	5	9	100
Human	Full Coverage	2	29	26	66	46	N/A	169	66
DOT	Full-Facial 1	2	5	0	0	0	0	7	0
ISO	Full-Facial 1	0	4	1	0	1	1	7	29
Human	Full-Facial 1	58	68	2	1	0	N/A	129	0.8
DOT	Full-Facial 2	0	6	2	0	0	0	8	0
ISO	Full-Facial 2	0	8	0	1	0	0	9	11
Human	Full-Facial 2	29	76	7	1	0	N/A	140	0.7

Table 3.
Comparison of Human Subject and Test Headform Ejection Data

Count (%)	Retained, minimal movement	Retained, some movement	Retained, possibly ejected with greater force	Ejected with resistance	Ejected with minimal resistance		Total Ejected Count, (%)
Helmet			*Human Subjects*				
Partial 1	0	6 (5.7)	12 (7.3)	70 (42.6)	76 (46.3)		146 (89.0)
Partial 2	8 (4.8)	55 (33.5)	22 (13.4)	27 (16.5)	15 (9.1)		42 (33.0)
Partial 3	5 (6.0)	36 (42.9)	3 (3.6)	11 (13.1)	29 (34.5)		40 (47.6)
Full Coverage	2 (1.2)	29 (17.2)	26 (15.4)	66 (39.1)	46 (27.2)		112 (66.3)
Full Facial 1	58 (45.0)	68 (52.7)	2 (1.6)	1 (1.2)	0		1 (0.8)
Full Facial 2	56 (40.0)	76 (54.3)	7 (8.0)	1 (1.1)	0		1 (0.8)
Test Headforms (DOT and ISO Combined)			* Failed retest with 10 kg weight. ** Passed retest with 10 kg weight			Retained on 4 kg test, ejected on 10 kg test	
Partial 1	1 (6.3)	2 (12.5)	*	2 (12.5)	1 (6.3)	10 (62.5)	13 (81.3)
Partial 2	4 (33.3)	6 (50.0)	2 (16.7)*	0	0	2 (16.7)	2 (16.7)
Partial 3	2 (25.0)	2 (25.0)	2 (25.0)*	0	2 (25.0)	2 (25.0)	4 (50.0)
Full Coverage	0	4 (22.2)	9 (50.0)*	1 (5.6)	4 (22.0)	9 (50.0)	14 (77.6)
Full Facial 1	2 (14.3)	9 (64.3)	1 (7.1)**	1 (7.1)	0	1 (7.1)	2 (14.2)
Full Facial 2	0	14 (82.4)	2 (11.8)**	1 (5.9)	0	0	1 (5.9)

Table 4.
Summary of 10 kg Laboratory Tests and Human Subject Test Results

	Human Subject Ejection %	DOT Headform 10kg Ejection %
Partial 1	89	86
Partial 2	33	33
Partial 3	48	50
Full Coverage	66	56
Full Facial 1	0.8	0
Full Facial 2	0.7	0

Comparison of the data for human subjects and test headforms shows that the 4kg-60cm test is not a rigorous test of positional stability for motorcycle helmets. It shows that helmets which passed that roll off test on headforms were easily ejected by the human subjects. Note in that for helmet "Partial 1" the ejection rate was 89% for human subjects, 86% for the 10kg-60cm tests, but only 19% for the 4kg-60cm test. Any acceptable laboratory test procedure for helmet retention should produce results which are approximately the same as for human subjects, thus providing real world protection for the motorcyclist. The 4kg-60cm test as promulgated by ASTM and used in the Snell M95 standard will not assure retention and the 10kg-60cm test appears to be required for rigorous testing. Table 4 shows the human subject and laboratory test data for the 10kg-60cm roll off test.

CONCLUSIONS

The application of the ASTM draft standard (ASTM, 1995) with DOT headforms can provide a suitable minimum performance requirement for positional stability of motorcycle helmets. This type of test is necessary to eliminate unsafe helmets from the current market offerings. This test is clearly justified by the high level of correlation with human subject test results.

The 4kg-60cm test as promulgated by ASTM and in use by Snell Memorial Foundation is not sufficiently rigorous to fail helmets that are susceptible to roll off ejection, and the 10kg-60cm test is the minimum necessary energy.

ACKNOWLEDGEMENT

This research was conducted for the U.S. Department of Transportation, National Highway Traffic Safety Administration under Contract DTNH22-97-P-02001. The authors gratefully acknowledge the cooperation and assistance of William J. J. Liu, Ph.D., the NHTSA Contract Manager, and Christopher Lash of NHTSA Safety Assurance.

REFERENCES

American National Standards Institute, “American National Standard for Protective Headgear for Motor Vehicle Users”. ANSI Z-90.1, ANSI, 1992.

American Society for Testing and Materials, “Standard Test Methods for Equipment and Procedures Used in Evaluating the Performance Characteristics of Protective Headgear”. ASTM F 1446-95a, 1995.

American Society for Testing and Materials, “DRAFT-Standard Specification for Helmet Stability and Roll-Off Testing”. ASTM, 1995.

British Standards Institution, “British Standard Specification for Protective Helmets for Vehicle Users”. BS 6658, 1985.

Canadian Standards Association, “Standard for Protective Headgear in Motor Vehicle Applications”. CSA CAN3-D230, 1985.

Federal Motor Vehicle Safety Standard No. 218, CFR 571.218, U.S. Department of Transportation, National Highway Traffic Safety Administration, 1988.

Gilchrist, A. & Mills, NJ, “Critical Assessment of Helmet Retention Test Methods, IRCOBI 1992.

Gilchrist, A, Mills, NJ, & Khan, T, “Survey of Head, Helmet and Headform Sizes Related to Motorcycle Helmet Design”. Ergonomics 31, No. 10, 1988, pp. 1395-1412.

Hurt, HH. “Logic Analysis of Helmet Ejection”. USC-HPRL Report, 1997

Hurt, HH. "Logic Analysis of Helmet Ejection". USC-HPRL Report, 1997

Hurt, HH, Ouellet, JV & Thom, DR, "Motorcycle Accident Cause Factors and Identification of Countermeasures"; Vol. I Technical Report, Vol. II Appendices and Supplemental Data, NTIS PB-206 443, PB-206 450, 1981.

Hurt, HH & Thom, DR, "Accident Performance of Motorcycle and Bicycle Helmets". ASTM STP 1229-Head and Neck Injuries in Sports, ASTM 1993.

Hurt, HH, Thom, DR & Smith, TA, "Updating the Twenty Year Old DOT Helmet Standard (FMVSS No. 218)". 40th Proceedings of the Association for the Advancement of Automotive Medicine, 1996.

Mills, NJ & Ward, RF, "The Biomechanics of Motorcycle Helmet Retention". IRCOBI, 1985.

Newman, JA, "The Dynamic Retention Characteristics of Motorcycle Helmets". Biokinetics/Ministry of Supply and Services, Ontario, Canada, September, 1979.

Otte, D, "Technical Demands of Safety in the Design of Crash Helmets for Biomechanical Analysis of Real Accident Situations". SAE 912911, 1991.

Otte, D & Felten, G, "Requirements on Chin Protection in Full-Face Helmets for Motorcyclist Impact and Injury Situations". Proceedings 1991 International Motorcycle Conference, Institut fur Zweiradsicherheit, 1991.

Otte, D, Appel, H & Suren, EG, "Recommendations for Improvement of the Injury Situation for the Users of Two-Wheel Vehicles". IRCOBI September 1986.

Snell Memorial Foundation, "1995 Standard for Protective Headgear for Use with Motorcycles and Other Automotive Vehicles". Snell Memorial Foundation, 1995.

Snively, GS, "Head Protection: Preventive Medicine in Traffic Safety, Proceedings AAAM pp. 69-80, 1978

Standards Association of Australia, "Methods of testing Protective Helmets". AS 2512.1-1984, AS 2512.2-1983, AS 2512.3-1981, AS 2512.5-1986

Thom, DR. Hurt, HH, Smith, TA & Ouellet, JV, "Feasibility Study of Upgrading FMVSS No. 218, Motorcycle Helmets". Final Report, US Department of Transportation, National Highway Traffic Safety Administration, DTNH22-97-P-02001, 1997.

United Nations, Uniform Provisions Concerning the Approval of Protective Helmets and of Their Visors for Drivers and Passengers of Motor Cycles and Mopeds, United Nations E/ECE/22.4, May, 1995.

AN ANALYTICAL ASSESSMENT OF PEDESTRIAN HEAD IMPACT PROTECTION

Abayomi Otubushin
John Green
Rover Group
United Kingdom
Paper Number 98-S10-W-17

ABSTRACT

In car-to-pedestrian collisions the lower limbs are usually struck first and the pedestrian's head arcs downward to strike the bonnet (hood) surface. Approximately 60% of pedestrian head strikes to vehicle front structures are to the bonnet, often supported by underlying reinforcement and engine bay structures. Pedestrian-friendly engine bay packaging and bonnet design has the potential to reduce the severity of the resulting head injuries. In order to achieve this aim, the important criteria for good pedestrian protection must be identified by understanding the physics of the impact and through impact testing. Much can still be learned from the protection levels offered by current vehicles especially in the bonnet regions where low Head Injury Criteria (HIC) are recorded during a headform impact.

In this paper the results of 70 headform impacts to the bonnets of seven European vehicles are examined. The vehicles represent the current European population and the tests were part of a series commissioned by ACEA (European Automotive Manufacturers Association). The effect of reinforcement and hard contact are described and the general principles of good structural design are given.

INTRODUCTION

In Europe pedestrian fatalities have been decreasing steadily in recent years but there are still approximately 7000 annually. Mackay recently estimated the proportion of pedestrian fatalities relative to all road user fatalities as being in the range 16-36% for motorised countries in Europe and the USA with the UK being at the high end of the range. In the UK 28% of the 3,598 road accident deaths reported by the Department of Transport in 1996 were pedestrians although the actual number of pedestrian fatalities had fallen by 43% with respect to the 1991 total. The reduction in pedestrian fatalities seen in the UK could be due in part to the increased use of traffic-calming measures in urban areas, city-centre pedestrian schemes and advertising campaigns and greater car use for short journeys. However, pedestrians still represent a substantial proportion of all road fatalities and, as such, their protection is being addressed by proposed vehicle safety legislation. The proposed sub-system test procedure was developed in an attempt to model a chaotic event (pedestrian/car impact) in a repeatable and meaningful manner and is still under development. It is therefore worth briefly considering the pedestrian kinematics before concentrating on the head/bonnet impact.

Pedestrian Accident Kinematics

The first point of contact is between the bumper and the lower extremities which are accelerated away breaking the frictional resistance between the pedestrian and the ground. A turning moment about the centre of gravity of the pedestrian is created by this first impact and causes the upper body to arc downwards. The next point of contact may be between the upper leg and the bonnet leading edge depending on the shape of the car, speed of impact and degree of braking. The third point of contact with the vehicle is usually between the bonnet top surface and the head although other parts of the body may also make contact. During this phase the bonnet usually deforms and may allow contact with underlying structures. In high speed impacts the head and upper body may contact the windscreen or header rail instead of the bonnet.

While the above impacts are occurring, the pedestrian is accelerated to the vehicle speed and as the vehicle stops, continues forwards and onto the ground where further injuries may be received.

Head injuries are among the most life threatening form of injury for pedestrians and are predominantly caused by a direct blow to the head or the face. The blows may cause fractures and/or give rise to accelerations causing relative motion of the brain and the skull. A common method of measuring the potential to cause head injury is the Head Injury Criterion (HIC). This was derived from the Wayne State tolerance curve that related the resultant head acceleration to the duration of exposure. Put simply, due to the response time of the brain, it is possible to sustain high levels of acceleration (of the order of 200-300g) for short periods of time (1-

2ms). The greater the length of time that the head is exposed to acceleration, the lower the tolerable magnitude of the acceleration. In this study the peak resultant acceleration is used to give an indication of peak forces experienced by the headform and HIC is also used as an indicator of head injury risk in line with the proposed legislation.

Proposed European Legislation

In October 1998 an EC proposal for regulation concerning the protection of pedestrians from vehicle fronts is expected. It will be based on the draft published earlier by the EC with additional modifications as recommended by the European Experimental Vehicles Committee (EEVC) working groups 17. The test procedure consists of a series of sub-system impactor tests that represent impacts between the pedestrian's leg, thigh/hip and head with the bumper, bonnet leading edge and bonnet top surface respectively. This paper considers only the headform impactor tests that represent child and adult head impacts. Details of the headform designs and test procedure are given in the references. The child and adult headforms are fired at impact angles of 50° and 65° to the horizontal respectively and both are fired at 40kph ($11.11ms^{-1}$). The nominal masses of the impactors are 2.5kg and 4.8kg for child and adult respectively.

Experience gained to date suggests that cost-effective, vehicle-based pedestrian protection should be designed in at the earliest concept stage to minimise risks to the appearance of the vehicle and costs associated with any modifications applied later in the design and development phase. In order to benchmark current vehicles and to assess the test proposals ACEA (European Automotive Manufacturers Association) commissioned a series of impact tests from which these headform impacts were drawn.

The vehicles selected were the Citroen XM, Fiat Punto, Range Rover, Renault Twingo, Renault Espace, Volvo 940, and VW Golf. A maximum of twelve impact points were chosen on each vehicle. Six of these points were judged to be "good" points in terms of estimated HIC values based on an inspection of the bonnet structure and under-bonnet layout. The other impact points were chosen as prescribed in the draft proposal at "positions judged to be the most likely to cause injury". These were labelled "bad" points. Two of the smaller vehicles did not have an adult impact test zone so only child headform impacts were conducted for these. For a further vehicle, only four adult impact points could be tested instead of six.

The impacts were filmed at 1000 frames per second and the trajectory of the headform was traced as it deformed the bonnet. The data acquisition rate from the instrumented headforms was 10,000 samples per second. It was therefore necessary to reduce the resultant headform acceleration data in order to achieve the same time interval as displacement data from the high speed film analysis. This was done by selecting 1 in every 10 samples and the procedure gave a good estimate of the crush into the engine bay at different times during the impact. However, the peak accelerations obtained using this method may be less accurate than those given in the tables which were obtained using the higher sampling rate. All figures for dynamic displacement given in this report were measured normal to the bonnet surface.

THEORY

Head Injury Tolerance

Hodgeson and Thomas conducted drop tests using adult cadaver heads onto rigid flat plates reported recently by Viano and King. Their results showed that a peak uniaxial force of 4.82kN and a peak acceleration of 201g can be sustained without skull fracture. Skull fractures were found to occur at peak forces of 5.8 kN and peak accelerations of 188g so an overlap existed at least for accelerations. For more localised impacts the force limits for skull fracture is more likely to be in the region of 2kN (for example see Aldman). Bearing in mind that it is possible to receive serious brain injury without skull fracture, particularly for children, a mean load of 4kN can be used to establish an approximate distance in which a head can be safely brought to rest when striking a large surface such as a car bonnet.

Adult
$$\frac{296\ \text{J}}{4.0\ \text{kN}} = 74\ \text{mm} \qquad (1.)$$

Child
$$\frac{154\ \text{J}}{4.0\ \text{kN}} = 38.5\ \text{mm} \qquad (2.)$$

The headform impactors used for the proposed impact tests are fired into the bonnet at 65° and 50° to the horizontal for adult and child headforms respectively to account for the different whole body trajectory observed in dummy tests. The impact angles can be used to estimate the vertical components of the displacements in the equations above as 67 mm and 30 mm respectively. These would be the amounts that the bonnets would have to displace. Greater bonnet displacement will give the scope for lowering forces and therefore accelerations. This method of estimating the required displacement does not take into account any dynamic effects which are automatically included in an acceleration-based estimate. Such an estimate can be derived from the HIC calculation shown in below.

$$HIC = \left[\frac{1}{t_2 - t_1} \int_{t_1}^{t_2} a\,dt \right]^{2.5} (t_2 - t_1) \qquad (3.)$$

Setting $t_1=0$ and HIC=1000, an expression can be written for the ideal acceleration-time curve:

$$a = 9.51t^{-0.4} \qquad (4.)$$

This curve was used to find that the theoretical minimum stopping distance for the headforms given an impact speed of 11.11 ms^{-1} was 51.1 mm. Accounting for the impact angles of the two headforms, the vertical displacements would be 46 mm and 39 mm for adult and child respectively (Figure 1).

The HIC calculation is very sensitive to slight changes in impact location and speed so in order to make sure that a design meets the HIC≤1000 specification an in-house specification should perhaps be somewhat lower.

Figure 2 shows a typical acceleration trace for HIC≤1000. An approximate response is also shown.

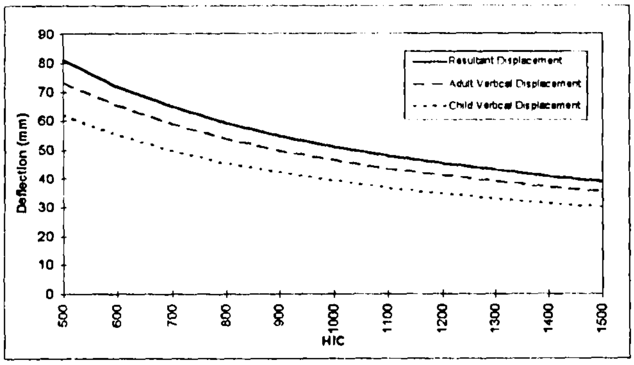

Figure 1. Minimum theoretical displacements for various HIC

Here the calculation is focused around the first peak because the rest of the response is at a relatively low level. The second peak in acceleration is due to the increased resistance caused by secondary contacts remote from the impact site. If this secondary peak is of sufficient magnitude it will be included in the HIC calculation.

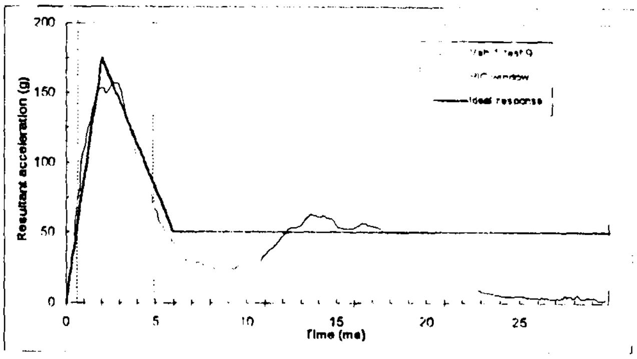

Figure 2. Typical adult acceleration result

This type of response is compared to other hypothetical responses in Figure 3 which can be used to determine a strategy for achieving low HIC values. Over a period of 10ms, various hypothetical acceleration traces have their HIC results compared.

Two strategies are suggested by the graph:-

- Strategy 1. Evolve the steel bonnet controlling the initial peak. In this case the post-peak response must be maintained at or below 60g.
- Strategy 2. Develop a structure to give a square pulse with a maximum of 100g. This may be possible with a low-density material that will not give an inertial spike.

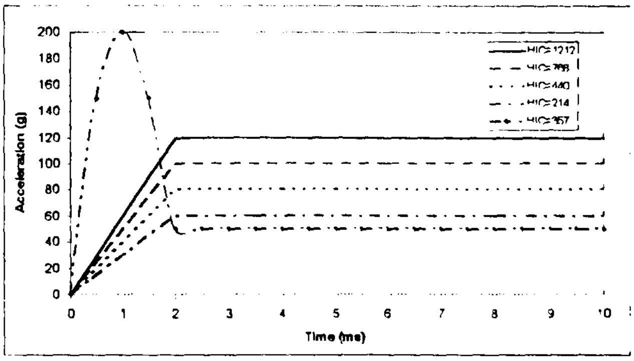

Figure 3. Hypothetical acceleration traces and resulting HIC

TEST RESULTS

An overview of the 70 impact test results is given in Figure 4. Approximately 23% of the targets resulted in HIC < 1000, 22% of the child headform impacts and 35% of the adult headform impacts. In Figure 5 individual results are compared to the theoretical minimum dynamic displacement as described above.

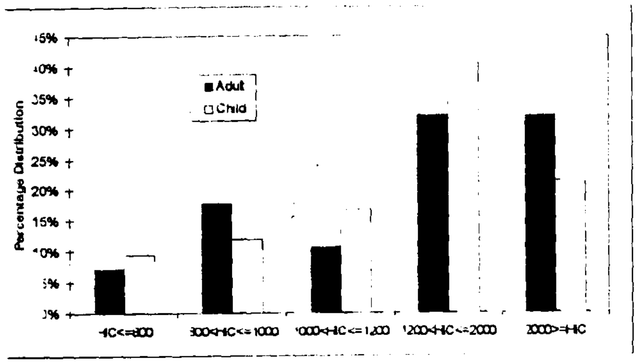

Figure 4. Summary of Test Results

Inspection of the bonnet and engine bay post test and analysis of the high speed films revealed that the main reason for HIC values much greater than 1000 was insufficient displacement of the headform. This applied when the headform contacted rigid structures such as windscreen wiper spindles, scuttle panels at the base of the windscreen and the bonnet surface close to the outboard edges. It is therefore more constructive to investigate the outcomes when sufficient displacement was possible. The remainder of this paper therefore concentrates on the impacts that resulted in HIC ≤ 1000 as these will indicate practices that can be carried over into new designs.

A brief description of the type of structure at the 16 impact sites resulting in HIC ≤ 1000 is given in Table 1. All the points were either in the middle third of the bonnet or close to the border between the mid- and outer thirds. None of the points were close to the fender tops or the front edge of the bonnet and all bonnets except for one vehicle were fabricated in steel with reinforcements under an outer skin . Vehicle 7 had a Fibre Reinforced Plastic (FRP) bonnet.

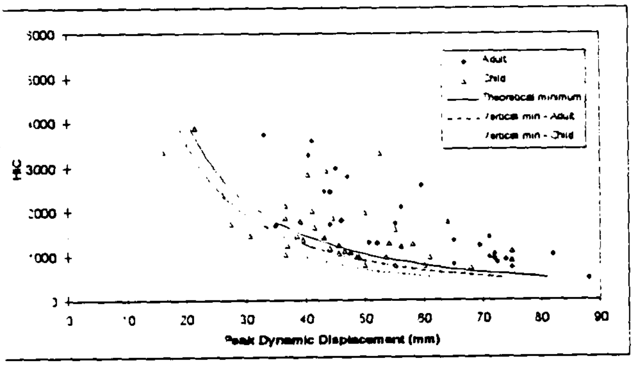

Figure 5. Comparison of Test Results with Theory

Tables 2 and 3 show the HIC, peak acceleration and maximum dynamic displacement for these impact tests. In these tables (G) and (B) represent "good" and "bad" points as previously defined.

In all tests except for test 7:5 above there was evidence of some under-bonnet contact either on the sound-proofing felt or on the bonnet reinforcement structure. The contact was not always directly below the impact point and its severity could be judged by the severity of any secondary peaks in the acceleration response.

The acceleration-time, acceleration-displacement, and speed-displacement curves for five of the above tests are given in the Appendix to demonstrate the main findings. The time window used to calculate the maximum HIC is indicated with vertical dashed lines (for the acceleration-displacement curves the window has been read across to displacement values for the given times). The speed indicated is an approximation from the resultant acceleration using the initial impact speed for the integration. Side by side comparison of the graphs permits the translation of acceleration peaks and troughs into physical events occurring in the vehicle structure.

DISCUSSION OF RESULTS

The peak acceleration recorded by the headform in the 16 tests with HIC≤1000 was in the range 110-201 g. The lowest HIC was recorded by the child headform into a non-metallic bonnet. Apart from that special case however it was generally observed that the child headform tended to experience higher peak accelerations. The initial peak occurs as the bonnet as a whole is accelerated and yields locally to the impact point. Although both headforms are fired at the same speed, the child headform has approximately half the momentum of the adult and so experiences a greater initial impulse arising from momentum transfer when impacting similar points. The amount of permanent deformation caused by the child impactor was also observed to be much less than that caused by the adult. This was especially true for impacts directly over reinforcements. Where the adult impactor would cause plastic deformation in the bonnet skin and reinforcements, the child impactor would tend to bounce off leaving only a small indentation in the skin.

The technique used to measure the dynamic displacement was accurate to within ±5 mm so worst-case figures can be calculated from the tables given. Adult and child headforms should be allowed a minimum of

70mm and 54 mm displacement if current bonnet technology is used.

The following refers to the responses shown in the Appendix:-

Vehicle 1 test 9 Adult: This response is close to the ideal. The HIC calculation was focused around the first peak and subsequent energy absorption took place at moderate accelerations.

Vehicle 2 test 2 Adult: Here the HIC calculation was spread over most of the trace because of the relatively low levels of acceleration. The result was the lowest of the test series in terms of HIC and the traces show no sign of a secondary hard contact. This impact point was on a bonnet reinforcement member.

Vehicle 2 test 7 Child: The good response of this test point derives from the low initial peak and subsequent acceleration history. Of the six child headform impact tests resulting in more than 50 mm dynamic displacement, four of them were on vehicle 2. This would seem to indicate that the child headform was able to cause large deformations in this steel bonnet. However, analysis of the test film revealed that the bonnet hinges permitted 20-30 mm of downward translation of the bonnet from the initial position. This would have occurred at lower forces than those required to cause plastic deformations.

Vehicle 2 test 8 Adult: The relatively low initial peak indicates that the headform was able to overcome the bonnet inertia and cause plastic collapse relatively easily. An under-bonnet contact was made at approximately 60 mm displacement however. This contact was sufficiently hard to cause a secondary peak large enough to be included in the calculation of the maximum HIC. It must be pointed out that, at the point of secondary contact the headform was travelling at approximately half the initial speed. The impact point was directly over a reinforcement which was observed to have been partially crushed after the impact.

Vehicle 7 test 5 Child: Of the 16 impacts reported in detail here, this test alone did not leave any evidence of secondary under-bonnet contacts either at or remote from the impact site. The secondary peak seen clearly in the acceleration-time graph was a result of the headform being accelerated back out of the FRP bonnet which bonnet was nearly perpendicular to the impact direction for this vehicle. Up to approximately 8 ms (55 mm) the response was close to the ideal for strategy 2 described above and would have continued well had the bonnet been designed to release the impact energy at a slower rate.

CONCLUSIONS

Seven European vehicles have been tested using the proposed legislative procedure for headform impact. Although 50% of the impact points chosen were expected to meet the pass criteria, only 23% actually did. For these results the following ranges were observed:-

- For adult headforms the maximum dynamic displacement ranged from 65mm (HIC=813) to 88mm (HIC=477).
- For child headforms the maximum dynamic displacement ranged from 49mm (HIC=955) to 68mm (HIC=728) for steel bonnets.
- For the successful child headform against a FRP bonnet the maximum dynamic displacement was 75mm but the HIC (886) was higher than the minimum for the steel bonnet due to a combination of the bonnet angle and the elasticity of the bonnet.

The theoretical minimum stopping distance normal to the bonnet surface to achieve a HIC of 1000 or less was calculated as 46 mm and 39 mm for adult and child headforms respectively so there is some scope for more efficient use of the under-bonnet package space where that space is available.

The tests confirm that (allowing 5mm for film analysis accuracy) the minimum under-bonnet package space required using current construction is 70 mm.

To minimise peak accelerations for the child headform impacts a combination of bonnet material specification and bonnet installation design may prove the most fruitful way forward. This way the response is not solely determined by the local stiffness of the bonnet structure. The elastic storage of impact energy is only advisable if the subsequent release of that energy is damped to prevent a second interaction between the bonnet and the headform.

REFERENCES

Mackay, M. "A review of the biomechanics of impacts in road accidents" in 'Crashworthiness of transportation systems: structural impact and occupant protection', 1997. p 118.

Department of Transport Statistics Bulletin (97)10, "Road Casualties Great Britain – Final Figures 1996", 1997.

Viano, D.C. "Injury mechanisms and biofidelity of dummies" in 'Crashworthiness of Transportation Systems: Structural impact and occupant protection', 1997. pp 28-30.

Aldman, B. " A method for the assessment of the load distribution capacity of protective helmets". Internal Report Chalmers University Gothenburg. 1984.

EEVC WG10, "Proposals for methods to evaluate pedestrian protection for passenger cars". Final Report. November 1994

EC DG III, "Draft proposal for a European Parliament and Council Directive relating to the protection of pedestrians and other road users in the event of a collision with a motor vehicle and amending Directive 70/156/EEC". February 1996

Table 1.
Description of the Structure at Analysed Impact Locations

Veh.:Test	Description of Structure
1:2	Single skin thickness, approx. 40 mm from reinforcement
1:6	Double skin thickness on reinforcement edge
1:7	Large area of single skin thickness, approx. 90 mm from reinforcement
1:9	On a joint of reinforcements
1:10	Small area of single skin thickness, approx. 50 mm from reinforcement
2:2	Directly over reinforcement
2:3	Double skin thickness, on edge of reinforcement near a joint of reinforcements
2:5	In the middle of a large area of single skin thickness
2:6	Double skin thickness, on reinforcement edge
2:7	In middle of a large area of single skin thickness
2:8	Directly over reinforcement
3:7	Approx. 10 mm from edge of reinforcement
5:3	Approx. 30 mm from reinforcement near a joint of reinforcements
5:9	Single skin thickness, approx. 40 mm from reinforcement
5:11	In the middle of a small area of single skin thickness, approx. 50 mm from reinforcement
7:5	FRP bonnet no under-bonnet contact was recorded

Table 2.
Results for HIC≤1000 – Adult Headform

Veh.: Test	Target	Bonnet Angle (°)	Impact Speed (ms^{-1})	HIC	Peak Acc. (g)	Max. Displ. (mm)
1:2	Between fan cowling and engine (G)	7.2	11.56	888	170	74
1:9	Over air intake transfer pipe (G)	5.9	10.86	734	158	75
1:10	Over area between fuse box and air/fuel intake system (G)	4.8	11.18	813	191	65
2:2	Between engine and brake fluid reservoir (G)	6.5	10.92	477	127	88
2:8	Over injector mechanism (G)	7.4	11.32	844	130	73
3:7	Between rear of engine and vehicle bulkhead (G)	9.8	11.37	929	164	72
5:3	Over rear corner of engine (G)	10.2	11.44	960	146	71

Table 3.
Results for HIC≤1000 – Child Headform

Veh.:Test	Target	Bonnet Angle (°)	Impact Speed (ms^{-1})	HIC	Peak Acc. (g)	Max. Displ. (mm)
1:6	Over transmission fluid reservoir (G)	9.2	11.05	959	191	54
1:7	Over fan cowling (G)	7.8	10.86	793	160	50
2:3	Over oil cap (B)	8.3	10.98	960	201	61
2:5	Between engine and ABS unit (G)	9.8	10.96	773	156	55
2:6	Over cooling hose (G)	11.1	11.00	728	182	68
2:7	Over air hose (G)	9.1	11.10	764	159	60
5:9	Over engine (B)	10.6	11.17	956	183	49
5:11	Over valve cover (G)	14.5	11.34	957	189	49
7:5	Over engine (G)	36.4	11.16	886	110	75

APPENDIX

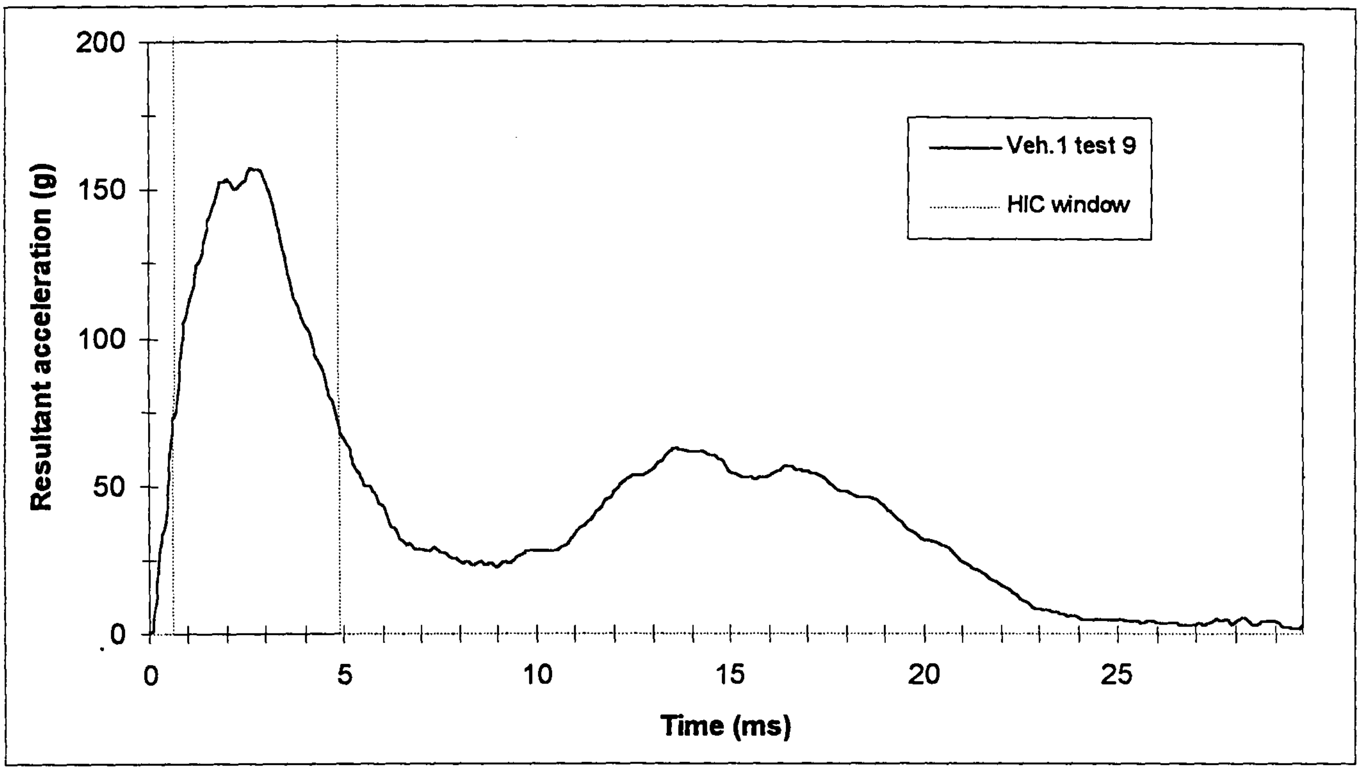

Resultant acceleration (g)
200
150
100
50
0
Time (ms)
0
5
10
15
20
25
Veh.1 test 9
HIC window

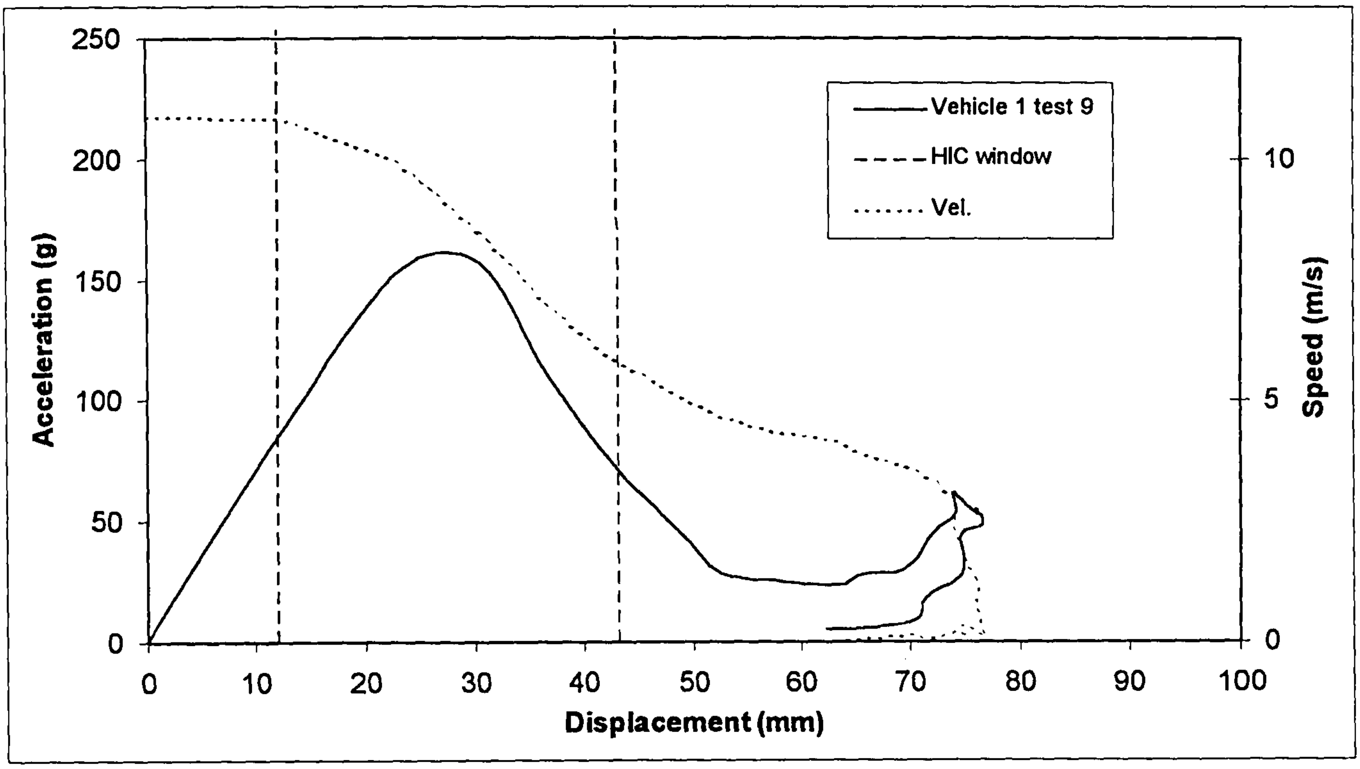

Acceleration (g)
250
200
150
100
50
0
Speed (m/s)
10
5
0
Displacement (mm)
0
10
20
30
40
50
60
70
80
90
100
Vehicle 1 test 9
HIC window
Vel.

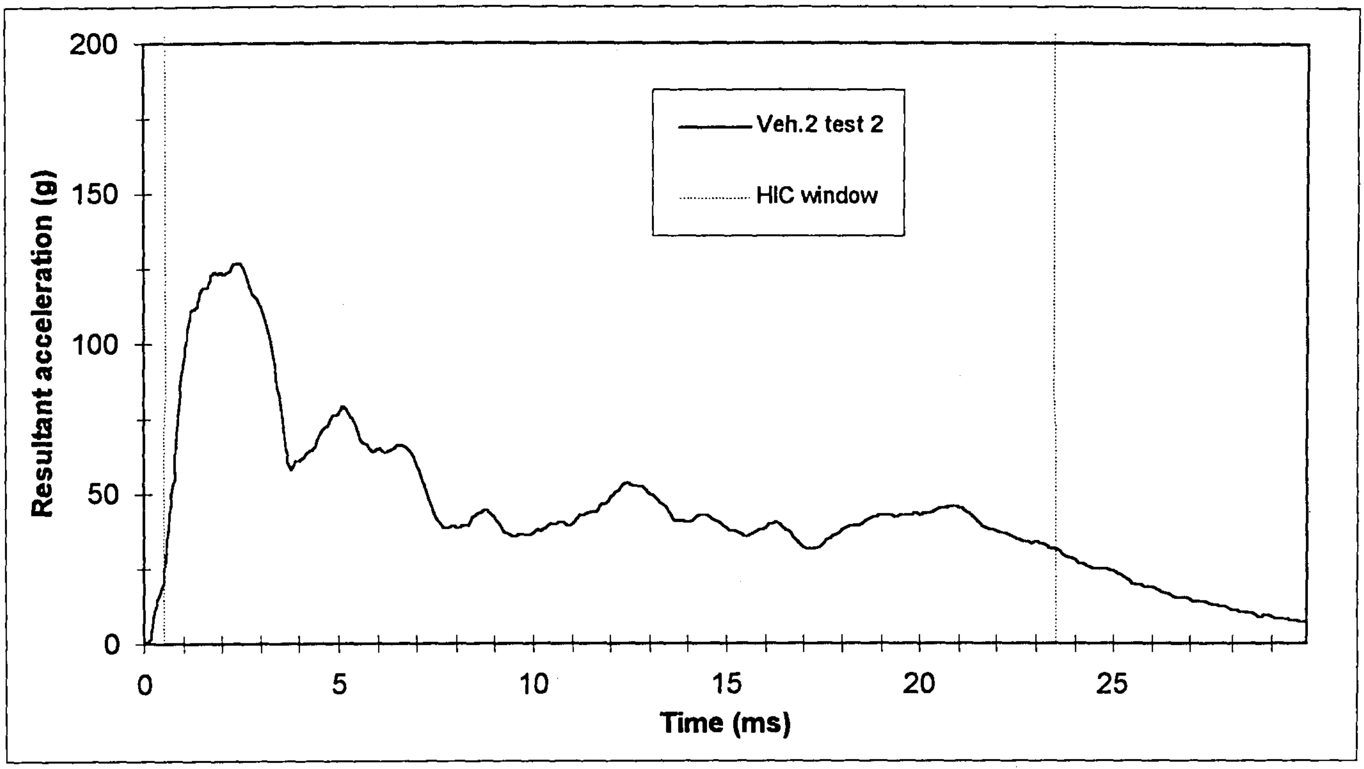
200
150
100
50
0
Resultant acceleration (g)
0
5
10
15
20
25
Time (ms)
Veh.2 test 2
HIC window

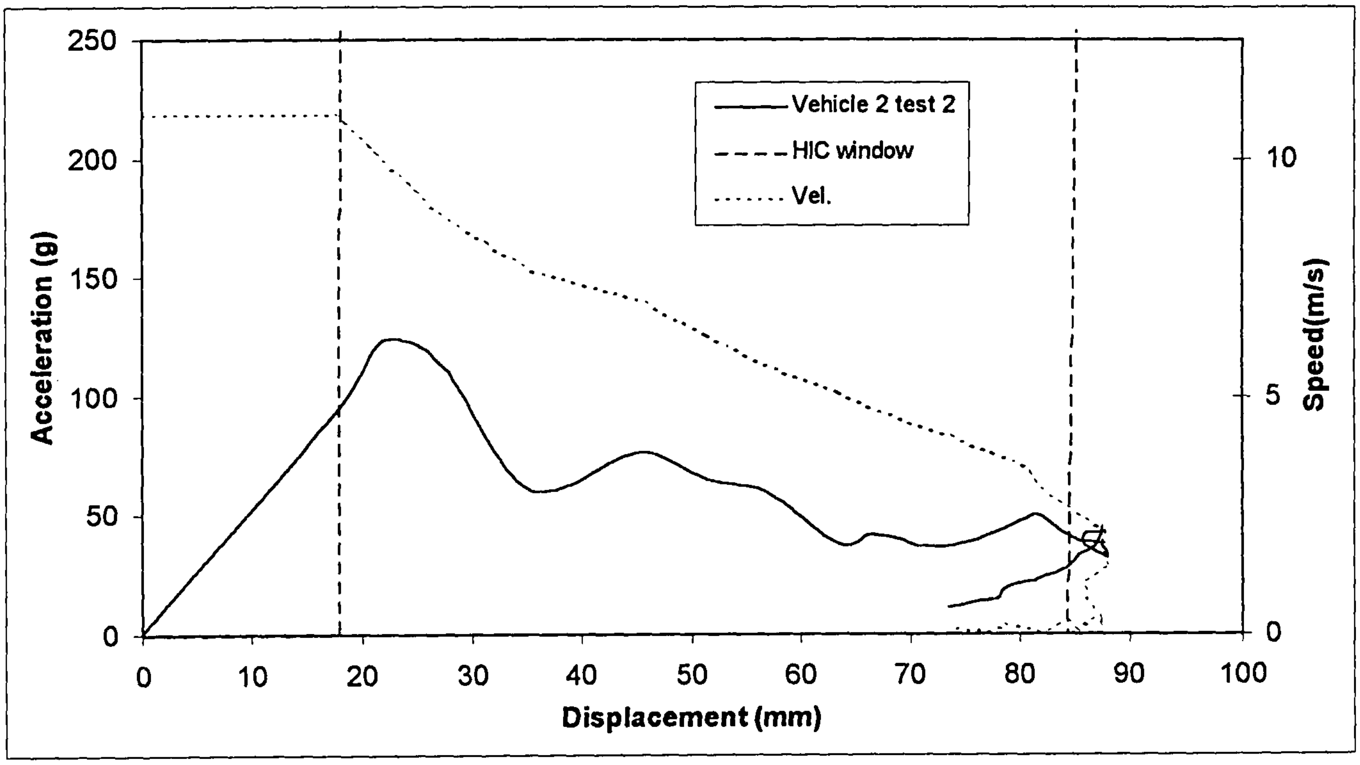
250
200
150
100
50
0
Acceleration (g)
0
10
20
30
40
50
60
70
80
90
100
Displacement (mm)
10
5
0
Speed(m/s)
Vehicle 2 test 2
HIC window
Vel.

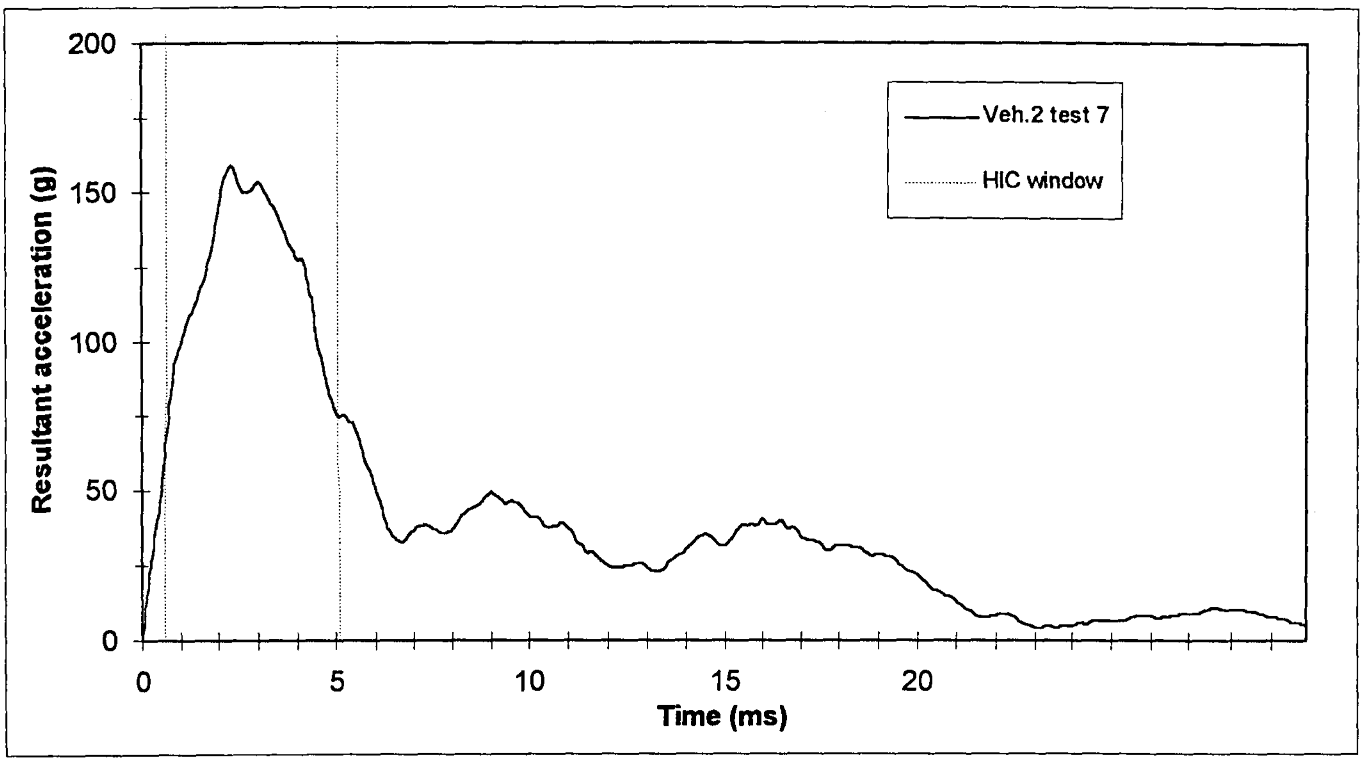
Veh.2 test 7
HIC window
Resultant acceleration (g)
200
150
100
50
0
0
5
10
15
20
Time (ms)

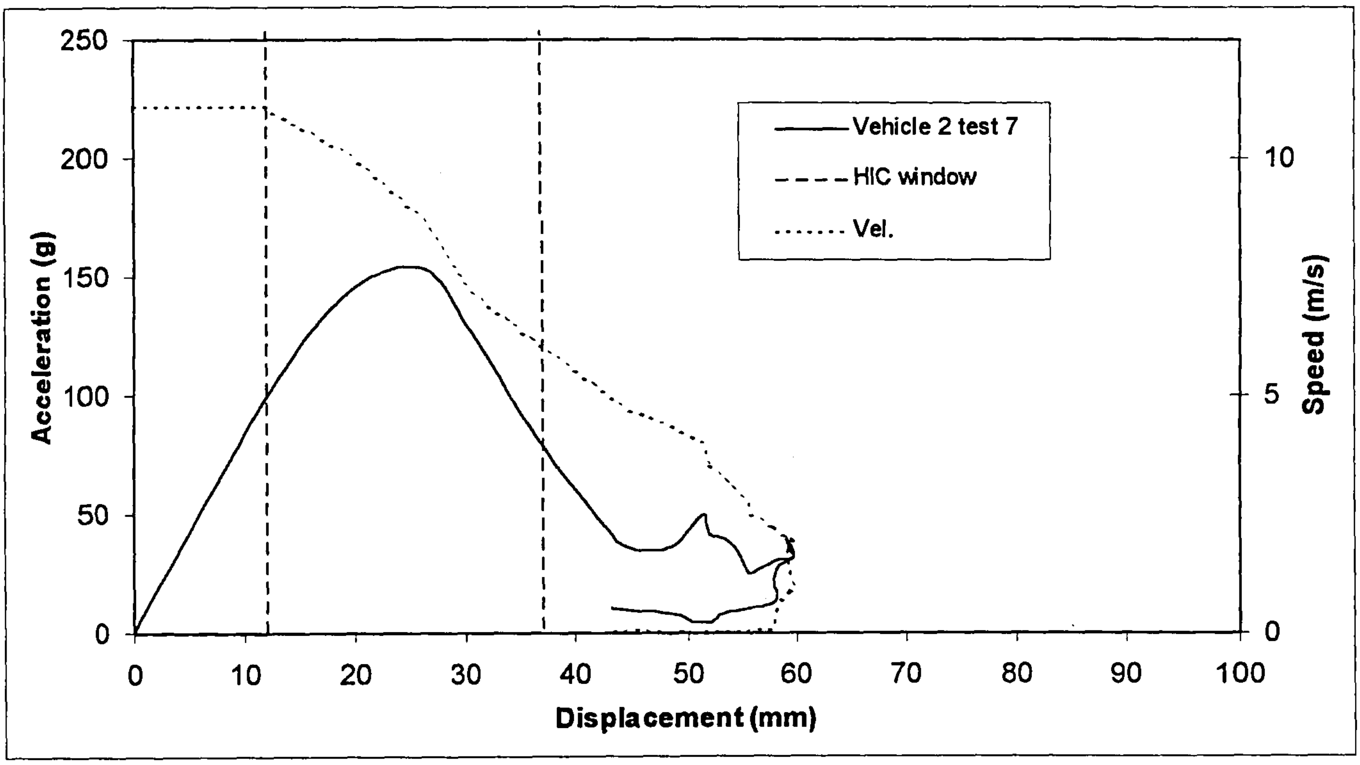
Vehicle 2 test 7
HIC window
Vel.
Acceleration (g)
250
200
150
100
50
0
Speed (m/s)
10
5
0
0
10
20
30
40
50
60
70
80
90
100
Displacement (mm)

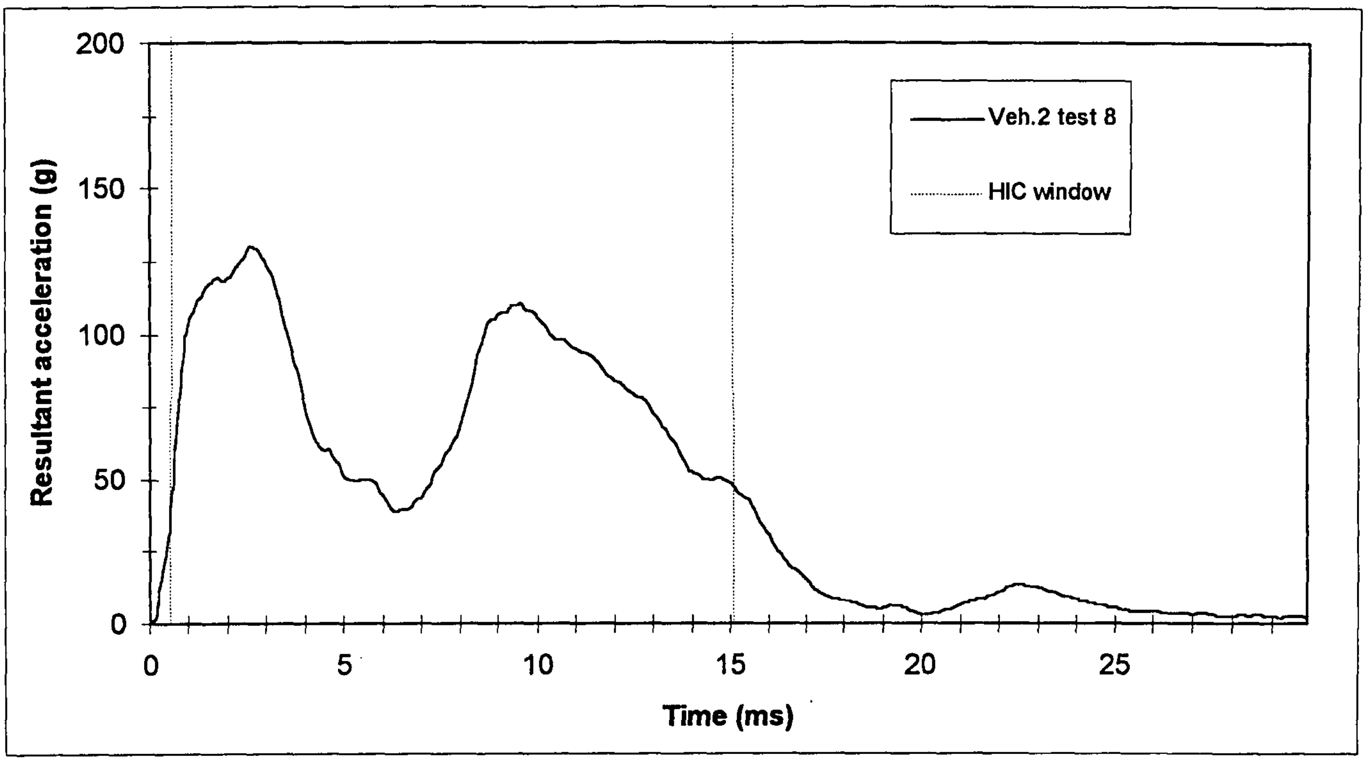
Resultant acceleration (g)
0
50
100
150
200
0
5
10
15
20
25
Time (ms)
Veh.2 test 8
HIC window

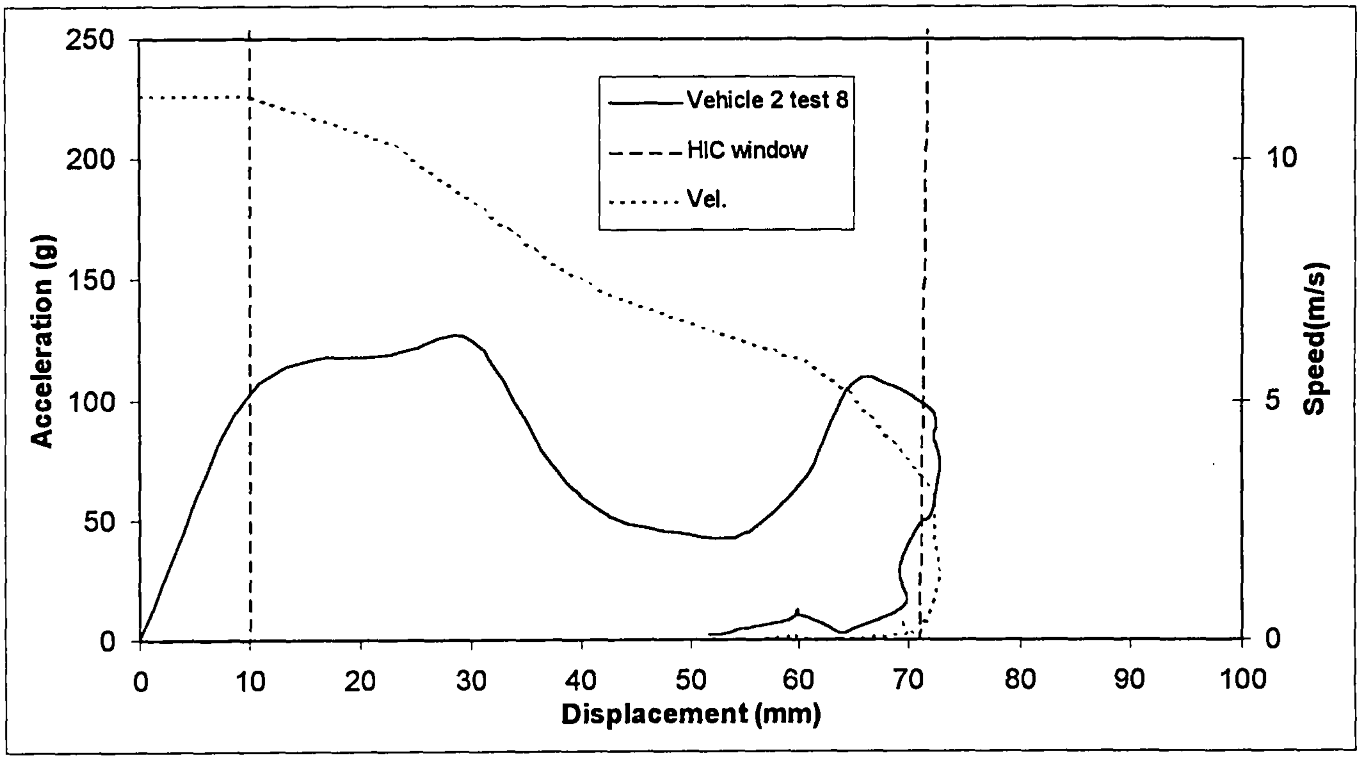
Acceleration (g)
0
50
100
150
200
250
Speed(m/s)
0
5
10
0
10
20
30
40
50
60
70
80
90
100
Displacement (mm)
Vehicle 2 test 8
HIC window
Vel.

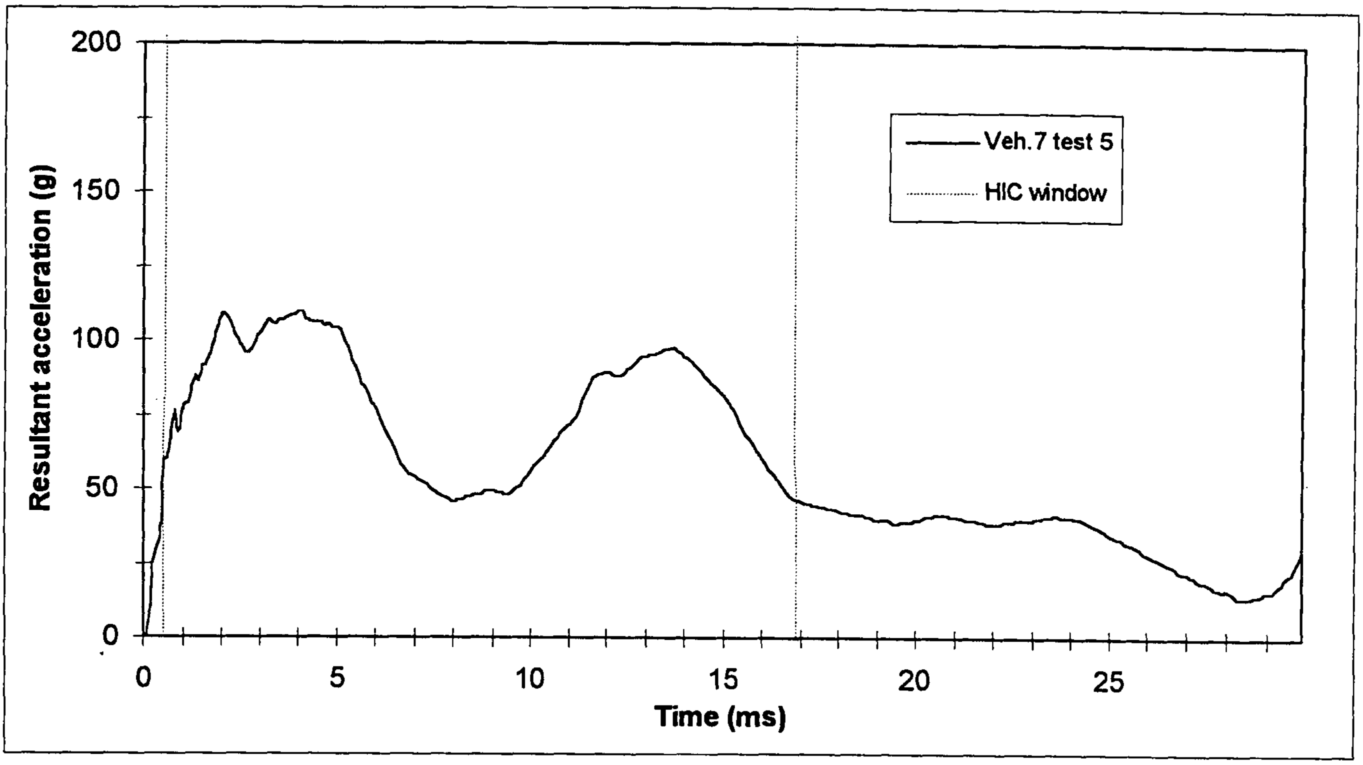
Resultant acceleration (g)
200
150
100
50
0
0
5
10
15
20
25
Time (ms)
Veh.7 test 5
HIC window

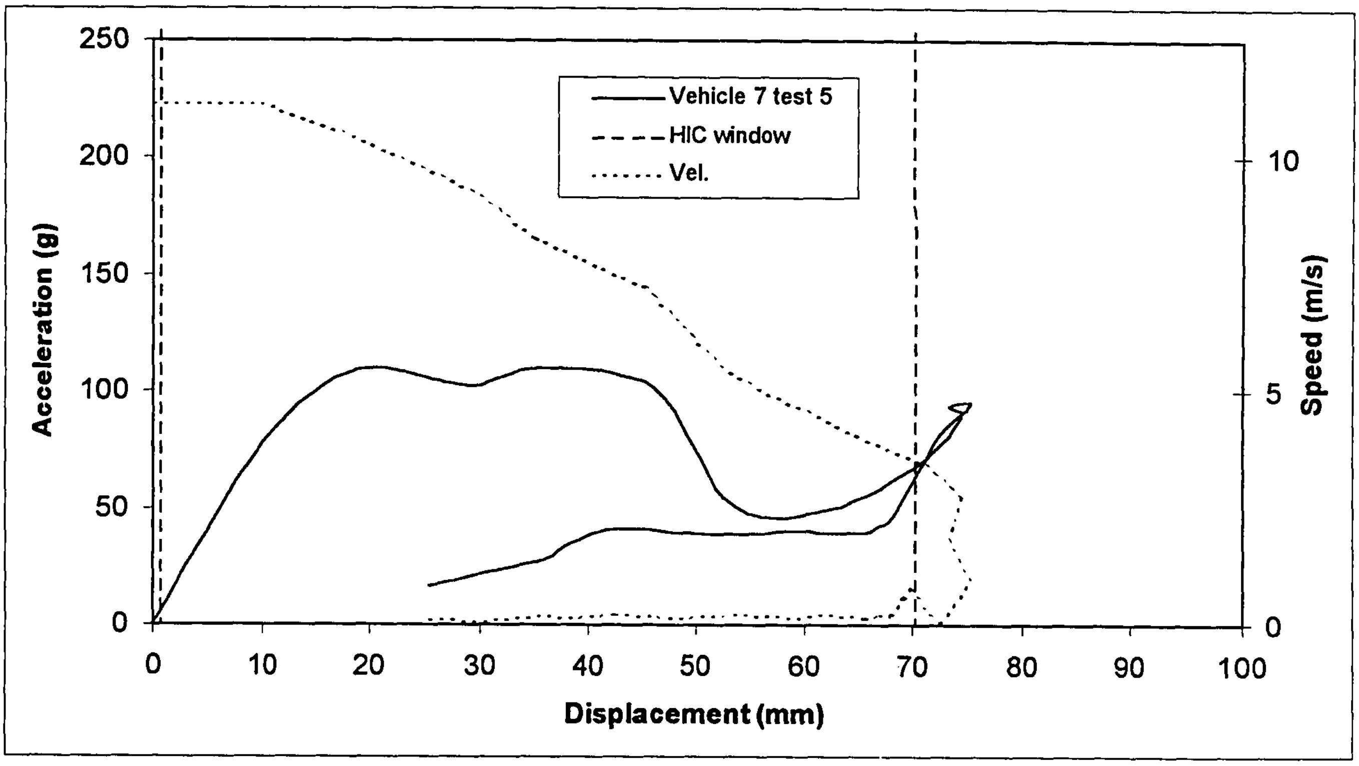
Acceleration (g)
250
200
150
100
50
0
0
10
20
30
40
50
60
70
80
90
100
Displacement (mm)
Speed (m/s)
10
5
0
Vehicle 7 test 5
HIC window
Vel.

SIMULATION OF CAR-PEDESTRIAN ACCIDENT FOR EVALUATE CAR STRUCTURE

Suguru Yoshida
Tetsuo Matsuhashi
Honda R&D Company, Ltd.
Yasuhiro Matsuoka
ESI Japan
Paper Number 98-S10-W-18

ABSTRACT

A new computer system and human body model to simulate the pedestrian road accidents involving vehicles were developed for evaluating vehicle structure and pedestrian injury. The aim of the simulation system is to predict the dynamic behavior of pedestrians and influence of car shape and structure on the pedestrian injury. To evaluate actual vehicle shapes and structures, this system carries simulations into an FEM environment. And new types of human body models were developed for the simulation. The character of human body model is to have a self-scaling modeling program for any pedestrian weight and height and particular joint characteristics obtained by the PMHS test. This paper describes the content of the simulation system and presents some results from the simulations.

INTRODUCTION

Pedestrians account for approximately one-third of those killed by traffic accident in Japan. There has been a desperate call for more effective structures of automobiles to reduce traffic accident casualties drastically. In recent years, responding to those demands, Honda proposed the ASV concept. And EURO-NCAP pedestrian tests are held using EEVC impactor method. To further enhance this safety improvement trend, it has been considered necessary to establish a simulation system for evaluate car structure and for analyze the phenomenon of car pedestrian accidents is desired.

The authors successfully developed one simulation system to reveal pedestrian body behavior. The major feature of the technique is having an analytical dummy of which behavior corresponds to the pedestrian PMHS test data. And it moves in the environment of FEM. This technique can evaluate the vehicle structure and identify phenomenon in car-pedestrian accident.

The new simulation system made it possible to comparatively study the influence of automotive body configuration on pedestrians, which could not otherwise be performed by impactor tests. This paper describes system description and examples of calculations conducted with mass production vehicles.

Simulation System

1. Analytical Dummy Model

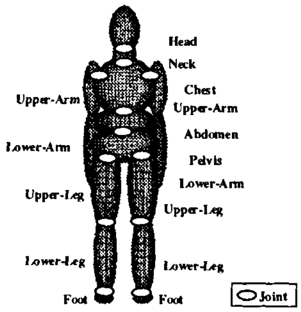

Figure 1. Ellipsoid Dummy

The dummy model described in this paper has 15 ellipsoids segments for each human body. And each geometric shape, center of gravity, inertia moment are created automatically by the program adjusting weight and height of every physiques. Physical properties of joint that connect adjacent segments were assumed to be common for every physique.

The geometrical properties, center of gravity, inertia moments were based on the measurement results of 32 body measurements used by the GEBOD.

This program was capable of creating various dummy models which differ in terms of height, weight, sex, and age (Figure 2.). Also standing initial positions and postures remain variable. It is necessary to determine new joint character in the process of corresponding with PMHS test data.

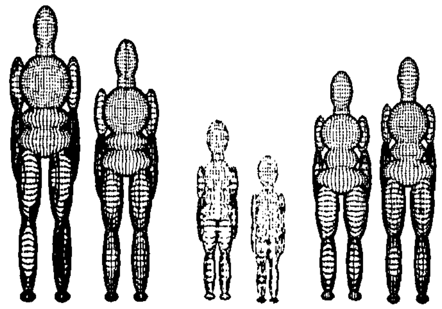

Figure 2. Child, Female, Male dummies

2. Vehicle Model

Two different vehicle models were available in this system. One was conventional ellipsoids and plane model (Figure 3.).

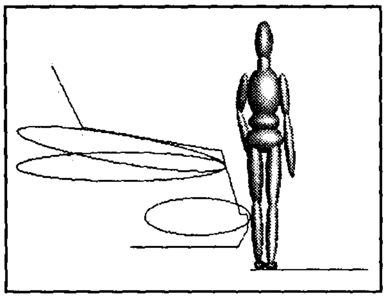

Figure 3. Ellipsoids and plane model

It defined contact forces with pedestrian body in terms of variable representing the amount of pedestrian invasion into vehicle body. This type of model was used to check the correlation with experimental PMHS test data. Another one was FEM model that represented the actual front-end structure of a vehicle (Figure 4.).

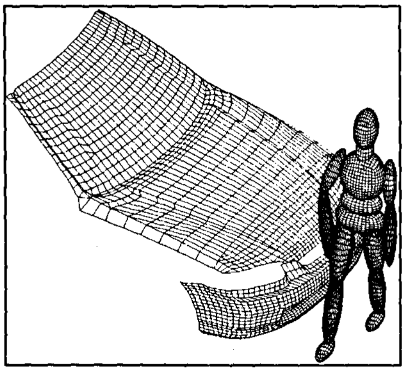

Figure 4. Finite element model

The FEM model enabled us to evaluate body structure using this simulation system.

Joint Character

1. PMHS Test Data

The correlation between simulation results and PMHS test data was studied, especially on joint character. The pedestrian test data used as a reference was that reported by Ishikawa et al(1). The summary of experimental condition was listed in table 1. The simulation were performed based on the conditions listed prior to comparing with experimental results.

Table 1. PMHS test cases

Case	Sex	Hight (m)	Weight (Kg)	Velocity (Km/h)
T2	Male	1.67	56	25
T6	Male	1.78	65	32
T9	Male	1.75	68	39

2. Simulation Model

The vehicle model used was simplified as shown in Figure 3. The bumper, hood edge, hood are modeled by ellipsoids and front windshield modeled by a plane.

All the components of the vehicle modeled as solid bodies featuring rigidity in terms of variable representing the amount of pedestrian invasion into vehicle body. And coefficient of friction between pedestrian and vehicle body was 0.25 and that between pedestrian and road surface was 0.67.

Each joint character could be determined by comparing the results of the PMHS tests and simulations. Those were described by comparison between that of Hybrid Ⅱ dummy which is widely used for frontal crash tests.

When compared with Hybrid Ⅱ properties, the one determined featured a Neck bending rigidity of approximately 25% and a Torso bending rigidity of approximately 50%. The lateral bending characteristics of Hip joint is free until it reached to 30 degree. And lateral bending of Knee is 200Nm at bending angle 15° Lateral bending of Ankle is 120Nm at bending angle 30°. The bending rigidity for the Shoulder and Elbow joints remained minimal. And Ishikawa (1) describes stretch behavior of human body. Then elongation type of spine model was produced and was included in the options. The elongation properties were identified by experimental result of several cases that achieved by varying vehicle velocity.

3. Simulation results

Figure 5. shows behavior of human model after crash at experimental condition T6 test for example of calculation.

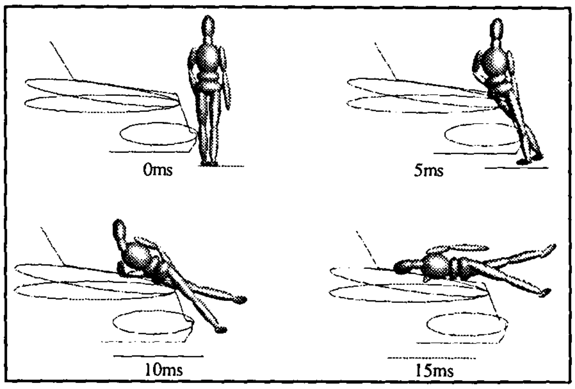

Figure 5. Simulation example

And Figure 6. explains trajectories of each pedestrian parts. Figure 7. shows Head velocities at different velocity conditions of T2, T6, T9.

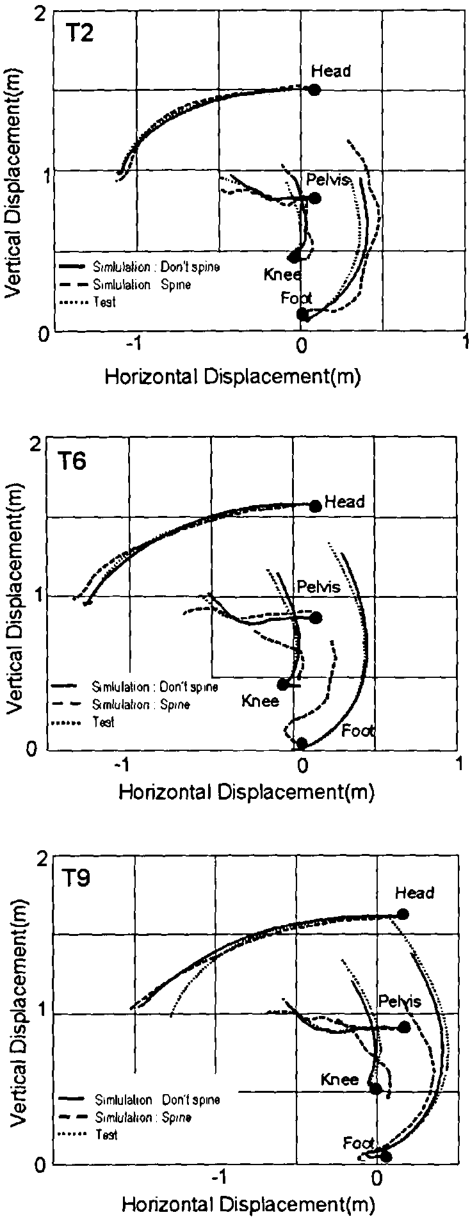

Figure 6. Trajectories of body segments (Fixed car body coordinate)

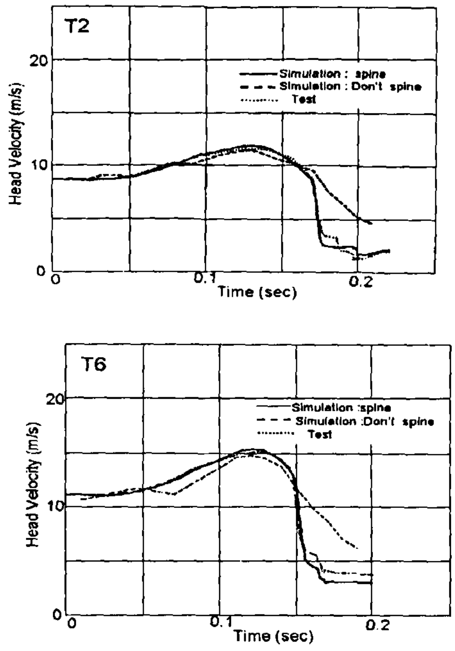

Figure 7. Head resultant velocity

In Figure 6. and 7., dotted lines represent the experimental results, whereas the solid lines shows simulation. Two combinations of the lines represent results that does not considering spine elongation. In Figure 6., each trajectory represent those of the Head, Pelvis, Knee, Foot in relation to vehicle coordinate.

Looking at trajectory of pedestrian after crash, in the case of T2 that has low velocity, simulation result shows good corresponding with experimental result. Oppositely in the case of T9 that has high velocity condition, ultimate difference reached approximately 220mm in Head trajectory.

Then considering the elongation of spine joint, adding the elongation properties correspond with test, we obtained the nearly trajectory of head at case T9.

And foot behavior shows difference between simulation and test in case T6. The reason for the difference in the leg trajectories under T6 condition was attributable to the fact that the simulation did not deal with a leg bone fracture which had occurred in the experiment.

In Figure 7., head velocity at low velocity condition shows better corresponding than that of high velocity cases. As same as trajectory of body parts, it shows consideration of spine elongation supply better corresponding for test result of T9.

Analytical Results with Mass Production Vehicles

1. Analysis with FEM Vehicle Model

As the examples of car-pedestrian crash simulation, examination was made to show the influence of configuration at mass product vehicles. Figure 8. and Figure 9. depict cross section of mass production models used in the simulation.

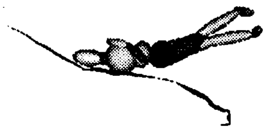

Figure 8. Vehicle A

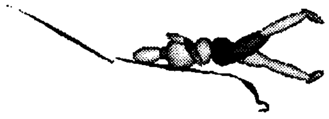

Figure 9. Vehicle B

There had been no significant differences in the striking potential between vehicles A and B in the impactor test similar to the EEVC.

At first he FEM models of car A and car B were made. And the analytical dummy models, described in the earlier sections, were set at between 140-160cm in height, which represent the majority of casualties in road traffic accident in Japan.

Calculation was executed using the dummy and FEM car model in environment of PAM-CRASH.

2. Difference of Head Trajectory

Firstly the comparison of head trajectory between car A and car B was investigated from results of accident simulation.

The analysis showed that there were differences in contact points and angles, though no significant difference was found with the head velocity at the moment of contact.

Showed by Figure 10., the head trajectory of Vehicle B finished relatively forward of area when compared with that observed with Vehicle A. Additionally, the contact angle was larger in case of Vehicle A. At the other hand velocity of head is almost same.

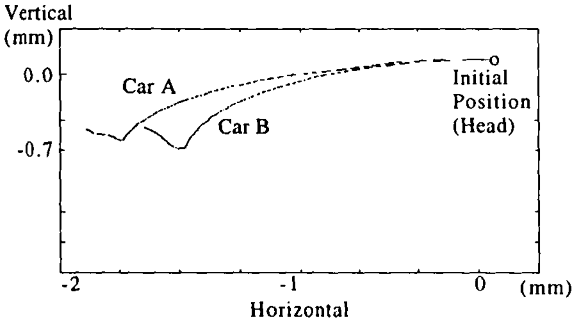

Figure 10. Head Trajectories

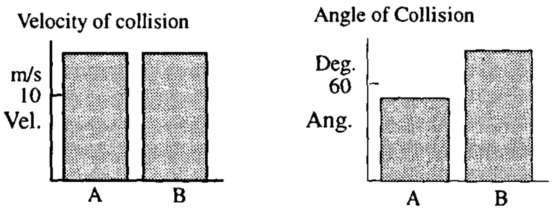

Fig 11. Head Velocities and Angles

This is presumed to be caused by the influence of the front-end design difference, which resulted in the differences in dummy behavior.

In the impactor test currently being carried out, the crash velocity and angle of the impactor to the vehicle are defined as constant.

3. Difference of Chest Trajectory

Secondly, the comparison of chest trajectory was investigated. As shown in Figure 12., the chest trajectory of the pedestrian with a height between 150-160cm tended to come into contact with the hood area above the cylinder head. Then it is possible that chest injury becomes different between Vehicle A and B.

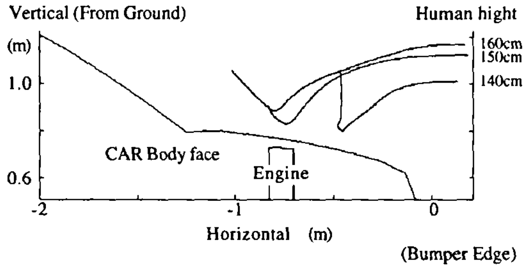

Figure 12. Chest trajectories

The difference of pedestrian behavior between car A and car B can be estimated by followings. One is difference of head angles when head contacts the car, and another is difference of contact position of chest that caused by frontal shapes of cars.

As a result, the simulation system was proved to be somewhat effective in revealing the difference in pedestrian body behavior due to the difference in front-end configuration, which had not been identified by the impactor test.

Conclusion

About the pedestrian behavior in the accident, described ellipsoidal simulation dummy could correspond to several experimental results. Also, the FEM analysis method which is basis for analytical evaluation of the vehicle body configuration and structure was established.

For future studies, the amount of data would be increased as much as possible in order to further improve the joint and elongation characteristics. And it is considered necessary to develop dummy model that can calculate injury seriousness, to predict injury of pedestrian. Then the measure for this problem, the dummy model build by FEM element is now considered (Figure 13.).

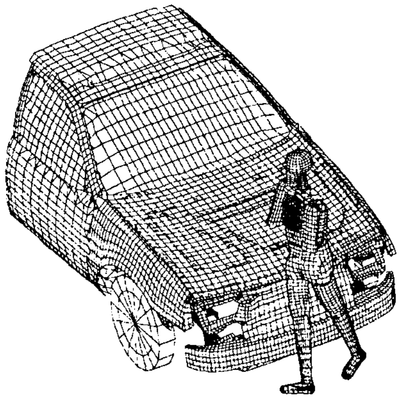

Figure 13. Finite Element Dummy

It can be made automatically for each height and weight. Basic model should be a EuroSID model with the 15 joints from the neck down to the hip. Upper leg, hip, chest, head, and arms are modeled using the FEM mesh. Injury analysis will be conducted with the model.

6. Acknowledgment

Finally, the authors would like to extend their gratitude to Dr. Hirotoshi Ishikawa of the Japan Automobile Research Institute (JARI) for valuable advice in developing the simulation system.

A STUDY ON PEDESTRIAN IMPACT TEST PROCEDURE BY COMPUTER SIMULATION

- The Upper Legform to Bonnet Leading Edge Test -

Atsuhiro Konosu
Hirotoshi Ishikawa
Japan Automobile Research Institute
Akira Sasaki
Japan Automobile Manufactures Association, Inc.
Japan

Paper Number 98-S10-W-19

ABSTRACT

EEVC/WG10 proposed three component pedestrian subsystem tests. Pedestrian subsystem impact tests with production cars have been conducted in Euro-NCAP according to the EEVC test method. From the Euro-NCAP the upper legform impact test has the most difficulty fulfilling the current injury criteria. However, recent accident analyses indicate that the priority of the upper legform test seems to be the lowest in the three EEVC subsystem tests.

The objective of this research is to validate the test conditions of the EEVC upper legform impact test using computer simulation models.

There is a possibility that the impact energy defined from the EEVC look-up graph may include significant errors. The values of the EEVC impact energy can be decreased about 30% for cars with a 650mm to 750mm bonnet leading edge height.

It is not necessary to use an impact velocity look-up graph which should be calculated directly using a specific impactor mass and an impact energy defined from an impact energy look-up graph.

INTRODUCTION

The European Experimental Vehicles Committee (EEVC/WG10) has proposed three component pedestrian subsystem tests for evaluating the vehicle safety performance in car-pedestrian accident. The three subsystem tests are headform impact to bonnet top, upper legform impact to bonnet leading edge, and legform impact to bumper.

Recently pedestrian impact tests with production cars have been conducted in the Euro-NCAP test program according to the current EEVC subsystem test method. The test results indicate that the upper legform impact test has the most difficulty fulfilling the current injury criteria. However, recent accident analyses indicate that the priority of the upper legform impact test seems to be the lowest in the three EEVC subsystem tests. This contradiction raised questions of whether the current upper legform impact test reflects the real world pedestrian accidents.

Accordingly, we validated the EEVC upper legform impact test conditions using computer simulation models. Both the car-pedestrian impact tests and the upper legform impact tests were simulated.

This paper outlines the computer simulation models and summarizes the parameter study concerning the EEVC test conditions of the upper legform impact test.

DEVELOPMENT OF COMPUTER SIMULATION MODELS

Car-Pedestrian Impact Model (Model A)

A car-pedestrian impact model was developed as shown in Figure 1 to understand the impact conditions at the bonnet leading edge when a car hits a pedestrian. MADYMO-5.3 was used in this study.

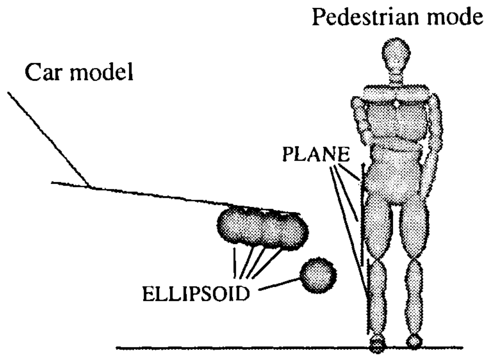

Figure 1. Computer simulation model of car-pedestrian impact (Model A).

To simplify the contact condition between car and pedestrian, the car-pedestrian impact model uses only two types of elements (ELLIPSOID and PLANE), and only ELLIPSOID-PLANE contact is defined. ELLIPSOID is used to represent the bumper and the bonnet leading edge. The pedestrian model is made by ELLIPSOID, however PLANEs are attached to the ELLIPSOIDs representing the pelvis, the upper leg, and the lower leg.

The model was validated by comparing the trajectories of the body segments in computer simulations and those from full-scale tests with PMHS (Post Mortem Human Subject)(1). The trajectories of the PMHS were normalized by their height. Their trajectory corridor was then made as shown in Figure 2. The trajectories obtained from the computer simulations were within the corridor. Accordingly, the car-pedestrian impact model can be used for this study.

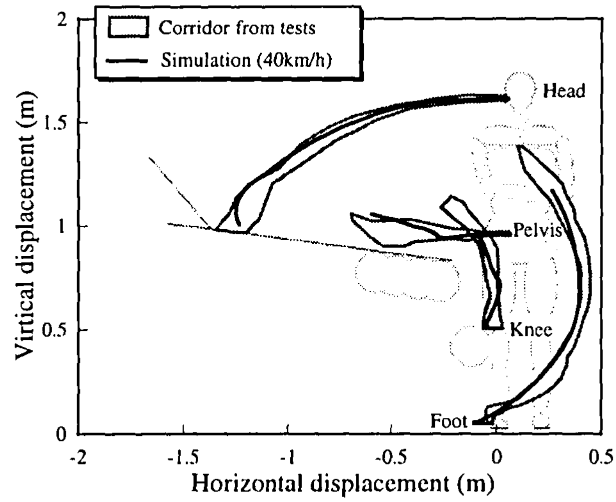

Figure 2. Validation of car-pedestrian impact model.

Upper Legform to Bonnet Leading Edge Test Model (Model B)

In order to understand the correlation between pedestrian full-scale tests and subsystem tests, an upper legform to bonnet leading edge test model was developed as shown in Figure 3. The impactor model has a translational joint to simulate the guiding system of the EEVC upper legform impactor. ELLIPSOID-PLANE contact is used to simplify the contact condition.

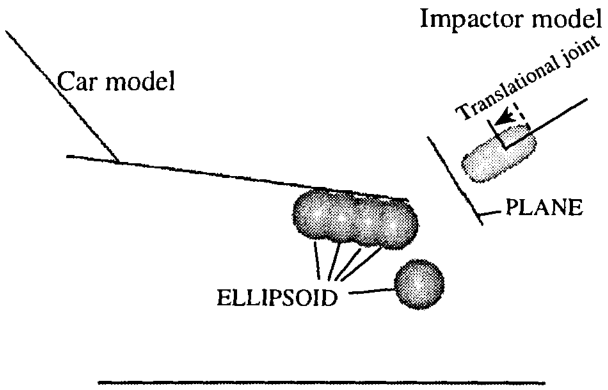

Figure 3. Computer simulation model of upper legform impact test (Model B).

PARAMETER STUDY

Parameter

In order to understand how the car front shape affects the test conditions of the EEVC upper legform test, simulations were performed for 42 cases. Figure 4 shows the definition of the car front shape. Table 1 shows the parameters used for the 42 simulations. Bumper center height is 390mm in all cases, since the bumper height doesn't cause significant differences on the test conditions. The EEVC upper legform test does not consider the bumper height in deciding its test conditions either.

The car impact speed is 40km/h. The car exterior stiffness is constant in all cases as shown in Figure 5. This stiffness is derived from the previous study using MADYMO-2D(2).

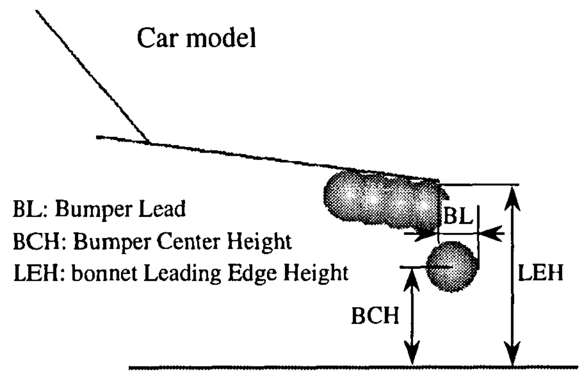

Figure 4. Definition of car front shape (BL, BCH, LEH).

Table 1. Parameters for 42 Simulations.

		BL (mm)					
		0	50	100	150	225	350
LEH (mm)	600	○	○	○	○	○	○
	650	○	○	○	○	○	○
	700	○	○	○	○	○	○
	750	○	○	○	○	○	○
	800	○	○	○	○	○	○
	850	○	○	○	○	○	○
	900	○	○	○	○	○	○

BCH: 390 mm

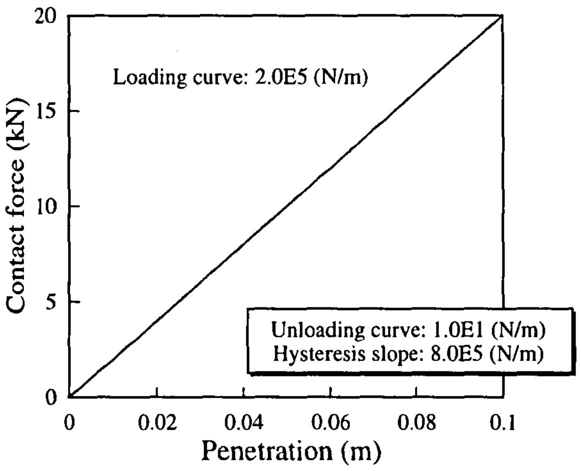

Figure 5. Car exterior stiffness used in all simulations.

Simulation Results

Impact Energy by EEVC Method

Impact energy was calculated by using two methods (EEVC method and new method). The first method or EEVC method was developed by EEVC to obtain the impact energy from their full-scale dummy tests(3). EEVC calculated values of horizontal energy from the measured forces and the relative displacements of the leg into the bonnet leading edge in the full-scale tests. They admit that accurate calculations of the deformation energy of the bonnet leading edge contact from full-scale tests is difficult.

There is a major problem in the EEVC method. Specifically, it should be noted that the direction of the relative displacement is not comparable to the direction of the resultant force vector in the EEVC method. The EEVC method assumes this difference is small. This assumption may be acceptable in calculating the impact energy for higher bonnet leading edge. However, this assumption cannot be used for the lower bonnet leading edge since there is significant sliding between the upper leg and the bonnet leading edge, and the directions of the relative displacement and the force vector are completely different.

The previously mentioned two computer simulation models were used in order to validate the EEVC method. The impact energy calculated from the car-pedestrian impact model was used to reconstruct the equivalent bonnet leading edge impact using the upper legform to bonnet leading edge test model.

The impactor force was divided by the femur/pelvis contact force to obtain the impact force ratio. If the subsystem test is equivalent to the full-scale test, the impact force ratio should become one. Figure 6 shows the impact force ratio obtained from the computer simulations using model A and model B at different bonnet leading edge

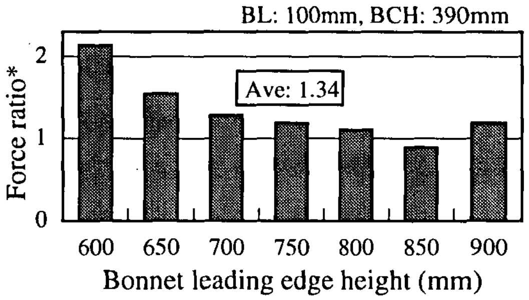

$$* \text{ Force ratio} = \frac{\text{Impactor force}}{\text{Femur/pelvis contact force}}$$

Figure 6. Impact force ratio from EEVC method.

heights. Most of the ratios exceed one. The average impact force ratio is 1.34. Note that the force ratio becomes nearly one when the bonnet leading edge height becomes higher. In contrast, the force ratio becomes more than 1.5 when the bonnet leading edge height becomes lower. This result suggests that the EEVC method may cause significant errors in calculating the impact energy, especially when the bonnet leading edge height becomes lower.

Impact Energy by New Method

Impact energy was also calculated by the new method. The new method uses normal impact force and penetration excluding tangential friction force to calculate the impact energy. This means that the friction energy is excluded in the new method. The friction energy should be excluded in the current EEVC upper legform impact test since the upper legform is guided and it is positioned perpendicular to the impact direction. The guided upper legform impactor cannot reconstruct the sliding mechanism at the contact surface.

Note that the direction of the penetration coincides with the direction of the normal impact force in the new method. This method can accurately calculate the impact energy in the normal direction even if there is significant sliding between the upper leg and the bonnet leading edge, although the energy due to the tangential sliding is not available.

The new method was also validated in the same way previously introduced for the EEVC method. Figure 7 shows the impact force ratio obtained from the computer simulations. Most of the ratios are close to one. The average impact force ratio is 1.01. This result clearly indicates that the impactor force in the subsystem test may become identical to the femur/pelvis contact force in the full-scale test if we use the impact energy defined by the new method.

Accordingly, the new method can be more realistic than the EEVC method in obtaining the impact energy look-up graph for the upper legform impact test.

Figure 8 shows the impact energy curves obtained from the computer simulations using the new method. When we compare the new impact energy curves with the EEVC look-up graph, the influence of bumper lead on the impact energy becomes less significant for lower bonnet leading edges. However, for higher bonnet leading edge, the bumper lead varies the impact energy significantly.

The impact velocity decreases inversely to the increase of bumper lead (see Figure 13). When the bumper lead increases, the contacting point may sift from femur to pelvis as shown in Figure 9. The effective mass at the contacting point may then increase accordingly. The decrease of impact velocity due to the increase of bumper lead does not necessarily decrease the impact energy, since the impact energy is decided from the combination of the impact velocity and the effective mass. The values of impact energy

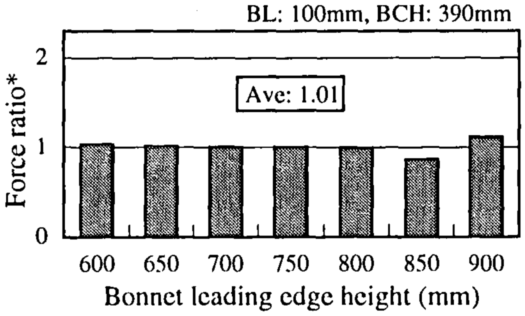

$$* \text{ Force ratio} = \frac{\text{Impactor force}}{\text{Femur/pelvis contact force}}$$

Figure 7. Impact force ratio from new method.

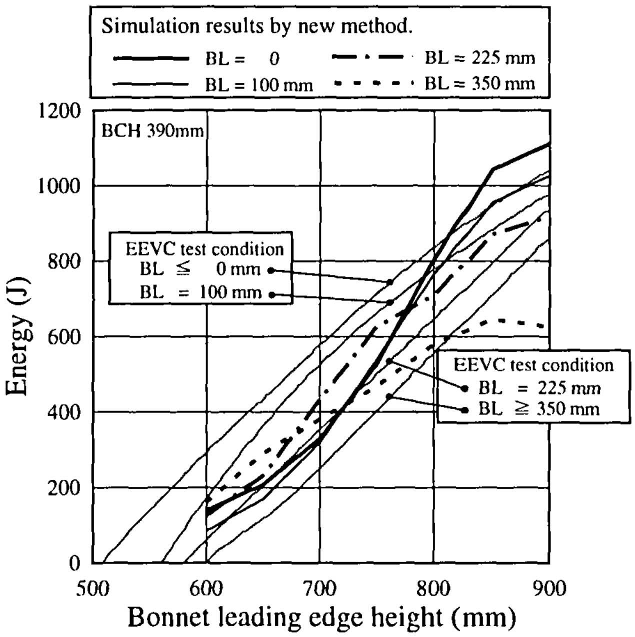

Figure 8. Impact energy curves by new method with the EEVC look-up graph.

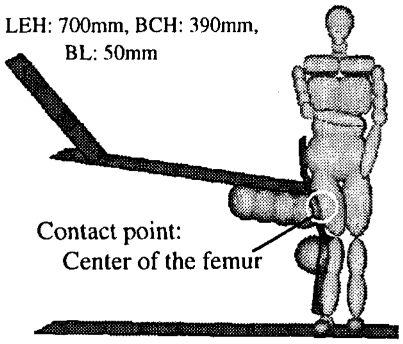

1) Contact at femur center. (BL:50mm)

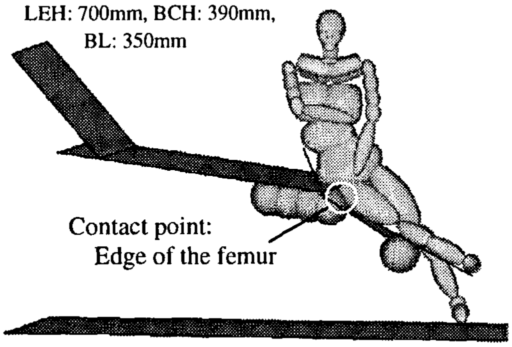

2) Contact near hip joint. (BL:350mm)

Figure 9. Contact point by bumper lead.

in the EEVC look-up graph always increase when the bumper lead decreases. This tendency is not seen in the new impact energy curves from the new method.

The femur/pelvis contact point can be determined geometrically considering the wrap around distance at the femur/pelvis contact point. If the bonnet leading edge is high or bumper lead is very long, the pelvis contacts the bonnet leading edge directly. The contact point shifts only on the pelvis, and the effective mass does not vary significantly, as compared to the femur-to-bonnet leading edge contact. If the contact point is on the pelvis, the variation of the impact energy can be mainly due to the variation of the impact velocity. If the contact point is on the femur, the variation of both the impact velocity and the effective mass cause the difference of the impact energy. Values of impact energy do not necessarily increase in relation to the decrease of bumper lead. However, the values of impact energy in the EEVC look-up graph always increase when bumper lead decreases.

The influence of bumper lead on the impact energy is insignificant when the bonnet leading edge is lower than 800mm and the bumper lead is less than 225mm. This zone may cover many production cars nowadays. Accordingly, one regression curve can be proposed to calculate the impact energy more simply as shown in Figure 10. This regression curve is expressed by Equation (1).

$$Energy(J) = -5.111\times10^{-5}LEH^3 + 1.149\times10^{-1}LEH^2 - 8.204\times10^{1}LEH + 1.901\times10^{4} \quad (1)$$

LEH: *Bonnet leading edge height (mm)*

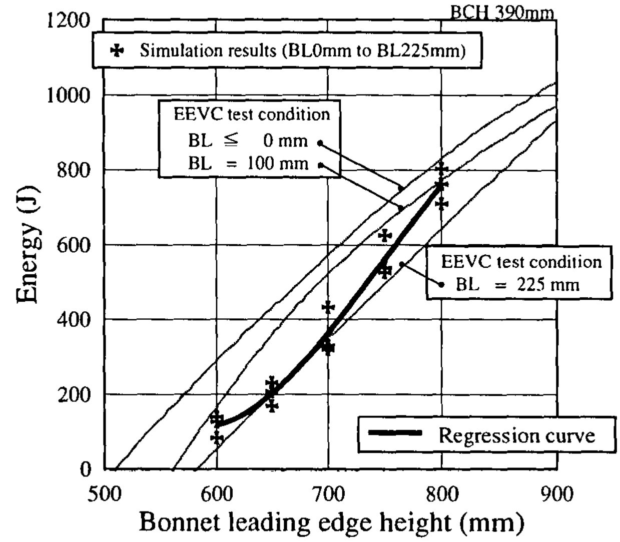

Figure 10. Impact energy regression curve by new method with the EEVC look-up graph.

Impact Angle by EEVC Method

Impact angle was calculated using two methods, the EEVC method and a new method. In the EEVC method, the horizontal and vertical contact forces relative to the ground coordinate system are integrated by time to obtain impulses in the horizontal and vertical directions(3). The impact angle is calculated from these horizontal and vertical impulses. The start and end angles are calculated from the horizontal and vertical impulses. Their average value is then used to produce an impact angle look-up graph. The start and end times are taken as the time at which the resultant force rises to 40% of the peak value and the time at which it falls below 40% of the peak force.

The horizontal and vertical contact forces include friction force caused by a sliding at the bonnet leading edge. The impact angle obtained from the EEVC method can be influenced by the friction force.

The impact angle curves from the computer simulations using the EEVC method are shown in Figure 11 with the EEVC impact angle look-up graph. The calculated values of the impact angle vary more significantly according to the bonnet leading edge height as compared to the EEVC impact angles. When the bonnet leading edge is higher than 800mm, the influence of the bumper lead on the impact angle becomes negligible. When the bonnet leading edge height is lower than 800mm, the extent of the bumper lead influence on the impact angle increases in relation to the decrease of the bonnet leading edge height.

Impact angle curves differ between the simulation results and the EEVC values as described previously. However, their general tendencies are comparable.

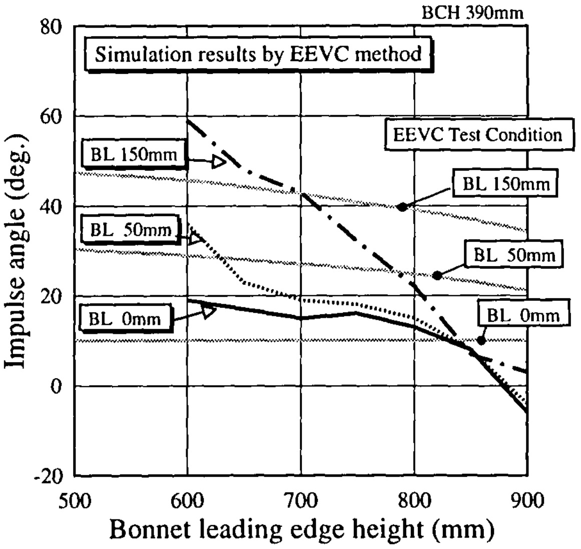

Figure 11. Impact angle curves by EEVC method with the EEVC look-up graph.

Impact Angle by New Method

The new method is almost the same as the EEVC method, but it excludes the friction force component. The friction force may affect the car deformation, but may not contribute to the femur lateral deformation. The impactor test is conducted against the perpendicular direction of the front member, so the impact angle should be calculated using only the impact force perpendicular to the front member.

The impact angle curves obtained from the computer simulations using the new method are shown in Figure 12 with the EEVC impact angle look-up graph. The impact angle curves calculated by the new method are similar but shift about 10 degrees upward relative to those from the EEVC method because the friction force works to decrease the impact angle.

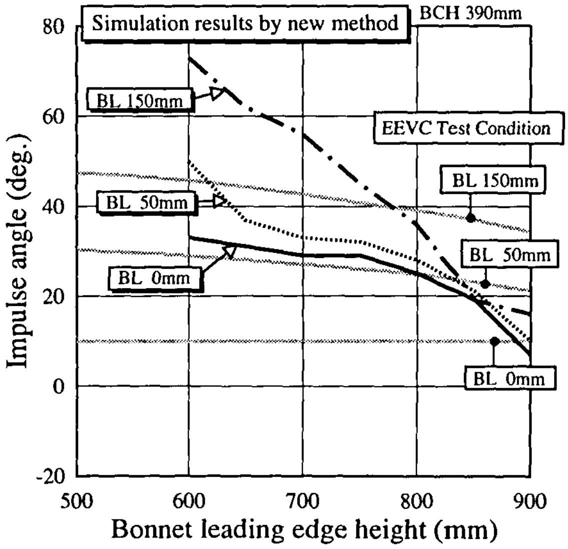

Figure 12. Impact angle curves by new method with the EEVC look-up graph.

Impact Velocity

Upper leg impact velocity against the bonnet leading edge depends strongly on the vehicle shape, especially the bonnet leading edge height and the bumper lead. Impact velocities calculated from the computer simulations of 42 cases are plotted in Figure 13 in which the EEVC impact velocity curves are also superimposed. The calculated impact velocities are nearly identical to the values in the EEVC look-up graph when a shaded zone is excluded.

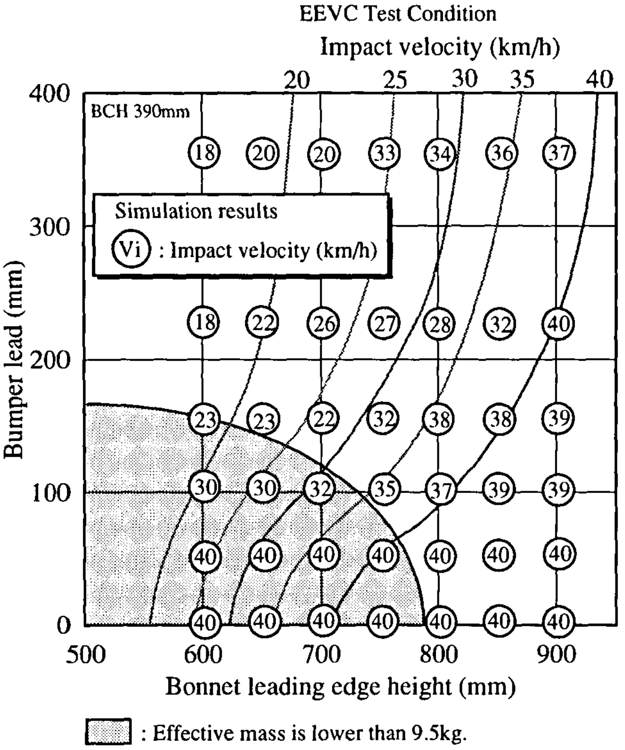

Figure 13. Calculated impact velocity with the EEVC look-up graph.

The effective mass at the bonnet leading edge contact was about 2kg to 25kg from the computer simulations. The effective mass is calculated from Equation (2).

$$M_{eff} = \frac{2E}{V_i^2} \qquad (2)$$

M_{eff} : Effective mass, E : Impact energy, V_i : Impact velocity

It is very difficult to develop a small impactor with the necessary instrumentation. EEVC selected a minimum impactor mass of 9.5kg to obtain the EEVC look-up graph$^{(4)}$. Accordingly, we modified our calculated values in the shaded zone by compensating for the mass ratio, using the minimum impactor mass of 9.5kg, under the same impact energy. Equation (3) explains this method.

$$V_{im} = \sqrt{\frac{M_{eff}}{9.5}} \times V_i \qquad (3)$$

(Effective mass < 9.5kg)

V_m : Modified impact velocity, M_{eff} : Effective mass (kg),

V_i : Impact velocity

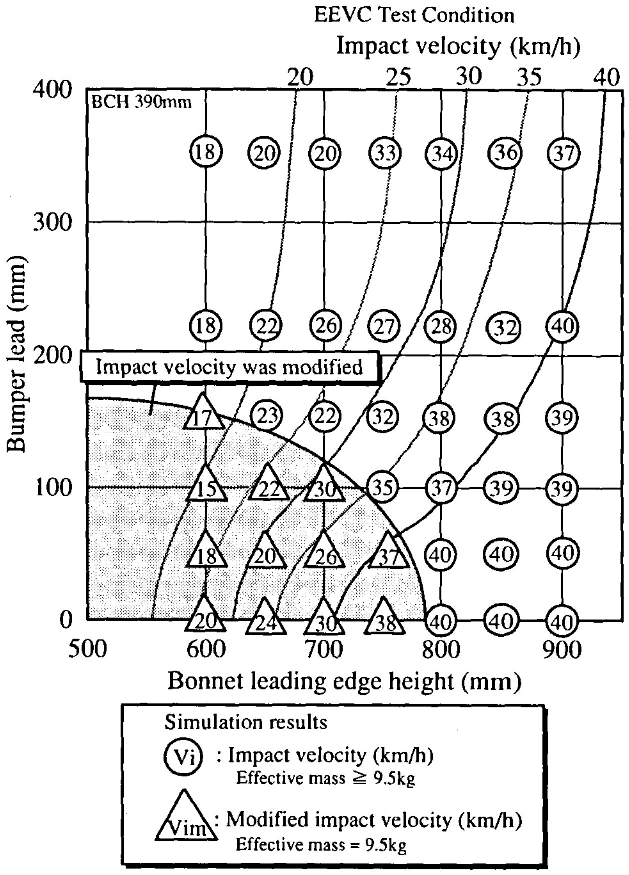

Figure 14. Calculated and modified impact velocities with the EEVC look-up graph.

Figure 14 shows the results of this modification. All values in the shaded zone are relatively smaller than those in the EEVC curves. Note that all cars included in the shaded zone are tested by the impactor mass of 9.5kg at the modified impact velocity.

Nowadays many cars with streamlined shape are included in the shaded zone. EEVC assumed that the modification of the impact velocity doesn't not affect the test results under the same impact energy. If this assumption is correct, the EEVC impact velocity look-up graph is not necessary. It should be noted that impactor mass can be constant in all tests. Impact velocity is calculated directly by Equation (2) with a specific impactor mass and an impact energy defined from the look-up graph.

Impact tests should be simple. It doesn't seem necessary to change the impactor mass in each test.

CONCLUSIONS

EEVC test conditions of the upper legform impact test were validated using computer simulation models. Conclusions are summarized below.

(1) Computer simulation results raised the possibility that the impact energy defined from the EEVC look-up graph may include significant errors, especially for cars with a lower bonnet leading edge. For example, the values of the EEVC impact energy can be decreased about 30% for passenger cars with a 650mm to 750mm bonnet leading edge height.

(2) It is not necessary to use an impact velocity look-up graph. Impact velocity should be calculated directly by Equation (2) using a specific impactor mass and an impact energy defined from an impact energy look-up graph.

(3) Impact angles from computer simulations vary more significantly according to the bonnet leading edge height and the bumper lead as compared to the values in the EEVC look-up graph. However, their general tendencies are comparable.

REFERENCES

(1) Ishikawa H., Kajzer J. and Schroeder G., "Computer Simulation of Impact Response of the Human Body in Car-Pedestrian Accidents". 933129, 37th Stapp Car Crash Conference Proceedings (P-269), 1993.

(2) Janssen E.G. and Nieboer J.J., "Protection of Vulnerable Road Users in the Event of a Collision with a Passenger car. Part 1 - Computer Simulations". TNO report No: 75405002/I, December 1, 1990.

(3) Lawrence G.J.L., "The Upper Legform Test Explained and Justified", EEVC WG17 Committee paper, 28/29 January, 1998.

(4) Lawrence G.J.L., Private Communication, March 1998.

(5)EUROPEAN COMMISSION, (1996). Draft proposal for a European Parliament Council Directive relating to the protection of pedestrians and other road users in the event of a collision with a motor vehicle. European Commission DG III/5021/96 EN, Brussels, 7 February 1996.

(6) European Experimental Vehicles Committee, "Proposals for Methods to Evaluate Pedestrian Protection for Passenger Cars", EEVC Working Group 10 report, November 1994.

(7) Lawrence G.J.L., Harris J. and Hardy B.J., "Development of a Bonnet Leading Edge Sub-Systems Test to Access Protection for Pedestrians". EC contract, ETD/89/7750/MI/28, TRRL, January 1991.

(8) Ishikawa H., Yamazaki K. and Ono K., "Current Simulation of Pedestrian Accidents and Research into Pedestrian Protection in Japan". 91-S3-O-05, The 13th International Technical Conference on Experimental Safety Vehicles, November 4-7, 1991.

INJURY RISK/BENEFIT ANALYSIS OF MOTORCYCLIST PROTECTIVE DEVICES USING COMPUTER SIMULATION AND ISO 13232

Scott. A. Kebschull
John W. Zellner
Michael Van Auken
Dynamic Research, Inc
United States
Nicholas M. Rogers
International Motorcycle Manufacturers Association
Switzerland
Paper Number 98-S10-W-26

ABSTRACT

International Standard 13232 provides common research methods for assessing the feasibility of proposed protective devices which might be fitted to motorcycles. This paper reviews the Part 7 computer simulation requirements of the Standard; and applies the simulation to an example injury risk/benefit analysis (Part 5) of a proposed UKDS motorcycle leg protector device. Overall, the computer simulation and injury risk/benefit analysis portions of the Standard were found to be practical and feasible. The analysis of the UKDS leg protector indicated that a motorcycle equipped with this device increases total injury costs to motorcycle riders in impacts with passenger cars, and therefore should not be fitted to motorcycles.

INTRODUCTION

During the last 25 years, research on the feasibility of rider crash protection devices which might be fitted to motorcycles has occurred in Great Britain, Japan, Germany, and the United States. One example of such research in the 1980's was the leg protector work of TRRL, the United Kingdom's Transport and Road Research Laboratory (now TRL), which led to a proposed Draft Specification (UKDS) for motorcycle leg protectors.

Subsequently, several UKDS leg protector designs were evaluated in full scale tests by TRRL and by the motorcycle industry, with generally opposite results [1,2,3]. In particular, one leg protector design was separately evaluated by TRRL and by the industry, using different test methods [4], and this resulted in large differences in measurements and conclusions.

An International Leg Protector Seminar [5] and the recommendation of experts in the crash protection field led to the conclusion that an internationally accepted motorcyclist crash dummy and research methodology were necessary first steps, before further objective and meaningful research could be pursued. This led to international development and approval of ISO 13232 [6].

Full scale tests involving the proposed UKDS leg protector were conducted using the Standard and reported by Rogers, et al [7]. This paper extends that work by reviewing the development, content, and status of a common research methodology for computer simulation which has been standardized in ISO 13232; and by illustrating the application of the Standard to an overall evaluation of the proposed UKDS leg protector device by means of computer simulation.

BACKGROUND

Development of ISO 13232

Recognizing the need for common test and evaluation methods, the United Nations Expert Group for General Vehicle Safety Provisions (UN/ECE/TRANS/WP29/GRSG) decided in March 1992, at the suggestion of the International Motorcycle Manufacturers Association (IMMA), to ask the International Organization for Standardization (ISO), to establish a common research methodology for motorcycle crash testing.

Six meetings of working group ISO/TC22/SC22/WG22 were held between November 1992 and April 1994 involving some 25 experts and observers from the United Kingdom, Germany, France, the Netherlands, Belgium, Italy, the United States of America, Japan, Canada, and China, with input from both the motorcycle industry worldwide and technical experts in the crash research field [8]. In summer 1994, a committee draft (CD) was balloted and approved within ISO/TC22/SC22. This was followed by balloting of a Draft International Standard (DIS); and final approval of the DIS by the ISO National Member Bodies in March

1996. Publication of ISO 13232 occurred in December 1996.

Review of ISO 13232 Provisions

ISO 13232 consists of eight interacting and mutually dependent parts:

Part 1:	Definitions
Part 2:	Definition of impact conditions in relation to accident data.
Part 3:	Motorcyclist dummy
Part 4:	Measurements
Part 5:	Injury indices and risk/benefit analysis
Part 6:	Full scale impact test procedures
Part 7:	Computer simulation procedures
Part 8:	Test and simulation documentation

The injury risk/benefit analysis enables an overall evaluation of the predicted effects on injuries of a given proposed protective device. This analysis is performed across a sample of the accident population, based on a calibrated computer simulation, and 200 pairs of simulated impacts (with and without the device fitted). A description of the provisions and rationale for each part of the Standard is given by Van Driessche [8]. In addition, specific rationale for the provisions is included in the Standard.

Continued Refinement of the Standard

It is anticipated that the Standard will be amended whenever necessary to take into account new research needs, technological progress, and practical experience.

Currently, WG22 technical work is continuing toward definition of a possible first revision of the Standard, taking into account practical experience and new technology.

EXAMPLE APPLICATION OF THE STANDARD TO IMPACT SIMULATION

Objectives of this Study

The objectives of the research reported herein were:

- To assess the practicality and feasibility of the ISO 13232 simulation requirements; and
- To apply ISO 13232 in an overall evaluation of UKDS leg protectors using computer simulation.

The UKDS leg protector device was designed and fitted by TRRL to a Kawasaki GPZ 500 motorcycle. This specific design has been the subject of previous reports, namely those of:

- Chinn [9], using test methods quite different from those of ISO 13232;
- Rogers [4], using test methods similar but not identical to those of ISO 13232;
- Rogers [7], using the test methods of ISO 13232.

Simulation Basis

The computer simulation was based on a proprietary version of the Articulated Total Body (ATB) program originally developed by Calspan for the National Highway Traffic Safety Administration [10]. The ATB simulation comprises generalized multi body equations of motion based on a Newton-Euler formulation, as required by the Standard. The software was executed on a Silicon Graphics Onyx Infinite Reality workstation containing eight 200 MHz R10000 CPUs for computation and a high-speed graphics pipeline for rendering the corresponding animations.

Simulation Models

An ISO Motorcyclist Anthropometric Test Dummy (MATD) was modeled, based on a modified Hybrid III 50th percentile male dummy in accordance with ISO 13232-3 and as summarized in Table 1.

The motorcycle that was modeled was a Kawasaki GPZ 500 with a summary given in Table 2.

The opposing vehicle that was modeled was a production Toyota Corolla 4 door sedan, Japan domestic model, model year 1988 to 1990, inclusive, as specified in ISO 13232-6. A summary appears in Table 3.

A summary of the UKDS leg protector that was modeled is found in Table 4.

Table 1.
MATD Dummy Description

Basis dummy:	M50 Hybrid III
Overall height:	1720 mm
Mass:	71 kg
Bodies:	30
Joints:	29
Ellipsoids:	28
Planes:	0

Table 2.
Motorcycle Description

Size:	Medium
UKDS category:	3a
Manufacturer:	Kawasaki
Model:	GPZ
Model year:	1988
Overall length:	2125 mm
Overall width:	675 mm
Overall height:	1165 mm
Mass - motorcycle with LP:	189 kg (dry)
Bodies:	7
Joints:	6
Ellipsoids:	18
Planes:	0

Table 3.
Opposing Vehicle Description

Type:	Sedan
Manufacturer:	Toyota
Model:	Corolla
Model year:	1988-1990
Overall length:	4200 mm
Overall width:	1660 mm
Overall height:	1340 mm
Mass:	1100 kg
Bodies:	7
Joints:	6
Ellipsoids:	26
Planes:	4

Table 4.
UKDS Leg Protector Description

Type:	UKDS
Components:	Primary Impact Element Rigid Support Element Knee Protection Element
Bodies (total left + right):	2
Joints (total left + right):	2
Ellipsoids (total left + right):	4
Planes (total left + right):	10

Basis for Simulation Model Parameters

The model parameters for the MATD dummy were based in part on Hybrid III measurements made by the US Air Force [11]. Modifications were made to that database to account for the frangible femurs, knees, and tibias that are specified in the Standard. In addition, a compliant chest and abdomen were added to the model to allow computation of the compression based injury measures of these body regions. The neck model was also modified to account for the special torsional module present in the MATD, as specified in the Standard.

Mass properties, dimensions, joint locations, and suspension properties for the motorcycle and opposing vehicle were determined by laboratory measurements of exemplar vehicles.

Model Calibration

ISO 13232-7 specifies that 20 dynamic and 11 static laboratory component tests be done and compared with the corresponding computer simulations of these tests in order to help indicate the quality of the computer simulation model. In addition, a motorcycle barrier test is specified in order to provide a comparison between the modelled and measured response characteristics related to the front wheel, front suspension, and front fork bending properties and their effects on the motorcycle forces and motions resulting from frontal impact.

For all static tests, the Standard requires plotting the force vs. displacement laboratory test results overlaid with the simulation results. For dynamic tests, the Standard requires plotting the force vs. displacement and force vs. time laboratory test results overlaid with the simulation results. The Standard requires that the simulation parameters used in these calibration tests be used for all subsequent simulation runs. The component calibration results for this analysis can be found in Appendix A.

The Standard also requires comparison and correlation of the simulation with full scale impact test results. For this analysis, the results of 14 full scale tests were available for correlation. Figure 1 shows a plot of peak resultant head acceleration correlation, for which the r^2 correlation coefficient was found to be 0.91. Figure 2 shows the correlation of the change in peak resultant head acceleration. This second plot is not required by the Standard, but was found to be important in quantifying the correlation of the effect of the protective device. If the points on the plot were mainly in the upper left portion of the plot, it would indicate that the simulation over predicts the harmful effects of a given device. If the points on the plot were mainly in the lower right portion, it would indicate that the computer simulation over predicts the beneficial effects of a given device. In this example, it was found that the simulation accurately predicted the change in head acceleration due to the leg protectors. The r^2 correlation coefficient for this plot was 0.84.

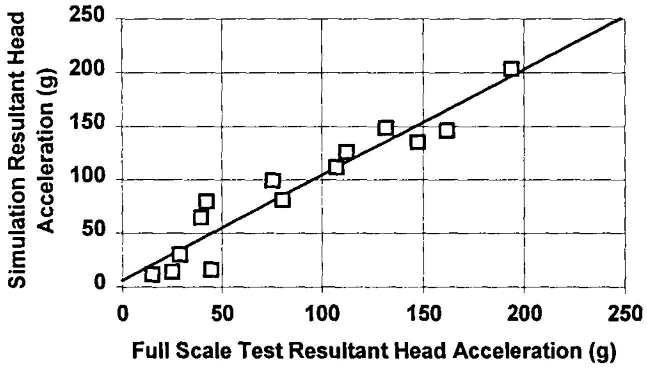

Figure 1. Correlation of peak resultant head acceleration.

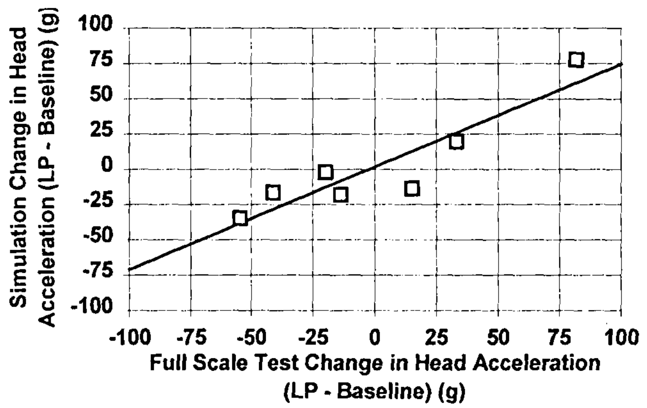

Figure 2. Correlation of change in peak resultant head acceleration due to fitment of leg protectors.

ISO 13232 also requires correlating femur and tibia fractures and knee dislocations for the 14 full scale tests to indicate the accuracy level of the simulation. Tables 5, 6, and 7 show the lower extremity injury results. The percentage of femur fractures correctly predicted by the simulation was 92.9%, the percentage of tibia fractures correctly predicted was 92.9%, and the percentage of knee dislocations correctly predicted was 100.0%.

Table 5.
Femur Fracture Correlation

		Full Scale Test	
		Fracture	No Fracture
Computer Simulation	Fracture	2	2
	No Fracture	0	24

Table 6.
Tibia Fracture Correlation

		Full Scale Test	
		Fracture	No Fracture
Computer Simulation	Fracture	2	2
	No Fracture	0	24

Table 7.
Knee Dislocation Correlation

		Full Scale Test	
		Fracture	No Fracture
Computer Simulation	Fracture	0	0
	No Fracture	0	28

The final calibration requirement is to plot various kinematic simulation parameters described in the Standard, overlaid with the corresponding full scale test variable. Maximum tolerances for the difference between the simulation variable and the full scale test variable at 10 ms before head contact are specified in the Standard. An example of this is shown in Figure 3. This portion of the Standard was found to have some limitations for full scale impact test comparisons, because it compares only the end points of the time histories. In some cases, this can result in acceptance of a simulation time history which has large deviations from full scale test results, during most of its duration; or it may reject a simulation time history which closely follows the full scale test result, except at one time instant. An alternate, revised method to compare these time history variables, has been proposed as an amendment to the Standard [12]. With this proposal, a correlation factor, analogous to an r^2 correlation coefficient, is calculated over the time history as follows:

$$C = 1 - \frac{\sum_{i,k}\left(d_{i,k} - \bar{d}_i\right)^2}{\sum_{i,k}\left(r_{i,k} - \bar{r}_i\right)^2} \qquad (1)$$

where:

C = correlation factor

i = subscript for each impact configuration

k = subscript for each time step

$d_{i,k} = r_{i,k} - \hat{r}_{i,k}$

$\bar{d}_i$ = average value (over time) of $d_{i,k}$

$r_{i,k}$ = value for test i at time k

$\bar{r}_i$ = average value (over time) of $r_{i,k}$

$\hat{r}_{i,k}$ = value for computer simulation i at time k

Using this method, the average correlation across all tests and all 13 variables was found to be 0.82.

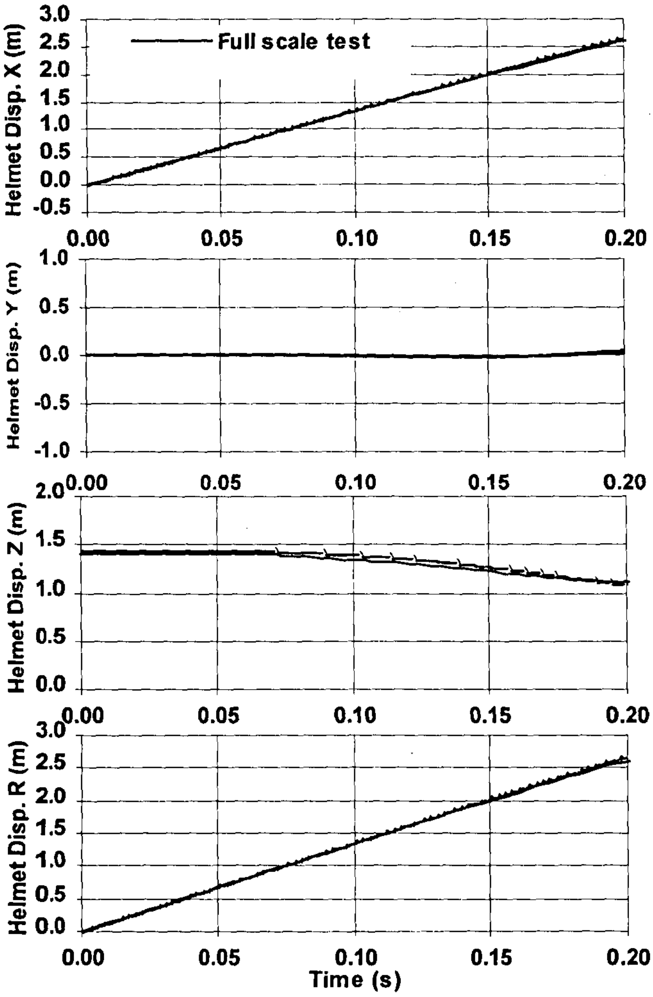

Figure 3. Example time history comparison overlay.

Simulation Output

As specified in the Standard, the computer simulation model was used to compute the following injury assessment variables and injury potential variables:

- Head maximum GAMBIT
- Head Injury Criterion (HIC)
- Head maximum resultant linear acceleration
- Sternum maximum normalized compression
- Sternum maximum velocity-compression (VC)
- Abdomen maximum penetration
- Femur fracture occurrence
- Knee dislocation occurrence
- Tibia fracture occurrence

The probability of each discrete AIS injury severity level was calculated for each of the four body regions: the head, thorax, abdomen, and lower extremities, in accordance with ISO 13232-5 requirements. These were used to calculate the Total Normalized Injury Cost (TNIC).

The computer simulation also generated three dimensional animations, in accordance with the provisions of ISO 13232-7, to display, graphically, the motions of the motorcycle, opposing vehicle, dummy, and protective device. The animation displayed only the actual modeled rigid body surfaces in their proper shapes, relative positions, and orientations, and these were useful in understanding the simulation results.

Injury Risk/Benefit Analysis

An injury risk/benefit analysis was performed via computer simulation using the procedures specified in ISO 13232-5. In summary, this portion of the Standard requires analyzing calibrated simulations of 200 impact configurations – with and without the protective device - which represent 501 accidents that occurred in standardized databases from Los Angeles and Hanover. The change in each injury index and injury assessment variable due to the fitment of the leg protector are tabulated and sorted for all 200 impact configurations. These are used to create cumulative frequency histograms for each injury index and injury assessment variable. The percentage of accidents that are beneficial, show no effect, and are harmful are tabulated for each of these histograms.

An additional injury risk/benefit definition has been proposed as an amendment to the Standard [13]. This amendment is needed because the current risk/benefit calculations, though useful, are not sufficient to describe the magnitude of the injury risks and benefits of a protective device and can lead to erroneous conclusions. Currently, the Standard requires reporting only the percentages of benefit, no effect, and harm without reporting the total magnitude of injury benefit and risk. The amendment proposes adding the calculation of risk/benefit and net benefit as follows:

$$BLI = \sum_{n=1}^{N_{total}} \left(x_{n,i} * FO_n \right) \tag{2}$$

$$r = \sum_{k=1}^{N_{risk}} \left(\Delta x_{k,i} * FO_k \right) \tag{3}$$

$$b = \sum_{l=1}^{N_{benefit}} \left(- \Delta x_{l,i} * FO_l \right) \tag{4}$$

where:

BLI = Sum of the values for the baseline vehicle injury index or injury assessment variable

b = Sum of the changes in injury index or injury assessment variable for the accidents in which the protective device decreased the injury (ie, a benefit)

r = Sum of the changes in injury index or injury assessment variable for the accidents in which the protective device increased the injury (ie, a risk)

$N_{benefit}$ = Number of configurations in which the protective device was beneficial for a given injury index or injury assessment variable

N_{risk} = Number of configurations in which the protective device was harmful for a given injury index or injury assessment variable

N_{total} = Total number of configurations

i = Subscript for each injury assessment variable

l = Subscript for each benefit configuration

k = Subscript for each risk configuration

n = Subscript for all configurations

Δx = Change in injury assessment variable (protective device - baseline)

x = Value of the injury assessment variable for the baseline motor cycle

FO = Frequency of occurrence

$$Benefit = \frac{b}{BLI} * 100\% \tag{5}$$

$$Risk = \frac{r}{BLI} * 100\% \tag{6}$$

Injury Risk/Benefit ratio is then defined as r/b * 100%, and Net Benefit is defined as Benefit - Risk. (A method for handling special cases, such as when r, b, or BLI are zero, is described in the proposed amendment.)

A plot of the Total Normalized Injury Cost cumulative frequency histogram for the leg protector device is presented in Figure 4, and a table of the injury risk/benefit analysis results is presented in Appendix D. The histogram plot for total normalized injury cost indicates that the total injury risk (area above the curve in the right half of the plot) is approximately equal to the total injury benefit (area below the curve in the left half of the plot). This is in agreement with the proposed injury risk/benefit calculations in which the risk/benefit ratio was found to be 116% and the net benefit was found to be -5%.

However, the percentage harmful was calculated to be only 17% of the accidents, and the percentage beneficial was calculated to be 26% of the accidents. Use of the latter indices alone, would lead to the incorrect implication that the overall effect of the leg protector would be beneficial, when, in fact, on an overall basis, it was found that the injury risks exceed the injury benefits. This example demonstrates why the proposed amendment to the Standard is necessary.

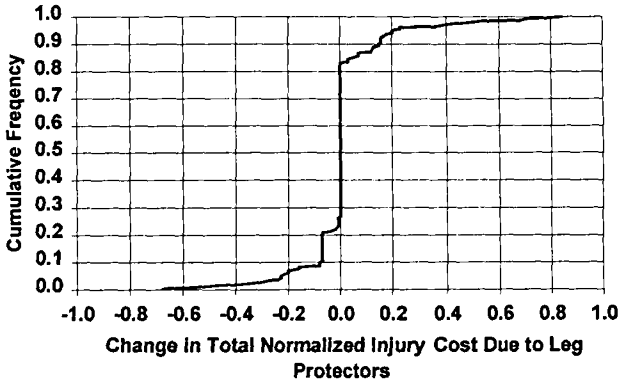

Figure 4. Total normalized injury cost cumulative frequency histogram.

The reasons that the UKDS leg protector is, overall, a harmful device can be observed in the second table of Appendix D. The leg protector is harmful (ie, has injury risk/benefit exceeding 100 percent) with respect to femur AIS, has little net effect on head AIS (ie, has nearly 100% risk/benefit), and is beneficial (ie, has small injury risk/benefit) with respect to chest, knee, and tibia AIS. However, the baseline motorcycle does not result in many injuries to the chest and knee, so the total possible number of leg protector benefits in these body regions is small. In addition, injury costs for each femur injury are much greater than those for each tibia injury, giving the femur body region more influence in the total normalized injury cost.

ISO 13232 Reporting Recommendations

ISO 13232 recommends the following to be reported in any publication which is intended to meet this International Standard:

- Injury Risk/benefit analysis data (provided in Appendix B);
- Injury Risk/benefit analysis basis (provided in Appendix C);
- Injury Risk/benefit analysis results (provided in Appendix D);
- Injury Risk/benefit analysis checklist (provided in Appendix E).

CONCLUSIONS AND RECOMMENDATIONS

Simulation According to ISO 13232

ISO 13232 computer simulation requirements were found to be practical and achievable, and the Standard appears to be useful for research in assessing the feasibility of proposed protective devices.

Experience with the Standard revealed two areas for possible refinement of the Standard. First, the injury risk/benefit calculations should be amended to include the magnitude of the risk and benefit, not just the percentage of cases having risk and benefit. Second, a "single point" time history comparison methodology is not useful. It is technically more descriptive to correlate the time histories over the entire period of time than to compare them only at the end points.

UKDS Leg Protectors

In an evaluation of UKDS leg protectors via computer simulation over the wide range of impact configurations defined in ISO 13232, the devices were found to increase the total normalized injury cost to the dummy in impacts with a passenger car. Specifically, the leg protectors increased costly femur injuries, and decreased less costly tibia injuries. This resulted in a risk/benefit ratio of 116% (ie, the ratio of total increases in normalized injury cost to the total decreases in normalized injury cost was 1.16). This means that the UKDS leg protectors increased rather than decreased total injury costs. The transference of injuries from the tibia to the femur and the net increase in injury cost is in agreement with previous full scale test results which were over a smaller sample of impact conditions.

Based on the overall evaluation of this device, using ISO 13232 procedures, it is recommended that such a device not be fitted to production motorcycles.

REFERENCES

1. Anon., "TRRL Review of Research on Motorcycle Leg Protection - 1991", Transport and Road Research Laboratory, Crowthorne, 1991.

2. Rogers, N.M., "Further Crash Tests of Motorcycle Leg Protectors as Proposed in the UK Draft Specification", 13th International Technical Conference on Experimental Safety Vehicles, Paris, November 1991.

3. Rogers, N.M., "A Technical Evaluation of Motorcycle Leg Protectors", 13th International Technical Conference on Experimental Safety Vehicles, Paris, November 1991.

4. Rogers, N.M., "Evaluation of TRL Designed Leg Protectors for a Medium Sized Sport Motorcycle", 14th International Technical Conference on the Enhanced Safety of Vehicles, Munich, May 1994.

5. Anon., "Leg Protectors: Do They Work", Proceedings of the International Seminar on Leg Protectors - Chantilly, France, International Motorcycle Manufacturers Association, Fresnes, France, November 1991.

6. Anon., Motorcycles - Test and Analysis Procedures for Research Evaluation of Rider Crash Protective Devices Fitted to Motorcycles, ISO 13232, International Organization for Standardization, Geneva, 1996.

7. Rogers, N.M., and Zellner, J., "Application of ISO 13232 to Motorcyclist Protective Device Research", 15th International Technical Conference on the Enhanced Safety of Vehicles, Melbourne, May 1996.

8. Van Driessche, H., "Development of an ISO Standard for Motorcycle Research Impact Test Procedures", 14th International Technical Conference on the Enhanced Safety of Vehicles, Munich, May 1994.

9. Chinn, B.P., and Karimi, H., "Leg Protection for a Sports Motorcycle", Society of Automotive Engineers Paper 900748, February 1990.

10. Obergefell, L.A., Fleck, J.T., Kaleps, I., and Gardner, T.R., "Articulated Total Body Model Enhancements", AAMRL-TR-88-009, January 1988.

11. Kaleps, I., White, R.P. Jr., Beecher, R.M., Whitestone, J., Obergefell, L.A., "Measurement of Hybrid III Dummy Properties and Analytical Simulation Data Base Development", AAMRL-TR-88-005, February 1988.

12. Kebschull, S., Van Auken, M., and Zellner, J., "Proposed Amendment to: Part 7, 4.5.4 and Table 4", ISO/TC22/SC22/WG22 N235, May 1997.

13. Kebschull, S., Zellner, J., Van Auken, M., "Proposed Amendment to: Part 5, 5.10.4", ISO/TC22/SC22/WG22 N236, May 1997.

Appendix A. Component calibration results

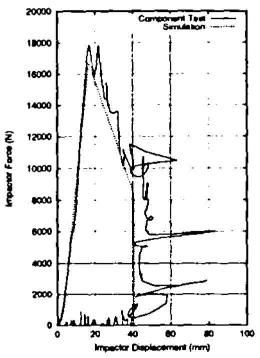

Sphere/OV roof rail

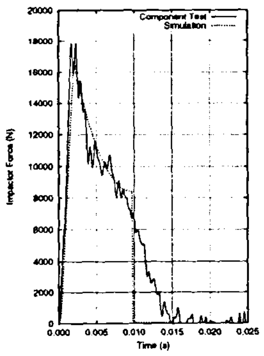

Sphere/OV roof rail

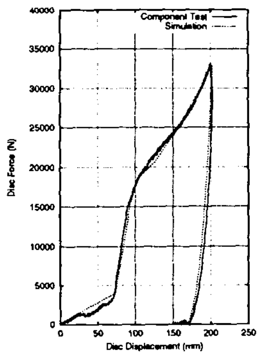

Disc edge/OV side

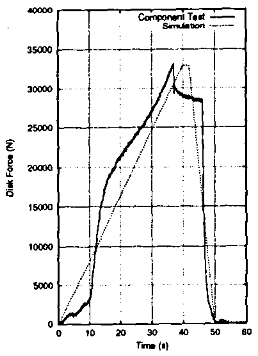

Disc edge/OV side

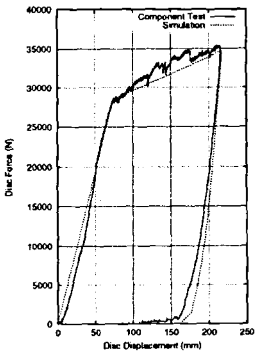

Disc side/OV side

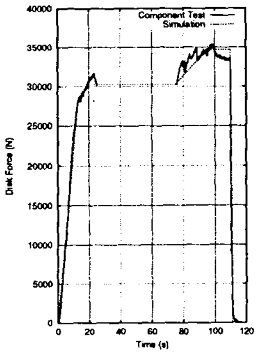

Disc side/OV side

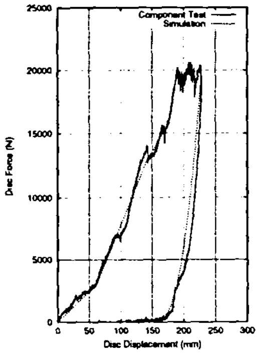

Disc edge/OV front bumper

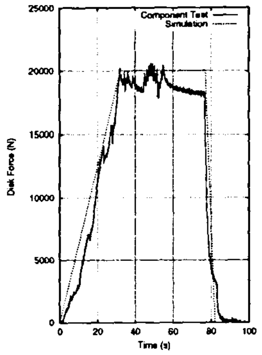

Disc edge/OV front bumper

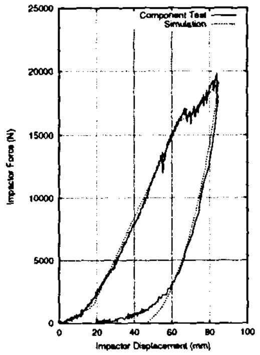

Disc side/OV front bumper

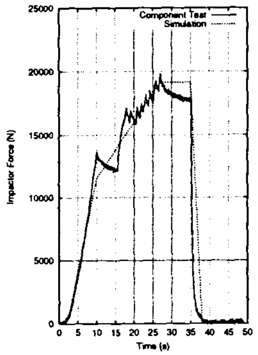

Disc side/OV front bumper

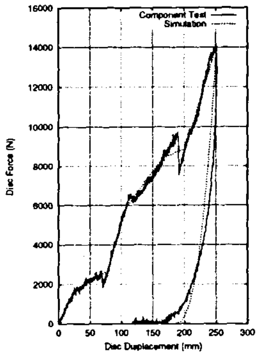

Disc edge/OV rear bumper

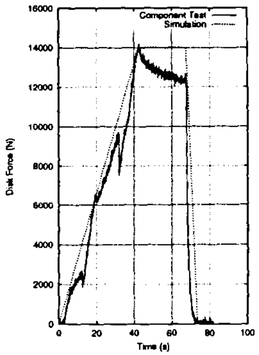

Disc edge/OV rear bumper

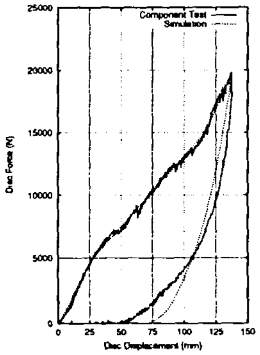

Disc side/OV rear bumper

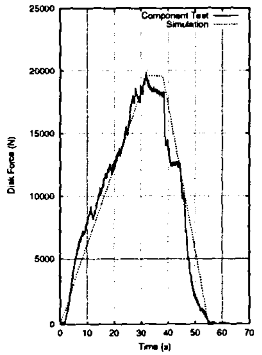

Disc side/OV rear bumper

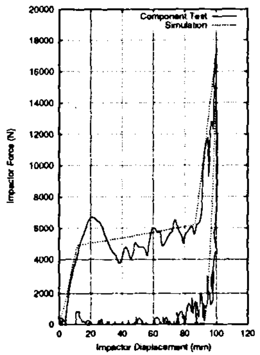

Sphere/OV bonnet

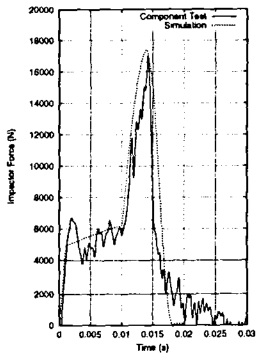

Sphere/OV bonnet

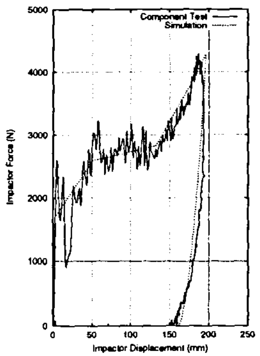

Sphere/OV front windscreen

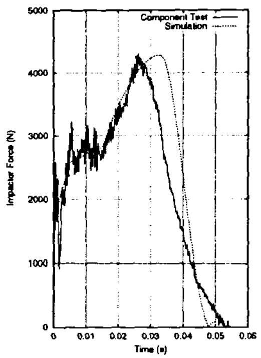

Sphere/OV front windscreen

Appendix A. Component calibration results (cont.)

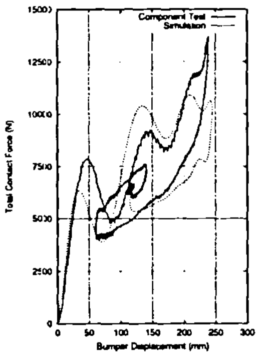

Ground/OV front suspension

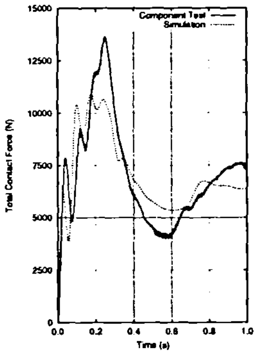

Ground/OV front suspension

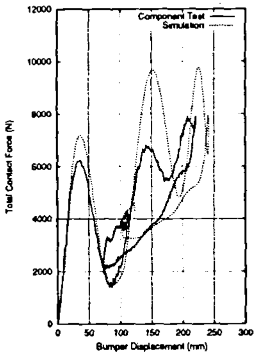

Ground/OV rear suspension

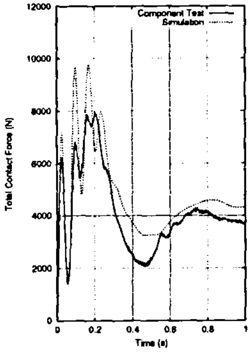

Ground/OV rear suspension

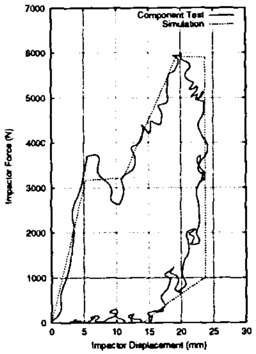

Cylinder/MC fuel tank

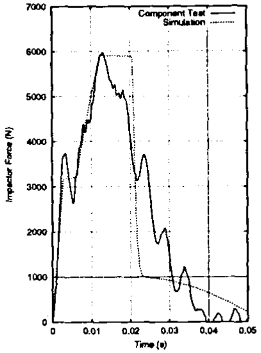

Cylinder/MC fuel tank

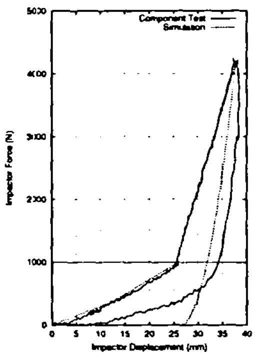

Cylinder/MC seat

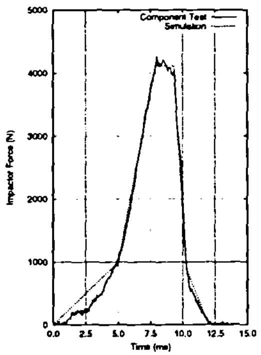

Cylinder/MC seat

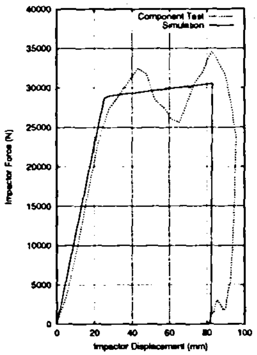

Flat/PIE

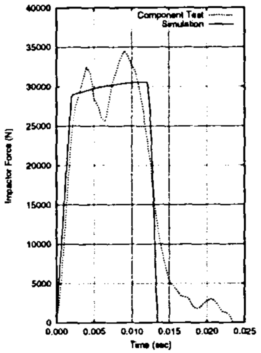

Flat/PIE

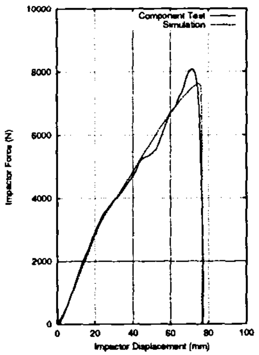

Knee form/KPE

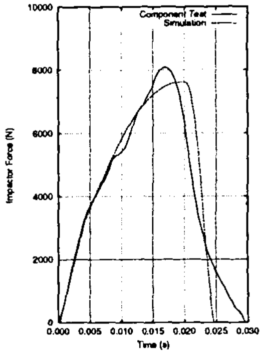

Knee form/KPE

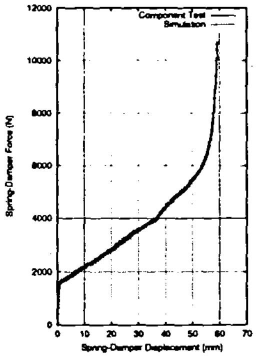

MC rear spring damper

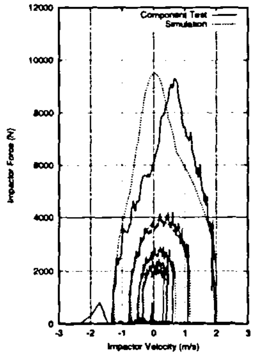

MC rear spring damper

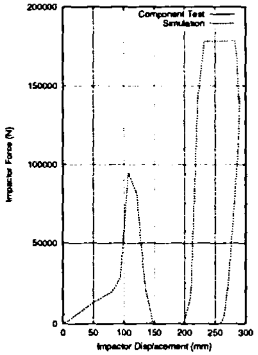

Barrier/MC front wheel

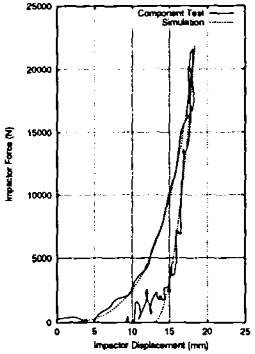

Flat anvil/Helmeted head

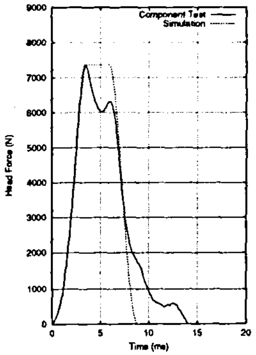

Flat anvil/Helmeted head

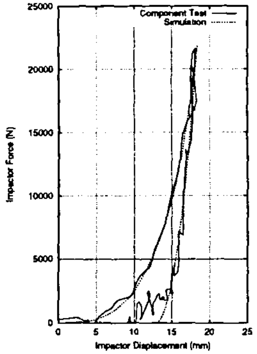

Flat/Upper arm

Appendix A. Component calibration results (cont.)

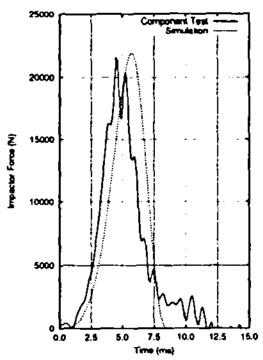

Flat/Upper arm

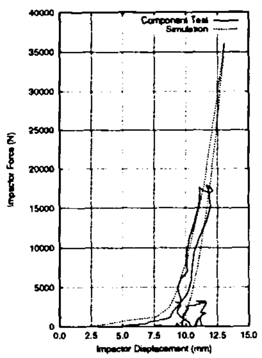

Flat/Lower arm

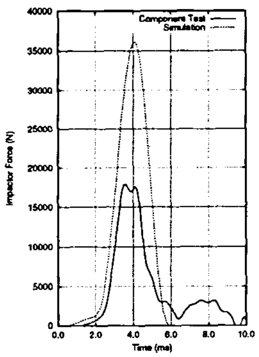

Flat/Lower arm

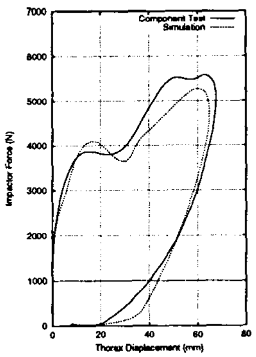

Cylinder/Dummy thorax

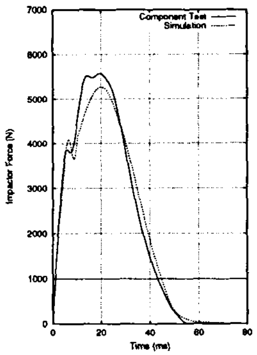

Cylinder/Dummy thorax

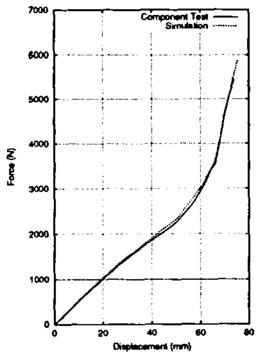

Cylinder/Abdomen

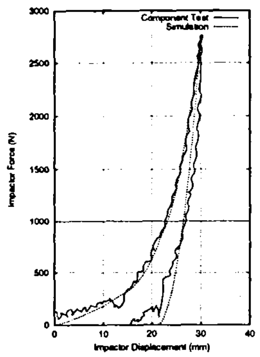

Flat/Pelvis

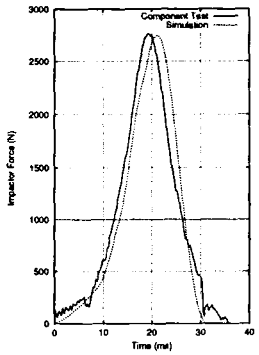

Flat/Pelvis

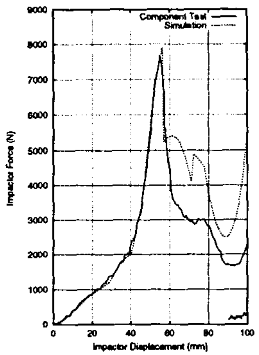

Cylinder/Upper leg

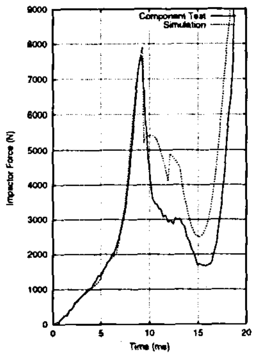

Cylinder/Upper leg

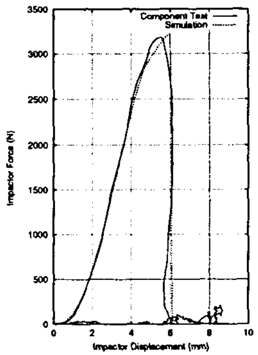

Flat/Knee

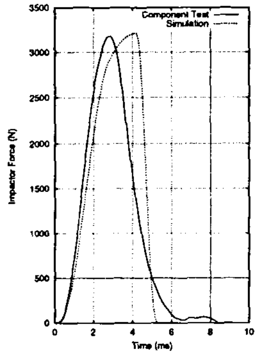

Flat/Knee

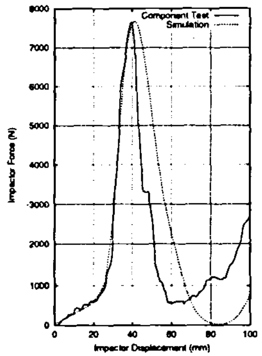

Cylinder/Lower leg

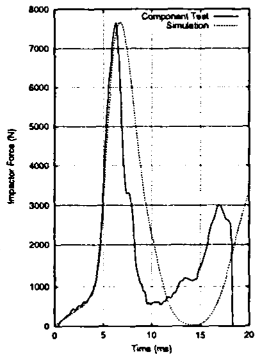

Cylinder/Lower leg

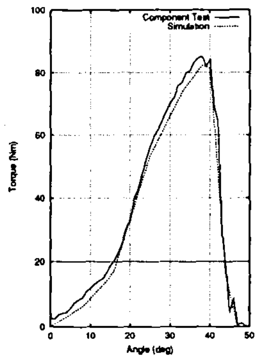

Dummy knee torsion

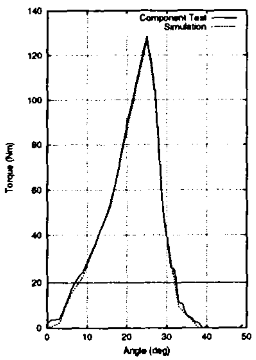

Dummy knee valgus

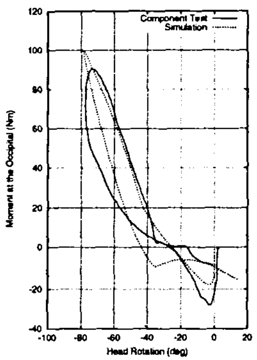

Forward neck flexion

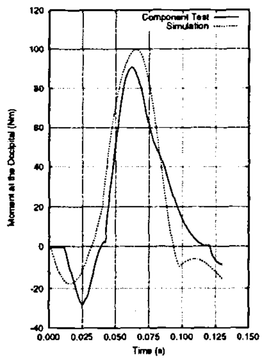

Forward neck flexion

Appendix A. Component calibration results (cont.)

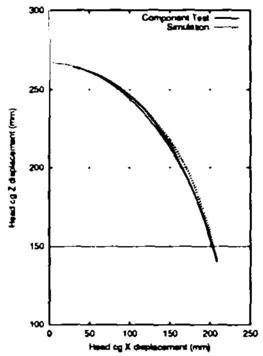

Forward neck flexion

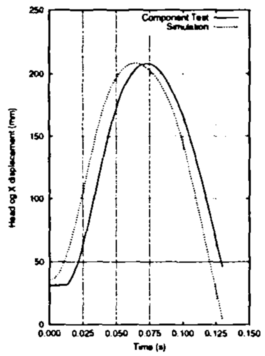

Forward neck flexion

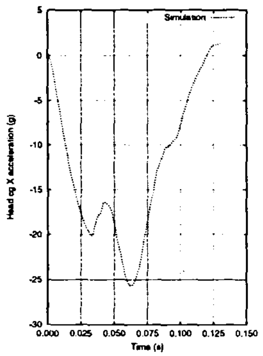

Forward neck flexion

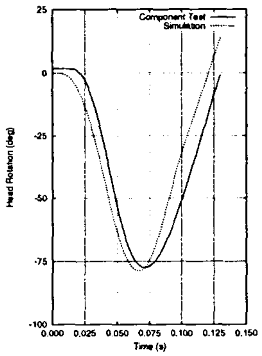

Forward neck flexion

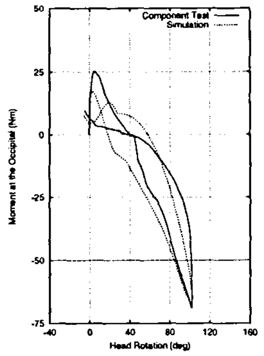

Rearward neck extension

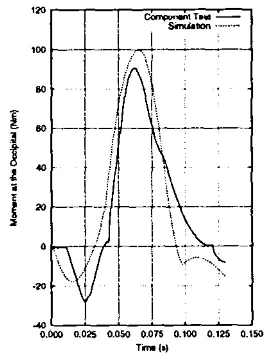

Rearward neck extension

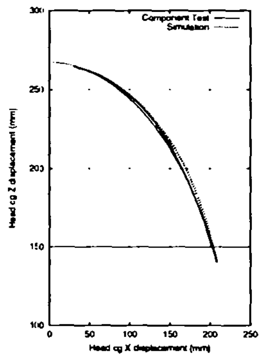

Rearward neck extension

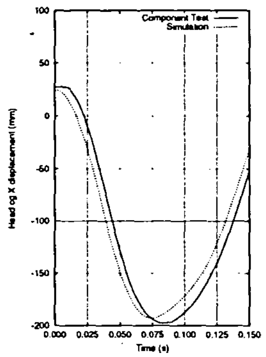

Rearward neck extension

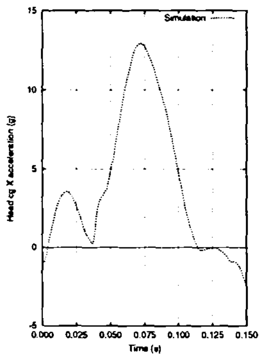

Rearward neck extension

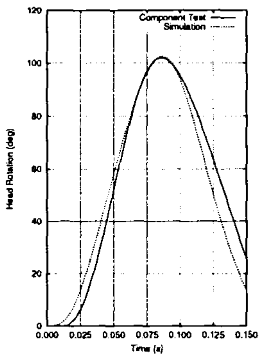

Rearward neck extension

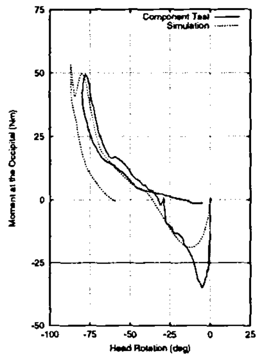

Lateral neck flexion

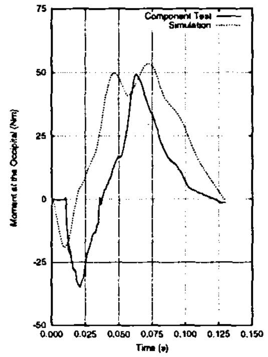

Lateral neck flexion

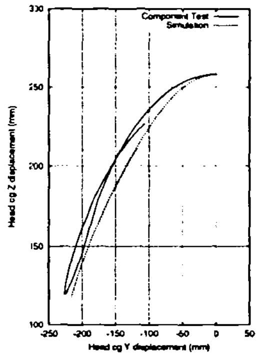

Lateral neck flexion

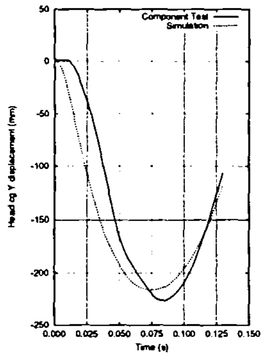

Lateral neck flexion

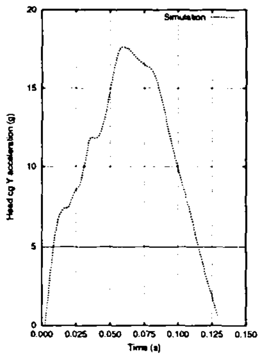

Lateral neck flexion

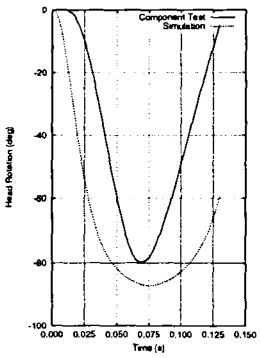

Lateral neck flexion

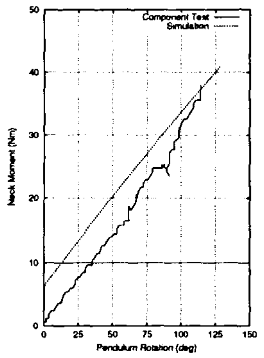

Neck torsion

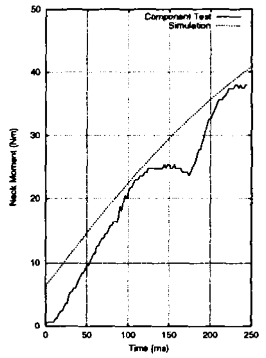

Neck torsion

Appendix B. Risk/benefit analysis data

Impact Configuration Code	Values																																		
	Head																	Chest PAIS			Abdomen PAIS			Femur (L+R) PAIS			Knee (L+R) PAIS			Tibia (L+R) PAIS			ICnorm		
	ar,H,max			Ar,H,max			Gmax			HIC			PAIS			hT	hV																		
	B	P	C	B	P	C	B	P	C	B	P	C	B	P	C	C	C	B	P	C	B	P	C	B	P	C	B	P	C	B	P	C	B	P	C
114- 0.0/ 6.7	26	11	-16	1.5	1.2	-0.3	0.1	0.1	-0.1	19	5	-14	0	0	0	-0.14	0.19	0	0	0	0	0	0	0	0	0	0	0	0	0	0	0	0.00	0.00	0.00
114- 0.0/ 9.8	10	6	-4	0.6	0.4	-0.2	0.0	0.0	0.0	13	4	-9	0	0	0	0.16	0.60	0	0	0	0	0	0	0	0	0	0	0	0	0	0	0	0.00	0.00	0.00
114- 0.0/13.4	14	7	-7	1.1	0.4	-0.7	0.1	0.0	0.0	29	7	-22	0	0	0	0.28	0.26	0	0	0	0	0	0	0	0	0	0	0	0	2	2	-2	0.07	0.00	-0.07
114- 0.0/20.1	21	13	-8	1.5	0.8	-0.7	0.1	0.1	0.0	90	29	-61	0	0	0	0.13	0.56	0	0	0	0	0	0	0	0	3	0	0	0	2	2	0	0.07	0.23	0.16
114- 6.7/ 0.0	63	23	-40	2.1	2.0	-0.1	0.3	0.1	-0.1	55	15	-40	0	0	0	-0.54	-1.22	0	0	0	0	0	0	0	0	0	0	0	0	0	0	0	0.00	0.00	0.00
114- 6.7/ 6.7	81	83	3	5.3	5.7	0.3	0.3	0.4	0.1	422	292	-130	0	0	0	-0.33	1.54	0	0	0	0	0	0	0	0	0	0	0	0	2	2	0	0.07	0.07	0.00
114- 6.7/ 9.8	82	65	-17	4.7	6.2	1.5	0.4	0.3	0.0	257	220	-37	0	0	0	-0.32	2.85	0	0	0	0	0	0	0	0	0	0	0	0	2	2	0	0.07	0.07	0.00
114- 6.7/13.4	79	99	20	8.0	6.5	-1.5	0.4	0.4	0.0	544	567	23	0	0	0	-0.24	2.36	0	0	0	0	0	0	3	3	0	0	0	0	2	2	0	0.23	0.23	0.00
114- 6.7/20.1	348	96	-253	23.0	10.7	-12.3	1.7	0.5	-1.2	4175	810	-3365	6	0	-6	-0.29	2.88	0	0	0	0	0	0	3	6	3	0	0	0	2	4	2	0.95	0.30	-0.65
114- 9.8/ 0.0	47	43	-4	3.9	2.3	-1.6	0.2	0.2	0.0	57	17	-40	0	0	0	-0.97	0.02	0	0	0	0	0	0	0	0	0	0	0	0	0	0	0	0.00	0.00	0.00
114- 9.8/ 6.7	61	71	10	6.6	7.3	0.6	0.3	0.3	0.0	243	246	2	0	0	0	-0.16	1.23	0	0	0	0	0	0	0	0	3	0	0	0	2	2	0	0.07	0.23	0.16
114- 9.8/ 9.8	100	66	-34	9.3	9.2	0.0	0.4	0.4	0.0	644	313	-331	0	0	0	-0.21	2.66	0	0	0	0	0	0	3	3	0	0	0	0	2	2	0	0.23	0.23	0.00
114- 9.8/13.4	126	76	-51	9.5	10.6	1.0	0.5	0.5	-0.1	1028	489	-539	0	0	0	-0.20	1.44	0	0	0	0	0	0	3	6	3	0	0	0	2	2	0	0.23	0.30	0.07
114- 9.8/20.1	364	126	-238	45.2	15.5	-29.7	1.9	0.7	-1.2	6552	1508	-5043	6	1	-5	-0.26	2.14	0	0	0	0	0	0	3	6	3	0	0	0	4	4	0	0.99	0.31	-0.68
114-13.4/ 0.0	52	19	-34	2.7	1.5	-1.2	0.2	0.1	-0.1	85	5	-80	0	0	0	-1.01	-0.26	0	0	0	0	0	0	0	0	0	0	0	0	0	2	2	0.00	0.07	0.07
114-13.4/ 6.7	163	161	-2	9.5	16.3	6.9	0.8	0.9	0.2	525	1191	666	1	3	2	-0.37	-0.54	0	0	0	0	0	0	0	0	3	0	0	0	2	2	0	0.10	0.39	0.29
114-20.1/ 6.7	334	249	-85	22.8	18.4	-4.4	1.6	1.1	-0.6	3240	4685	1446	6	4	-2	-0.44	-6.48	1	0	-1	0	0	0	3	3	3	0	0	0	2	2	2	0.94	0.59	-0.35
123- 6.7/ 0.0	37	35	-2	2.6	2.7	0.1	0.2	0.2	0.0	71	54	-17	0	0	0	-0.53	0.57	0	0	0	0	0	0	0	0	0	0	0	0	0	0	0	0.00	0.00	0.00
123- 6.7/ 6.7	7	7	0	0.4	0.8	0.4	0.0	0.0	0.0	9	7	-2	0	0	0	-0.13	0.34	0	0	0	0	0	0	0	0	0	0	0	0	2	2	-2	0.07	0.00	-0.07
123- 6.7/ 9.8	7	7	0	0.4	0.7	0.3	0.0	0.0	0.0	8	7	-1	0	0	0	-0.12	0.06	0	0	0	0	0	0	0	0	0	0	0	0	2	2	-2	0.07	0.00	-0.07
123- 6.7/13.4	7	6	-1	0.4	0.7	0.3	0.0	0.0	0.0	8	6	-2	0	0	0	-0.11	-0.13	0	0	0	0	0	0	0	0	0	0	0	0	2	2	-2	0.07	0.00	-0.07
123- 9.8/ 0.0	81	65	-17	3.9	3.6	-0.3	0.3	0.3	-0.1	356	297	-59	0	0	0	-0.48	0.46	0	0	0	0	0	0	0	0	0	0	0	0	0	0	0	0.00	0.00	0.00
123- 9.8/ 6.7	82	65	-17	3.4	1.7	-1.7	0.3	0.3	-0.1	143	62	-81	0	0	0	-0.18	0.10	0	0	0	0	0	0	0	0	0	0	0	0	2	2	-2	0.07	0.00	-0.07
123- 9.8/ 9.8	12	8	-3	0.7	0.6	-0.1	0.1	0.0	0.0	29	11	-17	0	0	0	0.14	0.33	0	0	0	0	0	0	0	0	0	0	0	0	2	2	-2	0.07	0.00	-0.07
123-13.4/ 0.0	202	118	-83	11.9	5.1	-6.8	0.8	0.5	-0.4	2760	617	-2142	2	0	-2	-0.36	3.44	0	0	0	0	0	0	3	3	-3	0	0	0	2	2	0	0.31	0.07	-0.24
123-13.4/ 6.7	161	109	-52	10.6	5.2	-5.4	0.8	0.5	-0.3	590	717	126	2	0	-2	0.13	-0.17	0	0	0	0	0	0	3	3	-3	0	0	0	2	2	0	0.27	0.07	-0.20
123-13.4/ 9.8	130	20	-109	7.5	0.8	-6.7	0.6	0.1	-0.5	290	44	-246	0	0	0	0.13	1.14	0	0	0	0	0	0	3	3	0	0	0	0	2	2	0	0.23	0.23	0.00
123-13.4/13.4	93	10	-82	4.2	0.6	-3.6	0.4	0.0	-0.3	167	25	-142	0	0	0	0.37	2.38	0	0	0	0	0	0	3	3	0	0	0	0	2	2	0	0.23	0.23	0.00
123-20.1/ 0.0	469	279	-190	26.4	7.7	-18.7	2.0	1.1	-0.9	13294	4731	-8563	6	5	-1	-0.35	6.38	0	0	0	0	0	0	6	3	-3	0	0	0	4	4	0	0.99	0.68	-0.31
123-20.1/ 6.7	286	247	-39	18.3	21.0	2.8	1.4	1.3	-0.1	3307	2743	-564	6	5	-1	0.19	4.59	0	0	0	0	0	0	3	3	0	0	0	0	4	4	0	0.85	0.82	-0.04
123-20.1/ 9.8	345	213	-132	28.6	16.7	-12.0	1.7	1.0	-0.7	4142	1681	-2461	6	4	-2	0.13	1.08	0	0	0	0	0	0	6	3	-3	0	0	0	4	4	0	0.97	0.56	-0.41
413- 0.0/ 6.7	64	54	-9	5.2	3.5	-1.7	0.3	0.3	-0.1	236	155	-82	0	0	0	-0.11	0.76	0	0	0	0	0	0	0	0	0	0	0	0	0	0	0	0.00	0.00	0.00
413- 0.0/ 9.8	166	84	-81	15.4	6.9	-8.5	0.9	0.4	-0.5	896	371	-524	3	0	-3	-0.08	-1.77	0	0	0	0	0	0	0	0	0	0	0	0	0	0	0	0.23	0.00	-0.23
413- 0.0/13.4	127	207	81	5.9	18.2	12.3	0.5	1.1	0.6	945	1362	418	0	4	4	-0.10	1.33	0	0	0	0	0	0	0	0	0	0	0	0	0	0	0	0.01	0.54	0.54
413- 0.0/20.1	124	319	195	5.7	10.2	4.5	0.5	1.3	0.8	453	3676	3223	0	5	5	-0.07	1.02	0	0	0	0	0	0	0	0	0	0	0	0	0	0	0	0.01	0.78	0.78
413- 6.7/ 6.7	103	86	-17	7.2	5.5	-1.8	0.5	0.4	-0.1	421	360	-61	0	0	0	-0.06	0.98	0	0	0	0	0	0	0	0	0	0	0	0	0	0	0	0.00	0.00	0.00
413- 6.7/ 9.8	95	98	3	6.3	9.1	2.9	0.5	0.5	0.1	542	494	-48	0	0	0	-0.11	0.50	0	0	0	0	0	0	0	0	0	0	0	0	0	0	0	0.00	0.01	0.00
413- 6.7/13.4	146	112	-34	7.7	10.9	3.1	0.7	0.6	0.0	809	450	-358	1	1	0	-0.11	1.14	0	0	0	0	0	0	0	0	0	0	0	0	0	0	2	0.02	0.07	0.05
413- 6.7/20.1	94	203	109	5.5	11.9	6.4	0.4	0.8	0.4	250	2447	2197	0	2	2	-0.07	0.05	2	0	-2	0	0	0	0	0	3	0	0	0	0	0	2	0.06	0.30	0.23
413- 9.8/ 6.7	9	12	3	0.6	1.0	0.4	0.0	0.1	0.0	8	9	1	0	0	0	0.31	0.22	0	0	0	0	0	0	0	0	0	0	0	0	0	0	0	0.00	0.00	0.00
413- 9.8/ 9.8	57	73	16	5.2	5.2	0.0	0.3	0.4	0.1	116	248	132	0	0	0	-0.11	1.51	0	0	0	0	0	0	0	0	0	0	0	0	0	0	0	0.00	0.00	0.00
413- 9.8/20.1	118	195	77	7.5	15.7	8.2	0.6	1.0	0.4	398	2134	1736	0	3	3	-0.07	-1.67	2	0	-2	0	0	0	0	0	3	0	0	0	0	0	2	0.05	0.45	0.40
413-13.4/ 6.7	8	6	-2	0.6	0.3	-0.2	0.0	0.0	0.0	7	6	0	0	0	0	0.11	1.17	0	0	0	0	0	0	0	0	0	0	0	0	0	0	0	0.00	0.00	0.00
413-13.4/ 9.8	9	10	2	0.5	0.9	0.4	0.0	0.1	0.0	16	18	3	0	0	0	-0.27	0.99	0	0	0	0	0	0	0	0	0	0	0	0	0	0	0	0.00	0.00	0.00
413-13.4/13.4	23	15	-8	1.4	1.2	-0.2	0.1	0.1	0.0	53	46	-7	0	0	0	0.45	0.97	0	0	0	0	0	0	0	0	3	2	0	-2	0	2	4	0.12	0.30	0.18
413-20.1/ 6.7	6	5	-1	0.5	0.4	-0.2	0.0	0.0	0.0	3	4	1	0	0	0	-0.08	1.37	0	0	0	0	0	0	0	0	0	0	0	0	0	0	0	0.00	0.00	0.00
711- 0.0/ 6.7	81	74	-7	3.7	3.9	0.2	0.3	0.3	0.0	334	267	-67	0	0	0	-0.06	-0.82	0	0	0	0	0	0	0	0	0	0	0	0	0	0	0	0.00	0.00	0.00
711- 0.0/ 9.8	89	87	-2	4.5	4.2	-0.3	0.4	0.4	0.0	468	434	-34	0	0	0	-0.11	-0.92	0	0	0	0	0	0	0	0	0	0	0	0	0	0	0	0.00	0.00	0.00

Appendix B. Risk/benefit analysis data (cont.)

Impact Configuration Code	Values																																		
	Head																	Chest PAIS			Abdomen PAIS			Femur (L+R) PAIS			Knee (L+R) PAIS			Tibia (L+R) PAIS			ICnorm		
	ar,H,max			Ar,H,max			Gmax			HIC			PAIS			hT	hV																	
	B	P	C	B	P	C	B	P	C	B	P	C	B	P	C	C	C	B	P	C	B	P	C	B	P	C	B	P	C	B	P	C	B	P	C
711- 0.0/13.4	61	17	-45	6.9	1.2	-5.7	0.3	0.1	-0.2	302	37	-265	0	0	0	-0.24	1.69	0	0	0	0	0	0	0	0	0	0	0	0	0	0	0	0.00	0.00	0.00
711- 0.0/20.1	62	73	11	2.7	5.3	2.6	0.3	0.3	0.0	406	580	174	0	0	0	-0.13	-0.15	0	0	0	0	0	0	0	0	0	0	0	0	4	2	-4	0.20	0.00	-0.20
711- 6.7/ 9.8	19	21	1	1.2	1.1	0.0	0.1	0.1	0.0	20	19	-1	0	0	0	-0.07	-0.13	0	0	0	0	0	0	0	0	0	0	0	0	0	0	0	0.00	0.00	0.00
711- 6.7/13.4	81	74	-7	3.7	3.9	0.2	0.3	0.3	0.0	340	267	-72	0	0	0	-0.06	-0.85	0	0	0	0	0	0	0	0	0	0	0	0	0	0	0	0.00	0.00	0.00
711- 9.8/13.4	27	13	-14	2.6	1.1	-1.5	0.2	0.1	-0.1	19	9	-10	0	0	0	-0.08	0.17	0	0	0	0	0	0	0	0	0	0	0	0	0	0	0	0.00	0.00	0.00
711- 9.8/20.1	98	89	-9	4.5	4.2	-0.3	0.4	0.4	0.0	508	458	-49	0	0	0	-0.11	-0.42	0	0	0	0	0	0	0	0	0	0	0	0	0	0	0	0.00	0.00	0.00
414- 0.0/ 6.7	188	68	-121	4.2	3.9	-0.3	0.8	0.3	-0.5	1023	170	-853	1	0	-1	-0.10	0.80	0	0	0	0	0	0	0	0	0	0	0	0	0	0	0	0.07	0.00	-0.07
414- 0.0/ 9.8	196	228	32	4.7	5.3	0.5	0.8	0.9	0.1	1358	1600	241	2	3	1	-0.09	0.42	0	0	0	0	0	0	0	0	0	0	0	0	0	0	0	0.11	0.27	0.17
414- 0.0/13.4	151	360	209	5.2	7.0	1.9	0.6	1.5	0.8	1309	4824	3516	1	6	5	-0.09	0.09	1	0	-1	0	0	0	0	0	0	0	0	0	0	0	0	0.02	0.86	0.84
414- 0.0/20.1	164	434	270	5.9	10.6	4.8	0.7	1.8	1.1	1530	7809	6279	1	6	5	-0.07	-0.08	2	2	0	0	0	0	6	6	-3	0	0	0	0	0	0	0.26	0.97	0.71
414- 6.7/ 6.7	6	13	7	0.8	1.1	0.3	0.0	0.1	0.0	2	3	1	0	0	0	-0.11	0.33	0	0	0	0	0	0	0	0	0	0	0	0	0	0	0	0.00	0.00	0.00
414- 6.7/ 9.8	9	10	0	1.0	1.0	0.0	0.0	0.1	0.0	4	4	-1	0	0	0	-0.10	1.97	1	0	-1	0	0	0	0	0	0	0	0	0	0	0	0	0.01	0.00	-0.01
414- 6.7/13.4	16	14	-2	1.4	0.9	-0.5	0.1	0.1	0.0	17	15	-2	0	0	0	-0.12	1.71	1	0	-1	0	0	0	0	0	0	0	0	0	0	0	0	0.02	0.00	-0.02
414- 6.7/20.1	98	165	67	3.8	5.1	1.4	0.4	0.7	0.3	190	993	803	0	1	1	-0.08	-0.73	0	0	0	0	0	0	6	3	-6	0	0	0	0	0	0	0.23	0.03	-0.20
414- 9.8/ 6.7	4	4	1	0.5	0.3	-0.2	0.0	0.0	0.0	1	1	0	0	0	0	-0.14	0.67	0	0	0	0	0	0	0	0	0	0	0	0	0	0	0	0.00	0.00	0.00
414- 9.8/ 9.8	24	16	-9	2.5	1.1	-1.5	0.1	0.1	-0.1	8	4	-4	0	0	0	-0.13	1.60	0	0	0	0	0	0	0	0	0	0	0	0	0	0	0	0.00	0.00	0.00
414- 9.8/13.4	12	12	0	2.2	1.7	-0.5	0.1	0.1	0.0	17	9	-8	0	0	0	0.35	0.83	0	0	0	0	0	0	0	0	0	0	0	0	0	0	0	0.00	0.00	0.00
414- 9.8/20.1	23	18	-4	2.0	1.2	-0.9	0.1	0.1	0.0	38	24	-14	0	0	0	0.24	1.16	1	0	-1	0	0	0	6	3	-3	0	0	0	0	0	0	0.23	0.15	-0.08
412- 0.0/ 6.7	59	87	28	3.0	4.2	1.2	0.2	0.4	0.2	172	223	51	0	0	0	-0.09	0.29	0	0	0	0	0	0	0	0	0	0	0	0	0	0	0	0.00	0.00	0.00
412- 0.0/ 9.8	57	65	7	2.1	3.5	1.4	0.2	0.3	0.0	134	174	40	0	0	0	-0.08	0.09	0	0	0	0	0	0	0	0	0	0	0	0	0	0	0	0.00	0.00	0.00
412- 0.0/13.4	45	58	13	2.4	2.8	0.4	0.2	0.2	0.1	162	143	-19	0	0	0	-0.08	-3.48	1	0	-1	0	0	0	0	0	0	0	0	0	0	0	0	0.01	0.00	-0.01
412- 0.0/20.1	63	87	24	4.1	3.3	-0.8	0.3	0.4	0.1	211	561	350	0	0	0	-0.13	2.48	5	1	-4	0	0	0	3	6	3	0	0	0	2	0	-2	0.51	0.23	-0.28
412- 6.7/ 6.7	10	24	14	0.8	1.8	1.1	0.1	0.1	0.1	14	16	2	0	0	0	-0.07	-0.20	0	0	0	0	0	0	0	0	0	0	0	0	0	0	0	0.00	0.00	0.00
412- 6.7/ 9.8	149	143	-6	5.9	4.6	-1.4	0.6	0.6	0.0	1013	524	-489	1	1	0	-0.08	-0.05	0	0	0	0	0	0	0	0	0	0	0	0	0	0	0	0.01	0.01	0.00
412- 6.7/13.4	149	135	-14	7.2	7.0	-0.1	0.7	0.6	-0.1	1226	1231	5	1	0	-1	-0.08	-0.29	0	0	0	0	0	0	0	0	3	0	0	0	0	0	0	0.02	0.15	0.13
412- 6.7/20.1	187	447	260	8.1	13.7	5.7	0.8	1.8	1.0	1830	7717	5887	2	6	4	-0.07	11.32	3	2	-1	0	0	0	3	6	0	0	0	0	0	0	0	0.30	0.98	0.68
412- 9.8/ 6.7	3	4	1	0.2	0.4	0.1	0.0	0.0	0.0	1	1	0	0	0	0	0.16	0.89	0	0	0	0	0	0	0	0	0	0	0	0	0	0	0	0.00	0.00	0.00
412- 9.8/13.4	142	126	-17	10.5	5.3	-5.2	0.7	0.5	-0.2	1006	986	-20	1	0	-1	-0.08	0.32	0	0	0	0	0	0	0	0	0	0	0	0	0	2	2	0.04	0.07	0.03
412-13.4/ 6.7	2	2	0	0.2	0.2	0.0	0.0	0.0	0.0	1	1	-1	0	0	0	-0.26	0.59	0	0	0	0	0	0	0	0	0	0	0	0	0	0	0	0.00	0.00	0.00
412-20.1/ 6.7	1	2	1	0.1	0.1	0.0	0.0	0.0	0.0	0	0	0	0	0	0	-0.12	0.73	0	0	0	0	0	0	0	0	0	0	0	0	0	0	0	0.00	0.00	0.00
115- 0.0/ 6.7	45	27	-18	1.8	1.4	-0.4	0.2	0.1	-0.1	52	28	-25	0	0	0	-0.10	0.13	0	0	0	0	0	0	0	0	0	0	0	0	0	0	0	0.00	0.00	0.00
115- 0.0/ 9.8	30	25	-5	1.6	1.4	-0.2	0.1	0.1	0.0	120	107	-13	0	0	0	-0.23	0.38	0	0	0	0	0	0	0	0	0	0	0	0	0	0	0	0.00	0.00	0.00
115- 0.0/20.1	130	105	-25	14.1	5.6	-8.6	0.6	0.5	-0.2	775	759	-16	1	0	-1	-0.32	1.00	0	0	0	0	0	0	0	3	6	0	0	0	0	0	0	0.02	0.23	0.21
115- 6.7/ 6.7	41	41	0	2.8	3.0	0.3	0.2	0.2	0.0	88	330	242	0	0	0	-0.52	-4.08	0	0	0	0	0	0	0	0	3	0	0	0	0	0	0	0.00	0.15	0.15
115- 6.7/ 9.8	56	55	-1	6.7	4.3	-2.4	0.3	0.2	-0.1	272	446	174	0	0	0	-0.43	-3.37	0	0	0	0	0	0	0	3	6	0	0	0	0	0	0	0.00	0.23	0.23
115- 6.7/20.1	148	122	-26	18.5	10.7	-7.8	0.8	0.5	-0.3	2255	1748	-507	2	0	-2	-0.24	0.07	0	0	0	0	0	0	6	6	0	0	0	0	4	4	0	0.38	0.30	-0.08
115- 9.8/ 0.0	12	14	2	1.3	1.4	0.2	0.1	0.1	0.0	22	44	22	0	0	0	-0.54	-2.84	0	0	0	0	0	0	0	0	0	0	0	0	0	0	0	0.00	0.00	0.00
115- 9.8/ 9.8	123	101	-22	10.8	7.8	-3.0	0.6	0.5	-0.1	1149	775	-374	0	0	0	-0.46	-2.67	0	0	0	0	0	0	0	3	6	0	0	0	2	2	-2	0.07	0.23	0.16
115- 9.8/13.4	119	124	5	6.5	5.5	-1.0	0.5	0.5	0.0	1120	947	-173	0	0	0	-0.25	-2.06	0	0	0	0	0	0	0	3	6	0	0	0	4	2	-4	0.20	0.23	0.03
115- 9.8/20.1	188	136	-51	16.1	11.2	-4.9	0.8	0.6	-0.3	3633	2539	-1094	2	0	-2	-0.29	1.58	0	0	0	0	0	0	6	6	0	0	0	0	4	4	0	0.37	0.30	-0.07
115-13.4/ 6.7	123	120	-3	10.9	7.9	-3.0	0.6	0.5	0.0	1105	1227	122	0	0	0	-0.47	-2.19	0	0	0	0	0	0	0	3	6	0	0	0	2	2	-2	0.07	0.23	0.16
115-13.4/ 9.8	104	124	21	7.0	4.5	-2.5	0.5	0.5	0.1	977	911	-65	0	0	0	-0.31	-2.26	0	0	0	0	0	0	0	3	6	0	0	0	4	2	-4	0.20	0.23	0.03
115-13.4/20.1	219	222	3	13.4	11.9	-1.5	0.9	1.0	0.1	4032	4316	283	3	4	1	-0.28	3.32	0	0	0	0	0	0	6	6	0	0	0	0	4	4	0	0.47	0.54	0.07
313- 0.0/ 6.7	31	31	0	3.0	3.0	0.0	0.1	0.1	0.0	52	59	7	0	0	0	-0.09	-3.27	0	0	0	0	0	0	0	0	0	0	0	0	0	0	0	0.00	0.00	0.00
313- 0.0/ 9.8	31	31	0	2.8	2.8	0.0	0.1	0.1	0.0	66	75	9	0	0	0	-0.21	-0.60	0	0	0	0	0	0	0	0	0	0	0	0	0	0	0	0.00	0.00	0.00
313- 0.0/13.4	27	39	12	2.2	2.7	0.5	0.1	0.2	0.1	47	100	54	0	0	0	-0.29	-1.26	0	0	0	0	0	0	0	0	0	0	0	0	0	0	0	0.00	0.00	0.00
313- 0.0/20.1	128	100	-27	6.9	5.0	-1.9	0.6	0.5	-0.1	366	268	-98	1	0	-1	-0.07	0.63	0	0	0	0	0	0	3	6	3	0	0	0	0	0	0	0.16	0.23	0.08
313- 6.7/ 6.7	255	66	-190	21.9	4.9	-17.0	1.3	0.3	-1.0	2747	222	-2525	5	0	-5	-0.15	0.13	0	0	0	0	0	0	0	0	3	0	0	0	2	2	0	0.79	0.23	-0.56

Appendix B. Risk/benefit analysis data (cont.)

Impact Configuration Code	Values																																	
	Head																	Chest PAIS			Abdomen PAIS			Femur (L+R) PAIS			Knee (L+R) PAIS			Tibia (L+R) PAIS			ICnorm		
	ar,H,max			Ar,H,max			Gmax			HIC			PAIS			hT	hV																	
	B	P	C	B	P	C	B	P	C	B	P	C	B	P	C	C	C	B	P	C	B	P	C	B	P	C	B	P	C	B	P	C	B	P	C
313- 6.7/ 9.8	88	94	6	5.1	11.6	6.5	0.4	0.6	0.2	214	474	261	0	1	1	-0.13	-3.97	2	0	-2	0	0	0	0	0	0	0	0	0	0	0	0	0.03	0.01	-0.01
313- 6.7/13.4	194	137	-57	9.8	6.7	-3.1	0.9	0.6	-0.3	1831	858	-973	2	1	-1	-0.11	-1.39	0	0	0	0	0	0	0	0	0	0	0	0	0	0	0	0.17	0.01	-0.16
313- 6.7/20.1	56	121	65	5.0	8.3	3.2	0.3	0.5	0.2	370	654	284	0	0	0	-0.12	2.43	2	3	1	0	0	0	0	3	6	2	2	-2	0	0	2	0.14	0.34	0.20
313- 9.8/13.4	145	301	157	9.5	20.3	10.9	0.7	1.5	0.8	727	3620	2893	1	6	5	-0.12	-2.71	4	0	-4	0	0	0	3	6	3	0	0	0	2	2	-2	0.46	0.88	0.42
313-13.4/20.1	215	397	182	14.7	16.1	1.3	1.0	1.6	0.6	2182	9292	7110	4	6	2	-0.08	-0.37	3	3	0	0	0	0	3	6	3	0	0	0	2	4	2	0.59	0.95	0.36
513- 0.0/ 6.7	65	59	-6	3.8	3.5	-0.3	0.3	0.2	-0.1	205	160	-46	0	0	0	-0.09	0.12	0	0	0	0	0	0	0	0	0	0	0	0	0	0	0	0.00	0.00	0.00
513- 0.0/ 9.8	128	93	-35	9.6	7.4	-2.2	0.6	0.5	-0.1	798	424	-374	1	0	-1	-0.07	3.30	0	0	0	0	0	0	0	0	0	0	0	0	0	0	0	0.02	0.00	-0.01
513- 6.7/ 6.7	6	7	0	0.5	0.4	-0.1	0.0	0.0	0.0	5	6	1	0	0	0	-0.30	1.42	0	0	0	0	0	0	0	0	0	0	0	0	0	0	0	0.00	0.00	0.00
513- 6.7/ 9.8	8	10	2	0.5	0.5	0.0	0.0	0.0	0.0	12	14	2	0	0	0	-0.19	0.38	0	0	0	0	0	0	0	0	0	0	0	0	0	0	0	0.00	0.00	0.00
513- 6.7/13.4	8	13	5	1.0	0.9	-0.1	0.1	0.1	0.0	11	31	20	0	0	0	-0.27	-2.39	0	0	0	0	0	0	0	0	0	0	0	0	0	0	0	0.00	0.00	0.00
513- 6.7/20.1	14	24	10	1.8	1.5	-0.3	0.1	0.1	0.0	26	111	85	0	0	0	-0.31	2.39	0	0	0	0	0	0	0	0	3	0	0	0	0	0	0	0.00	0.15	0.15
513- 9.8/ 6.7	4	4	0	0.3	0.4	0.1	0.0	0.0	0.0	2	2	0	0	0	0	-0.09	1.08	0	0	0	0	0	0	0	0	0	0	0	0	0	0	0	0.00	0.00	0.00
513- 9.8/ 9.8	8	8	0	0.6	0.6	0.0	0.0	0.0	0.0	10	12	3	0	0	0	-0.14	1.52	0	0	0	0	0	0	0	0	0	0	0	0	0	0	0	0.00	0.00	0.00
513-13.4/ 6.7	2	4	2	0.1	0.3	0.2	0.0	0.0	0.0	1	1	1	0	0	0	-0.14	0.68	0	0	0	0	0	0	0	0	0	0	0	0	0	0	0	0.00	0.00	0.00
224- 0.0/ 6.7	31	4	-27	1.8	0.4	-1.4	0.1	0.0	-0.1	10	3	-8	0	0	0	-0.38	-1.07	0	0	0	0	0	0	0	0	0	0	0	0	0	0	0	0.00	0.00	0.00
224- 0.0/ 9.8	11	4	-7	0.8	0.4	-0.4	0.1	0.0	0.0	8	2	-5	0	0	0	-0.07	-0.25	0	0	0	0	0	0	0	0	0	0	0	0	2	0	-2	0.07	0.00	-0.07
224- 0.0/13.4	8	3	-5	0.7	0.3	-0.4	0.0	0.0	0.0	7	2	-5	0	0	0	-0.06	-0.37	0	0	0	0	0	0	0	0	0	0	0	0	2	0	-2	0.07	0.00	-0.07
224- 6.7/ 6.7	20	74	54	1.7	4.0	2.3	0.1	0.3	0.2	28	72	44	0	0	0	0.40	0.18	0	0	0	0	0	0	0	0	0	0	0	0	2	2	0	0.07	0.07	0.00
224- 6.7/ 9.8	20	86	66	1.6	2.9	1.3	0.1	0.4	0.3	25	85	60	0	0	0	0.31	-1.26	0	0	0	0	0	0	0	0	0	0	0	0	2	2	0	0.07	0.07	0.00
224- 6.7/13.4	83	40	-43	5.9	1.6	-4.3	0.4	0.2	-0.2	107	25	-82	0	0	0	0.29	-0.34	0	0	0	0	0	0	3	3	0	0	0	0	2	2	0	0.23	0.23	0.00
224- 9.8/ 9.8	118	51	-67	6.3	3.6	-2.6	0.5	0.2	-0.3	207	39	-168	0	0	0	0.13	-2.21	0	0	0	0	0	0	3	3	0	0	0	0	2	2	0	0.23	0.23	0.00
224- 9.8/13.4	97	18	-79	5.7	1.4	-4.3	0.4	0.1	-0.3	127	6	-121	0	0	0	0.44	-0.63	0	0	0	0	0	0	3	3	0	0	0	0	2	2	0	0.23	0.23	0.00
224-13.4/ 6.7	132	56	-76	6.6	3.8	-2.8	0.6	0.3	-0.3	246	48	-199	1	0	-1	-0.57	0.01	0	0	0	0	0	0	3	3	0	0	0	0	2	2	0	0.23	0.23	0.00
131- 6.7/ 0.0	10	10	0	0.4	0.3	-0.1	0.0	0.0	0.0	4	5	0	0	0	0	0.38	1.70	0	0	0	0	0	0	0	0	0	0	0	0	0	0	0	0.00	0.00	0.00
131- 9.8/ 0.0	18	22	4	1.4	1.1	-0.3	0.1	0.1	0.0	55	43	-13	0	0	0	0.29	1.14	0	0	0	0	0	0	0	0	0	0	0	0	0	0	0	0.00	0.00	0.00
131- 9.8/ 6.7	4	3	-1	0.2	0.2	0.0	0.0	0.0	0.0	1	1	0	0	0	0	-0.25	-0.40	0	0	0	0	0	0	0	0	0	0	0	0	0	0	0	0.00	0.00	0.00
131-13.4/ 0.0	48	57	9	3.6	3.5	-0.1	0.2	0.3	0.0	516	188	-328	0	0	0	0.40	-0.01	0	0	0	0	0	0	0	0	0	0	0	0	0	0	0	0.00	0.00	0.00
131-13.4/ 6.7	11	17	6	0.8	0.3	-0.4	0.1	0.1	0.0	10	23	13	0	0	0	0.35	0.20	0	0	0	0	0	0	0	0	0	0	0	0	0	0	0	0.00	0.00	0.00
131-20.1/ 0.0	151	213	62	7.2	10.0	2.8	0.6	0.9	0.3	3066	5394	2327	1	3	2	-0.27	-2.37	0	0	0	0	0	0	0	3	3	0	0	0	4	4	0	0.20	0.44	0.23
131-20.1/ 6.7	41	50	9	3.2	5.3	2.1	0.2	0.3	0.1	327	161	-166	0	0	0	0.36	-0.99	0	0	0	0	0	0	0	0	0	0	0	0	0	2	4	0.00	0.20	0.20
131-20.1/ 9.8	30	28	-2	1.8	1.2	-0.6	0.1	0.1	0.0	81	53	-28	0	0	0	0.23	2.07	0	0	0	0	0	0	0	0	0	0	0	0	0	0	0	0.00	0.00	0.00
131-20.1/13.4	15	19	4	0.9	0.5	-0.5	0.1	0.1	0.0	14	29	15	0	0	0	0.37	-0.06	0	0	0	0	0	0	0	0	0	0	0	0	0	0	0	0.00	0.00	0.00
514- 0.0/ 6.7	17	29	12	0.7	2.2	1.5	0.1	0.1	0.1	6	12	6	0	0	0	-0.11	-0.19	0	0	0	0	0	0	0	0	0	0	0	0	0	0	0	0.00	0.00	0.00
514- 0.0/ 9.8	7	76	69	0.7	5.2	4.6	0.0	0.3	0.3	5	83	78	0	0	0	-0.10	0.45	0	0	0	0	0	0	0	0	0	0	0	0	0	0	0	0.00	0.00	0.00
514- 0.0/20.1	18	146	127	2.5	9.6	7.1	0.1	0.7	0.6	27	331	303	0	1	1	0.34	0.57	1	0	-1	0	0	0	3	3	0	0	0	0	0	0	0	0.15	0.16	0.01
514- 6.7/ 6.7	3	4	2	0.3	0.3	0.0	0.0	0.0	0.0	1	1	0	0	0	0	-0.18	0.35	0	0	0	0	0	0	0	0	0	0	0	0	0	0	0	0.00	0.00	0.00
514- 6.7/ 9.8	4	13	9	0.5	1.4	0.9	0.0	0.1	0.1	2	3	1	0	0	0	-0.20	1.04	0	0	0	0	0	0	0	0	0	0	0	0	0	0	0	0.00	0.00	0.00
514- 6.7/20.1	10	58	48	1.2	4.4	3.2	0.1	0.3	0.2	17	45	28	0	0	0	0.15	-0.10	0	0	0	0	0	0	3	3	0	0	0	0	2	0	-2	0.23	0.15	-0.08
514- 9.8/ 6.7	2	6	3	0.3	0.5	0.3	0.0	0.0	0.0	0	1	1	0	0	0	-0.13	0.49	0	0	0	0	0	0	0	0	0	0	0	0	0	0	0	0.00	0.00	0.00
514- 9.8/ 9.8	3	5	2	0.3	0.5	0.2	0.0	0.0	0.0	1	2	1	0	0	0	0.00	1.77	0	0	0	0	0	0	0	0	0	0	0	0	0	0	0	0.00	0.00	0.00
514- 9.8/13.4	5	20	15	0.5	1.4	0.9	0.0	0.1	0.1	3	5	3	0	0	0	-0.19	2.21	0	0	0	0	0	0	0	0	0	0	0	0	0	0	0	0.00	0.00	0.00
314- 0.0/ 6.7	86	112	26	3.5	4.3	0.9	0.4	0.5	0.1	273	479	206	0	0	0	-0.15	1.27	0	0	0	0	0	0	0	0	0	0	0	0	0	0	0	0.00	0.00	0.00
314- 0.0/13.4	71	199	128	2.9	5.6	2.7	0.3	0.8	0.5	200	1895	1695	0	2	2	-0.07	0.88	0	0	0	0	0	0	0	3	3	0	0	0	0	0	2	0.00	0.29	0.29
314- 6.7/ 6.7	76	46	-30	3.6	3.1	-0.5	0.3	0.2	-0.1	195	90	-106	0	0	0	-0.08	0.83	0	0	0	0	0	0	0	0	0	0	0	0	0	0	0	0.00	0.00	0.00
314- 6.7/ 9.8	344	237	-107	5.6	8.1	2.5	1.4	1.0	-0.4	3925	2071	-1854	6	3	-3	-0.08	0.25	0	0	0	0	0	0	0	0	0	0	0	0	0	0	0	0.82	0.35	-0.47
314- 6.7/13.4	650	702	52	24.9	37.2	12.3	2.0	2.0	0.0	19508	25304	5796	6	6	0	-0.06	0.00	0	0	0	0	0	0	3	0	-3	0	0	0	0	2	2	0.99	0.99	0.00
314- 9.8/ 6.7	8	13	5	0.9	0.9	0.0	0.0	0.1	0.0	3	5	2	0	0	0	0.21	0.50	0	0	0	0	0	0	0	0	0	0	0	0	0	0	0	0.00	0.00	0.00
314- 9.8/ 9.8	141	48	-94	4.8	2.2	-2.6	0.6	0.2	-0.4	961	46	-915	1	0	-1	-0.09	0.75	0	0	0	0	0	0	0	0	0	0	0	0	0	0	0	0.01	0.00	-0.01

Appendix B. Risk/benefit analysis data (cont.)

Impact Configuration Code	Values																																		
	Head																	Chest PAIS			Abdomen PAIS			Femur (L+R) PAIS			Knee (L+R) PAIS			Tibia (L+R) PAIS			ICnorm		
	ar,H,max			Ar,H,max			Gmax			HIC			PAIS			hT	hV																		
	B	P	C	B	P	C	B	P	C	B	P	C	B	P	C	C	C	B	P	C	B	P	C	B	P	C	B	P	C	B	P	C	B	P	C
223- 6.7/ 0.0	2	8	6	0.2	0.9	0.7	0.0	0.1	0.0	1	5	5	0	0	0	-1.35	-4.00	0	0	0	0	0	0	0	0	3	0	0	0	2	2	-2	0.07	0.15	0.08
223- 6.7/ 6.7	73	79	6	5.0	5.3	0.3	0.3	0.3	0.0	230	339	109	0	0	0	-0.26	0.44	0	0	0	0	0	0	0	0	3	0	0	0	0	0	0	0.00	0.15	0.15
223- 6.7/ 9.8	78	46	-32	5.8	5.5	-0.2	0.3	0.2	-0.1	365	168	-197	0	0	0	-0.29	0.46	0	0	0	0	0	0	3	3	0	0	0	0	2	2	0	0.23	0.23	0.00
223- 6.7/13.4	37	30	-7	4.5	2.1	-2.4	0.2	0.1	-0.1	109	112	2	0	0	0	-0.25	0.10	0	0	0	0	0	0	3	3	-3	0	0	0	2	2	0	0.23	0.07	-0.16
223- 9.8/ 6.7	37	28	-9	4.3	2.9	-1.4	0.2	0.1	-0.1	102	52	-51	0	0	0	-0.15	0.89	0	0	0	0	0	0	0	0	0	0	0	0	0	2	4	0.00	0.20	0.20
223- 9.8/ 9.8	50	80	30	6.7	6.0	-0.7	0.3	0.4	0.1	158	398	240	0	0	0	-0.17	0.59	0	0	0	0	0	0	0	0	0	0	0	0	0	0	2	0.00	0.07	0.07
223-13.4/ 9.8	98	79	-19	11.7	8.2	-3.6	0.6	0.4	-0.2	824	276	-548	1	0	-1	-0.07	0.69	0	0	0	0	0	0	0	0	0	0	0	0	0	0	2	0.01	0.07	0.06
223-20.1/ 6.7	312	315	3	19.5	33.4	13.9	1.3	1.6	0.3	2501	4029	1527	5	6	1	-0.06	1.16	0	0	0	0	0	0	3	3	0	0	0	0	0	0	0	0.76	0.93	0.17
223-20.1/ 9.8	390	286	-104	20.9	14.6	-6.3	1.6	1.2	-0.5	4081	2486	-1596	6	5	-1	-0.06	-0.53	0	2	2	0	0	0	6	3	-3	0	0	0	0	0	2	0.94	0.68	-0.26
222- 0.0/ 6.7	8	10	2	0.5	0.6	0.2	0.0	0.0	0.0	2	4	2	0	0	0	-0.74	0.69	0	0	0	0	0	0	0	0	0	0	0	0	0	0	0	0.00	0.00	0.00
222- 0.0/ 9.8	17	5	-12	0.7	0.6	-0.2	0.1	0.0	-0.1	6	3	-3	0	0	0	-0.51	1.01	0	0	0	0	0	0	0	0	0	0	0	0	0	0	0	0.00	0.00	0.00
222- 0.0/13.4	18	4	-14	0.9	0.4	-0.5	0.1	0.0	-0.1	6	3	-3	0	0	0	-0.42	0.07	0	0	0	0	0	0	0	0	0	0	0	0	2	2	-2	0.07	0.00	-0.07
222- 6.7/ 6.7	33	10	-24	2.7	1.3	-1.4	0.2	0.1	-0.1	38	5	-32	0	0	0	0.08	0.31	0	0	0	0	0	0	0	0	0	0	0	0	0	0	0	0.00	0.00	0.00
222- 6.7/ 9.8	10	4	-6	0.7	0.3	-0.4	0.1	0.0	0.0	7	4	-3	0	0	0	-0.06	-0.72	0	0	0	0	0	0	0	0	0	0	0	0	2	2	-2	0.07	0.00	-0.07
222- 6.7/13.4	69	5	-64	3.0	0.5	-2.5	0.3	0.0	-0.3	64	6	-58	0	0	0	-0.17	-1.21	0	0	0	0	0	0	0	0	0	0	0	0	2	2	-2	0.07	0.00	-0.07
222- 9.8/ 6.7	34	37	2	3.1	1.9	-1.1	0.2	0.2	0.0	56	70	14	0	0	0	-0.06	-0.48	0	0	0	0	0	0	3	3	0	0	0	0	0	0	0	0.15	0.15	0.00
222- 9.8/ 9.8	30	27	-3	2.1	1.7	-0.5	0.1	0.1	0.0	49	28	-21	0	0	0	0.11	-0.30	0	0	0	0	0	0	3	3	-3	0	0	0	0	0	0	0.15	0.00	-0.15
222- 9.8/13.4	8	7	-1	0.7	0.7	0.0	0.0	0.0	0.0	11	10	-1	0	0	0	-0.06	-0.27	0	0	0	0	0	0	0	0	0	0	0	0	2	2	0	0.07	0.07	0.00
312- 0.0/ 6.7	43	26	-17	3.2	2.0	-1.2	0.2	0.1	-0.1	44	10	-34	0	0	0	-0.08	1.25	0	0	0	0	0	0	0	0	0	0	0	0	0	0	0	0.00	0.00	0.00
312- 0.0/ 9.8	41	13	-28	1.7	0.7	-1.0	0.2	0.1	-0.1	20	4	-16	0	0	0	0.21	-0.21	0	0	0	0	0	0	3	3	0	0	0	0	0	0	0	0.15	0.15	0.00
312- 0.0/13.4	42	6	-36	3.4	0.3	-3.1	0.2	0.0	-0.2	26	6	-19	0	0	0	0.23	1.12	0	0	0	0	0	0	3	3	-3	0	0	0	0	0	2	0.15	0.07	-0.08
312- 6.7/13.4	32	58	26	1.8	4.4	2.7	0.2	0.3	0.2	51	118	66	0	0	0	-0.11	-1.76	0	0	0	0	0	0	0	0	0	0	0	0	0	0	0	0.00	0.00	0.00
312- 9.8/ 6.7	82	75	-7	8.4	6.8	-1.6	0.5	0.4	-0.1	221	148	-74	0	0	0	-0.09	0.98	0	0	0	0	0	0	0	0	0	0	0	0	0	0	0	0.00	0.00	0.00
312- 9.8/20.1	45	37	-8	4.1	2.7	-1.5	0.2	0.2	-0.1	128	171	43	0	0	0	-0.08	-0.12	2	0	-2	0	0	0	3	3	0	0	0	0	0	0	0	0.16	0.15	-0.01
312-13.4/ 6.7	6	3	-3	0.7	0.4	-0.3	0.0	0.0	0.0	3	2	-1	0	0	0	0.12	0.40	0	0	0	0	0	0	0	0	0	0	0	0	0	0	0	0.00	0.00	0.00
621- 0.0/ 6.7	25	3	-22	1.8	0.4	-1.5	0.1	0.0	-0.1	10	1	-9	0	0	0	0.58	-2.48	0	0	0	0	0	0	0	0	0	0	0	0	0	0	0	0.00	0.00	0.00
621- 0.0/ 9.8	24	3	-21	2.1	0.4	-1.7	0.1	0.0	-0.1	17	1	-15	0	0	0	0.66	-4.28	0	0	0	0	0	0	0	0	0	0	0	0	2	2	-2	0.07	0.00	-0.07
621- 0.0/20.1	33	10	-23	1.6	0.6	-1.0	0.1	0.1	-0.1	18	5	-13	0	0	0	-0.06	-2.22	0	0	0	0	0	0	3	3	-3	0	0	0	2	2	0	0.23	0.07	-0.16
621- 6.7/ 9.8	2	7	5	0.3	0.5	0.2	0.0	0.0	0.0	0	2	1	0	0	0	-0.26	0.33	0	0	0	0	0	0	0	0	0	0	0	0	0	0	0	0.00	0.00	0.00
621- 6.7/20.1	55	4	-51	2.8	0.4	-2.4	0.2	0.0	-0.2	108	3	-105	0	0	0	0.27	-3.77	0	0	0	0	0	0	0	0	0	0	0	0	2	2	-2	0.07	0.00	-0.07
621- 9.8/13.4	5	7	2	0.4	0.5	0.1	0.0	0.0	0.0	1	2	1	0	0	0	-0.20	0.33	0	0	0	0	0	0	0	0	0	0	0	0	0	0	0	0.00	0.00	0.00
132- 6.7/ 0.0	88	34	-53	3.6	1.7	-1.9	0.4	0.1	-0.2	268	49	-219	0	0	0	0.15	-0.36	0	0	0	0	0	0	0	0	0	0	0	2	0	0	0	0.00	0.12	0.12
132- 6.7/ 6.7	2	2	0	0.2	0.3	0.2	0.0	0.0	0.0	1	1	0	0	0	0	-0.09	-0.25	0	0	0	0	0	0	0	0	0	0	0	0	0	0	0	0.00	0.00	0.00
132- 9.8/ 6.7	5	3	-2	0.3	0.5	0.2	0.0	0.0	0.0	1	1	0	0	0	0	-0.24	-0.91	0	0	0	0	0	0	0	0	0	0	0	0	0	0	0	0.00	0.00	0.00
132-13.4/ 0.0	92	46	-46	6.6	3.3	-3.3	0.4	0.2	-0.2	466	404	-62	0	0	0	-0.39	-0.65	0	0	0	0	0	0	3	3	0	0	0	0	2	2	2	0.23	0.30	0.07
132-20.1/ 6.7	106	20	-86	5.6	1.4	-4.2	0.5	0.1	-0.4	176	97	-79	0	0	0	0.70	0.80	0	0	0	0	0	0	3	3	0	0	0	0	2	2	0	0.23	0.23	0.00
132-20.1/20.1	2	4	1	0.2	0.4	0.2	0.0	0.0	0.0	1	1	0	0	0	0	-0.08	-0.80	0	0	0	0	0	0	0	0	0	0	0	0	0	0	0	0.00	0.00	0.00
225- 0.0/ 9.8	29	5	-24	2.1	0.6	-1.5	0.1	0.0	-0.1	13	4	-9	0	0	0	-0.17	-1.09	0	0	0	0	0	0	0	0	0	0	0	0	2	0	-2	0.07	0.00	-0.07
225- 0.0/13.4	34	13	-22	2.3	0.8	-1.5	0.1	0.1	-0.1	31	5	-25	0	0	0	-0.06	-2.47	0	0	0	0	0	0	3	0	-3	0	0	0	2	0	-2	0.23	0.00	-0.23
225- 6.7/ 9.8	41	32	-9	2.9	1.9	-1.0	0.2	0.2	-0.1	24	15	-8	0	0	0	0.07	-3.49	0	0	0	0	0	0	3	0	-3	0	0	0	2	0	-2	0.23	0.00	-0.23
225- 6.7/13.4	49	39	-10	2.8	2.6	-0.2	0.2	0.2	0.0	33	24	-10	0	0	0	0.12	-3.13	0	0	0	0	0	0	3	3	0	0	0	0	2	2	0	0.23	0.23	0.00
225-20.1/ 9.8	93	45	-48	7.1	3.8	-3.3	0.5	0.2	-0.2	131	25	-105	0	0	0	-0.48	1.21	0	0	0	0	0	0	3	3	0	0	0	0	2	2	0	0.23	0.23	0.00
622- 0.0/ 6.7	4	8	4	0.2	0.4	0.2	0.0	0.0	0.0	1	3	2	0	0	0	-0.22	0.61	0	0	0	0	0	0	0	0	0	0	0	0	0	0	0	0.00	0.00	0.00
622- 0.0/ 9.8	6	10	4	0.5	0.4	-0.1	0.0	0.0	0.0	1	2	1	0	0	0	-0.23	-0.07	0	0	0	0	0	0	0	0	0	0	0	0	0	0	0	0.00	0.00	0.00
622- 0.0/13.4	2	9	7	0.2	0.3	0.1	0.0	0.0	0.0	0	1	1	0	0	0	-0.44	0.02	0	0	0	0	0	0	0	0	0	0	0	0	2	2	-2	0.07	0.00	-0.07
712- 0.0/ 6.7	8	35	28	0.7	2.2	1.4	0.0	0.1	0.1	4	36	32	0	0	0	-0.10	-3.01	0	0	0	0	0	0	0	0	0	0	0	0	0	0	0	0.00	0.00	0.00
712- 0.0/13.4	58	11	-46	1.7	0.9	-0.8	0.2	0.1	-0.2	90	10	-80	0	0	0	-0.08	-3.86	0	0	0	0	0	0	0	0	0	0	0	0	2	0	-2	0.07	0.00	-0.07
712- 6.7/ 9.8	1	1	0	0.1	0.0	-0.1	0.0	0.0	0.0	0	0	0	0	0	0	-0.09	-0.09	0	0	0	0	0	0	0	0	0	0	0	0	0	0	0	0.00	0.00	0.00

Appendix B. Risk/benefit analysis data (cont.)

Impact Configuration Code	Values																																		
	Head																	Chest PAIS			Abdomen PAIS			Femur (L+R) PAIS			Knee (L+R) PAIS			Tibia (L+R) PAIS			ICnorm		
	ar,H,max			Ar,H,max			Gmax			HIC			PAIS			hT	hV																		
	B	P	C	B	P	C	B	P	C	B	P	C	B	P	C	C	C	B	P	C	B	P	C	B	P	C	B	P	C	B	P	C	B	P	C
712- 6.7/13.4	15	8	-6	1.2	0.7	-0.4	0.1	0.0	0.0	11	3	-8	0	0	0	-0.10	-0.32	0	0	0	0	0	0	0	0	0	0	0	0	0	0	0	0.00	0.00	0.00
712- 6.7/20.1	6	7	0	0.4	0.4	0.0	0.0	0.0	0.0	4	3	-1	0	0	0	-0.08	-0.47	0	0	0	0	0	0	0	0	0	0	0	0	0	0	0	0.00	0.00	0.00
512- 0.0/ 6.7	112	51	-60	5.2	3.7	-1.4	0.5	0.2	-0.2	539	107	-432	0	0	0	-0.11	1.27	0	0	0	0	0	0	0	0	0	0	0	0	0	0	0	0.00	0.00	0.00
512- 6.7/ 9.8	55	34	-21	1.8	3.3	1.4	0.2	0.2	-0.1	46	35	-12	0	0	0	-0.08	-0.50	0	0	0	0	0	0	0	0	0	0	0	0	0	0	0	0.00	0.00	0.00
512-20.1/20.1	6	4	-3	0.8	0.4	-0.4	0.0	0.0	0.0	15	3	-12	0	0	0	0.12	6.76	0	0	0	0	0	0	3	3	-3	0	0	0	2	2	-2	0.23	0.00	-0.23
221-13.4/ 9.8	4	4	0	0.2	0.2	0.0	0.0	0.0	0.0	1	1	0	0	0	0	-0.11	-0.33	0	0	0	0	0	0	0	0	0	0	0	0	0	0	0	0.00	0.00	0.00
623- 0.0/ 6.7	25	3	-21	1.3	0.5	-0.8	0.1	0.0	-0.1	18	1	-17	0	0	0	0.22	-1.95	0	0	0	0	0	0	0	0	0	0	0	0	0	0	0	0.00	0.00	0.00
624- 6.7/20.1	2	2	1	0.3	0.3	0.0	0.0	0.0	0.0	0	1	1	0	0	0	-0.62	0.35	0	0	0	0	0	0	0	0	0	0	0	0	0	0	0	0.00	0.00	0.00

ar,H,max	Maximum linear resultant head acceleration
Ar,H,max	Maximum angular resultant head accelertaion
Gmax	Maximum GAMBIT
HIC	Head Injury Criterion
PAIS	Probable AIS
hT	Change in helmet trajectory in millimeters
hV	Percentage change in helmet velocity at helmet impact
ICnorm	Normalized injury cost
B	Baseline motorcycle
P	Motorcycle with protective device
C	Change due to protective device, i.e., "P" - "B"

Appendix C. Risk/benefit analysis basis

Impact configuration code	Basis is: (mark with "x")			Required documentation per ISO 13232 is attached	
	ISO 13232		Other (describe)		
	Full-scale test	Computer simulation		Yes	No
All		x		x	

Appendix D. Risk/benefit analysis results

Percentage of impacts which are:	Head							Chest PAIS	Abdomen PAIS	Femur (L+R) PAIS	Knee (L+R) PAIS	Tibia (L+R) PAIS	ICnorm
	$a_{r,H,max}$	$\alpha_{r,H,max}$	G_{max}	HIC	PAIS	hT	hV						
Beneficial	57	58	55	59	11	18	39	8	0	7	1	14	26
No effect	1	1	3	0	82	1	0	92	100	81	99	78	57
Harmful	42	42	42	41	7	81	61	1	0	12	0	8	17
Total	100	100	100	100	100	100	100	100	100	100	100	100	100

	Head						Chest PAIS	Abdomen PAIS	Femur (L+R) PAIS	Knee (L+R) PAIS	Tibia (L+R) PAIS	ICnorm
	$a_{r,H,max}$	$\alpha_{r,H,max}$	G_{max}	HIC	PAIS	hV						
Risk/Benefit	72	91	72	152	95	141	6	Undef.*	217	20	58	116
Net Benefit	6	2	6	-11	2	-3	72	None	-39	80	18	-5

* - Undefined (benefit = 0, risk = 0)

Appendix E. Risk/benefit analysis checklist

Part 5 Injury indices and risk/benefit analysis (all referenced tables are in ISO 13232-5)

	Req$^{1)}$	Rec$^{1)}$	Complied with: Yes	Complied with: No	Explanation, if not complied with (If necessary, attach additional pages)
5.10.1 Calculations of injury assessment variables and injury indices (see table 9)	x		x		
5.10.2 Change in head injury potential	x		x		
5.10.2.1 Change in helmet trajectory	x		x		
5.10.2.2 Percentage change in helmet velocity at helmet impact	x		x		
5.10.3 Distributions of injury assessment variables, change in head injury potential, and injury indices (see table 10)	x		x		
5.10.4 Risk/benefit calculations	x		x		

1) "Req" denotes a requirement of ISO 13232; "Rec" denotes a recommendation of ISO 13232

A NEW NECK FOR MOTORCYCLE CRASH TESTING

Christopher Withnall
Edmund Fournier
Biokinetics and Associates Ltd.
Canada
Paper Number 98-S10-W-27

ABSTRACT

A new test dummy neck has been developed specifically for motorcycle crash testing. This new neck is intended to replace the modified Hybrid III neck which is currently used with the Motorcyclist Anthropomorphic Test Device (MATD). The new neck is designed, with the aid of mathematical modeling, to address the unique posture and multi-directional biofidelity requirements of the MATD. It incorporates materials and features that are new to dummy neck design. It may be adjusted for a wide range of inclined torso angles that are typical of the large variety in motorcyclist riding postures. The performance of this neck is presented relative to established biomechanical neck data.

INTRODUCTION

The Motorcyclist Anthropomorphic Test Device (MATD), as the name suggests, is a dummy intended specifically for motorcycle crash testing. Based on the Hybrid III pedestrian dummy, the MATD has undergone several modifications in order to improve biofidelity, to improve injury sensing potential, to include an on-board data acquisition system, and to address the specific needs of the motorcyclist riding position [3, 4, 8].

The pedestrian model Hybrid III differs from the standard seated dummy in the areas of pelvis and lumbar spine. The pelvis soft tissue allows far greater articulation of the hip joints to accommodate a standing posture. The lumbar spine is straight rather than curved, and is less stiff in fore-aft and lateral bending. While these differences alone will allow the dummy to be positioned on a motorcycle, additional changes made to the Hybrid III in transforming it to an MATD include the following:

- Head skin extensions to accommodate a helmet and chinstrap,
- Widened and lightened spine box to house a self-contained data acquisition system,
- Hands that grip the handlebars,
- Crushable abdominal foam insert for penetration detection and measurement,
- String potentiometers for sternal deflection measurement,
- Frangible biofidelic knee assembly with fusible links for injury detection,
- Frangible femur and tibia for detecting leg fracture,
- Increased range of motion at upper and lower neck to accommodate riding posture,
- Addition of torsional module at the upper neck for biofidelic neck twist response.

The last two items are of primary interest here. Attention has been focused extensively on the dummy neck in order to investigate the potential for airbag systems to be used with motorcycles. With the recent widespread introduction of inflatable restraint systems in automobiles, there has become a new class of at-risk occupants called "out-of-position." The potential for airbags to offer motorcyclists protection in crash environments must be weighed against hazards similar to the "out-of-position" occupant in automobiles. Because there is no seat belt or pre-defined seating position for the motorcyclist, it becomes very likely that a rider will be out-of-position when a crash occurs. This, coupled with the added helmet, could put the motorcyclist at additional risk of neck injury.

Efforts to improve the biofidelity and function of the MATD neck have, to date, been based on the standard Hybrid III neck platform [4]. However, it was considered that further improvements to the MATD neck would require a more radical approach, such as the introduction of an all-new neck design. This paper describes the design and performance of such a new MATD prototype neck.

OBJECTIVES AND DESIGN FEATURES

One of the main differences between the motorcyclist riding position and that of the seated automotive driver is the angle of the torso. In an automobile, the torso is *reclined* from vertical, whereas the motorcyclist is *inclined* forwards. In both cases, the driver or rider tends to maintain his head level. Since most automobile seatbacks are set to roughly the same angle, and the driver sits at that angle at all times in the car, the range of neck angle adjustment for an automotive dummy is quite narrow. However, different motorcycles and riding styles dictate a wide range of motorcyclist postures, ranging from upright cruising to racing, requiring a test dummy neck with a wide adjustment range.

Research testing with the MATD has required positioning the dummy with back angles ranging from 15° to 65° forwards. This was confirmed by a brief investigation of volunteer riders on various styles of motorcycles in various riding postures [1]. Here, back angles were found to vary from 16° to 70° forwards. These back angles require that the neck be greatly extended in order to maintain the head level. The previous MATD neck had been modified at the upper and lower ends to allow more extension range, but this only allowed approximately 30°.

Additionally, this investigation of riders in various riding postures revealed that the location of the head relative to the torso changed with increased torso angle, not only the neck angle. Because the human neck curves in extension, it effectively gets shorter, and the position of the head migrates rearwards and downwards towards the torso. Plotting this location of the head relative to the torso, as the neck was progressively extended, revealed that the previous Hybrid III-based MATD neck, which pivoted at both ends, could not be positioned properly at large extension angles. It therefore became one of the primary goals of the new neck design to allow the neck to be set at large extension angles, and in doing so, position the head properly relative to torso[1].

The initial target range of neck positioning angles was chosen to be 15° to 65°. However, there was no biomechanical performance data available for these inclined postures that could be used to evaluate such a neck. The target range was therefore increased to 0° to 65°, allowing for validation at least in the most upright orientation.

The other primary goal was to achieve multi-directional biofidelity. Because the motorcycle dummy is not well coupled to its vehicle, the principal impact direction cannot be well predicted. For this reason, it is important that the dummy neck be biofidilic in several directions. The primary modes of biofidelity targeted for this neck design were in frontal flexion and extension, lateral flexion and torsion. While axial tension and compression were not identified as performance targets at this time, it was recognized that there should be the potential for at least some compliance in tension, precluding such features as a central neck cable.

The previous MATD neck incorporated an additional module at the upper end to increase the torsional compliance of the Hybrid III neck. It was intended that the new neck would not require such an additional module, and that torsional compliance would be built into the neck structure itself.

PERFORMANCE TARGETS

Described in the following are the biomechanical data that were the performance targets of the neck design. Graphical illustrations of this data are shown later under "Performance," in relation to the prototype neck response, in order to minimize repetition.

Frontal Flexion

Two criteria were chosen to measure neck performance in frontal flexion. The first was the kinematic data by Thunnissen et al [9] which describes the positions in time of the head centre of gravity and occipital condyles, based on upright seated volunteers with 0° back angles. This data illustrates the "head lag" phenomenon, based on the analog of the neck acting as a straight link between the first thoracic vertebra and the occipital condyles. A rearward acceleration to the base of the neck causes the head to translate forwards with little rotation, yet causing the neck to begin rotation, followed by coincident head and neck rotation.

The second criterion was the Mertz and Patrick [7] neck torque-angle relationship at the occipital condyles. However, this corridor was modified to account for the 0° initial position of the prototype neck, compared to the typically reclined seating position of the automotive occupant, upon which the corridor was based. It was modified by shifting the entire corridor by the approximate difference between the automotive seated back angle and the fully upright motorcycle rider. This was taken to be nominally fifteen degrees. The rationale was that if a seated automotive occupant's neck is already flexed more than a motorcyclist's, then the motorcyclist has more degrees of flexion available from their base position, and fewer degrees of extension. The corridor is simply shifted to account for this. However, it is recognized that this modification may be appropriate only within a modest range from the original Mertz corridor.

Extension

There is very little relevant kinematic data available for neck extension, so only dynamic criteria were chosen. The dynamic response target was the Mertz and Patrick [7] torque-angle relationship, again modified to account for the zero degree test posture.

Lateral Flexion

The ISO has developed response requirements for test dummies used in side impact [6]. Of these response requirements, peak lateral displacement of the head centre of gravity and the peak lateral head angle, based on volunteer experiments by Ewing et al [2], and analyzed by Wismans et al [10] were chosen as design targets.

Torsion

The same ISO requirements as above include a peak head twist angle, which occurs during lateral flexion, based on the above Ewing et al volunteer experiments. Additional requirements on neck twist are described in the ISO requirements for certification of a motorcycle impact dummy neck [5].

---

[1] This must accomplished with good stability, to resist neck sag and creep, especially with the added weight of a helmet.

DESIGN

Mathematical Modeling and Design Concept

A MADYMO model of a test dummy neck was created to assist in defining the component characteristics required of a new neck. The overall shape and length of the model were based on volunteer measurements mentioned earlier. The model joints were chosen with consideration for the eventual physical neck construction, which consists of elastomeric materials separated by thin aluminum disks, similar in concept to the Hybrid III. By iterating the stiffness functions of each elastomeric disk, the shape of each disk was designed for frontal and lateral directions.

The base of the neck attaches to the standard Hybrid III lower neck bracket, which is to be set permanently to its 7° extension mark. At the upper neck, a slider mechanism is used to allow an amount of fore-aft compliance, specifically in a forward flexion situation. The slider plate is attached to the standard Hybrid III upper neck load cell by a standard condyle pin. Front and rear nodding blocks are included to control head pivot at the occipital condyles.

Midway along the neck length, a locking adjustment is provided to set the head angle level for a given riding posture. This also changes the shape of the neck, and position of the head centre of gravity.

The neck and slider joint assembly total 1.63 kg. This compares favourably with the General Motors specification of 1.55 kg (GM drawing 78051-338) for the same assembly of the Hybrid III. However, it is anticipated that some parts of the slider mechanism in future prototypes could be made with aluminum, rather than steel, for weight reduction.

Deformable Disks

Four disks were chosen to represent bending of the human neck. Each disk is approximately 20 mm in thickness, and each has a unique cross-section. The shape of each disk was designed based on the required frontal versus lateral stiffness determined from the mathematical modeling. Laboratory material tests determined the basic bending responses of common geometric shapes, which were found to vary closely with the area moment of inertia of that particular shape. By scaling the desired response to the laboratory response, the desired moments of inertia for each disk in the frontal and lateral directions were obtained. Shapes were then designed to achieve these moments of inertia.

The result was a stack of disks that became progressively smaller from bottom to top, following the stiffness functions determined from the modeling. Additionally, the upper disks were made to be "egg-shaped" in cross-section, with the rear being wider than the front. The aim here was to encourage head twist with lateral bending.

The deformable disks were made from hot-cast Adiprene® urethane, by Uniroyal. An extensive review of candidate materials was conducted, which identified highly resilient materials with minimal damping as being desirable [1]. Such materials would likely result in a neck structure with good repeatability and reproducibility, due to the minimal viscoelastic characteristics in comparison to other elastomers. While human tissue tends to exhibit high damping and hysteresis, these qualities in a test device tend to introduce poor repeatability and rate sensitivity.

Slider Mechanism

The mathematical modeling demonstrated the impossibility for a stacked elastomeric neck to achieve the desired "head-lag" phenomenon in frontal flexion (see Figure 4). A stack of elastomeric disks, regardless of stiffness, tended to bend simply as a beam, causing the upper neck to travel in a circular arc, unless a rear control element pulled down on the rear of the skull. However, the presence of external control elements, such as cables or elastic bands, was undesirable due to the large extension set angles required for motorcyclist testing, and the presence of a helmet.

It was found that a relatively simple way to mimic the initial head translation in frontal flexion was by introducing a unidirectional sliding joint at the upper neck. The stiffness of this slider was determined by modeling to be relatively low compared to the neck structure, such that sliding of the head on the neck would occur before neck bending began. In this fashion, the head-lag would be observed without external control elements. The slider is controlled by a return spring made of the same material as the neck, and which acts as a bumper stop. A schematic of the slider is shown in Figure 1.

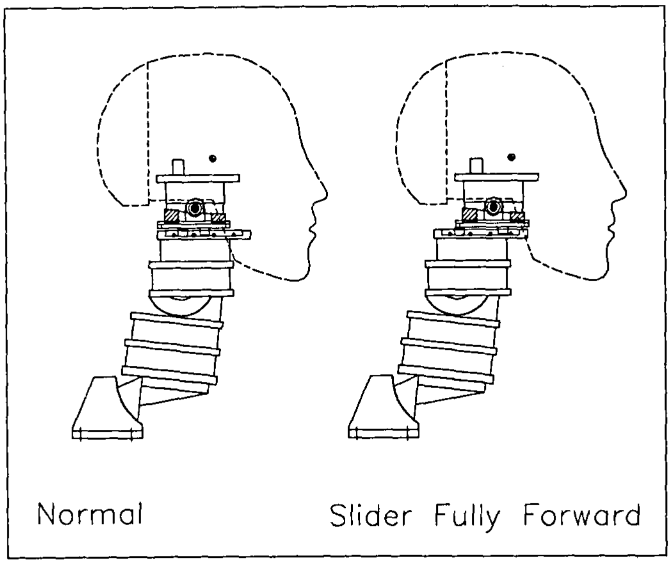

Figure 1: Slider mechanism.

Head Angle Adjustment

Head angle adjustment is provided by a spline-toothed interface and locking bolt. The splines form a circular arc, the centre of which is the virtual pivot location of the upper and lower neck that positions the head centre of gravity in the correct location for any head angle. Each spline tooth adjusts the head angle by 2.5°, from a 0° upright angle to a 65° inclined riding posture. Although infinite adjustment is not possible, the most that the head angle would be out of level would be half of the 2.5°, or 1.25°. A schematic of the head angle adjustment, together with the thoracic spine box, is shown in Figure 2.

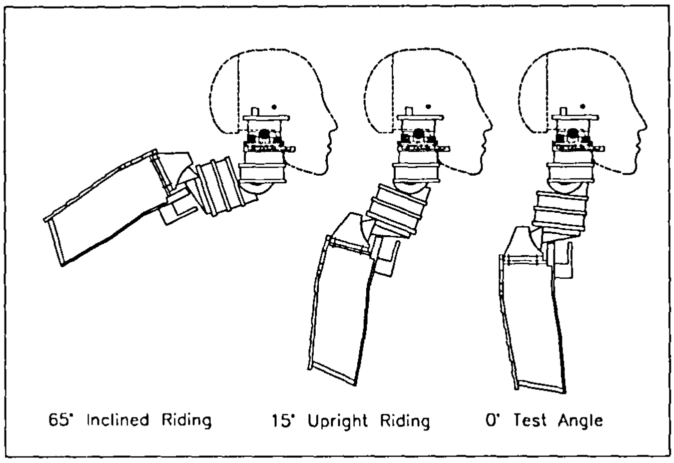

Figure 2: Head angle adjustment.

Nodding Blocks

Nodding blocks were incorporated into this design mainly due to compatibility with the existing Hybrid III upper neck load cell. The front nodding block is much stiffer than the rear, to assist with the "head lag" phenomenon. Both nodding blocks are made with the same urethane as the neck disks. Although the material properties of this urethane did not weigh heavily in this specification, it was felt that it would be better for manufacturing economics if the same urethane recipe could be used for all parts.

The rear nodding block was softened by making it triangular rather than rectangular, and by boring a hole through it. The nodding blocks sit in recessed pockets on the upper slider plate.

Neck Shroud

In order to meet the kinematic requirements for lateral flexion, the neck design calls for the neck to be rather slender in width. For this reason, it is felt that a shroud similar to that used with the current MATD neck shall be necessary for testing that might involve airbag interaction with the neck. The aim is to keep the airbag out from beneath the dummy's chin. The different profile of this new prototype, along with the articulation at the mid-length will not be compatible with current Hybrid III neck shrouds. It is intended that the shroud be designed only when all design iterations are finalized.

PERFORMANCE

Sled Testing

All acceleration-based testing was performed at the Defence and Civil Institute of Environmental Medicine (DCIEM) Impact Studies Facility, North York, Ont., Canada. Testing was conducted in forward flexion, lateral flexion and rearward extension. Note that DCIEM coded their tests in sequence. For this test series, test numbers ranged from 2960 to 2967

HyGe Sled Pin

The required acceleration pulse at the base of the neck for frontal and lateral flexion was based on the NBDL volunteer T1 acceleration measurements [9]. However, these pulses are very different than those normally achieved by a HyGe sled. This is because the T1 pulse is a function of the belt webbing and torso compliance of the volunteers. Therefore, it was necessary to have a custom sled pulse created.

This was accomplished by constructing a custom HyGe piston pin for the DCIEM facility. Although the frontal and lateral pulses are different, the characteristic shapes are similar, with a rapidly rising peak followed by a plateau of approximately half the peak (see Figure 3 and Figure 9). For economic reasons, it was felt that one pin could simulate both pulses by configuring the piston pressures accordingly. The following sections describe the actual sled pulses compared to the ideal T1 pulses. Note that the ideal T1 pulses [9] were used in the MADYMO modeling.

Instrumentation and Data Collection

The instrumentation and visual recording for this head/neck testing included the following:

- 3-axis head acceleration,
- 3-axis upper neck bending moments,
- 3-axis upper neck forces,
- 1 high-speed video camera (viewing lateral to sled travel),
- 2 high-speed film cameras (top and longitudinal views),

Data was collected at 8 kHz for 400 ms, following the protocol of SAE J211. Video was captured at exactly 500 fps, and film at nominally 500 fps. Targets were installed at the head centre of gravity, occipital condyles, and on the neck and lower neck bracket. For lateral flexion, where some head twist was expected, two outboard targets were mounted such that the head centre of gravity was exactly between them.

High Speed Video Analysis

All kinematic analysis was conducted by tracking targets with high-speed video. Software was used to track the targets on the dummy head and neck. This software provided the horizontal and vertical positions of each target relative to a chosen target on the sled. This data was then processed to compare the head-neck kinematics to the performance corridors.

Frontal Flexion (TESTS 2962, 2963)

Tests for frontal flexion were conducted at the zero degree (no extension) position of the neck adjustment. The Hybrid III lower neck bracket was set to 7° of extension, which is the permanent setting for this neck design.

Frontal Flexion Sled Pulse - The sled pulse for frontal flexion is shown below in Figure 3. The dashed line indicates the ideal volunteer average pulse of the NBDL volunteers. The custom pin reproduces this pulse quite closely, with notable differences being the slight plateau on the initial rise, the initial peak being slightly too low and narrow, and the third peak being higher and later. To prevent this third peak from being too high, the peak target sled acceleration was made 25 G with a velocity change of 17.0 m/s.

The sled pulse repeatablility is shown to be excellent (both pulses lie practically on top of each other).

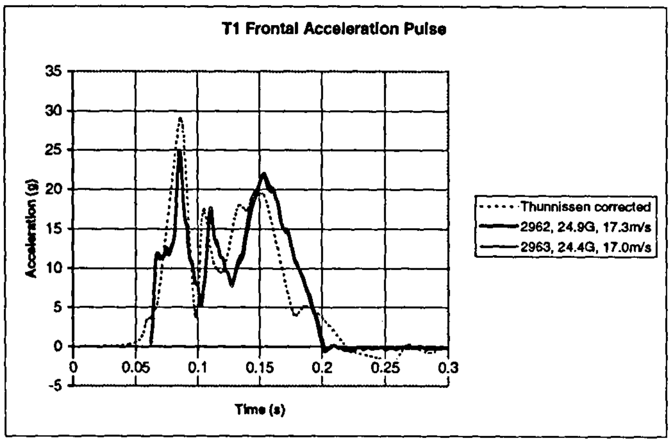

Figure 3: Frontal sled pulse.

Frontal Performance - The positions of the head centre of gravity and the occipital condyles are shown in Figure 4. The slider was tested both in the normal sliding and "locked" configurations, in order to investigate the effects of the slider joint. To lock the slider, the spring cavity was filled with a urethane block, limiting its sliding motion to no more than a few millimetres from its initial position.

The results for the sliding configuration show that the OC and CG follow the corridors very well until near full head excursion, where both demonstrate excessive forward travel. The locked configuration follows a similar path, except that it departs the corridor with excessive forward travel earlier, having less vertical travel.

From the high-speed video, the last acceleration peak is noticeably responsible for this excessive forward excursion late in the trajectory. The entire neck is seen to shear forwards as the head is pulled by this last peak. It is expected that if the acceleration profile had been more similar to the volunteer's pulse, where the predominance of the high acceleration was earlier in the event than later, the trajectory would not have shown such high forward travel.

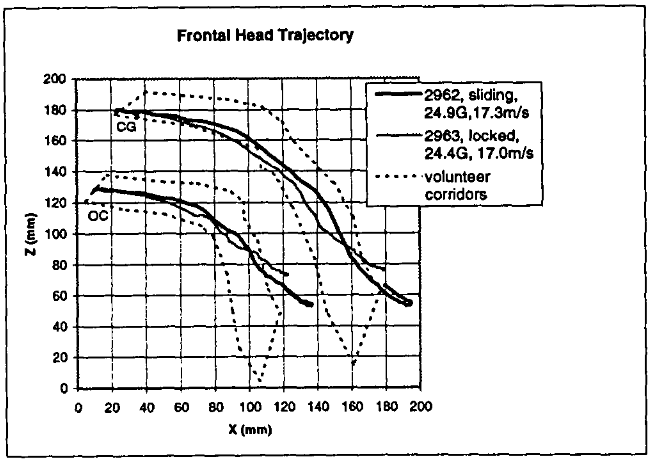

Figure 4: Frontal head and OC trajectories.

The difference between the locked and sliding configurations is illustrated better by Figure 5 where the head lag is more apparent. The slider mechanism allows the head to move forwards without rotating. Geometrically, this appears as the neck link pivoting through approximately twenty degrees, compared to the locked configuration where the neck link only pivots through approximately ten degrees before head rotation begins.

After the head begins rotating, the shape of both curves is nearly identical, and follows the shape of the corridor very well. It is anticipated that approximately 10 mm more sliding travel would situate the response inside the corridor.

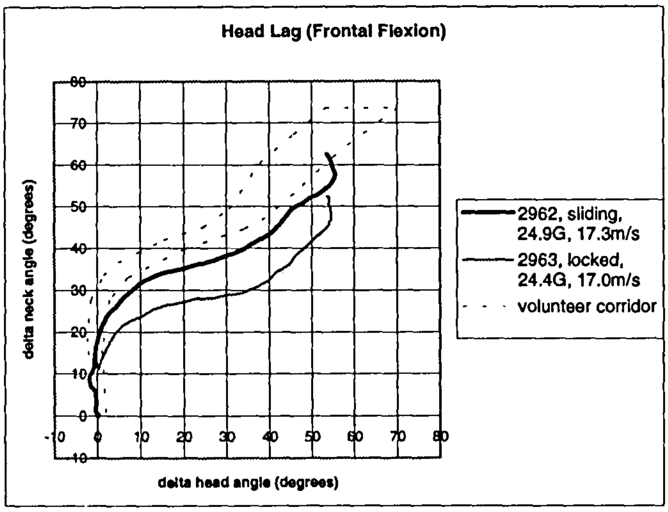

Figure 5: Frontal head lag.

The upper neck torque versus head angle response is shown below in Figure 6 compared to the Mertz modified bending response corridors. The reader will recall that the zero degree axis was shifted to account for the initial angle of the automotive seated occupant compared to a motorcycle rider. The results show that both the locked and sliding configurations satisfy this performance criterion. This corridor is for the loading condition only. Since the loading portion finishes at peak torque and head angle, the prototype neck is shown to fall completely within the corridor.

It should also be noted that the upper right portion of the corridor represents a person's chin contacting their chest. Since this prototype neck was mounted at the end of a cantilever, simulated chest contact was not possible, and therefore the latter half of the corridor is not relevant in the current testing.

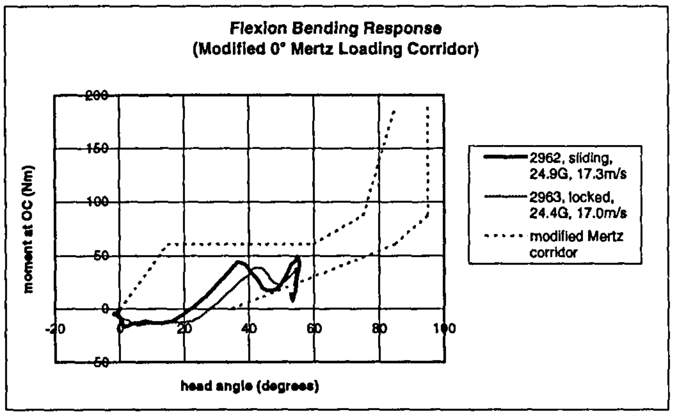

Figure 6: Flexion bending response.

Extension (TESTS 2966, 2967)

Tests for rearward extension were conducted at the zero degree (no extension) position of the neck adjustment.

Extension Sled Pulse - The extension sled pulse was intended to represent the Mertz and Patrick volunteer experiments, with a peak acceleration of 6G and velocity change of 4.4 m/s. While the exact shape of this pulse was unknown, the peak acceleration and velocity change were recreated well by the HyGe sled.

The standard HyGe "trapezoidal" pulse pin was installed for extension tests, as shown in Figure 7.

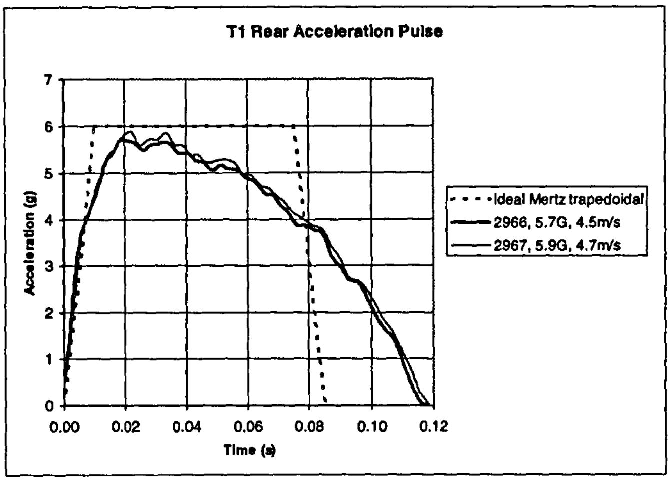

Figure 7: Extension sled pulse.

Extension Performance - The only criteria specified for rearward performance was the Mertz upper neck torque versus head angle relationship. The response of the prototype neck relative to this corridor, which is modified to adjust for the zero degree back angle of the upright motorcyclist, is shown in Figure 8.

Because the slider mechanism does not affect rearward response, there was no comparison made for a locked slider. The neck is shown to fall completely within the corridor, and to be repeatable in these two tests.

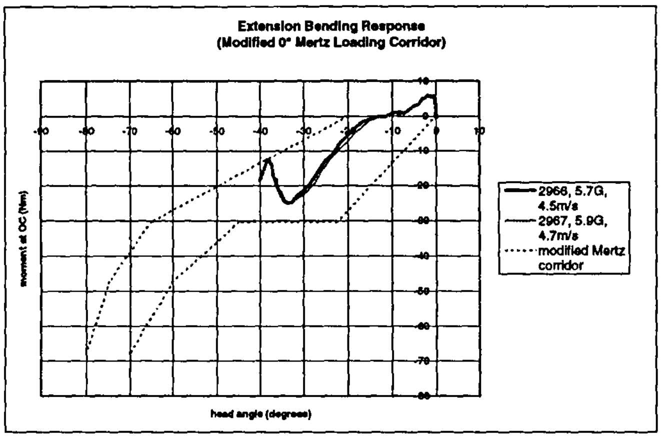

Figure 8: Extension bending response.

Lateral Flexion (TESTS 2960, 2961)

Tests for lateral flexion were conducted at the zero degree (no extension) position of the neck adjustment.

For forward flexion and rearward extension tests, it can be assumed that all motion will be in the mid-saggital plane, since the neck is symmetric about this plane, and the centre of gravity lies within it. But, for lateral flexion, where the head centre of gravity is not in line with the neck, and the neck is asymmetric, there is expected to be some out of plane motion, as well as torsion. For this reason, it becomes very difficult to resolve the position of the head centre of gravity from targets on the surface of the skull.

To remedy this, a thin rod was inserted through the skull's centre of gravity marking holes, and bent into "lollipops" on each side to mount targets. In this fashion, the video camera could see both targets, even if the head twisted. Having position data for the two targets throughout the event, the centre of gravity, which was exactly between the targets, could be tracked.

Lateral Flexion Sled Pulse - The lateral performance requirements, which comprise a series of peak measurements, do not necessitate as precise a test pulse as the frontal requirements. In fact, only a peak acceleration is dictated in the ISO lateral neck performance specifications [6]. However, the general characteristics of the frontal T1 pulse are also seen in the lateral pulse, where there is a sharp initial rise, followed by a series of lower peaks of relatively equal magnitude. Therefore, the HyGe pin that was designed for the frontal pulse was also used for the lateral pulse. The proper peak acceleration and velocity change set pressures for the sled were set after a few trial runs.

The resulting pulse is shown in Figure 9 relative to the NBDL volunteer pulse, corrected by Thunnissen et al. [9] to account for a non-rotating T1. The objective was to achieve a 14 G pulse with a velocity change of 7 m/s. In test 2960, the set pressure was too low, and the final velocity was too low. However, in the next test, the velocity change was very good. Peak accelerations were very good in both tests.

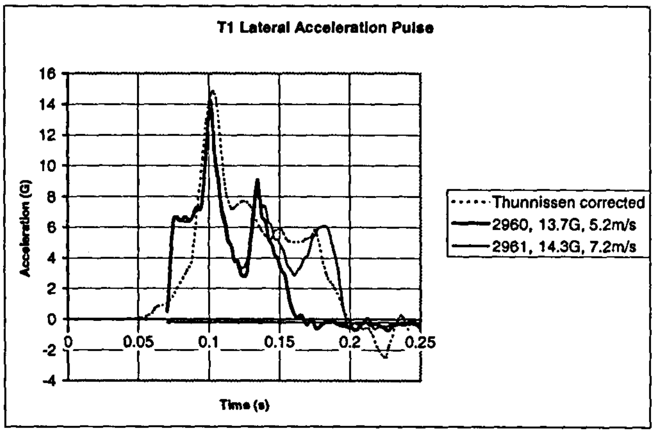

Figure 9: Lateral sled pulse.

Lateral Flexion Performance - The centre of gravity trajectory of the head is shown below in Figure 10. Run 2960 is shown to make it just to the volunteer window, but the velocity change of this pulse was too low. In run 2961, the centre of gravity trajectory fell within the window.

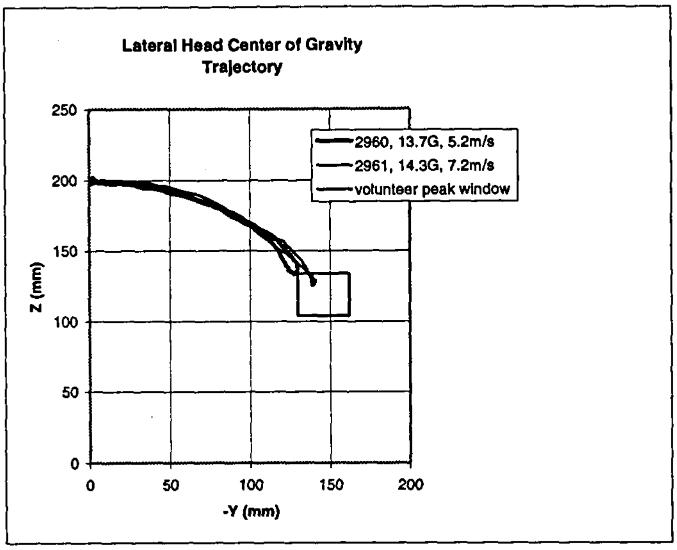

Figure 10: Lateral flexion head CG tragjectory.

The peak lateral flexion head angle achieved is shown in Figure 11. In both tests, the peak head angle exceeded the maximum allowable 59°, with 65° in test 2960 and 70° in test 2961.

The combination of the head CG being on the low side of the window and the peak head angle being over the limit suggests that the neck link should have rotated more, relative to the head link. In turn, this implies that the lower neck needs to be less stiff laterally, and the upper neck stiffer.

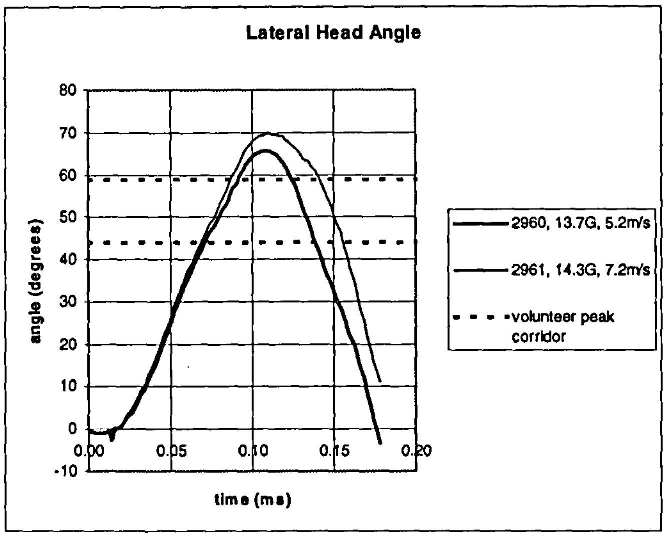

Figure 11: Lateral flexion head angle.

Torsion

Neck twist is specified in the ISO requirements as being from 32° to 45°, when tested in lateral flexion. However, film interpretation showed the neck twist, around the Z axis, to be only about 15°. This is supported by testing conducted in pure neck twist, similar to the certification tests for the MATD neck, specified by the ISO. Several tests were conducted at different torsion rates, and the resulting torque versus angle responses were very similar.

The response of the prototype in torsion is shown below in Figure 12. The two tests shown were done at a rapid twist rate (approximately 150°/second) shown in Test 1, and at a slower twist rate (approximately 60°/second) in Test 2. The results show that the neck is approximately 50% too stiff in torsion, compared to the target corridors. This excessive stiffness is supported by the lateral flexion test results, where the head needed to twist an additional 150% to fall within the established boundaries.

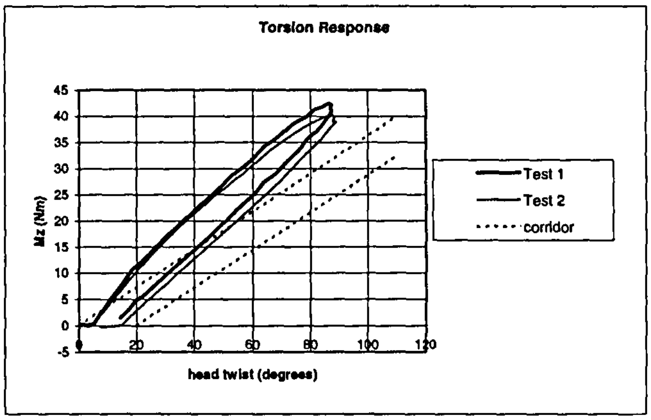

Figure 12: Torsion response.

Since the frontal, rearward and lateral responses of the neck are all reasonably good, there is the risk of upsetting these responses by changing the shape of the neck disks. Instead, it is felt that the torsional stiffness might be reduced by cutting selected disks through the midsaggital and/or coronal planes. In this manner, the torsional moment of inertia will be reduced, but the bending moments of inertia will remain unchanged. Some further experimentation shall be required to finalize the number and position of these cuts. There is a reluctance simply to add a torsional module, due to the combined complexity of a torsional/sliding joint.

SUMMARY

The following summarises the work completed, and provides recommendations for future work:

- A new prototype MATD neck has been designed, built and tested. This neck is intended to recognize a motorcyclist posture, as well as provide biofidelity in forward, rearward, and lateral bending, and in torsion.
- New features of this design include an adjustment for torso angles of 0° through 65°, as well as a slider mechanism to simulate the "head-lag" phenomenon
- The materials used in this design are hot-cast urethane for the deformable disks, aluminum for between these disks and for the adjustment mechanism, and steel for the slider mechanism.
- MADYMO modeling was used in designing the bending stiffness of the neck along its length.
- A customized HyGe sled pin was built to provide a reasonable representation of volunteers' T1 acceleration pulse.
- Testing was conducted in forward, rearward and lateral bending. Photographic and instrumentation data were collected.
- In forward flexion, the neck and slider mechanism showed good performance relative to the target corridors. A slight departure from the trajectory corridor is possibly due to deviation from the ideal acceleration pulse. Head-lag was introduced, although some increased sliding travel would be beneficial. Torque at the occipital condyles was within the corridors.
- In rearward extension, the torque at the occipital condyles was within the corridors. Kinematic performance data would be useful in complementing these requirements, but are not available at this time.
- In lateral flexion, the head centre of gravity traveled the correct distance, but head rotation was slightly excessive. This indicates that further optimization of the neck is required in lateral bending.
- Torsional response, both in lateral flexion as well as pure twist, showed the neck to be too stiff. It is anticipated that the torsional response might be softened by cuts in the urethane disks.
- A neck shroud similar to that currently used with the MATD shall be required for this neck to be used in airbag testing.

ACKNOWLEDGEMENTS

The author would like very much to thank Dynamic Research Inc., Torrance, California, for their support in the development of this dummy neck.

REFERENCES

1. Biokinetics Report R97-01, "Preliminary Design of the Next Generation MATD Neck," January, 1997.
2. Ewing, C. L., Thomas, D. J., Lustick, L., Becker, E., Willems, G., Muzzy III, W.H., "The Effect of the Initial Position of the Head and Neck on the Dynamic Response of the Human Head and Neck to –Gx Impact Acceleration," Proceedings of the 19th Stapp Car Crash Conference, 1975.
3. Gibson, T., Newman, J., Zellner, J., Wiley, K. "An Improved Anthropometric Test Device," Advisory Group for Aerospace Research and Development (AGARD), France, 1992.
4. Gibson, T., Shewchenko, N., Withnall, C.,/ "Biofidelity Improvements to the Hybrid III Neck," 14th International Technical Conference on Enhanced Safety of Vehicles (ESV), Paper 94-S1-O-13, Germany, 1994.
5. ISO/DIS 13232-3, "Draft Standard for Motorcycles – Test and Analysis Procedures for Research Evaluation of Rider Crash Protective Devices Fitted to Motorcycles; Part 3: Requirements for a Motorcycle Anthropometric Impact Dummy." August, 1995.
6. ISO/TC22/SC12 Document N455 – Revision 4 "Road Vehicles – Anthropomorphic Side Impact Dummy – Lateral Impact Response Requirements to Assess the Biofidelity of the Dummy," May, 1997.
7. Mertz. H., J., Patrick, L., M., "Strength and Response of the Human Neck." Proceedings of the 15th Stapp Car Crash Conference, SAE Paper No. 710995, SAE, Warrendale, PA, 1971.
8. St-Laurent, A., Szabo, T., Shewchenko, N., and Newman, J. A., "Design of a Motorcyclist Anthropometric Test Device," 12th International Conference on Experimental Safety Vehicle, Götberg, Sweden, 1989.
9. Thunnissen, J., Wismans, J., Ewing, C. L., Thomas, D. J., "Human Volunteer Head-Neck Response in Frontal Flexion: A New Analysis", Proceedings from the 39th Stapp Car Crash Conference, 1995. SAE paper no. 952721.
10. Wismans, J., Spenny, C.H., "Performance Requirements for Mechanical Necks in Lateral Flexion", Proceedings from the 27th Stapp Car Crash Conference, SAE Paper No. 831613, 1983.

Technical Session 11

New Car Assessment Programs

Chairperson: Bernd Friedel, Bundesanstalt für Straßenwesen (BASt), Germany

THE EFFECT OF REDESIGNED AIR BAGS ON FRONTAL USA NCAP

Brian T. Park
Richard M. Morgan
James R. Hackney
National Highway Traffic Safety Administration
Johanna C. Lowrie
Conrad Technologies, Inc.
United States
Paper Number 98-S11-O-01

ABSTRACT

In March 1997, the National Highway Traffic Safety Administration (NHTSA) temporarily amended Federal Motor Vehicle Safety Standard (FMVSS) No. 208 to allow manufacturers more flexibility in the use of less aggressive air bags. Beginning with the 1998 model year (MY), most vehicles produced for sale in the US market were equipped with these redesigned frontal air bags. This paper investigates how the safety ratings as developed in the New Car Assessment Program (NCAP) were affected by the introduction of these air bags.

Results from thirty-three MY 1998 vehicles crash tested for frontal NCAP were compared with the same make and models vehicles that were previously tested in NCAP. The only differences between the MY 1998 vehicles and the earlier vehicles are the redesigned air bags and other restraint system changes (i. e. , safety belt or steering assembly modifications). The head injury criteria (HIC), chest accelerations (chest G's), combined injury probability, and NCAP star ratings are examined for the driver and right front passenger. The neck responses of the driver and right front passenger between two model years also are examined relative to the new neck requirements that were included in the March 1997 amendment to FMVSS No. 208.

The average HIC values were lower for the MY 1998 vehicles. The lower average was primarily due to reductions in HICs that occurred in light truck and vans. Average chest G values were found to be nearly the same for the MY 1998 vehicles, as a group, when compared to the earlier models. Average neck loads were found to be approximately the same except for neck extension. The neck extension moments for the newer air bag vehicles were lower.

INTRODUCTION

Frontal crashes are the most prevalent fatality and severe injury-causing type of crash. Such crashes result in 51 percent of all driver and right front passenger fatalities. Air bags are proven to be effective in reducing fatalities in these types of crashes. NHTSA estimates that, between 1986 and May 1, 1998, air bags have saved over 3,000 drivers and passengers. Based on current levels of effectiveness, air bags will save more than 3,000 lives each year in passenger cars and light trucks when all light vehicles on the road are equipped with dual air bags.[1]

However, real world crash investigations have established that air bags are causing fatalities and injuries in some situations, especially to children and small-stature adults. [2] NHTSA's Special Crash Investigation program has identified 57 crashes in which the deployment of the passenger air bag resulted in fatal injuries to a child — unfortunately many cases were in low speed crashes.

Two adult passengers have also been fatally injured. In addition, 38 drivers are known to have been fatally injured. [1] Based on the 1998 - 1994 National Automotive Sampling System (NASS), a study of frontal collisions found that arm injuries to belt restrained drivers who had an air bag deploy are more likely than for drivers belt restrained without a deploying air bag. [3]

From NHTSA's ongoing study of adults and children who sustained fatal or serious injuries in low-to moderate severity crashes, it is found that the harm to these occupants is due to their close proximity to the air bag when it deployed. The most common reason for their proximity was the failure to use safety belts. In addition, infants in rear-facing child safety seats sustained fatal head or neck injuries from the deploying passenger air bags because they were positioned in the right front seat close to the dashboard. NHTSA continues to emphasize children under 12 years of age and infants in rear-facing child safety seats should not be in the right front seat where an air bag could deploy. By contrast, NHTSA studies concluded that such fatalities are very rare in comparison to the number of vehicles equipped with air bags (about 73 million vehicles had air bags by May 1, 1998).

To assist in reducing these problems, in March 1997, NHTSA temporarily amended FMVSS No. 208 to allow manufacturers more flexibility in the use of less aggressive air bags.[1] This amendment provided an option for manufacturers to use a generic sled test in place of the 48 kmph rigid barrier crash test to certify vehicle compliance with the unbelted 50th percentile male driver and passenger dummies. Based on the agency's research and analysis, the agency concluded that an average reduction in the power of air bag inflators of 20 to 35 percent would reduce the risk of air bag fatalities and injuries to out-of position occupants in lower speed crashes, while the life-saving capabilities of air bags in higher speed crashes may be reduced for unbelted occupants (particularly unbelted passengers). Manufacturers contended that the sled test would make it possible to more rapidly introduce these less aggressive air bags in their vehicles. Subsequently, most of the MY 1998 vehicles were equipped with redesigned air bags.

The objective of this paper is to investigate the effects of these air bag changes on MY 1998 vehicles crash tested for frontal NCAP by comparing with the same make and models vehicles tested in NCAP in previous years. The head injury criteria (HIC), chest accelerations (chest G's), combined injury probability, and NCAP star ratings are examined for the driver and right front passenger. The neck responses of the driver and right front passenger between two model years also are examined relative to the new neck requirements that were included in the March 1997 amendment to FMVSS No. 208.

Frontal USA New Car Assessment Program

In 1979, NHTSA began assessing the occupant protection capabilities of new cars by conducting high speed frontal, barrier crash tests. The primary goals of the USA NCAP is to provide consumers with a measure of the relative safety potential of automobiles and to establish market forces which encourage vehicle manufacturers to design higher levels of safety into their vehicles. The USA NCAP represents the first program ever initiated to provide relative crashworthiness information to consumers on the potential safety performance of passenger vehicles. [4,5,6]

Frontal USA NCAP test speeds and impact locations closely resemble the conditions in a large proportion of actual frontal crashes that result in fatalities or serious injuries. In these controlled crash tests, the levels of potential injury are assessed by measurements taken from two instrumented anthropomorphic test devices (dummies) that simulate 50th percentile adult males. These dummies are located in the front driver and front-right passenger seats and are restrained by the vehicle's safety belts and air bags, if available. [4]

During the crash, measurements are taken from each dummy's head, chest and upper legs. The injury potential to the head is measured by a composite of acceleration values known as the Head Injury Criterion or HIC. The injury potential to the chest is measured by a chest deceleration value known as chest G's. For the upper legs, the injury potential is measured by compressive axial forces on each of the femur bones. [4]

Beginning with the model year 1994 vehicles, the agency adopted a simplified nonnumeric format, the five star rating, for the frontal NCAP results. [6] NHTSA wanted to give the US consumer easily grasped vehicle safety performance information. This nonnumeric format is based on the use of injury risk functions, that relate the Hybrid III dummy measurements to injury probabilities. [7,8] The head and chest injury data are combined into a single rating, reflected by the number of stars with:[6]

☆☆☆☆☆ = 10% or less chance of any serious injury to the head or chest
☆☆☆☆ = 11% to 20% chance of serious injury
☆☆☆ = 21% to 35% chance of serious injury
☆☆ = 36% to 45% chance of serious injury
☆ = 46% or greater chance of serious injury

The relationship of the star rating system to injury probability and to the range of HIC and chest G values is shown in Figure 1.

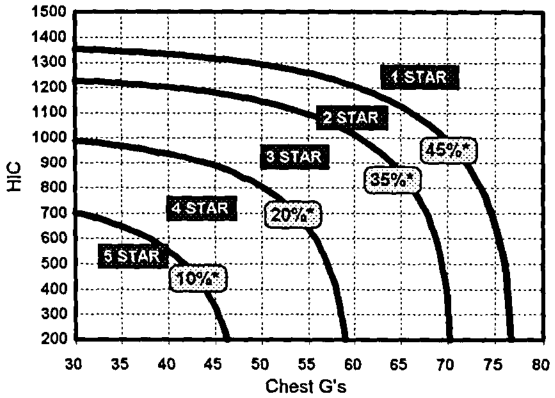

Figure 1. Relationship of the Star Rating and Probability to HIC and Chest G.

Consumers and interested parties may find the agency's safety information (i.e. star rating of vehicles) in several locations. World wide, one can reach the NCAP information on the agency's web site. The NHTSA web site address is www.nhtsa.dot.gov. NHTSA's web site provides a direct link to four other web sites world wide. The link reaches the (1) Insurance Institute for Highway Safety, (2) National Organization for Automotive Safety and Victim's Aid (Japan), (3) NRMA Crash Testing (Australia), and (4) Euro-NCAP (FIA Crash Testing).

RESULT AND DISCUSSION

For MY 1998, crash tests were conducted on fifty passenger cars, light trucks, vans, and sport utility vehicles in the frontal NCAP. In 1997, forty-two vehicles were tested. For this study, thirty-three vehicles have been selected and the pertinent dummy readings and star ratings are included in Table A1 of Appendix A. The thirty-three vehicles consist of different makes and models of twenty passenger cars and thirteen light trucks and vans (LTVs). A primary factor for selecting the vehicles is that the MY 1998 vehicles were reported by the manufacturers to have redesigned, or second generation, air bags for the driver and right front passenger as compared to the same make and model for MY 1997. Selected vehicles had no major structural changes between the two model years.

For the comparison, values of HIC, chest G's, and combined injury probability are examined. In addition, the redesigned air bag effects on the neck response of the 50th percentile Hybrid III dummy are studied (the neck readings for both years are included in Tables A2 and A3 of Appendix A). To examine the differences, the averages, standard deviations and ranges are calculated for the variables listed above for the two model years. The results are given for three vehicle groups: overall (combined passenger cars and LTVs), passenger cars, and LTVs. Calculated averages and standard deviation are tabulated in Table A4 of Appendix A.

Head Injury Criterion

The averages and standard deviations of HIC for the driver and right front passenger are illustrated in Figures 2 and 3. The results indicate that there is little difference for the overall and the passenger car groups for either the driver or right front passenger. However, marginal differences are exhibited for the LTV group, for both the driver and right front passenger. For the LTVs, the average driver HIC for MY 1998 is 137 less than the average HIC for MY 1997 and the average passenger HIC is 61 less for MY 1998. These differences in the LTV group for both driver and right front passenger are still considered to be small.

Figure 4 depicts the absolute difference in HIC value between the two model years. The comparison is made by calculating the difference from MY 1998 to MY 1997 for the same make and model for all thirty-three vehicles. Then, the difference is sorted and plotted in ascending order for driver and right front passenger. Therefore, the driver and passenger values do not occur at the same location in the figure. The decrease in HIC (indicated with negative sign) shows that the HIC value for MY 1998 is lower by the indicated amount. The figure shows that the trends for absolute change for driver and right front passenger are similar.

In Figure 5, HICs of the MY 1998 vehicles are plotted as a function of the HICs of the MY 1997 vehicles for the driver and right front passenger. Three HIC values exceed 1,000 which is the regulatory requirement in the 48 kph test of FMVSS No. 208. The values exceeding 1,000 are indicated with filled markers. Two readings above 1,000 in MY 1997 decreased in HIC value for MY 1998. One reading exceeded 1,000 in MY 1998, but was less than 1,000 in MY 1997. Most of the results are distributed along the 45 degree line and are well below 1,000.

In summary, from these comparisons, the differences in HIC between MY 1997 and MY 1998 vehicles are small. Therefore, it is expected that the level of head injury protection for the normally seated belt-restrained adult will be, at least, maintained in these MY 1998 vehicles.

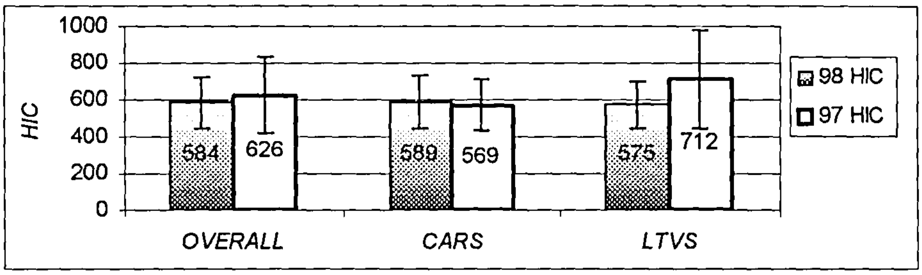

Figure 2. Average HIC values for the driver between MY 1998 and MY 1997.

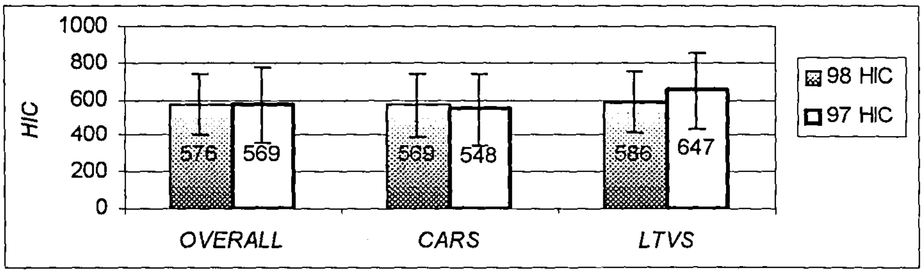

Figure 3. Average HIC values for the right front passenger between MY 1998 and MY 1997.

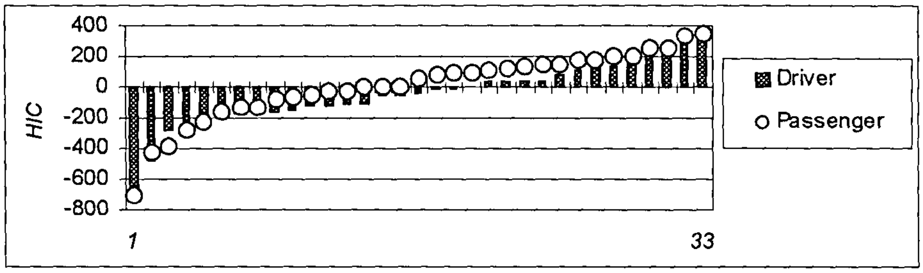

Figure 4. Absolute Difference in HIC between two Model Year vehicles for same vehicle.

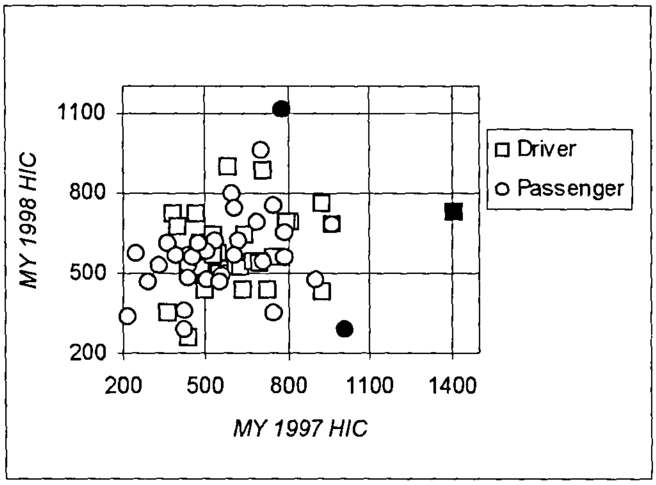

Figure 5. HIC distribution for the driver and right front passenger.

Chest G's (3 msec clip)

The averages and standard deviations of chest G's for the driver and right front passenger are illustrated in Figures 6 and 7. As can be seen, there is no difference in chest G's for the overall, the passenger cars, and the LTV groups for the driver. Similar results are found for the right front seat passenger; there is virtually no difference found in chest G's between the MY 1998 and MY 1997 vehicles.

Figure 8 depicts the absolute difference in chest deceleration values between the two model years. Again, the comparison is made by calculating the difference from MY 1998 to MY 1997 for the same make and model for all thirty-three vehicles. Then, the differences are sorted and plotted in an ascending order.

Figure 9 plots chest G's for MY 1998 as a function of chest G's for MY 1997 to show the overall chest G distribution for the driver and right front passenger. The

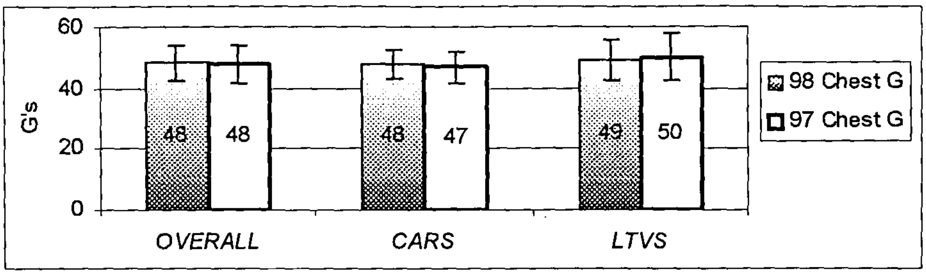

Figure 6. Average chest G's values for the driver between MY 1998 and MY 1997.

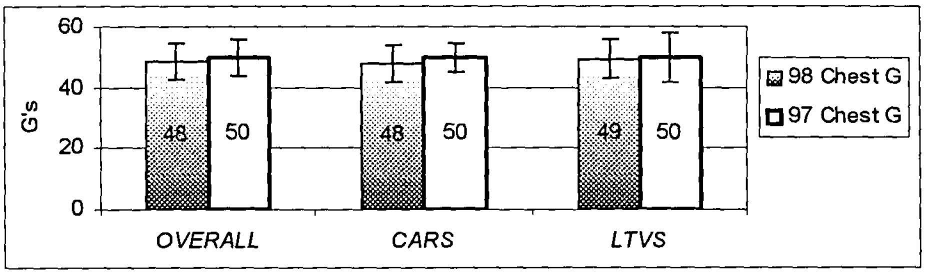

Figure 7. Average chest G's values for the right front passenger between MY 1998 and MY 1997.

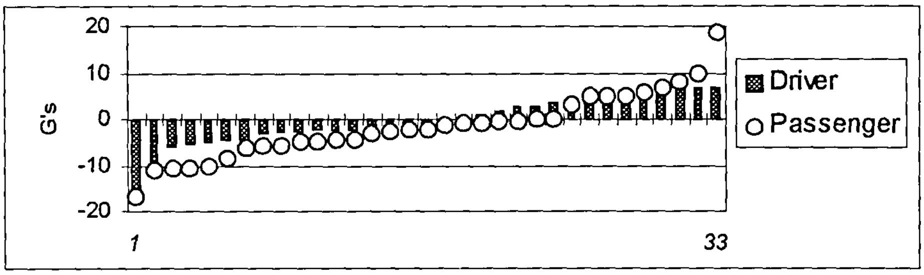

Figure 8. Absolute Difference in chest G's between two Model Year vehicles for same vehicle.

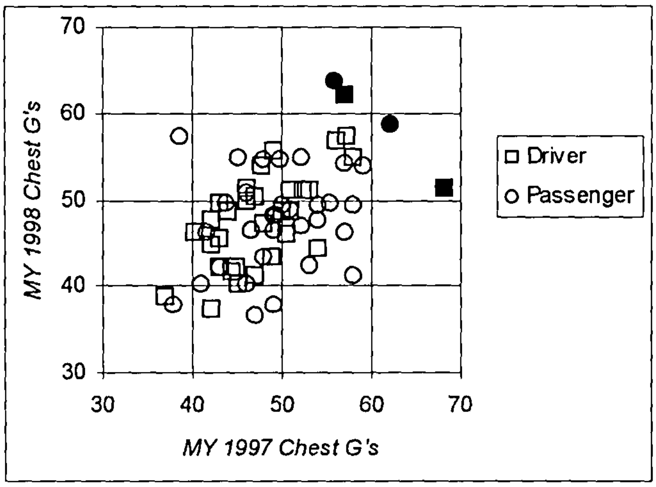

Figure 9. Chest G Distribution for the driver and right front passenger.

filled markers indicate the readings that exceed the 60 G's which is the regulatory requirement in the 48 kph test of FMVSS No. 208. Most of the results are distributed along the 45 degree line and no apparent difference is found. The figure shows that two chest readings that exceed 60 G's in MY 1997 are below 60 G's for MY 1998. Similarly, two chest readings that are below 60 G's in MY 1997 are now above 60 G's for MY 1998.

In summary, there is no difference in average chest G's between model years. Therefore, as for head injury protection, it is expected that the level of chest injury protection for the normally seated belt-restrained adult will be, at least, maintained in these MY 1998 vehicles.

Combined Injury Probability

As discussed before, the NCAP star rating is assessed based on the outcome of the combined injury probability that uses the dummy readings of HIC and chest G values. Figures 10 and 11 depict the comparison of the average combined injury probability for the driver and right front passenger, respectively. In general, in all three groups — overall, passenger cars, and LTVs — the injury probability for MY 1998 is generally lower than MY 1997 for both the driver and right front passenger. One notable change is in the LTV group. Since there is virtually no change in averaged chest G comparison, the difference reflects the slight change in average HIC. Nevertheless, no difference can be noted except for the LTV group.

To further examine the difference, Figure 12 depicts the absolute difference in combined injury probability between two model years for the driver and the right front passenger. Again, the comparison is made by calculating the difference from MY 1998 to MY 1997 for same makes and model for all thirty-three vehicles. Then, the difference is sorted and plotted in ascending order. For the driver, there is little variation for MY 1998 from MY 1997. One notable decrease in injury value is shown at the far left (of figure 12) for driver (lower by 45% for MY 1998). The variation is slightly more for the right front passenger. Nevertheless, most of the variation is less than 10 % for either decreased or increased injury probability values for the driver and the right front passenger. In summary, the trends for combined injury probability for driver and right front passenger are similar.

Since, the comparison of injury probability shows very little difference between MY 1998 and MY 1997, it is of interest to see how this is reflected by the nonnumeric five star rating. Figure 13 shows the difference in star rating results for two model years by plotting the difference. For instance, in the figure, a positive star means that the rating went up for MY 1998. The comparison shows that, for MY 1998, most of the star rating stayed the same or changed by no more than one star - up or down. In fact, 60 percent remained the same, whereas, only two ratings changed by more than one star. Fifteen star ratings increased for 1998 and 13 decreased.

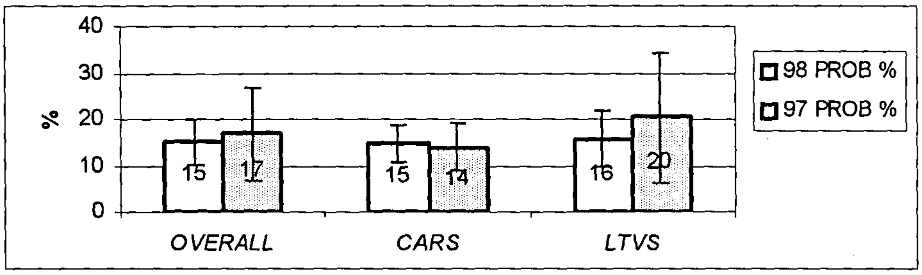

Figure 10. Average Combined Injury Probability values for the driver.

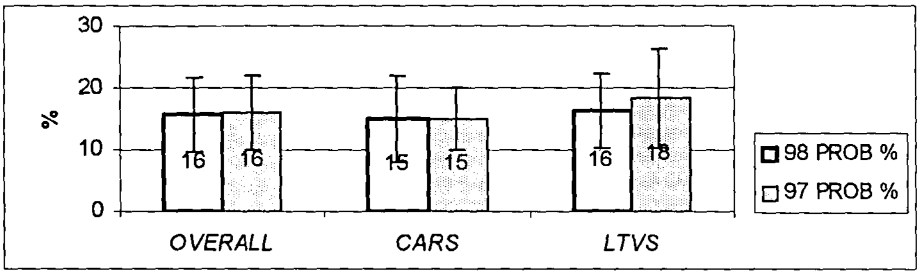

Figure 11. Average Combined Injury Probability values for right front passenger.

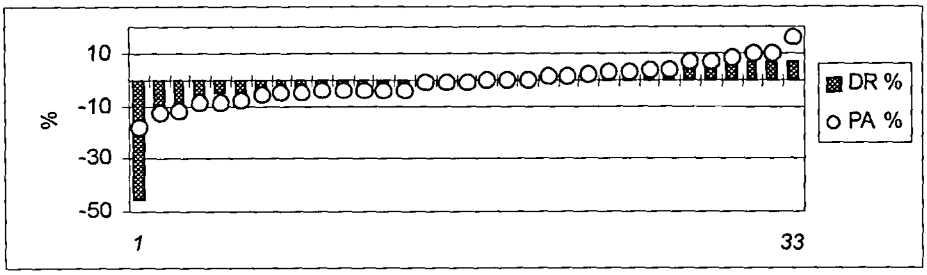

Figure 12. Absolute Difference in Combined Injury Probability between two Model Years.

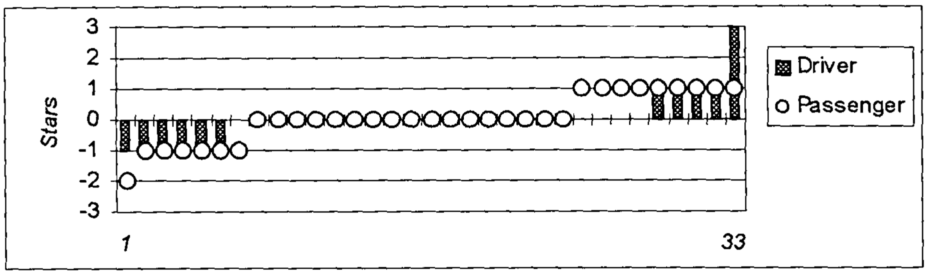

Figure 13. Difference in star rating for MY 1998 and MY 1997.

Neck Injury Criteria Comparison

Neck injury criteria are not used to determine the star rating. However, in the March 1997 temporary amendment to FMVSS No. 208, neck injury criteria were included as additional requirements in the optional sled test. The values for the neck injury criteria are shown in Table 1. With the occurrence of neck injuries associated with small stature adults and children in NHTSA's Special Crash Investigation Study, it is of interest to examine the effect of the redesigned MY 1998 air bags on the neck responses of the 50th percentile male test dummies in the NCAP tests.

Table 1.
Neck Injury Criteria for 50 % Dummy

Loading Mechanism	Neck Injury Criteria	SAE Electronic Filter
Flexion Bending Moment	190 Nm	600
Extension Bending Moment	57 Nm	600
Axial Tension	3300 N	1000
Axial Compression	4000 N	1000
Fore-and-Aft Shear	3100 N	1000

In Figures 14, 15, and 16, plots are shown of the neck force responses of MY 1998 as a function of MY 1997 for fore-and-aft shear, axial tension, and axial compression for both model years. All responses are below the FMVSS No. 208 requirements for both MYs except for the one response in 1998 that exceeds the axial tension criterion.

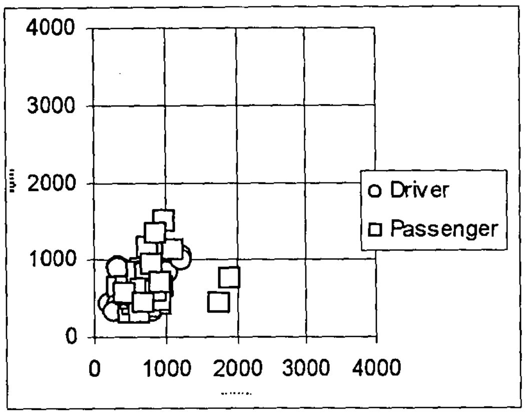

Figure 14. Neck fore-and-aft shear distribution

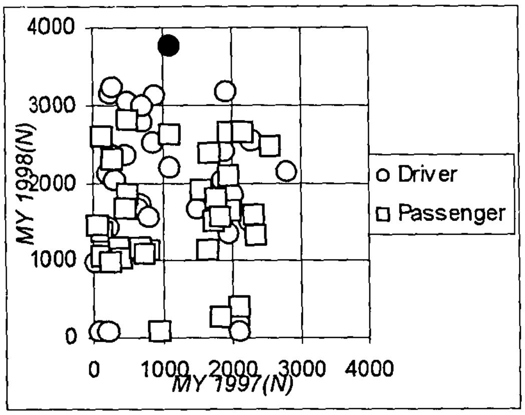

Figure 15. Neck axial Tension distribution

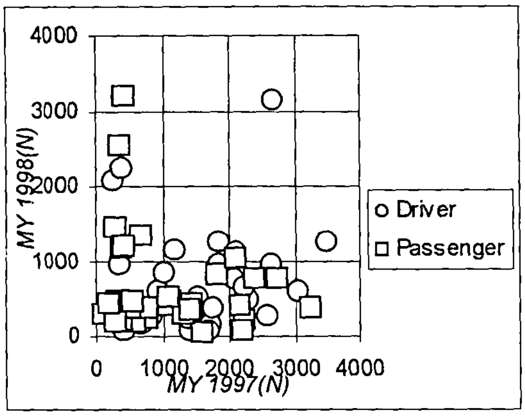

Figure 16. Neck axial Compression distribution

In Figures 17 and 18, plots are shown of the neck bending moments of MY 1998 as a function of MY 1997 for flexion and extension comparisons for the two model years. Here, most of the neck flexion bending moments are well below the FMVSS No. 208 injury criteria. However, for the neck extension bending, several readings exceed the criteria in both the MY 1998 and 1997 vehicles (indicated with filled markers).

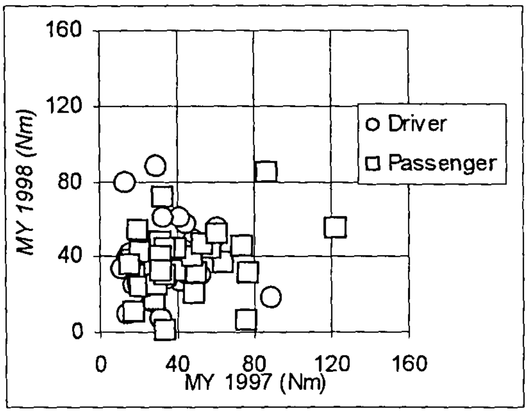

Figure 17. Neck Flexion Bending distribution

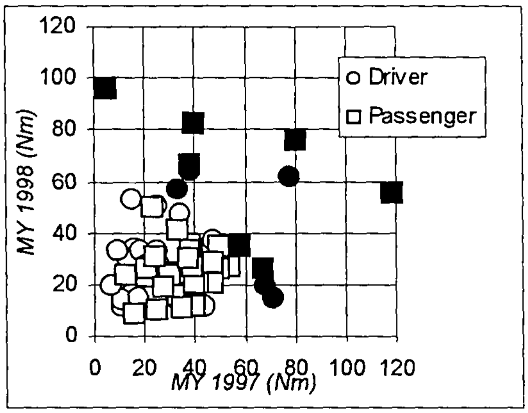

Figure 18. Neck Extension distribution

Figures 19 and 20 show the average neck extension for the driver and right front passenger for all groups. The comparisons show that the averaged readings for MY 1998 are somewhat lower than MY 1997 especially the passenger car group for both the driver and right front passenger. Furthermore, the difference can be discerned more in Figure 21 where it depicts the absolute difference in neck extension values between two model years for the driver and right front passenger. Again, the comparison is made by calculating the difference from MY 1998 to MY 1997 for the same makes and model for all thirty-three vehicles. Then, the difference is sorted and plotted in ascending order. For the driver, the number of neck extension responses that have decreased for the 1998 MY vehicles are about the same as that has increased. However, for the passenger, there are substantially more neck extension responses that have decreased for the 1998 MY vehicles than have increased — 24 of the 33.

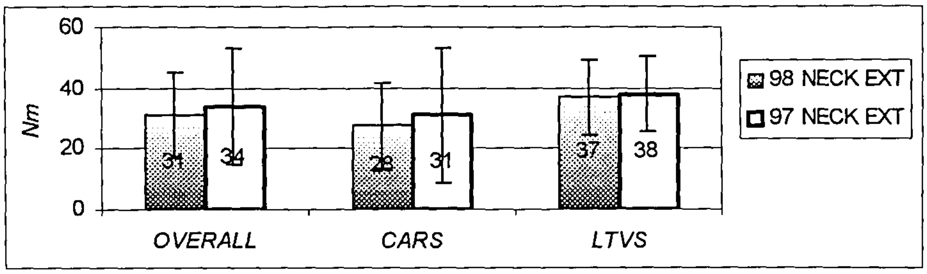

Figure 19. Average Neck Extension values for driver.

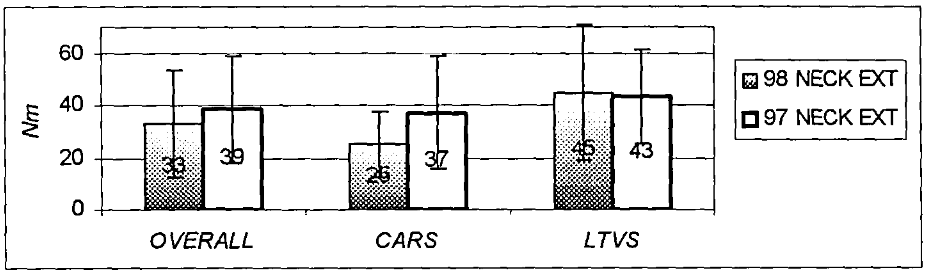

Figure 20. Average Neck Extension values for right front passenger.

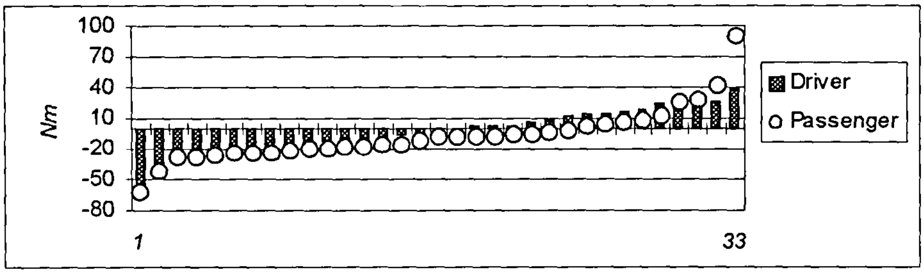

Figure 21. Absolute Difference in Neck Extension between two Model Years.

CONCLUSIONS

Beginning with the 1998 model year (MY), most vehicles produced for sale in the US market were equipped with redesigned frontal air bags. This paper investigates how the safety performance and ratings as developed in the New Car Assessment Program (NCAP) were affected by the introduction of these air bags.

Results from thirty-three MY 1998 vehicles crash tested for frontal NCAP were compared with the same make and models vehicles that were previously tested in NCAP. The only differences between the MY 1998 vehicles and the earlier vehicles are the redesigned air bags and other restraint system changes (i. e. , safety belt or steering assembly modifications). The head injury criteria (HIC), chest accelerations (chest G's), combined injury probability, and NCAP star ratings are examined for the driver and right front passenger. The neck responses of the driver and right front passenger between two model years also are examined relative to the new neck requirements that were included in the March 1997 amendment to FMVSS No. 208.

The average HIC values were lower for the MY 1998 vehicles. The lower averages were primarily due to reductions in HICs that occurred in LTVs. For the LTVs, the average driver HIC for MY 1998 is 575. This is 137 less than the average HIC for MY 1997. Overall only three HIC values exceeded the FMVSS No. 208 requirement of 1,000 — two in the MY 1997 vehicles and one in the MY 1998 vehicle.

Average chest G values were found to be the essentially the same for the MY 1998 vehicles when compared to the earlier models. All average values are between 48 and 50 G's. Two values for each MY exceeded the FMVSS No. 208 requirement of 60 G's.

The similarities in HIC and chest G's were reflected in the combined injury probabilities and the NCAP star ratings. For MY 1998, most of the star rating stayed the same or changed by no more than one star — up or down. In fact, 60 percent remained the same, whereas, only two ratings changed by more than one star.

Average neck loads were found to be approximately the same except for neck extension. The average neck extension moments for the newer air bag vehicles were lower for the passenger car group. For passenger cars, the average driver extension moment for MY 1998 is 28 Nm. This is 3 Nm less than the average extension moment for drivers in the MY 1997 passenger cars. The average passenger extension moment for MY 1998 is 25 Nm. This is 11 Nm less than the average extension moment for passengers in the MY 1997 vehicles.

These data indicate that the introduction of the redesigned air bags in the MY 1998 vehicles had little effect on the safety performance and ratings as measured and developed in NCAP. With average HICs of 584 for drivers, 576 for passengers, average chest G's of 48 for both drivers and passengers, and average neck responses well below those required in FMVSS No. 208, it is expected that the MY 1998 vehicles will provide high levels of protection to restrained occupants in frontal collisions that are represented by the NCAP tests.

REFERENCES

1. National Highway Traffic Safety Administration, U. S. Department of Transportation, Motor Vehicle Safety Standard No. 208, Docket No. 74-14 as amended by Notice 114 (Federal Register, Volume 62, No. 53, pp. 12960, 19 March 1997).

2. Winston, F. K., and Reed, R., " Air Bags and Children: Results of a National Highway Traffic Safety Administration Special Investigations into Actual Crashes," Fortieth Stapp Car Crash Conference, November 1996.

3. Kuppa, S. M., Olson, M. B., Yeiser, C. W., Taylor, L. M., Morgan, R. M., and Eppinger, R. H., " RAID - An Investigative Tool to Study Air Bag/Upper Extremity Interactions," Society of Automotive Engineers Paper No. 970399, February 1997.

4. Hackney, J. R., *The Effects of FMVSS No. 208 and NCAP on Safety as Determined from Crash Test Results,* Proceedings of the Thirteenth International Conference on Experimental Safety Vehicles, Paris, France, November 1991.

5. Kahane, C. J. , Hackney, J. R., and Berkowitz, A. M., *Correlation of NCAP Performance with Fatality Risk in Actual Head-On Collisions,* Report No. DOT HS 808 061, National Highway Traffic Safety Administration, Washington DC, 1994.

6. Hackney, J. R., Kahane, C. J., and Chan, R., *Activities of the New Car Assessment Program in the United States,* Proceedings of the Fifteenth International Conference on Experimental Safety Vehicles, Melbourne, Australia, May 1996.

7. Prasad, P., and Mertz, H., "The Position of the United States Delegation to the ISO Working Group 6 on the Use of HIC in the Automotive Environment," SAE Paper 851246, presented at the SAE Government/Industry Meeting and Exposition, Washington, DC, May 1985.

8. Viano, D. C., and Arepally, S., "Assessing the Safety Performance of Occupant Restraint Systems," Proceedings of the 34th Stapp Car Crash Conference, SAE Paper 902328, Warrendale, PA, November 1990.

9. Foster, J. K., Kortge, J. O., and Wolanin, M. J., "Hybrid III - A Biomechanically Based Crash Test Dummy," Twenty-First Stapp Car Crash Conference, SAE 770938, October 1977.

10. "Anthropomorphic Dummies for Crash and Escape System Testing," North Atlantic Treaty Organization, AGARD-AR-330, July 1996.

11. Mertz, H. J., "Anthropomorphic Test Devices," *Accidental Injury: Biomechanics and Prevention*, Nahum, A. M., and Melvin, J. M., eds., Springer-Verlag, New York, 1993.

Appendix A.

Table A1.

Head and chest readings and corresponding star rating for frontal New Car Assessment Program. The list below shows thirty-three vehicles chosen from the fifty crash tests conducted as MY1998. The results for MY1997 is either the result from MY1997 NCAP tests or from the prior year test result that carried over as MY1997. A primary factor for selecting the vehicles is that the MY1998 vehicles changed only the air bags for both driver and right front passenger—had no major structural changes.

		Model Year 1998 (Redesigned Air Bags)						Model Year 1997 (Fully Powered Air Bags)					
		Driver			Right Front Passenger			Driver			Right Front Passenger		
Make	Model	*HIC*	*ChestG 's*	*Stars*	*HIC*	*Chest G's*	*Stars*	*HIC*	*Chest G's*	*Stars*	*HIC*	*Chest G's*	*Stars*
Chevrolet	*Cavalier 2 Dr*	643	57	3	620	47	4	646	50	4	882	45	4
Chevrolet	*Cavalier 4 Dr*	514	54	4	751	48	4	552	48	4	749	54	3
Chevrolet	*Lumina*	679	48	4	495	40	5	394	42	5	560	46	4
Chevrolet	*Malibu*	691	42	4	473	50	4	810	44	4	546	44	4
Chevrolet	*CK Ext.*	726	46	4	693	57	3	468	40	5	689	39	4
Chevrolet	*Venture*	538	43	4	962	48	3	692	49	4	704	49	4
Dodge	*Dakota*	550	51	4	570	50	4	669	52	4	603	55	4
Dodge	*Ram Ext.*	691	47	4	295	49	4	793	48	4	1004	54	3
Ford	*Contour*	514	42	5	617	49	4	471	43	5	357	58	4
Ford	*Crown Victoria*	602	39	5	335	40	5	499	37	5	218	41	5
Ford	*Escort*	681	55	3	532	64	3	959	58	3	436	56	4
Ford	*Mustang*	436	41	5	364	47	4	493	47	4	419	52	4
Ford	*Taurus*	577	49	4	486	51	4	541	44	4	438	46	4
Ford	*Expedition*	544	45	4	569	42	4	693	42	4	393	43	5
Ford	*Explorer*	567	56	4	558	55	4	525	49	4	448	48	4
Ford	*F-150*	497	42	5	615	46	4	548	45	4	474	42	5
Ford	*Ranger*	442	51	4	545	43	4	724	53	4	711	53	4
Ford	*Windstar*	353	37	5	471	38	5	363	42	5	294	38	5
Honda	*Civic 4Dr*	619	50	4	531	55	4	480	46	4	329	45	5
Isuzu	*Rodeo*	650	62	3	561	54	4	528	57	4	782	59	3
Nissan	*Altima*	887	51	3	1119	55	2	710	51	4	777	52	4
Nissan	*Maxima*	565	49	4	654	54	4	747	50	4	783	57	3
Nissan	*Sentra*	898	49	3	797	49	4	583	51	4	599	50	4
Saturn	*SL*	435	40	5	585	44	4	633	45	4	506	48	4
Subaru	*Legacy*	525	51	4	623	49	4	482	46	4	532	51	4
Toyota	*Avalon*	504	50	4	577	37	5	517	47	4	243	47	5
Toyota	*Camry*	525	46	4	480	38	5	625	51	4	501	49	4
Toyota	*Corolla*	722	44	4	566	47	4	384	54	4	433	49	4
Toyota	*ES300*	512	50	4	478	48	4	432	43	5	902	49	3
Toyota	*4-Runner*	760	57	3	743	59	3	920	56	3	601	62	3
Toyota	*RAV-4*	434	49	4	355	46	4	919	51	3	747	57	3
Toyota	*Tacoma Ext.*	731	51	4	683	55	3	1411	68	1	962	50	3
Volvo	*S70*	259	46	5	294	41	5	434	43	5	421	58	4

Table A2.

Hybrid III dummy neck readings from frontal New Car Assessment Program for model year 1998.
Blank spaces indicate no data.

		Model Year 1998									
		DRIVER					RIGHT FRONT PASSENGER				
Make	Model	Shear (N)	Tension (N)	Comp (N)	Flex (Nm)	Exten (Nm)	Shear (N)	Tension (N)	Comp (N)	Flex (Nm)	Exten (Nm)
Chevrolet	*Cavalier 2 dr*	1053	1671	85	46	20	414	1137	181	30	27
Chevrolet	*Cavalier 4 dr*	840	2112	406	27	34	692	1054	444	32	23
Chevrolet	*Lumina*	440	2362	175	16	33	670	982	221	48	11
Chevrolet	*Malibu*	1011	1350	849	55	62	549	1516	214	35	24
Chevrolet	*CK Ext.*	358	2190	279	30	37	1171	2378	457	45	83
Chevrolet	*Venture*	912	2982	600	10	28	1339	2652	1212	1	76
Dodge	*Dakota*	550	3040	963	35	64	944	1814	194	45	35
Dodge	*Ram Ext.*	516	2528	760	8	36	1508	2608	525	36	96
Ford	*Contour*	338	89	178	49	12	666	1367	65	72	9
Ford	*Crown Victoria*	397	3174	600	43	17	902	1908	376	54	26
Ford	*Escort*	786	81	2241	25	51	667	1315	3207	7	12
Ford	*Mustang*	389	1728	513	32	14	776	1855	392	33	56
Ford	*Taurus*	415	3148	370	31	28		1307		45	19
Ford	*Expedition*	559	1843	392	61	25	318	1569	430	25	33
Ford	*Explorer*	924	3237	488	41	57	644	2314	820	47	21
Ford	*F-150*	438	2770	1113	40	34	480	2156	1048	31	27
Ford	*Ranger*	338	2045	654	30	29	617	1095	778	52	29
Ford	*Windstar*	620	993	241	50	20	452	1454	82	33	30
Honda	*Civic 4dr*	354	2140	1157	28	30	1138	92	524	85	24
Isuzu	*Rodeo*	609	2536	962	44	35	590	1597	1452	40	67
Nissan	*Altima*	616	187	2069	26	32	643	398	2559	38	10
Nissan	*Maxima*	338	1502	156	25	23	682	2459	459	11	36
Nissan	*Sentra*	651	2399	344	40	26	817	2097	315	24	21
Saturn	*SL*	721	1662	262	88	15	860	2643	396	42	35
Subaru	*Legacy*	672	1761	206	39	28	503	1632	1332	33	50
Toyota	*Avalon*	650	2034	291	36	14	427	1133	242	21	18
Toyota	*Camry*	608	78	1258	18	53	320	256	1182	17	25
Toyota	*Corolla*	863	2349	957	79	33	433	1168	478	37	26
Toyota	*ES300*	697	1435	85	58	12	528	1028	420	30	16
Toyota	*4-Runner*	752	3749	3156	61	48	542	2797	408	40	21
Toyota	*RAV-4*	485	1564	270	41	33	704	1660	361	46	41
Toyota	*Tacoma Ext.*	912	3124	1268	34	33	446	2610	774	55	26
Volvo	*S70*	530	1679	86	35	15	394	1161	305	32	31

Table A3.

Hybrid III dummy neck readings from frontal New Car Assessment Program for model year 1997. Blank spaces indicate no data.

		Model Year 1997									
		DRIVER					RIGHT FRONT PASSENGER				
Make	Model	Shear (N)	Tension (N)	Comp (N)	Flex (Nm)	Exten (Nm)	Shear (N)	Tension (N)	Comp (N)	Flex (Nm)	Exten (Nm)
Chevrolet	*Cavalier 2 dr*	1221	1480	415	32	68	922	1651	560	33	54
Chevrolet	*Cavalier 4 dr*	1015	197	1575	41	16	825	131	1436	77	21
Chevrolet	*Lumina*	200	264	1700	27	9	434	255	2213	31	35
Chevrolet	*Malibu*	1227	1945	1007	60	78	453	1733	395	28	30
Chevrolet	*Ck Ext.*	650	1100	1426	45	47	754	1666	550	39	40
Chevrolet	*Venture*	339	710	3033	14	52	851	2162	408	33	80
Dodge	*Dakota*	480	480	2630	24	38	800	1750	300	34	58
Dodge	*Ram Ext.*	666	843	2058	31	39	987	125	1092	15	5
Ford	*Contour*	796	215	1500	49	44	340	133	1600	32	16
Ford	*Crown Victoria*	391	1912	933	19	15	645	1559	749	19	50
Ford	*Escort*		2102	372	17	25	934	2320	400	76	40
Ford	*Mustang*	427	661	1520	33	11	1886	476	3247	39	118
Ford	*Taurus*	564	230	1733	24	21	684			57	27
Ford	*Expedition*	740	1999	685	32	37	617	1804	203	29	38
Ford	*Explorer*	320	278	2294	15	33	656	281	1800	53	40
Ford	*F-150*	333	700	2096	24	51	930		2101	34	39
Ford	*Ranger*	253	293	2237	52	37	846	718	2393	60	47
Ford	*Windstar*	436	42	1352	59	7	668	48	2176	31	37
Honda	*Civic 4dr*	425	2797	1175	35	13	1097	925	1086	86	12
Isuzu	*Rodeo*	584	2270	352	43	55	417	2299	286	31	38
Nissan	*Altima*	541	2076	240	21	43	449	2087	347	16	25
Nissan	*Maxima*	464	2250	678	19	37	815	2541	332	17	38
Nissan	*Sentra*	489	1867	214	27	45	709	1937	80	20	47
Saturn	*SL*	853	2013	813	29	71	589	1950	500	20	50
Subaru	*Legacy*	380	1816	449	14	26	499	1962	656	31	23
Toyota	*Avalon*	323	1850	364	41	33	796	776	772	49	39
Toyota	*Camry*	643	91	1827	89	15	472	1822	367	28	32
Toyota	*Corolla*	406	448	1851	13	18	545	364	1124	64	21
Toyota	*ES300*	426	199	1412	44	11	618	400	1095	19	33
Toyota	*4-Runner*	582	1082	2670	41	34	606	479	2152	48	41
Toyota	*RAV-4*	474	785	2579	28	25	911	468	1402	74	33
Toyota	*Tacoma Ext.*	354	886	3453	11	39	1742	1078	2722	122	67
Volvo	*S70*		628	1692	46	17	763	661	1286	50	24

Table A4.

Average, standard deviation, and range of dummy readings for the frontal New Car Assessment Program for model year 1998 and model year 1997. These calculations are made from the Table A1 based on the compared thirty-three vehicles.

			OVERALL				CARS				LTVS			
		Criteria	AVG	STD	MAX	MIN	AVG	STD	MAX	MIN	AVG	STD	MAX	MIN
MY 1998	**Dr**	*HIC*	584	139	898	259	589	149	898	259	575	128	760	353
		Chest G	48	6	62	37	48	5	57	39	49	7	62	37
		Prob %	15	5	27	7	15	4	23	9	16	6	27	7
		Shear	616	210	1053	338	618	219	1053	338	613	204	924	338
		Tension	1986	956	3749	78	1647	929	3174	78	2508	762	3749	993
		Comp	710	689	3156	85	614	635	2241	85	857	768	3156	241
		Flexion	39	18	88	8	40	19	88	16	37	16	61	8
		Extension	31	14	64	12	28	14	62	12	37	12	64	20
	Pa	*HIC*	576	173	1119	294	569	180	1119	294	586	169	962	295
		Chest G	48	6	64	37	48	7	64	37	49	6	59	38
		Prob %	16	6	36	8	15	7	36	8	16	6	25	8
		Shear	682	286	1508	318	636	206	1138	320	750	374	1508	318
		Tension	1612	710	2797	92	1325	661	2643	92	2054	551	2797	1095
		Comp	683	685	3207	65	701	837	3207	65	657	403	1452	82
		Flexion	37	17	85	1	36	19	85	7	38	14	55	1
		Extension	33	21	96	9	25	12	56	9	45	26	96	21
MY 1997	**Dr**	*HIC*	626	212	1411	363	569	148	959	384	712	268	1411	363
		Chest G	48	6	68	37	47	5	58	37	50	8	68	40
		Prob %	17	10	64	8	14	5	31	8	20	14	64	9
		Shear	548	255	1227	200	600	302	1227	200	478	155	740	253
		Tension	1106	818	2797	42	1252	901	2797	91	882	640	2270	42
		Comp	1465	867	3453	214	1074	591	1851	214	2067	897	3453	352
		Flexion	33	17	89	11	34	18	89	13	32	15	59	11
		Extension	34	18	78	7	31	21	78	9	38	13	55	7
	Pa	*HIC*	569	200	1004	218	518	181	902	218	647	210	1004	294
		Chest G	50	6	62	38	50	5	58	41	50	8	62	38
		Prob %	16	6	30	7	15	5	24	7	18	8	30	7
		Shear	765	329	1886	340	724	337	1886	340	830	317	1742	417
		Tension	1179	811	2541	48	1246	819	2541	131	1073	823	2299	48
		Comp	1102	844	3247	80	960	770	3247	80	1353	922	2722	203
		Flexion	42	14	122	15	40	22	86	16	46	27	122	15
		Extension	39	21	118	5	37	22	118	12	43	18	80	5

REPEATABILITY OF FRONTAL OFFSET CRASH TESTS

Susan L. Meyerson
David S. Zuby
Adrian K. Lund
Insurance Institute for Highway Safety
United States
Paper Number 98-S11-O-02

ABSTRACT

The Insurance Institute for Highway Safety publishes crashworthiness evaluations of passenger vehicles based on their performance in a 40 mi/h (64 km/h) frontal offset crash test. This paper describes the repeatability of vehicle and Hybrid III driver dummy responses for several pairs of vehicles in this type of crash test. Vehicle responses that were compared include interior intrusion measurements and vehicle accelerations. Driver dummy responses include dummy movement during the crash and electronic injury measures from the head, neck, chest, and upper and lower legs. The seven models that were tested twice are the 1997 Dodge Neon, 1997 Hyundai Elantra, 1994/95 Saab 900, 1995 Ford Taurus, 1997 Pontiac Trans Sport, 1996 Nissan Quest, and 1997 Infiniti Q45. Structural measures in the repeated tests were similar to those in the first tests for most models. Among injury measures, head injury criteria, neck tensions, chest compressions, femur and tibia axial forces, upper tibia indices, and foot accelerations also were similar in the repeated tests for most models. Neck bending moments and lower tibia indices were less consistent. Implications of these comparisons for the Institute's crashworthiness evaluations are discussed.

BACKGROUND

Crash tests are performed for a variety of reasons that include checking whether new designs meet engineering expectations and safety regulations, re-creating real-world crashes to study injury mechanisms, and comparing crashworthiness offered by different model designs. Because conducting a full-scale crash test is time consuming and costly, each of these endeavors relies on generalizing the results of a few tests, in many cases only one, to make inferences about other crashes under similar circumstances. Hence the issue of repeatability, or how closely the results of replicated tests resemble one another, is important.

Relatively little has been written on the subject of crash test repeatability. The most extensive study was reported by the National Highway Traffic Safety Administration (NHTSA), which conducted 12 full-overlap frontal crashes at 35 mi/h against a rigid barrier at three test sites.[1] In this study of the reliability of the agency's New Car Assessment Program (NCAP), the test vehicles were 1982 Chevrolet Citations identically equipped and built during the same shift at a single plant. The seats were welded in the correct adjustment position to minimize test setup differences. Head injury criterion (HIC) and chest acceleration were the two test results examined most closely.

Driver dummy HICs ranged from 522 to 954, and passenger dummy HICs ranged from 542 to 793, with one site consistently reporting the highest results and another consistently reporting the lowest. Reported chest accelerations were highest from the test site with the highest HICs and lowest from the site with the lowest HICs. Slight test procedure differences among the sites were noted, but none of these differences explained the particular pattern of results. For example, dummy head calibration results did not correlate with differences in crash test HICs.

Other differences among the tests were examined to try to explain some of the differences in the dummy injury measures. For instance, differences in dummy head contacts apparently explained some of the HIC variation observed. On the driver side, the head contacted the steering wheel rim in most tests because the 1982 Chevrolet Citations were not equipped with airbags. However, steering column intrusion varied enough among tests that the dummy's head contacted different parts of the steering wheel rim, and in two tests the dummy's head missed the steering wheel altogether. On the passenger side, the dummy's head sometimes contacted the right knee, which was pushed upward by floorboard buckling. The authors also noted that variation in torso rotation for both driver and passenger dummies may have been due to differences in seat belt placement.[1] However, a multivariate regression analysis did not find statistically significant relationships among vehicle response variables (amount of dynamic crush, floor buckling pattern, steering column movement) and dummy injury measures (HIC and chest acceleration). The many potential sources of test variability (procedure, test dummy condition, test vehicle) made it impossible to identify the specific contribution of any one source to the differences in dummy injury measures. Nevertheless, the authors made several recommendations that were intended to improve the reliability of NCAP results.

The need for a new frontal crash test standard in Europe led to the development by the European Experimental Vehicle Committee (EEVC) of the frontal offset crash test using a deformable barrier. The authors reasoned that offset tests with a deformable barrier face should be more repeatable than offset tests with a rigid barrier, in part because the weak edge of the soft barrier face would be less sensitive to lateral alignment.[2] The authors also suggested that the deformable barrier would reduce initial accelerations and increase the amount of time over which the acceleration is applied, compared with a rigid barrier. This increase in the duration of acceleration peaks would allow for more predictable onset of failure in structural components than the short, high acceleration peaks produced in rigid barrier tests. In support of these suggestions, the authors presented the results of three vehicles crashed into a deformable barrier at the same speed (56 km/h) with a 40 percent barrier overlap. Peak vehicle accelerations in these tests varied little and occurred at about the same time. Driver dummy injury measures were described as repeatable with HICs ranging from 374 to 427, maximum chest accelerations ranging from 70 to 96 g, maximum left femur loads ranging from 5 to 10 kN, and maximum right femur loads ranging from 5 to 8 kN.

The Bundesanstalt für Straßenwesen (BAST) submitted data on the repeatability of frontal offset deformable barrier tests to EEVC.[3] Three 1994 Volkswagen Golf VR6 A3s were tested at 56 km/h with a 40 percent barrier overlap. The authors reported good repeatability for the "classical" dummy measurements of HIC, chest acceleration, and chest compression, with coefficients of variation (standard deviation as a percent of the mean measured value) ranging from 2 to 8 percent. In addition, maximum head and chest accelerations as well as maximum chest compressions were recorded at about the same time in each of the repeated tests (within a range of 10 ms). The report stated that the dummies' leg measurements were more variable. Coefficients of variation calculated for the BAST leg injury data ranged from 2 to 108 percent, with most greater than 10 percent. Also, peak values from different tests were recorded at considerably different times, of which some occurred 50 ms apart. BAST also found that intrusion measurements were quite variable. Coefficients of variation for two of the measurements — vertical movement of the brake pedal and rearward movement of the left toepan — were comparable with those for the "classical" dummy measures. However, other toepan measures, steering column movement, and instrument panel rearward movement had coefficients that ranged from 12 to 185 percent.

The Japan Automobile Standards Internationalization Center (JASIC) also submitted data on the repeatability of frontal offset deformable barrier crash tests to EEVC.[4] Four midsize cars with two dummies, weighing approximately 1,400 kg per test setup, were tested at 56 km/h with a 40 percent barrier overlap. A measurement was judged repeatable if its range of observed values was no larger than 80 percent of its mean value. The JASIC tests showed good repeatability for all intrusion measurements except steering column vertical movement (range/mean = 3.2). HIC and chest acceleration results also were judged repeatable, but other injury measures (axial femur force, knee displacement, and neck extension moment) had range/mean values greater than 0.8.

INSTITUTE TESTS

The Insurance Institute for Highway Safety conducted two tests of each of seven vehicles at a nominal impact speed of 64.4 km/h (40 mi/h) and a nominal 40 percent overlap with a deformable barrier. Table 1 lists the vehicle weight, impact speed, and barrier overlap for each test. Although not conducted for the purpose of repeatability assessment, test conditions were similar enough for each pair of vehicles to provide further information about the repeatability of occupant protection performance in frontal offset deformable barrier crash tests.

Vehicle Response Measures

Vehicle acceleration and velocity history, occupant compartment intrusion, and action of restraint system components were compared between the first and second tests of each model. Vehicle acceleration was measured by

Table 1.
Repeated Frontal Offset Crash Tests

	Test Weight (kg)		Impact Speed (km/h)		Measured Overlap (%)	
Make/Model	**Test 1**	**Test 2**	**Test 1**	**Test 2**	**Test 1**	**Test 2**
Dodge Neon	1,312	1,308	64.0	64.3	41	41
Hyundai Elantra	1,340	1,355	64.4	64.8	45	40
Saab 900	1,476	1,489	64.5	64.2	40	40
Ford Taurus	1,565	1,599	64.5	64.5	41	40
Pontiac Trans Sport	1,836	1,852	63.4	64.2	41	41
Nissan Quest	1,846	1,862	64.2	64.0	40	40
Infiniti Q45	1,944	1,944	64.0	64.5	40	40

accelerometers inside the occupant compartment, and velocity history was either calculated from acceleration measures or obtained through film analysis from overhead cameras. Occupant compartment intrusion was characterized by the differences between precrash and postcrash positions of measurement targets on the instrument panel, toepan, and steering wheel hub. The maximum amount of seat belt spool-out was measured by stitching one end of a string to the belt webbing and attaching the other end to the B-pillar with tape so that as the webbing was pulled out of the retractor, the string was pulled out from under the tape. Airbag deployment time was characterized by noting when the airbag first was observed outside the module in the high-speed film.

Driver Dummy Responses

Hybrid III dummy injury measures and observed dummy kinematics were used to assess the repeatability of driver dummy responses. Dummy head contact locations, in addition to gross dummy kinematics, were used to compare dummy movement. Dummy injury measures include HIC, neck extension bending moment, neck tension force, chest compression, femur axial force, tibia-femur displacement, upper and lower tibia indices, tibia axial force, and foot acceleration.

RESULTS

Vehicle Responses

Table 2 lists the maximum vehicle longitudinal accelerations for the first and second tests of six models (vehicle acceleration was not recorded in the first Nissan Quest test). Acceleration differences in the repeated tests of the Saab 900, Pontiac Trans Sport, and Dodge Neon were less than 5 g, and the velocity histories calculated from the acceleration measurements in these tests follow each other closely. Despite somewhat larger peak acceleration differences (8-14 g) in the repeated tests of the Ford Taurus, Infiniti Q45, and Hyundai Elantra, these cars' occupant compartments experienced largely similar crash forces, as indicated by their occupant compartment velocity histories (Figures 1-3).

Table 2.
Maximum Vehicle Longitudinal Acceleration (g)

Make/Model	Test 1	Test 2
1997 Dodge Neon	35	33
1997 Hyundai Elantra	38	46
1994/95 Saab 900	32	28
1995 Ford Taurus	39	29
1996 Pontiac Trans Sport	24	25
1997 Infiniti Q45	30	44

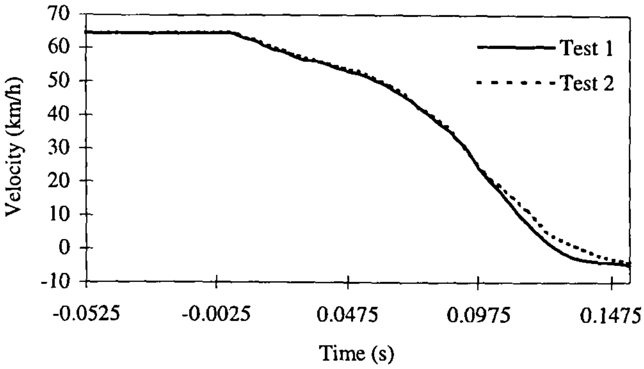

Figure 1. 1995 Ford Taurus Vehicle Longitudinal Velocity.

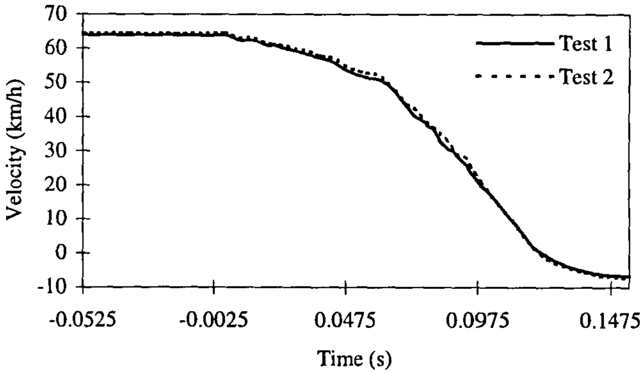

Figue 2. 1997 Infiniti Q45 Vehicle Longitudinal Velocity.

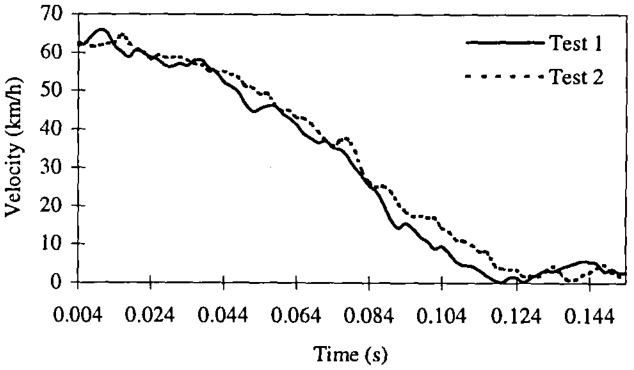

Figure 3. 1997 Hyundai Elantra Vehicle Longitudinal Velocity.

The peak vehicle acceleration differences in the repeated tests of the Ford Taurus and Infiniti Q45 were due to variation in high-frequency oscillations experienced by the accelerometers and did not indicate differences in the gross decelerations of the occupant compartments. Similarly, the apparent large acceleration difference in the Hyundai Elantra tests likely was due to differences in local accelerations caused by deformation of the occupant compartments near the accelerometer mounting locations, which were slightly different in the two tests. These differences developed later in the crashes as occupant compartments deformed. Acceleration histories for the first 60 ms of both crashes were quite similar. Because the accelerometer mounting locations were slightly different in the two tests, film analysis from an overhead camera was used to compute the velocity history shown in Figure 3.

Intrusion measurements in the repeated tests of the Dodge Neon and Hyundai Elantra, two small cars, as well as those in the Pontiac Trans Sport and Nissan Quest, two passenger vans, were very similar (Figures 4 and 5); some measures were exactly the same, and the largest differences were only 2-3 cm.

Intrusion differences among these models were much greater than differences between each model's first and second test. Intrusion measurements in the repeated tests of the Saab 900 and Ford Taurus, two midsize cars, were not very similar (Figure 6). Intrusion measurements in the repeated test of the Infiniti Q45 (Figure 7), a large luxury car, were not as similar as those for small cars and passenger vans but more similar than those for the Saab 900 and Ford Taurus.

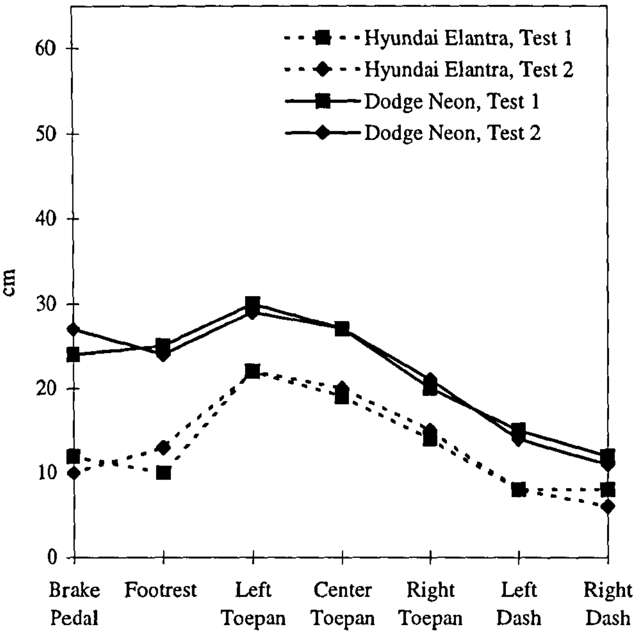

Figue 4. Small Car Intrusion.

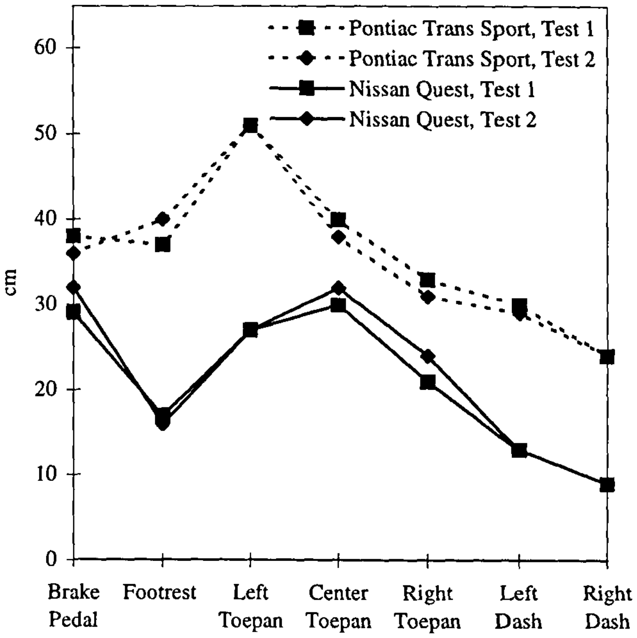

Figure 5. Passenger Van Intrusion.

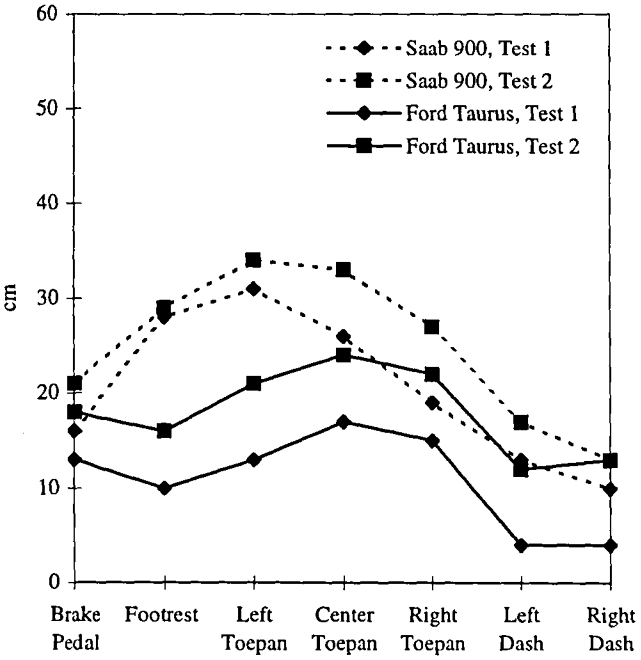

Figure 6. Midsize Car Intrusion.

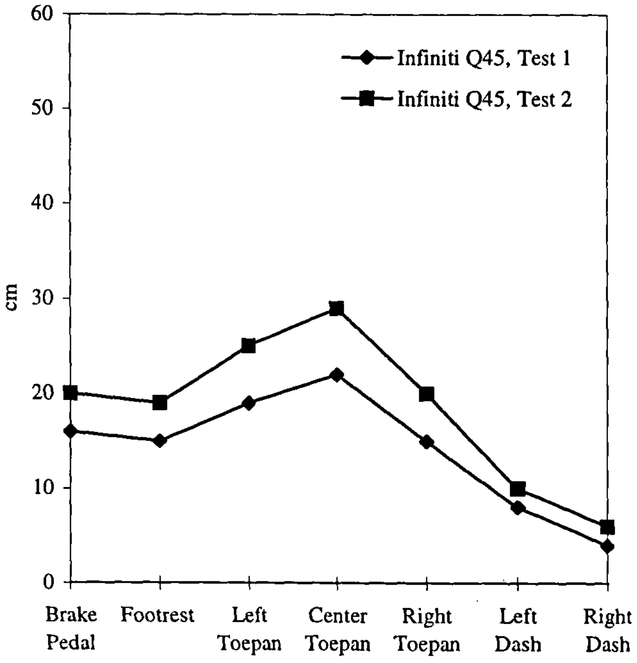

Figure 7. Large Luxury Car Intrusion.

Examination of underbody structures of the many models with repeatable intrusion measurements shows that crush zone components deformed in similar ways. For example, the engine cradles of the Pontiac Trans Sports did not deform but rather were pushed back into the occupant compartments, causing the same extreme level of intrusion in both tests (Figure 8). In contrast, the Infiniti Q45 tests show clear differences in the deformation patterns of crush zone components (Figure 9). The left side rail did not buckle in the second test, as it had in the first test, but remained straight and was driven rearward into the toepan, producing more toepan intrusion than in the first test.

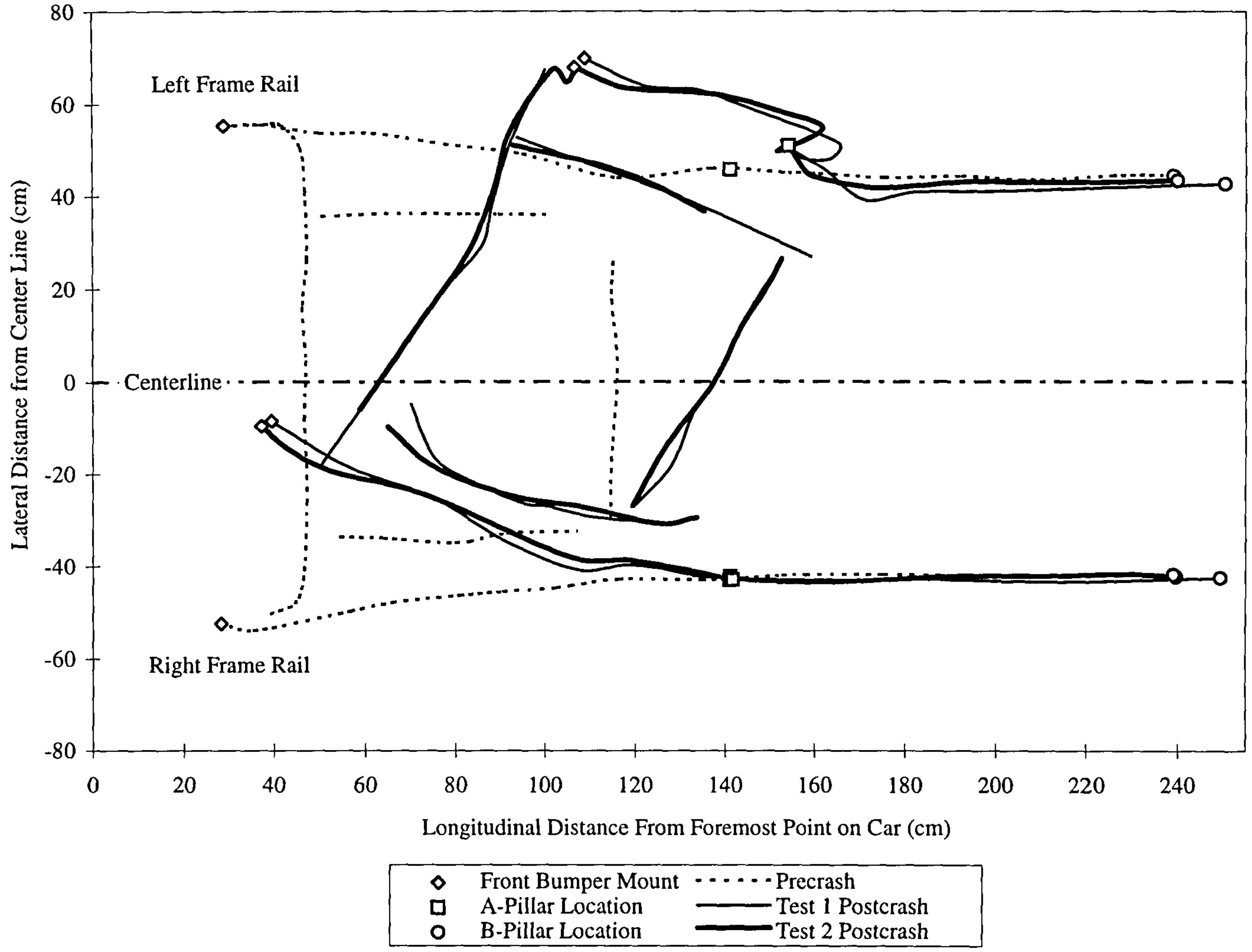

Figure 8. 1997 Pontiac Trans Sport Frame Rail Deformations, View from Below.

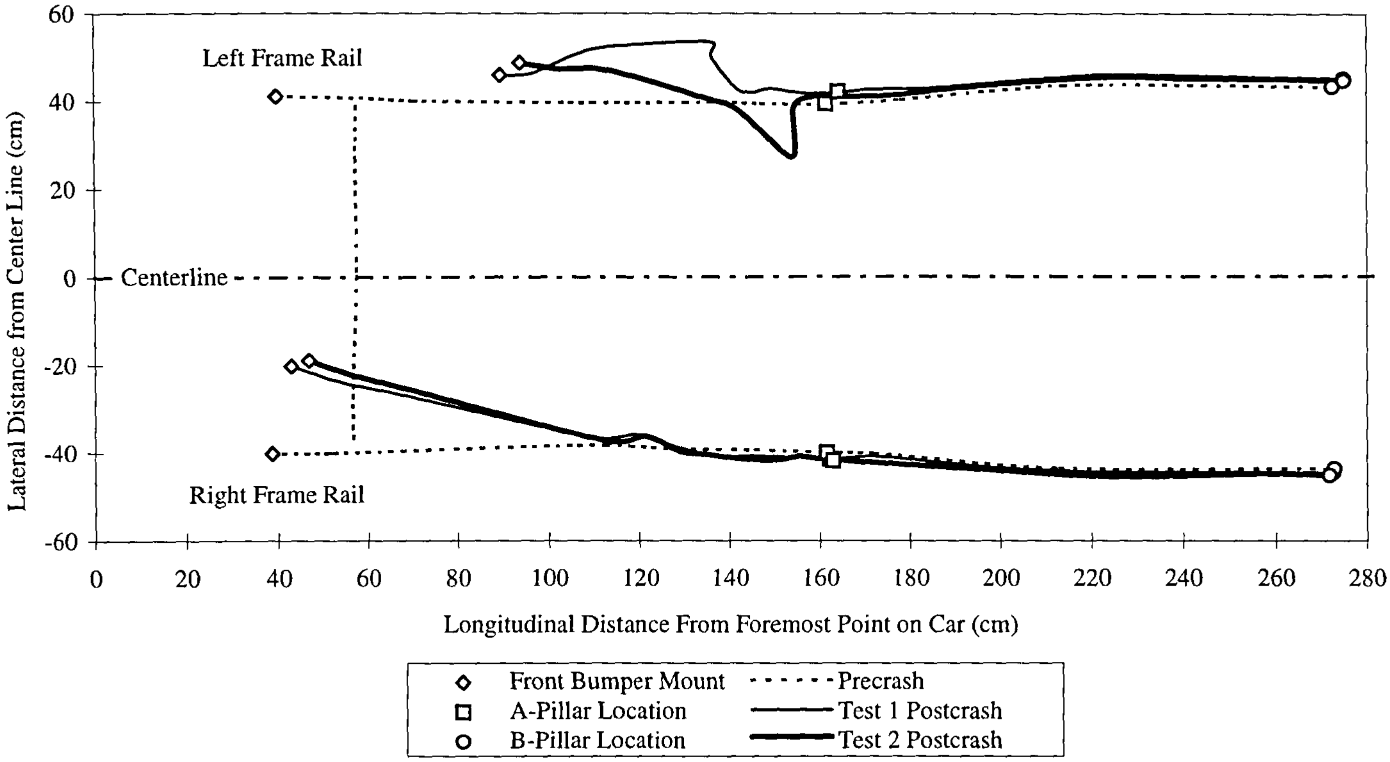

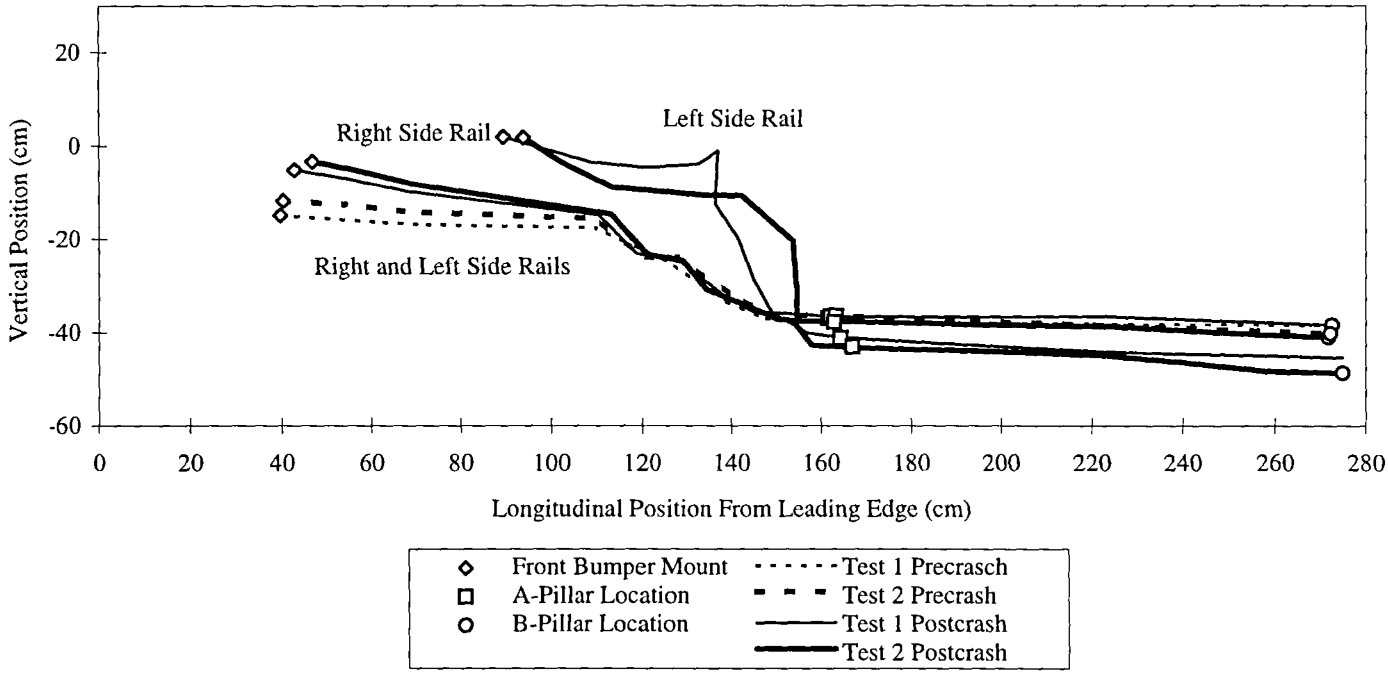

Figure 9. 1997 Infiniti Q45 Frame Rail Deformation, Views from Below and Side.

Longitudinal and vertical steering column movements were very similar (within 3 cm) in the repeated tests of all models except the Ford Taurus and Pontiac Trans Sport (Figures 10 and 11). Vertical movement was similar in the Ford Taurus tests, but longitudinal movement in the second test was 10 cm greater than in the first test. The Pontiac Trans Sport tests produced similar longitudinal steering column movement, but vertical measures differed by 5 cm.

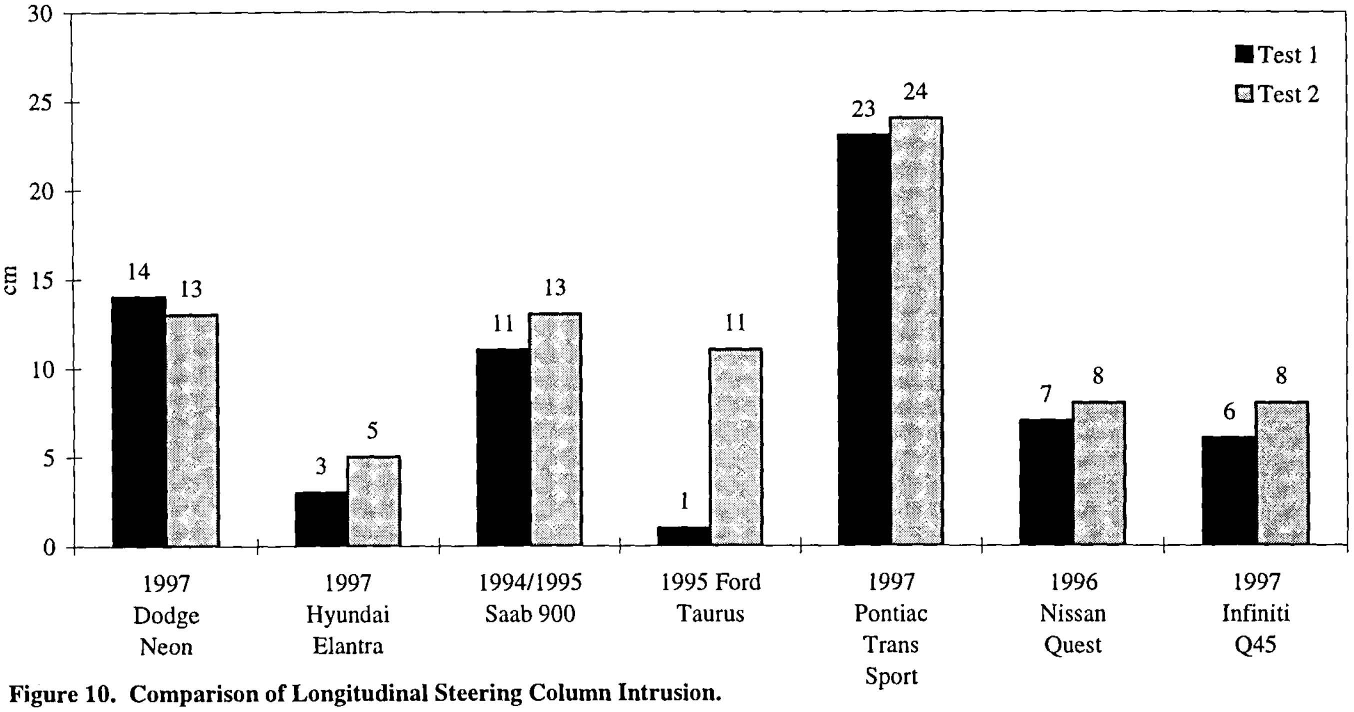

Figure 10. Comparison of Longitudinal Steering Column Intrusion.

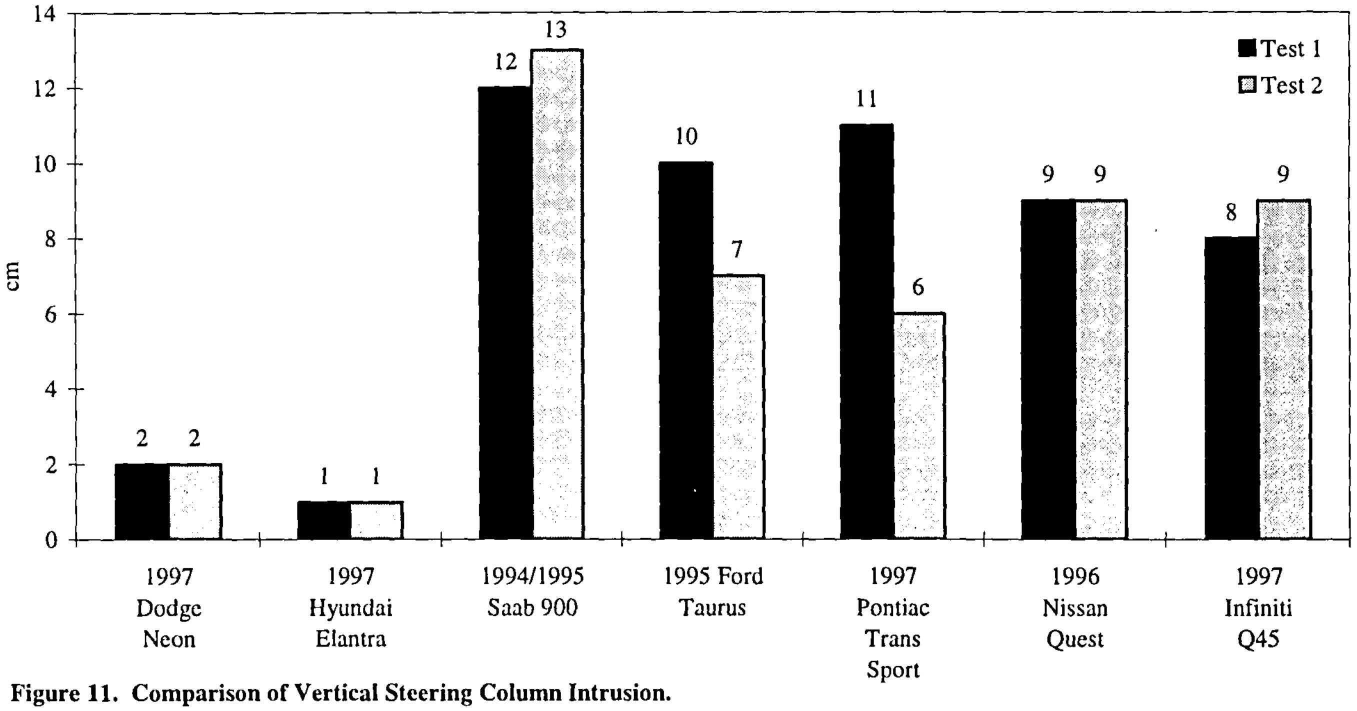

Figure 11. Comparison of Vertical Steering Column Intrusion.

Seat belt spool-out measures in the repeated tests of five models were very similar (differences of 2 cm or less), thus indicating seat belt system performance is repeatable (Table 3). The Saab 900 tests were not included in this comparison because retractor and pretensioner designs were changed between the 1994 and 1995 model years. The Infiniti Q45 tests were not included because spool-out measurements were not made in the first test.

Table 3.
Seat Belt Spool-out (cm)

Make/Model	Test 1	Test 2
1997 Dodge Neon	7	7
1997 Hyundai Elantra	6	7
1995 Ford Taurus	6	6
1997 Pontiac Trans Sport	6	8
1996 Nissan Quest	3	1

Airbag deployment times in the repeated tests of five models also were very similar (within 4 ms), but deployment times were 12 ms apart in the Hyundai Elantra tests (Table 4). A small difference in occupant compartment accelerations in the Hyundai Elantra tests may account for the larger difference in deployment times. Accelerations were slightly higher in the second test (average 8.1 g through 22 ms) than in the first test (average 6.1 g through 22 ms). The Saab 900 tests were not included in this comparison because the airbag sensor module was changed between the 1994 and 1995 model years.

Table 4.
Airbag Deployment Time (ms)

Make/Model	Test 1	Test 2
1997 Dodge Neon	40	42
1997 Hyundai Elantra	34	22
1995 Ford Taurus	26	26
1997 Pontiac Trans Sport	25	27
1996 Nissan Quest	20	18
1997 Infiniti Q45	52	56

Driver Dummy Responses

Table 5 lists the driver dummy head contact locations in the tests of five models. Despite head contact differences between the first and second tests, overall dummy movement patterns were very similar. For example, the dummy's head contacted the B-pillar in the first Ford Taurus test but narrowly missed contacting the B-pillar in the second test. Similarly, the dummy's head probably contacted the steering wheel through the airbag in the second Dodge Neon test, but this contact could not be verified because it was less forceful than in the first test. Dummy movement in the Hyundai Elantra tests also was very similar; however, after contacting the B-pillar, the dummy in the first test moved upward somewhat higher and brushed against the roof rail. The Saab 900 tests were not included in this comparison because of airbag and seat belt differences between the 1994 and 1995 models. The Pontiac Trans Sport tests were not included because of different driver seating positions.

Table 5.
Head Contacts Other Than Airbag
(in order of severity)

Make/Model	Test 1	Test 2
1997 Hyundai Elantra	B-pillar, roof side rail	B-pillar
1997 Dodge Neon	Steering wheel	None
1996 Ford Taurus	B-pillar	None
1996 Nissan Quest	None	None
1997 Infiniti Q45	B-pillar, side airbag	B-pillar, side airbag

Figures 12-16 show the upper body injury measures (HIC, neck tension force, neck extension bending moment, and chest compression) in the Dodge Neon, Hyundai Elantra, Ford Taurus, and Infiniti Q45 tests. Figures 17-22 show the lower body injury measures (axial femur force, tibia-femur displacement, upper and lower tibia indices, lower tibia axial force, and foot acceleration) in the Hyundai Elantra, Ford Taurus, and Infiniti Q45 tests. The Saab 900 tests were not included in these comparisons because of airbag and seat belt differences between the 1994 and 1995 models. The Nissan Quest tests were not included because data were not recorded in the first test. The Pontiac Trans Sport tests were not included because of different driver seating positions. The Dodge Neon tests were not included in the comparisons of leg injury measures because the first test was conducted using a dummy with ankles that had hard stops at the limits of the joint range of motion. The second Dodge Neon test was conducted using a newer foot/ankle design that had soft stops at the limits of the joint range of motion.

In the repeated tests of the Dodge Neon, Hyundai Elantra, Ford Taurus, and Infiniti Q45, HICs were very similar (Figure 12). The time intervals over which the HICs were calculated had the same duration to within 1 ms, and the largest difference between HIC-interval start times was 5 ms (Hyundai Elantra tests). Maximum neck tension forces also were similar and occurred at about the same time (Figure 13); the largest difference in maximum force was 0.3 kN (Hyundai Elantra tests), and the largest difference in the occurrence of maximum force was 7 ms.

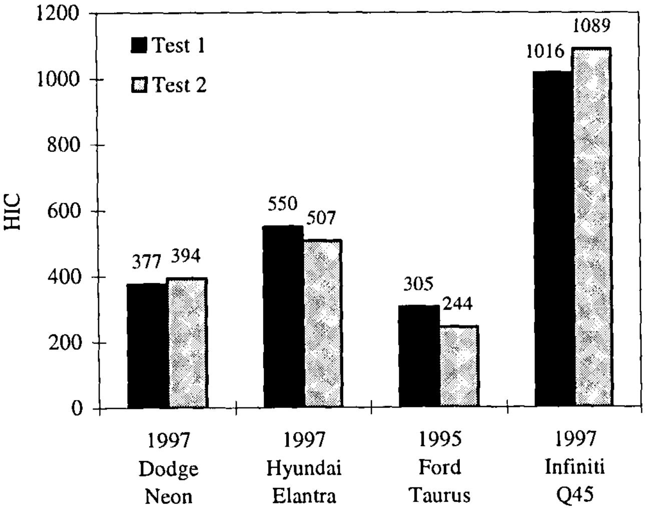

Figure 12. Comparison of HIC.

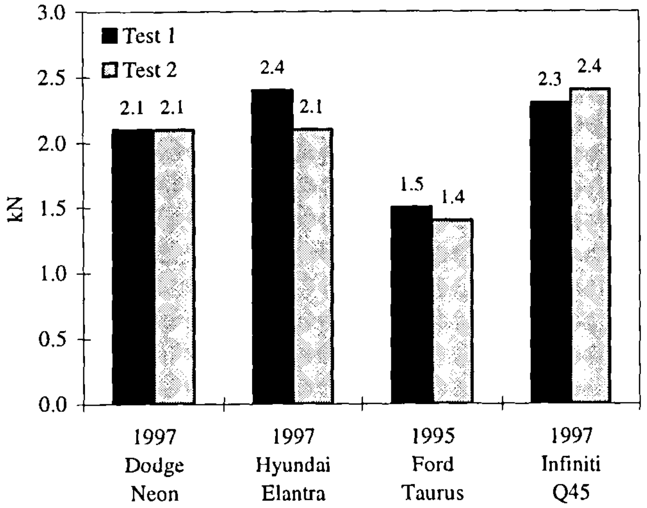

Figure 13. Comparison of Neck Tension.

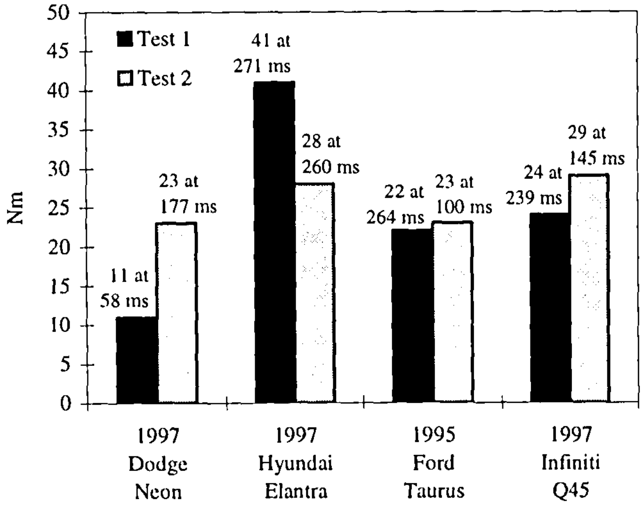

Figure 14. Comparison of Neck Extension Bending Moment.

Neck extension bending moments were more variable (Figure 14). The maximum values were similar but did not occur at the same time in the Ford Taurus and Infiniti Q45 tests. The maximum extension bending moment in the first Infiniti Q45 test occurred (at 239 ms) when the dummy's head contacted the B-pillar during rebound, but this measure in the second test was recorded (at 145 ms) before the head contacted the B-pillar (Figure 15). In the Hyundai Elantra tests, the maximum bending moments were recorded near the same time, but slight differences in the way the dummy's head contacted the B-pillar produced relatively large differences in the magnitude of the bending force. Extension bending moments in the Dodge Neon tests differed both in magnitude and time of occurrence.

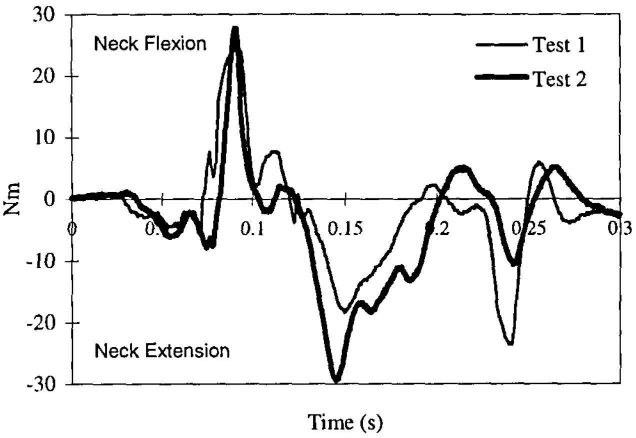

Figure 15. Neck Bending Moment - Infiniti Q45 Tests

Maximum chest compressions were very similar and occurred at about the same time (Figure 16); the largest difference in maximum compression was 6 mm, and the largest difference in the occurrence of maximum compression was 3 ms (Dodge Neon tests).

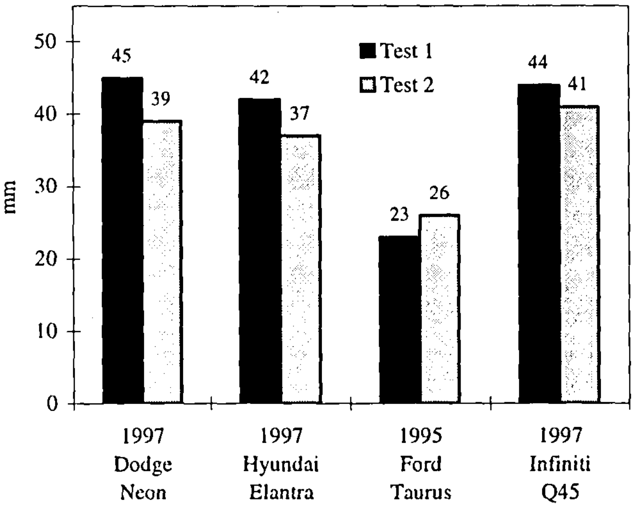

Figure 16. Comparison of Chest Deflection.

In the repeated tests of the Hyundai Elantra, Ford Taurus, and Infiniti Q45, the largest difference in femur forces (0.8 kN) occurred on the dummy's right leg in the Ford Taurus tests (Figure 17). Maximum femur forces occurred at about the same time except in the Ford Taurus tests, where maximum loads were recorded 43 ms apart. The largest difference in tibia-femur displacements (4 mm) occurred on the dummy's right leg in the Ford Taurus tests (Figure 18). Maximum tibia-femur displacements occurred at about the same time in the repeated tests. Upper tibia indices were similar, and the largest difference (0.13) was recorded on the dummy's left leg in the Infiniti Q45 tests (Figure 19).

Tibia axial forces were similar, and the largest difference (0.9 kN) was observed on the dummy's left leg in the Ford Taurus tests (Figure 20). Although the magnitudes of maximum tibia axial forces were similar, they did not occur at the same time. Maximum right tibia forces were recorded 38 ms apart in the Ford Taurus tests, and left tibia forces were recorded 41 ms apart in the Hyundai Elantra tests.

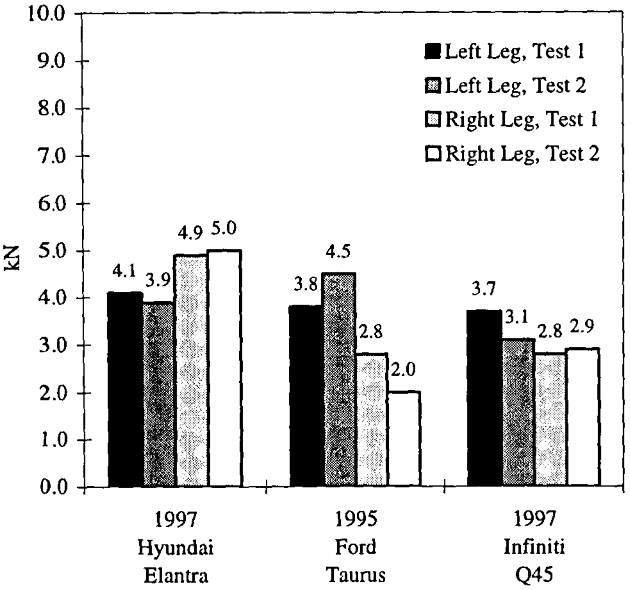

Figure 17. Comparison of Axial Femur Force.

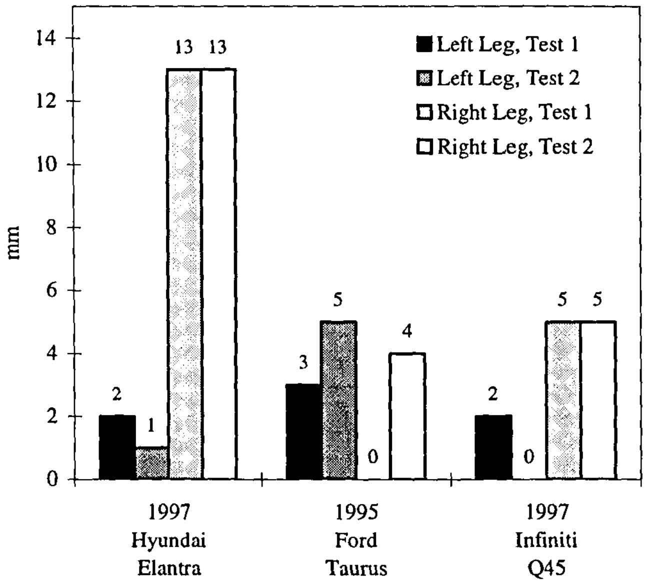

Figure 18. Comparison of Tibia-Femur Displacement.

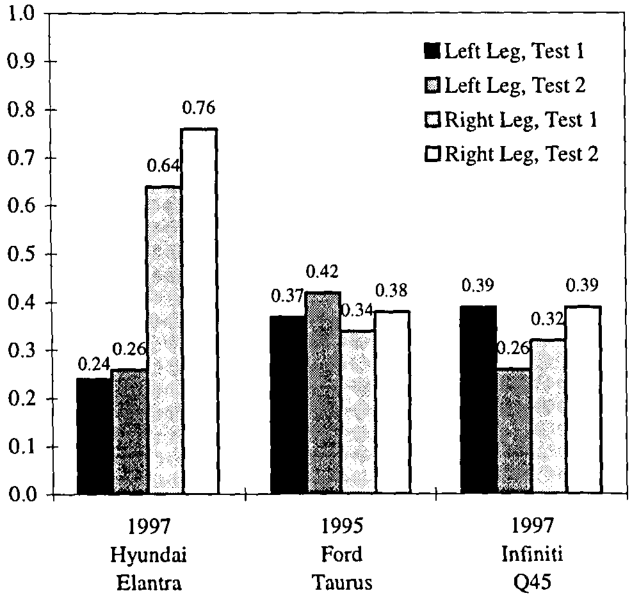

Figure 19. Comparison of Upper Tibia Index.

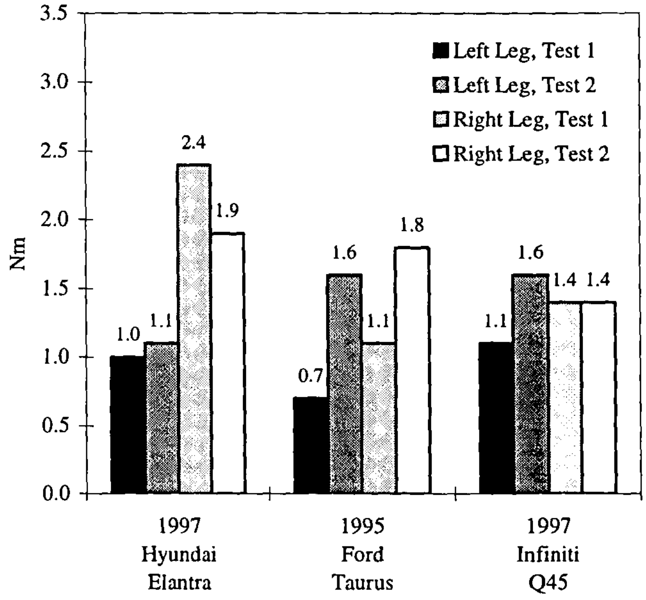

Figure 20. Comparison of Lower Tibia Axial Forces.

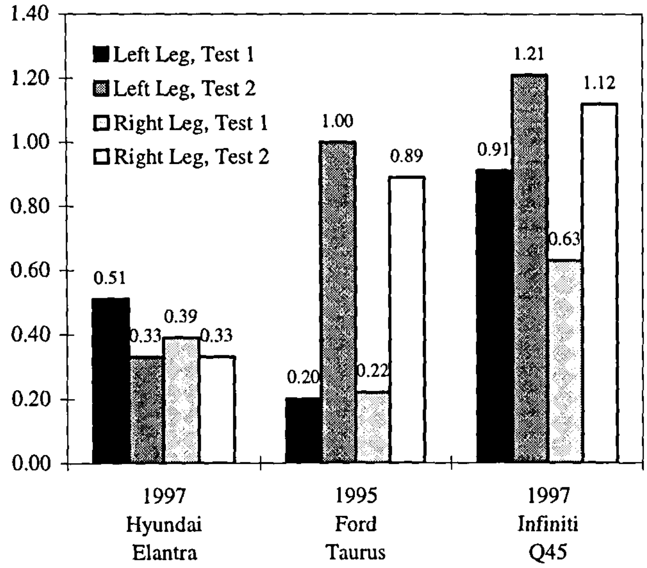

Figure 21. Comparison of Lower Tibia Index.

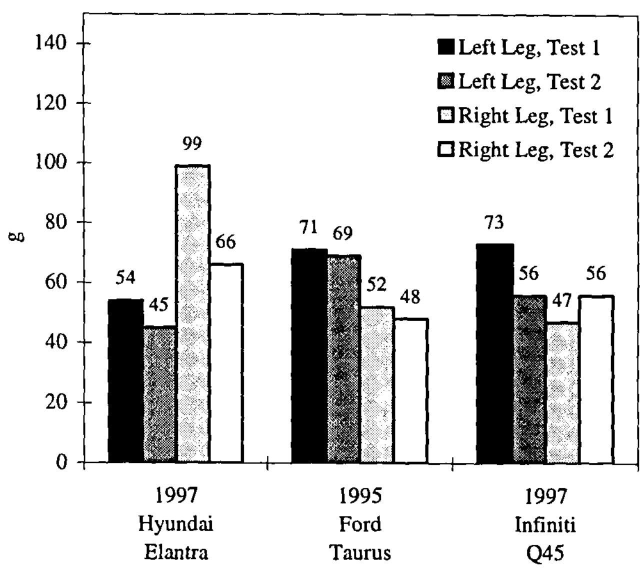

Figure 22. Comparison of Foot Accelerations.

Lower tibia indices show somewhat large differences in repeated tests (Figure 21). The smallest difference (0.06) was observed in the Hyundai Elantra tests, and the largest difference (0.80) was observed in the Ford Taurus tests. The occurrence of maximum tibia indices also was quite variable. Only the left indices occurred within 10 ms in the repeated tests of the Hyundai Elantra and Infiniti Q45. Foot accelerations were similar except in the Hyundai Elantra tests, where the difference between right foot accelerations was 33 g (Figure 22). Maximum foot accelerations occurred at about the same time except in the Ford Taurus tests, where maximum accelerations were recorded about 25 ms apart.

DISCUSSION

The results of repeated crash tests of the same vehicle model were very similar in this study. Vehicle accelerations, and hence the forces acting upon the occupants, were highly replicable, as were the performances of airbag and belt systems. Measurements of intrusion, a primary focus of offset crashes, were especially repeatable. Differences between pairs of vehicles in repeated tests were much smaller than the range of intrusion measurements seen for different vehicles of the same class. The Ford Taurus and Saab 900 showed the most intrusion variation, and only the Taurus intrusion difference would have given it a different rating in the Institute's evaluation of offset crash test performance (acceptable versus good). Similarly, occupant kinematics were highly similar, despite some minor differences in head contacts. Only the rearward steering column movements in the Ford Taurus tests and the airbag deployment times in the Hyundai Elantra tests exhibited appreciable differences. Because all seven models tested were equipped with driver airbags, differences in dummy head contacts with steering wheels, described in the NHTSA study, were not observed.

Dummy injury measures were reasonably repeatable as well. Only a few of the observed differences in the repeated tests would change the Institute's rating for the applicable body region. The greatest variability was observed for the lower tibia index. Interestingly, the vehicles with large differences, the Ford Taurus and Infiniti Q45, also exhibited less repeatable structural responses. A correlation between intrusion measurements and lower extremity injury measures has been established for this frontal offset test configuration,[5] and results from the Ford Taurus and Infiniti Q45 tests were consistent with this relationship. For each model, the test with greater intrusion also produced higher lower tibia bending forces. Toepan intrusion measurements in the Hyundai Elantra tests were considerably more repeatable, and the repeatability of the lower tibia index followed.

The Institute's crashworthiness evaluation combines results for three aspects of a vehicle's performance in an offset frontal crash test — structure/safety cage, injury measures (head/neck, chest, and left and right legs), and restraints and dummy kinematics — to derive an overall rating. The reliance on a combination of component ratings makes the overall evaluation even more consistent than component ratings alone. In the Institute ratings, even vehicles with a poor rating for one leg still can receive an acceptable rating if there is no other reason to rate the vehicle marginal or poor. In this test series, the vehicle showing the least repeatability (although performance still was reasonably similar) was the 1995 Ford Taurus. Nevertheless, intrusion measurements in the second test still would have been rated acceptable, and the leg injury ratings would have been acceptable and marginal. Dummy kinematics were similar, and good, in both tests, as was restraint system performance — airbags, belts, steering column, and seats. Overall, the rating for the Taurus in the second test would have been acceptable, only one category lower than its initial rating of good. For all other vehicles for which comparable information was available for all the rating components, the overall evaluation for the repeated test would have been the same as for the first test.

In summary, because differences between intrusion measurements, restraint system observations, and dummy injury measures in repeated tests generally were small compared with differences between rating categories, the Institute's overall crashworthiness evaluations would not be expected to change as a result of repeated tests. In cases where there is somewhat greater variability, a rating change of more than one category appears unlikely. Thus, the repeatability of modern vehicle performance in a frontal offset crash test is sufficient for making evaluations of the crash protection provided by different designs. It is anticipated that increasing manufacturer attention to designing for offset crash protection will further increase the predictability of structural performance, making offset crash test results even more repeatable.

ACKNOWLEDGMENT

This work was supported by the Insurance Institute for Highway Safety.

REFERENCES

1. Machey, J.M. and Gauthier, C.L., "Results, Analysis and Conclusions of NHTSA's 35 MPH Frontal Crash Test Repeatability Program." SAE Technical Paper Series 840201, Society of Automotive Engineers, Warrendale, PA, 1984.

2. Hobbs, A.C. and Williams, D.A., "The Development of the Frontal Offset Deformable Barrier Test." Proceedings of the 14th International Technical Conference on the Enhanced Safety of Vehicles, National Highway Traffic Safety Administration, Washington, DC, 1994, pp. 1352-58.

3. Bundesanastalt für Straßenwesen, "Report on Frontal Impact Test on VW Golf VR6 at 40 percent Overlap with EEVC Deformable Barrier (56 km/h)." Collaborative Frontal Impact Test Programme, Part Sponsored by the European Commission, Germany, 1994.

4. Oki, K., "Research for Frontal Impact Test Method in Japan." Paper presented at Meeting of EEVC WG11, Volvo Safety Center, Gothenburg, Sweden, 1995.

5. Zuby, D.S. and Farmer, C.M., "Lower Extremity Loads in Offset Frontal Crashes." Proceedings of the 15th International Technical Conference on the Enhanced Safety of Vehicles, National Highway Traffic Safety Administration, Washington, DC, 1996, pp. 414-21.

INTERNATIONAL NCAP PROGRAMS IN REVIEW

Michael Case
RACV
Michael Griffiths
Road Safety Solutions
Jack Haley
NRMA Ltd
Michael Paine
Vehicle Design & Research
Australia

Paper Number 98-S11-O-03

ABSTRACT

This paper summarises recent international NCAP programs and results. New Car Assessment Programs (NCAPs) are now running on four continents - Australia, United States, Japan and Europe. All use one or both of the standardised 56 km/h full frontal and the 64 km/h offset with deformable barrier tests.

Australian NCAP (ANCAP) commenced in 1992 and has now tested over 60 models. ANCAP has recognised the global nature of the car manufacturing industry and has developed the testing program to align with existing consumer crash testing programs operating overseas and to suit the types of crashes resulting in fatalities and serious injuries in Australia.

ANCAP will continue to push the bounds of technology to achieve improvements in occupant protection of passenger cars. ANCAP was the first consumer crash testing program that combined both full frontal and offset crash tests to produce a more accurate and meaningful result. The marked improvements in protection for occupants in passenger cars that are involved in frontal collisions in Australia shows that ANCAP has been very successful.

In the last few years NCAP programs have started in Europe and Japan and both include pedestrian impact tests that are not yet conducted in Australia. Side impact crash standards have been introduced in the US, Europe and in Australia. Pedestrian impact standards are under development in a number of countries. ANCAP intends to introduce a side impact test program in the near future.

Other NCAPs are also looking at enhancements to programs and possible future directions. For instance, research has begun in the US on a dynamic test that will provide a reliable measure of a vehicle's rollover susceptibility.

1 INTRODUCTION

1.1 Overview of Vehicle Safety in Australia

Australian vehicle safety standards consist of design rules for individual items and until recently did not provide for a test of the total occupant protection system.

A barrier test based on the 1987 US Federal Motor Vehicle Safety Standard (FMVSS) 208 was introduced from July 1995 and is known as Australian Design Rule (ADR) 69. This test has an impact speed of 48 km/h and the results are not made public.

Research by the Federal Office of Road Safety (FORS) and the Monash University Accident Research Centre (MUARC) shows that frontal crashes make up approximately 60 percent of the total serious and fatal injury crashes in Australia. Of all frontal crashes around half are offset.

Some of the Australian New Car Assessment Program (ANCAP) partners have funded MUARC to research real world accidents. MUARC has developed a vehicle crashworthiness rating system based on a method used by the Folksam Insurance company in Sweden. The method uses police crash reports from on-road crashes and registration databases from road authorities in NSW and Victoria.

The matching of the files is based on the registration number. The injuries received in each crash are matched with the vehicle model. The size of the database, greater than 350,000 crashes in the last analysis, provides statistical rigour to the results (MUARC 1998). The RACV, NRMA and NSW RTA publish this safety information as a guide for consumers considering the purchase of a used car.

MUARC has also been funded to evaluate the correlation between the ANCAP results and real world crash data. This research has been published in 1996 and 1997 and shows a good correlation between ANCAP scores and on-road occupant protection.

1.2 Australian New Car Assessment Program (ANCAP)

ANCAP was introduced to provide new car buyers with useful information about the relative occupant protection of popular vehicles on the Australian market. This information influences consumer demand and encourages manufacturers to design safer vehicles.

ANCAP commenced in 1992 using the US NCAP full frontal test. The first tests involved nine medium/large family vehicles and results were published in April 1993. From 1994 an offset test based on a draft European standard was also incorporated.

ANCAP is funded by Australian motoring clubs through the national Australian Automobile Association (AAA) and transport authorities in Queensland, New South Wales and South Australia. The program has a budget of A$1 million per year.

ANCAP has a management committee which is chaired by the AAA. The program is operated by a Technical Committee made up of stakeholder representatives who meet regularly. The testing is conducted by a contractor called Crashlab, located in Sydney, New South Wales.

ANCAP has released 13 sets of results so far, covering small, medium and large cars as well as light commercial vehicles, four wheel drives and passenger vans. Selection of vehicles for testing is based on sales volume. There are current results for over 30 of the most popular new vehicles presently on sale in Australia covering around 75% of the new vehicle market.

1.3 Testing

ANCAP has recognised the global nature of the car manufacturing industry and developed a crash testing program to align with existing overseas programs.

In addition to the full frontal test, an offset test using a deformable barrier was added in 1994. This test was developed for the European Experimental Vehicle Committee (EEVC) by the Transport Research Laboratory (TRL) in the UK. The test is recognised internationally and the barrier design is specified for both consumer crash test programs and for compliance with regulatory standards.

Each vehicle model tested in ANCAP undergoes a full frontal crash test into a solid concrete barrier and an offset crash test into a barrier with a deformable aluminium face.

The full frontal crash test simulates hitting a solid object or another vehicle exactly head-on and is conducted at a speed of 56 km/h. In this test the impact is spread evenly across the front of the vehicle. This test mainly evaluates the vehicle's restraint system.

The offset crash test simulates hitting another car and is conducted at a speed of 64 km/h. Forty percent of the width of the car makes contact with the barrier. In this test the crash forces are concentrated on the driver's side of the vehicle. This test mainly evaluates the vehicle structure's resistance to intrusion.

1.4 Results Presentation

The presentation of results has evolved by a process of continuous review including focus group evaluations. The current format is based on the US Insurance Institute for Highway Safety (IIHS) brochure and uses ratings of *Good, Acceptable, Marginal* and *Poor*.

This format was considered to be the best available by the organisations visited during an international ANCAP study tour. Market research in Australia has also shown that consumers find this presentation format relatively easy to understand.

Four areas of vehicle crashworthiness are evaluated - structure, restraints, injury measurements and head restraint design. These are combined into an overall evaluation which is based on both the full frontal and offset crash test results. The results are available on the internet (www.nrma.com.au/crashtests/).

1.5 Data Sharing

ANCAP is part of a global NCAP network. NCAP organisations are standardising on testing and are sharing results for similar vehicles in different markets. ANCAP, by agreement with the manufacturers, has used IIHS and NHTSA results for the Volvo 850 and Toyota Camry and a Euro NCAP result for the Volkswagon Polo. Japan NCAP is also republishing results from the US program.

The ANCAP ratings based on data provided by overseas organisations might differ from the ratings assigned by these organisations. In particular the ANCAP rating includes assessment of the results of full-frontal crash tests and takes into account the passenger injury measures and restraint performance in these tests. The ANCAP ratings also tend to place less emphasis on footwell intrusion and lower leg injury than IIHS ratings and more emphasis on structural performance than the Euro NCAP procedures.

Of 63 vehicles tested by IIHS or Euro NCAP and provisionally rerated under ANCAP procedures, 35 had the same rating, 18 had a better rating (mainly due to less emphasis on lower leg factors) and 10 had a worse rating (mainly due to the inclusion of the full-frontal test results).

Although it is desirable that the same rating system be used by all organisations this would have several disadvantages for the Australian new car fleet. All vehicles tested by IIHS and Euro NCAP had driver airbags and most (78 percent) had passenger airbags. In Australia less than half of the models tested in recent years have driver airbags and only one had a passenger airbag. The NCAP full frontal crash test is more likely to have an influence on the overall rating for vehicles which have no airbag.

Once the Australian new car fleet aligns more with the US and Europe in regard to airbag fitment and structural performance then harmonisation of the rating procedures will become more meaningful.

Data sharing means that duplication of effort and considerable costs can be avoided and more vehicles can be evaluated. Consumers will then be able to make a more informed choice at vehicle purchase on the basis of occupant protection performance.

1.6 Relationships

ANCAP consults with the automotive industry about the program through the Federal Chamber of Automotive Industries (FCAI), the group which represents the vehicle manufacturers and importers in Australia. Representatives from the vehicle manufacturing companies are invited to attend the test of their products and are able to review the results before publication. ANCAP meets with the FCAI before each public launch and in early 1997 conducted a technical briefing for FCAI members on the new IIHS-style rating system.

ANCAP is also working closely with the Federal Government through the Department of Transport's Federal Office of Road Safety (FORS) which administers the design standards for Australian vehicles. In 1996 the then Minister for Transport approved A$350,000 for a complementary FORS NCAP program to study airbag effectiveness on vehicles being tested by ANCAP. The Government has shown interest in continuing this level of support.

ANCAP has spent substantial time and effort briefing motoring journalists about the program to encourage a consumer perspective in the reporting of vehicle safety issues.

ANCAP has also made many presentations to fleet management groups on the implications of crash test results on vehicle selection for fleet managers.

1.7 Market Effect

In 1996 a benefit/cost analysis of NCAP was undertaken. Road trauma costs from the states of Queensland, New South Wales, Victoria and South Australia were used in the analysis. The potential benefit was defined as the likely savings in the social cost of passenger vehicle occupant trauma in full frontal and offset crashes in speed zones of 80 km/h or less. The estimate was therefore conservative as some benefit could also be expected in over 80 km/h speed zones.

The saving was calculated for each future year by multiplying the trauma costs by the injury risks of the improved Australian fleet for the year in question and dividing by the injury risk of the existing Australian fleet.

The costs associated with improving the ANCAP performance of the Australian fleet to the achieved USA level were determined by adding the total cost of the NCAP program to the cost of improving the level of safety of the vehicles.

The analysis was conducted using an estimated cost per vehicle of $200. After one year a benefit cost ratio of 2.48 is achieved. The benefit cost ratio continues to improve and after 15 years reaches a value of 3.61.

A sensitivity analysis was conducted on the average cost per vehicle to implement US protection standards. This showed that even with conservative assumptions and a 35 year fleet improvement time span, manufacturers can spend up to $750 per vehicle and still produce a positive benefit to the community.

A visible impact of the program is the amount of safety advertising used by manufacturers, often featuring a crash test dummy. There has also been a significant increase in the number of advertisements featuring airbags and structural details of vehicles.

Due to ANCAP and the consequent increase in safety advertising, Australian car buyers now rate safety as their third most important criterion after purchase and running costs. (ANOP 1997).

The proportion of the new car fleet fitted with at least a driver airbag has risen from 30 percent to 50 percent over four years. This shows the value of a consumer-orientated vehicle safety program and a strategy of promoting the results to influential groups such as vehicle fleet managers.

1.8 Future Directions

ANCAP is currently considering other possible programs, including side impact testing which Euro NCAP and US NCAP have already commenced. Euro NCAP is also carrying out pedestrian impact testing on vehicles while the US NCAP has recently announced a program to rate vehicle rollover susceptibility.

ANCAP will continue to network with other global programs and introduce new tests and improvements to results presentation according to international best practice where there is a benefit to consumers.

2 ANCAP STUDY TOUR

2.1 ESV Conference

The Enhanced Safety of Vehicles (ESV) Conference held in Melbourne during May 1996 had the theme of globalisation and harmonisation of vehicle safety standards. The discussion on international harmonisation of vehicle standards also included consumer crash testing programs, which in recent years have promoted improved occupant protection faster than regulations.

The ESV Conference demonstrated that much activity was occurring on a global scale with consumer crash test programs but there was a need to harmonise test protocols.

2.2 Study Tour

ANCAP saw benefits in reducing costs and enhancing the range of results provided by a more co-operative approach between global consumer crash test programs. An ANCAP sponsored overseas study tour was undertaken to follow up the potential benefits of data sharing.

The ESV Conference identified recent NCAP activity in Japan, Europe, United Kingdom and the United States. ANCAP independently discovered that South Korea is developing an NCAP. Visits to various vehicle manufacturers were also arranged in South Korea, Germany, Sweden and the United States.

3 UNITED STATES

3.1 National Highway Traffic Safety Administration (NHTSA)

NHTSA is part of the US Department of Transportation and has been conducting NCAP testing using the full frontal test at 56 km/h since 1978. About 35 new models are crash tested each year. NHTSA employs four contractors across the US to conduct its NCAP testing.

NHTSA uses a star system to provide consumers with vehicle safety performance information. The results are reported in a range of one to five stars. Five stars indicate the best protection within the same weight class. HIC scores are also reported.

The budget for 1997 was US $3.2 million which allowed 42 full frontal, 26 side impact and nine offset frontal tests. NHTSA estimated that this program provides safety information for consumers on almost 90% of the vehicles sold in the US during 1997.

The current US side impact standard FMVSS 214 applies to 1997 model year cars and for light trucks in 1998. Similarly to the full frontal program, NHTSA has added 5 mph to the regulatory impact speed, so the NCAP side impact test is run at 38.5 mph (62km/h). NHTSA released several sets of side impact test results during 1997. All US NCAP results are available on the internet (www.nhtsa.dot.gov).

NHTSA has agreed to supply ANCAP with US crash test information.

3.2 Insurance Institute for Highway Safety (IIHS)

The IIHS conducts the EEVC deformable barrier offset test with an impact speed of 64 km/h. This test is the same as that used by ANCAP and Euro NCAP. All IIHS tests are conducted at their vehicle research centre in Charlottesville, Virginia.

The IIHS vehicle crash test evaluation procedure uses a four level rating system (*Good, Acceptable, Marginal* and *Poor*). In addition to structure, restraints and injury measures, head restraints and bumper performance are also evaluated and reported. The IIHS provides an overall evaluation on vehicle safety performance but does not use a star rating system.

The IIHS crash test brochure is distributed to a mailing list of 16,000. The results are promoted using both a media release and video news release. Wide television coverage is achieved by an exclusive release on a 30 minute segment on the Dateline program, which has 24 million viewers.

IIHS commenced crash testing in 1994 and has since tested small and mid-size cars, utilities, passenger vans and luxury vehicles. The results are available on the internet (www.hwysafety.org).

IIHS has agreed to exchange crash test information with ANCAP.

4 JAPAN

4.1 Overview

The National Organisation for Automotive Safety and Victims' Aid (OSA) was established by the Japanese Government in 1973. OSA is funded yearly by the Ministry of Transport but is a separate legal entity. The primary objectives of OSA are to reduce road trauma through research and to offer assistance to 'victims' of vehicle accidents.

An increase in the road accident fatality rate in 1988 resulted in the Japan NCAP being established in 1991. After five years development the first results were published in March 1996. A second set of results were released in March 1997 and results from a third test program will be published in early 1998.

The "Automotive Safety Information" publication is distributed by both the OSA and the Ministry of Transport. The Japan Automobile Federation (JAF) publishes the results in its magazine JAF-MATE, which has a circulation of 12 million. The results are also promoted on television and are available on the internet (www.osa.go.jp).

OSA acknowledges that consumer tests are driving the vehicle safety agenda and international harmonisation of tests is important.

4.2 Test Programs

OSA has a Car Safety Assessment Committee with members from the Japan Automobile Research Institute (JARI) and Japan Automobile Manufacturers Association (JAMA). It also has regular discussions with JAMA members on NCAP related issues.

OSA conducts its full frontal crash test program at JARI. The test is the same as for US NCAP. The numerical test results are not published as OSA believes they are of little interest to consumers. A four category rating system (A/B/C/D) based on head injury criterion and chest acceleration is used. Recently the A category was split into A, AA and AAA levels to further discriminate vehicle safety performance.

The 1996 program tested the top selling nine vehicles across all classes and results were published early in 1997. A total of 18 models have now been reported on. OSA has tested 13 more passenger vehicles during 1997. Results were published in April 1998. The list of models is available on the OSA internet site (www.osa.go.jp).

OSA believes its options to provide more vehicle safety data to consumers include:-

- conduct more tests (subject to budget constraints);
- provide overseas NCAP data on vehicles which are sold in Japan; and/or
- provide vehicle manufacturer test data.

OSA is reproducing US NCAP data on similar vehicles sold in Japan. OSA believes that left hand drive data can be used for right hand drive vehicles if the vehicle manufacturer agrees the vehicles are similar.

Japan will have a national regulation for side impact this year. This will be based on the European test. OSA is interested in conducting a side impact test and is reviewing the UK DoT test. OSA is likely to increase the test speed over the regulatory speed by about 10 percent which is intended to show crash performance differences between vehicles. OSA expects to take up to three years to develop this test, which will be discussed through the Car Safety Assessment Committee.

OSA has agreed to exchange crash test information with ANCAP.

5 EUROPE

5.1 Overview

Euro NCAP is funded by the UK DoT, the Swedish National Road Administration, the FIA, the AA UK and the RAC. The Dutch government and the German motoring club, ADAC, have also recently joined the program.

TRL has been the only test contractor for the Euro NCAP up to the current program, when TNO Holland also became a contractor. The objective of Euro NCAP is to provide consumer information. EEVC test procedures for offset frontal impact (64 kmh, 40% overlap, deformable barrier), side impact and pedestrian impact are used

Two vehicles are required for each model tested. One is used for the pedestrian tests then the side impact test. The other is used for the offset frontal test.

5.2 Test Programs

The results from the small car program involving seven popular vehicles were released in February 1997 and those from the second program of 13 family cars were launched in July 1997.

6 COMPARISON OF GLOBAL NCAPs

6.1 Test Harmonisation

During the 1996 Enhanced Safety of Vehicles (ESV) Conference an invited speakers panel provided an opportunity for both industry and government representatives to put forward their view on the future direction of vehicle safety. Speakers representing the Association of International Automobile Manufacturers and the American Automobile Manufacturers Association indicated the need for global harmonisation of safety standards and tests.

The selection of types of tests to be conducted by ANCAP was determined by consideration of the types of crashes resulting in fatalities and serious injuries due to the nature of the Australian road and traffic environment.

Offset barrier testing as carried out by ANCAP is also conducted by the Insurance Institute for Highway Safety and NHTSA in the US, the Transport Research Laboratory in the UK and TNO in Holland. Many car manufacturers also perform offset crash tests but do not release the results. Volvo has conducted 65 km/h crash tests for over 10 years.

6.2 Evaluation/Presentation

In ANCAP, four areas of vehicle crashworthiness are evaluated - structure, restraints, injury measurements and head restraint design. These areas are also evaluated in other NCAPs but with slightly difference emphasis, partly due to the use by other groups of only one test, whereas Australia carries out two tests on each model.

ANCAP and IIHS have adopted a typical consumer rating system of *Good, Acceptable, Marginal* and *Poor* which NHTSA and Euro NCAP use a star system, five for NHTSA and four for Euro NCAP. Euro NCAP has combined offset frontal, side and pedestrian testing into one rating.

6.3 Information Exchange

There is agreement between all NCAPs that data is freely available to other groups once it has been quality checked and, in some cases, once a media launch has occurred.

ANCAP liaises with the Australian vehicle manufacturing or importing companies to determine the applicability of data from other NCAPs. Manufacturers have also been invited on many occasions to produce their own crash data for comparison but have so far declined to do so.

6.4 Future Directions

Generally NCAPs would like to be able to give as complete a guide as possible to consumers when buying a vehicle. Test types and protocols will be introduced and developed to achieve this aim. This would lead to a full evaluation using frontal, side, rear, rollover and pedestrian impacts.

7 SUMMARY

The main points relating to global NCAPs and harmonisation of consumer vehicle safety programs are:-

- Japan has established an NCAP based on the US program and is now planning side impact. An NCAP is being considered in South Korea. The Euro NCAP commenced in 1997 and involves frontal, side and pedestrian tests. The US NCAP was expanded in 1997 to include side impact.
- There is almost complete harmonisation between NCAP groups on test procedures except for the German Automobile Club ADAC and motoring magazine *Auto Motor und Sport*. There are some minor differences between NCAP groups in how results of vehicle safety performance are presented.
- There is now an agreement between Australia and other global NCAP groups to share data where vehicle and test specifications are compatible. There is also potential to further share data with the vehicle industry.
- Many manufacturers, including BMW, Mercedes-Benz and Volvo, have emphasised that vehicle safety is more than just dummy measurements and should include assessment of intrusion, head restraint design etc. ANCAP agrees and has developed criteria to provide a more comprehensive overall assessment of vehicle occupant safety.
- It is important to continue to compare NCAP results with real world crashes to validate consumer vehicle crash test programs. Research work conducted by MUARC on the correlation of ANCAP results with actual crash data is continuing (MUARC 1997).

- Compatibility between vehicles in different size categories is a very important issue for consumer occupant protection. The aggressivity of some types of vehicles, particularly 4WDs and vans, to other vehicle types is a major concern.
- Side impact testing has been introduced into the Euro and US NCAP crash test programs and is planned for Japan NCAP and ANCAP.
- ANCAP needs to further develop relationships with international NCAP groups, research organisations and vehicle manufacturers, both local and overseas.

ANCAP has provided consumers with the information necessary to make an informed decision on buying a new car on the basis of safety performance. This has generated market opportunities for the vehicle manufactures to produce and promote vehicles with improved crash test results. While the manufacturers' representative group has publicly criticised ANCAP, significant improvements in the crash test performance of new cars sold in Australia since the program commenced in 1992 have been able to measured.

ANCAP will continue to use consumer information to encourage vehicle manufacturers to further improve vehicle safety performance. ANCAP will also continue to consult with all stakeholders to ensure the ongoing relevance of the program.

REFERENCES

ANOP, Australian National Opinion Polls, 1997

MUARC, Newstead, Stuart, and Cameron, Max, "Correlation of results from the new car assessment program with real crash data," Report No 115, June 1997.

MUARC, Newstead, Cameron, and Le, Chau My, "Vehicle Crashworthiness ratings and crashworthiness by year of manufacture: Victoria and NSW crashes during 1987-96," March 1998.

EVOLUTION OF AUSTRALIAN NCAP RESULTS PRESENTATION

Michael Case
RACV
Michael Griffiths
Road Safety Solutions
Jack Haley
NRMA Ltd
Michael Paine
Vehicle Design & Research
Australia
Paper Number 98-S11-O-04

ABSTRACT

This paper traces the evolution of the methods of presentation of Australian NCAP (ANCAP) results to consumers.

ANCAP commenced in 1992 and has now tested over 60 vehicle models. The first two series of results in 1993 and 1994 were presented with an emphasis on NCAP criteria such as HIC and chest deflection measurements, with a colour-coded human figure included to indicate injury levels. The detailed dummy measurements were included in the back of the information brochure and this convention has been retained to the present.

The concentration on NCAP injury criteria was felt to be too technical for the intended general audience so for the next four releases of data the primary rating system became the *risk of life threatening injury* (>AIS 3) calculated as per the NHTSA algorithm, although the first three of these releases retained the colour-coded human figure.

At this time the US Insurance Institute for Highway Safety (IIHS) began NCAP offset tests and published the results in a more traditional consumer format. ANCAP focus group research revealed that this format was preferred by general readers, so ANCAP adopted this consumer format as of November 1996.

The Euro NCAP group began publishing its offset and side impact test data in February 1997 using a star rating similar to the NHTSA system. ANCAP is working with Euro NCAP and other international NCAP groups towards a common rating system.

1 INTRODUCTION

ANCAP was introduced to provide new car buyers with useful information about the relative occupant protection of popular vehicles on the Australian market. This information influences consumer demand and encourages manufacturers to design safer vehicles.

ANCAP commenced in 1992 with the full frontal test as used by the US NCAP since 1978. An offset test using the EEVC deformable barrier was added in 1994.

The first two series of ANCAP results were presented using head and chest injury criteria, with a human figure colour-coded included to indicate injury levels. The detailed dummy measurements were included in the back of the information brochure and this convention has been retained to the present (ANCAP [1] & [2]).

The first two ANCAP public brochures included both the results and the full technical report on each vehicle test. The third publication was separated into a mini-brochure for consumers and a detailed report for technicians (ANCAP [3] &[4]).

The full injury results presentation was felt to be too technical for most consumers so for the next four releases of data the primary rating system became the *risk of life threatening injury*. The first three of these releases retained the colour-coded human figure (ANCAP [5-7]).

In 1994 the US Insurance Institute for Highway Safety (IIHS) began conducting vehicle offset tests and publishing the results in a traditional consumer format of *Good, Acceptable, Marginal* and *Poor*. ANCAP focus group research revealed that the IIHS format was preferred by consumers and ANCAP adopted this format in late 1996 (ANCAP [8-13]).

2. PRESENTATION DEVELOPMENTS

2.1 Need for Improved Presentation

The first 1993 release of ANCAP results only reported the full frontal tests. The inclusion of offset tests in 1994 doubled the available information, which made useful interpretation by the average motorist more difficult. Although colour coded, the summary table of results in the ANCAP small car report presented a considerable amount of information.

NHTSA consumer focus group studies found that consumers wanted information on crash tests in a non-technical, easily understood form. NHTSA reported that consumers could understand information expressed simply in terms of 'risk of injury'. However, it indicated they were confused by technical data sheets and dummy output parameters that needed interpretation, particularly where these have a logarithmic relationship to the risk of injury.

2.2 Simplified Presentation

The on-going success of all NCAP groups relies on optimising consumer understanding. This could only be achieved in Australia by simplifying the format in which ANCAP presented test results. By adopting and extending some recent US NCAP developments in presentation, improved levels of consumer comprehension were expected.

In 1993, NHTSA began to publish NCAP results expressed as star ratings. These are calculated using injury risk functions which directly relate measured dummy parameters to figures of life threatening injury risk.

One disadvantage of the NHTSA star rating scheme is that the star cut-off values chosen result in discrete bands of safety performance. Vehicles with scores at either end of a performance band, if not ranked in some other way, are lumped together as having the one level of safety.

US NCAP only went as far as combining head and chest dummy parameters of full frontal tests. ANCAP needed to combine head and chest readings for full and offset frontal testing for both driver and front passenger.

Monash University Accident Research Centre (MUARC) research indicates that frontal crashes make up approximately 60 percent of the total serious and fatal injury car crashes in Australia. Of all frontal crashes around one half are of the offset type. Using these data, risk of injury scores for full and offset test cases were combined to establish an overall risk score which simulates 'real world' frontal crashes. This was achieved by applying the same injury risk functions used by NHTSA in calculating its star rating scores.

2.3 The 100 Point Injury Risk Scale

Injury risk values can be directly expressed on a 100 point scale. This represents the risk of life threatening injury for a weighted combination of full and offset frontal crashes based on relative real world incidence. A plot of Injury Risk scores based on the NCAP 4WD results, released in 1994 is shown in Figure 1 of the Appendix. Scores are shown ranked by driver results.

Interpretation is consistent with the test dummy output parameters themselves (ie higher scores mean a higher risk outcome) and with the real world MUARC Crashworthiness Ratings results (MUARC 1998).

2.4 Application of Simplified Presentation

Australian NCAP chose to use the 100 point risk rating in its four wheel drive and van release. This format was published in a mini-brochure titled *Buyer's Guide to Vehicle Crash Tests* (ANCAP [4]). A sample page is illustrated in Figure 2 of the Appendix. This brochure received favourable feedback from consumers about its "user-friendliness".

2.5 Industry Response

The motor vehicle industry in Australia supports the intention of ANCAP in providing consumer information on vehicle safety but has some reservations about the testing process. These include allegations that there is a lack of repeatability and that the impact speeds are too high.

2.5.1 Repeatability

ANCAP has some repeat data available which is summarised below. Tests conducted in Australia have shown good consistency of results. Table 1 below provides results of NCAP repeat tests for HIC which show that these results are repeatable within 10 percent.

Table 1 - ANCAP Report Test Data

Vehicle	HIC		Variation (%)
	Test 1	Test 2	
Daihatsu Charade	960	1050	9.4
Nissan Micra	820	900	9.8
Mitsubishi Mirage	640	608	5.0
Ford Laser	860	871	1.3
Ford Probe (US results)	724	784	8.3
Ford Probe (US results)	1025	994	3.0

2.5.2 Test speeds

Only about 17 percent of fatalities and 37 percent of AIS 4+ injuries occur at crash speeds up to 48 km/h (30 mph), the speed commonly used in regulatory tests around the world, including Australia. Up to the NCAP full frontal crash speed of 56 km/h (35 mph) the fatalities and injuries figures become 25 percent and 53 percent, and up to the NCAP offset tests speed of 64 km/h (40 mph), they are 59 percent and 73 percent respectively. NCAP test speeds therefore cover far more of the serious crashes experienced on-road than do the regulatory speeds.

Australian research shows that at the full frontal regulatory speed there is little difference in HIC between the models. Once the speed is raised the differences become much more significant and it is much clearer which vehicles protect their occupants better.

2.6 Marketing Plan

The ultimate aim of any NCAP is to provide marketing incentives for vehicle manufactures to build in state of the art/world's best practice occupant protection systems, by convincing consumers to give buying preference to above-average safety performance and particularly not to buy vehicles with below average crash test results.

Accordingly, there is not much point in having an NCAP unless:-

- it is easy for consumers to understand which is the safest car for their purposes;
- the relative safety information is presented in a compelling manner;
- consumers can make practical use of the information to effect their car buying decisions, and they are motivated to do so by the way the material is presented.

Most NCAP programs take some formal steps to publish their results, but the authors of this paper have not seen documentation of social marketing plans for other NCAP programs.

While it is common practice for inaugural NCAP programs to publish the results in a fairly innocuous manner to reduce the likelihood of litigation, it is important that once this settling in period is passed that the relative safety results are accessible and compelling in their presentation.

Like most NCAP programs, Australian NCAP was very cautious in its initial release, publishing mainly raw numbers for injury criteria for various parts of the body and avoiding overall vehicle safety summaries. Obviously, this mode of presentation is only of use to a very sophisticated user who can attempt to give different weightings to information on, say, injury criteria for head, chest and legs, relative injury information for driver and passenger and, where there is more than one test, somehow merging the results of an offset, head-on, or side-on test.

It is more useful to the consumer for the NCAP group itself to merge this information into a single outcome which takes into account the relative incidence of the various crash types and the relative occupancy of the different seating positions. In the past ANCAP has been aware of the need to make sure that the information actually got to consumers. It has done this by:-

- Media releases of the information as each batch of information becomes available through television, radio and newsprint. However, one-off media releases, whilst achieving a short term high profile, only provide communication span of approximately a day or so.
- Having brochures summarising the results on prominent stands in motoring organisations, and vehicle registering and driver licensing offices. These outlets provide long term access to the test results, but consumers need to be aware of their availability and have ready access to such offices.
- Conducting seminars specifically aimed at vehicle fleet managers, risk managers, occupational health and safety officers and the vehicle insurance industry. The response to these in Australia has been very good and the advantage of targeting fleet managers is that the control of a large number of vehicle purchases can be effected through one contact in a large organisation.
- Establishing an internet web site where all of the test results, including short segments of video of the crash tests, can be accessed (www.nrma.com.au)

ANCAP has now progressed to the formulation of a social marketing plan, in particular aimed at:-

- Fleet, occupational health and safety and risk, managers. In addition to specialised seminars this includes the placement of articles in fleet manager magazines etc.
- Presentation material and brochures to be available at new car sales outlets. This generally only occurs at those dealer outlets whose vehicles perform well in the tests. However, if a consumer is shopping around for a particular class of vehicle, they may be considering at least one make of vehicle which performs well.
- Better packaged, understandable information specifically aimed at non-technical audiences, particularly market growth sectors such as women purchasers.

The main task is to get the information to consumers in an understandable and compelling form so that they will act on it when buying a vehicle. Market testing has found that the credibility of those currently promoting the ANCAP program is very high. This is because motoring organisations are highly regarded and the significance of their merger with state government road safety divisions to put out consumer information is not lost on consumers.

Another important consideration is the occupational health and safety requirements to provide a safe workplace, under which a vehicle is included. This has the potential to provide powerful leverage to both government and industry fleet buying standards.

Our view is that, until an NCAP program has an audited/monitored sound marketing program, it is unlikely to achieve its full potential.

2.7 Media Launches

2.7.1 Media Releases

ANCAP has taken the common international approach of releasing a group of vehicle results at one time to maximise interest and to provide consumers with adequate comparative information.

A common media release , written by a member of the ANCAP Technical Committee and reviewed by one of the stakeholders media staff, is provided for all stakeholders. The release is subjected to rigorous legal review to ensure there are minimal grounds for legal action.

2.7.2 Questions & Answers

A summary of common Questions and Answers about the program is kept continually updated and included in the media kit for each launch.

2.7.3 Video Tapes/Photos etc

A Betacam compilation of all the crash tests for each launch is made up from the high speed and real-time film and video from the crash laboratory. This is supplied to any television journalist who attends the launch and on demand to other stations.

2.7.4 Video News Release (VNR)

For several releases ANCAP contracted a media company to produce a video news release consisting of a series of sample questions and answers featuring members of the Technical and Management Committees, with a compilation of the crash test video included. However it was found that the television stations preferred to conduct their own interviews and did not use the question and answer part of the VNR. As the process was quite expensive, involving a professional interviewer, it was abandoned and the video tape is now formatted as above by a contractor from original laboratory film and tapes.

2.7.5 Media Kit

All the above items are included in a media kit folder. Each stakeholder formats the folder to their own preference. The kit is distributed to a range of magazines, newspapers and periodicals.

2.8 International Data

The Enhanced Safety of Vehicles (ESV) Conference held in Melbourne during May 1996 had the theme of globalisation and harmonisation of vehicle safety standards.

The ESV Conference demonstrated that much activity was occurring on a global scale with consumer crash test programs but there was a need to harmonise test protocols, including presentation of crash test results. The Conference identified NCAP activity in Japan, Europe, Korea and the United States as well as Australia.

ANCAP saw benefits in reducing costs and enhancing the range of results provided by a more co-operative approach between global consumer crash test programs and gathered information from around the world to clarify the potential benefits of data sharing.

3. CURRENT SITUATION

3.1 Results Format

The ANCAP presentation of results has evolved by a process of continuous review, including focus group evaluations. The current format is based on the US IIHS brochure method and uses ratings of *Good, Acceptable, Marginal* and *Poor* (see Figs 2-4).

This format was considered to be the best available internationally in 1996. Market research in Australia has also shown that consumers find this presentation format relatively easy to understand.

Four areas of vehicle crashworthiness are evaluated - structure, restraints, injury measurements and head restraint design. These are combined into an overall evaluation which is based on both the full frontal and offset crash test results. The results are available on the internet (www.nrma.com.au/crashtests/).

3.2 Data Sharing

ANCAP is part of a global NCAP network. NCAP organisations are standardising on testing and are sharing results for similar vehicles in different markets. ANCAP, by agreement with the manufacturers, has used IIHS results for the Volvo 850 and Toyota Camry and a Euro NCAP result for the Volkswagon Polo. Japan NCAP is also republishing results from US NCAP. This will become more common as vehicle designs are increasingly globalised.

Data sharing means that duplication of effort and considerable costs can be avoided and more vehicles can be evaluated. Consumers can then make a more informed choice at the time of vehicle purchase on the basis of occupant protection performance.

3.3 Relationships

ANCAP consults with the automotive industry about the program through the Australian Federal Chamber of Automotive Industries (FCAI), the representative group for the vehicle manufacturers and importers in Australia. Representatives from the vehicle manufacturing companies are invited to attend the test of their own products and can review the results before publication. ANCAP meets with the FCAI before each public launch and in early 1997 conducted a technical briefing for FCAI members on the new IIHS-style rating system.

ANCAP has spent substantial time and effort briefing motoring journalists about the program to encourage the incorporation of vehicle safety ratings in the consumer perspective of road tests and reviews.

ANCAP has also made numerous presentations to fleet management groups on the implications of crash test results for vehicle selection for fleet managers. Industrial legislation in Australia requires employers to provide a safe workplace and a company vehicle is defined as a workplace. Due to Australian tax arrangements, about 50 percent of new vehicles are sold to fleets. Around 60-70 percent of production of the Holden Commodore and Ford Falcon is sold to fleets. The buying preferences of fleet managers therefore has a strong influence on vehicle manufacturers in Australia. The use by fleet managers of ANCAP ratings as a purchase criterion will further encourage vehicle manufacturers to provide safer vehicles.

3.4 Recent Releases

3.4.1 Large/Medium Car Class

In Australia, due to the dominance of four locally manufactured models, this category comprises about 40 percent of new car sales and is therefore a very important influence on the total market. Three out of the four large local models were updated in 1997 making an update very important.

Figure 3 in the Appendix reproduces the public brochure of the ratings for the vehicles currently on the Australian market. The airbag-equipped Camry and the Volvo 850 ratings are examples of overseas results being used with the agreement of the vehicle manufacturer. The Mitsubishi Magna is sold in the US and Japan as the Diamante.

3.4.2 Summary brochure

By the end of 1997, over 60 vehicle models had been tested by ANCAP. A summary brochure was then produced to present all these results together in an abbreviated format as an overall buyer's guide. Some of the models had been superseded but the results were useful for buyers of recent model second-hand vehicles. Figure 3 in the Appendix reproduces the brochure.

3.4.3 Four Wheel Drive Vehicles (4WDs)

The 4WD (SUV) category, as in the US, is growing in popularity in Australia. According to the manufacturers own survey data, most of these vehicles are rarely used off-road even though many, particularly the larger models, are designed for, and perform very well in, this role.

These vehicles are popular because they have a higher driving position, flexible interior space and an undeserved reputation as being safer due to their size and weight. While their occupants may come off better in a crash with a smaller vehicle, analysis of Australian on-road crash data shows that, when all crashes are considered, 4WDs are about as safe as a medium-sized sedan (MUARC 1998).

The ANCAP test results show that this class of vehicles lags well behind sedans in the introduction of better occupant safety. The highest rating vehicle, the Landrover Discovery with airbags, was only rated *Marginal* compared with some sedans now being rated *Good*.

Figure 4 in the Appendix reproduces the 4WD public information brochure.

3.5 Euro NCAP Ratings

The Euro NCAP test protocol includes offset frontal, side and pedestrian impact in its evaluation of each vehicle. Combining the results from these tests into an overall rating has been a challenge for Euro NCAP which other NCAP groups will also have to face.

Euro NCAP has adopted a star rating system similar to the NHTSA, whereas ANCAP and IIHS have adopted the *Good, Acceptable, Marginal, Poor* system. While efforts are being made to standardise NCAP presentation methods internationally, there are technical differences which require alternative presentations to be used in different markets.

Figure 5 in the Appendix shows an example of the Euro NCAP rating system.

3.6 Market Research

ANCAP commissioned focus group research (ANOP 1998) to evaluate how well the current brochure designs were communicating the ANCAP results, to canvass how the design and distribution could be improved and to suggest other avenues for promoting the program and the information.

The groups consisted of people who were soon to purchase, or had recently purchased, a new car. Both genders were represented (interviewed separately) and the groups were segregated into under and over 40 age groups.

The main results of the research were that-:

- despite considerable effort over the years to simplify the content of ANCAP brochures, even more simplified presentations were needed;
- the logos of the program sponsors needed to be given greater prominence as they contributed greatly to the credibility of the program;
- the rating system may need minor revision to add a category better than *Good. Excellent* was suggested;
- previous tests should be included wherever possible to provide a good comparison for readers;
- the distribution system should be broadened to include, for instance-:
    - -as an insert in motoring association magazines
    - -new car dealers
    - -service stations/garages
    - -supermarkets
    - -vehicle accessory stores and vehicle sections of supermarkets
    - -libraries

A public relations campaign was suggested including television current affairs and infotainment programs, particularly those with a consumer angle, radio programs featuring motoring personalities, and features in women's magazines which would be likely to reach a receptive audience. Cross promotions in these magazines with vehicle manufacturers were suggested.

Women are generally more concerned about safety than men and more often look for a wide range of information before reaching a purchasing decision. Women are involved in over half of all vehicle purchasing decisions, so they are an influential target group.

4 FUTURE DIRECTIONS

After frontal crashes, side impacts cause the most trauma on Australian roads. ANCAP therefore intends to adopt a side impact test in the near future. When this occurs the relevance and value of the full frontal test will be re-evaluated in the light of airbag penetration into the Australian new vehicle market.

The recent availability of an on-board data acquisition system by ANCAP's main test contractor means that the rear seat in vehicles can now be retained - previously it had to be removed to accomodate the junction boxes for the umbilical cord data acquisition system. This will allow a range of further test activities such as effectiveness of rear seatbelts/seat-pans, child restraints and seat latch strength. The exact tests to be run were still being decided at the time of writing.

5 CONCLUSIONS

ANCAP's experience with producing consumer ratings on vehicle safety is a useful guide to other groups attempting the same task. Of greatest importance are the periodic review of methods of presentation of information to the car buying public and methods of advertising, marketing and distributing the information.

Television has been found to be an excellent medium for promoting vehicle safety overall and ANCAP publications. However, television advertisements are expensive and a wider marketing program maintains interest in crash test results for a longer period.

REFERENCES

ANCAP [1], "Crash Test Report," Vol 1 Number 1, Large/Medium cars, April 1993.

ANCAP [2], "Crash Test Report," Vol 1 Number 2, Small cars, April 1994.

ANCAP [3], "Crash Test Report, Technical Summary," Vol 1 Number 3, 4 wheel drives and passenger vans, November 1994.

ANCAP [4], "Buyers Guide to Vehicle Crash Tests, 4 wheel drives and passenger vans," November 1994.

ANCAP [5], "Buyers Guide to Vehicle Crash Tests, Large/medium and small cars," June 1995.

ANCAP [6], "Buyers Guide to Crash Tests, Utes," November 1995.

ANCAP [7], "Buyers Guide to Crash Tests, Large/medium cars," March 1996.

ANCAP [8], "Buyers Guide to Crash Tests, Small car update," November 1996.

ANCAP [9], "Buyers Guide to Crash Tests, Large/medium car update," February 1997.

ANCAP [10], "Buyers Guide to Crash Tests, Small car update," July 1997.

ANCAP [11], "Buyers Guide to Crash Tests, Large/medium car update," December 1997.

ANCAP [12], "Buyers Guide to Crash Tests, Summary," January 1998.

ANCAP [13], "Buyers Guide to Crash Tests," 4WDs, April 1998.

ANOP, NCAP CRASH TEST BROCHURES, "Qualitative Research into New Car Buyers' Attitudes to Car Safety and the NCAP Brochures", ANOP Research Services Pty Ltd, April 1998.

MUARC, Newstead, Stuart, Cameron, Max, and Le, Chau My, "Vehicle Crashworthiness ratings and crashworthiness by year of manufacture: Victoria and New South Wales crashes during 1987-96," March 1998.

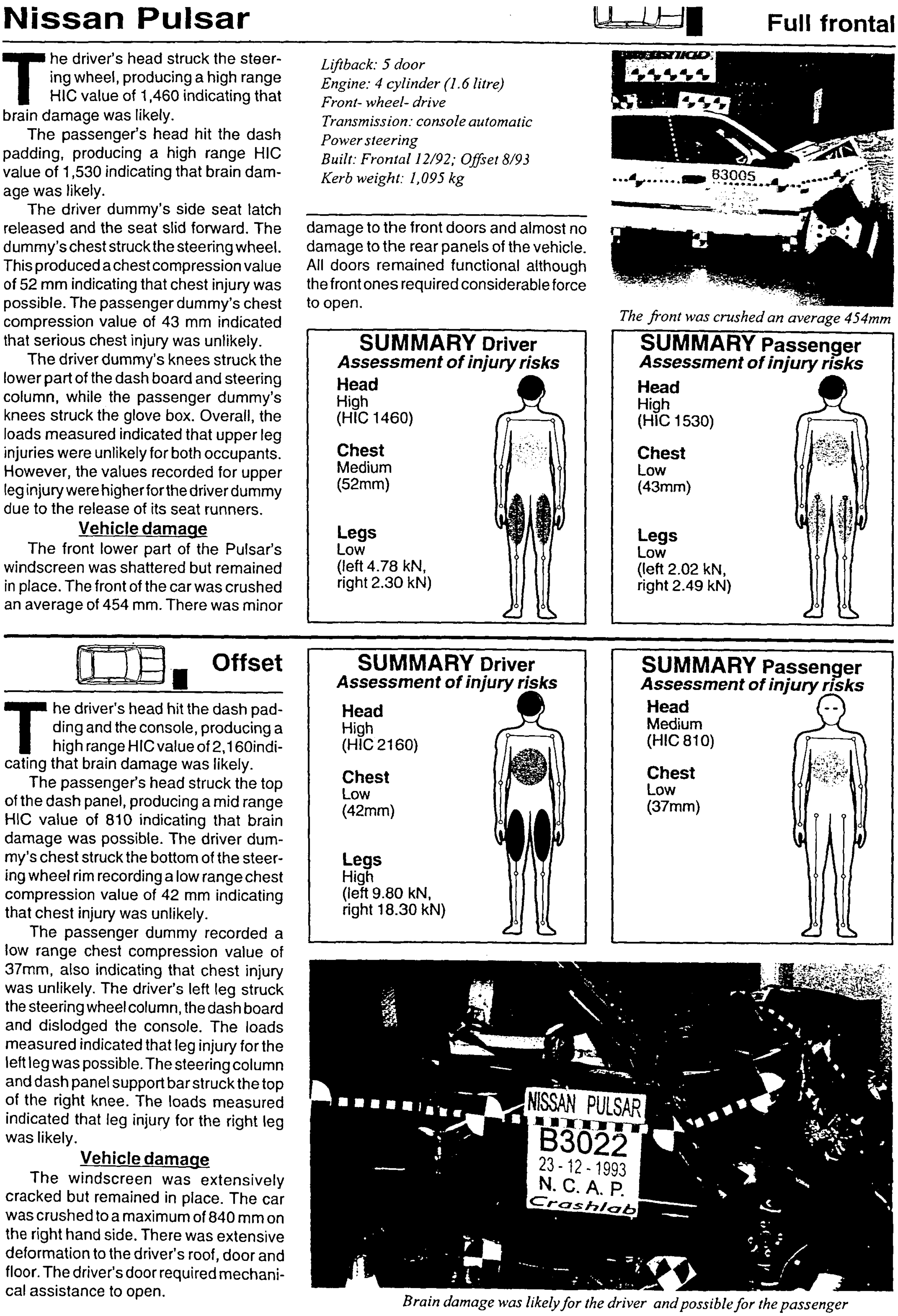
B3005
NISSAN PULSAR
B3022
23 - 12 - 1993
N. C. A. P.
Crashlab

Nissan Pulsar

Full frontal

The driver's head struck the steering wheel, producing a high range HIC value of 1,460 indicating that brain damage was likely.

The passenger's head hit the dash padding, producing a high range HIC value of 1,530 indicating that brain damage was likely.

The driver dummy's side seat latch released and the seat slid forward. The dummy's chest struck the steering wheel. This produced a chest compression value of 52 mm indicating that chest injury was possible. The passenger dummy's chest compression value of 43 mm indicated that serious chest injury was unlikely.

The driver dummy's knees struck the lower part of the dash board and steering column, while the passenger dummy's knees struck the glove box. Overall, the loads measured indicated that upper leg injuries were unlikely for both occupants. However, the values recorded for upper leg injury were higher for the driver dummy due to the release of its seat runners.

Vehicle damage

The front lower part of the Pulsar's windscreen was shattered but remained in place. The front of the car was crushed an average of 454 mm. There was minor damage to the front doors and almost no damage to the rear panels of the vehicle. All doors remained functional although the front ones required considerable force to open.

Liftback: 5 door
Engine: 4 cylinder (1.6 litre)
Front- wheel- drive
Transmission: console automatic
Power steering
Built: Frontal 12/92; Offset 8/93
Kerb weight: 1,095 kg

The front was crushed an average 454mm

SUMMARY Driver
Assessment of injury risks

Head
High
(HIC 1460)

Chest
Medium
(52mm)

Legs
Low
(left 4.78 kN,
right 2.30 kN)

SUMMARY Passenger
Assessment of injury risks

Head
High
(HIC 1530)

Chest
Low
(43mm)

Legs
Low
(left 2.02 kN,
right 2.49 kN)

Offset

The driver's head hit the dash padding and the console, producing a high range HIC value of 2,160 indicating that brain damage was likely.

The passenger's head struck the top of the dash panel, producing a mid range HIC value of 810 indicating that brain damage was possible. The driver dummy's chest struck the bottom of the steering wheel rim recording a low range chest compression value of 42 mm indicating that chest injury was unlikely.

The passenger dummy recorded a low range chest compression value of 37mm, also indicating that chest injury was unlikely. The driver's left leg struck the steering wheel column, the dash board and dislodged the console. The loads measured indicated that leg injury for the left leg was possible. The steering column and dash panel support bar struck the top of the right knee. The loads measured indicated that leg injury for the right leg was likely.

Vehicle damage

The windscreen was extensively cracked but remained in place. The car was crushed to a maximum of 840 mm on the right hand side. There was extensive deformation to the driver's roof, door and floor. The driver's door required mechanical assistance to open.

SUMMARY Driver
Assessment of injury risks

Head
High
(HIC 2160)

Chest
Low
(42mm)

Legs
High
(left 9.80 kN,
right 18.30 kN)

SUMMARY Passenger
Assessment of injury risks

Head
Medium
(HIC 810)

Chest
Low
(37mm)

Brain damage was likely for the driver and possible for the passenger

Figure 1 - Typical ANCAP Presentation

Frontal crash test performance – at a glance

					Protection from serious injury			
	Overall	Structure	Seat belt evaluation	Head	Chest	Upper legs	Lower legs	Head restraint
Toyota Camry (US)* (dual airbags)	G	G	A	G	G	G	G	A
Mitsubishi Magna 96-97 (driver's airbag)	A	■	G	G	A	■	P	P
Holden Commodore 97 (driver's airbag)	A	■	A	G	G	G	P	■
Toyota Camry 97 (no airbag)	■	A	■	■	G	G	P	A
Ford Falcon 94-97 (driver's airbag)	■	A	■	■	A	A	P	■
Mitsubishi Magna 96-97 (no airbag)	■	■	■	P	G	■	P	P

A driver's airbag typically halves the chance of a serious head injury

Key to ratings: Good G Acceptable A Marginal ■ Poor P

* Airbag equipped Camry tested in left-hand-drive form in the USA. A similar right-hand-drive specification is available in Australia. For more details about the crash tests contact one of the organisations listed on the back page or visit the Web site.

ncap

Figure 2 - ANCAP Large/Medium Vehicle Results

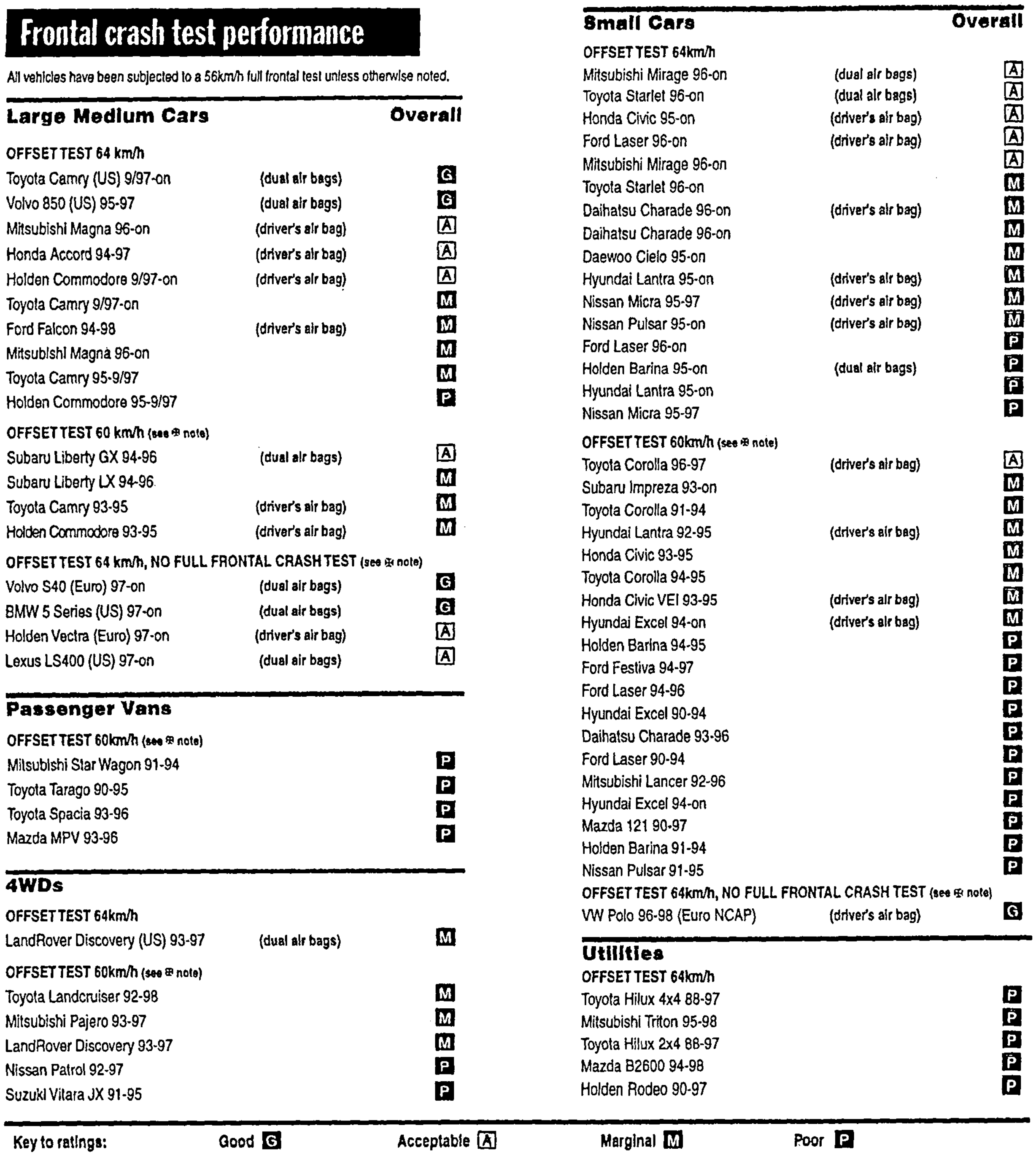

Frontal crash test performance

All vehicles have been subjected to a 56km/h full frontal test unless otherwise noted.

Large Medium Cars

OFFSET TEST 64 km/h

Vehicle		Overall
Toyota Camry (US) 9/97-on	(dual air bags)	G
Volvo 850 (US) 95-97	(dual air bags)	G
Mitsubishi Magna 96-on	(driver's air bag)	A
Honda Accord 94-97	(driver's air bag)	A
Holden Commodore 9/97-on	(driver's air bag)	A
Toyota Camry 9/97-on		M
Ford Falcon 94-98	(driver's air bag)	M
Mitsubishi Magna 96-on		M
Toyota Camry 95-9/97		M
Holden Commodore 95-9/97		P

OFFSET TEST 60 km/h (see ✱ note)

Vehicle		Overall
Subaru Liberty GX 94-96	(dual air bags)	A
Subaru Liberty LX 94-96		M
Toyota Camry 93-95	(driver's air bag)	M
Holden Commodore 93-95	(driver's air bag)	M

OFFSET TEST 64 km/h, NO FULL FRONTAL CRASH TEST (see ✱ note)

Vehicle		Overall
Volvo S40 (Euro) 97-on	(dual air bags)	G
BMW 5 Series (US) 97-on	(dual air bags)	G
Holden Vectra (Euro) 97-on	(driver's air bag)	A
Lexus LS400 (US) 97-on	(dual air bags)	A

Passenger Vans

OFFSET TEST 60km/h (see ✱ note)

Vehicle	Overall
Mitsubishi Star Wagon 91-94	P
Toyota Tarago 90-95	P
Toyota Spacia 93-96	P
Mazda MPV 93-96	P

4WDs

OFFSET TEST 64km/h

Vehicle		Overall
LandRover Discovery (US) 93-97	(dual air bags)	M

OFFSET TEST 60km/h (see ✱ note)

Vehicle	Overall
Toyota Landcruiser 92-98	M
Mitsubishi Pajero 93-97	M
LandRover Discovery 93-97	M
Nissan Patrol 92-97	P
Suzuki Vitara JX 91-95	P

Small Cars

OFFSET TEST 64km/h

Vehicle		Overall
Mitsubishi Mirage 96-on	(dual air bags)	A
Toyota Starlet 96-on	(dual air bags)	A
Honda Civic 95-on	(driver's air bag)	A
Ford Laser 96-on	(driver's air bag)	A
Mitsubishi Mirage 96-on		A
Toyota Starlet 96-on		M
Daihatsu Charade 96-on	(driver's air bag)	M
Daihatsu Charade 96-on		M
Daewoo Cielo 95-on		M
Hyundai Lantra 95-on	(driver's air bag)	M
Nissan Micra 95-97	(driver's air bag)	M
Nissan Pulsar 95-on	(driver's air bag)	M
Ford Laser 96-on		P
Holden Barina 95-on	(dual air bags)	P
Hyundai Lantra 95-on		P
Nissan Micra 95-97		P

OFFSET TEST 60km/h (see ✱ note)

Vehicle		Overall
Toyota Corolla 96-97	(driver's air bag)	A
Subaru Impreza 93-on		M
Toyota Corolla 91-94		M
Hyundai Lantra 92-95	(driver's air bag)	M
Honda Civic 93-95		M
Toyota Corolla 94-95		M
Honda Civic VEI 93-95	(driver's air bag)	M
Hyundai Excel 94-on	(driver's air bag)	M
Holden Barina 94-95		P
Ford Festiva 94-97		P
Ford Laser 94-96		P
Hyundai Excel 90-94		P
Daihatsu Charade 93-96		P
Ford Laser 90-94		P
Mitsubishi Lancer 92-96		P
Hyundai Excel 94-on		P
Mazda 121 90-97		P
Holden Barina 91-94		P
Nissan Pulsar 91-95		P

OFFSET TEST 64km/h, NO FULL FRONTAL CRASH TEST (see ✱ note)

Vehicle		Overall
VW Polo 96-98 (Euro NCAP)	(driver's air bag)	G

Utilities

OFFSET TEST 64km/h

Vehicle	Overall
Toyota Hilux 4x4 88-97	P
Mitsubishi Triton 95-98	P
Toyota Hilux 2x4 88-97	P
Mazda B2600 94-98	P
Holden Rodeo 90-97	P

Key to ratings: Good G Acceptable A Marginal M Poor P

Figure 3 - ANCAP Summary Brochure

Frontal crash test performance – at a glance

	Overall	Structure	Restraints	Head	Chest	Upper legs	Lower legs	Head restraint position
					Protection from serious injury			
Offset crash test speed 64km/h, full frontal 56km/h								
Landrover Discovery (US) 93-97 (dual airbags)	■†	■	■	A	G	G	A	■
Toyota RAV4 97 on	■	A	■	P	A	G	P	■
Toyota Prado 97 on	■	■*	■	P	G	G	P	■
Kia Sportage 97 on	P	■	P	P	A	G	P	A
Offset crash test speed 60km/h, full frontal 56km/h (not directly comparable with the vehicles above)								
Toyota Landcruiser 92-97	■	■	■	P	G	A	A	-
Mitsubishi Pajero 93-97	■	■	■	P	G	G	G	-
Landrover Discovery 93-97	■	■	■	P	G	G	G	-
Nissan Patrol 92-97	P	P	P	P	A	G	A	-
Suzuki Vitara JX 91-95	P	P	P	P	■	G	P	-

Key to ratings: Good G Acceptable A Marginal ■ Poor P

† If the restraints in the Discovery had performed slightly better the Overall rating would have been Acceptable. Landrover has confirmed that similar results can be expected from the equivalent Australian model

* In the offset test of the Toyota Prado there was a substantial leak from the fuel tank.

For more details about the crash tests contact one of the organisations listed on the back page or visit the Web site.

ncap

Figure 4 - ANCAP 4WD Results

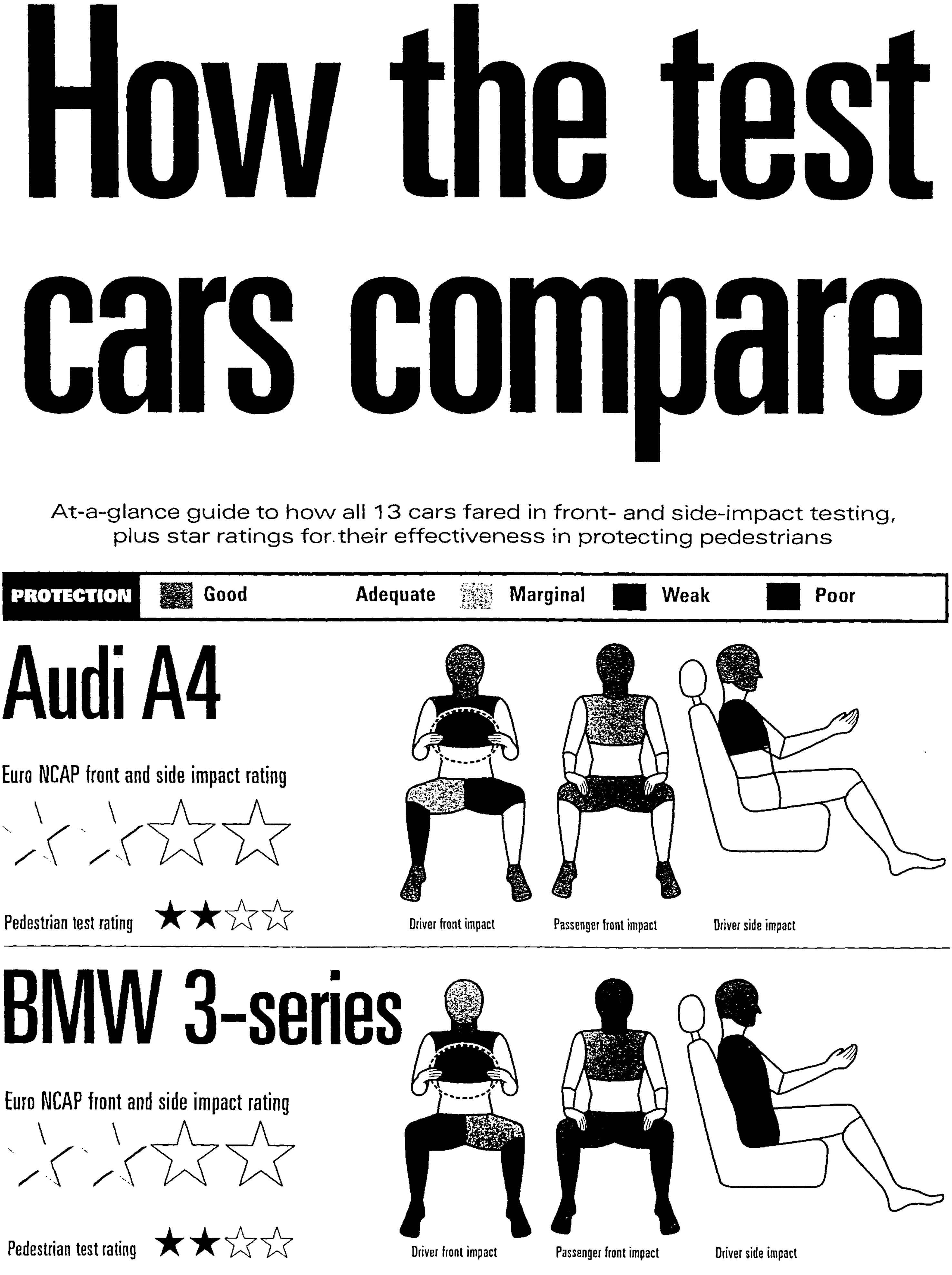

How the test cars compare

At-a-glance guide to how all 13 cars fared in front- and side-impact testing, plus star ratings for their effectiveness in protecting pedestrians

PROTECTION ▨ Good Adequate ▨ Marginal ■ Weak ■ Poor

Audi A4

Euro NCAP front and side impact rating

★★☆☆

Pedestrian test rating ★★☆☆

Driver front impact

Passenger front impact

Driver side impact

BMW 3-series

Euro NCAP front and side impact rating

★★☆☆

Pedestrian test rating ★★☆☆

Driver front impact

Passenger front impact

Driver side impact

Figure 5 - Example of Euro NCAP Rating System

A SCIENTIFIC METHOD FOR ANALYSING VEHICLE SAFETY

Craig Newland
Günther Scheffel
Mark Armstrong
Autoliv Australia Pty Ltd
AUSTRALIA
Keith Seyer
Federal Office Of Road Safety
Department of Transport & Regional Development
AUSTRALIA
Paper Number 98-S11-O-05

ABSTRACT

This paper describes an analytical technique that compares the actual performance of the vehicle structure in absorbing crash energy with an idealised (perfect) performance. The same methodology is applied to the restraint system performance. This can be used as basis of an objective assessment of the vehicle's crashworthiness within the constraints of its particular design. Such an analysis can direct designers to focus on areas of the vehicle that can be improved, such as crush structure and/or particular parts of the restraint system.

INTRODUCTION

Since the New Car Assessment Program began in the US nearly 20 years ago, people have wrestled with how to present the crash results in a form that is easily understood by the consumer.

There have been a number of rating systems used over the years but all have involved subjective assessments to one degree or another. With consumer crash testing occurring worldwide, it has become increasingly important to develop an objective, scientific method of rating vehicle crashworthiness. The aim of such a rating system should be to not only help the consumer make an informed choice but also to assist manufacturers in improving their vehicle designs.

To maximise the protection to an occupant during a crash, the vehicle structure and the restraint system must be optimised to achieve the minimum acceleration for the occupant over the longest possible time within the design constraints of the vehicle.

METHOD

The best restraint condition for an occupant during a crash is to have the minimum possible acceleration applied for the maximum possible duration in order to bring the occupant to rest. Minimum possible acceleration is achieved if the acceleration is held constant at a level sufficient to reduce the velocity from impact velocity to zero over maximum time. To achieve maximum time for this velocity change requires all available distance to be utilised. For restraint of an occupant's head, this ideal distance is from the head to the furthermost impacted extremity of the vehicle. Therefore, the vehicle's crush structure and the performance of the restraint system both have an effect on how well the occupant is protected.

Vehicle Analysis

From an occupant safety point of view, an ideal vehicle would crush progressively, with a constant force required to produce deformation and with the impacted surface of the vehicle displacing as far as possible without intruding into the occupant cell. Moreover, the occupant cell itself must not collapse or deform and all kinetic energy should be absorbed through deformation. In practical terms, if the deceleration of an "ideal" vehicle were measured, it would be constant over time and for the maximum possible duration as determined by the available crush before occupant cell deformation. This concept is illustrated schematically in Figure 1. For a frontal 90° impact against a rigid 0° barrier, an ideal vehicle would crush until the front bumper reached the firewall. The optimum (ideal) crush distance of the vehicle is denoted as S_{opt}. The vehicle has an initial (impact) velocity V_{imp}.

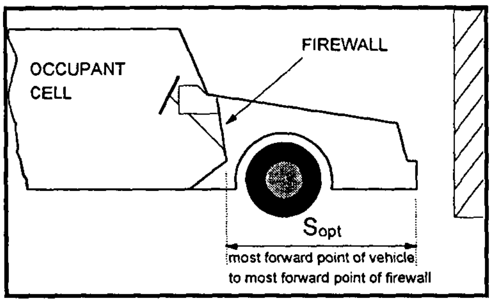
OCCUPANT
CELL
FIREWALL
S_{opt}
most forward point of vehicle
to most forward point of firewall

Figure 1. Optimum vehicle crush distance.

Given that minimum constant acceleration should be maintained, simple principles of the physics of motion under constant acceleration may be applied to calculate *ideal crash conditions* as follows:

$$\text{Velocity change} = \text{Final Velocity} - \text{Initial Velocity}$$
$$= 0 - V_{imp} \text{ (rebound should be avoided)}$$

Optimum acceleration (aopt) $= V_{imp}{}^2/(2*S_{opt})$.

Optimum crush time $(t_{max}) = V_{imp}/a_{opt}$.

The ideal instantaneous velocity at any time t is given by $V_i(t) = V_{imp} + a_{opt}*t$.

Hence the ideal specific (massless) energy at any time t is $E_i(t) = V_i(t)^2/2$.

The *actual* specific energy of a vehicle crash $E_a(t)$ can be calculated as $V_a(t)^2/2$, where $V_a(t)$ (the actual instantaneous velocity) is found by integration of the measured vehicle acceleration.

The actual specific energy (as a function of time) from a vehicle crash test can then be compared to the ideal specific energy, calculated based on the principles outlined above.

The typical natures of the ideal and actual energies for vehicle crush are shown in Figure 2.

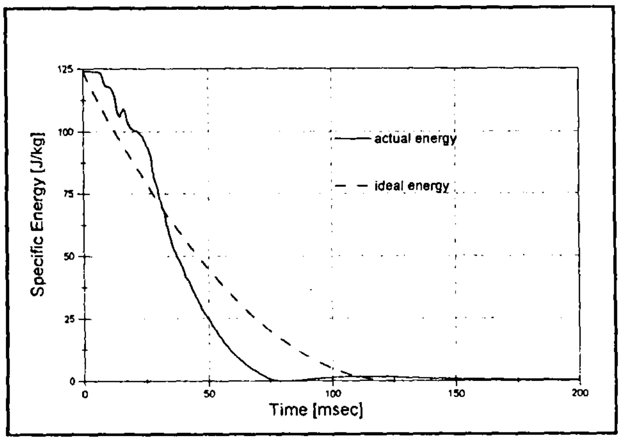

Figure 2. Typical Vehicle Crush Specific Energies For A Frontal 90° Impact Against A Rigid 0° Barrier.

The actual energy depicted in Figure 2 can be considered over three successive time periods as shown in Figure 3.

During the first phase, the actual energy decreases more slowly than ideal. During the second phase, the actual energy decreases more rapidly than ideal, with the vehicle coming to rest at the end of this period. The final phase represents rebound of the vehicle.

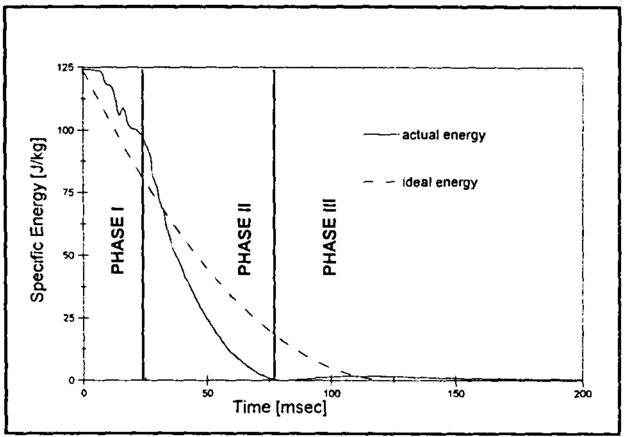

Figure 3. Division of the Typical Vehicle Specific Energy Curves into 3 distinct phases.

The performance of the actual vehicle against the ideal is assessed in each of the three phases. In the first phase, the maximum difference between the ideal and actual curves is divided by the ideal energy at the time that this maximum difference occurs. This resultant term is then subtracted from one. For the second phase the largest negative gradient of the actual energy curve and the ideal gradient at the same moment in time are determined. The ratio of ideal gradient to actual gradient is then used to characterise this phase. The final (rebound) phase is characterised by subtracting from one the ratio of the peak rebound energy divided by the initial energy (energy at time zero).

Occupant Head Analysis

The head analysis technique is based on the same philosophy as the vehicle analysis. A perfect restraint would operate to provide a minimum constant acceleration for the maximum possible time, which in turn is dictated by the available displacement. The occupant should be permitted to move, so long as contact to interior objects is avoided. Figure 4 illustrates the maximum available displacement relative to the ground for an occupant head during a frontal 90° impact against a rigid 0° barrier. The optimum head displacement is the sum of the vehicle crush distance, S_{opt} (bumper to firewall) and the distance from nose to occupant cell boundary, Snsw (usually the steering wheel).

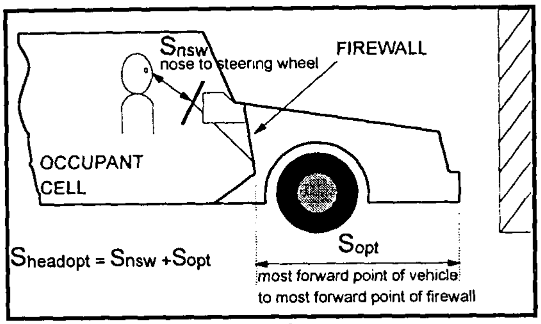

Figure 4. Optimum head displacement.

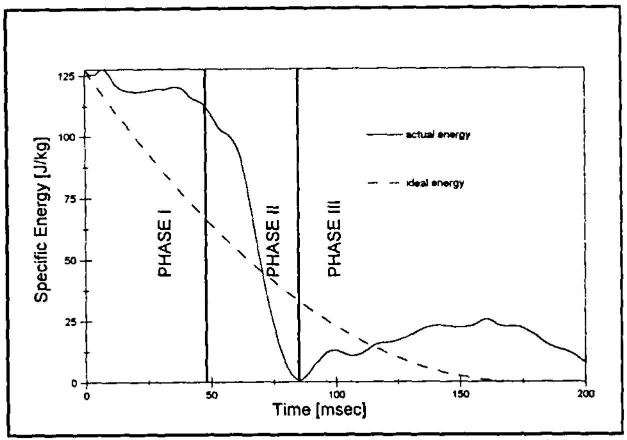

Figure 5. Typical curves showing occupant head specific energy with respect to ground.

The specific energy of the occupant head is considered in the same three phases as the vehicle specific energy as shown in Figure 5. This figure shows that during phase I the head is relatively uncoupled to the vehicle and continues with almost constant energy (constant velocity). In the second phase, the restraint system begins to slow the head and ultimately brings the head to rest. The third stage is the rebound of the head and is clearly more significant than for the vehicle. Performance indices are calculated in the same way as for the vehicle.

RESULTS

A series of 12 tests based on Australian Design Rule (ADR) 69/00 were conducted at a speed of 56 km/h at Autoliv Australia. These tests were 56 km/h frontal 90° impacts against a rigid 0° barrier, with belted occupants. This test condition was chosen to allow correlation with New Car Assessment Program (NCAP) test data. The vehicles tested are listed in Table 1. Unless otherwise stated, all vehicles were equipped with driver airbag.

The test results from the tests listed in Table 1 were analysed using the method described in this paper. The vehicle analysis results are listed in Table 2 and the driver head analysis results are listed in Table 3.

Table 1.
Vehicles Tested at 56 km/h Using ADR 69/00 Test Method

Test Number	Vehicle
TG6C0001	1996 Daihatsu Charade (no airbag)
TG6C0002	1995 Daihatsu Charade
TG6C0003	1996 Holden Commodore (no airbag)
TG6C0004	1996 Mitsubishi Magna
TG6C0006	1995 Hyundai Lantra
TG6C0007	1996 Hyundai Excel Sprint
TG6C0008	1996 Nissan Micra (no airbag)
TG6C0009	1996 Hyundai Excel
TG6C0010	1996 Toyota Corolla
TG6C0011	1997 Toyota Starlet
TG6C0012	1996 Mitsubishi Mirage
TG7C0001	1997 Ford Laser

Table 2.
Vehicle Energy Management Indices for 56 km/h ADR 69/00 Tests

Vehicle	Phase I	Phase II	Phase III
TG6C0001	0.7993	0.2302	0.9862
TG6C0002	0.8182	0.2433	0.9733
TG6C0003	0.8653	0.1549	0.9767
TG6C0004	0.9174	0.2695	0.9914
TG6C0006	0.8991	0.3180	0.9855
TG6C0007	0.8001	0.2690	0.9876
TG6C0008	0.8267	0.2285	0.9831
TG6C0009	0.7744	0.1606	0.9950
TG6C0010	0.8599	0.2637	0.9867
TG6C0011	0.9227	0.2800	0.9836
TG6C0012	0.9119	0.2017	0.9833
TG7C0001	0.8545	0.2728	0.9856

Table 3.
Driver Head Energy Management Indices for 56 km/h ADR 69/00 Tests

Vehicle	Phase I	Phase II	Phase III
TG6C0001	0.3870	0.1492	0.8001
TG6C0002	0.5062	0.1628	0.8606
TG6C0003	0.3857	0.1035	0.7395
TG6C0004	0.7591	0.2021	0.7275
TG6C0006	0.4377	0.1286	0.8195
TG6C0007	0.3948	0.0994	0.8266
TG6C0008	0.2720	0.1020	0.7881
TG6C0009	0.4665	0.1491	0.8256
TG6C0010	0.6258	0.1797	0.7958
TG6C0011	0.5050	0.1533	0.7366
TG6C0012	0.7545	0.2364	0.6803
TG7C0001	0.7370	0.2250	0.7096

DISCUSSION

General Comments

The analysis method detailed in this paper was developed after completion of the tests to which it was to be applied. Whilst the analysis philosophy and technique are clear, the pre-existence of the test data imposed certain difficulties on the calculation procedures adopted.

The performance indices calculated by this method indicate the actual energy management of a given vehicle, compared to the ideal that could be achieved for that vehicle. This must be kept in mind when comparing results from different vehicles as the numbers do not necessarily indicate the injury risk for an occupant, but rather the 'room for improvement' for a given design geometry.

Vehicle Analysis

The analysis method assesses actual energy management compared to ideal energy management. In order to calculate energy, the velocity of the vehicle must be determined. This has been achieved by integrating the longitudinal acceleration of the vehicle. However, the vehicle instrumentation for the 56 km/h ADR 69/00 tests measured longitudinal vehicle accelerations at the engine and rear seat crossmember. The measurements from these transducers reflect vehicle body crush occurring on all parts of the structure forward of the transducer mounting point. The engine acceleration is not useful for this analysis method, and unfortunately, any crush of the occupant cell, which is undesirable from an occupant safety point of view, would be incorporated in the measurements at the rear seat crossmember. In order to accurately characterise the actual vehicle crush behaviour compared to the ideal, it would be necessary to measure accelerations at the most forward point of the occupant cell. In an attempt to compensate for the fact the acceleration data cannot discriminate undesirable occupant cell deformation from desirable vehicle crush, a separate index is calculated to assess the amount of deformation of the occupant cell. This index is the relative crush of the occupant cell, calculated as:

$$\frac{\text{Occupant Cell Initial Size - Occupant Cell Final Size}}{\text{Occupant Cell Initial Size}}$$

Table 4 shows the results of the vehicle performance indices and the relative crush of the occupant cell. These relative crush values must be considered in conjunction with the performance indices. In some cases they may contradict good vehicle energy performance indices, but this is a reflection of the fact that the occupant cell suffered significant deformation, which may have been incorrectly assessed as a beneficial effect in the analysis due to the measurement difficulties.

Table 4.
Relative Crush and Vehicle Energy Management Indices for 56 km/h ADR 69/00 Tests

Vehicle	Relative Crush	Phase I	Phase II	Phase III
TG6C0001	0.8890	0.7993	0.2302	0.9862
TG6C0002	0.8780	0.8182	0.2433	0.9733
TG6C0003	0.9809	0.8653	0.1549	0.9767
TG6C0004	0.9482	0.9174	0.2695	0.9914
TG6C0006	0.9155	0.8991	0.3180	0.9855
TG6C0007	0.9386	0.8001	0.2690	0.9876
TG6C0008	0.9225	0.8267	0.2285	0.9831
TG6C0009	0.9883	0.7744	0.1606	0.9950
TG6C0010	0.9331	0.8599	0.2637	0.9867
TG6C0011	0.9102	0.9227	0.2800	0.9836
TG6C0012	0.9655	0.9119	0.2017	0.9833
TG7C0001	0.9015	0.8545	0.2728	0.9856

The vehicle analysis results indicate that the values from phase III (rebound) are all very similar and near ideal (that is, the actual vehicle rebound energies recorded for the sample vehicles are all very small). Hence, they are of little interest in this discussion, however, some interesting features are evident from the values calculated for phases I and II.

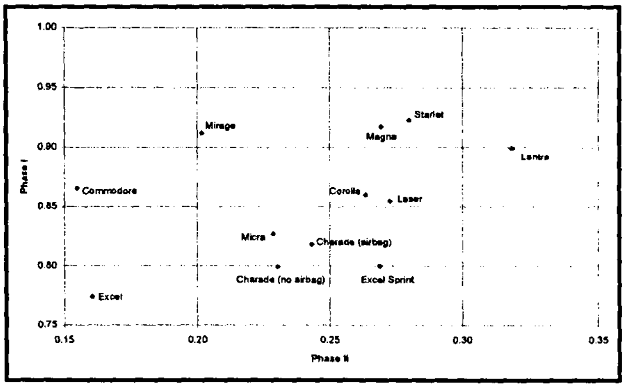

Figure 6. Vehicle Energy Management Indices for phases I and II.

Figure 6 shows the relationship between phases I and II for the vehicle analysis. The upper right corner of the graph represents best performance in both phases. This graph can be used to gain an impression of the overall structural performance of a vehicle and can be used as a means of ranking the structural performances, however, ranking is only valid for vehicles with a similar S_{opt}

(optimum crush distance). For example, it could be concluded that the structural performance of the Starlet was superior to that of the Excel, Excel Sprint and Charade, as these vehicles all have an optimum crush distance in the range 0.90 - 0.99m. The Micra could perhaps be considered in this group, with a crush distance of 0.86m.

It is interesting to note that the results in Figure 6 for the two Charade vehicles are in close agreement, whereas the Excel results are quite dissimilar. This statement is supported by the evidence from the accelerometers measuring the vehicle crash pulses. One possible explanation for this behaviour is that the Excel vehicles had very different crush modes. In other words, the collapse of the vehicle structure was fundamentally different in each of the Excel vehicles.

It would be possible to generate an overall Vehicle Energy Management Index, expressed as a number in the range 0 - 100 if the performance indices for each phase are averaged and multiplied by 100. Using this system, a value of zero would indicate the largest deviation from ideal and a score of 100 would correspond to ideal performance. However, the forming of a single number to characterise vehicle energy management loses the detailed information about individual aspects of the behaviour available for each phase, and could also dilute the significance of a particular phase. Equally, it could be argued that the relative importance of each of the phases are not the same and that weighting factors should be applied to add greater significance to particular phases, instead of simply averaging the individual phase performance indices. Therefore, a single number has not been used to characterise the overall performance.

Occupant Head Analysis

From a purely philosophical point of view, the maximum available displacement for an occupant head relative to the vehicle should be the distance from the initial position of the head to the boundary of the occupant cell. This definition suggests that the steering wheel reduces this idealised distance and that survival space for the occupant would be enlarged if the steering wheel and instrument panel were absent. This would clearly offer improvements in ideal restraint performance, however, to focus this work for realistic application using the sample data available, the distance from nose to steering wheel hub was chosen as the appropriate displacement for the occupant head relative to the vehicle.

The velocity of the driver head relative to ground needs to be determined in order to be able to calculate kinetic energy of the head. The accelerations at the centre of gravity of the head are not suitable for calculating velocity by integration, because the head undergoes angular motion. This angular motion of the head produces a centripetal acceleration that results in a change in angular velocity. However, the instantaneous centre of rotation is not usually known and the angular component of this motion cannot be removed from the total acceleration. Hence integration of the acceleration does not yield the true translational velocity. To overcome this difficulty, motion analysis from high speed films was used to determine the velocity time history of the driver head relative to the ground and this was used to calculate the actual energy of the head.

This film analysis method yields the head motion relative to ground, however, it does not indicate whether this motion is due to desirable vehicle crush or undesirable crush. To compensate for this fact, the relative steering wheel intrusion was chosen as a separate index to assess the extra risk imposed by steering wheel intrusion. Unfortunately, the dynamic steering wheel intrusion was unable to be measured in all vehicles, and hence static measurements taken before and after the tests were used. The relative steering wheel intrusion is calculated as:

$$\frac{\text{Snsw} - \text{Steering wheel intrusion}}{\text{Snsw}}$$

where Snsw is the distance from the driver dummy nose to the centre of the steering wheel hub, and steering wheel intrusion is the difference between the pre-test and post-test horizontal distances from the rear bumper to the centre of the steering wheel.

The result from this method is the potential for a relative steering wheel intrusion greater than one if the steering column had a residual displacement away from the occupant head. This is considered desirable as it allows an effective increase in survival space for the occupant, and this is reflected in the relative steering wheel intrusion. Table 5 shows the head restraint performance indices and relative steering wheel intrusion. Again, the relative steering wheel intrusion values should be considered in conjunction with the performance indices. A good head restraint performance index can be largely overshadowed by a poor result from the steering wheel intrusion.

Table 5.
Relative Steering Wheel Intrusion and Head Energy Management Indices for 56 km/h ADR 69/00 Tests

Vehicle	Relative Steering Wheel Intrusion	Phase I	Phase II	Phase III
TG6C0001	0.7175	0.3870	0.1492	0.8001
TG6C0002	0.9553	0.5062	0.1628	0.8606
TG6C0003	0.8677	0.3857	0.1035	0.7395
TG6C0004	1.1418	0.7591	0.2021	0.7275
TG6C0006	0.9816	0.4377	0.1286	0.8195
TG6C0007	0.9175	0.3948	0.0994	0.8266
TG6C0008	0.8048	0.2720	0.1020	0.7881
TG6C0009	0.8977	0.4665	0.1491	0.8256
TG6C0010	0.9380	0.6258	0.1797	0.7958
TG6C0011	0.9052	0.5050	0.1533	0.7366
TG6C0012	0.9321	0.7545	0.2364	0.6803
TG7C0001	1.0544	0.7370	0.2250	0.7096

The values for head restraint performance in phase III clearly indicate that the rebound energies for the head are much more significant than those for the vehicle.
The performance index for phase II is calculated using the peak gradient of the actual energy curve. This value represents the peak power applied to the head and therefore the performance index is the ratio of ideal power to peak actual power. For the vehicles tested the time of occurrence of the peak actual energy gradient (from motion analysis) was compared with the time window found for 36 millisecond Head Injury Criterion (HIC36) for the data obtained from accelerometers mounted at the centre of gravity of the dummy head. The peak energy gradient was always at a time within the HIC36 window, and was typically 5-10 ms after the beginning of the HIC36 window.

It is interesting to look at the relationships between each of the phases for the head restraint.
Figure 7 shows the relationship between phases I and II for head restraint. As a general trend, the better the phase I performance, the better the phase II performance. This indicates that a good performance in phase I acts as a firm basis for a good performance in phase II and a poor performance in phase I makes it difficult to achieve a good performance in phase II.

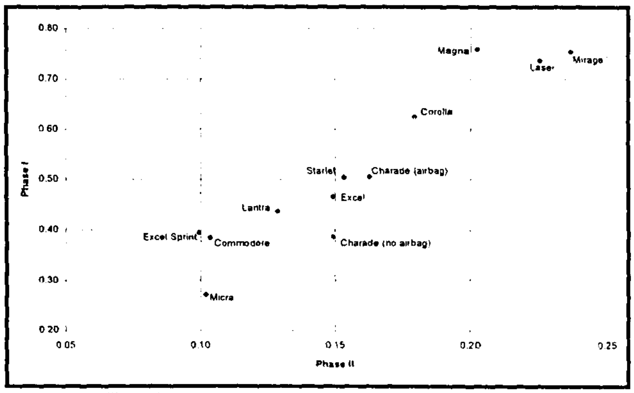

Figure 7. Head Energy Management Indices for phases I and II.

The relationship between phases II and III is shown in Figure 8. The features of most interest in this graph are the results for the Mirage, Magna and Laser. These three vehicles have the best performance indices for phase II and the worst for phase III. This indicates that the power applied to restrain the head was nearer optimum for these three vehicles than the other vehicles, but that the rebound energy was greater (i.e., a more severe rebound). This is in contrast to other airbag vehicles in the sample and may be an indication that the airbags in these vehicles are overpowered, resulting in a favourable HIC result, but a high rebound velocity. If the Magna, Mirage and Laser data are ignored in Figure 8, the general trend relationship between phases II and III is that a good performance in phase II corresponds to a good performance in phase III.

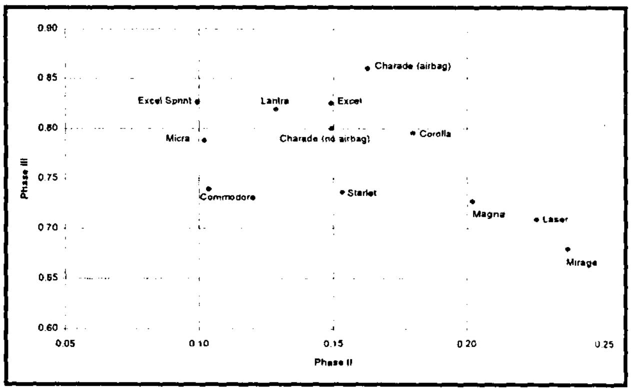

Figure 8. Head Energy Management Indices for phases II and III.

APPLICATION

This vehicle safety analysis method does not give a direct indication of the risk of injury of a given restraint system in a given vehicle. Instead, it quantifies the relationship between the actual restraint performance and an idealised perfect restraint for the physical dimensions of a particular vehicle and a particular test speed. A perfect restraint performance would yield the lowest possible injuries to any occupant. The calculated index gives an assessment of "how close to ideal" a restraint system may be and hence indicates the "room for improvement". This can be used to quantify improvements in restraint for various restraint systems in a given vehicle. It can also be used as a basis for ranking the restraint performances of various vehicles, provided the vehicles are of a similar size.

However, there is a great deal that may be revealed about the relative merits of different aspects of a particular restraint in a particular vehicle. For example, a poor vehicle structure performance and moderate head restraint performance would indicate that the belt and/or airbag system are working reasonably well, and that a more ideal restraint performance would be best achieved by improvements to vehicle crush behaviour.

The performance indices for each of the three phases can also indicate the characteristics that deviate the most from ideal and hence would yield the most benefit from an improvement. For example, a poor result for Phase I for the driver head may indicate excessive belt slack that could benefit from belt pretensioning. A poor result in Phase II is an indication that the restraint is too stiff and this should be targeted for improvement.

Such information is useful to restraint designers and safety performance analysts as it gives an objective reference and/or assessment of improvement with which to work when optimising restraint design.

CONCLUSION

The scientific method for analysing vehicle safety performance outlined in this paper:

1. Can be used to indicate the "room for improvement" of the restraint system and vehicle structure of any given vehicle in a frontal 90° impact against a rigid 0° barrier.
2. Does not directly indicate the injury risk to an occupant.
3. Can facilitate restraint development by indicating the relative merits of various aspects of the restraint system and vehicle structure to indicate the most beneficial area for improvement.

RECOMMENDATIONS

It is intended that this method will undergo further validation by analysing data from a controlled set of experiments.

It would be desirable to extend this method for body parts other than the head, to allow a more complete assessment of the performance of a restraint system.

ACKNOWLEDGEMENTS

Grateful thanks are extended to Brendan Chambers and Robert Judd (Autoliv Australia Pty Ltd) for useful discussions and to John Fabre (Psycorp Pty Ltd) for helpful discussion regarding characterising the actual data with respect to the ideal data. The authors also acknowledge the input from Robyn Attewell (INTSTAT Pty Ltd) for comments on the mathematics of the method, presentation and interpretation of results

DEVELOPMENT OF THE EUROPEAN NEW CAR ASSESSMENT PROGRAMME (EURO NCAP)

C. Adrian Hobbs
Paul J. McDonough
Transport Research Laboratory
United Kingdom
Paper Number 98-S11-O-06

ABSTRACT

For the first time in Europe, comprehensive consumer information on the crash performance of cars has been made available to the public, through the European New Car Assessment Programme (Euro NCAP). Cars have been tested in full scale offset frontal and side impacts and the aggressivity of the car front to pedestrians has been assessed. The test procedures used are based on those developed, by the European Enhanced Vehicle-safety Committee, for legislation in Europe. In order to show how well the car and the recommended child restraints work together, restrained child dummies were seated in the rear of the car, in both the frontal and side impact tests.

An assessment protocol has been developed to provide an objective evaluation of the protection provided by the cars. The assessment protocol uses occupant trajectory, vehicle deformation and inspection data, in addition to the dummy instrumentation data, to provide an evaluation of the protection provided by the car for a range of occupant sizes. This paper outlines the objectives of Euro NCAP and gives details of the test and assessment procedures used. Test results for the completed phases are presented along with the ratings for occupant and pedestrian protection.

INTRODUCTION

Consumer information crash test programmes have proved effective in improving car safety in a number of countries. The European New Car Assessment Programme (Euro NCAP) was developed in the United Kingdom with the aim of bringing about such improvements throughout the European Union. Euro NCAP has grown with sponsorship from other European countries, the European Commission, European consumer groups and international motoring organisations. Euro NCAP carries out frontal, side and pedestrian impact tests and includes an assessment of how well the car and the manufacturer's recommended child restraints protect young children. After initial hostility, most manufacturers have become more positive about Euro NCAP and the industry is now contributing to the development of the programme. More importantly, many manufacturers are responding rapidly by improving their cars and by standardising safety features throughout the European Union. The rate of improvement in occupant protection is such that reductions in car occupant casualties should soon be identifiable in accident statistics. Improvements for the pedestrian are developing more slowly but there is a clear indication that manufacturers are at last taking the protection of pedestrians seriously.

A summary of the results of the first two phases of Euro NCAP tests is given in Appendix I.

EURO NCAP AIMS

Legislative safety standards set a minimum level, below which no car's performance is allowed to fall. However, they provide no incentive to encourage manufacturers to provide higher standards of safety. Manufacturers do respond to consumer demands and, for many years, consumers have been provided with a wealth of information to help them make their choice. Absent from this information has been comprehensive data about the crash performance of cars. Euro NCAP is now starting to provide this information which, in combination with other data, can be used by consumers to help in their car choice. The use by consumers, of crash safety information, provides a strong incentive to manufacturers to improve the safety of their products. Those manufacturers who choose to excel at crash protection, obtain recognition for their efforts and this can result in increased market share.

EURO NCAP INFRASTRUCTURE

Euro NCAP is sponsored by: the European Commission, the governments of the Netherlands, Sweden and the United Kingdom; motoring organisations, through the Alliance International de Tourisme (AIT) and Federation International de l' Automobile (FIA); the German motor club Allgemeiner Deutscher Automobile Club (ADAC) and European consumer groups, through International Testing. Further sponsors are expected to join in the future.

Policy is determined by a Steering Committee, acting through a Secretariat. Technical aspects are dealt with by a Technical Working Group, which is also responsible for rating the cars. Protocols have been developed which detail the testing (1) and assessment procedures (2).

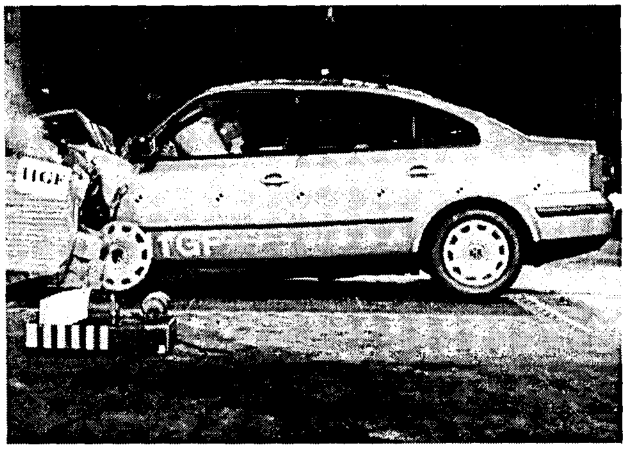

Figure 1. Euro NCAP Offset Deformable Barrier Test at 64 km/h.

Currently, two laboratories carry out the testing: TNO, in the Netherlands and TRL, in the United Kingdom. Vehicle inspections are carried out by Vehicle Safety Consultants. As Euro NCAP grows, it is expected that additional organisations will be approved to carry out the testing and inspection tasks.

CAR SELECTION AND PURCHASE

As the frontal impact test is designed to simulate a car to car impact between two similar cars, car size is not accounted for. Euro NCAP tests and compares cars within size categories. No attempt is made to compare the performance of cars from different size categories. In frontal impacts between heavy and light cars, it is clear that momentum effects favour the occupants of the heavy car. Other characteristics also tend to favour larger cars. However, in impacts with substantial roadside obstacles, the advantages of being in a heavier car are less clear. In side impacts mass has a more limited effect, whereas size, in particular seat height, has a greater effect. In this test, the impact simulates the car being hit by a fixed size of "bullet" car.

Once a size category is chosen for testing, the sponsors choose which cars to include in the programme. With most car models, there are a variety of body style, engine, transmission and safety related options available. Euro NCAP aims to test the variant with the largest sales within the European Union. It is recognised that differences within a model range have some effect on crashworthiness, just as it is recognised that there are differences in the performance of right and left hand drive cars. Euro NCAP can take no account of this. It is a manufacturer's responsibility to ensure that a car's performance is not unduly compromised by such factors.

From the third phase, Euro NCAP will only test cars with safety equipment fitted as standard throughout all fifteen member states of the European Union. However, the manufacturer is given the option of funding additional tests, with optional safety equipment fitted. Manufacturers also have the option to fund tests, if tests on their car are not being funded by Euro NCAP. If a car is updated or superseded, the manufacturer can again fund a set of tests. In these circumstances, Euro NCAP will also publish the results from the tests funded by manufacturers.

No matter how the test is funded, care is taken to ensure that the cars tested are built to normal standards on the usual production line. This is usually achieved by purchasing the cars anonymously, through normal retail outlets. Other methods of selecting a car are possible, provided that Euro NCAP is satisfied that the car has not been specially prepared. Two examples of each car model are obtained. One is used for the frontal impact test and the other is used for the pedestrian tests and then the side impact test.

In both the frontal and side impact tests, child restraints recommended by the car manufacturer are used. Where the manufacturer does not recommend any particular child restraint, locally obtained restraints are used. Euro NCAP aims to encourage car manufacturers to take responsibility for providing good child protection in their cars.

TEST PROCEDURES

Euro NCAP assesses the protection for car occupants, in frontal impact and side impact and the protection afforded by the car's front to pedestrians. The test procedures used are based on those developed by the European Enhanced Vehicle-safety Committee (EEVC), for legislation in Europe. In the frontal and side impact tests, child dummies are installed in child restraints in the rear of the car. The installation and assessment procedures for the child restraints are based on those developed for ECE Regulation 44.03 (3).

Frontal Impact

In the frontal impact test, the car is impacted into an offset deformable barrier (ODB) at 64 km/h. The car is offset so that 40 percent of its width aligns with a deformable honeycomb barrier face mounted on a rigid block (Fig 1). In the front seats of the car are two instrumented Hybrid III dummies. Seated in the rear child restraints are a P1½ and a P3 dummy. With the exception of the impact speed and the presence of the child dummies, the test is the same as that specified in the new European Frontal Impact Directive (4).

Table 1.
Frontal Impact Car to Car Accident Impact Speed Related to the Proportion of Serious and Fatal Casualties Addressed

Accident Impact Speed* km/h	Casualties Addressed AIS≥3
50	Few
55	Just under ½
60	About ⅔

* 55 km/h approximates to an ODB test at 64 km/h

The impact speed of 64 km/h was chosen on the basis of accident analyses carried out for EEVC Working Group 11, which developed the European test procedure. An analysis of available frontal impact accident research concluded that a crash test, which replicated a car to car crash at 55 km/h, would address just under half of the serious and fatal casualties (AIS≥3). Reducing that speed to 50 km/h would address few such casualties, whereas, increasing the speed to 60 km/h would address about two thirds of them (Table 1). No direct comparison exists to relate the impact speed in an ODB test to its equivalent speed in a car to car crash, between similar cars. In the car to car impact, each car has to absorb its own impact energy. In an ODB test, the deformable barrier absorbs some of the impact energy. The amount of energy it absorbs depends upon how the car's structure loads the honeycomb. In comparative tests using a modern family size car, a car to car crash at 55 km/h was more severe than an ODB test at 65 km/h. This car loaded the deformable barrier relatively uniformly, such that the barrier would be quite efficient in absorbing energy. Future car designs are likely to load the deformable barrier at least as well. In this way, the designer can minimise the amount of energy his car has to absorb. Based on the available data, it can be seen that the Euro NCAP frontal impact test speed of 64 km/h is equivalent to a car to car impact at a speed of about 55 km/h.

Side Impact

The Euro NCAP side impact test is similar to that specified in the European Side Impact Directive (5). In the test the car is impacted on the driver's door by a 950 kg mobile deformable barrier (MDB), at 50 km/h (Fig 2). A EUROSID dummy, positioned in the driver's seat, is used to assess the car's performance. Again, child dummies are seated in the rear of the car. Although the European Directive allows different designs of barrier face to be used, Euro NCAP uses the same design for all its tests. Currently, the Cellbond Multi 2000 barrier face is specified.

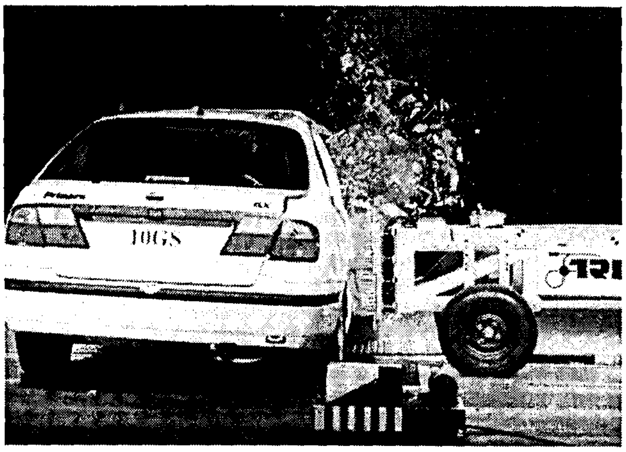

Figure 2. Euro NCAP Mobile Deformable Barrier Side Impact Test at 50 km/h

Child Restraints

In order to ensure consistency in the securing of the child and the restraint, the procedures developed for ECE Regulation 44.03 are used. The force used to install the restraints are limited to those that research has shown are used by parents. Instructions to use abnormal force during installation are ignored. In some cars, the rear seat belts can

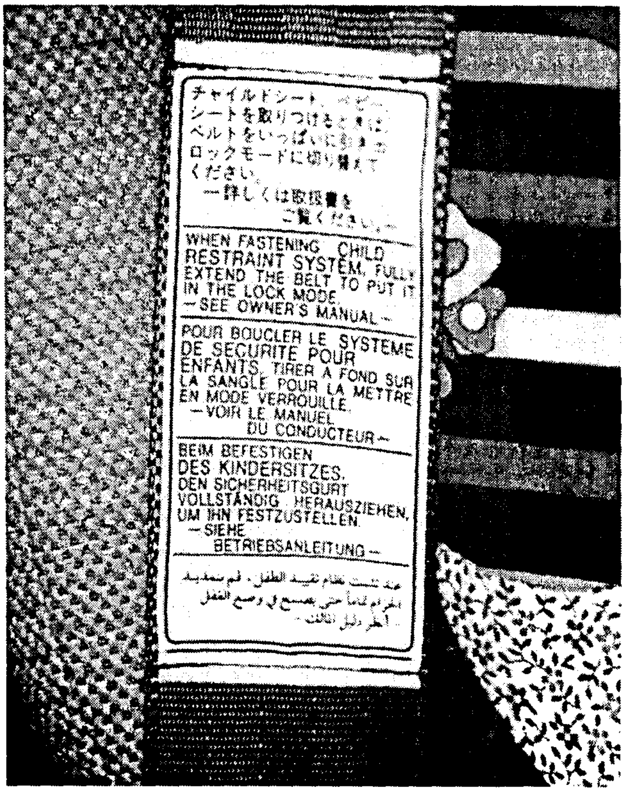
WHEN FASTENING CHILD RESTRAINT SYSTEM, FULLY EXTEND THE BELT TO PUT IT IN THE LOCK MODE
—SEE OWNER'S MANUAL—
POUR BOUCLER LE SYSTEME DE SECURITE POUR ENFANTS, TIRER A FOND SUR LA SANGLE POUR LA METTRE EN MODE VERROUILLE.
—VOIR LE MANUEL DU CONDUCTEUR—
BEIM BEFESTIGEN DES KINDERSITZES, DEN SICHERHEITSGURT VOLLSTÄNDIG HERAUSZIEHEN, UM IHN FESTZUSTELLEN.
—SIEHE BETRIEBSANLEITUNG—

Figure 3. Multi-language Label on Rear Seat Belt Giving Instructions about Use with Child Restraints

be switched from emergency locking to automatic locking mode, for use with child restraints. Euro NCAP only uses such features, if there are clear use instructions on the belt (Fig 3).

The danger associated with the use of rearward facing child restraints, on seats equipped with airbags, is well established. Euro NCAP aims to see this hazard avoided. At some stage in the future, Euro NCAP may downgrade the rating of cars where this hazard exists. To avoid being downrated, cars with passenger seat airbags could be required to have automatic provision to disable the airbag when a child restraint is in place. A less significant downrating may be used where cars that have no automatic system but do have a clearly visible, explicit text warning. Currently, Euro NCAP is reporting what provision exists to avoid this hazard.

Pedestrian Testing

Pedestrian protection is assessed using the procedures recommended by the EEVC, for European legislation. A total of eighteen component tests are performed. Three leg form tests are carried out on the bumper and three upper leg form tests are performed on the bonnet leading edge. Head injury risk is assessed separately for adults and for children. For each, six head impact tests are performed in the relevant parts of the bonnet top area (Fig 4).

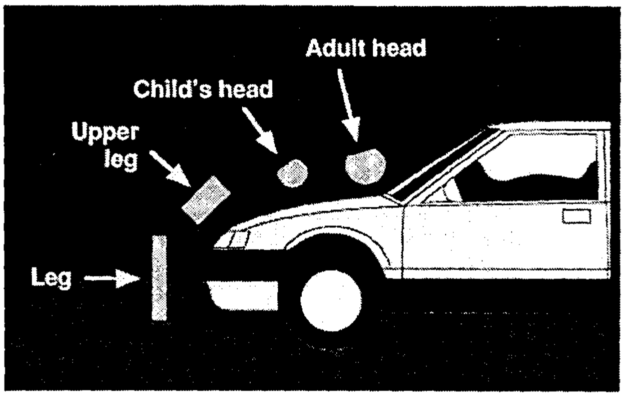

Figure 4. Euro NCAP Pedestrian Body Form Tests

The EEVC procedure requires the assessor to seek out aggressive structures to test. However as most current car designs provide poor protection, Euro NCAP has instigated a change from phase three. To provide a reward to those who make some early improvement, manufacturers are allowed to choose nearly one half of the test sites. This enables them to benefit from areas that they have improved.

ASSESSMENT PROCEDURES

Frontal and Side Impact

In the frontal and side impact tests, fiftieth percentile male dummies are used, in the standard seating position. In the frontal test, the measured data is adjusted by the use of "modifiers" to extend the applicability of the assessment to different sized occupants and those sitting in different seating positions. Modifiers are also used in some cases where the dummies have no relevant instrumentation. Although the same concerns apply to some aspects of the side impact test, no methods have currently been developed to properly modify the side impact dummy data. After each test, the cars are measured and given a detailed examination. This examination provides the information upon which the modifiers are based.

The first stage of the assessment is based on the dummy data and deformation measurements. In the case of the frontal impacts, the modifiers are applied to the rating for the most relevant body region.

In the frontal and side impact tests, the rating for each body region falls within a colour coded band. These bands are coloured green, for best performance, through yellow, orange and brown, to red for worst performance (Table 2). In most cases, the boundaries between the brown and red bands are the criteria established by the EEVC. Where possible, the boundary between the green and yellow bands is set at the five percent probability level, for the same injury. Where there was no data to establish this boundary, it was set pragmatically, following discussions with industry representatives.

Table 2
Individual Body Region Rating in Frontal and Side Impact

Rating	Colour Code	Points Phases 1-2	Points Phases 3 >
Good	Green	4	4.00
Adequate	Yellow	3	2.67-3.99
Marginal	Orange	2	1.33-2.66
Weak	Brown	1	0.01-1.32
Poor	Red	0	0.00

After the modifiers are applied, an overall rating is established for frontal and side impact. For this purpose, body regions are grouped together and the rating for the grouped region is that of the worst performing sub-region. The grouped body regions are:

FRONTAL IMPACT
- Head and Neck
- Chest
- Knee, femur and Hip
- Leg, Foot and Ankle

SIDE IMPACT
- Head
- Chest
- Abdomen
- Pelvis

For each of these body regions points are awarded: four points for green down to zero points for red. In the first two phases of Euro NCAP, there were step changes in the points scale between the green/yellow and brown/red boundaries. From phase three, a linear scale has been adopted. In order to generate the final rating, the points for the two driver dummies are totalled and converted into a star rating (Table 3). If in the frontal impact, any part of the passenger obtains a lower score than for the driver, the passenger's score for that body region is used in the overall rating. A maximum score of 32 points is possible, for frontal and side impact protection.

Table 3
Conversion from Points to Overall Star Rating for Frontal and Side Impact

Star Rating	Points
★★★★	25 - 32
★★★	17 - 24
★★	9 -16
★	1 - 8
No Star	0

No attempt is made to weight the injury parameters on the basis of importance and no attempt is made to convert the test findings into measures of injury risk. It would be possible to apply different weights to life threatening and disabling injuries. This could also be done for severe and slight injuries and for frequently occurring and infrequently occurring injuries. However, it is unlikely that general agreement could be obtained for such weighting values. For example, individuals are more likely to be concerned about severity than frequency, whereas society has concerns for frequent and therefore costly injuries.

For conversions between test measurements and injury risk to be made, it is necessary for injury mechanisms to remain broadly similar. For car occupants, injury mechanisms have changed significantly in the recent past and can be expected to change in the future. It would, for example, be inappropriate to apply old data on injuries arising from hard contact with intrusion, to test data where the occupant loading came solely from the restraint system.

Euro NCAP makes no attempt to make such conversions. It simply presents the data on the basis of performance in crash tests. The intention is to encourage manufacturers to make improvements in all areas and to avoid concentrating attention on any individual area of the car.

Struck Through Stars

A change, introduced in phase three, results from concern that some cars are obtaining a relatively good final rating, despite poor performance in individual important body regions. This has most frequently been seen in the side impacts, where the chest was poorly protected. This concern is indicated by the final star being struck through, where the dummy data justifies a red rating, for a body region where fatal injuries are possible. These body regions are the head and chest, in frontal impact and the head, chest, abdomen and pelvis, in side impact.

Frontal Impact Injury Parameters

The measured parameters used in the frontal impact assessment are:

HEAD
- HIC_{36}
- Resultant acceleration, 3 msec exceedence

Note: Where there is no hard contact the rating is green

NECK
- Shear
- Tension
- Extension

CHEST
- Compression
- Viscous Criterion

UPPER LEG
- Femur force
- Knee slider

LOWER LEG
- Tibia Index
- Tibia compression

FOOT & ANKLE

Brake pedal rearward displacement

Footwell intrusion (not yet implemented)

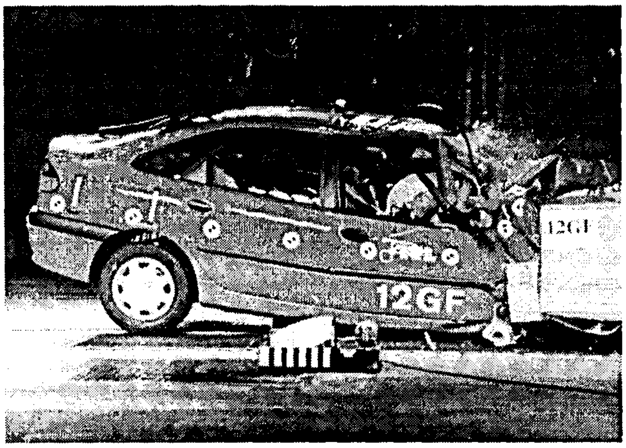

Figure 5. Unstable Head Contact on the Driver's Airbag.

Frontal Impact Modifiers

The measured parameters are adjusted, where necessary, by modifiers. In addition to their other functions, the modifiers allow some account to be taken of small vehicle and impact variations. Each modifier may reduce the score, for a body region by one or two points. These penalties are cumulative, but for any body region the maximum penalty is limited to two points. The frontal impact modifiers are:

HEAD

Unstable airbag head contact or airbag missed (-1 point)

If the centre of gravity of the head moves laterally outside the outer edge of the airbag, during the head's forward motion, contact is said to be unstable. In these circumstances, there is concern that the airbag might fail to protect in slightly different impact situations (Fig 5).

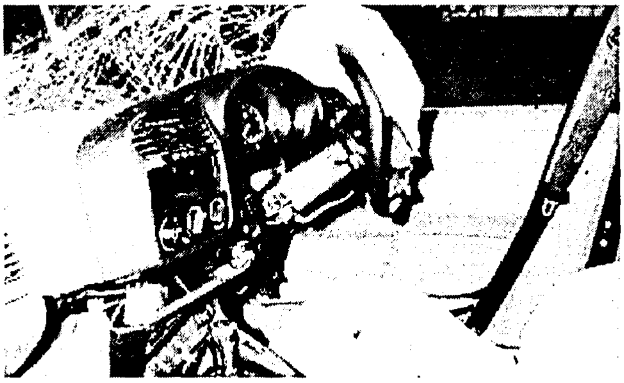

Figure 6. Steering Wheel Bent from Driver Chest Contact.

Steering wheel displacement > 80mm upwards or 100mm rearwards (0 points up to 10% below both limits to -1 point from 10% above either limit*)

This requirement is intended to help ensure that the airbag launch platform remains near to the design position

CHEST

Chest contact with the steering wheel (-1 point)

Direct chest loading from the steering wheel is poses an increased risk of injury (Fig 6).

A pillar displaced rearwards (0 points up to 100mm to –2 points from 200mm*)

A pillar displacement is used as an indicator of facia level intrusion. Intrusion is highly correlated with injury risk

Passenger compartment integrity (-1 point)

Where the passenger compartment becomes unstable, due to overloading, intrusion is likely to increase rapidly for small increases in impact severity and the repeatability is expected to be poor (Fig 7).

UPPER LEG

Stiffer structures in the knee impact area (-1 point)

The dummy's knees are set to a fixed spacing. Human occupants might sit with their knees in a variety of positions. If stiffer structures were impacted, knee loads would be greater (Fig 8).

Concentrated loading on the knee (-1 point)

Instrumentation in the upper leg check the protection for the femur, hip joint and pelvis. There is no

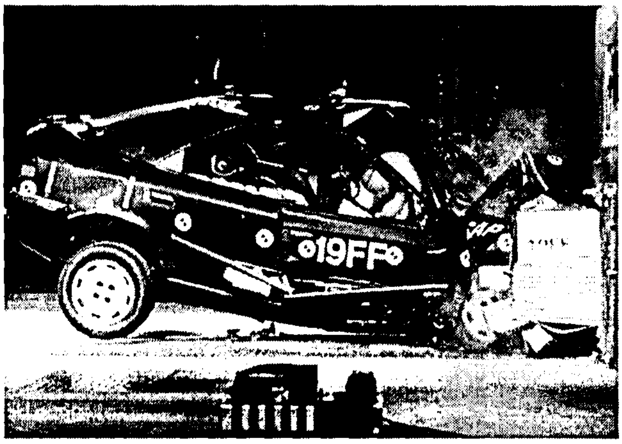

Figure 7. Loss of Passenger Compartment Integrity due to Overloading.

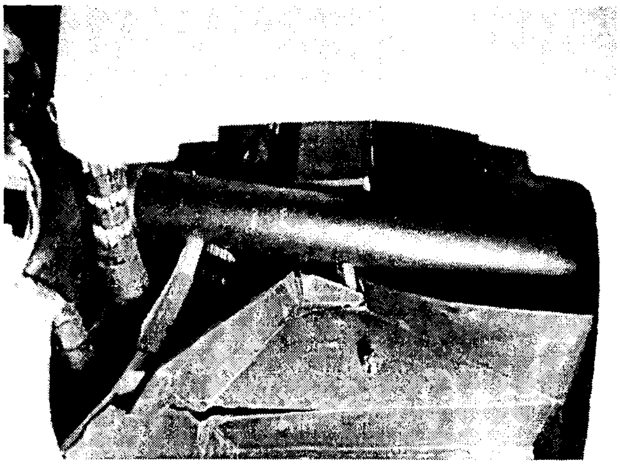

Figure 8. Steering Column Support in the Knee Impact Area Increases the Risk of Injury.

instrumentation to assess the risk to the knee from direct concentrated loading. Concentrated loading can injure the knee itself (Fig 9).

LOWER LEG

Upward brake pedal displacement > 80mm (0 points up to 10% below the limit to –1 point from 10% above the limit*)

Where the brake pedal is displaced upwards, the end of the pedal may impale the leg.

FOOT & ANKLE

Rupture of the footwell (-1 point)

Where there is significant rupture of the footwell area, there is an increased risk of injury from possible ingress of external objects

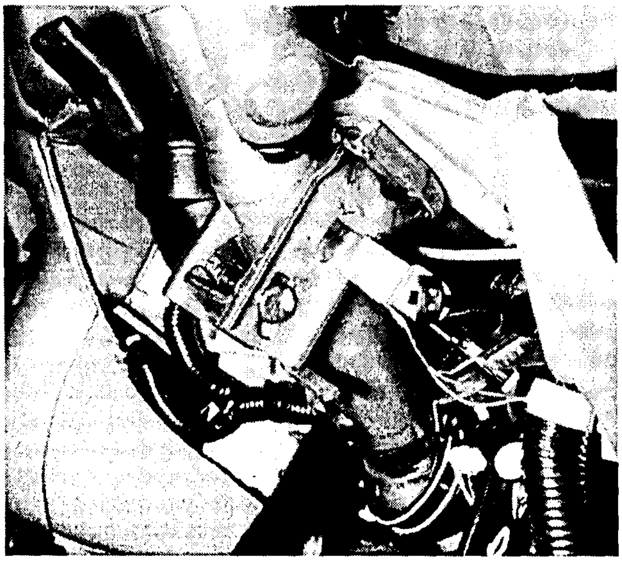

Figure 9. Column Adjuster Bracket Could Concentrate Loading on Part of the Knee.

* These assessments have changed slightly following the adoption of sliding scales for Phase 3.

Side Impact Injury Parameters

The measured parameters used in the side impact assessment are:

HEAD
HIC_{36}
Resultant acceleration, 3 msec exceedence
Note: Where there is no hard contact the rating is green

CHEST
Compression
Viscous Criterion

ABDOMEN
Total abdominal force

PELVIS
Pubic symphysis force

Note: No modifiers are applied in side impact.

Child Injury Parameters

The assessment of child protection has developed through the early phases of Euro NCAP. Currently, the child protection assessment is not included within the overall assessment of occupant protection. The child protection parameters are:

Frontal Impact

1½ year old (P1½ dummy) and 3 year old (P3 dummy)

HEAD
Forward head excursion

NECK
Head vertical acceleration (P1½ only)

CHEST
Resultant acceleration
Vertical acceleration

Side Impact

1½ year old (P1½ dummy) and 3 year old (P3 dummy)

HEAD
Containment within the child restraint
Resultant acceleration, 3 msec exceedence

Pedestrian Injury Parameters

With the current level of pedestrian protection provided by most cars, it would be inappropriate to use the proposed EEVC requirements as a lower performance boundary along with an additional higher performance boundary. So that differences between cars can be identified and to increase the incentive for manufacturers, Euro NCAP, uses the EEVC limits as the upper performance boundary and has generated an additional lower performance boundary. During the first two phases, this lower boundary was taken to be the median of the results from test sites which failed to meet the EEVC limits. From phase three, the lower limits have been fixed. The parameters used to assess pedestrian protection are:

ADULT AND CHILD HEAD FORM
HIC_{36}

UPPER LEG FORM
Bending Moment
Sum of Forces

LEG FORM
Tibia Acceleration
Knee shear displacement
Knee bending angle

Each of the eighteen individual test sites are rated and awarded up to two points (Table 4). The points are then totalled, to obtain the overall star rating (Table 5). A problem arises when there is insufficient space to carry out the adult head impacts. For this reason, there have been small differences in the rating procedures used for each of the early phases.

Details of the assessment criteria are given in Appendix II.

Table 4
Pedestrian Body Form Ratings*

Rating	Colour Code	Points
Fair	Green	2.00
Weak	Yellow	0.01-1.99
Poor	Red	0.00

* This rating is for Phase 3 onwards. Slight differences exist for Phases 1 and 2.

Table 5
Conversion from Points to Overall Star Rating for Pedestrian Body Form Impacts*

Star Rating	Points
★★★★	28 - 36
★★★	19 - 27
★★	10 - 18
★	1 - 9
No Star	0

* This rating is for Phase 3 onwards. Slight differences exist for Phases 1 and 2.

MANUFACTURER INVOLVEMENT

When a decision has been made to test a particular size category of car, each manufacturer marketing a car in that size category is advised that his car might be chosen for test. The biggest selling variant is identified and the manufacturer is asked to confirm this. For those models selected for test, the manufacturer is asked what safety equipment is fitted as standard, on that variant, in all the fifteen member states of the European Union. As Euro NCAP only selects standard fit safety equipment, the manufacturer is given the option to fund additional tests on cars with optional safety equipment. If Euro NCAP decides not to include a car, again the manufacturer has the option of funding the tests. Whoever funds the test, Euro NCAP will publish the results.

Each manufacturer is asked to supply test set up data and they are invited to witness the set up and the test. They are asked to confirm that they are satisfied that both were carried out correctly. Following the test, they are supplied with a complete set of data and asked to report any concerns to the test laboratory.

When the assessment has been completed, the manufacturer is invited to a meeting to discuss the results of the tests, the inspection findings and to be advised of the assessment. The purpose of the meeting is to ensure that there were no undetected problems that might invalidate the rating. If there are concerns, manufacturers are invited to provide comparative data. This data is not published, nor is it intended to be used to modify the results from the Euro NCAP test. If problems cannot be resolved, the possibility exists for a further test to be performed, either at the expense of Euro NCAP or the manufacturer. Where a repeat test is carried out, the rating will be based on the results from that test alone. The manufacturer does not have the option to choose which data are published. The meeting is also used to discuss what data the manufacturer might be prepared to supply, for possible future developments of Euro NCAP.

In general, the data provided by manufacturers has shown that the test procedures have good repeatability. Where there have been differences between the manufacturer's and Euro NCAP's data, they can usually be explained. Loss of integrity of the passenger compartment, in frontal impact, is most commonly associated differences in deformation extent. This was expected and was one of the reasons for the inclusion of this criterion. In side impact, variations in the distribution of rib loading can often be related to small areas of stiff structure that load the chest slightly differently.

MEETINGS WITH THE MOTOR INDUSTRY

The Technical Working Group has regular meetings with the industry. Formally, it is through these meetings that information exchanges between Euro NCAP and the industry take place. Any manufacturer can be represented at these meetings, through their appropriate association. Initially these meetings were hostile, with industry representatives arguing against the existence of Euro NCAP. Over time the meetings have developed and have now become very useful. Euro NCAP seeks the industry views on its testing and assessment procedures and from this, a number of useful improvements have been made.

FUTURE DEVELOPMENTS

Although the test procedures used by Euro NCAP are comprehensive, they cannot fully assess the protection provided by a car. There are some particular deficiencies that Euro NCAP would like to address. It has always been recognised that the European side impact test does not adequately assess the protection provided for the head. Usually the head only impacts the side glass and possibly the B pillar. No assessment is made of the risk of injury from other parts of the car's interior or from structures outside the car. With the introduction of head protecting side impact airbags, Euro NCAP needs to be able to give due credit for effective systems. Consideration is currently being given to how this might be achieved. No such procedures exist to extend the applicability of the side impact results to different sized occupants and seating positions. What is clear is that some manufacturers are developing much of their protection to suit the standard seating position. There is also concern over the installation of "pelvis pushers," some of which may be used to unload the dummy's chest, in a manner that might not work for a human occupant. Euro NCAP may try to measure the shear force transmitted up the spine, with a view to developing a limit for it, in the future. When more is known about what influences Compatibility and when techniques are available to measure it, Euro NCAP would expect to adopt them. As car safety develops, it will be necessary for Euro NCAP to develop, whilst providing a consistent and stable environment for manufacturers to work within.

CRITICISMS OF EURO NCAP

As with other consumer information crash test programmes, the industry has voiced many criticisms of Euro NCAP. Although there has been substance to some of these, many have been unfounded or based on misunderstandings. Perhaps the most valid criticism is that Euro NCAP has not yet been able to test every available make of car, in a chosen size category. As funding increases, from additional sponsors, more cars can be tested and more complete coverage should be possible. As new models are launched, they may be tested, with their results added to that already published.

There has been criticism that only three test procedures are used, when car manufacturers test with many different configurations. Manufacturers do need to test using a range of impact configurations, if they are to ensure that their safety systems work correctly. Those who do this satisfactorily should produce cars that perform well in the Euro NCAP tests. Unfortunately, not all manufacturers carry out such extensive test programmes and the results of their tests are not available to the consumer.

It has been suggested that a frontal impact test speed of 64 km/h is unfair to large cars, because a smaller proportion of their kinetic energy can be absorbed by the deformable barrier face and because they will frequently impact lower mass cars. Such a test speed will make the cars stiffer and more aggressive to other cars. However, the deformable barrier face was introduced to overcome problems generated from the use of a rigid barrier. The deformable barrier test creates its own new problems but these have been minimised by limiting its depth and energy absorption capability. If large cars were to be tested at a lower speed, their ability to protect in the many crashes into immovable roadside obstacles would be reduced.

One reason for the development of the deformable barrier test was to highlight the problems caused by very non-homogenous front structures. Research is showing that such geometrical factors have a dominant influence over compatibility. In the short term at least, it is expected that the benefits from designing for the deformable barrier will outweigh any possible disadvantages of designing for the higher test speed. For the car's own occupants, there are clear advantages from testing at this speed.

There has been some concern over the subjective assessment used in the generation of some of the modifiers. In particular, those for passenger compartment integrity and the knee impact areas. Wherever possible, a clear objective definition has been given for each modifier. Where this has not been possible, a list of the aspects considered has been detailed. In most cases, the assessment is clear and unquestioned. In borderline cases, the manufacturer would be given the benefit of the doubt.

EURO NCAP TEST PHASES

The first phase of Euro NCAP covered seven cars in the supermini category. The results of these tests were published in February 1997. The second phase included tests on thirteen family cars and was published in July 1997. Small family cars have been tested for phase three, with the results being published in May 1998. Phase four will follow, with publication in September 1998, and will cover executive cars. Beyond that, additional phases and tests of models, which were not tested in the first four phases, are planned.

MANUFACTURER RESPONSE

From its first announcement, Euro NCAP has created a positive response from most manufacturers. They have immediately tried to make improvements to existing models and have increased the safety specifications of new designs. The rate of improvement has far exceeded expectations and the introduction of improvements has created problems for Euro NCAP regarding when cars are bought for testing. In a significant number of cases, optional safety equipment has been made standard throughout the European Union. In private discussions, many manufacturers state that a design requirement for new models is that the car will obtain four stars for occupant protection. This situation for pedestrians is not quite so good. However, it is clear that a number of manufacturers are taking positive steps towards improved pedestrian protection.

A number of manufacturers have also opted to fund Euro NCAP tests, either of new cars models or of cars with additional safety equipment. In some cases, manufacturers have requested that cars are tested in time for the results to be used when the car is first launched. Such arrangements are possible, provided that the cars meet the Euro NCAP requirements regarding how the cars for testing are obtained.

CONCLUSIONS

Euro NCAP was established to bring the benefits of consumer crash testing to the whole of Europe. Despite objections, the industry has responded by making rapid improvements to the cars they produce. Although some manufacturers are still negative about the programme, many others are positive. They have identified the marketing advantages which can be obtained by performing well and they appear determined to take advantage of them. There are still improvements which are necessary and difficult decisions have to be taken about how they can be incorporated. It can already be seen that the Euro NCAP tests have been accepted by most as the tests which are setting the standard for future crash protection. This places a great responsibility upon Euro NCAP to ensure that its requirements are both well founded and effective.

ACKNOWLEDGEMENTS

The assistance is gratefully acknowledged of the Euro NCAP Technical Working Group and particularly Vehicle Safety Consultants, funded by International Testing, in developing the Euro NCAP procedures.

REFERENCES

1 Williams, D A, and C C Parkin, *European New Car Assessment Programme (Euro NCAP) - Testing Protocol, Version 1.3*, Unpublished Project Report PR/SE/249/97, Transport Research Laboratory, 1997.

2 Hobbs, C A, P F Gloyns and S J Rattenbury, *European New Car Assessment Programme (Euro NCAP) - Assessment Protocol and Biomechanical Limits, Version 1.0*, Unpublished Project Report PR/SE/245/97, Transport Research Laboratory, 1997.

3 Economic Commission for Europe, *Regulation No 44.03 Uniform Provisions Concerning the Approval of Restraining Devices for Child Occupants of Power-driven Vehicles ("Child Restraint System")*, United Nations, Geneva 1996.

4 The European Commission, *Directive 96/97/EC of the European Parliament and of the Council of 16 December 1996 - On the Protection of Occupants of Motor Vehicles in the Event of a Frontal Impact and Amending Directive 70/156/EEC*, The European Commission, Brussels, 1997.

5 The European Commission, *Directive 96/27/EC of the European Parliament and of the Council of 20 May 1996 - On the Protection of Occupants of Motor*

Vehicles in the Event of a Side Impact and Amending Directive 70/156/EEC, The European Commission, Brussels, 1996.

© Copyright TRL Limited 1998. This paper has been produced by the Transport Research Laboratory, as part of a contract placed by the Department of the Environment, Transport and the Regions. Any views expressed are not necessarily those of the Department. Extracts from the text may be reproduced, except for commercial purposes, provided the source is acknowledged.

APPENDIX I

SUMMARY RESULTS FROM EURO NCAP PHASE 1 SUPER-MINIS

Fiat Punto		Occupant		Pedestrian
Overall Rating		★★		★
Frontal and Side Impact Rating by Body Region				
Frontal Impact			Side Impact	
	Driver	F Pass		Driver
Head/Neck	**Marginal**	**Good**	Head	**Good**
Chest	**Weak**	**Adequate**	Chest	**Weak**
Upper Leg	**Weak**	**Good**	Abdomen	**Adequate**
Leg/Foot	**Poor**	**Adequate**	Pelvis	

Ford Fiesta		Occupant		Pedestrian
Overall Rating		★★★		★
Frontal and Side Impact Rating by Body Region				
Frontal Impact			Side Impact	
	Driver	F Pass		Driver
Head/Neck	**Adequate**	**Good**	Head	**Good**
Chest	**Marginal**	**Adequate**	Chest	**Weak**
Upper Leg	**Marginal**	**Adequate**	Abdomen	**Good**
Leg/Foot	**Weak**	**Good**	Pelvis	

Nissan Micra		Occupant		Pedestrian
Overall Rating		★★		★★
Frontal and Side Impact Rating by Body Region				
Frontal Impact			Side Impact	
	Driver	F Pass		Driver
Head/Neck	**Good**	**Good**	Head	**Good**
Chest	**Marginal**	**Adequate**	Chest	**Adequate**
Upper Leg	**Poor**	**Good**	Abdomen	**Poor**
Leg/Foot	**Poor**	**Good**	Pelvis	**Adequate**

Renault Clio		Occupant		Pedestrian
Overall Rating		★★		★
Frontal and Side Impact Rating by Body Region				
Frontal Impact			Side Impact	
	Driver	F Pass		Driver
Head/Neck	**Marginal**	**Good**	Head	**Good**
Chest	**Weak**	**Adequate**	Chest	**Poor**
Upper Leg	**Poor**	**Good**	Abdomen	**Marginal**
Leg/Foot	**Weak**	**Adequate**	Pelvis	

Rover 100		Occupant		Pedestrian
Overall Rating		★		★★
Frontal and Side Impact Rating by Body Region				
Frontal Impact			Side Impact	
	Driver	F Pass		Driver
Head/Neck	**Poor**	**Good**	Head	**Good**
Chest	**Weak**	**Good**	Chest	**Poor**
Upper Leg	**Poor**	**Adequate**	Abdomen	**Poor**
Leg/Foot	**Poor**	**Good**	Pelvis	**Adequate**

Vauxhall/Opel Corsa	Occupant	Pedestrian		
Overall Rating	★★	★		
Frontal and Side Impact Rating by Body Region				
Frontal Impact			Side Impact	
	Driver	F Pass		Driver
Head/Neck	**Adequate**	**Poor**	Head	**Good**
Chest	**Marginal**	**Adequate**	Chest	**Adequate**
Upper Leg	**Poor**	**Weak**	Abdomen	**Weak**
Leg/Foot	**Marginal**	**Adequate**	Pelvis	

VW Polo	Occupant	Pedestrian		
Overall Rating	★★★	★		
Frontal and Side Impact Rating by Body Region				
Frontal Impact			Side Impact	
	Driver	F Pass		Driver
Head/Neck	**Adequate**	**Good**	Head	**Good**
Chest	**Marginal**	**Adequate**	Chest	**Poor**
Upper Leg	**Adequate**	**Good**	Abdomen	**Adequate**
Leg/Foot	**Poor**	**Good**	Pelvis	**Adequate**

SUMMARY RESULTS FROM EURO NCAP PHASE 2 FAMILY CARS

Audi A4	Occupant	Pedestrian		
Overall Rating	★★	★★		
Frontal and Side Impact Rating by Body Region				
Frontal Impact			Side Impact	
	Driver	F Pass		Driver
Head/Neck	**Good**	**Good**	Head	**Good**
Chest	**Weak**	**Marginal**	Chest	**Poor**
Upper Leg	**Weak**	**Good**	Abdomen	**Adequate**
Leg/Foot	**Poor**	**Adequate**	Pelvis	**Adequate**

BMW 3 Series	Occupant	Pedestrian		
Overall Rating	★★	★★		
Frontal and Side Impact Rating by Body Region				
Frontal Impact			Side Impact	
	Driver	F Pass		Driver
Head/Neck	**Marginal**	**Good**	Head	**Good**
Chest	**Poor**	**Marginal**	Chest	**Weak**
Upper Leg	**Poor**	**Good**	Abdomen	**Poor**
Leg/Foot	**Poor**	**Good**	Pelvis	**Good**

Citroen Xantia	Occupant	Pedestrian		
Overall Rating	★★	★		
Frontal and Side Impact Rating by Body Region				
Frontal Impact			Side Impact	
	Driver	F Pass		Driver
Head/Neck	**Marginal**	**Good**	Head	**Poor**
Chest	**Weak**	**Marginal**	Chest	**Poor**
Upper Leg	**Poor**	**Good**	Abdomen	**Marginal**
Leg/Foot	**Poor**	**Adequate**	Pelvis	**Good**

Ford Mondeo	Occupant	Pedestrian		
Overall Rating	★★★	★★		
Frontal and Side Impact Rating by Body Region				
Frontal Impact			Side Impact	
	Driver	F Pass		Driver
Head/Neck	**Good**	**Good**	Head	**Good**
Chest	**Weak**	**Marginal**	Chest	**Poor**
Upper Leg	**Poor**	**Good**	Abdomen	**Good**
Leg/Foot	**Poor**	**Adequate**	Pelvis	**Good**

Mercedes Benz C Class	Occupant	Pedestrian
Overall Rating	★★	★★

Frontal and Side Impact Rating by Body Region				
Frontal Impact			Side Impact	
	Driver	F Pass		Driver
Head/Neck	**Adequate**	**Good**	Head	**Good**
Chest	**Weak**	**Marginal**	Chest	**Weak**
Upper Leg	**Poor**	**Good**	Abdomen	**Marginal**
Leg/Foot	**Poor**	**Adequate**	Pelvis	**Good**

Renault Laguna	Occupant	Pedestrian
Overall Rating	★★★	★★

Frontal and Side Impact Rating by Body Region				
Frontal Impact			Side Impact	
	Driver	F Pass		Driver
Head/Neck	**Adequate**	**Good**	Head	**Good**
Chest	**Adequate**	**Good**	Chest	**Poor**
Upper Leg	**Poor**	**Good**	Abdomen	**Adequate**
Leg/Foot	**Poor**	**Adequate**	Pelvis	**Good**

Nissan Primera	Occupant	Pedestrian
Overall Rating	★★★	★★

Frontal and Side Impact Rating by Body Region				
Frontal Impact			Side Impact	
	Driver	F Pass		Driver
Head/Neck	**Good**	**Good**	Head	**Good**
Chest	**Adequate**	**Marginal**	Chest	**Weak**
Upper Leg	**Marginal**	**Good**	Abdomen	**Adequate**
Leg/Foot	**Poor**	**Good**	Pelvis	**Adequate**

Rover 600	Occupant	Pedestrian
Overall Rating	★★	★★

Frontal and Side Impact Rating by Body Region				
Frontal Impact			Side Impact	
	Driver	F Pass		Driver
Head/Neck	**Adequate**	**Good**	Head	**Good**
Chest	**Poor**	**Adequate**	Chest	**Poor**
Upper Leg	**Poor**	**Good**	Abdomen	**Poor**
Leg/Foot	**Poor**	**Adequate**	Pelvis	**Good**

Peugeot 406	Occupant	Pedestrian
Overall Rating	★★	★★

Frontal and Side Impact Rating by Body Region				
Frontal Impact			Side Impact	
	Driver	F Pass		Driver
Head/Neck	**Adequate**	**Good**	Head	**Good**
Chest	**Marginal**	**Marginal**	Chest	**Weak**
Upper Leg	**Poor**	**Good**	Abdomen	**Good**
Leg/Foot	**Poor**	**Good**	Pelvis	**Marginal**

Saab 900	Occupant	Pedestrian
Overall Rating	★★	★★

Frontal and Side Impact Rating by Body Region				
Frontal Impact			Side Impact	
	Driver	F Pass		Driver
Head/Neck	**Adequate**	**Good**	Head	**Good**
Chest	**Poor**	**Marginal**	Chest	**Poor**
Upper Leg	**Weak**	**Good**	Abdomen	**Weak**
Leg/Foot	**Weak**	**Good**	Pelvis	**Adequate**

Vauxhall/Opel Vectra	Occupant	Pedestrian
Overall Rating	★★★	★★

Frontal and Side Impact Rating by Body Region				
Frontal Impact			Side Impact	
	Driver	F Pass		Driver
Head/Neck	**Adequate**	**Good**	Head	**Good**
Chest	**Marginal**	**Weak**	Chest	**Poor**
Upper Leg	**Good**	**Good**	Abdomen	**Marginal**
Leg/Foot	**Poor**	**Adequate**	Pelvis	**Good**

VW Passat	Occupant	Pedestrian
Overall Rating	★★★	★★

Frontal and Side Impact Rating by Body Region				
Frontal Impact			Side Impact	
	Driver	F Pass		Driver
Head/Neck	**Adequate**	**Good**	Head	**Good**
Chest	**Good**	**Marginal**	Chest	**Adequate**
Upper Leg	**Marginal**	**Adequate**	Abdomen	**Weak**
Leg/Foot	**Poor**	**Adequate**	Pelvis	**Adequate**

Volvo S40	Occupant	Pedestrian
Overall Rating	★★★★	★★

Frontal and Side Impact Rating by Body Region				
Frontal Impact			Side Impact	
	Driver	F Pass		Driver
Head/Neck	**Good**	**Good**	Head	**Good**
Chest	**Marginal**	**Marginal**	Chest	**Adequate**
Upper Leg	**Good**	**Good**	Abdomen	**Adequate**
Leg/Foot	**Marginal**	**Good**	Pelvis	**Adequate**

Note: The ratings used in Phases 1 and 2 are slightly different from those adopted for Phase 3 onwards.

APPENDIX II

Injury Parameters

The main injury parameters are based on biomechanical data. Others use vehicle deformation data. For frontal and side impact a lower performance boundary has been set at the limits proposed by EEVC. An upper performance boundary has also been set. Where possible, this has been set to the five percent probability level, for the same injury. The lower performance boundary is the point at which the rating changes from Poor (Red) to Weak (Brown). The upper performance boundary is at the point at which the rating changes from Adequate (Yellow) to Good (Green).

For pedestrian protection, the EEVC limits are used for the upper performance boundary with a lower limit generally set at around the average value for cars in phases one and two.

Frontal Impact Performance Boundaries

Head	Lower	Upper
HIC_{36}	1000	650
Res acc (3 msec)*	72 g	88 g

* This criterion has changed slightly, with the adoption of sliding scales for phase three.

Neck	Lower	Upper
Shear	3.1 kN @ 0 msec 1.5 kN @ 25 – 35 msec 1.1 kN @ from 45 msec	1.9 kN @ 0 msec 1.2 kN @ 25 - 35 msec 1.1 kN @ from 45 msec
Tension	3.3 kN @ 0 msec 2.9 kN @ 35 msec 1.1 kN @ from 60 msec	2.7 kN @ 0 msec 2.3 kN @ 35 msec 1.1 kN @ from 60 msec
Extension	57 Nm	42 Nm

Chest	Lower	Upper
Compression	50 mm	22 mm
Viscous Criterion	1.0 m/sec	0.5 m/sec

Upper Leg	Lower	Upper
Femur force	9.07 kN @ 0 msec 7.56 kN @ from 10 msec	3.8 kN
Knee slider	15 mm	6 mm

Lower Leg	Lower	Upper
Tibia Index	1.3	0.4
Tibia compression	8 kN	2 kN

Foot & Ankle	Lower	Upper
Brake pedal rearward displacement	200 mm	100 mm
Footwell intrusion**	200 mm	100 mm

** This criterion has not yet been implemented

Side Impact Performance Boundaries

Head	Lower	Upper
HIC_{36}	1000	650
Res acc (3 msec)*	72 g	88 g

* This criterion has changed slightly, with the adoption of sliding scales for phase three.

Chest	Lower	Upper
Compression	42 mm	22 mm
Viscous Criterion	1.0 m/sec	0.32 m/sec

Abdomen	Lower	Upper
Total Force	2.5 kN	1.0 kN

Pelvis	Lower	Upper
Pubic Symphysis Force	6.0 kN	3.0 kN

Child Injury Performance Boundaries

Frontal Impact

Head	Lower	Upper
Forward Excursion (forward facing) (rearward facing)	550 mm* 600 mm**	550 mm* 600 mm**

* and shall not contact the car interior

** no compression load is to be imposed on the crown of the head

Neck	Lower	Upper
Head Vert Comp Acc (3 msec)*	None	20g

* P1½ dummy only

Chest	Lower	Upper
Resultant Acceleration	55 g	41 g
Vertical Acceleration	30 g	23 g

Side Impact

Head	Lower	Upper
Containment	None	Within the restraint
Res acc (3 msec)	None	80 g

Pedestrian Injury Parameters

Head Form	Lower*	Upper
HIC_{36}	1500	1000

Upper Leg Form	Lower*	Upper
Bending Moment	400 Nm	220 Nm
Sum of Forces	7.0 kN	4.0 kN

Leg Form	Lower*	Upper
Tibia Acceleration	230 g	150 g
Knee Shear Displacement	7.5 mm	6 mm
Knee Bending Angle	30°	15°

OBJECTIVES AND EXPERIENCE OF PUBLISHING CRASH-TESTS RESULTS IN A EUROPEAN MAGAZIN

Alexander Gulde
Dr. Lothar Wech
TÜV Automotive GmbH, Group TÜV Süddeutschland
Bernd Ostmann
auto motor und sport
Germany
Paper Number 98-S11-O-07

ABSTRACT

Since 1990, "auto motor und sport" has published the results of over 70 crash tests. All tests were carried out under extremely realistic conditions with the aid of the TÜV Süddeutschland ECV system. The main advantage of this system is that the test vehicles are driven under their own engine power. A 50% offset collision into a 15° angled solid barrier at a speed of 55 kph was selected as the test configuration. This has allowed conclusions to be drawn concerning the behaviour of the restraint system and of the vehicle structure. Since the test conditions were maintained exceptionally accurately during the series, developments and tendencies could be drawn from the data. The following tendencies could clearly be seen from the database:

- The stiffness of the occupant compartment has increased
- Restraint systems have become noticeably more efficient
- The pattern of injury has changed, with injuries of the lower extremities now becoming more important

The series of published crash tests has therefore significantly contributed to turn the attention of the car driver towards vehicle passive safety. In the future the problem of compatibility will increasingly be taken into consideration in the area of personal safety. Vehicle-vehicle crash tests, which have also been presented for publication, have contributed to clarifying some of these issues. These publications may also lead to further objective conclusions.

INTRODUCTION

In our times of highly complex traffic and high sensitivity on the part of the individual concerning an enlightened attitude towards technology and safety awareness, vehicle safety forms an important element of technology and everyday life.
Technically-interested people can form their own opinion with the aid of a great number of available media, such as reports in daily newspapers, statements by consumer protection associations, television broadcasts or also specialised and independent magazines dealing exclusively with the subject of automotive engineering. In view of this large variety of information sources, a test procedure characterised by a clear evaluation pattern and continuous realistic test conditions is advantageous for the final consumer. For this reason, "auto, motor und sport" has selected a test procedure which -- with the aid of ECV technology -- gives highly realistic results.

ECV CONTROL

In order to allow driverless control, the TÜV Süddeutschland ECV (Electronically controlled vehicle) system is used for the test.

The particular advantage of this test method is that the vehicle can be driven under its own power. The ECV system can further be distinguished from other current test methods as follows:

- high longitudinal and transverse precision through electronic steering and control system;
- complete transportability, i.e. the ECV system is universally applicable to enclosed test tracks;
- the greatest possible flexibility with respect to crash configuration and vehicle combination include the collision of two moving vehicles;
- adjustable for different passenger cars and trucks.

The required speed is entered into the on-board vehicle controller before the test. The vehicle is constantly and steadily accelerated to the desired speed by an actuator. The actual speed signal comes from a tacho hub, normally mounted on a non-driven wheel. System accuracy is ensured by means of control measurements on comparison trips with the help of an external speed measurement system. An automated gear shifter can be incorporated to cover large speed ranges or for use in heavy trucks. Passenger cars are normally driven in second gear.

Path control is achieved by driving the vehicle along an electrical pilot cable. The cable is an emitter with a 10 kHz A/C signal, generating a concentric electromagnetic field. An antenna mounted on the front of the vehicle detects lateral deviations by measuring the field intensity and communicates these to the onboard computer. The required steering corrections are automatically calculated and transmitted to the steering shaft by an electric motor. Figure1 shows a functional schematic of the ECV Crash System. Detailed information about this technology can be gained from the fourth reference.

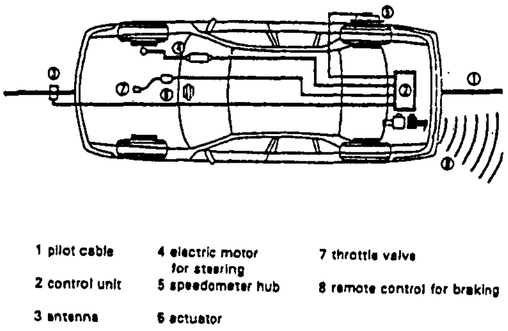

Fig. 1

CONFIGURATION

For "auto, motor sport" tests the following configuration was selected:
- 55 km/h
- 50% offset
- 15° barrier with ASD
- 2 Hybrid III dummies on the front seats
- if necessary, 2 child dummies FTSS representing children of 3 and 6 years of age
- car driven via ECV with its own engine power

Figure 2 presents the test configuration in a diagram.

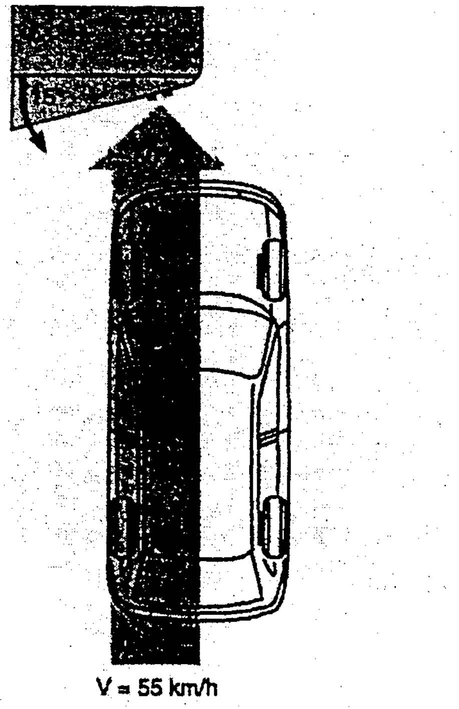

Fig 2

EVALUATION PATTERN

Vehicle evaluation is divided into three main categories. If a vehicle has low scores in all evaluation criteria, then the vehicle is evaluated as having a "low injury risk". Should one of the criteria be assessed within the range of "medium injury risk", the entire vehicle will be classified as having a "medium injury risk". Analogously, cars that achieve poor results will also be evaluated as having a "high injury risk". Figure 3 shows the limit values for dummies and vehicles. The evaluation covers the following parts: HIC (head), the acceleration values over 3 milliseconds (head, chest, pelvis), the peak load value acting on the upper thigh and the rotation of the head around the Y-axle (not including the yaw movement). At the vehicle, the following parts are included in the evaluation: footwell intrusion, belt force (shoulder belt), door opening behaviour and the displacement of the steering wheel during the test.

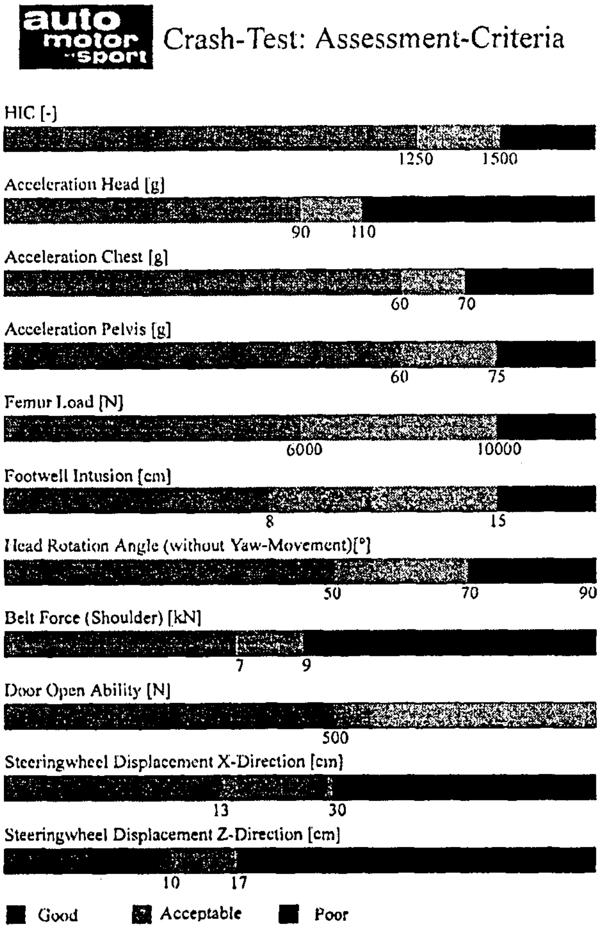

Fig. 3

IMPROVEMENT IN CAR-BODY STIFFNESS

With respect to the stiffness and strength of the car body and, in particular, the passenger compartment, the data that has been collected since 1990 allow the following conclusions:
The stiffness of the passenger compartment has increased due to improved deformation behaviour. Figure 4 shows a vehicle with a collapsing passenger compartment (especially in the area of the A-pillar) from an early (1990) "auto motor und sport“ crash test. In contrast, Fig. 5 shows a current model of today's vehicle population with good stiffness performance.

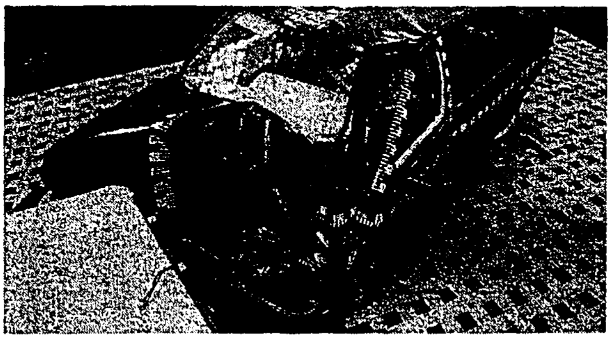

Fig. 4

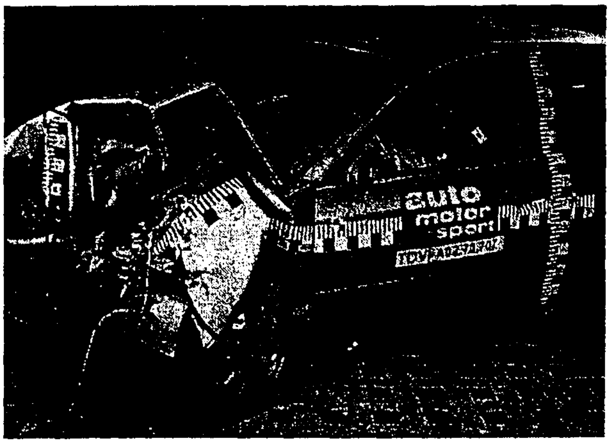

Fig. 5

The two interior pictures taken of the aforementioned vehicles' passenger compartments also reflect considerable improvement. In addition, the driver's door of the vehicle tested in 1990 could only be opened after 20 minutes and with the aid of rescue tools. Figure 6 also shows that, on account of insufficient stiffness in the passenger compartment, there were marked intrusions into the body interior. The displacement of the steering wheel in X-direction, for example, was 28 cm. The fact that the passenger compartment at the driver's side was shortened by 35 cm also points to insufficient survival space for the driver. In contrast, Fig. 7 presents a modern vehicle that was tested only 7 years later. Apart from the inflated airbag, this picture could be mistaken for a picture taken before the test. The deformation values, too, speak for themselves. A horizontal steering-wheel displacement of only 4 cm and the shortening of the passenger compartment by 10 cm represent today's state of the art.

Fig. 6

Fig. 7

IMPROVEMENT IN RESTRAINT SYSTEMS

Not only in the vehicle structure but also with respect to the efficiency of passenger restraint systems, does the data that have been collected over recent years allow statements to be made evidencing a continuous improvement in this field. From the Head Injury Criterion (HIC) to the loads acting on the upper thighs, the characteristics outlined in the following become evident.

Figure 8 shows the HIC values measured on a selection of vehicles. A decrease in divergence over the course of the years is very clearly recognisable. In this area, where HIC values of more than 1000 were not uncommon back in 1990, today's values are concentrated around a HIC value of 500. Vehicles in the sub A-range still form the exception in this case because -- due to their short deformation potential -- they have reached the limits of today's restraint systems.

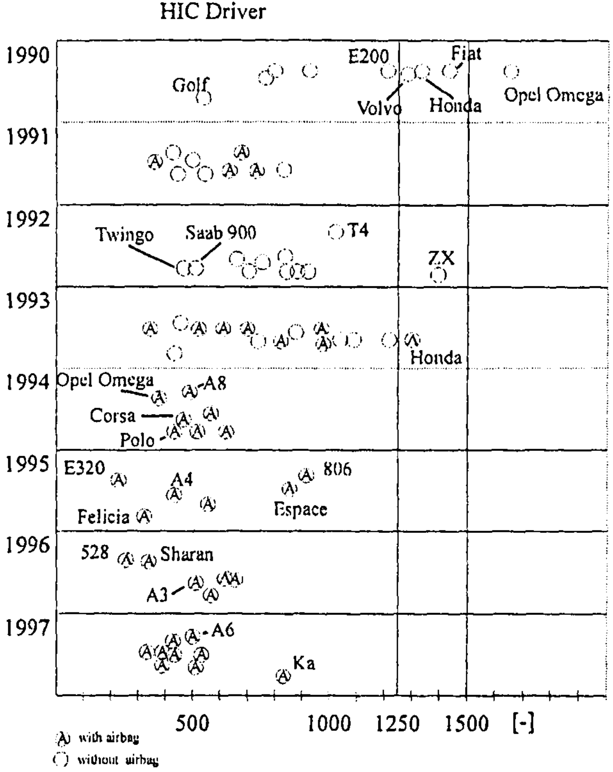

Fig. 8

Due to the same measurement point (head) similar tendencies can be seen for the head acceleration as shown in Figure 9. In this respect, where in 1990 acceleration values (3 ms) of more than 110g were measured, today's values are in the 60g-range and sometimes even far smaller than this.

With respect to chest acceleration as presented in Figure 10, only a slight tendency can be shown. Apart from some exceptions, chest acceleration (3ms) was already under the magic limit of 60 g for the majority of vehicles when crash tests began. Since in the first years tests exclusively covered vehicles which were only equipped with a 3-point seat belt and since the airbag only arrived on the scene gradually, the following conclusions can be made. In addition to vehicle deceleration characteristics, the 3-point belt has a primary influence on chest acceleration. It seems that the influence of the airbag in this field is only secondary. However, this does not mean that the airbag does not possess an improvement potential in this field, too. Another reason for this behaviour seems to lie in the laws of physics. Due to increasing vehicle decelerations partly caused by the constantly decreasing space reserves in the engine compartment and on account of the increased stiffness resulting from the vehicles' higher dead weight, no essential improvement can be achieved if the passengers participate early in the deceleration of the car body.

Acceleration Head Driver, 3 ms

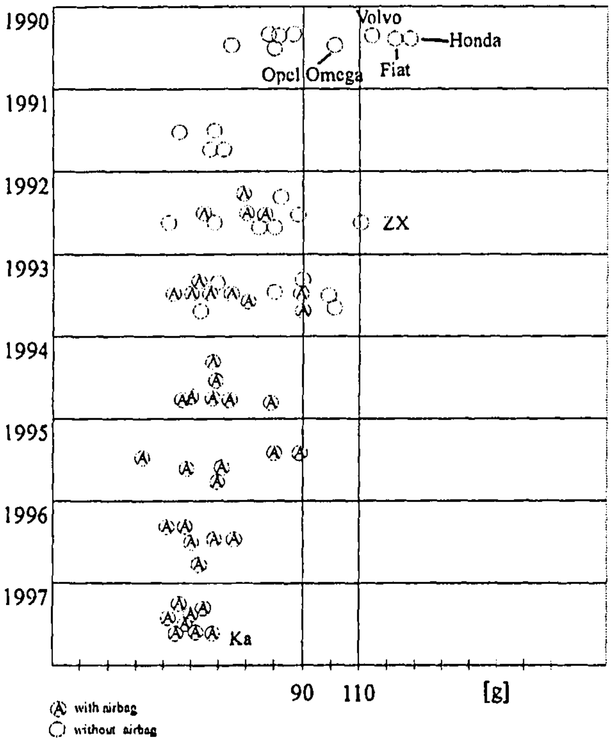

Fig. 9

Accelaration Chest Driver, 3ms

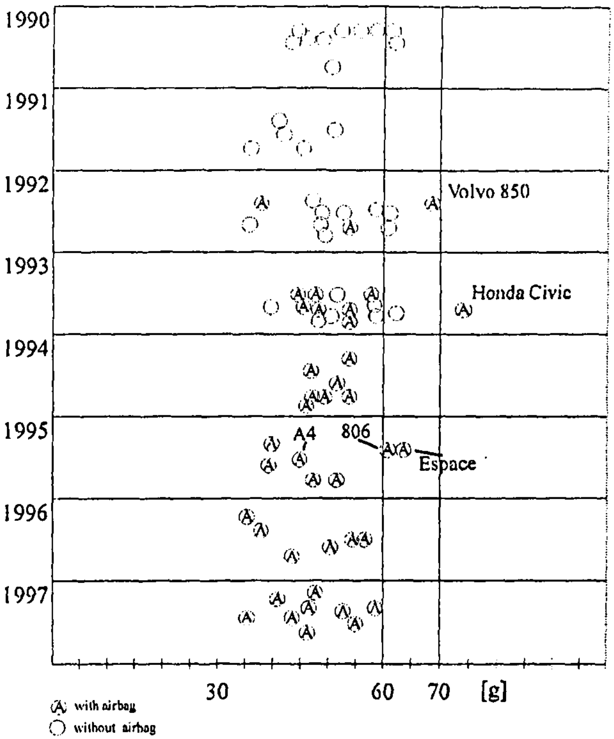

Fig. 10

Another continuous improvement in the field of passive safety is presented in Figure 11. In 1992 pelvis acceleration (3ms) peaked in values exceeding 75 g. From then on continuous improvement has been achieved. Seat-belt tensioners, airbag, car-body stiffness and the reduced intrusion resulting from this, as well as optimised design and material selection for the passenger compartment are some of the causes for this development. One exception to this is a vehicle that was tested in 1995 in which the unfavourably positioned reinforcement of the instrument panel resulted in high pelvis acceleration values.

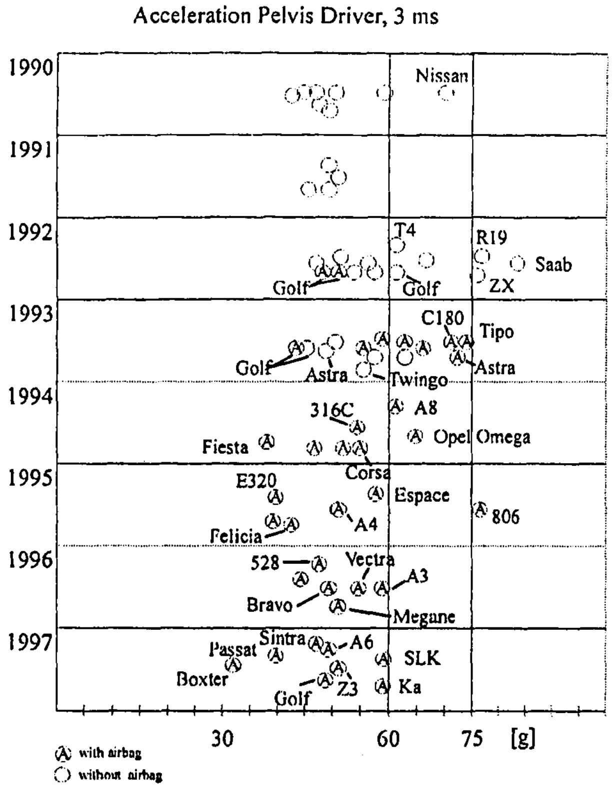

Fig. 11

The load acting on the upper thigh shown in Figure 12, as in the case of chest acceleration, do not show a significant tendency to improve. Categorisation into vehicles with and without airbags is not applicable since these values depend primarily on seat-belt function, knee-restraint quality, potential submarining effects and passenger-compartment reduction. It can also be seen that vehicles in which higher loads are acting on the upper thighs also show increased pelvis acceleration. This is caused by the direct transmission of force from the upper thigh to the pelvis. The improved design characteristics of restraint systems and knee restraints make "blunders", which were still recorded before 1996, appear unlikely in today's vehicle population.

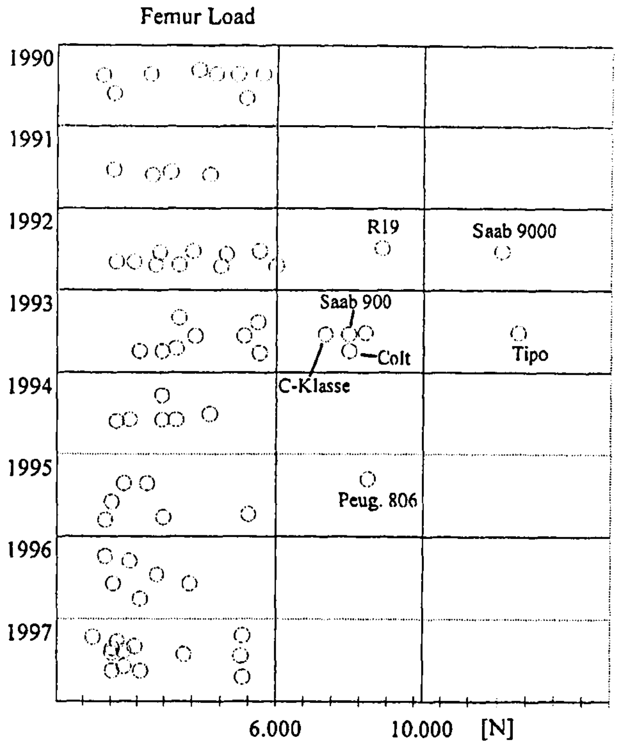

Fig. 12

INJURY PATTERN

The volume of loads has continuously decreased since the "auto motor und sport" tests began. On the account of various restraint systems which, however, act differently on the individual body regions of the dummies (passengers), the loads did not decrease equally for all body regions. As already explained in the aforementioned paragraph, the decrease in loads acting on the head was especially high. Figure 13 also shows injury traces on dummy head surfaces that often occurred in the early years. As a rule, such traces of injuries are not observed any longer today. Pelvis acceleration also considerably decreased. Since, however, there was not such a significant decrease in the loads acting on the upper thigh, it can be assumed that the injury risk has shifted to the lower extremities. Although most of the forces measured that act on the upper thigh were within the uncritical range, the limit value may easily be exceeded in case of a higher collision energy as occurs in real accidents.

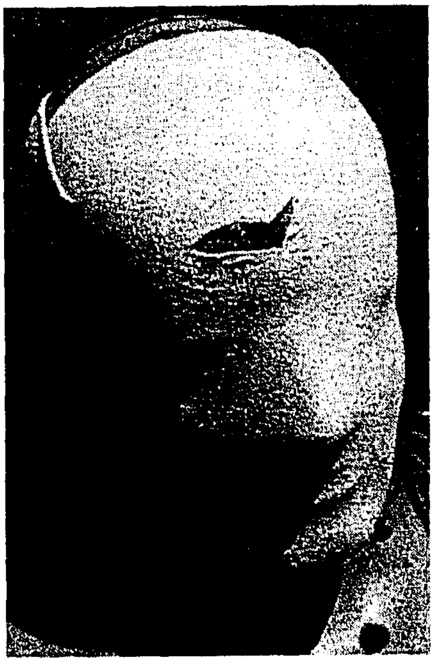

Fig. 13

Figure 14 shows traces of injuries that were caused by insufficient protection through the knee restraints. Thanks to technical progress such pictures have become less common.

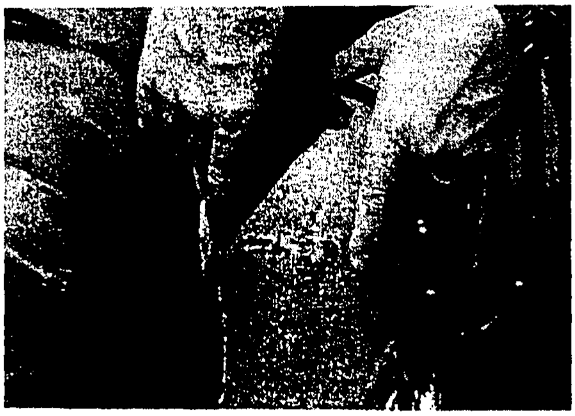

Fig. 14

CONCLUSION

Thanks to more than 70 tests performed under the same marginal conditions and configuration, a large pool of data is now available which allows us to interpret the changes in passive vehicle safety that have developed over the last 8 years.

Because of continuous improvement in the structural stiffness of vehicle bodies, material quality, the design-related arrangement in the passenger compartment and the restraint systems, one can speak of a considerable reduction in passenger risk. Nowadays, small vehicles with design-related short deformation, such as the Ford Ka, achieve head acceleration values which, some years ago, some of the large vehicles could only dream of.

Since the restraint systems for standard seat positions (50%) have already been highly optimised, the future focus will certainly be directed to the injury mechanisms pertaining to the lower extremities.

Since end consumers with the power gained through their purchasing decisions can decisively influence the actions of the automobile industry, media do play a major role in the passive vehicle safety improvement process. The crash test as used by "auto motor und sport" , which in the beginning was often described as being too stringent, thanks to the public interest does not represent an insurmountable obstacle any longer, for most vehicles nowadays.

Besides all these introduced criteria of the passenger safety currently the matter of compatibility becomes more important. Therefore „auto motor und sport“ realized apart the already mentioned tests against the rigid barrier also a lot of vehicle-vehicle-tests. This method of tests will complete the present test configuration.

REFERENCES

Hupfer, P.; Richter, R.; Wech, L.: Das ECV-Crashsystem des TÜV Bayern. ATZ 94 (1992) 5, pp. 260-268

auto motor und sport, issue 19/90, pp. 127-150

auto motor und sport, issue 23/97, pp. 86-92

auto motor und sport, issue 19/97, pp. 42-47

Ostmann, B.; Koch, M.; Wech, L.; Jakob, B.: Euro-NCAP im Vergleich zur ams-Konfiguration am Beispiel VW Golf IV; CRASH-TECH special '98, Munich, 1998

auto motor und sport, issue 18/95, pp. 48-52

auto motor und sport, issue 6/97, pp. 42-46

QUALITY CRITERIA FOR CRASHWORTHINESS ASSESSMENT FROM REAL ACCIDENTS

Klaus Langwieder, Hans Bäumler
German Insurance Association
Institute for Vehicle Safety
Germany
Brian Fildes
Monash University Accident Research Centre
Australia
Paper Number 98-S11-O-08

ABSTRACT

The Institute of Vehicle Safety of the German Insurance Association (GDV) conducted a review of the possibilities and the limits to vehicle safety rating systems. The review included four workshops held from 1995 to 1998 that involved a number of international experts who examined existing systems to highlight key issues. Important criteria for the establishment of a high-quality safety rating system have been defined. This paper describes the findings, future developments and activities planned by this committee.

INTRODUCTION

In the past few years, the Institute of Vehicle Safety has studied some 20,000 automobile accidents involving personal injury /9/. The results of these analyses have formed the basis for several studies which have been published and presented at earlier ESV conferences and elsewhere.

Stimulated by the growing public debate as to how to objectively assess automobile safety, the GDV created a group of experts who were to define quality criteria for such assessments. The reason for the creation of this team of experts was that existing safety evaluation procedures have given rise to often inconsistent results. It is possible to classify one and the same vehicle as either "very safe" or "very unsafe", depending on the rating method used.

This discrepancy is due on the one hand to the fact that it is only possible to compare the results from crash tests with the results of retrospective accident analyses when defined conditions are used. On the other hand, since the methodologies of such retrospective accident studies vary considerably, this necessarily causes the results of such studies to deviate as well.

The definition of quality standards appears to be a suitable way of bringing about improvements in the comparability of retrospective methods, although existing methods will first have to be analyzed before new criteria can be defined.

REVIEW OF PUBLISHED SAFETY ASSESSMENTS

In order to be able to integrate into the study the approaches taken by existing methods, the literature was first evaluated /1/. The methods below were included in the study:

- Folksam Car Model Safety Rating /2/
- Traffic Accidents by Car Model, study by the University of Oulu, Finland /3/
- Driver Death rates by Make and Model from IIHS /4/
- Injury, Collision and Theft Losses by Make and Model from HLDI /5/
- Used Car Safety Ratings, Monash University, Australia /6/
- Injury Accident and Casualty Rate, UK Department of Transport /7/
- Two-car Accidents in Germany Involving Personal Injury, University of Cologne /8/

One important differential feature of such methods is the parameters used to assess vehicle safety. Of utmost importance is the need to differentiate between systems involving crashworthiness and crash involvement, as they are fundamentally different and can lead to different evaluations of car safety.

Crash involvement refers to the likelihood of being involved in a crash (either generally or at different crash severities). A crash over-involvement rate reflects not only active and to a certain extent passive safety aspects of a vehicle, but also the behavioural and travel characteristics of its driver and other active safety deficiencies.
Crashworthiness, on the other hand, has to be a pure evaluation of the passive safety characteristics of a vehicle, as it measures the inherent ability of the vehicle to protect its occupants from injury in a crash.

Crashworthiness information is what the general public usually desires when purchasing a new or used car. However, crash involvement information, too, is valuable for setting enforcement strategies, insurance rates, and establishing other road safety countermeasures.

Table 1 provides an overview of the parameters used by the various methods. In addition, it also shows the factors used to categorize the vehicles, the normalization parameters used and the way in which the vehicles reviewed were grouped together.

THE APPROACH USED IN ANALYZING THE METHODS

The published scientific literature served as a basis on which to examine the structure of existing methods. In order to make a comparison of the methods possible, a "Standardized Presentation" was created for each of the selected assessment methods based on the description of the approaches and the mathematical models contained in the studies. Table 2 shows one example of this standardized presentation for the rating procedure used by the UK Department of Transport (DoT). The standardized presentations of all methods reviewed can be found in Annex 1.

Particular importance was placed on the analysis and processing of the mathematical models used in order to make it possible to program and apply them at a later date to uniform accident material. In addition to the detailed description of the models, a formalized description of the different calculation steps was developed quite similar to the "Standardized Presentation". This is named as the "Formalized Process of Calculation", an example of which can be found in Table 3. This approach benefits from the following advantages:

- description of the database
- clearly organized presentation of the systematic sequence of calculations
- description of important risk exposure parameters
- description of the categorization
- description and presentation of the results.

The formalized methods of presentation made it possible to present and compare the approaches used by the different rating methods in a clearly arranged manner. The formalized presentation of the mathematical models considerably facilitated the programming of the individual methods used in the various studies. The possibility of computerizing the mathematical models, however, was a prerequisite for applying the method to uniform accident material.

Table 1. Overview of various rating systems currently available

Publishing organisation	Rating measure used in the publication	Dimensions covered by the measure Crash involvement (CI) Crashworthiness (CW)	Factors used to adjust the ratings before comparison between models	Factors used to categorise the [adjusted] ratings into car groups
Insurance Institute for Highway Safety (USA)	Driver death rate per 10,000 registered vehicle years	CI and CW	None currently (previously included car wheelbase and driver age & sex)	wheelbase body style
Highway Loss Data Institute (USA)	1. Occupant injury rate per insured vehicle year a) by injury b) injury cost >$500	CI and CW	* driver age	Wheelbase body style
	2. Vehicle damage payments per insured vehicle year	CI	* driver age * excess deductable	
Folksam Insurance (Sweden)	1. Relative risk of driver injury in two-car crashes	CW	Car weight	Car Weight
	2. Risk of death or permanent disability to front seat occupants	CW	None	
	3. Combinations: 1 by 2	CW	Car weight	
Department of Transport (UK)	Rate of driver injury (and severe injury) in two-car crashes with at least one injured driver	CW	* speed limit * point of impact * driver sex * driver age	size of car
University of Oulu (Finland)	1. Relative risk of driver injury in two-car crashes in built-up areas	CW	* driver age * driver sex * car mass	car mass
	2. Relative number of drivers injured in two-car crashes in built-up areas to that expected	CW (includes a measure of aggressivity of the make/model)	* driver age * driver sex * car mass	car mass
	3. Total driver injury rate per 100 million km.	CI and CW (includes aggressivity)	Km drivern by type of area + driver age	crash type
Monash University Accident Research Centre (Australia)	1. Rate of driver injury in tow-away crashes	CW	For all comparisons: * driver sex * driver age * speed limit * No. vehicles	Market group (related to mass, size and cost)
	2. Rate of death or hospitalisation of injured drivers	CW		
	3. Combination: 1 by 2	CW		
University of Cologne (AFO) (Germany)	Degree of injury and average cost of injury	CW	* innocent drivers	car mass

Table 2.
Standardized Presentation of the UK DoT Method

Safety Assessment Method **Estimates**	**Cars: Make and Model: The Risk of Driver Injury and Car Accident Rates In Great Britain: 1992** Department of Transport, UK, 1994
Dataset	• England • Two-car crashes including at least one injured driver • Number of accidents: >100.000 • Number of injured individuals: >100.000
Required Frequency for each Car Model	• > 150 accidents
Considered Parameter	• Number of accidents in which the driver of the assessed car was injured exclusively • Number of accidents in which both drivers were injured • Number of accidents in which the driver of the opposite car was injured exclusively -> determination of the injury risk D_i for each car model i
Safety Rating Values	Relative safety value P_i calculated with the aid of D_i and $D_{all\ cars}$
Data Adjustment and Adaptation	• Speed limit at the scene of the accident to describe the accident severity • Age group and sex of the driver • Type of collision (first point of impact) -> calculating adjustment factors for D_i
Formation of Groups, Categorizing	• Dividing the models of car into groups based on length • Relative rating within every weight class depending on the percentage deviation of P_i compared to P-mean of the class

Table 3.
Formalized Process of Calculation, Example Method used by the University of Oulu, Finland

Comprehensive accident database Finnish Insurance Companies	Finland

Selection of all accidents involving 2 private cars with damage > 3000 FIM within city limits

Determination of factors A-F:

Relative risk of injury

$$RR_{ic}=\frac{N(I_{ic})}{N(I_{ic})+N(I_{oc})}$$

$N(I_{ic})$ = number of injured drivers in the inspected car model i

$N(I_{oc})$ = number of injured drivers in the opposite car

ic = inspected car model
oc = opposite car

Number of injured drivers in the inspected car model per driven kilometer $=\frac{N(I_{ic})}{M_{ic}}$

Number of all drivers injured in accidents involving the inspected car model per distance travelled annually $=\frac{N(I_{ic})+N(I_{oc})}{M_{ic}}$

Number of injured drivers based on the total number of accidents involving the inspected car model $=\frac{N(I_{ic})}{N(A_{ic})}$

Number of injured drivers in the opposite cars of the inspected car models based on the total number of accidents involving the opposite car. $=\frac{N(I_{oc})}{N(A_{ic})}$

Assessment:

$RR_{ic} < 0,5$: above-average passive safety of car model i

Injured drivers per expected number of injured drivers with 95% confidence interval categorized in 3 classes based on the Poisson distribution; statistical test parameter for significance Q_i:

$Q_i < 1,96$:	Above-average safety	(+)
$-1,96 =< Q_i =< 1,96$	Average safety	(0)
$Q_i > -1,96$	Below-average safety	(-)

APPLICATION OF THE METHOD TO UNIFORM ACCIDENT MATERIAL

The GDV Institute of Vehicle Safety collects data at periodic intervals on traffic accidents involving personal injury from large-scale studies as a basis for accident research. The following large-scale analyses have been carried out, among others, since the institute was founded:

- IS ´69 - Internal automobile safety
- FS ´74 - Analysis of two-car collisions involving personal injury in 15,000 cases
- FS ´80 - Analysis of two-car collisions involving personal injury in 5,500 cases
- FS ´90 - Analysis of two-car collisions involving personal injury in 15,000 cases

The FS 90 accident material, which was used as the basis for the model calculations, comprises 15,000 two-car collisions in which a total of 30,000 automobiles were involved. Approximately 80 parameters were collected per case in what was termed the basic assessment. The analysis covered accident files on two-car accidents involving personal injury provided by the German automobile insurers. There is an in-depth description of this material in /9, 10/. The parameters that were entered included:

- location
- sex and age of the driver
- type of vehicle
- severity of injury sustained by passengers
- type of collision
- extent of damage to the vehicles involved
- etc.

This made it possible to use most of the rating methods described and apply them to this accident material /11/. We were unable to calculate either of the two American methods, since the data structure used in the FS 90 study gives no information about how many cars of one model are insured within one year.

For calculating the other methods the GDV has been extended. The annual mileage of the respective vehicles had to be integrated into the database in order to assess the method used by the University of Oulu. The method used by the UK DoT required the entry of vehicle lengths. It was possible to adapt the FS 90 database in this instance as well.

In order to calculate a ranking of the vehicles with respect to their passive safety, the following twelve car types were selected:

Small car class:
VW Polo
Opel Corsa
Fiat Uno
Peugeot 205

Compact car class:
VW Golf
Opel Kadett
Ford Escort
Mazda 323

Luxury class:
Mercedes-Benz 200 - 300
BMW 5 Series
Audi 100
Opel Rekord

These 12 vehicles were calculated on the basis of their passive safety for each of the methods. It was found that there was great differences in the assessment of automobile safety despite the use of uniform accident material. The BMW 5 Series, for example, was evaluated as being both the safest vehicle (ranked 1st in the Folksam car model safety rating) on the one hand and as the least safest car (ranked 12th by Monash University) on the other hand, refer to Figure 1. A similar spread was also found for the Opel Corsa and the Peugeot 205).

EVALUATING THE RESULTS OF THE MODEL CALCULATION

The model calculations based on uniform accident material demonstrated that the results of the current rating systems clearly have a different outcome irrespective of the accident material used. Two systems (Folksam and DoT) come very close as far as their results are concerned, whereas the Monash method (1992) provided entirely different results. It must also be taken into consideration, however, that all methods reviewed have experienced continuing development during the intervening period.

Furthermore, it was also found that a database containing 30,000 cars (15,000 car-car accidents) as is the case with the FS-90 database, is limited for a safety ranking intended to evaluate less common models of cars. A safety ranking of the 50 most common models, for instance, would require several times the amount of data material contained in the FS 90 database. This means that in Germany for instance, it would only be possible to rely on the data from official statistics.

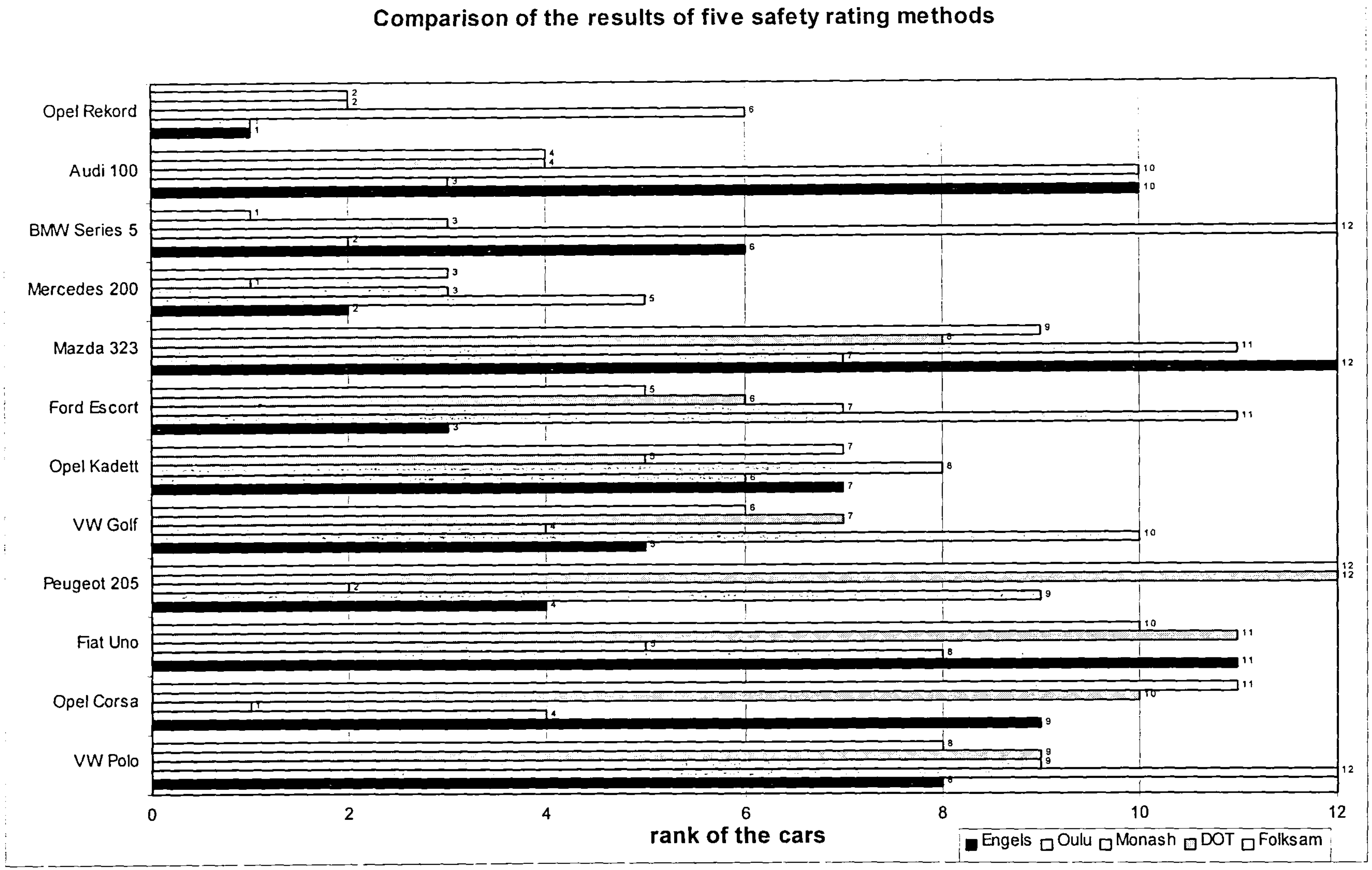

Figure 1. Total ranking of 12 car models using different ranking procedures (uniform accident material FS 90)

These data, however, do not have enough structure available for a ranking.

RESULTS OF THE EXPERT'S DISCUSSION

One important issue in evaluating the results of the calculated rankings is the question of the extent to which the mathematical models used are actually representative of passive safety.
This issue was discussed among a team of experts in four different workshops. Annex 2 contains a list of the names of participants. There are plans to transform this group of experts into a ongoing project to allow the work already begun on the comparison of the various methods to be continued and updated. It would also make it possible to institutionalize the work on quality criteria for safety assessments.

The previous workshops have been devoted to a discussion of the topics below which, among other things, have been incorporated into resolutions, recommendations and guidelines.

Database Requirements for Safety Rating Assessments - A high quality database was seen as an essential basic requirement for a reliable and accurate rating system. The data need to be comprehensive and have sufficient detail to enable adequate control of possible extraneous factors.

The most reliable and comprehensive data format for these evaluations is that adopted by crash investigators, but these data are limited in number because of extraordinary costs.

Police and insurance databases are usually of sufficient size but some of their parameters are limited in quality and key parameters like impact severity and type of collision are often not available.

The number of cases necessary to make reliable assessments per model is another important issue and one that requires further research. Equally important, the distribution of cases should be by random selection and representative of the types and severity of crashes that occur in the real world.

The prospect of sharing data within Europe and even on an international scale is one possibility of obtaining sufficient data for a high quality rating. This would also allow vehicle types with a small population to be rated. For such data it would be necessary to internationally standardize the parameters used by the different investigators.

Controlling for Risk Exposure and Substitutes for Impact Severity - One essential element in car safety assessment is to collect and input the parameters required for an assessment of impact severity. These parameters are, among others:

- type of accident (car to car, car to truck, etc)
- type of collision
- Energy Equivalent Speed - EES
- Change of speed Δv
- impact angle
- overlap

Both the age and the sex of the passengers involved play another important role in the assessment of the passive safety of a vehicle on the basis of a retrospective accident analysis, since these parameters have a very decisive effect on the extent of injury a person sustains.

Since the cited parameters are not contained in every data record, as explained above, methods must be developed to replace these and to validate the substitution using a "reference data record", for instance. High-, medium- and low-priority parameters which have a very decisive effect on the quality of a safety rating would be defined in a first step. These parameters are contained in Table 4 below.

Table 4. Safety Rating Parameters of high, medium and low priority

High Priority	***Medium Priority***	***Low Priority***
Vehicle mass or size	Vehicle model year	Mileage (total + annual)
Crash Severity	Vehicle Identification Number	No. registered cars
Injury severity (AIS scale)	Use of safety systems*	Years of insurance
Type of crash	Two or four doors	Marital status of the driver
Age of the driver	Trim and transmission	No. of occupants
Sex of the driver	Crash location	
Guilt of the driver	Driver size and weight	

It is obvious that a safety rating that uses only low- and medium-priority parameters will be less valid and less relevant than a method that is based on high-priority parameters.

As already discussed above, it is feasible, however, to substitute parameters such as impact severity by a combination of other less relevant parameters, provided that there is proof that these parameters have a "similar impact". Continued research work, however, is necessary in this respect.

Outcome Measures - Current systems include assessments of safety based only on property damage, minor and major injury. While most crashes have relatively minor outcomes, it is the severe cases that are more likely to reflect on a vehicle's inherent crashworthiness characteristics, provided that control mechanisms are in place to avoid negative selection.

A high quality rating system needs to include sufficient injury detail to permit meaningful analysis. It is desirable for these data to be coded in terms of injury description and severity using the Abbreviated Injury Scale (AIS). The addition of long term outcome details such as rehabilitation and impairment would also be useful in determining safety outcomes.

The cost of injury or harm associated with the crash is a promising means of incorporating all these aspects but should only be used on databases of sufficient size and representativeness to ensure that extreme outcomes do not unduly influence the ratings.

Publishing Results from Rating Systems - In the existing safety rating methods, different strategies can be envisioned when presenting the results of the investigations to the public. Some authors publish the ratings as *"safety assessments"*, others as differences in performance and let the reader interpret these in terms of which is more safe.

An allied issue is the degree of sophistication that can be attributed to minor differences in outcome and hence what is an appropriate rating scale. Current systems vary from simple 3 or 5 point classifications scales up to continuous rating scales, although the latter often include a 95th percentile band along with the single point score.

Experience seem to suggest that, irrespective of how these ratings are published, the media will always interpret these results in terms of simple ratings of which car is the safest. This needs to be taken into account when deciding on how to publish results.

Future Steps & Research Needs - From the discussions within the expert's group, a number of limitations, data shortcomings and items requiring further research were identified. Some of the systems reviewed have been recently updated and analysis techniques modified. The expert's group will review these latest versions to gain additional insights into high quality criteria for safety rating systems. Based on the present status, the major research needs are listed below:

- There was considerable discussion about the quality of travel speed information for determining and controlling crash severity. It was proposed that a small sample of representative crashes where data is available from police, insurance and crash investigations should be evaluated in an attempt to answer this question.
- This might also include the feasibility and accuracy of collecting closing speed data combined with speed limit information to get a feeling of how these parameters are interconnected.
- There is clearly a need for a comprehensive European database of sufficient size and detail to enable scientifically robust comparative ratings of passenger cars. The European Commission is currently examining the feasibility of establishing a European Community Road Accident database (CARE) which would seem to offer considerable potential for assessing crash involvement and even crashworthiness of cars, if there are necessary safety data in sufficient quality availible.
- Nineteen exposure items including 7 high priority items were identified in Table 4 that need to be checked for in any future safety assessment. It would be useful to refine this list even further to identify those that are essential from those that are desirable, thus minimizing analysis effort and maximizing the chances of locating a suitable database.
- There is growing interest in addressing not only self-protection of passenger car occupants but also partner protection. Several Europen projects are analysing which description systems are available.
  It would be useful to examine the possibilities of assessment systems to highlight vehicle aggressivity and the desirability of including this aspect in any future safety rating system.
- Sample size will be a key issue for providing a robust and reliable ranking, yet this was not able to be resolved totally during the expert's discussions. There was consensus on the need for further work in this area, but only in the light of a clearer understanding of what is achievable in establishing suitable databases and criteria.
- Consumers need clear, unambiguous information of the relative safety of the various makes and models of cars available. Crash tests and real world accident data will inevitably provide differing ratings of passive safety due to their limitations. It is absolutely essential that further consideration be given to how these different procedures can be better compared in future and that information of both systems could be combined into a general report on car safety.

ACKNOWLEDGEMENTS

The Authors wish to thank all participants of the workshops and their companies for their excellent work and support.

REFERENCES

/1/ H. Keller, W. Huber: „Analyse von Safety Rating-Verfahren für Pkw", Technische Universiät München, February 1996

/2/ B. Aldman, H. Gustafson, A. Nygren, C. Tingvall, J. Wersall: „Injuries to Car Occupants - Some Aspects of the Interior Safety of Cars" Folksam Insurance Company, Stockholm 1984 and
H. Gustafson: „Folksam Car Model Safety Rating 1989 - 1990, Folksam Research, Stockholm

/3/ T. Ernvall, J. Tapio: „Injure Risk by Car Models in Two-Car-Crashes", University of Oulu, Road and Transport Laboratory, Finland

/4/ Insurance Institute for Highway Safety: „Shopping for a Safer Car", Arlington USA, 1990

/5/ Highway Loss Data Institute: „Insurance Collision Report", Arlington, USA, 1993

/6/ M. Cameron et. al.: „Vehicle Crash Worthiness Ratings from Victoria and New South Wales Crash Data", Road and Transport Research, Vol. 1, No. 3, Sept. 1992, Australia

/7/ Department of Transport: „Cars: Make and Model: The Risk of Driver Injury and Car Accident Rates in Great Britain", Government Statistical Service, London, UK, 1995

/8/ K. Engels: „Rangreihenfolge von Pkw-Typen hinsichtlich ihrer passiven Sicherheit bzw. inneren Sicherheit", Universität Köln 1993

/9/ HUK-Verband: „Vehicle Safety 90", Munich 1994

/10/ K. Langwieder, H. Bäumler: „Priorities of Real Car Crashes and the Agreement of Real Accidents with Results from Crash Testing", 14th ESV-Conference, Munich 1994

/11/ H. Wolff, O. Widmaier: „Modellrechnungen mit der Datenbank FS 90", Universität Ulm, Ulm 1995

ANNEX 1: STANDARDIZED PRESENTATIONS OF THE REVIEWED SAFETY RATING METHODS

Standardized Presentation: Folksam Car Model Safety Rating, Folksam Insurance Company

safety assessment method	**car model safety rating**
study	FOLKSAM insurance company, 1989/90 FOLKSAM insurance company, 1991/92
database	• Sweden • car-versus-car collisions including at least one injured driver (starting in 1991) • number of accidents: 26527, 1985-1990 (for the 1991/92 study including at least one injured driver) • number of injured individuals 28153, 1986-1990 (only adult drivers/front-seat passengers)
required frequency of each vehicle type	• no information given
considered parameter	• number of accidents where both drivers (in the assessed and in the opposite vehicle) were injured • number of accidents where only the driver in the assessed vehicle was injured • number of accidents where only the driver in the opposite vehicle was injured -> determining the relative injury risk R_i for each vehicle type i • risk of fatal injuries for the driver of the assessed vehicle (as a function of the ISS value) • risk of permanent injury after-effects for the driver of the assessed vehicle (as a function of the AIS value) -> determining the mean risk of serious consequences MRSC for each vehicle type
safety values of reference	• safety value **Z** calculated with the help of - MRSC (mean risk of serious consequences) - R (relative injury risk)

data correction and data adaptation	• different weight proportions of the accident vehicles; increasing or reducing the R_i value by a "**weight effect**". This effect is calculated on the basis of all the vehicles available in the data base (e.g. for the 1990/91 study: 0,035) • considering passenger influence with the help of the "**passenger factor**"
formation of the classes	• creating an average Z with the help of the vehicle types and subordinating Z into four weight classes
categorizing	• developing a relative rating within every weight class depending on the percentage deviation of Z_i in contrast with Z

Standardized Presentation: Cars: Make and Model, Department of Transport, UK

Safety Assessment Method **Estimates**	**Cars: Make and Model: The Risk of Driver Injury and Car Accident Rates In Great Britain: 1992** Department of Transport, UK, 1994
Dataset	• England • Two-car-crashes including at least one injured driver • Number of accidents: >100.000 • Number of injured individuals: >100.000
Required Frequency for each Car Model	• > 150 accidents
Considered Parameter	• Number of the accidents in which the driver of the assessed car was injured exclusively • Number of the accidents in which both drivers were injured • Number of the accidents in which the driver of the opposite car was injured exclusively -> determining the injury risk D_i for each car model i
Safety Rating Values	Relative safety value P_i calculated with the help of D_i and $D_{\text{all cars}}$
Data Adjustment and Adaptation	• Speed limit at the scene of the accident to describe the accident severity • Age group and sex of the driver • Collision type (first point of impact) -> calculating adjustment factors for D_i
Formation of Groups, Categorizing	• Dividing the models of car into groups based on length • Relative rating within every weight class depending on the percentage deviation of P_i compared to P-mean of the class

Standardized Presentation: Injury Risk Rates, University of Oulu

safety assessment method **examination**	**Injury Risk Rates by Car Models in Two-Car-Crashes** University of Oulu, T. Ernvall, 1994
database	• Finland • two-car-crashes in build-up areas plus damage value of > 3000 FIM • number of accidents: 119899, 1987-1992 • number of injured individuals: 10 267 injured drivers
required frequency of each car model	• no information given
considered parameter	• number of **injured drivers** in the **assessed vehicle** • number of **injured drivers** in the **opposite vehicle** -> determining the relative injury risk RR_i for each car model i • number of injured drivers in relation to the **driven mileage** of the car model i -> injure risk rate for each car model i • number of all injured drivers involved in **accidents** with car model i -> injure risk rate for each car model i • number of injured drivers for each number of accidents of the inspected car model i -> injure risk rate for each car model i • number of all injured drivers in opposite vehicles for each car model i accidentsi -> injure risk rate for the opposite individual in car model i
safety values	RR_{ic}: relative injury risk Q_i : statistical test result to signify the expected number of injured individuals and the actual number of injured individuals in a car model (95% reliability)
data correction and data adaptation	none
formation of classes, categorizing	$RR_{ic} < 0{,}5$ within all of the car models identifies a vehicle as safe above average Q_i functions as a standard to assess whether the safety of the vehicle is above average, average, or below average

Standardized Presentation: Vehicle Crashworthiness Ratings, Monash University

safety assessment method **examination**	**Vehicle Crashworthiness Ratings from Victoria and New South Wales Crash Data** Monash University, M. Cameron et al, 1992
database	• Australian States of Victoria and New South Wales • car accidents including medical expenses for one injured individual of > Aus$ 317 (Victoria) and cars which were sufficiently damaged to require towing (New South Wales), respectively • number of accidents: unknown, 1983-1990 (Victoria); 1989-90 (New South Wales) • number of injured individuals: 12 867 injured drivers (Victoria), 10097 (New South Wales)
required frequency for each vehicle type	• no information given
considered parameter	• number of injured drivers in the assessed car model • number of all (including drivers) accidents including car model i -> determining the injury risk IR_i for each car model i • number of all fatally injured drivers of the assessed car • number of all hospitalized drivers of the assessed cars • number of all (truly) injured drivers of the assessed cars ->determining the injury severity IS_i for each car model
safety reference values	• CR_i = combined value from $IR_i * IS_i$ (in analogy to FOLKSAM)
data correction and adaptation	• standardization of the injury risk IR and the injury severity IS by considering the influence of the driver's sex and speed limit at the scene of the accident
formation of the classes, categorizing	• categorizing the car models into seven vehicle classes (remark: this was not done with the help of criteria like wheel-base or car weight but according to the understanding common to the Australian market - large, medium and small cars, luxury cars, sports cars, four-wheel drive vehicles and passenger vans. • relative rating within every vehicle class due to CR • additionally, a summing-up and an assessment according to the manufacturers was implemented.

Standardized Presentation: Status Report, Insurance Institute for Highway Safety

Safety Assessment Method **Estimates**	**Status Report** Insurance Institute for Highway Safety, USA, 1992
Dataset	• USA • All the accidents including fatal injures (concerning passengers in cars registered 1984-1988) • Number of accidents: no information, 1986-88 • Number of injured passengers: no information
Required Frequency of Car Models	• no information given
Considered Parameter	• Number of fatally injured passengers in the assessed car model i • Number of registered vehicles of the car model i ->Determining the [killing rate] for each 10,000 registered vehicles of the car model i • Wheel-base of car model i • Proportion of fatally injured passengers in car model i (passengers > 30 years) • Proportion of fatally injured female passengers in car model i -> Forecasting the [killing rate] for car model i
Safety Rating Values	• [killing rate] R_i • Forecasted [killing rate] R'_i • Proportion of R_i to R'_i
Data Adjustment and Adaptation	none
Formation of the Groups, Categorizing	• Dividing the car models into 5 groups of car (four-door, two-door, sports car, luxury cars, station wagons) and differentiating 3 wheel-base groups for each group of car • Determining the number of R_i in the ranking/rating list compared to all the car models and grading of R_i according to this rank within every group of car • Determining the number of the proportion of R_i to R'_i in the rankings

ANNEX 2: MEMBERS OF THE EXPERT'S GROUP

Prof.Dr. Klaus Langwieder, Chairman, GDV, Institute for Vehicle Safety, Munich, Germany;
Mr. Hans Bäumler, GDV, Institute for Vehicle Safety, Munich, Germany;
Mr. Wolfgang Barth, President, Kraftfahrt-Bundesamt, Flensburg, Germany;
Mr. Andrew Brown, VSE Division, Ministry of Transport, London, UK;
Mr. Max Cameron, Monash University Accident Research Centre, Australia.
Prof. Dr. Timo Ernvall, University of Oulu, Finland;
Prof. Brian Fildes, Monash University Accident Research Centre, Australia.
Prof. Dr. med. Bernd Friedel, Bundesanstalt für Straßenwesen, Gladbach, Germany;
Mr. Josef Haberl, BMW, München, Germany;
Mr. Lasse Hantula, Finnish Motor Insurers' Centre, Helsinki, Finland;
Mr. Kim Hazelbaker, Highway Loss Data Institute, Arlington, Virginia, USA;
Mr. Werner Huber, Technical University of München, Germany;
Prof. Dr. Hartmut Keller, Technical University of München, Germany;
Mr. Anders Kullgren, Folksam Insurance, Stockholm, Sweden;
Mr. Anders Lie, Swedish National Road Administration, Borlänge, Sweden;
Mrs. Pauline Masurel, Department of Transport, London, UK
Mr. Brian O'Neill, Insurance Institute for Highway Safety, Arlington, USA;
Prof. Dr. Claes Tingvall, Swedish National Road Administration, Borlänge, Sweden;
Mr. Peter Wilding, Department of Transport, London, UK;
Prof. Dr. Hans Wolff, University of Ulm, Germany;
Dr. Falk Zeidler, Mercedes-Benz, Sindelfingen, Germany;
Dr. Robert Zobel, Volkswagen, Wolfsburg, Germany;

FUTURE DIRECTIONS FOR AUSTRALIAN NCAP

Christopher G.M. Coxon
Transport South Australia
James W. Hurnall
Queensland Transport
Australia

Paper Number 98-S11-O-10

ABSTRACT

Consumer research shows new car buyers want to consider vehicle safety before making a vehicle purchase decision. Vehicle safety practitioners can consider additional factors than the minimum standards set by regulations. These additional safety factors must be relevant to the requirements of an increasingly educated customer who has access to a wide range of safety data including that available on the Internet. To maintain relevance, Australian NCAP (ANCAP) must react to new customer issues, such as changes in new vehicle regulations, improvements in crash performance of cars in certain types of crashes, and the types of road crashes that contribute to road trauma. ANCAP must adapt to change and improve published material. It must add relevant tests that research shows contributes to improved occupant protection against vehicle crash injury.

This paper also considers the future of Australian NCAP and the relevance to consumers of including car to car tests, European side impact test, American side impact test, pedestrian impacts, and rollover tests. Vehicle manufacturers' criticisms of ANCAP are similar to those of other international NCAP groups and some responses are given. Consumers are asking for relevant product safety information to make an informed vehicle selection choice. ANCAP information must adapt and change to meet these changing consumer demands.

INTRODUCTION

Researchers have been asking new car buyers for a long time what factors are important when they make a new car purchasing decision. Most specific consumer research information is carried out in small focus group sessions where the detailed feeling of consumers can be explored. In this way motorists' priorities and attitudes can be recorded. If the research is carried out over several years, then the changes to attitudes and priorities can be measured. The feedback from research study groups is very important for Australian NCAP, which has a goal to publish relevant vehicle safety material.

Misconceptions about what makes a car safe continue, as many consumers still equate a strong vehicle with safety. Accident prevention features, or active safety items such as ABS brakes rate a minority mention. Airbags are commonly mentioned as a safety feature, but the trickle of unfavourable news stories, mostly from the United States, have undermined their credibility for Australians in the last two years.

Fleet managers are major purchasers of new vehicles who have become increasing informed about vehicle safety issues. New occupational health and safety legislation defines the rights of people who are injured while working, which includes using a company vehicle while at work. There exists possible liability for a fleet manager if they knowingly supply a new vehicle with poor performance in independent crash rating programs. Manufacturers must take notice of this change to fleet managers' possible legal liability and build vehicles which perform well in consumer crash tests, or risk losing business with this large segment of the market.

Fleet Manager and Consumer Vehicle Safety Needs:

- Consumers want clear simple, non technical advice on vehicle safety.
- The information should be applicable to the most frequent vehicle occupant injury crash types.
- Consumers want consistent, knowledgeable safety messages from authoritative sources.
- Regulatory safety requirements meet minimum consumer safety needs, but are not useful to select a safer new vehicle.

ANCAP CONSUMER BROCHURE FORMAT SMALL CARS

Model	Airbags	Rating
Mitsubishi Mirage 96-on	(D&P Airbag)	A
Toyota Starlet 96-on	(D&P Airbag	A
Honda Civic 95-on	(D airbag)	A
Ford Laser / Mazda 323	(D airbag)	A
Mitsubishi Mirage 96-on		A
Toyota Starlet 96-on		M
Daihatsu Charade 96-on	(D Airbag)	M
Daihatsu Charade 96-on		M
Daewoo Cielo 95 -98		M
Hyundai Lantra 95-on	(D airbag)	M
Nissan Micra 95-97	(D airbag)	M
Nissan Pulsar 95-on	(D airbag)	M
Ford Laser 95-on		P
Holden Barina 95-on	(D& P airbag)	P
Hyundai Lantra 95-on		P
Nissan Micra 95-97		P

Key to Overall Ratings:
G Good A Acceptable. M Marginal. P Poor.

DISCUSSION

Market research with people who have recently purchased a new vehicle show there is an expectation that all vehicles will be safe. This is seen as a combined responsibility for governments to make necessary safety regulations and vehicle manufacturers to test and ensure the safety regulations have been met. New vehicle buyers also wanted safety ratings to be available at car dealers, which is not presently the case.

Regulations

Safety regulations require manufacturers to certify that vehicles are designed and tested to meet the minimum safety standards. These standards are often many years old and while providing a basic level of occupant protection, consumers now expect a more adequate level of protection. Much has been debated about the need for uniform international occupant protection safety standards, but in practice they remain an unrealised goal. Full-frontal tests differ in detail in most major markets, with the United States requiring an unbelted 48 km/h crash test. Aggressively deploying airbags, which have been reported as causing injury to belted occupants in crashes, have resulted in changes to reduce head and neck injuries.

In international automotive markets, manufacturers must choose front and side impact specifications that meet market regulatory requirements. This means that consumer safety test data could give different safety ratings, depending on the source country of the consumer test. An example is the Euro NCAP side impact crash test program and the NHTSA side impact NCAP test program in the United States, where the tests are to different standards, at a different test speed and with different dummies.

Side Impact Crash Testing

Consumers researching published data or through the Internet, may be confused with the different ratings that result on the same vehicle model. Side Impact data are available on the Internet for both the Mercedes C-class sedan and the Ford Modeo/ Contour.

Table 1.
Internet Consumer Side Impact Safety Data 1998

	NHTSA Side Impact Rating Front Occupant	NHTSA Side Impact Rating Rear Occupant	Euro NCAP Side Impact Driver
Mercedes C- class	★★★ 11-20% Chance of serious injury	★★★★ 6-10% chance of serious injury	Head & Pelvis Good Chest Weak Abdomen Marginal
Mondeo/ Contour	★★★ 11-20% chance of serious injury	★★★★ 6-10% chance of serious injury	Head Abdomen & Pelvis Good Chest Poor

Consumers may find that United States side impact crash test consumer results are different, as in Table 1, for the same models when tested by EuroNCAP.

Australia has regulated to allow certification to either the European or the FMVSS side impact standard. Manufacturers of similar vehicles could choose to certify the vehicles with either side impact standard. ANCAP will eventually adopt one side impact test, as it may confuse consumers to test similar competitive vehicles to two different tests. ANCAP will review available published side impact crash test data, and discuss issues with both the international consumer crash test community, and manufacturers' before commencing side impact crash testing.

Airbags Regulation & Head Injury Risk

Australian regulations require manufacturers to certify vehicles to meet Australian Design Rule 69 (ADR69) which is similar to FMVSS 208 but without the need to test for unbelted occupants. ADR69 is not design specific but is performance based. Many manufacturers can meet the requirements with or without driver or front passenger airbags. This has allowed the price sensitive sectors of the small and medium passenger car market to have vehicles available in the Australian marketplace without frontal airbags. In a frontal crash, the absence of the driver airbag can increase the risk of head and chest injury between two and nine times for the same basic model. Consumers need to be aware of this significant difference, even if all vehicles meet the basic regulated standard.

Table 2.
Airbags reduce the chance of head injury

Head injury Risk. % of a life threatening injury.			
	Driver airbag	No driver airbag	Ratio of risk
Large Cars	17 %	40 %	2.4
Small Cars	6 %	28 %	4.6

In Table 2 the advantage of driver airbags in frontal crashes for small cars is very clear. The risk of a life threatening head injury requiring hospital treatment average is 4.6 time as great for small cars not fitted with driver airbags. The average ratio of head injury risk for large cars is 2.4 times as great without the driver airbag.

Consumer issues that flow from market research are the unfavourable news stories from the United States on airbag injuries to children. One United States media story, republished in the Australian media reported a parking lot low speed crash in which the passenger airbag inflated resulting in fatal injuries to the child who was a front seat passenger. No material was presented that explained the child was not wearing a seatbelt. The resulting damage to consumer confidence in airbags is dramatic. It is especially true for women who read and believe the story could happen to their children. Research shows women have a considerable influence in the issue of safety in vehicles, especially if they transport children. They may use this media information to change from buying an airbag equipped vehicle, to making a firm decision to not specify an airbag next time they buy a new vehicle. Subsequent press and media information on the original crash has little effect on the person's belief that airbags can fatally injure a child.

The new role for vehicle consumer safety groups is to take up safety issues of unfavourable news media reported crashes and then maintain a constant media flow of the benefits of vehicle safety equipment. This requires monitoring of the print media and effort to produce a flow of good news where safety equipment has been effective in reducing occupant injury in vehicle crashes.

Manufacturers' Safety Information

There needs to be more consistent safety information from sources where consumers receive occupant safety information.

At present, manufacturers do not publish material which would allow a reasonable person to make a knowledgeable comparison of vehicle safety, by model against a competitive product. However, it is acknowledged that safety of vehicles covers an enormous range of topics to ensure all safety areas are adequately addressed. The lack of availability of factual material from manufacturers on consumer safety material is not expected to change in the near future.

Often, there has been conflict from manufacturers where a poor ANCAP frontal crash test result is dismissed by a manufacturer as a one-only test, and therefore not representative of the model. Manufacturers, or their representatives in international markets, have not been prepared to make available crash test data that they have generated, so that both test results can be published. A manufacturers' dismissal of an independent crash safety test may confuse some consumers. Mostly, conflict with manufacturers is from models that have performed poorly in ANCAP tests.

Some manufacturers who perform well in consumer crash tests use the ANCAP results to show consumers the model has performed well in independent crash tests. Their advertising, and sales information packages to buyers, and prospective new buyers, reinforce the need to make a safe purchasing new car decision.

Car to Car Crash Testing

Some car to car crash tests are carried out as basic research to validate the speed used in offset crash test programs developed by NHTSA, Insurance Institute for Highway Safety (IIHS), and EuroNCAP. Budget restrictions have not allowed this research testing to be considered as part of the Australian consumer program. It is not considered necessary to repeat this type of crash as a consumer information program at this time.

Information for Consumer Groups

There is a need for consumers to have access to material about many aspects of vehicle safety if they are to make a knowledgeable choice in selecting a new vehicle:

Future Consumer Safety Tests.
Frontal Crash test results.
Side impact crash test data.
Rollover tests.
Child Seat crash test results.
Pedestrian impact crash test data.
ABS Brakes, and effectiveness.

Frontal crashes into other vehicles, large trees or poles and fixed objects account for two thirds of Australian fatal vehicle crashes. For this reason frontal crashes remain the prime consideration for ANCAP. Later in 1998 ANCAP will consider if the past practice of testing two vehicles of each model, one at 56 km/h into a solid barrier, and another 40% offset test at 64km/h into a deformable barrier will continue. Should one of the tests be replaced with a side impact test? One area that has not progressed is publishing the ADR69 48 km/h crash test results in place of the Full frontal 56 km/h NCAP test. Confidentiality of test results submitted to the Government for certification purposes is no longer an acceptable reason for withholding valid consumer safety information.

Side impacts after frontal crashes are the next most serious crash causing serious injury, and is expected to be the included in our future consumer crash test programs.

Four Wheel Drive vehicles are over represented, by a factor of four, in rollover crashes that often cause severe occupant injury. An international test is needed to allow this group of vehicles to be evaluated for rollover resistance and occupant injury, with results published for consumers to make a knowledgeable choice.

Pedestrian test programs that publish results similar to those in place in Euro NCAP are seen as worthwhile to reduce unprotected road user injuries.

International Safety Specification Differences

It is recognised that using international crash testing data also needs to be referred to manufacturers' vehicle specifications for the model tested, and differences in specification in each market that could make a difference to the results.

One example is the use of Euro airbags for the European market and the specification of a full-size airbag in the Australian market. Head injury data may be significantly different in an offset test where the vehicle rotates, and the smaller Euro airbag may not capture the driver's head fully in an offset crash.

Consumers who now have access to international crash test data through Internet facilities, may be misled about vehicle safety when a particular vehicle is not constructed to the same specification as that presented in the electronic media. Manufacturers do not make differences in construction specification available to consumers in their Internet pages. Some are also reluctant to make specification detail differences available to crash testing groups.

ANCAP must consider specification differences in safety equipment that may contribute to different results on crash tests. Would the consumer be aware that for the same looking vehicle model sold in a different international market, different safety equipment levels than those supplied to Australian consumers are made available? This is particularly true for driver and passenger airbags that are not specified as standard equipment in Australia for many small or medium cars and 4WD vehicles.

International Crash Tests

With 38 international manufacturers producing vehicles, it is financially difficult to maintain up to date consumer safety tests to ensure all data are relevant to vehicle models available in the market. There is a need to share crash test data among consumer testing countries to ensure access to relevant safety material.

With increasing availability of crash test data from NHTSA, IIHS, EuroNCAP and Japan NCAP, there is great potential to republish vehicle model crash test data in other countries. This is a great benefit in Australia, where the passenger market is supplied by 38 different suppliers selling around 500,000 vehicles a year, ref Fig 3.

Figure 3.
Manufacturer, Market Share, Models sold and ANCAP Available Consumer Material

	Market share % 1997 data	Models	NCAP Publish-ed material (by volume)
GM	22.8	9	95.6
Ford	20.9	6	99.5
Toyota	13.8	8	95
Hyundai	9.9	4	93
Mitsubishi	9.3	5	96
Mazda	4.2	9	80
Honda	3.3	8	80
Nissan	2.9	7	75
Daewoo	2.6	6	50
Others	10.3	127	10

ANCAP material covers 73% of the passenger segment by volume. Many models in the luxury market imply they are safer that the mass produced high volume vehicles. Consumers may not have available any comparative crash safety material on these models. Australian NCAP tests from 10 to 15 vehicles a year. With data sourced from other crash testing countries, consumers in Australia can have more comparable occupant safety information on which to base a purchasing decision.

It is important to ANCAP that the consumer crash test specifications are the same to enable the use of international crash test results. ANCAP will align its testing where possible with international consumer crash tests. An area of difference will be the result presentation format, where each country will choose the presentation format that best suits the home market.

SUMMARY

ANCAP must develop its future direction to make easily available, in a consumer friendly format, vehicle safety information required by an information society.

ANCAP should make public vehicle safety information linkages for consumers and fleet managers who use and purchase vehicles as part of their work.

Frontal airbags are effective in reducing head injury, and more action is needed to increase fitment in all vehicles.

ANCAP must work with international vehicle safety programs and manufacturers to provide consumers with best practice vehicle safety information.

There is a need for ANCAP to investigate other types of vehicle injury crashes to improve consumer safety material.

Review developments, applicability and feasibility of introducing side impact crash tests to enhance consumer vehicle safety material.

ANCAP to continue work with manufacturers and their agents to ensure correct safety information is available to consumers purchasing new vehicles, where overseas safety data may be different due to specification differences.

REFERENCES

Highway & Vehicle Safety report. NHTSA Crash test results, 1996-7

EuroNCAP Crash Test Program. UK Department of Transport of Transport. Crash test results, 1996-7

Australian NCAP. Buyer's Guide to Crash tests, March 1996, November 1996, & February 1997.

Australian NCAP. Buyer's Guide to New Car Safety Crash Tests, July 1997 & December 1997.

Australian NCAP. Buyer's Guide to Car Safety Crash Tests. An at a glance summary of crash tests to December 1997.

ANOPS Market survey, 1997. Australian Automobile Association.

ANOPS Qualitative Research Into ANCAP Crash Test Brochures, April 1998. ANCAP.

Federal Office of Road Safety Airbags Enhance Safety Popular Small Cars, 1997

Federal Office of Road Safety Airbags Enhance Safety Popular Large Passenger Cars, 1997

Glass's Guide, Australian Automotive Industry Directory / Federal Chamber of Automotive Industries, 1998 Black & White Data Book.

IMPROVEMENTS IN NCAP RESULTS FOR AUSTRALIAN VEHICLES

Christopher G.M. Coxon
Transport South Australia
James W. Hurnall
Queensland Transport
Australia
Paper Number 98-S11-O-11

ABSTRACT

Since 1993 Australian NCAP has been crash testing vehicles and publishing results to provide new vehicle consumers, when making a purchasing decision, independent advice on occupant protection. During the life of the program there have been significant improvements in the occupant safety performance of some vehicles while other models have shown only small improvements.

This paper reviews the performance of those vehicles crash tested in the Australian NCAP (ANCAP), highlighting models that have shown significant improvements in performance. An analysis of crash test data, known changes to vehicle specification and change in price for the vehicle, is undertaken to review the improvements in occupant protection offered and any associated increase in costs.

In 1997 Australian NCAP calculated an expected community benefit to cost ratio of 3.3 for improvements in occupant protection in passenger cars. This was based on assumptions contained in earlier work including an estimated increase in cost of $200 per vehicle for improvements in occupant protection and the expected reduction in social costs of crashes. This analysis is reviewed in light of the actual improvements in occupant protection in the new car fleet since the start of NCAP in Australia

INTRODUCTION

As the Australian new car market is dominated by a small number of passenger cars in the Large / Medium and Small Car categories the ANCAP has conducted three programs for testing each of these categories.

This paper reviews the process used by ANCAP to select vehicles for testing and the results of the test conducted for each of the three Large / Medium Car and Small Car programs. The results are reviewed in terms of the impact on improvements in occupant protection in the new car fleet since the start of NCAP in Australia.

VEHICLES SELECTED FOR NCAP

Selection Criteria

The vehicle selection procedure for NCAP must be compatible with the NCAP mission:

"To facilitate improvements in motor vehicle occupant protection through consumer education and buying power influenced by crash testing popular motor vehicles sold on the Australian market and publishing the relevant performance of the total occupant protection section."

Based on the NCAP mission and the goals of influencing buying decisions of new car buyers and manufacturing strategies of vehicle manufactures to increase the level of passive safety in passenger cars the following selection criteria are used:

1. sales figures (or projected sales) : to target those cars that are the most popular,
2. model : to account for standard or deluxe models which may contain airbags,
3. body configuration : to select the body configuration that is the most popular or to allow for direct comparisons across different manufacturers vehicles,
4. market segment : to target individual segments of the market to allow comparison of results,
5. cost : to make the most cost effective use of NCAP funds.

The selection procedure allows long term planning, ie. a test program up to 12 months in advance and addresses different sections of the vehicle market based on sales volumes.

Makeup of Australian New Car Fleet

Until recently the Australian new car fleet has been dominated by four vehicles, General Motors - Holden Commodore, Ford Falcon, Mitsubishi Magna and Toyota Camry. These four cars account for approximately 40% of new cars sold in Australia each year. The Large / Medium Car category accounted for approximately 45 % of all new passenger cars sold in Australia in 1998.

Table 1 below has details on sales volumes for 1993, 1995 and 1997 for the different segments as grouped by ANCAP.

The next main group of car sales is in the Small Car category which in 1997 accounted for 42% of the new car market. There are a number of these models which consistently sell approximately 20,000 units per year and hence become the basis for any ANCAP Small Car Program. The largest increase in any vehicle category during this period was in this category which saw an increase in sales of 110,000 units from 1993 to 1997.

Table 1
Sales Volume of Australian New Car Market

ANCAP Categories	Sales in Calender Year		
	1993	1995	1997
Large / Medium	246,395	257,533	248,433
Small	118,146	145,506	228,178
Passenger 4WD	49,961	43,778	50,269
People Movers	6,481	7,065	6,702
Prestige / Luxury	20,064	35,973	33,710
Utilities	50,857	71,370	70,394

The ANCAP uses vehicle categories that align closely with the Federal Chamber of Automotive Industries (FCAI) market segments. The FCAI segments of Micro, Light and Small are all combined into the NCAP Small Car category while the FCAI Medium and Upper Medium Segments are combined into the NCAP Large / Medium Car categories.

The ANCAP Small Car category contains passenger cars up to 1100 kg kerb weight while the Large / Medium Car category continues on from this with passenger cars up to approximately 1600 kg kerb weight.

Most cars in other market categories sell less than 10,000 units per year, with many makes selling less than 5,000 units per year. Additionally, more development work appears to be carried out in these categories and new or upgraded models are offered more frequently. Consequently the ANCAP has concentrated on crash testing the volume sellers in the Large / Medium and Small Car categories.

Three programs have been conducted on each of these categories while other categories have had only a single program conducted, ie people movers and commercial utilities. The ANCAP are just starting a second program on passenger four wheel drives.

RESULTS OF NCAP TESTS

Coverage of Australian New Car Fleet

To analyse ANCAP results to determine if there has been any improvements in front seat occupant protection, the Life Threatening Injury Risk (LTIR) value is calculated from results published by ANCAP during 1993, 1995 and 1997 for large / medium cars and for small cars.

Due to the high coverage of the Australian new car fleet by the models tested by ANCAP (between 60 % and 70 % as shown in Table 2) it is assumed that range of models tested are representative of the entire fleet

Table 2
ANCAP Coverage of the Australian New Car Market

Calendar Year	Total Sales	ANCAP tested	Coverage
1993	555,306	334,067	60 %
1995	488,372	309,038	63 %
1997	540,353	395,243	73 %

Life Threatening Injury Risk

The Life Threatening Injury Risk (LTIR) is the probability of sustaining a life threatening injury), ie AIS 4 or greater, and is obtained by combining the results of both HIC and chest compression for both full frontal and offset crash tests.

LTIR was calculated separately for driver and passenger. This showed a reduction in LTIR for those cars tested by ANCAP over this period. The average LTIR for Large / Medium cars (called L / M in the following tables), Small cars and a total for each of the three years are summarised in Table 3 below;

Table 3
Average LTIR of the Australian New Car Fleet

Year	L / M		Small		Total	
	D	P	D	P	D	P
1993	54	49	54	46	54	47.5
1995	26	28	49	27	37.5	27.5
1997	25	21	34	26	29.5	23.5

From these results it is obvious that there has been improvement in the level of occupant protection offered by new cars available for sales in Australia. It is interesting to note that this type of analysis shows more improvement in the Large / Medium Car category than the Small Car category.

Using a fleet weighted average technique based on models tested by ANCAP will present a picture of the level of occupant protection offered in the new car fleet as the Australian new car market is dominated by the small number of models represented in ANCAP tests.

The LTIR fleet weighted averages were calculated from VFACTS data which shows the number of units sold in that calendar year, ie 1993, 1995 and 1997.

A fleet weighted LTIR for a model can be calculated using:

Fleet LTIR = (model sales / ANCAP volume) x LTIR (1.)

where:
model sales = total sales of the test model throughout the calendar year
ANCAP volume = the total sales of all ANCAP test models throughout the calendar year

Table 4
Fleet Weighted LTIR of the Australian New Car Fleet

Year	L / M		Small		Total	
	D	P	D	P	D	P
1993	42	39	19	15	61	54
1995	24	26	20	11	44	37
1997	18	15	17	15	35	30

This method also shows there has been substantial improvements in the level of occupant protection offered by the Australian new car fleet over this period.

It is interesting to note that a fleet weighted analysis shows there has only been improvements in the Large / Medium Car category, not the Small Car category. This is because the Australian market is dominated by 4 models in the Large / Medium Car category while the Small Car category has a larger number of lower selling vehicles, with a wider range of LTIR, which results in a low fleet weighed LTIR.

This leads to two questions;

What is the cost of the improvements in occupant protection?

How are the improvements achieved?

COST OF IMPROVEMENT

The costs of improvements in occupant protection are part of the overall cost of a new car and therefore can be gauged by considering the total cost of the Australian new car fleet. This will be determined using sales volumes for cars tested by ANCAP and calculated using total cost for volume of cars sold.

The cost of cars fluctuates throughout the year and with options. To achieve a consistency for comparisons the new model price contained in "The Red Book" has been used and the most popular variant has been chosen, ie for large car this will be a sedan with automatic transmission and for a small car this will be a variant with manual transmission.

Where ANCAP has tested both an airbag and non-airbag model the additional cost for the airbag is included.

The average cost of a new car for both car categories and the total are calculated and recorded in Table 5 below.

Table 5
Average Cost of New Australian Cars

Year	L / M ($)	Small ($)	Total ($)
1993	25745	17910	22606
1995	29000	20087	25997
1997	29703	17407	24402

An interesting point that Table 5 highlights is the decrease in average cost of a new small car which may be due to the influence of Korean made cars on the new car market. The highest selling car in this category is the Hyundai Excel which accounts for 17 % of all small cars and outsells its nearest rival by almost 2 to 1. This has resulted in a lower average cost for 1997 new cars when compared with 1995 new car costs.

To take into account inflation, the average weekly wage will be used and the cost of the cars in terms of the average weekly wage will put the increase in price into perspective.

Table 6
Australian Average Weekly Wage

Year	1993	1995	1997
Wage	522.30	554.50	591.40
% Increase	0	6.2	13.2

Table 6 has the Australian average weekly wage for all employees as at November for each year and the corresponding increase over the 1993 figure.

The cost of a new car can then be expressed in terms of the number of weeks required to purchase (Figure 1);

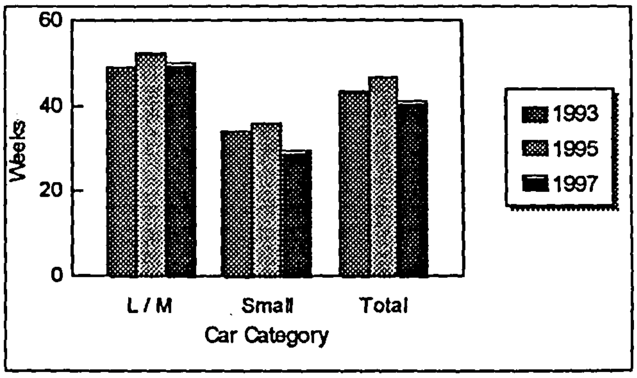

Figure 1. Weeks to purchase a new car

From the above graph it can be seen that the affordability of a new passenger car in Australia has not changed very much from 1993 to 1997. For example, to purchase a large cars in 1993 required 49.3 weeks while in 1997 it required 50.2 weeks, ie an extra week.

However, the cost of a new small car actually decreased from 1993 to 1997 (after an increase in 1995) from 34.3 weeks to 29.4 weeks.

The overall cost of purchasing a new car also had a slight decline from 43.3 weeks in 1993 to 41.3 weeks in 1997. A major factor in this was obviously the decrease in cost of small cars and the increase in sales of small cars. While the volume of large car sales remained fairly static at approximately 250,000 units the small car sales increased by 90 % from 118,000 units (1993) to 228,000 units in 1997.

While the overall level of occupant protection offered in the Australian new car fleet has improved the affordability of new cars has also increased.

SAFETY IMPROVEMENTS

There have been obvious improvements to occupant protection in Australian passenger cars during the life of the NCAP. These include improvements in the restraint systems to existing floor pans and body shells through the addition of items such as airbags, webbing grabbers and pretensioners with model upgrades.

When manufacturers have designed a new car they have taken the opportunity to introduce leading edge automotive safety technology. Consideration of the two main sellers in the Australian new car market, General Motors Holden Commodore and Ford Falcon will highlight this.

General Motors - Holden Commodore

1993: The 1993 Commodore (6 cylinder VP Executive), as one of the two largest passenger car sellers in the Australian car market was included in the initial ANCAP tests in 1993. This test was a 56 km/hr full frontal test which resulted in a Driver HIC of 1690 and chest compression of 52 mm, while the passenger HIC was 2410 with chest compression of 45 mm.

1995: In 1995 the upgraded model, VR Commodore was tested. The VR was a face-lift for the Commodore which included seat belt webbing grabbers as standard equipment and both driver and passenger airbags were offered as options. The model tested by ANCAP was fitted with a driver airbag.

1997: In 1997 a new model, the VT Commodore, was released. This was a completely new vehicle with an increased wheelbase and increase in width over the previous model. To improve the occupant protection the VT Commodore's front structure was improved. Also a driver airbag was included as standard and both front seats have lap sash seat belts fitted with both webbing grabbers and pretensioners.

Table 7
ANCAP Full Frontal Test Results for Commodore

Year	Driver		Passenger	
	HIC	Chest (mm)	HIC	Chest (mm)
1993	1690	52	2410	45
1995	1170	41	1110	45
1997	441	38	710	44

As seen from Table 7 the improvements in occupant protection technology that were designed and manufactured into the successive models of Commodore resulted in improvements in ANCAP test results.

Ford Falcon

1993: As the other of the two largest selling cars in Australia the Ford Falcon was included in the initial ANCAP in 1993. The Falcon tested, a 6 cylinder EB Series 2, was fitted with seat belt webbing clamps and performed slightly better than the Commodore as seen from the summary of the HIC and chest deformation measurements in Table 8.

1995: In 1995 the upgraded EF Falcon was tested. The EF Falcon was fitted with a driver airbag as standard equipment and both front lap sash seat belts were fitted with webbing grabbers.

1997: In 1997 another upgraded model, EL Falcon was available. This model had no further occupant protection improvements over the EF model. A completely new model Falcon is due out in late 1998.

Table 8
ANCAP Full Frontal Test Results for Falcon

Year	Driver		Passenger	
	HIC	Chest (mm)	HIC	Chest (mm)
1993	1340	54	780	47
1995	910	59	1280	48

As seen from Table 8 the improvements in occupant protection technology that were designed and manufactured into the upgraded EF model Falcon resulted in improvements in ANCAP test results for the driver. This is expected to continue with the new model Falcon due for release late in 1998.

COST BENEFIT ESTIMATE

Previous Analysis

In 1994 an analysis of the occupant protection afforded by the vehicles tested by ANCAP up to that time was undertaken and included in the Report to Stakeholders. The analysis intended to determine if it was cost effective to improve the front seat occupant crash protection in the Australian new passenger car fleet to a level at least equal to world's best practice which was considered to be the USA new car fleet.

The potential benefit was defined as the likely savings in the social costs of passenger vehicle occupant trauma in full frontal and offset crashes in speed zones of 80 km/hr or less. Road trauma costs from Queensland, New South Wales, Victoria and South Australia were used.

The saving was calculated for each future year by multiplying the trauma costs by the injury risks of the improved Australian fleet for the year in question and dividing by the injury risk of the existing Australian fleet.

The costs associated with improving the NCAP performance of the Australian fleet to the achieved USA level were determined by adding the total cost of the NCAP program to the cost of improving the level of safety of the vehicles.

The analysis was based on the fleet weighted driver LTIR as this was higher than the passenger LTIR.

The analysis was conducted using an estimated cost per vehicle of $200 for improvements in occupant protection. A 7 % discount rate and 10 year introduction for new vehicles was used.

Under these assumptions, after one year a benefit cost ratio of 2.48 is achieved. The benefit cost ratio continues to improve and after 15 years reaches a value of 3.61.

A sensitivity analysis was conducted on the average cost per vehicle to implement US protection standards. The sensitivity analysis showed that even with conservative assumptions and a 35 year fleet improvement time span, manufacturers could spend up to $750 per vehicle and still produce a positive benefit to the community.

Updating for 1997 Results

The expected new vehicle fleet average driver LTIR in 1997 was 43 %, which has been exceeded by the new models sold in 1997. The benefit cost analysis prediction did not expect a new vehicle fleet average driver LTIR of under 35 % until 2000. The Australian vehicle manufacturers have reached this target 3 years earlier than predicted.

Recalculating the potential BCR using the values used previously and bringing the 2000 benefits forward, ie:

Annual cost to community
- if current fleet is unchanged, 1997, $1,163 million
- if fleet average LTIR reduced to US levels, 2000 value, $847 million

Reduction in annual cost through improved fleet occupant protection levels, $316 million

Cost to improve occupant protection levels, (adding costs previously used for 1993 up to 2000), $127 million

Then BCR aggregate = 2.5

It is estimated that an aggregate BCR of 2.5 has been achieved through improved occupant protection levels of the new passenger car fleet.

SUMMARY

Since the commencement of the New Car Assessment Program in Australia there has been improvements in the occupant protection levels for front seat occupants in new passenger cars offered for sale.

Several factors have contributed to this improvement;

1. ANCAP
2. Introduction of ADR 69/00 in 1995
3. Introduction of cars that were primarily designed for the US and European markets.

By considering the results of the ANCAP tests in terms of the new car fleet there has been an improvement in the overall level of occupant protection for purchasers of new cars in Australia. With the increase in levels of occupant protection there has been a small increase in relative cost of a new large car, while there has been a decrease in relative cost of a small car. This has resulted in an overall relative reduction in the cost of new cars.

By updating a prior analysis it is estimated that the improvement in front seat occupant protection has shown a cost to benefit ratio of 2.5.

One of the large contributors to the reduction in cost of new cars has been the increase in volume of sales of small cars. What impact this will have on the overall level of safety offered by the Australian car fleet is not known.

REFERENCES

"New Car Assessment Program, 1992 - 1995, Report to Stakeholders", January 1995

VFACTS, Vehicle Retail Sales, Complied by Ferntree Computer Corporation for the Federal Chamber of Automotive Industries

New Car Assessment Program, "Crash Rating Report", Vol 1 Number 1, April 1993

New Car Assessment Program, "Crash Test Report", Vol 1 Number 2, April 1994

New Car Assessment Program, "Buyer's Guide to Vehicle Crash Tests - Large / Medium Cars and Small Cars", June 1995

New Car Assessment Program, "Buyer's Guide to Crash Tests - Small Car Update", November 1996

New Car Assessment Program, "Buyer's Guide to Crash Tests - Small Car Update", July 1997

New Car Assessment Program, "Buyer's Guide to Crash Tests - Large & Medium Car Update", February 1997

New Car Assessment Program, "Buyer's Guide to Crash Tests - Large & Medium Car Update", December 1997

Stolinski, Richard, "The Development of Result Presentation in Australia's New Car Assessment Program", Proceedings of the 15th ESV Conference, Melbourne, Australia, May 1996

Reilly-Jones, Carleen, et al, "Australian NCAP Program Reviewed - A Comparison of Performance of 1995 Australian and US Vehicles", Proceedings of the 15th ESV Conference, Melbourne, Australia, May 1996

"The Red Book Mar 1998 - Apr 1998, Australia's Premier Guide to New and Used Passenger and Light Commercial Vehicle Values and Identification", Published by Automated Data Services Pty Ltd, Canterbury, Australia, 1998

Seyer, K "Airbag Verses Non-Airbag Passenger Cars - A Discussion Paper", Federal Office of Road Safety, Australia,

Average Weekly Earnings, States and Australia, Australian Bureau of Statistics Catalogue No. 6302.0

"Autospec - 1993 Auto Market Guide" Published by Autospec Pty Ltd, East Malvern, Victoria, Australia.

"Autospec - 1995 Auto Market Guide" Published by Autospec Pty Ltd, East Malvern, Victoria, Australia.

"Autospec - 1997 Auto Market Guide" Published by Autospec Pty Ltd, East Malvern, Victoria, Australia.

AN ANALYSIS OF NCAP SIDE IMPACT CRASH DATA

Hansun Chan
James R. Hackney
Richard M. Morgan
National Highway Traffic Safety Administration
Heather E. Smith
Conrad Technologies, Inc.
United States
Paper Number 98-S11-O-12

ABSTRACT

Since 1990, the National Highway Traffic Safety Administration (NHTSA) implemented a dynamic side impact compliance test. This compliance test, Federal Motor Vehicle Safety Standard (FMVSS) No. 214, is a nearly right angle side impact in which the striking vehicle moves at 53.6 kmph into the struck vehicle. In 1997, NHTSA began testing passenger cars in side impact in the New Car Assessment Program (NCAP). In the USA NCAP side impact, the striking vehicle is towed at a 8 kmph higher speed than in the compliance test.

An analysis has begun on the data from the first NCAP side impact tests, thirty-two in number. In the crashes, accelerometers were installed in the door and door frames of the struck vehicle. Using the accelerometers on the vehicle structure and in the side impact dummy, the crash event was investigated. One tool used in the investigation was the velocity-versus-time diagram.

First, the crush of the interior door and its relationship to the severity of the occupant injury readings was examined. A correlation was found between the single independent variable, amount of the interior door crushed by the occupant, and the Thoracic Trauma Index. Second, the data was examined to determine the extent to which the pelvis of the dummy was loaded initially before loading the torso. A weaker correlation was found between the time duration (that the pelvis was loaded before the torso) and the Thoracic Trauma Index. Finally, the effect of the two independent variables together was examined.

INTRODUCTION

Based on the most harmful event, side impact accounts for 25 percent of fatalities for passenger car and light truck crashes in the USA. [1] For passenger cars, side impact accounts for approximately 30 percent of the fatalities in passenger car crashes. Likewise, side impact accounts for roughly 15 percent of light truck fatalities. Since the use of dynamic Federal safety standards in side protection began, in recent years occupant protection in side impact crashes has received increasing interest. This interest comes from both the consumers and the automotive industry. [2,3]

In comparison with frontal collisions, the space between the occupants and the intruding element in side crashes is extremely small. In addition, the side impact crash occurs much more rapidly. Consequently, occupant protection in side crashes presents a challenge to engineers designing a vehicle for safety.

Significant research work, both theoretical and experimental in nature, has been performed to characterize the safety performance of vehicles in side crashes. Gabler et al. [4] analyzed data of 28 production vehicles that underwent side impact crash testing. They found that these vehicles varied dramatically in their ability to protect the occupant in the struck car. They were able to identify a design parameter – the door effective padding thickness (DEPTH) – that strongly correlated with occupant thoracic injury potential.

Hobbs [5] investigated the influence of car structure and padding on side injuries. He analyzed more than 40 full scale vehicle impact tests. His findings revealed that a most important factor, in influencing protection, is the vertical intrusion profile of the incoming door. It appeared that controlling the vertical intrusion profile of the door is much more important than the prevention of the intrusion itself. Hobbs says "The degree of door tilt has been found to influence the way loads are transferred to the occupant. When the door tilts in at the top, loads are concentrated on the thorax. Where it (door tilt) remains upright, the loads are more evenly distributed and it may be that earlier loading of the pelvis reduces thoracic loading, by helping to accelerate the occupant sideways." Along the same line, Saab engineers developed a collapse behavior for the B-pillar that reduces the injury readings of the occupants in a side impact. It allows the lower part of the B-pillar to behave more softly than the upper part. Saab feels this "collapse" diverts crash loading to the parts of the body that can withstand them the most, the pelvic region. Saab feels this "collapse" protects the parts more susceptible to trauma: the head, rib cage, and chest. [6]

Lau et al. pointed out that the maximum velocity of the intruding door (of the stuck car) is important because the door strikes the occupant directly. [7] They compared the door's motion to a powerful "punch" to the dummy. In their paper, they pictured the velocity of the intruding door as rising as high (in magnitude) as the velocity of the striking barrier. Strother et al. presented data from another crash that suggested the velocity of the intruding door rose to a lower level, roughly the terminal velocity of the struck car. [8]

Finite element modeling has been successfully and extensively used to simulate collision events. Using the finite element program code DYNA3D, Rao et al. [9] simulated different impact scenarios at 45 kmph for a mid-size car being impacted in the side by a moving barrier. Their simulation results indicate that one can gain an understanding of how the interior door might respond to structural changes made in the struck car. Blaisdell et al. [10], in their comprehensive examination of collision performance of automotive door system , concluded that "...merely increasing door and latch strength without considering the entire system will not necessarily provide additional occupant protection, and may be counterproductive ...." They recommend that designers graph the velocity changes for different portions of the structure with respect to the occupant. This recommended approach parallels the method used in Reference 4.

Since 1997, the NHTSA has carried out forty-six full scale side impact tests under NCAP. These tests were conducted with extensive instrumentation so as to provide data needed for conducting research aiming at improving vehicle side protection. Accelerometers were installed in various locations of the test vehicle including the door panels, A- and B-pillars, sills and floor, and vehicle center of gravity (CG). This information, combined with data recorded from occupants, is used in this study to investigate the differences in safety performance and identify design parameters that influence vehicle side crash protection. The velocity-versus-time analysis as previously referenced [4, 7, 8, 10] was used in this study. The authors feel it helps in the visualization of the kinematics of the occupant and the behavior of the intruding vehicle structure.

TEST PROCEDURE

The vehicle impact tests that generated the data used in this analysis were conducted in accordance with the test procedure of the side impact NCAP. The NCAP side impact test is based on the dynamic requirements of FMVSS No. 214, but is conducted at a higher speed. The NCAP tests, which simulate an intersection collision, were conducted with a moving deformable barrier (MDB), as the striking vehicle. The 1360 kg MDB was moving at a speed of 61 kmph and at an angle of 27 degrees off the perpendicular to impact a stationery vehicle, as shown in Figure 1.

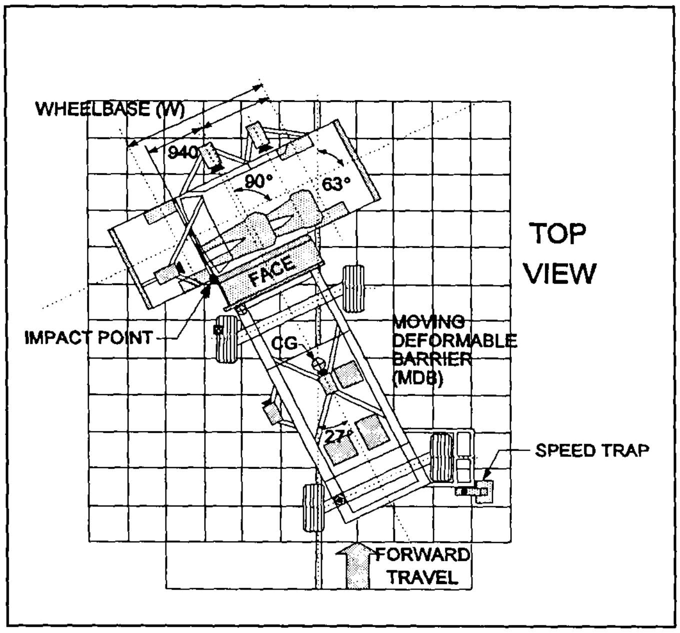

Figure 1. Test Setup.

Each impact test used two side impact dummies (SIDs) as specified in FMVSS No. 214. One SID was positioned in the driver seat, and a second SID was positioned in the rear passenger seat behind the driver, as shown in Figure 1. The dynamic response of each SID was recorded by accelerometers installed at the upper rib, lower rib, lower spine, and pelvis of each SID, as shown in Figure 2.

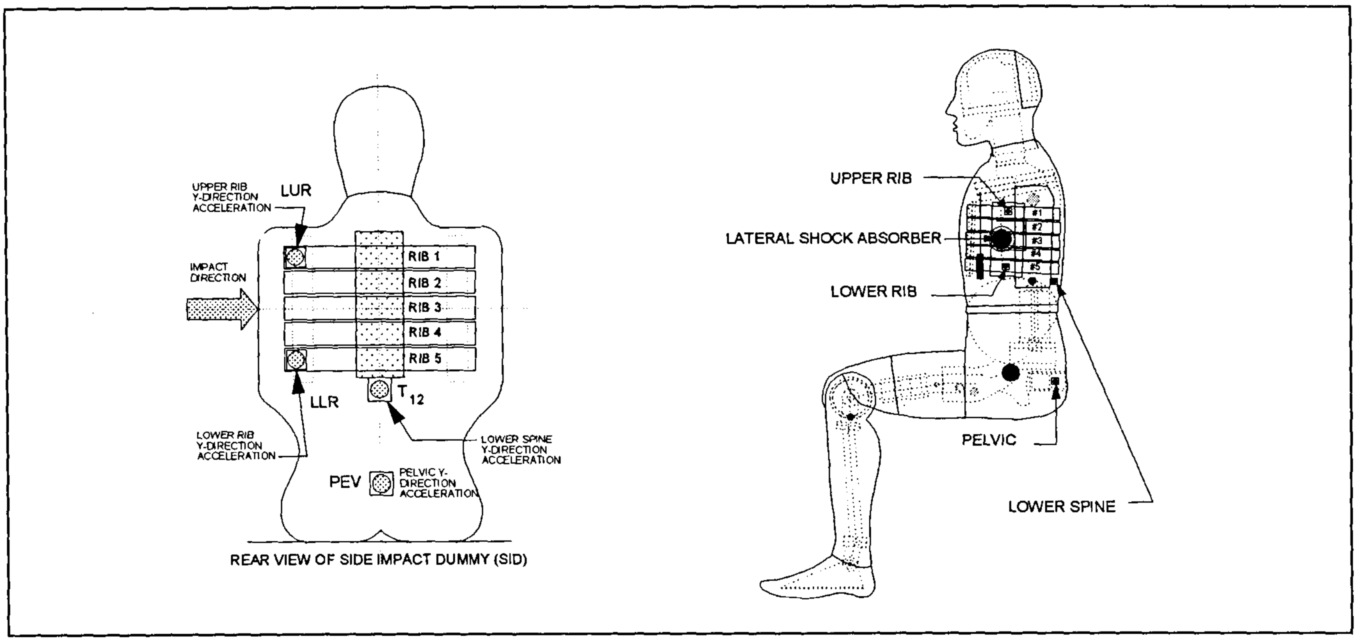
UPPER RIB Y-DIRECTION ACCELERATION
LUR
IMPACT DIRECTION
RIB 1
RIB 2
RIB 3
RIB 4
RIB 5
LLR
T12
LOWER RIB Y-DIRECTION ACCELERATION
LOWER SPINE Y-DIRECTION ACCELERATION
PEV
PELVIC Y-DIRECTION ACCELERATION
REAR VIEW OF SIDE IMPACT DUMMY (SID)
UPPER RIB
LATERAL SHOCK ABSORBER
LOWER RIB
PELVIC
LOWER SPINE

Figure 2. Rear and Side View of SID.

Twenty or so accelerometers were installed at various locations of the test vehicle to monitor the motion of the test vehicle and its structural components. Since the vehicle side doors and the door frames play an important role in side impact protection, special instrumentation was used to capture the dynamic responses o these components. For the front door, three accelerometers were installed on the interior surface of the inner door panel. For the B-pillar, two accelerometers were mounted on the interior surface of the inner door panel. Shown in figure 3 are the general locations of these accelerometers. Actual locations of these accelerometers may vary with the individual test because of the variations in vehicle design. Two accelerometers each were installed in the A-pillar and B-pillar. One accelerometer was located in the base and the other in the mid-section of the B-pillar.

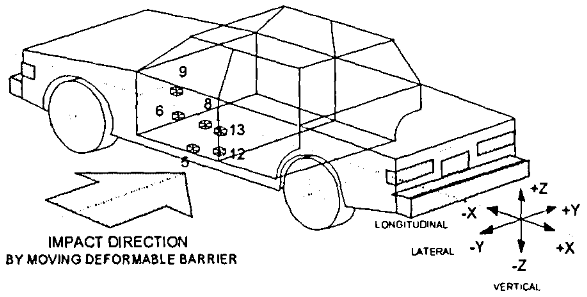
9
6
8
13
12
5
IMPACT DIRECTION BY MOVING DEFORMABLE BARRIER
+Z
-X
+Y
LONGITUDINAL
LATERAL
-Y
+X
-Z
VERTICAL

#5	Left Side Sill @ Front Seat
#6	Left Front Door on Centerline
#8	Mid-rear on Left Front Door
#9	Left Front Door on Upper Centerline
#12	Left Lower B-Post
#13	Left Mid B-Post

Figure 3. Location of Accelerometers.

PHYSICAL EVENT OF A SIDE CRASH AND THE VELOCITY-VERSUS-TIME DIAGRAM

During a car-to-car side collision, the physical event is a complicated transfer of momentum from the striking car to the struck car. To a large extent, the severity of the crash event, as seen by the occupant in the struck vehicle, is determined by the time rate of change for this momentum transfer. The time rate of momentum transfer, in turn, is dependent upon the relative structural stiffness and effective mass distribution, among other factors, of the individually struck cars. Because of their proximity to the impacting car and the occupant, the doors (front and rear) and the pillars (essentially the A- and B-pillars) of the struck vehicle are among the components that play a critical role in deciding how the momentum transfer is being carried out around the occupant. The doors and the pillars use their energy-absorbing capability and their material strength to channel the momentum transfer. In addition, the intruding door structure can provide an interior surface that crushes at a non-injurious level and acts to protect the occupant. The characteristics of the dynamic interaction between these components and the vehicle occupants (the SID test dummies) determine the effectiveness of the vehicle side crash protection performance.

One useful tool, to understand the dynamic interaction between the intruding door structure and the vehicle occupants during the impact, as well as to assess the efficiency of the door design in collision performance, is the velocity-versus-time diagram. This diagram graphically traces these critical structural components and the responses of the occupant. Shown in Figure 4 is a simplified illustration of a typical door construction. The door is generally comprised of the outer and inner panels (usually made of sheet metal) and the interior trim panel (usually made of plastic with or without energy-absorbing padding). Housed between the inner and outer panels (skins) are the window mechanism, remote actuating levers and rods, as well as reinforcing guard beam(s), if so equipped. The door is attached to the door frame, which is comprised of the pillar structure, roof rail, and door sill. The door frame is designed to resist collision forces and also serves to transmit crash loads from the region around the occupant (essentially the doors) to other vehicle structures during the crash. In the NCAP side tests, the motions of the striking vehicle; the doors, pillars, and occupant of the struck car; and the struck car were electronically monitored using accelerometers.

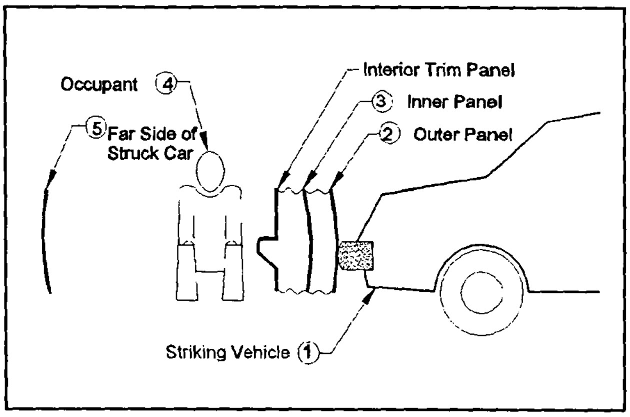

Figure 4. An Illustration of Door Cross Section and Essential Locations of the Velocity-versus-Time Diagram.

A velocity-versus-time plot, typical of the NCAP side tests, is shown in Figure 5. The outer panel (skin) is struck by the impactor (MDB) and moves together with the MDB almost immediately after contact, as shown by the curve denoted as ②. Within 3 to 5 milliseconds (msec), the velocity of the inner panel (together with the interior trim panel) rises to the speed of the striking vehicle as it (the door) continuously undergoes deformation. Sometimes the speed of the inner door panel overshoots that of the impactor, as shown by curve ③. In fact, curve ③ is representative of the velocities of the pillars as well. Dynamic contact between the door inner surface and the SID (in the area of the ribs, spine, or pelvis) generally starts 10 to 20 msec after the impact event began. After the dynamic loading of the occupant (SID) by the intruding door structure has begun, the occupant usually reaches its peak velocity around 20 to 40 msec after initial impact. Curve ④ shows a typical velocity - time trace of the SID response. This response typifies the motion of the SID's rib, spine, and pelvis. As shown in the diagram, the occupant was contacted and loaded by the intruding door structure starting at time t_0. The intruding door continued in contact with the occupant until the two separated at time t_1. The continuous deformation of the door structure can also be visualized as a two-sequence event. First, the door starts to deform under the influence of the impactor. As this deformation continues, the interior door encroaches until striking the SID which resists the door's motion with its inertia force. This inertial loading of the door by the SID and the impact loading of the occupant starts at t_0 and lasts until time t_1 when the two separates. The velocity of the impactor, curve ①, and the velocity of the struck car, curve ⑤, generally move to a common velocity, v_f. The velocity-versus-time diagram not only documents (with a high degree of clarity) the key interactions of the crash event but also supplies the necessary data needed for analyzing and assessing the vehicle's collision performance in a side crash. In the sections that follow, the data in the velocity-versus-time diagram are used in an analysis and assessment of the NCAP side impacts.

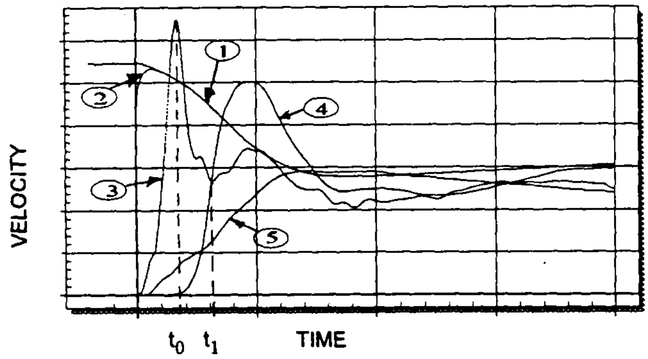

Figure 5. Velocity-versus-Time Diagram.

MAXIMUM SPEED OF THE INTRUDING DOOR

Figure 6 graphically presents the velocities of many essential points during the NCAP side impact test of the 1997 two-door Ford Thunderbird. To construct Figure 6, accelerometers at critical locations – the locations shown in Figure 3 – were integrated to obtain the velocities. During the first 140 msec, all the velocities progress to a common velocity, v_f, which is 32 kmph in the case of the Ford Thunderbird.

The velocity of the interior door goes from rest to 56 kmph in 11 msec. In the case of the Ford Thunderbird, the velocity rises quite high, above the velocity of the striking barrier. The occupant is not moving at all during these initial 23 msec. As suggested by Lau et al., the dummy is at rest and must receive quite a punch when the door intrudes inward about 132 mm.

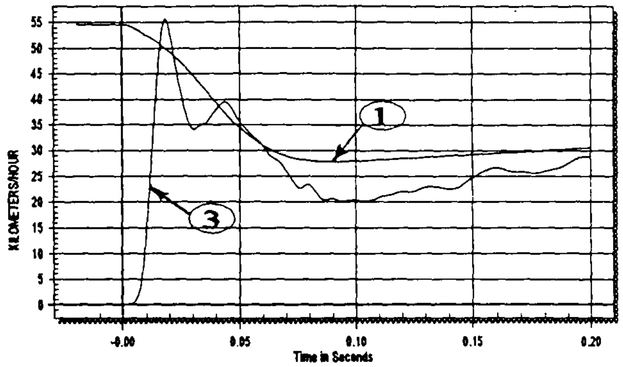

Figure 6. Interior Door Velocities of Ford Thunderbird.

In analyzing all thirty-two NCAP side impact tests, the maximum speed of the interior door varied over a range from a low of roughly 32 kmph to a high of about 59 kmph. For example, Figure 7 gives the velocity-versus-time diagram for the 1997 Toyota Corolla. In the case shown by Figure 7, the maximum speed of the door appears to rise only to about the final velocity, v_f, of the two vehicles around 10 msec.

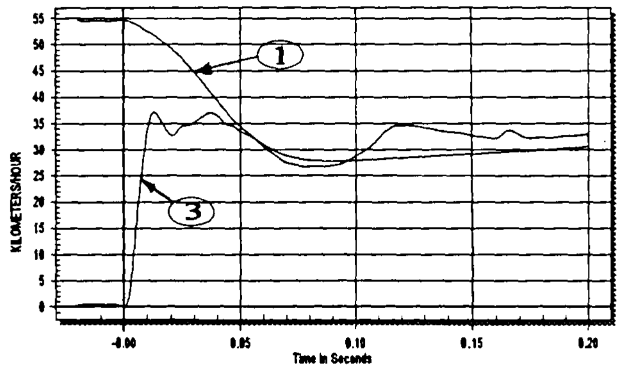

Figure 7. Velocity of the MDB and Toyota Corolla.

To quantify the range in door velocities, consider Figure 8. Shown is a corridor for the door velocity observed in twenty-seven NCAP side impact crash tests. The velocity of twenty-seven vehicles was computed at the mid B-pillar location of the struck vehicle. The two curves of the corridor are the plus one and minus one standard deviation curve for the twenty-seven tests. For perspective, the average velocity of the center of gravity of the striking vehicle – the moving deformable barrier – is drawn.

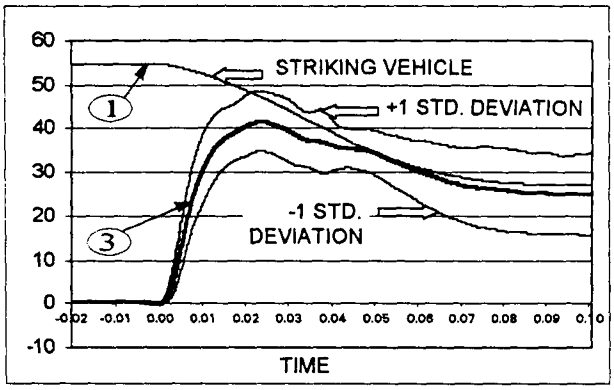

Figure 8. Average Velocity of Mid B Pillar with ± 1 Standard Deviation.

There are a possible choice of six door accelerometer locations: the left front sill, the left front door centerline, the left front door mid-rear, the left front door upper centerline, the left lower B-post, and the left mid B-post. The vehicles' mid-B pillar was chosen because, in general, this sensor performed satisfactory. Other sensors may have rotated or had curves that did not approach the final velocity. It is important to realize that for some vehicles, the peak velocity may have occurred at another accelerometer location.

Generally speaking, the maximum velocity of the door varied between two peaks for the set of all door velocities observed in these laboratory tests. One is a maximum velocity that has an apogee around the final velocity of the striking and struck vehicle. This is commonly termed the *soft stroke* of the impacting door. The second type of peak velocity occurs when the door velocity exceeds the striking vehicle's velocity. At this time, a *punch* is said to have occurred.

OCCUPANT CRUSH OF THE INTERIOR DOOR

Looking back at Figure 5, (or Figure 6 in the case of a specific car, the Ford Thunderbird), one sees the door's velocity, curve ③, rise to a maximum. In part, the interior door begins to decrease its velocity because occupant and door collide, and reaction forces are directed from the occupant, curve ④, onto the door, curve ③. The initiation of this interaction is indicated by time t_0 in Figure 5. It is 17 msec in Figure 6.

The distance between the door and the occupant is determined by computing the area between the door velocity curve and the velocity curve of the occupant (which is zero at the moment the door contacts the occupant). Integrating the velocity curve of the door, curve ③, in Figure 9, from t=0 to $t=t_0$, will compute the distance. This distance is also reported as the arm-to-door or hip-to-door distance.

At some point in time, the occupant and the interior door reach a common velocity. In Figure 5, this is marked by t_1. By computing the area between the occupant and door velocity curves from time t_0 to time t_1, one can determine the amount of door padding and structure crush and occupant chest crush. Gabler et al. [4] define Door Effective Padding Thickness (DEPTH) as the relative displacement between the door and occupant from the time of occupant-door contact until the time of occupant-door separation. Figure 9 below illustrates these areas. From the crash observer's perspective, DEPTH is the amount which the occupant's torso deforms plus the amount which the occupant crushes the door's padding and interior structure.

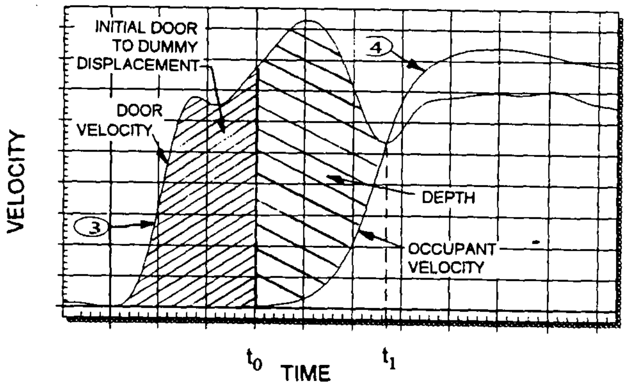

Figure 9. Door and Occupant Velocity Curves.

Figure 10 shows a plot of the Thoracic Trauma Index, TTI, for the thirty-two cars versus the occupant crush of the interior door. The data is included in Appendix 1. of this paper. A linear regression routine was compiled through the thirty-two data points and the R-value was computed to 0.48. Equation 1., below, describes this relationship. These data suggest that there is a correlation between TTI and the single variable, occupant crush of the interior door. [11]

$$\mathrm{TTI} = -0.146\ \mathrm{DEPTH} + 103.99 \qquad (1.)$$

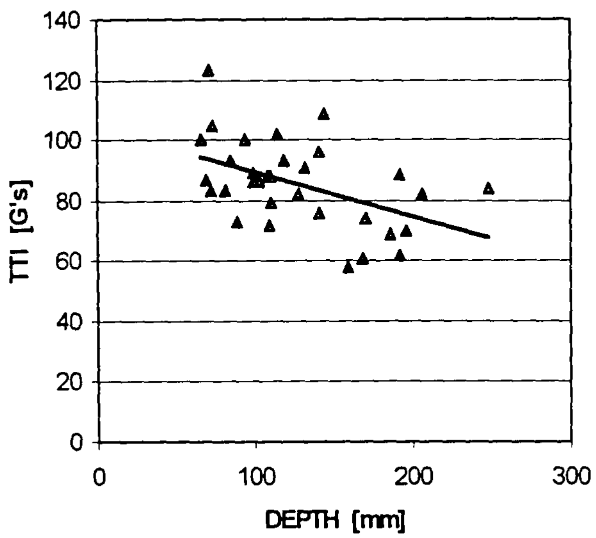

Figure 10. DEPTH vs TTI.

VERTICAL INTRUSION PROFILE OF THE INTERIOR DOOR

As Reference 6 suggests, it makes sense, from a biomechanical point of view, to have the intruding door load the parts of the occupant's body that can withstand the forces the most without trauma. Reference 6 advises that it is important to load the pelvic region during the initial occupant-door contact. As Hobbs explains, it is better to distribute the loading along the entire torso of the occupant, beginning first with the pelvis, than to have the intruding structure only strike the shoulder and torso, where many important organs are located. [5]

By referring to Figure 2, it can be seen that the dummy, SID, has a lateral accelerometer in the pelvis. There are two lateral accelerometers on the upper and lower ribs. The pelvis is a relatively rigid structure while the torso has a soft simulated arm over a stiff rib cage. If the dummy is being loaded by an interior door that is vertically aligned, then the pelvis accelerometer should have an initial response at the same time or slightly before the beginning of the rib cage acceleration. Should the pelvic signal start significantly before the signal at the rib cage, then the pelvis is contacting the door first. This *lead* is commonly referred to as the pelvic lead. The pelvic lead phenomenon has been applied to the design of some vehicles. [6] Basically, it amounts to the pelvis being impacted ahead of the thorax.

To determine the pelvic lead, one calculates the difference in time between the peak acceleration of the pelvis and the thorax (caused by impact with the intruding door), as shown in the equation below. Figure 11 shows two typical acceleration curves for the pelvis and spine.

$$\text{Pelvic Lead} = t_{\text{torso}} - t_{\text{pelvis}} \qquad (2.)$$

where,

t_{torso} = time at maximum torso acceleration, and
t_{pelvis} = time at maximum pelvic acceleration.

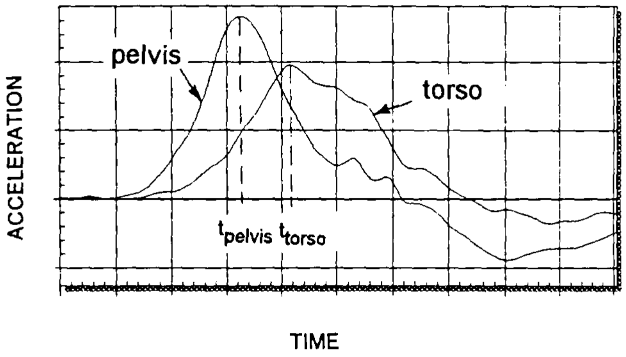

Figure 11. Occupant Response of Pelvis and Thorax.

For the thirty-two NCAP side impact tests, Figure 12 shows a plot of the Thoracic Trauma Index, TTI, versus the pelvic lead. These test data suggested that the pelvic lead will introduce beneficial effects to the thoracic portion of the SID. In other words, more pelvic lead lessens the severity of thoracic injury. These data suggest that there is a modest correlation between TTI and the single variable, pelvic lead. A linear regression routine was compiled with thirty-two data points and the R-value was computed to be 0.37, with the equation below, describing the relationship. [11]

$$\text{TTI} = -0.509 \text{ Pelvic Lead} + 95.05 \qquad (3.)$$

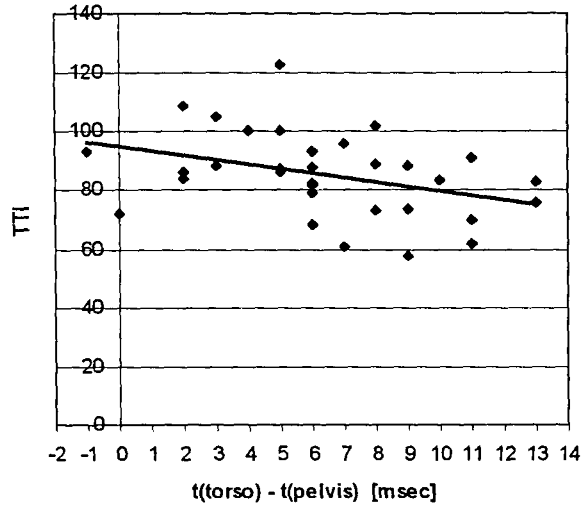

Figure 12. Pelvic Lead vs TTI.

Figure 13 plots the Pelvic Lead vs the maximum pelvic acceleration value. As shown, the Pelvic Lead and maximum pelvic acceleration are not necessarily related to each other. In other words, greater Pelvic Lead may not necessarily develop large pelvic acceleration.

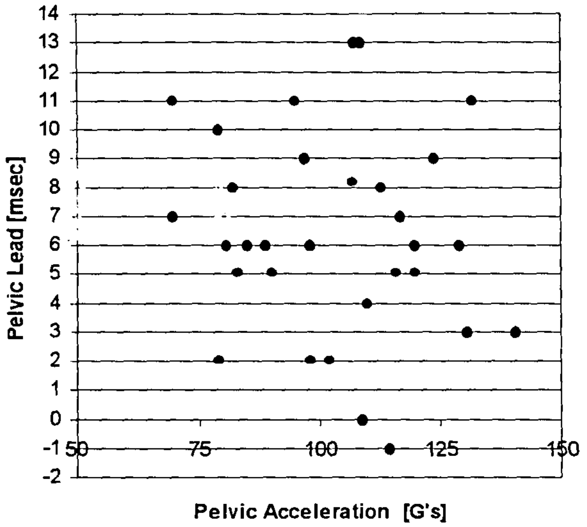

Figure 13. Pelvic Lead vs Pelvic Acceleration.

EFFECT OF COMBINING DEPTH AND PELVIC LEAD

In the Introduction section and the previous two sections, two important considerations for protecting an occupant in side impact were discussed. Using the data from thirty-two NCAP side impact tests, the dummy's response was examined first as a function of DEPTH and then as a function of pelvic lead. Alone, neither of these variables satisfactorily explains the response of the dummy in these tests. The next step in this study is to investigate if the two variables together increase our ability to explain the dummy's response.

A linear regression analysis was performed using a routine to determine the regression coefficients and confidence levels. [11] Two independent parameters, DEPTH and pelvic lead, were chosen for the regression analysis.

A relationship between these two independent variables and the Thoracic Trauma Index, TTI, was computed. The R-value for the combination of variables, DEPTH and pelvic lead, is 0.60 with the relationship described by Equation 4. [11] Figure 14 graphs the TTI, recorded in the NCAP tests, versus the linear combination of DEPTH and pelvic lead. Figure 14 illustrates that TTI increases, monotonically, as the linear combination of DEPTH and pelvic lead increases. This linear model explains about a third of the variability in the data.

$$\text{TTI} = -1.42\ \text{Pelvic Lead} - 0.14\ \text{DEPTH} + 112.5 \quad (4.)$$

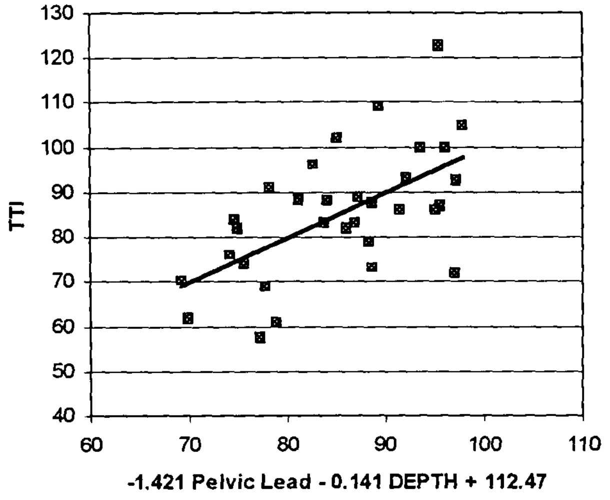

Figure 14. Linear Combination of Pelvic Lead and DEPTH.

To understand how the two independent variables interact to mechanically affect the dummy's response, the data in Figure 13 may be plotted as DEPTH versus pelvic lead. A data point would then be the value of TTI recorded in the NCAP crash test. For this type of cross plot, greater clarity is obtained by arranging the TTI values into groups and giving each group a nemonic symbol. On the cross plot, a data point would then appear under the symbol of the group to which its value belongs. To plot DEPTH versus pelvic lead, the TTI value was first converted to a star rating.

For those readers not familiar with the star rating methodology, the side star rating system is based on the thoracic injury function curve developed for the Thoracic Trauma Index. This thoracic injury function curve is contained in the final regulatory evaluation for FMVSS No. 214 [12] and is shown in Figure 15. This function relates the probability of an AIS ≥ 4 thoracic and upper abdominal injury to TTI in a lateral impact.

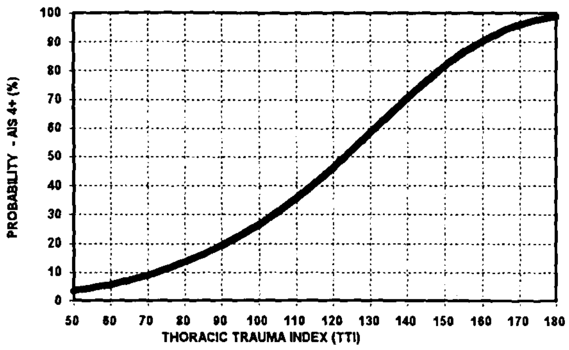

FIGURE 15. Thoracic Trauma Index Risk Function (Reference 12).

From the probability values, a star rating for an occupant was developed. The following levels are used to designate the stars:

☆☆☆☆☆ = 5% or less chance of serious thoracic and upper abdominal injury

☆☆☆☆ = 6% to 10% chance of serious injury

☆☆☆ = 11% to 20% chance of serious injury

☆☆ = 21% to 25% chance of serious injury

☆ = 26% or greater chance of serious injury

Using the risk curve, the star ratings correspond to a range of TTI values.

☆☆☆☆☆ = TTI ≤ 57

☆☆☆☆ = 57 < TTI ≤ 72

☆☆☆ = 72 < TTI ≤ 91

☆☆ = 91 < TTI ≤ 98

☆ = TTI > 98

In short, the star rating methodology converts the continuous TTI into a categorical variable. Appendix 2. provides star ratings for forty-six NCAP side impact vehicles.

Figure 16 shows the test data on a graph of DEPTH versus pelvic lead. For each of the thirty-two

NCAP tests, the dummy's response is represented by its star rating. Superior descriptors, of the mechanical input into the dummy, should partition different star ratings further apart with minimal overlaps. For poorer descriptors, the star ratings should be intermixed without clear separation. In Figure 16, it can be seen that DEPTH and pelvic lead begin to separate the outcome variable, representing the dummy's response. Those dummy responses with three stars are grouped together. The four star ratings are generally higher than the three star ratings but are mixed with the three star ratings. Figure 16 suggests that for a given value of crushing door padding, a lower thoracic response may be obtained by impacting the pelvis roughly 10 ms before the torso.

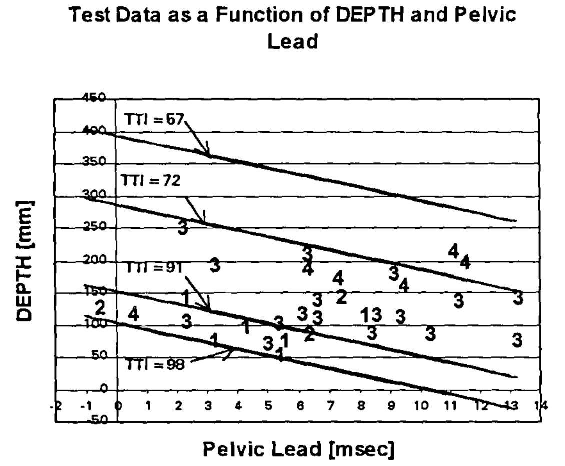

Figure 16. Linear Combination of Pelvic Lead and DEPTH at a Constant TTI.

CONCLUSIONS

The USA NCAP conducted thirty-two side impact crash tests. These tests were based on the testing methodology of FMVSS No. 214. The deformable moving barrier was traveling at 61.6 kmph just before hitting the struck vehicle. Accelerometers were installed in a variety of locations about the door panel, A-pillar, and B-pillar of the struck vehicle. In previous side impact testing, struck door accelerometers frequently exhibited anomalies because they were subjected to severe impact loading. An analysis was conducted of the accelerometers used in the thirty-two NCAP tests. It was determined that many of the accelerometers survived the side impact and produced satisfactory signals.

Using the accelerometers in the interior door, A-pillar, and B-pillar, the maximum velocity of the interior door in the struck vehicle was calculated. It was found that the speeds of the thirty-two intruding doors appeared to vary over a wide range. Some doors had a maximum speed that reached only as high as the velocity of the struck vehicle. Other intruding doors reached a speed roughly twice the final velocity of the struck vehicle.

The Door Effective Padding Thickness (DEPTH) is the relative displacement between the door and occupant from the time of occupant-door contact until the time of occupant-door separation. The DEPTH was calculated for thirty-two cars crashed in NCAP side impact. The correlation between the dummy's response and the DEPTH was modest for this data set.

The side impact dummy has accelerometers in the torso and an accelerometer in the pelvis. In a side impact, a pelvic signal starting significantly before the torso would indicate a pelvic lead and mean the door is contacting the pelvis before the torso. The pelvic lead is defined as the time of the pelvic response subtracted from the time of the thoracic response. The pelvic lead was calculated for the thirty-two cars crashed in NCAP side impact. A weak correlation between the dummy's response and the pelvic lead was found for this data set.

No single variable fully explains the response of the dummy during a side impact event. The linear combination of DEPTH and pelvic lead account for about a third of the variation of this data set. The next step in this study will be to investigate other variables with the objective of more completely describing the intensity of the mechanical input and the response of the occupant in the struck vehicle.

REFERENCES

1. *Traffic Safety Facts 1996*, National Highway Traffic Safety Administration, U.S. Department of Transportation, Report No. DOT HS 808 649, pp. 71 and 73, December 1995.

2. *NHSA Releases Side Crash Test Results in New Consumer Information Program*, National Highway Traffic Safety Administration, U. S. Department of Transportation, Press Release No. NHTSA 21-97, 11 April 1997.

3. *Euro NCAP Crash Tests*, UK Department of Transport and *What Car?*, January 1997.

4. Gabler, H.C., Hackney, J.R., Hollowell, W., " DEPTH: A Relationship Between Side Impact Thoracic Injury and Vehicle Design," 12th International Technical Conference on Experimental Safety Vehicles, Gorteborg, Sweden 1989.

5. Hobbs, C.A., "The influence of Car Structures and Padding on Side Impact Injuries," 12th International Technical Conference on Experimental Safety Vehicles, Gorteborg, Sweden 1998.

6. "Saab 9-5 is packed with innovations," *Automotive Engineering*, The Society of Automotive Engineers, 400 Commonwealth Drive, Warrendale, Pennsylvania 15086, September 1997.

7. Lau, I. V., Capp, J. P., and Obermeyer, J. A., "A Comparison of Frontal and Side Impact: Crash Dynamics, Countermeasures and Subsystem Tests," Thirty-fifth Stapp Car Crash Conference Proceedings, November 1991.

8. Strother, C. E., and Morgan, R. M., "A fundamental look at side impact," Proceedings of the American Association for Automotive Medicine, Louisville. Kentucky, October 1979.

9. Rao, A., Thompson, G.J., Mucino, V.H., and Smith, J.E., "Crash Analysis Response of a Mid-size Car Subjected to Side Impact," SAE International Congress & Exposition, Detroit, Michigan, February 1997.

10. Blaisdell, D., Stephens, G., and Meissner U., "Collision Performance of Automotive Door Systems," SAE Publication No. SP-1045, 1994.

11. Littell R. C., Rudolf F. J., and Spector P. C., SAS System for Linear Models, 3rd Ed., SAS Institute Inc., Cary, North Carolina, 1991.

12. *Final Regulatory Impact Analysis: New Requirements for Passenger Cars to Meet a Dynamic Side Impact Test FMVSS 214,* National Highway Traffic Safety Administration, Report No. DOT HS 807 641, August 1990.

Appendix 1.
Test Data for Thirty-two NCAP Side Impact Tests

Test No.	Make & Model	Model Year	Vehicle Test Wt. kg	TTI g(s)	LUR Depth mm	Pelvic Lead msec
1	Cadillac Deville 4-dr	1997	2085	57.8	159	9
2	Chevrolet Camaro 2-dr	1997	1744	86	99	5
3	Chevrolet Cavalier 2-dr	1997	1450	123	71	5
4	Chevrolet Lumina 4-dr	1997	1758	61	168	7
5	Chevrolet Malibu 4-dr	1997	1618	100	94	4
6	Dodge Intrepid 4-dr	1997	1741	72	109	0
7	Dodge Stratus 4-dr	1997	1538	75.8	141	13
8	Ford Contour 4-dr	1997	1506	73	88	8
9	Ford Crown Victoria 4-dr	1997	1995	68.6	186	6
10	Ford Escort 4-dr	1997	1328	88	108	6
11	Ford Taurus 4-dr	1997	1756	74	171	9
12	Ford Thunderbird 2-dr	1997	1814	91	132	11
13	Honda Accord 4-dr	1997	1470	96	141	7
14	Honda Civic 4-dr	1997	1241	83.1	72	13
15	Hyundai Sonata 4-dr	1997	1543	102	114	8
16	Kia Sephia 4-dr	1997	1305	93	84	6
17	Mazda 626 4-dr	1997	1424	92.9	118	-1
18	Mitsubishi Galant 4-dr	1997	1496	84	249	2
19	Nissan Maxima 4-dr	1997	1618	70	196	11
20	Pontiac Grand AM 4-dr	1997	1581	109	144	2
21	Saturn SL 4-dr	1997	1267	88.2	110	9
22	Subaru Legacy AWD 4-dr	1997	1562	88.4	192	3
23	Toyota Camry 4-dr	1997	1601	82.2	127	6
24	Toyota Corolla 4-dr	1997	1312	89	99	8
25	Toyota Tercel 2-dr	1997	1149	83.3	81	10
26	Volvo 850 4-dr	1997	1723	62	192	11
27	Buick Century	1998	1766	82	206	6
28	Buick LeSabre	1998	1805	79	110	6
29	Chevrolet Cavalier 4DR	1998	1592	105	73	3
30	Ford Escort ZX2	1998	1344	100	66	5
31	Ford Mustang	1997	1601	87	69	5
32	Mercedes Benz C-230	1998	1626	86	103	2

Appendix 2.
Star Ratings for Forty-six NCAP Side Impact Tests

Test No.	Make & Model	Model Year	Driver Upper Rib G's	Driver Lower Rib G's	Driver Spine G's	Driver Pelvic G's	Driver Star Rating	Passenger Star Rating
1	Cadillac Deville 4-dr	1997	47.2	44.3	68.3	96.9	☆☆☆☆	☆☆☆☆
2	Chevrolet Camaro 2-dr	1997	83.3	81.9	88.4	83.0	☆☆☆	☆☆☆☆
3	Chevrolet Cavalier 2-dr	1997	107.5	135.8	110.2	115.8	☆	☆☆
4	Chevrolet Lumina 4-dr	1997	54.4	61.1	61.4	69.5	☆☆☆☆	☆☆☆
5	Chevrolet Malibu 4-dr	1997	82.9	95.2	105.6	109.8	☆	☆☆☆
6	Dodge Intrepid 4-dr	1997	78.3	80.4	64.5	108.9	☆☆☆☆	☆☆☆
7	Dodge Stratus 4-dr	1997	74.0	75.8	75.8	108.7	☆☆☆	☆☆
8	Ford Contour 4-dr	1997	63.9	69.5	76.4	82.0	☆☆☆	☆☆☆☆
9	Ford Crown Victoria 4-dr	1997	69.3	65.5	67.8	80.9	☆☆☆☆	☆☆☆☆
10	Ford Escort 4-dr	1997	78.0	99.0	77.0	120.0	☆☆☆	☆☆☆
11	Ford Taurus 4-dr	1997	71.0	78.0	70.0	97.0	☆☆☆	☆☆☆
12	Ford Thunderbird 2-dr	1997	71.5	87.7	93.4	131.8	☆☆☆	☆
13	Honda Accord 4-dr	1997	94.4	78.0	97.4	117.0	☆☆	☆☆☆
14	Honda Civic 4-dr	1997	78.5	86.9	79.3	107.2	☆☆☆	☆☆☆
15	Hyundai Sonata 4-dr	1997	113.9	109.1	89.7	112.8	☆	☆☆
16	Kia Sephia 4-dr	1997	79.0	90.9	95.1	84.7	☆☆	☆
17	Mazda 626 4-dr	1997	70.7	90.4	95.4	114.5	☆☆	☆☆☆
18	Mitsubishi Galant 4-dr	1997	70.0	74.0	94.0	98.0	☆☆☆	☆☆
19	Nissan Maxima 4-dr	1997	65.9	63.3	73.7	95.3	☆☆☆☆	☆☆☆
20	Pontiac Grand AM 4-dr	1997	104.0	94.5	114.4	102.2	☆	☆☆☆
21	Saturn SL 4-dr	1997	86.0	83.9	90.4	123.8	☆☆☆	☆☆☆
22	Subaru Legacy AWD 4-dr	1997	84.5	81.2	92.2	130.8	☆☆☆	ND
23	Toyota Camry 4-dr	1997	76.4	82.0	82.4	88.6	☆☆☆	☆☆☆
24	Toyota Corolla 4-dr	1997	81.8	75.3	96.4	106.9	☆☆☆	☆☆☆
25	Toyota Tercel 2-dr	1997	86.7	91.6	74.9	79.2	☆☆☆	☆☆☆☆
26	Volvo 850 4-dr	1997	57.4	50.5	66.5	70.5	☆☆☆☆	ND
27	Buick Century	1998	76.0	77.0	86.8	128.8	☆☆☆	☆☆☆
28	Buick LeSabre	1998	63.3	64.8	93.2	98.1	☆☆☆	☆☆☆
29	Chevrolet Cavalier 4DR	1998	99.2	74.4	110.7	140.7	☆	☆☆☆
30	Ford Escort ZX2	1998	85.9	99.2	100.9	119.8	☆	☆☆☆☆
31	Ford Mustang	1997	76.5	80.4	94.3	90.1	☆☆☆	☆☆☆
32	Mercedes Benz C-230	1998	67.1	80.8	91.0	79.5	☆☆☆	☆☆☆☆
33	Mazda 626	1998	56.7	67.5	93.3	135.7	☆☆☆	☆☆☆
34	Dodge Neon	1998	93.7	87.0	94.0	102.0	☆☆	☆☆☆
35	Pontiac Bonneville	1998	74.4	72.9	94.1	111.5	☆☆☆	☆☆
36	Honda Civic 2DR	1998	85.1	107.9	78.9	92.1	☆☆	☆☆☆
37	Nissan Altima	1998	81.5	89.8	87.1	93.0	☆☆☆	☆☆☆
38	Toyota Avalon	1998	47.6	51.4	61.1	106.3	☆☆☆☆☆	☆☆☆☆
39	Toyota Corolla	1998	76.1	75.5	74.6	108.2	☆☆☆	☆☆☆
40	Mitsubishi Eclipse	1998	111.2	98.3	132.4	108.6	☆	ND
41	VW Jetta	1998	46.5	61.0	89.9	115.6	☆☆☆	☆☆
42	Nissan Sentra	1998	82.0	78.0	98.0	116.0	☆☆☆	☆☆☆
43	Honda Accord 4DR	1998	67.7	71.4	67.9	77.4	☆☆☆☆	☆☆☆☆
44	Olds Intrigue	1998	79.1	59.9	90.4	98.2	☆☆☆	☆
45	Toyota Lexus ES300	1998	53.0	54.0	61.0	107.0	☆☆☆☆☆	☆☆☆☆
46	Hyundai Elantra	1998	73.6	77.4	97.1	127.7	☆☆☆	☆

IMPROVING US NCAP CONSUMER INFORMATION

Noble N. Bowie
Roger Kurrus
Mary Versailles
National Highway Traffic Safety Administration
United States

Paper Number 98-S11-0-13

ABSTRACT

This paper provides an overview of the National Highway Traffic Safety Administration's (NHTSA) recent and planned future activities to improve the content and delivery of the consumer information it provides as part of the New Car Assessment Program (NCAP). Many of NHTSA's activities respond to the recommendations of the National Academy of Sciences' study "Shopping For Safety: Providing Consumer Automotive Safety Information." The activities discussed in this paper are organized under four categories: Better Understand Customers' Needs; Improve Existing NCAP Information; Develop New NCAP Information of Value; and Improve Awareness and Use of NCAP Information.

INTRODUCTION

Does safety sell? The results of a 1995 Customer Satisfaction Survey conducted by the National Highway Traffic Safety Administration suggests that safety does sell. Seventy-five percent of the survey respondents consider safety a "very important" consideration in their purchase decision. Another 20 percent consider safety "somewhat important."[1]

Given this level of consumer interest in vehicle safety, its no surprise that ads touting "Highest Government Rating In Class," "The Crash Test that Made the Stars Come Out," are being used to market today's vehicles.

To respond to the public's growing interest in motor vehicle safety, NHTSA has created a new division, the Consumer Automotive Safety Information Division, to increase its focus on vehicle safety consumer information complimenting the traditional engineering focus of the agency's rulemaking function. This new division is responsible for the effective development and delivery of NCAP and other vehicle safety consumer information. Prior to the formation of this division, the NCAP engineering staff had this responsibility along with the responsibility for technical aspects of NCAP. NHTSA has requested a separate line item in its 1999 budget to fund this division, which has been operating with funds from the NCAP program and other offices. In crafting its motor vehicle safety consumer information agenda, NHTSA is using the recommendations of a 1996 National Academy of Sciences study as a guide.

BACKGROUND

Historically, NCAP information has been distributed through the use of press releases and video news releases. Consumers could obtain a copy of the results by calling NHTSA's Hotline. Beginning in 1995, NHTSA also began publishing the "Buying a Safer Car" brochure which included the NCAP results and other information on vehicle safety features for purchasers of new vehicles.

As part of the Department of Transportation and Related Agencies Appropriations Act, 1995 (P.L. 103-331; September 30, 1994), Congress provided NHTSA funds "for a study to be conducted by the National Academy of Sciences (NAS) of motor vehicle safety consumer information needs and the most cost effective methods of communicating this information." The NAS study was completed and released to the public on March 26, 1996. It is titled "Shopping for Safety - Providing Consumer Automotive Safety Information," TRB Special Report 248. Based on its findings, the study makes recommendations to NHTSA on ways to improve automobile safety information for consumers. Many of these recommendations pertain to the NCAP program.

On May 20, 1997 NHTSA published a notice summarizing the NAS study and requesting comments on NHTSA's response to the recommendations of this study and on programs

---

[1] The Customer Satisfaction Survey was repeated in late 1997. Preliminary results of the survey are similar to these results - 74% consider safety "very important" while 21% consider safety "somewhat important."

NHTSA has begun or is considering to address these recommendations. NHTSA requested comments because it wishes to develop these programs in cooperation with other interested parties.

Comments were received from 12 individuals and organizations. Commenters included the three American automobile manufacturers, the American Automobile Manufacturers Association (AAMA), the Association of International Automobile Manufacturers (AIAM), Advocates for Highway and Traffic Safety, Volvo, and the Insurance Institute for Highway Safety. In general, commenters supported NHTSA's efforts in response to the NAS study.

INITIATIVES ORGANIZED UNDER 4 CATEGORIES

The Consumer Automotive Safety Information Division has organized its NCAP activities into four categories: Better Understand Customers' Needs; Improve Existing NCAP Information; Develop New NCAP Information of Value; and Improve Awareness and Use of NCAP Information.

Better Understand Customers Needs

In the past, NHTSA has conducted research for specific projects, such as the development of the star rating system for NCAP, air bag labels, or utility vehicle warning labels.

The NAS study recommended that NHTSA conduct research into consumer decision making and safety information requirements. The research would examine how consumers conceptualize auto safety, how consumers use safety information in choosing a vehicle, and how safety information can best be communicated and disseminated.

All commenters on NHTSA's notice concerning the NAS study encouraged NHTSA to do fundamental research to better understand the needs and motivations of consumers. Commenters did differ in their opinions as to whether this research needed to be conducted before any further activity is undertaken or whether this research could be conducted simultaneously with other activities.

On June 12, 1997 NHTSA awarded a contract to a marketing and research firm to conduct general research on what consumers know about vehicle safety and how they go about obtaining and using information in making automobile purchasing decisions. The first activity conducted consisted of a literature search to determine the scope of knowledge regarding these issues and identify gaps that may be addressed by future research. The literature search was completed on November 6, 1997.

The second activity was a series of fifteen focus groups among consumers and auto salespeople in Tampa, Northern New Jersey, and Kansas City. The focus groups with consumers sought to explore the perceptions of and predispositions to consult vehicle safety information among different consumer segments; the priority consumers place on safety when purchasing a vehicle and how safety information affects or influences purchase decisions; ways to increase the urgency consumers associate with vehicle safety performance. Focus groups were also conducted with new and used vehicle salespeople to gather feedback about consumer use of vehicle safety data. The final report on the focus groups was completed on March 5, 1998.

The final activity under this contract, currently being conducted, is the development of a general marketing plan that will identify target audiences, recommend strategies to improve the dissemination of consumer information, recommend marketing activities to motivate consumers to seek information, and methods to evaluate the effectiveness of the marketing plan. The marketing plan should be completed soon.

Some general findings to date from this research are:

•vehicle safety concerns vary from person to person, but are most influenced by the presence of children in a household;

•for most, vehicle safety considerations are confined to a few specific factors (air bags, anti-lock brakes, etc.); and

•consumers are misinformed about the source of crash tests, although they are interested in the results.

In 1995, NHTSA conducted a telephone survey to determine the public's attitudes toward the federal role in promoting vehicle safety. This survey was repeated in late 1997. Final results of the second survey are not yet available, however, additional questions were asked concerning the use of safety information in purchasing new vehicles. These results should also add to the knowledge in this area, and future follow-up surveys could be one means of determining the effectiveness of new efforts.

Once the current general research program is completed, NHTSA will examine the results of all research conducted over the last few years to determine the need for further research. Along with the NAS study, the results of this research will be used to guide future improvements to the NCAP consumer information. NHTSA also intends to continually monitor research needs and conduct further research as needed.

Improve Existing NCAP Information

Since its beginnings for Model Year 1979 vehicles, the only changes that has been made to enhance the program for consumers was the presentation of results in the form of a "star rating," rather than the numerical presentation of the data and the addition of side impact crash test information.

The NAS study recommends that NHTSA provide consumers with more explicit information on: the importance of vehicle size and weight; the benefits of (and proper use of) safety features such as seat belts and anti-lock brakes; the frequency of crash types for which test results are available; and the uncertainties associated with crash test results.

Commenters to the NHTSA notice were divided on whether additional information on the importance of vehicle size and weight should be provided to consumers. Some commenters supported this recommendation, while others believe it is premature to provide such information or believe that such information must also include information on the effect that larger/heavier vehicles have on occupants of smaller/lighter vehicles in a crash.

NHTSA intends to ensure that current statements on size/weight are highlighted in all appropriate materials and will consider adding statements concerning the disbenefits to occupants of other vehicles. NHTSA will also explore other means to inform consumers about the effects of size and weight in the future.

NHTSA agrees with the NAS recommendation to provide consumers with more information on the benefits and proper use of safety features. The agency typically couples safety feature information with NCAP materials. For example, the "Buying A Safer Car" brochure includes information on air bags, advanced safety belt features, traction control, and anti-lock brakes. The agency will continue this practice as well as develop consumer information materials and campaigns dedicated to specific safety features.

Some commenters to the NHTSA notice believed that NHTSA was not doing enough to provide consumers with information on the reliability of crash test results and the real-world frequency of crash types. In response, NHTSA intends to quantify the actual number of real-world crashes that occur for each crash test mode in appropriate materials. In addition, NHTSA will include a statement with information on crash test results advising consumers only one test per vehicle is conducted and that it is not possible to assess how well a vehicle provides protection in all circumstances using a single test which cannot reflect all crash situations. In addition, materials will explain that while the test procedures and environment are tightly controlled, the ratings assigned to the vehicle for that specific set of circumstances may not always be exactly reproduced in subsequent tests. The first materials to include these new statements was the 1998 issue of the "Buying a Safer Car" brochure.

Develop New NCAP Information of Value

The NAS study recommended that NHTSA expand the types of comparative information that was available to consumers, develop a summary safety rating for new vehicles, and recommended that such information be provided in the form of a safety label, with additional more detailed information in other forms.

Beginning with Model Year 1997 vehicles, NHTSA has begun testing vehicles for side impact crash protection as part of the NCAP program. Accordingly, side impact crash test ratings are now provided to consumers along with the frontal ratings. As an outgrowth of the NCAP program, NHTSA has recently published a new companion brochure to the "Buying a Safer Car" brochure titled "Buying a Safer Car for Child Passengers." This brochure includes information on vehicle safety features and designs of particular importance to families with children, and is designed to help them make an informed decision when purchasing a vehicle for their family. This information responds to the research finding that it is consumers with children who are most interested in safety when purchasing a vehicle.

In the area of comparative rollover information, NHTSA is testing 12 vehicles to see if selected driving maneuvers accurately identify rollover propensity. NHTSA is also analyzing the data on the rollover experience of each of these 12 vehicles to allow NHTSA to compare the real-world experience with the experience predicted from the testing. This evaluation will be completed in the fall. After completion of the research, an agency decision will be made about possible use of the information, including possible labeling requirements on the propensity of vehicles to roll over. As recommended by the NAS study, such a label could also be expanded to include existing NCAP information or a recommended summary safety rating.

Another area of possible new information for the NCAP program is braking. NHTSA is conducting research on braking performance, and again, the results of that research are expected in the fall. If the research is promising, the NCAP vehicles could be tested for braking performance prior to the crash test, providing additional information to the public. Such a program has already been implemented by Japan's National Organization for Automotive Safety and Victim's Aid..

Finally, the new information program with the greatest potential to impact the NCAP program is in response to the NAS study recommendation to develop one overall measure that combines relative importance of crashworthiness[2] and crash avoidance[3] features for a vehicle. The study recognizes however, that, for the foreseeable future, summary measures of crashworthiness and crash avoidance must be presented separately due to differences in current level of knowledge, and differences in the roles of vehicle and driver in the two areas. For now, the NAS study recommends that the agency develop a summary measure of a vehicle's crashworthiness which incorporates quantitative information supplemented with the professional judgment of automotive experts, statisticians, and decision analysts. NHTSA should provide information with this measure to reflect the range of uncertainty in those judgments. For crash avoidance, the study recommends the development of a checklist of features for the near future.

Development of a summary crashworthiness measure was the major interest of commenters on the NHTSA notice. All commenters expressed a willingness to work collaboratively with NHTSA toward the goal of a summary crashworthiness rating, although some expressed concerns about the complexity of this endeavor. Two commenters outlined possible approaches to a summary crashworthiness rating. General Motors suggested an approach that combines information on vehicle mass, motor vehicle safety standard certification data, and a measure of the margin of compliance with the motor vehicle safety standards. Volvo suggested that a rating should combine laboratory test results, expert judgments, and real life crash data. Little support was expressed for combining the current front and side NCAP scores. Support was also expressed for other comparative safety information in the areas of rollover and crash avoidance. Commenters also expressed an interest in working with other countries with consumer information programs to harmonize any vehicle rating scheme.

In September, 1997, NHTSA conducted

---

[2] Crashworthiness refers to a vehicle's ability to protect occupants from serious injury or death when a crash occurs.

[3] Crash avoidance refers to a vehicle's ability to prevent a crash from occurring.

a series of seven focus groups in Washington DC, Boise, Idaho, Dallas, Texas, and Frederick, Maryland to explore consumers' need for information about motor vehicle safety, specifically their need for crash and braking test data. Participants in these focus groups showed an interest in crash test data. Most participants, however, felt most vehicle brakes behave similarly and therefore did not believe that comparative braking information would be meaningful. However, participants did express an interest in such information if there were appreciable differences in braking performance between vehicles.

Based on the comments to the NHTSA notice and the results of focus group research, NHTSA does not, at this time, intend to pursue combining the existing front and side NCAP scores into a single rating. Instead, NHTSA is considering examining the development of a summary crashworthiness rating, which would likely combine front and side crash protection information as well as information on the crash protection offered in other crash modes. If this effort is undertaken, NHTSA intends to work with interested parties on the development of this rating, perhaps under the auspices of the existing Motor Vehicle Safety Research Advisory Committee as suggested by some commenters.

Improve Awareness and Use of NCAP Information

The NAS study recommends that NHTSA present a summary crashworthiness rating in a hierarchically organized approach. Such an approach would have the most highly summarized information on a vehicle label with a graphical display or on a checklist. This could be part of the current labels on new vehicles, or, preferably, a separate label focusing on safety information. The next level of information would be an accompanying brochure with more detailed explanations of the summary measures, information on the assumptions used in those calculations, etc. The most detailed level would be a handbook with complete comparisons of all vehicles.

The September focus groups conducted by NHTSA support the concept of presenting consumer information in different hierarchical levels of detail, as results indicate that consumers vary in the amount of detail they want. NHTSA intends to use this concept whenever appropriate in its consumer information programs.

Finally, the NAS study recommends the development of a multichannel approach to the dissemination of information, including NHTSA's Auto Safety Hotline, the Internet, asking the insurance industry and automobile clubs to include information in their mailings, having NHTSA information printed in consumer journals, having safety information included in driver education courses, and public service announcements.

NHTSA has been working to expand the dissemination of NCAP and other vehicle safety consumer information materials, by improving its Internet site; by using video news releases, radio public service announcements and print articles; and by working in partnership with dealerships, special interest groups, and states. The new Consumer Automotive Safety Information Division hopes to emulate some of the communication strategies that have been successfully used by NHTSA's Office of Traffic Safety Programs in addressing safety belt usage and impaired driving.

As mentioned previously, the third portion of the current research program is the development of a general consumer information marketing plan to recommend additional ways to disseminate consumer information. NHTSA has already developed individual marketing plans for the "Buying a Safer Car for Child Passengers" brochure and the NCAP program. Some of the new promotional activities being pursued under those plans are distributing media packages to print publications, and securing partnerships to distribute and/or reprint the brochure.

SUMMARY

In summary, NHTSA has reorganized to focus on the improvement of its vehicle safety consumer information programs. NHTSA supports the general thrust of the recommendations of the NAS study, and is pursuing an agenda to implement those recommendations. NHTSA is using consumer research (surveys, focus groups, and systematic field studies) to guide the development and delivery of consumer information products. NHTSA is taking steps to improve existing consumer information, as well as developing new consumer information. Finally, NHTSA is expanding the distribution of its consumer information through the use of comprehensive marketing plans.

REFERENCES

Boyle, John M., "National Highway Traffic Safety Administration 1995 Customer Satisfaction Survey". May 1996.

Equals Three Communications, "Research Report to the National Highway Traffic Safety Administration: Results of Focus Groups Among Adult Drivers and New and Used Salespeople in Tampa, FL; Ridgewood, NJ; and Kansas City, KS About Vehicle Safety Data". March 1998.

Global Exchange, Inc., "Motor Vehicle Safety Overview: Customer Perceptions and Information Needs". November 1997.

Global Exchange, Inc., "Research Report to the National Highway Traffic Safety Administration: Results of Seven Focus Groups Among Car Buyers in Washington, Boise, Dallas and Frederick, Maryland". September 1997.

Transportation Research Board, "Shopping For Safety: Providing Consumer Automotive Safety Information". TRB Special Report 248. 1996.

PHILOSOPHY AND STRATEGY OF NEW CAR ASSESSMENT PROGRAM TO RATE CRASHWORTHINESS

Gerhard Lutter
Hermann Appel
ISS Automotive Research
Andre Seeck Bernd Friedel
Federal Highway Research Institute
Germany

Paper Number 98-S11-O-14

ABSTRACT

A means of assessing the passive safety of automobiles is a desirable instrument for legislative bodies, the automobile industry , and the consumer. As opposed to the dominating motor vehicle assessment criteria, such as engine power, spaciousness, aerodynamics and consumption, there are no clear and generally accepted criteria for assessing the passive safety of cars.

The proposed method of assessment combines the results of experimental safety tests, carried out according to existing legally prescribed or currently discussed testing conditions, and a biomechanical validation of the loading values determined in the test.

This evaluation is carried out with the aid of risk functions which are specified for individual parts of the body by correlating the results of accident analysis with those obtained by computer simulation.

The degree of conformance to the respective protection criterion thus deduced is then weighted with factors which take into account the frequency of occurrence and the severity of the accident on the basis of resulting costs.

Each of the test series includes at least two frontal and one lateral crash test against a deformable barrier.

The computer-aided analysis and evaluation of the simulation results enables a vehicle-specific overall safety index as well as partial and individual safety values to be determined and plotted graphically.

The passive safety provided by the respective vehicle under test can be defined for specific seating positions, special types of accident, or for individual endangered parts of the body.

INTRODUCTION

In the frame of the research project "Quantification of Passive Safety of Passenger Car Occupants" [1] on behalf of the Bundesanstalt für Straßenwesen (Federal Highway Research Institute), a procedure has been developed, that investigates and assesses the safety of passenger cars on the basis of accident analysis, statistical biomechanics, and crash tests.

In several expert meetings this procedure has been introduced and developed. The test program comprises three different crash tests:

- Frontal crash similar to FMVSS 208 (US-NCAP) (testing restraint systems)
- Offset-test, frontal, similar to 96/79/EG (testing vehicle front structure)
- Side impact according to 96/27/EG with moving deformable barrier (testing restraint systems as well as vehicle structure)

PROCEDURES FOR SAFETY ASSESSMENT

During the last fifteen years, different solution attempts for safety assessment have been proposed and partially have been realized, with basic differences in size of assessment, selection and weighting of criteria, as well as possibilities of application. In principle, the following concepts can be distinguished.

Retrospective Analytical Procedures

Assessment of a specific vehicle type is done by valuation of actual data of available data bases from state and insurance companies, which have been collected and stored over a sufficiently long period of time with statistical certainty. The size of the usable data arises from the frequency of accidents in the survey period. Surveys can be divided into two basic categories. One category is based on the reason of the accident, which mostly considers the pre-crash phase and so is a matter of active safety, while the other category deals with crash and post- crash phase, thus relating to passive safety.

A further distinction feature of retrospective accident analysis is the number of the analyzed accident material and their depth. They are classified as large case studies and in-depth studies.

In large case studies a great number of accidents is being collected, so that these accident data usually do not have the necessary depth for extracting specific statements about severity and mechanism of injury and crash behaviour.

In-depth studies only collect a restricted number of accidents, but they try to analyze the data as exact and in-depth as possible, and so offer the possibility to examine the questions mentioned intensively. Quite often, these data are not representative of the entire accident events, as they usually are collected in local investigations where infrastructural influences of the region of investigation can have a great influence. Additionally, vehicles, which are on the market in only a small number, are not or hardly available in those studies. For this reason, large case studies are used for examinations aimed at ranking the safety of vehicles.

The following institutions judge the passive safety of cars with retrospective procedures:

- Highway Loss Data Institute Report (USA)

- FOLKSAM Report (Schweden)
- Department of Transport Rating System (UK)
- Insurance Institute for Highway Safety (USA)
- Univercity of Oulo [Finnland]
- Monash Univercity (Australien)

Prospective Procedures - Experimental Procedures

To be able to make a statement predicting the state of the passive safety, one cannot proceed by means of retrospective methods with new vehicles. Derivation of the level of safety of the current model from the behaviour of the predecessor model is not possible, as the actual model can be significantly different from the predecessor. Therefore, results from experimental safety tests are used as criteria in relation to the level of protection criteria.

Selection of crash tests determines, which part of the real-world accident events will be covered. At present, the following institutions investigate the safety of passenger vehicles by the use of crash tests:

- ADAC (BR Germany)
- New Car Assessment Program (USA)
- Auto Motor und Sport (BR Germany) [15]
- „European" New Car Assessment Program („Euro" NCAP) (UK)
- Insurance Institute for Highway Safety (USA)
- OSA (Japan)
- NCAP (Australia)

Combined procedures

Combination of experimental safety tests and in-depth accident analysis tries to avoid the conceptually caused disadvantages of retrospective procedures on the one hand and purely experimental procedures on the other hand.
The following procedures are being used or in the development stage:

- Crashworthiness Rating System for Cars (GB)
- Secondary Safety Rating System for Cars (GB)
- Pilot study "Quantifizierung der Passiven Sicherheit" TU-Berlin

Valuation of existing or proposed procedures

Retrospective procedures do not make it possible to make predictions of the passive safety of new vehicles, neither in the real-world accident events nor in the laboratory, as those vehicles are not found in the accident events, when they come to market. Only after several years of presence on the roads, the amount of collected accident data is large enough to make reliable statements about the passive safety, at least this is true for vehicles with a great number of registrations. Therefore it is necessary to investigate the potential of protection in simulated tests, so-called crash tests.

A sole examination of results from crash tests, as done in the prospective procedures, is not sufficient for assessment of passive safety, as they often are only selective assessment attempts that do not reflect the entire real accident events. Moreover, single tests with e.g. very high test speed can lead to an excessive reinforcement of structures, which can have adverse consequences in regard of compatibility in the entire accident events.

Combined procedures try to take into account information from the accident events as well as from constructive design properties of the vehicle. This is done by weighting the results achieved with an additional weighting factor. Assessment of the loading of occupants is carried out by squaring the quotient, according to the "Crashworthiness Rating System for Cars". There is no biomechanical explanation for that. The "Secondary Safety Rating System for Cars" examines the constructive lay-out of the vehicle without subjecting it to a dynamic test. The elements examined are being selected on the basis of data from the accident events. Values attained in every assessment phase become weighted with a factor determined from the accident events. Since a dynamic test is not being performed, no statements can be made about the dynamic behaviour of the structure, the efficiency of the restraint system, etc.

These here introduced procedures contain many good features of a safety assessment. However, none of the assessment procedures mentioned so far shows a clear attempt to build up on the accident statistics. Also the assessment of passenger loadings or further assessment quantities is not or only insufficiently well-founded. An objective, transparent and comprehensible assessment algorithm is not available in most procedures. The attempt of TU Berlin, which was developed in the context of a research project of the German Road Research Institute shows a good basis due to the clear structure and the systematic construction, which will be further extended in the context of this project.

REQUIREMENTS ON A RELIABLE ASSESSMENT SYSTEM

The bandwidth of already existing assessment possibilities of an in principle identical aim, namely the assessment of passive safety, reflects the difficulties and necessary restrictions of such a procedure. Provision of transparent, comprehensible and quantifiable criteria is of basic significance. Following requests and main tasks will build the experimental/analytical attempt of an assessment algorithm:

Table 1:
Specifications for Safety Assessment

Specifications for Safety Assessment of Self and Partner Protection for an Analytical Procedure		
REQUIREMENTS	BASIS	MEASURES
realistic test conditions	data base, in-depth study	accident analysis equivalent accidents
measurement location	data base, in-depth study	accident analysis occupant loadings
assessment criteria, protection criteria	biomechanics, numerical simulation	physical loadings, injury severity/risk function assessment function
limiting value	standards	ECE regulations, FMVSS
relevance factors	data base, in-depth study	data base, relevance factor
statistical confirmation	reference tests, numerical simulation	measurement scatter, statistical evaluation

The specifications for an assessment procedure must contain demands that cover the real accident events under consideration of singular points of view. Doing this, results of accidents related to the occupant in physiological, physical and economic view and the translation of the assessment attempt into a practicable procedure have to be considered.
The following requests to a safety assessment shall be made from these aspects:

- Reproduction of and validation at the real-world accident
- Integration of assessment of self and partner protection
- predictability
- transparency, comprehensability, biomechanical justification
- consideration of measurement scatter
- integration of standards
- modular structure

The necessity to analyze and simulate experimentally the reality as extensively as possible is the dominating of the posed requests. All aspects of vehicle safety with regard to protection of occupants as well as to protection of exterior road-users shall be included. A substantial benefit can be expected if a procedure could be developed which shows a quantitative, reality referring forecast ability. To obtain necessary acceptance of such a procedure, in spite of the variety of the influence parameters, a solution attempt must be worked out which can provide a transparent, comprehensible, checkable consistent procedure. Necessary temporal and financial conditions shall more over allow the realization of the safety assessment. The procedure to be suggested shall make use of frequency and results of an accident event as weighting factor for the experimental test constellation, which is equivalent to the accident. Already existing, legally specified safety test shall also be taken into account when formulating test conditions. These represent a discontinuous assessment measure and play a decisive role due to their compulsory nature for vehicle design. The same holds for the specified protection criteria levels in these tests. The provision of the functional coherence between loading values measured in the tests and injuries of occupants in the form of risk functions is necessary for the striven continuous assessment.

TEST PROCEDURE FOR ASSESSMENT OF PASSIVE SAFETY OF PASSENGER CARS

The newly developed assessment technique combines the methods used so far [2, 3, 4, 5, 6, 7, 8] and provides for inclusion of biomechanics of occupants as well as economic consequences in an experimental-analytical procedure.

Accident Analysis

The main task had to be solved by the accident analysis, based on the data material [9] of the Medizinische Hochschule Hannover (MHH; Medical Highschool Hannover):

– Provision of input data for numerical simulation.

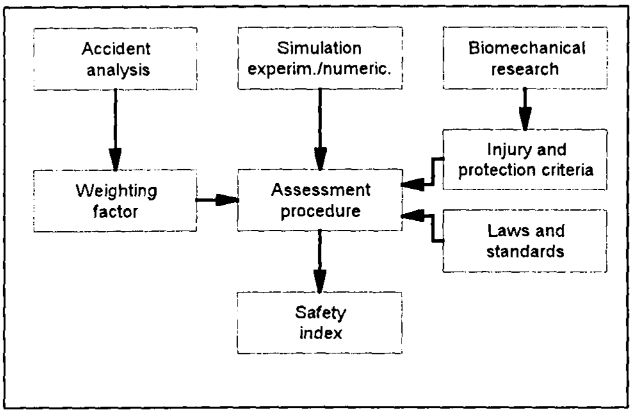
Accident analysis
Simulation experim./numeric.
Biomechanical research
Injury and protection criteria
Weighting factor
Assessment procedure
Laws and standards
Safety index

Figure 1: Assessment method

- On the basis of the material of the accident research unit of MHH, an accident data set has been ascertained, that is used as an input data set for numerical simulation. With this accident data set, assessment functions are established in computer simulations.
- Ascertainment of distribution functions of different parts of the body in order to deduce assessment functions [10, 11]. Numerically evaluated functional relations between accident characteristics and load factor on the one hand and distribution functions of injury severity on the other hand are correlated. Correlation is made according to the EAC-method [12], where the result is made mathematically describable by statistic means.
- Determination of relevance factors for weighting measurements at different parts of the body. Relevance factors are used to compare measurements one to another on the basis of injury costs.

Experimental Simulation

When establishing test procedures for the experimental part of the assessment, it was proceeded from the compulsory homologation test similar to FMVSS 208 (a frontal impact against a rigid barrier) [13], an offset test with 40% overlap (a frontal test against a deformable barrier) close to 96/79/EG, and the European side impact test with a moving deformable barrier similar to 96/27/EG [14]. These three tests serve mainly as a judgement of self- protection.

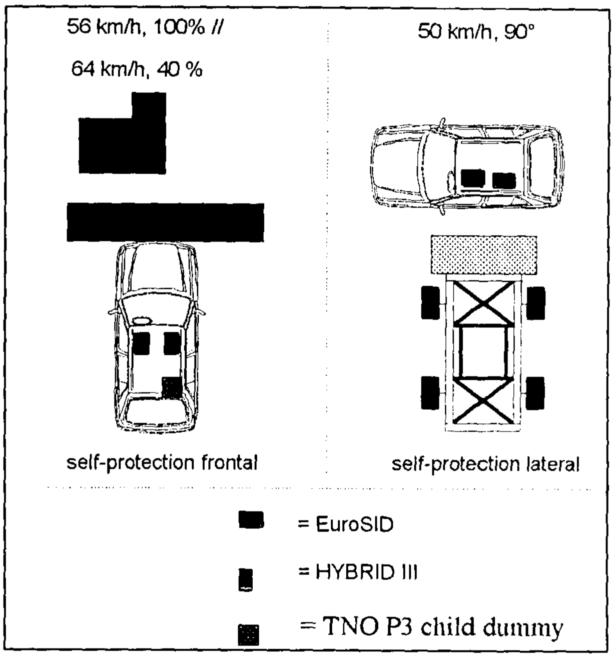
56 km/h, 100% //
64 km/h, 40 %
50 km/h, 90°
self-protection frontal
self-protection lateral
= EuroSID
= HYBRID III
= TNO P3 child dummy

Figure 2: Test-procedure

Instrumentation of the dummies correspond to 96/79/EG and 96/27/EG.

Test Conditions -The following conditions were laid down:

Table 2:Frontal crash similar to FMVSS 208 (US-NCAP)

Collision object	rigid barrier
Impact speed	56 km/h
Impact angle	0°
Overlap	100%
Loading	Hybrid III on driver's and passenger's seat and TNO P3 dummy with child restraint system behind the passenger

Table3: 40%-offset test similar to 96/79/EG

Collision object	deformable barrier
Impact speed	64 km/h
Impact angle	0°
Overlap	40%
Loading	Hybrid III on driver's and in the back behind the front passenger seat

Table 4:Side impact according to 96/27/EG

Collision object	moving deformable barrier (EEVC)
Impact speed	50 -2 km/h
Impact angle	90° left
Impact point	seat reference point
Loading	EuroSID on driver's seat and on the back seat (both struck side)

Measurements and Protection Criteria - Type and position of transducers are in accordance with the customary equipment used with the respective proposed dummies.

For valuation of intrusion into the foot well, use of 5-axial transducers in the lower leg is recommended.

Table 5
Side impact
Transducers in dummy type EuroSID

Body part	Type of measurement	Protection criterion
Head	acceleration 3-axial	HPC 1000
Thorax	deformation and deformation speed	VC 1 m/s
Thorax	deformation of ribs	42 mm
Abdomen	force 3-axial	$\Sigma F_{Abd.}$ 2,5 kN
Pelvis	force in symphysis	$F_{symp.}$ 6 kN

Table 6
Frontal crash
Transducers in dummy type Hybrid III

Body part	Type of measurement	Protection criterion
Head	acceleration 3-axial	HIC_{36} 1000
Head	acceleration 3-axial	a_{3ms} 80 g
Neck	forces	limiting curves
Neck	torque	My < 57 Nm
Thorax	acceleration 3-axial	a_{3ms} 60 g
Thorax	deformation speed	VC 1,3 m/s
Thorax	deformation	< 50 mm
Upper leg	longitudinal force	F_{max} < 10 kN
Lower leg	Tibia Index (TI)	TI < 2 kN

Table 7
Frontal crash
Transducers in child dummy type TNO P3

Body part	Type of measurement	Protection criterion
Head	acceleration 3-axial	HIC_{36} 1000
Head	acceleration 3-axial	a_{3ms} 80 g
Thorax	acceleration 3-axial	a_{3ms} 60 g
Thorax	acceleration z-axial	a_{3ms} 35 g

Rule of Procedure

A finite number of safety tests is necessary to achieve statistically secured test results. However, only one single test is assigned for tests of homologation and type approval, so, the measured value will deviate from the true value with a certain degree of probability.

In order to reduce test expenditures, a rule of procedure takes this into account.

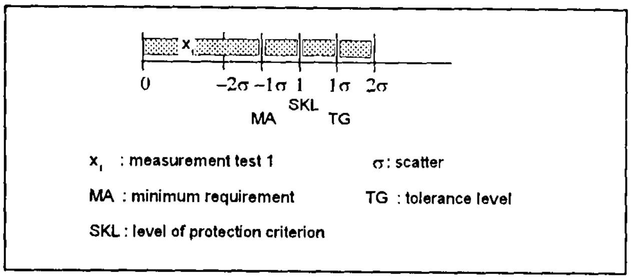

Figure 3: Rule of procedure

The rule includes the definition of a minimum requirement

MA = protection criterion - measurement scatter

and an upper tolerance level

TG = protection criterion + measurement scatter

The relation of the respective loading to these quantities determines whether the values are accepted for assessment, whether one further repeat test with assessment of the mean values is required, or whether the results are excluded from the assessment procedure.

Determination of Assessment Functions

The measurements obtained from a minimum of three or a maximum of six integral safety tests can now be proceeded for assessment.

The physical loading values are first related to the protection criterion, which is the tolerance level of the respective body part. These normalized values are input data to the body part related assessment functions [1].

By combining accident analysis results with those of computer simulation, these functions represent a relationship between the real accident damage and the experimentally deduced loading values.

In the statistical evaluation (figure 4), the severity of the injuries, coded according to the AIS, are plotted for frontal and for lateral collisions (figures 5 and 6) as functions of the equivalent accident characteristics [10, 15], analogous to the values measured by the transducers in the head, thorax, ribs, abdomen, pelvis thighs, and lower legs of the dummy.

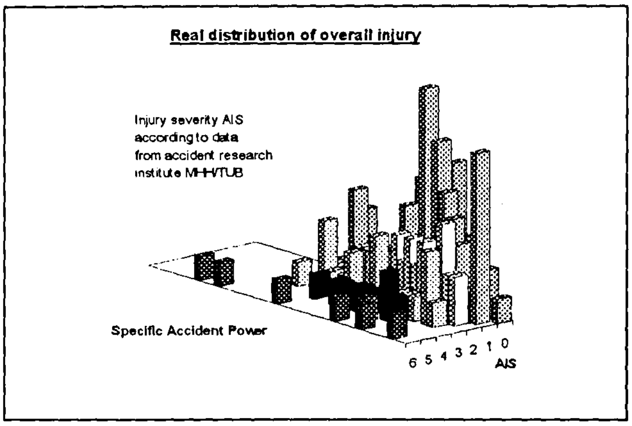

Figure 4: Real distribution of overall injury severity MAIS

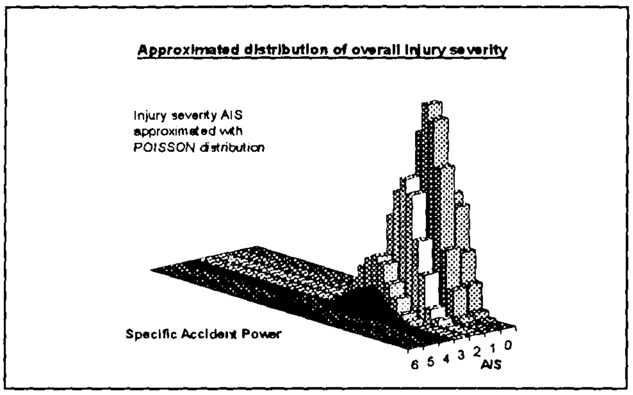

Figure 5: Approximated distribution of overall injury severity MAIS

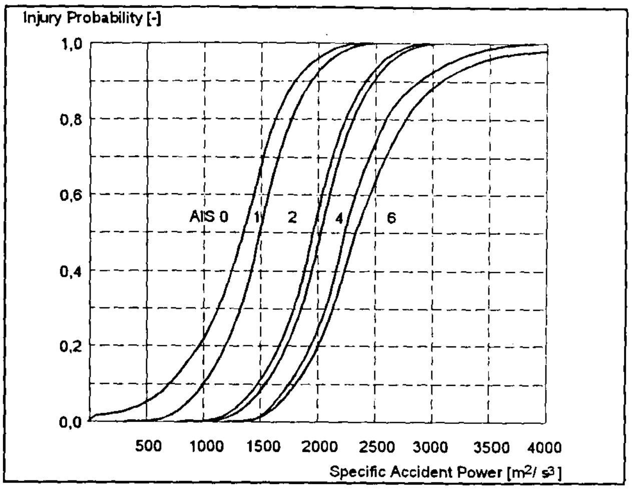

Figure 6: Injury probability of the head (AIS injury scale)

As a result, a distribution function is obtained for the probability of reversible or irreversible injuries to each part of the body in frontal or lateral application of load (figure 7).

The results of this statistical evaluation of real accidents are utilized to determine boundary values as input data for computer simulation, which are to ensure a uniform distribution and to specify the required number of simulation passes.

The physical occupant loading quantities deduced from the equivalent accident characteristics by using occupant simulation models can be correlated to the statistical evaluations. By eliminating the equivalent accident characteristics, which are common to the models, a direct relationship between the loading and the severity of the injuries is established.

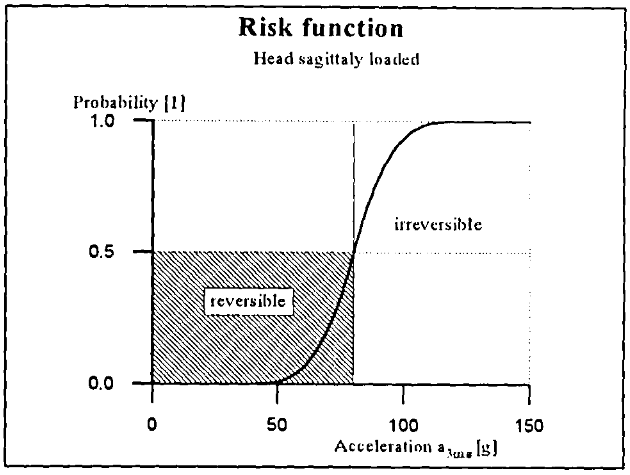

Figure 7: Risk function for occupant loading

Assessment

The assessment function, the central element of the proposed algorithm, provides the ability to carry out a continuous validation of the test results, i.e. the normalized individual measured value is assessed below the protection criterion level within the range defined by the risk function. This degree of compliance with the respective criterion is calculated for every measured value and is weighted with the corresponding relevance factors (figure 8).

The areas of safety assessment described before can be expressed in the following formal relation (figure 9).

The transformation of this method into a computer program [16] enables calculation of both an overall safety index for the whole vehicle and of partial safety indices for the passive safety of the vehicle under test in frontal or lateral collisions. Also, safety values related to seat position and body parts can be established (figure 10).

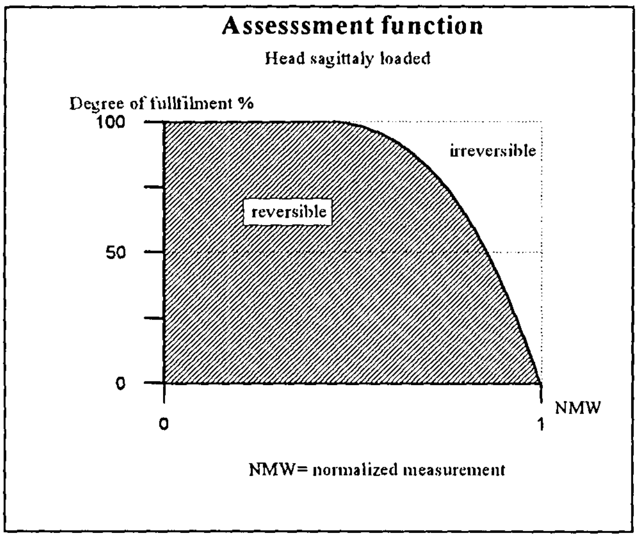

Figure 8: Assessment function

$$\text{Safety index} = \sum_{k=1}^{n}\sum_{j=1}^{m}\sum_{i=1}^{l} RF_{ijk}\left[f_i\left(\frac{MW_i}{SK_i}\right)\right]_{jk}$$

i : point of measurement
j : seating position
k : single test
RF : relevance factor
SK : protection criterion
MW : measurement value

Figure 9: Algorithm for safety assessment [16]

VALIDATION OF THE ASSESSMENT PROGRAM

The philosophy of the validation was to test cars which are on the market for several years to see if there is any correlation between the real world accidents and the results of the crash tests.

The material is the accident database of North Rhine-Westphalia (NRW-data). The BASt performed the accident analysis [20] for those cars which were used in the crash tests with the task to compare these cars with each other regarding the passive safety. The cars which the expert group chose, expecting that these cars were represented in a sufficient number in the accident data material, were the following four cars, which are as well as the results of the two comparisons of passive safety documented in table 8.

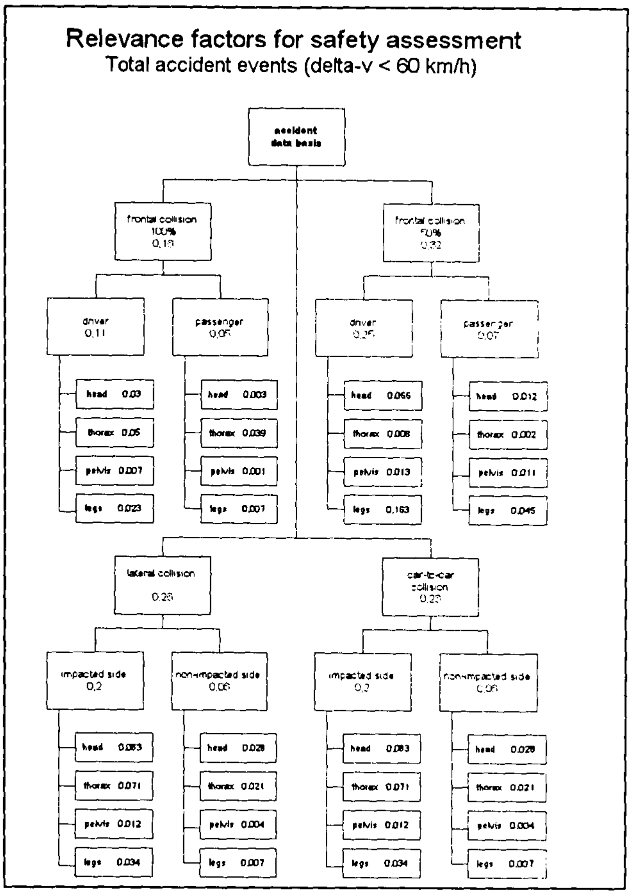
Relevance factors for safety assessment
Total accident events (delta-v < 60 km/h)
accident data basis
frontal collision 100% 0,16
frontal collision 50% 0,32
driver 0,11
passenger 0,05
driver 0,25
passenger 0,07
head 0.03
thorax 0.05
pelvis 0.007
legs 0.023
head 0.003
thorax 0.039
pelvis 0.001
legs 0.007
head 0.066
thorax 0.008
pelvis 0.013
legs 0.163
head 0.012
thorax 0.002
pelvis 0.011
legs 0.045
lateral collision 0.26
car-to-car collision 0.26
impacted side 0,2
non-impacted side 0,06
impacted side 0,2
non-impacted side 0,06
head 0.083
thorax 0.071
pelvis 0.012
legs 0.034
head 0.028
thorax 0.021
pelvis 0.004
legs 0.007
head 0.083
thorax 0.071
pelvis 0.012
legs 0.034
head 0.028
thorax 0.021
pelvis 0.004
legs 0.007

Figure 10: Example of a structure of relevance factors

The safest car both analysis detected was the BMW 5 E34 followed by the VW Golf II, Opel Kadett E, and the FIAT Uno. The comparison on the basis of the NRW-accident data described the value in relation to the medium safe car. This car has the ranking number 100.

Cars with a ranking number greater than 100 are less and lower than 100 more safe than the medium safe car.

Table 8: Comparision between accident and TUB-NCAP ranking

test car	mass class	accident data ranking	TUB-NCAP (SI) ranking
FIAT Uno	sub compact	101	0.1426
OPEL Kadett E	compact class	99	0.2070
VW Golf II	compact class	92	0.3371
BMW 5 E34	large	74	0.5130

The TUB-NCAP algorithm which calculates the safety index (SI) in comparison shows the same ranking. The maximum safety index is 1.0.

At a first glance it seems that the assessment program is working very well.

SUMMARY AND OUTLOOK

Within the scope of this work, the project "Quantification of Passive Safety of Passenger Car Occupants" describes an assessment method for passive safety of cars.

The ranking calculated by the TUB-NCAP is the same as in the NRW-real world accident data analysis of the BASt. This is one more evidence that this assessment program works.

The methodology of validation which is used (that means the comparison between real world accidents and the assessment of the tests) seams to be the only possibility to create a sure assessment program which gives all groups, who are interested in the passive safety of cars, right information about the level of the passive safety of the car. The necessity of repeatability and transparency of the assessment procedure is given by a biomechanically based algorithm.

In this period of validation an offset-crash against the rigid barrier was used. According to the philosophy of this assessment program the new 96/79/EG offset-crash with a deformable element should be used in the future because this test is closer to accident reality. ,Every test which is closer to accident reality makes the validation of this assessment program safer.

For the validation a special attention was given to the assessment of compatibility by means of a car-to-car test. It has to be investigated, wether a less expensive test constellation possibly could give a more complete assessment of the compatibility of passenger cars.

Physical boundary conditions like

- collision speed,
- stiffness of barrier,
- length of barrier at primary impact,
- length of barrier at secondary impact,
- definition of step depth

as well as the behaviour of vehicles of different weight, different front structures and driving concepts have to be investigated.

The EU sponsors two projects which are working on the field of compatibility. The aim of these projects is the development of a test procedure for examination of the compatibility protection potential. On the basis of such a test procedure it should be possible to develop a functional correlation between forces or geometric deformation behaviour of the car and the barrier and the loadings of the dummy to evaluate the compatibility of cars.

Partner protection of the other exterior road users is not included in this procedure at this time. Further research should be done with the view to pedestrians and drivers of bicycles and motorcycles.

For the pedestrian protection an EU working group is developing a test procedure. At this moment the proposal is not validated so that it seems to be necessary to wait for the validation of a suitable test procedure for pedestrian protection.

At this time the assessment algorithm of TUB-NCAP uses only the biomechanical assessment functions for the calculation of the safety index. In the future, functions or assessment criteria will be developed for the opening behaviour of the door, the behaviour of the fuel system (leakage), remaining survival space etc. to put more information into the assessment algorithm. But for all these parameters it is necessary to develop such assessment functions to avoid a subjective assessment which is not reproducible and not transparent.

In this way, the procedure can be optimized concerning the number of necessary crash test and the incidental costs of tests and vehicles.

LITERATURE

[1] APPEL, H.; KRAMER, F.; GLATZ, W.; LUTTER, G.: Quantifizierung der passiven Sicherheit für Pkw-Insassen (FP8517/2), Forschungsbericht Bundesanstalt für Straßenwesen, Bergisch Gladbach, Februar 1991

[2] KRAMER, F.; GLATZ, W.; LUTTER G.: Quantifizierung der passiven Sicherheit (FP8517), Pilotstudie, Bericht: TUB 8517/2

[3] JOHN, MACHEY AND CHARLES, L. GAUTHIER: Results, Analysis and Conclusions of NHTSA's 35 mph Frontal Crash Test Repeatability Program, Office of Market Incentives NHTSA, Washington, DC

[4] U.S. GOVERNMENT PRINTING OFFICE: The Car Book 1981-0-335-248

[5] FOLKSAM INSURANCE COMPANY: Säkra och farliga bilar, Viking Books, 1984

[6] PENOYRE, S.: Transport and Road Research Laboratory, A Crashworthiness Rating System for Cars, 9 th ESV-Conference Kyoto

[7] VEHICLE SAFETY CONSULTANTS LTD.: Car Safety Rating Scheme, Internal Paper, 1988

[8] ADAC: ADAC-Motorwelt, offizielles Mitteilungsblatt des ADAC e.V., Heft 11/88

[9] OTTE, D.: Erhebung am Unfallort MHH/TUB, Projekt FP7263/7506/7813-4/8200-1 BASt

[10] KRAMER, F.: Schutzkriterien für den Fahrzeuginsassen im Falle sagitaller Belastung, Dissertation, TU Berlin, 1989

[11] LUTTER, G.: Ermittlung der Risikofunktion für den lateral belasteten Insassen, Diplomarbeit 16/1989 TU Berlin, September 1989

[12] KRAMER, F.; APPEL, H.; RICHTER, B.; OBERDIECK, W.; LANGWIEDER, K.; SCHMELZING, W.: Evaluation of Protection Criteria by Combining Results of Computer and Experimental Simulation with Accident Investigation, Vth. IRCOBI Conference Birmingham (UK), 1980

[13] FMVSS 208, USA FEDERAL REGISTER VOL NO. 156, 14.8.73

[14] ECONOMIC COMMISSION FOR EUROPE: Proposal for Draft Regulation: Uniform provisions concerning the approval of vehicles with regard to the protection of the occupants in the event of a lateral collision, TRANS/SC1/ WP29/GRSP/R.48/Rev.1, 23-Jan-1991

[15] HOFMANN, J.: Rechnerische Untersuchung zur optimalen Seitenstruktur von Personenkraftwagen, Dissertation, TU Berlin, 1980

[16] LUTTER, G.: Algorithmus zur Bewertung der Quantifizierung der Fahrzeugsicherheit mit Hilfe eines Rechenprogramms, Studienarbeit Nr. 8/87, TU Berlin, 1989

[17] VERGLEICHENDE BEWERTUNG DER SICHERHEIT VON PKW: Niederschrift der Besprechung am 24.2.1992 in der Bundesanstalt für Straßenwesen, Bergisch Gladbach

[18] LUTTER, G.: Quantifizierung der passiven Sicherheit im Hinblick auf das reale Unfallgeschehen, derzeit unveröffentlicht, Berlin 1994

[19] HOBBS, A.: Essential Requirements for An Effective Full Scale Frontal Impact Test, SAE Congress 1990, Detroit

A SIMULATION STUDY ON INFLATION INDUCED INJURY AND NCAP WITH DEPOWERED AIR BAG

Toru Kiuchi
Toyota Motor Corporation
Japan
Paper Number 98-S11-O-15

ABSTRACT

In the United States, air bags are required in all passenger cars and light trucks. The National Highway Traffic Safety Administration (NHTSA) has estimated that almost 2,800 lives have been saved by the air bags. However, air bags designed to protect passengers have, in some situations, caused serious injuries, especially in moderate impacts. Last year, in order to reduce injuries caused by air bag inflation, NHTSA revised the requirements for FMVSS 208 unbelted testing to allow the sled test protocol as a temporary alternative to the frontal barrier vehicle crash test. It is believed that this decision will allow manufacturers to depower air bags by about 20-35 percent, decreasing aggressiveness of air bags during inflation. The NHTSA continues to use the New Car Assessment Program (NCAP) 35mph frontal barrier test as a "measure" of vehicle crashworthiness. The NCAP test report data are widely disseminated to the public as vehicle safety information.

This paper evaluates the effects of air bag depowering on dummy measurements under both moderate frontal impact and severe 35mph frontal barrier impact using MADYMO simulations. These simulations suggest that the aggressiveness of the air bag deployment can be greatly reduced in moderate impacts, without compromising occupant protection performance in more severe impacts.

INTRODUCTION

About a quarter century has passed since air bags were first offered on a few vehicles in the 1970s. NHTSA has required air bags on the driver side from 1991, and on both the driver and passenger sides from 1998. There has been high consumer demand for air bags, and consequently automobile manufacturers have actively introduced new vehicles equipped with air bags. According to the data published on Feb. 1, 1998, by NHTSA, in the United States 70.6 million vehicles (48.6 million passenger cars and 22 million light trucks) are equipped with air bags. In this report, NHTSA estimates that 2,474 drivers' and 370 passengers' lives have been saved by air bags. However, it is also reported that air bags designed to protect occupants have induced some serious injuries, especially in crashes of moderate impact. The Special Crash Investigation (SCI) showed that 37 drivers, 13 children in rear facing child safety seats, 42 children not in rear facing child safety seats, and 4 adult passengers were killed by air bags. These reports led to an increase in public awareness that air bag may cause unnecessary automobile fatalities. As a result, in March 1997, NHTSA revised the requirements for FMVSS 208 unbelted testing to allow the sled test protocol as a temporary alternative to the frontal barrier vehicle crash test. In November 1997, NHTSA also allowed cut-off switches for short stature drivers and other occupants deemed at-risk by the agency. As of April 1998, an estimated 22,000 users have obtained permission to install these switches to deactivate the air bags in their cars.

OBJECTIVE

The first aim of this study is to clarify that depowering of the driver side air bag reduces its aggressiveness, and the second aim is to demonstrate how occupant protection performance is influenced by depowering of air bags, which are designed as a supplemental restraint system, using MADYMO simulations. For the air bag aggressiveness study, a moderate impact condition was used in the MADYMO simulations. For the occupant protection study, a severe frontal barrier crash test was selected to assess occupant protection performance in the consumer information NCAP test. Finally, we investigated occupant protection performance using HIC(15) and chest deflection, which are more suitable criteria of occupant protection than HIC(36) and chest g's, especially in cases where occupants are restrained by both air bags and seat belts.

MADYMO Simulation Study

Moderate Frontal Impact Model - To evaluate the air bag deployment and its relative aggressiveness, we carried out MADYMO(Ver. 5.2) simulations. As mentioned above, a moderate frontal impact was selected for this study. The model had no intrusion of either the steering column or the toe board, and the deceleration of a vehicle in a moderate barrier frontal crash was used (Figure 1). The TNO original AF-05 dummy database was used for the driver dummy and the seat was placed in the most forward position in these cases. FEM seat belt models were used instead of conventional belt models. Depowering of the air bag was modeled by reducing mass flow rate. As shown in Figure 2, air bag "B" was about 20 percent depowered, compared with air bag "A." Graphic output from the simulation using air bag "A" (Figure 3) demonstrates that the dummy experiences hyper-extension of its neck as the air bag deploys. However, the simulation with the depowered air bags shows the dummy sustaining less hyper-extension, relative to the baseline air bag (Figure 4). In addition, HIC (36), chest g's, and the neck extension moment were all reduced by air bag depowering (Figure 5, 6, and 7).

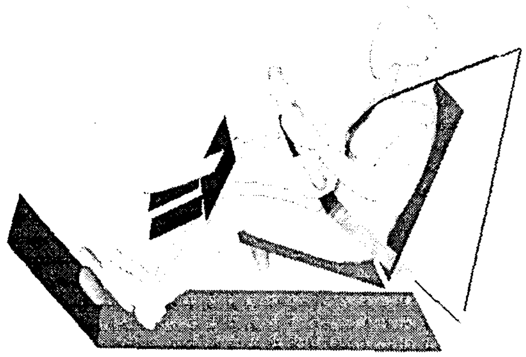

Figure 1. MADYMO Model in Moderate Impact.

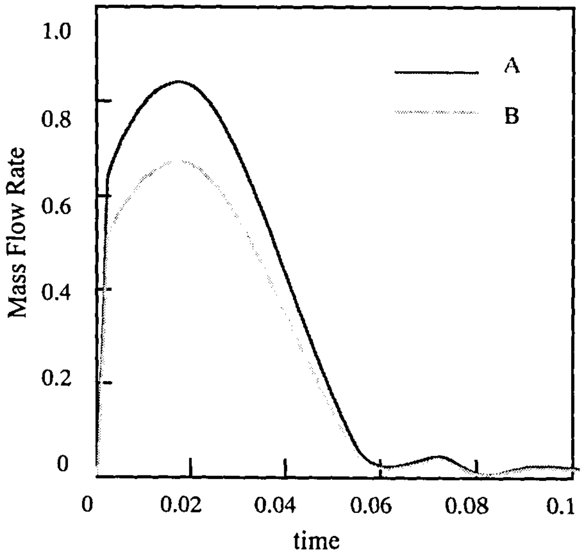

Figure 2. Comparison of Mass Flow Rate.

Severe Frontal Impact Model - Using the same models for baseline and depowered air bags as in the previous study, we carried out MADYMO simulations under a 35mph frontal impact condition. However, the dummy database was changed from the TNO original AF05 to the TNO original AM50, and 2 different seat belt systems were used in these simulations. The AM50 dummy was seated according to FMVSS 208 test procedures. One seat belt was modeled as being equipped with a conventional retractor, and the other was modeled as being equipped with both a pretensioner and a force limiter. The level of limiting force was about 4 kN. Figure 7 shows graphic output of the simulation with air bag "B", pretensioner and force limiter. Figures 9-12 show comparisons of dummy measurements, HIC(36), HIC(15), chest g's, and chest deflection. Results show that a change from air bag "A" to air bag "B" produced somewhat higher HIC scores, but the addition of the pretensioner and the force limiter reduced the dummy measurements.

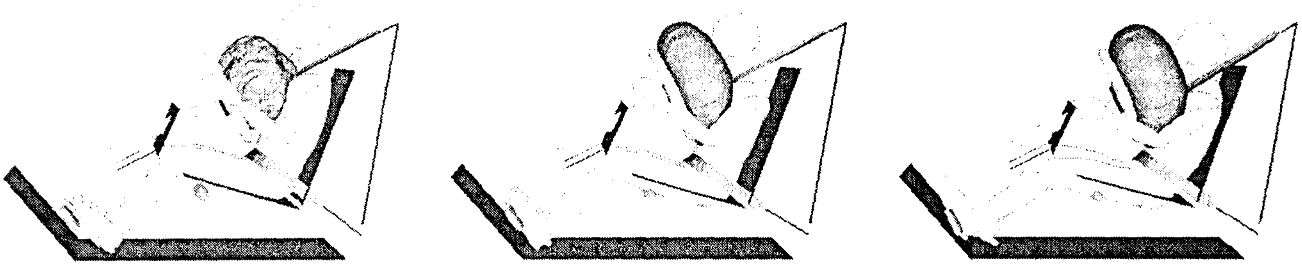

25msec 50msec 75msec

Figure 3. Graphic Output of MADYMO Simulation in case of Air Bag "A".

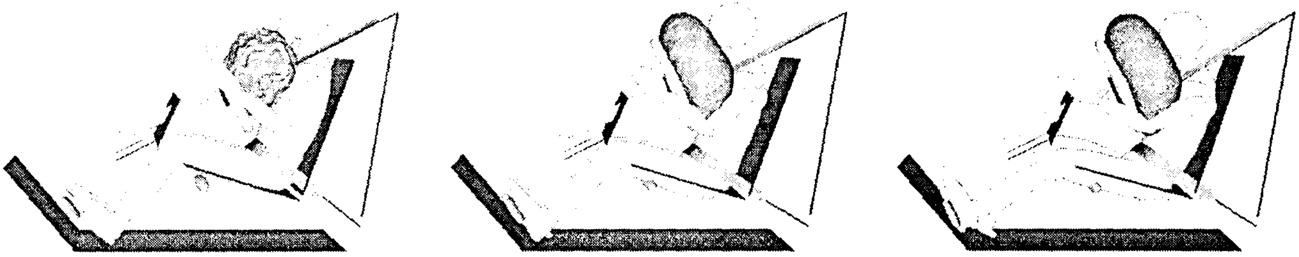

25msec 50msec 75msec

Figure 4. Graphic Output of MADYMO Simulation in case of Air Bag "B".

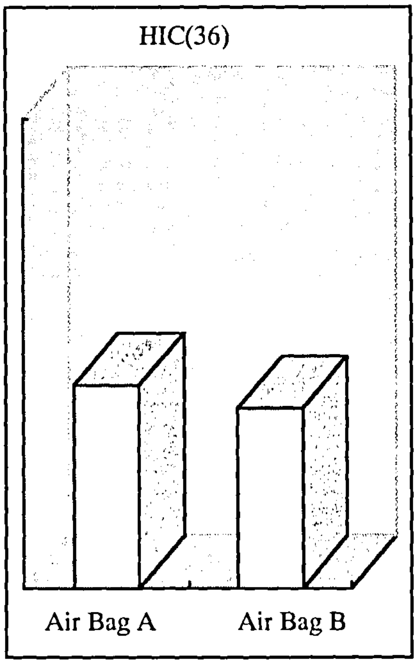

Figure 5. HIC(36) of MADYMO Simulation.

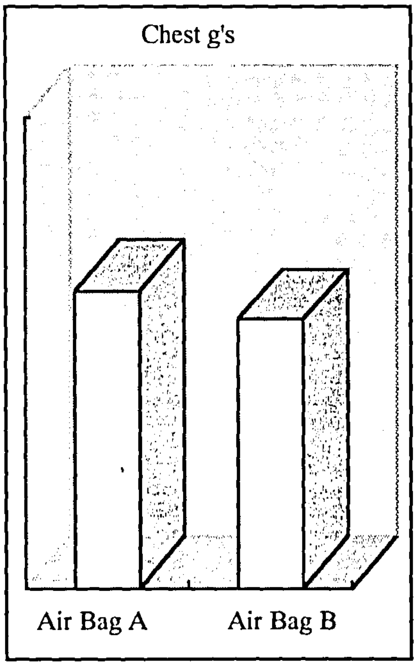

Figure 6. Chest g's of MADYMO Simulation.

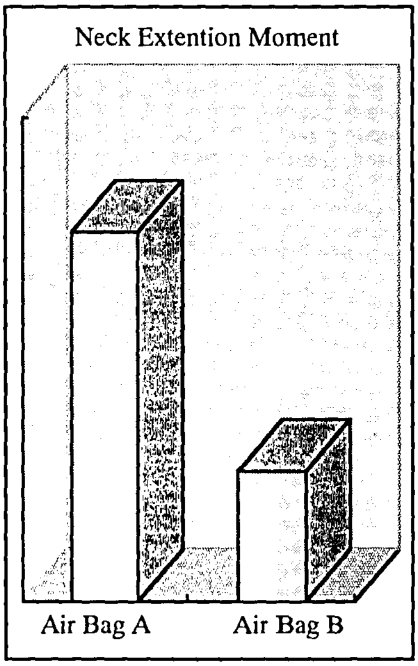

Figure 7. Neck Extension Moment of MADYMO Simulation.

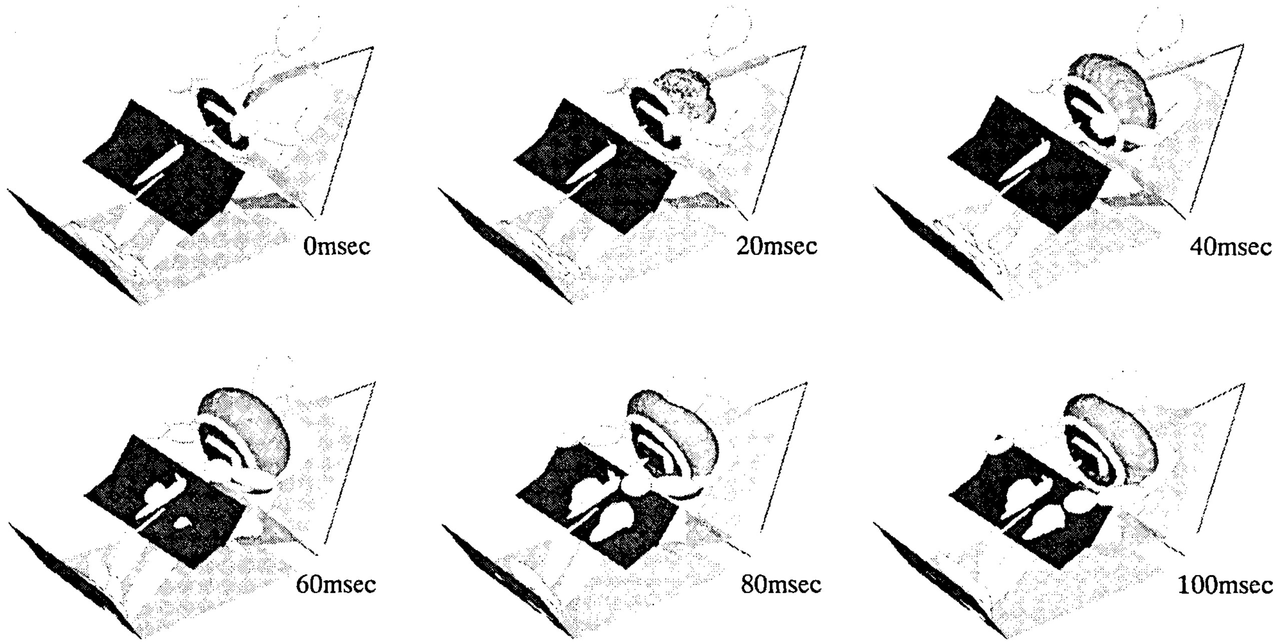
0msec
20msec
40msec
60msec
80msec
100msec

Figure 8. Graphic Output of MADYMO Simulation in case of Air Bag "B" with Pretensioner and Force Limiter.

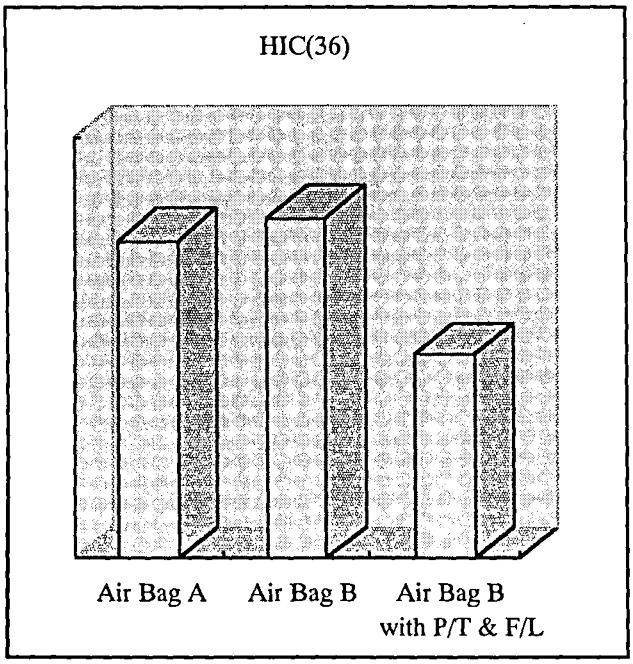

Figure 9. HIC(36) of MADYMO Simulation.

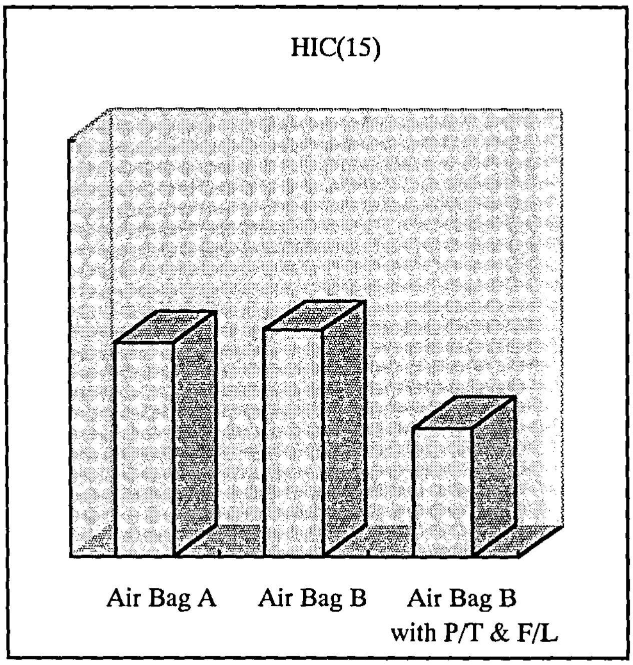

Figure 10. HIC(15) of MADYMO Simulation.

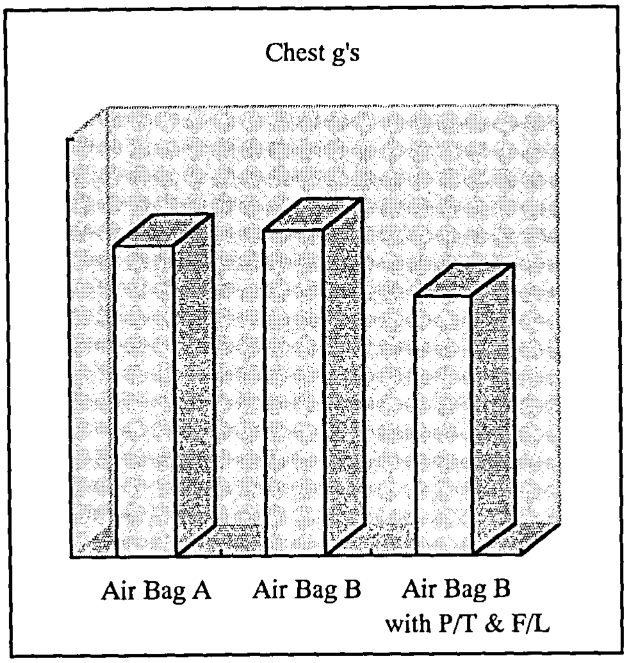

Figure 11. Chest g's of MADYMO Simulation.

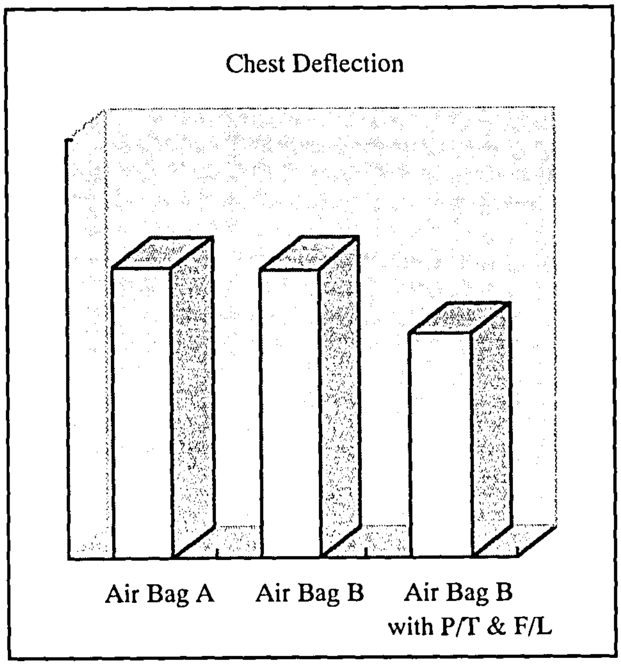

Figure 12. Chest Deflection of MADYMO Simulation.

DISCUSSION

The results of the MADYMO simulations indicated that depowering of air bags reduces aggressiveness under a moderate impact condition. It is also showed that depowered air bags may produce slightly higher dummy measurements than baseline air bags in MADYMO simulations of a 35mph frontal impact. NHTSA has also conducted a MADYMO simulation study evaluating air bag aggressiveness, and their results were published in the Final Regulatory Evaluation in Feb. 1997. The report included the results of 35mph frontal impact vehicle tests with AM50 dummy restrained by both the air bag and the seat belt. The vehicle tests and MADYMO simulations conducted by NHTSA showed the same tendency as our results (Table 1 and Table 2). Based on these results, they concluded that air bag depowering makes little difference on HIC and chest g's in the 35mph frontal tests.

On the other hand, various crash tests, whose results are widely reported, are currently carried out to produce vehicle safety information for consumers. As shown in Tables 3 and 4, many of these ratings are based on HIC(36) and chest g's (which are used for injury criteria

Table 1.
Vehicle to Barrier Tests by NHTSA

	Baseline	25% Depowered
HIC	814	857
Chest g's	52	59.6

Table 2.
Simulations by NHTSA

	Baseline	20% Depowered
HIC(36)	600.5	678.5
Chest g's	42.3	44.6

Table 3.
Various Rating Test Conditions

		Configuration	Impact Velocity	Dummy	Measurements						
					Head				Chest		
					HIC(36)	HIC(15)	3msG	peakG	3msG	Deflection	V*C
United States	NHTSA	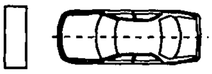	35mph	H-Ⅲ	○				○		
	IIHS	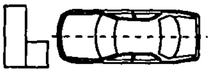	40mph		○	○	○	○	○	○	○
Japan	MOT	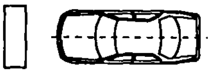	55kph		○				○		
Australia	Queensland, NSW, South Australia	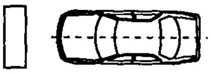	56kph		○				○		
		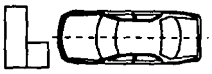	64kph								
United Kingdom	TRL	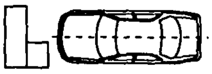	64kph		○		○	○		○	○
Germany	AMS	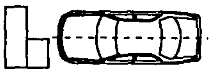	55kph		○		○		○		
	ADAC	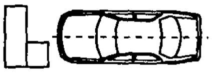	60kph		○		○		○		

Table 4.
Compliance Test Conditions

	Configuration	Impact Velocity	Dummy	Measurements						
				Head				Chest		
				HIC(36)	HIC(15)	3msG	peakG	3msG	Deflection	V*C
United States	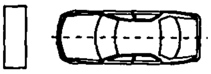	30mph	H-Ⅲ	○				○	○	
Canada	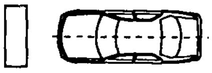	30mph			○		○		○	
Japan	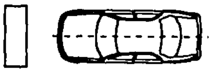	50kph		○				○		
Australia	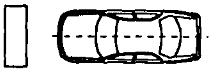	50kph		○				○	○	
Europe	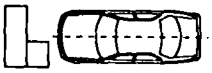	56kph		○*		○			○	○

* in case with head contact only

in most compliance tests as well).

The concept of HIC was proposed by Versace in 1971. It is a value based upon the head acceleration vs. time curve. In 1972, NHTSA proposed the use of HIC for assessing the potential of head injury with HIC < 1000 being acceptable values. In 1986, NHTSA proposed a time limitation of 36msec for calculating HIC value. This limitation was applied because high HIC values were being produced by low acceleration of long duration. That did not represent a likelihood of head injury. At that time, two alternative methods of HIC calculation were proposed. The first was to calculate HIC for the duration of head contact only. This option was rejected because of the difficulty in measuring the head contact duration. The second alternative was to set a limit for the time duration during which HIC is calculated. Although a number of researchers had proposed to use a time limitation in the order of 15-17msec, NHTSA finally selected 36msec as the time limitation to be used for HIC calculation based on their study. Prasad and Mertz proposed HIC(15) and also developed a life-threatening brain injury risk curve based on an analysis of HIC(15) values. The method of calculating HIC(15) has been accepted by the International Standards Organization. We calculated HIC(15) values using head resultant acceleration of MADYMO simulations for the 35mph frontal impact. The injury risk of each simulation was calculated and charted using the Prasad and Mertz curve (Figure 13). A comparison of injury risk using HIC(15) revealed no significant difference between the baseline air bag and the depowered air bag.

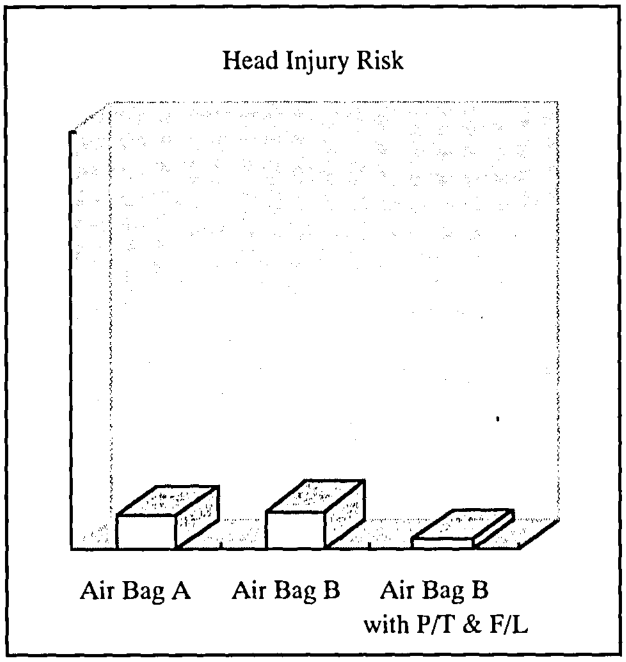

Figure 13. Head Injury Risk of MADYMO Simulation.

Finally we are of the opinion that chest deflection measures are the most appropriate criterion for chest injuries. In NCAP, as in FMVSS 208, chest g's have been used as chest injury criteria since its introduction in 1971. However, recently chest deflection is considered to a better chest injury measure and has been used since the H-III dummy was proposed for FMVSS 208 to reduce concentrated rib deflection by the seat belt. It will also be used for the Euro-frontal impact rule in 1998. In general, it is believed that most life threatening chest injuries are due to mechanical internal organ damage caused by rib deformation. Therefore, using chest deflection for chest injury criteria is thought to be more realistic. In this study, FEM belt with and without a force limiter were modeled in the MADYMO simulations. Results of similar cadaver tests conducted by Kallieris are shown in Figure 14. They reported that the force limiter prevented partial rib deformation under a severe crash condition. Our simulation of both a depowered air bag and a belt system with a force limiter predicted reduced chest deflection compared with baseline (Figure 8).

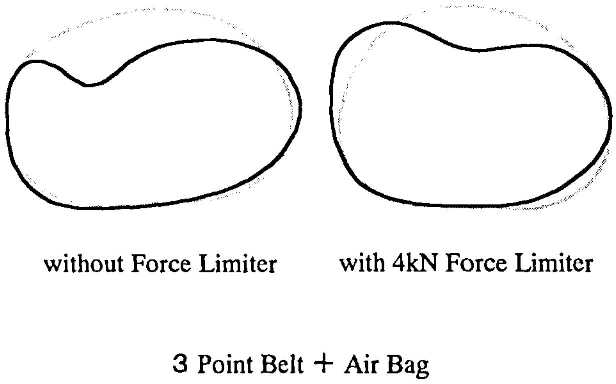

Figure 14. Rib Deformation with and without Force Limiter (Kallieris et al.).

CONCLUSION

The results of the MADYMO simulations indicate that depowered air bags reduce AF05 dummy measurements in some moderate frontal impacts.

In the study modeling a 35mph frontal impact, values of HIC and chest g's were slightly higher with depowered air bags than with baseline air bags, but the probability of injuries based on these values were not significantly different. HIC(15) and chest deflection are considered to be biomechanically more appropriate for assessing injury potential than HIC(36) and chest g's, which are widely used in tests such as NCAP. Similar trends were observed using these injury criteria. In specific situation, where depowered air bags result in unacceptable injury measures in 35mph frontal barrier tests, the simulations suggest that the addition of a pretensioner, or a force limiter, or both, may be an appropriate alternative.

REFERENCES

1. NHTSA, "Safety Fact Sheet", February 1, 1998
2. NHTSA, "Special Crash Investigation", April 1, 1998
3. Federal Register. January 6, 1996(Volume 62, Number 3). Docket 74-14; Notice 108. Notice of Proposed Rulemaking: Depowering of Air Bags.
4. Federal Register. March 19, 1997(Volume 62, Number 53). Docket 74-14; Notice 114. Depowering of Air Bag Final Rule.
5. "Air Bag On-Off Switches". Docket NHTSA-97-3111, RIN 2127-AG61
6. NHTSA, "Final Regulatory Evaluation, Actions to Reduce the Adverse Effects of Air Bags - FMVSS No. 208 DEPOWERING", February 1997
7. Digges, K., et al., "Benefits of Depowering Present Day Air Bags", Prepared for AIAM, May 28, 1997
8. Versace, J., "A Review of the Severity Index", SAE 710881, Fifteenth Stapp Car Crash Conference, 1971.
9. Federal Register. October 17, 1986(Volume 51, Number 201). Docket 74-14; Notice 47. Occupant Crash Protection and Automatic Restraint Phase-in Reporting
10. Prasad, P., and Mertz, H. J., "The Position of the United States Delegates to the ISO Working Group 6 on the Use of HIC in the Automotive Environment", SAE 851246, 1985.
11. Mertz, H. J. and Irwin, A. L., "Brain Injury Assessment of Frontal Crash Test Results", SAE 941056, 1994.
12. Mertz, H. J., Horsch, J., Horn, G. and Lowne, R., "Hybrid III sternal deflection associated with thoracic injury severities of occupants restrained with force-limiting shoulder belts", SAE 910812, 1991.
12. Kallieris, D., Rizzetti, A., et. al., "On the Synergism of the Driver Air Bag and the 3-Point Belt in Frontal Collisions", SAE 952700
13. Crandall, J. R., Bass, C. R., et al. "Thoracic response and injury with belt, driver side airbag, and force limited belt restraint systems", IJCrash 1997 Vol. 2 No. 1

DEVELOPMENT OF A METHOD OF ESTIMATING THE COSTS OF INJURIES PREDICTED BY ANCAP TESTING IN AUSTRALIA

G. Anthony Ryan
Delia Hendrie
Narelle Mullan
Road Accident Prevention Research Unit
Department of Public Health
The University of Western Australia
Australia
Paper Number 98-S11-P-16

ABSTRACT

A database of comprehensive injury costs was developed using data from finalised personal injury claims where a single injury was sustained. A method of combining costs for cases with multiple injuries was developed. Injury Assessment Functions were used to predict the probability of head, chest and lower limb injury from measurements taken from Hybrid III dummies in Australian New Car Assessment Program full frontal and offset tests. Costs for injury to each body region were obtained by summing the product of the probability of injury and the cost of injury for each level of injury and body region. These costs were then combined for each of driver and passenger position and for each vehicle. Results showed a wide range of costs in the initial ANCAP tests in 1992 and 1993, with a considerable reduction in subsequent testing, in both full frontal and offset tests. Injury costs in offset tests were lower than in frontal tests and were higher for passengers than drivers.

INTRODUCTION

Testing for the Australian New Car Assessment Program (ANCAP) has been carried out in Australia since 1992. Griffiths (1996) demonstrated that there was a reduction in the probability of head injury in large and medium vehicles between 1992 and 1994, and that the performance of Australian vehicles was inferior to US vehicles of similar mass. Another method of comparing the occupant protection performance of different vehicles, and of the same vehicle over time, is to use estimates of the costs of injuries predicted from crash testing, in this case, from the Australian ANCAP program.

AIM

The aims of this project were to:

1. Develop a database of comprehensive injury costs by body region and injury severity;
2. Estimate the costs of injuries predicted by measurements obtained from anthropometric test devices in different models of vehicles in full frontal and offset crash tests;
3. Analyse changes in the costs of injuries for the same vehicle model in different tests, and for groups of vehicles.

METHOD

A series of steps were involved in the process of estimating injury costs for ANCAP tests.

1. Comprehensive costs of injury by level of severity for each body region were established.
2. The probability of injury for a given body region at various impact levels was established using appropriate Injury Assessment Functions.
3. For a particular vehicle in a particular test, the cost of injury was determined from the product of the probability of injury of a particular severity and the cost of that injury, summed over all injury severities.
4. A method of combining the costs of injuries to several body regions into a single sum was developed for cases with multiple injuries.
5. Cost estimates were developed separately for driver and front seat passenger in each of frontal and offset frontal impact tests.
6. Comparisons were made between successive tests of the same vehicle, and between classes of vehicles.

INJURY COSTS

Comprehensive costs for road injury by injury severity level for each body region were developed using data from 49,755 personal injury insurance claims from New South Wales and from other sources. The claims data included the Abbreviated Injury Scale (AIS) (1985 revision) coding for up to five injuries per person. The components of these costs included hospital and medical, rehabilitation, modifications to home etc, aids and appliances, economic loss, general damages, legal and investigations, long term and home care, insurance administration, property damage, travel delay, accident investigation, motor vehicle insurance, unpaid earnings, non-victim costs, and other costs. These costs were estimated for cases with finalised claims for single injuries.

Table 1
Injury costs by component, body region and severity (A$ 000s)

Severity	Costs A$ 000					
	Head			**Chest**		
	Additive	Non-additive	Total	Additive	Non-additive	Total
AIS 1	1.9	16.5	18.4	1.2	6.8	8.0
2	4.6	25.4	30.0	3.9	14.1	18.0
3	14.8	56.8	71.6	5.4	18.7	24.1
4	75.2	648.0	723.2	15.6	18.7	34.3
5	75.2	648.0	723.2	15.6	18.7	34.3

Severity	Costs A$ 000					
	Upper leg			**Lower leg**		
	Additive	Non-additive	Total	Additive	Non-additive	Total
AIS 1	2.1	17.2	19.3	1.7	11.2	12.9
2	8.7	34.2	42.9	8.5	33.5	42.0
3	16.3	47.8	64.1	18.9	53.8	72.8
4	16.3	47.8	64.1	-	-	-
5	16.3	47.8	64.1	-	-	-

A method of combining costs was developed for cases with multiple injuries. It was assumed that some costs could be attributed to each individual injury; these were termed additive costs, while other costs could only be attributed to either the crash event or would apply equally to all injuries, and could only be counted once. These were termed non-additive costs. Additive costs included hospital and medical, rehabilitation, modifications to home etc, and aids and appliances, while non-additive costs included the remainder. In cases where there were injuries to more than one body region, the additive costs for each region were summed, and added to the largest non-additive cost from any body region. Costs for fatal injuries were not included. Average total costs for the four body regions used in evaluating vehicle design changes and their additive and non-additive components are set out in Table 1.

PROBABILITY OF INJURY

For each body region the probability of injury was estimated using an appropriate Injury Assessment Function (IAF). The Australian ANCAP test program provided measurements from the Hybrid III dummies used, for the head (Head Injury Criterion (HIC)), the chest (deflection in millimetres and acceleration in g), upper leg (knee impact force, kN), and for the lower leg (Tibial Index).

Head Injury

A search for an appropriate IAF revealed that Newman, Tylko and Miller (1992) had proposed an IAF for head impacts which used Gmax, a measure which combined linear and angular accelerations. As these values were not available from the ANCAP test results, the family of curves proposed by Newman et al (1992), were transferred to a base of HIC values, by extrapolation from a curve for AIS 4 head injury proposed by Mertz (1994). These curves were then compared with those proposed by NHTSA (1995), which were based on work by Prasad and Mertz (1985). The curves developed from Newman were steeper and provided greater discrimination between impacts of similar magnitude. Although the assumptions made in developing both sets of curves were equally tenuous, the NHTSA curves have been used in estimating the probability of head injury as they have been widely used and have become accepted as the industry standard (Figure 1).

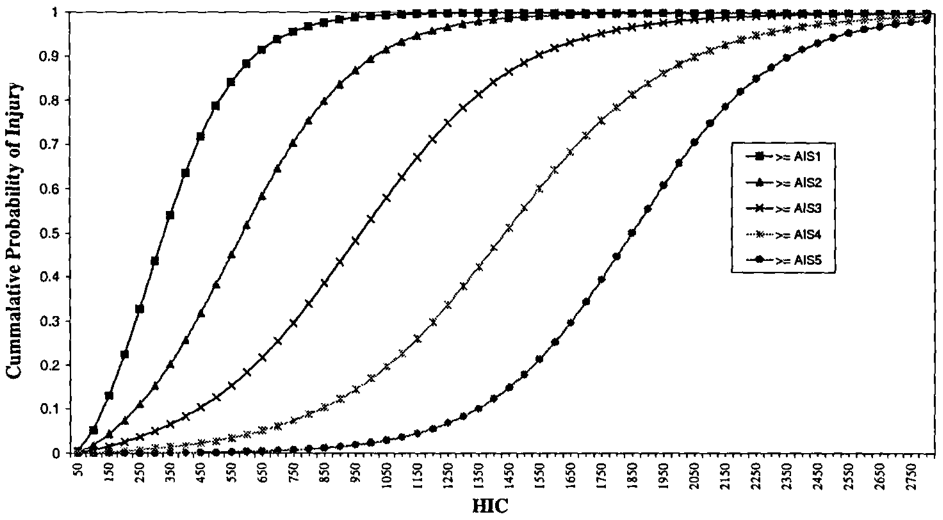

Figure 1 Probability of head injury severity as a function of HIC.

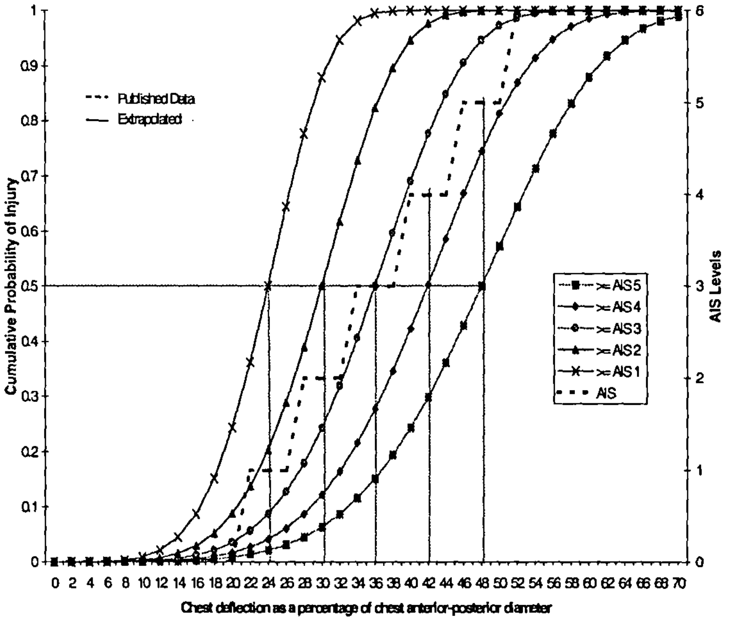

Figure 2 Probability of chest injury as a function of chest deflection

Chest Injury

The probability curves for chest injury of Newman et al (1992), based on chest deflection as a percentage of chest anterior-posterior diameter were adopted (Figure 2). The anterior-posterior diameter of the Hybrid III chest was assumed to be 223mm.

Upper Leg

The knee impact force criterion of Mertz (1994) was adopted, where a knee impact force of 7.5kN indicated AIS3 upper leg injury, equivalent to a fracture of the femur or pelvis.

Lower Leg

The Tibial Index of Mertz (1994) was used for lower leg injury. Peak bending moment for the upper and lower tibia (M) and peak axial compression force for the lower tibia (P) were used in the equation:

Tibial index = M/225Nm+P/35.9kN

A Tibial Index greater than 1.0 indicates an injury of AIS2, which is equivalent to a fracture of the tibia.

COST OF INJURY

For each body region, the cost of the injury was obtained by summing the product of the probability of occurrence of each level of severity of injury (as predicted by the injury assessment functions) by the cost of the injury of that severity, divided into its additive and non-additive components. That is, for each body region:

$$\text{Additive Injury Cost} = \Sigma\ (P_i\,.Ca_i)$$

Where $i = AIS1, AIS2, AIS3, AIS4, AIS5$
P = probability of injury
Ca = additive cost

and

$$\text{Non-additive Cost} = \Sigma\ (P_i.\ Cna_i)$$

Where $i = AIS1, AIS2, AIS3, AIS4, AIS5$
P = probability of injury
Cna = non-additive cost

Cost For Each Seated Position

Having determined the appropriate cost for all four body regions, a cost was calculated for each driver and front passenger position. Additive costs were summed across all body regions and added to the maximum of the non-additive costs for any region. That is, for each driver and front passenger:

$$\text{Occupant Cost} = \Sigma(\text{Additive Injury. Cost})_j + \text{MAX}(\text{Non-additive Injury. Costs})_j$$

j = *Head, Chest, Upper Leg and Lower Leg*

Cost Per Vehicle

A total cost per vehicle was obtained, by adding the driver cost and passenger cost. The full-frontal and offset tests were treated independently. That is, for each full-frontal and offset test;

$$\text{Vehicle Cost} = \Sigma(\text{Occupant costs})_k$$

Where k = Driver, Passenger

NEW CAR ASSESSMENT PROGRAM (ANCAP)

The first ANCAP tests of Australian cars were carried out in 1992 and 1993 as full frontal tests at 56km/h. Offset tests with 40% overlap, using a deformable barrier, at 60km/h were introduced in 1994. The impact speed for the offset tests was subsequently raised to 64km/h. Additional tests on the same model were carried out when there was thought to have been a substantial change in occupant protection performance. Therefore, while the majority of vehicles had been tested at least twice in the five years 1992 - 1997, there were a number for which only one test had been performed. Only the first and the latest test have been included when discussing changes in individual vehicles, regardless of how many tests were performed. If only one test was performed, then it was considered in the first set of tests. Results for full frontal and offset tests are presented separately. Large and medium cars were grouped together, being vehicles with a mass of 1200kg and over.

RESULTS

For the 80 vehicle tests published by the ANCAP program, injury costs were calculated for driver and passenger for frontal and offset tests. Due to the large volume of data, results are only presented for large and medium cars, ie, those with a mass of 1200kg and over. Frontal and offset tests are presented separately.

Figure 3 presents the estimated costs of the predicted injuries to driver and passenger for frontal tests for large/medium cars.

The total injury cost for the initial test ranged widely, from over A$1.2 million to under A$100,000. For all except one of the six models where at least one or more test was performed, there were substantial differences. All the latest models tested were equipped with driver airbags.

These results are summarised in Figure 4, which shows the large spread of costs in the initial tests, with four models having costs over A$600,000. This compares with the latest tests where all but one were under A$400,000.

The mean cost for the six models which were tested at least twice was A$757,080 for the first test and A$257,520 for the latest, a difference of A$499,560. For all full frontal tests of large and medium vehicles the mean total cost was A$488,190.

Figure 5 shows the results for the offset frontal tests. In general these costs were lower than for the full frontal tests. The mean total cost was A$153,000 per test. It is notable that the improvement in costs in successive tests seen in the full frontal tests is not seen in the offset tests where costs in some models were higher in later tests.

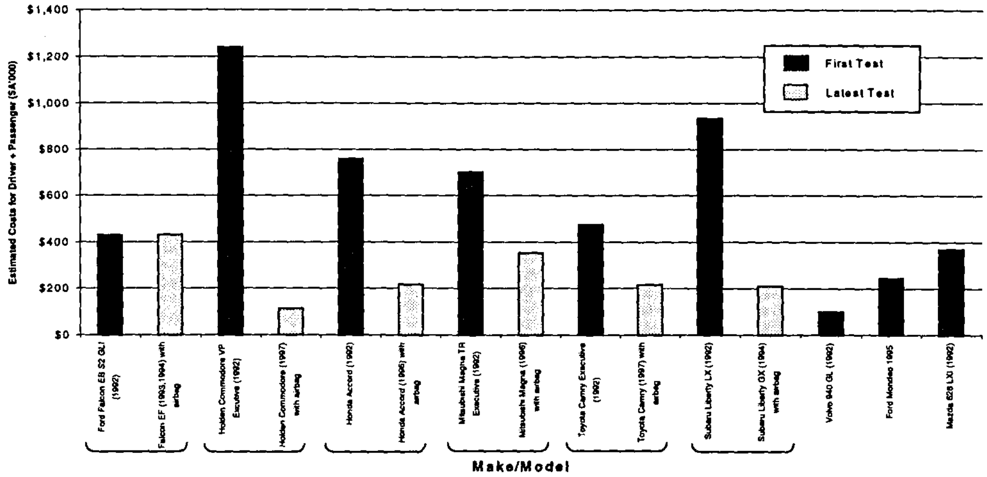

Figure 3 Estimated total cost of injuries for large/medium cars in full frontal tests (A$ 000s)

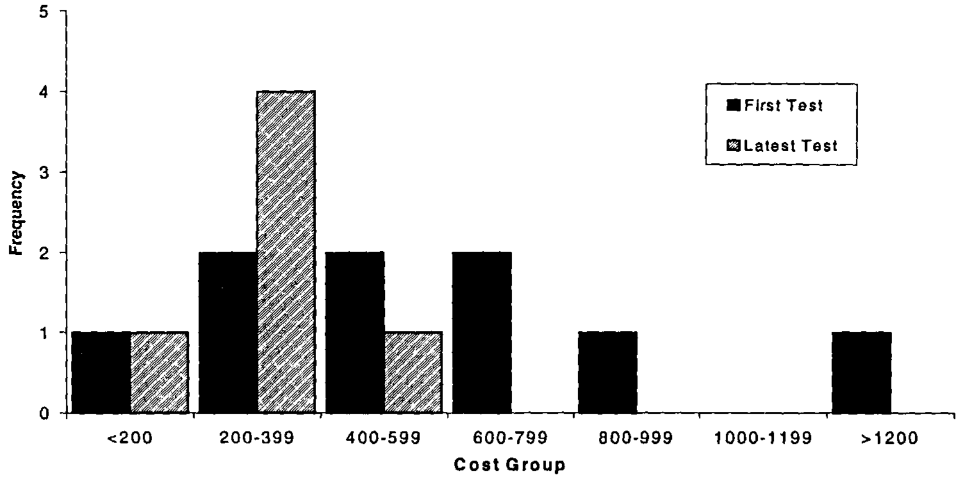

Figure 4 Comparison of costs between the first and latest tests, large/medium cars, full frontal tests(A$ 000s)

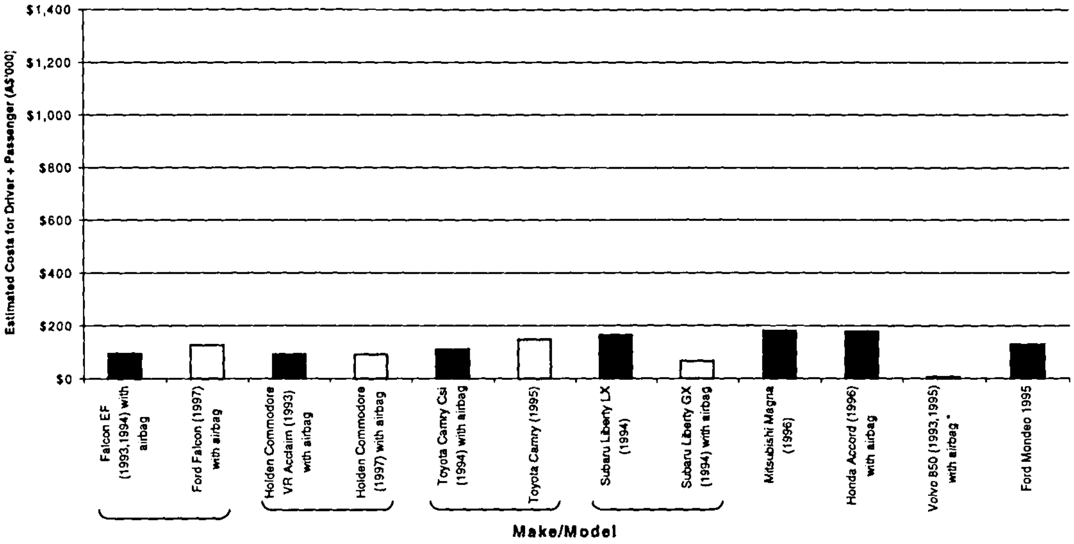

Figure 5 Estimated total cost of injuries for large/ medium cars in offset tests (A$ 000s)

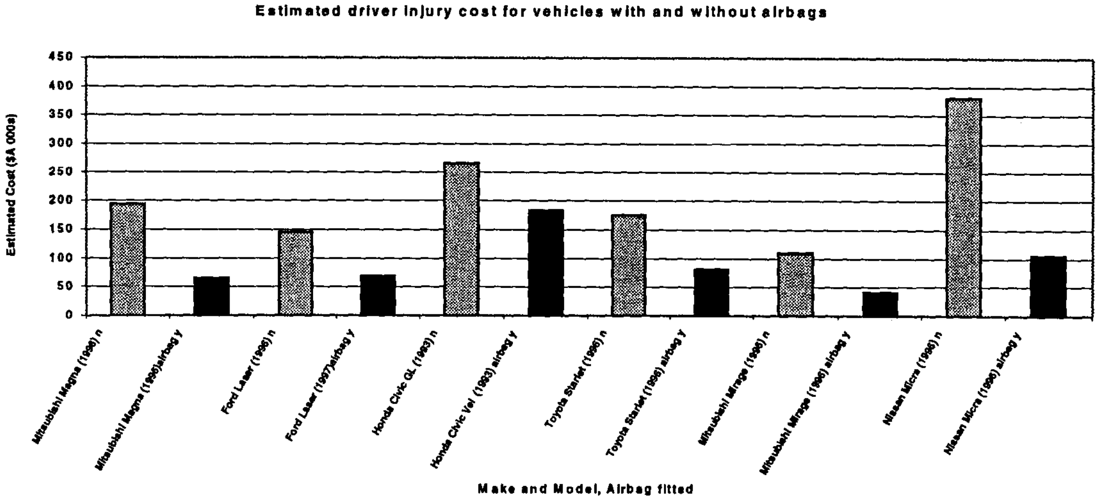

Figure 6 The effect of a driver airbag on estimated cost of injury (A$ 000s)

Mean Driver, Passenger and Total Costs

In 14 (63.6%) of the 22 frontal tests where data were available, passenger injury costs were higher than driver costs. This is reflected in the respective mean costs for all tests, where the driver mean cost was A$210,360 and for the passenger, A$277,830. For offset tests, the mean cost for drivers was A$114,000 and for passengers, A$39,400.

The Effect of Airbags

Six models were tested with and without driver side airbags. The results are shown in Figure 6. In each case there was a considerable decrease in costs of driver injury, although the magnitude of the change depended to some extent on the initial cost in the no airbag state. The mean difference was A$121,000 with a range from A$69,000 to A$276,000. In percentage terms, the difference ranged from 27.7% to 69.2% of the initial cost.

DISCUSSION

A number of assumptions were made in the course of this project, all of which may affect the magnitude of the costs estimates. With regard to the Road Injury Cost Database, the cost estimates were largely based on finalised personal injury claims over a seven year period. The estimates for the more severe head injuries will be considerably lower than they should be, because these claims can take up to five years to be settled. The IAFs used were the best estimates available but they are dependent on a number of assumptions that may later be shown to be inaccurate. Notwithstanding these problems, the method has been applied consistently for all vehicles and provides an indication of the relative performance of vehicles with each other and over time. The results also show that it is possible to greatly reduce the costs of injuries, as demonstrated in standardised crash tests, through appropriate changes in vehicle construction.

ACKNOWLEDGMENTS

This study was supported by research grants from the Roads and Traffic Authority of New South Wales, the NRMA Ltd, and the Royal Automobile Club of Victoria.

The authors wish to acknowledge the generous assistance provided by the Motor Accidents Authority of New South Wales, and by the Australian New Car Assessment Program.

REFERENCES

Association for the Advancement of Automotive Medicine. Abbreviated Injury Scale, 1985 Revision. Des Plaines Il. 1985

Griffiths M. Consumer crash test programs: international harmonisation and scope for injury reduction. Proceedings, Fifteenth Technical Conference on the Enhanced Safety of Vehicles. US National Highway Traffic Safety Administration. 1996 2040-2044.

Newman JA, Tylko S, Miller T. Toward a comprehensive biomechanical injury cost model. Accident Analysis and Prevention 26 305-314 1994

Mertz HJ Injury assessment values used to evaluate Hybrid III response measurements. The First Human-Life Crash Test Dummy. Warrendale, PA. Society of Automotive Engineers Inc 287-422 1994

National Highway Traffic Safety Administration. Final economic assessment, FMVSS No. 201, Upper Interior Head Protection. Office of Regulatory Analysis, Plans and Policy. Washington DC. June 1995

ESV
WINDSOR98

U.S. Department
of Transportation
National Highway
Traffic Safety
Administration

DOT HS 808 759
October 1998

Transport Canada
Road Safety

Transports Canada
Sécurité routière